Controls on the Enrichment of the Serra Verde Rare Earth Deposit, Brazil

Carmen Pinto-Ward

December 2017

Department of Earth Science and Engineering

Imperial College London

A thesis submitted in part fulfilment of the requirements for the degree of Doctor of Philosophy of Earth Science and Engineering Department of Imperial College London and the diploma of Imperial College London.

Declaration of Authorship

I declare that this thesis, titled “Controls on the Enrichment of the Serra Verde Rare Earth deposit, Brazil”, is entirely my own work under the supervision of Prof. Richard Herrington and Dr. Jamie Wilkinson. All published and unpublished materials used in the thesis have been given full acknowledgement. This work has not been previously submitted, in whole or in part, to any other academic institution for a degree, diploma, or any other qualification.



Carmen Pinto-Ward

Department of Earth Sciences and Engineering

Imperial College

Copyright Notice

The copyright of this thesis rests with the author and is made available under a Creative Commons Attribution Non-Commercial No Derivatives licence. Researchers are free to copy, distribute or transmit the thesis on the condition that they attribute it, that they do not use it for commercial purposes and that they do not alter, transform or build upon it. For any reuse or redistribution, researchers must make clear to others the licence terms of this work.

Abstract

Ion-adsorption rare earth element deposits (IADs) are weathered granites that contain economically exploitable REE-bearing clays, hosting 90 % of world HREE resources, and thus a vital supply of critical metals. The mechanisms that lead to the enrichment of REE, and the controls on the development of the host weathered profile are poorly understood. The Serra Verde deposit in Brazil is one of the few IADs discovered outside China, and therefore provides a valuable case study in understanding the factors that lead to their formation.

Samples from the weathered profile and bedrock were analysed by SEM, EMP, and XRD to characterise the deposit and assess the controls on the enrichment. The Serra Verde IAD developed over a strongly REE-enriched, phosphate-poor, and weakly peraluminous A-type granite. The REE-mineral assemblage of the granite is largely hydrothermal, formed of REE-fluorcarbonates, altered zircons, metamict niobiates, F-rich xenotime-Y, and monazite-La. Breakdown of the granite under wet, tropical conditions, produced a strongly REE-enriched saprolite. Mass balance analysis indicates that enrichment occurred through efficient mass transfer of REE from the upper profile.

Lateral variations in ore grade, REE mineralogy, and saprolite thickness are attributed to variable drainage across the profile. LREE-fluorcarbonates are the principle source of mobilised REE, and show complex dissolution and re-precipitation patterns across the saprolite. The formation of supergene fluorcarbonates reduces the amount of REE adsorption on clays, and are distinguished by their negative Ce anomalies.

Leaching experiments were carried out to quantify the percentage of ion-exchangeable REE (PER), the REE residence in ore minerals, and the sensitivity to both leaching time and pH. The PER at Serra Verde is controlled by REE mineralogy, clay content and composition. Leaching times over 10 minutes result in a significant decrease in extracted REE, while lower pH increased the PER at the expense of introducing additional impurities from clay breakdown.

Acknowledgements

This thesis was completed with the organisational, logistical and financial support from Serra Verde Mining and their partners. I am thankful for the experiences I had in Brazil at the site, and for their willingness to have this unique deposit studied from an academic perspective. The technical field team showed patience and shared their insight while showing me around the deposit area. Their assistance in locating drill core and shipping samples back to London were invaluable.

I would like to thank my supervisors, Prof. Richard Herrington and Dr. Jamie Wilkinson, for offering me the opportunity to work on such an interesting project and for providing their support, guidance and encouragement throughout the duration of the PhD project. It has been a privilege to be a member of the LODE research group in the Natural History Museum, and I have learnt greatly from my fellow scientists in the group.

The Natural History Museum has been an enjoyable base for the duration of my study, and I am very fortunate to have access to a wide range of analytical instruments, sample preparation rooms, and chemical laboratories, which facilitated the spectrum of scientific investigation that formed the core of this thesis.

Much of this work would not have been possible without the help of several staff members of the NHM, who provided the training, technical support, and shared their expertise on the challenges faced in analysing REE and weathered samples. I would especially like to thank John Spratt for his patience in setting up the EMP to analyse the long list of rare earth elements, and the additional time he gave in order to explain how to process the data. Furthermore, I extend great thanks to Jens Najorka who provided helpful XRD training, and let me use the centrifuge to its design limit for separating clay fractions. I want to express how grateful I am to Rachel Norman – for going through my leaching experiment plan and giving honest advice from a chemist's perspective, and to both Emma Humphreys-Williams and Stanislav Strekopytov who assisted with experimental set ups in all of the leach experiments and analysis of the leach solutions. The patience and skill in preparing resin blocks of weathered material shown by Tony Wighton, Enrica Bonato and Callum Hatch made all the difference. Finally, Tomasz Goral's knowledge and skill in setting up the Quanta enabled us to capture the really very cool chemical analyses of nano-scale REE minerals for the first time.

And lastly, thank you to my dear family. You have always been supportive of my projects and my decisions, and it has given me much freedom in choosing my path. Above all I would like to thank my partner and tea-maker Tom, whose unrelenting support and love gave me the motivation and confidence to complete this project.

Table of Contents

Declaration of Authorship **2**
Abstract **3**
Acknowledgements **4**
List of Figures **12**
List of Tables **21**
Abbreviations **23**
Appendix List **24**
Chapter 1: Introduction **25**
1.1 General Introduction 25
1.2 Thesis Scope 26
1.3 Thesis structure 28
Chapter 2: A Review of Ion-Adsorption REE Deposits **30**
2.1 Ion Adsorption Rare Earth Deposits 30
2.1.1 Distribution 31
2.1.2 Classification 32
2.2 Chinese Ion adsorption REE deposits 35
2.2.1 Weathered profile 35
2.2.2 Mineralogy 38
2.3 Controls on the Formation of Ion-Adsorption Deposits 39
2.3.1 Climate and Geomorphology 39
2.3.2 Parent Rock Lithology 40
2.3.3 Minerals hosting the REE 41
2.3.4 Hydrothermal alteration 43
2.4 Mechanisms of Formation and Modification 44
2.4.1 Mobilisation of REE 44
2.4.2 Clay ion adsorption 45
2.4.3 Fractionation of REE 45
2.5 REE recovery from ion-adsorption clays 46
2.5.1 Ion-exchange theory 46
2.5.2 Experimental studies 47
2.6 Summary and Conclusions 48

Chapter 3: Geology of the Study Area **52**
3.1 The Serra Verde REE deposit and Study Area 52
3.2 Regional Geological Setting 53
3.3 The Serra Dourada Granite 58
3.3.1 Geochronology 58
3.3.2 Lithologies and Mineralogy 59
3.3.3 Geochemistry 61
3.3.4 REE-minerals 66
3.4 Exploration and Mining History 68
3.5 Summary 68
Chapter 4: Methods **70**
4.1 Introduction 70
4.2 Sample Collection 70
4.3 Whole Rock Geochemistry 71
4.3.1 Sample Preparation 72
4.3.2 Analytical methods 72
4.3.3 Quality control (accuracy and precision) 75
4.3.4 SV Assay samples 80
4.4 Scanning Electron Microscopy 80
4.4.1 Sample preparation 81
4.4.2 Sample analysis 81
4.5 Electron Microprobe Analysis 81
4.5.1 Sample preparation 82
4.5.2 Sample analysis 82
4.6 X-Ray Diffraction 85
4.6.1 Sample preparation and analysis 86
4.6.2 Instrument calibration 86
4.6.3 Swelling clay test 86
4.7 Optical Microscopy 87
Chapter 5: Mineralogy and Geochemistry of the Serra Verde REE Deposit Parent Bedrock **88**
5.1 Introduction 88
5.2 Methods 90

5.2.1 Samples 90
5.2.2 Analytical methods 92
5.2.3 Assay data processing for geochemical maps 92
5.3 Petrology 95
5.3.1 Plateau samples 95
5.3.2 Granite rim samples 100
5.4 Whole-Rock Geochemistry 101
5.4.1 Serra Dourada geochemistry 101
5.4.2 Sample geochemistry 102
5.5 REE Mineralogy 114
5.5.1 Zircon 115
5.5.2 REE phosphates 121
5.5.3 LREE-fluorcarbonates 132
5.5.4 Niobiates 136
5.5.5 Amorphous REE silicates 144
5.5.6 Other accessory minerals 146
5.6 Discussion 149
5.6.1 Serra Dourada granite 145
5.6.2 Geochemistry of the Serra Verde parent bedrock 151
5.6.3 REE-bearing minerals of parent bedrock of Serra Verde REE deposit 153
5.6.4 Hydrothermal alteration 159
5.6.5 Proposed model for REE enrichment and hydrothermal alteration of the bedrock granite 161
5.7 Conclusions 163
Chapter 6: Characterisation and Mass Balance Analysis of the REE-enriched Weathered Profile of the Serra Dourada granite 164
6.1 Introduction 164
6.2 Study Area 165
6.3 Methods 167
6.3.1 Sample selection 167
6.3.2 Analytical methods 168
6.3.3 Calculations 168
6.4 General Characteristics of Weathered Profile 176

6.4.1 Vertical variations 176
6.4.2 Lateral variations 181
6.5 Whole-Rock Geochemistry 184
6.5.1 Chemical weathering intensity 184
6.5.2 Major element distribution along the weathered profile 186
6.5.3 Trace element distribution along the weathered profile 191
6.6 Bulk Mineralogy 202
6.7 Mass balance Analysis 204
6.7.1 Identification of immobile elements 204
6.7.2 Bulk density 207
6.7.3 Volumetric strain 209
6.7.4 Mass transfer 211
6.8 Discussion 219
6.8.1 Bulk characteristics of the weathered profile 219
6.8.2 REE distribution and fractionation 223
6.8.3 Mass balance model of REE enrichment 224
6.8.4 Physico-chemical conditions along the weathered profile 227
6.9 Conclusions 232
Chapter 7: Mineralogical Characterisation of the REE-rich Saprolite Horizon including the Residency and Distribution of REE 233
7.1 Introduction 233
7.2 Materials and Methods 235
7.2.1 Sample selection 235
7.2.2 Analytical methods 238
7.2.3 Mineral modal analysis 239
7.2.4 Calculating the proportion of REE in minerals 241
7.3 Geochemical Composition 243
7.3.1 REY-enriched saprolite samples 243
7.3.2 Internal variation in the saprolite 249
7.3.3 Clay-rich fracture-fill samples 253
7.4 Bulk Mineralogy 254
7.4.1 REY-enriched saprolite samples 254
7.4.2 Saprolite sub-horizon variation (DDH0161) 257

7.4.3 Clay-rich fracture-infill samples 259
7.5 REE Mineralogy 260
7.5.1 REE fluorcarbonates 260
7.5.2 Phosphates 272
7.5.3 Niobiates 278
7.5.4 Cerium oxides and silicates 280
7.5.5 Other minerals 280
7.6 REE-Mineral Abundances in the Clay Fraction 284
7.6.1 SEM-BSE imagery 284
7.6.2 REE-mineral maps 284
7.6.3 Proportion of REE held in resistant and supergene minerals 285
7.7 Discussion 290
7.7.1 Chemical and mineral characteristics of the saprolite ore horizon 290
7.7.2 REE distribution and mineral residence 291
7.7.3 Occurrence and composition of supergene REE-fluorcarbonates 293
7.7.4 Proportion of REE held in resistant and supergene minerals 295
7.7.5 Clay-rich fracture fillings 297
7.8 Conclusions 298
Chapter 8: Rare Earth Recovery by Ion-Exchange Leaching 299
8.1 Introduction 299
8.2 Experimental and Analytical Methods 300
8.2.1 Experimental samples 300
8.2.2 Experimental procedure 305
8.2.3 Analytical methods 306
8.2.4 Extraction calculations 307
8.2.5 Preliminary experiment to determine leaching time 309
8.3 Results 312
8.3.1 EMP and SEM analysis of clay minerals 312
8.3.2 Supernatant solutions 316
8.3.3 Residual material 336
8.4 Discussion 342
8.4.1 Ion-exchangeable REE in Serra Verde ore 342
8.4.2 Non-REE impurities 345

8.4.3 Effect of supergene minerals on extraction of REE 345
8.4.4 Effect of clay mineralogy on ion-exchangeable REE 347
8.4.5 Effect of pH on the leaching of REE and other elements 350
8.5 Conclusions 352
Chapter 9: Controls on the Formation and Enrichment of the Serra Verde REE Deposit 353
9.1 Assessment of the Controls on Formation and Enrichment 353
9.1.1 Composition and mineralogy of the protolith 353
9.1.2 Climate 354
9.1.3 Topography and drainage 355
9.2 The Mechanisms of REE Mobilisation, Fractionation, and Enrichment in the Serra Verde Deposit 357
9.3 Proposed model of formation and evolution of the Serra Verde REE Deposit 360
9.4 Exploration and Geometallurgical Implications 363
9.5 Conclusions and Further Work 364
Reference List 366
Appendix 380

List of Figures

Figure 1.1. Diagram showing the different aspects of the Serra Verde IAD that were investigated to achieve the aim of this PhD study. 28
Figure 2.1. Map highlighting the locations of currently known ion-adsorption REE deposits around the world. 32
Figure 2.2. REE distribution patterns in typical LREE and HREE clay-dominated IADs 33
Figure 2.3. Pie charts divided by REE-Y composition REE recovered from the ore from the Longnan deposit and from Xunwu. 33
Figure 2.4. Schematic diagram showing the main horizons that develop in weathering profiles. 36
Figure 2.5. A. REE fractionation developed on the Longnan, Huashan, Heling, and Helukou weathering profiles in southern China. B. Ce anomaly variations in the weathering profiles C. Main horizons of the weathering profile in ion-adsorption type deposits 37
Figure 2.6. Chart comparing the occurrence and abundance of LREE and HREE in different mineral classes. 41
Figure 2.7. Schematic of the cationic exchange process at clay surfaces during leaching 47
Figure 3.1. Outline of the Serra Dourada Granite and location study area of the plateau. 53
Figure 3.2. Crustal provinces of South America 54
Figure 3.3. Map depicting the main geological groups of northern Tocantins Province 55
Figure 3.4. Geological map of the Goiás Tin Province. 57
Figure 3.5. Simplified geochronological scale of events that affected central Brazil and the SDG. 57
Figure 3.6. Classification plots for A-type granite (A) 1000 Ga/Al vs Zr, and A1 vs A2 granites (B) Nb-Y-Ce ternary diagram. 63
Figure 3.7. Chondrite-normalised REE patterns of the different rock types in the SDG 65
Figure 3.8. Chondrite-normalised REE chart showing patterns for biotite granite and albitite samples from the SDG. Data from Marini et al. (1992). 65
Figure 3.9. Chondrite-normalised REE chart showing patterns of biotite granite, albitite and biotitite samples from SDG. Data from Teixeira & Botelho (2006). 66
Figure 3.10. SEM images from Santana 2013, showing bastnäsite and chamosite replacing allanite. 67
Figure 4.1. Work flow showing steps followed by ALS during whole rock geochemistry 74
Figure 4.2. Work flow showing steps followed by NHS during whole rock geochemistry 74
Figure 4.3. Reproducibility charts for two standards (left SY-4, and right GRE-3) analysed by the ME-ICP06 method at ALS. 77
Figure 4.4. Mean bias charts for each of the elements, plotted on separate graphs for each of the analytical methods used by ALS. 78

Figure 4.5. Mean bias charts for each of the elements, plotted on separate graphs for each of the analytical methods used by NHM. 79
Figure 4.6. Sum of the WDS spectral scans for each standard, showing the peak positions of elements detected by the LLIF and LPET crystals. 83
Figure 4.7. Schematic of the expected peak position on XRD patterns collected from Normal, Air-dried and EG solvated smectite clay mineral. 87
Figure 5.1. Location map showing the drill holes sampled and studied in this chapter by geochemical analysis. The inset figure shows the locations of drill holes that were sampled for fresh granite beneath the main plateau area. 91
Figure 5.2. Cumulative distribution of SiO_2 values coloured by the percentage bins used for colour scale cut-offs on gridded element maps. 93
Figure 5.3. Plots showing the non-weathered CIA cut-offs for Ti and Na from drill hole assay data, and corresponding filtered sample maps showing the included and excluded samples. 94
Figure 5.4. DDH0004 graphic core log (left) with sample locations marked by yellow dots, and photographs of the main lithologies (photos taken by Serra Verde Mining). 95
Figure 5.5. Photograph of three representative drill core sections studied from the top, middle, and lower portions of DDH0004. 97
Figure 5.6. Photographs comparing two representative pale-coloured biotite granite samples, and two pink-coloured biotite granite samples. 97
Figure 5.7. Thin section micrographs of biotite granite. 99
Figure 5.8. Photographs of two representative granite samples collected from the rim of the biotite granite. 100
Figure 5.9. Selected element maps that best highlight the variable geochemistry of the southern Serra Dourada granite 102
Figure 5.10. Geochemical classification map of the filtered CIA drill hole data (left), using bin values from the individual element maps in a simple decision tree (right). 103
Figure 5.11. Granite classification diagrams using major elements. 104
Figure 5.12. Major element plots for granite bedrock samples, showing the relationships between selected major elements for the three groups. 105
Figure 5.13. Trace element plots for granite bedrock samples, showing relationships between selected elements for the three groups of bedrock samples. 109
Figure 5.14. Chondrite-normalised REE patterns for granite samples. 110
Figure 5.15. Downhole drill hole assay data (black) and samples analysed in this study for both major and trace elements 111
Figure 5.16. SEM-BSE image showing the abundance of bright REE-bearing accessory phases in a typical granite bedrock sample. 114

Figure 5.17. SEM-BSE images or representative zircon grains and their textures found in granite samples. 116
Figure 5.18. Selected element plots of EMP analysis on zircons. 118
Figure 5.19. Back-scattered electron images of representative zircon grains that exhibit the dark altered patches and corresponding chondrite-normalised REE patterns..... 119
Figure 5.20. SEM-BSE images of monazite-Ce. 122
Figure 5.21. SEM-BSE images showing analysis points, and corresponding EDX spectra showing monazite replacement of titanite and replacement of apatite..... 121
Figure 5.22. Chondrite-normalised REE patterns of monazite-II analyses with published data. 124
Figure 5.23. Apfu element plots for EMP analyses, showing monazite-I and -II compositions, and monazite analyses by Teixeira & Botelho (2002)..... 126
Figure 5.24. SEM-BSE images of F-rich xenotime(-Y). 129
Figure 5.25. Apfu element plots showing differences in analysed composition between F-rich and normal F-poor xenotime varieties in the bedrock. 131
Figure 5.26. Chondrite-normalised REE patterns showing representative analyses for F-rich xenotime and normal xenotime. Xenotime patterns from Teixeira & Botelho, 2006 and Forster, 1998 are included for reference. 131
Figure 5.27. Ternary plot for Th-Ca-REE showing the compositions of fluorcarbonates analysed by EMPA in this study. 132
Figure 5.28. SEM-BSE images of bright REE-fluorcarbonates present in plateau granite samples, showing the variety of mineral textures and pseudomorphic habits. 134
Figure 5.29. Chondrite-normalised REE patterns showing representative results for Ce-bastnäsite and La-bastnäsite. 136
Figure 5.30. Diagram showing the classification of analytical data points of Nb minerals from this study using the statistical approach of Ercit (2005). 137
Figure 5.31. SEM-BSE images of samarskite minerals, showing their range occurrence and metamictic state. 138
Figure 5.32. Ternary diagrams 1 and 2 show A-site occupancy in analyses classified as samarskite, and diagram 3 shows B-site occupancy. 139
Figure 5.33. SEM-BSE and corresponding EDX element map showing the internal variation in composition of a metamictic samarskite grain..... 140
Figure 5.34. Chondrite-normalised REE patterns of several representative samarskite-Y analyses. . 141
Figure 5.35. SEM-BSE images of uranopyrochlore minerals found in the albitised section of drill hole DDH0004. Note the large grain size of these minerals..... 142
Figure 5.36. SEM-BSE images of nioboaeschynite-Ce and rare fergusonite-Y. 142
Figure 5.37. SEM-BSE images of representative fine grained amorphous Y-Ce silicates (possibly britholite-Ce) observed throughout the granite bedrock samples. 145

Figure 5.38. Chondrite-normalised REE patterns of representative Ce & Y silicate EMP analysis... 145
Figure 5.39. SEM-BSE images showing the typical occurrences and habit of fluorite in the biotite granite. ... 147
Figure 5.40. SEM-BSE images of thorites, occurring as inclusions or small grains proximal to zircons, and elongate ilmeno-rutile needles associated with biotite. ... 148
Figure 5.41. Interpretative 2D lithological map based on geochemical element maps and draped over hill-shaded digital elevation model. ... 151
Figure 5.42. Classification of rocks (left) and chondrite-normalised REE patterns, including published whole rock data, for SD granite samples. ... 152
Figure 5.43. Generalised interpretative cross-section of the Southern SDG. ... 163
Figure 6.1. Map of the study area. ... 166
Figure 6.2. Photographs of remaining plateau. ... 167
Figure 6.3. Schematic showing the three main processes controlling element enrichment within a weathering profile. ... 171
Figure 6.4. Schematic diagram showing the use of isocon analysis for the identification of conservatively behaving elements in weathered profile. ... 175
Figure 6.5. Schematic diagram showing the strip logs of the downhole profile from each of the six principal drill holes studied in this chapter. ... 176
Figure 6.6. Photographs of an exposed section of the weathering profile on the plateau. ... 178
Figure 6.7. Photographs showing white clay rich material infilling joint spaces in the mottled and saprolite horizons and coating fractures surface of saprock drill core sections. ... 180
Figure 6.8. Photographs of top section of weathered profile. ... 181
Figure 6.9. Cross sections of the weathered profile, contour maps of the surface elevation (5m) and the underlying bedrock on the central plateau. ... 183
Figure 6.10. A) Molar A-CN-K plot and CIA and B) SAF ternary plots illustrating the degrees of weathering along the profile. ... 184
Figure 6.11. Two plots showing covariation of loss of ignition wt % with the a) chemical index of alteration and b) the index of laterisation. ... 185
Figure 6.12. Major element trends along the six different drill holes studied. ... 188
Figure 6.13. Average REE proportions in the saprolite horizon of drill holes DDH0099 and DDH0266 shown as pie charts for a) LREE, HREE and Y, and b) individual REE. ... 192
Figure 6.14. Trace element distribution trends along profile the six drill holes studied a) REY b) La, Ce and Y c) La_N/Y_N d) enrichment factor. ... 194
Figure 6.15. REE enrichment ($C_{j,w}/C_{j,p}$) and fractionation trends (La_N/Yb_N and Ce_N/Ce^*_N) along the weathered profile of six drill holes studied. ... 199
Figure 6.16. Chondrite-normalised REE patterns and parent rock normalised REE patterns of the different horizons in each drill hole ... 201

Figure 6.17. XRD patterns of representative samples from different horizons in DDH0161..... 202
Figure 6.18. SEM-BSE images of weathered rock in each of the horizons. 203
Figure 6.19. Down-hole C_{iw}/C_{io} down-hole and isocon diagrams for selected 'immobile' candidates (for Al, Zr, Nb, Ti and Th) in ferruginous zone and mottled zone. 205
Figure 6.20. SEM-BSE images and EDS spectrum of zircon crystals found preserved in ferruginous zone. 206
Figure 6.21. SEM-BSE images and EDS spectrums showing the occurrence of Ti in the fine fraction and associated with Fe minerals. 207
Figure 6.22. Recorded dry bulk density for each horizon of the Serra Dourada weathered profile preserved on the central plateau area. Error bars show outliers..... 208
Figure 6.23. Volumetric strain (ε) trends plotted for along each drill hole studied. Calculations made using Zr as immobile element. 210
Figure 6.24. Depth profiles for Tau values for major elements in the six drill holes studied. The vertical dashed vertical line at τ (Zr) = 0, represents the point of no element gains or losses relative to parent granite. 214
Figure 6.25. Depth profiles for Tau values for P_2O_5, MnO, La, Ce, and Y in the drill holes studied. 215
Figure 6.26. Absolute REY mass changes per unit rock volume ($\delta_{i,j}$ (kgm^{-3})) and total mass gains or losses REY (($M_{j,flux}$ ($kg\ m^{-2}$)) calculated for each horizon in each of the drill holes studied..... 218
Figure 6.27. Summary of main features of the weathered profile. 220
Figure 6.28. Schematic diagram showing effect of drainage across the plateau..... 222
Figure 6.29. Downhole charts for the drill holes studied showing comparison of close system enrichment ($C_{Zr,w}/C_{Zr,p}$) and open system enrichment factors ($\tau_{REY,\ Zr}$). 226
Figure 6.30. REE mass gains and losses vs strain in the different horizons. 230
Figure 6.31. Summary diagram of interpreted pH and redox conditions along the profile. 229
Figure 6.32. Depth hole Redox sensitive Ce and Mn trends. 231
Figure 6.33. Eh pH stability field diagram for Mn-O-H system, Ce-O-H system and Fe-O-H system, superimposed. 231
Figure 7.1. Schematic diagram showing the location of the samples collected within the saprolite and saprock horizons of each drill hole studied. 237
Figure 7.2. Photographs of drill core fragments of saprolite samples analysed from the drill holes .. 237
Figure 7.3. Photographs of clay-rich veinlet samples 238
Figure 7.4. X-ray image processing workflow used for calculating modal abundance estimates, showing the steps for producing a mineral map. 242
Figure 7.5. Four images of the same area of a CSF sample. A. BSE image B. BSE image with the filter applied highlighting the REE-minerals as bright spots. C. Validation map of Al, Si and K. D. High intensity pixel-filtered element map of La, Y and Ti. 243

Figure 7.6. Chondrite-normalised REE distribution patterns showing the bulk and clay fraction saprolite sample compositions for each drill hole. 246
Figure 7.7. Distribution factor index (DFx) for individual REE in clay size fraction of saprolite samples relative to the bulk saprolite from different drill holes. 248
Figure 7.8. Chondrite-normalised REE distribution patterns Bulk and clay size fraction saprolite and transition zone samples from DDH0161 249
Figure 7.9. Distribution factor index (DFx) values for individual REE in the clay size fraction of transition zone and saprolite horizon samples from DDH0161. 250
Figure 7.10. Chondrite-normalised REE patterns of clay-rich fracture infill samples 254
Figure 7.11. X-ray diffraction patterns of randomly-oriented, glycol-impregnated samples. 255
Figure 7.12. X-ray diffraction patterns of randomly-oriented bulk and CSF samples from REE-enriched saprolite from six drill cores. 256
Figure 7.13. XRD patterns in the 2 – 70˚ (2θ) response for CSF samples CS7 and CS14 from DDH0266 and DDH0161. 257
Figure 7.14. XRD patterns of bulk samples collected along the saprolite horizon, transition zone and base of mottled zone from drill core DDH0161. 258
Figure 7.15. Stacked XRD patterns of CSF samples from the transition zone and saprolite horizon of DDH0161 258
Figure 7.16. Representative X-ray diffraction patterns of fracture-infill samples collected from an exposed section of preserved weathered profile on the plateau and a kaolinite standard. 259
Figure 7.17. XRD patterns of white clay-rich material coating fracture surfaces in bedrock/saprock samples from drill cores DDH0099 and DDH0161 260
Figure 7.18. SEM-BSE images of saprock samples showing the occurrence of fluorcarbonates infilling microfractures and spaces left behind by the dissolution of Na-feldspar. 261
Figure 7.19. SEM-BSE images showing LREE-fluorcarbonate rosettes, intergrown clay minerals..262
Figure 7.20. Photographs of resin blocks and SEM-BSE images of saprolite samples. 263
Figure 7.21. SEM-BSE images showing the distribution and morphology of LREE-fluorcarbonates at different levels of the saprolite horizon of drill hole DDH0161. 264
Figure 7.22. High-resolution SEM-BSE images showing the dissolution and re-crystallisation of REE-fluorcarbonates into clay-rich areas and along fractures. 265
Figure 7.23. High-resolution SEM-BSE images showing the morphologies of REE-fluorcarbonates in micro-fractures from drill hole DDH0161. 267
Figure 7.24. False-colour SEM-EDX map showing composition of nano-scale LREE-fluorcarbonate grains, found intermixed with clays in DDH0161. 269
Figure 7.25. False-colour SEM-EDX map showing composition of LREE-fluorcarbonate rosettes intermixed with clays in sample SV11. 269

Figure 7.26. Element plots showing the compositions of REE-fluorcarbonates in saprolite, saprock and bedrock samples from DDH0161 and DDH0266. 271
Figure 7.27. Chondrite-normalised REE patterns of LREE-fluorcarbonates present in saprolite, saprock, and bedrock samples of DDH0161. 272
Figure 7.28. BSE images showing the variety of phosphate occurrences and habits in the saprolite. 274
Figure 7.29. SEM-BSE images of fine REE-phosphate grains found in the upper saprolite and transition zone samples of DDH0161. 275
Figure 7.30. SEM-BSE and false-colour EDX element maps showing the dissolution and reprecipitation of intergrown Y- and Ce-rich phosphates 276
Figure 7.31. SEM-BSE and false-colour EDX element maps showing the representative habit and composition of bastnäsite-La and rhabdophane-Ce. 276
Figure 7.32. SEM-BSE images of acicular phosphates intergrown with clay minerals in clay-rich fracture-infill material collected in the weathered profile. 277
Figure 7.33. SEM-BSE image, false-colour EDX element maps and EDS spectrum showing composition of phosphate in a clay-rich fracture fill. 277
Figure 7.34. High resolution SEM-BSE and EDS false-colour maps of small niobiate grain intermixed with clay minerals from the saprolite, DDH0121. 278
Figure 7.35. SEM-BSE images, enlargements, and EDS spectra of niobiates in saprolite samples... 279
Figure 7.36. Britholite minerals intergrown with LREE-fluorcarbonates in lower saprolite sample SV6.1 from drill core DDH0161. 281
Figure 7.37. SEM-BSE images and EDS spectra of Ce-silicate minerals found in the upper-most part of the saprolite. 281
Figure 7.38. SEM-BSE image, element maps and EDS spectra showing Ce oxide and Y-phosphate clusters occurring in transition zone samples. 282
Figure 7.39. SEM-BSE images of Ce oxides associated with botryoidal Ba-Mn oxides (psilomelane) from DDH0099. 283
Figure 7.40. Representative SEM-BSE images of CSF samples from the saprolite. 287
Figure 7.41. Mineral maps and grain size distribution analysis of La-rich and Y-rich mineral grains present in CS7. 288
Figure 7.42. Mineral maps and grain size distribution analysis of La-rich and Y-rich mineral grains present in CS7. 289
Figure 7.43. Schematic diagram of the occurrence and breakdown of LREE-fluorcarbonates in the different horizons. 295
Figure 8.1. Representative X-ray diffraction patterns of bulk saprolite samples. 302
Figure 8.2 Representative X-ray diffraction patterns of < 2 micron fraction separates. 302
Figure 8.3 Representative X-ray diffraction patterns of clay veinlets samples collected from exposed sections of the weathered profile. 303

Figure 8.4. Photographs of prepared bulk saprolite, clay fraction and clay veinlet sample material used for the batch leach experiment. 304
Figure 8.5. Photographs showing the three 0.5 M ammonium sulphate solutions at different pH, and mechanical test tube roller used to agitate the solid-liquid mixture during leaching..... 305
Figure 8.6. Work flow for single-step extraction experiments, using de-ionised water and ammonium sulphate solutions at varying pH..... 308
Figure 8.7. Plots showing the results of measured concentrations in the supernatant solution for sample SV7 at different leaching times. 311
Figure 8.8. Changes in the proportion of REY and selected individual REE extracted in the supernatant solutions, over different leaching times. 312
Figure 8.9. SEM-BSE image and corresponding false-colour EDX element map for a clay sample from drill hole DDH0099. 314
Figure 8.10. SEM-BSE images showing examples of clay rich areas analysed by EMPA in polished blocks of saprolite samples SV9 and SV7. 315
Figure 8.11. Extracted concentrations of REY in filtered supernatant solutions from leached bulk saprolite samples and corresponding extracted percentages of REY..... 316
Figure 8.12. Extracted percentages of individual REE from bulk saprolite samples by leaching with ammonium sulphate solution at different pH values. 318
Figure 8.13. Chondrite-normalised REE patterns of untreated bulk saprolite samples and the REE extracted from these samples by ammonium sulphate solutions from batch experiments at different pH values. 319
Figure 8.14. Extracted concentrations of alkali and alkaline earth metals in filtered supernatant solutions from leached bulk saprolite samples and corresponding extracted percentages of REY at different pH values. 323
Figure 8.15. Extracted concentrations of selected elements in filtered supernatant solutions from leached bulk saprolite samples and corresponding extracted percentages of REY at different pH values. 324
Figure 8.16. Extracted concentrations of REY in filtered supernatant solutions from leached bulk saprolite with corresponding clay separates and extracted percentages of REY at different pH values, and for D.I. water. 325
Figure 8.17. Percentage of REE extracted from saprolite clay separates at different pH values showing the influence of pH on the extraction level. 326
Figure 8.18. Chondrite-normalised REE patterns for REY extracted in filtered supernatant solutions from leached bulk saprolite samples and the corresponding clay separate samples (CS) by ammonium sulphate solutions from batch experiments at pH 5.5. 326
Figure 8.19. Extracted concentrations of REY in filtered supernatant solutions from leached clay veinlets and extracted percentages of REY at different pH values, and for D.I. water. 328

Figure 8.20. Percentage extracted of individual REE in filtered supernatant solutions from clay veinlet samples at different pH values, showing the influence of pH on extraction..... 329
Figure 8.21. Chondrite-normalised REE patterns of REY extracted in both the filtered supernatant solutions from clay veinlet samples with ammonium sulphate under different pH conditions, and the corresponding untreated bulk clay veinlet samples. 330
Figure 8.22. Extracted concentrations of Ca, Mg, Na, K in filtered supernatant solutions from leached clay veinlets and corresponding extracted percentages of REY at different pH values, and for D.I. water. 332
Figure 8.23. Extracted concentrations of Al, Fe, Th, U from leached clay veinlets and corresponding extracted percentages of REY at different pH values, D.I. water. 333
Figure 8.24. Representative XRD patterns of untreated bulk saprolite samples and corresponding washed and filtered leach residues..... 337
Figure 8.25. Representative XRD patterns of untreated clay separate samples and corresponding washed and filtered leach residues..... 338
Figure 8.26. Representative XRD patterns of untreated clay veinlet samples and corresponding washed and filtered leach residues..... 339
Figure 8.27. SEM-BSE image and corresponding false-colour EDS element map showing undissolved Y-phosphate amorphous grains within washed and filtered residue material from sample SV13. 340
Figure 8.28. SEM-BSE image and corresponding false-colour EDS element maps overlaid over SEM-BSE imagery to show residual LREE-fluorcarbonates, Ce-oxides, REE-niobiates, and very fine-grained precipitated sulfur-bearing phase in the residual solid from sample CS7 after leaching with ammonium sulphate solution at pH 3. 341
Figure 8.29. SEM-BSE imagery and corresponding false-colour EDS element maps showing preserved supergene La-phosphates and Y-phosphates grains in leach residue solids of S3 after leaching with ammonium-sulphate solution of pH 3..... 341
Figure 8.30. REE ratio plots comparing untreated bulk saprolite samples and corresponding ion-exchangeable REE for saprolite and clay veinlet samples..... 344
Figure 8.31. Plot showing the MgO content of bulk saprolite and clay veinlet samples, and corresponding percentages of extracted ion-exchangeable REY..... 347
Figure 8.32. Plots showing the CIA and LOI of bulk saprolite and clay veinlet samples, and corresponding percentages of extracted ion-exchangeable REY..... 349
Figure 8.33. Plots showing the CIA and LOI of bulk saprolite samples, and corresponding La/Yb ratios of extracted ion-exchangeable REY. 349
Figure 8.34. REE/Al ratio plot for the extracted Al and REE in the supernatant solutions for all leach experiments run under different pH conditions. 351
Figure 9.1. Summary of the relationship between drainage setting, and REE fractionation and residence in the saprolite..... 356

Figure 9.2. Schematic summary of the mineral breakdown pathways for the Serra Verde profile. ... 358
Figure 9.3. Plots of phosphate contents vs ion-exchangeable REYs as a percentage of total REE content in weathered granites and Ce anomalies vs ion-exchangeable REYs. ... 359
Figure 9.4. Schematic diagram illustrating the proposed genetic evolution that led to the formation of the Serra Verde REE deposit. ... 362

List of Tables

Table 2.1. Ion-adsorption REE deposit sub-types as defined by Chi & Tian (2008). ... 34
Table 2.2. Summary of parent bedrock features of IADs in southern China and weathering profiles with REE potential in southeast Asia and Japan. ... 38
Table 2.3. List of REE-hosting accessory minerals of potential economic interest and their chemical formulae ... 42
Table 2.4. Published studies of recovery results from ion-exchange leaching of REE enriched weathered granite samples. ... 48
Table 3.1. Geochemical composition of SDG granites from Bilal et al. (1997). ... 62
Table 3.2. Chemical composition of the main REE host minerals identified in SDG. ... 67
Table 4.1. List of samples and sample types sent to ALS and NHM for geochemical analysis. ... 71
Table 4.2. Summary of elements, analysing crystal, count times, background position and primary standards used in EMP analysis. ... 84
Table 5.1. Samples collected and analysed for geochemical and mineralogical characterisation. ... 91
Table 5.2. Geochemical composition of granite samples collected from 100 m of DDH0004 drill core, analysed at NHM and ALS. ... 112
Table 5.3. Geochemical composition of Serra Dourada granite drill core samples that were analysed at ALS. ... 113
Table 5.4. EPMA of selected zircon grains from biotite granite samples underlying SV deposit, including representative zircon grains that show REE-enrichment zones, as well as non-altered and normal grains. ... 117
Table 5.5. EMP analyses of Th-poor and Th-rich Monazite-(Ce) grains. Monazite analyses from Teixeira and Botelho (2002) are also included for comparison. ... 125
Table 5.6. Representative EMPA of xenotime and their formulae, calculated on the basis of 4 oxygens to apfu cation proportions. ... 130
Table 5.7. Representative EMP analysis and structural formula of bastnäsite-Ce and bastnäsite-La in samples from drill hole DDH0004. ... 135
Table 5.8. Chemical formulae of key niobiate minerals. ... 136

Table 5.9. EMP results for niobiates, sorted into analyses for bright and dark patches determined by SEM-BSE response..... 143
Table 5.10. EMPA results from apatite and Ce- and Y-silicate minerals. 148
Table 6.1. Definition of parameters used in mass balance equations. 175
Table 6.2. Mean values of each horizon for major elements, REE and HFSE for each drill hole. 190
Table 6.3. Calculated mass transfer coefficients ($\tau_{i,j}$) and absolute mass changes per unit volume rock ($\delta_{i,j}$) for major elements and trace elements for each horizon. 216
Table 7.1. Summary of the samples collected and analysed for geochemical and REE-mineralogical characterisation. 236
Table 7.2. Whole-rock chemical composition of studied saprolite samples. 244
Table 7.3. Major and trace element concentrations in the < 2 µm size fractions (CSF) of the saprolite samples studied. 251
Table 7.4. Major and trace element composition of clay-rich fracture-filling material collected from mottled zone, saprolite and bedrock. 252
Table 7.5. Representative EMPA results of REE-fluorcarbonates found in saprolite and saprock samples from drill cores DDH0161 and DDH0266, and from bedrock. 270
Table 7.6. Representative EMP analyses of phosphates, niobiates and Ce minerals from saprolite samples. 283
Table 7.7. Estimates of total REY (REE+Y) residency in phosphates for the bulk samples of the saprolite, and corresponding clay size fraction separates. 286
Table 7.8. Calculated estimates of total REE (REY) residency in fluorcarbonates for the mapped CSF samples of the saprolite..... 286
Table 8.1. List and composition of samples used in ion-exchange experiment. 300
Table 8.2. Experimental conditions of the batch ion-exchange. 307
Table 8.3. EMPA results from clay-rich areas in saprolite samples. 314
Table 8.4. Extracted element concentrations in filtered supernatant solutions for all leached samples in the ion-exchange experiments. 334

Abbreviations

IAD	=	Ion-adsorption deposit
SV	=	Serra Verde
SDG	=	Serra Dourada granite
NHM	=	Natural History Museum
IAC	=	Imaging and Analysis Centre
REE	=	Rare earth elements
REY	=	Rare earth elements and yttrium
LREE	=	Light rare earth elements
HREE	=	Heavy rare earth elements
MREE	=	Middle rare earth elements
TREE	=	Total rare earth elements
TREO	=	Total REE oxides
PER	=	Percentage of ion-exchangeable rare earth elements
DDH	=	Diamond drill hole
CSF	=	Clay separate fraction
D.I.	=	De-ionised [water]
CIA	=	Chemical index of alteration
LOI	=	Loss on ignition
IOL	=	Index of lateritisation
(b)dl	=	(Below) detection limit
a.s.l.	=	Above sea level
DEM	=	Digital elevation model
SEM	=	Scanning electron microscope
BSE	=	Back-scattered electron
XRD	=	X-ray diffraction
EDS	=	Energy dispersive spectrum
EDX	=	Energy dispersive X-rays
EMPA	=	Electron microprobe analysis

Mineral Abbreviations

Ap	=	Apatite
Bst	=	Bastnäsite
Bt	=	Biotite
Fl	=	Fluorite
K fsp	=	Potassium-series feldspar
Mnz	=	Monazite
Pcl	=	Pyrochlore
Sm	=	Samarskite
Thr	=	Thorite
Ti min	=	Ti-bearing minerals
Xtm	=	Xenotime
Zrn	=	Zircon

Appendix List

Appendix A Field Drill Core Logs **380**

Appendix B Bulk Geochemical Data **386**

B1. Reference standards and duplicates 386

B2. Serra Verde assay results for drill holes studied 391

B3. Bedrock element maps 397

Appendix C Electron Microprobe Data **399**

C1. Standards and correction factors 399

C2. EMP Mineral analysis 403

C3. EMP Clay analysis 429

Appendix D Isocon Analysis Tables **434**

Appendix E SEM Analysis **437**

E1. Clay separate analysis 437

E2. Mineral maps 439

Appendix F Leaching Experiments Raw Data **441**

Chapter 1

Introduction

1.1 General Introduction

The rare-earth elements (REE) are a group of seventeen elements that comprise the lanthanides, scandium and yttrium. These elements are grouped together because they have similar chemical behaviour and often occur in the same minerals. When they were first discovered, REE were thought to be rare in nature. However, as better analytical techniques developed it was found that they are in fact relatively abundant in the earth's crust. Nevertheless, because of their wide distribution due to their tendency to substitute into various mineral phases (Castor & Hendrick 2006), occurrences of REE minerals and economic REE deposits are rare.

Rare earth elements are increasingly being integrated into modern technology and some sectors are already highly reliant on these elements. In the green energy sector for example, REEs are found in many of the crucial components such as batteries and high strength magnets used to build hybrid cars and wind turbines. At the time of writing this thesis, the main REE applications are in: permanent magnets, catalysts, metal alloys, polishing powders, phosphors, glass additives, and ceramics (Walters et al. 2011). The highest demand for REE comes from the first three (magnets, catalysts, and metal alloys) with an estimated combined consumption of 58 % of the total volume of REE demand (Walters et al. 2011). The total global demand for REE oxide in 2011 was 105,000 tonnes and by 2025 it is projected to double to 210,000 tonnes (Alonso et al. 2012). This rapid growth in the demand of REE will be driven by the development of new applications for REE in advanced technologies, the growth of the renewable energy sector and the increasing consumption expected in developing nations.

Up until the 1980's, the United States and Australia were the principal REE producers and suppliers to the world market. However, the closure of the majority of historic REE mining operations, and the development several Chinese deposits, resulted in a geographical shift of supply. Since the 1990's, China has been the main REE producer, supplying more than 90 % of the global REE production (Kynicky et al. 2012). China's success can be attributed largely

to the contribution of Bayan Obo, the largest REE deposit in the world located in northern China, and also the unique, low cost HREE-enriched ion adsorption type clay deposits found in southern China (Kynicky et al. 2012). The increasing demand for REE and the dependence on a single supplying country has led to the identification of REE as a critical resource by scientific and governmental panels, and has motivated an increasing drive for both the development of known deposits, and the identification of new REE resources.

Ion-adsorption type REE deposits (IADs) are weathered granites that contain economically exploitable REE-bearing clays. The lateritic weathering profiles result from the breakdown of feldspars into clays and the dissolution of REE-bearing minerals. To date, IADs have only been mined in China and account for 80% of the world's economic HREE reserves (Chi & Tian 2008). Ion-adsorption type REE deposits are of great interest because of their heavy rare earth element (HREE) enrichment, low mining and processing costs, and low radioactive element content (Kanazawa & Kamitani 2006). The lack of economic targets of this type outside China, and the paucity of published information regarding the Chinese deposits, means there is a limited understanding of IADs. Finding new ion-adsorption type deposits worldwide relies on improving the understanding of known deposits.

The Serra Verde REE deposit is a 30-35 m thick lateritic weathering profile with economic concentrations of REE bearing clays, which developed over a Proterozoic age alkali granite in the Goías province of Brazil. The deposit has an NI43-101 compliant resource of 911 Mt at 0.12 % of total rare earth oxides (TREOs). The formation of the deposit is suggested by Serra Verde Mining LLC to have occurred in three stages: (i) emplacement of the Serra Dourada tin granite; (ii) metasomatism of the granite; (iii) and laterization during the Miocene. However, to date, no studies have been published on the mineralogical and chemical composition or the formation of the Serra Verde REE deposit. If the Serra Verde deposit is one of the few ion-adsorption type rare earth element deposits that has been discovered outside China, it would offers a unique opportunity to investigate a rare and poorly understood source of REE and further scientific understanding in this small field.

1.2 Thesis Scope

Ion-adsorption REE deposits are highly important sources of HREE but a poorly studied type of deposit. Overall there are few general deposit studies of IADs and most published work to date has focused on characterising particular parts of the system, such as the parent granites, or REE extractability from a given deposit resource. As a result, only simplified models of these

deposits have been developed, which fail to explain the global scarcity of IADs, and variations between known deposits. The recently discovered and resourced Serra Verde deposit has not been studied before and, together with its accessible location and preserved drill core, offers a good opportunity to carry out a general deposit study. A full characterisation is carried out downhole and at surface, allowing the roles of different components and processes associated with the deposit to be investigated and compared. This thesis aims to firstly present the main geochemical and mineralogical characteristics of the Serra Verde REE deposit, and to secondly determine the main controls involved in its formation and enrichment.

This thesis presents the first scientific characterisation undertaken for this deposit. The detailed descriptions will not only provide the foundation for answering questions related to its formation and metallurgy, but also to help determine if the deposit is a true IAD and whether it can be compared with the Chinese IADs. The characterisation involves bulk mineral and geochemical descriptions of the parent granite and the different horizons of the weathered profile, as well as more detailed characterisation of the REE -mineralogy of the parent granite and ore zone.

Once the deposit is characterised, an assessment will be made of the roles that different controls have on the formation of this deposit, such as parent granite type, weathering intensity, and mineralogy. Furthermore, an interpretation of the formation and enrichment history will be presented based on the geological investigation of this work and previous studies of the region (figure 1.1). This study focuses on the controls of formation because the conditions and settings under which IADs form remain unclear. By understanding more about how the main controls interact during IAD formation, not only do the genetic models for IADs improve, but the predictability of these deposits in exploration and geometallurgy increases.

Based on the aims described above, the main objectives of this PhD project are to:

1. Characterise the bulk geochemical and mineral composition of the parent granite.
2. Assess the effect of the starting parent granite composition on the REE enrichment of the deposit.
3. Characterise the geochemical and mineral composition of the weathered profile.
4. Assess the effect of tropical weathering on REE grades and distribution.
5. Identify the residence of the REE within primary, secondary and supergene minerals in weathered profile.
6. Determine the proportion of REE adsorbed onto clay minerals in the deposit.

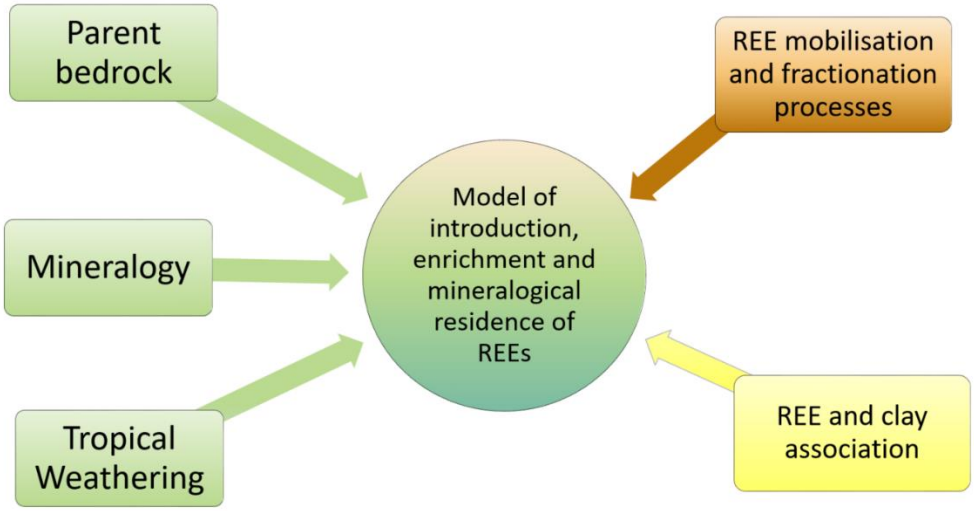


Figure 1.1 Diagram showing the different aspects of the Serra Verde IAD that were investigated to achieve the aim of this PhD study.

1.3 Thesis structure

The thesis is composed of nine chapters. A short description of the content and goals of each chapter which relate to the objectives stated above are provided:

Chapter 1 – Introduction: A general introduction and outline of the main objectives and structure of this thesis.

Chapter 2 – Literature review: A review of the scientific knowledge concerning REE IADs that summarise and contextualises the work that has been carried out. Assessments of the current level of scientific understanding and remaining questions around IAD are included.

Chapter 3 – Geology of the Study Area: Description of the Serra Verde REE deposit and local study area of the southern Serra Dourada Granite, as well as a review of the geological setting.

Chapter 4 – Analytical Methods: Description of the samples collected, sample preparation, and details pertinent to the data quality and analytical methods applied in this study.

Chapter 5 – The Mineralogy and Geochemistry of the Serra Verde REE Deposit Parent Bedrock: Presentation of data from the bedrock, to (1) characterise the chemical and mineral composition of the parent granite that weathered to form the Serra Verde deposit, and (2) to identify and study the composition of the minerals hosting the REE in the parent granite, and interpret the origin of the REE mineral assemblage.

Chapter 6 – Characterisation and Mass Balance Analysis of the REE-Enriched Weathered Profile of the Serra Dourada Granite: Presentation of downhole data from the profile, and evaluation of vertical and lateral variation with mass balance analysis. This is in order to (1) examine and describe the weathered profile hosting the Serra Verde deposit, in order to determine its maturity, vertical and lateral variation, REE distribution and development history. In addition, to (2) quantify the redistribution and mass flux of REE in the weathered profile, in order to assess the effects that the tropical weathering regime has had on the distribution and enrichment of REE.

Chapter 7 – Mineralogical Characterisation of the REE-rich Saprolite Horizon: Presentation of a detailed study of saprolite samples to establish the residence of the REE within primary, secondary and supergene minerals in the saprolite and their contribution to the total REE budget of the Serra Verde deposit. This will help map out the mineral weathering pathways of the REE from the granite bedrock into clay minerals.

Chapter 8 – Rare earth recovery by ion-exchange leaching: Presentation of results from ion-exchange leaching experiments, in order to measure the amount of exchangeable REE ion in the ore material and identify any factors affecting the recovery of REE from this ion-adsorption deposit.

Chapter 9 – *Discussion, Conclusions and Further work:* Integration of the findings from each chapter to present a general model for the formation and enrichment of the Serra Verde REE deposit. Furthermore, an identification of suitable areas for future research, and implications of this study for both exploration and metallurgical processing are presented.

Chapter 2

A Review of Ion-Adsorption REE Deposits

2.1 Ion Adsorption Rare Earth Deposits

Ion-adsorption rare earth element (REE) deposits are supergene deposits that contain economically exploitable REE-bearing clays. The clays develop due to the weathering of REE-enriched granites and contain over 50 % ion-exchangeable REEs relative to their bulk REE content (Wu et al. 1989; Bao and Zhao 2008; Sanematsu et al. 2013). These deposits, which are mostly found, and only mined, in southern China to date, are typically small in their spatial extent, and have grades in the range of 0.05 - 0.2 % oxides (REE_2O_3; Wu et al. 1996).

Despite their low grades, REE ion-adsorption deposits (IADs) are a key source of heavy rare earth elements (HREEs); they account for more than 80% of the world's economic HREE reserves (Chi and Tian 2008), due to being one of the few recognised HREE-bearing ore types (Sanematsu 2013). Carbonatites, alkaline complexes, and placer deposits from which REEs are also typically extracted, are all normally enriched in light rare earth elements (LREE). The lower mining and processing costs than other REE deposits, and the low radioactive element content of IADs has contributed to their pre-eminence as a source of HREEs (Kanazawa and Kamitani 2006). Today, the majority of HREE produced worldwide come from IADs deposits in the southern provinces of China (Sanematsu and Watanabe 2016). Large resources of HREE deposits were discovered in the 1970's and 1980's, and by 1992 accounted for 14 % of China's total REE production (Zhang et al. 1995).

Despite the recognition of REE-bearing clays in Chinese IAD weathered granitic profiles since the early 1970s, outside of China IADs are viewed as a new type of REE deposit due to the small number of scientific publications (e.g. Walters et al. 2011). The limited understanding of IADs is due to the lack of economic targets of this type outside China and the lack of distributable scientific data regarding the Chinese deposits. Interest in these low grade IADs deposits outside China has largely been sparked by increasing demand for REE and concerns over monopolisation of their long-term supply (Goodenough et al. 2016).

The first reports on IADs were published in the 1980s and early 1990s in Chinese journals and describe the deposits from the Jiangxi province and surrounding areas (e.g. Yang et al. 1987, Wu et al. 1989, Wu et al. 1993). Chi and Tian (2008) stated that much of this early work was not systematic, partly due to confidentiality issues. Nothing beyond reviews of previous work were published between the mid-1990s and mid-2000s (e.g. Zhang et al. 1995, Wu et al. 1996). Since the late 2000s, there has been a slow re-emergence of new publications as economic interest in rare earth deposits has grown. More recent literature has examined the REE-bearing clay potential of weathered granites in southeast Asia and Japan (e.g. Imai et al. 2008, Murakami and Ishihara 2008, Sanematsu et al. 2009, Sanematsu et al. 2013) and has also investigated both the geochemistry and genetic controls of the Chinese deposits for the first time (e.g. Bao and Zhao 2008, Sanematsu and Watanabe 2013, Sanematsu et al. 2015).

Although focused research into individual IADs has been limited, several studies of the behaviour of REE during development of weathering profiles were carried out in the 1980's (e.g. Nesbitt 1979, Duddy 1980, Alderton et al. 1980, Middelburg et al. 1988, Braun et al. 1990). These studies highlighted the mobilisation and fractionation processes of REE during weathering and cautioned the use of REE as parent rock tracers for sediments and for palaeo-environmental reconstructions.

Research into the interactions between clays and REE has mostly focused on sorption mechanisms (e.g. Coppin et al. 2002, Aja 1998, Bruque et al. 1980, Miller et al.1982). Much of this work was carried out for either soil, environmental or engineering applications, but is still applicable to developing the understanding of IADs. Finally, residual lateritic REE deposits, which form over alkaline complexes and carbonatites and have received more attention are believed to share some similarities with IADs (Morteani and Preinfalk 1996).

2.1.1 Distribution

All the economically productive IADs that have been found to date are located across the southern provinces of Jiangxi, Guandong, Fuijan, Guangxi, Hunan, and Yunnan in China (Bao and Zhao 2008, Sanematsu and Watanabe 2016; see Figure 2.1). The majority of these deposits are concentrated in the low-lying, northeast-trending Nanling Mountains and are mostly small (< 0.01 Mt ore) to medium in size (0.05 – 0.5 Mt ore; Kanazawa 2006, Zhu 1999, Sanematsu and Watanabe 2016). This region of southern China experiences a sub-tropical climate and low

denudation rates (Zhang et al. 1995). The ages of the weathering profiles in this part of China range from modern to early Palaeogene (Meyerhoff et al. 1986).

Outside of China, a few deposits and occurrences have been identified. They are distributed between Brazil, Madagascar, Malawi, Japan and countries in southeast Asia (Laos, Myanmar, Thailand; see potential map Figure 2.1). All of these areas, including the Chinese deposits, share similar climatic conditions, being found throughout modern tropical and sub-tropical belts. Similarly, all of the IADs and occurrences have been found in the last two decades, which shows that the formation of IADs are not restricted to China. To date, none of these deposits have reached commercial production. The Serra Verde deposit in Brazil, and Tantalus deposit in Madagascar are the two deposits outside of China that are currently being developed.

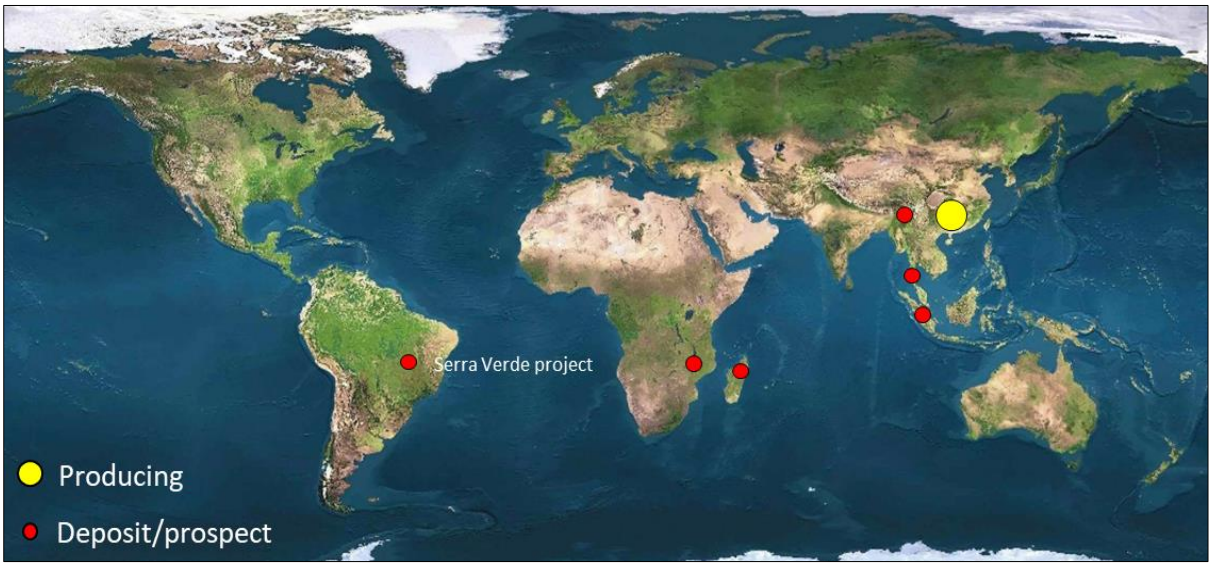


Figure 2.1. Map highlighting the locations of currently known ion-adsorption REE deposits around the world. Note that most of the deposits are located in tropical and temperate regions at low latitudes.

2.1.2 Classification

IADs are commonly divided into HREE- or LREE-enriched types based on the REE distribution pattern of the ore (e.g. Kynicky et al. 2012, see Figure 2.2). HREE deposits show a 'left-dipping' chondrite normalised REE pattern, with preferential enrichment in HREE and Y, whereas LREE deposits show a 'right–dipping' trend with a preferential enrichment of LREE. The boundary between LREE and HREE is commonly placed between Eu and Gd. Yttrium is grouped with the HREE because it exhibits similar chemical behaviour (Walters et al. 2011).

The Longnan and Xunwu deposits are the most cited examples of the HREE, and LREE types respectively. The ore from Longnan contains >70 % HREE+Y, with Y accounting for the majority of the REE content (Figure 2.3). The ore from Xunwu is instead primarily enriched in La and Nd. Compared to other REE deposits such as Bayan Obo and Mount Weld (Australia), LREE IADs are slightly more enriched in HREE (see Figure 2.2).

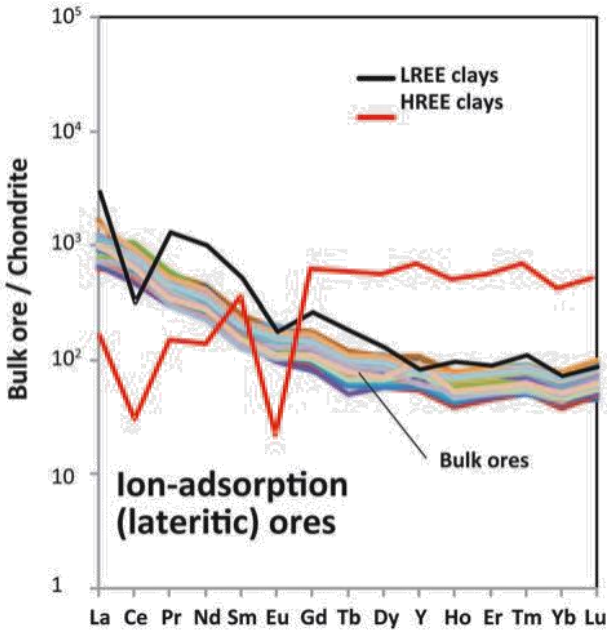


Figure 2.2. REE distribution patterns in typical LREE and HREE clay-dominated IADs (Source: Kynicky et al. 2012). The bulk ores signature refers to other non-IAD REE deposits found in China such as Bayan Obo, Maoniuping, and Huanglongpu.

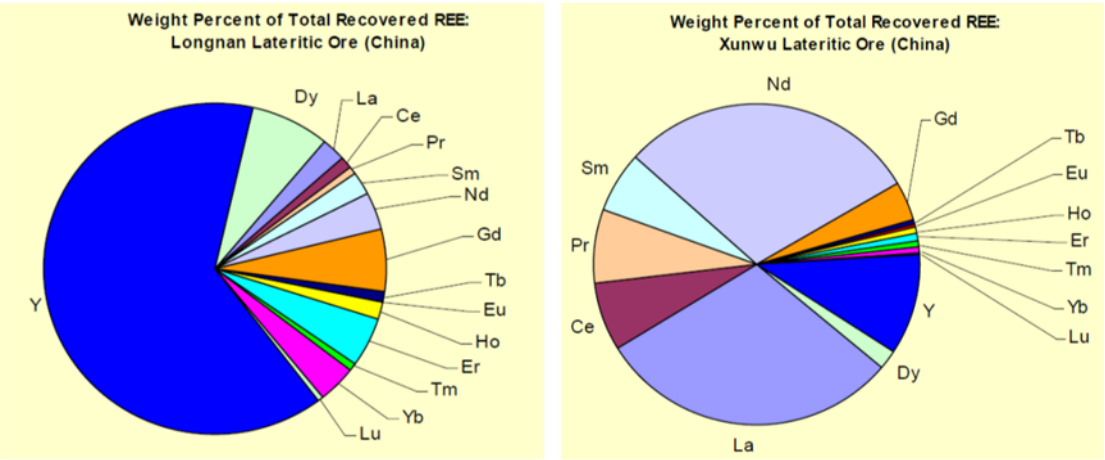


Figure 2.3. Pie charts divided by REE-Y composition REE recovered from the ore from the Longnan deposit (left) and from Xunwu (right; modified from Hedrick 2010).

Ruan and Guocai (1998) argued that HREE-type deposits are less common than the LREE-types based on the analysis of 338 samples from weathered granites in China. Of these samples, 71 % fell into the LREE category. So far, the REE content of weathered granites studied from Thailand, southwest Japan and Laos have also shown LREE enrichment (Imai et al. 2008, Murakami and Ishihara 2008, Sanematsu et al. 2009, Sanematsu et al. 2013). Further subdivisions within these two enrichment types can be made based on Eu anomalies and Y content (Chi and Tian 2008; summarised in Table 2.1).

Another way to differentiate IADs is by using the ore mineralogy present in the weathering profile. Bao and Zhao (2008) distinguished deposits that contain only REE-bearing clay mineralisation and those that contain mineralisation consisting of REE-bearing clays and REE-rich resistant minerals in their study of four Chinese IADs. Separating IADs based on their mineralogy (REE in clays or in both clays and resistant minerals) could be useful to help identify parental rock types and their accessory minerals that favour the development of deposits with a higher percentage of REE-bearing clays. Several of the REE-enriched weathering profiles studied outside China appear to fall within such a mixed category. For example, the Japanese weathering profiles studied by Murakami et al. (2008) contain LREE-bearing clays and HREE residual minerals such as zircon, and the most prospective weathering profiles in Laos contain REE bearing clays and resistant REE phosphates such as monazite and rhabdophane (Sanematsu et al. 2009).

No other criteria such as bedrock lithology, primary REE minerals, age of formation, morphology or drainage have been applied to distinguish deposits. As more weathered granites are investigated around the world, more differences, and consequently new classification schemes, are likely to emerge.

Table 2.1. Ion-adsorption REE deposit sub-types as defined by Chi and Tian (2008).

Deposit type	**Geochemical Sub-type**
HREE	High Y
HREE	Intermediate Y
LREE	High La and Eu
LREE	Intermediate Y and low Eu
Non-selective partitioning	No selective enrichment

2.2 Chinese Ion-Adsorption REE deposits

2.2.1 Weathered profile

A weathered or weathering profile represents a layer of loose and unconsolidated material at the Earth's surface that has developed from the breakdown of rocks through their exposure to the atmosphere, water, and biological organisms. The weathering of rock progresses downwards, with the most intensely weathered material found at the top (soil) and the least weathered at the base of the profile at the fresh rock interface. This vertical variation results in visually, chemically, and texturally distinct layers, which are known as horizons. Most weathered profiles follow a similar vertical pattern of mineral breakdown and a general classification system has been developed which helps identify, describe, and compare weathered profiles. There are three main horizons: A (top soil), B (sub-soil), and C (weathered parent rock; (Velde & Meunier 2008). The A horizon represents the top layer that is leached, where organic material accumulates, and biological activity occurs. The B horizon is the principal mineral layer where clay minerals and Fe or Al oxides accumulate. Finally, the C horizon is composed of partly-weathered rock where the original fabric of the rock is still retained (Figure 2. 4).

Although the weathering of rocks follow similar trends, it is important to note that characteristics of the individual horizons described above can vary greatly, depending on the degree of weathering, bedrock type, climatic conditions and tectonic setting. For example, in regions of humid tropical climate that have been tectonically stable for long periods of time, deep lateritic weathered profiles with intensely leached and Al and Fe oxide-rich soils commonly develop (Modesi-Gauttieri et al. 2011). The horizons of weathered profiles developed in these settings have been given different names to highlight the unique characteristics of the regolith that develops in these climates (Figure 2. 4).

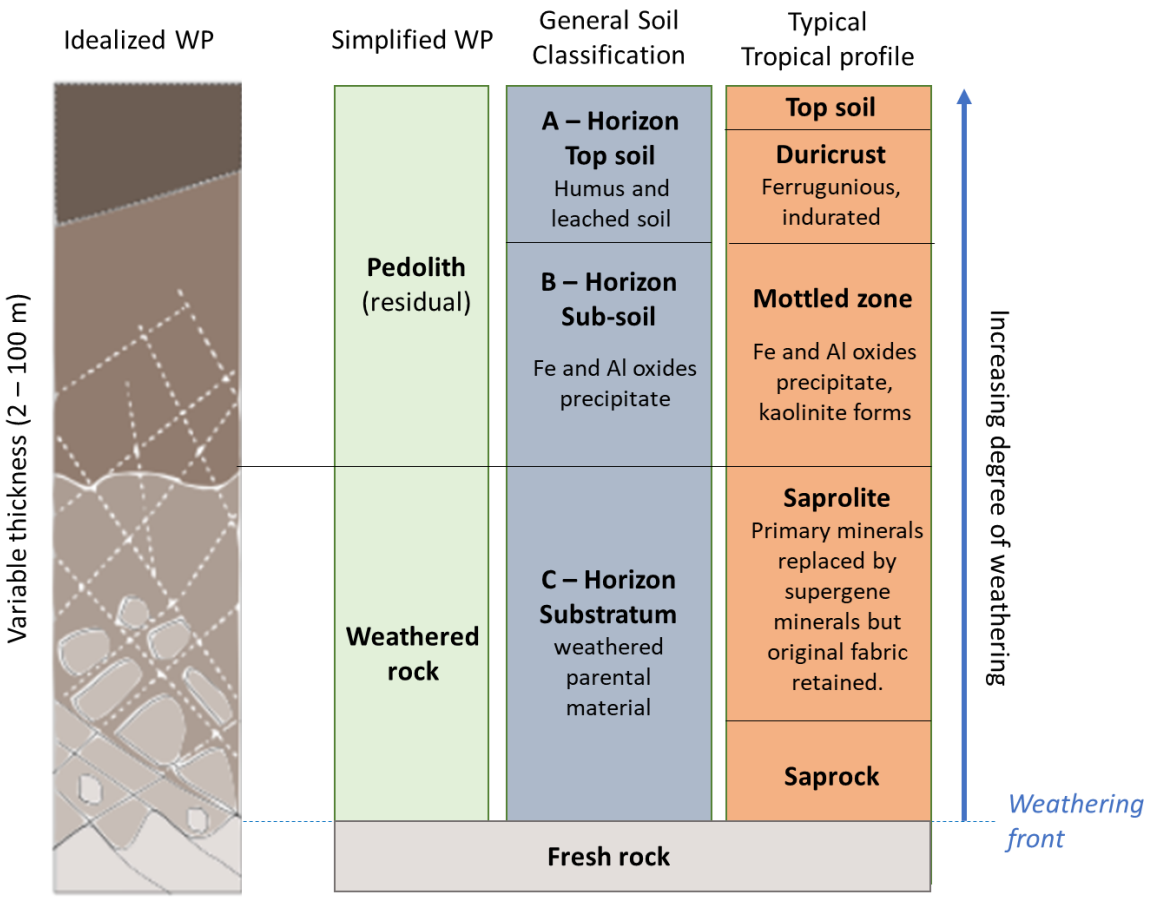


Figure 2. 4 Schematic diagram showing the main horizons that develop in weathering profiles.

The weathering profile of ion-adsorption type deposits described from China have thicknesses that typically range between 6 to 10 m but can locally reach up to 60 m. The profiles are divided into four main horizons based on mineral assemblage and texture (Sanematsu and Watanabe 2016, NPCS Board of Consultants and Engineers 2009; see Figure 2.5). From top to bottom the horizons are: a reddish eluvium composed mainly of clay (> 40 %), quartz, Fe oxides, and organic matter (1-2 m thick); a reddish to light grey, completely weathered saprolite horizon composed primarily of clay minerals and quartz, as well as minor K-feldspar and mica (5 – 10 m); a semi-weathered horizon which retains the original texture of the bedrock and contains primarily clays (< 30 %), quartz, feldspars, and biotite (3 – 5 m); and finally the granitic bedrock composed of quartz, plagioclase, K-feldspar, biotite or muscovite, and accessory minerals (Zhang et al. 1995, Chi and Tian 2008, Kanazawa and Kamitani 2006). The most developed weathered profiles are found on topographic highs, with the thickest deposits generally found preserved on mountainous ridges, and the thinnest in eroded valleys (Chi and

Tian 2008). The top most lateritic horizons, do not appear to be strongly developed in these weathered profiles, suggesting they are not intensity weathered.

REE concentrations are highest in thick, clay-rich horizons, usually within a 3 – 8 m sub-horizon towards the lower half of the saprolite horizon. The REE are enriched by a factor of up to 3 times above that of the parent rock (Table 2.2). The upper part of the profile within the eluvium horizon is depleted in REE, and only low REE enrichment is observed in the underlying saprock horizon (Wu et al. 1996). One distinguishing characteristic in ion-adsorption REE deposits is the variation in the Ce anomaly down the profile (Figure 2.5); Ce is typically enriched in the eluvium layer but depleted in the lower section of the profile relative to the neighbouring REE. Another characteristic is the fractionation of LREE and HREE (Figure 2.5); relative to the parent rock, the eluvium layer is slightly LREE-enriched whereas the fully-weathered and semi-weathered horizons are HREE enriched.

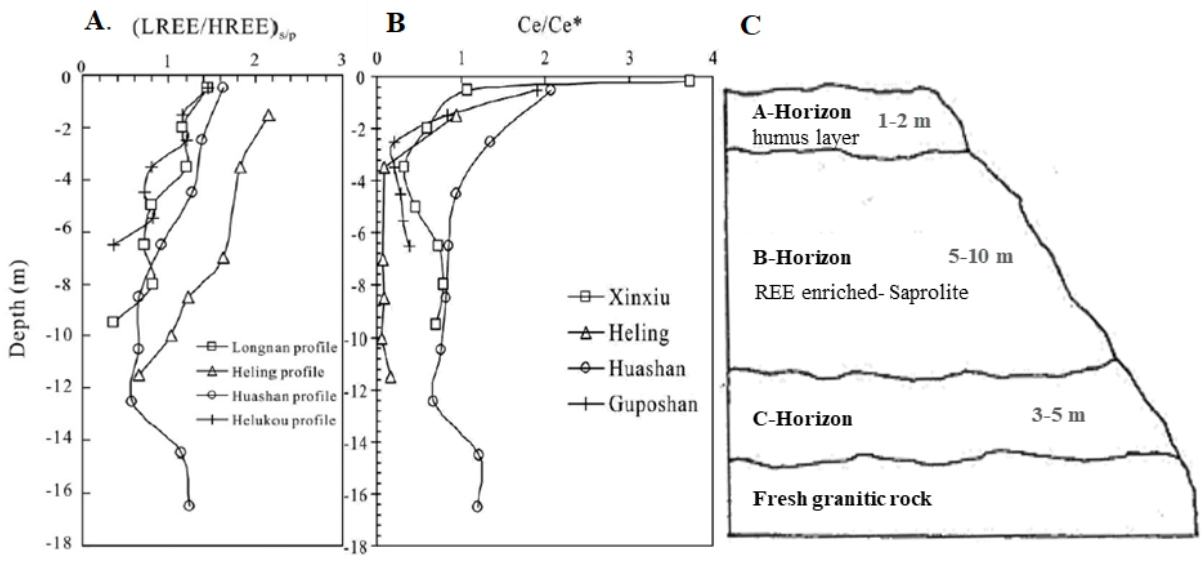


Figure 2.5. A. REE fractionation developed on the Longnan, Huashan, Heling, and Helukou weathering profiles in southern China. $(LREE/HREE)_{s/p}$ represents the LREE/HREE ratio of samples (s) relative to the same ratio in the parent rock (p; source is Bao and Zhao 2008). B. Cerium anomaly variations in the weathering profiles (Source: Bao and Zhao 2008). C. Main horizons of the weathering profile in ion-adsorption type deposits (modified from NPCS Board of Consultants and Engineers 2009).

Table 2.2. Summary of parent bedrock features of IADs in southern China and weathering profiles with REE potential in southeast Asia and Japan.

Name	Country	Parent Rock and REE (ppm)	REE host minerals	REE (ppm)	Type	Reference
Longnan	Jiangxi, China	Granite	-	1122 -1547	HREE	Yang (1987)
Dignan	Jiangxi, China	Biotite granite 286 ppm	Zircon, apatite, trace REE synchysite	317 - 466	LREE	Ishiara *et al.* (2008)
Zudong	Jiangxi, China	Muscovite - biotite granite 264 ppm	Y-REE-fluoro-carbonates (e.g. synchisite) 60 % of REE	-	HREE	Huang et al. (1989)
Xinxiu	Jiangxi, China	Muscovite granite	Doverite (65 %), fluorite (3 %), xenotime, monazite, apatite	200 - 592	HREE	Bao & Zhao (2008)
Heling	Jiangxi, China	Granite	Bastnaesite-(Ce), apatite, zircon; minor monazite, tourmaline, fergusonite, doverite fluorite.	1125 - 2799	LREE	Bao & Zhao (2008)
Huashan	Guanxi, China	Biotite granite	Monazite, allanite, and xircon apatite, fergusonite-(Y), xenotime.	410 - 561	LREE	Bao & Zhao (2008)
Guposhan	Hunan, China	Biotite granite	Fergusonite-(Y), allanite, xenotime, monazite,apatite, zircon, gadolinite.	797 - 1113	LREE	Bao & Zhao (2008)
Naegi	Sanyo, Japan	Biotite granite 142-245 ppm	Fluorite, apatite, ilmenite, zircon, monazite, fergusonite, allanite and rutile.	171 – 530	LREE	Murakami & Ishihara (2008)
Tanakami	Sanyo, Japan	Biotite granite 142-245 ppm	Allanite, monazite, zircon and xenotime.	182	LREE	Murakami & Ishihara (2008)
Kata Beach	Thailand	Biotite granite 592 ppm	Allanite, titanite, apatite, zircon, and LREE-fluorocarbonate.	578 - 1,084	LREE	Sanematsu *et al.* (2013)
-	Attapu and Xaisumboun, Laos	Biotite granite - biotite granodiorite 123 ppm	-	80 - 1050	LREE	Sanematsu *et al.* (2009); Menati (2011)

2.2.2 Mineralogy

The main clay minerals that are found in both the semi-weathered and completely weathered horizons are kaolinite and halloysite (Wu et al. 1996). Other clays that have been found in minor proportions include montmorillonite, gibbsite, illite and vermiculite (Zhang et al. 1995, Sanematsu et al. 2013). The percentage and crystallinity of kaolinite and halloysite decreases up-profile and both minerals are eventually replaced by gibbsite in the eluvium horizon (Chi and Tian 2008). A small amount of iron oxide can also be found in the eluvium horizon and is responsible for its red-pink colouration (Zhang et al. 1995).

Kaolinite and halloysite are quoted as the main clays that retain REE in the profile (Yang et al. 1981, Huang et al. 1989, Wu et al. 1989, Murakami and Ishihara 2008). These were identified by determining REE concentrations in the different grain size fractions and characterising the clays present in each fraction using X-ray diffraction (Chi and Tian 2008). In the eluvium horizon, secondary REE minerals such as cerianite, rhabdophane, and Ce-bearing ferro-manganese oxides are common (Sanematsu et al. 2013). Overall there is little information available on the mineralogy and geochemical composition of the Chinese IAD profiles.

2.3 Controls on the Formation of Ion-Adsorption Deposits.

The development of laterite deposits is controlled by climate, climatic history, tectonic setting, bedrock lithology, age of weathering, and geomorphology (Freyssinet et al. 2005). Investigations of IADs have concentrated primarily on climate and bedrock lithology as the likely primary controls.

2.3.1 Climate and Geomorphology

Climatic conditions and the geomorphology of the landscape determine the intensity of chemical weathering processes. Marker and Oliviera (1994) compared the weathering profiles of alkaline rocks in different climatic regions of Brazil and found that humidity and drainage conditions significantly influenced the development of weathering profiles and the distribution of REE. Their main findings can be summarised into three observations:

1) Weathered alkaline rock profiles in tropical humid climates and with intense drainage displayed strong Ce enrichment in the upper parts of the profiles and had HREE enrichment in the saprolite;
2) Weathered alkaline rock profiles in moderate drainage settings with high groundwater levels exhibited minor REE fractionation and enrichment;

3) Weathered profiles in sub-humid climates and with restricted drainage showed limited liberation of REE from primary minerals and fractionation/enrichment of REE did not occur.

The humid and warm climatic conditions of southern China and hilly setting of the Nanling Mountains have provided the optimal conditions for the development of deep weathering profiles with strong REE enrichment and fractionation. The thickest and most enriched deposits are found where the best drainage conditions and lowest denudations rates occur (Chi and Tian 2008). The annual rainfall in the Longnan district is 1580 mm yr^{-1}, with a relatively dry summer (Wu et al. 1990).

Murakami and Ishiara (2008) suggested that seasonal fluctuations may enhance the leaching and precipitation processes involved in the formation of IADs. The weathering profiles of southwest Japan exhibit lower levels of maturity compared to those from southern China, believed to be related to the higher annual rainfall of 1800 $mmyr^{-1}$ and absence of a dry season. It is thought that the dry summer in Longnan plays a role in REE enrichment by allowing meteoric water to reach deep into the profile when the water table is at a low level.

2.3.2 Parent Rock Lithology

The characteristics of the bedrock on which laterites develop have a significant influence on the grade and quality of the ore (Freyssinet et al. 2005). For ion-adsorption type deposits, the abundance of REE, the normalised REE distribution pattern, the accessory minerals hosting the REE and the feldspar content of the rock are considered to be the most important bedrock features that influence the degree of REE enrichment and the type of deposit that develops (LREE vs HREE, or clay-hosted REE ore vs mixed mineral-hosted REE ore).

The granites in the Jiangxi province have Indosinian (Permian) and Yanshanian (Jurassic to Cretaceous) ages and are intruded into Proterozoic and Palaeozoic folded sedimentary rocks (Murakami and Ishiahara 2008). The most common granites found in the Nanling Mountains are Yanshanian (dated at 130-195 Ma) and are associated with tin and tungsten mineralisation (Zhang et al. 1995).

The rocks over which Chinese IADs have formed include medium- to fine-grained muscovite granites, fine- to coarse-grained biotite granites, granite porphyries, rhyolites and tuffs (Zhang et al. 1995). The muscovite granites are typically associated with HREE-type deposits whereas granite porphyry and volcanic rocks produce LREE-type deposits. Biotite granites may be associated with both HREE- and LREE-type IADs (Chi and Tian 2008). All granites that host

IADs have an initial REE content ranging between 200 – 400 ppm (Table 2.2). Sanematsu and Watanabe (2013) state that these granites are typically metaluminous to weakly peraluminous, have medium to high alkali composition and have low P_2O_5 concentrations (< 0.08 %).

2.3.3 Minerals hosting the REE

The majority of the REE in granites are held in accessory minerals (Bao and Zhao 2008). REE substitute for major ions such as Na^{+}, Ca^{2+}, Th^{4+} and U^{4+} and can be found in a wide range of minerals classes including carbonates, silicates, phosphates, oxides and halides (Walters et al. 2011, Kanazawa and Kamitani 2006). The small difference in ionic radii between HREE and LREE is enough to produce preferential substitution in different minerals (Figure 2.6). Oxides preferentially incorporate HREE, due to their smaller ionic radii, whereas carbonates, halides and phosphates preferentially concentrate LREE (Kanazawa and Kamitani 2006). Silicates can be enriched in either HREE or LREE depending on the coordination number of the REE in the mineral (Kanazawa and Kamitani 2006).

There are over 200 accessory minerals that host REE but only a small number are considered to be of economic significance (Walters et al. 2011). The main host minerals identified in the granites below IADs include bastnaesite, parisite, gadolinite, doverite, allanite, xenotime, monazite, zircon, synchysite, apatite, fergusonite and Ti-oxides (Table 2.3). The importance of these minerals in accounting for the total REE content varies because their presence and abundance differs between granites (Bao and Zhao 2008).

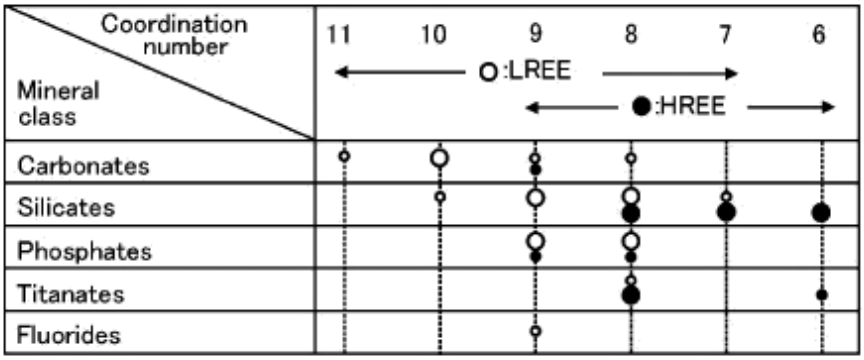


Figure 2.6. Chart comparing the occurrence and abundance of LREE and HREE in different mineral classes. The size of the circle is proportional to the average abundance of REE in each mineral class (Source: Kanazawa and Kamitani 2006).

The dissolution or partial dissolution of accessory minerals during chemical weathering plays an important role in the development of IADs. The degree of dissolution will influence the degree of REE enrichment, the type of enrichment (LREE vs HREE) and type of REE mineralisation (REE bearing clays vs a mixture of clay and resistant minerals). In Chinese deposits, the REE bearing accessory minerals identified in the parent granite have variable susceptibilities to weathering; xenotime and zircon are strongly resistant to weathering; fergusonite, monazite and allanite are moderately resistant; and bastnaesite, parisite, gadolinite and doverite are weakly resistant (Wu et al. 1993, Bao and Zhao 2008). HREE tend to be hosted in very resistant minerals such as zircon and xenotime, and several studies have found accumulations of these resistant minerals in the weathering profiles (e.g. Middleburg et al. 1988, Mongelli 1993, Murakami and Ishihara 2008, Sanematsu et al. 2013).

Table 2.3. List of REE-hosting accessory minerals of potential economic interest and their chemical formulae (Walters et al. 2011).

Mineral	Formula	Approximate REO %
Aeschynite-(Ce)	$(Ce,Ca,Fe,Th)(Ti,Nb)_2(O,OH)_6$.	32
Allanite-(Ce)	$(Ce,Ca,Y)_2(Al,Fe^{3+})_3(SiO_4)_3OH$.	38
Apatite	$Ca_5(PO_4)_3(F,Cl,OH)$	19
Bastnäsite-(Ce)	$(Ce,La)(CO_3)F$	75
Brannerite	$(U,Ca,Y,Ce)(Ti,Fe)_2O_6$	9
Britholite-(Ce)	$(Ce,Ca)_5(SiO_4,PO_4)_3(OH,F)$	32
Eudialyte	$Na_4(Ca,Ce)_2(Fe^{2+},Mn,Y)$ $ZrSi_8O_{22}(OH,Cl)_2$(?).	9
Euxenite-(Y)	$(Y.Ca.Ce,U,Th)(Nb,Ta,Ti)_2O_6$	24
Fergusonite-(Ce)	$(Ce,La,Nd)NbO_4$	53
Gadolinite-(Ce)	$(Ce,La,Nd,Y)_2Fe^{2+}Be_2Si_2O_{10}$.	60
Kainosite-(Y)	$Ca_2(Y,Ce)_2Si_4O_{12}CO_3.H_2O$.	38
Loparite	$(Ce,La,Na,Ca,Sr)(Ti,Nb)O_3$	30
Monazite-(Ce)	$(Ce,La,Nd,Th)PO_4$	65
Parisite-(Ce)	$Ca(Ce,La)_2(CO_3)_3F_2$.	61
Xenotime	YPO_4.	61
Yttrocerite	$(Ca,Ce,Y,La)F_3.nH_2O$.	53
Huanghoite-(Ce)	$BaCe(CO_3)_2F$.	39
Cebaite-(Ce)	$Ba_3Ce_2(CO_3)_5F_2$.	32
Florencite-(Ce)	$CeAl_3(PO_4)_2(OH)_6$.	32
Synchysite-(Ce)	$Ca(Ce,LA)(CO_3)_2F$.	51
Samarskite-(Y)	$(Y,Ce,U,Fe^{3+})_3(Nb,Ta,Ti)_5O_{16}$.	24
Knopite	$(CaTi,Ce_2)O_3$	na

In order to produce an IAD with a high percentage of REE-bearing clays, the parent granite must contain REE-bearing accessory minerals that are susceptible to weathering. However, there are different theories on the most favourable accessory mineralogy for the production of IADs. Bao and Zhao (2008) suggested a wide variety of accessory minerals including REE fluorcarbonates, phosphates (monazite, apatite, and rarely xenotime), oxides (pyrochlore, aeschynite, and other Nb–Ti phases), and members of the epidote group (especially allanite). Whereas Sanematsu and Watanabe (2013) proposed a much narrower range, suggesting granites that are rich in allanite, titanite and REE fluorcarbonates and poor in phosphates (monazite and xenotime) are required to produce IADs. The evident trend in these mineral assemblages is that deposits with a high percentage of REE-bearing clays appear to have developed from granites containing fluorcarbonate accessory minerals. For example, the Heling deposit, which contains 98 % of its REE adsorbed onto clays, was developed from a porphyritic biotite granite with bastnaesite as the principal REE mineral (Bao and Zhao 2008).

2.3.4 Hydrothermal alteration

Several granites which host IADs exhibit signs of hydrothermal alteration (e.g. Huang et al. 1989, Bao and Zhao 2008, Ishiara et al. 2008). The hydrothermal alteration involves albitisation, muscovitisation and fluoritisation and is believed to be the result of late stage magmatic fluids interacting with the granite (Huang et al. 1989). The hydrothermal alteration causes changes in the REE distribution and REE-hosting accessory minerals of the parent rock and consequently can influence the development of IADs. One case study where changes to parent rock and the effects of REE distribution on the weathering profile can be observed is the Xinxiu biotite granite in Jiangzi province which has been partly altered. The fresh biotite granite is enriched in LREE (2.4 LREE/HREE) and has a simple assemblage of REE-hosting accessory minerals (monazite-xenotime-zircon-apatite-fluorite) whereas the altered part of the granite shows enrichment of HREE (0.74 LREE/HREE) and a more varied REE-hosting accessory assemblage (monazite-xenotime-zircon-fluorite-doverite-gadolinite-chernovite; Bao and Zhao 2008). The formation of fluorcarbonate and phosphate minerals during the alteration of granites has also been noted by Huang et al. (1989) and Ishiara et al. (2008). In the Dignan granite REE-fluorcarbonates infilling cracks and apatites with REE-enriched rims have been observed (Ishiara et al. 2008).

The alteration of granites may play an important role in the development of the less common HREE IADs by changing the REE distribution patterns of the parent rock towards a more

HREE-enriched pattern, and by forming accessory minerals enriched in HREE that are more susceptible to weathering (Xu et al. 2017).

2.4 Mechanisms of Formation and Modification

The formation of IADs is thought to require granitic rocks with elevated initial REE content and the presence of REE-hosting accessory minerals that are weakly resistant to weathering. However, deposit grades are determined by the mobilisation and fractionation of REE into solution, and the adsorption behaviour of residual clay minerals in the weathering system.

2.4.1 Mobilisation of REE

The REE-depleted upper profile and the strongly enriched lower profile that characterise the weathering profile of IADs indicate that REE have been mobilised within the weathering system (Nesbitt 1979). It has been suggested that acidic surface waters percolate through the weathering mantle and transport available REE ions from the top of the profile towards to the lower horizons. During this process, alkalinisation of the water through mineral reactions reduces its ability to carry ions and eventually leads to precipitation of REE as hydroxides and carbonates or the absorption of REE ions onto clays (Nesbitt 1979).

Several authors have highlighted that the mobility of the REE is controlled not only by the availability of ions from dissolution of accessory minerals but also by the pH and oxidation conditions of the environment (e.g. Wu et al. 1989, Nesbitt 1989, Braun et al. 1990). The pH of solutions percolating through the ground is determined by acids acquired at, and near, the surface and the interaction with major mineral phases such as feldspars. The acids are obtained from CO_2 uptake (carbonic acid) and the breakdown of organic material (Nesbitt 1979). The humus-rich eluvium layer above the Chinese weathered granites provides a source of organic acids that can lower the pH of solutions filtering down. Vegetation cover may therefore play a role in weathering of ground rock by helping to produce more corrosive solutions with a higher capacity to carry REE.

The effect of redox conditions on the mobility of Ce can explain positive and negative anomalies of Ce in the weathered profile. Unlike the other trivalent REE (except Eu), Ce can exist as Ce^{3+} or Ce^{4+} in the weathering environment depending on the oxygen fugacity. When conditions are strongly oxidising, as is typically the case in the shallow subsurface, Ce has a valency of 4+ and tends to precipitate, typically in an oxide form. When conditions are reducing, Ce is trivalent and is relatively mobile, behaving similarly to the neighbouring LREE.

As a result, during weathering it is common to observe Ce accumulating in the upper horizons as cerianite or being taken up by Fe-Mn oxides, while the other REE migrate further down the profile (Braun et al. 1991). This produces the observed fractionation of Ce relative to other REE in IADs.

2.4.2 Clay ion adsorption

Clays are effective at adsorbing high concentrations of ions because of their charged surfaces and high specific surface area (Coppin et al. 2002). Adsorption can occur either through cation exchange on the crystal layer surfaces or chemisorption of anions at the layer edges (Aide and Aide 2012). The ability of clays to adsorb ions is determined not only by their abundance but also by others factors such as pH, ionic strength, and degree of crystallinity. One of the reasons clay behaviour is unpredictable is because the surface charge along the edges of the mineral can vary (Aide and Aide 2012). In kaolinite, the charge along the edges is related to reactions between ionisable surface groups and the ions present in aqueous solution, with sorption coefficients exhibiting a linear increase with increasing pH (Coppin et al. 2002). This finding may help to explain why clays in the lower part of the profile, where conditions are less acidic due to the lower degrees of mineral weathering, can concentrate greater amounts of REE. The lower crystallinity of clays observed up-profile could also limit their ion adsorption capacity.

2.4.3 Fractionation of REE

The subtle chemical differences within the REE group are sufficient to cause fractionation during weathering processes. The weathering profiles of ion-adsorption type deposits show clear evidence of fractionation, with LREE enrichment in the eluvium horizon and HREE enrichment in the lower part of the profile. Exactly how this fractionation occurs is still not well understood or constrained (Mongelli 1993). Some of the mechanisms that may be involved in the fractionation of REE in weathering profile include preferential dissolution of REE-hosting minerals, preferential mobilisation of HREE due to complex formation or physio-chemical conditions of percolating solutions, and the preferential adsorption by different clays.

The interaction between clay minerals and REE has been studied for over 20 years (Coppin et al. 2002). However, results have produced contradictory results, and complete understanding remains elusive. It has been suggested that cations with a higher charge-to-size ratio (i.e. HREE) would be preferentially adsorbed onto clays (Bau 1991). This is supported by one sequential leaching study which showed preferential adsorption of HREE (Sanematsu 2009). However, other experiments have shown preferential adsorption of LREE (Bao and Zhao

2008). The contradictions may be explained by different physiochemical conditions: HREE have been observed to be more strongly adsorbed on to kaolinite at high ionic strengths but not in relation to a specific pH range (tested at pH 3 – 9; Coppin et al. 2002). Organic species may also have a role to play; high concentrations of humic acids in solution have been found to increase the adsorption of LREE onto kaolinite (Wan and Liu 2006).

2.5 REE recovery from ion-adsorption clays

Adsorbed REE ions in the clays that compose IAD ores can be recovered by simple ion-exchange leaching, with the use of mono-valent salt solutions at ambient temperature (Ru'an 1988, Moldoveanu and Papangelakis 2012). Ion-exchange REE extraction methods have been mainly developed in China which, until recently, hosted the only known occurrences of ion-adsorption type deposits. The Chinese operations have mined REE from IADs for over four decades and during this time their ion-exchange leaching technology has developed from batch leaching using NaCl in the 1970's, to modern in situ leaching with ammonium sulphate starting during the 2010's (Moldoveanu and Papangelakis 2016).

2.5.1 Ion-exchange theory

The chemical mechanism proposed for the REE ion-exchange extraction is a cationic exchange. Trivalent REE cations adsorbed onto clay aluminosilicate surfaces become desorbed and released when exposed to an inorganic salt solution by exchanging position with monovalent cations that have a greater affinity for the clay surface (see Figure 1). The exchange occurs because the small monovalent cations have a higher charge density than the large trivalent REE cations, and are preferentially adsorbed by the negatively charged clay surfaces. For efficient ion-exchange to occur, the molar concentration of the monovalent salt solution needs to be higher than the concentration of the adsorbed cations. In the case of ion-adsorbed REE, a 3:1 stoichiometric ratio between the clay-hosted cations and the monovalent cation substrate is required (see equation 1 below, using kaolinite as the clay host).

$$[Al_2Si_2O_5(OH)_4]_{clay}\cdot REE^{3+}\ (s) + 3M^{+}\ (aq) \quad \leftrightarrow \quad [Al_2Si_2O_5(OH)_4]_{clay}\cdot 3M^{+}\ (s) + REE^{3+}\ (aq) \qquad \text{[Eq. 1]}$$

Experimental conditions for leach exchange must be maintained at acidic pH in order to ensure that REE^{3+} ions are retained in solution. Optimal pH ranges for REE ion-exchange experiments involving clay minerals are considered to be pH 3 to 6 (Moldoveanu and Papangelakis 2016). At acidities below pH 3 there is a risk of clay mineral dissolution, while at acidities above pH

6 REE cations begin to hydrolyse, converting from trivalent cations to insoluble hydroxide complexes ($REE(OH)_3$), and precipitating (Moldoveanu and Papangelakis 2016).

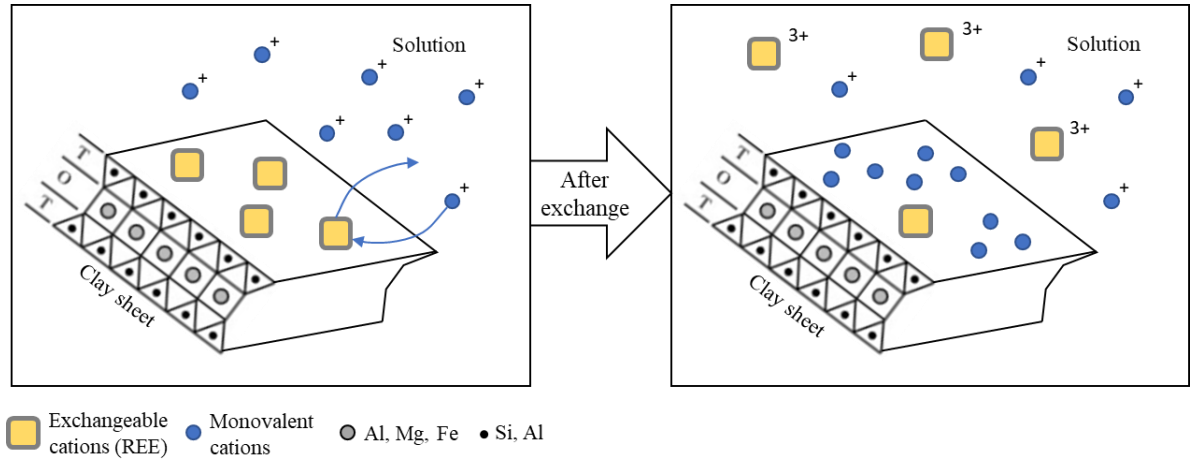


Figure 2.7. Schematic plot of the cationic exchange process at the clay surface during leaching, after Xiao et al. 2015.

2.5.2 Experimental studies

Overall, there is little published research on ion-exchange REE extraction from IAD ores. Most of the studies available were published after 2008 when REE became a popular research topic due to the increasing global demand of REE. The few studies that have been published are mostly all carried out at ambient temperatures and pressures, and favour the use of ammonium sulphate as the monovalent salt exchange cation at slightly acidic conditions (e.g. Sanematsu and Kon 2013, Moldoveanu and Papangelakis 2013, Xiao et al. 2015).

Most of extraction studies on ion-adsorption ore material have focused on improving the methods of extraction; identifying the optimum experimental leaching conditions, testing the capability of different leach solution, and suppressing the concentration of non-REE impurities (Moldoveanu and Papangelakis 2012, 2013, and 2016, Zhang et al. 2013, Yang and Zang 2015, Xiao et al. 2015). In recent years, environmental considerations have also been included in the development of leaching methods, due to the negative impacts that heap leaching and in situ leaching practises are having on local soil nutrients and plant growth (Xiao et al. 2015). Of the few studies that have measured and published REE recoveries from IADs around the world, the results are highly variable both within and between different ore samples (14 to 95 %; see Table 2.4).

Very few studies have looked closely at the controls on the adsorption and desorption of REE onto clays. Much of what is known about the interaction between REE and clay minerals comes

from studies outside economic geology. Most of this research has been carried out since the 1980's and focused on the use REE as geochemical tracers for surface water drainage, and the storage of nuclear waste.

Table 2.4. Published studies of recovery results from ion-exchange leaching of REE enriched weathered granite samples.

Author	Location & Samples	Recovery	Reagent
Sanematsu et al. 2009	Laos; weathered granite samples	14 – 72 %	Sodium acetate
Sanematsu et al. 2013	Thailand; weathered granite samples	34 – 85 %	Ammonium sulphate
Sanematsu et al. 2013	China; Dignan province IAD ore	42 – 64 %	Ammonium sulphate
Moldoveanu & Papangelakis 2012	REE enriched clay samples from Africa, Asia, and South America.	60 – 90 %	Ammonium sulphate
Xiao et al. 2015	China; Guangzi province IAD ore from Chaongzuo	95 %	Ammonium sulphate

2.6 Summary and Conclusions

Ion adsorption REE deposits are supergene deposits that contain commercially exploitable REE-bearing clays and commonly develop over REE-enriched granites in regions with warm, humid climates and low denudation rates. Despite the low grades of these deposits (0.05 – 0.2 wt % REE oxides), their low mining and processing costs, low radioactive element concentrations, and relatively high HREE content make them economical. IADs are currently the main source of HREEs which are critical elements for many advanced and renewable technologies such as high-strength magnets and electronics.

Until recently IADs were considered unique to southern China. However, in the last decade new deposits have been identified in Southeast Asia, Japan, Madagascar, and Brazil. Of these discoveries the Serra Verde deposit in Brazil and the Tantalus deposit in Madagascar are the largest and both are currently under development. As the demand of REE increases and the understanding of their formation improves, more IADs are likely to be discovered. Based on the distribution of known deposits, future deposits are most likely to be found in regions that are tectonically stable, have long histories of warm climate, and granite bedrock exposed at surface.

The current understanding on the formation of IADs derives from a small body of published work focusing on the Chinese deposits and has been complemented with knowledge from other areas of research such as nuclear waste management, clay mineralogy and regolith geology. The present genetic model proposes that IADs develop from the weathering of REE-enriched granites, where the breakdown of REE-bearing minerals allows mobilised REE ions to become adsorbed onto clays, themselves derived from the weathering of primary minerals such as feldspar. Over time, and given the right conditions, the continuous breakdown of bedrock and downward mobilisation is believed to allow sufficient concentrations of REE to accumulate in the lower clay-rich horizons of the profile to form a deposit. The main controls on the development of this supergene deposit are the parent bedrock, geomorphology, climate and tectonic conditions. However, the role and importance of these different controls and the processes involved in the formation of IAD are yet to be studied in detail.

Most of the work that has been published has focused on the granites over which IAD have formed or are thought to form on. The parent granite is the source of the REEs and clay minerals and is therefore considered an important control on the likelihood of ore formation. REE-enriched granites are thought to be necessary but not all weathered REE-enriched granites develop profiles with REE-enriched ionic clays. This selective occurrence suggests that certain types of granites are mineralogically and geochemically more favourable for the formation of IADs. A review of literature by Sanematsu et al (2017) shows that the granites of the Chinese IADs are typically metaluminous to weakly peraluminous, with medium to high alkali composition, and low P_2O_5 concentrations (<0.08 %). These granites also tend to be muscovite- or biotite-bearing and are commonly associated with tin and tungsten mineralisation. In order to determine whether these features are common to all IADs, the parent granites of IADs outside of China need to be characterised.

The REE content, REE distribution and accessory mineral assemblages of the granite protolith is also hypothesised to influence the degree of REE enrichment and the type of IAD that develops. However, how these features influence and contribute to the mineralogical and geochemical characteristics of IADs is only beginning to be understood. For example, the Chinese IADs parent granites exhibit a variety of REE-hosting accessory minerals but those with fluorocarbonates, allanite and titanite are considered to be more favourable compared those that hold REE in phosphate minerals. Another observation that has been highlighted is that HREE- dominant deposits appear to form more commonly over hydrothermally-altered granites produced by fluorine-rich fluids. These fluids are thought to modify the REE

composition and mineralogy of the granite and impact its susceptibility to weathering. The role, importance and prevalence hydrothermal alteration for the development of HREE-dominant IADs therefore needs to be investigated further.

There are other controls on the development of IADs that have been highlighted but are less well-studied. These include climate, geomorphology (drainage), and tectonic conditions. The Chinese IADs are known to have formed under stable tectonic conditions with low erosional rates, a sub-tropical and seasonal climate, and good drainage. These conditions, together with a prolonged period of weathering, encouraged the development of deep mature profiles, and the breakdown of a sufficient volume of rock to produce REE-enrichment by a factor of up to 3, relative to protolith composition. It is unclear whether these conditions are necessary, or if they fit within a wider range of conditions under which IADs may form. Some researchers believe that tropical conditions may prevent IAD formation due to an intense leaching regime, and that a lack of seasonal variation may prevent good drainage. However, the effect of weathering intensity and drainage regimes on the mobilisation and retention of REE has not been studied in the context of these deposits. Another question that has yet to be answered is how vulnerable these deposits are to changes in climatic conditions and drainage regimes over time and therefore how likely are they to be preserved. Notably, the Chinese deposits all formed in recent geological history (Miocene). Without comparable data from deposits in other parts of the world, it remains unknown whether IADs are constrained to the recent geological record, or if we may expect to find these deposits further back in the geological record.

The formation and enrichment of IADs involves the liberation, mobilization, and capture of REE in the weathered profile. These processes are the least studied components of IADs and much of what is known has been transplanted from other fields of research.

The liberation of REE requires the breakdown of REE-bearing minerals in the bedrock which itself depends on the susceptibility of primary mineralogy to weathering. Once released, the REE ions are assumed to move freely down through the profile, to become adsorbed or removed from the system. However, no known studies have tracked the accessory minerals in the profile to observe their breakdown and the pathways that released REE ions take before clay adsorption. It is not known whether the REE remain as ions in solution until they interact with clay minerals or if they form intermediate secondary phases such as carbonates, phosphates or oxides. Overall very little is published on the mineralogy and geochemical composition of these Chinese IAD profiles to assess the progression mineral weathering.

Downward mobilisation of REE from the top of the profile by percolating water is considered the main mechanism for REE transport and enrichment in IADs. However, published works merely describe this process, and no mass balance calculations have been attempted in order to quantify the enrichment process for this deposit type. As a result, the volume of granite that has broken down, the relative contributions of different weathering processes (mobilisation, residual vs compaction) have not yet been assessed, and the percentage of REE retained in the weathering system is unknown.

The capture and retention of REE in weathered profiles is determined by the clay mineralogy and controlled by physiochemical conditions in the profile. While there is little published information regarding the mineralogy of these deposits, in some Chinese IADs kaolinite and halloysite have been determined to be the main REE host as the dominant clay mineral. Other clay types are present, but only in minor proportions.

Much of what is known about the interaction between REE and clay minerals derives from adsorption and leaching experiments. These studies show adsorption and desorption behaviour of clay minerals is largely dependent on physiochemical conditions (pH and Eh) as well as the composition of percolating water. It is generally accepted that alkaline conditions in the saprolite horizon are favourable for the adsorption of REE, and that Ce can be retained higher up in the profile due to its variable solubility under different oxidation states. Laboratory studies also show that clays can preferentially adsorb particular REE causing fractionation. However, mixed results for adsorbed LREE/HREE composition indicate that clays may shift between different adsorption states, and therefore their influence on the development of HREE vs LREE IADs is not yet clear.

In summary, IADs are currently the principal sources of global HREE supply but have only recently been given academic attention due to increasing demand for REE. There is currently a simple model that explains their formation. This is based on the small amount of work published from the known Chinese deposits. The limited number of deposits and their poor characterisation means there are many questions that remain unanswered regarding the controls and processes of adsorption, enrichment and fractionation. Newly discovered IADs from other parts of the world are a great opportunity to improve the characterisation of these deposits, determine controls on mechanisms of formation, and assess if the Chinese IAD model is representative.

Chapter 3

Geology of the Study Area

This chapter outlines the geology of the Tocantins province and briefly reviews previous work on the Serra Dourada granite complex which composes the bedrock of the Serra Verde deposit, as well as the location and climate of the study area.

3.1 The Serra Verde REE deposit and Study Area

The Serra Verde deposit is located in the middle of the southern half of the Serra Dourada granite (SDG); an elongate, dome-shaped Proterozoic granitic complex situated in the northern part of the state of Goiás, central Brazil. The Serra Verde deposit is hosted in the thick weathered laterite profile that developed over the granite during the Miocene, and is today partly preserved (Braun 1971, Trescases et al 1981). The deposit is being explored and developed by Serra Verde Mining who reported a resource in 2012, of 911 Mt REY oxide with a cut of grade of 0.12 % (measured, indicated, and inferred; NI 43-101 data from company website).

Today there are only a few areas where the complete weathering profile with its flat geomorphology is still preserved, mainly located at the plateaus located on topographic highs (Figure 3.1). It is one of these plateaus, the central plateau (see), that has been selected as the focus of this study. The plateau falls in the middle of the deposit and is large enough to look at lateral variations.

The study area is currently covered with cerrado (a woodland savannah vegetation) and is characterised by hilly terrain with mean elevations ranging between 400 and 900 m a.s.l. The region has a humid tropical climate with marked dry (April – September) and wet (October – March) seasons. Annual rainfall is 1500 mm and temperatures range between 21 C and 26 C throughout the year (INMET).

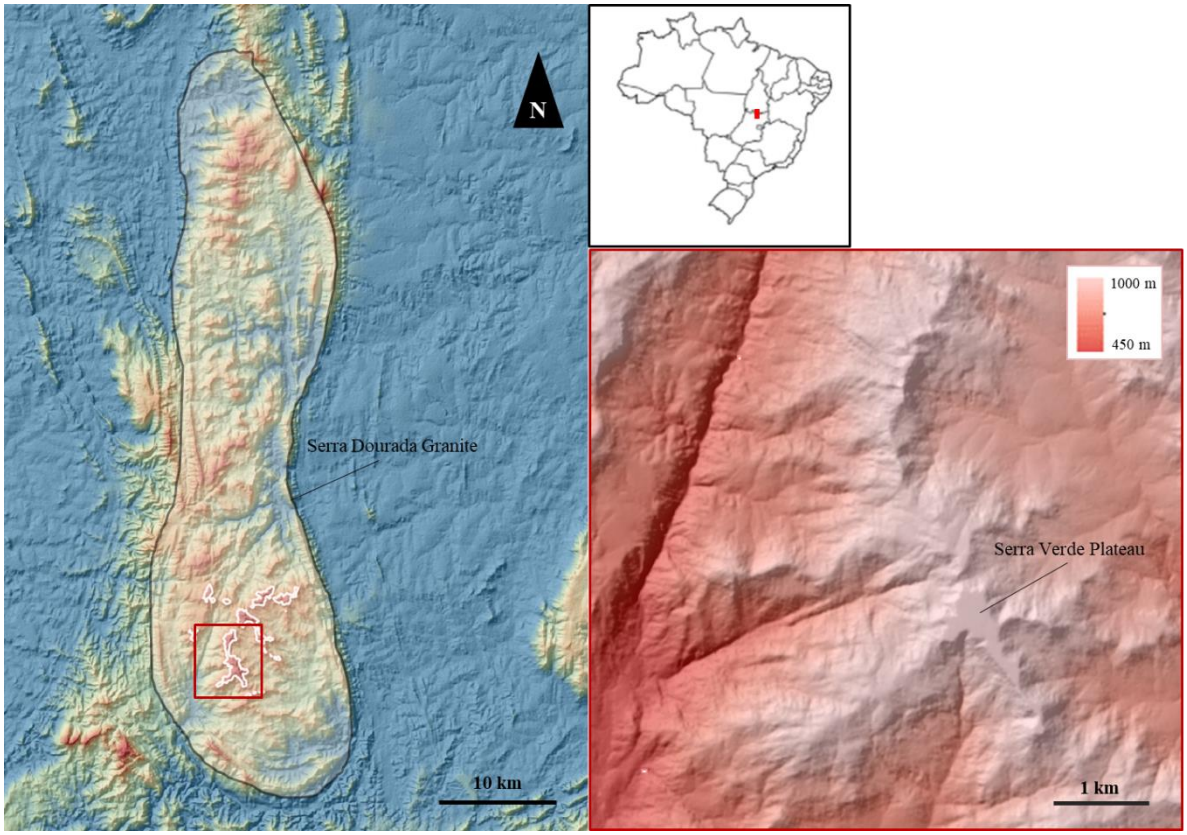


Figure 3.1. Outline of the Serra Dourada Granite (left; pale orange) and location study area of the plateau (white outlines are areas with preserved profile). Inset map of LiDAR hill-shaded digital terrain model (15 m resolution) on the right shows the preserved plateau.

3.2 Regional Geological Setting

The Proterozoic granites of northern Goiás are situated in the Tocantins metamorphic province, which is itself buttressed between the São Francisco, Amazonian and Paraná cratons (Figure 3.2). Within the Tocantins province, the granites are located in the Goiás Massif between the Araguaia belt to the west and the Brasilia belt to the east (see Figure 3.3).

The granites that compose much of the Goiás Massif have been split into two groups by Mariani & Botelho (1986); the Rio Tocantins Sub-Province (RTS) in the west, and the Rio Paraná Sub-Province (RPS) in the east (Figure 3.4). The RPS granites, which have been more extensively studied, are small ovoid shaped bodies that are surrounded by the Arai rift group meta-sediments. Within the RPS two distinct granitic suites have been identified; the 1.77 Ga alkaline g1 suite, and the 1.6 – 1.57 Ga metaluminous to peraluminous tin-mineralised G2 suite (Pimentel et al. 1999). The RTS granites are instead elongate ellipsoid bodies surrounded by

Serra da Mesa Group meta-sediments. The Serra Dourada granite, which is the largest of all the granites, running 45 km from N – S, belongs to the RTS group (Mariani & Botelho 1986). Locally, the SDG is surrounded by quartzites and mica-schists of the Serra da Mesa.

The RTS and RPS were intruded at the end of the Paleoproterozoic Trans-Amazonian orogenic event (see Figure 3.5). The post-orogenic crustal relaxation and extensional processes that followed the Trans-Amazonian orogeny are cited to have caused rifting and associated magmatism (Almeida et al. 2000). The hypothesis for a rift setting comes from the 1.77 Ga Arai rift volcano-sedimentary sequence which lies unconformably on the Archean-Paleoproterozoic basements (Pimentel et al. 1999). The evolution of the Arai rift basin is still debated because it is not yet clear whether it developed into a large open oceanic basin (Pimentel et al. 1999). Rhyolites found within the Arai sequence which are geochemically linked to RPS granites, confirm that the RPS intrusions were coeval with the development of the rift basin (Pimentel et al. 1991).

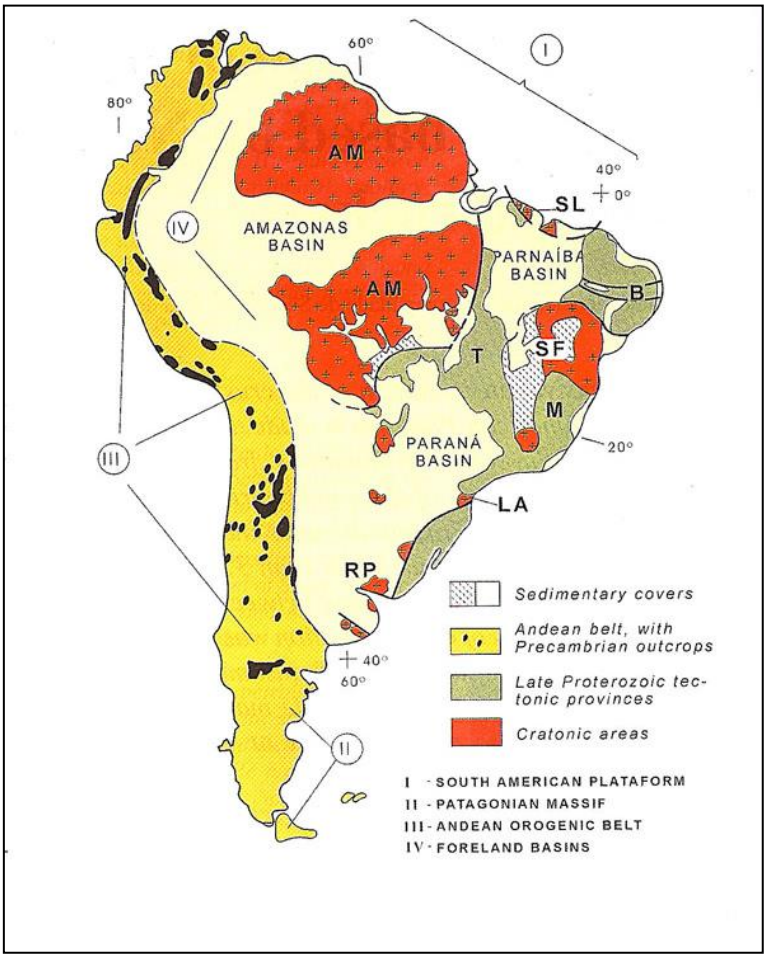


Figure 3.2. Crustal provinces of South America; AM: Amazonian craton; SF: Sao Francisco craton; RP: Rio de la Plata craton; SL: Sao Luis cratonic fragment; LA: Luis Alves cratonic fragment; T: Tocantins Province; M: Maitiqueira; B: Borborema. (Source: Cordani & Sato 1999).

Pelitic and arenitic sediments of the Serra da Mesa Group are considered to be the lateral equivalent of the upper part of the Arai sequence (Pimentel & Botelho 2001). The intrusive relationship between RTS granites and the Serra da Mesa Group are however controversial. Macambira (1983) and Pimentel et al. (1991) argue that their field observations suggest the granites intruded and deformed sediments of Serra da Mesa Group. Contrarily, Marini & Botelho (1986) argue that there is no clear intrusive relationship and suggest instead that the Serra da Mesa Group sediments were deposited on top of the granite after it had intruded into the Archean-Paleoproterozoic basement. One of the reasons that the relationships may be unclear is due to the strong deformation and extensive recrystallization found along the margins of the granites (Dall'Agnol et al. 1999).

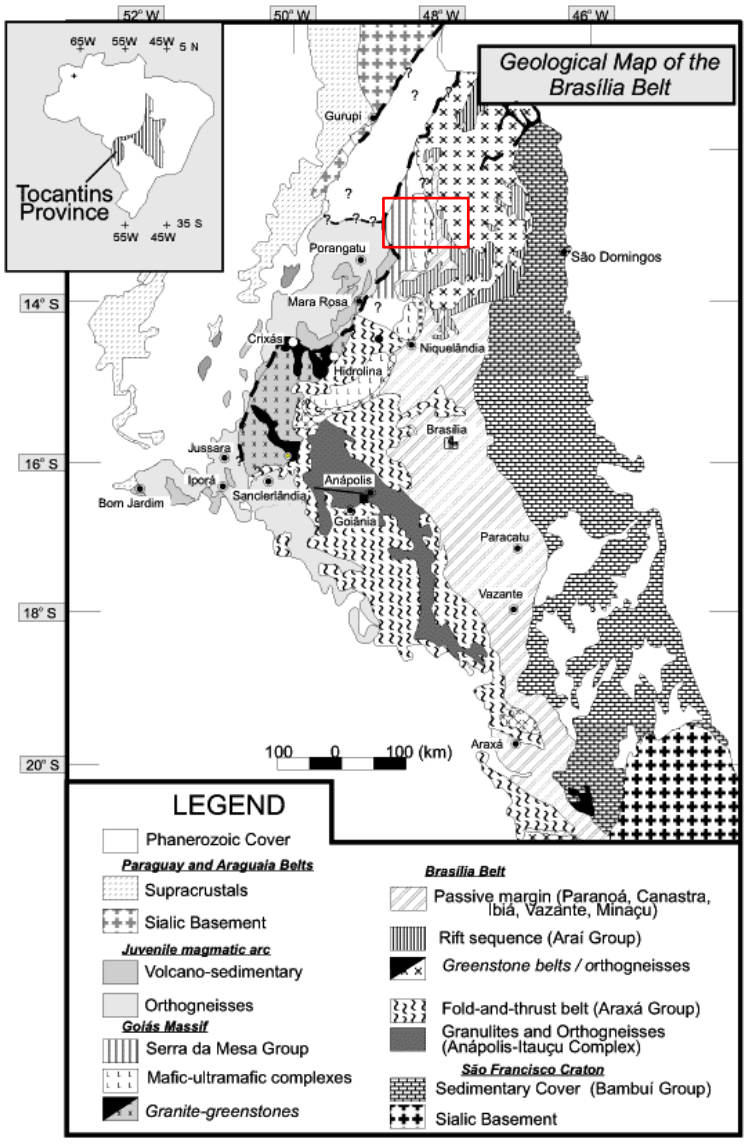


Figure 3.3. Map depicting the main geological groups of the northern Tocantins Province. The location of the Tocantins granites (detailed in Figure 3.4) discussed in this review are shown by the red box. (Source: Pimentel & Botelho 2001)

Two orogenic events in the late Mesoproterozoic (formation of Rodinia) and in the Neoproterozoic (formation of Western Gondwana) strongly deformed the rocks of the Tocantins Province. Very little is known about the effect of the late Mesoproterozoic orogenic event in this region because the metamorphism of the rocks was later overprinted and structures further reworked by subsequent events (Almeida et al. 2000). The Neoproterozoic orogenic event that followed was caused by a collision of the São Francisco and Amazonian cratons. It is known as the Brasiliano Pan-African orogeny and was responsible for the formation of the Brasilian fold-thrust belt that runs ca. 1000 km north-south along the São Francisco Province (Pimentel et al. 1999). Bilal (1991) estimates that the rocks in the RTS were metamorphosed to amphibolite facies in metamorphic conditions of 540 ºC and 5 – 7 kbar, estimated from geothermometric analysis of biotites. The rocks in the RTS are more strongly deformed than in the RPS because according to Marini et al. (1992), the RTS rocks were closer to the Uraçu fault which accommodated significant deformation.

The Tocantins Province has remained very stable since the Brasiliano Pan-African orogenic event (Almeida et al. 2000). The last thermo-tectonic event to have affected the region is recorded by the 530 Ma minimum K-Ar age biotites obtained from basement rocks (Reis Neto 1983). Uplift and erosion during this quiescent period likely caused the SDG to become exhumed sometime during the Cretaceous. This first erosion cycle is associated with the development of a major continental-scale peneplane extending over much of Brazil, and is still visible today in the tabular and flat-topped topography of central Brazil (King 1956). A deeply weathered lateritic profile then developed as climatic conditions became increasingly wetter during the Paleogene (Braun 1971). A second erosion cycle known as the Velhas erosion cycle started in the Late Paleogene which incised and eroded much of the Cretaceous peneplane. The erosion has continued into the Neogene and is still active today (Trescases et al. 1981).

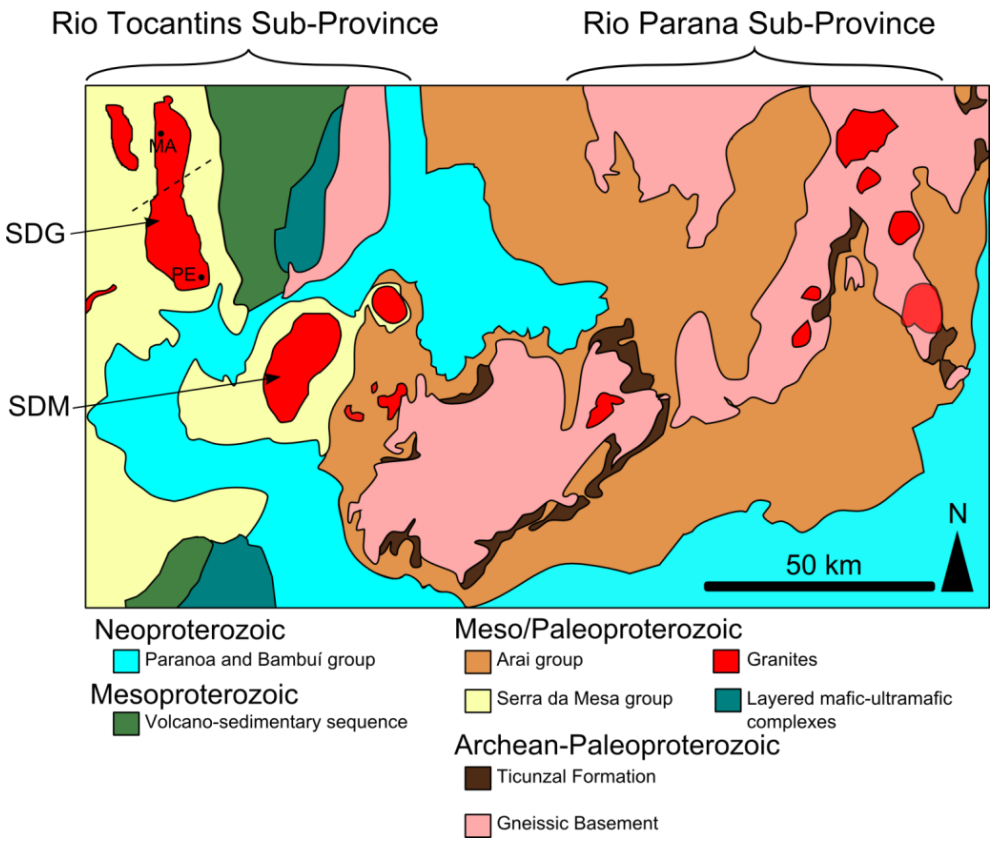


Figure 3.4. Geological map of the Goiás Tin Province; SDG: Serra Dourada granite, SDM: Serra da Mesa granite, PE: Pela Ema, and MA: Mata Azul. (Source: modified from Goiás State geological map and Pimentel & Botelho 2001).

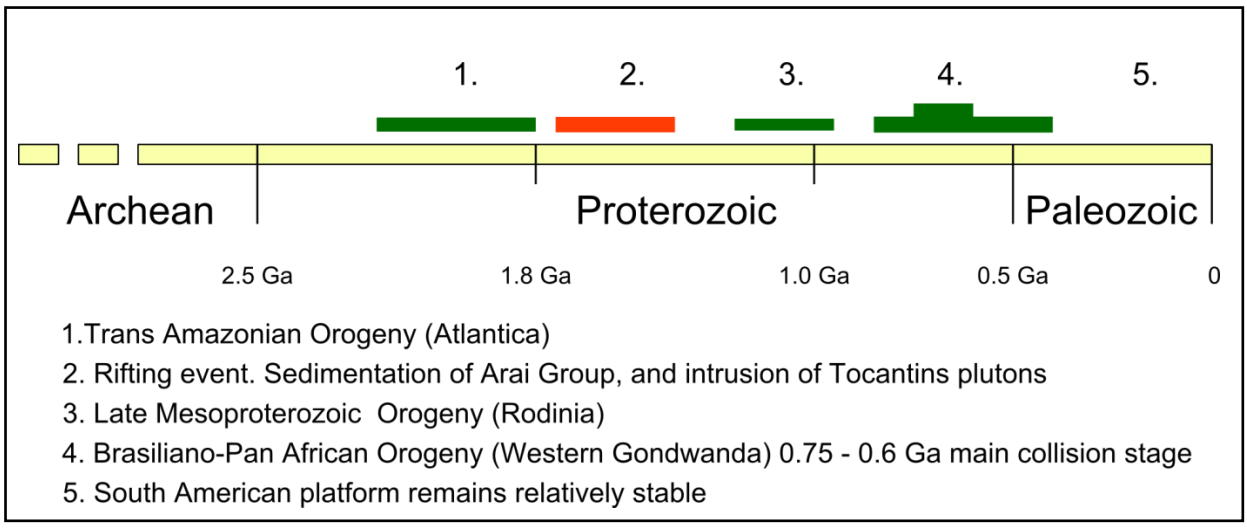


Figure 3.5. Simplified geochronological scale of events that affected central Brazil and the SDG.

3.3 The Serra Dourada granite

The Serra Dourada granitic complex is the largest of several highly evolved anorogenic granites that intruded the Archean-Paleoproterozoic basement between 1.7 – 1.5 Ga (Pimentel et al. 1991) and which have been historically known for their tin and gem mineralisation. During the 1980's cassiterite was extracted from the SDG, at the only underground tin mine developed in Goiás; Pela Ema. In recent years, the high REE content of these granites has been recognised and economic interest in the SDG as a potential host of placer and clay-bearing REE deposits has been revived. Serra Verde Mining LLC, a private company, is currently completing a resource evaluation of clay-bearing REEs in the SDG weathered profiles, and has plans to develop a mine in the near future in the southern part of the granite.

Although the SDG has not been extensively studied, there are a few studies that provide a general insight into its geology. Macambira (1983) produced the first detailed description of the SDG by mapping the area and carrying out petrographic and metallogenic work. This was followed by Bilal (1991) who focused on understanding the tin and beryllium mineralisation occurrences in the granite. These studies developed the first academic foundations of the SDG. However, the high REE content of the SDG was not recognised until geochemical data from the granite was published by Marini et al. (1992). Since then, the studies that have followed have increasingly focused on the granite's REE mineralogy and geochemistry (e.g. Bilal et al. 1997, Teixeira 2002, Teixeira & Botelho 2002 and 2006, and Santana 2013).

The following sections introduce the available work regarding the SDG in order to contextualise and inform the discussion presented in this thesis. Particular attention is given to data that is relevant to the enrichment of the clay-bearing REE deposit at Serra Verde.

3.3.1 Geochronology

Few isotopic studies that define the age of emplacement of the SDG have been carried out, and all reported dates come from studies from the 1970's and 1980's which used the whole rock Rb - Sr dating method (Hasui & Almeida 1970, Reis Neto 1983, and Macambira 1983). Reis Neto (1983) reported an emplacement date of 1.43 ± 0.24 Ga and Macambira (1983) reported an emplacement date of 1.68 Ga. Unfortunately, these ages are now considered unreliable because the Rb-Sr system in rocks is now known to be susceptible to isotopic resetting during metamorphism (Rollinson 1993) and at least one large tectonic event is known to have affected the Tocantins Province after the likely emplacement age of the granites (the Brasiliano-Pan African orogenic event). One of the strong critics of the Rb-Sr dates is Pimentel et al. (1991)

who notes that the considerable scatter of the data observed on the isochron plot can be attributed to the open system behaviour of the Rb-Sr isotopic system during the Brasiliano-Pan African orogenic event. Marini et al. (1992) writes that only indicative emplacement dates of 1.6 - 2.0 Ga for the RTS can be inferred from the Rb - Sr isotope data.

Evidence for the homogenisation of isotopic systems by the Brasiliano-Pan African orogenic event, estimated to have been at its collisional peak around 600 Ma (Almeida et al. 2000), comes from the Neoproterozoic to early Palaeozoic dates obtained from biotite and monazite crystals from SDG and surrounding rocks. Reis Neto (1983) reported K - Ar biotite ages of 513 Ma for SDG and 513 Ma and 530 Ma for the basement gneisses. Teixeira (2002) reported U-Pb ages 571 ± 24 Ma from monazite crystals for the SDG.

The most reliable dates obtained from RTS come from lead isotope studies on Serra da Mesa Granite located a few kilometres south - east of SDG (Reis Neto 1983, Pimentel et al. 1991, Rossi et al. 1992). Consequently, these dates are commonly used to represent the age of emplacement of all RTS granites (e.g. Pimentel & Botelho 2001 and Petersen et al. 2002). Combining the whole rock data of Serra da Mesa and Serra Branca, Reis Neto (1983) reported an age of 1658 ± 44 Ma. Pimentel et al. (1991) obtained a U-Pb zircon age of 1.57 - 1.61 Ga and Rossi et al. (1992) obtained Pb-Pb evaporation age of 1580 ± 20 Ma for Serra da Mesa. If the dates of Serra da Mesa are representative of the sub-province, the RTS granites coincide with the younger 1.6 - 1.5 Ga G2 suite identified in the RPS.

If the intrusion relationships cited by Macambira (1983) and Pimentel et al. (1991) are correct, the depositional age of Serra da Mesa Group meta-sediments surrounding the SDG can also be used to constrain the maximum age of intrusion. According to Dardenne (2000) the sediments of Serra da Mesa Group were deposited between 1.7 Ga and 1.5 Ga thus giving the granites of RTS a maximum age of 1.7 Ga.

3.3.2 Lithologies and Mineralogy

Three granite rock types have been identified in the SDG by Bilal et al. (1997). From the least to the most evolved they consist of: an amphibole granite, a biotite granite, and a fine grained porphyritic granite. The biotite granite is the main rock type making up the bulk of the intrusive body. The amphibole granite is found mostly around the edges of the granite complex, and the porphyritic granite occurs as fine veins cutting through the biotite granite. Bilal et al. (1997) interpreted these three rock types as a differentiating series produced by the fractional crystallisation of the magma. All three rock types have been sheared and metamorphosed into

gneissic rocks with the strongest deformation found around the edges (Teixeira & Botelho 2006, Pimentel et al. 1991). Macambira & Villas (1984) also identified two types of late pegmatites; one found along the border containing tantalite-columbite, emerald, muscovite, and monazite, while the other found in the drill core beneath Serra Verde contains aquamarine.

The biotite granite is described as a pink, coarse grained granite composed of quartz, perthitic microcline, oligoclase, and biotite with zircon, apatite, monazite, xenotime, thorite, fluorite, ilmenite, pyrite, and chalcopyrite as accessory minerals (Macambira 1983, Bilal 1991, Bilal et al. 1997, Teixeira & Botelho 2006). The other two granite rock types are mineralogically similar to the main intrusion, the key difference between them being an occurrence of calcium-amphibole in the amphibole granite, and an occurrence of late microcline phenocrysts in the porphyritic granite. The porphyritic granite also appears to contain fewer accessory minerals, with allanite mentioned as the only accessory phase (Teixeira & Botelho 2006).

As well as the main lithologies, altered rocks hosting tin mineralisation have been identified in SDG. The altered rocks include muscovite-biotite granite, albitites, biotitites (rocks containing > 98 % biotite), and quartz-muscovite greisens, with albitites being the most common (Teixeria & Botelho 2006). The first study of the SDG by Macambira (1983) proposed that the albitites (then called 'soda gneisses') and biotitites, which occurred as lenses inside the granite, were partly assimilated trondhjemite enclaves. This hypothesis was later rejected by Marini & Botelho (1986) who argued instead that these rocks represented intermediate alteration stages towards a greisen. Their argument was based on the fact that the albitites were surrounded by muscovite-biotite granite and that the biotites composing the biotitites were identical to metasomatised biotites associated with albitites in other parts of the Tocantins province. Marini et al. (1992) provided support for the second interpretation by presenting data that showed that the albitites and enclosing biotite granites had the same rare earth pattern therefore negating the trondhjemite interpretation.

3.3.3 Geochemistry

Excluding REE data, the only major and trace element data available from the SDG comes from unaltered samples analysed and published by Bilal et al. (1997). The data shows that the SDG is a highly evolved felsic granite with high silica (66 – 75 % SiO_2), high alkali content (2.16 – 2.91 % Na_2O, and 4.8 – 6.3 % K_2O), and low Fe content (1.98 – 6.48 % Fe_2O_3; Table 1). Like other Proterozoic granites in the Goiás tin province, the SDG is characterised by elevated concentrations of high field strength elements (HFSE) namely Th, Zr, Nb, and REE, and low Ca, P, and Sr. The results also show that all three rock types exhibit high fluorine contents (> 800 ppm).

Comparing results between the different granite types, an evolution of the geochemical composition can be observed from the least to the most evolved granites. From the amphibole granite to the porphyritic granite, SiO_2 content increases while Fe_2O_3, MgO, and P_2O_5 decrease. Likewise, Ba, Zr, Nb and Sr become more depleted while U, Th, Rb, and Y become more enriched. Contrarily, the REE and the fluorine show no systematic variation. No major or trace element data for the altered rocks has been published for comparison.

Analyses by four different studies confirm the REE content of SDG is high with values for the biotite granite ranging between 400 ppm and 778 ppm TREE and 545 and 826 ppm REY (TREE + Y; Bilal et al. 1997, Marini et al. 1992, Teixeira & Botelho 2006, and Santana 2013). This range excludes one sample reported by Marini et al. (1992) identified as a mineralised biotite granite with values of 1,334 ppm TREE and 1,713 ppm REY. The sample was collected from the southern part of the granite in the Pela Ema area. However, Marini et al. (1992) do not publish its location nor a detailed description for this sample and as a result it is difficult to speculate on the reason for such an enriched composition. REE data of albitites show similar values to those found in biotite granites with values ranging between 690 ppm and 1145 ppm (Teixeira & Botelho 1996 and Marini et al. 1992). Again, no description or coordinates for these samples are provided in the published studies.

3.3.3.1 Classification

The SDG has been classified as a slightly peraluminous to metaluminous (0.92 – 1.07 [Al/Ca+Na+K]), subalkaline, anorogenic-type granite by Bilal et al. (1997). More specifically it is considered a sub-type A2 granite based upon its high Y/Nb ratio (Figure 3.6). Sub-type A2 granites are considered to be anorogenic granites which are derived from continental crust, or have incorporated a significant proportion of continental crust (Eby 1992).

Table 3.1. Geochemical composition of SDG granites from Bilal *et al.* 1997**.**

	Amphibole granite		Biotite Granite					Porphyritic Granite		
SiO2	66.6	65.9	71.3	73.8	73.25	73.3	74.53	74	75.2	75.4
TiO2	1.28	1.1	0.504	0.35	0.363	0.49	0.293	0.27	0.29	0.222
Al2O3	12.44	13.4	13.1	12.9	12.5	12.9	12.2	12.5	12.7	12
Fe2O3	6.48	5.71	3.29	3.19	2.88	3.21	2.38	2.16	2.11	1.98
MnO	0.1	0.074	0.049	0.036	0.038	0.047	0.03	0.022	0.069	0.023
MgO	1.32	1.06	0.44	0.195	0.28	0.403	0.214	0.238	0.251	0.159
CaO	2.93	2.47	1.3	0.765	1.02	1.02	0.49	0.81	1.12	0.84
Na2O	2.43	2.63	2.34	2.3	2.53	2.91	2.5	2.16	2.54	2.85
K2O	4.9	4.98	5.83	6.34	5.61	4.82	5.72	5.93	5.62	5.76
P2O5	0.41	0.36	0.07	0.04	0.05	0.06	0.03	0.04	0.05	0.03
H2O	0.74	0.8	0.8	0.96	0.23	0.7	0.42	0.66	0.37	0.32
Total	99.63	98.48	99.02	100.8	98.75	99.86	98.81	98.79	100.32	99.58
Ba	700	981	489	430	321	504	233	336	339	237
Be	3.01	2.64	3.12	3	5.4	3.67	1.96	3.04	4.03	4.03
Co	11.5	5.67	1.84	1.6	1.06	10.2	1.7	0.63	1.55	0.05
Cs	10.5	9.9	13.8	11.6	5.7	7.9	10.3	14	8.4	6.9
F	1925	2830	1610	2685	1900	1340	1246	2165	1750	812
Ga	22.8	19.4	22.6	24.6	23	22.3	24	21.9	21.5	22.5
Hf	13	12.2	13.7	15	15.7	13.8	9	11.7	13.3	9.5
Li	16.5	13.8	23.3	19.5	28.8	29.2	19.9	27.4	23.8	21.6
Ni	10.2	4.9	6	2	5.7	7	3.2	3.2	2.4	4.9
Nb	39.9	43.2	40	33	27	33	29.2	23	26.2	22.8
Pb	30.5	35.4	35	34	41	38.6	33.3	38.6	38	46.6
Rb	236	259	268	303	324	313	356	358	309	306
Sc	15	11.1	4.96	4	4.45	4.72	3.27	3.07	3.98	2.04
Sn	5.8	4.3	4.7	4.8	7.8	5.4	7.8	7.8	6	8.3
Sr	118	117	70	72	75	57	58	60	59	55
Th	44.9	43	46.8	64	67	53.1	69	77	59.3	82
Ta	2.7	0.9	2.7	5.1	2.9	4.2	5.5	6.2	3	6.6
U	2.8	3.64	6.2	9.9	13.3	18.8	10.4	18.9	12.7	16.8
V	27.3	18.6	5.86	0.18	6.2	9.7	0.98	3.55	3.28	1.55
Y	82.5	76.1	88	76	91	78.9	90	131	109	119
Zn	100	71	60.9	67	50	81	59	38	28	39
Zr	400	576	459	425	348	431	330	228	260	256
La	127	137	151	141	169	131	157	147	126	136
Ce	255	272	254	230	270	229	282	294	250	271
Nd	110	101	103	70	94	67	87.5	135	116	125
Sm	21	21.2	20	14	19	14.6	17.7	17	15	16
Eu	2	1.9	1.6	1	0.69	1.04	0.5	0.83	0.82	0.6
Gd	16.4	16.2	14.7	12.2	14.7	12.8	12.3	16.4	16.3	16.3
Tb	2.6	2.5	2.4	2.3	2.3	2.2	2.1	3.1	3.1	3
Yb	7	6.17	7.2	6.9	8.2	8.7	7.5	11.7	11.5	10.9
Y	82.5	76.1	88	76	91	78.9	90	131	109	119

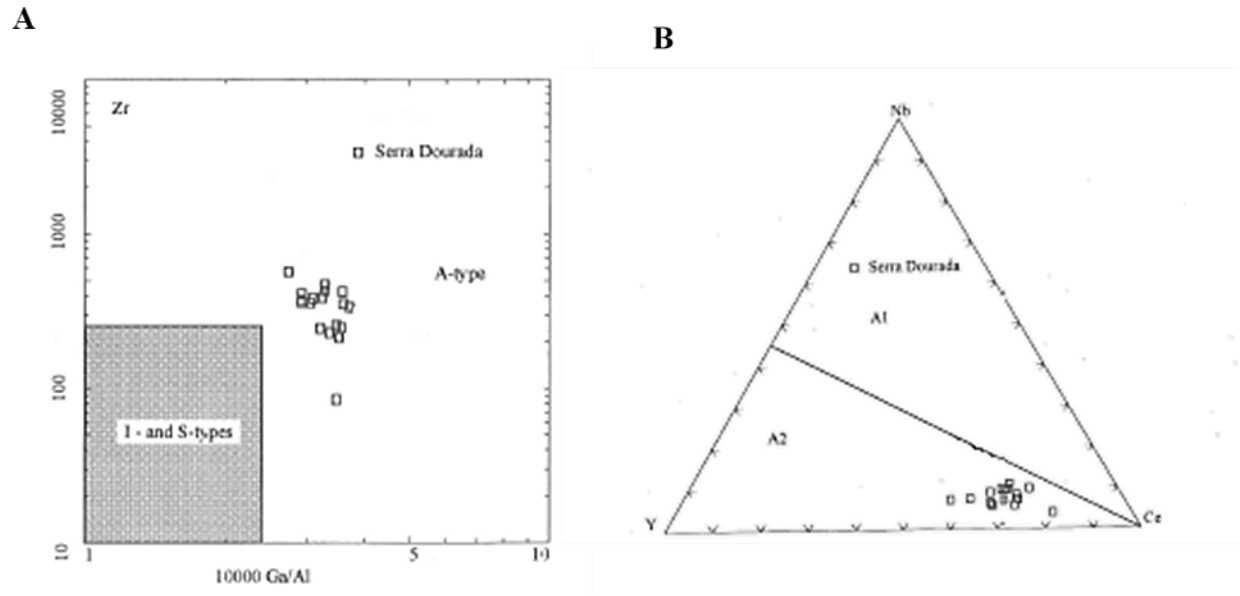


Figure 3.6. Classification plots for A-type granite (A) 1000 Ga/Al vs Zr, and A1 vs A2 granites (B) Nb-Y-Ce ternary diagram. Both plots from Bilal et al. (1997).

3.3.3.2 Normalised REE patterns

Chondrite-normalised REE data show that the SDG is more than 100 times enriched in REE with light REEs (LREE) showing the greatest enrichment (Figure 3.7, Figure 3.8, Figure 3.9). The normalised REE patterns of the SDG are characterised by a moderate LREE/HREE fractionation [$7.4 < (La/Yb)_N < 15.1$] and a strong negative Eu anomaly [$0.11 < Eu/Eu^* < 0.30$]. The strongest LREE/HREE fractionation is observed within the LREE, with a trend inclined towards the HREE and 4.7 – 6.2 La_N/Sm_N ratio. In contrast, the HREEs show a low degree of fractionation with a near horizontal chondrite-normalised trend and a low 1.19 – 1.65 Gd_N/Yb_N ratio. The chondrite-normalised patterns of the SDG are compared with the high silica peralkaline rhyolites from the Kenya rift valley and the Finnish rapakivi granites (Bilal et al. 1997).

The chondrite-normalised REE patterns of the amphibole granite, the biotite granite, and the porphyritic granite have the same trends and same degree of enrichment (Figure 3.7, Figure 3.8). The only observable differences between the three rock types is that the negative Eu anomaly becomes more pronounced and the HREE become slightly more enriched between the amphibolite granite towards the porphyritic granite. Bilal et al. (1997) attribute this

variation to a product of the fractionation of allanite, which preferentially accommodates LREE in its crystal lattice.

The 'mineralised biotite granite' presented by Marini et al. (1992) has a similar REE pattern to the other biotite granite but is 2 – 3 times more enriched in REE (Figure 3.9). Small differences between the patterns are a small negative Ce anomaly and stronger HREE-fractionated trend in the mineralised sample. It is unclear whether the main biotite granite represents a local anomaly or if it represents an enriched zone within the biotite granite because it is the only sample that has been reported with such high REE values.

The effect of hydrothermal alteration on the REE distribution and content of the SDG is unclear because the interpretations of the geochemical effects caused by albitisation by Marini et al. (1992) and Teixeira (2006) are contradictory. The former writes that albitised rocks become LREE enriched and are characterised by an inclined pattern to the lightest REEs, while the latter argues that albitisation results in REE enrichment which is dominated by the HREE.

The normalised REE pattern of the albitite sample analysed by Marini et al. (1992) shows a more strongly fractionated trend with 17.16 La/Yb_N compared to 9.22 La/Yb_N in the host biotite granite due to its higher LREE content (Figure 3.8). The normalised REE pattern of the albitite samples analysed by Teixeira & Botelho (2006) on the other hand show a seagull-shape pattern with elevated REE content (Figure 3.9). In these samples, the HREE are strongly enriched and the LREE/HREE fractionation is very low with 1.53 La/Yb_N compared to the biotite granite used as a reference. In both studies, the strong Eu anomaly is retained.

Neither study presents a description nor a geochemical composition of the albitite samples analysed for REE. Teixeira & Botelho (2006) also do not explain the spatial relationship between the reference biotite granite and the albitised samples. Without this information it is difficult to compare the results of each study and begin to understand the differences between the normalised REE patterns obtained. Factors such as differences in the extent of alteration or variations in the initial REE content of altered biotite granite may explain the differences between these samples.

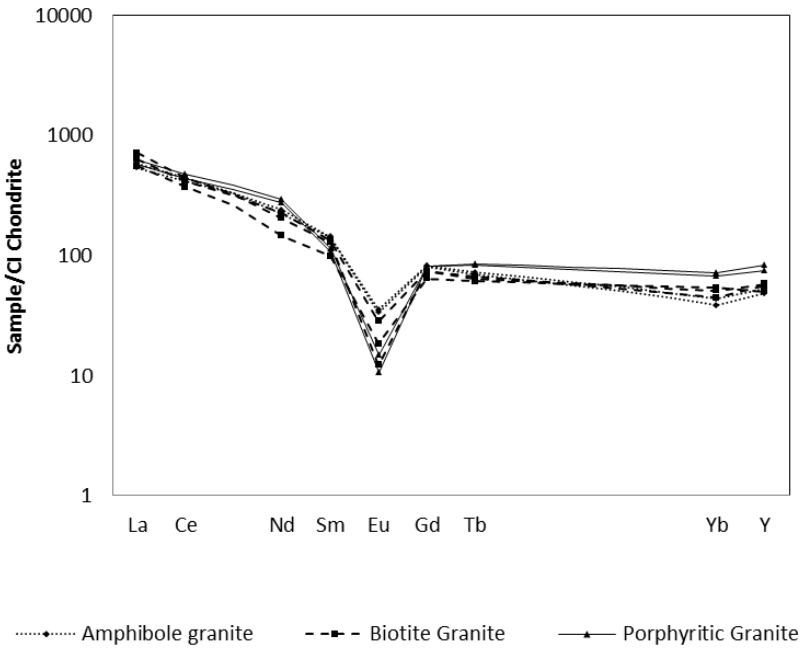


Figure 3.7. Chondrite-normalised REE chart showing patterns of the different rock types in the SDG (amphibole granite, biotite granite and porphyritic granite). Data from Bilal et al. (1997).

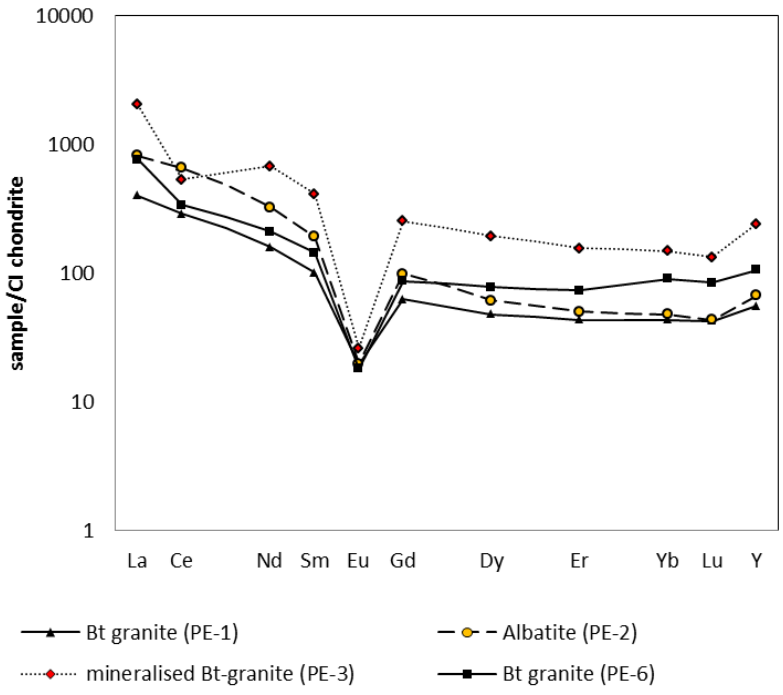


Figure 3.8. Chondrite-normalised REE chart showing patterns for biotite granite and albitite samples from the SDG. Data from Marini et al. (1992).

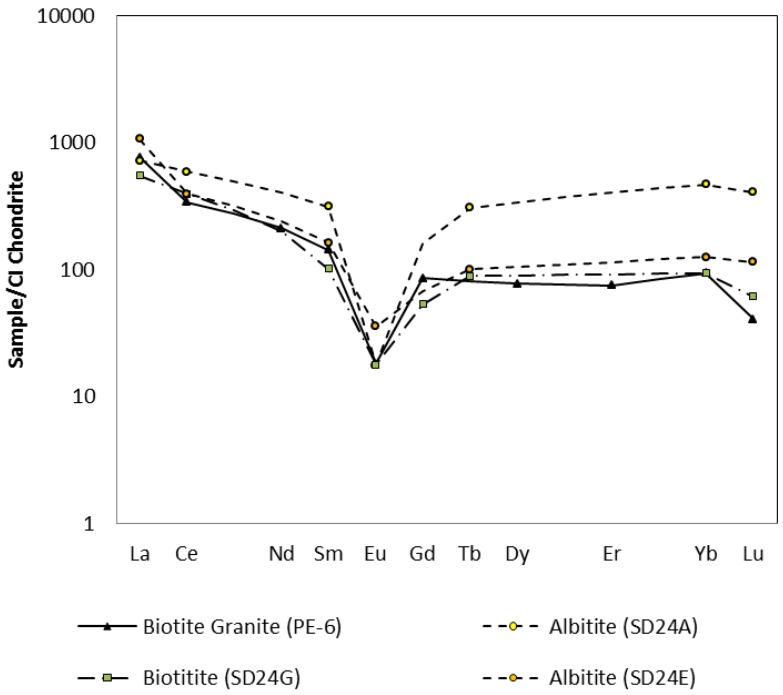


Figure 3.9. Chondrite-normalised REE chart showing patterns of biotite granite, albitite and biotitite samples from SDG. Data from Teixeira & Botelho (2006).

3.3.4 REE minerals

Monazite, xenotime and allanite have been identified as the primary REE minerals in the SDG (Macambira 1983, Teixeira & Botelho 2006, Santana 2013). Monazite and xenotime are reported to occur as colourless anhedral to subhedral crystals that range between 10-100 microns in rock samples but grains up to 1.5 mm have been found as residual grains in streams (Santana 2013). Monazite and xenotime are found as inclusions in quartz and feldspars or associated with zircon, thorite and biotite (Teixeira & Botelho 2006). Allanite is present as euhedral to anhedral grains up to 2 mm in size. Based on estimates of the abundances of individual rare earth minerals, Teixeira & Botelho (2006) argue that allanite is the principal LREE carrier in the granite.

Secondary rare earth minerals such as bastnäsite and fluorite have also been identified from more detailed mineralogical studies using XRF and SEM-EDS (Teixeira & Botelho 2006, Santana 2013). SEM images of biotite granite sections show that bastnäsite occurs as acicular to massive crystals overgrowing and replacing allanite (Figure 3.10). These secondary REE minerals are thought to have been produced by hydrothermal fluids interacting with the granite (Bilal et al. 1997).

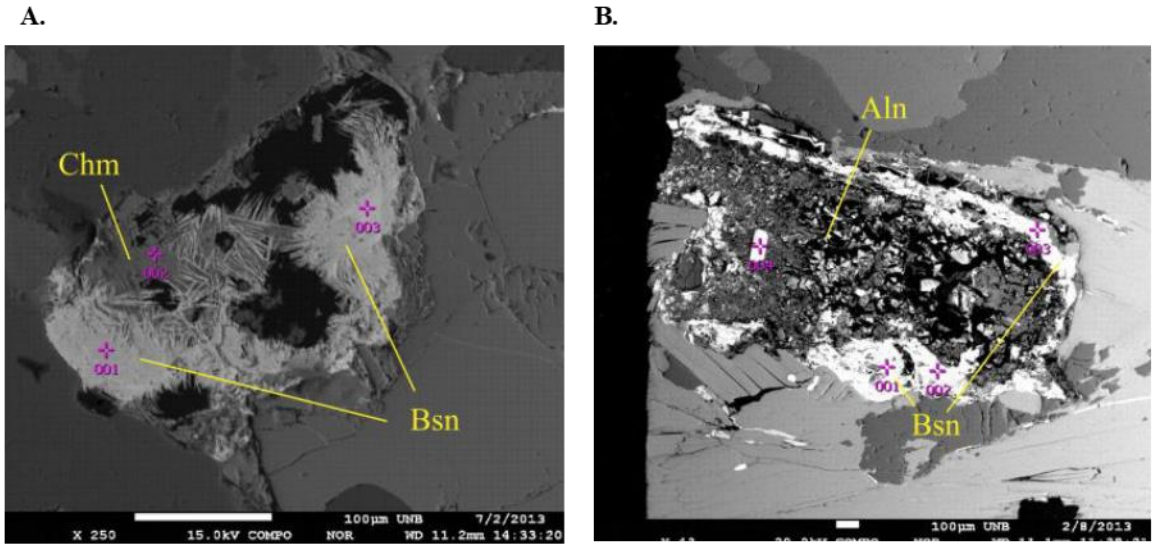


Figure 3.10. SEM-BSE mages from Santana 2013, showing bastnäsite and chamosite replacing allanite.

Table 3.2. Chemical composition of the main REE host minerals identified in SDG.

Mineral	Chemical composition
Monazite	$(Ce,La)PO_4$
Xenotime	$(Y)PO_4$
Allanite	$(Ce,Ca,Y,La)_2(Al,Fe^{III})_3(SiO_4)_3(OH)$
Zircon	$ZrSiO_4$
Bastnaesite	$(Ce,La,Y)CO_3F$

Variations in the geochemistry of unaltered biotite granite, albitised biotite granite and greisen have led Teixeira & Botelho (2002) to propose that some of the monazites present in altered rocks are secondary. Monazite crystals from altered rocks were found to contain lower REE and Th but have higher Ca concentrations compared to monazite crystals in unaltered rock samples. Teixeira et al. (2002) explain that secondary monazite can form by the destruction of apatite and allanite, and precipitation of phosphate and REE by hydrothermal fluids.

The normalised pattern of REE in the individual accessory minerals analysed by Teixeira & Botelho (2006) shows that allanite and monazite are the main LREE carries while xenotime is the main carrier for the HREE. Bastnäsite is enriched in LREE but also carries middle REE and some HREE. Zircon, the most abundant accessory phase, is found to be depleted in REE. Teixeira & Botelho (2006) found that, apart from a small fraction of zircon grains enriched in Y and HREE, zircon has little influence on the REE content of the granite.

3.4 Exploration and Mining History

Interest in the mineral resources of northern Goiás region began in the late 1950's when roads from the new capital of Brasilia were being constructed. Artisanal miners ('garimperios') were the first to arrive and explore the area, and soon discovered cassiterite, columbite, tantalite, wolframite, mica, beryl and emeralds in the SDG (Hains 2013). The garimperios extracted alluvial and colluvial cassiterite, and followed mineralised pegmatite veins that outcropped at the surface. Several of the pits and trenches that were dug can still be found today around the southern portion of the granite and the Mata Azul prospect in the northern part of the granite.

A systematic geological mapping program by the National Department of Mineral Production (DNPM) in the late 1960's identified SDG as potential host of Sn, Nb, Ta, and W mineralisation (Hains 2013). This led to more focused exploration and the development of an underground tin mine called Pela Ema by Goiás Estanho S.A. that operated throughout the 1980's, extracting disseminated Sn in greisen skarns and albitised granite endogreisen. Unfortunately for the company, the discovery of tin placer deposits in Rodinia lowered the market prices, and made the Pela Ema mine uneconomical forcing its closure at the end of 1980's and bringing tin mining to an end at Serra Dourada. Serra Verde Mining LLC is the first company to resume exploration and resource evaluation work in the SDG.

3.5 Summary

The Serra Dourada granitic complex (SDG) is a Proterozoic intrusive body located in northern Goiás in Central Brazil that has historically been mined for tin and is now the focus for REE exploration by Serra Verde Mining LLC. Geographically located within the Goiás Tin Province, the SDG belongs to the Rio Tocantins Sub-Province (RTS) which is characterised by larger and elongated granites.

The SDG is one of a cluster of granites that intruded into Archaean-Paleoproterozoic basement after the Trans-Amazonian orogeny in a post-orogenic extensional setting. The granites were subsequently deformed and recrystallized during orogenic events in the Meso- and Neoproterozoic, namely the Brasiliano-Pan African orogeny, which left the strongest overprint shown by the K-Ar biotite ages. Throughout the Phanerozoic, the Tocantins region has remained relatively stable.

Geochemical correlation between volcanic layers from rift sequences age these Proterozoic granites between 1.77 and 1.50 Ga. A precise and reliable age of SDG is not available because

Rb – Sr isotopes used in previous studies experienced re-setting during later metamorphic events and intrusive relationship of the granite and the surrounding Serra da Mesa meta-sediments remains controversial. The age of the neighbouring granite, Serra da Mesa, has been commonly used to define the age of the SDG and other granites in the RTS subgroup.

The SDG is composed primarily of biotite granite, and more minor occurrences of amphibolite and porphyritic granite lithologies. These rock types are cut by late-stage pegmatites and overprinted by albitisation from associated fluorine-rich fluids. The tin that was historically mined from SDG came primarily from albitised lenses.

The SDG is an evolved granite, enriched in HFSE. It has been classified as meta- to peraluminous and an A-type granite with continental crust contribution (Eby 1992).

The SDG is enriched in REE with concentrations of 500 – 900 ppm and over 100 times enriched with respect to the chondritic value. Values of up to 1400 ppm have been reported for the biotite granite but it remains unclear whether these samples are representative of a local anomaly or a larger enriched zone within the biotite granite. The chondrite-normalised REE patterns show that the SDG is LREE enriched with a moderate LREE/HREE fractionation, and a strongly negative Eu anomaly. The albitised rocks also have high REE concentrations, although the role of hydrothermal alteration in the enrichment and distribution of REEs remains unclear.

REE-bearing minerals that have already been identified in the SDG include monazite, xenotime, allanite and bastnäsite. Bastnäsite has also been found replacing allanite. Individual analyses of these minerals have revealed that monazite and allanite are the main LREE hosts and xenotime and bastnäsite the main HREE carriers. Zircon, the most abundant accessory mineral, carries no REEs.

This review illustrates the lack of work undertaken to date that investigates the weathered profile that has developed over the SDG. The REE carrier minerals identified by previous studies can be traced into the minerals that make up the weathered profile of the IAD. Altered minerals such as bastnäsite should be identified in the bedrock because these alteration products may be more susceptible to weathering. Examining the relative REE enrichments above hydrothermally altered and unaltered bedrock may reveal important controls on the grades of IADs.

Chapter 4

Analytical Methods

4.1 Introduction

The Serra Verde IAD REE deposit was studied through a combination of geological profile mapping in the deposit area, detailed logging of diamond drill core, and detailed geochemical, petrographic, and mineral analysis on collected samples in the laboratory facilities of the Natural History Museum, London.

The main analytical techniques used in this study include inductively coupled plasma spectrometry (ICP-MS) and inductively couple plasma atomic emission spectroscopy (ICP-AES) geochemical analysis, scanning electron microscope imaging, electron probe micro analysis and X-ray diffraction analysis. In addition, ion-exchange leaching experiments on a selected subset of samples was conducted in the chemistry laboratory of the IAC. Details of the samples collection, preparation, and the methodology are described in this chapter for each of the analytical techniques. The ion-exchange experiments are described in Chapter 8.

4.2 Sample Collection

The samples used in this study include field samples and diamond drill core samples from Serra Verde Mining plc exploration drilling campaign. The field samples were mainly taken from sections of weathered profile that are exposed along road cuts.

Drill core samples include visually unweathered granite samples, and samples of each of the different horizons in the weathered profile. Samples collected represent 10 cm long sections of quarter HQ drill core. A higher density of samples was collected from the saprolite section because it represents the ore zone of the REE deposit. The drill core has dried since it was collected. Efforts were made to sample the most cohesive core sections, where the texture and fabric of the drill core were preserved. Samples used to study the weathered profile are from the central plateau, which represents the centre of the deposit and is where the weathered profile can still be found fully preserved. Most of the samples used to study the granite are also from the plateau area, but a few additional samples from fringe of the southern half of the granite were also examined.

4.3 Whole Rock Geochemistry

A total of 68 samples were analysed for geochemistry. The samples include 35 granite samples, 14 weathered granite samples (mainly saprolite samples), 8 clay veinlet material samples, and 11 clay size fraction separates (CFS). All samples were prepared in the preparation laboratory at the NHM and then submitted for geochemical analysis at a certified laboratory.

Geochemical analysis of the samples was carried out by the IAC laboratory at the Natural History Museum in London, and by ALS Minerals in Ireland; an external commercial laboratory. All samples were initially going to be analysed at the NHM but due to high turn around time, it was decided to send the remaining samples to a commercial laboratory. ALS minerals is a certified geochemical laboratory (the quality assurance certificate can be found at http://alsglobal.com/en/our-services/minerals/Geochemistry/Downloads). Table 4. 1 shows which samples were sent to each laboratory. The analytical methods were kept consistent between laboratories so that all of the results obtained are comparable.

Table 4. 1 List of samples and sample types sent to ALS and NHM for geochemical analysis.

Laboratory	Batch #	Sample #	Sample Type			
			Granite	Weathered granite	Fracture infill	CSF
IAC, NHM UK	1	3	3			
	2	10		10		
ALS, Ireland	1	25		25		
	2	30	5		14	11

The concentrations of different groups of elements in the samples were assayed by different methods. The sample preparation and analytical methods used for the different groups of elements are described in this section. A summary of elements analysed, and analytical methods used by each laboratory, are presented in Figure 4.1 and Figure 4.2.

4.3.1 Sample Preparation

Bulk samples were dried, crushed, and milled in the sample preparation laboratories of the Natural History Museum (NHM), London. Samples were air-dried for 10 days, crushed to < 2 mm using a jaw crusher and then milled to < 75 μm using a planetary ball grinder mill.

The clay size fraction (CSF), < 2 μm material, was separated from the bulk weathered granite samples by wet-sieving and centrifugation. Weathered granite samples were first sieved down to < 53 microns using D.I. water. The < 53 μm slurry was then centrifuged in a two-step process to obtain the clay fraction. First, centrifuged for 4 minutes at 1000 rpm to separate the coarsest fraction by decanting into a new container, and secondly centrifuged a second time for 20 minutes at 4000 rpm to concentrate the fine fraction. The process was repeated several times until ~0.5g of CSF material had been recovered. No dispersants or deflocculants were used, because the chemical composition of the clay minerals is vulnerable to modification by these chemicals.

4.3.2 Analytical methods

4.3.2.2 Major elements

Major elements (SiO_2, Al_2O_3, Fe_2O_3, CaO, MgO, Na_2O, K_2O, Cr_2O_3, TiO_2, MnO, P_2O_5, SrO, BaO) were analysed using the same ICP-AES method at ALS and IAC laboratories. The method involves adding 0.2 g of sample pulp material to a lithium metaborate flux (0.9 g), fusing the mixture in a furnace at 1000 $^{\circ}C$ and subsequently dissolving the resulting glass bead in 100 mL of nitric acid (4 % NHO_3), and hydrochloric acid (2 % HCl_3). The resulting solution was then analysed by inductively coupled plasma-mass spectrometry (ICP-AES) and corrected for spectral inter-element interferences. Oxide concentrations were calculated from the determined elemental concentrations. The reference code for major element analysis by this method at ALS Minerals is ME-ICP06.

4.3.2.3 Trace elements

Trace elements (Ba, Ce, Cr, Cs, Dy, Er, Eu, Ga, Gd, Hf, Ho, La, Lu, Nb, Nd, Pr, Rb, Sm, Sn, Sr, Ta, Tb, Th, Tm, U, V, W, Y, Yb, Zr) of samples sent to ALS were analysed using method ME-MS81. The method involves the same fusion and dissolution techniques described for major elements analysis, but the final solutions are analysed by inductively coupled plasma-mass spectrometry (ICP-MS). The same method was applied to samples submitted to IAC laboratory in NHM. However, the list of trace elements analysed differs: Cs, Ga Sn V and W

were not analysed for clay veinlet samples or granite samples. For these samples only REE elements, Pb, Th and U trace elements were analysed.

4.3.2.3 Base elements

The granite and weathered granite samples sent to ALS were also analysed for base metals using method ME-4ACD81. Samples were fused with lithium metaborate, dissolved by four acid digestion and ICP-AES analysis. The four-acid digest was applied to ensure sulphides and oxides in the sample were fully dissolved. The base metals analysed include Ag, Cd, Co, Cu, Mo, Ni, Pb, and Zn.

4.3.2.4 Fluorine content

The fluorine content of granite sample and weathered granite samples was measured by K-OH fusion and ion-chromatography (F-IC881 method code) at ALS laboratories in Vancouver, Canada. Fluorine analysis was requested because of the abundance of fluorite and other fluorine containing minerals observed in the samples.

4.3.2.5 Volatile content

The volatile content of samples sent to ALS was determined by a loss on ignition test. The test involves heating 1 g of sample material in an oven at 1000 $^{\circ}$C for one hour, cooling and weighing. The difference in weight before and after heating is used to estimate the percentage of volatile content in the sample.

The volatile content of samples sent to IAC lab in NHM were determined by CHN elemental analysis using an vario EL cube. CHN elemental analysis involves sample combustion at 1800 $^{\circ}$C and analysis of individual combustion products (H, C, N and S) in the emitted gases using separate infra-red and thermal conductive cell detectors. The H and C values are given in wt % and have been converted to H_2O (wt %) and CO_2 (wt %values).

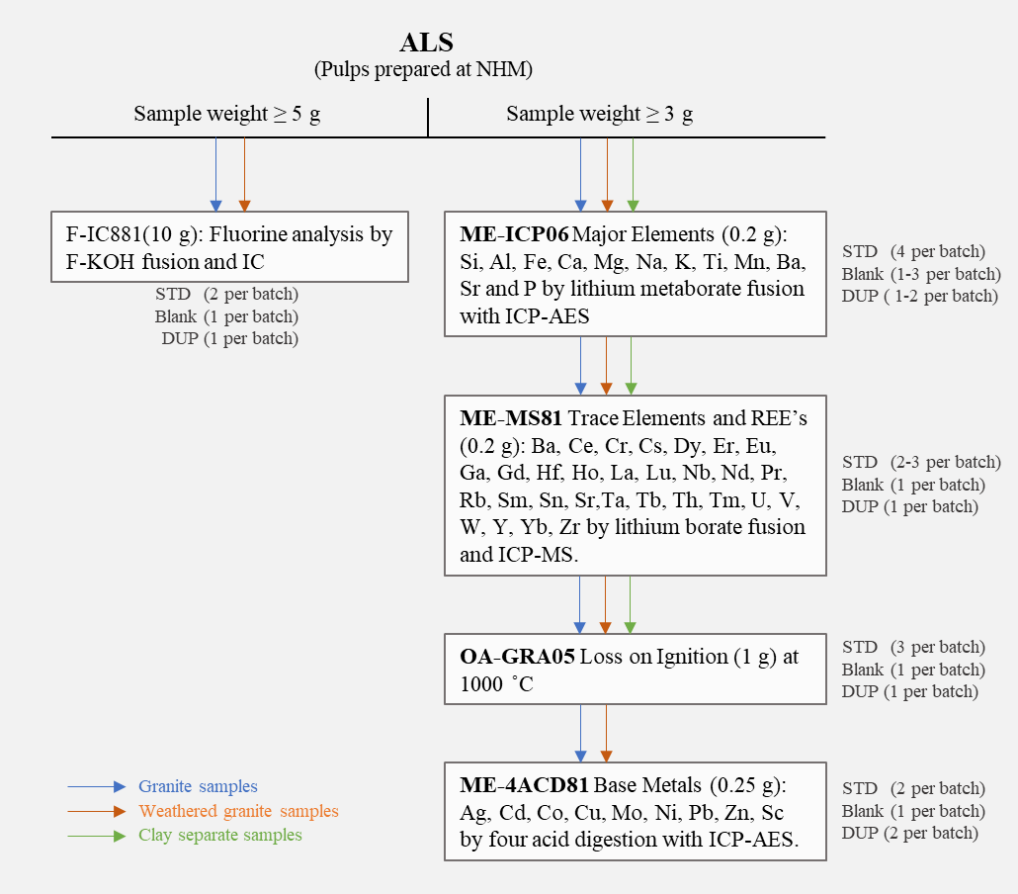


Figure 4.1. Work flow sheet showing steps followed by ALS during whole rock geochemistry

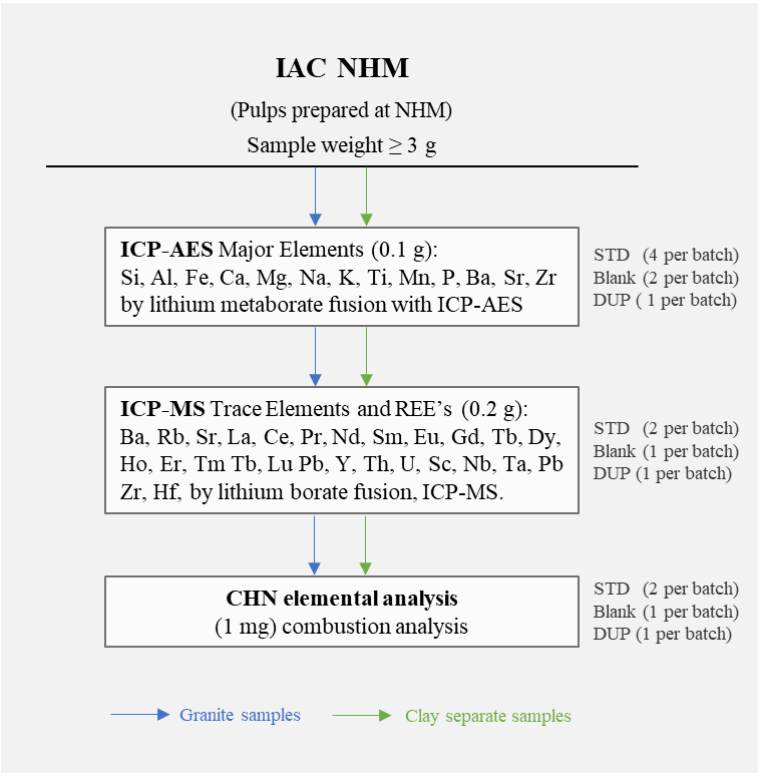


Figure 4.2. Work flow sheet showing steps followed by NHS during whole rock geochemistry

4.3.3 Quality Control (accuracy and precision)

The accuracy and precision of the chemical analysis results for each method was assesssed using the results of the standard materials. The accuracy of the data obtained from each method was determined by calculating the percentage mean bias from the reference values of the standard using the following formula:

$$Mean\ Bias\ (\%) = \frac{100}{n}\sum \frac{\left(X^i_{measured} - X^i_{reference}\right)}{X^i_{reference}}$$

where $X^i_{measured}$ is the concentration of element *i* measured in the standard, $X^i_{reference}$ is the known concentration of element *i* in the standard, and *n* is the number of analyses. Mean bias is a useful statistical tool to determine whether the mean of a given population of analytical measurments is an under- or over-estimate of the true value.

The precision of analytical measurements was calculated using relative standard deviation (RSD) of standard analyses, expressed as:

$$RSD(\%) = \left[\frac{\sigma}{\bar{X}^i_{measured}}\right] \times 100$$

where $\bar{X}^i_{measured}$ and σ are the mean concentration of element *i* and the standard deviation, respectively. RSD is widely used in analytical chemistry for reporting the precision and repeatability of a measurement. It also has the advantage of allowing direct comparison between elements of different concentrations.

4.3.3.1 ALS Laboratory

For each batch of samples of approximately 30 samples, 2 to 4 standards, 1 to 2 duplicates of selected samples, and one blank sample were analysed. Specific numbers for each method are presented in Appendix B1.

For each analytical method several certified standard materials were used. They include: OREAS-121, SY-4, GRE-3 and AMIS0304 for major elements; AMIS0304, SY-4 and GRE-3 for trace element analysis; SARM-1, SARM-3 and CCU-1d for fluorine analysis; and GBAP-3, OREAS-90 and OREAS-93 reference materials for LOI. The reference values and analysed values of these standards can be found in Appendix B1.

The major elements have mean percentage bias values within ± 10 % of reference values (Figure 4.4). The only element that falls outside the control limits is Cr_2O_3 which shows +41

% bias. The large bias is due to Cr_2O_3 concentrations being at or below the detection limit in all standards analysed for major element analysis (Appendix B1).

The majority of the trace elements have mean bias values and error bars within ± 10 %. With the exception of Sn, Nb, Cr, Ta, V, and W, all other trace elements have mean bias values within ± 5 %. V and W are the only two elements which fall outside the control limits with bias values of +12.5 % and -28.9 % respectively. The mean percentage bias for Cr falls within ±10 % but the error on this value is large. Again, the concentration in most of the standards analsed for trace elements have Cr concentrations close to the detection limit. The low accuracy of results for Cr, V and W leads to the recommendation that the assays of these three elements will not be considered further.

All base metals, except Sc, have a mean percentage bias falling within ± 10 %. The bias value of Sc is -12 % and therefore will not be evaluated or discussed further. Finally, the LOI and F analysis have bias values within ± 10 %. Fluorine and LOI contents measured in the reference standards in this study were consistent with reported values.

The RSD values for major elements show that there is little variation between samples. RSD values calculated from standard SY-4 and GR 3, both of which were analysed four times in method ME-ICP06, are < 5 % for nearly all elements. BaO, Cr_2O_3 and SrO have RSD values between 5 and 10 %. The RSD value for LOI, using OREAS-90 results is 2.72 %.

For trace elements and base metals, insufficient repeats of the sample standard were carried out to make a quantitative accuracy assessment. Comparison of the standards that were analysed multiple times, and the assays from the main original and duplicates for trace elements, show that the majority of assays fall within ± 5 wt %, when concentrations in the samples are sufficiently above detection limits (Figure 4.3 Appendix B1). The only trace elements that show poor reproducibility are W, Cr and V. These elements will not be discussed in the results chapters.

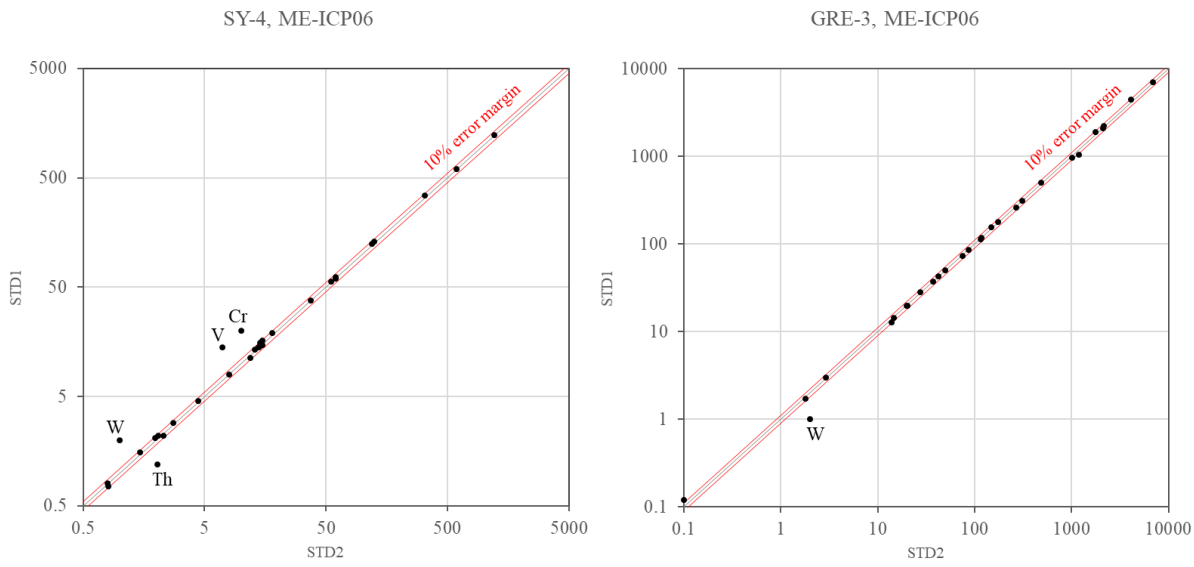


Figure 4.3. Reproducibility charts for two standards (left SY-4, and right GRE-3) analysed by the ME-ICP06 method at ALS. A 10% error margin on analysed values is indicated by the red lines. All assays and scales are in ppm. Outlier elements have been labelled.

The duplicates results show that samples are well homogenised. All major elements and trace elements analysed with the exception of P_2O_5, Zr, and Hf have differences of < 10 wt %. Fluorine, LOI, and base metal results that are present above detection limit also have differences of < 10 wt %.

Zr and Hf show a difference of 15 % and 13 % between the main and duplicate granite samples but a difference of < 5 % in the CSF main and duplicate samples. The larger difference in granite samples is likely due to zircon crystals which are relatively coarse and mostly absent in the CSF. Zircon are the hard minerals that can resist breakdown during milling, and as a result may be variably distributed in pulp rock. Therefore, an error margin of ±15 % will be considered when analysing the Zr and Hf results from these assays in this study.

The difference in phosphate concentrations between main and duplicate samples ranges between 0 and 66 %, with the largest values found in samples with the lowest phosphate concentrations. Overall, the phosphate concentrations are low in the samples analysed in this study, and many are close to, or at, the detection limit of the analytical method (0.01 wt %). Comparison of phosphate concentrations between samples with concentrations below 0.1 wt % will be avoided.

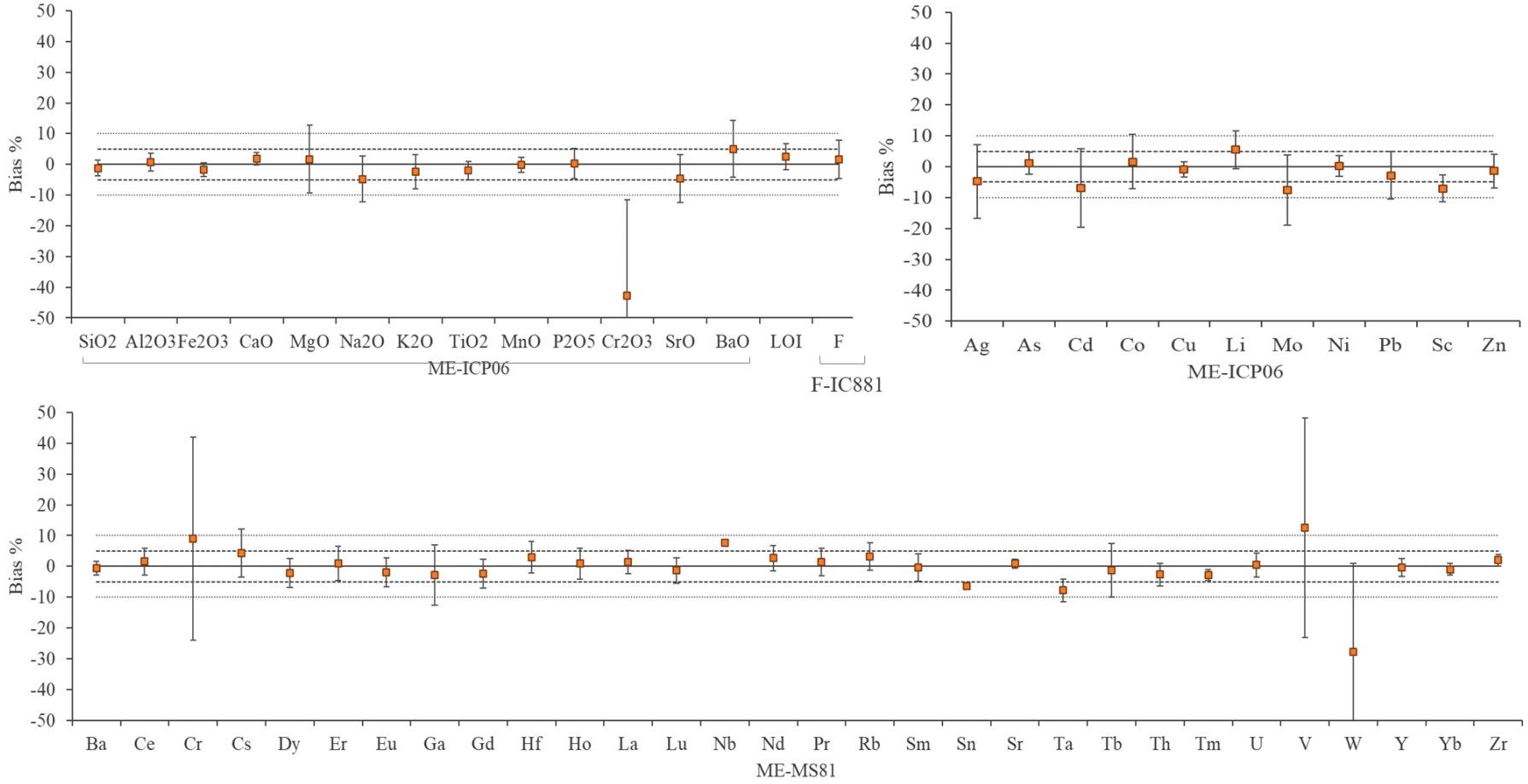


Figure 4.4. Mean bias charts for each of the elements, plotted on separate graphs for each of the analytical methods used by ALS. Note the outlier samples with large error bars.

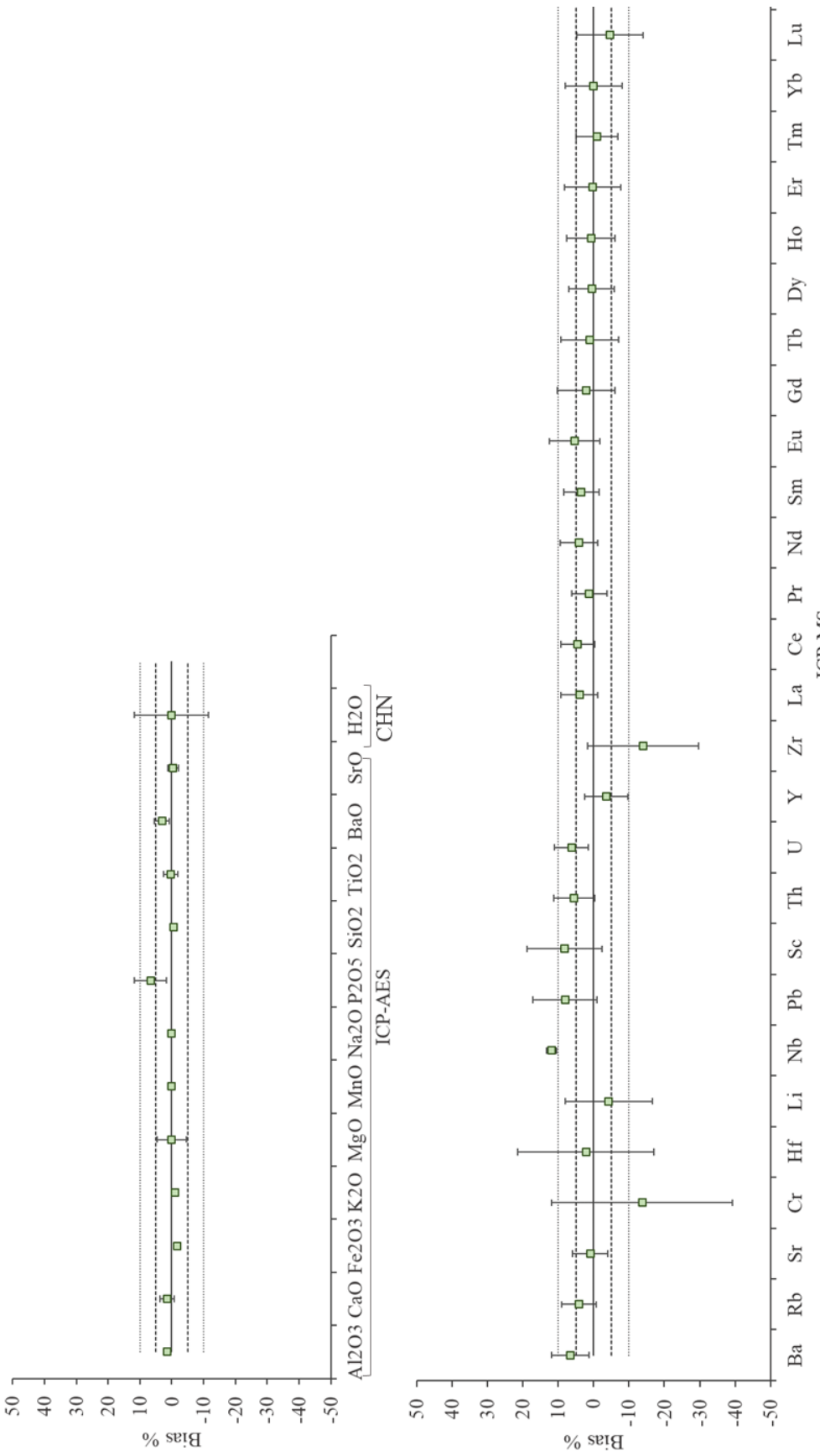


Figure 4.5. Mean bias charts for each of the elements, plotted on separate graphs for each of the analytical methods used by NHM. Note the outlier samples with large error bars.

4.3.3.2 NHM laboratory

The standards used for checking the accuracy and precision of geochemical analysis include: G-2, NIM-G, STM-1, GSP-2, SY-4 and W-1 for major elements, BCR-2, JLK-1, SCo-1 for trace elements, and SY-3, and GA for CNH analysis.

The mean percent bias of all major elements, except P_2O_5, fall within ± 5 %; P_2O_5 has values falling within ±10 % (Figure 4.5). All trace elements analysed, excluding Zr, Hf, Nb, Pb, and Sc have mean bias percentages < ± 10 % (figure X). Zr and Hf appear to be underestimated with mean percent bias values of - 14 %, and Nb, Pb, and Sc values are generally overestimated with mean percent values of + 11 %. SY-3 and GA standards used for CNH analysis have mean percent bias of < ±5 %, but display large errors (Figure X). Due to the low volume of samples, no repeat analyses of NHM laboratory standards were carried out to calculate a repeatability.

4.3.4 SV Assay samples/ company data

Drill core assay data from Serra Verde Mining was also used in this study. The drill core was assayed by ALS, Belo Horizonte, Minais Gerais using the following analytical packages:

ME-XRF26 - major elements analysis by lithium metaborate fusion and XRF

ME-MS81 - trace elements and REE analysis by lithium metaborate fusion with ICP finish.

OA-GRA05 - volatile content by loss on ignition at 1000 °C.

For every 40 samples analysed, two standards, one blank sample and one duplicate sample were analysed. The standards inserted include OREAS-146and AMIS-0185 both of which are certified reference materials. Details of QA/QC can be found in Technical report NI-43-101 from 15th October 2013.

4.4 Scanning electron microscopy

Scanning electron microscopy (SEM) was carried out on selected samples for mineral identification, for acquisition of backscatter electron (BSE) images and for acquisition of element distribution maps. All SEM work was carried out on the Zeiss EVO 15LS SEM and the FEI Quanta 650 SEM in the Imaging and Analysis Centre at the Natural History Museum.

4.4.1 Sample preparation

Saprolite fragments were mounted in 30 mm resin blocks and polished. CSF were prepared into solid clay discs using a manually-operated hydraulic pellet press. The press produced discs of 6 mm radius and ~1 mm thickness, with 0.3 g of sample material per disc. Each solid CSF disc was mounted onto a glass slide using double-sided conductive tape and conductive silver paint was applied at the side to prevent the surface from charging. Samples from fracture infill were mounted as powder onto metal stubs using double sided carbon tape. Both CSF discs and polished resin blocks were carbon coated before loading into the SEM chamber. All samples except those mounted onto stubs were carbon coated.

4.4.2 Sample analysis

SEM micro-analysis was carried out in the IAC research labs at the Natural History Museum, London with two SEM instruments. The Zeiss EVO 15LS SEM was used for imaging and compositional analyses of minerals in carbon-coated polished blocks, and pressed CSF discs. BSE images and EDS analyses were obtained with 20 kV acceleration voltage and 3 ± 0.3 nA beam current. The FEI-Quanta 650 FEG SEM was used for high-resolution backscattered (BSE) imaging and hyperspectral X-ray mapping of fine-grained minerals. Carbon-coated samples were analysed under high vacuum conditions at 12 kV. Samples mounted on stubs were analysed under low pressure conditions at 9 kV.

4.5 Electron probe microanalysis

Microscale quantitative element analysis of the REE bearing minerals present in the samples studied was performed by electron microprobe analysis (EMPA). Analyses were carried out in the Imaging and Analysis Centre at the Natural History Museum using a Cameca SX-100 electron microprobe equipped with a wavelength dispersive system. EMPA is a non-destructive method that uses a high-energy focused beam of electrons to generate X-rays characteristic of the elements within the sample. The adjustable spot size down to 1 micron, and the high accuracy beam positioning with the use of an optical microscope allows very small grains in the order of 10's of microns diameter to be analysed. The Electron microprobe can quantitatively analyse elements from B to U at resolutions and detection limits as low as 100 parts per million.

A laser ablation ICP-MS technique was also considered because it offers lower detection limits than EMP. However, the small size of the target grains precluded its application to collect elemental analyses for discrete REE mineral grains at sufficient spatial resolution in this study.

4.5.1 Sample preparation

EMPA measures the counts of characteristic X-rays of specific wavelengths that relate to the chemical composition of the sample, released under excitation by an applied electron beam, focused onto a flat surface of the sample material. The samples under analysis must therefore first be polished to minimise surface relief, and carbon coated to ensure that the charge from the electron beam can be adequately dissipated while ensuring maximum beam energy incident onto the sample surface. Sample types analysed under the EMP include carbon coated polished blocks, carbon coated thin sections, and carbon coated pressed clay discs.

4.5.2 Sample analysis

4.5.2.1 Running conditions

The Cameca SX-5 EMP is equipped with four multi-crystal wavelength-dispersive spectrometers and was operated with a configuration involving one TAP, one LLIF, one PET, and one LPET diffracting crystal. The elements detected by each crystal are presented in Table 4.2.

Operating conditions included an accelerating potential of 20 kV, a beam current of 20 nA (measured on the Faraday cup), and a beam diameter ranging between 1 and 10 microns depending on the mineral grain size. Only individual grains, or clusters of grains of the same composition with sizes greater than 5 times the diameter of the spot size were analysed to ensure accurate mineral results. These analytical conditions were maintained throughout and between analytical sessions.

The peak count times and background count times for each element analysed are presented in Table 4.2. The peak counting time ranged between 20 and 60 s and background counting time was made equal to half the peak count time.

The peak and background positions with minimum interference and leach correction were used to measure element concentrations. The peak and background position for each element are presented in Table 4.2.

Due to the large number of elements analysed, and the numerous wavelengths of x-rays released by some the elements, in particular the REE, there are few sections along the X-ray spectrum that are 'peak-free' to facilitate background measurement. WDS spectral scans were carried out on all of the laboratory standards to identify the best background peak positions with minimum interference (Figure 4.6).

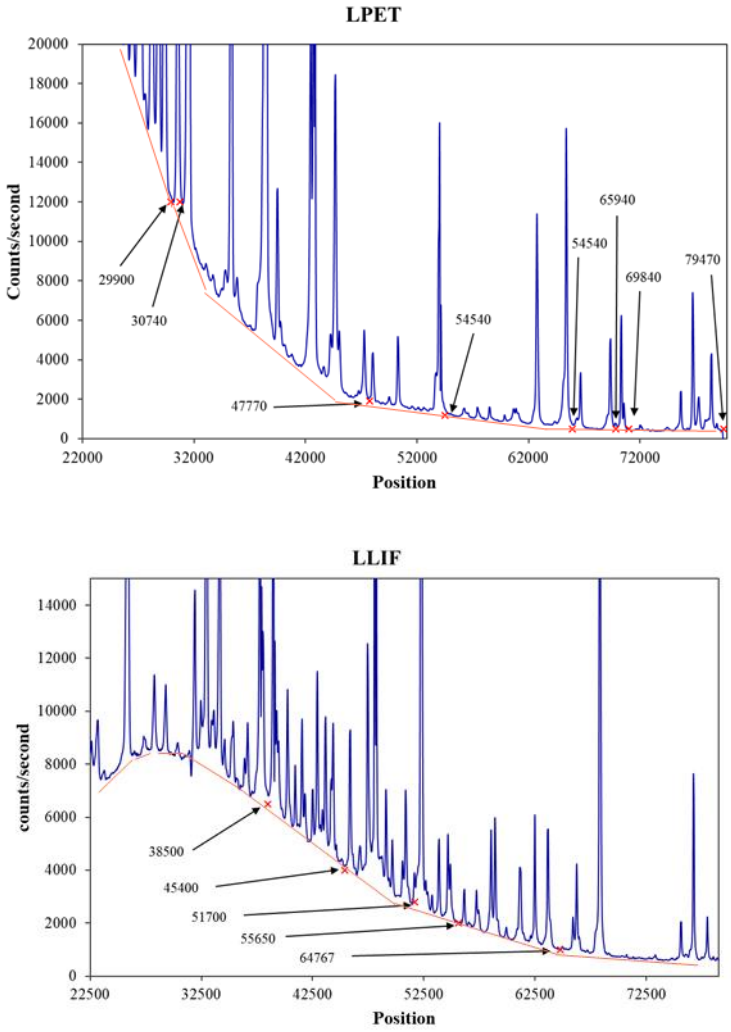


Figure 4.6. Sum of the WDS spectral scans for each standard, showing the peak positions of elements detected by the LLIF (lower) and LPET (top) crystals. The peak-free sections identified and used for background measurement are marked by red crosses.

4.5.2.2 Calibration

Primary standards used to calibrate the instrument include synthetic REE glass standards, natural minerals, synthetic oxides, and pure metal (Table 4.2). Accuracy of the calibration was checked using a secondary standard. A natural monazite standard was run as an unknown and the results compared with expected values which were determined by ICP-MS analysis.

Table 4.2. Summary of elements, analysing crystal, count times, background position and primary standards used in EMP analysis.

Element	Line	Analysing crystal	Peak count time (s)	Background time (s)	Peak positions	Background position 1	Background position 2	Estimated Slope	Primary Standard
K	Kα	PET	20	20	42766	43366		1.1	KBr
Ca	Kα	PET	20	20	38388	38988		1.1	Wolastonite
Ti	Kα	PET	20	20	31419	31919		1.1	SrTiO3
Ba	Laα	PET	20	20	31728	32328		1.1	Baryte
F	Kα	LPC0	60	60	41020	41370	40670		Topaz
P	Kα	LPET	20	20	70370	70970		1.1	Monazite
La	Laα	LPET	30	30	30474	30739	29779		LA-Glass
Ce	Laα	LPET	30	30	29302	29902		1.1	CE-Glass
Cl	Kα	LPET	20	20	54040	54540		1.1	NaCl
Sr	Laα	LPET	20	20	78477	79477		1.1	SrTiO3
Nb	Laα	LPET	30	30	65438	65938		1.1	PNb
Th	Mα	LPET	30	30	47274	47774		1.1	Monazite
U	Mβ	LPET	20	20	42458	500		1.1	Uranium Oxide
Zr	Laα	LPET	30	30	69343	69843		1.1	Zircon
Pb	Mα	LPET	20	20	60364		59564	1.1	Vanadanite
Na	Kα	TAP	10	10	46353	47153	45553		Jadeite
Mg	Kα	TAP	20	20	38487	39587	37387		Forsterite
Al	Kα	TAP	20	20	32457	33257		1.2	Corundum
Si	Kα	TAP	20	20	27736	28486		1.2	Fayerlite
Y	Laα	TAP	60	60	25108	25608		1.2	Y-Glass
Mn	Kα	LLIF	20	20	52204	45406	55656		MnTiO3
Fe	Kα	LLIF	20	20	48082	64767		1.1	Fayerlite
Pr	Lβ	LLIF	60	60	56116	64767	55667		PR-Glass
Nd	Laα	LLIF	30	30	58882	64762	45412		ND-Glass
Sm	Laα	LLIF	30	30	54639	51702	45403		SM-Glass
Gd	Lβ	LLIF	60	60	45869	51702	45403		GD-Glass
Hf	Laα	LLIF	30	30	38975	39475		1.1	PHF
Ta	Laα	LLIF	20	20	37789	38289	37289		PTA
Tb	Laα	LLIF	30	30	49077	51700	45400		TB-Glass
Dy	Lβ	LLIF	30	30	42481	45403	38503		DY-Glass
Ho	Lβ	LLIF	30	30	40908	45400	38500		HO-Glass
Er	Lβ	LLIF	30	30	39413	45400	38500		ER-Glass
Tm	Laα	LLIF	30	30	42885	45405	38505		TM-Glass
Yb	Laα	LLIF	30	30	41522	38506	45406		YB-Glass
Lu	Laα	LLIF	20	20	40213	45388	38488		LU-Glass

4.5.2.3 Background and Peak Overlap Corrections

X-ray spectrometry involves measurement of characteristic X-ray peak intensities corrected for background. The background level is obtained by interpolating background intensities measured on either side of the peak of interest. Measurement of the peak and background X-ray intensities must therefore be free of peak overlaps.

Peak overlap occurs when the peak of more than one element coincide, while background overlap occurs when the tail or peak of another element falls on the position selected for background measurement (Figure 4.6). Contributions from these overlaps must be corrected in order to obtain true spectral intensities.

Although peak and background positions were carefully selected to minimise peak interferences, the large number of elements, and the numerous energy lines of REE mean that some interference is unavoidable.

Peak interferences between the elements analysed were identified by analysing the full suite of calibration standards with the EMP as unknowns. The differences between the raw values and the expected composition were used to identify the peak interferences. The positive, and negative values for elements that are absent in the standard material were respectively identified as peak and background overlaps (Appendix C1).

The results from the standards were used to calculate empirical correction factors. The correction factors were validated by applying them to raw standard data. A list of these correction factors can be found in Appendix C1.

The empirical correction factors were applied to all mineral data sets. Corrections were applied in two stages. Cameca software was employed to correct the largest peak overlaps (e.g. CeLα on SmLα, and BaLα on Ce) during data collection. The remaining interference corrections were applied afterwards during processing of the raw data.

4.5.2.4 Limits of detection and analytical error

The limit of detection (LOD) and the analytical error were calculated automatically by the Cameca software. The detection limit is taken as the concentration equivalent to three standard deviations (3σ) of the background counts. The error of each analysis is calculated as two standard deviations (2σ) of the number of counts in an analysis peak. The LODs and analytical errors for each element in each mineral are presented in (Appendix C1). For most REE bearing minerals, EMP detection limits are not low enough to analyse the full suite of REE; only the most abundant REE were accurately quantified.

4.6 X-Ray diffraction

Qualitative powder X-ray diffraction (XRD) analysis were performed on fine-grained weathered samples to determine their main mineral composition and identify the different clay mineral species present. XRD analysis was also conducted on the solid residues of all samples leached to identify any mineral alterations or the formation of new phases caused by reaction with the leach solution.

4.6.1 Sample preparation and analysis

Samples were hand ground into fine powders using an agate mortar and pestle, and prepared into randomly-oriented powder mounts on a sapphire substrate. The mounted powders were analysed with Cobalt Kα-1 X-ray radiation using an Enraf-Nonius Powder Diffraction Systems 120 with an INEL 120º curved position sensitive detector (PSD) at the X-ray diffraction laboratory at the Natural History Museum in London. XRD patterns were recorded from 4º to 120º 2θ for 1 hour. Horizontal and vertical slits were used to restrict the beam to a size of 0.14 by 5mm respectively. The measurements were made in reflection geometry with powder sample surface at an angle of 4º to the incident beam. Minerals were identified by comparing and matching energy peaks with reference mineral stick 2θ patterns from the mineral database ICDD (international centre for diffraction data). Small degrees of mismatch in peak position and intensity is considered acceptable experimental error for this technique.

Co radiation was selected over the more commonly used Cu radiation because it is more suited for samples containing Fe phases. Fe minerals, particularly if they are amorphous, cause fluorescence which results in a raised background level that dampens the peaks of other mineral phases in the XRD pattern. The fluorescence produced by Fe minerals is much lower in the Co target than in a Cu target.

4.6.2 Instrument calibration

Different instrument configurations can change the peak position. It is therefore important to calibrate the data collection by using a standard before running samples in order to ensure that peaks intensities are recorded in the correct, and consistent positions. For this study silver behenate (AgBeh) standards and silicon (Si) standards were used to calibrate small offsets. Siver behenate produces 13 evenly spaced peaks at low angle that are used for low angle peak calibration.

4.6.3 Swelling clay test

Ethylene glycol solvation was used to test for the presence of smectite minerals in samples that presented very low angle peaks. Randomly oriented samples mounted on sapphire substrate were solved in ethylene glycol in a glass chamber for 12 hours in an oven at 60°C. Glycolated samples were then run for an hour under the same X-ray conditions as the air-dried samples, with snap-shots taken every 15 minutes to check for any peak position shifts due to glycol evaporation. The low angle peaks of untreated and glycol solvated XRD patterns were compared to determine if smectite was present. Samples containing smectite should exhibit a

change in the low angle basal diffraction peak position from 14-15 Å to 17 Å. The incorporation of ethylene glycol molecules into the double sheet interlayer of smectites causes them to swell, which in turn results in an increase of the d-spacing in the basal diffraction peaks (Figure 4.7). Non-swelling clays do not exhibit lattice expansion after being treated with ethylene glycol and should therefore have no appreciable effect on the basal peak position.

In XRD patterns collected from randomly oriented samples reflections are produced which can be used to help the identification of clay minerals (Moore & Reynols 1997). Diagnostic reflections at high angles were therefore used to help distinguish between different smectite mineral species, dioctahedral vs trioctahedral types, in samples where swelling clays were confirmed. Reflectance values from Table 7.4 in Moore & Reynolds 1997 were used.

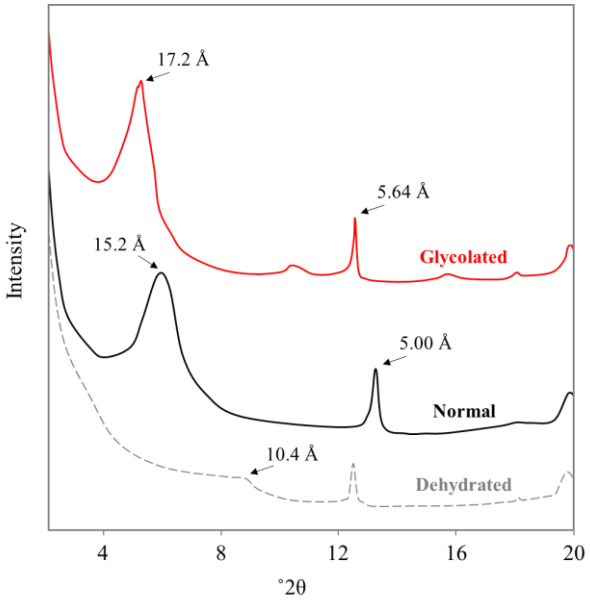


Figure 4.7. Schematic showing the expected peak position on XRD patterns collected from Normal, Air-dried and EG solvated smectite clay mineral (image modified from Tilley & Eggleton, 2005).

4.3 Optical Microscopy

Transmitted and reflective light microscopy was used to carry out petrographic study of the bedrock underlying the weathering profiles of SDG. Samples selected were prepared into polished thin sections and were studies using microscopes at the NHM.

Chapter 5

The Mineralogy and Geochemistry of the Serra Verde REE Deposit Parent Bedrock

5.1 Introduction

IADs are supergene REE deposits that form through the weathering of granitic rocks. Formation of this type of deposit requires both the breakdown of REE-bearing minerals to release REE ions, and also the breakdown of bulk rock-forming minerals into clay minerals that adsorb the REE ions. The mobilisation of REE in the weathering system is strongly controlled by the weathering resistance of primary REE minerals in the parent granite. The development of an IAD and the degree of REE-enrichment is therefore largely determined by the mineralogy of the parent rock (Sanematsu et al. 2016). Few granites that develop a weathering profile develop REE IADs, which suggests that IAD-hosting granites have special compositional features.

Most of the IAD deposits found in southern China developed over highly differentiated biotite or muscovite granites that have I-type affinities and classify as ilmenite series intrusions. These granites are typically metaluminous to weakly peraluminous, have low phosphate contents and medium to high alkali contents (Sanematsu & Watanabe 2016). Previous publications have shown that granites hosting IADs contain a large range of REE-hosting minerals in the parent rocks; the main REE-minerals that have been identified include bastnäsite, parisite, gadolinite, doverite, allanite, xenotime, monazite, zircon, synchysite, apatite, fergusonite, samasrkite and Ti-oxides (Sanematsu et al. 2016). The abundance of each of these minerals, and the total percentage of REE hosted by the minerals, varies between different granites (Bao & Zhao 2008).

However, it does appear that granites with a hydrothermal mineral assemblage are more favourable for the development of IADs, particularly the HREE-rich deposits (Sanematsu & Watanabe 2016). From the few studies published, hydrothermal alteration of primary mineralogy appears to play a key role in the development of IADs by changing the REE

distribution and the REE mineralogy to one that is more susceptible to weathering (Huang et al. 1989). The types of hydrothermal alteration that have been observed at Chinese IAD-hosting granites include albitisation, muscovitisation, and fluoritisation (e.g. Huang et al. 1989, Bao & Zhao 2008, Ishiara et al. 2008), which are believed to be the result of late stage magmatic fluids interacting with the granite (Huang et al. 1989).

The Serra Verde ion adsorption deposit is located at the southern side of the Serra Dourada granite complex (SDG). The Serra Verde deposit was discovered over the last decade, and no mineralogical and geochemical information is published about the parent granite directly beneath the deposit, particularly the REE mineral assemblage. Previous studies on surface grab samples from other parts of the SDG complex have identified monazite, xenotime, and zircon as the main REE carriers; all of which are highly resistant minerals (Teixeira and Botelho 2006). More minor REE minerals such as bastnäsite and allanite have been reported previously (Santana 2013). Due to the tropical climate, it is likely that other important but physiochemically weaker REE-hosting minerals present in the granite have not survived in the surface environment, and may therefore never have been sampled by previous studies. In addition, none of the samples analysed by previous studies include granite samples where the deposit is located.

The Serra Dourada is an extensive granitic complex, and the few samples from other studies that investigated the margins and northern parts of the complex may not provide representative information about the granite bedrock from which the Serra Verde REE deposit formed. Furthermore, these studies make no mention of hydrothermal alteration to the mineralogy of the bedrock. A detailed mineral study of the granite underlying the Serra Verde REE deposit in order to properly determine the geochemical and mineralogical starting point for weathering is therefore justified.

The aim of this chapter is to characterise both the bulk and mineralogical composition the parent granite of the Serra Verde REE deposit in order to understand what role it played in the development of a REE-enriched profile. The results of this investigation will establish the mineralogical starting point from which subsequent work focusing on the weathered profile can build upon.

Specific questions that will be addressed are:

- What are the main characteristics and classification of the granite underlying Serra Verde, and how does its composition compare to previous classifications of the SDG?
- What is the REE content and mineralogy of the fresh bedrock?
- Is there any enrichment of REE, and is this largely a product of magmatic, hydrothermal, or other processes?

Addressing the aim of this chapter will be achieved by, firstly, analysing the Serra Verde downhole assay database to produce 2D geochemical maps of the bedrock, in order to visualise the variability in chemical composition and geometry of the southern SDG intrusive body, and give context to the granite lithology beneath the Serra Verde REE deposit.

Secondly, by carrying out a detailed geochemical and mineralogical study of 'fresh' samples of granite underlying the deposit from core samples collected from diamond drilling beneath the Serra Verde deposit. Observations of the petrology, textures, and occurrences of the major and REE mineralogy are integrated with geochemical analyses of the bulk rock and REE-minerals.

5.2 Methods

5.2.1 Samples

In order to examine the mineralogy and geochemistry of the granite underlying the plateau where the profile is preserved, 24 samples were collected from 10 Serra Verde Mining drill holes, including detailed sampling along the deepest drill hole, DDH0004, which extends 70 m into the unweathered granite. Only single samples could be collected from the other drill holes because of their shallow penetration into the fresh bedrock of 1 – 2 m. To compare the composition of this granite to historic work in the SDG complex, 3 additional drill holes were selected for further sampling close to the edges of the granite complex (see Figure 5.1 for the locations of all sampled bedrock drill holes). These holes were selected for detailed study because they also extend further into unweathered bedrock (up to 80 m).

A total of 10 samples were collected from sections at 26 – 100 m depth in DDH0004, each measuring approximately 10 cm long. A further 12 samples were collected from the remaining holes. The sampling depths for each drill hole can be found in Table 5.1. Pegmatites that were observed in the bedrock were not sampled because assay results show they contain very low REE concentrations.

Table 5.1. Samples collected and analysed for geochemical and REE-mineralogical characterisation.

#	Sample ID	Drill Hole	Depth (m)	Bulk Geochem	SEM	EMP
1	SD1	DDH0009	37.2	x		
2	SD3	DDH0009	97.1	x		
3	SD4	DDH0004	26.5	x	x	x
4	SD5	DDH0004	27.5	x	x	x
5	SD6	DDH0004	28.7	x	x	x
6	SD7	DDH0004	44.9	x	x	x
7	SD8	DDH0004	82.8	x	x	x
8	SD9	DDH0004	93.1	x	x	x
9	SD10	DDH0004	99.5	x	x	x
10	SD12	DDH0002	9.5	x		
11	SD14	DDH0007	17.7	x		
12	SD15	DDH0121	26.7	x		
13	SD16	DDH0099	99.3	x	x	x
14	SD17	DDH0061	61.4	x	x	x
15	SD18	DDH0020	35.9	x	x	
16	SD19	DDH0075	12.5	x	x	x
17	SD20	DDH0266	21.3	x	x	x
18	SD21	DDH0096	41.9	x	x	x
19	SD22	DDH0040	14.2	x		
20	SD23	DDH0028	6.38	x	x	x
21	SD24	DDH0071	17	x		
22	SD25	DDH0004	74.4	x	x	x
23	SD26	DDH0004	33.1	x	x	x
24	SD27	DDH0004	51.1	x	x	x

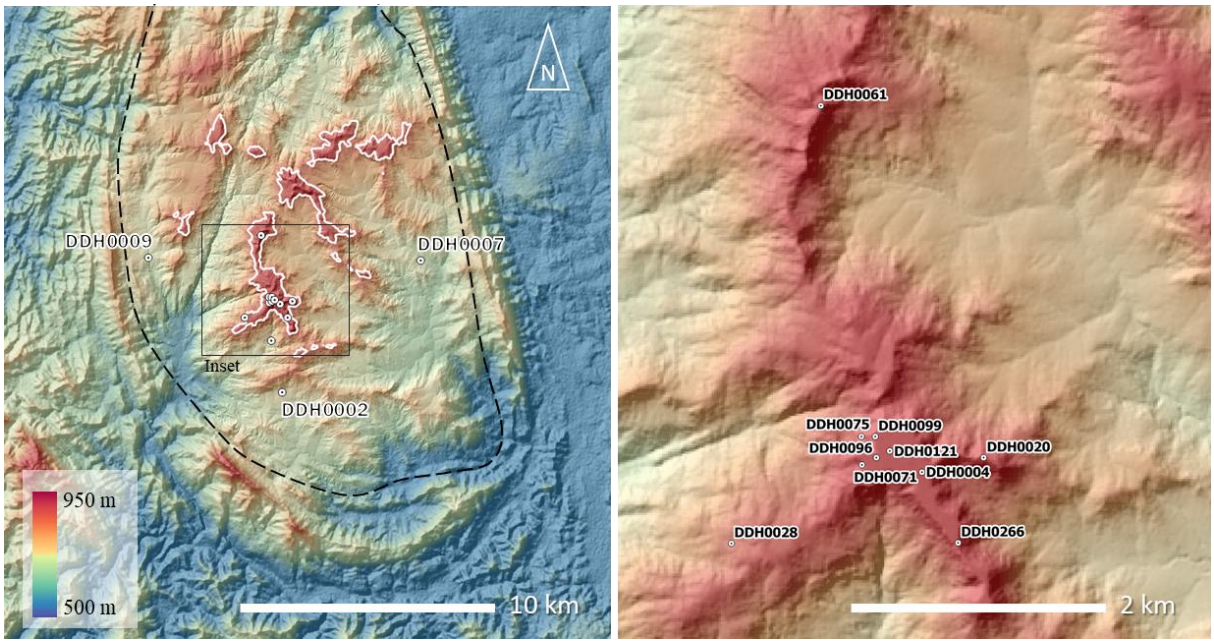


Figure 5.1. Location map showing the drill holes sampled and studied in this chapter by geochemical analysis (left). White outlines demarcate the approximate extents of preserved weathered profiles. The inset figure (right) shows the locations of drill holes that were sampled for fresh granite beneath the main plateau area.

5.2.2 Analytical methods

Geochemical analysis on whole rock samples was carried out at ALS Ireland and NHM London by ICP-MS, ICP-AES, LOI, and ion chromatography, in order to determine the chemical composition of the granite bedrock.

SEM work was carried out to identify and examine the textures of the REE-bearing accessory mineral phases in the bedrock samples, and electron microprobe analysis was carried out in order to determine the chemical composition of these minerals. REE-bearing accessory phases were principally identified by their bright response in SEM-BSE imagery, and EDS analyses. A list of the analytical work that was carried out on each sample can be found in Table 5.1. Detailed descriptions of the methodology, analytical conditions, data handling, and apparatus can be found in Chapter 4.

5.2.2 Assay data processing for geochemical maps

The lack of fresh bedrock exposure at surface, the high relief, and large area of the Serra Verde deposit have posed a challenge to mapping the granite bedrock. The downhole assay database enables a geochemical map of the granite to be made by filtering those drill holes that intersect fresh rock, and then classifying the assay points by major and trace element concentrations. The maps were made to show spatial geochemical variation across the southern half of the Serra Dourada Granite, extending beyond the boundaries of the plateau study area.

The chemical index of alteration (CIA) is a calculated index that can be used to quantify the degree of weathering of a feldspar-bearing rock, and is appropriate here to filter granite assay samples based on the degree of feldspar weathering. The next chapter includes further details of this index, where it is used to assess weathering intensity through the profile, and sets it into context with other weathering indices.

The grids were generated by the following steps:

1. Calculating CIA values for all samples and filtering the assay database for samples below 66 CIA to produce a fresh bedrock filter, which correspond mainly to bedrock and saprock lithologies. Fresh granite values typically fall near a CIA of 50, a CIA cut-off value of 66 was selected to include the saprock samples because of an insufficient number of fresh bedrock samples to produce continuous element maps.
2. For drill holes with multiple fresh bedrock assays, the values were averaged to allow gridding of a 2D map.

3. The grid was generated at a 20 by 20 m cell size, and a maximum search radius of 180 meters. All elements were displayed using the same colour scale of population percentage cut-offs (see Figure 5.2). The colour scale was applied with unequal assay bin sizes starting from 30 % for the lowermost values, then progressively at 60, 80, 90, 95, 98, and 100 percent cumulative bins. The advantage of this scale is to enhance the visualisation of anomalously high values of individual elements within the granite while comparing equally sized data populations. However, any anomalously low values will not be highlighted.
4. The elements were selected for gridding based on their weathering mobility. Elements with concentrations that vary independently with increasing CIA, up to 66, were selected as appropriate to map the in-situ granite composition (e.g. Zr, Ti, Ba). Elements which decrease in concentration at higher CIA values were not used to produce maps, due to their mobile behaviour in the filtered data (e.g. Na, Ca, P). An example of an immobile and mobile element – CIA relationship is shown in Figure 5.3. REE maps were not made because of the weathering enrichment observed in the saprock samples.

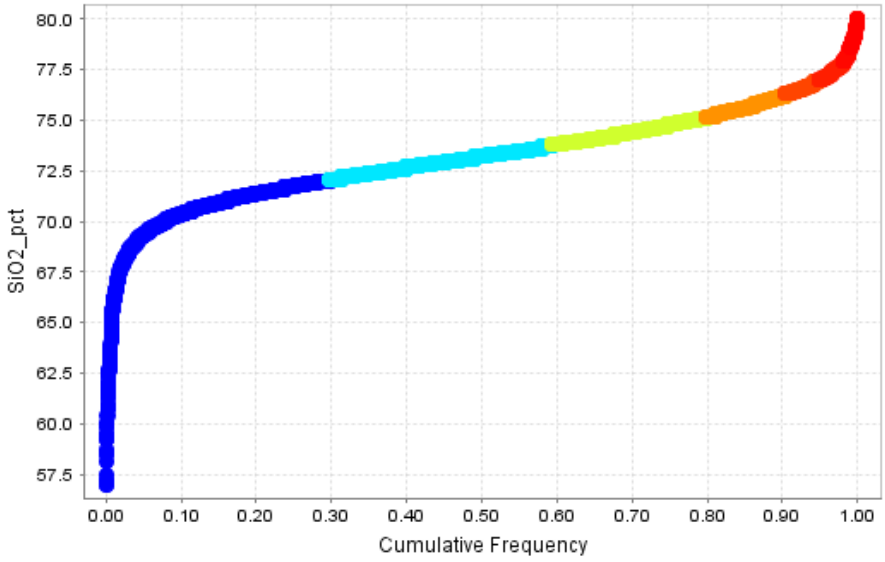


Figure 5.2. Cumulative distribution of SiO_2 values coloured by the percentage bins used for colour scale cut-offs on gridded element maps.

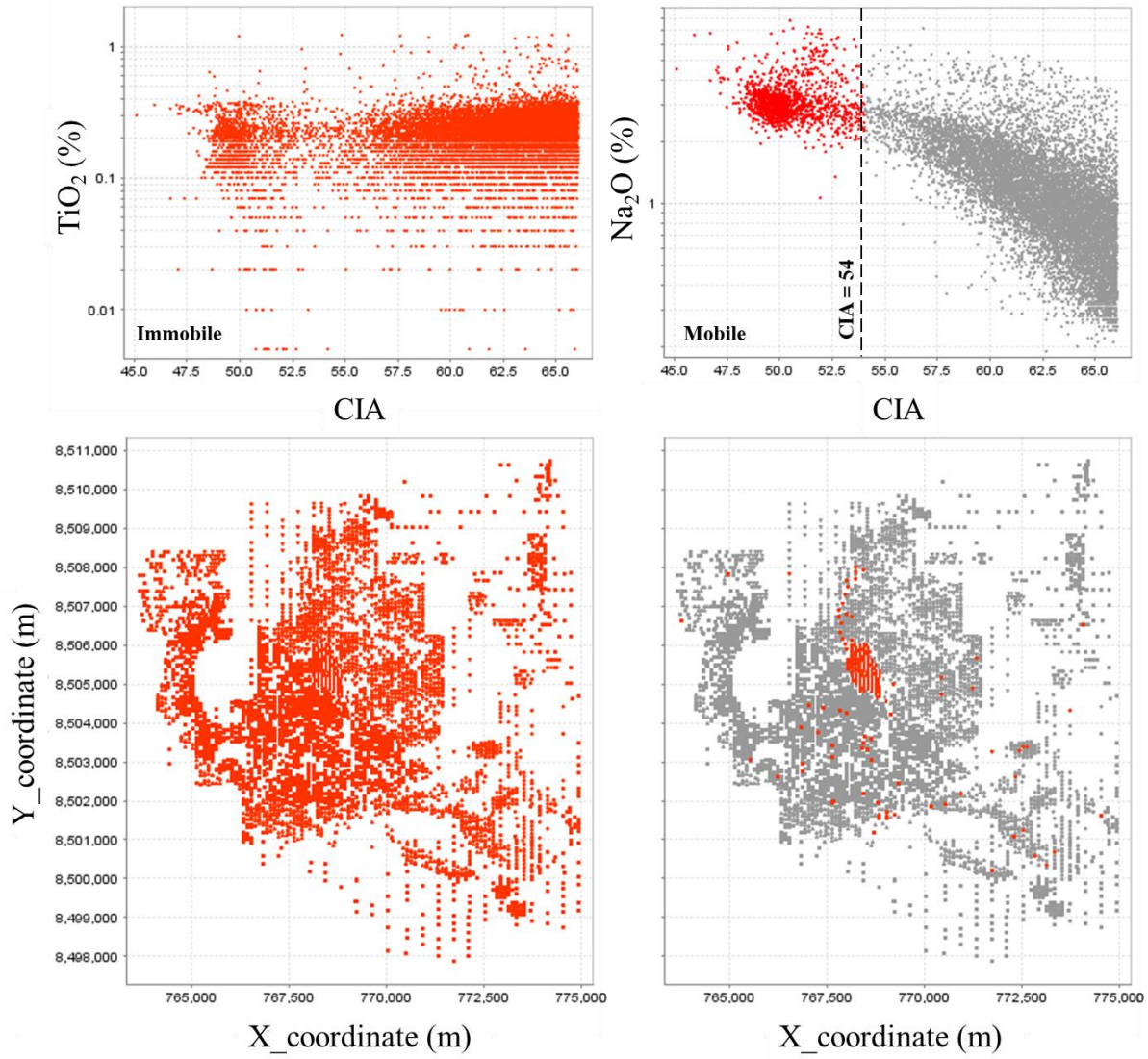


Figure 5.3. Plots showing the non-weathered CIA cut-offs for Ti and Na from drill hole assay data (top), and corresponding filtered sample maps showing the included (red) and excluded (grey) samples below. The CIA cut-off value is taken where the Na_2O concentration is independent from CIA i.e. no weathering effect on Na_2O concentration. Note the limited spatial distribution of samples in the filtered data for Na centered on the plateau area.

5.3 Petrology

5.3.1 Plateau samples

DDH0004 downhole log

DDH0004 is a deep drill hole situated in the centre of the plateau area and is presented here to show the variability of the fresh bedrock granite under the SV deposit. The downhole geology log (Figure 5.4) and petrological examination shows that most of the intersected bedrock is composed of biotite granite, and the remainder is composed of several pegmatites that cut though the granite in the lower half of the core (below 60 m), and an albitised granite zone of ~ 10 meters between 80 and 90 m depth.

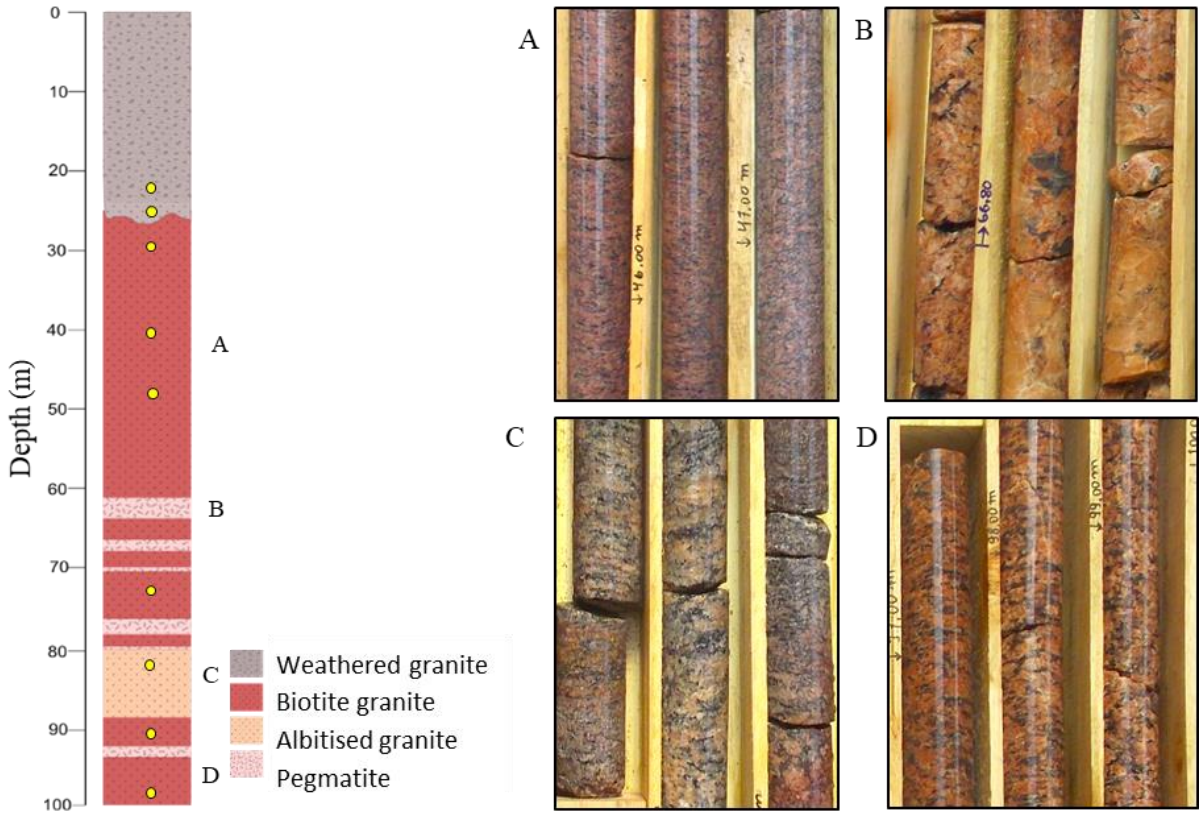


Figure 5.4. DDH0004 graphic core log (left) with sample locations marked by yellow dots, and photographs of the main lithologies (photos taken by Serra Verde Mining). Letters denote the downhole locations of the photographs.

The biotite granite is more strongly deformed at depth; images in Figure 5.5 show how biotite granite is progressively more foliated and layered at greater depths. Samples from the top are weakly foliated, while samples near to the base are coarser grained, and exhibit strong compositional layering. A colour difference is also noted between paler pink biotite granite in

the upper half of the hole (< 60 m), in contrast to the brighter red biotite granite below. Similar differences are observed between drill holes (Figure 5.6). The albitised granite zone is paler than the rest of the biotite granite.

Numerous pegmatites of variable thicknesses up to ~5 m are readily identifiable in the drill holes by their very coarse grain size, lower biotite content, and paler colour than the hosting biotite granite. The intrusive contacts are sharp, linear, and undeformed.

Biotite granite description

Petrography shows that the rock is a coarse-grained, foliated, metamorphosed, alkaline feldspar-quartz-plagioclase-biotite granite composed of quartz (40 %), orthoclase (20 %), microcline (20 %), plagioclase (10 %), perthite (5 %), and biotite (4 %). Fine-grained silicate mosaics and accessory minerals typically make up less than 1 % by volume, and include zircon, fluorite, Fe oxides, ilmeno-rutile, and unidentified pale grains (see Figure 5.7). The bulk mineral composition would classify this granite as an alkali feldspar- to syeno-granite using the IUGS felsic ternary system (Le Maitre 2002).

The hand samples have a bright reddish pink colour, characteristic of the alkaline feldspars, and is mosaiced with glassy grey quartz. Samples collected from the top of DDH0004, and in drill holes 0020, 0061, 0099, and 0121 are consistently paler in colour than those occurring elsewhere (Figure 5.6). These samples are all from the bedrock located under the north-east side of the plateau. Black shiny aligned biotite sheets carry the foliation, highlighting the deformation in the granite.

Quartz composes anhedral crystals up to 5 mm in diameter. In some places quartz grains exhibit undulose extinction, or are composed of fused grains with uneven fracture boundaries. Small (20 micron) rounded grains are also present as isolated or clustered interstitially between feldspars. Biotite, accessory minerals, and fluid inclusions are present within some crystals. Quartz frequently presents elongated geometries with a preferred orientation parallel to the foliation of the biotites.

Plagioclase grains are subhedral laths to anhedral grains with well-developed polysynthetic twinning. The extinction angle shows the composition as dominantly oligoclase. Some grains show a mottled texture with shiny fine flakes in fractures interpreted as weak sericitization. Microcline grains are subhedral to anhedral, mostly poikiolitic and have quartz inclusions. They often exhibit characteristic tartan twinning extinction.

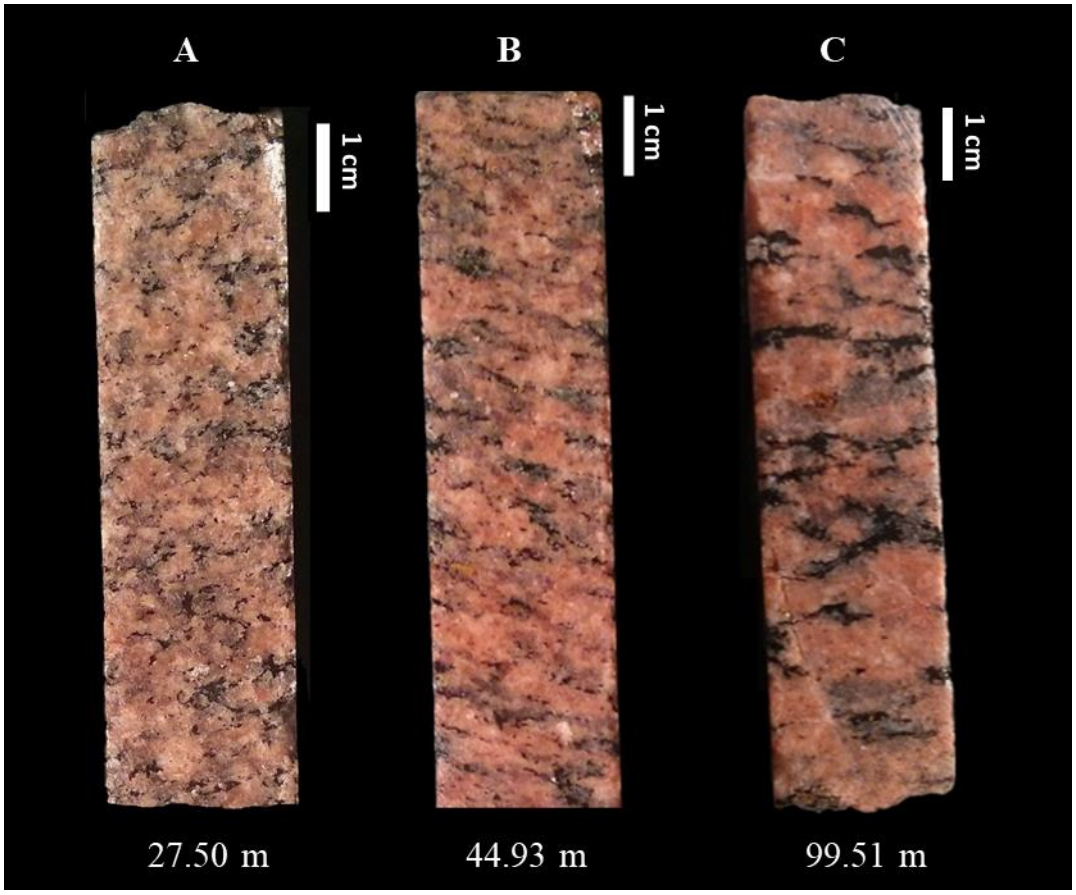


Figure 5.5. Photograph of three representative drill core sections studied from the top, middle, and lower portions of DDH0004, showing an increase in metamorphic strain with depth.



Figure 5.6. Photographs comparing two representative pale-coloured biotite granite samples (top), and two pink-coloured biotite granite samples (below).

Orthoclase and perthite are subhedral to anhedral, and mostly poikiolitic. Some grains show well-developed perthitic exsolution textures, which do not align to the foliation or elongation of other minerals.

Biotites occur as subhedral tabular grains varying in size from 0.05 to 5 mm in the longest axis. They are overgrown in places by quartz, and share the preferential orientation seen in hand samples forming discontinuous layers in between feldspars, and as clusters entirely surrounding feldspar crystals (auguen). Very rarely they exhibit red colouration, replacing the more common dull brown colour, perhaps due to compositional variation.

Accessory minerals generally form as grains 50 – 500 microns in diameter and are commonly associated with biotite, and less commonly between feldspar and quartz crystals, as fine-grained inclusions within fused grain boundaries.

Zircons are observed as euhedral to subhedral fractured crystals up to 500 microns diameter. Several grains exhibit concentric zoning, and inclusions are clearly visible in transmitted and cross-polarised light. All grains are either completely or partially enclosed by biotite, or occur between quartz and feldspar crystals.

Fluorite is present as clear anhedral crystals, interstitial to feldspar and biotite. The grains are readily identifiable in hand specimen from their violet to transparent colour.

Titanite occurs as large, mm-sized, subhedral to anhedral stubby crystals of a greenish yellow colour, always spatially associated with biotite, but only present in some of the drill hole samples.

Iron oxides are present as fine inclusions in feldspar crystals, surrounding other accessory phases, and infilling crystal fractures, and probably have a hematitic to goethitic composition based on their brownish-red colouration.

Unidentified accessory phases have mottled, or powdery textures with irregular relief and carry variable subhedral, pseudomorphic habits. They are almost opaque and occur in two main colours: brown and whitish-red grains. Brown grains occur throughout the rock, but powdery whitish-red grains occur exclusively within biotite or fractures in quartz adjacent to biotite.

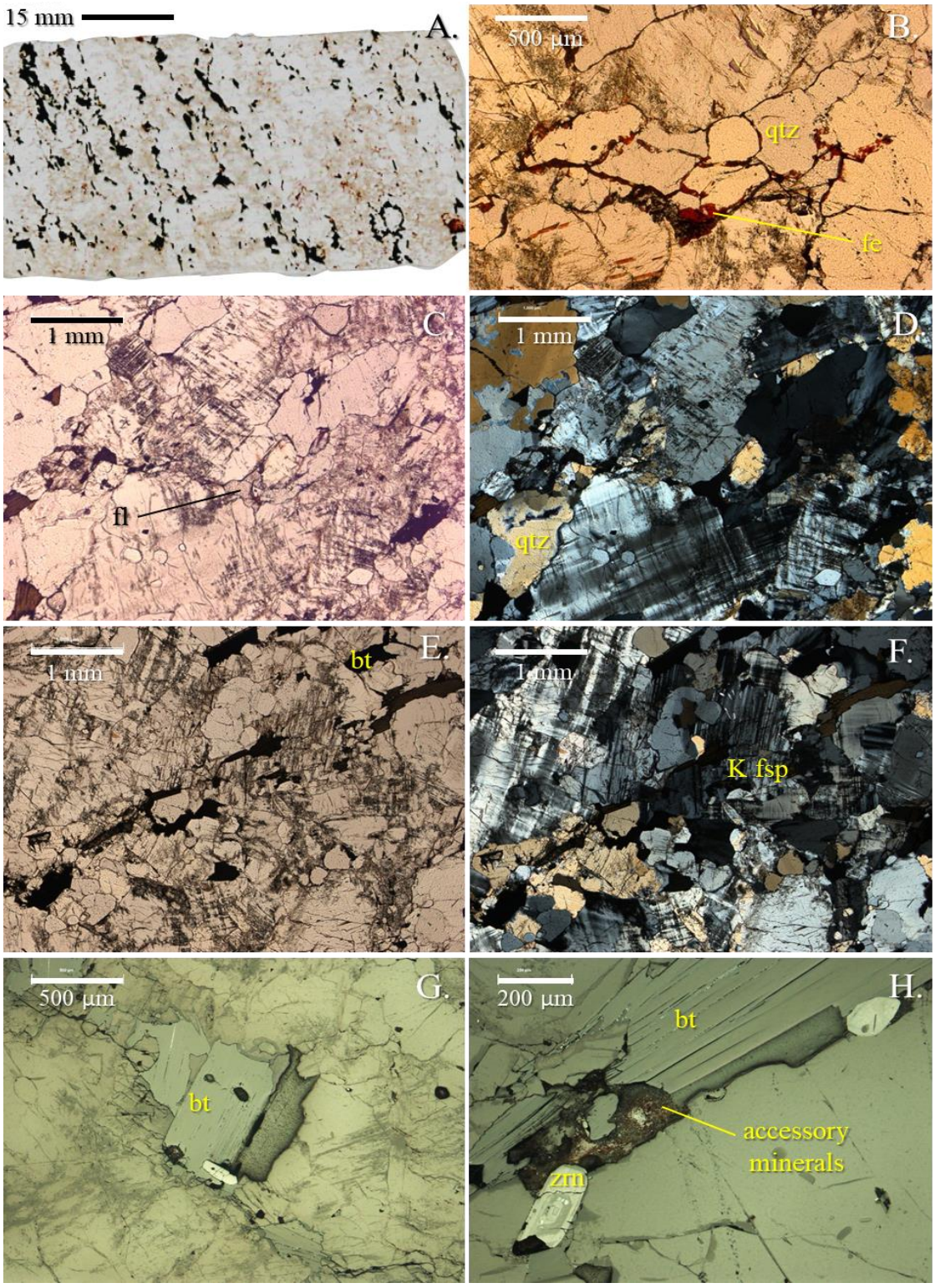


Figure 5.7. Thin section micrographs of biotite granite; A. Macro image of typical thin section with aligned biotite streaks and trace Fe oxides (far right); B. Fe oxides between quartz grain boundaries (PPL); C. and D. Poikiolitic microcline and perthite, quartz grains with undulose extinction and interstitial fluorite (PPL and XPL); E. and F. Preferentially oriented biotite and fractured feldspar (PPL and XPL); G. and H. Zircon and altered accessory minerals included or concentrated around biotite flakes (REF). Note thin section prepared to 40 micron thickness for SEM and EMP analysis, causing interference colours to shift slightly to higher birefringence in XPL.

5.3.2 Granite rim samples

At the periphery of the biotite granite, the bedrock samples are generally finer grained, contain slightly higher proportions of quartz, and lower biotite than the granite underlying the plateau area. The rock is similarly foliated, and some samples contain small amounts of visible muscovite sitting alongside biotite in the darker mica clusters. Rare interstitial dull brassy pyrite (up 2 mm diameter) sit between mica and quartz crystals. Crystals of pale purple fluorite up to 1 mm are also present in these samples, mostly interstitial between feldspar grains.

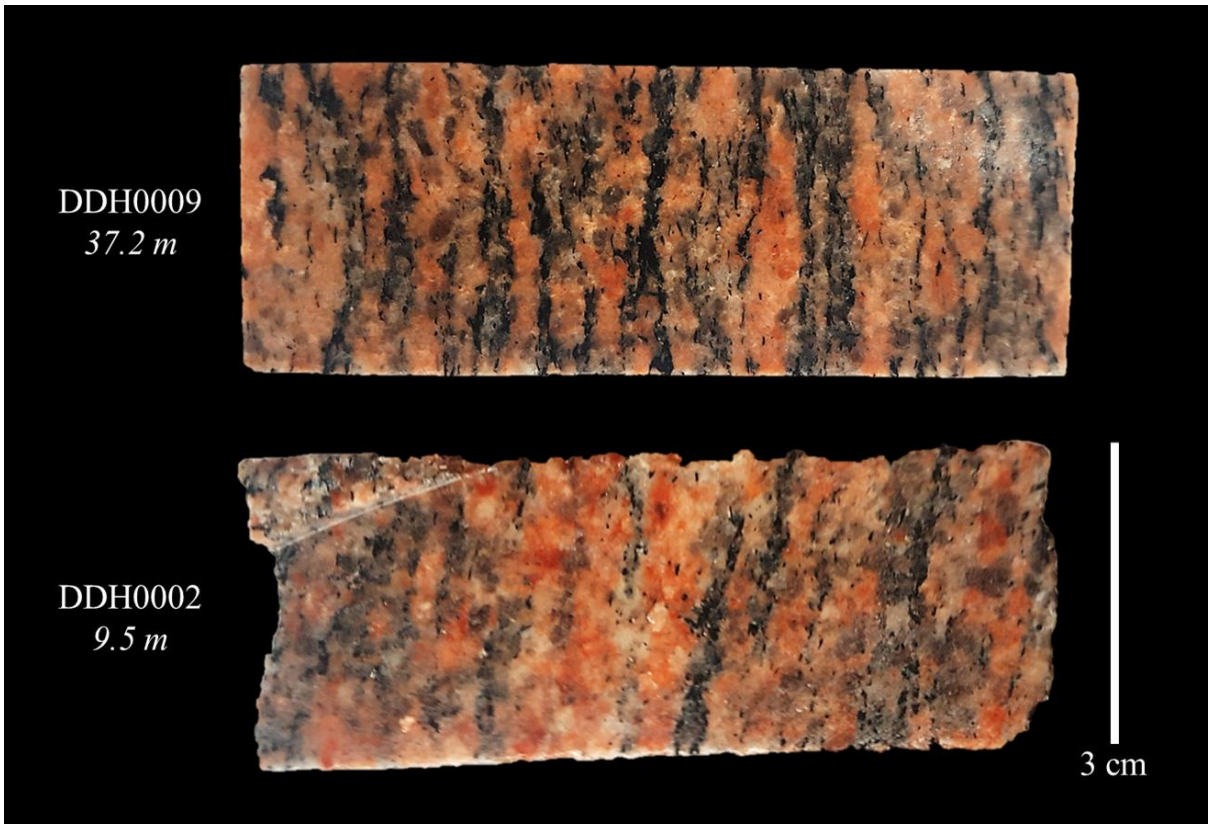


Figure 5.8. Photographs of two representative granite samples collected from the rim of the biotite granite, showing the significantly finer bulk grain size and higher abundance of quartz.

5.4 Whole-Rock Geochemistry

5.4.1 Serra Dourada geochemistry

The geochemical maps show strong compositional variation within the granite area delineated by previous geological mapping of the southern region of the SDG. This variation is interpreted to outline a concentric core and rim geometry, as well as more linear features cutting across the area. Element maps that best show these features are presented in Figure 5.9 (for all other maps see Appendix B3).

The major element maps reveal a sub-circular core of granite with elevated Ti, Zr, and Fe at the north-western quadrant of the element maps approximately 8 km in diameter, and a rim with elevated Si and Rb, and low K, Fe, and Zr. The widest part of the rim is visible at the south-eastern side of the core (ca. 3 km at surface), and continues along the south-western and north-eastern flanks of the core, decreasing to a surface width of less than 1 km. This rim also has elevated Sn and W values.

The Ba, Nb, Ta, Ga, K and Th element maps do not reflect the core and rim geometry, but reveal a strikingly clear partition between the north-eastern and south-western halves of the area covered by the core and rim. The north-eastern half is characterised by elevated Nb, Ta, and Ga. The south-western half is characterised by elevated Th, K and Ba. The boundary zone between these halves is highlighted by elevated Ba and Sr which demarcate a sub-linear zone striking NW-SE, continuing for at least 7 km, and up to 1 km across at surface.

Finally, anomalously high Ti, Sr and Ba, as well as anomalously low Nb, Ga, Ta and Rb define an outermost zone at the southern and eastern edges of the element maps. This zone sits within the area mapped as part of the SDG complex (1:500,000 Map, CPRM 2008), and may correspond to the edge amphibolite granite referred to by Bilal 1997.

The filtered assay data was classified to define the boundaries between the different compositional zones, using the results from the Zr, Th, Nb, Rb, and Ba element maps described above by applying a decision tree. The results are presented in Figure 5.10 and highlight the different zones.

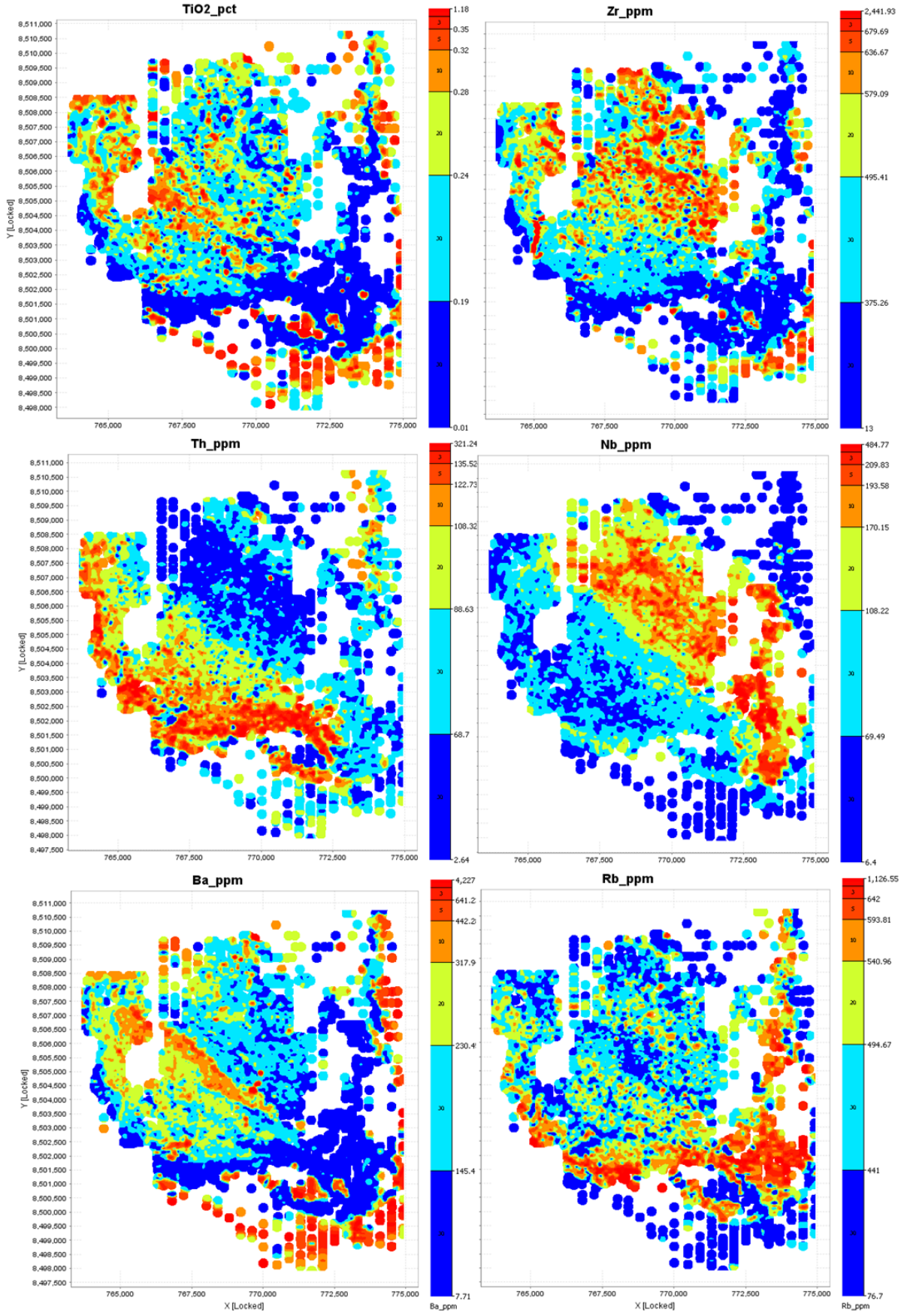


Figure 5.9. Selected element maps that best highlight the variable geochemistry of the southern Serra Dourada granite.

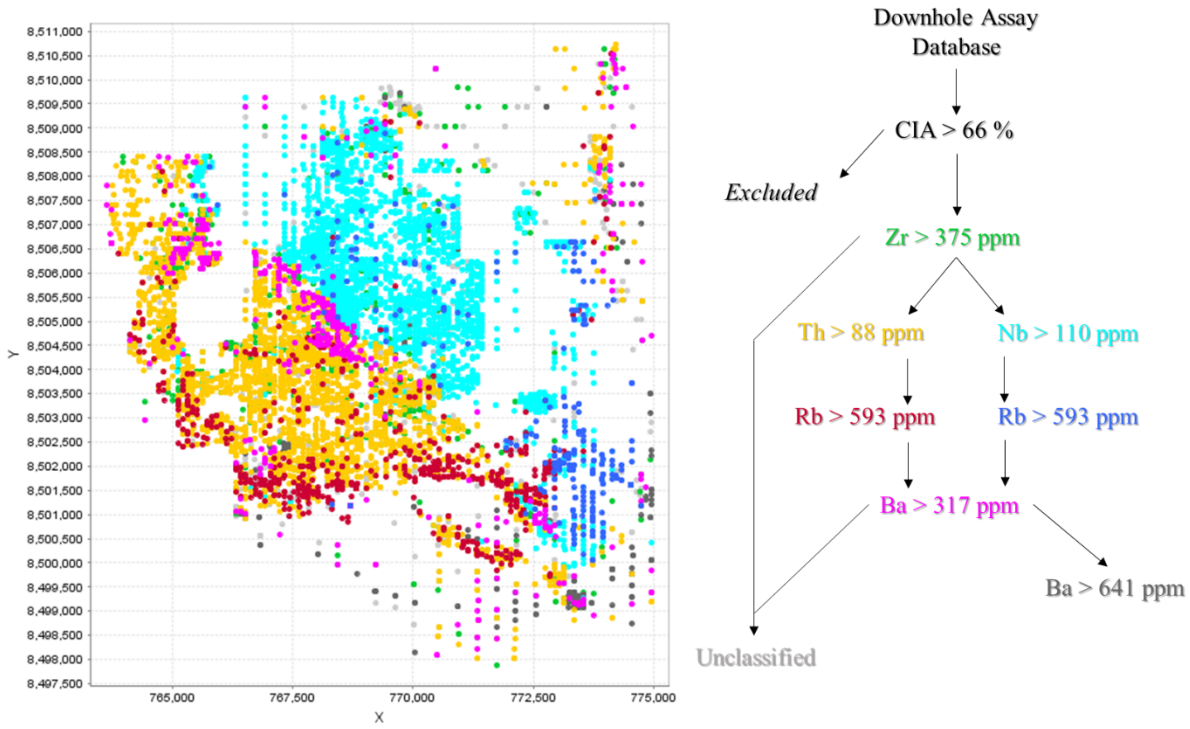


Figure 5.10. Geochemical classification map of the filtered CIA drill hole data (left), using bin values from the individual element maps in a simple decision tree (right).

5.4.2 Geochemistry samples analysed

Geochemical analysis results for granite samples sent for analysis are presented in Table 5.2 and Table 5.3.

The samples are first evaluated in terms of their rock type classification, followed by more detailed description of their chemical composition, and the main variation between different granite samples groups.

Following the results from the geochemical granite maps, samples are grouped into Nb-rich (> 100 ppm) and Nb-poor (< 100 ppm); both groups falling within holes from the core of the granite located in the plateau area. The remaining samples are termed rim samples (collected from drill holes 2, 6, and 9) based on their location outside the geochemical core of the granite.

5.5.2.1 Granite Classification

A chemical classification of samples analysed was carried out by using the Fe-number, aluminium saturation indices, silica content, and alkali content. The granite classification diagrams presented in Figure 5.11 show that the Serra Dourada granite is a highly evolved alkali-rich granite. It contains high K and Fe contents, which classify the granite as both a

shoshonitic series (strongly potassic rock), and ferroan granite. According to the ASI values, all samples may also be classified as weakly peraluminous granites (<1.1 ASI). These results are consistent with other A-type granites sampled in the Goiás province, as described and analysed by Pimental (2001).

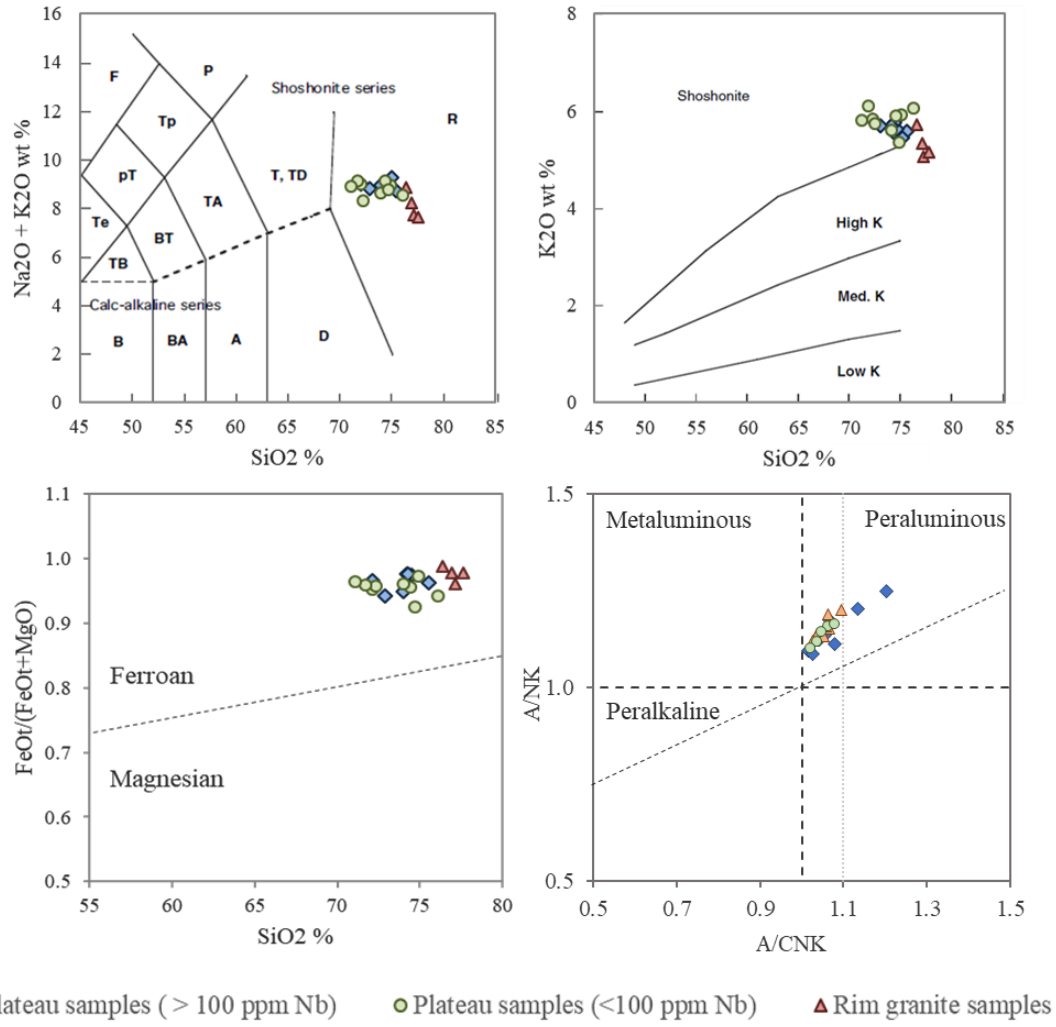


Figure 5.11. Granite classification diagrams using major elements; alkali element wt % vs SiO_2 wt % plot and K_2O wt % vs SiO_2 wt % plot (top left and top right, both after Peccenillo and Taylor 1976). Fe* (molar) vs SiO_2 wt % plot (lower left); A/NK vs A/CNK (molar) plot (lower right, after Shand 1943).

5.5.2.1 Major elements

Major element plots show the main variations in major element compositions for the samples analysed (Figure 5.12):

Plateau samples have high silica values that range from 70 to 76 wt % SiO_2. The rim granite samples have values from 76 to 78 wt % SiO_2. Fe_2O_3 values range from 1.9 to 3.9 wt %, and

exhibit a negative correlation to silica; rim samples have the highest silica and the lowest Fe concentrations of the three groups (see central upper element plot in same Figure 5.12).

Together Na_2O and K_2O make up between 8.3 and 9.1 wt % of samples in the Nb-rich and Nb-poor samples, and 7.61 to 8.86 wt % in the rim samples. A sample from the deep drill hole DDH0004 has the lowest alkali content of 6.43 wt % (5.28 wt % Na_2O and 1.15 wt % K_2O), making it an anomalously sodic sample, and corresponds to the albitised section of core log. Most of the alkali content is attributed to K, which is present in concentrations of ~ 6 wt % K_2O in the granite samples. Na values are ~ 3 wt % Na_2O for Nb-rich and Nb-poor plateau samples, and slightly lower at ~ 2.8 wt % Na_2O for rim samples.

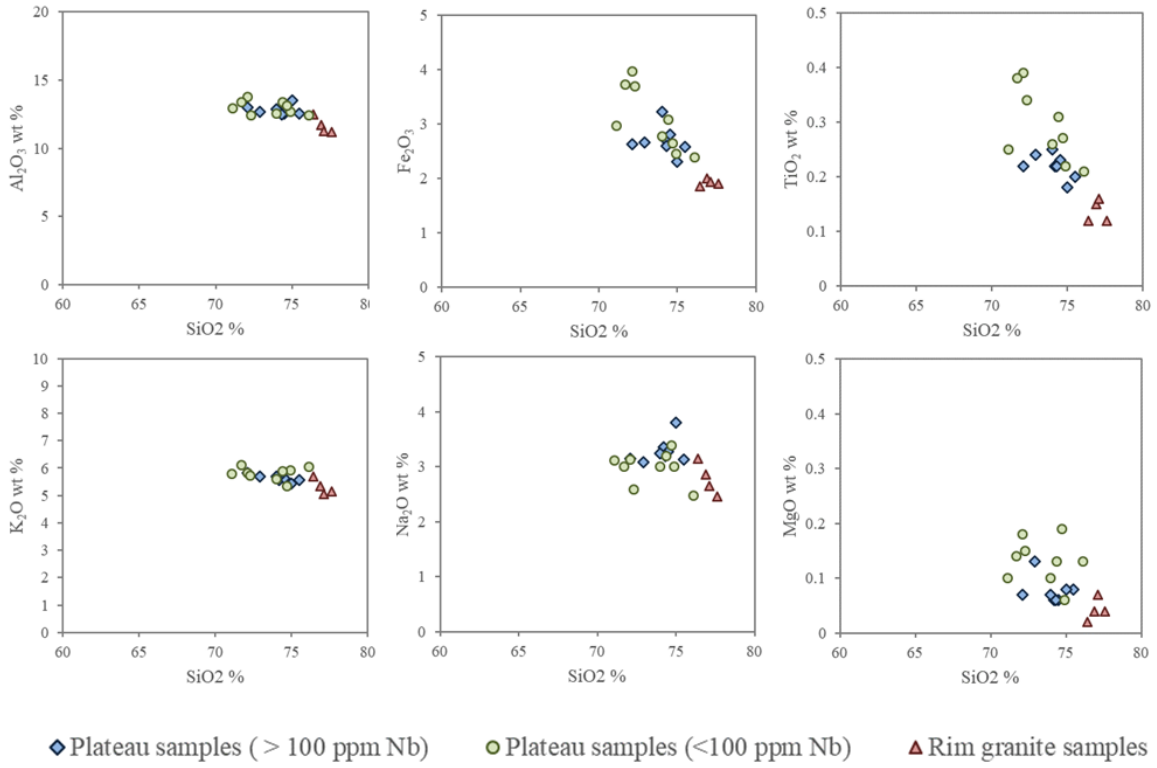


Figure 5.12. Major element plots for granite bedrock samples, showing the relationships between selected major elements for the three groups.

The granite samples have average concentration ranges of 0.63 – 1.2 wt % CaO, 0.05 – 0.2wt % MgO, < 0.01 – 0.04 wt % P_2O_5, and 0.12 – 0.39 wt % TiO_2. The values are also comparable to previously published biotite granite analyses by both Bilal (1997) and Santana (2013), which were also collected from the SDG complex. Ti and Mg concentrations show the same negative correlation to Si, with the lowest values occurring in rim samples.

Although concentrations of phosphate are low in all samples analysed, Nb-poor samples have slightly higher average phosphate contents than Nb-rich samples; < 0.01 wt % vs 0.03 wt %. Nb-poor samples also appear to have slightly higher Fe, Ti, and Mg contents (Figure 5.12). On the whole however, Nb-rich and Nb-poor samples are not very different in terms of their major element composition, reflecting their similar primary mineralogy.

5.5.2.1 Trace elements

The trace element plots presented Figure 5.13 show the main variations in trace element compositions for the granite bedrock samples analysed. The results show the following:

The trace element compositions of the samples confirm the spatial geochemical zones of the gridded element maps presented in section 5.4.1; the two groups of plateau samples have significantly different trace element compositions to both the rim granite samples, and each other. The absolute assay values are also comparable to CIA filtered samples in the drill hole assay database.

Each of the elements Ba, Rb, and Sr show variable concentrations in the sample groups with large ranges in values. Average concentrations are 200 ppm, 450 ppm and 25 ppm for Ba, Rb, and Sr respectively. However, the range of Ba for the Nb-poor sample group (~ 200 – 550 ppm) is significantly higher than both the Nb-rich sample group (~ 100 – 230 ppm) and the rim granite sample group. Similarly, Sr values are ~35 – 70 ppm for the Nb-poor group, ~20 – 35 ppm for the Nb-rich sample group, and 10 – 22 ppm for the rim granite sample group. Rb values are similar for the Nb-rich and Nb-poor sample groups (~350 – 500 ppm), but significantly higher in the rim granite group (~450 – 650 ppm).

For the plateau samples, Th concentrations range between 80 and 100 ppm, and U concentrations range between 8 and 12 ppm U. Th values are only slightly more elevated in the some of the Nb-poor group than the Nb-rich group, and there is no significant variation in either Th or U within DDH0004. Most of the rim granite samples have higher Th and U with concentrations of ~120 ppm Th, and 12 to 19 ppm U.

Granite samples have high abundances of high field strength elements (Nb, Ta, Zr) in comparison to previous granite sampling work carried out in the same area by Bilal et al (1997).

The samples are clearly split into two groups based on their Nb content and reflect the terms of the sample groups (Figure 5.13). Samples with < 100 ppm Nb are located at the rim of the granite, and south-west side of the plateau, while samples with > 100 ppm Nb are all located

at the north-east side of the plateau. This distribution matches the Nb element granite map at similar concentrations.

Samples along DDH0004 also show a downhole trend in Nb concentrations; higher concentrations occur in the upper half of the drill hole than in the lower half (~140 ppm vs ~80 ppm respectively, see Figure 5.15). Nb concentrations remain unchanged in the albitised section of the core log, but pegmatites have lower Nb concentrations.

Although Ta concentrations are much lower than Nb at < 10 ppm, they show similar variation between samples to Nb, with Ta/Nb ratios remaining near-constant in all analysed bedrock samples. Ta/Nb ratios are 0.04 – 0.06, and are characteristic of anorogenic alkaline granites (Pollard 1989).

All samples analysed have high Zr concentrations. Plateau samples contain an average of ~500 ppm Zr, most ranging between ca. 400 and 600 ppm. Two samples have notably high concentrations of 679 and 861 ppm, from drill holes 75 and 266 respectively, both falling in the Nb-poor sample group. Along DDH0004, Zr remains constant in the biotite granite at ~520 ppm, and values are elevated in the albitised section at 757 ppm.

Rim granite samples have much lower Zr concentrations averaging 260 ppm, and the values in this group coincide closest with the values obtained by Bilal et al 1997 and Santana 2013; 400 ppm and 270 ppm mean Zr respectively.

Analysis results for F show that all granite samples analysed are enriched in fluorine. All granite samples have very high fluorine values of around 5000 ppm, except for three samples that have values of ~1000 ppm. Lower Ca values in these three samples may indicate that the bedrock has been weakly weathered by percolating fluids which may have removed some of the F. Rim samples appear to have on average slightly higher fluorine contents than plateau samples (Table 5.2, Table 5.3).

Fluorine values in granite analysed are much higher than those reported by Bilal et al 1997, with obtained values of 810 – 2830 ppm. Bailey 1977 notes that high fluorine contents of over 800 ppm are typical of alkaline granites, and may be indicative of roof zones and granite margins.

5.5.2.3 Rare earth elements in the bedrock

REY concentrations in plateau samples are high and range between 766 and 1800 ppm. Samples from drill holes 20 and 266 have the highest fresh concentrations (1600 and 1800 ppm

respectively) and display negative Ce anomalies (Ce/Ce* 0.69 and 0.72). The petrological observations of these two samples indicate that subtle weathering textures have formed at grain edges, which, together with the negative Ce anomaly, is considered to reflect some additional REY enrichment through early weathering. Downhole in DDH0004, the uppermost sample located nearest to the base of the weathering profile has REY concentrations of 1644 ppm, and strong negative Ce anomaly (Ce/Ce* = 0.56). The extremely high REY values (> 1500 ppm) are, therefore, probably not indicative of the fresh bedrock protolith, which has an average REY concentration of 1010 ppm by excluding these three values.

Nb-rich samples are on average slightly more enriched in REE than the Nb-poor and rim samples (1156 ppm REY vs 981 ppm REY, excluding samples with suspected contribution from weathering). Rim granite samples have similar REE concentrations to Nb poor samples. (940 ppm REY)

All samples are LREE-enriched, LREE values are constant across the samples, but HREE values more variable. Nb-rich samples are more enriched in HREE and Y than Nb-poor samples (see Y/Nb plots in Figure 5.13). Excluding samples with weathering contributions, Y and HREE concentrations range from 132 – 318 ppm Y and 56 – 138 ppm HREE for Nb-rich samples, and 112 – 197 ppm Y and 43 – 85 ppm HREE for Nb-poor samples. The rim granite samples have Y and HREE concentrations that are comparable to the Nb-poor samples.

Chondrite-normalised REE patterns show that all fresh granite samples have the same REE trend, and are strongly enriched above chondritic values by factors of 100 – 1,000 (Figure 5.14). All biotite granite samples exhibit a LREE-enriched trend with La_N/Yb_N values between 5.4 and 18.3, and have strongly negative Eu anomalies ($0.05 < Eu_N/Eu^*_N < 0.3$). LREE are strongly fractionated ($3.9 < La_N/Sm_N < 7.9$), while HREE trends are nearly flat ($0.9 < Gd_N/Yb_N < 1.5$).

There are small differences between the samples groups; rim samples have more pronounced negative Eu anomalies than granite samples under the plateau area (0.05 – 0.12 Eu_N/Eu^*_N vs 0.14 – 0.3 respectively), and Nb-rich samples are less fractionated than Nb-poor samples with La_N/Yb_N values of 5.4 – 8.5 vs 8.5 – 18.3 respectively.

The downhole element plots in Figure 5.15 also show that the samples collected in this study are consistent with the drill hole assay database, and therefore can be reliably compared with the assay data collected by the company.

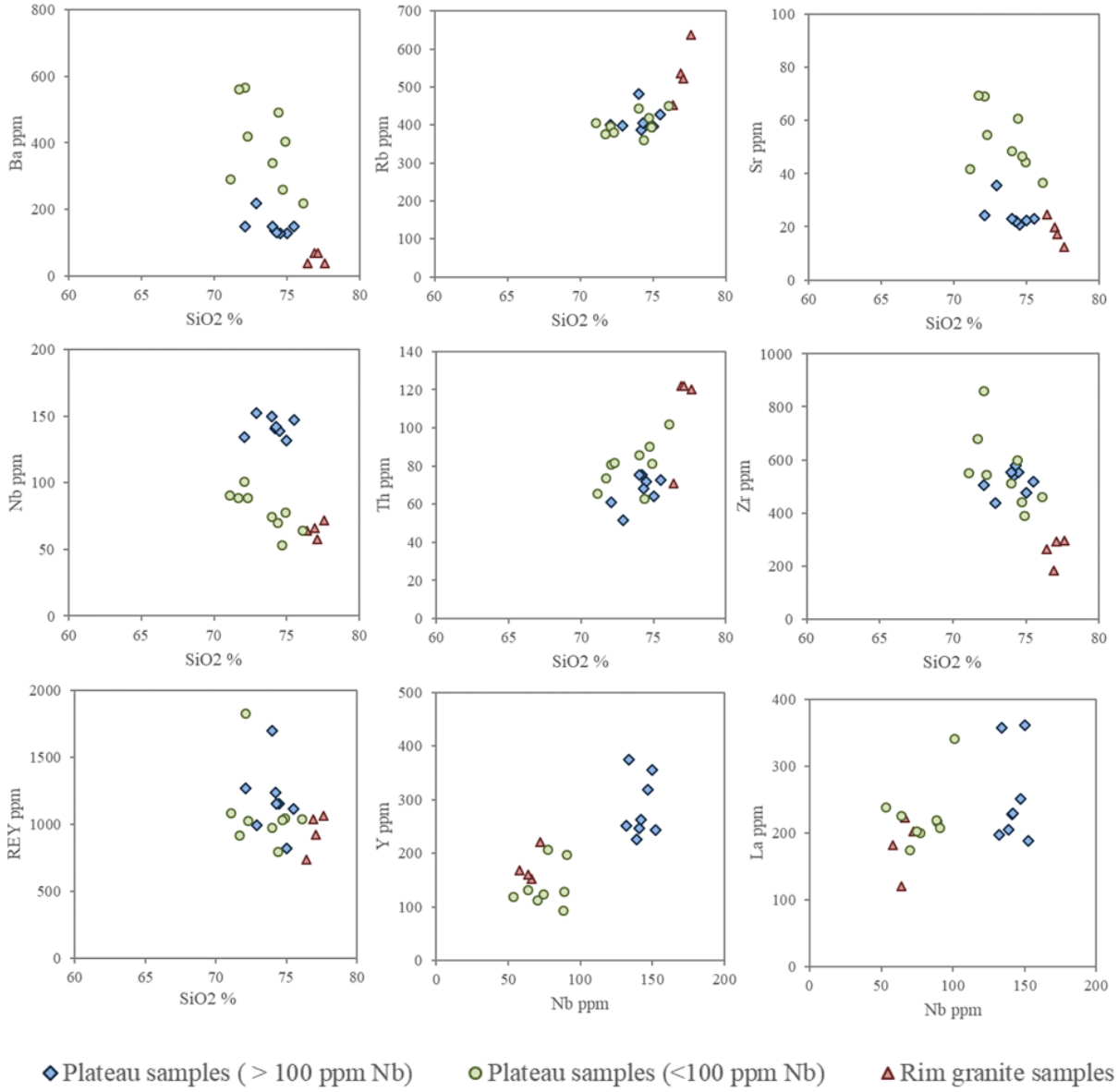


Figure 5.13. Trace element plots for granite bedrock samples, showing relationships between selected elements for the three groups of bedrock samples.

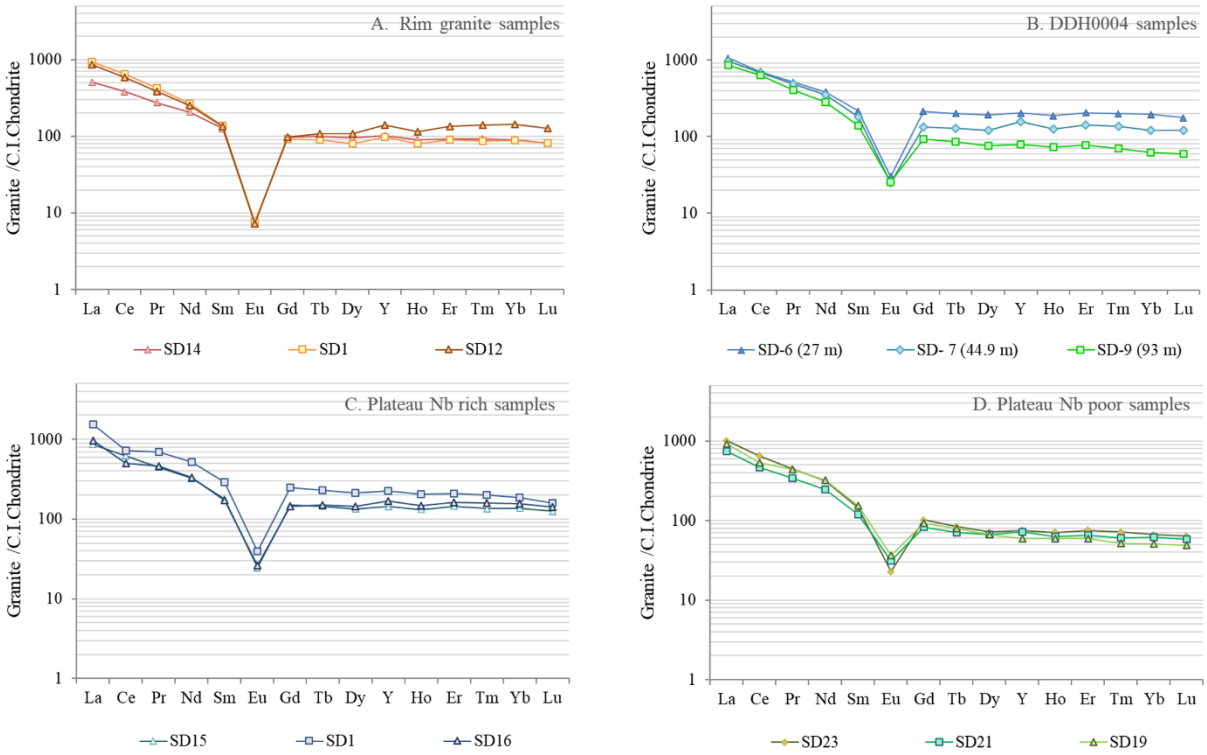


Figure 5.14. Chondrite-normalised REE patterns for granite samples. Note Y is plotted as a pseudolanthanide with atomic mass intermediate between Dy and Ho.

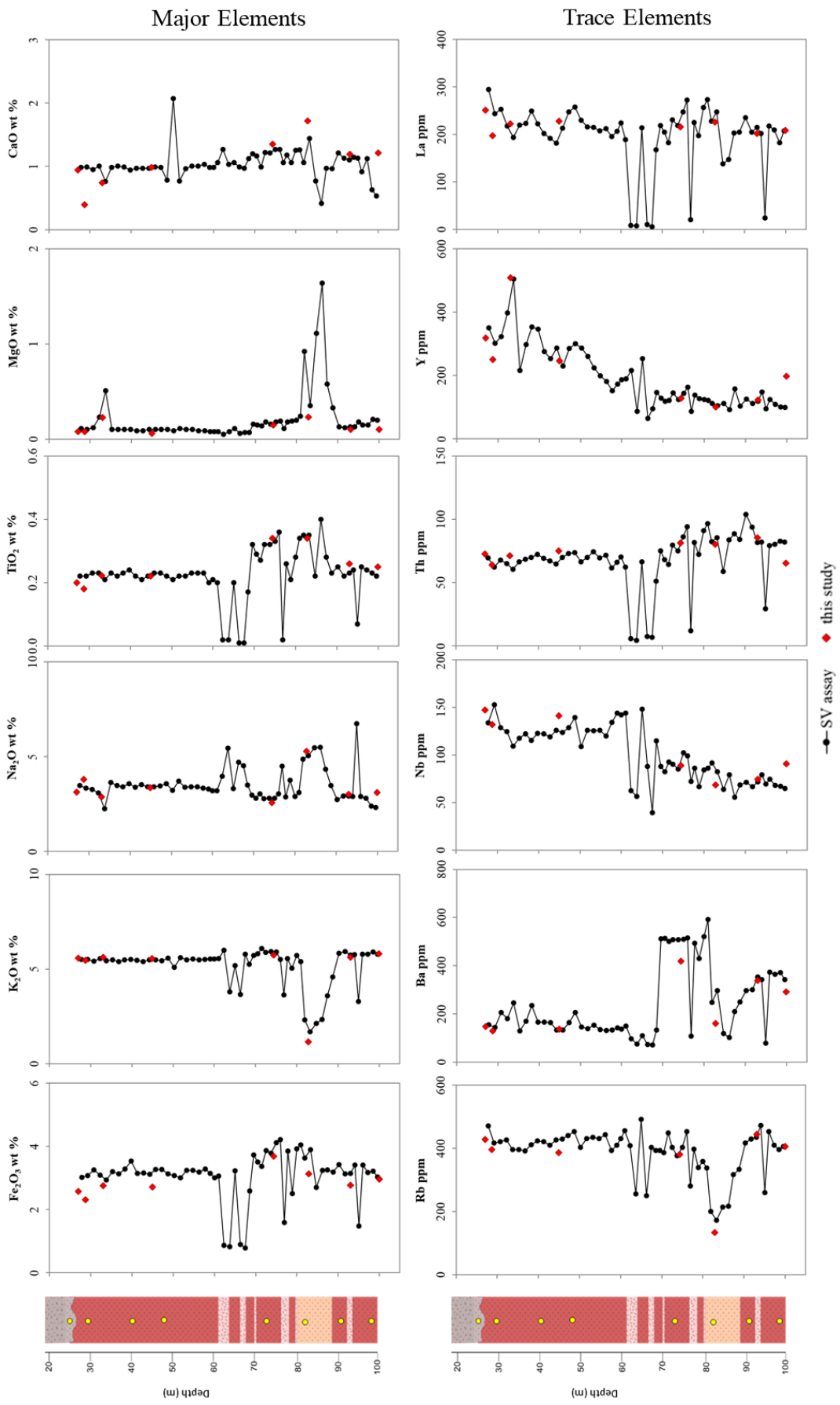


Figure 5.15. Downhole drill hole assay data (black) and samples analysed in this study (red) for both major (top) and trace (below) elements.

Table 5.2. Geochemical composition of granite samples collected from 100 m of DDH0004 drill core, analysed at NHM (SD26 and SD27 only) and ALS.

			Whole Rock									
Sample #			SD4	SD5	SD6	SD26	SD7	SD27	SD25	SD8	SD9	SD10
drill core			4	4	4	4	4	4	4	4	4	4
depth			26.50	27.50	28.73	33.00	44.93	51.00	74.35	82.82	93.05	99.99
Element	Unit	LOD										
SiO_2	%	0.01	72.1	75.5	75	71.688	74.2	72.464	72.3	75.2	74	71.1
Al_2O_3	%	0.01	13	12.55	13.5	13.023	12.65	13.427	12.4	13.7	12.55	12.95
Fe_2O_3	%	0.01	2.63	2.58	2.31	2.7536	2.72	2.7546	3.69	3.13	2.77	2.97
CaO	%	0.01	0.93	0.94	0.39	0.7418	0.98	0.4466	1.35	1.72	1.19	1.21
MgO	%	0.01	0.07	0.08	0.08	0.2254	0.06	0.1836	0.15	0.23	0.1	0.1
Na_2O	%	0.01	3.15	3.13	3.8	2.8751	3.36	2.3751	2.58	5.28	3.01	3.11
K_2O	%	0.01	5.81	5.58	5.45	5.6246	5.56	6.3312	5.73	1.15	5.61	5.8
Cr_2O_3	%	0.01	<0.01	<0.01	<0.01	n.a.	<0.01	n.a.	<0.01	0.01	<0.01	<0.01
TiO_2	%	0.01	0.22	0.2	0.18	0.2221	0.22	0.2384	0.34	0.34	0.26	0.25
MnO	%	0.01	0.04	0.05	0.03	0.1309	0.03	0.0326	0.05	0.04	0.04	0.04
P_2O_5	%	0.01	0.01	<0.01	0.01	<0.02	0.02	<0.02	0.03	0.03	0.02	0.03
SrO	%	0.01	<0.01	<0.01	<0.01	<0.01	<0.01	0.0055	<0.01	<0.01	<0.01	<0.01
BaO	%	0.01	0.02	0.02	0.02	0.04	0.02	0.0426	0.05	0.02	0.04	0.03
LOI	%	0.01	0.63	0.89	0.38	1.07	0.6	0.949	0.64	0.4	0.48	0.7
Nb	ppm	0.2	134	147	132	n.a.	141	n.a.	88.8	68.5	74.5	90.8
Ta	ppm	0.1	8.5	9	9.1	n.a.	8.8	n.a.	5.8	4.5	4	7.7
Ga	ppm	0.1	39.4	39.6	40.6	n.a.	37.4	n.a.	34	34.9	33.9	38
Ba	ppm	0.5	149.5	147.5	128.5	n.a.	136	n.a.	418	159.5	339	291
Rb	ppm	0.2	401	428	396	n.a.	386	n.a.	381	133	444	405
Sr	ppm	0.1	24.3	23.1	22.4	n.a.	22.1	n.a.	54.6	78.6	48.5	41.6
Th	ppm	0.05	60.8	72.8	63.9	71.354	75.2	91.811	81.4	80.3	85.5	65.4
U	ppm	0.05	6.51	9.85	8.6	10.203	10.75	7.2047	10.3	7.15	9.8	8.36
V	ppm	5	10	11	9	n.a.	5	n.a.	7	11	8	12
Sn	ppm	0.03	14	13	9	n.a.	8	n.a.	19	16	9	16
W	ppm	1	3	4	6	n.a.	5	n.a.	5	1	3	4
Zr	ppm	2	505	518	477	n.a.	539	n.a.	545	759	513	549
Hf	ppm	0.2	17.2	18.5	16	n.a.	19.5	n.a.	16.7	21.5	14.7	16.7
Cr	ppm	10	10	20	10	n.a.	10	n.a.	20	20	10	20
Cs	ppm	0.01	1.68	2.3	2.04	n.a.	1.81	n.a.	2.29	1.4	2.02	2.39
La	ppm	0.5	358	251	197.5	222.35	228	209.35	216	226	202	208
Ce	ppm	0.5	343	428	308	994.29	415	236.3	393	422	390	360
Pr	ppm	0.03	62	47.5	38.2	37.416	44.6	32.003	40.7	44	37.5	39.6
Nd	ppm	0.1	246	174	137	138.19	161	104.8	142.5	154.5	127.5	144
Sm	ppm	0.03	45.5	31.9	24.4	27.887	26.9	17.543	23.2	24.8	20.4	24.2
Eu	ppm	0.03	2.83	1.69	1.23	1.5909	1.4	1.2876	1.57	2.02	1.45	1.6
Gd	ppm	0.05	58	42.3	24.6	38.621	26.5	14.628	21	21.8	18.45	25.7
Tb	ppm	0.01	9.62	7.21	4.61	8.492	4.6	2.5946	3.42	3.37	3.07	4.45
Dy	ppm	0.05	58.1	47.2	29.7	68.104	29.7	16.964	19.8	18.85	18.5	28
Ho	ppm	0.01	11.85	10.25	6.91	16.771	6.92	3.6013	4.34	3.66	3.94	6.13
Er	ppm	0.03	34.8	32.7	23.6	55.48	22.5	10.952	13.55	9.81	12.3	18.15
Tm	ppm	0.01	4.97	4.89	3.45	8.6708	3.39	1.6932	2	1.32	1.73	2.91
Yb	ppm	0.03	30	31.3	21.1	54.825	19.4	10.97	12.9	7.48	10.05	18
Lu	ppm	0.01	4.11	4.34	3.03	8.043	2.95	1.6186	1.84	1.07	1.45	2.59
Y	ppm	0.5	375	318	251	507.96	246	102.17	128.5	100.5	123	197.5
REY	ppm		1644	1432	1074	1074	1239	1239	1024	1041	971	1081
LREE	ppm		1115	976	731	731	903	903	838	895	797	803
HREE	ppm		153	138	92	92	89	89	58	46	51	80
Cu	ppm	1	1	<1	2	n.a.	<1	n.a.	4	6	1	1
Li	ppm	10	30	40	20	n.a.	30	n.a.	50	40	40	30
Pb	ppm	2	42	43	35	60.071	39	45.38	40	18	49	46
Sc	ppm	1	1	1	1	1.3457	1	3.1623	4	4	2	3
Zn	ppm	2	103	108	76	n.a.	103	n.a.	90	62	63	90
F	ppm	20	4570	5470	870	n.a.	4910	n.a.	5710	1170	5690	5320
Total	%		98.61	101.52	101.15	98.395	100.42	99.251	99.31	101.25	100.07	98.29
LaN/YbN			8.11	5.45	6.36	2.8	7.98	13.00	11.37	20.53	13.65	7.85
Eu/Eu*			0.17	0.14	0.15	0.15	0.16	0.25	0.22	0.26	0.23	0.20

Table 5.3. Geochemical composition of Serra Dourada granite drill core samples that were analysed at ALS.

			Whole Rock										Whole Rock			
Sample #			SD15	SD16	SD18	SD22	SD17	SD20	SD24	SD19	SD21	SD23	SD1	SD3	SD12	SD14
Drill core			121	99	20	40	61	266	71	75	96	28	9	9	2	7
Depth (m)			26.67	29.79	35.88	14.21	35.49	21.30	17.00	12.51	41.91	6.38	37.20	97.05	9.50	16.17
Element	Unit	LOD														
SiO_2	%	0.01	74.5	74.3	74	72.9	76.1	72.1	74.9	71.7	74.4	74.7	76.9	77.1	77.6	76.4
Al_2O_3	%	0.01	12.6	12.5	12.9	12.7	12.5	13.8	12.7	13.4	13.4	13.2	11.7	11.25	11.2	12.5
Fe_2O_3	%	0.01	2.8	2.6	3.22	2.66	2.39	3.96	2.45	3.72	3.08	2.64	2	1.93	1.9	1.86
CaO	%	0.01	0.96	0.73	1.01	0.91	1.19	1.21	1.12	1.2	0.63	1.16	0.88	1.01	0.83	0.98
MgO	%	0.01	0.06	0.06	0.07	0.13	0.13	0.18	0.06	0.14	0.13	0.19	0.04	0.07	0.04	0.02
Na_2O	%	0.01	3.28	3.2	3.24	3.08	2.47	3.13	3	3	3.2	3.39	2.86	2.65	2.46	3.15
K_2O	%	0.01	5.62	5.77	5.7	5.7	6.05	5.83	5.92	6.11	5.9	5.35	5.33	5.06	5.15	5.71
Cr_2O_3	%	0.01	<0.01	<0.01	<0.01	<0.01	0.01	<0.01	<0.01	<0.01	<0.01	0.01	<0.01	0.01	0.01	0.01
TiO_2	%	0.01	0.23	0.22	0.25	0.24	0.21	0.39	0.22	0.38	0.31	0.27	0.15	0.16	0.12	0.12
MnO	%	0.01	0.04	0.04	0.04	0.04	0.03	0.05	0.03	0.04	0.04	0.04	0.02	0.02	0.02	0.02
P_2O_5	%	0.01	0.01	0.02	0.01	0.02	<0.01	0.03	0.02	0.04	0.03	0.03	0.02	<0.01	0.01	<0.01
SrO	%	0.01	<0.01	<0.01	<0.01	<0.01	<0.01	<0.01	<0.01	<0.01	<0.01	<0.01	<0.01	<0.01	<0.01	<0.01
BaO	%	0.01	0.01	0.01	0.02	0.02	0.02	0.07	0.05	0.06	0.06	0.03	0.01	0.01	<0.01	<0.01
LOI	%	0.01	0.74	0.52	0.58	0.53	0.55	0.82	0.52	0.78	0.41	0.57	0.39	0.47	0.57	0.65
Nb	ppm	0.2	139	142	150	152.5	63.8	101	77.3	88.6	70.2	53.4	66.3	57.9	72.1	63.9
Ta	ppm	0.1	10.2	9.8	9.4	8.5	3.7	6.5	5.8	5.7	4.7	5.3	5	2.5	4	7.8
Ga	ppm	0.1	38.9	38.5	40	42.3	32	37.7	34	37.5	32.8	32.9	32.3	30.5	34.3	34.9
Ba	ppm	0.5	128	129.5	149.5	217	217	567	403	562	492	260	68.2	68.6	37	38.4
Rb	ppm	0.2	407	406	481	399	451	397	393	375	359	418	535	522	638	453
Sr	ppm	0.1	20.8	22.2	23.2	35.6	36.7	69.2	44.2	69.5	60.7	46.7	19.9	17.4	12.3	24.8
Th	ppm	0.05	71.7	68.2	75.2	51.6	102	80.8	81.3	73.4	62.8	90.3	122	122	120	70.9
U	ppm	0.05	11.1	10.95	11.95	8.63	12.5	10.35	11.3	8.58	8.32	10.7	18.55	11.8	17.45	12.85
V	ppm	5	<5	10	7	9	9	6	5	7	10	14	6	<5	5	8
Sn	ppm	0.03	9	7	15	5	8	15	9	14	10	13	15	7	13	26
W	ppm	1	4	34	4	1	1	3	2	4	2	2	3	1	2	2
Zr	ppm	2	552	579	554	439	460	861	389	679	600	440	184	292	296	265
Hf	ppm	0.2	19.7	20.2	18.3	14.9	15.8	22.5	12.4	18.8	16.9	13.7	7.6	11.6	11.4	12.3
Cr	ppm	10	10	20	20	20	30	10	20	10	20	20	20	20	20	20
Cs	ppm	0.01	2.05	1.73	3.23	1.87	1.68	2.73	1.7	2.11	2.34	1.78	1.25	0.77	0.98	1.9
La	ppm	0.5	205	230	362	189	226	341	200	219	174.5	238	223	182.5	203	120.5
Ce	ppm	0.5	380	306	441	280	411	425	368	328	285	400	399	329	362	235
Pr	ppm	0.03	41.4	43.1	65.1	33.2	40.5	59.5	36.1	41	31.8	41.2	39.1	31.9	35.8	25.5
Nd	ppm	0.1	148	151	237	119.5	134.5	219	123.5	148	111.5	143	123	104.5	116	94.2
Sm	ppm	0.03	26.5	25.4	43.3	20.5	21.3	39.3	19.2	22.9	17.55	21.6	20.5	18.45	20.1	18.7
Eu	ppm	0.03	1.38	1.48	2.22	1.41	0.93	3.3	1.4	2.06	1.75	1.28	0.43	0.46	0.41	0.42
Gd	ppm	0.05	29.8	28.6	49.2	22	17.45	44.8	18.45	18.55	16.3	20.2	18.25	17.4	19.5	19.4
Tb	ppm	0.01	5.26	5.4	8.28	4.12	3.08	7.82	3.22	2.85	2.53	3.02	3.27	3.25	3.93	3.56
Dy	ppm	0.05	33.2	35.3	52.1	27.4	18.7	52	22.5	16.3	16.25	17.65	19.7	21.6	26.6	23.5
Ho	ppm	0.01	7.19	8.11	11.15	6.36	4.13	12.8	5.52	3.24	3.46	3.86	4.35	4.85	6.2	4.95
Er	ppm	0.03	23.3	26.1	33.5	21.6	13.5	39.5	18.4	9.42	10.4	12	14.3	16	21.4	14.75
Tm	ppm	0.01	3.36	3.94	4.92	3.09	1.98	5.13	2.73	1.27	1.5	1.77	2.15	2.62	3.49	2.28
Yb	ppm	0.03	22.1	25.1	29.7	19.4	12.35	27.1	16.3	8.13	9.96	10.7	14.25	18.25	22.9	14.4
Lu	ppm	0.01	3.1	3.47	3.94	2.72	1.8	4.19	2.42	1.21	1.44	1.56	2.01	2.5	3.13	2
Y	ppm	0.5	225	263	355	244	131.5	546	206	93.2	112.5	118.5	152	168	221	160
REY	ppm		1155	1156	1698	994	1039	1826	1044	915	796	1034	1035	921	1065	739
LREE	ppm		832	786	1200	666	852	1132	767	780	638	865	823	684	757	514
HREE	ppm		97.5	107	144	84.7	55.5	149	71.1	42.4	45.5	50.6	60.0	69.1	87.7	65.4
Cu	ppm	1	6	2	1	1	2	2	3	2	3	5	2	3	4	3
Li	ppm	10	40	20	50	40	30	30	20	30	20	40	40	30	40	20
Pb	ppm	2	41	42	44	37	53	31	40	31	30	46	50	47	68	61
Sc	ppm	1	1	1	1	2	2	5	2	4	4	3	2	2	2	1
Zn	ppm	2	99	98	141	79	54	124	58	91	94	55	35	29	65	62
F	ppm	20	5110	3490	5480	4260	5180	4080	4690	4100	1140	4470	5780	5880	6080	5250
Total	%		100.8	99.97	101.04	98.93	101.6	101.52	100.99	100.57	101.59	101.53	100.3	99.74	99.91	101.42
LaN/YbN			6.30	6.22	8.28	6.62	12.43	8.55	8.34	18.30	11.90	15.11	10.63	12.05	6.02	5.68
Eu/Eu*			0.15	0.17	0.15	0.20	0.15	0.24	0.23	0.30	0.32	0.19	0.07	0.12	0.06	0.07

5.5 REE Mineralogy

This section examines the mineralogy of the samples underlying the plateau area, and provides descriptions of their occurrence, morphology and measured chemical composition (complete table of EMP analyses can be found in Appendix C2).

In the granite samples that were studied, REE are concentrated in the accessory minerals, which are more chemically and texturally variable than the major minerals. The accessory mineral phases identified in this study include apatite, Ce-minerals, fluorite, fluorcarbonates, rutile, niobiates, monazite, thorite, zircon and xenotime. There is also an unknown Y-silicates present. Except for fluorite, all of these minerals occur in clusters, and are spatially associated with biotite crystals. These minerals are abundant, which can be seen from the bright phases in Figure 5.16.

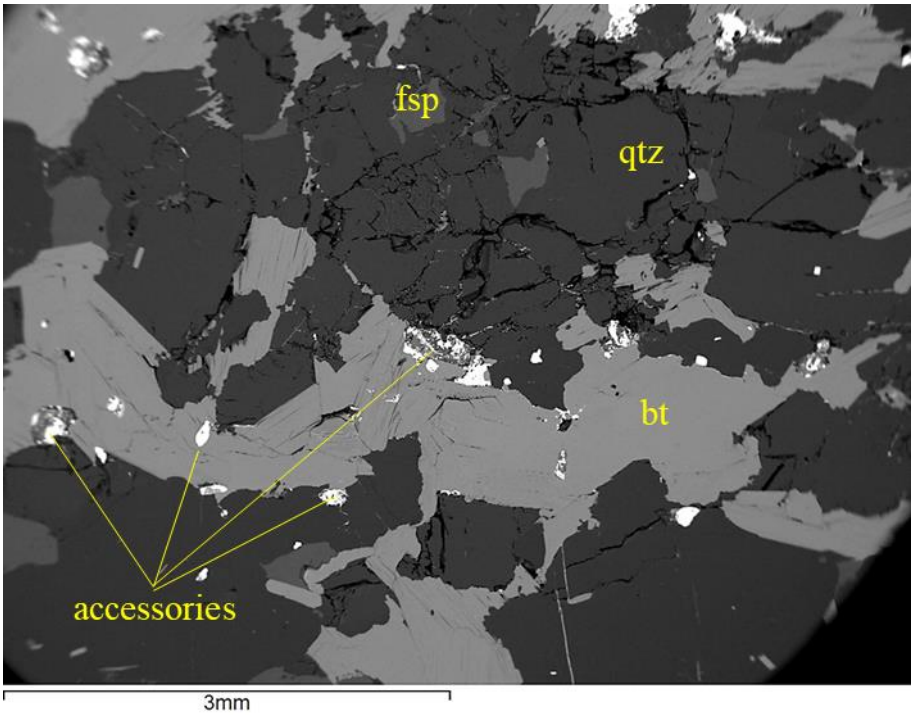


Figure 5.16. SEM-BSE image showing the abundance of bright REE-bearing accessory phases in a typical granite bedrock sample. Mineral abbreviations on pg 23.

5.5.1 Zircon

Petrography

Zircon is the most common accessory mineral found in the biotite granite and occasionally occurs throughout the granite as inter-granular crystals, but is most concentrated around, or included within, biotite crystals. The grains are euhedral to subhedral and are on average 100 μm in size. Larger grains are typically elongate and are observed in sizes up to 300 μm. The majority of the zircons have smooth edges and rounded corners, but some have rough edges suggestive of corrosive-interaction at the grain edges, and are sometimes engulfed by other accessory minerals such as fluorite, niobiate, or xenotime (Figure 5.17; panels E, G). Many of the imaged zircon grains are fractured and contain inclusions of thorite and monazite (Figure 5.19). Fractures cutting across zircons are frequently infilled with Ce oxides. In the SEM-BSE imagery, two kinds of internal textures can be observed in the zircon grains:

The first is characterised by concentric, well-defined rims that zone outwards from a homogenous core and can be distinguished by small differences in BSE response. Rims are a typical primary feature of zircon crystals which represent growth zones with slight chemical variations (Hoskin & Schaltegger 2003).

The second texture, which is present in the majority of the zircons imaged, is characterised by low BSE responses, and irregular patches that overprint the primary growth rims. These darker patches tend to preferentially replace individual growth zones, or the core, and are connected to cracks that run through the crystal. They have a more complex shape, have sharp edges that appear ragged, and exhibit lower relief. These irregular patches with low BSE response have been observed in zircons from other parts of the world (e.g. Nasdala et al. 2009) where they are recognised as secondary features produced by hydrothermal alteration or radiation damage.

Analytical results

A total of 65 zircon crystals were analysed by EMP, and both the normal and the patchy zircons occur throughout the drill holes that were sampled (representative grains from three depths are presented in Table 5.4). The clean cores and rims have a stoichiometric composition with ~32 wt % SiO_2 and ~65 wt % ZrO_2, minor concentrations of Hf and trace quantities of Th, U, Y and P. The Hf content in the zircon averages 1.66 wt % HfO_2 and the atomic ratio Hf/(Hf+Zr), which is sensitive to the proportion of the Hf end-member ($HfSiO_4$), varies from 0.011 to 0.022 indicating that the zircon compositions are normal according to the classification of Neves et al. (1974).

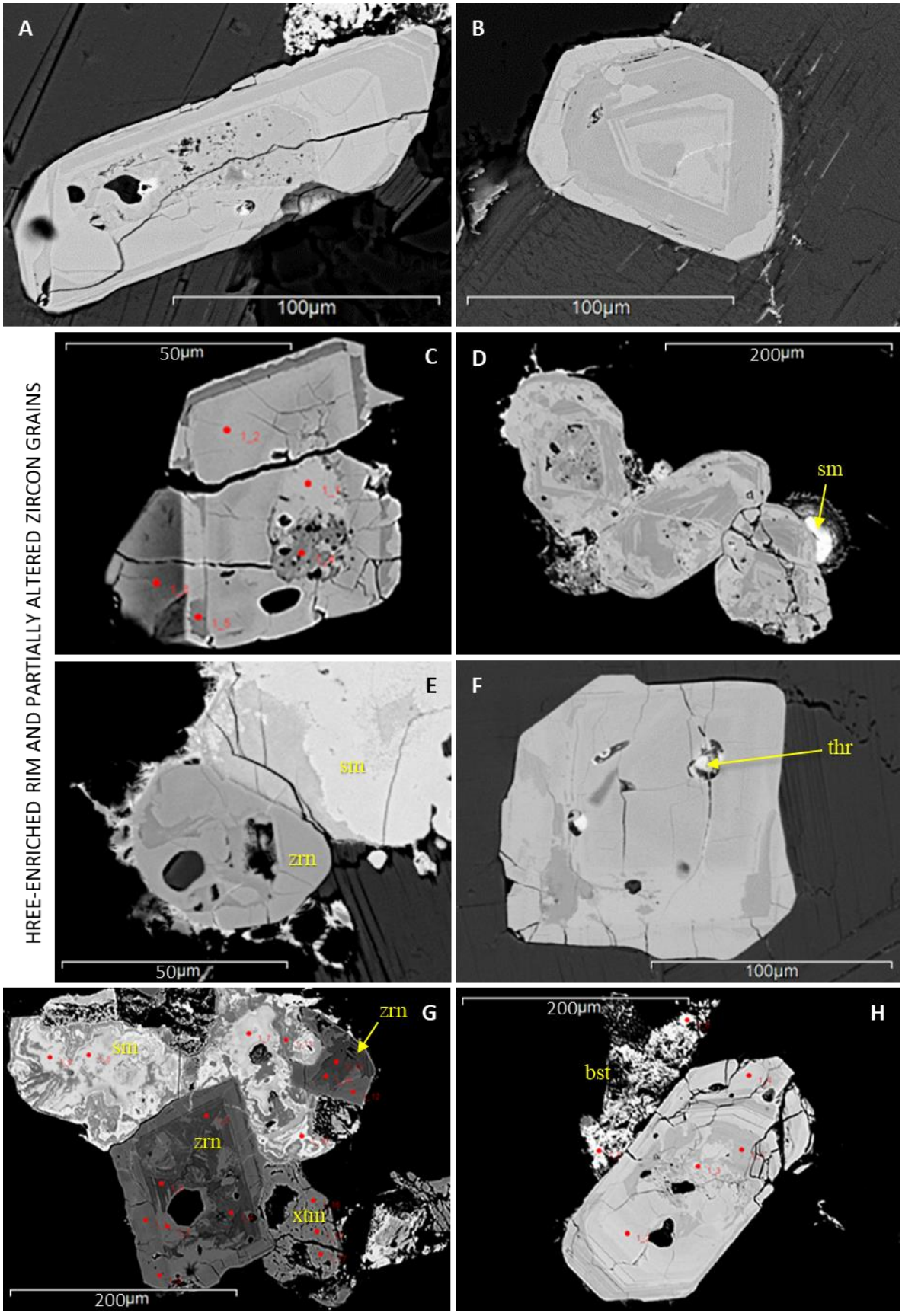


Figure 5.17. SEM-BSE images or representative zircon grains and their textures found in granite samples analysed, showing zonation (A and B), alteration and inclusion features (C, D, E, F) and association with niobiate, phosphate, and fluorcarbonate minerals (G and H). Mineral abbrv. on pg 23.

Table 5.4. EPMA of selected zircon grains from biotite granite samples underlying SV deposit, including representative zircon grains that show REE-enrichment zones, as well as non-altered and normal grains.

	Zircon - unaltered										Zircon - altered patches									
Sample	SD19	SD23	SD24	SD25	SD27	SD4	SD5	SD6	SD7	SD9	SD21	SD23	SD24	SD24	SD27	SD4	SD5	SD6	SD7	SD9
#	Z-296	Z-282	Z-354	Z-355	Z-107	Z-14	Z-25	Z-55	Z-98	Z-232	Z-348	Z-290	Z-128	Z-142	Z-122	Z-7	Z-29	Z-67	Z-95	Z-218
ZrO_2	64.2	64.4	66.5	65.9	62.7	64.3	65.8	64.8	64.8	62.2	43.4	47.4	38.8	58.3	42.6	45.0	42.9	33.4	47.1	39.3
HfO_2	1.99	1.66	1.52	1.55	2.01	3.01	1.55	1.55	1.42	4.43	1.21	0.77	1.38	1.41	1.36	1.44	1.67	0.86	1.07	1.08
SiO_2	31.4	31.6	31.5	31.6	31.2	31.7	31.9	31.4	31.9	31.4	28.2	26.5	27.2	28.7	27.8	27.7	24.6	26.3	27.2	26.1
Al_2O_3	0.15	<dt	<dt	<dt	<dt	<dt	<dt	<dt	<dt	<dt	1.15	1.79	1.61	0.19	1.27	0.62	1.00	1.49	1.66	1.76
P_2O_5	<dt	0.07	<dt	<dt	<dt	0.08	<dt	<dt	<dt	<dt	0.68	<dt	0.36	0.23	0.24	0.78	0.51	<dt	0.37	0.40
CaO	<dt	<dt	<dt	<dt	0.05	<dt	<dt	<dt	<dt	<dt	0.43	1.30	0.84	0.19	0.90	0.39	0.28	0.53	0.61	0.97
FeO	0.77	0.33	<dt	0.20	0.16	<dt	0.17	<dt	0.21	0.04	0.41	0.91	1.39	0.32	0.71	0.84	1.01	3.42	0.39	0.20
MnO	<dt	<dt	<dt	<dt	<dt	<dt	<dt	<dt	<dt	<dt	<dt	<dt	0.09		0.23	0.10	0.05	0.23	0.54	0.39
Nb_2O_5	<dt	<dt	<dt	<dt	<dt	<dt	<dt	<dt	<dt	<dt	0.14	<dt	0.59	0.20	0.41	0.41	1.13	0.55	0.45	<dt
Ta_2O_5	<dt	<dt	<dt	<dt	<dt	<dt	<dt	<dt	<dt	<dt	<dt	<dt	<dt	<dt	<dt	<dt	<dt	<dt	<dt	<dt
ThO_2	<dt	0.13	<dt	<dt	0.11	<dt	<dt	<dt	0.08	<dt	0.19	0.35	0.10	0.25	<dt	0.11	0.40	0.17	0.24	0.21
UO_2	<dt	0.27	<dt	<dt	0.31	<dt	<dt	<dt	<dt	<dt	0.62	1.37	0.89	0.55	0.70	0.30	0.47	0.77	0.50	1.10
Y_2O_3	0.09	0.31	0.16	0.15	0.62	0.29	0.38	0.40	0.50	0.26	4.09	4.14	3.61	0.98	2.27	2.73	6.53	4.98	4.51	4.37
La_2O_3	<dt	<dt	<dt	<dt	<dt	<dt	<dt	<dt	<dt	<dt	<dt	<dt	<dt	<dt	<dt	<dt	<dt	<dt	<dt	<dt
Ce_2O_3	<dt	<dt	<dt	<dt	<dt	<dt	<dt	<dt	<dt	<dt	0.09	0.98	0.82	<dt	<dt	0.29	1.11	1.07	1.03	0.76
Pr_2O_3	<dt	<dt	<dt	<dt	<dt	<dt	<dt	<dt	<dt	<dt	<dt	<dt	<dt	<dt	<dt	<dt	<dt	<dt	<dt	0.07
Nd_2O_3	<dt	<dt	<dt	<dt	<dt	<dt	<dt	<dt	<dt	<dt	<dt	<dt	0.09	<dt	0.11	<dt	<dt	<dt	<dt	<dt
Sm_2O_3	<dt	<dt	<dt	<dt	<dt	<dt	<dt	<dt	<dt	<dt	<dt	<dt	0.10	<dt	0.09	0.07	0.05	0.05	<dt	0.06
Gd_2O_3	<dt	<dt	<dt	<dt	<dt	<dt	<dt	<dt	<dt	<dt	<dt	0.36	0.08	<dt	0.09	<dt	<dt	<dt	<dt	<dt
Tb_2O_3	<dt	<dt	<dt	<dt	<dt	<dt	<dt	<dt	<dt	<dt	0.05	0.05	0.08	<dt	<dt	0.05	<dt	<dt	<dt	<dt
Dy_2O_3	<dt	<dt	<dt	<dt	<dt	<dt	<dt	<dt	<dt	<dt	0.37	0.55	0.47	<dt	0.24	0.34	0.60	0.54	0.45	0.55
Ho_2O_3	<dt	<dt	<dt	<dt	<dt	<dt	<dt	<dt	<dt	<dt	0.12	<dt	<dt	<dt	<dt	<dt	0.17	0.14	0.15	<dt
Er_2O_3	<dt	<dt	<dt	<dt	<dt	<dt	<dt	<dt	<dt	<dt	0.49	0.82	0.37	0.15	0.25	0.31	0.95	0.69	0.49	0.52
Tm_2O_3	<dt	<dt	<dt	<dt	<dt	<dt	<dt	<dt	<dt	<dt	0.07	0.10	0.07	<dt	<dt	<dt	0.17	0.13	0.10	0.07
Yb_2O_3	<dt	<dt	<dt	<dt	0.12	<dt	<dt	<dt	<dt	<dt	0.68	0.96	0.54	0.25	0.20	0.43	1.83	1.26	0.96	0.70
Lu_2O_3	<dt	<dt	<dt	<dt	<dt	<dt	<dt	<dt	<dt	<dt	0.07	0.12	0.09	<dt	<dt	<dt	0.32	0.20	0.13	0.09
F	<dt	<dt	<dt	<dt	<dt	<dt	<dt	<dt	<dt	<dt	2.18	2.16	0.74	0.32	0.55	1.22	1.10	0.80	1.25	1.47
(-O)=F											0.92	0.91	0.31	0.13	0.23	0.52	0.46	0.34	0.53	0.62
Total	98.7	99.5	99.8	99.0	97.7	99.6	100.2	98.4	99.3	96.7	88.3	92.7	83.4	92.7	84.2	87.6	92.4	86.6	93.1	83.6
Cation proportions (based on 4 oxygen atoms)																				
Zr	1.05	1.05	1.08	1.07	1.04	1.05	1.06	1.06	1.05	1.03	0.82	0.88	0.78	1.03	0.85	0.87	0.85	0.71	0.87	0.80
Hf	0.02	0.01	0.01	0.01	0.02	0.03	0.01	0.01	0.01	0.04	0.01	0.01	0.02	0.01	0.01	0.02	0.02	0.01	0.01	0.01
Si	0.92	0.92	0.91	0.91	0.93	0.92	0.92	0.92	0.93	0.93	0.96	0.87	0.98	0.91	0.99	0.95	0.87	1.00	0.90	0.95
Al	0.01	0.00	0.00	0.00	0.00	0.00	0.00	0.00	0.00	0.00	0.05	0.07	0.07	0.01	0.05	0.03	0.04	0.07	0.06	0.08
P	0.00	0.00	0.00	0.00	0.00	0.00	0.00	0.00	0.00	0.00	0.02	0.00	0.01	0.01	0.01	0.02	0.02	0.00	0.01	0.01
Ca	0.00	0.00	0.00	0.00	0.00	0.00	0.00	0.00	0.00	0.00	0.02	0.05	0.03	0.01	0.03	0.01	0.01	0.02	0.02	0.04
Fe	0.02	0.01	0.00	0.00	0.00	0.00	0.00	0.00	0.01	0.00	0.01	0.03	0.04	0.01	0.02	0.02	0.03	0.11	0.01	0.01
Mn	0.00	0.00	0.00	0.00	0.00	0.00	0.00	0.00	0.00	0.00	0.00	0.00	0.00	0.00	0.01	0.00	0.00	0.01	0.02	0.01
Nb	0.00	0.00	0.00	0.00	0.00	0.00	0.00	0.00	0.00	0.00	0.00	0.00	0.01	0.00	0.01	0.01	0.02	0.01	0.01	0.00
Ta	0.00	0.00	0.00	0.00	0.00	0.00	0.00	0.00	0.00	0.00	0.00	0.00	0.00	0.00	0.00	0.00	0.00	0.00	0.00	0.00
Th	0.00	0.00	0.00	0.00	0.00	0.00	0.00	0.00	0.00	0.00	0.00	0.00	0.00	0.00	0.00	0.00	0.00	0.00	0.00	0.00
U	0.00	0.00	0.00	0.00	0.00	0.00	0.00	0.00	0.00	0.00	0.00	0.01	0.01	0.00	0.01	0.00	0.00	0.01	0.00	0.01
Y	0.00	0.00	0.00	0.00	0.01	0.00	0.01	0.01	0.01	0.00	0.07	0.07	0.07	0.02	0.04	0.05	0.12	0.10	0.08	0.08
La	0.00	0.00	0.00	0.00	0.00	0.00	0.00	0.00	0.00	0.00	0.00	0.00	0.00	0.00	0.00	0.00	0.00	0.00	0.00	0.00
Ce	0.00	0.00	0.00	0.00	0.00	0.00	0.00	0.00	0.00	0.00	0.00	0.01	0.01	0.00	0.00	0.00	0.01	0.01	0.01	0.01
Pr	0.00	0.00	0.00	0.00	0.00	0.00	0.00	0.00	0.00	0.00	0.00	0.00	0.00	0.00	0.00	0.00	0.00	0.00	0.00	0.00
Nd	0.00	0.00	0.00	0.00	0.00	0.00	0.00	0.00	0.00	0.00	0.00	0.00	0.00	0.00	0.00	0.00	0.00	0.00	0.00	0.00
Sm	0.00	0.00	0.00	0.00	0.00	0.00	0.00	0.00	0.00	0.00	0.00	0.00	0.00	0.00	0.00	0.00	0.00	0.00	0.00	0.00
Gd	0.00	0.00	0.00	0.00	0.00	0.00	0.00	0.00	0.00	0.00	0.00	0.00	0.00	0.00	0.00	0.00	0.00	0.00	0.00	0.00
Tb	0.00	0.00	0.00	0.00	0.00	0.00	0.00	0.00	0.00	0.00	0.00	0.00	0.00	0.00	0.00	0.00	0.00	0.00	0.00	0.00
Dy	0.00	0.00	0.00	0.00	0.00	0.00	0.00	0.00	0.00	0.00	0.00	0.01	0.01	0.00	0.00	0.00	0.01	0.01	0.00	0.01
Ho	0.00	0.00	0.00	0.00	0.00	0.00	0.00	0.00	0.00	0.00	0.00	0.00	0.00	0.00	0.00	0.00	0.00	0.00	0.00	0.00
Er	0.00	0.00	0.00	0.00	0.00	0.00	0.00	0.00	0.00	0.00	0.01	0.01	0.00	0.00	0.00	0.00	0.01	0.01	0.01	0.01
Tm	0.00	0.00	0.00	0.00	0.00	0.00	0.00	0.00	0.00	0.00	0.00	0.00	0.00	0.00	0.00	0.00	0.00	0.00	0.00	0.00
Yb	0.00	0.00	0.00	0.00	0.00	0.00	0.00	0.00	0.00	0.00	0.01	0.01	0.01	0.00	0.00	0.00	0.02	0.01	0.01	0.01
Lu	0.00	0.00	0.00	0.00	0.00	0.00	0.00	0.00	0.00	0.00	0.00	0.00	0.00	0.00	0.00	0.00	0.00	0.00	0.00	0.00
F	0.000	0.000	0.000	0.000	0.000	0.000	0.000	0.000	0.000	0.000	0.233	0.225	0.085	0.032	0.062	0.133	0.122	0.096	0.131	0.169
Σ cations	2.01	2.00	2.00	2.00	2.01	2.00	2.00	2.00	2.00	2.00	1.99	2.03	2.05	2.00	2.04	2.00	2.04	2.10	2.03	2.03
Σ A	1.09	1.08	1.09	1.09	1.08	1.08	1.08	1.08	1.08	1.07	1.01	1.15	1.06	1.09	1.04	1.03	1.16	1.10	1.12	1.07
Σ B	0.92	0.92	0.91	0.91	0.93	0.92	0.92	0.92	0.93	0.93	0.97	0.87	0.99	0.91	1.00	0.98	0.88	1.00	0.91	0.96

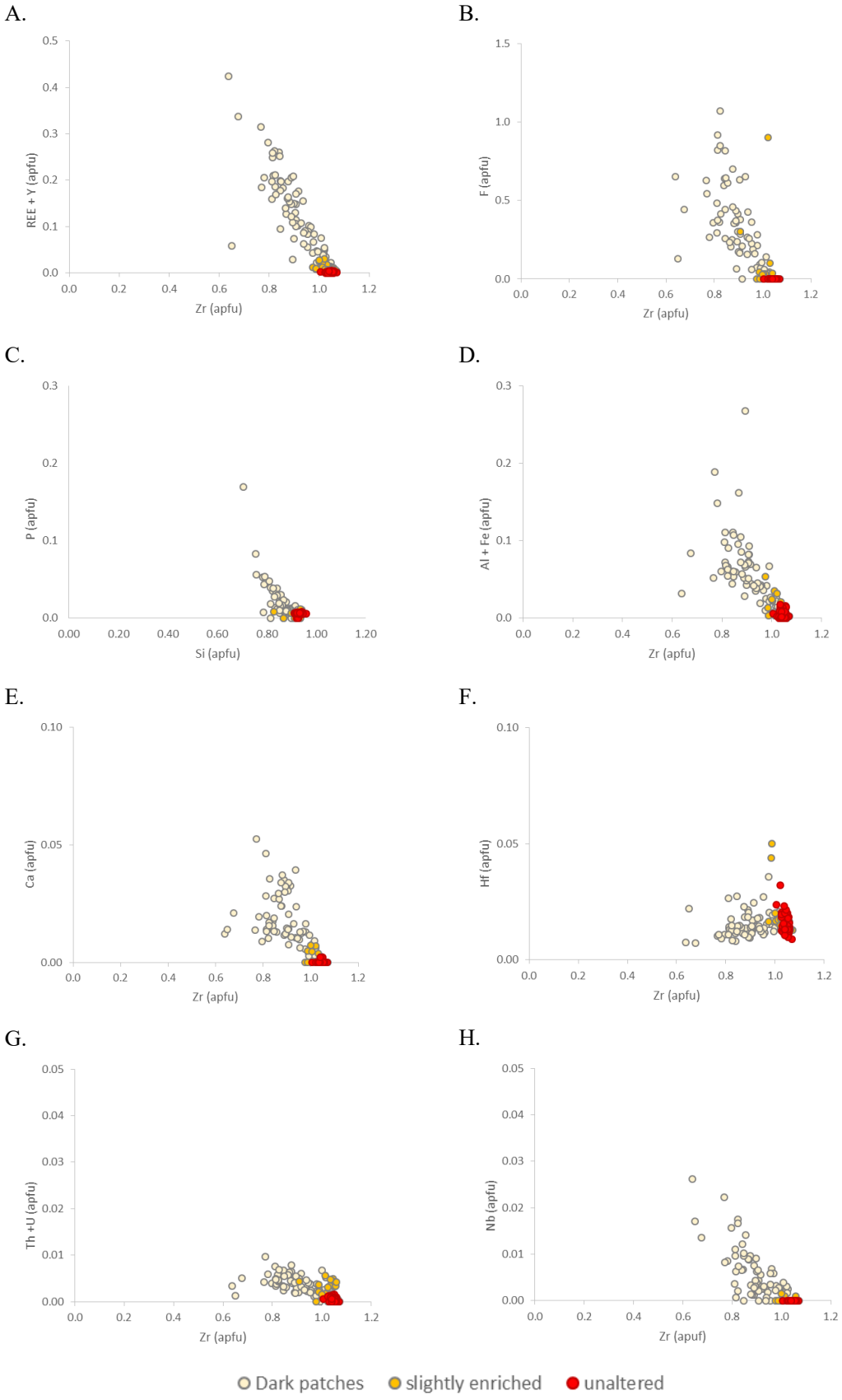


Figure 5.18. Selected element plots of EMP analysis on zircons. A. to G. REE + Y, F, Al + Fe, Ca, Nb, Th + U are plotted versus Zr; H. P versus Si. All plots in cations per formula unit (apfu).

Th and U, which preferentially concentrate in the thorite inclusions, are present in low concentrations in the zircon. Th values fall below the detection limit of the micro-probe and the UO_2 values range between below detection limit to 0.57 wt % with an average of 0.18 wt %. The average concentrations of Y_2O_3 and P_2O_5 in the zircons are 0.27 wt % and 0.25 wt % respectively, and are probably present as xenotime inclusions within the grains. REE may also be present in trace quantities, but values fall below the detection limit of the microprobe.

The chemical composition of the dark patches differs strongly from the normal zircon composition of Hoskin & Zchaltegger (2003) (Table 5.4, Figure 5.18). There are three main differences:

1. The dark patches have lower SiO_2 (24 – 28 wt %) and ZrO_2 (42 – 58 wt %) concentrations, and are characterised by strong enrichment of REE and Y. Up to 7 wt % $TREE_2O_3$ and up to 13 wt % Y_2O_3 have been measured. Magmatic zircons generally contain < 1 wt % TREE+Y, and grains with values above this threshold are considered to be altered zircons (Hoskin & Schaltegger 2003).

2. As well as REE and Y, the dark patches are composed of elevated levels of P_2O_5 (> 0.58 wt %) and small amounts of non-formula elements such as F (< 2 wt %), CaO (< 0.6 wt %), FeO (< 1.5 wt %), Al_2O_3 (< 2 wt %), Nb_2O_5 (< 1.6 wt %), and ThO_2 (< 0.44 wt %). Fe, Al, Nb, and P are known to substitute with REE and Y into zircon to help balance charge (see equations below). These coupled substitutions in the altered zircon are supported by the strong negative correlation observed between the non-formula elements and Zr (Figure 5.18).

$$(Al, Fe)^{3+}{}_{[interstitial]} + 4\,(Y, REE)^{3+} + P^{5+} = 4\,Zr^{4+} + Si^{4+}$$

$$(Y, REE)^{3+} + P^{5+} = 2\,Zr^{4+}$$

$$(Y, REE)^{3+} + (Nb, Ta)^{5+} = 2\,Zr^{4+}$$

(Source: Hoskin & Schaltegger 2006)

3. The dark zircon patches are characterised by low analytical totals with values ranging between 90 – 98 wt %. EDS-SEM of these dark patches confirm that the low totals are real and that no other elements were missed from the EMP analysis. The low totals therefore indicate altered zircon is hydrated and porous due to intra-crystal voids. Radiation damage from U and Th is the most common way to increase porosity in the zircon crystal structure. However, Nasdala et al. (2009) argue that radiation damage alone cannot explain such low totals in zircon

crystals, and that crystal damage by fluid-replacement alteration is more likely. High water content in the structure can be achieved by water substituting for SiO_4, or flooding pre-existing pore spaces with water.

Chondrite-normalised REE patterns of EMP point analysis on different parts of zircon grains clearly show the REE enrichment in the dark altered patches (Figure 5.19). The unaltered zircon has 100 – 1,000 times chondrite values of Y and Yb, which is typical for zircons (Hoskin & Schaltegger 2003) whereas the altered zircon has an order of magnitude higher with up to 10,000 times the chondrite-normalised value. The normalised pattern shows that the dark patches are strongly enriched in Y, HREE and Ce, and have a left-inclined REE trend. The incline is shallow with Lu_N/Gd_N values between 3 and 30. LREE are usually too large to fit within the zircon crystal structure, so to incorporate the concentration of Ce found by this analysis, the cation must be present as the smaller Ce^{4+} which has a similar ionic radius to Lu and may thereby substitute into the zircons (Hoskin & Schaltegger 2003).

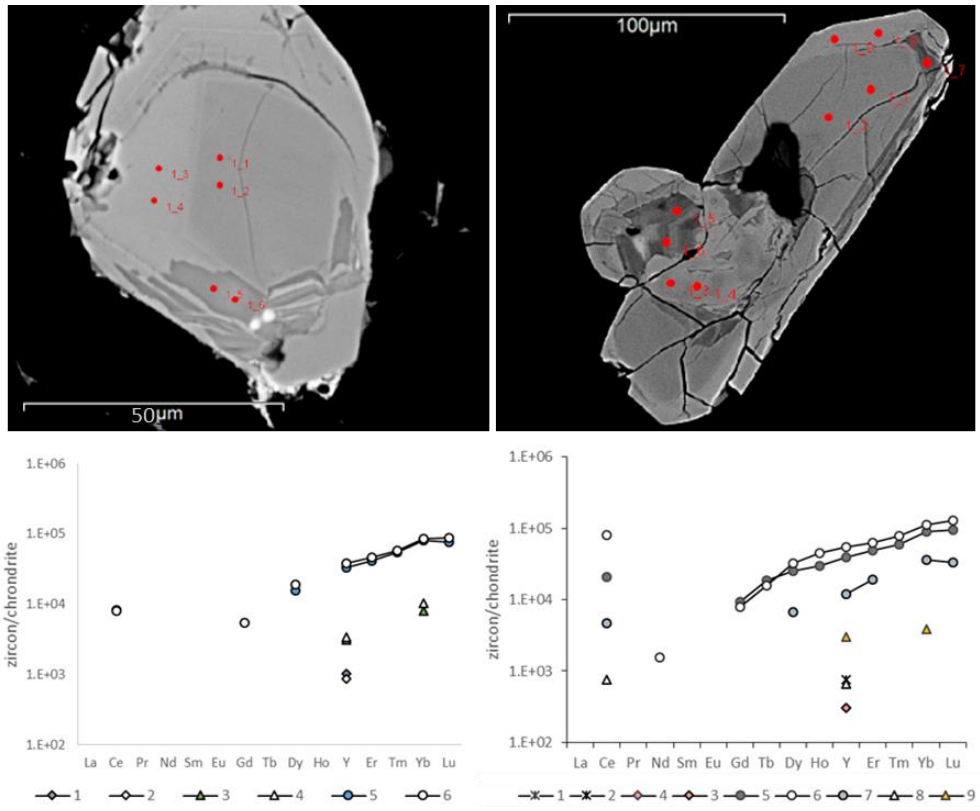


Figure 5.19. Back-scattered electron images of representative zircon grains that exhibit the dark altered patches (top) and corresponding chondrite-normalised REE patterns (below) of numbered EMP analysis points. Chondrite-normalising values are from McDonough & Sun 1995.

5.5.2 REE phosphates

REE phosphate minerals are scarce in all samples analysed, reflecting the low P_2O_5 contents in whole rock geochemistry of the granite.

5.5.2.1 Monazite

Two populations of monazite-(Ce) were distinguished on the basis of chemical composition and texture using SEM-BSE images. Monazite-I, which has a similar composition to the monazite analysed by Teixeira and Botelho (2002) from a different part of the Serra Dourada Complex, is very rare in samples analysed. The two grains that were found are subhedral crystals, ~0.5 mm in size, fractured and spatially associated with biotite (see panel H in Figure 5.20). Electron microprobe analyses show that this Monazite-I has high contents of Th (13.1 wt % ThO_2) and Si (2.4 wt % SiO_2; Table 5.5).

Monazite-II is the dominant monazite population in the drill core samples. Monazite-II can be found as subhedral to rounded grains, up to 300 μm in size, clustered with other accessory minerals around biotite, or sometimes within as inclusions. They are also found as anhedral < 50 μ interstitial grains between quartz and feldspars, as small inclusions in zircons, and as replacement rims on fluoro-apatites or titanites (Figure 5.20 and Figure 5.21), the last of which are most common in the samples with lower Nb concentrations (e.g. DDH0096, DD0075 and DDH0028).

Monazite-II is an Nd-rich monazite-Ce, depleted in Th (Table 5.5). Except for a few analyses that show values between 2 – 6 wt % ThO_2, Th is always below detection limit. Monazite-II has between 11.5 and 16 wt % Nd_2O_3 and a Ce/Nd atomic ratio of 1.8, while Monazite-I has ~9 wt % Nd_2O_3 and a 2.9 Ce/Nd atomic ratio. The second monazite population also has elevated CaO (1.7 – 4 wt %), $HREE_2O_3$ (1.1 – 3.0 wt %), Y_2O_3 (2.8 – 7.0 wt %), and lower than average CeO_2 (20 – 24 wt %) and SiO_2 (< 1.99 wt %). Small amounts of F (< 1.20 wt %), SO_3 (0.17 – 0.50 wt %), FeO_t (< 0.56 wt %), Al_2O_3 (< 1 wt %), and BaO (< 0.24 wt %) are also present in Monazite-II. In both EMPA and EDS-SEM analysis, the element totals for Monazite-II are low (90 – 96 wt %). From the uneven texture that can be observed in SEM-BSE images, the low total can be attributed to high crystal porosity. Despite the low totals, the stoichiometry fits well with the monazite chemical formula.

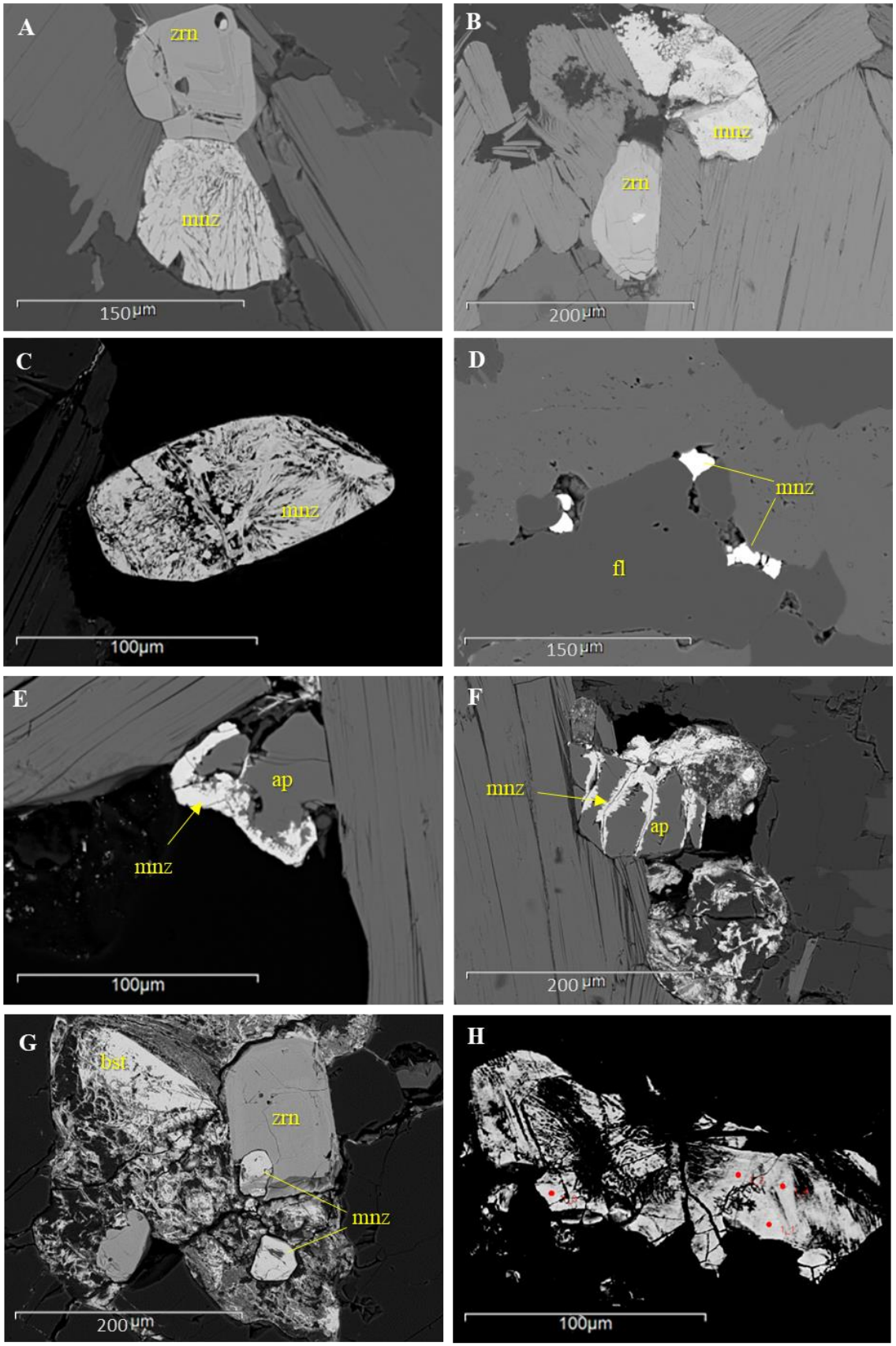


Figure 5.20. SEM-BSE images of monazite-Ce. A., B., and C. partly dissolved monazites; D. interstitial monazite associated with fluorite; E. and F. monazite replacing apatite; G. monazite included in zircon and LREE-fluorcarbonate with pseudomorphic texture; H. Th-rich monazite. Min. abbrv. pg 23.

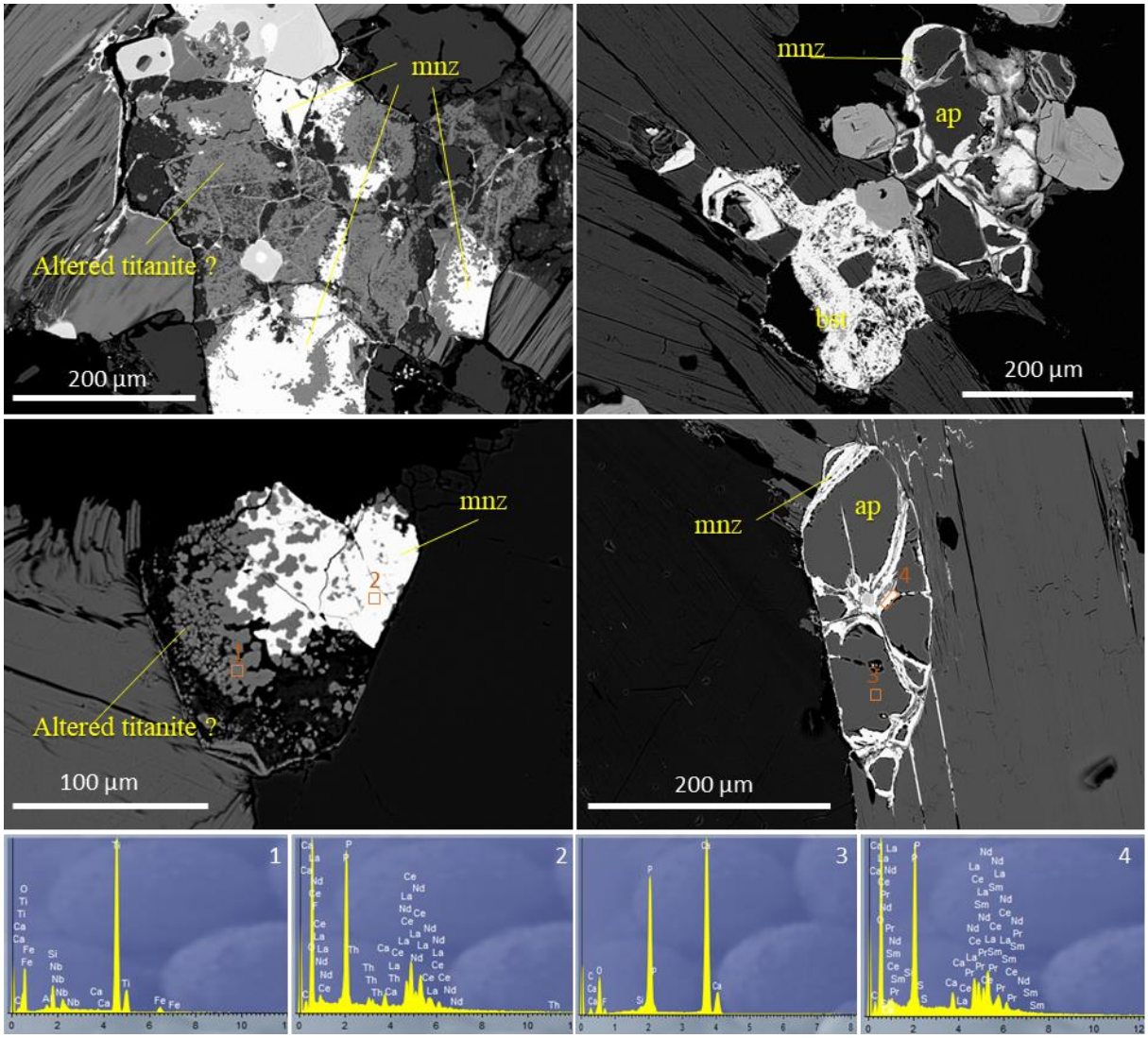


Figure 5.21. SEM-BSE images showing analysis points (red), and corresponding EDX spectra showing monazite replacement of titanite (images on the left) and replacement of apatite (images on the right). Mineral abbreviations on pg 23.

Representative chondrite-normalised REE patterns of the Monazite-I and Monazite-II are shown in Figure 5.22. Monazite-I has a steep LREE inclined pattern with a La/Gd_N ratio of 49 and matches that of the Monazite-(Ce) patterns obtained by Teixeira and Botelho (2002) and appears to be typical for high Th monazites (Catlos et al. 2013). The chondrite-normalised pattern of Monazite-II has a LREE inclined trend but is not so strongly fractionated with La_N/Gd_N ratios of 8 – 21. This is due to the strong HREE enrichment which flattens the pattern. Comparing the two patterns it is noticeable how, except for La and Ce, all the REEs are more enriched in the monazite-II than monazite-I. It also a noticeable that a small LREE discontinuity exists in the Monazite-II pattern; a convex-upward curved segment between Ce and Sm. A similar feature was observed by F rster (1998) in Th-poor Nd-rich hydrothermal monazite-(Ce) from granites from the Ergebirge-Fichtelgebirge region in Germany. Although

unusual for a monazite, the chondrite-normalised pattern for Monazite-II presented in Figure 5.22 were found to be consistent in 30 analyses carried out on different grains from different samples along the drill core and in core samples across the granite. Finally, it should be noted that the chondrite-normalised REE pattern of Monazite-II is very similar to that of the LREE-fluorcarbonates also found in the samples (see Figure 5.22).

Calcium can substitute into the monazite structure through coupled substitution with Si and Th. However, Monazite-II has a Ca content (0.8 – 0.15 apfu) in excess of both Th (< 0.003 apfu) and Si (< 0.006) which means Ca is not present in monazite as cheralite (Ca, Th)(P, Si)O_4. A strong positive correlation exists between both Ca and F, and Ca and LREE which suggests that Ca may be present in LREE-fluorcarbonates (Figure 5.23). The presence of fine intergrowths of LREE-fluorcarbonate with Nd-rich monazite would also explain some of the low element totals (as CO_2 is not measured during analysis) and the slightly higher ∑ A-site values (~1.04 apfu) than ∑ B site (~0.97 apfu). Unfortunately, this intergrowth cannot be verified with SEM-BSE images because both monazite and LREE-fluorcarbonates have similarly high reflectances. Carbonates have been observed together with altered monazites in other studies, for example Mariano et al. (1979) found fine carbonate veins in altered monazites from Araxa, Brazil. Although less significant, some of the excess Ca may also be associated with S in sulphate.

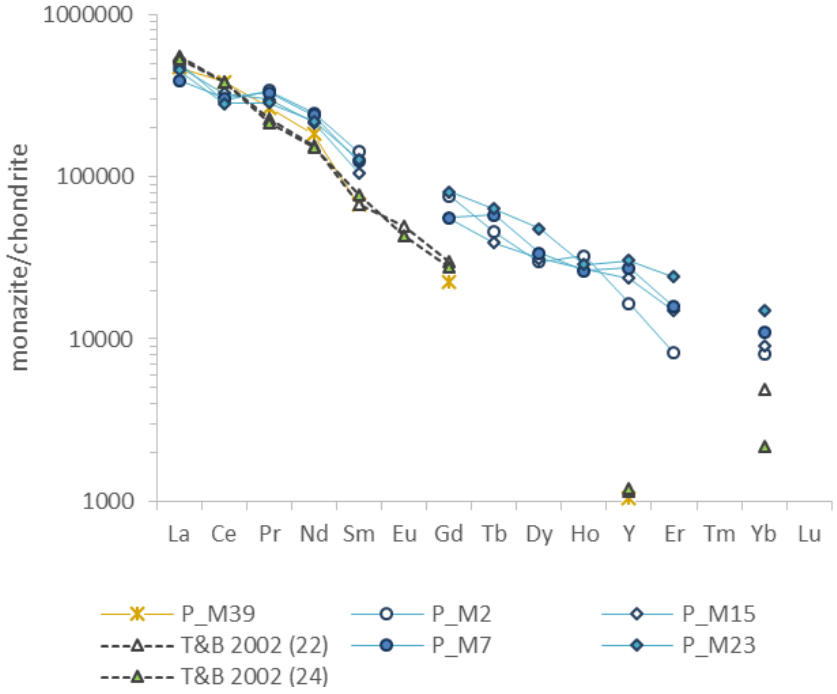


Figure 5.22. Chondrite-normalised REE patterns of monazite-II analyses and previously published data.

Table 5.5. EMP analyses of Th-poor and Th-rich Monazite-(Ce) grains. Monazite analyses from Teixeira and Botelho (2002) are also included for comparison.

Mineral	Monazite-I						Monazite-II						
Source	T&B 2002		SD21	SD21	SD21	SD4	SD4	SD4	SD4	SD5	SD25	SD10	SD10
Analitical No.	22	24	PM-90	PM-94	PM-96	PM_39	PM-9	PM-18	PM-20	PM-28	PM-45	PM-63	PM-68
P_2O_5	24.47	24.74	28.2	26.1	25.8	27.1	29.8	29.3	29.0	27.6	27.6	29.2	29.6
SiO_2	2.47	2.8	<dt	3.44	3.59	2.44	0.2	0.1	0.2	0.9	0.3	0.5	0.2
Y_2O_3	0.23	0.24	5.9	<dt	<dt	0.21	3.01	3.61	3.71	3.36	3.91	4.78	4.28
La_2O_3	15.41	14.84	7.4	16.9	16.7	13.1	12.0	13.1	12.8	14.1	14.8	13.1	13.1
Ce_2O_3	27.71	27.31	14.1	30.0	29.7	27.5	27.8	28.7	28.5	21.4	17.3	23.4	23.9
Pr_2O_3	2.46	2.32	1.97	2.34	2.43	2.88	3.09	2.72	2.73	3.67	4.16	3.25	3.30
Nd_2O_3	8.18	8.06	6.3	5.5	5.3	9.7	10.9	9.6	9.9	13.1	14.3	11.5	11.7
Sm_2O_3	1.16	1.32	1.40	0.50	0.46	1.2	1.97	1.61	1.65	2.46	2.86	2.11	2.16
Gd_2O_3	0.69	0.64	1.21	0.13	0.18	0.51	0.94	0.80	1.02	1.52	1.72	1.38	1.40
Tb_2O_3	n/a	n/a	0.23	0.06	<dt	<dt	0.17	0.19	0.22	0.19	0.20	0.16	0.20
Dy_2O_3	0.32	0.28	1.00	<dt	<dt	<dt	0.74	0.78	0.80	0.84	0.88	0.88	0.86
Ho_2O_3	n/a	n/a	<dt	<dt	<dt	<dt	<dt	0.20	<dt	0.20	<dt	0.17	0.15
Er_2O_3	n/a	n/a	0.37	<dt	<dt	<dt	0.17	0.30	0.31	0.33	0.20	0.27	0.31
Tm_2O_3	n/a	n/a	<dt	<dt	<dt	<dt	<dt	<dt	<dt	<dt	<dt	<dt	<dt
Yb_2O_3	0.09	0.04	0.31	<dt	<dt	<dt	0.09	0.15	0.13	0.16	0.15	0.17	0.17
Lu_2O_4	n/a	n/a	<dt	<dt	<dt	<dt	<dt	<dt	<dt	<dt	<dt	<dt	<dt
ThO_2	11.03	13.4	11.5	14.8	15.0	13.1	<dt	<dt	<dt	<dt	<dt	<dt	<dt
UO_2	0.14	0.28	0.54	0.53	0.60	0.2	0.55	0.27	0.33	0.52	0.43	0.34	0.35
CaO	0.43	0.44	3.22	0.11	0.11	1.0	3.37	3.26	2.81	3.46	2.94	3.20	3.26
Al2O3	n/a	n/a		<dt	<dt	<dt	0.11	0.14	0.11	0.26	<dt	0.21	0.11
FeO	n/a	n/a	0.2	<dt	<dt	<dt	0.06	0.12	0.06	0.09	<dt	0.33	0.27
F	n/a	n/a	<dt	<dt	<dt	<dt	0.96	1.08	1.11	0.81	0.80	0.70	0.55
(-O)=F							0.41	0.46	0.47	0.34	0.34	0.30	0.23
REE	56.0	54.8	34.3	55.5	54.7	54.9	57.8	58.2	58.0	57.9	56.6	56.3	57.3
REY	56.3	55.1	40.2	55.5	54.7	55.1	60.9	61.8	61.8	61.3	60.6	61.0	61.6
Total	94.8	96.7	83.8	100.5	99.8	98.8	95.5	95.7	94.9	94.6	92.3	95.2	95.7
Cation proportions (based on 4 oxygen atoms)													
P	0.84	0.88	1.04	0.89	0.88	0.92	0.98	0.97	0.97	0.93	0.96	0.96	0.98
Si	0.16	0.12	0.00	0.14	0.15	0.10	0.01	0.01	0.01	0.04	0.01	0.02	0.01
Σ site B	1.01	1.00	1.04	1.03	1.03	1.02	0.99	0.97	0.98	0.97	0.97	0.98	0.99
Y	0.003	0.005	0.136	0.000	0.000	0.004	0.062	0.075	0.078	0.072	0.086	0.099	0.089
La	0.228	0.231	0.114	0.135	0.138	0.120	0.000	0.000	0.000	0.000	0.000	0.000	0.000
Ce	0.413	0.421	0.005	0.004	0.005	0.002	0.004	0.002	0.003	0.004	0.004	0.003	0.003
Pr	0.034	0.036	0.119	0.250	0.248	0.194	0.172	0.188	0.186	0.207	0.225	0.188	0.188
Nd	0.111	0.121	0.225	0.440	0.439	0.406	0.395	0.410	0.410	0.312	0.260	0.334	0.342
Sm	0.013	0.019	0.031	0.034	0.036	0.042	0.044	0.039	0.039	0.053	0.062	0.046	0.047
Gd	0.004	0.004	0.097	0.079	0.077	0.140	0.151	0.134	0.140	0.187	0.210	0.160	0.163
Tb	0.008	0.009	0.021	0.007	0.006	0.016	0.026	0.022	0.022	0.034	0.041	0.028	0.029
Dy	0.001	0.004	0.000	0.000	0.000	0.000	0.000	0.000	0.000	0.000	0.000	0.000	0.000
Ho	-	-	0.017	0.002	0.002	0.007	0.012	0.010	0.013	0.020	0.023	0.018	0.018
Er	-	-	0.003	0.001	0.000	0.000	0.002	0.002	0.003	0.002	0.003	0.002	0.003
Tm	-	-	0.014	0.000	0.000	0.000	0.009	0.010	0.010	0.011	0.012	0.011	0.011
Yb	0.001	0.001	0.000	0.000	0.000	0.000	0.000	0.002	0.000	0.002	0.000	0.002	0.002
Lu	0.000	0.000	0.005	0.000	0.000	0.000	0.002	0.004	0.004	0.004	0.003	0.003	0.004
Th	0.16	0.13	0.000	0.000	0.000	0.000	0.000	0.000	0.000	0.000	0.000	0.000	0.000
U	0.003	0.002	0.004	0.000	0.000	0.000	0.001	0.002	0.002	0.002	0.002	0.002	0.002
Ca	0.01	0.02	0.150	0.005	0.005	0.041	0.140	0.136	0.119	0.148	0.130	0.134	0.136
Al	-	-	0.000	0.000	0.000	0.000	0.004	0.005	0.004	0.009	0.000	0.007	0.004
Fe	-	-	0.006	0.000	0.000	0.000	0.002	0.004	0.002	0.003	0.000	0.011	0.009
Σ site A	0.99	1.00	0.948	0.958	0.956	0.972	1.03	1.05	1.03	1.07	1.06	1.05	1.05
F	-	-	0.000	0.000	0.000	0.000	0.119	0.134	0.138	0.102	0.104	0.087	0.068

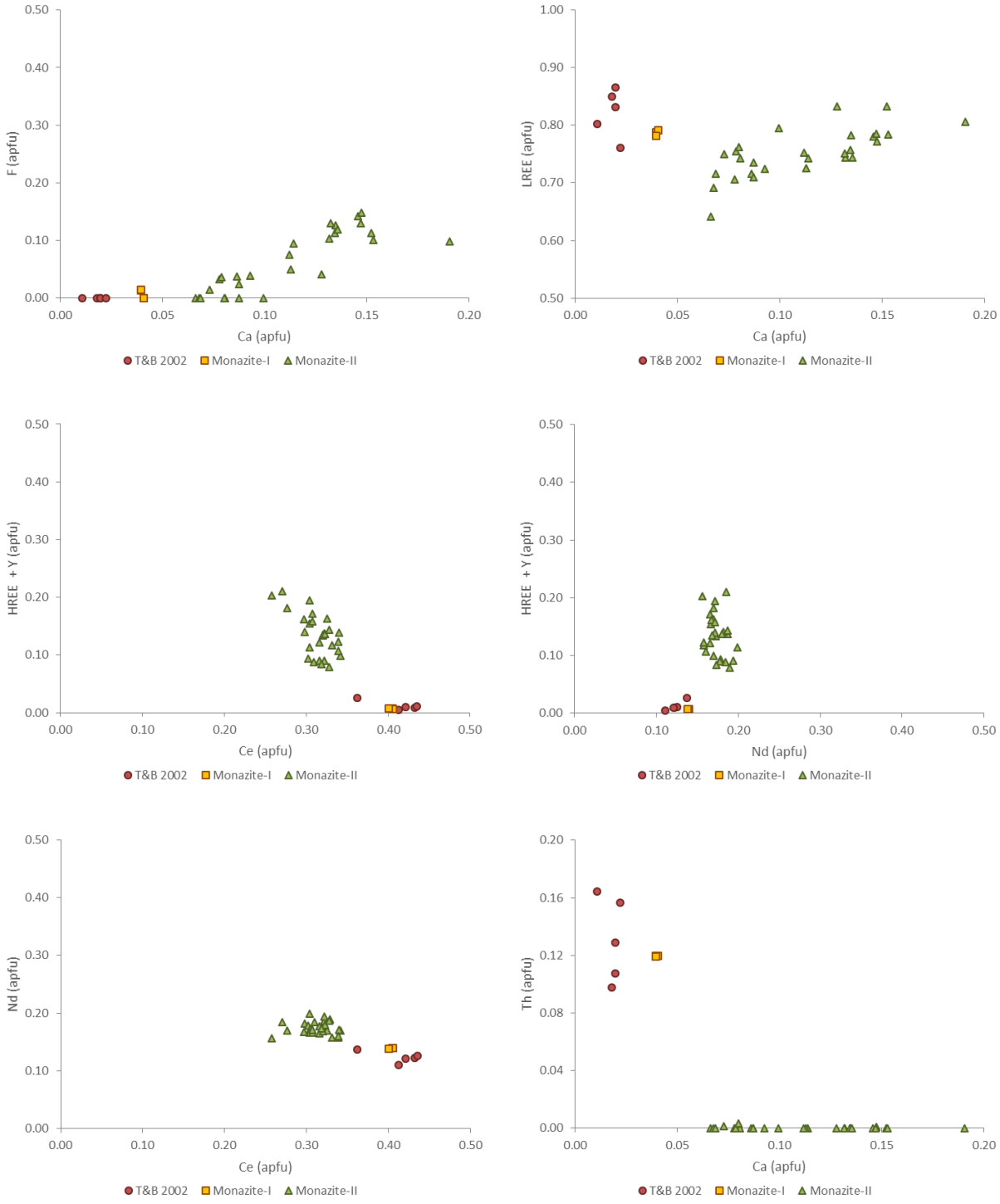


Figure 5.23. Apfu element plots for EMP analyses, showing monazite-I and -II compositions, and monazite analyses by Teixeira & Botelho (2002).

5.5.2.2 Xenotime

In the biotite granite underlying the Serra Verde deposit, xenotime occurs as subhedral elongate grains (Figure 5.24; panels A, B), as replacement rims or patches on apatite crystals (Figure 5.24; panels C, D), outer growths on monazites (Figure 5.24; E), inclusions in zircon, and anhedral grains associated with fluorite (Figure 5.24; F). The first two occurrences are the most common. Elongated subhedral grains are up to 200 microns in length and are frequently found in contact with, or engulfing, zircons. SEM-BSE images also show that the majority of these grains exhibit corrosive textures, and have Nb-rich crosscutting micro-veinlets, and fine LREE-fluorcarbonate overgrowths (Figure 5.24; panels G, H).

Electron microprobe analysis show that Y is the most abundant oxide, with values ranging between 43.7 -56 wt % Y_2O_3 (Table 5.6). The total REE concentrations range between 7 and 17 wt % REE_2O_3 and are dominated by HREE; Dy, Er, Yb account for > 70 % of the total REEs. The xenotimes also contain small amounts (< 1 wt %) of Ca, Fe, Si, Th, and U. Small but variable FeO contents are present, but have been omitted from Table 5.6 because previous studies have shown that Fe detected in xenotimes that are found next to biotites may be influenced by secondary fluorescence from biotite crystals (Franz et al. 1996).

The xenotimes analysed in this study can be divided into two groups: normal xenotime and fluorine-rich xenotime. The composition of the normal xenotime matches closely to chemical composition of xenotime grains from other parts of biotite granite in Serra Dourada Complex analysed by Teixeira & Botelho (2006), and the calculated composition of A-type biotite granite (Foster 1998). The only difference is that xenotime grains analysed in this study have lower Gd_2O_3 concentrations (~1.5 wt % vs ~3.35 wt %; Teixeira & Botelho (2006)).

The F-rich xenotimes are more common, and have an unusual composition characterised by five properties:

1. Very high F contents, that range from 5.8 to 10.5 wt % F. These are unusually high levels of F for xenotime, but still chemically feasible; similar compositions are noted in the Madiera Nb-Ta-Sn deposit of Pitianga, Brazil where Bastos-Neto & Pereira (2012) reported xenotimes with up to 5.1 wt % F in albitised parts of the granite.
2. Low P contents of 15 – 25 wt % P_2O_5. The concentration of P in the structural formula, even after adding Si, which can substitute for P, is below 1.0 (apfu). Other studies have found that P can be slightly underdetermined due to interferences with HREE (Franz et al. 1996). However, this effect is not sufficient to account for the missing P in F-rich

xenotimes, because P values for the normal xenotimes are within the expected formula range. Therefore, the P in these F-rich xenotimes is most likely depleted. Although there is a weak, negative correlation between P and F, it is not clear how the stochiometric deficiency in P is being compensated for in the crystal structure.

3. Low analytical totals of 90.2 – 96.0 wt %, which suggest F-rich xenotimes are likely porous or hydrated. The irregular and patchy textures of many of the grain observed in SEM-BSE images may indicate the presence of higher than average volatile contents.
4. Higher Y_2O_3 (49.43 – 56.00 wt %), and lower REE_2O_3 contents than normal xenotimes (8.9 – 12.5 wt %; see Figure 5.25).
5. Slightly higher U and Ca, but lower Th contents than normal xenotimes. In most analyses Th is below the detection limit, and UO_2 ranges between 0.19 – 0.58 wt %. The CaO content ranges between 0.28 – 0.66 wt %, and is negatively correlated with F (Figure 5.25).

Chondrite-normalised REE patterns for the normal xenotime group follows the flat HREE-enriched pattern of published data closely, with a steep LREE decline present in all xenotime analyses beginning at Dy, reflecting a stronger HREE fractionation (Yb_N/Gd_N = 2.43 ratio) than previously published analyses (Forster, 1998). However, F-rich xenotimes have strong HREE fractionation with Yb_N/Gd_N = 7.10 – 12.77 (Figure 5.26). The pattern appears to be shifted to the right, with the position of the steep decline starting at Ho rather than Gd. It is only the smaller HREE ions (Er-Lu) which remain enriched and exhibit flat patterns. The larger HREE ions (Gd to Ho) are instead depleted. It would appear that an increase of Y in the xenotime structure favours the incorporation of smaller HREE ions.

The pattern also highlights the strong fractionation between Y and Ho in F-rich xenotime; two elements considered to behave as a geochemical pair due to their similar ionic size and charge (Bau 1996). The Y/Ho for F-rich xenotimes ranges between 46 and 71, compared to a chondritic ratio of 28.

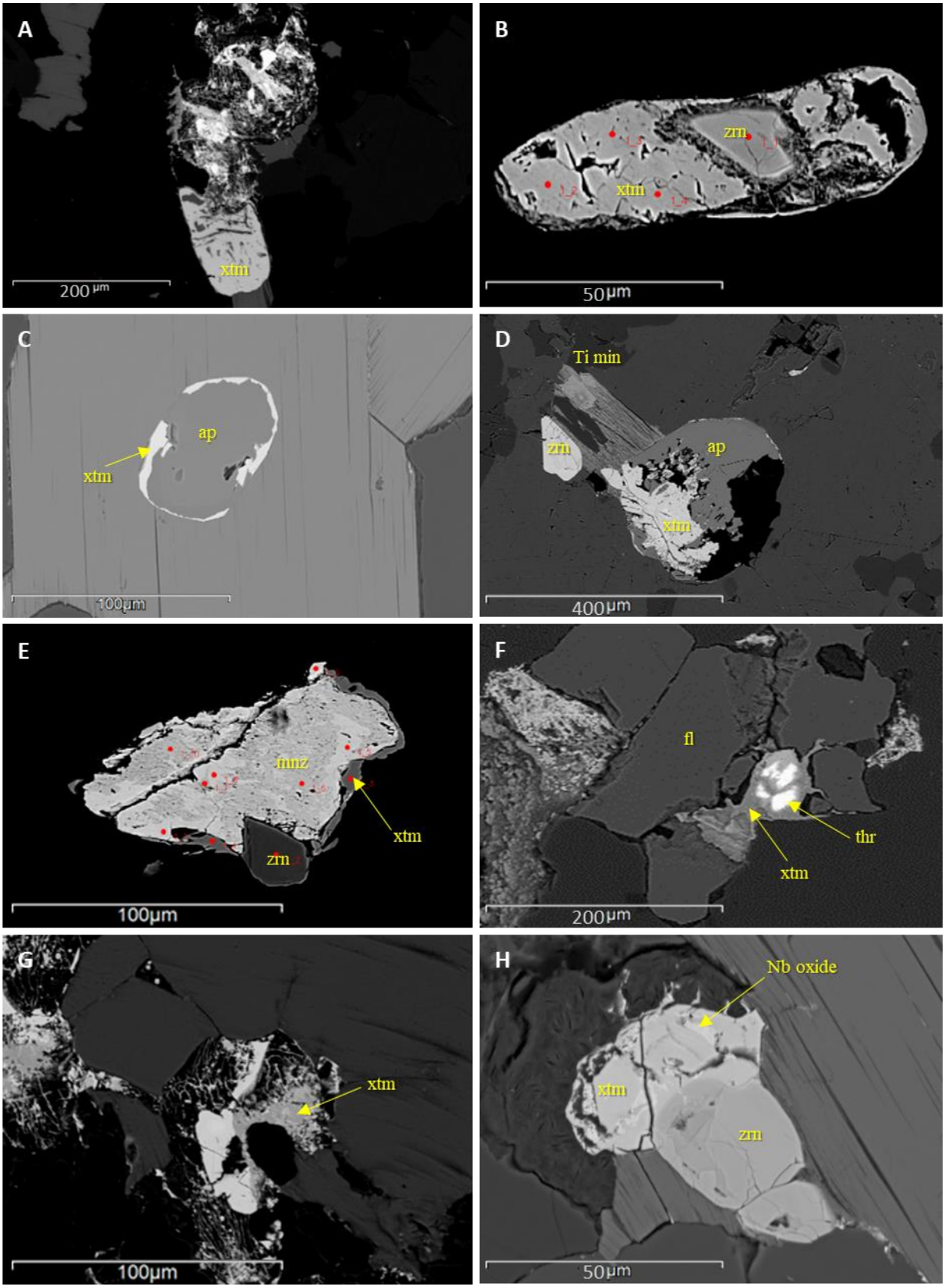


Figure 5.24. SEM-BSE images of F-rich xenotime(-Y): A. partly dissolved xenotime; B. elongate xenotime with zircon inclusion; C. and D. xenotime apparently replacing apatite; E. xenotime growth rim surrounding monazite; F. anhedral xenotime with a thorite inclusion associated closely with fluorite; G. partly dissolved xenotime overgrown with LREE-fluorcarbonate; H. partly dissolved xenotime cut by Nb-rich veins. Mineral abbreviations on pg 23.

Table 5.6. Representative EMPA of xenotime and their formulae, calculated on the basis of 4 oxygens to apfu cation proportions.

Mineral	F-rich Xenotime					Xenotime			
Source	SD5	SD6	SD7	SD9	SD27	SD20	SD20	SD9	T&B 2006
Analitical No.	PX-2	PX-4	PX-6	PX-16	PX-10	PX-44	PX-47	PX-12	
P_2O_5	25.6	19.2	20.2	36.8	34.7	34.7	21.6	36.8	34.3
SiO_2	5.00	0.08	1.83	0.17	1.43	1.43	<dt	0.66	0.17
CaO	0.55	3.79	0.26	<dt	0.41	0.41	0.83	0.06	n.a
ThO_2	<dt	<dt	0.18	0.94	<dt	<dt	<dt	1.18	0.33
UO_2	0.38	0.28	0.70	0.26	<dt	<dt	0.23	0.50	0.56
Y_2O_3	52.1	52.5	51.2	43.7	44.1	44.1	55.9	46.1	47.8
La_2O_3	<dt	<dt	<dt	<dt	1.52	1.52	<dt	<dt	n.a
Ce_2O_3	0.08	0.08	0.25	<dt	2.40	2.40	<dt	<dt	0.03
Pr_2O_3	<dt	<dt	<dt	<dt	0.31	0.31	<dt	<dt	n.a
Nd_2O_3	<dt	<dt	<dt	0.10	1.17	1.17	<dt	<dt	0.01
Sm_2O_3	<dt	0.07	<dt	0.41	0.48	0.48	<dt	0.20	n.a
Gd_2O_3	<dt	<dt	<dt	<dt	0.53	0.53	1.66	<dt	3.35
Tb_2O_3	0.12	0.15	0.08	0.56	0.36	0.36	0.19	0.42	n.a
Dy_2O_3	1.78	1.88	1.74	5.63	3.26	3.26	2.54	4.44	4.05
Ho_2O_3	0.69	0.65	0.68	1.53	0.72	0.72	0.88	1.18	n.a
Er_2O_3	2.92	2.39	2.55	4.69	2.53	2.53	3.00	3.83	3.39
Tm_2O_3	0.41	0.33	0.36	0.59	0.42	0.42	0.35	0.55	n.a
Yb_2O_3	1.99	2.08	2.55	3.77	3.42	3.42	1.86	3.54	3.59
Lu_2O_3	0.32	0.34	0.38	0.46	0.58	0.58	0.24	0.51	n.a
F	6.94	8.29	9.94	<dt	0.19	0.19	8.59	<dt	<dt
(-O)=F	2.92	3.49	4.19		0.08	0.08	3.62	<dt	
Total	98.9	92.1	93.0	99.6	98.6	98.6	97.8	97.8	97.6
HREE	60.3	60.3	59.5	60.9	55.4	55.4	65.0	65.0	58.9
REY	60.4	60.5	59.8	61.4	61.8	61.8	66.6	66.6	62.3
Cation proportions (based on 4 oxygen atoms)									
P	0.707	0.634	0.693	0.996	0.969	0.729	0.683	1.016	0.930
Si	0.163	0.003	0.074	0.005	0.047	0.000	0.000	0.017	0.005
Ca	0.019	0.158	0.011	0.000	0.015	0.065	0.033	0.000	
Th	0.000	0.000	0.002	0.007	0.000	0.000	0.000	0.006	0.002
U	0.003	0.002	0.006	0.002	0.000	0.004	0.002	0.003	0.004
Y	0.859	1.026	0.861	0.902	0.842	0.987	1.059	0.789	0.816
La	0.000	0.000	0.000	0.000	0.000	0.000	0.000	0.000	0.000
Ce	0.000	0.003	0.002	0.000	0.000	0.000	0.003	0.000	0.000
Pr	0.000	0.000	0.000	0.000	0.000	0.000	0.000	0.000	0.000
Nd	0.000	0.000	0.000	0.000	0.000	0.000	0.000	0.000	0.000
Sm	0.001	0.000	0.001	0.000	0.002	0.000	0.000	0.002	0.000
Gd	0.000	0.000	0.000	0.016	0.000	0.016	0.018	0.000	0.036
Tb	0.002	0.001	0.001	0.002	0.004	0.002	0.002	0.004	0.000
Dy	0.032	0.025	0.021	0.021	0.039	0.027	0.025	0.046	0.042
Ho	0.010	0.010	0.009	0.007	0.010	0.009	0.010	0.012	0.000
Er	0.039	0.039	0.033	0.023	0.031	0.031	0.030	0.039	0.034
Tm	0.007	0.006	0.005	0.003	0.005	0.003	0.003	0.005	0.000
Yb	0.058	0.039	0.033	0.012	0.035	0.016	0.014	0.035	0.035
Lu	0.009	0.006	0.005	0.002	0.005	0.002	0.002	0.005	0.000
∑cations	1.91	1.95	1.76	2.00	2.00	1.89	1.88	1.98	1.904
F	0.71	1.02	1.27	0.00	0.02	0.93	1.02	0.00	0.000

*T&B 2006 average value of xenotime analyses at Serra Dourada, from Teixeira & Botelho, 2006.

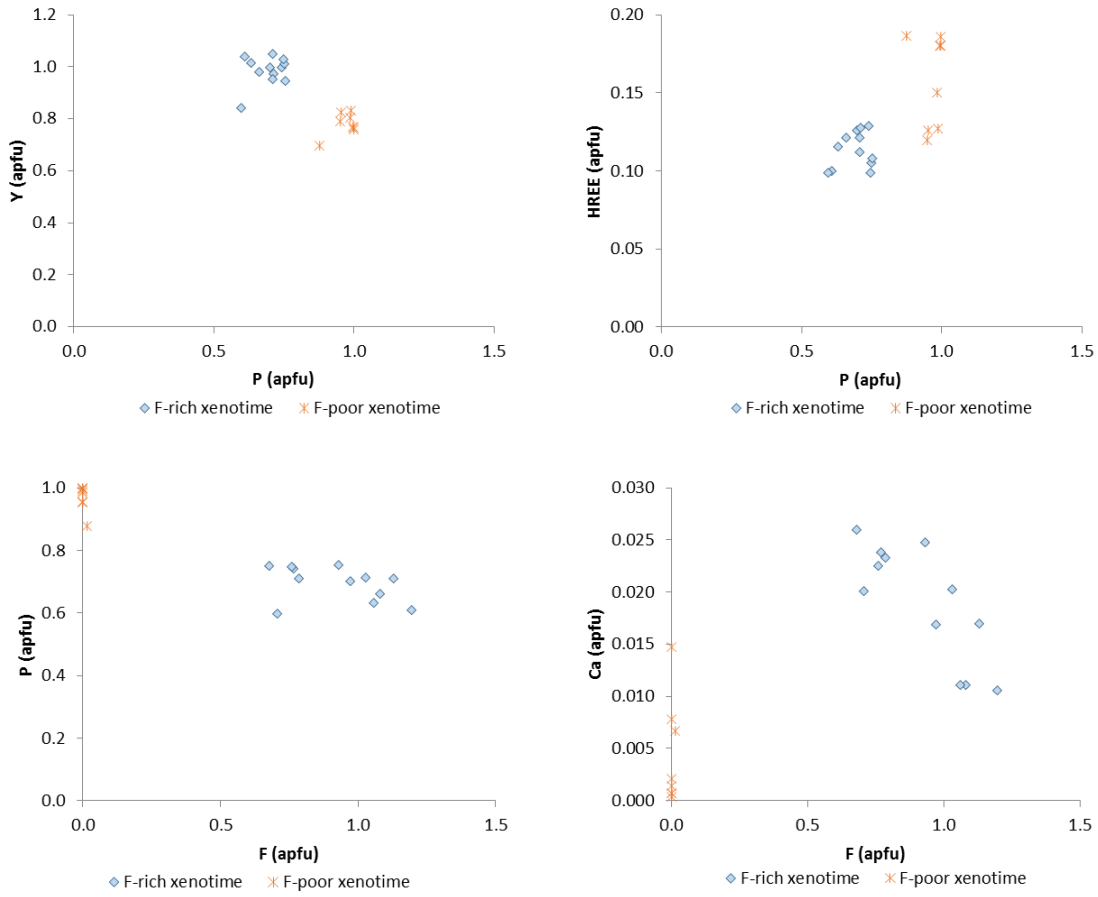


Figure 5.25. Apfu element plots showing differences in analysed composition between F-rich and normal F-poor xenotime varieties in the bedrock.

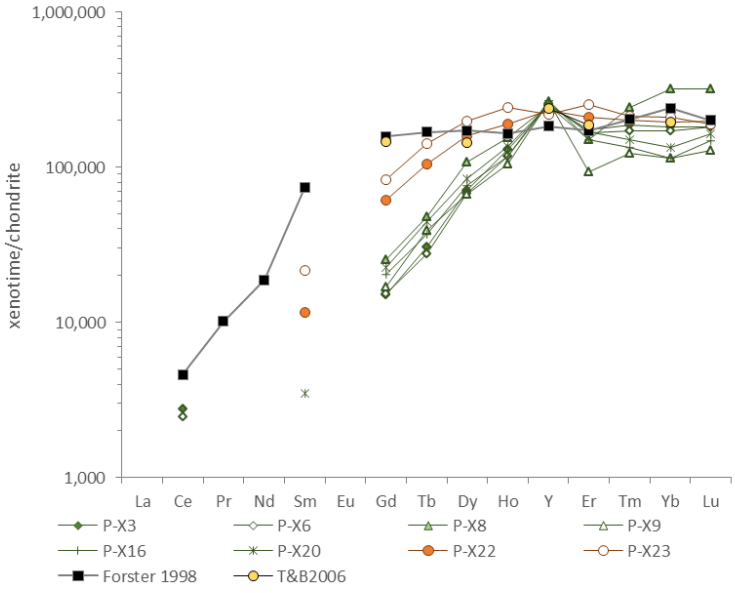


Figure 5.26. Chondrite-normalised REE patterns showing representative analyses for F-rich xenotime (green points; P-X3 to P-X20) and normal xenotime (orange circles; P-X22 and P-X23). Xenotime patterns from Teixeira & Botelho, 2006 (yellow circles) and Forster, 1998 (black squares) are included for reference.

5.5.3 LREE-fluorcarbonates

The most abundant and common REE minerals found in the samples studied are LREE-fluorcarbonates, which are abundant in the Nb-rich granite, but scarce in the Nb-poor granite.

Bastnäsite grains and aggregates are visible in hand specimen as opaque, pale, hazy yellow-red minerals up to 2 mm in diameter, and occur as fine intergrown needle-like aggregates, in fine veins, or with pseudomorphic euhedral textures up to 0.5 mm in diameter (Figure 5.28). They are intergrown with other minerals such as iron oxides, unidentified Ce- and Y-silicates, niobiates, and phosphates.

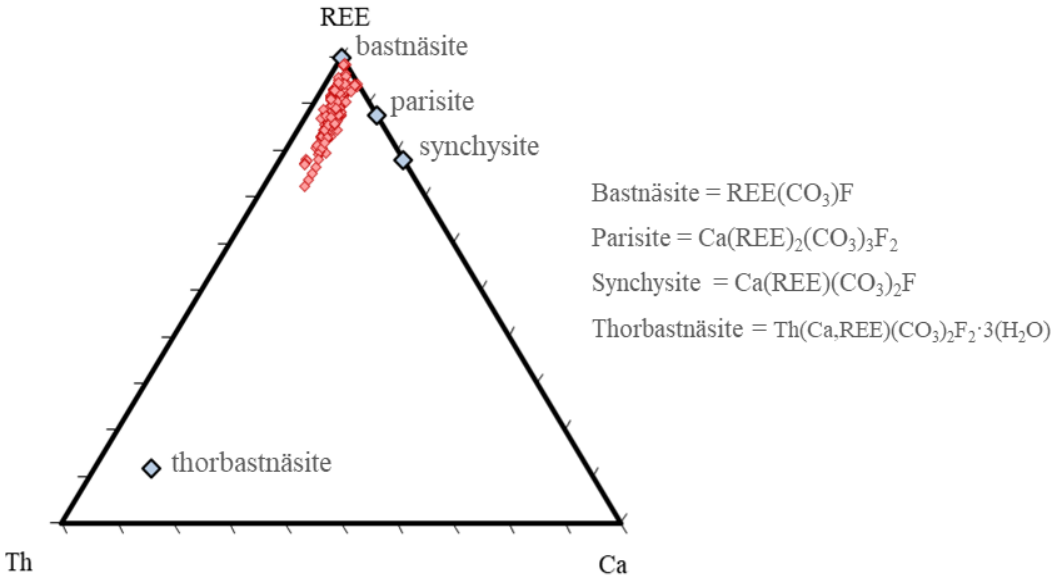


Figure 5.27. Ternary plot for Th-Ca-REE showing the compositions of fluorcarbonates analysed by EMPA in this study. Formula compositions for the end-members of different mineral species are indicated.

The fine grained intergrown nature of fluorcarbonates makes reliable spot analyses difficult and may account for the range in compositions (Figure 5.27). Low concentrations of non-formula trace elements in the analysis probably represent mineral impurities at the scale of the spot size. The best analyses were obtained from large or aggregate bastnäsite crystals.

The bastnäsites are of varying composition between bastnäsite (REE-rich), parisite (REE and Ca-bearing), and thorbastnäsite (Th-rich). All fluorcarbonate analyses fall in the REE-

bastnäsite classification; REE are dominant, while Th and Ca are present in minor concentrations (see ternary plot in Figure 5.27). Th contents are up to 12 wt %, with mean values of 3.8 wt %. Ca contents are up to 5 wt %, with mean values of 1.96 wt %. The REE are commonly present in significant concentrations of 50 – 60 wt % REY, and dominated by the LREE.

Ce- and La-dominant varieties are found in both Nb-rich and Nb-poor granite samples (Table 5.7) but no differences in morphology, texture, or habit are observed; these varieties can only be discriminated by their geochemical composition. Bastnäsite-(Ce) and bastnäsite-La show similarly LREE-fractionated chondrite-normalised patterns, with La_N/Yb_N ranging between 92 and 225. The principal difference between these varieties is that all La-bastnäsites have slightly negative Ce anomalies with values as low as 0.02 Ce/Ce* (Figure 5.29). The HREE and Y content of these samples varies between 0.38 and 6.9 wt %, and 2.46 – 12 wt % respectively. Analysis from both species show minor quantities of Sr and Ba which correlate with Ca content. The results indicate lower individual La, Ce, Pr and Sm than expected, and unusually high HREE and Y contents relative to published REE-fluorcarbonate analyses (Ruberti et al. 2008, Styles and Young 1983, Hoshino et al. 2012).

Low concentrations of non-formula elements in bastnäsite are also present in analyses, they include P, Si, Al, and Fe, each present in variable amounts up to 3 wt % and show no correlation to REE, Y or Ca content. These are interpreted as impurities or contamination originating from other finely intergrown minerals observed in SEM-BSE imagery such as iron oxides.

Both Ce- and La-bastnäsite species are present in all samples. However, bastnäsite-(La) is more commonly found in samples at the top of DDH0004, and in samples that show incipient weathering nearer to the base of the weathering profile (e.g. DDH0266).

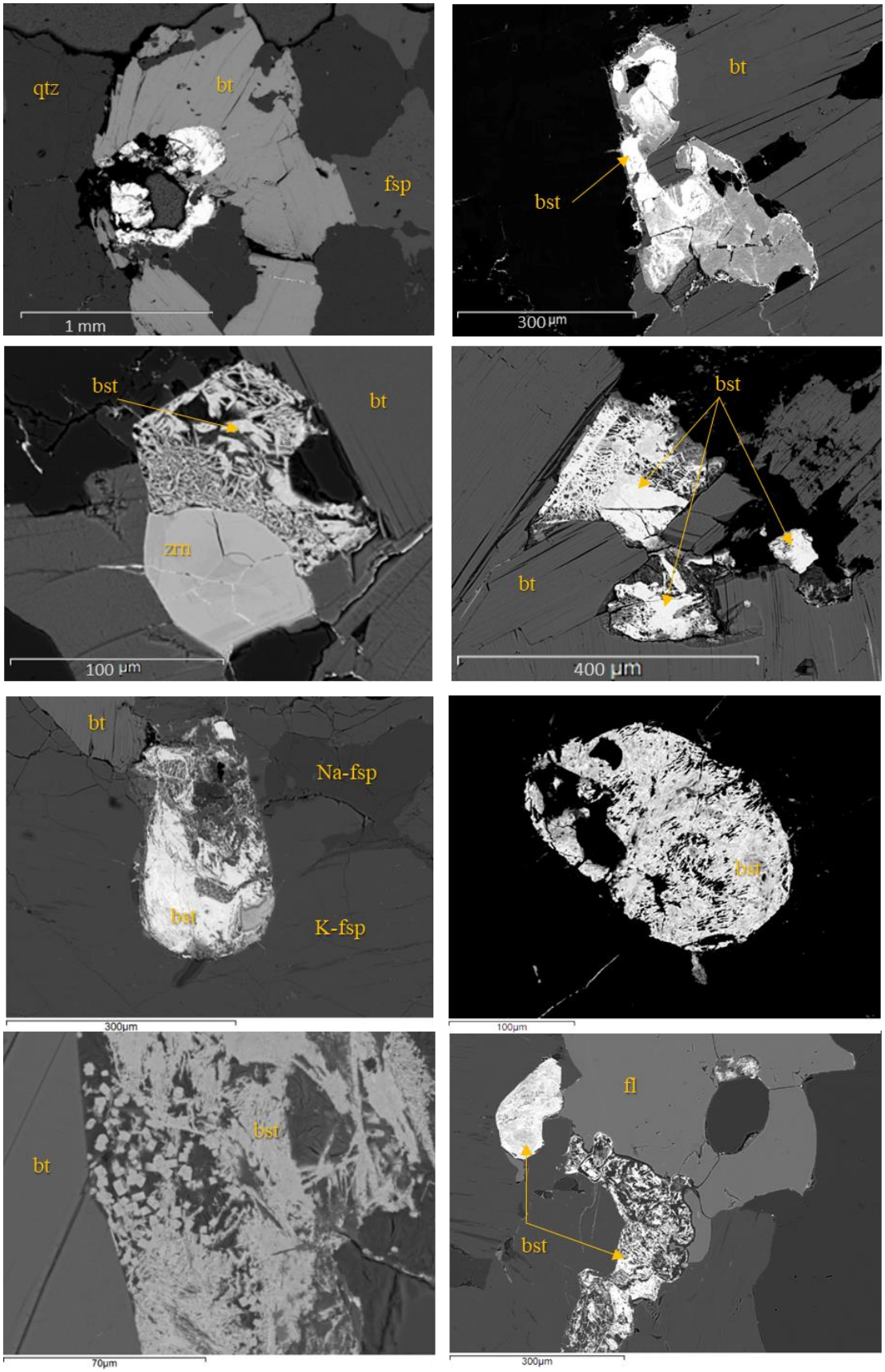


Figure 5.28. SEM-BSE images of bright REE-fluorcarbonates present in plateau granite samples, showing the variety of mineral textures and pseudomorphic habits. Mineral abbreviations on pg 23.

Table 5.7. Representative EMP analysis and structural formula of bastnäsite-Ce and bastnäsite-La in samples from drill hole DDH0004. Structural formula based on O = 4 structural formula $(A)(CO_3)F$, where A = REE, Y, Ca, Th, Fe.

	Bastnasite - Ce						Bastnasite - La							
Sample	SD4	SD6	SD7	SD25	SD8	SD19	SD10	SD21	SD4	SD27	SD25	SD9	SD6	SD10
Analysis No.	B-3	B-34	B-57	B-84	B-90	B-143	B-129	B-148	B-11	B-71	B-87	B-106	B-52	B-127
SiO_2	0.15	0.23	0.53	1.25	0.18	1.30	0.30	0.36	0.18	0.23	0.31	4.06	0.19	1.29
Al_2O_3	<dt	<dt	0.09	0.07	<dt	0.34	<dt	<dt	<dt	<dt	<dt	1.38	<dt	0.52
Y_2O_3	3.64	4.45	3.51	4.15	5.38	5.08	2.00	10.33	3.21	2.01	4.18	3.14	4.75	9.38
La_2O_3	19.6	16.8	13.3	15.3	14.6	13.6	29.0	26.9	24.6	24.2	21.4	22.2	19.2	14.0
Ce_2O_3	25.3	24.9	29.0	26.4	29.8	26.3	7.06	5.06	13.7	17.1	15.1	10.8	16.9	18.8
Pr_2O_3	3.55	2.95	3.05	2.85	2.95	2.89	4.71	3.44	4.84	3.63	3.86	3.65	3.95	2.63
Nd_2O_3	12.4	10.2	10.3	9.94	10.2	9.44	17.1	14.5	15.8	11.9	13.2	12.4	13.7	9.2
Sm_2O_3	1.94	1.70	1.68	1.53	1.80	1.57	2.42	2.61	2.38	1.64	2.18	1.98	2.39	1.51
Gd_2O_3	1.14	1.11	1.01	0.98	1.04	1.20	1.14	2.82	1.32	0.86	1.16	1.05	1.29	1.07
Tb_2O_3	0.18	0.22	0.21	0.20	0.22	0.24	0.09	0.39	0.17	0.11	0.20	0.13	0.20	0.23
Dy_2O_3	0.57	0.66	0.72	0.85	1.00	0.92	0.24	2.03	0.51	0.35	0.69	0.65	0.74	1.31
Ho_2O_3	<dt	<dt	<dt	<dt	<dt	0.18	<dt	0.37	<dt	<dt	<dt	0.18	0.15	0.23
Er_2O_3	0.23	<dt	0.19	0.39	0.37	0.45	<dt	0.78	0.18	0.17	0.25	0.18	0.19	0.49
Tm_2O_3	<dt	<dt	<dt	<dt	<dt	<dt	<dt	<dt	<dt	<dt	<dt	<dt	<dt	<dt
Yb_2O_3	<dt	<dt	<dt	0.14	0.10	0.20	<dt	0.47	<dt	<dt	0.09	<dt	0.09	0.27
Lu_2O_3	<dt	<dt	<dt	<dt	<dt	<dt	<dt	<dt	<dt	<dt	<dt	<dt	<dt	<dt
CaO	1.85	3.58	3.29	3.40	2.98	4.31	2.07	1.36	2.51	2.99	3.92	4.76	3.96	3.24
SrO	<dt	0.87	0.35	1.12	0.31	2.17	0.58	<dt	0.24	0.60	1.02	0.91	0.46	0.19
FeO	<dt	<dt	<dt	<dt	<dt	<dt	<dt	<dt	<dt	<dt	<dt	0.25	<dt	0.23
ThO_2	3.33	3.13	2.18	3.24	1.72	2.49	1.70	1.62	2.59	4.26	5.06	7.07	3.86	5.21
UO_2	<dt	0.21	0.19	0.28	<dt	0.15	<dt	<dt	<dt	0.24	0.23	0.44	<dt	0.28
CO_2 (cal.)	20.8	21.4	20.9	22.1	21.6	23.5	19.7	21.3	20.8	20.4	21.9	25.1	21.6	21.9
F	7.35	6.64	7.78	6.54	8.62	7.20	7.16	9.16	8.89	6.92	7.60	8.44	7.95	7.11
(-O)=F	3.10	2.80	3.27	2.75	3.63	3.03	3.02	3.86	3.74	2.92	3.20	3.55	3.35	2.99
Total	98.9	96.2	95.0	98.0	99.3	100.5	92.2	99.6	98.2	94.6	99.2	105.2	98.3	96.2
REE	64.9	58.5	59.6	58.6	62.2	57.0	61.8	59.4	63.5	59.9	58.2	53.1	58.8	49.8
REY	68.5	62.9	63.1	62.7	67.6	62.1	63.8	69.7	66.7	61.9	62.3	56.3	63.6	59.2
Cation proportions (based on 4 oxygen atoms)														
Ca	0.07	0.14	0.13	0.13	0.11	0.16	0.09	0.05	0.10	0.12	0.15	0.17	0.15	0.12
Sr	0.00	0.02	0.01	0.02	0.01	0.04	0.01	0.00	0.00	0.01	0.02	0.02	0.01	0.00
Y	0.070	0.086	0.068	0.079	0.100	0.092	0.041	0.191	0.061	0.040	0.078	0.055	0.089	0.179
La	0.262	0.225	0.180	0.202	0.188	0.170	0.414	0.346	0.324	0.335	0.278	0.267	0.250	0.185
Ce	0.336	0.331	0.389	0.346	0.381	0.328	0.100	0.064	0.179	0.235	0.194	0.129	0.217	0.247
Pr	0.047	0.039	0.041	0.037	0.037	0.036	0.066	0.044	0.063	0.050	0.049	0.043	0.051	0.034
Nd	0.161	0.132	0.135	0.127	0.127	0.115	0.235	0.180	0.202	0.159	0.166	0.144	0.172	0.118
Sm	0.024	0.021	0.021	0.019	0.022	0.018	0.032	0.031	0.029	0.021	0.026	0.022	0.029	0.019
Gd	0.014	0.013	0.012	0.012	0.012	0.013	0.015	0.032	0.016	0.011	0.013	0.011	0.015	0.013
Tb	0.002	0.003	0.003	0.002	0.003	0.003	0.001	0.005	0.002	0.001	0.002	0.001	0.002	0.003
Dy	0.007	0.008	0.009	0.010	0.011	0.010	0.003	0.023	0.006	0.004	0.008	0.007	0.008	0.015
Ho	0.000	0.000	0.000	0.000	0.000	0.002	0.000	0.004	0.000	0.000	0.000	0.002	0.002	0.003
Er	0.003	0.000	0.002	0.004	0.004	0.005	0.000	0.009	0.002	0.002	0.003	0.002	0.002	0.006
Tm	0.000	0.000	0.000	0.000	0.000	0.000	0.000	0.000	0.000	0.000	0.000	0.000	0.000	0.000
Yb	0.000	0.000	0.000	0.002	0.001	0.002	0.000	0.005	0.000	0.000	0.001	0.000	0.001	0.003
Lu	0.000	0.000	0.000	0.000	0.000	0.000	0.000	0.000	0.000	0.000	0.000	0.000	0.000	0.000
Fe	0.000	0.000	0.000	0.000	0.000	0.000	0.000	0.000	0.000	0.000	0.000	0.007	0.000	0.007
Si	0.005	0.008	0.019	0.045	0.006	0.044	0.012	0.013	0.007	0.009	0.011	0.133	0.007	0.046
Al	0.000	0.000	0.004	0.003	0.000	0.014	0.000	0.000	0.000	0.000	0.000	0.053	0.000	0.022
Th	0.110	0.103	0.073	0.106	0.054	0.077	0.060	0.051	0.084	0.146	0.162	0.210	0.124	0.170
U	0.000	0.007	0.006	0.009	0.000	0.004	0.000	0.000	0.000	0.008	0.007	0.012	0.000	0.008
Σ cations	1.11	1.13	1.10	1.16	1.06	1.13	1.08	1.05	1.08	1.15	1.17	1.28	1.13	1.20
C	1.03	1.06	1.04	1.08	1.03	1.09	1.04	1.01	1.01	1.05	1.05	1.12	1.04	1.07
F	0.84	0.76	0.90	0.74	0.95	0.77	0.87	1.01	1.00	0.82	0.84	0.87	0.88	0.80

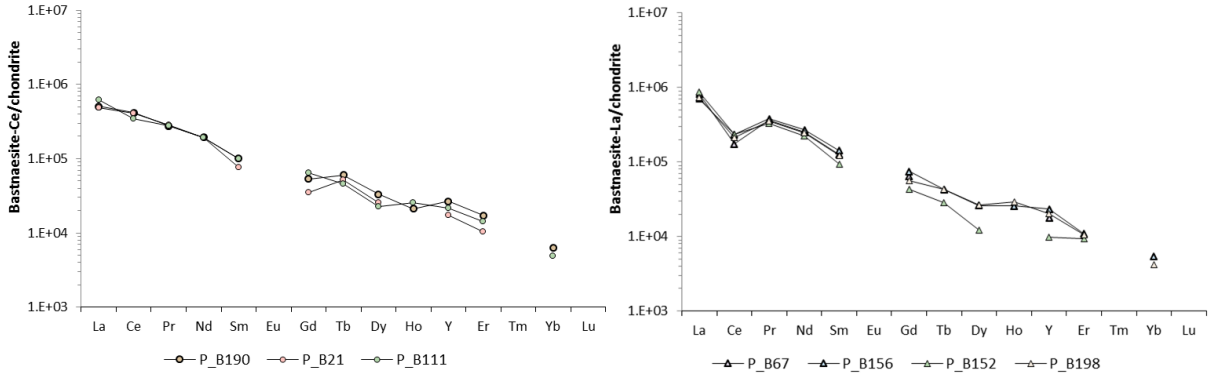


Figure 5.29. Chondrite-normalised REE patterns showing representative results for Ce-bastnäsite (left) and La-bastnäsite (right). Note the difference in negative Ce anomalies between the two mineral varieties.

5.5.4 Niobiates

Niobiates have not been reported in the Serra Dourada granite before but are found to be relatively common in the granite that underlies the Serra Verde deposit, especially in the Nb-rich samples. Three varieties of Nb minerals were identified: they include the samarskite-(Y), nioboaeschynite-(Ce), and pyrochlore groups. Samarskite-(Y) is the most abundant in the Nb-rich biotite granite samples, while pyrochlore is the dominant Nb-mineral in the albitised section of drill core in DDH0004.

Due to the similar and complex chemical formulae of the REE niobates, and their metamictic nature, different species of niobiate are sometimes difficult to identify and differentiate (Table 5.8). Classification of Nb minerals was aided by Ercit's (2005) statistical approach with the calculation on two geochemical canonical variables using the niobiate formula elements (Figure 5.30).

Table 5.8. Chemical formulae of key niobiate minerals.

Mineral	Formula
Samarskite-(Y)	(Y, Ce, Fe, Ca) (Nb, Ta, Ti) O_4
Yttrocolumbite	(Y, U, Fe^{2+}) (Nb, Ta) O_4
Fergusonite-(Y)	$YNbO_4$
Uranopyrochlore	$(U, Ca, Ce)_2(Nb, Ta)_2O_6(OH, F)$
Yttpyrochlore-(Y)	$(Y, Na, Ca, U)_{1-2}(Nb, Ta, Ti)_2O_6(OH)$
Columbite-(Fe)	$FeNb_2O_6$
Nioboaeschynite-(Ce)	$Ce, Ca\ (Nb, Ti)_2(O, OH)_6$

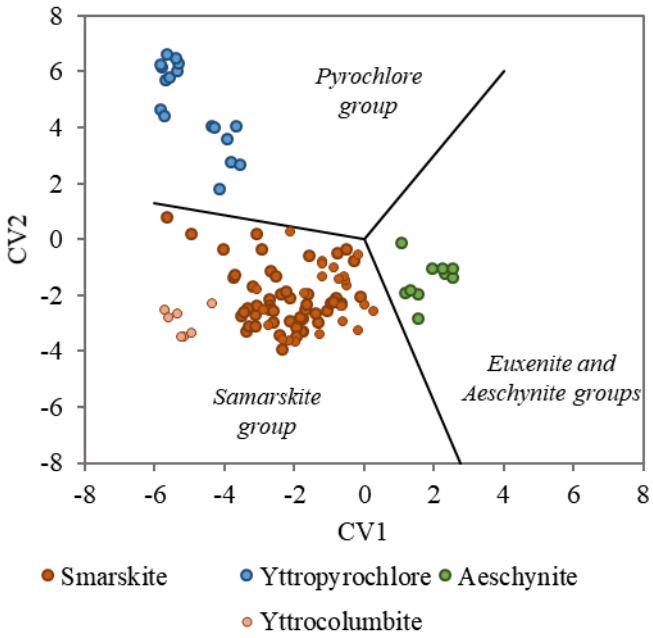


Figure 5.30. Diagram showing the classification of analytical data points of Nb minerals from this study using the statistical approach of Ercit (2005), where CV1 = 0.245 Na + 0.106 Ca – 0.077 Fe + 0.425 Pb + 0.220 Y + 0.280 LREE + 0.137 HREE + 0.100 U + 0.304 Ti + 0.097 Nb + 0.109 Ta – 12.81, and CV2 = 0.102 Na – 0.113 Ca – 0.371 Fe – 0.167 Pb – 0.395 Y – 0.280 LREE – 0.265 HREE – 0.182 U – 0.085 Ti – 0.166 Nb – 0.146 Ta + 17.29 (all numbers as oxide wt %).

5.5.4.1 Samarskite-Y [Y,Ca,Fe (NbO_4)]

Samarskite-(Y) is the most common niobiate species found in the biotite granite. The range of observed grain sizes is quite large at 20 – 200 µm diameter. Their habits most frequently occur as rounded or elongate subhedral grains, or as irregular pseudomorphs of other minerals intergrown with LREE-fluorcarbonates and Fe oxides.

Samarskites are commonly found in contact with, engulfing, or replacing zircons (see Figure 5.31), adjacent to or included in both biotite sheets and quartz, and are also found associated with fluorite. No concentric zonation or compositional banding in samarskite crystals are observed. SEM-BSE images of samarskite show patchy internal textures with variably bright and mid reflectance, which are interpreted as evidence of strong alteration and metamictic crystal composition likely due to radiation damage (Heroldová 2011).

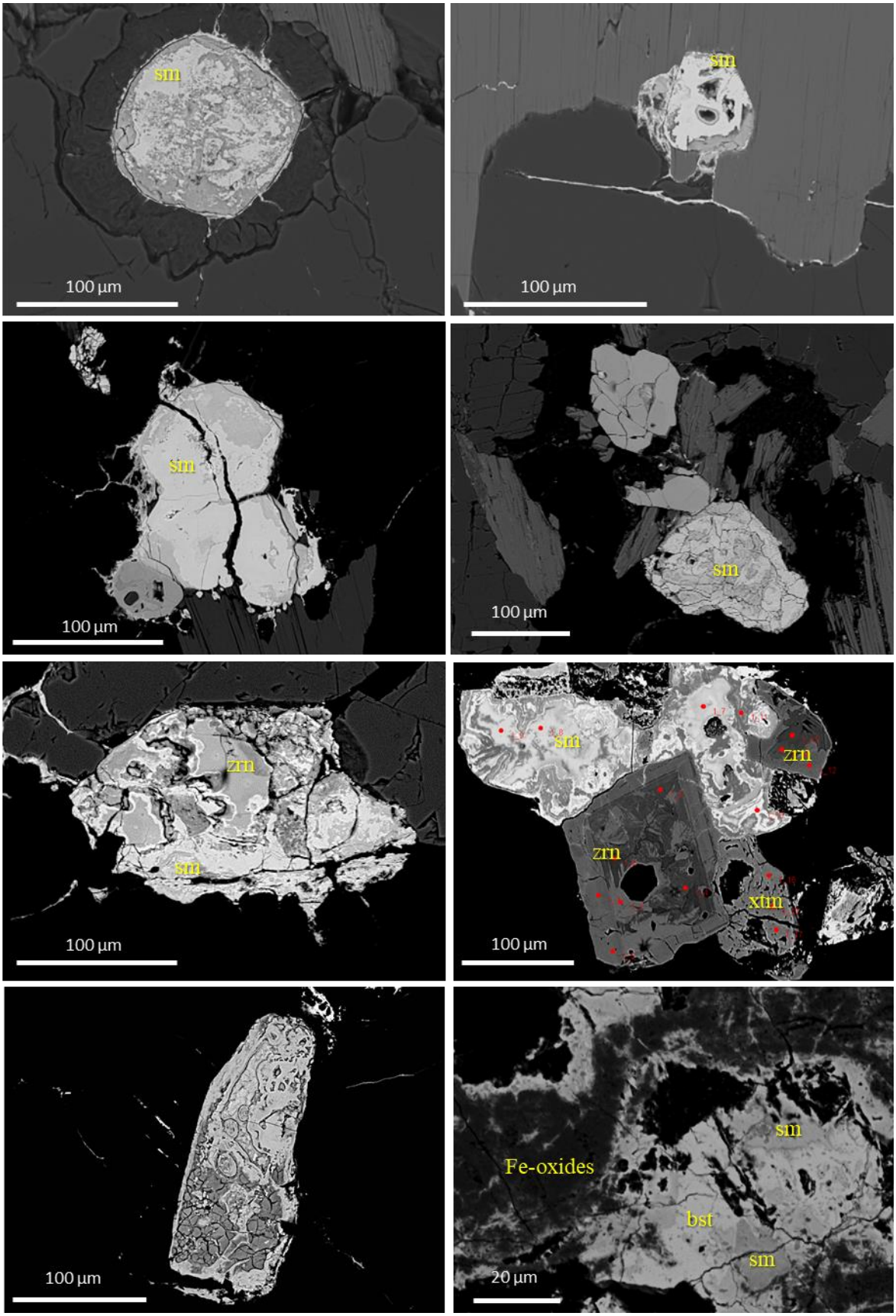


Figure 5.31. SEM-BSE images of samarskite minerals, showing their range occurrence and metamictic state. Note the close associations with zircon, and internal textural variability indicative of varying composition. Mineral abbreviations on pg 23.

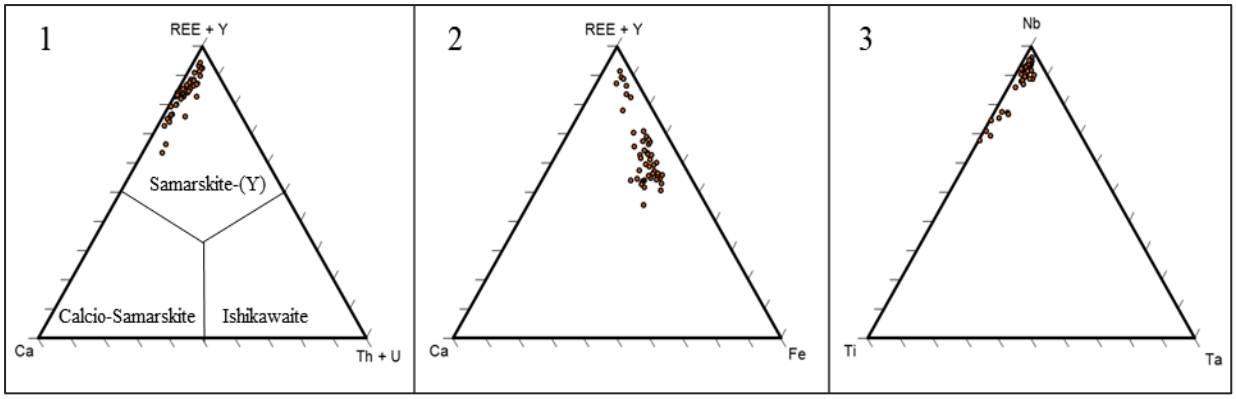


Figure 5.32. Ternary diagrams 1 and 2 show A-site occupancy in analyses classified as samarskite, and diagram 3 shows B-site occupancy. Note how all analyses fall within the Samarskite-(Y) plot area of the Samarskite group species. Ternary diagram from Hanson et al. 1999.

Samarskites are a complex group of niobiate minerals that have the structural formula of ABO_4. In the A site several elements such as Y, REE, Fe, U, Th, Ca, Fe can be present, while Nb, Ti, Ta are present in the B site. Samarskite minerals are chemically complex and generally completely metamict and pervasively altered where they have been identified (Hanson et al. 1999).

Samarskite group minerals are divided into three end members samarskite-(Y), calcio-samarskite and ishikawaite. All samarskite analyses from this study fall in the samarskite-(Y) (Figure 5.32). All of the samarskites analysed hold variable amounts of REE and Y and are characterised by low Ta and TiO_2 concentrations; Ta is consistently found < 5 wt %, and Ti is present in highly variable concentrations up to 9 wt %. REY contents range between 17 – 30 wt % (Y_2O_3 + REE_2O_3). The most abundant REE in all analyses are Y and Ce. CaO content ranges between 0.5 and 4 wt %, and Fe_2O_3 content ranges between 1 and 10 wt %.

In the samarskite analyses, low UO_2 contents (< 3 wt %), and low concentrations of BaO (up to 1 wt %) are ubiquitous, while ThO_2 is present up to 3 wt %, MnO up to 1 wt %, and both Na_2O and K_2O are also present at low concentrations slightly above the detection limit. A few grains also contained trace amounts of Pb. Si and Zr are consistently present in the samarskites, and strongly correlate. Small amounts of Zr and Si can be explained by the observed replacement of zircons containing quartz inclusions.

The irregular patches in samarskites with contrasting reflectance in SEM-BSE imaging suggest internal compositional variation; the majority of minerals appear to be metamictic. Chemical analysis show that the variation in SEM-BSE response can be explained by differences in Y,

Nb and REE content. Darker patches are usually more Y-enriched, have lower Nb concentrations, and higher Si concentrations. Analytical totals are also lower, suggesting increased porosity in the dark patches. Y-rich and REE-rich species of samarskite have been described by Hanson et al. 1999 in similar geological settings, but the controls on the composition of these minerals remain poorly understood.

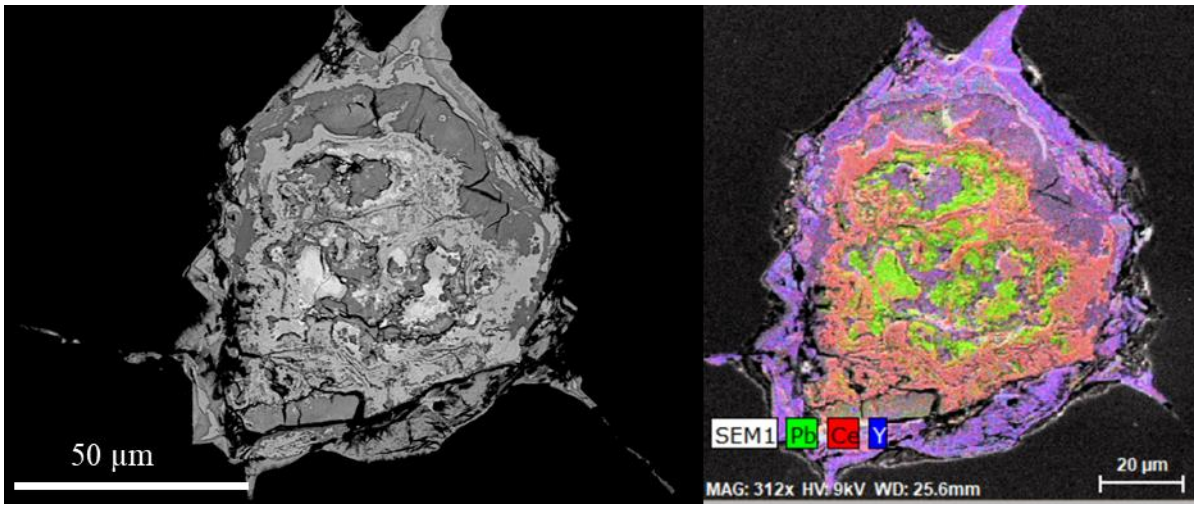


Figure 5.33. SEM-BSE (left) and corresponding EDX element map (right) showing the internal variation in composition of a metamictic samarskite grain, typical of the grains observed in granite bedrock samples.

The chondrite-normalised REE pattern of samarskite minerals are presented in Figure 5.34. The pattern shows a left-inclined trend with HREE preferentially enriched relative to LREE ($La_N/Yb_N = 0.16$). The HREE exhibit a relatively flat trend, and the steep inclination starts after Dy.

A strong positive Ce anomaly is also present; Ce/Ce* ranges from 5 to 20. Ce is the only REE that is present in significantly high concentrations. Ce anomalies are not described by published studies and may not be typical of samarskite, which may suggest the composition has been further modified by alteration by Ce-bearing fluid.

The Y_N/Ho_N ratio shows non-chondritic values of ~ 0.5; Y and Ho are fractionated, which reflects that other HREE are preferentially incorporated into niobiates compared to Y. Non-chondritic Y_N/Ho_N whole rock and mineral values have been showed to be the result of interaction with an aqueous fluid, causing precipitation and fractionation due to the contrasting complexation of Y and Ho in solutions (Bao and Zhao 1996). Taken together with the

anomalously high Ce, this suggests that the samarskites in the Serra Verde granite are hydrothermal. This observation compliments the analysed composition of F-rich xenotimes, which preferentially incorporate more Y than Ho and may therefore also be a product of hydrothermal fluid interaction with the bedrock.

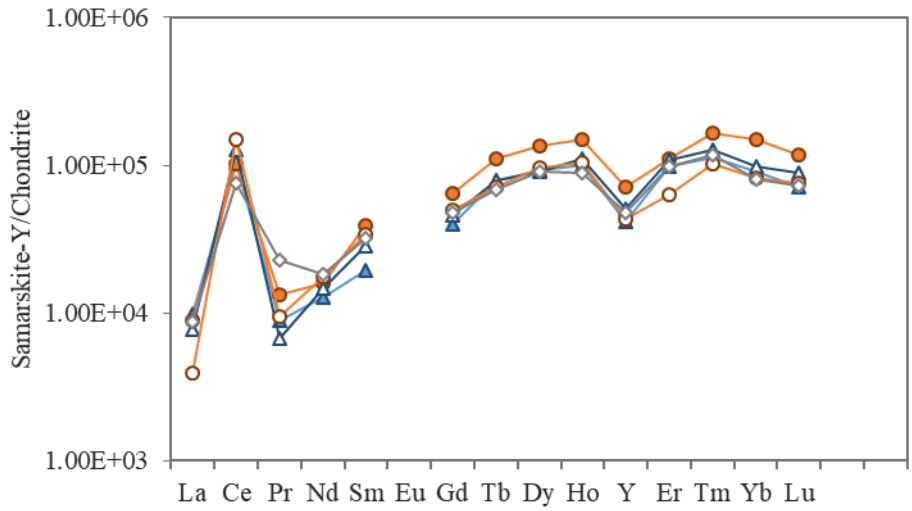


Figure 5.34. Chondrite-normalised REE patterns of several representative samarskite-Y analyses.

5.5.4.2 Pyrochlore [U,Ca,Ba)$_2$(Nb)$_2$O$_6$(OH,F)]

Pyrochlore is also a large group of niobium mineral species with the chemical formula $A_2B_2O_6(OH,F)$, and may incorporate similar elements to samarskite in the respective A and B sites. Pyrochlore grains are found to occur as interstitial crystals and partial replacements, and are spatially associated with both fluorite and biotite. The most common species identified is uranopyrochlore where U, Ca, and Ba are the dominant A site cations.

The analyses show that pyrochlore can be characterised by its low REE content, up to 10 wt % REY, with the MREE composing most of the REY. Pyrochlores were only found in the albitised granite sample of DDH0004 (82.82 m), and adjacent sections (72 m and 93 m).

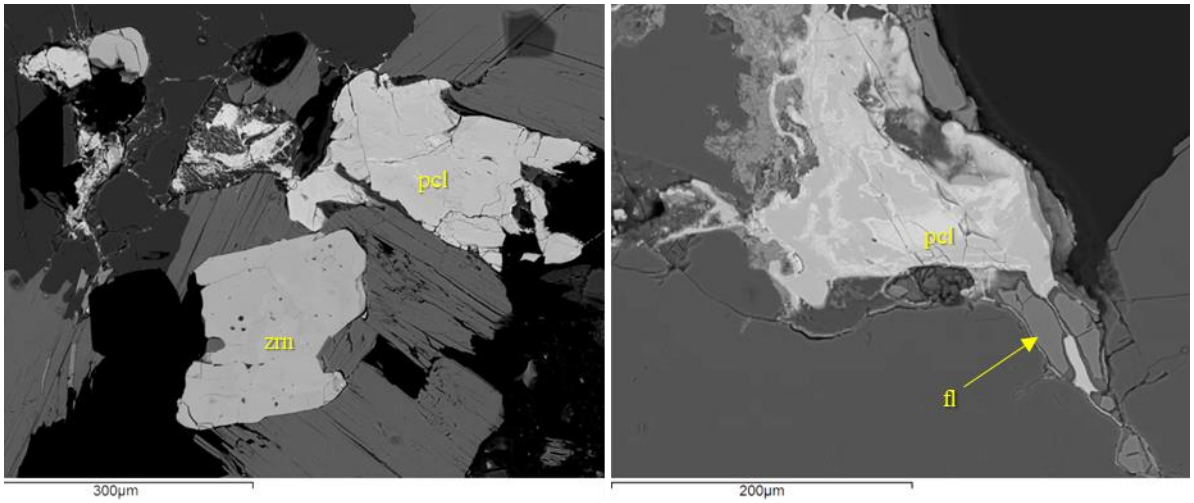


Figure 5.35. SEM-BSE images of uranopyrochlore minerals found in the albitised section of drill hole DDH0004. Note the large grain size of these minerals. Mineral abbreviations on pg 23.

5.5.4.3 Other niobates

Only a few grains of other niobates minerals were found in the samples analysed. These include yttro-columbite, which was found in the albitised section of DDH0004, aeschynite (nioboaeschynite –(Ce)), and fergusonite both present in the biotite granite. The nioboaeschynite-(Ce) was found spatially associated with LREE-fluorcarbonates, and a single fergusonite grain was found preserved in a quartz crystal Figure 5.36. The chemical analyses of these minerals are presented in Table 5.9.

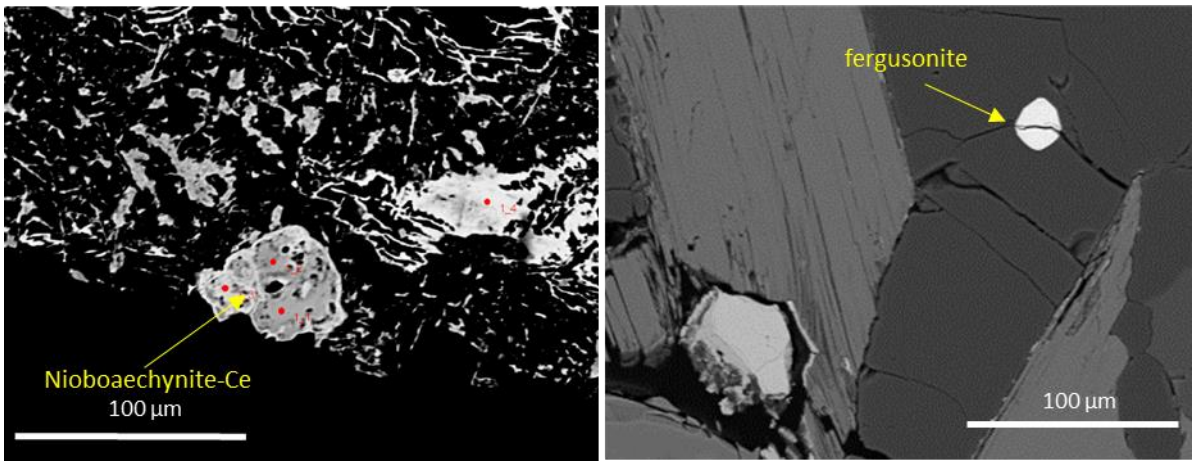


Figure 5.36. SEM-BSE images of representative nioboaeschynite-Ce and rare fergusonite-(Y).

Table 5.9. EMP results for niobiates, sorted into analyses for bright and dark patches determined by SEM-BSE response.

Mineral	Fergusonite-Y	Samarskite-Y				Samarskite-Ce					Nioboaeschynite-Ce				Columbite		Pyrochhlore	
Source	SD6	SD4	SD5	SD10	SD4	SD4	SD9	SD10	SD16	SD6	SD16	SD5	SD6	SD4	SD8	SD8	SD8	SD8
Analitical No.	Nb49	Nb3	Nb26	Nb102	Nb9	Nb6	Nb87	Nb93	Nb109	Nb34	Nb114	Nb22	Nb30	Nb11	Nb71	Nb73	Nb80	Nb61
wt %																		
Nb_2O_5	46.1	47.6	36.3	37.4	34.0	36.6	49.7	36.4	37.0	39.1	25.0	26.4	30.7	32.3	45.4	44.2	62.8	56.6
Ta_2O_5	1.94	2.53	1.14	3.59	1.12	0.64	1.25	1.39	2.80	1.94	1.11	<dt	2.28	0.27	1.30	0.52	0.85	1.32
TiO_2	1.02	1.08	1.05	1.23	1.41	7.00	1.25	6.44	6.64	4.85	11.23	11.98	11.36	17.00	0.72	0.36	1.12	2.40
ZrO_2	0.49	0.81	1.35	0.24	1.69	0.23	0.87	1.01	0.31	0.32	0.00	0.77	0.64	0.11	1.65	1.74	0.80	0.69
SiO_2	<dt	3.49	5.78	4.44	6.59	3.22	3.36	4.97	2.72	3.89	4.13	4.00	5.19	4.45	4.85	5.06	6.60	5.25
Al_2O_3	<dt	0.19	0.17	0.16	<dt	0.21	0.14	0.37	0.30	0.16	0.96	0.20	0.13	0.24	0.07	0.07	0.42	0.50
FeO	0.13	7.79	1.81	5.43	2.00	7.04	7.30	9.22	7.80	9.46	5.35	4.97	8.84	4.13	21.26	29.26	1.11	1.59
MnO	<dt	0.44	0.17	0.13	0.11	0.44	0.59	0.56	0.35	0.57	0.30	0.35	0.34	0.84	<dt	<dt	0.11	<dt
CaO	0.50	1.44	1.15	1.02	0.74	1.30	3.93	2.77	1.25	2.38	1.05	1.15	1.67	1.48	2.09	1.24	6.38	5.36
Na_2O	<dt	0.08	<dt	0.38	<dt	<dt	0.15	0.13	<dt	<dt	0.09	<dt	<dt	<dt	0.11	0.09	0.43	0.18
BaO	<dt	0.18	<dt	0.46	<dt	0.13	0.96	0.44	<dt	0.36	<dt	0.25	0.44	0.17	0.79	0.78	1.44	0.98
ThO_2	2.05	1.73	1.55	0.97	1.75	2.64	0.90	2.30	6.80	1.26	3.92	3.02	1.69	1.57	0.83	0.74	0.68	1.83
UO_2	0.79	0.72	0.30	2.61	0.24	<dt	0.63	0.24	0.39	<dt	0.22	0.24	<dt	0.24	0.67	0.58	2.27	1.42
Y_2O_3	26.65	10.19	15.43	11.46	17.39	9.17	0.86	1.50	5.58	6.35	4.93	8.59	5.60	13.66	3.82	3.98	4.50	3.98
La_2O_3	0.07	0.17	1.12	0.36	0.19	0.75	0.18	0.31	0.13	<dt	0.13	2.94	0.13	0.25	0.13	0.12	0.22	0.23
Ce_2O_3	0.64	5.91	7.77	6.93	9.35	10.19	20.30	24.25	13.08	14.21	14.31	14.52	17.28	3.61	5.85	1.71	0.86	2.87
Pr_2O_3	0.18	0.20	0.30	<dt	<dt	0.32	<dt	0.13	0.18	0.14	0.15	0.53	0.12	0.26	<dt	<dt	<dt	0.17
Nd_2O_3	1.59	1.32	1.51	0.50	0.76	1.95	0.84	0.79	0.95	0.84	0.94	2.15	0.81	1.72	0.50	0.26	0.32	1.52
Sm_2O_3	1.22	0.94	0.85	0.26	0.58	0.90	0.31	0.36	0.59	0.59	0.63	0.69	0.55	1.27	0.24	0.07	<dt	1.03
Gd_2O_3	1.31	0.45	0.45	<dt	0.24	0.43	0.49	0.49	1.04	0.23	0.85	0.38	0.37	0.77	<dt	<dt	0.07	0.50
Tb_2O_3	0.54	0.40	0.37	0.23	0.41	0.31	<dt	<dt	0.29	0.27	0.24	0.32	0.25	0.46	0.12	<dt	0.13	0.43
Dy_2O_3	4.32	3.49	3.55	2.49	4.00	2.81	<dt	<dt	2.68	2.27	2.03	2.74	2.30	3.81	1.63	1.04	1.60	3.56
Ho_2O_3	0.89	0.77	0.86	0.62	0.85	0.68	<dt	<dt	0.53	0.54	0.43	0.58	0.44	0.91	0.31	0.24	0.25	0.56
Er_2O_3	3.00	2.13	2.71	2.20	3.06	1.98	<dt	<dt	1.64	1.41	1.26	1.96	1.37	2.31	1.11	0.96	1.19	1.84
Tm_2O_3	0.42	0.25	0.38	0.33	0.42	0.20	<dt	<dt	0.23	0.19	0.17	0.30	0.17	0.27	0.15	0.15	0.16	0.23
Yb_2O_3	2.87	1.69	2.58	2.54	2.71	1.46	<dt	<dt	1.38	0.93	1.10	1.73	0.83	1.87	0.93	0.97	0.97	1.12
Lu_2O_3	0.36	0.14	0.30	0.35	0.26	0.12	<dt	<dt	0.13	0.11	0.08	0.23	0.11	0.17	0.09	0.08	0.11	<dt
F	<dt	0.22	0.75	0.52	1.08	0.42	<dt	<dt	<dt	<dt	<dt	0.44	<dt	0.52	<dt	0.12	0.38	0.73
Total	97.08	96.36	89.69		90.92	91.12	94.04	94.05	94.75	92.34	80.58	91.40	93.61	94.61	94.57	94.35	95.79	96.82
atoms per unit formula																		
Nb	0.963	0.936	0.772	0.828	0.713	0.789	0.988	0.747	0.795	0.815	0.927	0.889	0.965	0.980	0.868	0.834	1.628	1.539
Ta	0.024	0.030	0.015	0.048	0.014	0.008	0.015	0.017	0.036	0.024	0.025	0.000	0.043	0.005	0.015	0.006	0.013	0.022
Ti	0.044	0.044	0.047	0.057	0.062	0.314	0.052	0.275	0.297	0.211	0.867	0.841	0.743	1.074	0.029	0.014	0.060	0.136
Zr	0.013	0.020	0.036	0.007	0.044	0.006	0.021	0.026	0.008	0.008	0.000	0.032	0.025	0.004	0.039	0.041	0.026	0.023
Si	0.000	0.152	0.272	0.218	0.306	0.154	0.148	0.226	0.129	0.179	0.340	0.298	0.361	0.299	0.205	0.211	0.379	0.316
Al	0.000	0.010	0.009	0.009	0.000	0.012	0.007	0.020	0.017	0.009	0.093	0.018	0.010	0.019	0.003	0.003	0.029	0.035
Fe	0.005	0.285	0.072	0.224	0.078	0.282	0.270	0.352	0.312	0.367	0.369	0.311	0.516	0.233	0.757	1.025	0.054	0.081
Mn	0.000	0.016	0.007	0.005	0.004	0.018	0.022	0.021	0.014	0.022	0.021	0.022	0.020	0.048	0.000	0.000	0.005	0.000
Ca	0.025	0.067	0.058	0.053	0.037	0.066	0.185	0.135	0.063	0.118	0.092	0.092	0.124	0.107	0.095	0.056	0.392	0.346
Na	0.000	0.007	0.000	0.036	0.000	0.000	0.013	0.012	0.000	0.000	0.015	0.000	0.000	0.000	0.009	0.007	0.047	0.021
BaO	0.000	0.003	0.000	0.009	0.000	0.002	0.017	0.008	0.000	0.007	0.000	0.007	0.012	0.004	0.013	0.013	0.032	0.023
Th	0.022	0.017	0.017	0.011	0.018	0.029	0.009	0.024	0.074	0.013	0.073	0.051	0.027	0.024	0.008	0.007	0.009	0.025
U	0.008	0.007	0.003	0.027	0.002	0.000	0.006	0.002	0.004	0.000	0.004	0.004	0.000	0.003	0.006	0.005	0.027	0.018
Y	0.655	0.236	0.386	0.299	0.429	0.233	0.020	0.036	0.141	0.156	0.216	0.341	0.207	0.488	0.086	0.088	0.137	0.127
La	0.001	0.003	0.020	0.007	0.003	0.013	0.003	0.005	0.002	0.000	0.004	0.081	0.003	0.006	0.002	0.002	0.005	0.005
Ce	0.011	0.094	0.134	0.124	0.159	0.178	0.327	0.403	0.228	0.240	0.430	0.397	0.440	0.089	0.091	0.026	0.018	0.063
Pr	0.003	0.003	0.005	0.000	0.000	0.006	0.000	0.002	0.003	0.002	0.005	0.014	0.003	0.006	0.000	0.000	0.000	0.004
Nd	0.026	0.021	0.025	0.009	0.013	0.033	0.013	0.013	0.016	0.014	0.028	0.057	0.020	0.041	0.008	0.004	0.006	0.033
Sm	0.019	0.014	0.014	0.004	0.009	0.015	0.005	0.006	0.010	0.009	0.018	0.018	0.013	0.029	0.003	0.001	0.000	0.021
Gd	0.020	0.006	0.007	0.000	0.004	0.007	0.007	0.007	0.016	0.003	0.023	0.009	0.009	0.017	0.000	0.000	0.001	0.010
Tb	0.008	0.006	0.006	0.004	0.006	0.005	0.000	0.000	0.005	0.004	0.006	0.008	0.006	0.010	0.002	0.000	0.002	0.008
Dy	0.064	0.049	0.054	0.039	0.060	0.043	0.000	0.000	0.041	0.034	0.054	0.066	0.052	0.082	0.022	0.014	0.030	0.069
Ho	0.013	0.011	0.013	0.010	0.013	0.010	0.000	0.000	0.008	0.008	0.011	0.014	0.010	0.019	0.004	0.003	0.005	0.011
Er	0.044	0.029	0.040	0.034	0.045	0.030	0.000	0.000	0.024	0.020	0.033	0.046	0.030	0.049	0.015	0.013	0.021	0.035
Tm	0.006	0.003	0.006	0.005	0.006	0.003	0.000	0.000	0.003	0.003	0.004	0.007	0.004	0.006	0.002	0.002	0.003	0.004
Yb	0.040	0.022	0.037	0.038	0.038	0.021	0.000	0.000	0.020	0.013	0.028	0.039	0.018	0.038	0.012	0.012	0.017	0.021
Lu	0.005	0.002	0.004	0.005	0.004	0.002	0.000	0.000	0.002	0.001	0.002	0.005	0.002	0.003	0.001	0.001	0.002	0.000
C	0.000	0.000	0.000	0.000	0.000	0.000	0.000	0.000	0.000	0.000	0.000	0.000	0.000	0.000	0.000	0.000	0.000	0.000
F	0.000	0.030	0.112	0.080	0.158	0.063	0.000	0.000	0.000	0.000	0.000	0.103	0.000	0.110	0.000	0.015	0.069	0.138
Σ cations	2.02	2.09	2.06	2.11	2.07	2.28	2.13	2.34	2.27	2.28	3.69	3.67	3.66	3.69	2.30	2.39	2.95	3.00
Σ A	0.99	1.08	1.22	1.18	1.28	1.17	1.07	1.30	1.14	1.23	1.87	1.94	1.91	1.63	1.38	1.53	1.25	1.30
Σ B	1.03	1.01	0.83	0.93	0.79	1.11	1.05	1.04	1.13	1.05	1.82	1.73	1.75	2.06	0.91	0.85	1.70	1.70
O	4	4	4	4	4	4	4	4	4	4	6	6	6	6	6	6	6	6

5.5.5 Amorphous REE silicates

Throughout the granite samples, grains exhibiting a bright SEM-BSE response, and with a Y-Ce silicates composition are identified. These grains are found as fine to coarse grained, 200micron amorphous pseudomorphs commonly intergrown with REE-fluorcarbonates with an irregular patchy habit (Figure 5.37). EMP analyses show that these Y-Ce silicates are mainly composed Ce, Y, Si, and P with minor amounts of Th, U, Ca, Fe, and F (Table 5.10). Although, concentrations of each element vary between the points analysed, the overall composition of these grains are similar to the britholite group of minerals $(REE,Ca,Th)_5(SiO_4,PO_4)_3(OH,F)$. The low CaO (1 wt % mean), and high REE (55 wt % mean REY) and F contents (2.3 wt % mean) means they are best classified as fluorobritholite-(Ce) and fluorobritholite-(Y) species. Britholites typically form as secondary minerals and have been observed replacing allanite in other A-type granites (e.g. Uher et al. 2015).

In most of the analyses, Ce_2O_3 is the dominant REE with concentrations ranging between 15 and 40 wt %. In the remaining analyses, Y_2O_3 is the most abundant with concentrations ranging between 8.3 and 24.5 wt %. The other REE make up 5 and 15 wt % of the measured britholite compositions. Chondrite-normalised patterns presented in Figure 5.38 show that the Y-Ce fluorbritholites have either flat or HREE-enriched patterns, and that all exhibit a strong positive Ce anomaly (Ce/Ce*). The HREE are consistently unfractionated, while LREE are variably fractionated. Analyses with more HREE-enriched chondrite-normalised patterns correlate positively with more strongly developed Ce anomalies.

ThO_2 concentrations in Ce-Y silicates range from 0.1 to 12 wt %, and UO_2 concentrations range from 0.3 to 2 wt %. Point analysis where Ce > Y contain notably higher Th contents. Elevated actinide element concentrations are also characteristic of britholite group minerals analysed in other granites (Uher et al. 2015).

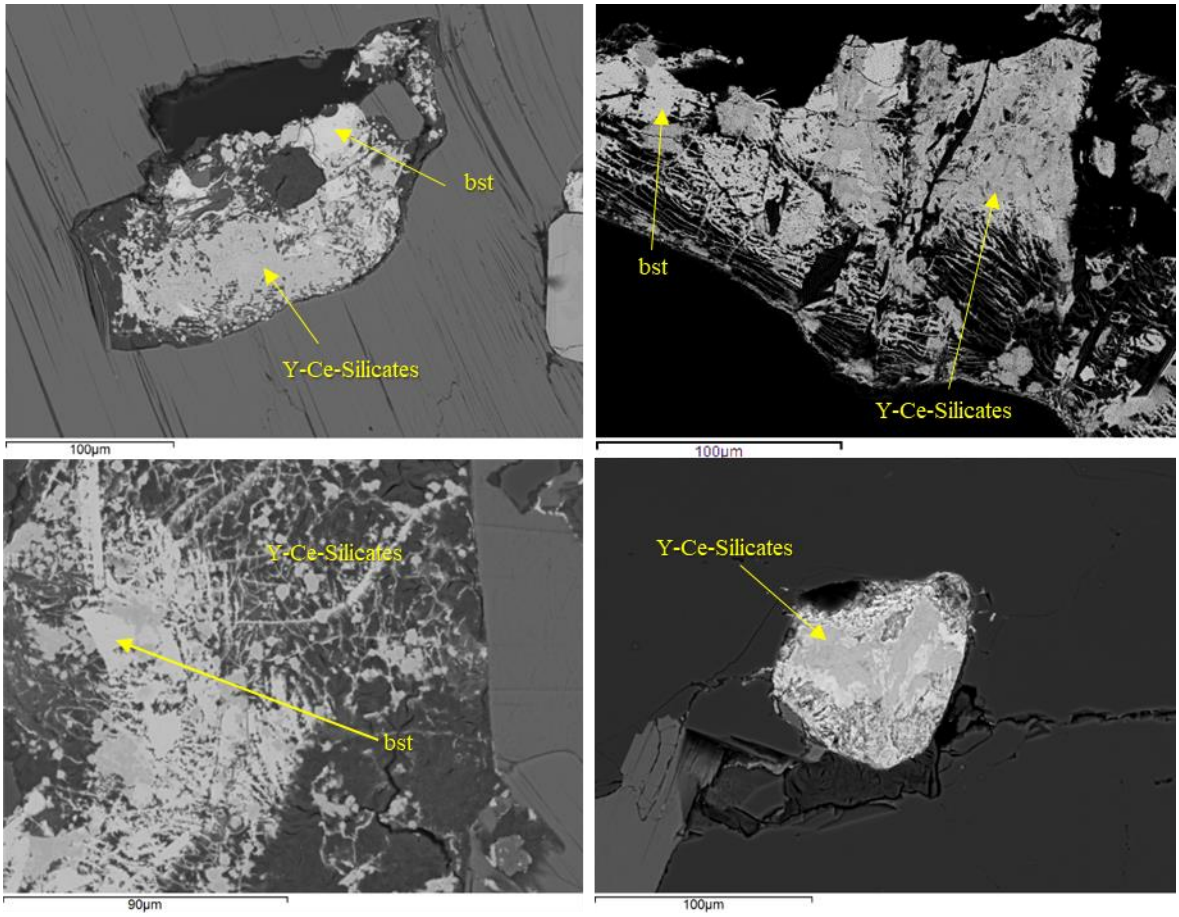


Figure 5.37. SEM-BSE images of representative fine grained amorphous Y-Ce silicates (possibly britholite-Ce) observed throughout the granite bedrock samples. Mineral abbreviations on pg 23.

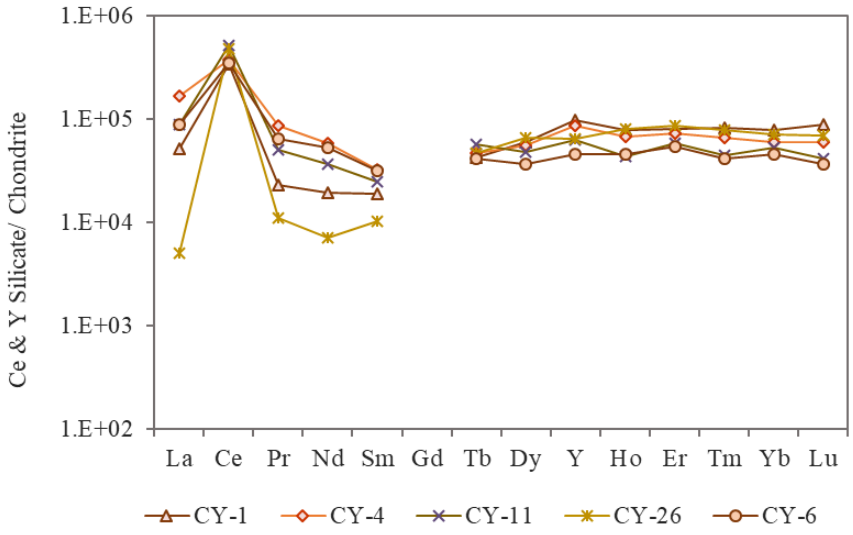


Figure 5.38. Chondrite-normalised REE patterns of representative Ce & Y silicate EMP analysis.

5.5.6 Other accessory minerals

There are several other accessory minerals present in the biotite granite with small or trace quantities of REE and Y. They include fluorite, apatite, thorite, ilmeno-rutile and titanite. Except for fluorite, all three occur in low abundance, reflecting the low P, Ti and Th whole-rock assay results.

5.5.6.1 Fluorite

Fluorite is a common accessory phase in the biotite granite. It is mostly interstitial, commonly found between feldspars and quartz crystals but also surrounding accessory phases such as zircon and samarskite (Figure 5.39; panels A, B). A few rounded grains of fluorite, up to 300 microns diameter, were also found as inclusions in K-feldspar (Figure 5.39C). The interstitial fluorites range in size, with larger grains easily discernible in hand samples. The interstitial fluorite is commonly pale to purple in visible light. Backscatter images show that fluorites in the samples are homogenous and occasionally contain inclusions (Figure 5.39 D). Unlike other accessory minerals present in biotite granite, the texture or composition of fluorite does not appear to be significantly different from its typical habit and composition.

EMPA results show that the fluorite in the biotite granite contain up to 0.46 wt % Y_2O_3. All the other trace elements are below the detection limit of the EMP.

5.5.6.2 Apatite

Round to elongate subhedral apatites, up to 300 μm in diameter, are most commonly found included in biotite crystals. SEM-BSE images show that the grains are internally homogeneous and have smooth, rounded, subhedral but defined edges. Several grains have been partially replaced by monazite and xenotime (see section 5.5.2).

The grains analysed have a fluor-apatite end-member composition, characterised by their high F and low Cl contents (below detection limit). Concentrations of TREE oxides and Y_2O_3 are < 1.2 wt % and < 2 wt % respectively, and chondrite-normalised patterns show little fractionation, with the La_N/Dy_N ratio, ranging between 0.2 – 0.8. The apatites also contain trace quantities of Fe, Mn, Na and Si (Table 5.10).

5.5.6.3 Thorite

Thorite is found in association with zircon, either as inclusions or as subhedral grains adjacent to zircon crystals (Figure 5.40; panels A, C). Due to their small size it was difficult to obtain good analyses of these thorites. However, consistent small quantities of P, Y, Ca, and F in the

larger grains found suggest they contain small inclusions or intergrowths of xenotime. The variable reflectance of the thorite grains in SEM-BSE imaging also indicates that they have internally variable compositions.

5.5.6.4 Ilmeno-rutile and titanite

Ilmeno-rutile is found most commonly in the albitised section of the drill core (in samples of lower half of the DDH0004, and in low-Nb granite samples). It is found included within or between biotite crystals as elongate needle-like crystals, oriented parallel to biotite cleavage planes (Figure 5.39; panels B, D). EMPA results show that ilmeno-rutile has variable FeO contents with values ranging between 1.9 and 25.8 wt %. This could be produced by variable numbers of ilmenite lamellae in a dominantly rutile composition mineral, as described by Meinhold (2010). The results also show that the ilmeno-rutile is Nb-rich and Ta-poor, hosting up to 4.5 wt % Nb_2O_5 but < 0.12 wt % Ta_2O_5. Trace quantities of Al, Ca, Ba, Mn, Ta, and Zr were also detected. Titanite is present as a very scarce phase, often occurring as thin needles and enclaves in biotites and in contact with ilmeno-rutile needles.

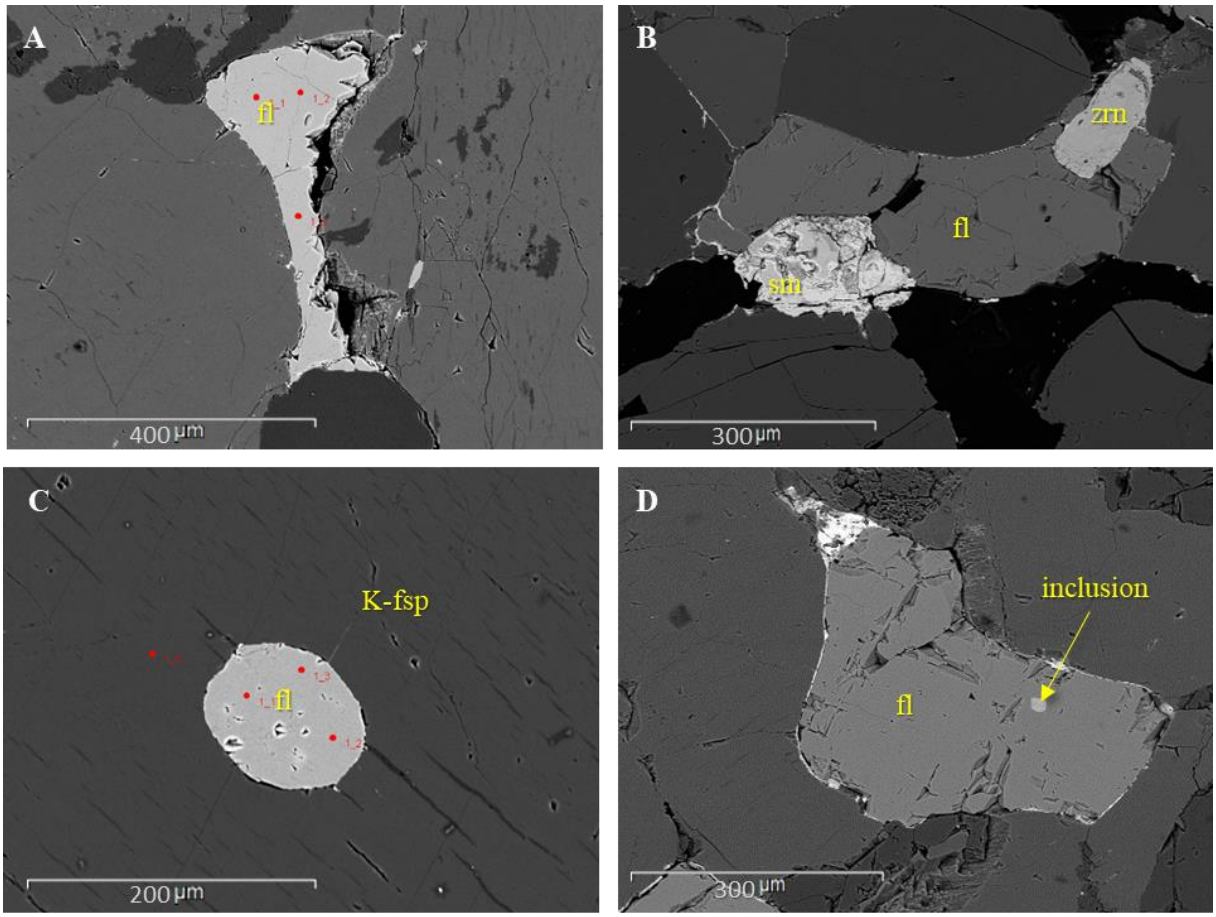


Figure 5.39. SEM-BSE images showing the typical occurrences and habit of fluorite in the biotite granite. Mineral abbreviations on pg 23.

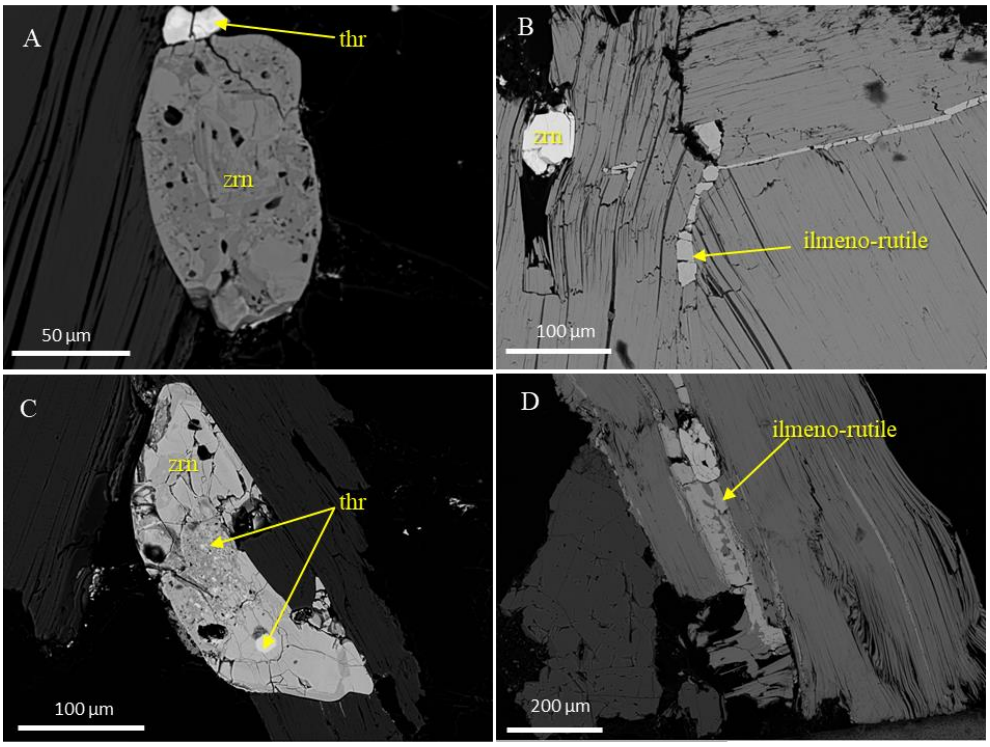


Figure 5.40. SEM-BSE images of thorites, occurring as inclusions or small grains proximal to zircons (both left), and elongate ilmeno-rutile needles associated with biotite (both right).

Table 5.10. EMPA results from apatite and Ce- and Y-silicate minerals.

	Apatite								Ce & Y silicate				
Sample	SD5	SD19	SD25	SD8	SD9	SD23	SD19	SD20	SD5	SD6	SD6	SD25	SD9
#	AP1	AP4	AP10	AP26	AP33	AP38	AP40	AP46	CY-1	CY-4	CY-11	CY-17	CY-26
wt %													
P_2O_5	35.3	42.6	42.2	42.3	42.6	44.8	40.3	44.9	5.75	7.60	3.30	4.07	4.44
CaO	49.7	54.1	51.9	54.1	52.2	53.8	53.7	56.0	0.80	1.97	1.15	0.76	1.26
Na_2O	0.1	0.1	0.1	0.1	0.3	0.1	<dt	<dt	0.00	0.00	0.00	0.00	0.00
SiO_2	0.5	0.2	0.4	0.3	0.6	0.5	0.4	0.4	12.6	10.0	16.2	20.7	16.0
FeO	0.11	0.15	0.05	0.08	0.14	0.39	0.67	0.09	0.16	0.26	0.61	5.08	6.48
MnO	0.10	0.09	0.09	0.06	0.12	0.09	0.06	<dt	<dt	<dt	<dt	<dt	<dt
Y2O3	4.07	0.68	0.96	0.78	1.35	1.03	0.53	0.46	19.5	17.0	12.6	12.9	9.2
La_2O_3	0.21	<dt	<dt	<dt	0.15	0.14	<dt	<dt	1.4	4.7	2.5	0.1	2.4
Ce_2O_3	0.25	0.12	<dt	<dt	0.35	0.11	<dt	<dt	24.5	26.96	37.20	34.31	24.74
Pr_2O_3	<dt	<dt	<dt	<dt	0.08	0.07	<dt	0.07	0.25	0.93	0.54	0.12	0.70
Nd_2O_3	0.18	<dt	<dt	<dt	0.17	0.10	<dt	<dt	1.02	3.13	1.95	0.37	2.81
Sm_2O_3	<dt	<dt	<dt	<dt	0.08	<dt	<dt	<dt	0.33	0.56	0.42	0.17	0.54
Gd_2O_3	<dt	<dt	<dt	<dt	<dt	0.18	<dt	0.10	<dt	<dt	<dt	<dt	<dt
Tb_2O_3	<dt	<dt	<dt	<dt	<dt	<dt	<dt	<dt	0.17	0.19	0.24	0.20	0.17
Dy_2O_3	<dt	0.12	0.16	<dt	0.18	0.15	<dt	0.12	1.69	1.55	1.34	1.84	1.04
Ho_2O_3	<dt	<dt	<dt	<dt	<dt	<dt	<dt	<dt	0.49	0.42	0.27	0.51	0.29
Er_2O_3	<dt	<dt	0.15	<dt	0.14	0.17	<dt	<dt	1.46	1.34	1.06	1.60	1.00
Tm_2O_3	<dt	<dt	<dt	<dt	<dt	<dt	<dt	<dt	0.23	0.19	0.12	0.22	0.12
Yb_2O_3	0.27	<dt	<dt	<dt	<dt	<dt	<dt	<dt	1.43	1.09	0.97	1.30	0.83
Lu_2O_3	<dt	<dt	<dt	<dt	<dt	<dt	<dt	<dt	0.25	0.17	0.12	0.20	0.10
ThO_2	<dt	<dt	<dt	<dt	<dt	<dt	<dt	<dt	11.4	2.1	3.0	2.5	2.56
UO_2	<dt	<dt	<dt	<dt	<dt	<dt	<dt	<dt	1.37	0.88	1.66	1.00	0.92
Cl	<dt	<dt	<dt	<dt	<dt	<dt	<dt	<dt	<dt	<dt	<dt	<dt	<dt
F	4.19	4.76	4.64	4.95	4.12	4.98	4.40	3.78	3.39	3.66	3.09	1.23	2.64
-O=F	1.76	2.00	1.95	2.08	1.74	2.10	1.85	1.59					
Total	93.3	101.0	98.7	100.6	100.8	104.6	98.2	104.2	88.2	84.8	88.3	89.2	78.2
TREE	0.91	0.24	0.31	0.00	1.15	0.92	0.00	0.29	33.28	41.21	46.73	40.97	34.76
REY	4.99	0.92	1.27	0.78	2.50	1.95	0.53	0.75	52.83	58.25	59.29	53.89	43.95

5.6 Discussion

5.6.1 Serra Dourada Granite

There have been few published studies that examine the composition of the Serra Dourada granite. Some published data exist for the margins, and northern half of the SDG complex, located ~25 km from the Serra Verde study area. No public geochemical data exist that traverse the granite interior where the Serra Verde deposit is located.

Drill hole data has been useful to build a continuous picture of the geochemical variations of the bedrock across the southern Serra Dourada granite complex. Integration of the geochemical element maps has shown that the biotite granite is more geochemically complex than has previously been presented; the results indicate that the biotite granite can be divided into several distinct compositional lithologies. In addition, the geochemical maps delineate discrete boundaries within the granite complex, namely within the core of the biotite granite, and between the inner biotite and outer amphibole granites. A summary map showing the interpretation of the geochemical maps is presented in Figure 5.41.

The outermost geochemical lithology is characterised by elevated concentrations in both Ba and Ti. Reference to the national CPRM aero-geophysics datasets indicates that the outermost area is significantly more similar to the granite than the surrounding Serra da Mesa sediments, and is therefore interpreted to be part of the SDG granite complex, representing the edge amphibole granite described by Bilal (1997). The mineral composition of this lithology could not be confirmed by the drill hole assay database due to a lack of fresh core samples in this area, and because this area was not visited for sampling.

Within the margin of the amphibole granite, a core and rim of a later, single biotite granite body is interpreted to have intruded. Both the core and the rim of the biotite granite have been shown to exhibit the same REE patterns, which shows that there has been no fractionation of REE, and supports the conclusion of a single intrusion.

The core of the biotite granite is characterised by its Zr, Fe, and Ti-rich whole rock composition, and coarse-grained texture. The rim is characterised in general by a more evolved felsic composition; exhibiting higher concentrations of Si, Rb, lower Ba, Ti, and Fe as well as a notably fine-grained texture. Based on this, the rim is interpreted as the edge of the biotite granite intrusion, as the chilled contact zone of the core granite. This rim zone also contains elevated Sn and W, and therefore may relate to the development of the endo-greisen Sn

mineralisation controlling the location of a small historic working to the south-east (Macambira and Villas 1984).

The geochemical maps also show that the north-eastern half of the biotite granite has a strong Nb-, Ta- and Ga-enrichment overprint. This geochemical overprint is well-defined and clearly separates the biotite granite into two halves. Similar Nb-enriched zones have been commonly identified in A-type granites and are interpreted to relate to the fluid rich zone that concentrates the upper portion of A-type granite intrusions (Pollard 1989). The Nb-rich half of the granite is divided from the south-western Nb-poor (Th-rich) half, by a narrow linear boundary zone trending NW-SE. This boundary appears to offset the NW edge of the core, and coincides closely with linear zones of elevated Ba and Sr, suggesting the action of a fault zone that transects the core and rim of the biotite granite.

The difference in composition between the two halves may be explained by vertical movement on this fault, where the north-eastern half is interpreted as the down-thrown hanging wall of the fault. Fluids likely percolated through this structure to produce local precipitation of Ba- and Sr-bearing minerals, most probably sulphates and carbonates. Mineralogical results from DDH0004 show that only the samples from the top section of that drill hole contain niobiate and LREE-fluorcarbonate minerals. Therefore, DDH0004 appears to have intersected the fault boundary between these two granite halves, most likely occurring at the zone of elevated Ba and Mg geochemistry, coincident with visible albitisation and strain, occurring at 70 to 86 m depth.

Mapping and study work at other granites in the Tocantins province have shown that multiple intrusive complexes are common (e.g. Serra Branca (Pinto-Coelho et al. 2007), Sucuri (Machado de Mello & Bilal 2009)). Without geochronological dating in this area, a more complex multiple intrusive history to explain the differences in granite composition cannot be ruled out and should be the focus of further work.

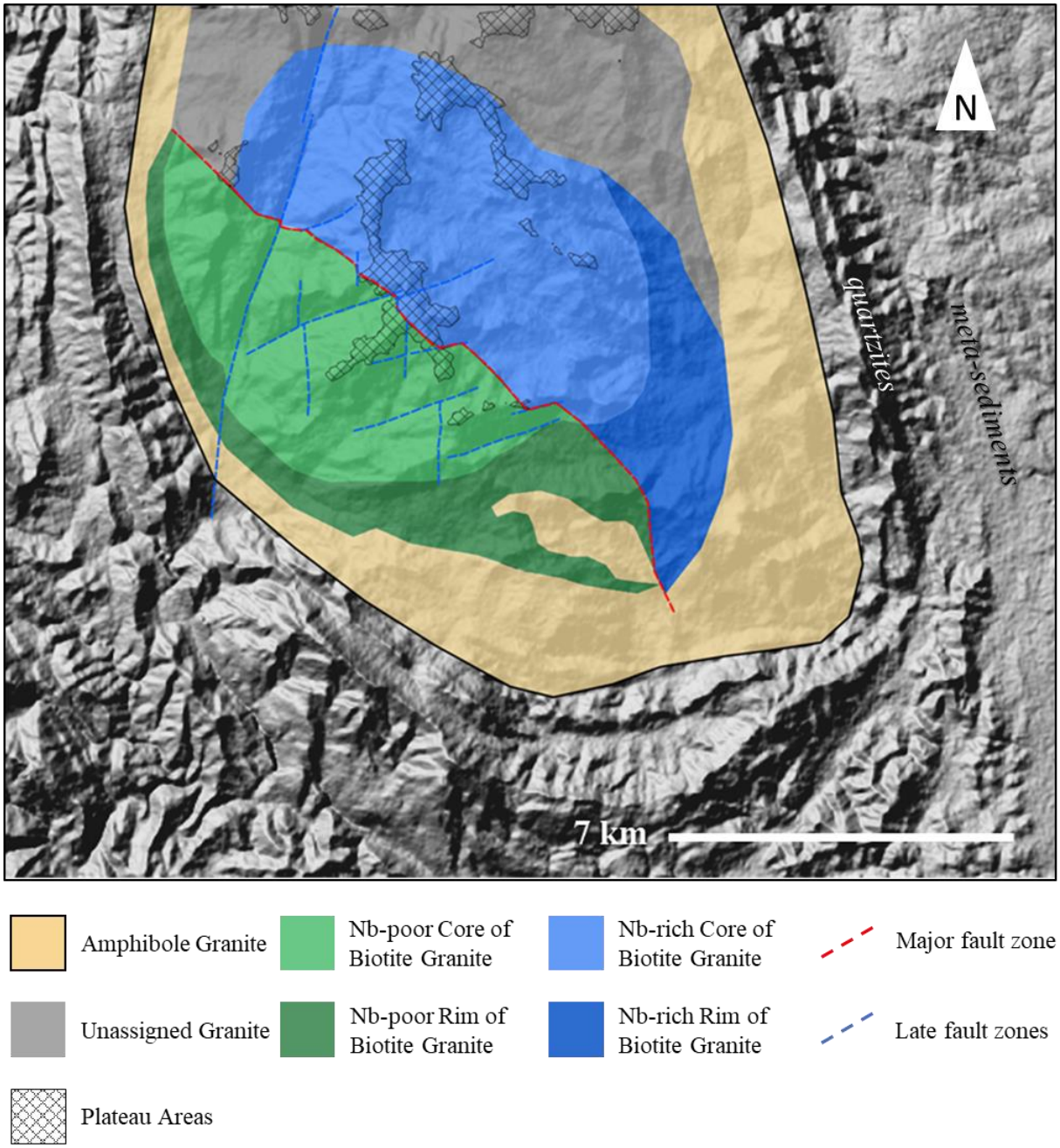


Figure 5.41. Interpretative 2D lithological map based on geochemical element maps and draped over hill-shaded digital elevation model.

5.6.2 Geochemistry of the Serra Verde parent bedrock

The central plateau, which is the focus of this study, is located in the center of the biotite granite body and mostly sits over the Nb-rich core zone. The granite samples collected from the plateau show that the parent rock of the Serra Verde REE deposit is a highly evolved alkali rich coarse grained feldspar-quartz-biotite granite. Geochemically the parent rock is REE-enriched, contains abundant F, has elevated concentrations Zr and Fe, and is generally low in P, Ti and

Ca concentrations which are reflected in the compositions of the accessory mineralogy. The main differences observed between the Nb-rich and Nb-poor biotite granite samples are the that the Nb-rich biotite granite is slightly finer and paler in colour, has elevated Nb, Ta, Ga and HREE, and has a more intesely altered REE mineral assemblage than the Nb-poor biotite granite (see also section 5.6.3).

The parent bedrock of the Serra Verde deposit is strongly enriched in REE. The REE content samples analysed from the biotite granite range from 800 to 1500 ppm REY with higher concentrations found in samples that fall in the Nb-rich side of the biotite granite north of the fault boundary. These concentrations are generally higher than previously published biotite granite data from other parts of the Serra Dourada granite (Figure 5.42). Marini et al. (1992), Bilal et al. (1997), and Teixeira & Botelho (2006) report values of 500 ppm to 850 ppm REY in samples, mainly collected from the edge and northern half of the complex. The chondrite-normalised patterns of the enriched bedrock underlying the SV deposit exhibit the same patterns as those from the publications cited above. The main difference to results from this study is the identification of more elevated REE concentrations, and slightly stronger HREE enrichment relative to LREE in the granite underlying SV deposit. The composition of the biotite granite in the centre of the southern half of the complex is also less peraluminous than published data from elsewhere in the SDG (Figure 5.42).

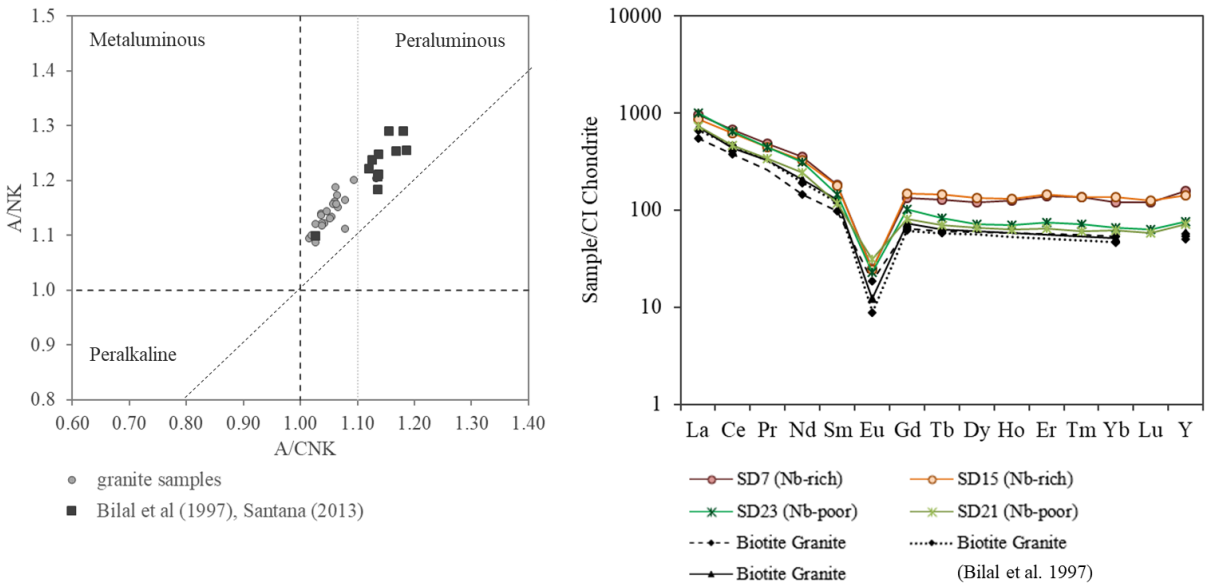


Figure 5.42. Classification of rocks (left) and chondrite-normalised REE patterns, including published whole rock data, for SD granite samples.

The elevated HFSE, alkali element, and REE composition of the biotite granite in the centre of the lower half of the SDG compared to other parts of the complex suggest the Serra Verde deposit developed over a geochemically and mineralogically distinct part of the complex. The only other granite in the Tocantins region that has been found to hold comparably high REE contents is Pedra Branca, located 120 km from Serra Verde (Marini et al. 1992). Both belong to the 'g2' sub-group; an evolved group of felsic intrusives with metaluminous to peraluminous characteristics which may have undergone similar REE-enrichment events.

5.6.3 REE-bearing minerals of parent bedrock of Serra Verde REE deposit

Detailed SEM and EMP mineralogical work on samples collected was carried out to determine the residency of REE in the parent bedrock of the Serra Verde REE deposit. The results show that the REE in the granite samples studied are held in a variety of accessory minerals which are found most concentrated around biotite clusters. They include monazite, REE-fluorcarbonates, zircon, xenotime, metamict niobiates, unidentified Y- and Ce-silicates, fluorite, and apatite. The first two minerals listed concentrate the LREE, whilst the remaining minerals, especially niobiates, host the HREE.

Zircon, fluorcarbonates, niobiates, and Y- and Ce-silicates are the most abundant REE accessories and are therefore concluded to be the principal REE host minerals in the Serra Verde parent bedrock. Xenotime and monazite also contain high concentrations of REE, but are scarce in the rock samples studied, while fluorite and apatite hold low concentrations of REEs most of which were below the microprobe detection limit.

REE bearing minerals display pseudomorphic, and internal patchy textures, and have atypical compositions, which suggests that they represent new phases that have replaced extant minerals in the bedrock granite. This is interpreted to be due to remineralisation by, or precipitation from a hydrothermal fluid that interacted with the granite. A short discussion for each mineral is given below:

5.6.3.1 Zircon

Zircon is the most abundant accessory mineral in the biotite granite underlying the Serra Verde deposit. The grains appear to be primary with oscillatory zoning and formed before most other accessory phases. The dark alteration patches which overprint the primary texture reveal that

the zircons were most likely altered and enriched in HREE by corrosive hydrothermal fluids after their formation.

Corrosive textures along fractures and the localised patches of HREE-enrichment suggest that fluids penetrated zircons through cracks, and alteration was focused on particular growth zones, generally including the mineral core. This preferential alteration may be related to variations in chemical composition of the zircon, in addition to radiation damage caused by the decay of Th and U, or physical disturbances to the original crystal structure.

Teixeira & Botelho (2006) have argued that zircon has little influence on the REE content of the Serra Dourada biotite granite based on their findings that only a few zircon grains were enriched in Y and HREE in the samples they analysed. However, comparable zircon compositions are not observed in the granite underlying the Serra Verde deposit. The majority of zircons analysed contain REE-enriched zones, and therefore a significant percentage of the bulk Y and HREE are likely to be locked in this accessory mineral in the southern part of the granitic complex. In order to calculate the REE locked in these minerals, it would be necessary to measure the abundance of zircon in the rock, and analyse mineral separates from known masses of granite.

Zircons presenting similarly dark, low analytical totals, and REE-enriched patches have also been observed in other granites such as the Ririwai biotite granite in Nigeria (Pointer et al. 1988) and La Pedraza in Spain (Perez-Soba et al. 2007). Both of these granites are highly fractionated alkali-rich granites and are REE-enriched. Studies of these granites attribute the development of the dark patches to hydrothermal alteration by F-rich and alkali rich fluids. Fluorine is known to be sufficiently corrosive to breakdown zircon and transport Zr (Rubin et al. 1993). A similar fluid event in the bedrock at Serra Verde may also have facilitated alteration of the zircons, and carried elements such as Al, Fe, Nb and P, which allowed coupled cation substitution for Zr and Si. Such an alteration would likely have resulted in the hydration and increased porosity that are observed in these zircons.

5.6.3.2 Monazite

Monazite is an uncommon accessory mineral, and therefore a minor REE carrier in the Serra Verde biotite granite. The relatively low abundance of monazite to other accessory phases means that it likely hosts a low proportion of the total REE. This finding contrasts with those from studies on other parts of the SDG which have identified monazite as the primary LREE-bearing phase (Santana 2013).

Two types of monazite have been identified; a primary magmatic Th-rich monazite-(Ce) and a secondary, Th-poor, Nd-rich monazite-(Ce), with the latter being dominant in the granite bedrock. The Th-rich monazite species, has been identified in other parts of the biotite granite by Teixeira and Botelho (2002) where it is also interpreted to be magmatic, but is observed in high abundance. The low abundance of Th-rich monazite in samples from Serra Verde, together with the low whole rock phosphate contents, suggests that the magmatic REE mineralogy of the centre of the biotite granite is markedly different from other parts of the Serra Dourada complex. The lack of primary Th-rich monazites may also help towards explaining the low Th spatial anomaly centred on the Serra Verde deposit.

The fine-grained occurrence, and chemical composition of the dominant, albeit scarce Th-poor, Nd-rich monazite-(Ce), indicates a hydrothermal origin. Very low concentrations of Th are not commonly observed in igneous monazites, which have typical concentrations of > 3 wt % ThO_2, because both Th and REE fractionate into similar minerals (Catlos 2013). As a result the Th-poor monazites (< 1 wt % ThO_2) are considered to be of a hydrothermal fluid origin (Forster 2000; Schandl & Gordon 2004). The ragged and patchy appearance of the Th-poor, Nd-rich monazites in SEM-BSE imagery supports this hydrothermal interpretation. Monazites with Th values below detection limit have also been found in the Llallagua tin deposit in Bolivia (Kempe et al. 2008), in REE-mineralised lamprophyre dykes intruding the Aby Reish shear zone in Egypt, and metasomatic metamorphic terranes (Harlov & Forster 2002)

Monazite is clearly observed replacing partially preserved apatites and titanites. The sharp replacement rims on the apatites suggest that the Th-poor, Nd-rich monazite-(Ce), formed by the dissolution and replacement of the apatite in the biotite granite, while rounded grains of Th-poor, Nd-rich monazite-(Ce), may represent complete apatite pseudomorphs. This monazite replacement process has been observed in other deposits and rocks (e.g. Araxa dolomitised carbonatite by Marino et al. 1979, Variscan Schwarzwalk metapelites by Harlov & Foster 2002), re-created in laboratory experiments (e.g. Betkowski et al. 2014; using alkali rich fluids), and simulated by thermodynamic geochemical modelling using fluorine- and sulphate-bearing fluids (e.g. Migdiv & William-Jones 2014). Both fluorine and sulphate are known complexation ligands that transport REE in fluids. Replacement of apatite is thought to occur through preferential removal of Ca and the complexation of less mobile phosphate with complexed REE to precipitate monazite (Migdiv & William-Jones 2014). The interpretation that hydrothermal monazite alteration of the biotite granite was caused by an F-bearing fluid, is consistent with the observations in this study and would explain the small the F contents

detected in monazite EMP analyses due to co-precipitating F-phases. Th partitions more strongly into monazite than LREE, suggesting that Th-poor monazites present in the bedrock are unlikely to be magmatic, and that the hydrothermal fluids were also Th-poor (Stepanov et al. 2012).

The analyses in this study show that the monazites have unusually high Ca, HREE and Y contents (1.69 wt % $HREE_2O_3$). Natural monazites are cited to be able to substitute 1 – 2 wt % HREE + Y and rarely up to 4 wt % HREE + Y at higher temperatures of 700 – 800 ˚C (Catsol 2013). This is attributed to the different ionic sizes of HREE (8-coordinated) compared to LREE (9-coordinated) resulting in preferential LREE accommodation within the larger 9-coordinated monazite sites. One explanation possible explanation, is that lower Ce and higher Nd contents in these monazites cause the crystal lattice to shrink and therefore accommodate greater amounts of HREE in the mineral structure. HREEs in these monazites are negatively correlated with Ce and positively correlated with both CaO and F contents (Figure 5.23). This observation, together with the detection of F and low analytical totals, may be partly explained by the presence of finely inter-grown fluorcarbonates.

The chemical composition of the Nd-rich monazite-(Ce), have not been reported previously in the Serra Dourada granite complex. However, Teixeira and Botelho (2002) have described monazite-Ce in albitites and greisens, found in the south-eastern end of the granitic complex, with higher CaO (0.15 – 1.6 wt %) and lower ThO_2 (2 – 10 wt %) contents. The conclusion of this study corroborates with that of Teixeira et al. (2002) where they propose that these secondary monazites formed by the destruction of primary apatite and allanite by a REE-bearing hydrothermal fluid.

5.6.3.3 Xenotime

Like monazite, xenotime is present in small abundances and two different varieties were been identified in the granite: a 'normal' composition xenotime species, and a F-rich xenotime. The normal xenotime is very rare and its composition matches that of typical magmatic xenotimes, and xenotime analyses carried out by previous studies of the SDG (Teixeira and Botelho 2006). Contrastingly, the more abundant F-rich xenotimes have not been reported before in the SDG, and have an unusual chemical composition characterised by enrichment of Y and F, lower MREE and P contents, and fractionated Y_N/Ho_N values. These xenotimes are commonly found replacing apatite crystals.

The replacive occurrence and unusual composition of F-rich xenotimes in the Serra Verde bedrock suggest that they are of hydrothermal origin, and most likely formed from the interaction of a REE- and F-bearing fluid with primary apatite grains. Although rare, occurrences of F-rich xenotimes have been reported before at the world-class Nb-Ta-Sn deposit in the Madeira granite at Pitinga, Brazil (Bastos-Neto & Pereira 2012), with reported F contents up to 5 wt %.

5.6.3.4 Niobiates

Niobiates in the SDG have previously only been found as residual minerals, mainly fergusonite, identified in alluvial sediment samples (Santana 2013). The niobiates described in this study are the first known niobiates to have been found and described in-situ in the biotite granite of the SDG.

The main niobiate species identified in the granite is samarskite; a complex REE-Nb-oxide that is difficult to characterise due to its metamict nature. The grains analysed are HREE-, Y- and Ce-enriched, with small concentrations of Th, and are usually found either replacing zircon or xenotime, or intergrown with REE-fluorcarbonates.

The abundance of niobites was not measured, but the positive correlation between Nb and HREE concentrations in whole rock samples compared to the poor correlation between Zr and HREE, suggests they are more important HREE carriers than zircon in the Serra Verde parent rock. A positive Nb - Y correlation in Serra Dourada granite had previously been noted by Bilal et al. (1996) but had not been confirmed with mineral composition data until now.

The occurrence of niobiates in part of the biotite granite, together with non-chondritic Y/Ho values and the atypical positive Ce anomalies suggests that they most likely of hydrothermal origin rather than magmatic. The mobilisation and behaviour of Nb in hydrothermal fluids is still not fully understood, but experiments carried out by Zaraisky et al. (2010) indicate that Nb behaves as a soluble cation in F-rich fluids, in the form of F- or F-OH- aqueous complexes.

In other alkali granites, pyrochlore and fergusonite are more commonly reported than samarskite, which is typically associated with pegmatites (Cerny and Ercit 1989). However, there are reports documenting samarskite as an accessory mineral in Sn-W granites from Thailand (Praditwan 1988), Indonesia (Clarke and Beddoe-Stephens 1987), and the IAD-hosting granites in China (Sanematsu et al. 2016). In the SV bedrock, the absence of pyrochlore from most samples other than the albitised section of DDH0004, suggests that this phase is a

by-product of localised albitisation, perhaps coinciding with the location of the fault that separates the Nb-rich and Nb-poor compositions of granite.

5.6.3.5 LREE-fluorcarbonates

Pseudomorphic LREE-fluorcarbonates are abundant in the samples studied, and analyses identify bastnäsite-(Ce) as the dominant species. These fluorcarbonates are interpreted to be secondary minerals, which have likely replaced extant allanite and titanite minerals based on the large size and habit of pseudomorphs. Allanite-(Ce) and titanite may be feasible precursor candidates to the bastnäsite; no allanite was found in samples analysed but descriptions of allanite and titanite from detrital mineral studies elsewhere in the SDG bedrock by Santana (2013 & 2015) match the shape and size of bastnäsite pseudomorphs observed in this study. Furthermore, allanite and titanite are common REE minerals found in metaluminous to weakly peraluminous granites (e.g. Bea 1996, Vlach 2007), and conversion of allanite to LREE-fluorcarbonates and iron oxides was observed by Vlach (2007).

In the northern SDG, Santana (2013) found bastnäsite replacing allanite in the granite bedrock, and the transformation of allanite to secondary REE carbonates has been reported in other granites (e.g. Berger et al. 2008, Forster 2000, Littlejohn et al. 1981). Fluorcarbonates are known to precipitate from HF and CO_2 fluids (Jones & Wood 1992) and are therefore interpreted to indicate that the hydrothermal fluid interacting with this bedrock was CO_2- and F-bearing.

5.6.3.6 Ce- and Y-silicates

Y- and Ce-fluorbritholites are frequently intergrown with LREE-fluorcarbonates, and are therefore likely to be of similar hydrothermal origin. The irregular patchwork formed by these two minerals define large pseudomorphic grains comparable to the habits of allanite and apatite, which are interpreted to be the precursor minerals. The variable P contents measured in these minerals are probably inherited from extant apatite.

5.6.3.6 Primary magmatic accessory minerals

SEM and EMP analysis of thin sections from the granite bedrock of the Serra Verde REE deposit have shown that the accessory mineral assemblage is dominantly hydrothermal, originating from the alteration and replacement of original magmatic titanite, allanite, and apatite. Primary zircons show signs of severe textural damage by alteration, but were present as an abundant primary accessory mineral, while magmatic REE phosphates are partially preserved, but their low abundances indicate that they were minor REE carriers in the unaltered

granite. This interpretation is consistent with the occurrence and chemical compositions of secondary phases, and other published occurrences and experiments of hydrothermal mineral replacement by a corrosive, F-bearing, aqueous fluid. The highest preservation of partially preserved apatite and titanite occurs in the drill holes in the south-western Nb-poor half of the granite, and this likely indicates that the hydrothermal alteration only acted through some sectors of the granite body at surface today.

5.6.4 Hydrothermal alteration

5.6.4.1 Composition of the hydrothermal fluid

The presence of LREE-fluorcarbonates and fluorite together with the variable quantities of F in other the other accessory minerals support the theory of alteration by F- and CO_2-bearing fluids. Except for the Nb oxides, all accessory minerals were found to contain fluorine in variable quantities above the detection limit, indicating that this fluid has pervasively metasomatised the mineralogy of the granite bedrock.

The whole rock geochemistry together with mineralogical observations of the accessory minerals in biotite granite underlying the Serra Verde deposit suggest the metasomatising F-CO_2 fluid has transported and introduced Nb and HREE into the bedrock. Geochemically this is shown by the large mappable Nb bedrock anomaly, positive Nb - HREE correlation, and HREE-enrichment with no accompanying LREE-enrichment shown by the chondrite-normalised patterns. Mineralogically the presence of Y in fluorite, the Ho/Y fractionation in several mineral groups, and the identified occurrence of both samarskite and F-rich xenotime, is supporting evidence that the HREE were a constituent of the F-rich fluid. In contrast, SEM images of secondary LREE and Th phases show that they have formed in close proximity to their precursor minerals, and were likely not mobile constituents of the hydrothermal fluid. Preferential enrichment and transport of HREE and Nb in late-stage fluids has been reported in other A-type granites. In the Mesozoic aged Young granites in Nigeria for example, alkaline rich F-bearing hydrothermal have also been correlated to the disseminated Nb, Ta, U, Sn and HREE mineralisation (Ogunleye et al., 2006, Pirajno, 2009).

Fluorine-rich fluids are considered very efficient phases for concentrating and transporting HFSE (Zaraisky et al., 2010), as well as having the ability to attack minerals that are otherwise considered to be relatively inert. The interaction of fluorine-rich fluid with crystallising magma

would explain the intensely corroded texture of the altered zircons observed in SEM-BSE imagery.

However, transportation of REE is still not well-understood, and the mechanisms of complexation remain unclear. The abundance of fluorite associated with REE-enrichment was initially used to argue that fluoride (F^-) was the main complexing agent responsible for REE transport (Migdisov & William-Jones 2014). However, recent experimental results (Migdisov & William-Jones 2014) suggest that in most fluids, F^- has a very low REE carrying capacity and that other complexing agents such as Cl^- have far higher REE capacities in ore fluids. This work would suggest that another anion in the fluid, possibly sulphate, provides the carrying capacity for the REE in the metasomatising fluid. The presence of sulphate in the hydrothermal fluid is suggested by the S content of secondary Th-poor monazite, and the anomalously high Ba concentrations in the central fault zone at Serra Verde, probably representing localised barite precipitation from a sulphate-bearing fluid.

Although, Migdisov & William-Jones (2014) do not consider F as an important transporting agent, they do view F concentrations playing a key role in the precipitation of REE from the fluid. As well as lowering crystallisation temperatures, reducing viscosity, and increasing ion diffusivity of magmas and associated fluids (Manning 1991, Giordano et al. 2004), it has been shown that fluorine concentrations can influence the activity coefficients of high field strength elements by increasing their solubility (Agangi et al. 2010, Keppler 1993). The precipitation of fluorite can therefore be viewed as a trigger for the precipitation REE from solution by reducing their solubility and destabilising REE-complexes.

What is clear is that a F-rich hydrothermal fluid interacted with parts of the biotite granite, altered its REE mineralogy, and increased its bulk HREE content. As most of the samples exhibit the same chondrite-normalised patterns, and show similar degrees of REE enrichment, the majority of the REE content in both the Nb-rich and Nb-poor biotite granite can be attributed to the primary magmatic composition of the granite.

5.6.4.2 Source and migration of the fluid

The abundance of fluorite and occurrence of fluorite inclusions found in feldspars suggests that these minerals first crystallised from a fluorine- and volatile-rich magmatic intrusion. A high volatile content is associated with more hydrous melt compositions, which have long been known to lower the solidus temperature of granitic intrusives (Tuttle & Bowen, 1958). This increases the time for volatile-rich fluids to accumulate and separate from the melt during

crystallisation and cooling. As the volatile fluids migrate, they pick up incompatible elements (HFSE, U, HREE) from the granitic melt. The low density of the volatile-rich fluid causes it to rise to the roof of the intrusive body, and concentrate beneath the carapace.

The Nb-rich zone of the biotite granite most likely represents this roof zone of the biotite granite intrusion, this is indicated by the finer crystal grainsize of the granite in the Nb-rich zone, the presence of Nb rich pegmatites that frequently cross-cut the biotite granite, and the Nb zonation in DDH0004 which shows the upper portion to be significantly more Nb-rich. Pollard (1989) suggests that vertical geochemical and textural zonation is commonly observed in granites associated with rare metal mineralization.

The preferential accumulation of HREE in fluids can be explained by the difference in compatibility behaviour of LREE and HREE during magmatic crystallization. In felsic magmas, LREE act as compatible elements and become incorporated into LREE-rich accessory phases, such as monazite and allanite (Miller and Mittlefehldt 1982). This causes HREE to accumulate in the increasingly hydrous melt during crystallisation. Thus, fractionation of REE allowed HREE to become enriched in the volatile fluids that were be transported into the top of the granite body.

These volatile fluids may also be responsible for the tin mineralisation in and around the south-eastern portion of the biotite granite. In the 2D geochemical maps, a distinct Nb-rich zone of the biotite granite extends towards the periphery of most intense greisen alteration and cassiterite occurrences (Macambira & Villas 1984).

5.6.5 Proposed model for REE enrichment and hydrothermal alteration of bedrock granite

Petrographic, geochemical and mineral chemistry data suggest that the REE enrichment in the parent granite bedrock of the Serra Verde deposit is the product of the combination of magmatism, post-magmatic hydrothermal metasomatism, and subsequent deformation. A schematic cross-section presented in Figure 5.43 shows the proposed impact of this metasomatism and deformation on the granite, using the observations of the mineralogical and geochemical compositions from samples across the southern SDG.

The following sequence of events is proposed to explain the results of this study:

1. Amphibole granite intrusion into Serra da Mesa Group sediments.

2. Biotite granite intrusion emplaced into amphibole granite, cooling slowly to produce a relatively more evolved, felsic rim.
3. Development of late stage F-CO_2-H_2O fluid from the biotite granite, which mobilises Nb, Ta, W, Sn and HREE.
4. Migration and concentration of the late stage fluid upwards to the cupola of the biotite granite.
5. Metasomatisation of the granite by action of the late stage fluid reacting with the cupola and rim of the biotite granite, resulting in enrichment Nb, Ta, W, Sn and HREE and formation of hydrothermal accessory mineral assemblage from magmatic phases.
6. Deformation producing large faults through the biotite granite (NW – SW trending fault), bringing the metasomatised upper portion of the biotite granite in contact with the unaltered granite core.
7. Subsequent erosion of the overlying sediments and exposure of granite, leading to the removal of the metasomatised cupola at the south-west side of the biotite granite.
8. Development of a thick weathering profile over the exposed biotite granite.

Other regional metamorphic events post-dating the intrusion of the granite are well-documented (e.g. Suita 1998, Pimental et al 1991), and the impact of these events has not been investigated in this study. However, these events are not considered to have had significant impact on the chemical composition of the granite bedrock.

The proposed history is simplified model of the intrusive and fluid alteration history of one part of the SDG. The history of this complex is likely to be more complex, perhaps involving multiple phases of fluid-granite interaction. More work is needed to present a more detailed history of the evolution of the Serra Dourada granite, specific chemical controls on REE mineral alteration and the source and timing of the F-CO_2-H_2O hydrothermal fluids.

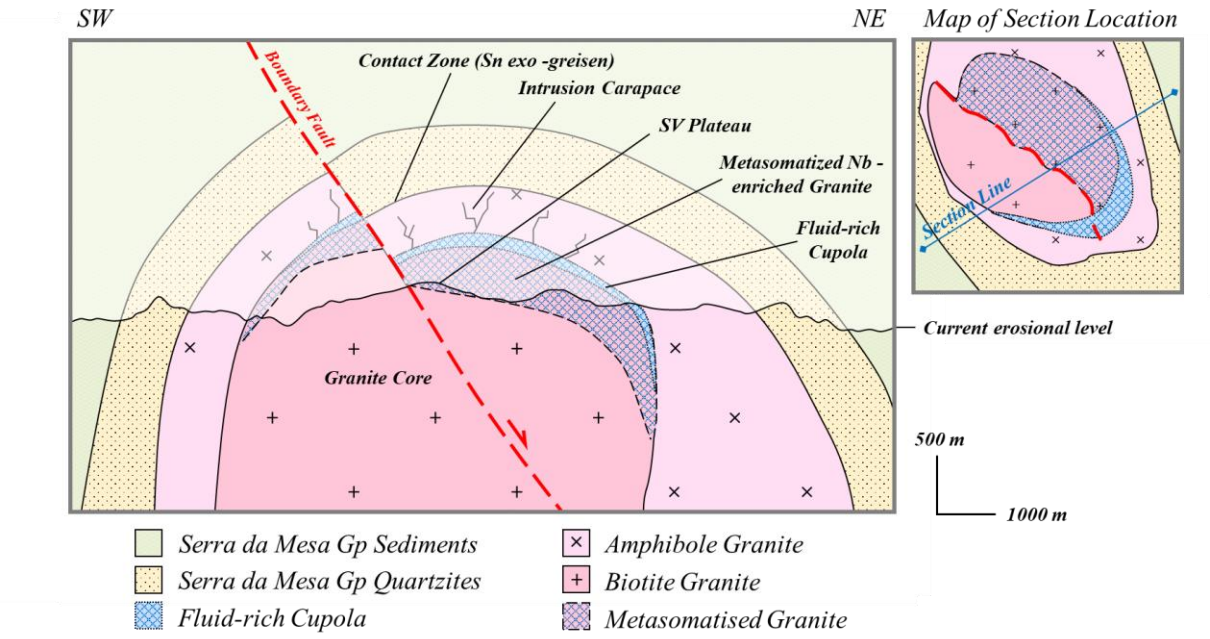


Figure 5.43. Generalised interpretative cross-section of the Southern SDG, showing an estimated offset of the central fault, and the extent of hydrothermal metasomatism in the upper portion and roof of the biotite granite body, based on geochemical bedrock element maps and published mapping data in the SDG area.

5.7 Conclusions

1. The core of the bedrock underlying Serra Verde is composed of a highly evolved, weakly peraluminous alkali feldspar granite, rich in both HFSE and REE, but poor in phosphate. The rim of this granite is more fine-grained and silica-rich than the surrounding amphibole granite described by previous studies.
2. The REE assemblage of the parent granite is the product of hydrothermal alteration, which introduced significant HREE and Y, resulting in the replacement of primary allanite, apatite, and titanite with a more complex accessory assemblage. LREE-fluocarbonates and complex niobiates are the principal REE host minerals.
3. Variations in geochemistry and mineralogy indicate that only some parts of the SDG are REE-enriched and hydrothermally altered. The Serra Verde REE deposit developed directly over the most strongly REE-enriched part of the SDG.
4. The chemical composition of altered minerals, and the abundance of fluorite suggests that a F- and CO_2-rich fluid was responsible for modifying the primary granite mineralogy, and is likely to have originated from late stage metasomatim of the biotite granite intrusive, before subsequent deformation events.

Chapter 6

Characterisation and Mass Balance Analysis of the REE-enriched Weathered Profile of the Serra Dourada Granite

6.1 Introduction

Rocks exposed on the surface of the earth undergo chemical and physical weathering. The breakdown and transformation of their primary minerals together with mobilisation of their constituent elements leads to their eventual transformation into soil or sediments. Chemical weathering is the dominant process in humid and warm environments, and is caused by acidified surface waters, from the dissolution of atmospheric CO_2 and organic acids, interacting with a mineral substrate (White 2003). The breakdown of minerals occurs mainly through hydrolysis, oxidation and dissolution reactions. In areas where the rate of chemical weathering is faster than erosion, vertical, stratified weathering profiles develop with distinct horizons between the fresh bedrock and the surficial soil. Weathered profiles are best developed in the tropics, where thicknesses between 30 and 100 m may be found (Gutierrez 2013).

The role of chemical weathering as a mechanism for enrichment has long been recognised in economic geology (Freyssinet et al. 2005). Several deposit classes are hosted entirely within weathered rock material (e.g. Al bauxites, Ni laterites, and REE deposits), and form either by residual enrichment or element re-distribution mechanisms. In the case of Chinese IADs, the latter is considered to be the main mechanism of enrichment, causing mobilisation and accumulation of REE into the middle and lower sections of the weathered profiles (Sanematsu and Watanabe 2016). In the profiles of these IADs, the mobilisation of REE has advanced to such a degree that separate zones of REE accumulation and depletion have developed. Deposits in China reportedly have grades from 500 to over 3000 ppm REE, representing 3 to 5 times the concentration in the parent rock (Bao and Zhao 2008), highlighting the role of these

mechanisms in determining the magnitude of enrichment. Assessing the contribution of different weathering processes to the REE enrichment is therefore crucial to understanding the formation of IADs.

The Serra Verde REE deposit is hosted in a thick weathered profile that developed over the Serra Dourada granite under tropical climatic conditions during the Tertiary (Braun 1971). There are no published studies of the SV weathered profile and therefore very little is known about its general mineralogy, the distribution of REE and other elements throughout the profile, or the mechanisms responsible for REE enrichment within the deposit. This information is needed to understand how weathering processes contributed to enrichment of the REE and therefore the formation of the profile and deposit at Serra Verde. In addition, it provides a valuable case study to compare with Chinese IADs, and whether the same enrichment processes and profiles are responsible for forming IADs in other parts of the world.

The aim of this chapter therefore is to, firstly, examine and describe the weathered profile hosting the Serra Verde deposit, in order to determine its maturity, vertical and lateral variation, REE distribution, and development history. Secondly, to quantify the redistribution and mass flux of REE in the weathered profile, in order to assess the effects that the tropical weathering regime has had on the distribution and enrichment of REE.

6.2 Study Area

The weathered profile that developed over the Serra Dourada granite is best preserved on the central topographic highs of the Serra Dourada granitic complex. This study focuses on the main plateau and associated ridges located in the middle of the southern half of the complex (Figure 6.1). The top surface of the plateau has an elevation of 970 m a.s.l., has a long axis trending northwest by southeast of 1.6 km and a maximum width of 650 m. The weathered profile on this plateau is fully preserved and is sufficiently extensive to examine lateral variations.

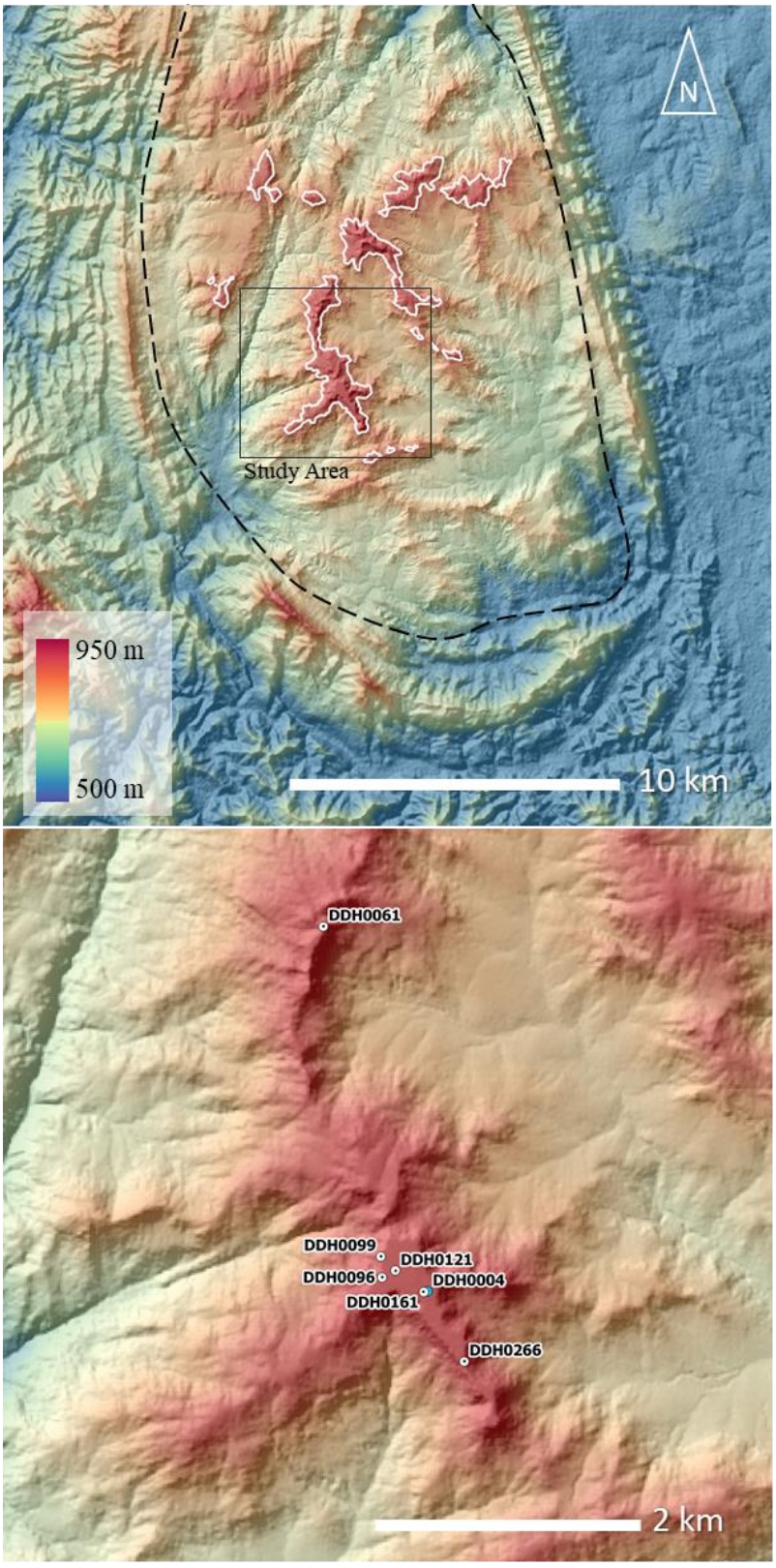


Figure 6.1. Study area. Top: Hill-shaded DEM of the southern half of the Serra Dourada granite (black dashed outline) showing the remaining topographic highs (white outlines) where weathered granitic profiles are still preserved. Bottom: A detailed view of the main plateau in the Serra Verde deposit area with the location of the drill holes studied (location of DDH0004 is also given, marked by blue dot).

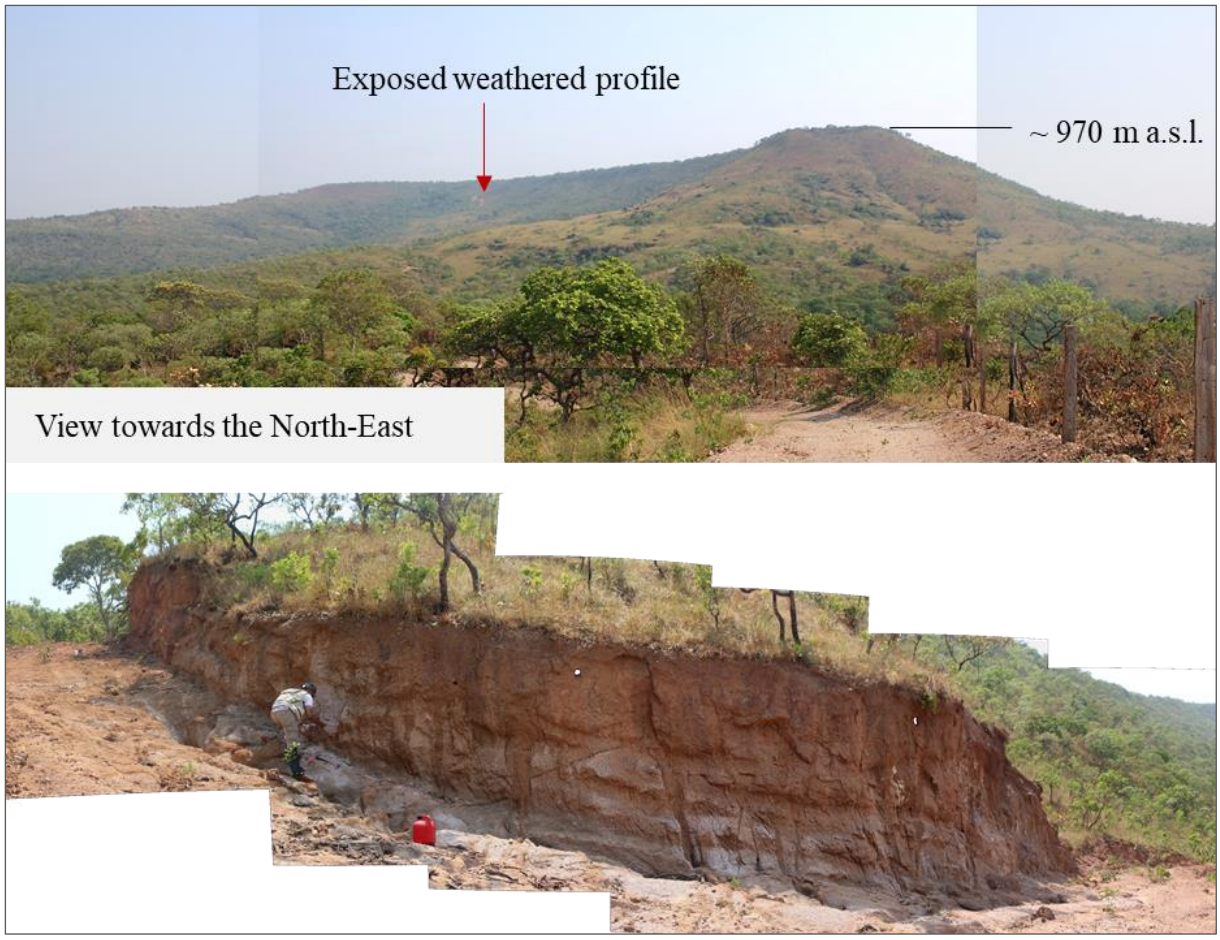


Figure 6.2. Photographs of the preserved profile on the plateau; top: aspect of the plateau; bottom: road-cut, exposing the weathered profile.

6.3 Methods

6.3.1 Sample selection

A total of 6 drill holes located on the main plateau were selected and sampled for detailed geochemical and mineralogical analysis (Figure 6.1). Each of these holes intersects the full weathered profile down to the top of bedrock, with a strongly REE-enriched saprolite. The thickness of the profile preserved on the plateau varies considerably, and therefore two short, two medium and two long profiles were selected to study the range in variation.

Mapping and some further sampling (studied in Chapters 7 and 8) was carried out along road exposures of the profile on the plateau to examine macro-textures of the weathered material, and lateral variation of the horizons (Figure 6.2).

6.3.2 Analytical methods

Whole rock geochemical data used in this chapter was provided by Serra Verde Mining, and includes major and trace element concentrations determined by ICP-MS, ICP-AES, LOI. This data was used to examine the distribution of elements along the profile and for mass balance analysis. The full logs and corresponding assay datasets for each sampled drill hole can be found in Appendix A.

Due to the fragility of weathered material, drill core of the weathered material had dried and lost integrity by the time the field work was carried out (2014-2015). Density data was provided by Serra Verde Mining, obtained by the following method: 10 – 20 cm sections of diamond drill core were weighed and coated with cling film. Core sections were then immersed in water to measure the displaced weight of water, repeating for both wet and dried samples. The wet and dry densities were then calculated using Archimedes' principle.

SEM work was carried out to examine the weathering textures of bulk minerals and identify resistant minerals in the profile. XRD analysis was carried out on weathered samples to track composition and changes in bulk mineralogy along the profile. Detailed descriptions of the methodology, analytical conditions, data handling, and apparatus can be found in Chapter 4.

6.3.3 Calculations

6.3.3.1 Weathering intensity indices

Chemical indices are commonly used to evaluate the weathering intensity or degree of weathering of a rock sample. In this study, the chemical index of alteration (CIA) and the index of laterisation (IOL) were used assess and quantify the extent of weathering along the weathered profile of the Serra Dourada granite.

Chemical Index of Alteration (CIA)

The chemical index of alteration (CIA) was developed by Nesbitt & Young (1982). The ratio uses the concentration of mobile elements relative to the Al content in a rock, tracking the removal of mobile elements from a feldspar-like aluminosilicate reference composition in order to determine the degree of weathering. When aluminosilicate framework minerals break down, mobile elements are released and removed from the crystal while aluminium is retained in the breakdown products. The CIA index therefore measures the extent to which silicate minerals,

in particular tectosilicates and phyllosilicates, have been converted to clay minerals with no capacity for Na, K or Ca; i.e. the degree of kaolinitisation. The CIA is calculated using molecular proportions of CaO, Na_2O, K_2O and Al_2O_3 and expressed as a percentage, in the formula:

$$CIA = [Al_2O_3/(Al_2O_3 + CaO^* + Na_2O + K_2O)] \times 100\ (molar)$$

where CaO^* represents the amount of CaO hosted in silicates only.

CaO values were corrected using the methodology proposed by McLennan et al. (1993) whereby the CaO values of the sample are accepted only if CaO < Na_2O; when CaO > Na_2O the concentration of CaO is assumed to be equal to that of Na_2O.

Fresh rock samples and feldspar minerals have CIA values that fall near ~ 50, while weathered products such as kaolinite and illite have CIA values between 80 and 100. Rock samples with CIA values above 50 are therefore considered to have experienced some degree of weathering. Nesbitt and Young (1982) proposed the following classification: values < 60 represent incipient weathering, values 60 - 80 represent intermediate weathering, and values > 80 represent intense weathering. Samples with CIA values > 80 have experienced near-complete removal of mobile elements and are dominantly composed of weathering breakdown products.

Index of Lateritisation (IOL)

The CIA index is not suitable for quantifying advanced stages of chemical weathering as it only focuses on the breakdown of primary minerals. Laterisation processes that occur after complete kaolinitisation are not taken into account. These include iron and aluminium oxide accumulation, and the loss of Si from the dissolution of quartz and clay minerals. Instead, indices that measure the retention of residual elements (Fe, Si and Al) are needed to evaluate more weathered sections of the profile.

In this study the 'index of lateritisation' (IOL) proposed by Babechuk et al. 2014 is used. The IOL is calculated using wt % averages and the following equation:

$$IOL = 100 \times \left[\left(Al_2O_3 + Fe_2O_{3(t)}\right)/\left(SiO_2 + Al_2O_3 + Fe_2O_{3(T)}\right)\right]$$

The index builds on the $SiO_2/(Al_2O_3 + Fe_2O_3)$ laterite ratio proposed by Schellman (1981, 1982 and 1998). As a result, Babechuk et al. 2014 suggest the IOL index should be used together with Schellman's chemical classification of laterites and the SiO_2-Al_2O_3-$Fe_2O_{3(T)}$ (SAF)

ternary plot which can distinguish between kaolinitised, lateritised and bauxitised weathering residues. Similarly to CIA, a starting value for the unweathered rock is needed and higher IOL values represent more intensely weathered samples.

6.3.3.2 Mass balance calculations

Changes in the element composition of weathered rocks are typically expressed as the ratio of the chemical concentration of an element in the weathered sample to its concentration in the parent material $C_{j,w}/C_{j,p}$. This ratio is known as the enrichment factor, and is the result of both chemical transformation and physical deformation processes that occur during weathering. More specifically, the enrichment factor in a sample volume is mainly the product of three processes: residual enrichment, volumetric strain and mass transfer. Quantification of these enrichment processes is of particular interest for the REE and bulk elements in the SV deposit, and understanding their relative contribution in producing the varying degrees of elemental enrichment or depletion measured in the profile are one of the key objectives of this chapter.

Quantification of each of these processes is the basis for a chemical mass balance model. Equations to calculate the contribution of these processes were first developed in the 1980's by Brimhall and co-workers, and are still used today with small adjustments (Brimhall et al. 1985, 1991, 1992, Brimhall and Dietrich 1987). The equations require the identification and characterisation of the parent rock as well as chemical composition of the weathered sample and in some cases bulk dry densities.

The mass balance equations used for mass balance calculations have also the following assumptions:

1. There is a genetic relationship between the regolith and the parent material.
2. One or more elements have remained immobile during chemical weathering. The mass flux of these elements must be equal to zero. These elements are used to calculate the volumetric strain.
3. Lateral mobilisation and external fluxes (e.g. atmospheric inputs) are assumed to be negligible so that only the vertical dimension is considered, and water or fluid movement is downwards.

Contributions to chemical enrichment

The enrichment factor is derived from equation 1, (Chadwick et al. 1990):

$$\frac{C_{j,w}}{C_{j,p}} = \frac{\rho_p}{\rho_w} \times \frac{1}{(\varepsilon_{i,w} + 1)} \times (\tau + 1) \quad (1)$$

Where ρ_p and ρ_w are the densities of the parent rock and the weathered sample respectively, $\varepsilon_{i,w}$ is the volumetric strain and τ is the coefficient of mass transfer. A schematic illustration of these terms is given in (Figure 6.3) below. Residual enrichment is the process whereby density changes caused by removal or addition of mobile elements results in element concentration changes. Volumetric strain is the volume collapse or expansion caused by mass gains or losses, or caused by transformation in the mineralogy. Density changes caused by volume change can change the element concentration. Finally, mass transfer changes in element concentration occur as a result of element mobilisation and redistribution, resulting in mass gain or losses along the profile

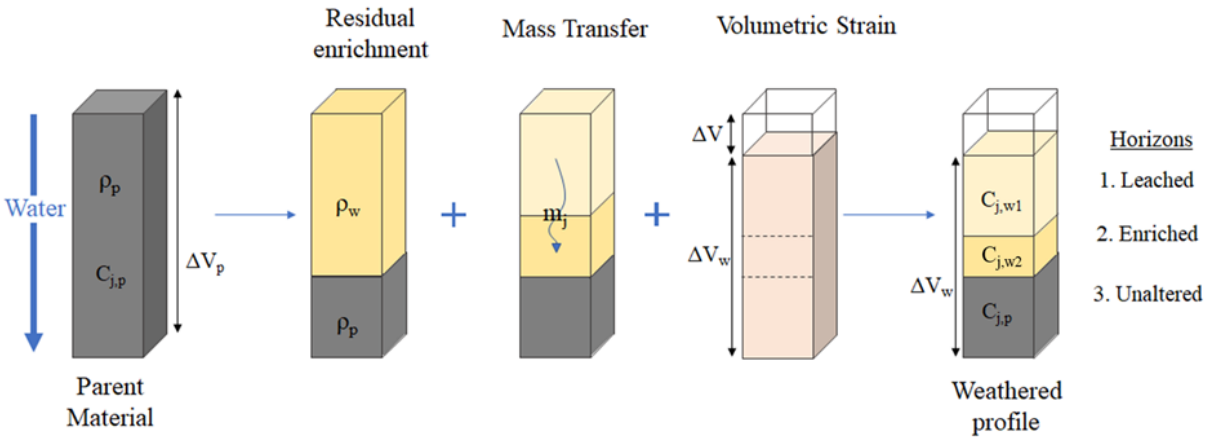


Figure 6.3. Schematic showing the three main processes controlling element enrichment within a weathering profile. Diagram modified from Brimhal and Dietrick (1987) and Amundson (2003).

The first two processes, residual enrichment and volumetric strain, are described as closed system contributions; where changes in element concentration involve no mass movement. The total mass of the element remains unchanged, but its concentration may be enriched or diluted by bulk density changes. The contribution from closed system enrichment can be estimated

with the use of 'immobile' element data. The conservative behaviour of 'immobile' element means the mass transfer term (1+ τ) in eq. 1 is equal to zero and only residual enrichment and strain contribute to the immobile element ratio (eq 2). Note that in the equation below, subscript *i* is used to instead of *j* to represent immobile element.

$$\frac{C_{i,w}}{C_{i,p}} = \frac{\rho_p}{\rho_w} \times \frac{1}{(\varepsilon_{i,w} + 1)} \tag{2}$$

The third process, mass transfer, is considered an open system process as it involves mass fluxes into and out of the system. The contribution from mass transfer is shown in eq (3)

$$m_{j,w} = m_{j,\mathrm{p}} + m_{j,\mathrm{flux}}$$

$$\frac{1}{100}(V_w \rho_w C_{j,w}) = \frac{1}{100}(V_p \rho_p C_{j,p}) + m_{flux} \tag{3}$$

Where $m_{j,w}$ and $m_{j,p}$ is the mass of element j in weathered sample and the parent rock respectively. The term $m_{j,flux}$ represents the addition or loss of mass of element through transportation.

Volumetric strain

The volumetric strain was calculated using bulk density ratios and concentrations of immobile element *i* in the weathered rock and protolith using the equation for strain (Brimhall & Drietrich 1987 Brimhall et al. 1992):

$$\varepsilon_{i,w} = \frac{\Delta V}{V_p} = \frac{\rho_p C_{i,p}}{\rho_w C_{i,w}} - 1 \tag{4}$$

Strain values that are greater than zero indicate expansion relative to initial rock volume, and values less than zero indicate the weathered rock has collapsed. Values ≈ 0 indicate no volume changes have taken place and the weathering is thus isovolumetric.

Calculation of net gains and losses

The elemental mass gains or losses in the weathered profile can be expressed as a fractional mass change relative to the mass of the element in the parent rock with the dimensionless

element-mass transfer coefficient, $\tau_{i,w,}$ (e.q. 5) (Brimhall et al. 1992, Anderson et al. 2002)). The mass transfer coefficient can be calculated using only the chemical composition of the parent rock ($C_{i,p}$) and the weathered sample ($C_{i,j}$) and therefore can be applied to both the isovolumetric and non-isovolumetric weathered profile regardless of bulk density.

$$\tau_{i,j} = \frac{m_{j,flux}}{m_{j,p}} = \frac{\rho_w C_{j,w}}{\rho_p C_{j,p}}\left(\varepsilon_{i,w} + 1\right) - 1$$

$$= \frac{C_{ip} C_{j,w}}{C_{i,w} C_{j,p}} - 1 \qquad (5)$$

When $\tau_{i,j}$ values are positive, net addition of mass has occurred, and when $\tau_{i,j}$ values are negative removal of mass has occurred. If $\tau_{i,j}$ = - 1, total removal of element *j* has occurred, and when $\tau_{i,j}$ = 0 no gains or losses have taken place and the rock can be characterised as having undergone isomass weathering.

The mass gains or losses in the weathered profile can also be expressed as absolute mass changes of an element per unit volume of parent rock, $\delta_{i,j}$ (eq.6). The calculation of this expression requires density data. (Brimhall et. 1992, Anderson et al. 2002)

$$\delta_{i,j} \equiv \frac{m_{j,flux}}{V_p} = \frac{1}{100}\left(\varepsilon_{i,w} + 1\right)\left(\rho_w C_{j,w}\right) - \frac{1}{100}\left(\rho_p C_{j,p}\right)$$

$$= \frac{1}{100}\left(C_{j,w}\rho_p \frac{C_{i,p}}{C_{i,w}} - \rho_p C_{j,p}\right) \qquad (6)$$

Both the mass transfer coefficient and the absolute mass changes per unit volume were calculated for the six drill holes studied.

Finally the total mass gains and losses of REE per unit area (kg m^{-2}) from each horizon were calculated by integrating the $\tau_{i,j}$ plot results over the thickness of a given horizon (Chadwick et al. 1990; Egli and Fitze, 2000; Brantley and Lebedeva 2011):

$$\Delta M_{j,flux} = \rho_p C_{j,p} \int_{Z=0}^{Z=L} \frac{\tau_{j,w(z)}}{(\varepsilon_{i.w}(z) + 1)} dZ \quad (7)$$

Here, L is the thickness of the horizon which was defined from drill core logging. $M_{j,flux}$ is the total mass of element j added or lost to the horizon and z is the depth interval of the sample.

6.3.3.3 Isochon analysis for immobile element identification

Mass balance calculations are highly dependent on immobile element concentrations. High field strength elements (HFSE) and Al are the most commonly used reference elements to evaluate mass fluxes in weathered profile because they are highly insoluble and tend to occur in resistant minerals (Du et al. 2012 and references there in). However, Du et al. 2012 have shown that in the most intensely weathered horizon these elements can become mobilized at different scales, particularly if they have been released from their primary host minerals. As a result, the immobile element used in mass balance calculations must be carefully selected.

The isocon analysis, developed by Grant (1986) for evaluating the mass gains and losses of hydrothermally altered rocks, can be used to identify the most conservatively behaving elements in a weathering profile. The method involves comparing the chemical composition of the altered and original rocks.

The choice of immobile element can be determined from the clustering of C_i^a/C_i^o data or the best fit data forming a linear array through the origin of the isochon diagram (Grant 2005) (Figure 6.4Figure 6.3Figure 6.4). The C_i^a/C_i^o is the ratio between the most altered, in this case the most weathered, and the original rock (the parent bedrock) for a specific element. Elements that share the same C_i^a/C_i^o will fall along the same line and will represent the most conservative elements.

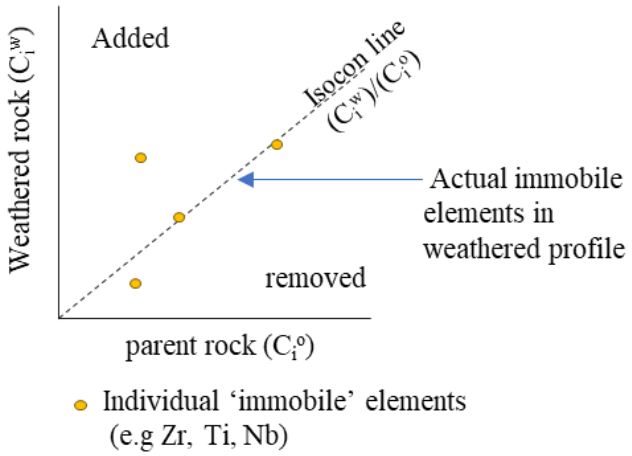


Figure 6.4. Schematic diagram showing the use of isocon analysis for the identification of conservatively behaving elements in weathered profile (marked by the isocon line).

Table 6.1. Definition of parameters used in mass balance equations.

Parameter	*Definition*
i	Immobile chemical element
j	mobile chemical element of interest
w	Weathered rock
p	Parent rock
$m_{j,flux}$ *(kg,g)*	Mass of element gained or lost /mass of element in or out of parent rock
$m_{j,w}$	Mass of element (j) in weathered material volume.
$m_{j,p}$	Mass of element (j) in parent material volume.
V_p *(cm^3)*	Volume of parent material
V_w *(cm^3)*	Volume of weathered horizon of interest. of a given thickness and unit area.
L_w *(m)*	Thickness of weathered horizon
ρ_p *(g cm^{-3})*	Parent rock bulk density
ρ_w *(g cm^{-3})*	Weathered rock bulk density
$C_{j.w}$ *(%, ppm)*	Concentration of element (j) in the weathered sample.
$C_{j.p}$ *(%, ppm)*	Concentration of element (j) in the parent rock.
$C_{i,w}$ *(%, ppm)*	Concentration of immobile element in the weathered sample
$C_{i,p}$ *(%, ppm)*	Concentration of immobile element (i) in parent rock.
$\varepsilon_{i,w}$	Net strain determined using immobile element (i) in weathered zone.
$\tau_{j,w}$	Fractional mass gain or loss of element of interest (j) relative to immobile element (i)
$\delta_{j,w}$ *(g cm-3)*	Mass gain or loss per unit volume of element j relative to immobile element i.
$\Delta mj_{,flux}$ *(kg/m^{-2},g/cm^{-2})*	Total mass gains or losses of element (j) for each horizon or profile thickness (L_w) relative to immobile element (i)

Source: Brimhall and Dietrich (1987), Brimhall *et al.* (1992), and Chadwick *et al.* 1990

6.4 General Characteristics of the Weathered Profile

6.4.1 Vertical variations

The weathered profile preserved on the central plateau of the Serra Dourada granite is a mature profile that can be divided into four well-developed horizons (the saprock, saprolite, mottled zone, and ferruginous zone), which are commonly capped by ferruginous soil. Weathered pegmatites and fractures infilled with clay material also commonly cross-cut through these horizons.

The absence of erosional surfaces, and lack of evidence for transported material along the profile were observed during field mapping or drill core logging, which suggests the profile on the plateau is an autochthonous profile that developed continuously with no clear unconformities.

A description of each horizon from the base of the profile, as well as a description of the pegmatites and infilled fractures observed, is given below. The observations are based on field descriptions and drill hole logs (Figure 6.5).

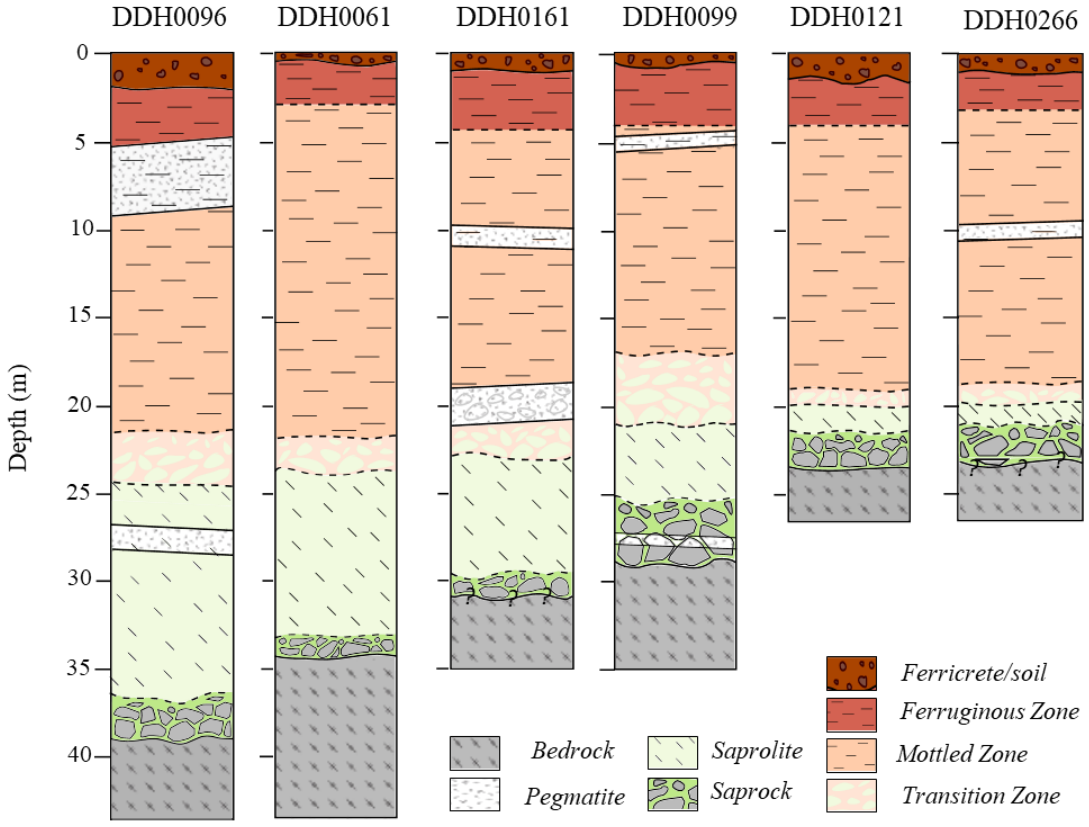


Figure 6.5. Schematic diagram showing the strip logs of the downhole profile from each of the six principal drill holes studied in this chapter.

The saprock

The saprock horizon represents the weathering front of the profile where granite breakdown begins. The saprock displays incipient to moderate weathering where the original fabric is still preserved, and the rock is still relatively competent. In the drill holes logged the saprock sections have a pale and dusty appearance, produced by the initiation of feldspar weathering, and is usually fractured. Preferential weathering along these fracture planes is observed with many of them infilled with clays (Figure 6.6). Of the feldspar minerals Na-feldspars show preferential weathering while biotite and quartz minerals remain unaffected in this horizon.

The saprock horizon in Serra Dourada granite weathered profile has variable thickness. In drill holes logged thicknesses of up to ~4 m were observed (Figure 6.5). In some drill holes the saprock is so thin that it gives the appearance of sharp pale transition from bedrock to saprolite, without any clear saprock sequence.

The saprolite

The rock material in the saprolite horizon is highly to moderately weathered. The original foliated texture and structure of the granite is still preserved but a large proportion of the feldspars have been replaced by white, secondary clay minerals. Quartz and biotite minerals are still present, but unlike in the saprock, biotite crystals have dull appearance and the rock material is friable.

The mottled zone

The mottled zone is the thickest horizon in the profile, and it is characterized by a progressive destruction of the rock fabric and increase in the formation of iron oxides. In the mottled zone, the weathered rock has a reddish mottled appearance produced by the development of iron oxides within masses of pale coloured clay minerals (Figure 6.6). Except for quartz minerals, the mottled zone is composed mainly of secondary clay minerals and Fe-oxides. The rock-forming feldspars and biotite minerals have all been weathered in this horizon.

The boundary between the mottled zone and saprolite can be either sharp or gradual. In the drill holes logged the transition zone ranges between 0.5 and 4 m thickness and is characterized by a transitional brown colour. In the transition zone the breakdown of biotite minerals from dull looking flakes to biotite ghosts of iron oxides and clay can be observed.

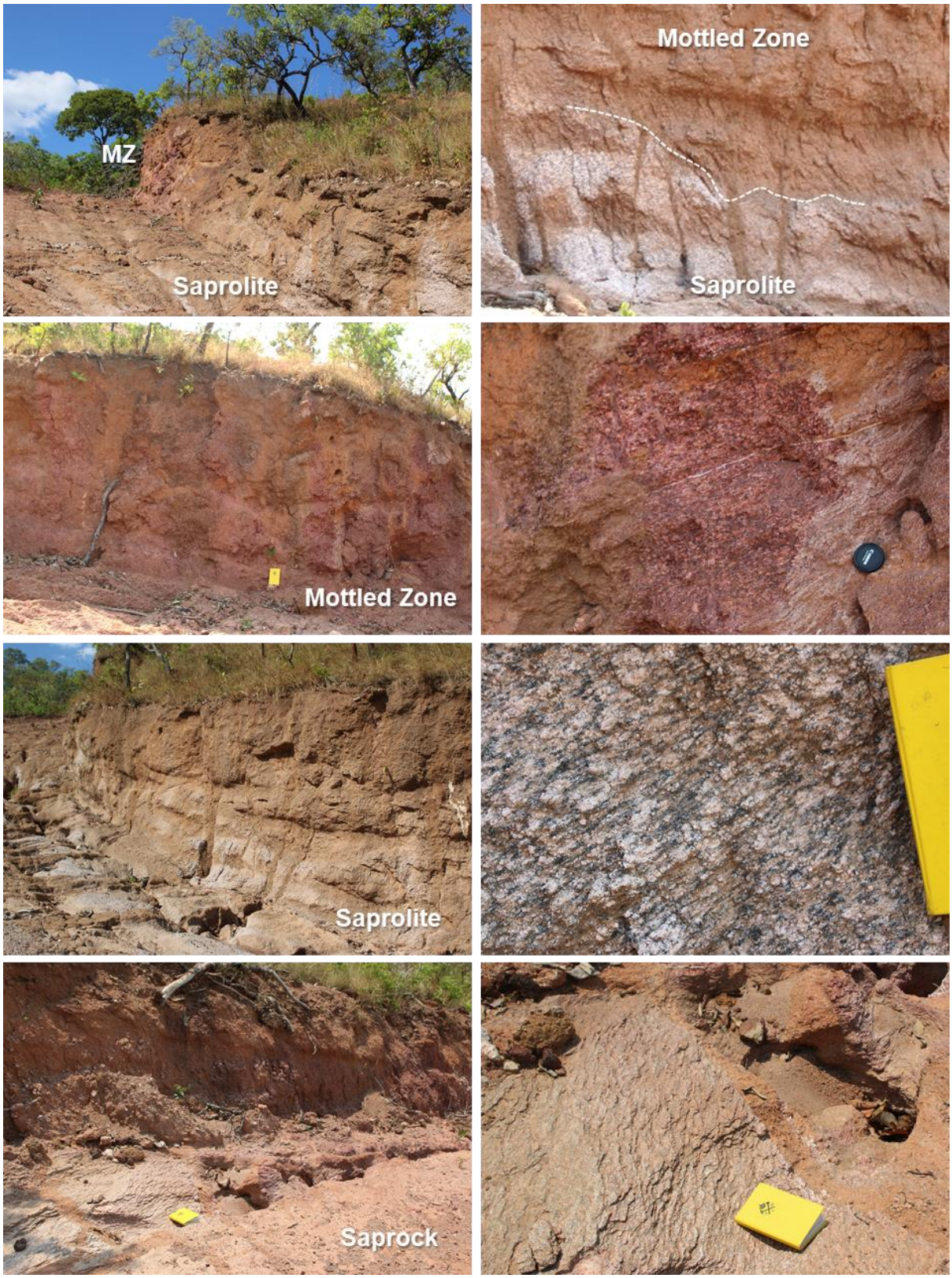


Figure 6.6. Photographs along an exposed section of the weathering profile preserved on the plateau.

The ferruginous zone

The contact between the mottled zone and ferruginous zone is transitional, extending over ca. 1 m and is mainly characterised by a colour change from pale brown to dark red. The ferruginous zone is characterised by a higher iron oxide content than the mottled zone and loss of mottled texture. In the drill holes studied, the ferruginous zone is consistently restricted to the top 5 meters of the profile.

Ferricrete soil

The ferricrete soil is the upper-most layer of the weathered profile. It is primarily composed of centimetre-sized irregularly-shaped iron nodules, and residual quartz crystals in a fine matrix of iron oxides (Figure 6.8). A small amount of organic matter, usually plant roots, can also be found in this horizon. The soil can be up to 2 m thick, but is not always present.

This layer of ferricrete appears to acts as a protective layer from erosion. In places where it is no longer present the weathered profile has become more susceptible to removal by heavy rain.

Pegmatites

Pegmatites are observed cutting through fresh bedrock and are preserved in the weathered profiles. They are easily discriminated from the weathered granite by their paler white colour, and coarser mica and quartz crystals.

Infilled fractures

Along exposed sections of the profile, joints and localised faults can be seen cutting across the weathered profile. These joints and fractures are often infilled with indurated < 0.5 cm thick, white to grey-coloured clay-rich material. Residual coarse sand-sized to silt-sized quartz is also present in these fractures. In fractures at the saprolite horizon, biotite and feldspar minerals occur. The fractures are most clearly observed in the mottled zone where the pale infill material contrasts strongly with the red colour of the horizon. In saprock drill core sections, clay veinlets and infilled fractures are also commonly observed. Figure 6.7 show examples of these infilled fractures observed in different horizons of the profile.

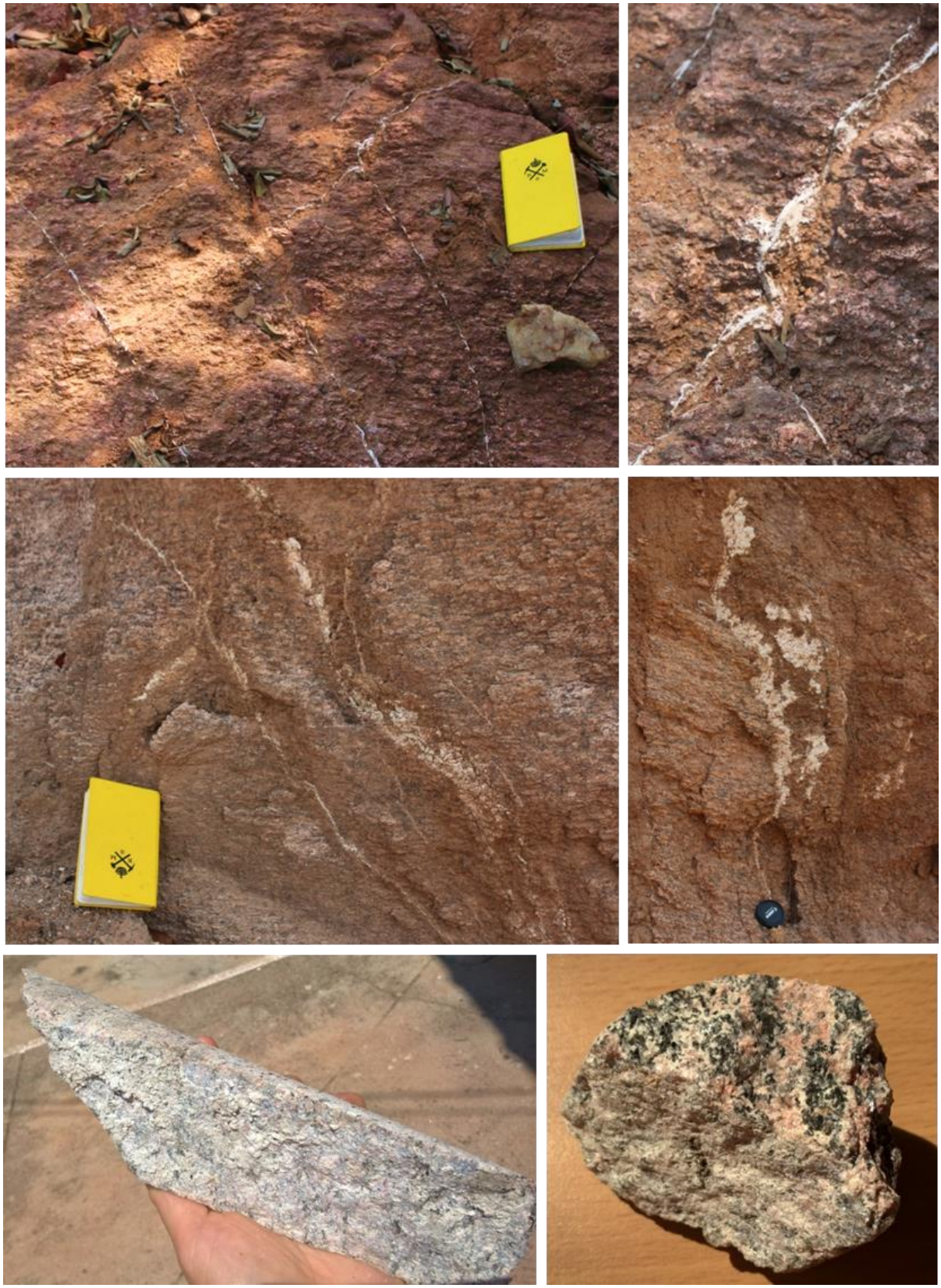


Figure 6.7. Photographs showing white clay rich material infilling joint spaces in the mottled horizon (top) and saprolite horizon (middle) and coating fractures surface of saprock drill core sections (bottom).

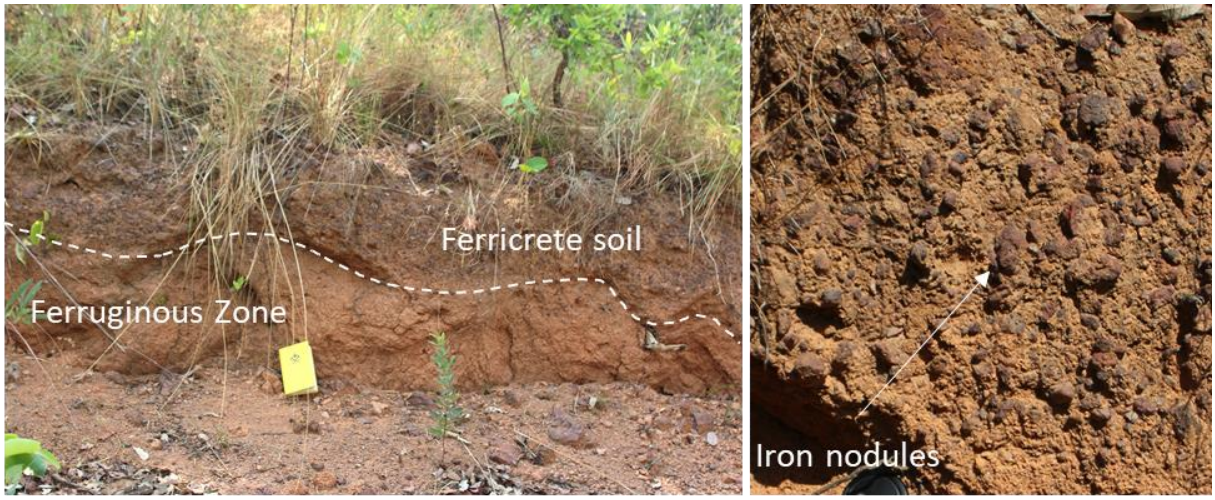


Figure 6.8. Photographs of top section of weathered profile. Left photograph showing ferricrete soil covering ferruginous horizon and right photograph showing iron nodules characteristic of ferricrete soil.

6.4.2 Lateral variations

6.4.2.1 Weathering profile thickness across the plateau

The plateau surface is relatively flat, with less than 10 m variation in relief (between 965 and 975 m a.s.l.). However, the thickness of the weathered profile underlying the plateau surface is considerably more variable. This shows that the weathering front; the contact between the bedrock and the saprock horizon underlying the plateau, is highly irregular. A contour map of the weathering front confirms this irregularity, and reveals that the variation is mainly the result of a ridge and channel feature oriented NW-SE running through the middle of the plateau area (Figure 6.9).

The elevation contour map of the weathering front shows that the lowest and highest points on the plateau are 920 and 960 m a.s.l., which translate into profile thickness variations of between 15 and 55 m across the plateau. The drill holes studied capture this range with the shortest downhole profile measuring 20 m, and the thickest measuring 45 m.

The cross sections presented in Figure 6.9 show that the channel section, which has probably experienced preferential weathering to develop its current geometry, contains the thickest profiles (e.g. DDH0096), while the ridge section appears to be more resistant to weathering and hosts the thinnest profiles (e.g. DDH0121). Towards the flanks of the plateau the profile becomes thinner, partly due to erosion of the mottled and ferruginous zones.

6.4.2.2 Lateral variation of the main horizons

The main horizons described in the previous section are all laterally continuous across the profile, but with thickness variation. Cross sections presented in Figure 6.9 show the lateral variations of individual horizons across the central plateau.

The saprolite and saprock horizons are the most variable horizons; their thickness ranges between 0.5 – 8 m, and 0.5 – 6 m respectively. The thickest and best developed saprolite and saprock horizons are found in the more deeply weathered profiles. Over the channel, where the deepest profiles are found, average thicknesses of these two horizons are 6 m and 4 m respectively. Over the ridge feature, where the shallowest weathered profiles are found, average saprolite and saprock thicknesses are 2.9 m and 2 m.

The mottled zone thickness shows similar patterns to the saprolite and saprock horizons, but has less variation as a proportion to the total thickness. The thickest mottled zone horizons are found in deeper profiles, with thicknesses of 19 – 22 m, and thins-out in shallower profiles with thicknesses varying between 13 – 18 m. By contrast, the ferruginous zone has the most uniform thickness across the plateau, with thicknesses varying between 3 and 5 m.

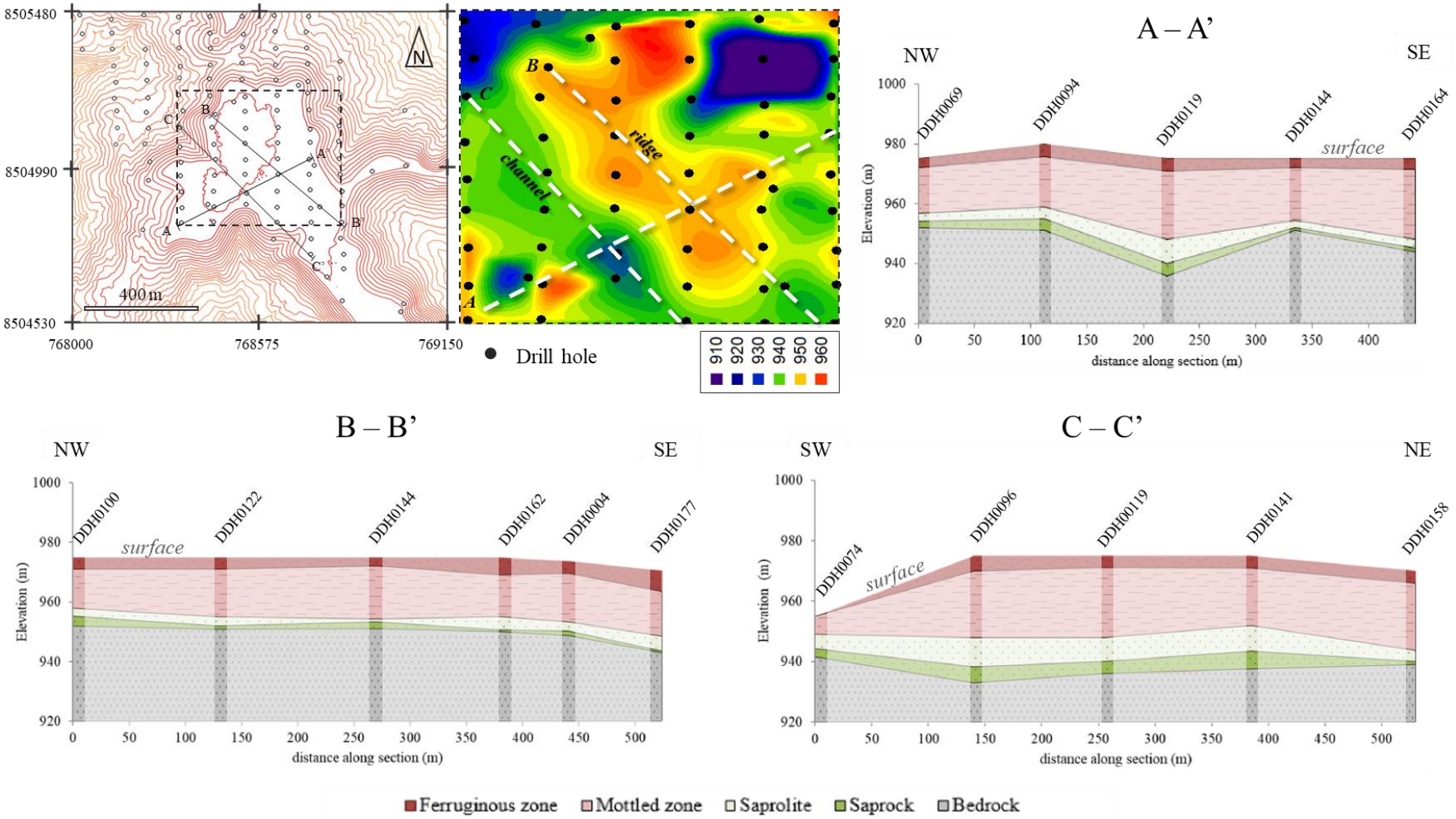


Figure 6.9. Cross sections of the weathered profile, contour maps of the surface elevation (5m) and the underlying bedrock on the central plateau. Note: Saprolite horizon presented contains transition zone. Drill hole data used to construct cross sections and underlying contour map.

6.5 Whole-Rock Geochemistry

6.5.1. Chemical weathering intensity

The unweathered granite samples from the plateau area of the Serra Dourada Complex have CIA values that range between 49 and 51. This is consistent with the < 50 CIA value expected for most unweathered igneous rocks. The samples from the six drill holes have CIA values that extend from 50 in the least weathered rocks at the base of the profile, to > 99 in the most weathered samples in the top half of the profile.

The CIA value ranges for each horizon are consistent between different drill holes. Samples from saprock horizon have CIA values from 50 – 52, 52 – 95 in the saprolite, and > 95 in the mottled and ferruginous zones. This distribution of CIA values across the horizons suggests that breakdown of primary minerals occurs primarily in the saprolite. The > 90 CIA values in mottled zone samples indicate that alkaline and alkali elements have been nearly completely removed, and the weathered rock is completely kaolinitised.

The A-CN-K ternary plot shows there are two trends associated with increasing CIA values in the saprolite horizon (Figure 6.10). The first is a Ca- and Na-depletion trend in the lower half of the saprolite, and the second trend is K-depletion trend. These two trends match field observations of preferential breakdown of plagioclase beginning in the saprock samples followed by the progressive breakdown of k-feldspar and biotite along the saprolite.

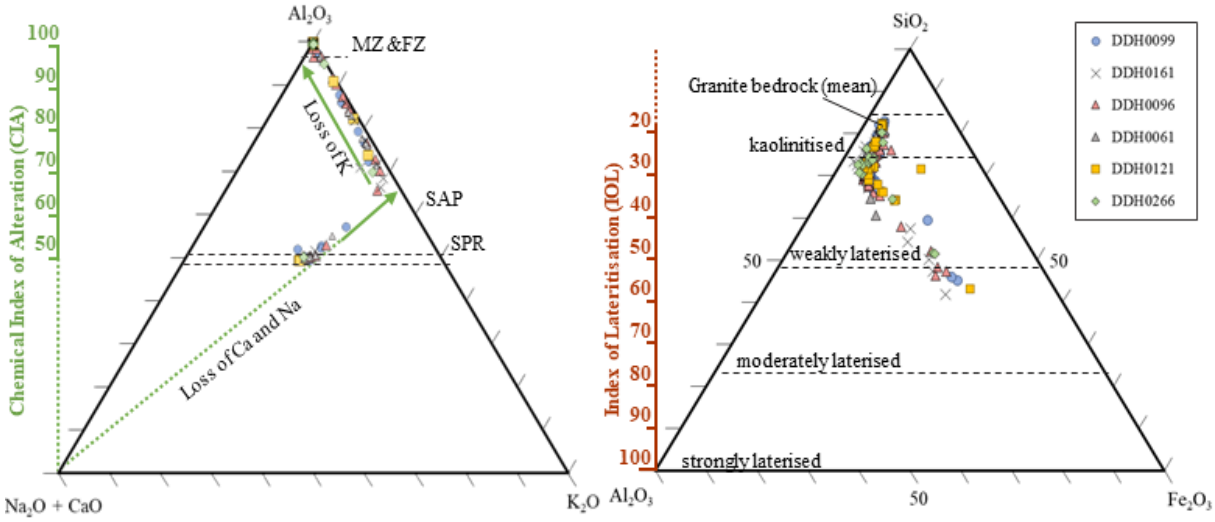


Figure 6.10. Molar Al_2O_3 - Na_2O+CaO - K_2O ternary (A-CN-K plot) with vertical CIA axis (left) and mass % SiO_2-Al_2O_3-$Fe_2O_{3(total)}$ ternary (SAF plot) with vertical IOL axis (right) illustrating the degrees of weathering along the profile. In the SAF plot, the kaolinitisation and lateritisation boundaries used are from Schellman (1983).

The CIA weathered index in not useful for assessing advanced weathering. The index of laterisation and the SAF ternary plots are used to assess the extent of weathering in the samples of the mottled and ferruginous zones. The SAF plot presented in Figure 6.10 shows that samples classed as kaolinitised and lateritised show two different trends. Samples in the kaolinitised category show moderate loss of SiO_2 accompanied by an increase of Al_2O_3 relative to the parent granite. Samples passing the boundary between kaolinitisation and weak laterisation continue to lose SiO_2, but the trend shifts from aluminium to an increase of Fe_2O_3. This shift is consistent with observations of iron oxides modal abundances increasing in the mottled zone. Only a few points from each drill hole enter the moderately lateritised category where SiO_2 is < 50 wt %. These points represent samples approaching the top of the profile. In general, the SAF plot shows that the weathered profile reached weak to moderate degrees of laterisation.

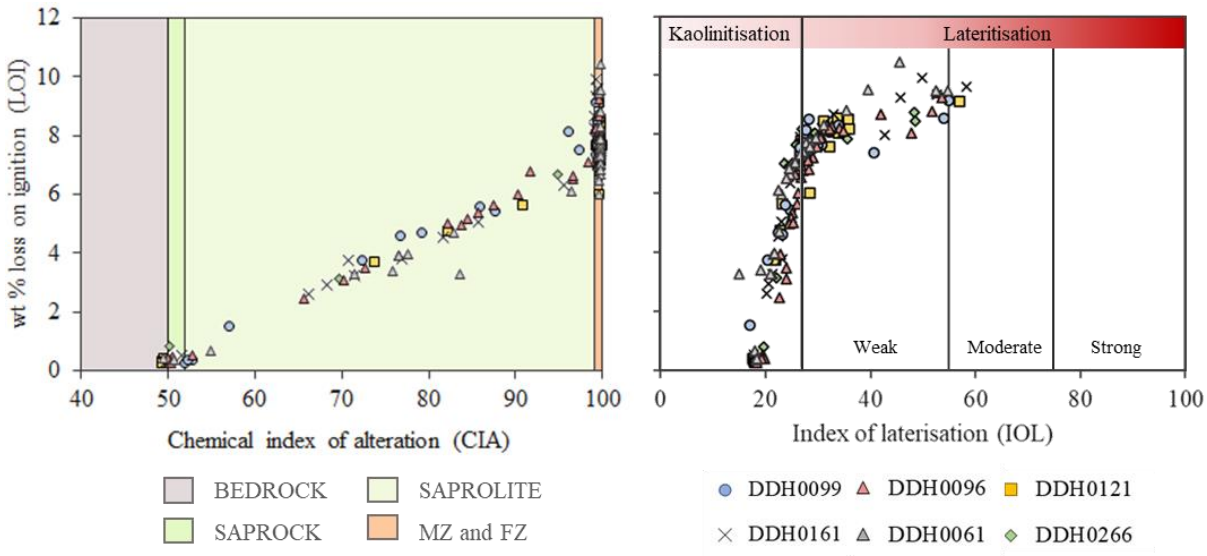


Figure 6.11. Two plots showing covariation of loss of ignition wt % with the chemical index of alteration (left) and the index of lateritisation (right). Boundaries from Figure 6.10 used in both plots.

In the saprolite samples, the LOI values increase from ~0.5 to 7 wt % and show a positive correlation with CIA values (Figure 6.11). In samples with CIA values > 99 the LOI are highly variable, with values ranging from 6 to 11 wt %.

The LOI values also show a positive relationship with samples that fall under the kaolinitisation category in IOL classification (Figure 6.11). For the LOI in samples that are classified as lateritised, this relationship is weaker and appears to become independent. The most lateritised samples have LOI values between 9 and 11 wt %. These results suggest that no strong

breakdown and replacement of hydrous clay minerals for oxides is taking place, even in the most weathered sections of the profile.

6.5.2 Major element distribution along the weathered profile

Major element concentrations along the weathered profile of six assayed drill holes examined in this study are presented in Figure 6.12, and described in this section. Mean concentrations for the different horizons in each drill hole are also presented in Table 6.2.

The silica in the weathered profile decreases gradually from the bedrock (71 – 73 wt % SiO_2) to the top of the mottled zone (62 – 67 wt % SiO_2) and then sharply in the ferruginous zone (39 – 47 wt % SiO_2). The Al and Fe contents show the opposite trend to silica, with concentrations increasing from the base to the top of the profile. The increase in Al_2O_3 concentrations occurs mainly between the bedrock and the saprolite horizon, where concentrations increase from ~13 to 20 wt %. Above the saprolite Al_2O_3 values remain mostly constant. The Fe_2O_3 trend on the other hand shows a continuous increase throughout the profile, first gradually between the bedrock and the top of the mottled zone, from ~ 3 wt % to 10 wt %, and then sharply in the ferruginous zone where values can reach 35 wt %. The significant shift in Si and Fe values at the top of the profile can be used to map the thickness and maturity of the ferruginous soil cap.

The element distribution trends show that Na, Ca, Mg, and K are only found in the lower half of the weathered profile and all exhibit decreasing trends between the bedrock and transition zone (Figure 6.11). Above the transition zone, all of the alkali and alkaline elements are depleted and are present in concentrations of < 0.05 wt %. Concentrations of Na, Ca, and K begin to decrease in the saprock horizon, but their depletion occurs at different points. Complete Ca removal occurs in the saprock, followed by Na in the saprolite and K in the transition zone. This is consistent with observations of the CIA mineral weathering trends throughout the profile.

Magnesium is also restricted to the lower half of the weathered profile, but exhibits a different trend compared the other alkali and alkaline elements. Instead, the MgO distribution shows a curved trend with concentrations increasing by a small amount between the bedrock and saprolite, and then gradually decreasing in the transition zone. In the majority of these drill holes the highest MgO concentrations found in the saprolite are double that of the bedrock, which ranges from 0.07 – 0.2 wt %. The only exception is DDH0099 where concentrations increase from 0.08 wt % in bedrock to up to 0.6 wt % in the saprolite. Peak concentrations are

usually found in the middle or lower half of the saprolite horizon and can be used to map out the position of the saprolite along the profile.

Phosphate concentrations in the bedrock are low (< 0.05 wt %) and remain low throughout the weathered profile at under 0.2 wt % P_2O_5. The P_2O_5 distribution trends presented in Figure 6.12 show a small increase in concentration within the saprolite, with concentrations doubling relative to initial bedrock values, and then decreasing again at the base or middle of the mottled zone to values of ca. 0.01 wt % P_2O_5. Phosphate concentrations increase again in the ferruginous zone to ~0.06 wt %, possibly due to addition from transported cover, or residual enrichment. The only notable peak in phosphate is found in DDH0061 where the concentration increases to 0.15 wt % for a short interval in the saprolite. It is worth noting that many of the assay values are near the detection limit of the analytical method used.

Overall, manganese concentrations are elevated in the lower half of the profile and depleted in the upper half of the profile relative to starting bedrock concentrations which are characteristically less than 0.05 wt %. The distribution and concentration of Mn in the lower half varies between drill holes but can be divided into two main groups. In the weathered profile of the thicker drill holes, DDH0096, DDH0061 and DDH0161, multiple and sharp MnO peaks can be found between the saprolite and lower half of the mottled zone. These peaks vary in concentration but can be up to 0.3 wt %. In the shorter drill holes, DDH0161, DDH0121 and DDH0266, there are fewer and less discrete MnO peaks. In the top half of the weathered profile MnO concentrations are under 0.01 wt % for all drill holes.

Finally, the TiO_2 trends show that concentrations along the weathered profile increase gradual to from concentrations of ~ 0.2 wt % to ~ 0.5 wt % in the ferruginous zone. In each drill hole, one or two sharp depletion peaks can be observed. These negative peaks match the position of pegmatites that were logged in the drill cores (Figure 6.12).

The weathered pegmatites found along the profile of the six drill holes can be geochemically identified by an increase of Al, and significant drop in HFSE and Fe. Depletion peaks of TiO_2 can be used to accurately map the location of these pegmatites.

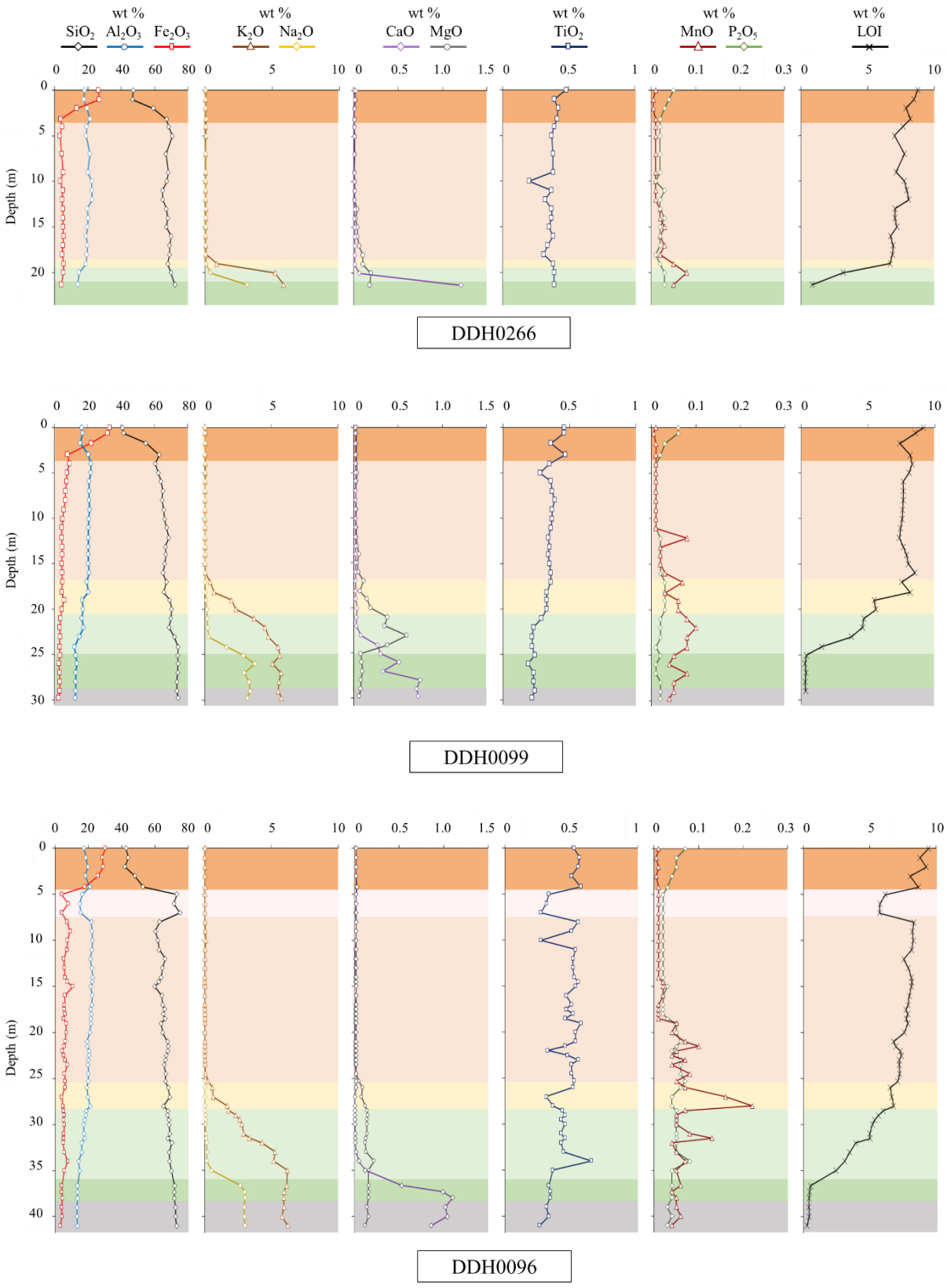
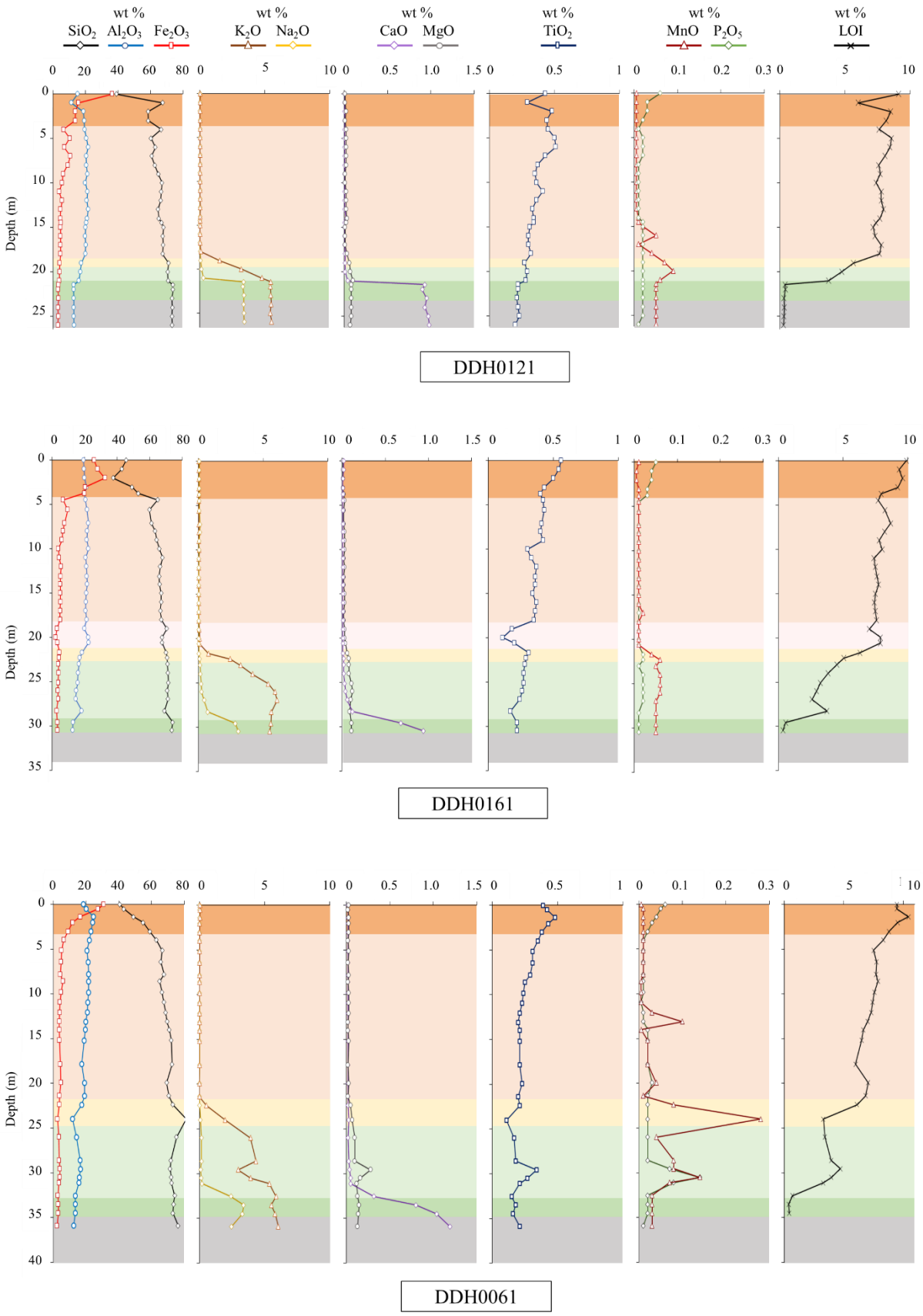


Figure 6.12. Major element trends along the six different drill holes studied.



...Figure 6.12. continued.

Table 6.2. Mean values of each horizon for major elements, REE, and HFSE for each of the 6 drill holes.

		Thickness	Major elements (wt %)										Trace elements (ppm)							
Drill hole	Horizon	(m)	Si_2O	Al_2O_3	Fe_2O_3	K_2O	Na_2O	CaO	MgO	MnO	P_2O_5	TiO_2	Th	U	Zr	Nb	REY	La	Ce	Y
	Soil/Ferricrete	1.0	39.0	15.10	36.47	0.03	0.01	0.01	0.01	0.01	0.06	0.46	178	7.33	906	113	137	19.1	48.9	29.1
	Ferruginous Zone	3.0	58.6	18.95	13.73	0.02	0.01	0.01	0.02	0.01	0.03	0.43	122	5.32	1243	162	100	7.95	33.4	33.0
	Mottled Zone	15	60.9	19.15	5.79	0.02	0.01	0.01	0.02	0.01	0.01	0.36	97.9	7.69	948	205	1328	6.4	1260	27.5
DDH0121	Transition Zone	0.9	71.2	17.45	4.13	1.53	0.06	0.01	0.06	0.07	0.02	0.34	85.7	12.9	556	180	1212	145	706	135
	Saprolite	1.5	70.6	16.57	4.03	3.68	0.17	0.02	0.08	0.08	0.02	0.24	89.2	12.8	637	192	2946	895	459	416
	Saprock	2.6	73.5	12.79	3.28	5.45	3.36	0.93	0.08	0.05	0.02	0.22	67.2	11.1	490	146	1702	375	412	367
	Bedrock		73.3	13.0	3.07	5.52	3.42	0.98	0.070	0.050	0.020	0.22	63.1	9.36	474	137.5	1184	203	372	273
	Soil/Ferricrete	1.1	47.1	18.0	26.2	0.03	0.01	0.020	0.005	0.010	0.050	0.48	174	5.35	606	86	147	16.2	88.5	18.3
	Ferruginous Zone	2.2	53.6	18.6	19.1	0.02	0.01	0.007	0.012	0.005	0.034	0.41	218	6.92	739	108	141.2	8.99	90.8	19.5
	Mottled Zone	16	67.7	20.2	4.38	0.03	0.03	0.007	0.024	0.015	0.020	0.35	115	10.00	717	117	1791	4.8	1738	21.5
DDH0266	Transition Zone	1.0	67.8	18.8	5.40	0.86	0.050	0.010	0.100	0.050	0.020	0.38	144.0	12.7	732	130	2975	376	2050	82
	Saprolite	0.9	69.7	14.6	5.23	5.19	0.37	0.060	0.190	0.080	0.030	0.39	165.5	21.5	1050	140	12863	4860	1805	1080
	Saprock	3.0	72.1	13.8	3.96	5.83	3.13	1.21	0.180	0.050	0.030	0.39	80.8	10.4	861	101.0	1826	341	425	546
	Soil/Ferricrete	1.0	45.4	19.2	25.90	0.03	0.05	0.02	0.010	0.010	0.050	0.56	139	5.94	978	131	116	17.3	32.8	31.3
	Ferruginous Zone	3.5	44.6	20.0	25.93	0.02	0.05	0.01	0.012	0.007	0.036	0.48	162	7.04	877	165	96.2	11.77	24.9	29.8
	Mottled Zone	15	60.3	19.8	5.54	0.01	0.04	0.01	0.024	0.010	0.009	0.35	102	5.74	834	219	200	2.9	135	34.4
DDH0161	Transition Zone	1.3	70.3	17.6	4.32	1.68	0.05	0.02	0.071	0.051	0.020	0.30	92.4	10.30	747	214	1840	253	981	192
	Saprolite	6.6	71.0	15.2	3.74	5.21	0.27	0.04	0.098	0.054	0.018	0.21	79.9	11.0	623	172	3793	1169	537	574
	Saprock	2.1	73.7	12.7	3.23	5.55	2.97	0.83	0.110	0.050	0.010	0.22	68.8	9.97	503	146.9	2211	572	435	438
	Bedrock																			
	Soil/Ferricrete	0.6	41.0	16.5	33.4	0.05	0.02	0.02	0.030	0.010	0.060	0.46	185	5.48	900	129	146	17.0	73.5	26.3
	Ferruginous Zone	3.4	52.9	17.5	21.2	0.02	0.02	0.02	0.030	0.008	0.037	0.43	144	5.41	839	148	133	10.8	77.5	21.4
	Mottled Zone	13	66.5	20.9	5.45	0.02	0.02	0.02	0.034	0.021	0.014	0.36	111	9.32	896	225	602	3.88	522	36.0
DDH0099	Transition Zone	4.0	68.3	18.5	5.02	1.36	0.08	0.03	0.132	0.056	0.030	0.34	101	13.7	790	207	1335	256	485	174
	Saprolite	4.1	71.2	15.4	3.42	4.62	0.56	0.10	0.432	0.085	0.018	0.24	69.1	10.6	554	152	5040	1410	608	1063
	Saprock	3.9	73.9	13.0	3.13	5.50	3.24	0.48	0.088	0.055	0.015	0.22	66.4	10.5	504	143	1734	381	367	398
	Bedrock		74.3	13	3.30	5.77	3.20	0.73	0.060	0.040	0.020	0.22	68.2	10.05	579	142.0	1156	230	306	263
	Soil/Ferricrete	0.5	40.6	18.3	30.74	0.04	0.01	0.02	0.030	0.005	0.060	0.39	137	6.20	643	172	222	32.5	100.5	44.9
	Ferruginous Zone	2.5	49.1	22.7	18.50	0.03	0.01	0.02	0.026	0.010	0.040	0.44	154	6.75	736	228	257.3	33.03	147.9	38.3
	Mottled Zone	18.3	67.9	20.2	4.75	0.01	0.01	0.02	0.025	0.019	0.015	0.25	83	5.87	566	217	426	6.7	341	40.0
DDH0061	Transition Zone	3.6	77.4	14.3	3.02	1.32	0.05	0.03	0.061	0.191	0.020	0.15	62.4	5.85	424	183	1006	123	589	108
	Saprolite	7.5	73.2	15.1	3.53	4.39	0.45	0.07	0.135	0.063	0.047	0.21	69.4	7.8	486	184	1486	378	365	275
	Saprock	1.0	73.3	13.4	3.09	5.52	3.38	0.80	0.15	0.03	0.02	0.18	59.6	6.28	398	163.5	1011	243	321	153
	Bedrock		73.0	13.4	3.07	5.81	3.29	1.04	0.14	0.03	0.02	0.16	56.1	7.60	413	155.0	1012	209	299	220
	Soil/Ferricrete	2.0	43.2	17.9	29.21	0.03	0.01	0.02	0.020	0.008	0.060	0.54	146	5.29	958	110	107	17.8	37.0	24.3
	Ferruginous Zone	3.0	47.2	19.3	24.63	0.02	0.01	0.02	0.020	0.008	0.041	0.54	191	6.28	1012	124	79.0	8.44	31.0	19.0
	Mottled Zone	18.0	64.2	21.2	6.54	0.05	0.01	0.02	0.015	0.029	0.035	0.49	117	7.64	989	129	580	22.5	489	24.9
DDH0096	Transition Zone	2.5	67.7	19.7	4.80	0.83	0.01	0.01	0.092	0.136	0.048	0.40	91.6	9.65	813	108	1710	261	921	136
	Saprolite	8.2	68.8	16.3	5.57	4.20	0.20	0.04	0.150	0.059	0.052	0.45	95.7	12.1	928	128	1650	370	503	255
	Saprock	2.4	71.6	13.4	4.13	5.99	2.92	0.90	0.160	0.050	0.040	0.34	78.3	9.55	661	92.8	1648	389	422	316
	Bedrock		72.5	13.2	3.65	5.99	2.99	0.97	0.140	0.050	0.033	0.30	76.6	9.55	587	86.5	1122	225	404	183

6.5.3 Trace element distribution along the weathered profile

6.5.3.1 High field strength elements

The distribution of Th, Nb, and Zr along the six drill cores is presented in Figure 6.14. In general, all three show increases upwards through the weathered profile.

The Zr trends show that concentrations increase from 500 – 600 ppm at the base of the profile to ~1000 ppm in the ferruginous zone. Concentrations begin to increase in the saprolite and in general show a continuous increasing upward trend. In most of the drill holes, the Zr concentrations in the ferruginous soil is markedly lower than the rest of the profile.

The Th trends show that concentrations increase gradually along the profile. Concentration increase from ~ 75 ppm Th in the bedrock to ~ 140 ppm in upper mottled zone and then more steeply to up to 250 ppm in the ferruginous zone. The only significant Th peak found in the drill hole trends is a 266 ppm peak in the middle of the mottled zone of DDH0266.

The Nb trends show that niobium concentrations increase by a small amount between the bedrock (~100 – 140 ppm) and mottled zone (~140 – 240 ppm), and then decrease towards the top of the profile to concentrations of ~100 ppm. The point along the mottled horizon where concentrations begin to fall varies between drill holes. In DDH0266 Nb concentration begin to decrease at the base of the mottled zone, in DDH121, DDH0099, and DDH161 concentrations decrease in the middle of mottled zone, and in drill holes DDH0096 and DDH0061 concentrations only start to decrease at the contact with the ferruginous zone.

The HFSE concentrations in the top of the profiles are highly variable between drill holes. This coincides with the ferricrete soil horizon where additional modification of the geochemistry may arise due to external input, or removal, of material due to mass transport. HFSE trends in this part of the profile should therefore be interpreted with caution.

Discrete negative shifts in concentrations of Nb, Th and Zr are comparable to Ti and coincide with the logged positions of pegmatites, and can be attributed to a local change in the protolith material.

6.5.3.2 REE distribution

The REY distribution trend in Figure 6.13 shows that REE mainly concentrate in two parts of the weathered profile; in the saprolite horizon and in the lower half of the mottled zone. The saprolite is enriched in all REE, whereas elevated REY concentrations in the lower half of the mottled zone are mostly attributed to Ce. All other REE in the lower half of the mottled zone are present at very low concentration. The upper mottled zone and ferruginous zone have low concentrations of REE, which are significantly lower than the parent bedrock material, making these horizons relatively REE-depleted.

Average REY concentrations for the saprolite horizons of the six drill holes range widely from 0.16 to 1.2 wt % REY and appear to correlate with saprolite horizon thicknesses. Drill holes with the thinnest saprolite horizon (DDH0121 and DDH0266; 1 – 2 m thick) have the highest REY concentrations, up to 1.2 wt %. In contrast, drill holes DDH0096 and DDH0061, which have the thickest saprolite horizons (8 – 10 m), have the lowest concentrations at 0.17 wt %. Overall, the REE composition of the saprolite horizon is LREE dominant, with the proportion of LREE composing 65 to 85 % of the total REY (Figure 6.13 A). The most abundant individual REE are La and Nd followed by Ce and Y (Figure 6.13 B).

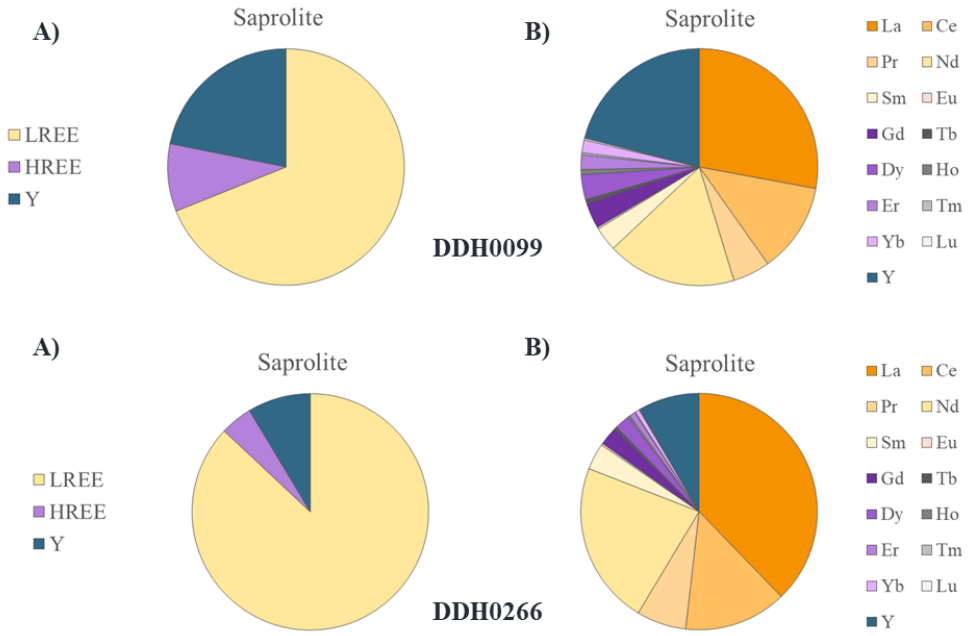


Figure 6.13. Average REE proportions in the saprolite horizon of drill holes DDH0099 and DDH0266 shown as pie charts for A) LREE, HREE and Y; B) individual REE. Percentages are calculated using the average assay composition of saprolite horizon samples from the six drill holes examined in this chapter.

The distribution of REY within in the saprolite horizons is not homogenous and large variations in REY concentration in the order of 100 to several 1000 ppm are exhibited. Downhole REY trends in Figure 6.14 show that, except for DDH0096, REY are more strongly concentrated in the middle and lower half of the saprolite horizon. The distribution of REE within the saprolite also appears to be correlated with thickness of the horizon. The largest and most narrow REY peaks are most strongly developed in the thinnest saprolite horizons (DDH0266 and DDH0121, 0.6 – 1.2 wt %) whereas the broadest and least well-defined REY peaks occur in the drill holes with thick saprolite horizons (DDH0096 and DDH0061, at 0.2 and 0.3 wt % respectively).

The distribution of La and Y presented Figure 6.14 show that although they have different concentrations in the saprolite, they share very similar downhole trends along the saprolite and their peak concentrations coincide in all drill holes. This indicates that both LREE and HREE are preferentially accumulating together in the same part of the saprolite.

Elevated REY concentrations observed in the lower half of the mottled zone are produced by one of multiple Ce peaks that can be found along the weathered profile. Each drill hole has between two and three well-defined Ce peaks, located between the saprolite and the lower mottled zone. The shape and magnitude of these Ce peaks can be observed in the downhole Ce trend in Figure 6.14.

The largest Ce concentration peak in each drill hole, with the exception of DDH0161, occurs in the lower half of the mottled zone, at depths between 10 and 20 m below the surface. Broad peaks may cover sections 5 – 10 m thick, with average concentrations between 0.06 – 0.33 wt % Ce. The highest peak Ce concentrations are found in the shortest drill holes; 0.8 wt % in DDH0266, and 0.72 wt % in DDH0121. The maximum concentrations in other drill holes are considerably lower, ranging between 0.13 and 0.18 wt % Ce. Short drill holes generally have more discrete Ce peaks; concentrations of Ce shift rapidly between samples intervals. Concentrations of Ce in longer drill holes decrease gradually throughout the mottled zone.

Ce concentration peaks are also found in the transition zone and saprolite. These peaks are consistently narrower, and have relatively lower average concentrations. In the saprolite, none of these Ce peaks coincide with other REE concentration peaks. Above the Ce peaks in the lower mottled zone, the mottled and ferruginous zones have very low REE concentrations, with values below 200 ppm REY.

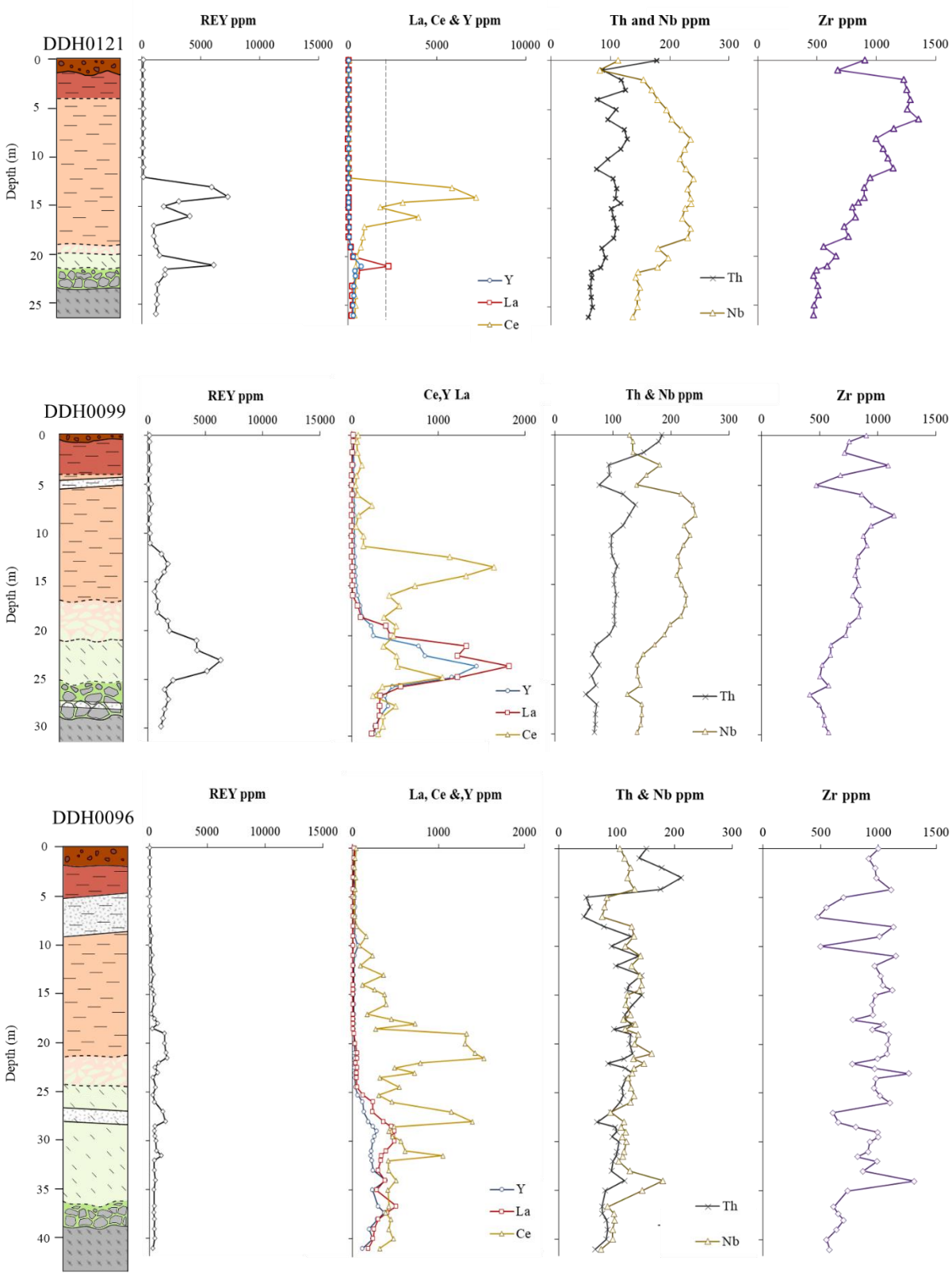
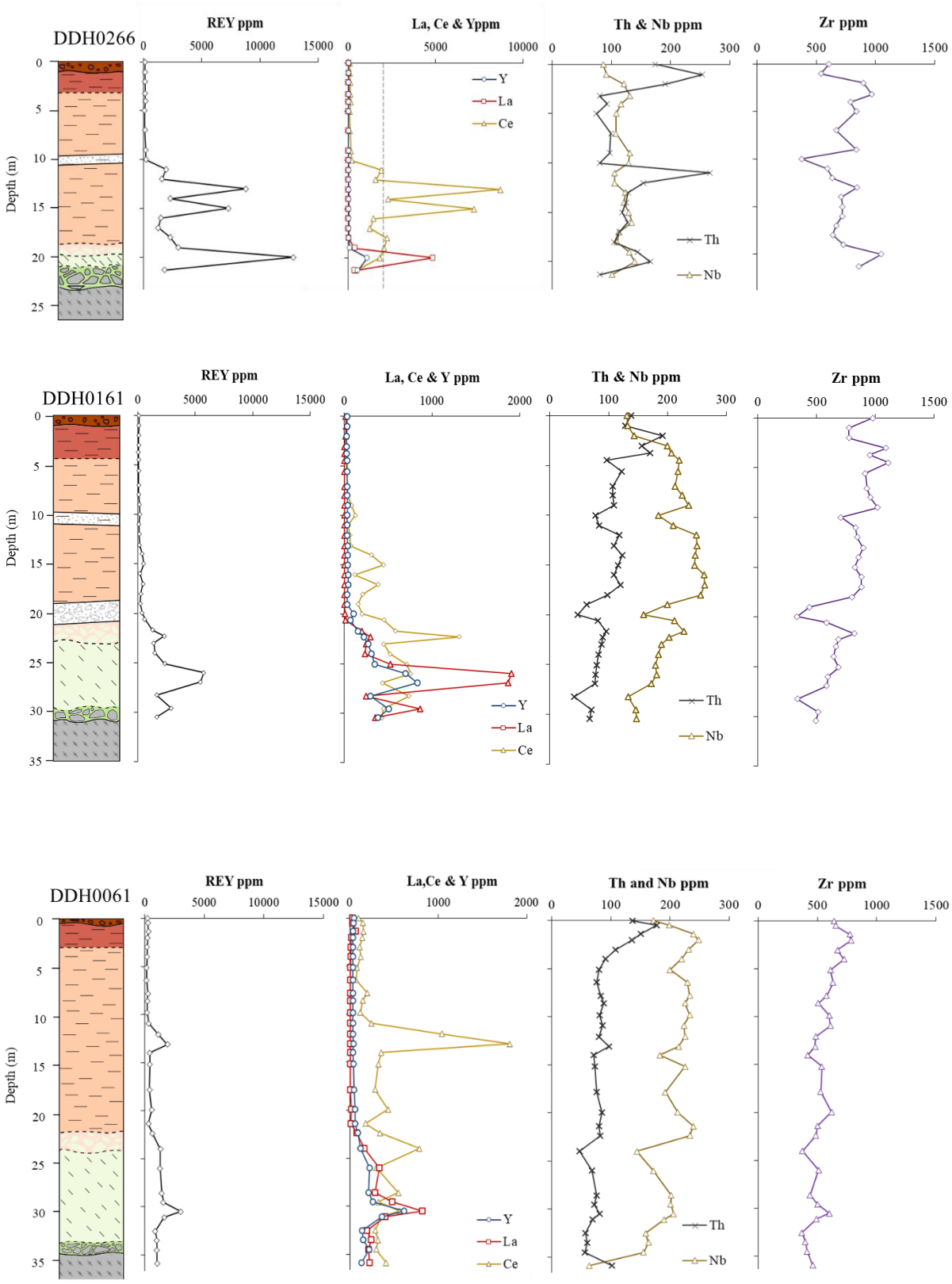


Figure 6.14. Trace element distribution trends along profile the six drill holes studied a) REY b) La, Ce and Y c) La_N/Y_N d) enrichment factor shown by Zr. Note the different concentration scales used for La, Y & Ce ppm in the graph for DDH0121 (top).



...Figure 6.14. Continued. Note the different concentration scales used for La, Y & Ce ppm trends in the graph for DDH0266 (top).

6.5.3.3 REE enrichment

The bedrock-normalised element enrichment patterns in Figure 6.16 and the downhole enrichment factor trends for REY, La, Ce and Y in Figure 6.15 show the degree and variation of REE enrichment and depletion along and between the weathered profiles of the drill holes studied.

The results show that positive REY enrichment factors are found from the base of the profile up to the middle of the mottled zone. Above this point REE become strongly depleted. The most strongly REY-enriched part of the weathered profile is the saprolite horizon where average REY concentrations of up to 10 times the bedrock REY concentration can be found. In contrast, the most strongly depleted horizon is the ferruginous zone, which has average REY enrichment factors ranging between 0.06 – 0.25.

The downhole REY enrichment trends in Figure 6.15 show that the degree of enrichment in saprolite horizon is highly variable between drill holes. The average REY enrichment factor values fall between 1.5 and 10 and can be divided into three groups: weak, moderate, and high enrichment. The least enriched and least variable saprolite horizons are found in DDH0061 and DDH0096, which have average REY enrichment factors of 1.5 and 2.0 respectively and maximum and minimum values of 1 and 2.99. The second group includes drill holes DDH0161, DDH0121 and DDH0099 which have higher average REY enrichment factors of 2.43, 2.49 and 4.4 respectively and also display greater variation with values ranging between 1.13 and 5.5. Finally, the third group is represented by DDH0266 which has the most enriched saprolite REY enrichment factor of 10.

The bedrock normalised pattern in Figure 6.16 and the downhole La and Y enrichment trends in Figure 6.15show that in the saprolite horizon LREE are more strongly enriched relative to bedrock than the HREE. However, the difference in the degree of individual REE enrichment varies between drill holes and within saprolite horizon. In the saprolite of drill holes DDH0121, DDH0266 and DDH0161 LREE concentrations are several times more enriched than HREE. For example, in the saprolite of DDH0161 La has an enrichment of 10.5 times while Yb is only 2.8. In drill holes DDH0096, DDH0099 and DDH0061 the difference in enrichment in the saprolite is not as large. In these drill holes LREE are only 1 or 2 times more enriched than HREE.

The downhole Ce enrichment trend in Figure 6.15 show that the Ce concentration peaks in the mottled zone have enrichment factor values of between 4 and 22. The highest Ce enrichments are found in DDH0121 and DDH266.

6.5.3.3 REE fractionation

The saprolite and saprock material has inherited the LREE-enriched chondrite-normalised patterns of the parent rock, with its strong negative Eu anomaly (Figure 6.16). However, saprolite and saprock can be distinguished from parent rock by more elevated REE abundances, negative Ce anomalies, and more strongly fractionated LREE patterns.

In contrast, the chondrite-normalised REE patterns of the mottled zone and ferruginous zone are consistently depleted relative to the parent rock, exhibit positive Ce anomalies, and are HREE enriched (left inclined; Figure 6.16). Excepting for the negative europium anomaly that has been retained throughout the profile, the upper parts of the weathered profile have an inverse chondrite-normalised REE pattern, which mirrors that of the saprolite.

The downhole La_N/Yb_N trends presented in Figure 6.15 shows that the LREE to HREE fractionation in saprolite varies between the drill holes. The drill holes can be divided into two groups, strongly LREE/HREE fractionated saprolite (La_N/Yb_N = 13 – 41) and moderately fractionated saprolite (La_N/Yb_N = 8 – 14). The first group include drill holes DDH0266, DDH0161 and DDH121, and the second group DDH0099, DDH0096 and DDH0061.

The La_N/Yb_N trend also shows that in the strongly fractionated group LREE-HREE fractionation along the saprolite is highly variable, with the highest La_N/Yb_N values coinciding with the most enriched interval of the saprolite. In the moderately fractionated group, La_N/Yb_N ratios remain relatively constant throughout the profile intersection.

The cross-over point along the weathered profile between LREE-fractionated and HREE-fractionated weathered rock occurs at, or slightly above, the transition zone. Above this cross-over point La_N/Yb_N values range between 0.2 and 1.0, and remain relatively constant through the mottled zone. Towards the top of the profile, the degree of fractionation becomes less pronounced, before becoming LREE-fractioned (La_N/Yb_N < 3) at the top of the ferruginous horizon. However, relative to the bedrock, the ferruginous zone remains more HREE-fractionated.

The downhole (Ce_N/Ce^*_N) trend presented in Figure 6.15 show the contrasting Ce anomalies between the lower and upper portions of the weathered profile. The negative Ce anomaly that

characterises the lower profile is most strongly developed in the saprolite horizon. Ce anomaly values in saprolite of drill holes studied range between 0.95 and 0.11 Ce_N/Ce^*_N. The most negative Ce values in each drill hole coincide with the most REE-enriched section.

Drill holes DDH0099, DDH0161, DDH0121 and DDH0266, which have better developed REY peaks, contain Ce anomalies ranging between 0.11 and 0.2 Ce_N/Ce^*_N (Figure 6.15). DDH0096 and DDH0061 have poorly defined REY peaks in their saprolite, and have less pronounced negative Ce anomalies with maximum values of 0.46 and 0.41 Ce_N/Ce^*_N respectively. The most negative Ce anomalies in the saprock, from the drill holes studied, range between 0.36 and 0.94 Ce_N/Ce^*_N, with more REE-enrichment saprock showing more pronounced Ce anomalies. The saprock intersected by DDH0099 has the strongest negative Ce anomaly at 0.36.

A positive Ce anomaly that characterises the upper half of the profile begins to develop within the transition zone. Ce anomaly trends through the profile shows that the positive anomaly increases throughout the mottled zone and reaches a peak at 10 – 15 m below the surface. This depth coincides with the maximum absolute Ce concentration values along these profiles. The highest positive Ce anomalies in the drill holes studied are 388 Ce_N/Ce^*_N in DDH0121, and 490 Ce_N/Ce^*_N in DDH0266. For the other four drill holes the highest Ce_N/Ce^*_N values are ~100. Above this peak, the Ce anomaly trend decreases toward the top of the profile and returns to $Ce_N/Ce^*_N < 5$. This decreasing trend can also be observed in the decreasing height of the Ce peaks in chondrite-normalised patterns between lower mottled zone and ferruginous zone in Figure 6.16.

Chondrite-normalised patterns show that the negative Eu anomaly present in the bedrock is retained throughout the weathered profile, albeit, at increasingly less negative values. The Eu anomaly remains fixed in lower half of the profile (around 0.2 Eu_N/Eu^*_N) and then becomes less negative from the base towards the centre of the profile.

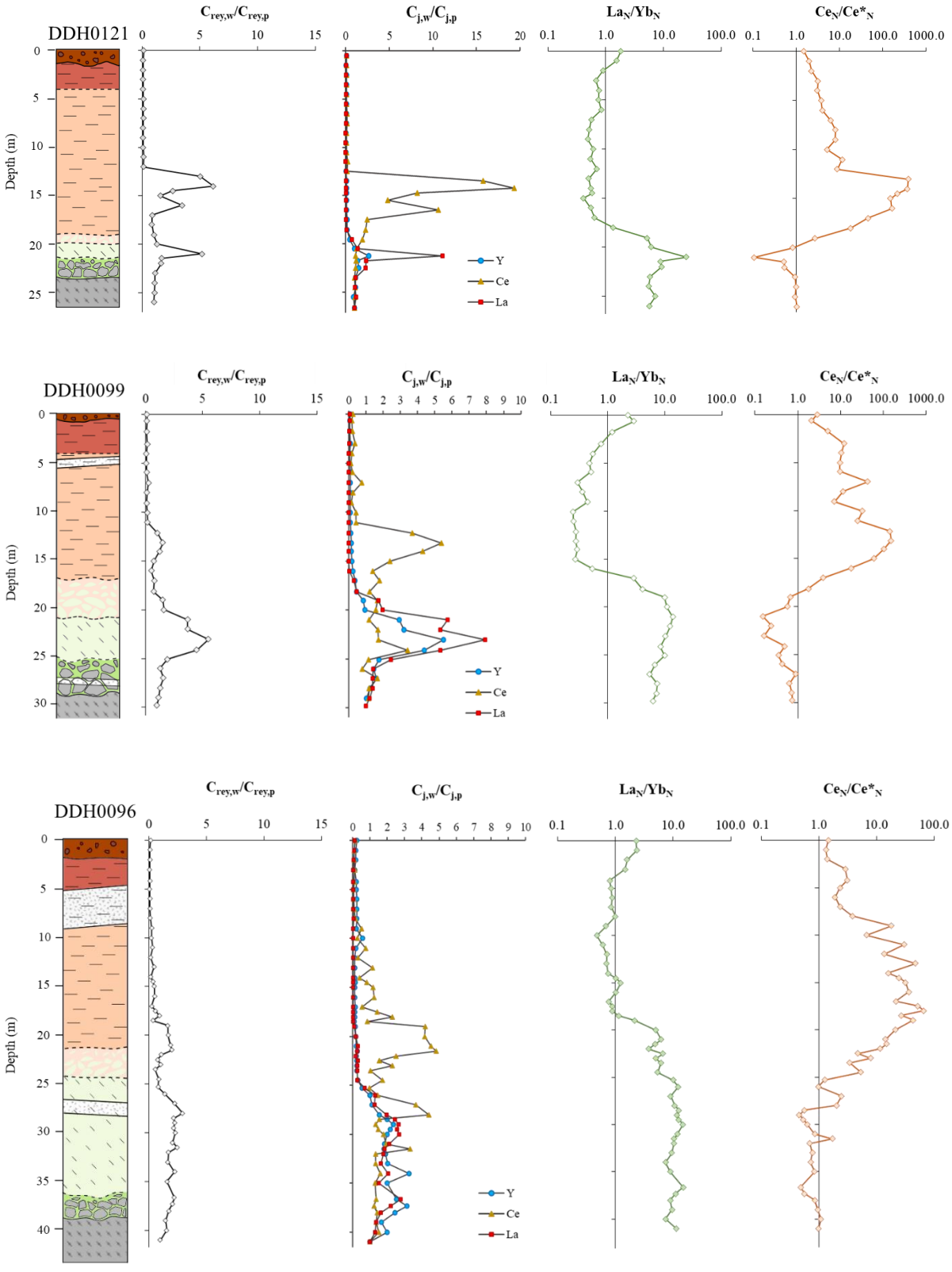
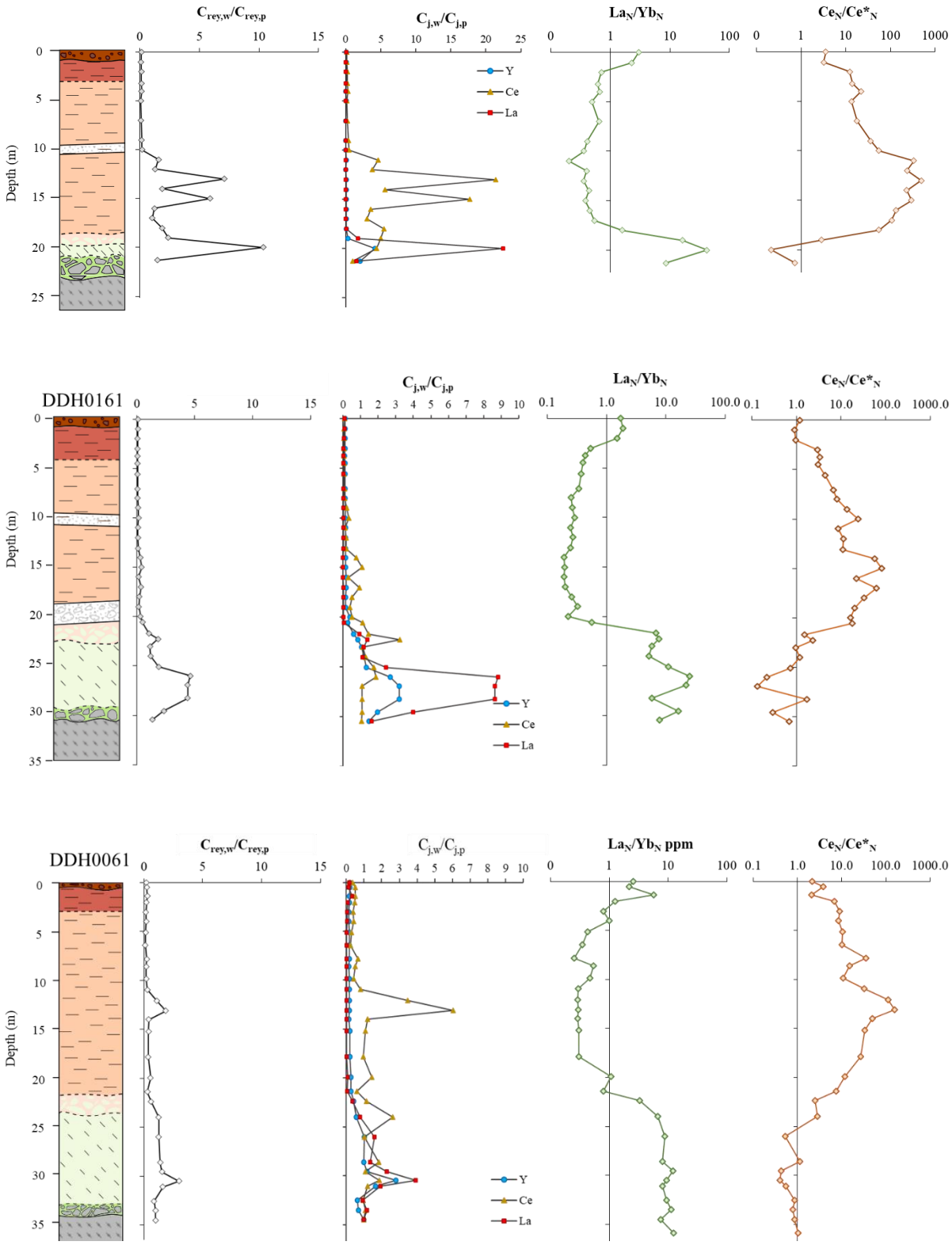


Figure 6.15. REE enrichment ($C_{j,w}/C_{j,p}$) and fractionation trends (La_N/Yb_N and Ce_N/Ce^*_N) along the weathered profile of six drill holes studied.



...Figure 6.15. Continued.

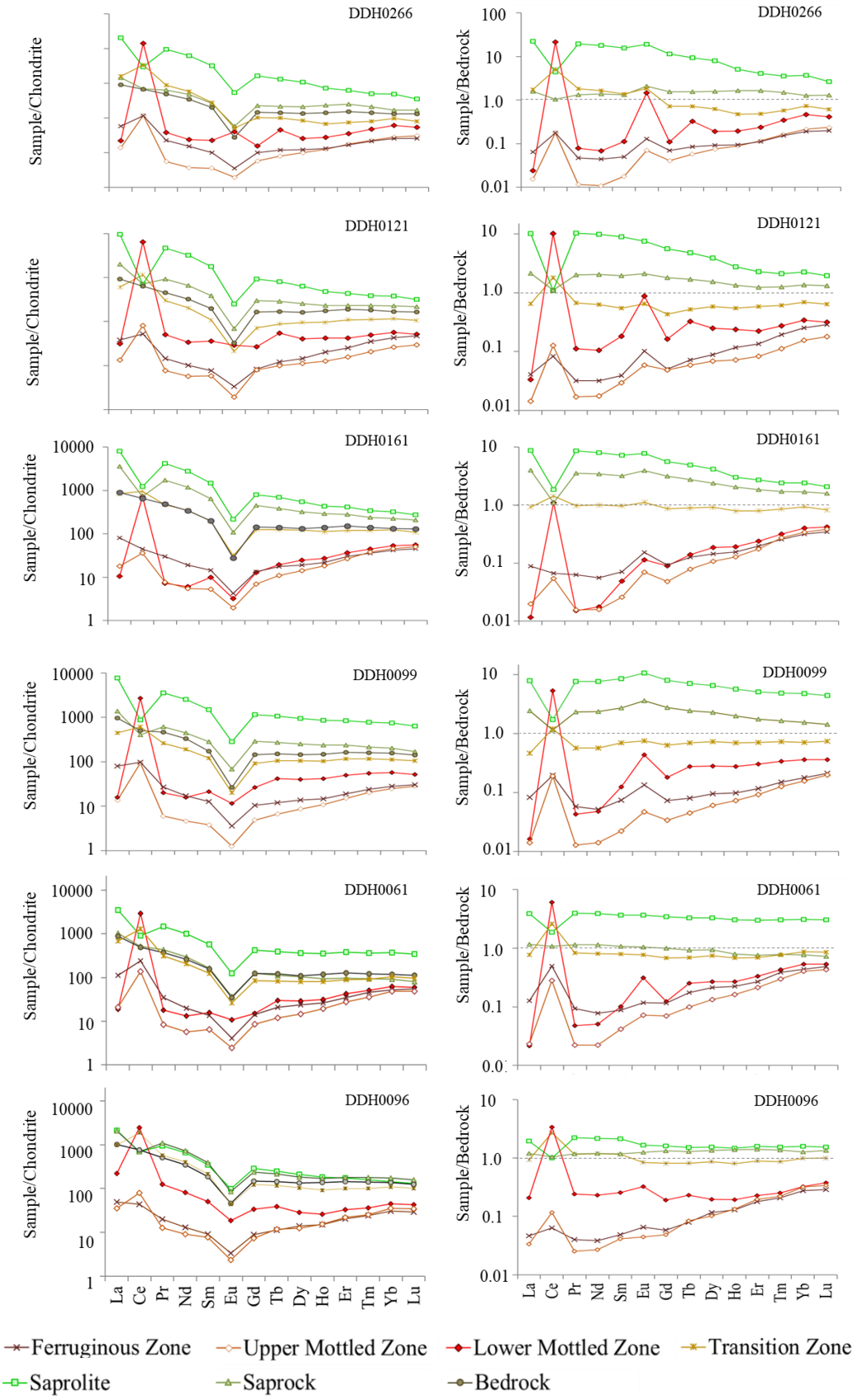


Figure 6.16. Chondrite-normalised REE patterns (left) and parent rock normalised REE patterns (right) of the different horizons in each drill hole. Representative sample of each horizon are displayed. Chondrite-normalisation values calculated after McDonough & Sun (1995).

6.6 Bulk Mineralogy

Bulk XRD analysis and SEM analysis was carried out on representative samples from each of the horizons of DDH00161. The results show clear bulk mineralogy differences between horizons and a mineralogical evolution along the weathered profile (Figure 6.17 and Figure 6.18).

Mineralogical analysis show that the breakdown of primary minerals is constrained to the lower half of the weathered profile. In XRD patterns, feldspar and biotite peaks are no longer present above the saprolite and only quartz peaks are retained up to the top the profile. In SEM-BSE images of the saprolite and transition zone, biotites can be seen to be preferentially breaking down along cleavage planes and feldspar display dissolution textures. SEM analysis also shows that Na feldspars are preferentially weathered to K-feldspars. Na-feldspars begin to weather in the saprock and are rarely observed in saprolite samples. K-feldspar on the other hand only begin to weather in the saprolite (Figure 6.18 C and D).

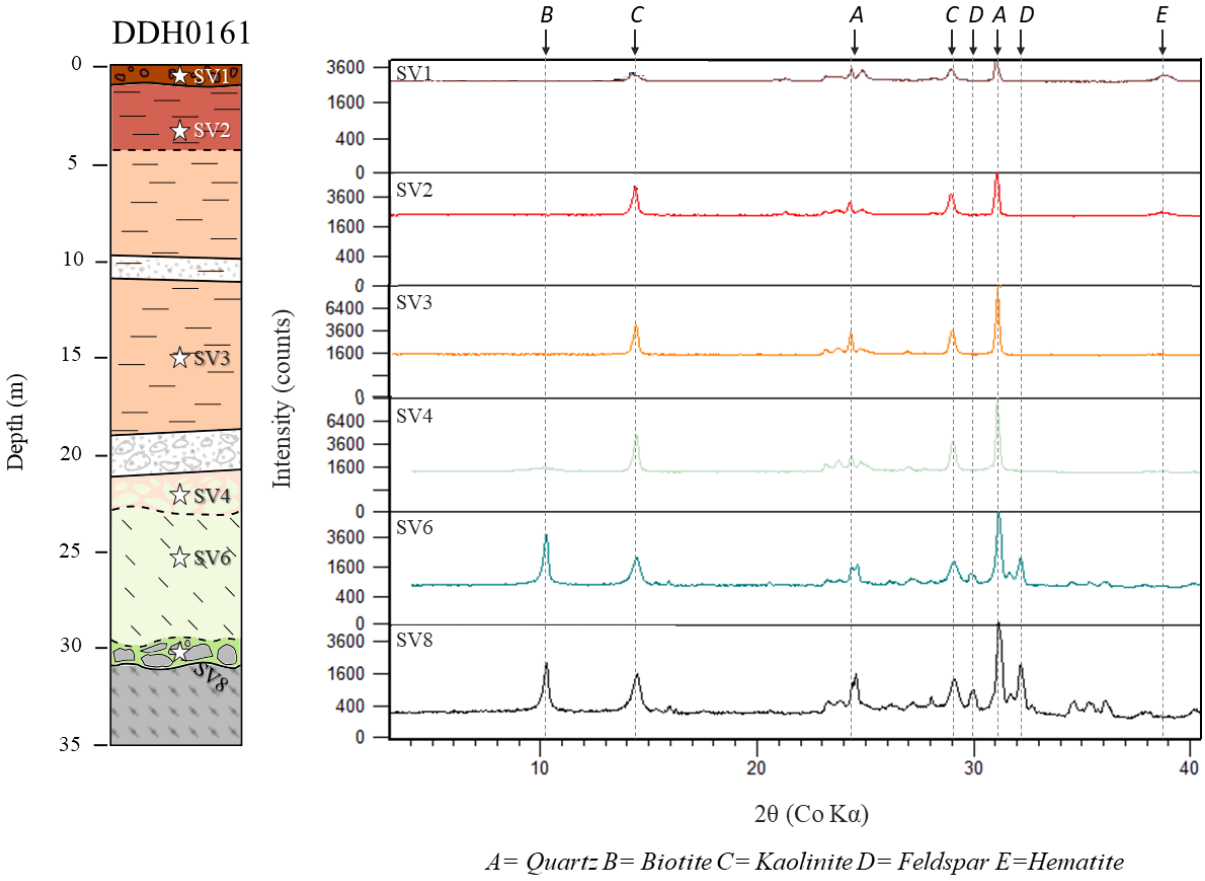


Figure 6.17. XRD patterns of representative samples of the different horizons from DDH0161.

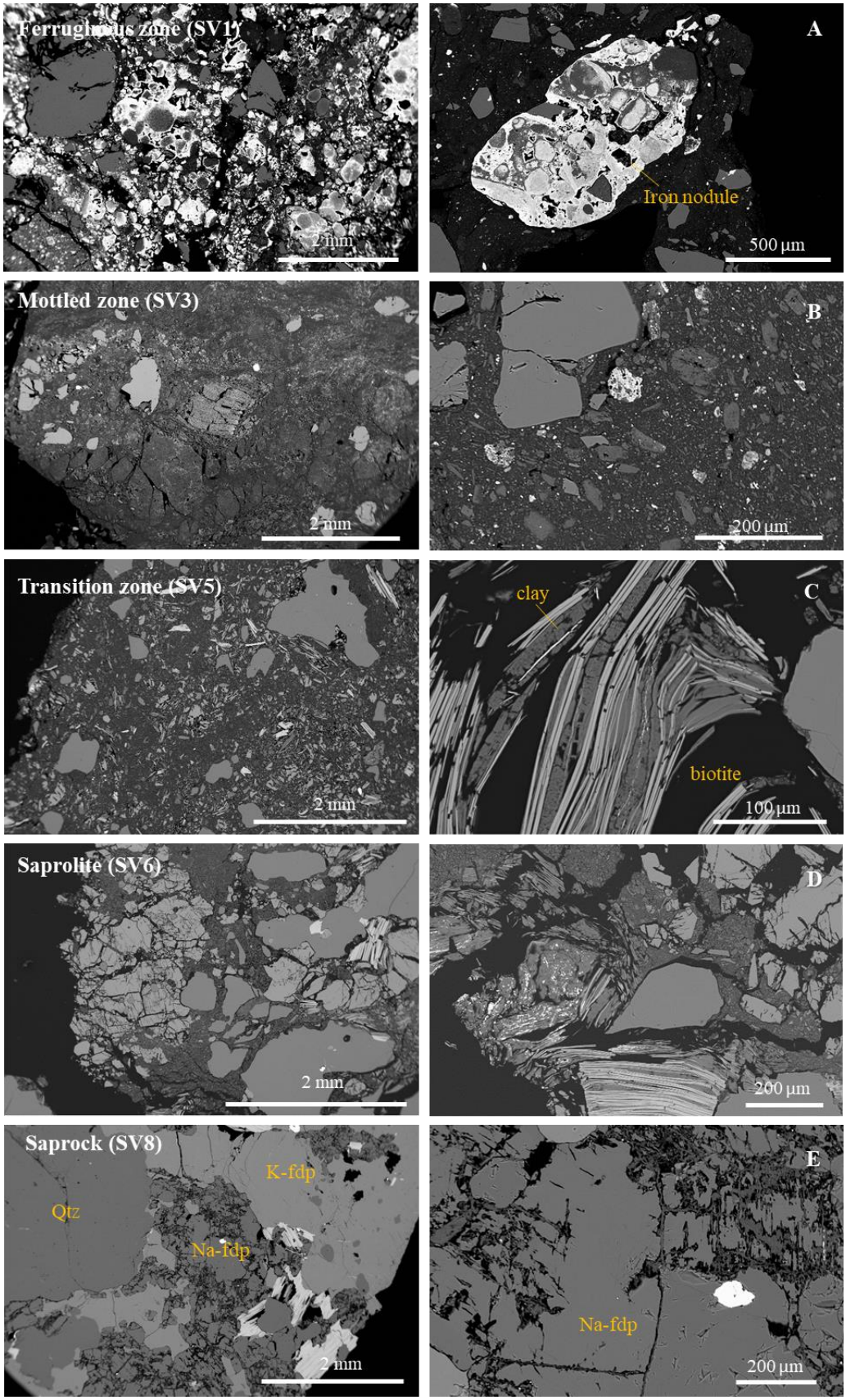


Figure 6.18. SEM-BSE images of weathered rock in each of the horizons. Samples from DDH0161. Note the decreasing particle size and the breakdown of feldspars and biotite minerals in the lower horizons.

The main breakdown products of weathering appear to be kaolinite and iron oxides. Kaolinite peaks are found in the XRD patterns of all the samples analysed and is therefore the dominant clay mineral in the profile. Other clays may also be present but their concentration is not high enough to be detected in bulk sample. Although, iron oxide peaks are not observed in XRD patterns, the elevation of background line from 400 counts in saprolite to > 1600 counts in ferruginous zone, caused by iron fluorescence, indicates the presence of increasing amounts of amorphous iron minerals. Crystalline hematite is only detectable by XRD in the ferruginous soil. The increase in iron oxide is also apparent from SEM analysis, where fine iron oxides can be observed in the matrix of mottled zone and formation of iron nodules in the ferruginous soil (Figure 6.18 A and B).

6.7 Mass Balance Analysis

6.7.1 Identification of immobile elements

Immobile element candidates in this weathered profile include: Zr, Al, Th, Nb and Ti. These are all considered highly immobile in low temperature conditions and are present at Serra Verde in concentrations significantly above analytical detection limit. Isocon graphs and isocon ratios, together with SEM analysis, were used to determine the best immobile elements for mass balance calculations.

6.7.1.1 Isocon analysis

The Ciw/Cio trends presented in Figure 6.19 show that Zr, Al, Th, Nb and Ti behave conservatively between the bedrock and lower half of the mottled zone. Along this section of the profile, the Ciw/Cio values of these different elements are highly similar. The isocon diagrams for samples from the lower mottled zone of each studied drill hole show that these elements fall along or near to the isocon line.

In the top half of the mottled zone, the C_i^w/C_i^o ratio trends of individual elements begin to diverge, and upon reaching the ferruginous horizon, these elements have clearly contrasting C_i^w/C_i^o values. This means that in the more advanced weathered part of the profile, not all of the selected elements are behaving conservatively.

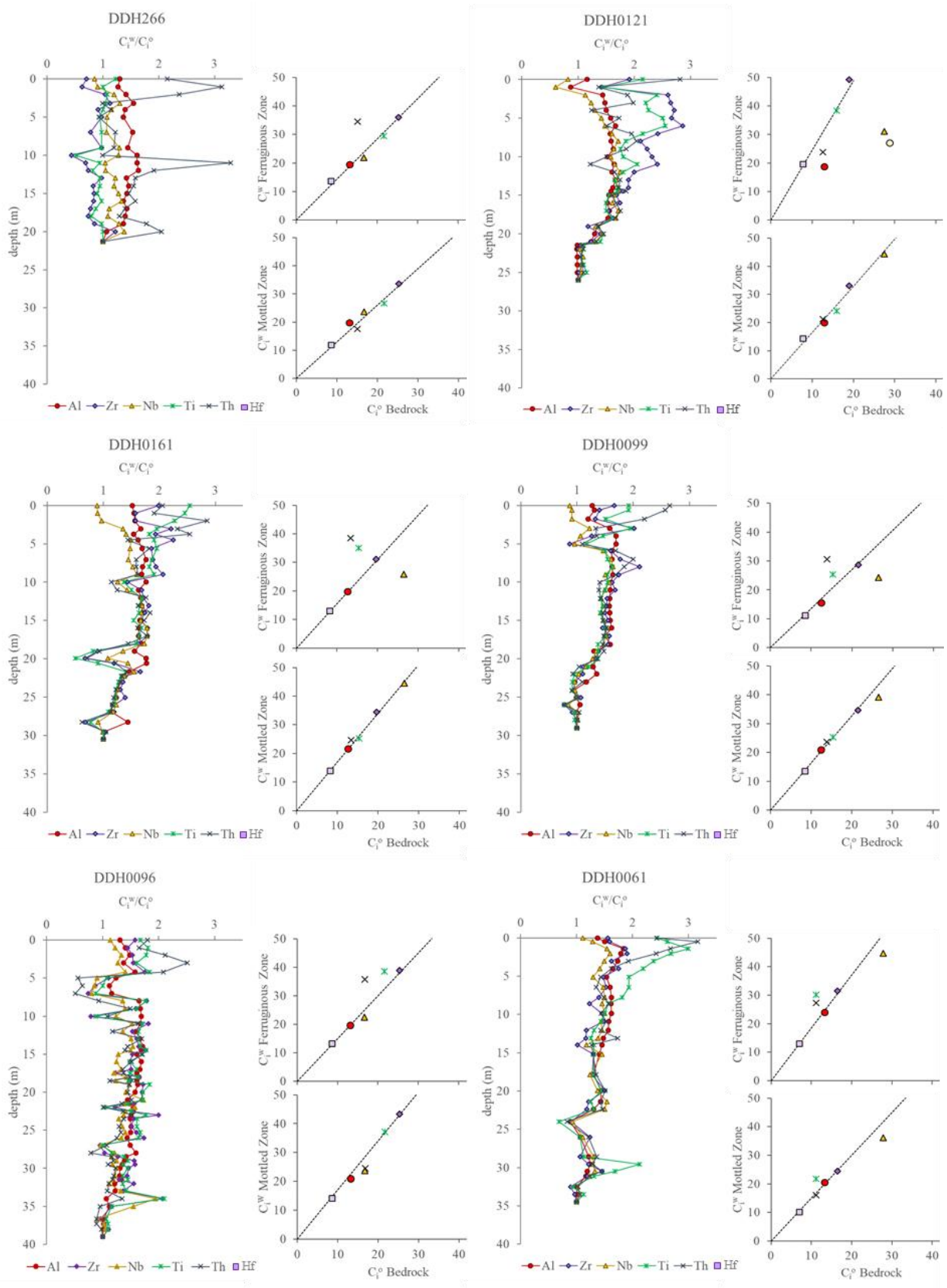


Figure 6.19. Down-hole C_i^w/C_i^o down-hole and isocon diagrams for selected 'immobile' candidates (Al, Zr, Nb, Ti and Th) in ferruginous zone and mottled zone. The same element scaling factors are applied to all isocon diagrams (see Appendix D). Pegmatite lithologies have been omitted.

The isocon graphs for ferruginous samples, show that Zr, Hf and Al are the most conservative, Nb is generally depleted in ferruginous horizon, and both Ti and Th become enriched. The only exception to this behaviour is DDH0121, where Al is depleted relative to the isocon line, and the most conservative elements are Ti and Zr. The isocon graphs also show that Zr and Hf have not fractionated in the weathering profile, which suggest they remain retained within zircon crystals throughout the profile.

6.7.1.2 SEM analysis

SEM analysis show that zircon and quartz are the only remaining minerals from the parent granite that can be found in the most intensely weathered section of the weathered profile (Figure 6.20). Zircon grains found in ferruginous zone are fractured but show with no sign of weathering, including the hydrothermally-altered patches of bedrock. Zircon is the main host of zirconium and hafnium in the granite, and in the weathered profile.

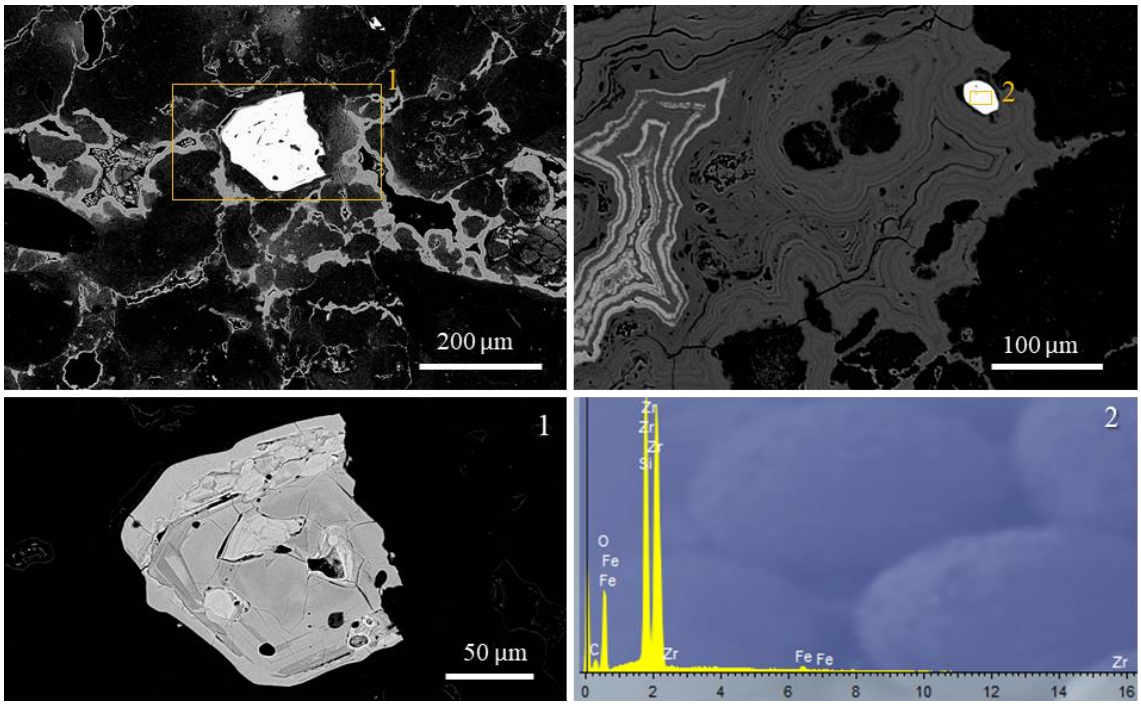


Figure 6.20. SEM-BSE images and EDS spectrum of zircon crystals found preserved in ferruginous zone.

Biotite, metamictic niobiates, phosphates and REE fluorcarbonates, which are the main hosts of Ti, Nb and Th in the parent granite, were not found in the ferruginous zone. SEM analyses of ferruginous material shows that Ti is associated with Fe minerals, and is most likely present

as a minor element in Fe-oxides such as hematite. Nb and Th concentrations are too low to be detected in the ferruginous zone, but are assumed to be concentrated in the fine fraction because there are no visible minerals in the SEM images. The release of Ti, Nb and Th from their hosting minerals means they are more likely to be mobilised through dissolution or fine particle transportation and sorting within the profile.

Out of the five 'immobile' elements considered, Zr appears to behave the most conservatively throughout the weathered profile, both in its isochon behaviour in whole rock assays, and zircon crystal preservation throughout the profile. Zirconium will therefore be used as reference element to evaluate mass flux of other elements in the following sections.

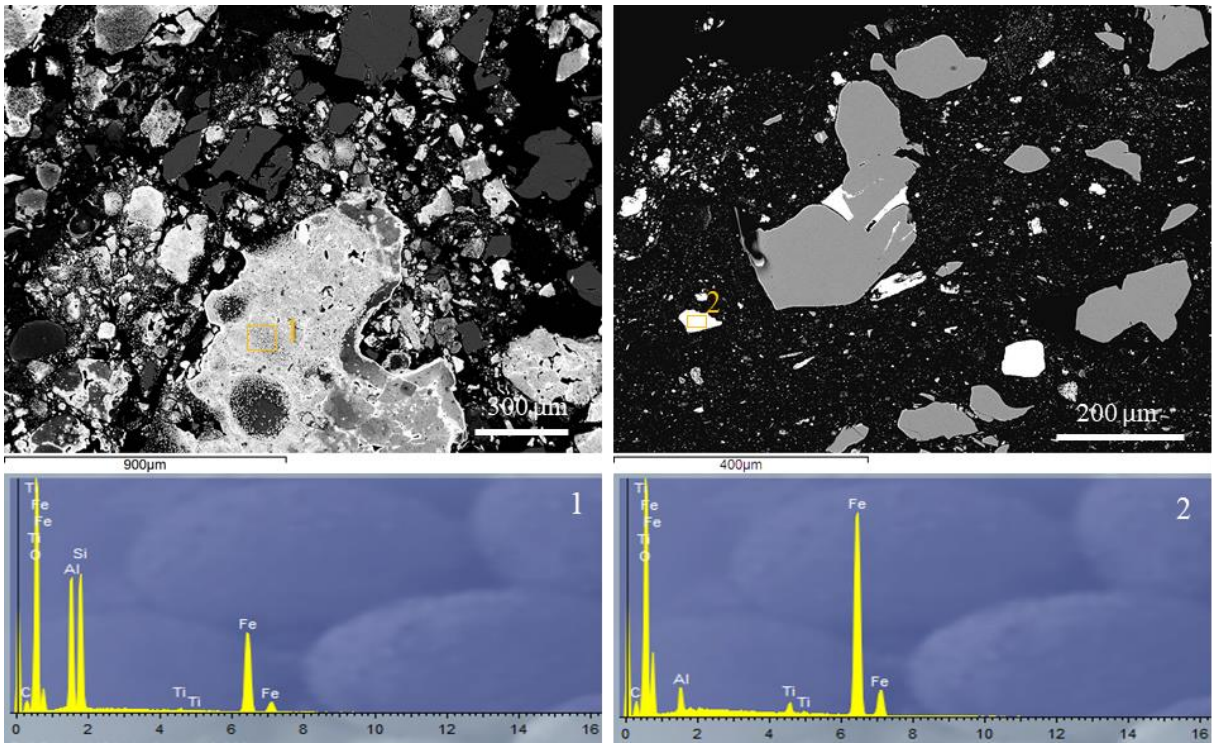


Figure 6.21. SEM-BSE images and EDS spectrums showing the occurrence of Ti in the fine fraction and associated with Fe minerals.

6.7.2 Bulk density

Dry bulk density results for the central plateau were gathered and collated from the Serra Verde drill hole database in order to determine an average bulk density value for each of the different horizons along the profile. The data for each horizon is plotted in box and whisker charts in Figure 6.22, showing the average and range of values from each horizon across the central plateau.

The density results show that the weathered rock in the saprock horizon has a mean bulk density of 2.39 (± 0.11 σ) g cm^{-3}, which is similar to the granite bedrock bulk density of 2.5 (± 0.02 σ) g cm^{-3}. This equates to a density ratio of 0.96 (ρ_w/ρ_p) between the saprock and bedrock. Above the saprock horizon, there is a marked decrease in bulk density with values dropping to 1.71 (± 0.13 σ) g cm^{-3} for the saprolite horizon, and 1.56 (± 0.11 σ) g cm^{-3} for the mottled zone. The saprolite and mottled zone have similar density ratios of 0.68 and 0.62 to the bedrock respectively.

Bulk density appears to increase slightly in the ferruginous zone, although very little data is available for this horizon; only 3 samples are recorded in the database.

The variation in the bulk densities for each horizon across the plateau is low. Of the available density results for the six drill holes studied here, all data fall within one standard deviation of the mean bulk densities.

Bulk densities are used in the mass balance calculations for each of the horizons in the following sections. Where no available bulk density data was recorded for a particular horizon in the drill holes studied here, an average horizon bulk density for the missing horizon was used.

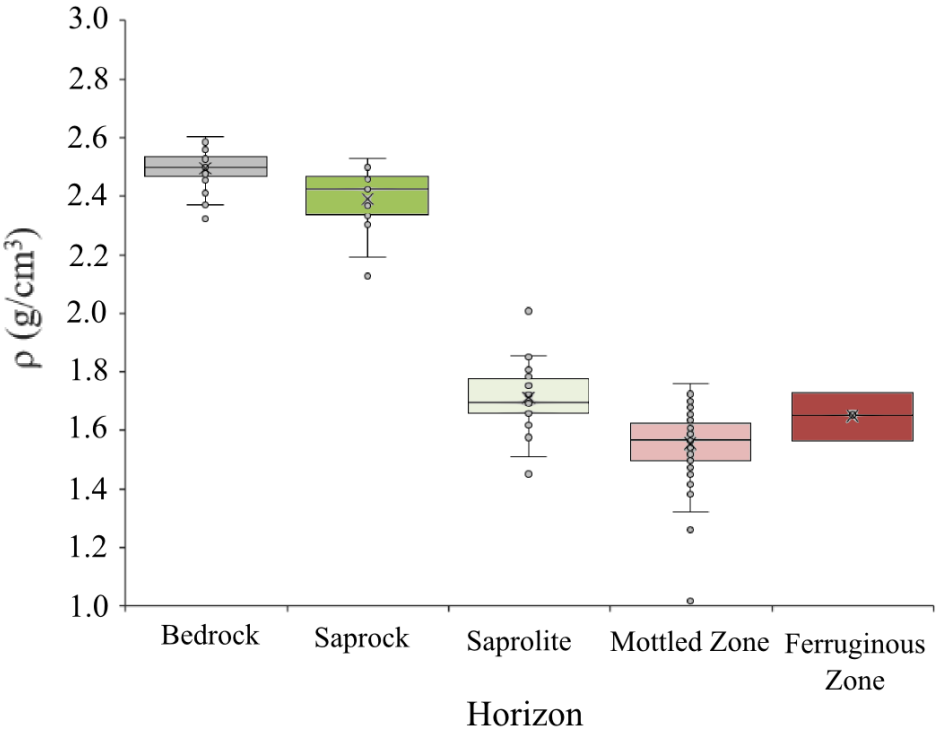


Figure 6.22. Recorded dry bulk density for each horizon of the Serra Dourada weathered profile preserved on the central plateau area. Error bars show outliers.

6.7.3 Volumetric strain

The volumetric strain index for each drill hole was calculated using Zr as the immobile element and density data described in the previous section of this chapter. The results are presented in Figure 6.23. Individual calculated strains for each horizon show the following physical changes along the profile:

Saprolite

The most dilated horizon in the weathered profile is the saprolite horizon. The volumetric strain trends in Figure 6.23 show that weathered material in the saprolite horizon of all six drill holes has undergone positive strain ($\varepsilon > 0$). Average positive strain values for saprolite horizon ranges between factors of 0.0 and + 0.53. The drill holes displaying the highest and lowest average volumetric dilation are drill holes DDH0099 and DDH0096 respectively.

The trends through each profile also show sub-horizon volumetric expansion variations within the saprolite horizon. Drill holes with thick saprolite horizons, where more than one sample was assayed, show that the most dilated material is located closer to the base of this horizon. The highest individual sample positive strain factors are found in DDH0099 and DDH0061with maxima of + 0.68 and + 0.63 respectively.

Mottled zone

The tops of the weathered profiles, the mottled zone and ferruginous zone, have experienced volumetric collapse. The trends show that strain values decrease towards the surface and are consistently negative in the ferruginous horizon. Strain values within the ferruginous zone are ca. - 0.2 for all drill holes except DDH0121 drill hole, which has undergone greater volumetric collapse with a factor of - 0.4.

All trends show that the cross-over point between volumetric expansion and volumetric collapse along the weathered profiles occurs in the mottled zone. However, within the mottled zone, the position of this cross-over point varies between different drill holes. In the strain trends of DDH0121 and DDH0161 volumetric collapse begins at the base of the mottled zone. For DDH0266 and DDH0099 it can be found towards the middle of the mottled horizon and for DDH0061 and DDH0096 definite volumetric collapse does not occur until the top of mottled zone at, or near to, the contact with the ferruginous zone. As a result, the mean index of volumetric strain for this horizon can be positive, negative or zero.

Overall, the data shows that the lower sections of the profile have undergone dilation, while upper sections of the profile have undergone volumetric collapse. For the drill holes studied, it appears that in shorter weathered profiles, the cross-over between dilated and collapsed weathered material occurs lower down in the mottled horizon compared to thicker weathered profiles.

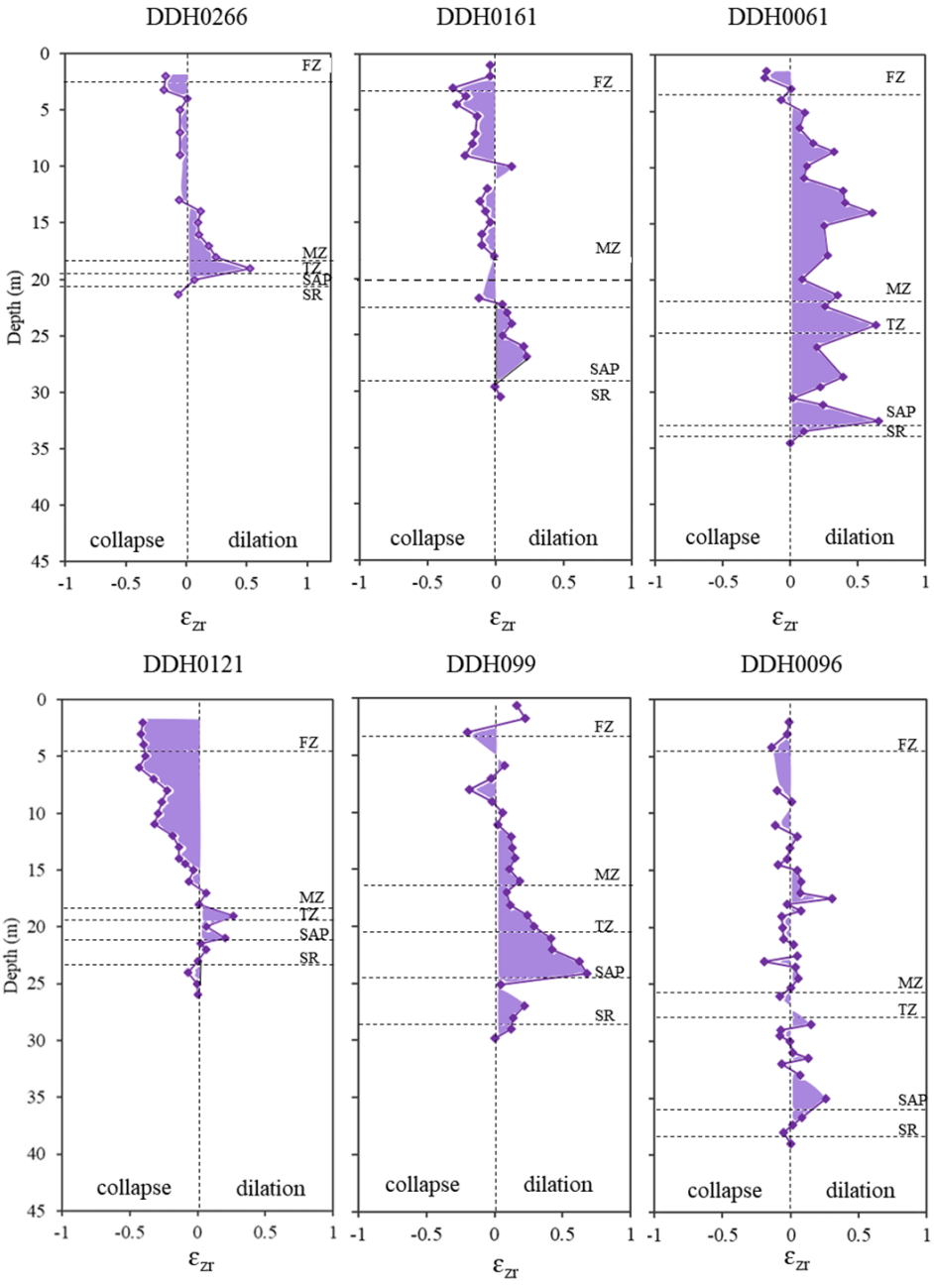


Figure 6.23. Volumetric strain (ε) trends plotted for along each drill hole studied. Calculations made using Zr as immobile element. Note that samples from pegmatite sections are omitted. Average zircon compositions from DDH0004 were used as the parent material Zr concentration ($C_{i,p}$) for drill holes DDH0266 and DDH0161.

6.7.4 Mass transfer

Mass gains and losses of major elements and REE were calculated for each depth interval as well as for each horizon using Zr as the immobile element.

6.7.4.1 Fractional mass gains and losses

The fractional mass gains and losses ($\tau_{i,j}$) results are presented in Figure 6.24 and Figure 6.25 as downhole trends and in Table 6.3 as average values for each horizon.

Major and minor elements

The results show that SiO_2, CaO, Na_2O and K_2O have $\tau_{Zr,j} < 0$ which indicates that these elements are dominantly removed during weathering. The depletion of Si begins in the saprolite horizon, where Tao values for SiO_2 range from -0.39 to -0.07, and decrease gradually towards the top of the profile. Tao values for SiO_2 in the ferruginous zone range between -0.5 and -0.7.

The removal of alkali and alkaline elements occurs in the lower half of the profile and is mostly concentrated in the saprolite horizon. Tao trends in show that the degree of weathering at the mottled zone marks where most of the alkali and alkaline earth elements have been leached out. Tao values at the base of the mottled zone are < -0.98 for K_2O, Na_2O and CaO and < -0.62 for MgO.

Of the alkali and alkaline elements, MgO has the least consistent $\tau_{zr,j}$ values between drill holes. The first variation that can be observed is the maximum degree of Mg removal. Drill holes DDH0121, DDH0266 and DDH0161, have $\tau_{Zr,Mg}$ values ranging between -0.96 and -0.92 in the ferruginous zone which indicate Mg has been strongly depleted in these profiles. In comparison, DDH0096, DDH0099 and DDH0061 have $\tau_{Zr,Mg}$ values ranging between -0.9 and -0.61 which indicate that Mg leaching has been less intense and Mg has not been fully removed from the bulk rock material.

The second variation that can be observed between $\tau_{Zr,Mg}$ trends is in the degree of Mg addition in the saprock and saprolite before depletion dominates. DDH00266 and DDH0161 drill holes show no addition of Mg, drill holes DDH0096, DDH0121 and DDH0061 present small enrichment of Mg in saprock (+0.11 to +0.28), and in DDH0099 a large amount of Mg has accumulated. The saprolite of DDH0099 has $\tau_{Zr,Mg}$ values ranging between + 4.69 and +10 with the strongest addition occurring in the lower half of the saprolite.

The downhole $\tau_{Zr,j}$ trends show that Fe_2O_3 is the only major element to show gains towards the top of the profile. Addition of Fe_2O_3 begins in upper half of the mottled zone and is strongest in the top 5 m of the weathered profiles. Fe_2O_3 gains are highest in the ferricrete soil where maximum $\tau_{Zr,Fe}$ values reach +6. The $\tau_{Zr,Fe}$ values for the Ferruginous horizon are also high, ranging between 0.71 and 4.16. In the lower sections of the profile Fe_2O_3 appears to behave relatively conservatively, with Tao values fluctuating around zero.

Although the concentrations of phosphate are low enough to cause large fluctuations of Tao values, a general trend can still be observed in the downhole $\tau_{Zr,j}$ values. Phosphate shows small to no gains in the saprolite and transition zone, depletion in the mottled zone and positive trends in the ferruginous zone and in the ferricrete soil. The only drill holes to show phosphate gains in the saprolite are drill holes DDH0161 and DDH0061 with maximum Tao values of 0.68 and 4.8 respectively. The depletion of phosphate in the mottled zone is moderate with average Tao values for the horizon ranging between -0.3 and -0.64.

Overall $\tau_{Zr,j}$ values for MnO show a depletion trend from the base to the top of the profile. However, in half of the drill holes the trend is interrupted by large positive peaks. These positive Tao peaks are only observed in the thicker drill holes, DDH0099, DDH0096 and DDH0061 and can be found in the saprolite, transition zone and mottled zone. In both DDH0096 and DDH0061 the largest peak occurs in the transition zone and has $\tau_{Zr,Mn}$ values of 4.6 and 10.3. In DDH0099 Mn gains are concentrated in the saprolite. The peak $\tau_{Zr,Mn}$ in this drill hole is broad, covering most of the saprolite, with a value of 1.4. At the top of the profile MnO exhibits near-complete removal by leaching in all drill holes.

Rare earth elements

The average horizon $\tau_{Zr,REY}$ values presented in Figure 6.25 show a clear upward REE addition and depletion trend along the weathered profile. The saprock and saprolite horizons have positive $\tau_{Zr,REY}$ values ranging from +0.04 to +0.88, and +0.25 to +9.21 respectively. The mottled zone and the ferruginous zone have overall negative $\tau_{Zr,REY}$ values ranging from +0.44 to -0.90 and -0.86 to -0.97 respectively. The strongly negative Tao values in the ferruginous zone indicate that there is a near complete removal of REY at the top of the profile.

The downhole La, Ce and Y Tao trends show that the REE gains are not uniform throughout the saprolite, and that $\tau_{zr,REY}$ peak values are found towards the lower half of this horizon.

Furthermore, the peak $\tau_{Zr,REY}$ values appear to correlate with the saprolite horizon thickness. The trends show that the drill holes with the highest $\tau_{Zr,REY}$ values correspond to the thinnest saprolite horizons; drill holes DDH00266 and DDH0161.

The peak position of the downhole La and Y Tao trends coincides in the saprolite horizon, indicating that LREE and HREE accumulate together. However, the peak $\tau_{Zr,La}$ value is higher than $\tau_{Zr,Y}$ in all drill holes which mean greater gains of LREE compared to HREE. The difference between peak $\tau_{Zr,La}$ and $\tau_{Zr,Y}$ values are largest in drill holes DDH0121, DDH0266 and DDH0161 where $\tau_{Zr,La}$ have values ranging from +5 to +13 and $\tau_{zr,Y} < +3$. This difference is significantly smaller in the other drill holes, and decreases rapidly within the profile either side of the peak values.

The drill hole with the highest HREE gains is DDH0099 where peak $\tau_{Zr,Y}$ is +5.11. In all other drill holes maximum $\tau_{zr,Y}$ values are < 3.5. In a couple of drill holes, the HREE addition in the saprock is greater than LREE. These drill holes are DDH0266 (+1.7 $\tau_{Zr,Y}$ vs +0.4 $\tau_{Zr,La}$) and in DDH096 (+2.06 $\tau_{Zr,Y}$ vs +1.13 $\tau_{Zr,La}$).

The $\tau_{Zr,Ce}$ trend shows Ce gains over several meters in the lower half of the mottled zone. The peak $\tau_{Zr,Ce}$ values range from 2.09 and 11.5, again with highest values occurring in the shorter drill holes; DDH0266 and DDH0121. The only exception is DDH0161 where Ce is preferentially gained in the transition zone and has a much lower Tao value compared to other drill holes.

In the upper sections of the mottled zone and the ferruginous zone, all REE are depleted and the no variations between drill holes are observed. Comparison of La and Y Tao values indicates that LREE are slightly more strongly depleted than HREE.

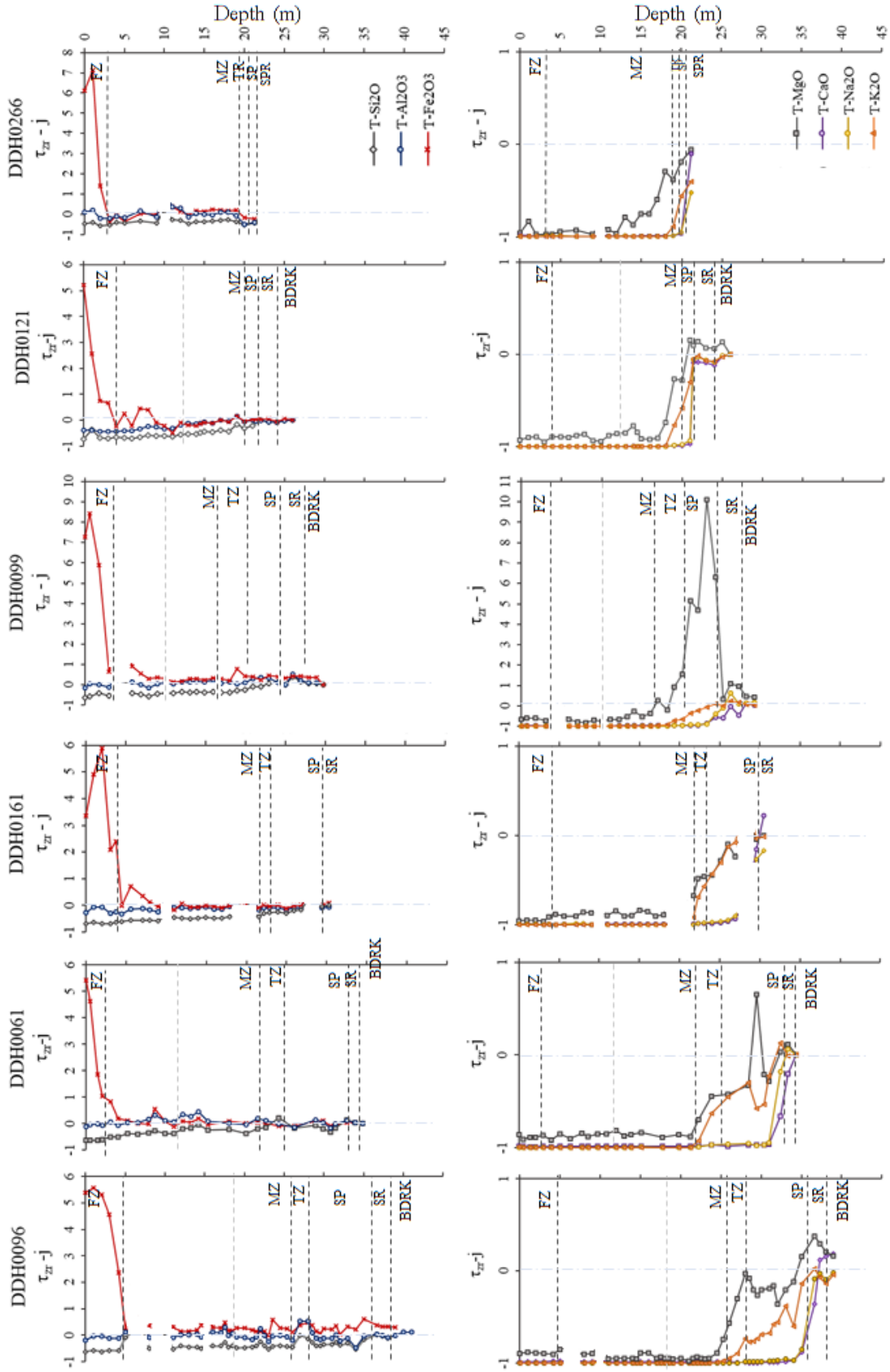


Figure 6.24. Depth profiles for Tau values for major elements in the six drill holes studied. The vertical dashed vertical line at $\tau_{(Zr)} = 0$, represents the point of no element gains or losses relative to parent granite.

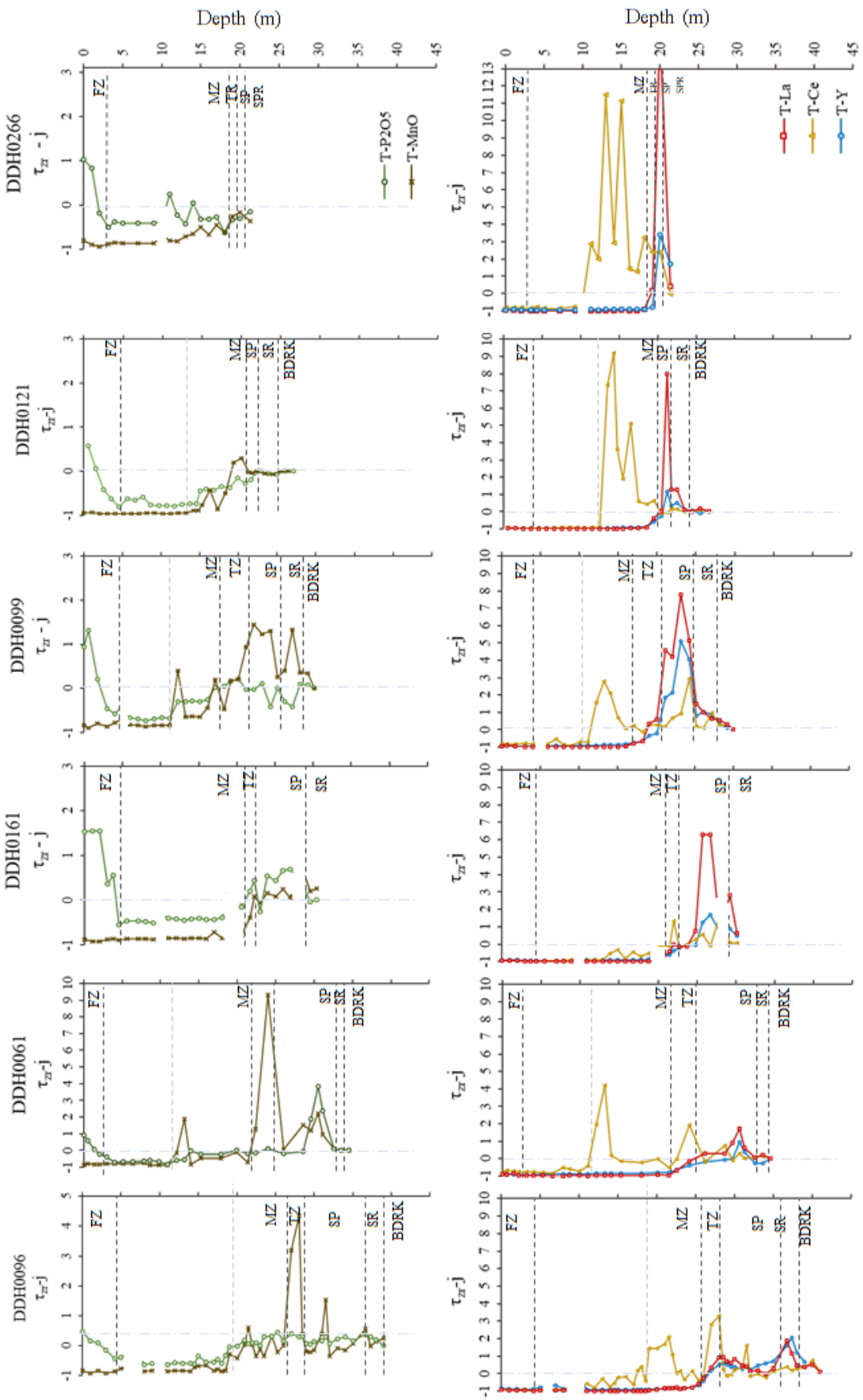


Figure 6.25. Depth profiles for Tau values for P_2O_5, MnO, La, Ce and Y in the six drill holes studied. The vertical dashed vertical line at $\tau_{(Zr)} = 0$, represents the point of no element gains or losses relative to parent granite.

Table 6.3. Calculated mass transfer coefficients ($\tau_{i,j}$) and absolute mass changes per unit volume rock ($\delta_{i,j}$) for major elements and trace elements for each horizon.

		Thickness	$\tau_{z,j}$									$\tau_{z,j}$						$\delta_{zr,j}$				
Drill hole	Horizon	(m)	Si_2O	Al_2O_3	Fe_2O_3	K_2O	Na_2O	CaO	MgO	MnO	P_2O_5	REY	La	Ce	Y	Th	Nb	REY	La	Ce	Y	Th
	Soil/Ferric	1.0	-0.72	-0.39	5.22	-1.00	-1.00	-1.00	-0.93	-0.95	0.57	-0.94	-0.95	-0.93	-0.94	0.47	-0.57	-2.83	-0.49	-0.88	-0.65	0.08
	Ferruginou	3.0	-0.70	-0.44	0.71	-1.00	-1.00	-1.00	-0.92	-0.96	-0.52	-0.97	-0.99	-0.97	-0.95	-0.26	-0.55	-2.91	-0.51	-0.91	-0.66	-0.04
	Mottled Z	15.1	-0.58	-0.26	-0.06	-1.00	-1.00	-1.00	-0.88	-0.88	-0.64	-0.44	-0.98	0.69	-0.95	-0.22	-0.25	-1.32	-0.51	0.66	-0.66	-0.04
DDH0121	Transition	0.9	-0.17	0.14	0.15	-0.76	-0.99	-0.99	-0.27	0.19	-0.15	-0.13	-0.39	0.62	-0.58	0.16	0.12	-0.38	-0.20	0.58	-0.40	0.03
	Saprolite	1.5	-0.28	-0.05	-0.02	-0.50	-0.96	-0.99	-0.16	0.20	-0.26	0.85	2.28	-0.08	0.13	0.05	0.04	2.56	1.18	-0.08	0.09	0.01
	Saprock	2.6	-0.03	-0.05	0.04	-0.04	-0.05	-0.09	0.11	-0.03	-0.03	0.39	0.79	0.07	0.30	0.03	0.03	1.18	0.41	0.07	0.21	0.01
	Soil/Ferric	1.05	-0.47	0.09	6.12	-1.00	-1.00	-0.98	-0.96	-0.80	1.04	-0.90	-0.94	-0.82	-0.94	1.03	-0.32	-2.05	-0.51	-0.82	-0.42	0.08
	Ferruginou	2.15	-0.51	-0.08	3.25	-1.00	-1.00	-0.99	-0.93	-0.92	0.15	-0.90	-0.97	-0.85	-0.95	1.08	0.01	-2.05	-0.52	-0.82	-0.42	0.16
	Mottled Z	15.8	-0.36	0.04	0.01	-1.00	-0.99	-0.99	-0.85	-0.74	-0.31	0.34	-0.98	1.94	-0.94	0.13	0.26	0.78	-0.53	2.01	-0.41	-0.01
DDH0266	Transition	1.00	-0.36	-0.04	0.04	-0.90	-0.99	-0.99	-0.39	-0.52	-0.55	1.18	0.17	2.55	-0.69	0.17	0.30	2.71	0.09	2.47	-0.31	0.03
	Saprolite	0.9	-0.29	-0.19	0.09	-0.56	-0.95	-0.96	-0.19	-0.17	-0.27	9.21	15.44	2.38	3.38	0.45	0.36	21.09	8.30	2.31	1.52	0.09
	Saprock	3.00	-0.10	-0.07	0.01	-0.40	-0.52	-0.10	-0.06	-0.36	-0.11	0.77	0.41	-0.03	1.70	-0.14	-0.02	1.76	0.22	-0.03	0.76	-0.03
	Soil/Ferric	1.00	-0.69	-0.22	3.36	-1.00	-0.99	-0.99	-0.95	-0.90	1.53	-0.95	-0.96	-0.96	-0.94	0.06	-0.47	-2.93	-0.51	-0.97	-0.60	0.01
	Ferruginou	3.48	-0.66	-0.10	3.87	-1.00	-0.99	-0.99	-0.94	-0.92	1.02	-0.96	-0.97	-0.97	-0.94	0.38	-0.26	-2.94	-0.52	-0.97	-0.60	0.06
	Mottled Z	14.5	-0.51	-0.06	0.09	-1.00	-0.99	-0.99	-0.87	-0.88	-0.45	-0.90	-0.99	-0.80	-0.92	-0.09	0.03	-2.78	-0.53	-0.81	-0.59	-0.01
DDH0161	Transition	1.32	-0.37	-0.07	-0.05	-0.80	-0.99	-0.99	-0.57	-0.33	0.32	-0.02	-0.22	0.59	-0.51	-0.07	0.12	-0.07	-0.12	0.60	-0.33	-0.01
	Saprolite	6.56	-0.23	-0.03	-0.01	-0.26	-0.95	-0.96	-0.29	-0.14	0.47	1.42	3.29	0.05	0.75	-0.04	0.08	4.36	1.76	0.05	0.48	-0.01
	Saprock	2.06	-0.01	0.00	0.06	-0.02	-0.21	0.06	-0.02	-0.02	-0.02	0.75	1.60	0.05	0.66	0.02	0.15	2.30	0.86	0.05	0.42	0.00
	Soil/Ferric	0.62	-0.64	-0.15	5.51	-0.99	-1.00	-0.98	-0.68	-0.84	0.93	-0.92	-0.95	-0.85	-0.94	0.74	-0.42	-2.65	-0.55	-0.65	-0.61	0.13
	Ferruginou	3.38	-0.54	-0.10	3.43	-1.00	-1.00	-0.99	-0.65	-0.86	0.28	-0.92	-0.97	-0.83	-0.94	0.46	-0.28	-2.66	-0.56	-0.63	-0.62	0.08
	Mottled Z	13	-0.46	0.01	0.07	-1.00	-1.00	-0.98	-0.64	-0.66	-0.53	-0.66	-0.99	0.10	-0.91	0.05	0.02	-1.91	-0.57	0.08	-0.60	0.01
DDH0099	Transition	4.02	-0.37	0.01	0.12	-0.83	-0.98	-0.97	0.61	0.03	0.10	-0.15	-0.18	0.16	-0.52	0.08	0.07	-0.44	-0.11	0.12	-0.34	0.01
	Saprolite	4.06	-0.07	0.20	0.08	-0.16	-0.82	-0.86	6.53	1.22	-0.08	3.56	5.41	1.08	3.23	0.06	0.12	10.26	3.11	0.82	2.12	0.01
	Saprock	3.92	0.07	0.12	0.09	0.09	0.16	-0.25	0.68	0.58	-0.14	0.72	0.90	0.38	0.74	0.12	0.15	2.09	0.52	0.29	0.48	0.02
	Soil/Ferric	0.5	-0.64	-0.12	5.43	-1.00	-1.00	-0.99	-0.86	-0.89	0.93	-0.86	-0.90	-0.78	-0.87	0.56	-0.29	-2.21	-0.48	-0.59	-0.48	0.08
	Ferruginou	2.52	-0.62	-0.04	2.38	-1.00	-1.00	-0.99	-0.89	-0.81	0.11	-0.86	-0.91	-0.72	-0.90	0.54	-0.17	-2.20	-0.48	-0.55	-0.50	0.08
	Mottled Z	18.3	-0.32	0.11	0.13	-1.00	-1.00	-0.99	-0.87	-0.55	-0.45	-0.69	-0.98	-0.17	-0.87	0.07	0.02	-1.78	-0.52	-0.13	-0.48	0.01
DDH0061	Transition	3.62	-0.18	0.14	0.01	-0.96	-1.00	-0.98	-0.78	0.37	-0.16	-0.03	-0.43	0.92	-0.52	0.08	0.15	-0.09	-0.23	0.70	-0.29	0.01
	Saprolite	7.49	-0.15	-0.04	-0.02	-0.36	-0.88	-0.94	-0.18	0.77	1.02	0.25	0.54	0.04	0.06	0.05	0.01	0.64	0.29	0.03	0.03	0.01
	Saprock	1.00	0.04	0.04	0.04	-0.01	0.07	-0.20	0.11	0.04	0.04	0.04	0.21	0.11	-0.28	0.10	0.09	0.09	0.11	0.09	-0.16	0.01
	Soil/Ferric	2	-0.61	-0.09	5.47	-1.00	-1.00	-0.98	-0.89	-0.88	0.32	-0.92	-0.94	-0.92	-0.86	0.52	-0.01	-1.92	-0.43	-0.73	-0.26	0.08
	Ferruginou	3	-0.60	-0.07	4.16	-1.00	-1.00	-0.98	-0.90	-0.87	-0.15	-0.94	-0.97	-0.94	-0.90	0.89	0.05	-1.97	-0.44	-0.74	-0.27	0.14
	Mottled Z	18	-0.46	0.00	0.36	-1.00	-1.00	-0.99	-0.93	-0.54	-0.27	-0.56	-0.92	-0.01	-0.88	0.17	0.09	-1.18	-0.42	-0.01	-0.26	0.03
DDH0096	Transition	2.5	-0.46	-0.16	0.11	-0.95	-1.00	-0.99	-0.57	0.01	0.15	-0.20	-0.26	-0.16	-0.43	-0.04	-0.03	-0.43	-0.12	-0.13	-0.13	-0.01
	Saprolite	8.15	-0.36	-0.08	0.27	-0.53	-0.95	-0.97	-0.15	0.05	0.15	0.40	0.46	0.16	0.45	0.07	0.19	0.83	0.21	0.12	0.13	0.01
	Saprock	2.35	-0.06	-0.01	0.33	-0.08	-0.07	0.01	0.28	0.20	0.28	0.88	1.03	0.28	1.56	0.19	0.21	1.85	0.47	0.22	0.46	0.03

6.7.4.2 REE mass transfers

The absolute mass changes per unit volume of parent rock ($\delta_{Zr,j}$) and the total mass fluxes ($M_{j,flux}$) in each horizon were calculated for REY, La, Ce, and Y and are presented in Table 6.3 and Figure 6.26.

The results show that in the saprolite horizon absolute REY mass gains per unit volume of parent rock range widely between 0.64 – 21.1 kgm^{-3}. The drill holes with the highest $\delta_{Zr,REY}$ values are DDH0266 (21.09 kgm^{-3} REY) and DDH0099 (10.29 kgm^{-3}), while drill holes with the lowest $\delta_{Zr,REY}$ values are DDH0096 (0.64 kgm^{-3}) and DDH0061 (0.84 kgm^{-3}).

The total mass REY gains in the saprolite horizon for the six drill holes fall into two groups and do not correlate well with saprolite thickness. In the first group, which includes drill holes DDH0099, DDH0161 and DDH0266, the $M_{REY,flux}$ values are relatively high and range from 16 to 27 kgm^{-2}. In the second group, which includes DDH0096, DDH0061 and DDH0121, REY mass gains are much lower ranging from 3.36 and 5.8 kgm^{-2}. The drill holes with the highest REE mass additions have both very thin and thick saprolite horizons.

The saprolite $\delta_{Zr,j}$ results for La and Y also show that mass gains are higher for LREE than for HREE. The largest difference is found in DDH0121 where absolute $\delta_{Zr,La}$ are 13 times higher than $\delta_{Zr,Y}$ (1.18 kgm^{-3} for La vs 0.09 kgm^{-3} for Y), and the lowest difference is in DDH0099 where $\delta_{Zr,La}$ gains are only 1.5 times higher than $\delta_{Zr,Y}$ (3.11 kgm^{-3} for La and 2.12 kgm^{-3} for Y).

The large variation in the $\delta_{Zr,REY}$ in the mottled zone (-2.78 to 0.78 kgm^{-3}) is due to variations in the mass gains of Ce in the lower mottled zone (itself 0.72 to 4.8 kgm^{-3}). The Ce addition in DDH0266 and DDH0121 is so high that it results in a positive $\delta_{Zr,REY}$ value. All other REE are strongly depleted in the mottled zone, as indicated by La (-0.43 to -0.57 kgm^{-3}) and Y (-0.26 to -0.66 kgm^{-3}).

Both $\delta_{Zr,REY}$ mass change per volume values and $M_{REY,flux}$ flux values become increasingly negative above the transition zone (Figure 6.26), and values in the ferruginous zone are similar between drill holes for both variables (-1.92 to -2.94 kgm^{-3}). This means that the degree of REE mass loss is uniform laterally across the deposit, and that values at the top do not reflect and are not indicative of variations observed in the lower sections of the profile.

Comparison of the total gains and losses along the profile show that the total losses are overall greater than total gains. The drill hole where the difference is smallest is DDH0099 (96 % retained), followed by DDH266, DDH161 and DDH96 (36 – 41 %), and finally DDH0121 and

DDH0061 (only 11 % retained). This difference applies to all individual REE except for Ce. In drill holes DDH0266 and DDH121, Ce gains are overall greater than the losses.

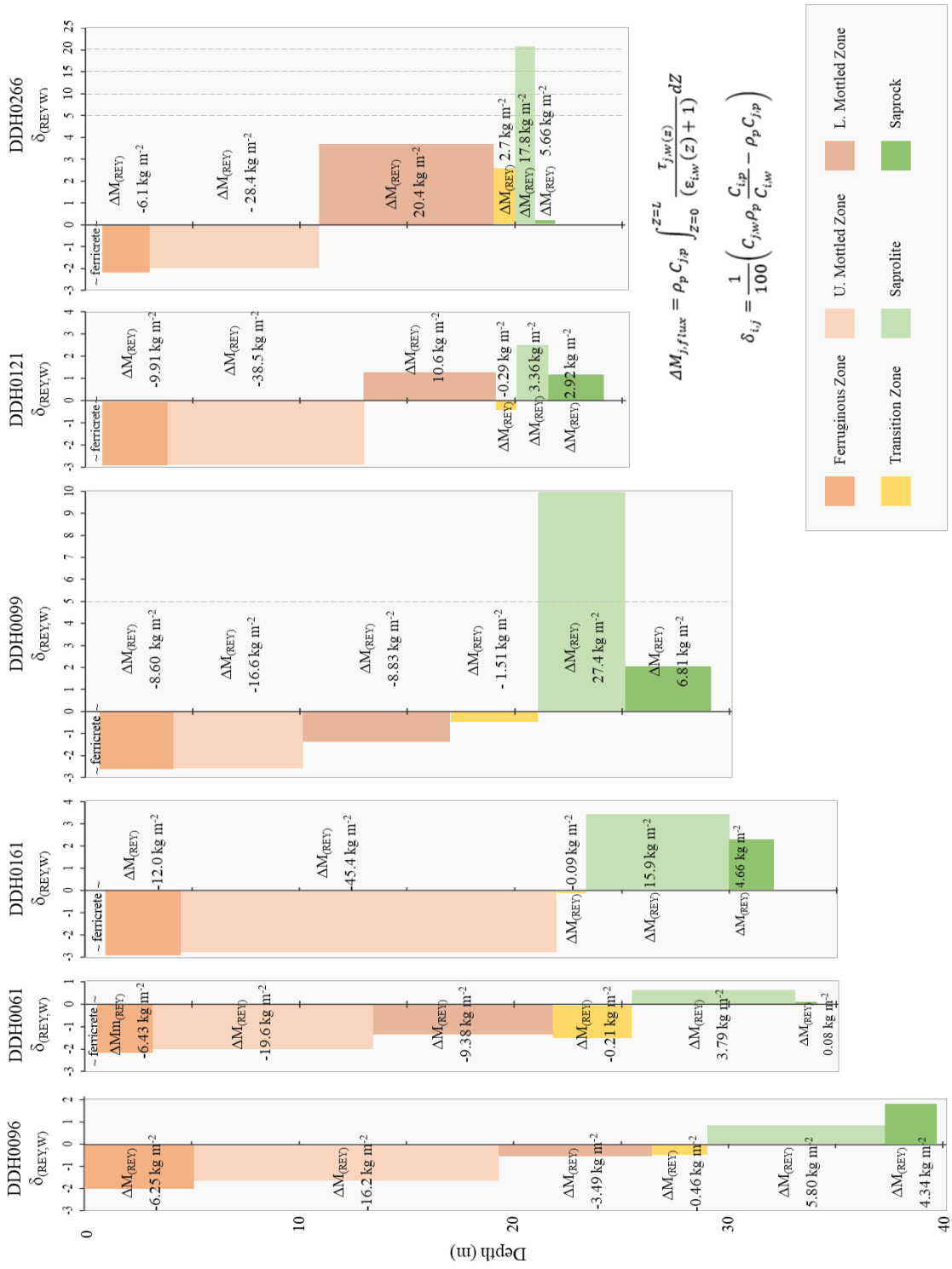


Figure 6.26. Absolute REY mass changes per unit rock volume ($\delta_{i,j}$ (kg m^{-3})) and total mass gains or losses REY ($M_{j,flux}$ (kg m^{-2})) calculated for each horizon in each of the drill holes studied

6.8 Discussion

6.8.1 Bulk characteristics of the weathered profile

The weathered profile of the Serra Verde deposit is a thick and mature profile defined by its distinct weathering horizons that has undergone weak to moderate laterisation. From bottom to top, the saprolite and saprock horizons represent the principal zones of kaolinitisation and REE accumulation, while the mottled and ferruginous zones above are where laterisation and REE-depletion processes dominate. A schematic summary of the geochemistry and mineralogy through the profile is presented in Figure 6.27.

6.8.1.1 Mineralogy and geochemistry

In the lower profile, the saprolite and saprock are characterised by gradual breakdown of aluminosilicates into clay minerals and the gradual loss of elements such as Ca, Na, K, and Mg. Primary mineral breakdown occurs in the following order: Na-feldspar is broken down to kaolinite in the saprock and lower saprolite, K-feldspar and biotite are broken down to kaolinite, Fe-oxides, and probably a small amount of smectite in the upper half of the saprolite, and quartz remains resistant. This differential mineral breakdown matches the differences between trends of major elemental concentrations within the saprolite, and an increase in the moisture content due to clay formation. This breakdown sequence is common for igneous rocks exposed at the earth's surface and reflects the different stabilities of these magmatic minerals when exposed to atmospheric pressure and temperature conditions (Goldich 1938, Berner & Berner 1996).

Although, no smectite was found in XRD analysis of DDH0161 samples, the small Mg peak observed in all the saprolites studied, especially DDH0099, suggest a small amount of smectite is forming from the breakdown of biotite at particular points along the saprolite. Biotite can convert into smectite first before turning into kaolinite under conditions of restricted drainage (Fordham 1990). Formation of smectite at specific levels in the saprolite may therefore reflect locally poor drainage conditions.

Between the saprolite and the mottled zone, there is a clear geochemical and mineralogical boundary, defined by the complete loss of alkali and alkaline elements and the complete breakdown of primary aluminosilicates. Above the saprolite, the mottled and ferruginous zone are characterised by gradual accumulation of Fe and Al oxides, moderate loss of Si, and a depletion of labile elements (< 0.05 wt % Ca, Na, K, and Mg). Kaolinite, quartz and iron

oxides are the main minerals that compose these upper horizons. The ferruginous zone distinguished from the mottled zone by the rapid loss of Si from the breakdown of kaolinite and the formation of pisolithic Fe nodules.

Overall, the weathered profile that developed over the Serra Dourada granite is typical of granites that have weathered in tropical humid climatic conditions and the dominance of kaolinite throughout the profile has been suggested to indicative of good drainage conditions (Melfi et al 1983, Marker and Oliviera 1994).

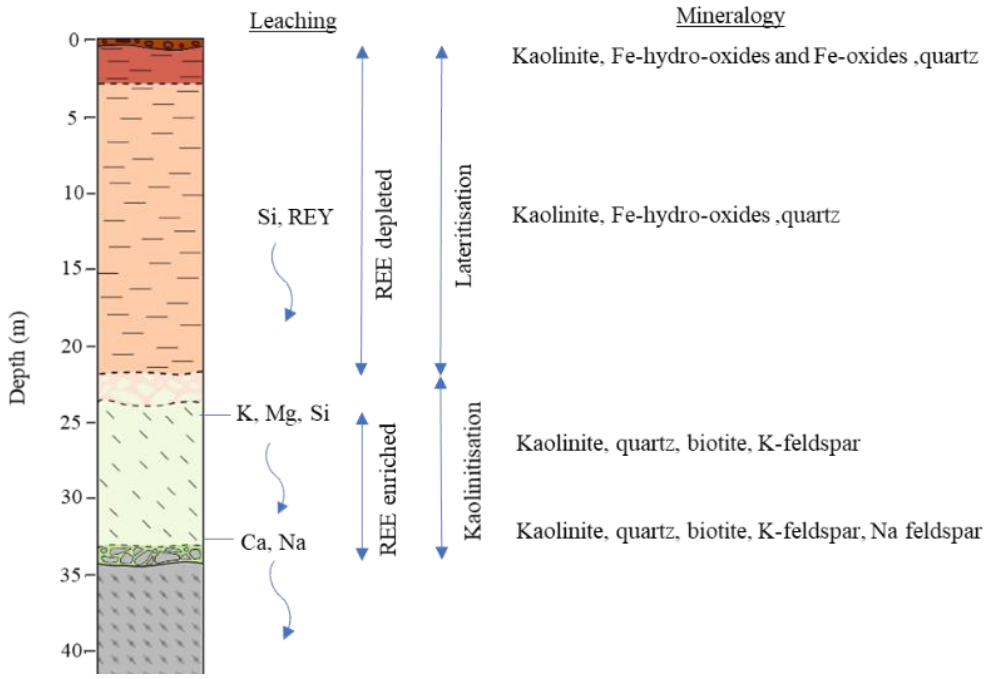


Figure 6.27. Summary of main features of the weathered profile.

6.8.1.2 Volumetric strain

Volumetric strain is a measure of the volume changes experienced by weathered material relative to the bedrock, and it is important for identifying the processes that cause physical changes in the weathered profile. The weathered profile of the Serra Verde deposit has undergone little deformation; strain results show that only the top of the mottled zone and ferruginous zone near the top of the profiles have experienced compaction (negative strain), while the lower half of all profiles have remained unchanged or are slightly dilated (positive strain). Dilation can occur through addition of mass, physical increases in void space or clay

swelling (Anderson et al. 2002, Parizek & Girty 2014). The only notable dilation occurs in DDH0099, and is coincident with a section of Mg accumulation which suggest it is the result added mass and the presence of swelling clays such as montmorillonite.

Compaction of material in soil profiles is considered to represent the collapse of weathered rock volume as a result of mass removal through leaching (Brimhall and Dietrich 1987, Brimhall et al. 1988). In the weathered profile of the Serra Verde deposit the negative strain coincides with strong removal Si in the upper mottled zone and ferruginous zone of most drill holes. Through the removal of silicate material, the compressive strength of the rock decreases as small cavity spaces are left behind and the porosity increases. The decreased strength eventually leads to a collapse of the rock volume from the weight of the overburden.

All drill holes studied show compaction at the top of their profile however the strain cross-over point, from dilation to collapse, varies between them with the most notable difference between the longest and the shortest drill holes. In the former, the first samples to exhibit collapse occur much higher in the mottled zone compared to the latter. Difference in cross over position between drill holes could reflect variations in drainage conditions, where profiles with poor drainage are unable to develop negative strain indices further down the profile due to a lack of mass removal by water. This would suggest relatively poor drainage of the profile in drill holes DDH0061, and DDH0096.

6.8.1.3 Lateral variations in saprolite thickness

Cross sections of the weathered profile and mapping of the bedrock underlying the plateau show that while the plateau surface has a relief of < 5 m, the thickness of the weathered profile varies by up to 20 m. The total thickness variations are mainly attributed to the saprolite and saprock horizons which exhibit the greatest range. The variations of saprolite and saprock thickness follow the variations of the underlying bedrock topography, with the thinnest sections of 0.5 m or less found directly above bedrock topographic ridges, and the thickest sections of up to 8 m found above bedrock channels. The mottled and ferruginous zones have comparatively consistent thicknesses across the plateau, and follow the plateau surface more closely.

The thickness of the saprock and saprolite horizons is determined by the weathering rate of aluminosilicate minerals, and the vertical gradient of alkali loss, which in turn are dependent on the rate of water flow through the soil (White 2003, Clow & Drever 1996). As meteoric waters percolate and flow through the permeable weathering profile, the water interacts with

minerals and removes any accumulated solutes in pores. The higher the water flow rate, the faster the removal of cations by flushing, and the less buffered and more acidic the water becomes, which promotes faster hydrolysis and breakdown of aluminosilicates (Clow & Drever 1996). Horizons that have experienced higher weathering rates due to higher flow rates, have higher gradients of cation concentrations, and are therefore expected to be thinner than horizons with lower weathering rates (see schematic in Figure 6.28).

The rate of water flow through the profile will be controlled by several factors, including meteoric water input, the height of the ground-saturated water table, and bulk permeability of the different profile horizons and underlying fresh bedrock. In the case of the Serra Verde deposit, the crystalline bedrock underlying the weathered profile is relatively competent and impermeable. The variable shape and slope of the topographic bedrock surface can therefore influence the drainage pattern at the base of the profile by causing increased water flow away from topographic highs, while directing water towards channels and causing ponding. By influencing the water drainage, the bedrock topography affects the flow rate of percolating water through the overlying profile, and in turn the chemical weathering gradient of the saprolite and saprock horizons to produce the variable thickness observed across the plateau. The development of bedrock channels may be due to preferential weathering of discrete areas, perhaps controlled by rock type, faulting, or pre-existing topography.

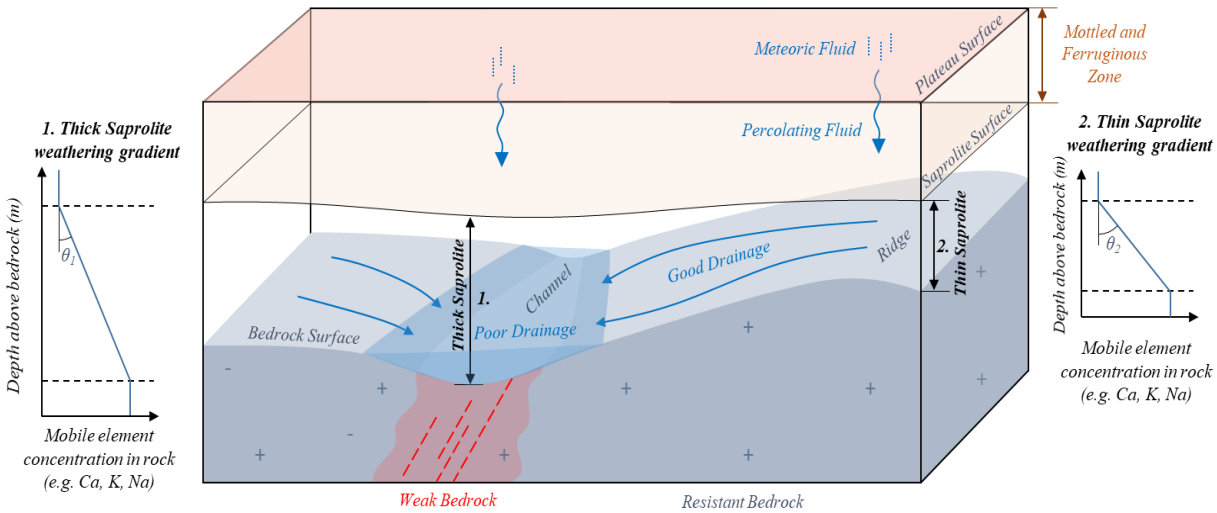


Figure 6.28. Schematic diagram showing the proposed effect of drainage on saprolite thickness across the profile on the plateau.

6.8.2 REE distribution and fractionation

The REE distribution down the drill holes show that the weathered profile is divided into a REE enriched zone, which includes the saprock and saprolite, and a REE depleted zone in the mottled and ferruginous zones (Figure 6.27). The most enriched horizon is the saprolite horizon, containing between 0.16 to 1.2 wt % mean REY, and represents the REE ore zone. The mean REE grades in the saprolite are closely related to saprolite thickness, drill holes with the thinnest saprolites have the highest mean REE grades. This increase in concentration is due to the REE precipitation process operating in a smaller volume, and with a higher weathering gradient.

Within the saprolite, REE are not equally distributed and grades commonly increase towards the lower half of the horizon. In most drill holes, peak REE concentrations coincide with the level of most intense plagioclase weathering. This preferential concentration of REE is likely to be related to the more alkaline conditions found at the base of the saprolite and the formation of kaolinite from the breakdown of plagioclase that can adsorb the REE from solution. REE are significantly more soluble in acidic solutions, and clay minerals have higher REE adsorption capacities in more alkaline conditions (Coppin et al. 2002, Ma and Eggleton 1999). The preferential enrichment of REE at the base of the saprolite was observed to be more pronounced and more discrete in the drill holes with thinner saprolites. In drill holes with thicker saprolites REE were found to be more dispersed across the horizon.

In terms of composition, both the saprolite and saprock retain the chondrite-normalised REE signature of the bedrock; the REE are LREE-fractionated, the negative Eu anomaly is preserved, and HREE exhibit flat trends. The key differences are the development of strong negative Ce anomalies and slightly more LREE-fractionated trends. The drill holes with the most pronounced Ce anomalies and largest difference in LREE fractionation were those with the thinnest saprolite (DDH0121, DDH0266). Within the saprolite no strong REE fractionation was observed; in all drill holes, the maximum individual REE peaks coincide.

The negative Ce anomaly in the saprolite is produced by the retention of Ce in the mottled zone. In all drill holes, Ce is found strongly concentrated in the lower mottled zone with values up 8000 ppm Ce. This fractionation is due the mobility of Ce being redox sensitive (Braun 1990). Ce has two valencies: Ce^{3+} which is soluble and Ce^{4+} which is insoluble. As weathering progresses, oxidation causes Ce^{4+} to be retained at higher levels, while other REE with a single 3+ valency are mobilised down into the saprolite where they concentrate. The retention of Ce^{4+}

in the mottled zone explains both the positive anomaly in the chondrite-normalised REE patterns of the mottled zone, and negative anomalies in the underlying saprolite.

6.8.3 Mass balance model of REE enrichment

Mass balance analysis was carried out to measure the contributions of different enrichment processes and better understand how tropical weathering led to the enrichment of REE in the Serra Verde deposit. The mass balance results show that the majority of the enrichment, which ranges between a factor of 1.5 to 10, relative to bedrock, and can be attributed to mass transfer of REE from the mottled zone and ferruginous zone down into the saprolite and saprock. This process is principally an open system enrichment, which has increased REE concentrations by a factor of 1.25 to 10.21 ($\tau + 1$; average 3.62).

Mass transfer is achieved through the breakdown of primary REE bearing minerals and the downward mobilisation of free REE^{3+} ions by percolating acidic meteoric waters. In order to retain and accumulate the REE in the lower half of the profile, meteoric waters need to be sufficiently buffered by mineral interaction, and saturated in cations to cause the REE to precipitate before the water leaves the profile. These chemical mechanisms of REE migration are described by Nesbitt (1979), Duddy (1980), Prudencio et al. (1993) and Aubert et al. (2001) for studies at different weathering profiles.

Leaching processes in the mottled zone and ferruginous zone of in the Serra Verde weathered profile have been highly efficient, with removal of more than 90 % of the REE from these horizons. The efficiency of this REE mass removal can be explained by a high and constant input of rainwater that would have maintained the acidity required to mobilise and transfer REE down through the upper profile. Good drainage of the profile would also have been required to flush the water through the upper profile and maintain sufficiently high concentration gradients.

However, the retention of REE across the plateau does not appear to have been as effective. Comparison of the total net losses and gains between the upper and lower profile show that the amount of REE lost is consistently greater than the amount gained. The net retention of REE varies between 10 – 90 %, which indicates that a proportion of mobilised REE left the weathering system in outflowing groundwater. However, some lateral mobilisation of REE may also be occurring as indicated by the net gain of Ce in DDH0266.

The large variation in mass gains observed between drill holes could be expected to relate to saprolite thickness, as with mean REE grades; with thicker saprolites having greater accommodation capacities and therefore higher mass gains. However, no clear relationship between saprolite thickness and mass gains was observed. In fact, the drill holes DDH0061 and DDH0096 with the thickest saprolite horizons have had the lowest REE mass gains. As has been discussed above, these two drill holes are located in areas of relatively poor drainage. It is possible that this poorer drainage may have reduced the efficiency of REE delivery into saprolite. The mass gains in the REE in the ore zone at Serra Verde are therefore not directly controlled by the thickness of the saprolite. Other factors such as drainage or physiochemical conditions may have had a stronger control.

Comparison of LREE and HREE mass balance results shows that the net losses of HREE are greater than LREE in the weathered profile. This difference suggests that LREE are preferentially retained in the saprolite horizon while HREE preferentially remain in solution. Other studies have previously found that HREE are preferentially retained in percolating fluids, thought to be due to the higher stability of aqueous HREE complexes in weathered profiles (Braun 1990, Duddy 1980; Gouveia et al. 1993, Galan 2007 Scheepers & Rozendall 1993). The preferential accumulation of LREE in the saprolite may also be explained by the differences in leaching of LREE and HREE in the mottled zone. Results show that LREE are more strongly depleted than HREE. Retention of HREE in the mottled zone can be explained by a combination of the higher susceptibility of LREE-bearing mineralogy to acidic weathering in the upper profile compared to HREE-dominant minerals, and by the adsorption of HREE onto Fe oxides (Peasecki et al.2008). The degree of HREE mass loss is found to vary between drill holes. In the relatively thinner profiles of DDH0121, DDH0266 and DDH0161 the net HREE losses were greater, which suggests that improved drainage directly results in a greater removal of HREE from the upper profile due to higher flushing rates, and preferential retention of HREE in the fluid.

Contributions by volumetric strain and residual enrichment of REE, which represent closed system enrichment processes, are relatively small (enriching by a factor of 0.98 to 1.58 in the saprolite; see Figure 6.29), with the lowest contributions at the base of the profile. The low contributions are likely due to the lack of collapse occurring in the saprolite, and because relatively small proportion of the total mass has been removed by the percolating fluid. A simple model can be proposed for the mass balance of REE enrichment at Serra Verde where REE mass losses occurring in the upper profile correlate with higher degrees of compaction,

and REE mass gains in the lower profile correlate with higher degrees of dilation with the cross-over point occurring at lower mottled zone (Figure 6.30).

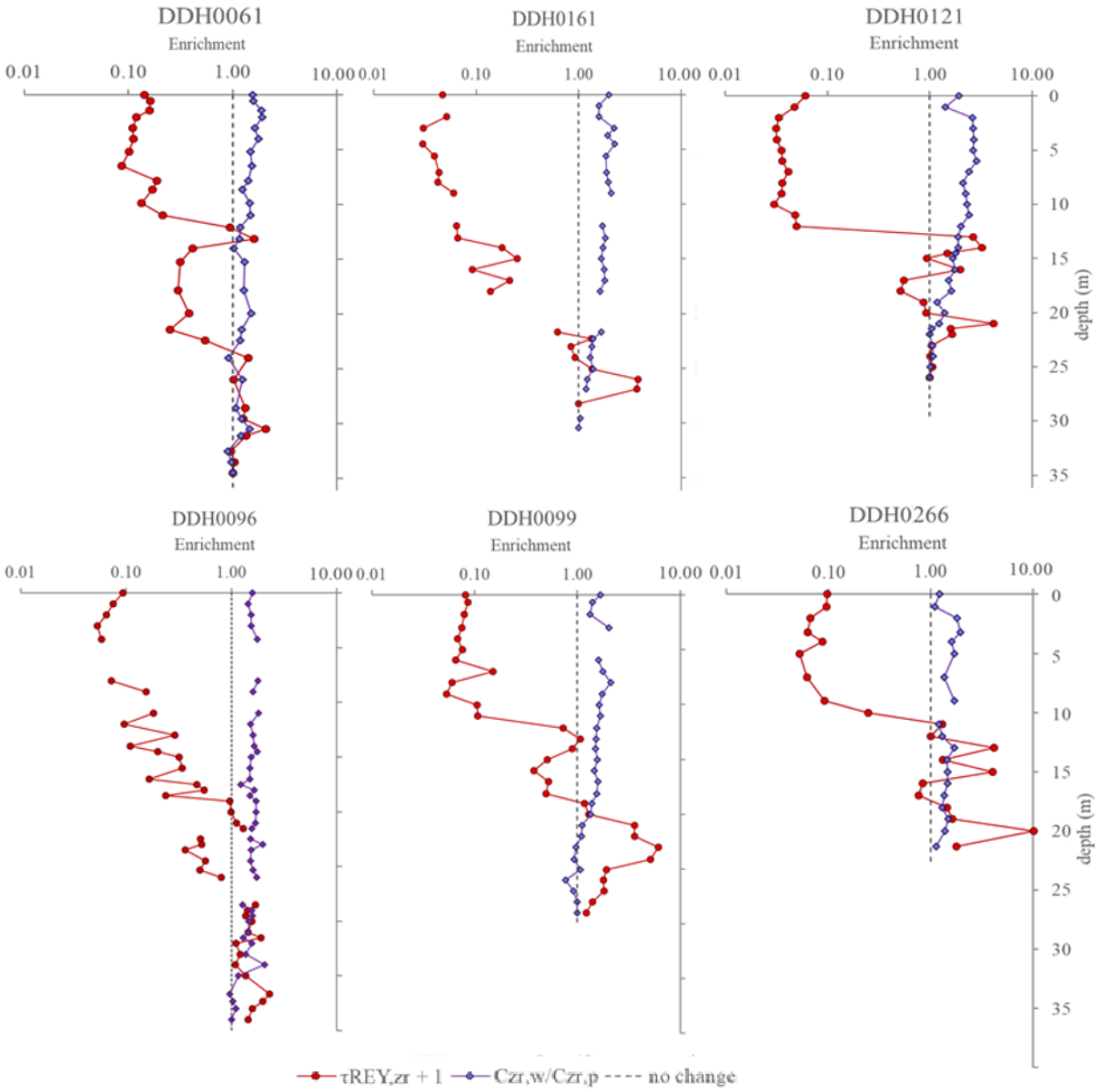


Figure 6.29. Downhole charts for the drill holes studied showing comparison of close system enrichment ($C_{zr,w}/C_{Zr,p}$) and open system enrichment factors ($\tau_{REY,zr}$).

In many primary and residual REE deposits, REE are enriched together with deleterious radioactive elements (Th and U) due to their close association in primary bedrock minerals (Kanazawa and Kamitani 2006, Dostal 2017). In the Serra Verde profile, Th is clearly decoupled from REE, and REE enrichment in saprolite has not been accompanied by Th or U

enrichment. This can be explained by the low mobility of Th compared to REE in the weathering profile which causes Th to behave conservatively and accumulate at the top of the profile while REE are accumulate in the base of the profile, producing a low-Th REE ore in the saprolite. The enrichment of REE by mass transfer processes has the added benefit of producing low-Th ores in IADs.

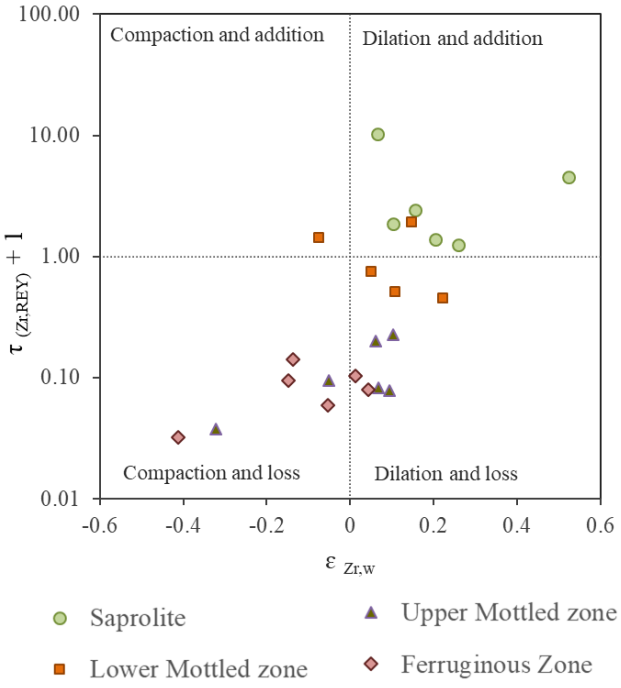


Figure 6.30. REE mass gains and losses vs strain in the different horizons.

6.8.4 Physico-chemical conditions along the weathered profile

The mobilities of Ce, Fe and Mn are redox- and pH-sensitive as their mobility depends primarily on their oxidation state (Brooking 1988). Ce, Fe, and Mn form insoluble species when they are oxidised (Ce^{4+}, Fe^{3+}, and both Mn^{3+} and Mn^{4+}) and tend to precipitate out of solution. The vertical distribution of these elements in the profile can therefore be used to track the variation of physiochemical conditions (redox and acidity conditions) along the profile.

6.8.4.1 Redox front

The redox conditions along the profile are controlled by aeration, percolating meteoric water, and groundwater levels. At the top of the profile aeration and rainwater input help maintain highly oxidised and slightly acidic conditions. Down into the profile, oxidation decreases with

depth as the ground becomes increasingly water saturated and the oxidised rainwater interacts with relatively reduced primary minerals.

The sharp Ce concentration peaks observed in all the downhole Ce trends suggests there is a strong redox boundary just below the Ce peaks at the base of the mottled zone. Above this boundary conditions are sufficiently oxidised to have Ce occur as Ce^{4+} and cause its accumulation, while below this boundary oxidation conditions are reduced enough to allow Ce to remain dominantly as mobile Ce^{3+} (Figure 6.31). The position of this boundary varies between drill holes but in general is found between 15 and 30 m below the surface. Other studies have also used Ce to interpret the location of a redox boundary (e.g. Braun 1990, Banfield and Eggleton 1989, Ma et al. 2007).

The formation of these peaks is likely produced by past fluctuation of the water table level in the permeable weathering profile. The reduced water from the lower half of the profile is able to transport Ce^{3+} as the level fluctuates with seasonal variation, rising during high rainfall periods (Bilong 1988). When the position of the water table stabilises, Ce oxidises and precipitates at the top of the water level due to contact with oxygen, and forms a discrete concentration peak (Braun 1990). As the weathering and redox fronts move downwards with progressive weathering, so does the Ce peak, and the upper section of the profile is left depleted of Ce. Due to the dependence on the level of the water table, short periods of stability can produce multiple Ce peaks. The unique oxidation behaviour of Ce at this redox boundary causes its fractionation from the other REE.

At the mottled zone-saprolite boundary a large amount of Fe oxide minerals accumulates, associated with the distinct colour change from the pale pink saprolite where the biotite is largely unweathered, to the bright pink-red colour of the mottled zone where the biotite is mostly weathered and thus releases Fe as Fe oxides. The location of this change in Fe oxidation state matches and corroborates the Ce redox boundary.

6.8.4.2 pH conditions

The pH conditions along a weathered profile are expected become more neutral and alkaline as the slightly acidic meteoric water that percolate through profile is gradually buffered by interacting with silicate minerals. The largest change in pH is expected to occur in the lower part of the profile where primary minerals are being dissolved by hydrolysis which consumes a large proportion of H+ ions and releases cations such as Na and K into solution.

The distribution of REE along the profile suggest that the top half of the weathered profile is relatively acidic while the lower half is relatively neutral to alkaline (Figure 6.31). This is because REE are more soluble and mobile in acidic conditions and begin to precipitate when solution approaches pH 6 (Moldoveanu & Papanglakis 2016). The lack of REE in the ferruginous and mottled zones therefore suggest this part of the profile is maintained at more acidic conditions by the influx of meteoric water.

The adsorption capacities of clay minerals are also affected by pH conditions. Experiments have shown that clay minerals, including smectites and kaolin groups, have greater adsorption capacities when conditions are more neutral or alkaline (Coppin et al. 2002, Ma and Eggleton 1999). In very acidic conditions, clay minerals may cease their cation adsorption behaviour entirely (Plant and Raiswell 1994). The more acidic conditions in the mottled zone may therefore help explain why despite large amounts of kaolinite this horizon is strongly depleted in REE and the lower saprolite and saprock which have a smaller proportion of clay material are strongly enriched in REE. The pH conditions along the weathered profile are therefore important controlling factor in the distribution of free REE^{3+} ions along the profile.

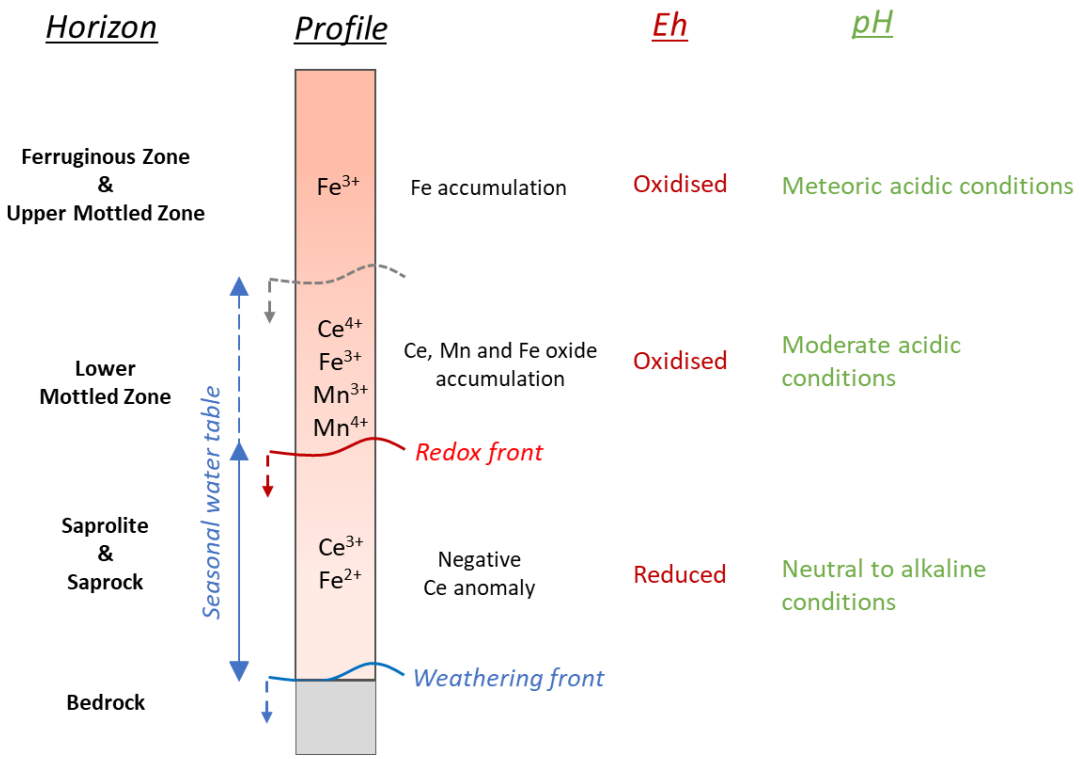


Figure 6.31. Summary diagram of interpreted pH and redox conditions along the profile.

6.8.4.3 Differences between drill holes

The patterns of redox-controlled Ce and Mn peaks in the mottled zone divide the drill holes into two groups; those with multiple, coincident peak values (DDH0099, DDH0096, and DDH0061), and those where only Ce peaks are found and no Mn accumulation has developed (DDH0161, DDH0121, and DDH0266; see Figure 6.32). The differences in the Mn and Ce distribution between these drill holes could be produced by differences in oxidation and pH conditions controlling the mobility of Ce and Mn. The Eh-pH stability field for these elements shows that boundaries between soluble and insoluble Mn and Ce ionic species exist at different conditions. Two percolating fluid Eh-pH trajectories (see arrows A and B in Figure 6.33), are proposed to explain the differences in Ce and Mn accumulation in different parts of the weathering profile. Trajectory A tracks a fluid that is only slightly neutralised by interaction with the weathering zone, resulting in Ce precipitating and Mn remaining mobile. In trajectory B, the fluid pH advances to a more alkaline composition, such that both Ce and Mn precipitate together.

Variations in the drainage across the plateau can produce the proposed trajectories of the percolating water, where poorer drainage leads to less flushing and more equilibration of the percolating water with the weathering zone, and thus generating the higher alkalinity of trajectory B. The profiles that contain these coincident Ce and Mn peaks are also those with the thickest saprolites which has been shown to be the result of poorer drainage (see above). The presence or absence of Mn together with Ce can therefore be used to diagnose the drainage at a particular part of the Serra Verde plateau.

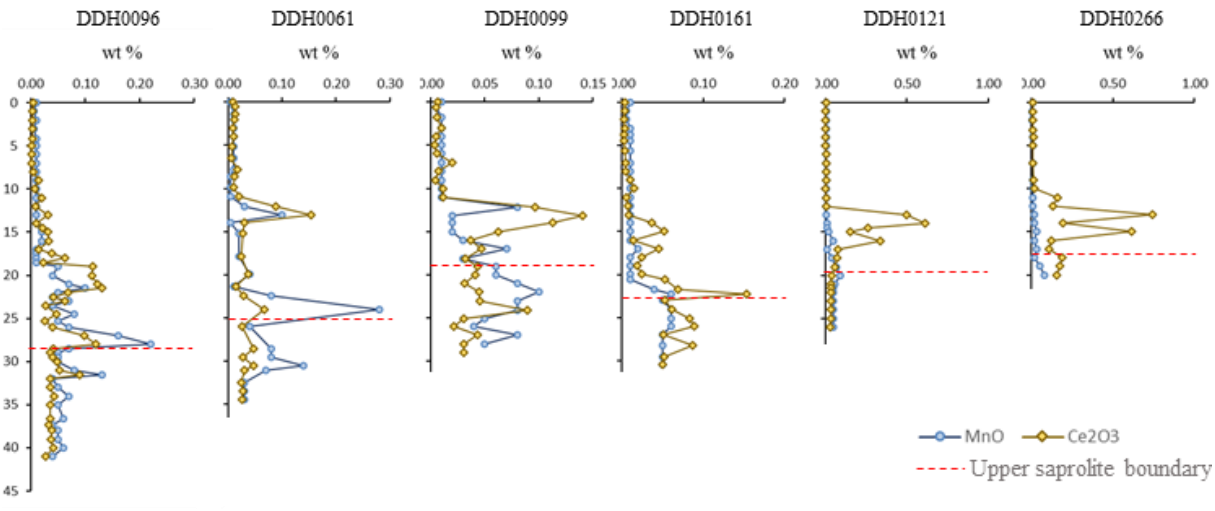


Figure 6.32. Downhole redox-sensitive Ce and Mn trends.

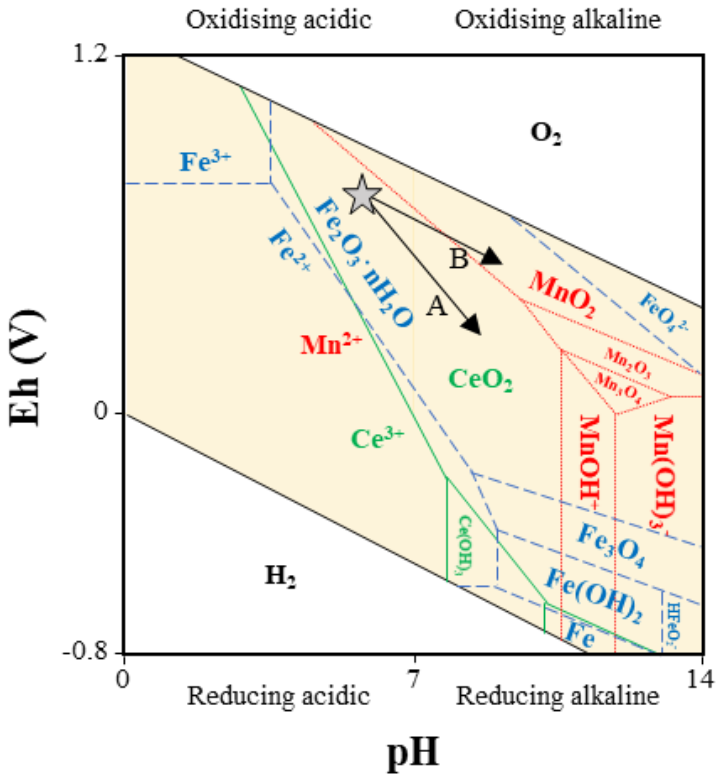


Figure 6.33. Eh-pH stability field diagram for Mn-O-H system, Ce-O-H system and Fe-O-H system, superimposed. Assumed activities Mn = 10^{-10} mol Ce =10^{-6} mol and Fe = 10^{-5} mol at 25 ˚C and 1 atm pressure (Brooking 1983, Takeno 2015). Star represents rain water conditions. Arrows indicate possible water trajectory of percolating water weathered profile preserved on the plateau of the Serra Dourada granite. Trajectory A – representing an estimated fluid for drill holes DDH0099, DDH0096 and DDH0061; and trajectory B – representing DDH0266, DDH0161 and DDH0121.

6.9 Conclusions

1. The Serra Verde weathered profile is mature, weakly to moderately lateritised in the upper profile, and kaolinitised in the saprolite, with well-defined geochemical and mineralogical horizons.
2. The REE are most concentrated in the saprolite horizon, forming an ore zone of 0.16 to 1.2 wt % REY, which is 1.5 – 10 times more REE-enriched that the parent bedrock. REE are most strongly enriched at the base of the saprolite that coincides with pH-Eh buffering to more neutral-reduced conditions. The mottled and ferruginous zones are depleted in REE with respect to bedrock concentrations.
3. Ce is strongly fractionated from other REE and concentrates at the lower half of the mottled zone due to its oxidation, producing a distinct negative Ce anomaly in the saprolite. Th is also fractionated from the REE due to its immobile behaviour.
4. Mass balance analysis of REE shows that the weathered profile can be divided into an upper leached zone, and a lower enriched zone with the transition occurring at the saprolite-mottled zone boundary. The majority of REE enrichment is the result of open system mass transfer, which has enriched the REE by an average factor of 3.62, while enrichment occurring due to residual processes only contributed an average factor of 1.3. Of the REE transferred from the upper profile, an average of 39 % of REE are retained by the lower profile.
5. Mass gains of LREE are 1.5 to 13 times greater than HREE, due to the preferential precipitation of LREE, and the preferential retention of HREE in the percolating fluid.
6. Variations in the profile thicknesses, the presence of intermediate weathering products, and the estimated Eh-pH trajectories necessary to explain variations in geochemistry suggest that drainage conditions had a major control on saprolite variation across the plateau. Thinner saprolites, which have higher REE grades and mass transfers, but lower bulk clay contents are shown to be the product of a relatively high drainage setting. The bedrock surface topography is interpreted to be the principal control on drainage in the overlying profile. The highest net enrichment of REE occurs in intermediate drainage settings overlying slopes in bedrock topography where coincident higher retention of REE, and high REE grades occur. Ce fractionation is suggested to be the product of fluctuation of the groundwater table.

Chapter 7

Mineralogical Characterisation of the REE-rich Saprolite Horizon including the Residency and Distribution of REE

7.1 Introduction

The enrichment and adsorption of REE onto clay minerals in IADs is largely the result of primary REE-mineral breakdown and REE ion mobilisation into clay-bearing sections of the weathered profile (Bao and Zhao 2008). REE in the parent granites are usually hosted by an assemblage of accessory minerals, which have different solubilities during weathering. Allanite, titanite, apatite, and LREE-fluorcarbonates are considered good sources of REE due to their relatively high solubilities during weathering, while some REE-phosphates (e.g. monazite), niobiates and zircons are considered to be resistant (Wu et al. 1993, Sanematsu & Watanabe 2016). The REE mineral assemblage, and the proportions of specific mineral species will therefore influence the amount of REE available for mobilisation and clay absorption.

However, the mineral pathways of REE from primary REE-bearing minerals in the bedrock to ion-adsorbed REE on clays are poorly understood. Detailed studies of mineral breakdown from saprolite samples have not been published and the behaviour of minerals in supergene conditions has largely been determined by experimental work on individual minerals. For example, it has been shown that primary apatites dissolve significantly faster than monazites and xenotimes (Valsami-Jones et al. 1998, Oelkers and Poitrasson 2002), and typically result in the formation of supergene phosphates such as rhabdophane and florencite (Banfield and Eggleton 1989, Aubert et al. 2001, Sanematsu et a 2013). The breakdown of LREE-fluorcarbonates has not been investigated, but are assumed to be highly susceptible to dissolution based on their observed absence from IAD ore materials, and are therefore considered a major potential source of REE (Bao and Zhao 2008, Sanematsu & Watanabe 2016).

In chapter 5, the primary mineralogy of the granite protolith underlying the Serra Verde deposit was shown to contain a hydrothermal assemblage of LREE-fluorcarbonates, altered zircons, metamict niobiates, as well as small amounts of phosphates and Ce-silicates. This represents an accessory mineral assemblage that includes REE-minerals both resistant and highly susceptible to weathering.

In chapter 6, characterisation of the weathered profile showed that a REE-enriched saprolite with grades up to 1.2 wt % has developed from deep weathering of the granite protolith. Mass balance analysis showed that the enrichment was primarily the result of mass transfer, indicating that some or all of the primary REE-minerals were broken down in the profile, liberating REE and allowing them to mobilise into the ore zone. Considerable lateral and vertical geochemical variation of the saprolite was also observed, and may indicate differences in the supergene mineral assemblage.

The ore mineralogy of the REE-enriched saprolite horizon of the Serra Verde deposit has not been characterised before. This is therefore a good opportunity to investigate the breakdown behaviour of the accessory minerals identified in the parent bedrock, and the mineral pathways of liberated REE from the bedrock assemblage, into supergene minerals in the saprolite. Identifying and determining the distribution of REE-hosting minerals and their behaviour in the weathering profile will help to characterise the REE ore zone, and improve understanding of IAD formation. Finally, studying the residency of REE in the ore zone may highlight REE-bearing phases that are not leachable by ion-exchange processing.

The aims of this chapter are therefore to:

1. Present a detailed chemical and mineralogical description of the saprolite ore zone;
2. Determine the REE distribution and residency in saprolite minerals;
3. Identify and explain any lateral or vertical mineral variations within the saprolite;
4. Understand the breakdown of primary REE minerals in the enriched protolith, and chart the pathways that REE take from being concentrated in discrete accessory phases to being more widely dispersed during secondary processes and becoming more loosely bound to clay minerals.

7.2 Materials and Methods

7.2.1 Sample selection

A total of 19 samples that comprise quarter-core fragments from the drill holes already described in Chapter 6 were selected as a subset and analysed by a range of methods described below. The locations of samples from each drill hole, their allocated sample numbers and the analysis carried out on each are presented in Figure 7.1 and Table 7.1.

The quarter-core samples include:

- Six saprock samples from drill cores DDH0096, DDH0161, DDH0099, and DDH0266.
- Four samples from the saprolite horizons of DDH0061, DDH0099, DDH0121 and DDH0266. Each of these samples was collected from the most REE-enriched section of their respective saprolite horizon by using the assay data.
- Two saprolite samples from drill hole DDH0096. An extra sample was collected due to the high thickness of the profile here, and the consequent lack of a well-defined REE-enrichment peak within the broader REE-rich saprolite horizon in this drill hole (see Chapter 6).
- Seven saprolite and transition zone samples from DDH0161.

Drill hole DDH0161 was selected for more detailed sampling; six samples from the saprolite and one from the transition zone were chosen and studied in detail. This closely-spaced sampling enabled sub-horizon variation within the saprolite to be assessed. The geochemistry of the weathering profile shows the most variation within the saprolite, but the REE concentration often shows discrete layers of consistently enriched REE (see Chapter 6). DDH0161 was selected for detailed study because it is located closest to the drill hole examined in the detailed bedrock study (DDH0004; see Chapter 5), which permitted a continuous evaluation of mineral breakdown pathways from totally fresh bedrock, through the weathering zone, to the surface of the profile.

In addition to the bulk quarter-core samples, samples were collected from clay-filled fractures observed cutting through the weathered profile. A total of seven samples were prepared and analysed (Table 7.1). Five samples were collected from an exposed section of weathered profile on the plateau (on coordinates 48.51882 deg. South and 13.51383 deg. West) and another two samples were collected from drill core. Of the field samples, S1 and S8 were taken from infilled

fractures running through mottled zone horizon and S3, S5 and S9 were collected from infilled fractures running through the saprolite horizon. The drill core samples were taken from clay coatings on fracture surface of bedrock sections from drill holes DDH0099 and DDH0161 labelled S10 and S11 respectively.

Photographs of the samples of core fragments from saprolite and infilled fractures are presented in Figure 7.2 and Figure 7.3. Note the bright white colour of the material infilling the clay fractures in Figure 7.3 compared to the more mixed and dull colours of the bulk samples in Figure 7.2.

Table 7.1. Summary of the samples collected and analysed for geochemical and REE-mineralogical characterisation.

Sample ID	Sample Type	Horizon	Drill Hole	Depth (m)	Bulk Geochem	Clay Fraction Separate (< 2μm)	SEM	XRD	EMP
SV5	core fragments	Transion zone	DDH0161	22.3	x	x	x	x	
SV5.1	core fragments	Saprolite	DDH0161	24.3			x	x	
SV6	core fragments	Saprolite	DDH0161	25.5	x	x	x	x	x
SV6.1	core fragments	Saprolite	DDH0161	25.8			x	x	x
SV6.2	core fragments	Saprolite	DDH0161	26.1			x	x	x
SV7	core fragments	Saprolite	DDH0161	26.9	x	x	x	x	x
SV8	core fragments	Saprolite	DDH0161	28.5	x	x	x	x	
SV8.1	core fragments	Saprock	DDH0161	29.5			x		x
SV8.2	core fragments	Saprock/Bedrock	DDH0161	31.0			x		x
SV9	core fragments	Saprolite	DDH0099	23.0	x	x	x	x	
SV9.1	core fragments	Saprock	DDH0099	25.0			x	x	
SV9.2	core fragments	Saprock/Bedrock	DDH0099	29.8			x		
SV10	core fragments	Saprolite	DDH0096	34.1	x	x	x	x	
SV11	core fragments	Saprolite	DDH0096	29.8	x	x	x	x	
SV11.1	core fragments	Saprock	DDH0096	37.0	x	x	x		
SV12	core fragments	Saprolite	DDH0121	21.0	x		x	x	
SV13	core fragments	Saprolite	DDH0061	30.5	x				
SV15	core fragments	Saprolite	DDH0266	20.1		x	x	x	
SV16	core fragments	Saprock	DDH0266	21.3			x		
S1	field sample	Mottled zone clay infilled fracture			x		x	x	
S8	field sample	Mottled zone clay infilled fracture			x		x	x	
S3	field sample	Saprolite clay infilled fracture			x		x	x	
S5	field sample	Saprolite clay infilled fracture			x		x	x	
S9	field sample	Saprolite clay infilled fracture			x		x	x	
S10	core fracture surface	Saprock clay infilled fracture	DDH0099	29.8	x		x	x	
S11	core fracture surface	Saprock clay infilled fracture	DDH0161	31.0			x	x	

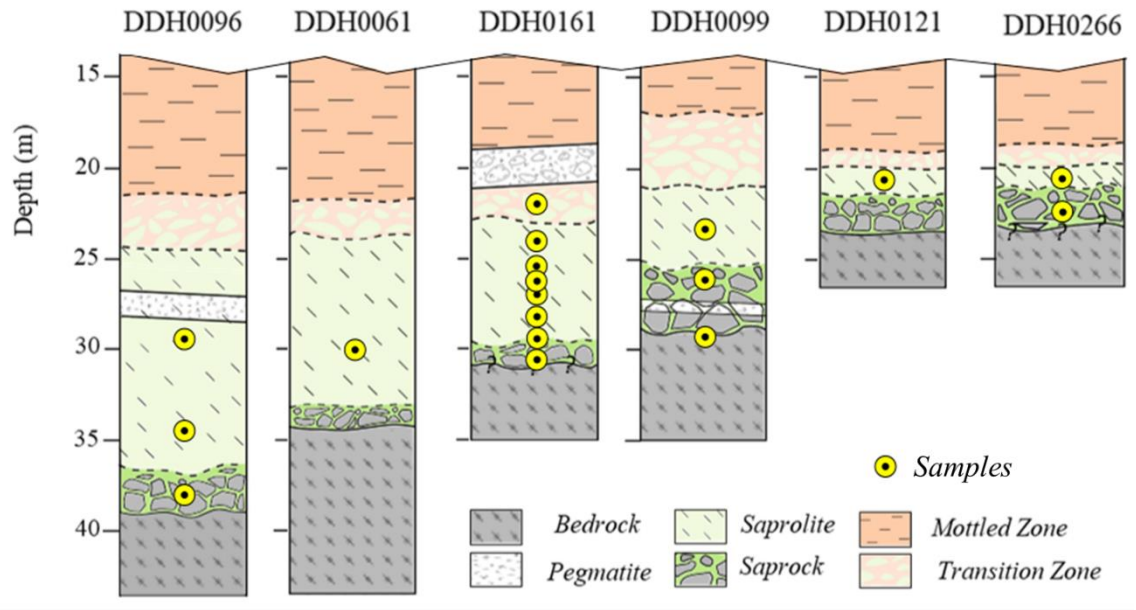


Figure 7.1. Schematic diagram showing the location of the samples collected within the saprolite and saprock horizons of each drill hole studied. Note that pegmatite lithologies are similarly weathered to their host horizon, but are compositionally different and have therefore not been sampled in the study of the profile.

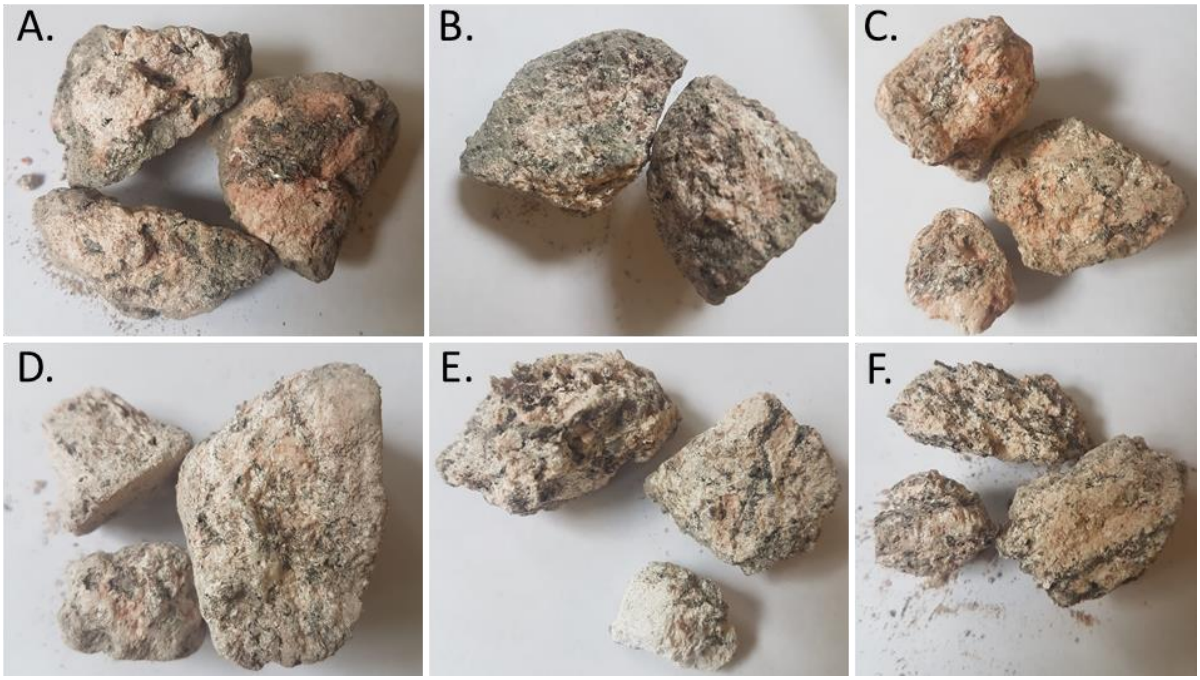


Figure 7.2. Photographs of drill core fragments of saprolite samples analysed from the following drill holes: A. SV15 (DDH0266; 20.1 m), B. SV7 (DDH0161; 26.9 m), C. SV11 (DDH0096; 29.8 m), D. SV12 (DDH0121; 21.0 m), E. SV9 (DDH0099; 23.0 m), F. SV13 (DDH0061; 30.5 m). Field of view for each photograph is 6 cm.



Figure 7.3. Photographs of clay-rich veinlet samples collected from the weathered profile in outcrop; left panel: S1; central panel: S3; and right panel: S5. The field of view for each photograph is ~ 5 cm.

7.2.2 Analytical methods

7.2.2.1 Bulk geochemical analysis

All samples, except S8 - S10 and the CSF samples, were sent to ALS (Australian Laboratory Services P/L) in Ireland. The clay vein samples (S8 to S10) were analysed at the NHM for bulk geochemical analysis.

In order to determine whether REE are preferentially concentrated in the clay size fraction, the distribution factor (DFx) was calculated by the following equation (Acosta et al. 2009):

$$\boldsymbol{DFx} = \boldsymbol{X}_{fraction} / \boldsymbol{X}_{bulk}$$

Where $X_{fraction}$ and X_{bulk} are the concentrations ($mgkg^{-1}$) of individual REE in a given particle size fraction, and in the bulk sample respectively. If $DFx > 1$ the element is interpreted to accumulate more in the clay size fraction.

7.2.2.2 Mineral identification and composition analysis

X-ray diffraction (XRD), scanning electron microscopy with energy dispersive spectrometer (SEM-EDS) and electron microprobe analyses were used to mineralogically characterize the saprolite and clay fracture infill samples in both the bulk and < 2 μm fractions. All samples selected were analysed by XRD and SEM. Only 6 bulk saprolite samples from drill holes DDH0161 were analysed by EMPA (Table 7.1).

Qualitative powder X-ray diffraction (XRD) analysis was performed to determine the main minerals present in the samples. The identification of clay minerals was of particular interest.

SEM micro-analysis was carried out in the Imaging and Analysis Centre (IAC) at the Natural History Museum, London, using two SEM instruments. The Zeiss EVO 15LS SEM was used for imaging and compositional analyses of minerals in carbon-coated polished blocks, and pressed CSF discs. The FEI-Quanta 650 FEG SEM was used for high-resolution backscattered (BSE) imaging and hyperspectral X-ray mapping of fine-grained minerals.

The compositions of REE-mineral grains in saprolite samples were determined using the Cameca SX-5 electron microprobe housed in the IAC at the NHM.

Ethylene glycol solvation was used to test for the presence of smectite minerals in XRD analysis. Details of the preparation, mechanism and analysis of this test are given in Chapter 4.

7.2.3 Mineral modal analysis

The low abundance and fine-grained nature of the REE minerals present in the saprolite samples prevented the use of quantitative XRD analysis or point counting methods for estimating mineral abundances. Similarly, normative mineral calculations, where estimates are made using the geochemical composition of a sample, could not be used for REE-rich minerals because the formula elements from these minerals also occur throughout minerals composing the bulk rock composition. For example, in the case of fluorcarbonates, the bulk F concentration is controlled by both biotite and fluorite, which are present in much higher abundances than fluorcarbonate, and the abundances of these minerals cannot be estimated reliably from other elemental concentrations.

The abundance of resistant and supergene REE minerals in saprolite samples were therefore calculated using a modal analysis method in which La, Y and Ce element concentration maps were produced for CSF samples using the FEI Quanta 650 FEG SEM at the Natural History Museum. These were then processed into La-, Ce- and Y-rich mineral maps used for calculating the abundance of REE minerals. Because the bulk samples have a grain size range over several orders of magnitude (micron to several millimetres), this method could only be applied to the CSF samples which have narrow grain size ranges, and therefore allow representative variations to be captured in the mapped areas.

Modal analysis using SEM analysis could be carried out because high concentrations of heavy REE means that REE minerals stand out clearly from other minerals, in both BSE images and element maps (Figure 7.5). In BSE images, REE minerals appear as the brightest grains, while in the Quanta element maps these grains exhibit the highest pixel intensities of the mineralogy.

Instrument and analytical conditions

X-ray element mapping of small areas (approximately 100 μm x 80 μm) of the carbon-coated surface of the CSF pressed samples were collected using a Bruker Flat Quad 5060F energy dispersive X-ray detector (EDS) under high vacuum conditions at 9 kV and ~ 24 mm working distance. The resolution of the resulting map was able to image individual grains in the range 90 nm and 150 nm. However, due to drift and other interactions, the resolution is expected to be slightly lower: in the order of ~0.5 micron radius and 0.9 micron depth for a pixel size of 90 nm. Each element map was imaged over 2 to 6 hours in order to collect sufficient X-ray counts.

Processing data

The raw element maps were processed using Esprit 1.9 Bruker analytical software and the modal abundance (volume %) and grain size distribution analysis were done using Image-J and QGIS v2.18 image processing software. A work-flow diagram showing how X-ray element maps were converted into mineral maps is presented in Figure 7.4. The main processing steps included:

1. Average 3x3 filter - to reduce the noise to signal ratio of the X-ray map and better distinguish the individual grains from the background composition;
2. Pixel intensity filter - only pixels with the highest intensity (255 value) and therefore only the strongest elemental X-ray signal that relate to the mineral of interest were passed;
3. Element overlap corrections - the X-ray energy level used to identify Ti and La are very close to each other and the signals of these elements can sometimes overlap causing misidentification because Ti-rich grains can appear as La-rich grains and vice versa. An element interference correction was therefore applied to the La map in order to remove any Ti grains that have been included;
4. Vectorisation of filtered and corrected La, Y and Ce maps - the raster image was converted to a vector image (polygons) to calculate grain size distributions and abundances;
5. Quantification of mineral abundances - the processed image vectors are used to quantify a minimum true coverage of only the high REE-concentration grains. The distribution of grain sizes was calculated from a grain size histogram
6. Validation - mineral maps of La-, Y- and Ce-rich grains were checked using a BSE image of the same area (e.g. see Figure 7.5).

Uncertainties of the modes have not been calculated. However, results are given confidence by verifying grains in element maps with BSE images and by running several maps per sample to make sure results were consistent. One key consideration is that grains that cover less than a pixel will not be picked up by this method, and because noise cannot be fully removed from the data, 1 pixel grains were excluded from mineral abundance calculations.

7.2.4 Calculating the proportion of REE in minerals

The REE grades in the saprolite horizon, which vary both vertically and laterally, will be controlled by the nature and abundance of REE mineral phases. Determining the proportion of REE held within these phases is useful for understanding the pathways that REE are taking in the weathering profile, the processes of enrichment, and the geometallurgical implications for clay leachability. This is achieved by integrating the REE composition and mineral abundance information of each REE mineral phase.

This calculation can be made for phosphates because all phosphates in the saprolite are associated with REE, and for fluorcarbonates which have measured abundances from the X-ray mineral maps. The following equation states the total REE as a sum of the REE fractions held in each mineral phase:

$$X_{total} = X_A + X_B \ldots + X_n$$

$$X_{total} = (M_A C_A) + (M_B C_B) \ldots + (M_n C_n)$$

$$X_{total} = (M_{Bast} C_{Bast}) + (M_{REEPO4} C_{REEPO4}) + \left(M_{remaider\ clay\ rich} C_{remainder\ clay\ rich}\right)$$

Where :

X_{total} = measured individual or total REE abundance in the bulk sample.
$X_{(A,B\ldots n)}$ = REE contribution by each phase, where the sample has *n* phases.
M = Mineral phase abundance in the sample.
X = REE concentration in mineral phase.

The REE residency for niobiates and zircons could not be estimated because the abundance of niobiates cannot be estimated from the Nb content of the bulk rock due to the incorporation of Nb in Ti-minerals, and a representative REE concentration in zircon was not measured.

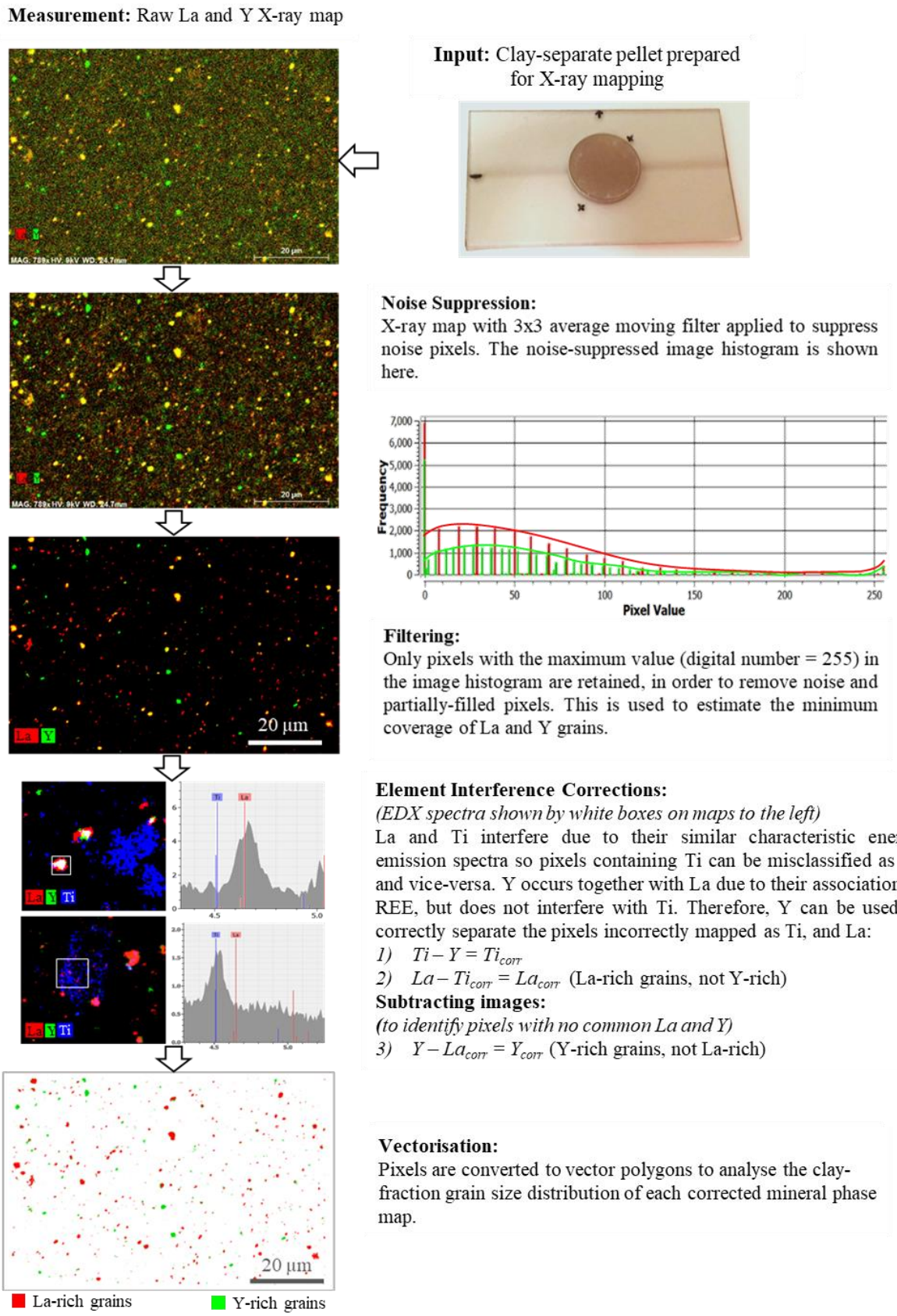


Figure 7.4. X-ray image processing workflow used for calculating modal abundance estimates, showing the steps for producing a mineral map. The histogram shows the number of pixels (frequency) images at each energy level, normalised to 256 levels. Note the small population at maximum energy which passed filtering.

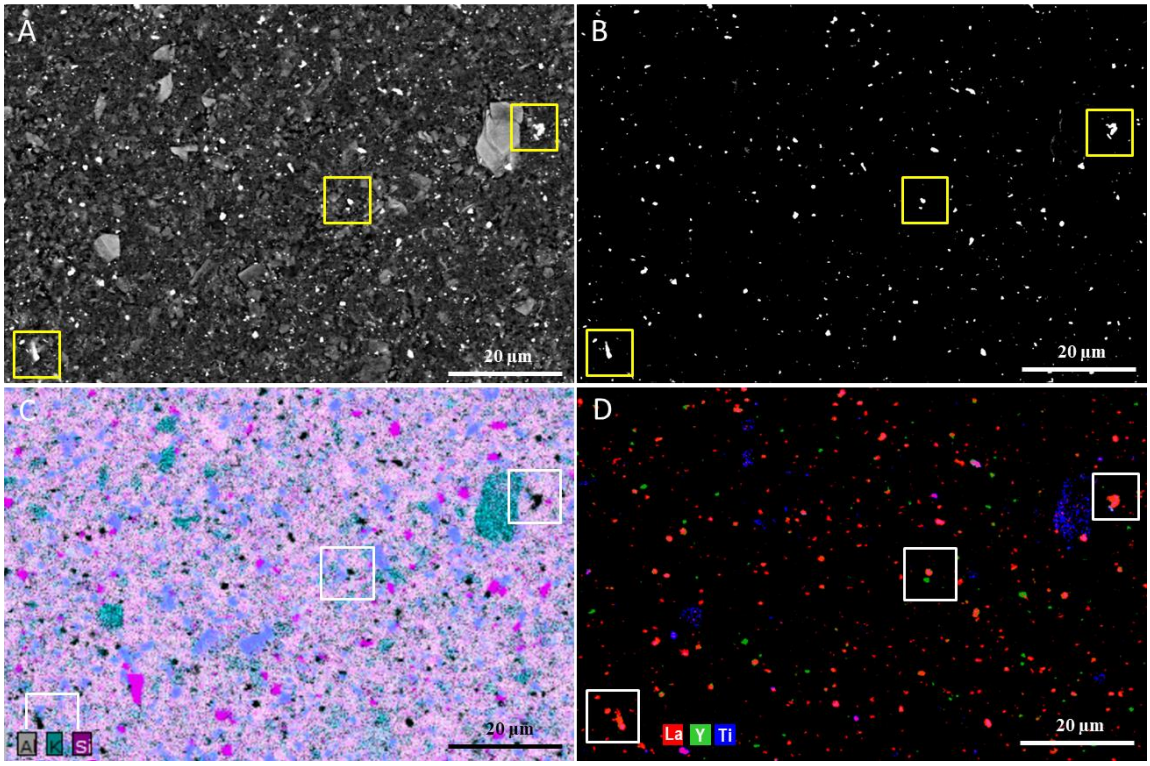


Figure 7.5. Four images of the same area of a CSF sample. A. BSE image B. BSE image with the filter applied highlighting the REE-minerals as bright spots. C. Validation map of Al, Si and K here showing that the bright grains in the BSE image are not aluminosilicates. D. High intensity pixel-filtered element map of La, Y and Ti as an RGB.

7.3 Geochemical Composition

7.3.1 REY-enriched saprolite samples

The chemical compositions of the bulk and CSF saprolite samples from the most REE-enriched sections of the six studied drill holes are presented in this section (Table 7.2, Table 7.3).

7.3.1.1 Bulk geochemical composition

The whole-rock geochemistry of the bulk saprolite samples is dominated by Si and Al; the SiO_2 content ranges from 66 to 72 wt %, and the Al_2O_3 content from 15 to 18 wt %. The samples can be divided into two groups based on their silica content: SV9, SV10, SV11 and SV13 with 66 – 69 wt % SiO_2, and SV7, SV12 and SV14 with 70 -72 wt % SiO_2.

The most abundant elements after Si and Al are Fe and K, but both are present in variable concentrations (2.5 - 7.72 wt % Fe_2O_3, and 2.77 - 6.72 wt % K_2O). Samples SV10 and SV14 contain the highest Fe_2O_3 concentrations at > 5 wt %, whereas SV9 has the lowest. Samples SV7, SV10 and SV14 have the highest K_2O concentrations, also > 5 wt %. In comparison, the average parent rock K_2O content is 5.6 wt % and Fe_2O_3 content is 3 wt %.

Table 7.2. Whole-rock chemical composition of studied saprolite samples.

		whole rock									
Sample #		**SV5**	**SV6**	**SV7**	**SV8**	**SV9**	**SV10**	**SV11**	**SV12**	**SV13**	**SV14***
drill core		161	161	161	161	99	96	96	121	61	266
depth		22.28	25.4	26.93	28.5	23.04	34.14	29.75	121.21	30.5	20.13
Major (%)	Det. Limit										
SiO_2	0.01	70.8	71.2	70.9	63.1	67.1	66.8	65.5	71.8	68.8	69.7
Al_2O_3	0.01	17.5	15.6	15.15	21.1	17.35	15.2	17.85	15.95	16.15	14.6
Fe_2O_3	0.01	3.73	3.2	2.99	1.9	2.5	7.72	4.84	3.37	3.96	5.23
CaO	0.01	0.01	0.01	0.04	0.08	0.08	0.06	<0.01	0.01	0.02	0.06
MgO	0.01	0.05	0.1	0.1	0.07	0.66	0.23	0.13	0.07	0.15	0.19
Na_2O	0.01	0.06	0.17	0.27	0.49	0.25	0.15	0.08	0.15	0.14	0.37
K_2O	0.01	2.57	5.54	6.72	6.64	4.5	5.72	2.77	4.33	4.31	5.19
TiO_2	0.01	0.31	0.27	0.25	0.15	0.2	0.75	0.46	0.28	0.35	0.39
MnO	0.01	0.04	0.09	0.05	0.04	0.05	0.1	0.05	0.05	0.08	0.08
P_2O_5	0.01	0.01	0.03	0.02	<0.01	0.02	0.09	0.05	0.02	0.09	0.03
SrO	0.01	<0.01	0.01	<0.01	<0.01	<0.01	0.01	<0.01	0.01	<0.01	0.01
BaO	0.01	0.01	0.02	0.02	0.02	0.02	0.07	0.03	0.01	0.03	0.04
LOI	0.01	6.2	4.26	3.65	5.49	8.04	4.32	6.87	4.9	4.98	3.14
Total		101.3	100.5	100.2	99.1	100.8	101.2	98.6	101.0	99.1	99.1
Trace (ppm)											
Rb	0.2	610	604	532	490	354	625	477	568	483	566
Ba	0.5	71.8	167.5	168	208	155.5	643	292	128	244	277
Sr		5.2	11.6	14.8	18.4	15.9	34.1	16.3	9.7	29.8	20.5
Cs	10	5.91	2.54	2.23	1.88	2.78	3.86	4.72	3.35	3.28	3.92
Zr	2	687	643	493	263	429	1420	886	630	599	1050
Hf	0.2	23.4	22	16.7	9	13.6	35.6	24.4	23	21.2	31.5
Ta	0.1	10.2	10	9	5.4	6.7	9.2	6.3	10.6	9.9	9.2
Nb	0.2	210	179.5	171.5	128	139	194	124	190.5	214	139.5
U	0.05	11.25	10.2	14.05	9.85	10.85	18.45	12.4	14.35	13.1	21.5
Th	0.05	90	91.2	80.3	31.4	69.7	146.5	96.2	91.6	79.3	165
Pb	2	61	182	67	69	41	32	33	49	47	
Ag	0.5	<0.5	<0.5	<0.5	<0.5	<0.5	39.4	33.1	<0.5	<0.5	
As	5	7	12	32	6	23	5	<5	<5	8	
Cu	1	6	5	3	14	12	70	55	20	13	3.92
Co	1	2	4	3	1	4	6	4	1	6	
Mo	1	1	1	3	<1	1	6	3	2	1	
Ni	1	7	14	34	7	28	16	14	8	8	
Sn	1	9	9	8	7	6	21	17	10	7	14
Zn	2	119	122	90	106	125	234	161	152	101	
Ga	0.1	47.6	48.5	48.9	56.1	46	46.3	45.4	47.3	48.4	55.1
Sc	1	2	1	1	1	1	10	6	2	4	
Li	10	30	40	40	20	30	30	30	20	30	
F	20	1270	1070	1740	720	2050	1340	710	720	1530	
REE (ppm)											
La	0.5	302	866	2840	185	2170	453	507	245	531	4860
Ce	0.5	488	1305	667	623	444	697	362	712	373	1805
Pr	0.03	67.7	191	599	31.8	402	93.1	103.5	55.7	94.3	874
Nd	0.1	224	564	1835	104	1300	297	331	178.5	300	2870
Sm	0.03	41.5	102	320	19.1	244	61.8	58.4	32.9	57.6	466
Eu	0.03	2.28	5.48	18	1.39	14.8	3.71	4.45	2.13	4.92	30.2
Gd	0.05	34.7	72	235	21.7	251	60.3	46.9	27.7	67.5	329
Tb	0.01	5.89	12.2	36.4	4.54	41.6	11.1	7.58	5.84	12.6	47.8
Dy	0.05	38.9	67.6	188	32.5	245	73.9	45.8	42.9	84.1	262
Ho	0.01	8.79	14.5	35.2	8.35	55.8	18.15	9.98	10.8	20.8	39.8
Er	0.03	26	41	86.5	25.7	151	53	28.2	34.3	64.6	99.8
Tm	0.01	3.9	5.68	10.95	3.95	20.2	7.76	4.24	5.38	9.5	12.25
Yb	0.03	25.4	37.6	66.1	26	127	48.4	27.4	38.6	64.5	78.9
Lu	0.01	3.57	5.06	8.67	3.74	17.6	7.17	4.05	5.5	8.74	8.62
Y	0.5	225	375	993	258	1655	558	276	268	615	1080
REE wt %		*0.127*	*0.329*	*0.695*	*0.109*	*0.548*	*0.189*	*0.154*	*0.140*	*0.169*	*1.178*
REEY wt %		*0.150*	*0.366*	*0.794*	*0.135*	*0.714*	*0.244*	*0.182*	*0.167*	*0.231*	*1.286*
LREE/HREE		7.65	11.87	9.42	7.62	5.03	5.74	7.85	7.17	4.09	12.42
La_N/Yb_N		8.07	15.65	29.19	4.83	11.61	6.36	12.57	4.31	5.59	29.81
La_N/Sm_N		4.54	5.30	5.54	6.05	5.55	4.58	5.42	4.65	5.76	6.51
Nd_N/Yb_N		3.10	5.29	9.78	1.41	3.61	2.16	4.26	1.63	1.63	12.81
Gd_N/Lu_N		1.20	1.76	3.35	0.71	1.76	1.03	1.43	0.62	0.96	4.72
$(Eu/Eu^*)_N$		0.18	0.19	0.20	0.21	0.18	0.19	0.26	0.22	0.24	0.24
$(Ce/Ce^*)_N$		0.83	0.78	0.12	1.97	0.12	0.82	0.38	1.47	0.40	0.21
Y_N/Ho_N		0.89	0.90	0.98	1.07	1.03	1.07	0.96	0.86	1.03	0.94

N = normalised using CI chondrite (McDonough & Sun 1995) * drill core assay data

Both Ca and Na are strongly depleted in all saprolite samples, with concentrations of < 0.1 wt % CaO and < 0.4 wt % Na_2O. Mg contents are also low (< 0.2 wt % MgO) but very close to parent rock values. The only exception is SV9, which has an elevated Mg value of 0.66 wt % MgO, equivalent to ten times the bedrock concentration.

Phosphate contents are low at < 0.1 wt % P_2O_5. The samples with the highest phosphate contents are SV10 and SV13 with concentrations of 0.09 wt % P_2O_5. All other samples have < 0.05 wt % P_2O_5 which is very close to the analytical detection limit.

The trace elements Ba, Rb and Cs are not depleted in the saprolite samples and instead have slightly higher concentration values compared to parent rock (see Chapter 5), ranging 354 – 625 ppm Rb, 128 – 648 ppm Ba, and 1.88 – 3.92 ppm Cs. In felsic igneous rocks, these large ion lithophile elements are typically concentrated in K-feldspar (Rhodes 1969).

Of the high field strength elements, Zr is the most abundant but concentrations vary widely from 429 to 1420 ppm. Samples from drill hole 96 are the most enriched with concentrations of > 800 ppm Zr. All other samples have Zr concentrations that fall between 430 to 630 ppm. Niobium concentrations range from 139 to 214 ppm. The radioactive elements Th and U, are present in low concentrations with values ranging from 70 to 146 ppm, and 9.9 to 14.3 ppm respectively. The ratio Th/U varies from 5.7 to 7.9. Nb contents are relatively consistent between samples with concentrations of 124 – 214 ppm.

The fluorine content of these saprolite samples was also analysed. Results show concentrations ranging from 710 to 2050 ppm, significantly lower than parent rock granite of ~4000 ppm F. Samples with the highest F contents include SV14 (1530 ppm), SV7 (1740 ppm), SV10 (2030 ppm), and SV9 (1340 ppm). The other samples have an average concentration of 710 ppm.

The total REY content in these enriched REE-enriched saprolite samples ranges widely from 0.17 wt % to 1.29 wt % REY. Samples can be divided into two groups: SV7, SV9 and SV14 with concentrations above 0.7 wt % and SV10, SV11, and SV12 with concentrations below 0.3 wt % REY. Chondrite-normalised patterns presented in Figure 7.6 show that the saprolite samples exhibit the same LREE-enriched patterns with negative Ce and Eu anomalies. All samples, except for SV12, have significant negative Ce anomalies (Ce/Ce* = 0.12 to 0.82). SV12 shows a positive Ce anomaly 1.47. Samples with higher REY contents have more pronounced negative Ce anomalies.

The degree of LREE/HREE fractionation varies widely between the samples. La_N/Yb_N ratios range from 4.13 to 29.19. The most fractionated patterns are from samples SV7 and SV14. The range of La_N/Sm_N values (4.5 – 6.51) is much narrower than the range of Gd_N/Lu_N (0.62 – 4.72), which indicates that the fractionation is mainly limited to the HREE. Samples with higher REY also have a higher Gd_N/Lu_N ratio.

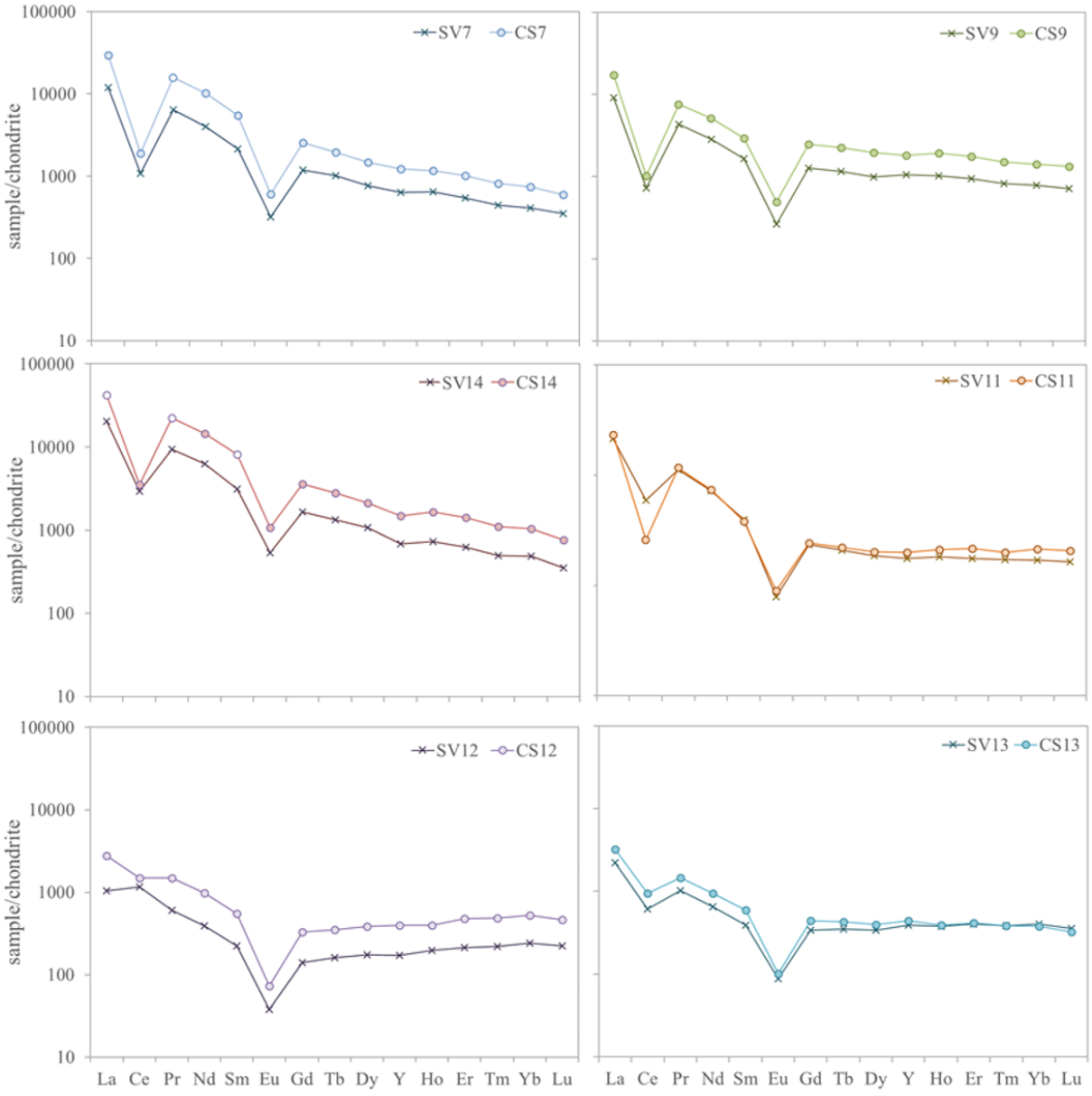


Figure 7.6. Chondrite-normalised REE distribution patterns showing the bulk and clay fraction saprolite sample compositions for each drill hole. DDH0161 (SV7, CS7); DDH0099 (SV9, CS9); DDH0266 (SV14, CS14); DDH0096 (SV11, CS11); DDH0121 (SV12, CS12); and DDH0061 (SV13, CS13). Some REE concentrations for samples CS7 and CS14 are above the analytical detection limit (points with white fills in left-side, upper two charts), and have therefore been calculated from regression to the neighbouring element concentrations in the same sample. Chondritic values are from McDonough & Sun (1995). Y is plotted as a pseudolanthanide with atomic mass intermediate between Dy and Ho.

7.3.1.2 Clay size fraction (CSF) composition

The compositions of the CSF samples are dominated by high SiO_2 and Al_2O_3. The geochemical results (Table 7.3) show that the SiO_2 content in the CSF is lower (41.8 – 46.0 wt %) while the Al_2O_3 content is higher (30.5- 35.2 wt % Al_2O_3) than the bulk geochemistry. The average molar Si/Al in CSF samples is 2.4 compared to 7.3 in the bulk samples. The low Si content is likely due to the removal of coarse quartz crystals observed in hand sample.

The element analysis show that CSF samples have lower concentrations of K_2O (0.7-2.5 wt %) and Na_2O (< 0.06 wt %) and higher CaO (0.02 - 0.16 wt %), MgO (0.12 -1.3 wt %), and Fe_2O_3 (2.38 - 11 wt %) concentrations than their respective bulk samples. The CSF also show significantly higher volatile contents with LOI values ranging from 12 to 17 wt %.

All CSF samples have low phosphate concentrations with values below 0.15 wt % P_2O_5. Compared to bulk samples, a few samples show higher phosphate concentrations such as CS12 (0.05 wt %), CS13 (0.13 wt %) and CS14 (0.14 wt %), while the rest maintain the same, or show slightly lower concentrations. Phosphate grains of different sizes were observed in bedrock by SEM analysis, which may explain why these grains are not preferentially represented by a single grain size fraction (see Chapter 5).

In terms of major element composition, CFS samples are very similar to each other. However, the SV9 sample stands out for its relatively elevated CaO, MgO and LOI values, and its lower Fe_2O_3 and K_2O contents.

The most notable difference in trace element composition between the CFS and bulk saprolite samples is the Zr content; element analysis show that CFS samples have < 110 ppm Zr compared to higher Zr (consistently above 200 ppm) observed in the bulk saprolite. This suggests that zircon, which is the main mineral host of Zr, is preferentially retained in grain size fractions > 2 μm. Other trace elements that have lower concentrations in CFS are Ba and Rb. Lower concentrations in these two elements may be explained by a large fraction of feldspar content in the bulk sample being retained in the coarse separate. Nb, Th, and U are instead preferentially concentrated in the CFS with concentrations ranging between 100 – 500 ppm, 140 – 400 ppm, and 13 - 66 ppm respectively.

The total REE concentration of the CSF samples ranges widely from 0.14 to 2.64 wt % REY. With the exception of two samples, the CSF samples have higher REE contents than the bulk saprolite with DF_{REE} index values ranging from 1.33 to 2.05. The two CFS samples with lower

REE concentrations are CS10 and CS11 which come from the same drill core, DDH0096. The samples with the highest DF_{REE} index values are CS7, CS12 and CS14 (see Table 7.4).

The chondrite-normalised REE patterns presented in Figure 7.6 show that CSF share broadly the same REE patterns as their respective bulk samples. However, the CFS REE patterns have more strongly pronounced negative Ce anomalies and are overall slightly more LREE/HREE fractionated. Samples CS7 and CS14 show the greatest difference with La_N/Yb_N values of 40 compared to 29 in bulk samples. All other La_N/Yb_N values remain below 15 and are only 1 – 3 higher than the bulk sample.

The fractionation of individual REE between fine clay size fraction and coarser size fractions in the saprolite samples can be observed in Figure 7.7. The DFx for individual REE shows that: 1) Ce is the REE element which partitions the least into the CSF and in the case of samples from DDH0096 it is preferentially held in coarser fraction. 2) Preferential accumulation of LREE vs HREE is variable between samples. For saprolite samples from drill holes 161, 266 and 121, the LREE partition more strongly into the CSF with DF_{La} of ~2.5 vs DF_{Yb} of ~ 2.0X. In contrast, REE in the CSF from saprolite samples from DDH0099 and DDH0096 are instead not fractionated, or hold HREE preferentially. Finally, it should be noted that in CSF samples where LREE are preferentially accumulated Eu has a lower DF_X.

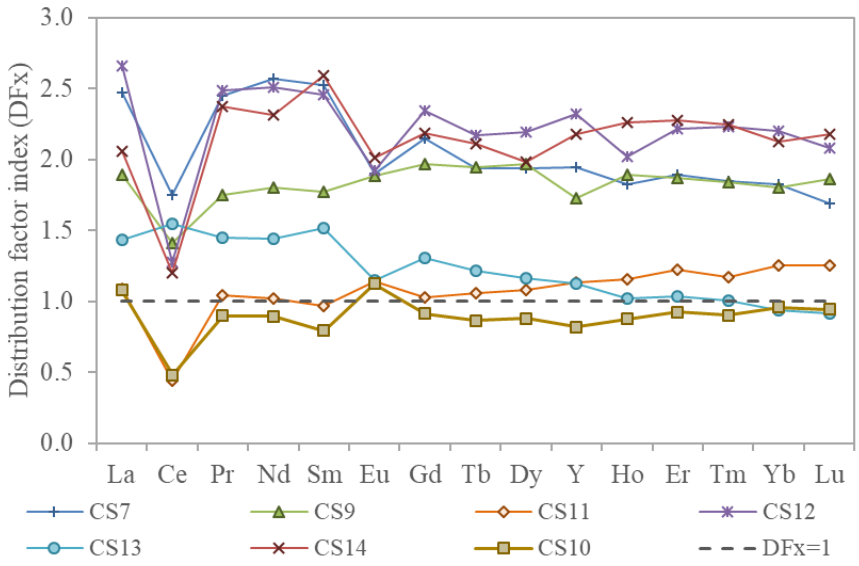


Figure 7.7. Distribution factor index (DFx) for individual REE in clay size fraction of saprolite samples relative to the bulk saprolite from different drill holes. (DFx) = $X_{fraction}$ / X_{bulk} , where X is the concentration of a given element. Note Y is plotted as a pseudolanthanide with atomic mass intermediate between Dy and Ho.

7.3.2 Internal variation in the saprolite

Four samples along the saprolite and transition zone horizons from DDH0161 were analysed in order to study the chemical variations within these horizons (Table 7.3).

7.3.2.1 Bulk geochemical composition

SV8, collected from the lower saprolite, has a bulk elemental composition which resembles that of a pegmatite and is therefore excluded from the sample comparison. The paragraphs below mainly discuss samples SV5, SV6 and SV7 which represent the transition zone, the upper saprolite and the middle to lower saprolite of DDH0161.

The bulk composition does not vary significantly between SV5, SV6 and SV7 does not change significantly. The main compositional differences observed are an overall decrease in the alkali and alkaline element content, a small increase of < 1 wt % for Fe_2O_3, Al_2O_3 and TiO_2, and thirdly, an increase in the volatile content from 3.65 wt % to 6.2 wt%. SiO_2 remains constant. Of the trace elements analysed, Nb, Zr and Th all show elevated concentrations relative to the parent bedrock.

REE concentrations show a greater degree of variability between these three samples. The total REY content decreases linearly with distance from 0.79 wt % in SV7, to 0.37 wt % in SV6, and to 0.15 wt % in SV5. All three samples have similar LREE-enriched chondrite-normalised patterns with negative Eu anomaly similar to the parent rock. However, the degree of LREE/HREE and Ce fractionation varies between samples. SV7 is the most fractionated sample followed by SV6 and SV5 with La_N/Yb_N ratios decreasing from 29.19 to 8.07 and Ce/Ce* increasing from 0.012 to 0.83.

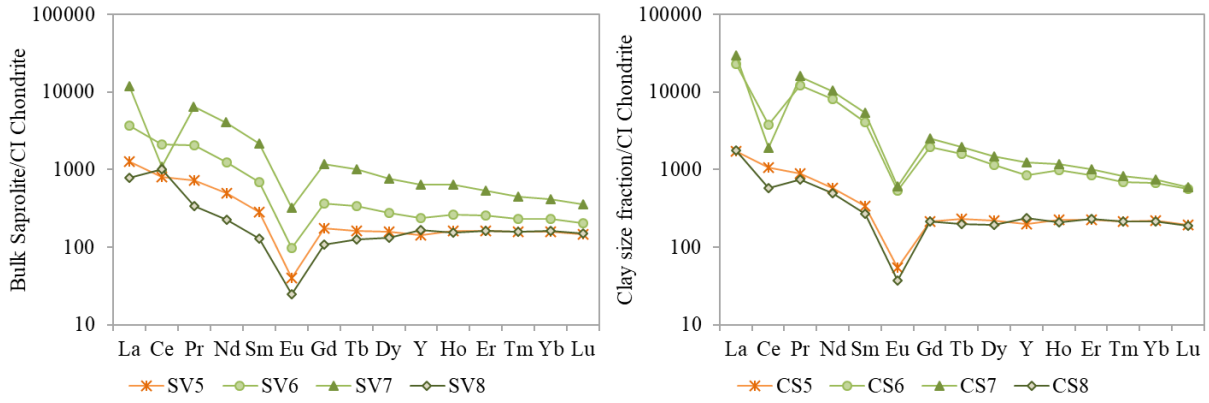


Figure 7.8. Chondrite-normalised REE distribution patterns Bulk (left) and clay size fraction (right) saprolite and transition zone samples from DDH0161. Note Y is plotted as a pseudolanthanide with atomic mass intermediate between Dy and Ho.

7.3.2.2 Clay size fraction composition

Similar to the CSF of the enriched saprolite samples described previously, all four CSF from DDH0161 have lower SiO_2, K_2O, and Na_2O contents but higher Al_2O_3, Fe_2O_3, MgO, CaO and volatile (LOI) contents compared to the bulk saprolite. Although the phosphate content also remains low in all samples, a noticeable increase is observed in the upper saprolite with up to 0.14 wt % P_2O_5 in the CSF (CS6). All other CSF samples from DDH0161 have concentrations < 0.02 wt % P_2O_5. Trace element results show that the CSF samples from DDH0161 have higher concentrations of Th, U, Nb and lower concentrations of Zr, Ba, Rb than the bulk saprolite.

REE concentrations in the CSF of DDH0161 range from 0.2 to 1.9 wt %, higher than their respective bulk samples, with DF_{REE} index values of 1.20 to 4.28. In contrast to the bulk samples, REE concentrations in CSF samples decrease from the middle saprolite towards the transition zone. However, both the upper and lower saprolite CFS samples are strongly REE-enriched (1.58 wt % and 1.89 wt % respectively) and have much more similar REE compositions to the bulk saprolite. The chondrite-normalised patterns (Figure 7.8) show the differences between bulk and CSF; the patterns for SV7 and SV6 show that these samples have similar degrees of enrichment, large negative Ce anomalies and the same degree of LREE/HREE fractionation (La_N/Yb_N = 34 in SV7 vs. La_N/Yb_N = 39 in SV6).

DF_{REE} index values (Figure 7.9) indicate that REE, and particularly LREE, in the upper saprolite of DDH0161 are more strongly accumulated in the CSF than in the lower saprolite (4.28 vs 2.33 DF_{REE}).

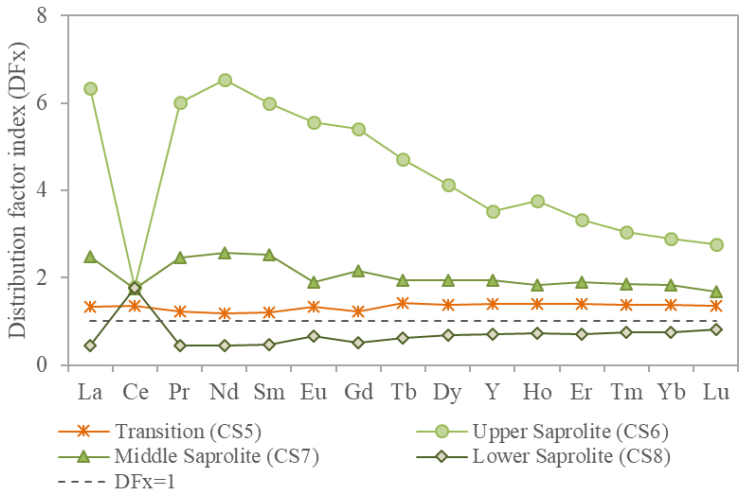


Figure 7.9. Distribution factor index (DFx) values for individual REE in the clay size fraction of transition zone and saprolite horizon samples from DDH0161. Note Y is plotted as a pseudolanthanide with atomic mass intermediate between Dy and Ho.

Table 7.3. Major and trace element concentrations in the < 2 μm size fractions (CSF) of the saprolite samples studied. Analytical methods include ICP-AES and ICP-MS analysis (see Chapter 4 for details).

		< 2 micron fraction									
Sample #		**CS5**	**CS6**	**CS7**	**CS8**	**CS9**	**CS10**	**CS11**	**CS12**	**CS13**	**CS14**
Drillcore		161	161	161	161	99	96	96	121	61	266
Depth		22.28	25.4	26.93	28.5	23.04	34.14	29.75	121.21	30.5	20.13
Major (%)	Det. limit										
SiO_2	0.01	45	46.1	46	46.8	48.6	41.8	42.7	44.3	43.5	44.6
Al_2O_3	0.01	34.2	31.5	30.5	34.7	29.3	29.8	33.5	33.5	35.2	32.1
Fe_2O_3	0.01	4.34	4.18	5.05	1.87	2.38	11.15	6.6	6.81	4.24	4.6
CaO	0.01	0.01	0.08	0.1	0.11	0.16	0.12	0.02	0.03	0.05	0.1
MgO	0.01	0.06	0.3	0.25	0.14	1.29	0.3	0.17	0.14	0.12	0.18
Na_2O	0.01	0.01	0.02	0.06	0.04	0.05	0.02	0.01	0.02	<0.01	0.04
K_2O	0.01	0.79	1.25	2.36	1.02	0.77	2	1.4	2.03	0.87	1.54
TiO_2	0.01	0.25	0.24	0.34	0.11	0.16	0.77	0.57	0.52	0.27	0.32
MnO	0.01	0.04	0.05	0.07	0.02	0.04	0.1	0.06	0.09	0.04	0.03
P_2O_5	0.01	0.02	0.14	0.02	0.01	0.03	0.04	0.03	0.05	0.13	0.07
SrO	0.01	<0.01	0.01	<0.01	<0.01	<0.01	<0.01	<0.01	<0.01	<0.01	0.01
BaO	0.01	0.01	0.01	0.01	0.01	0.01	0.04	0.02	0.01	0.01	0.01
LOI	0.01	13.95	14.35	13	14.35	16.85	12.3	13.2	12.6	14.8	14.65
Total		*98.68*	*98.23*	*97.76*	*99.18*	*99.65*	*98.44*	*98.28*	*100.1*	*99.23*	*98.25*
Trace (ppm)											
Rb	0.2	435	468	528	168.5	106.5	487	472	841	219	286
Ba	0.5	46.9	65.2	127	58.5	69.6	286	156.5	120.5	60.7	106
Sr	0.1	2.5	9.5	9	6.3	11	11.8	6	3.9	18	7.8
Cs	10	4.51	2.37	2.84	0.93	1.61	3.73	5.76	6.41	2.12	2.43
Zr	2	63	151	74	23	71	32	27	42	87	111
Hf	0.2	2.4	5.9	2.4	1	2.5	1.5	1	1.9	3.2	4.1
Ta	0.1	8.9	13.2	11.5	5.5	7.7	7.3	6	24	14.8	8.4
Nb	0.2	280	305	317	151.5	154	173.5	140	400	376	176.5
U	0.05	12.6	28	37.1	25.2	17.75	14.2	13.05	30.3	13.9	66.3
Th	0.05	159.5	391	179	49.4	106	198	125	228	101.5	500
Ga	0.1	89.3	94.6	107	86.5	60.5	69.1	71.8	90.9	89.9	99.5
Sn	1	10	13	15	6	5	30	20	21	6	11
REE (ppm)											
La_2O_3	0.5	404	5480	7020	416	4110	489	551	652	761	>10000
Ce_2O_3	0.5	658	2320	1165	354	627	334	159	911	578	2170
Pr_2O_3	0.03	83	1148	1470	70	702	84	108	139	137	>1000
Nd_2O_3	0.1	265	>1000	>1000	228	2340	266	338	448	432	6640
Sm_2O_3	0.03	49.9	612	808	40.3	432	49	56.7	80.9	87.3	>1000
Eu_2O_3	0.03	3.04	30.40	34.20	2.11	27.90	4.17	5.08	4.10	5.65	60.80
Gd_2O_3	0.05	42.5	389.0	505.0	42.5	494.0		48.2	65.0	88.3	720.0
Tb_2O_3	0.01	8.31	57.4	70.6	7.26	80.9	9.56	8.02	12.7	15.35	101
Dy_2O_3	0.05	53.5	279	365	48.2	483	65.1	49.5	94.1	97.7	520
Ho_2O_3	0.01	12.35	54.4	64.2	11.4	105.5	15.9	11.5	21.8	21.3	89.9
Er_2O_3	0.03	36.5	136.5	163.5	36.9	282	49	34.5	76.1	66.8	227
Tm_2O_3	0.01	5.4	17.3	20.2	5.3	37.1	7.0	5.0	12.0	9.5	27.5
Yb_2O_3	0.03	35.2	108.5	120.5	34.5	229	46.3	34.3	85.1	60.5	168
Lu_2O_3	0.01	4.8	14.0	14.7	4.7	32.8	6.8	5.1	11.5	8.0	18.8
Y_2O_3	0.5	315	1320	1935	369	2860	457	312	622	692	2350
REE wt %		*0.166*	*1.43**	*1.65**	*0.130*	*0.998*	*0.143*	*0.141*	*0.261*	*0.237*	*2.40**
REY wt %		*0.198*	*1.57**	*1.85**	*0.167*	*1.284*	*0.188*	*0.173*	*0.323*	*0.306*	*2.64**
LREE/HREE		7.37	*12.57**	*11.5**	5.82	4.72	6.14	6.21	5.91	5.44	11.83*
$DF_{(REY)}$ [1]		*1.32*	*4.28*	*2.33*	*1.24*	*1.80*	*0.79*	*0.95*	*1.94*	*1.33*	*2.05*
La_N/Yb_N		*7.80*	*34.31*	*39.58*	*8.19*	*12.19*	*7.17*	*10.91*	*5.20*	*8.54*	*40.44*
La_N/Sm_N		*5.06*	*5.59*	*5.43*	*6.45*	*5.94*	*6.23*	*6.07*	*5.03*	*5.44*	*5.17**
Nd_N/Yb_N		*2.65*	*11.95*	*13.77*	*2.33*	*3.60*	*2.02*	*3.47*	*1.85*	*2.52*	*13.92*
Gd_N/Lu_N		*1.10*	*3.43*	*4.26*	*1.13*	*1.86*	*1.00*	*1.17*	*0.70*	*1.36*	*4.73*
$(Eu/Eu^*)_N$		*0.20*	*0.19*	*0.16*	*0.16*	*0.18*	*0.24*	*0.30*	*0.17*	*0.20*	*0.20*
$(Ce/Ce^*)_N$		*0.87*	*0.22*	*0.09*	*0.50*	*0.09*	*0.40*	*0.16*	*0.73*	*0.43*	*0.12*
Y_N/Ho_N		*0.89*	*0.84*	*1.05*	*1.13*	*0.94*	*1.00*	*0.94*	*0.99*	*1.13*	*0.91*

N = normalised using CI chondrite. *Value used for La, Sm or Nd calculated using regression from adjacent REE elements.
1. Distribution Factor index for REY in clay fraction

Table 7.4. Major and trace element composition of clay-rich fracture-filling material collected from mottled zone, saprolite and bedrock.

		Clay rich fracture infill					
		S1[1].	S8[2].	S3[1].	S9[2].	S5[1].	S10[1].
		MZ	MZ	SAP	SAP	SAP	DDH0099_BDRK
Size Fraction		< 53 µm	< 100 µm	< 53 µm	< 100 µm	< 53 µm	< 100 µm
Major (%)	Det. Limit						
SiO_2	0.01	39.8	47.3	45.8	48.7	52	58.5
Al_2O_3	0.01	37.7	38.6	33.4	35.8	29.7	18.1
Fe_2O_3	0.01	0.59	0.14	0.3	1.20	0.87	1.81
CaO	0.01	0.01	<dt	0.02	<dt	0.03	1.04
MgO	0.01	0.7	0.24	0.69	0.46	0.6	2.0
Na_2O	0.01	<0.01	<dt	<0.01	<dt	0.02	0.26
K_2O	0.01	0.06	0.18	0.05	0.30	0.73	1.11
TiO_2	0.01	0.04	<dt	0.01	0.14	0.06	0.12
MnO	0.01	<0.01	<dt	<0.01	0.01	0.01	0.02
P_2O_5	0.01	0.02	<dt	0.21	0.17	0.04	<0.01
SrO	0.01	<0.01	n.a	0.01	n.a	<0.01	<0.01
BaO	0.01	<0.01	n.a	<0.01	n.a	<0.01	0.01
LOI	0.01	20.1	n.a	19.6	n.a	15.05	16.75
Total		99.0	86.8	100.1	87.9	99.1	99.6
Trace (ppm)							
Rb	0.2	16.3	n.a.	12.9	n.a.	71.5	115
Ba	0.5	11.8	3.42	17.3	21.8	41.2	120
Sr	0.1	0.9	< dt	4.5	4.67	4.7	28.5
Cs	10	0.33	n.a.	0.25	n.a.	0.99	1.76
Zr	2	57	< dt	32	104	155	235
Hf	0.2	2	n.a.	1	n.a.	5.2	7.5
Ta	0.1	0.7	n.a.	0.2	n.a.	4	3.8
Nb	0.2	25.6	n.a.	9.6	n.a.	46.3	98.8
U	0.05	14.4	4.58	17.1	30.5	8.06	36
Th	0.05	75.6	1.96	88.9	188	82	27.5
Sn	0.1	2	n.a.	1	n.a.	5	4
Ga	1	51.4	n.a.	49.2	n.a.	42.2	67.8
REE (ppm)							
La_2O_3	0.5	1500	1792	5270	3987	3470	2290
Ce_2O_3	0.5	1065	25.4	1605	1419	344	178
Pr_2O_3	0.03	269	308	950	738	612	336
Nd_2O_3	0.1	819	967	2800	2272	1920	1220
Sm_2O_3	0.03	118	143	436	346	293	244
Eu_2O_3	0.03	6.59	9.31	20.7	20	20.9	14.1
Gd_2O_3	0.05	98.3	108	319	237	233	389
Tb_2O_3	0.01	14.7	15.1	44.1	33	31.4	66.7
Dy_2O_3	0.05	89.3	91.2	256	187	188	458
Ho_2O_3	0.01	21.6	19.1	52.7	37	38.3	115
Er_2O_3	0.03	67.4	57.4	158.5	108	112	362
Tm_2O_3	0.01	9.26	8.21	20.5	15	15.2	48.9
Yb_2O_3	0.03	57.2	47.9	125	92	92.8	303
Lu_2O_3	0.01	7.84	6.33	17.1	12	14.2	43.0
Y_2O_3	0.5	723	613	1885	1147	1325	4040
ΣREE wt %		*0.41*	*0.36*	*1.21*	*0.95*	*0.74*	*0.61*
ΣREY wt %		*0.49*	*0.42*	*1.40*	*1.07*	*0.87*	*1.01*
La_N/Yb_N		17.8	29.5	25.4	25.4	28.6	5.13
La_N/Sm_N		7.94	7.20	7.85	7.40	7.55	5.86
Nd_N/Yb_N		5.04	8.72	7.11	7.29	7.89	1.42
Gd_N/Lu_N		1.55	2.50	2.11	2.04	2.31	1.12
$(Eu/Eu^*)_N$		0.19	0.21	0.23	0.24	0.17	0.14
$(Ce/Ce^*)_N$		0.41	0.20	0.01	0.06	0.17	0.05
Y_N/Ho_N		1.16	1.07	1.12	1.20	1.24	1.23

N = normalised using CI Chondrite (McDonough & Sun 1995)

1. Samples analysed by ALS. 2. Samples analysed at NHM.

7.3.3 Clay-rich fracture-fill samples

The clay-rich material infilling fractures in different horizons (see Chapter 6) is composed primarily of SiO_2 (39.8 – 58.5 wt %), Al_2O_3 (18.1 – 38.6 wt %) and volatiles (16.8 – 20 wt % LOI; see Table 7.4). The results also show that samples collected from fractures in the mottled zone (S1 and S8) and the saprolite horizon (S3, S5 and S9) are strongly depleted in Fe_2O_3 (0.14 – 1.2 wt %), CaO (<0.03 wt %), Na_2O (<0.02 wt %), and K_2O (<0.73 wt %). The sample collected from drill core DDH0099 (S10) also contains low concentrations of K_2O (1.11 wt %), Fe_2O_3 (1.81 wt %) and Na_2O (0.26 wt %) but has relatively high CaO (1 wt %).

The MgO content of fracture infill samples ranges from 0.24 to 2 wt %. These values are much higher compared to the average composition of the host horizons that the fractures are found in, suggesting mobility and enrichment of Mg in these domains. The phosphate content however, is low and variable between samples. Samples with the lowest concentrations are S1 and S10 with < 0.02 wt % P_2O_5. Samples with the highest P_2O_5 are S3 and S9 with 0.21 wt % and 0.17 wt % respectively.

One of the main geochemical feature of these clay-rich fracture infill samples is their high REE content which ranges from 0.4 to 1.4 wt % REY. The samples with the highest REE concentrations are those collected from fractures in the saprolite horizon. All three samples have values > 0.87 wt % REY.

Chondrite-normalised REE distribution pattern show that the REE composition of the clay-rich fracture infill samples is very similar to that of the REE-enriched saprolite samples described in section 7.3.1 (Figure 7.10). They are all LREE enriched, display strong negative Ce anomalies and have negative Eu anomalies.

LREE/HREE fractionation in the mottled zone and saprolite fracture samples is high, with La_N/Yb_N values ranging from 17.8 to 29.5. Sample S10 which was collected from the saprock, exhibits a much lower degree of LREE/HREE fractionation with La_N/Yb_N = 5.13. The strongest fractionation is in the LREE, which show a steeply inclined trend (Figure 7.10) and have La_N/Sm_N values of 5.89 to 7.94. The HREE display instead a relatively flat trend with Gd_N/Lu_N values of 1.12 – 2.31. The negative Ce anomaly is also strongly pronounced with values up to 0.4.

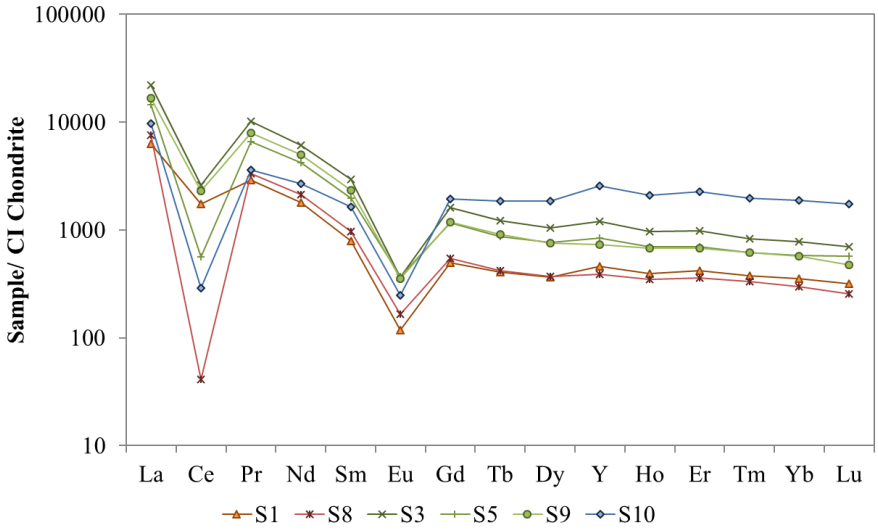


Figure 7.10. Chondrite-normalised REE distribution patterns of clay-rich fracture infill samples collected from the mottled zone (S1, S8), saprolite (S3, S5 & S9) and saprock (S10) horizons. Note Y is plotted as a pseudolanthanide with atomic mass intermediate between Dy and Ho.

7.4 Bulk Mineralogy

7.4.1 REY-enriched saprolite samples

XRD analyses show that the REE-enriched saprolite samples each have similar XRD patterns with bulk mineral compositions dominated by quartz, K-feldspar, biotite and kaolinite (Figure 7.12). The XRD pattern of sample SV9 has two additional broad but well-defined peaks at 15 Å (6.8 *2θ*) and 5 Å (20.*6 θ*), which are not observed in the patterns of the other samples. These two peaks, particularly the low angle peak at 15 Å (6.8θ), suggest smectite clay minerals are also an important constituent. A glycol test was carried out to confirm the presence of swelling clays; in this test, a diffraction peak was observed at 1.5 Å (73.2 *2θ*) indicating that the smectite clay mineral in SV9 is montmorillonite (Figure 7.11).

Although the mineral compositions are comparable, there are differences in the intensity and shape of the powder diffraction peaks, indicating variations in mineral crystallinity and abundance. Overall, the XRD patterns can be divided into three groups. In group 1, which includes SV14, SV7 and SV12, the XRD patterns have well-defined biotite and K-feldspar peaks while the kaolinite peaks appear relatively broad. In this group kaolinite peak 7.18 Å (14.3 *2θ*) is less intense than the biotite peak. In group 2, which includes SV11 and SV13, the XRD patterns show the opposite relationship; the kaolinite peaks are very intense and narrow while the biotite peak is broad, not well-defined and has much lower counts. In this group, only low intensity peaks of K-feldspar are measured. Finally, group 3 (SV9 only), contains smectite

as the primary constituent of the sample and the intensities of the biotite 10 Å (10.2 *2θ*), kaolinite7.18 Å (14.3 *2θ*) and smectite 15 Å (6.8 *2θ*) peaks are similar.

X-ray analyses of the CSF samples were also carried out to determine the mineralogy of fine fraction saprolite samples. The results show that the CSF samples have similar mineralogy to the bulk samples but in different proportions. In the CSF, kaolinite has by far the most intense diffraction peaks (Figure 7.12) and is therefore considered to be the dominant mineral. K-feldspar, quartz and biotite are also present but have peak intensities that are much lower compared to the bulk sample.

CS9 is not the only sample with smectite present; XRD patterns of CS14 and CS7 show very broad low intensity peaks at around 15 Å (6.8 *2θ*), which glycol tests confirm is caused by smectite (Figure 7.11). Although the analysis does not allow an estimate of the proportion present, the fact that smectites are only detectable in the CSF, itself a concentrate of the fine-grained minerals, means that the smectite content of CS14 and CS7 is much lower than in CS9.

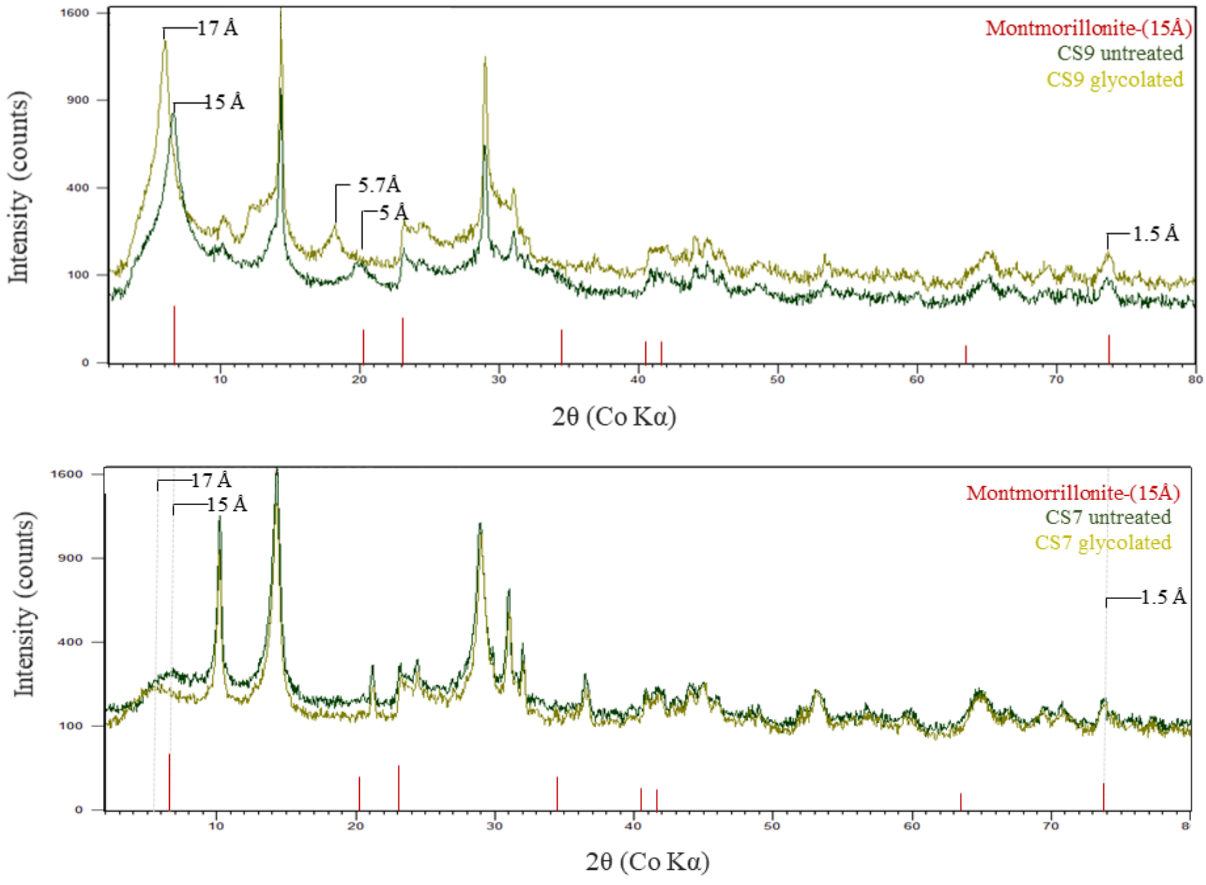


Figure 7.11. X-ray diffraction patterns of randomly-oriented, air-dried sample (dark green) and glycol-impregnated (pale green) of samples CS9 (above) and CS7 (below). Both treated and untreated samples were run for 1 hour under the same conditions. A red stick pattern for montmorillonite (15 Å) is also shown for reference.

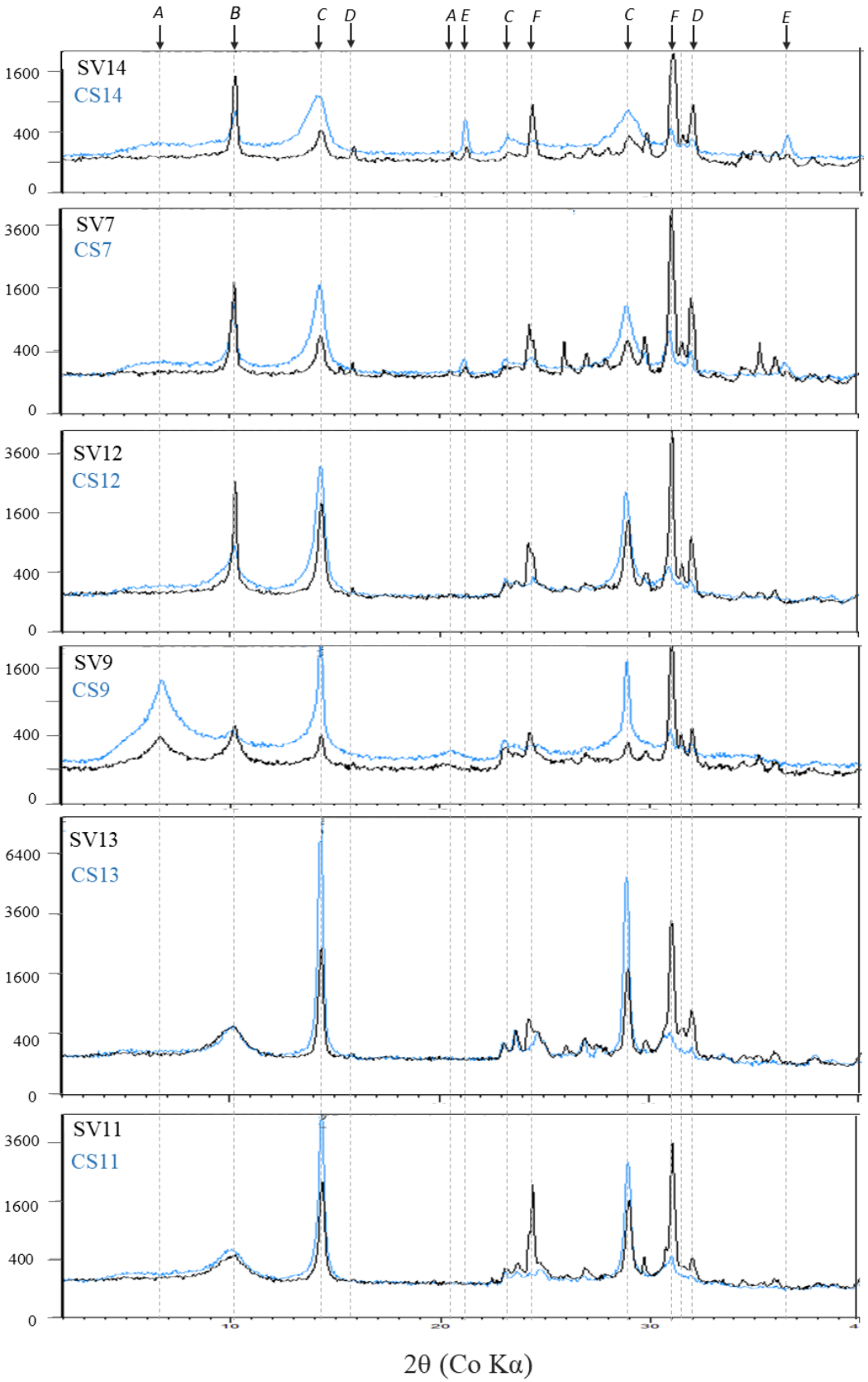


Figure 7.12. X-ray diffraction patterns of randomly-oriented bulk (black) and CSF (blue) samples from REE-enriched saprolite from six drill cores. All samples run for 1 hour.

The XRD patterns of CS14 and CS7 have peaks at 4.9 Å (21.1 *2θ*) 2.89 Å (36.5 *2θ*) and 1.99 Å (53.42 *2θ*) which do not correspond with any primary rock minerals or their breakdown products. A mineral search in the ICDD mineral database suggests the best match for the unknown phase is a REE carbonate, either bastnäsite or hydroxyl-bastnäsite (see Figure 7.13). These peaks are not observed in the other CSF samples and are not intense enough to stand out from the background in the equivalent bulk samples SV14 and SV7.

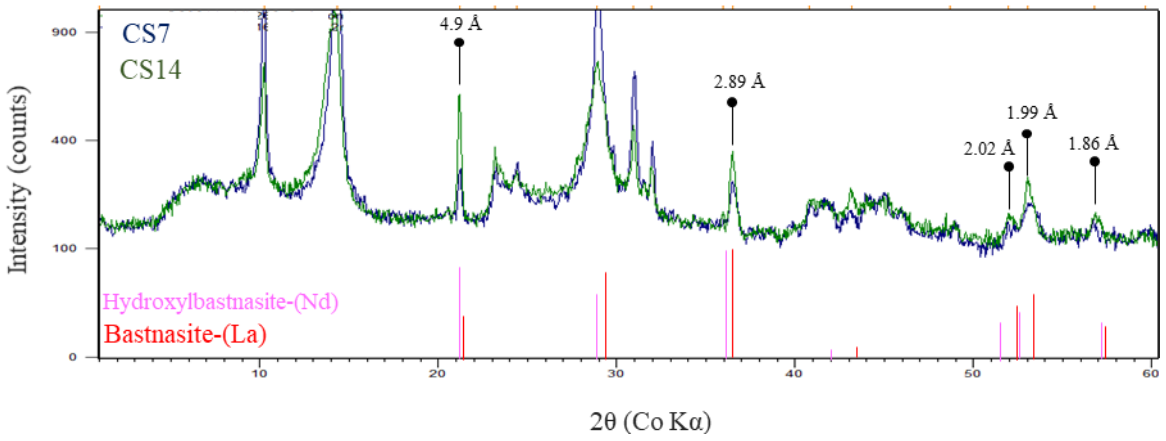


Figure 7.13. XRD patterns in the 2 – 70° (2θ) response for CSF samples CS7 and CS14 from DDH0266 and DDH0161. Stick patterns show that sample peaks correspond to bastnäsite and hydroxyl bastnäsite species.

7.4.2 Saprolite sub-horizon variation (DDH0161)

XRD patterns of samples taken along the saprolite horizon in DDH0161 show that the bulk mineral composition within this zone remains approximately consistent. All four XRD patterns reveal that the principal minerals in the saprolite are kaolinite, biotite, K-feldspar and quartz (Figure 7.14). Samples from the transition zone and from the base of the mottled above show that the only observable changes up the profile are a gradual increase in the intensity and definition of the kaolinite peaks and a decrease in the intensity and sharpness of the biotite and K-feldspar diffraction peaks until they are no longer present. This trend shows that the breakdown of biotite and K-feldspar occurs mainly in the transition zone.

The XRD patterns of CSF samples from DDH0161 confirm that kaolinite is the dominant clay mineral (Figure 7.15). However, some smectite is also present in the saprolite. Both upper and lower saprolite samples show a broad and very low intensity peak at 15 Å (6.8 *2θ*) and interference peak at 1.5 Å (73.2 *2θ*), characteristic of montmorillonite (Figure 7.11). No smectite was detectable in samples from the transition zone or the base of the mottled zone.

The XRD patterns also reveal the occurrence of REE-fluorcarbonates in both the upper and lower saprolite samples in this drill core.

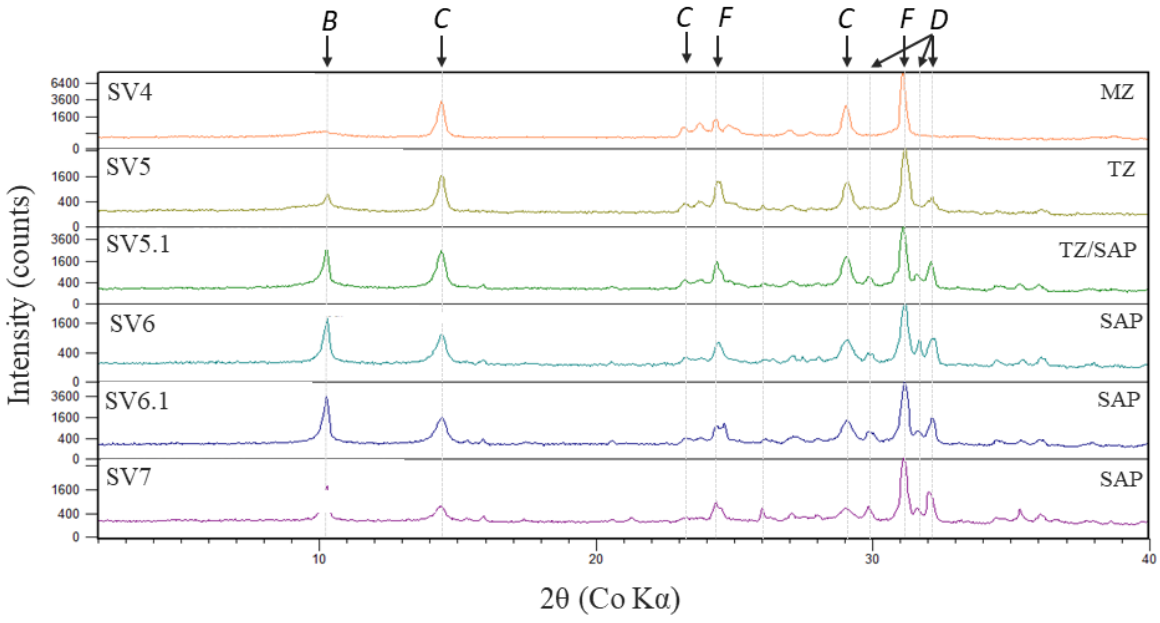


Figure 7.14. XRD patterns of bulk samples collected along the saprolite horizon (SV6, SV6.1 and SV7), transition zone (SV5 and SV5.1) and base of the mottled zone (SV4) from drill core DDH0161. Diagnostic peak positions are marked with dashed lines and arrows. Note that no smectite or bastnäsite peaks were detected in this sample.

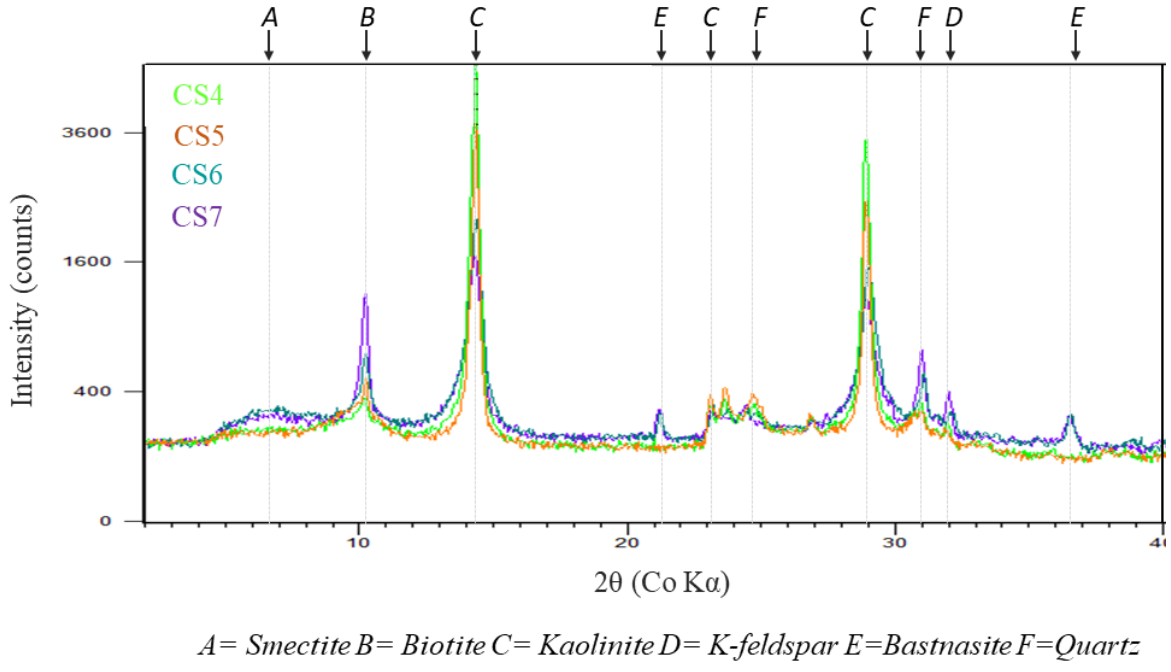


Figure 7.15. Stacked XRD patterns of CSF samples from the transition zone and saprolite horizon of DDH0161.

7.4.3 Clay-rich fracture-infill samples

The clay-rich, fracture-infill samples collected from an exposed section of the weathered profile all have very similar X-ray diffraction patterns (Figure 7.16). They are composed of mainly kaolin clays and some smectite and quartz. It is unclear from the XRD patterns whether the kaolin clay is kaolinite or meta-halloysite (de-hydrated halloysite) because, although the positions of the dominant peaks coincide with those of the kaolinite standard, their shape and intensity are different. For example, the sharp characteristic peaks at 7.18 Å (14.3 *2θ*) and 3.58 Å (29 *2θ*) in the kaolinite standard pattern are broad and defined in the samples, suggesting poor crystallinity. The only differences that can be observed between these three samples is that S1, which was collected from a fracture in the mottled zone, contains gibbsite, and that S5 has a higher quartz content.

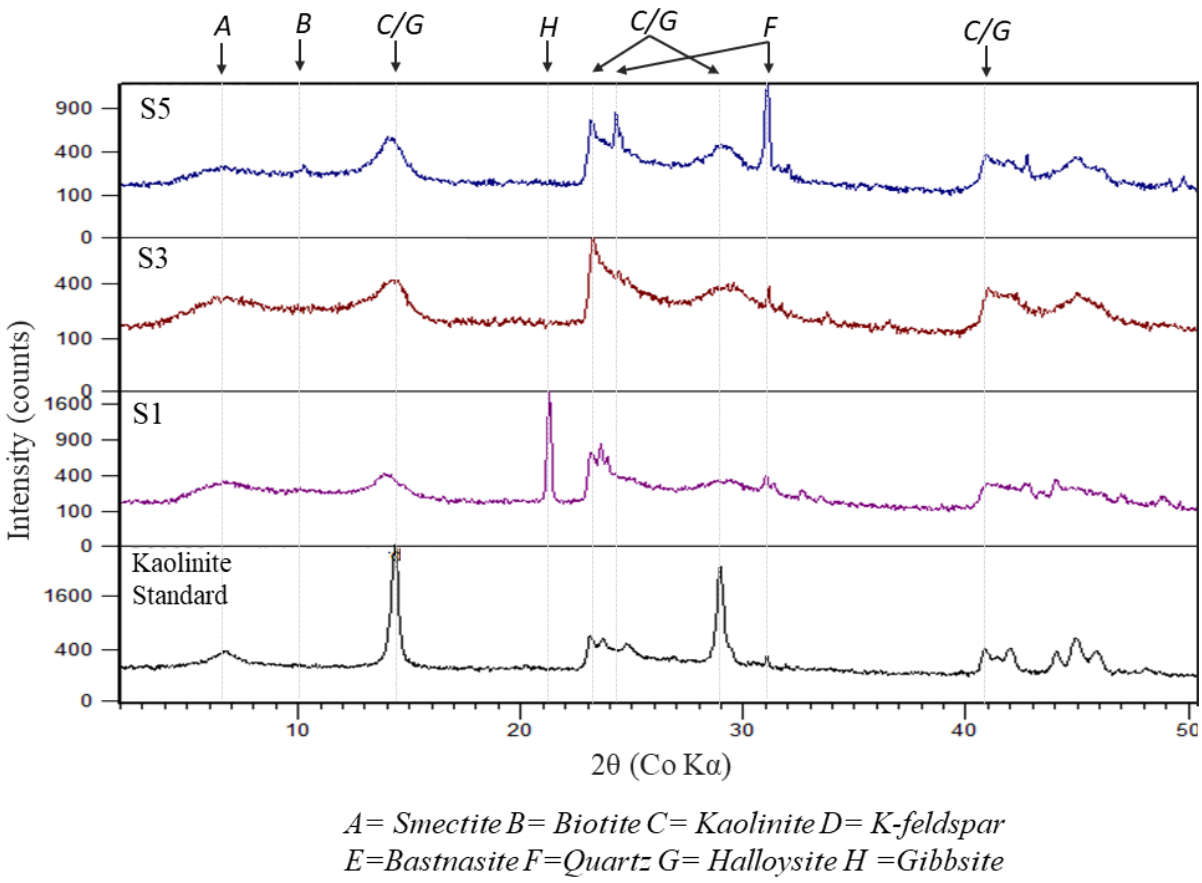


Figure 7.16. Representative X-ray diffraction patterns of clay-rich, fracture-infill samples (S1, S3, S5) collected from an exposed section of preserved weathered profile on the plateau and a kaolinite standard.

Representative patterns for the clay-rich material coating fracture surfaces in bedrock and saprock samples from DDH0099 and DDH00161 confirm the presence of smectite, kaolinite, biotite, quartz and K-feldspar (Figure 7.17). Unlike other samples analysed, the dominant clay in S10 and S11 appears to be smectite (montmorillonite) with significantly higher smectite peak intensities than those for kaolinite. In sample S11, kaolinite peaks are only slightly higher than the background. Another mineral pattern present in sample S11 confirms the presence of bastnäsite.

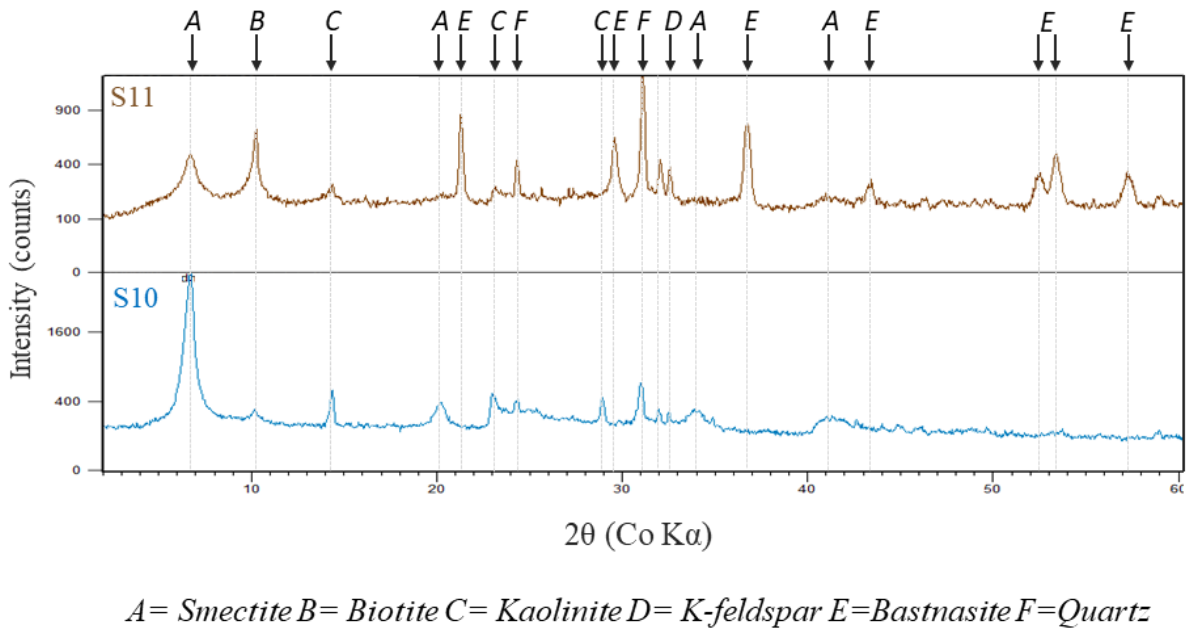


Figure 7.17. XRD patterns of white clay-rich material coating fracture surfaces in bedrock/saprock samples from drill cores DDH0099 (S10) and DDH0161 (S11).

7.5 REE Mineralogy

7.5.1 REE-fluorcarbonates

7.5.1.1 Distribution and Morphology

SEM analyses on saprock samples show that REE-fluorcarbonate grains have ragged and fractured edges. Accessory mineral grains are present, with veinlets of bright REE-fluorcarbonate occurring in fracture-filling colloform textures extending away from them. These grains are also present in the bedrock and described in Chapter 5. In saprock samples where weathering has progressed further, and where REE are more strongly enriched (SV8.2,

SV9.1, SV11.1 and SV16), REE-fluorcarbonates can also be found infilling fractures and pores within partially dissolved Na-feldspar crystals (Figure 7.18).

REE-fluorcarbonates also occur in larger fractures in the saprock. In sample S10, REE-fluorcarbonates are abundant and occur as well-crystallised discs, up to 20 microns across (Figure 7.19; panels A, B). These discs are found in clusters, forming rosettes, and are usually mixed with other clay. In sample S11, REE-fluorcarbonates are much less common and occur as amorphous grains concentrated in a few clay-rich clumps (Figure 7.19 C).

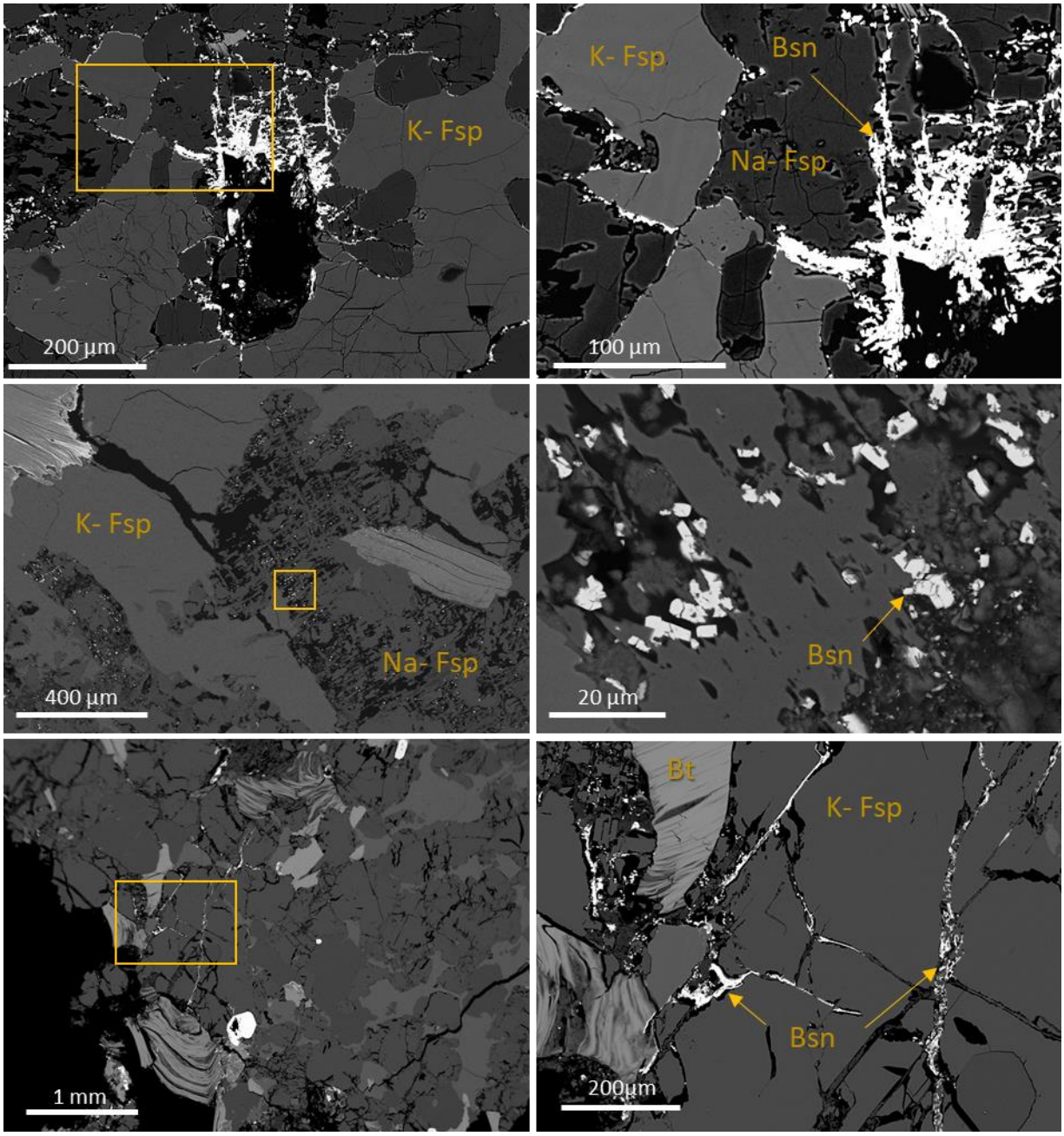


Figure 7.18. SEM-BSE images of saprock samples showing the occurrence of LREECO_3F infilling microfractures and spaces left behind by the dissolution of Na-feldspar.

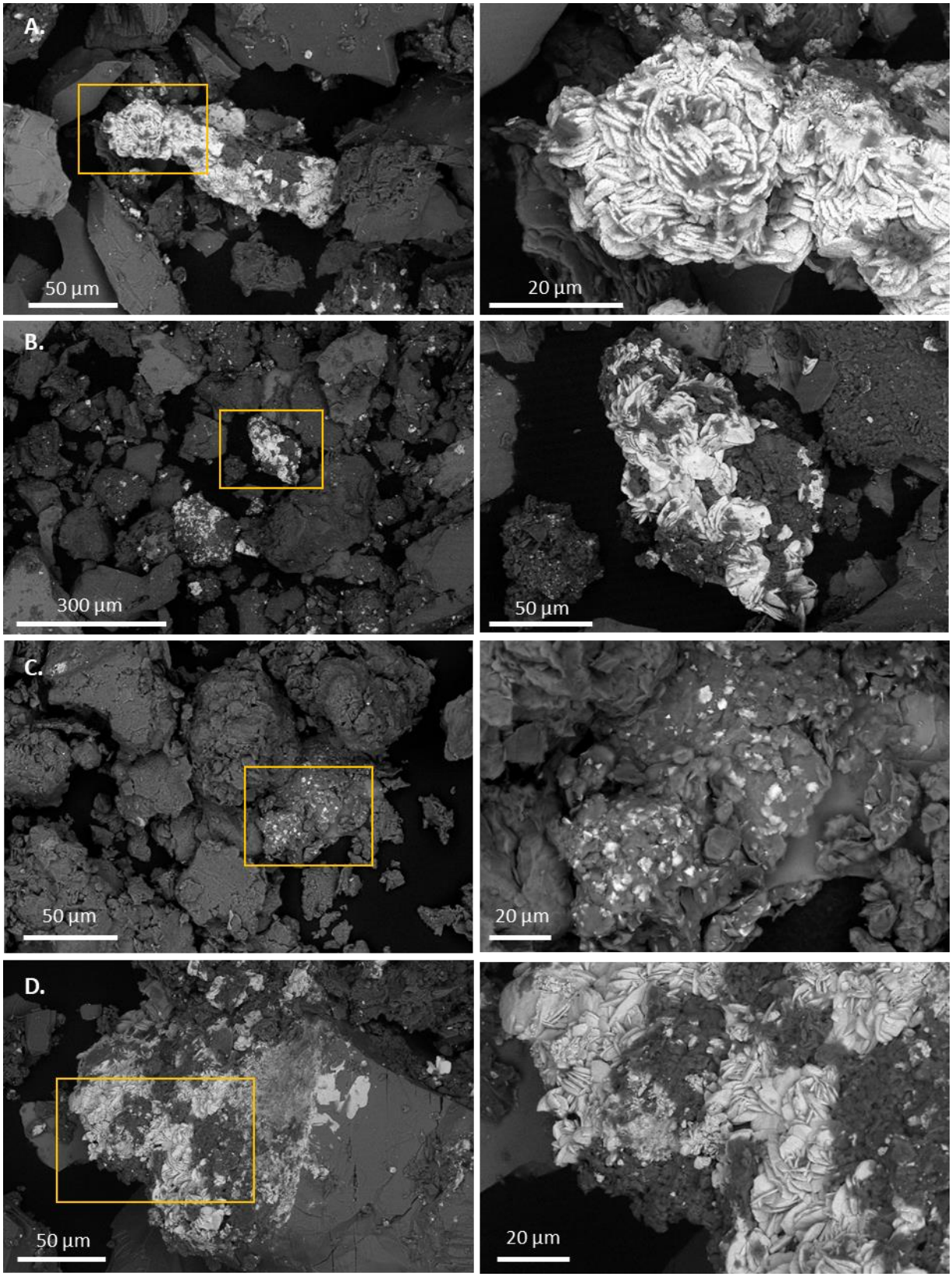


Figure 7.19. SEM-BSE images showing LREE-fluorcarbonate rosettes, intergrown with clay minerals in samples S10 (A), S11 (B) and S9 (C).

REE-enriched saprolite samples

In the REE-enriched saprolite samples collected from different drill holes, there are several different occurrences of REE-fluorcarbonates. In samples SV7 and SV14 they are abundant and easily identified; SEM analysis shows that they occur as fine, bright veinlets running through the weathered, clay-rich areas (Figure 7.20). In these samples the REE-fluorcarbonates are most commonly found in areas that appear as white patches in hand sample.

In comparison, only traces of REE-fluorcarbonates were found in SV9, SV11, SV12 and SV13. Sample SV9 has similar REE concentrations to SV7, but BSE imaging shows no bright veinlets running through SV9 (Figure 7.20, lower panels). A close inspection of the clay clumps, however, reveals that these have bright REE-enriched rims. It is possible that these are relicts of previous REE-fluorcarbonate veinlets that have now fully dissolved. The other samples, SV11, SV12 and SV13, have much lower REE concentrations compared to SV7 and SV14, so REE fluorcarbonates may still be present in these samples but in such low concentrations that they are hard to find.

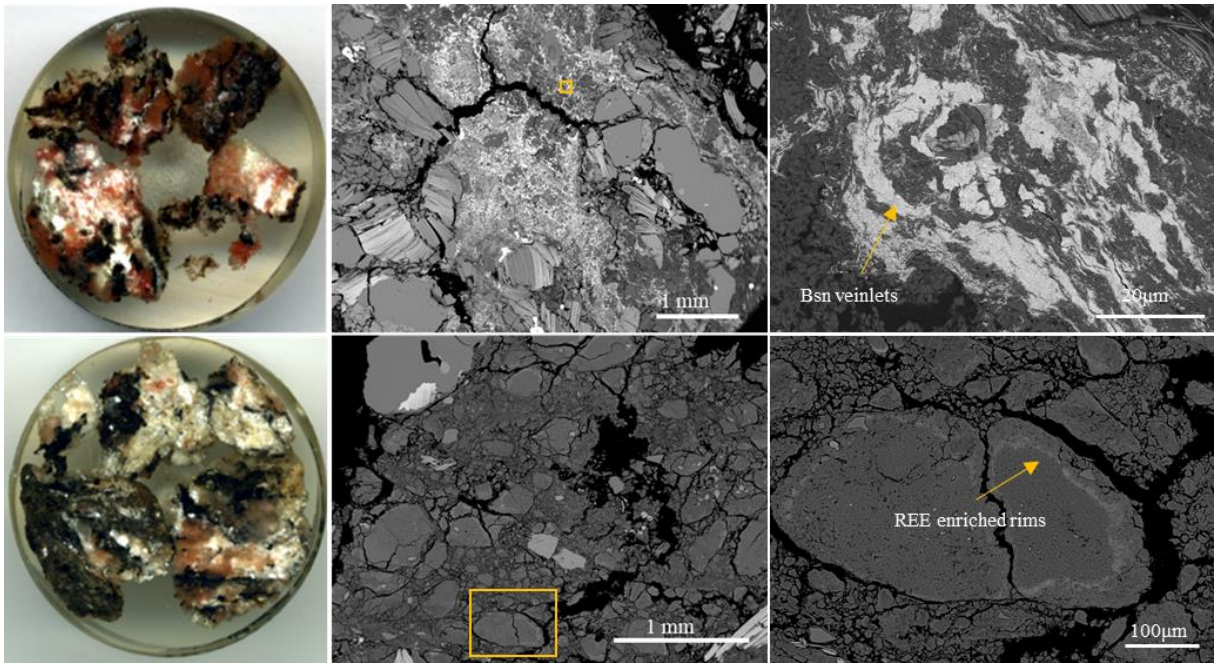


Figure 7.20. Photographs of resin blocks and SEM-BSE images of saprolite samples. Upper images show abundant REE-fluorcarbonate in SV7, and lower images show REE-enriched rims in clay clumps in SV9, perhaps relic enrichment associated with earlier REE-fluorcarbonates (not dissolved).

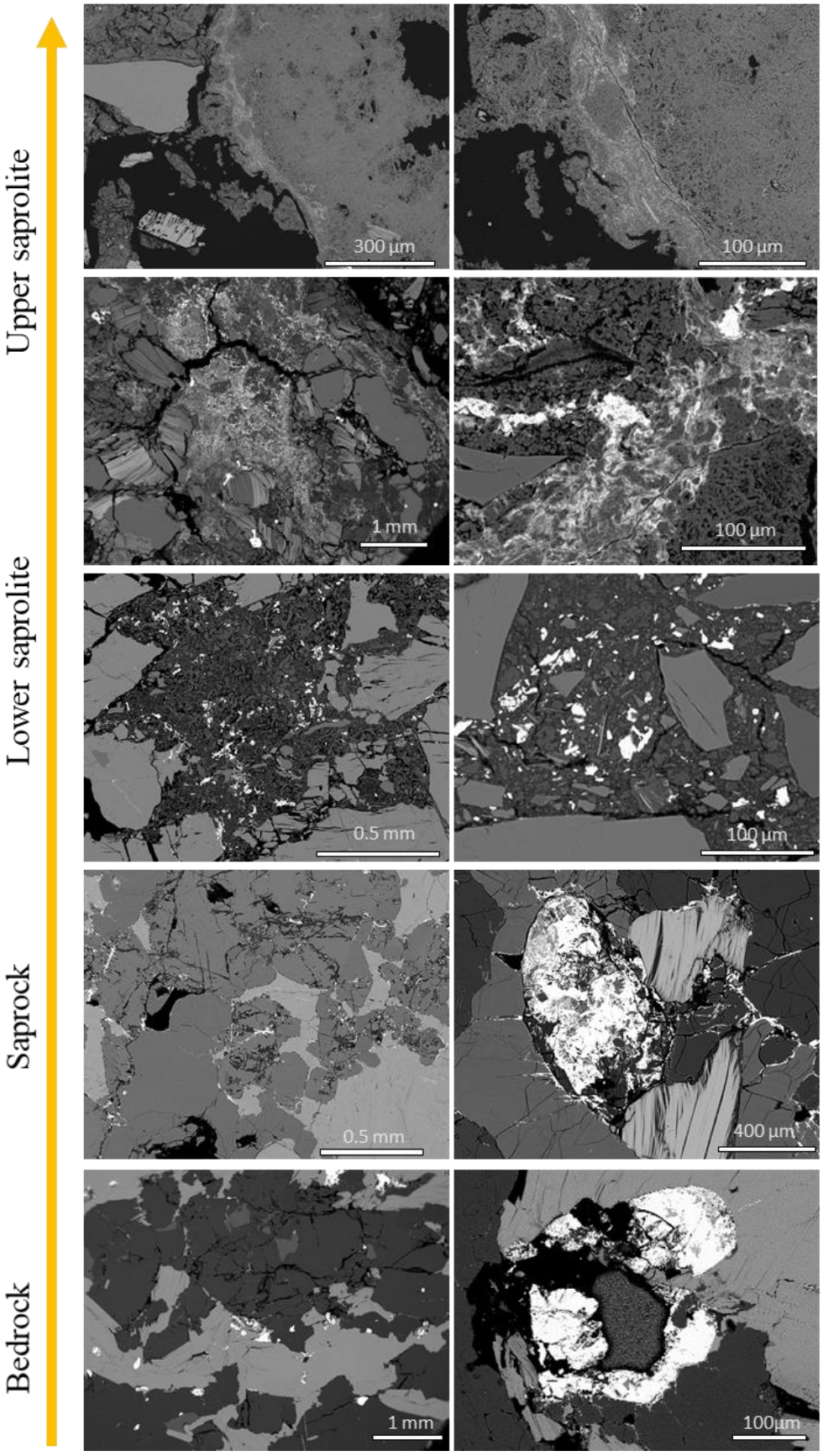


Figure 7.21. SEM-BSE images showing the distribution and morphology of LREE-fluorcarbonates at different levels of the saprolite horizon of drill hole DDH0161.

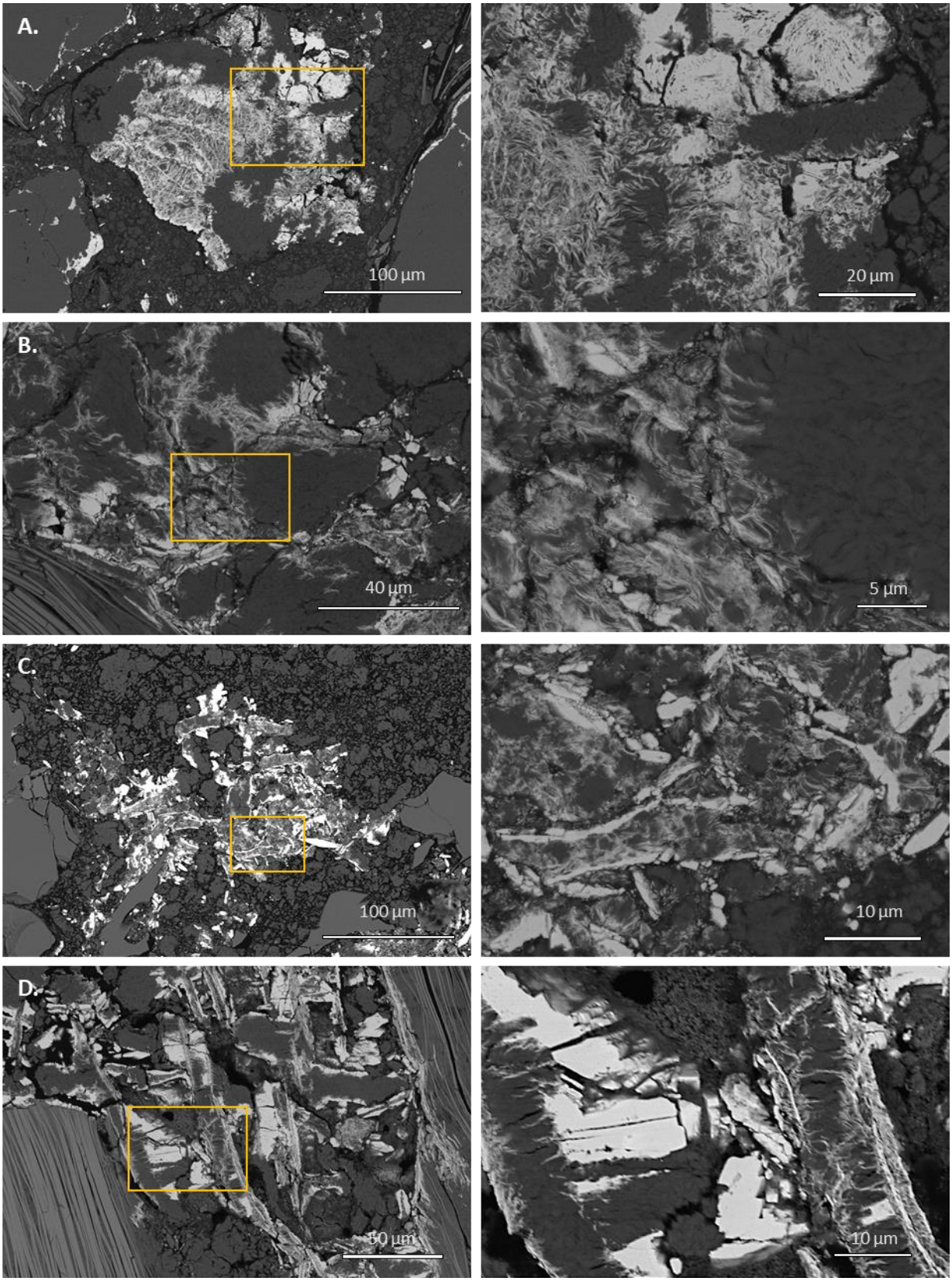


Figure 7.22. High-resolution SEM-BSE images showing the dissolution and re-crystallisation of REE-fluorcarbonates (bright phases) into clay-rich areas and along fractures. Images taken from saprolite samples SV6 and SV7.

DDH0161 samples

Samples taken along saprock, saprolite and transition zone horizons of DDH0161 show an evolution in form, distribution and abundance of REE fluorcarbonates throughout the weathering profile. This evolution is from discrete, relatively large accessory phases in the bedrock, to the more widely-dispersed, nano-scale grains closely intermixed with clay minerals at the top of the saprolite.

SEM-BSE imaging (Figure 7.21) shows the following:

- In the bedrock, REE-fluorcarbonates were found as discrete accessory minerals several 100 microns across in size, with pseudomorphic textures, and spatially associated with biotite.
- In the saprock, the original REE-fluorcarbonate phases are still present, but show signs of early breakdown, and are accompanied by REE-fluorcarbonates that have formed along micro-fractures in the rock.
- In the lower saprolite, REE-fluorcarbonates are found broken up into smaller fragments (up to 50 microns across). Some of these fragments also exhibit corrosion textures.
- In the middle saprolite, extensive dissolution and reprecipitation of the LREE-fluorcarbonates has occurred. Re-crystallised REE-fluorcarbonates form fine veinlets a few microns thick that cut across the sample. Veinlets are found extending throughout the weathered material in the sample.
- In the upper saprolite, very few veinlets are observed. These are very fine and not well-defined in SEM-BSE images. Disseminated REE-fluorcarbonate abundance is low in these samples and the grains are extremely small and strongly intermixed with clay minerals. No REE-fluorcarbonate grains were found in the transition zone.
- The samples with the most abundant REE-fluorcarbonates are in the middle to lower saprolite, and coincide with the highest bulk REE concentrations. Overall, REE-fluorcarbonates become less common, increasingly dispersed, and finer grained towards the top of the saprolite horizon as far as the transition zone.

High resolution SEM-BSE images capture the dissolution, mobilisation, and reprecipitation of REE-fluorcarbonates in saprolite samples from DDH0161 (Figure 7.22). They form increasingly fine veinlets, composed of nano-scale (< 1 micron) anhedral grains, that branch out into the surrounding weathered material and concentrate in clay-rich areas.

Clay-rich fracture-filling samples

REE-fluorcarbonates were found in two of the clay-rich fracture infill samples - samples S5 and S9 - which were collected from lower parts of an exposed saprolite section. In sample S9, REE-fluorcarbonates are common and have disc-shaped habits, comparable to S11 (Figure 7.19). No REE-fluorcarbonates were found in samples S1, S3, and S8, which come from fractures in the mottled zone and upper parts of the exposed saprolite sections.

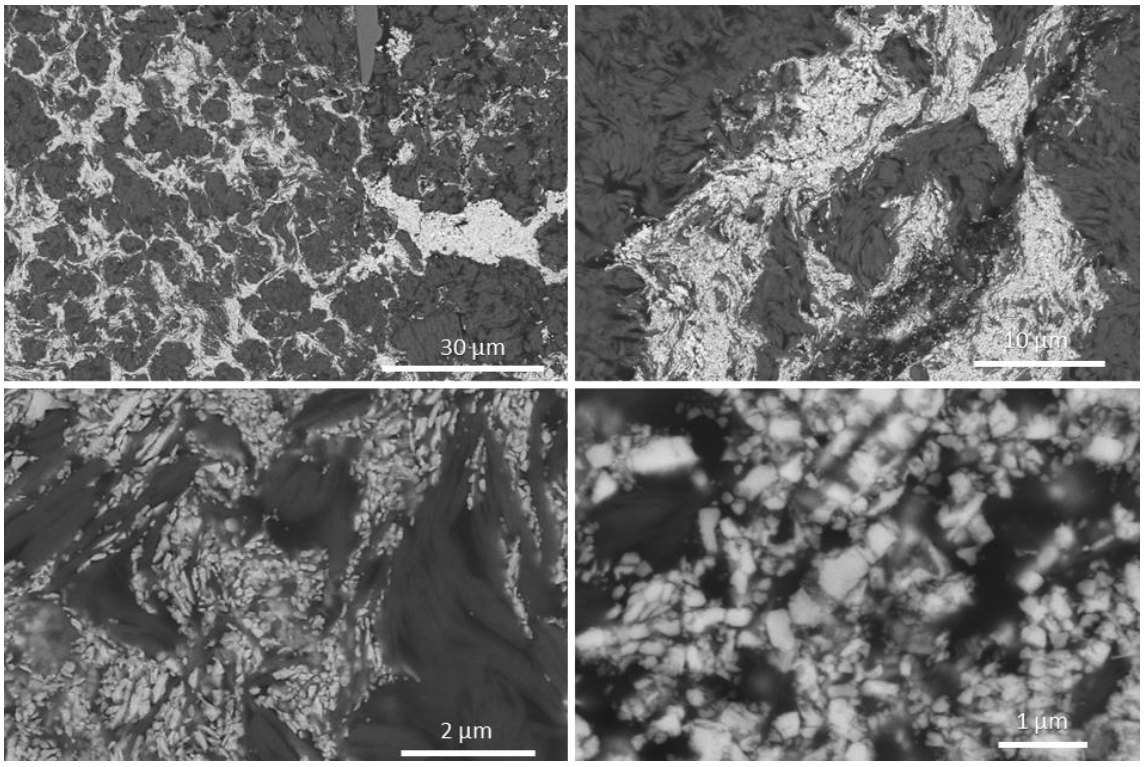


Figure 7.23. High-resolution SEM-BSE images showing the morphologies of REE-fluorcarbonates in micro-fractures from drill hole DDH0161.

7.6.1.2 Mineral Composition

The REE-fluorcarbonates found in the saprolite and saprock samples have chemical compositions that are distinct from the REE-fluorcarbonates present in the bedrock. SEM-EDX and EMP analysis results show that the REE-fluorcarbonates from the weathering zone are bastnäsite group minerals with La and Nd as the dominant REE, and negative Ce anomalies (Table 7.5, Figure 7.24). Compositions are variable, falling between bastnäsite-(La) and bastnäsite-(Ce). However, in the bedrock, bastnäsite-(Ce) is the dominant species, and no fractionation of LREE is observed (see Chapter 5). Ca and Th contents are also higher.

From the variations observed here, three naturally discrete compositional populations in the mineral chemistry can be identified (see Figure 7.26, Table 7.5, and Figure 7.27).

The Type-I population represents the bastnäsite-(La) end member, with the highest La concentrations and lowest Ce concentrations (< 0.5 wt %). This population has very strongly negative Ce anomalies (0.04 on average), low Ca and Th contents (< 1 wt % Ca and < 0.2 wt % Th) and relatively high HREE concentrations (~11 wt % HREE+Y).

The data points that fall between bastnäsite-(La) (Type-I), and bastnäsite-(Ce) (bedrock source) compositions have been divided into two groups: Type-II and Type-III. The Type II population is the more compositionally similar to Type-I, similar La, Nd, and Ca concentrations, but with less depletion in Ce (1 - 20 wt % Ce) and higher Ce anomalies (< 0.2). The Type III population falls closer to bastnäsite-(Ce); Ce concentrations in this group range between 10 – 16 wt %, the negative Ce anomaly ranges between 0.20 and 0.50, and Ca concentrations fall between 1- 3 wt %. Both Type-II and Type-III have variable Th concentrations that range between 0.30 to 3.47 wt % and HREE+Y contents of ~3.5 wt %.

Comparing the types of bastnäsite species with the types of sample analysed, it appears that Type-I and Type-II are most commonly found in saprolite samples. The REE-fluorcarbonates found in clay veinlet samples are also La-rich bastnäsite, with strong negative Ce anomalies (Figure 7.25). Type-III bastnäsite is more common in saprock samples, indicating an upward progression with increasing weathering from bastnäsite-(Ce) to bastnäsite-(La).

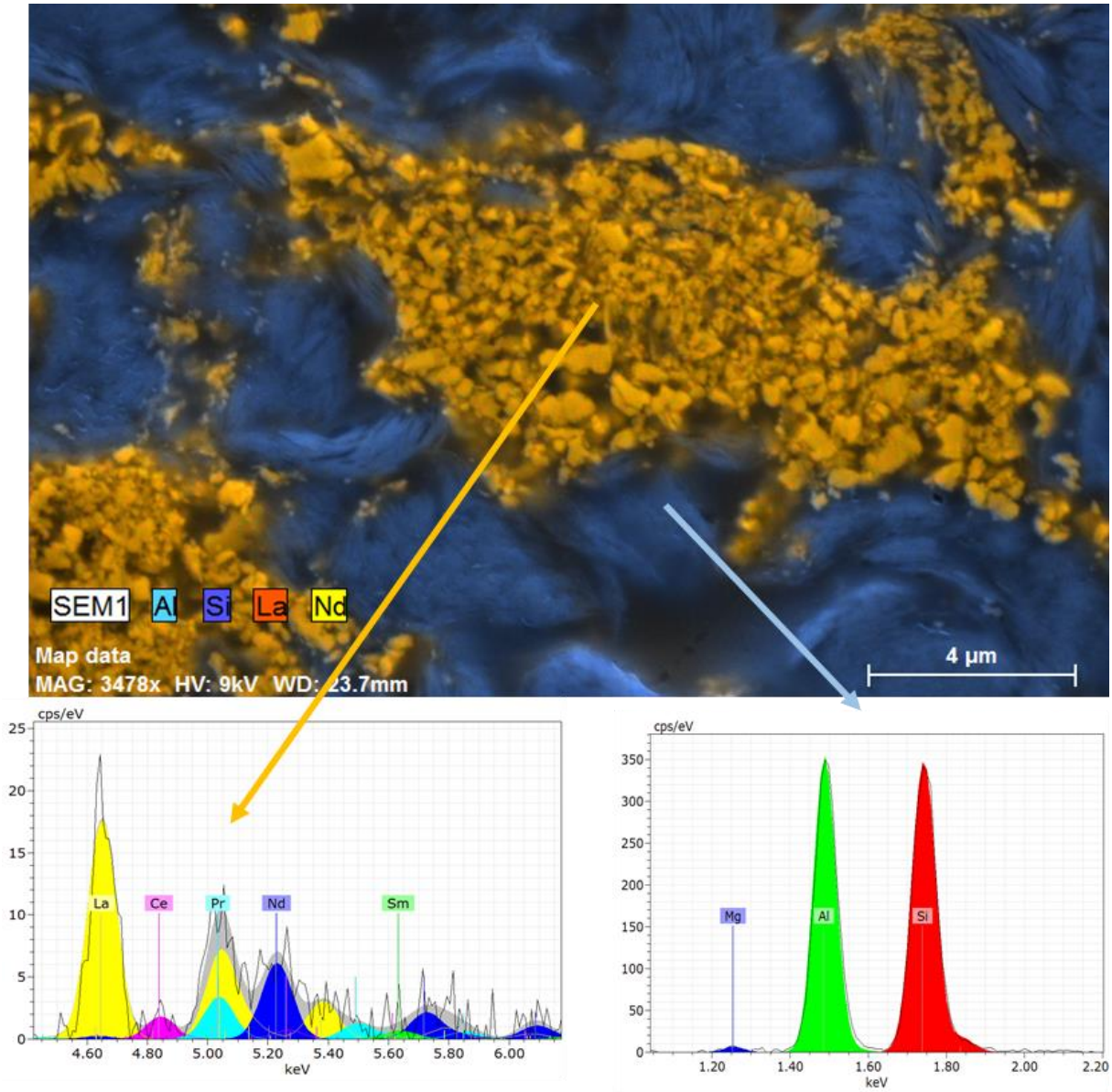


Figure 7.24. False-colour SEM-EDX map showing composition of nano-scale LREE-fluorcarbonate grains, found intermixed with clays in DDH0161.

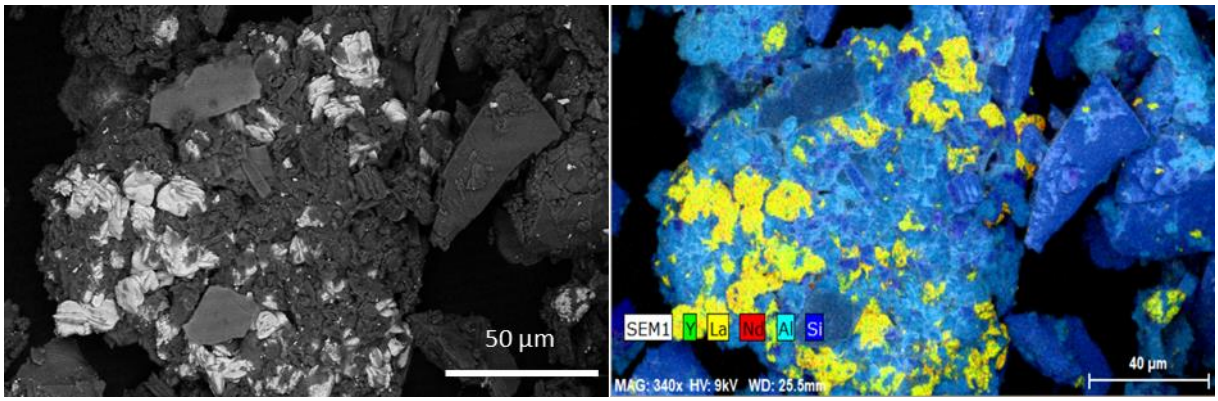


Figure 7.25. False-colour SEM-EDX map showing composition of LREE-fluorcarbonate rosettes intermixed with clays in sample SV11.

Table 7.5. Representative EMPA results of REE-fluorcarbonates found in saprolite and saprock samples from drill cores DDH0161 and DDH0266, and from bedrock.

	Saprolite and Saprock									Bedrock		
	Bastnasite-La									Bastnasite-Ce		
	Type I			Type II			Type III					
Sample	SV6	SV7	SV8.2	SV6	SV6.1	SV6	SV14	SV8.2	SV8.2			
Analysis No.	P_B	P_B	P_B	P_B	P_B	P_B	P_B	P_B	P_B	P_B	P_B	P_B
SiO_2	0.39	0.12	0.17	0.68	0.80	3.57	0.81	0.98	0.18	0.77	0.60	0.23
Al_2O_3	0.17	<dt	<dt	0.12	0.32	2.57	0.07	<dt	<dt	0.07	0.39	<dt
Y_2O_3	**11.2**	**10.6**	**14.3**	2.34	1.94	6.71	6.63	4.31	3.21	8.16	7.33	8.05
La_2O_3	**29.0**	**29.3**	**28.1**	**27.9**	**31.7**	**24.7**	**21.6**	**22.2**	**24.6**	**19.1**	**13.0**	**15.7**
Ce_2O_3	0.53	0.46	0.90	3.01	2.36	3.19	**16.8**	**18.7**	**13.7**	**23.2**	**25.3**	**28.1**
Pr_2O_3	4.87	4.70	4.43	5.61	6.14	4.40	3.35	3.92	4.84	3.39	2.48	2.96
Nd_2O_3	**17.4**	**17.7**	**16.8**	**18.0**	**20.5**	**15.9**	12.1	14.0	15.8	11.9	8.55	9.65
Sm_2O_3	3.08	3.24	3.07	2.67	3.15	2.73	2.03	2.21	2.38	1.71	1.45	1.52
Gd_2O_3	2.55	2.78	2.41	1.09	1.30	1.99	2.02	1.21	1.32	0.95	1.24	1.54
Tb_2O_3	0.33	0.35	0.41	0.16	0.15	0.24	0.28	0.14	0.17	0.14	0.21	0.21
Dy_2O_3	1.78	1.94	2.26	0.49	0.69	1.42	1.30	0.67	0.51	0.60	1.15	0.90
Ho_2O_3	0.32	0.31	0.45	<dt	0.19	0.17	0.22	0.16	<dt	<dt	0.19	0.19
Er_2O_3	0.56	0.66	0.96	<dt	<dt	0.44	0.60	0.31	0.18	0.22	0.47	0.37
Tm_2O_3	0.08	<dt	<dt	<dt	<dt	<dt	<dt	<dt	<dt	<dt	<dt	<dt
Yb_2O_3	0.46	0.41	0.49	0.10	0.14	0.38	0.25	0.15	<dt	0.12	0.23	0.15
Lu_2O_3	<dt	<dt	<dt	<dt	<dt	0.07	<dt	<dt	<dt	<dt	<dt	<dt
CaO	1.20	1.32	2.06	0.43	0.69	0.57	1.92	2.66	2.51	2.10	3.40	3.32
SrO	<dt	0.07	<dt	<dt	<dt	<dt	<dt	<dt	0.19	0.16	<dt	0.13
FeO	0.37	<dt	<dt	0.10	0.71	0.10	<dt	0.53	0.24	0.11	3.64	0.66
P_2O_5	<dt	<dt	0.55	0.23	<dt	<dt	<dt	0.26	0.17	0.28	<dt	<dt
ThO_2	<dt	<dt	0.56	2.35	2.16	0.34	2.89	1.72	2.43	3.77	4.74	2.08
UO_2	<dt	<dt	<dt	<dt	<dt	<dt	<dt	<dt	<dt	0.19	0.21	0.09
CO_2 (calc.)	17.9	20.3	22.2	21.4	20.8	22.9	20.8	22.0	20.7	20.8	22.7	21.9
F	8.61	9.06	7.07	6.88	7.53	6.80	8.96	8.24	8.89	8.16	7.33	8.05
(-O)=F	2.71	2.90	2.31	3.63	3.82	2.98	3.77	3.09	3.74	3.44	3.09	3.39
Total	74.3	74.0	77.9	65.3	72.9	69.5	72.9	74.1	72.5	76.9	74.6	75.8
REE	61.0	61.9	60.3	59.1	66.3	55.6	60.6	63.7	63.5	61.3	54.3	61.3
REY	72.2	72.5	74.5	61.4	68.3	62.3	67.2	68.0	66.7	69.4	61.7	69.3
Structural formula based on 4 anions.												
Ca apfu	0.019	0.028	0.024	0.045	0.050	0.074	0.074	0.100	0.096	0.082	0.126	0.124
Sr	0.000	0.000	0.000	0.000	0.000	0.000	0.000	0.000	0.004	0.003	0.000	0.003
Y	0.053	0.039	0.137	0.210	0.200	0.253	0.127	0.081	0.061	0.073	0.099	0.109
La	0.436	0.443	0.349	0.376	0.383	0.346	0.287	0.288	0.326	0.255	0.166	0.202
Ce	0.047	0.033	0.045	0.007	0.006	0.011	0.222	0.241	0.180	0.307	0.321	0.358
Pr	0.087	0.085	0.061	0.062	0.061	0.054	0.044	0.050	0.063	0.045	0.031	0.038
Nd	0.272	0.278	0.217	0.218	0.224	0.200	0.155	0.176	0.203	0.154	0.106	0.120
Sm	0.039	0.041	0.036	0.037	0.039	0.035	0.025	0.027	0.029	0.021	0.017	0.018
Gd	0.000	0.000	0.000	0.000	0.000	0.000	0.000	0.000	0.000	0.000	0.000	0.000
Tb	0.002	0.002	0.003	0.004	0.004	0.004	0.003	0.002	0.002	0.002	0.002	0.002
Dy	0.007	0.008	0.018	0.020	0.022	0.024	0.015	0.008	0.006	0.007	0.013	0.010
Ho	0.000	0.000	0.000	0.000	0.000	0.000	0.000	0.000	0.000	0.000	0.000	0.000
Er	0.000	0.000	0.005	0.006	0.007	0.010	0.007	0.003	0.002	0.002	0.005	0.004
Tm	0.000	0.000	0.000	0.001	0.000	0.000	0.000	0.000	0.000	0.000	0.000	0.000
Yb	0.001	0.002	0.004	0.005	0.004	0.005	0.003	0.002	0.000	0.001	0.002	0.002
Lu	0.000	0.000	0.000	0.000	0.000	0.000	0.000	0.000	0.000	0.000	0.000	0.000
Fe	0.007	0.004	0.023	0.003	0.011	0.000	0.019	0.000	0.016	0.022	0.004	0.106
Si	0.029	0.030	0.137	0.014	0.005	0.006	0.029	0.035	0.007	0.028	0.021	0.008
Al	0.006	0.014	0.116	0.007	0.000	0.000	0.003	0.000	0.000	0.003	0.016	0.000
Th	0.088	0.068	0.010	0.000	0.000	0.016	0.091	0.053	0.077	0.120	0.144	0.064
U	0.000	0.000	0.000	0.000	0.000	0.000	0.000	0.000	0.000	0.005	0.006	0.002
Σ cations	1.09	1.08	1.18	1.01	1.02	1.04	1.10	1.06	1.07	1.13	1.08	1.17
C	1.03	1.05	1.16	1.02	1.01	1.04	1.02	1.05	1.01	1.03	1.07	1.04
F	0.86	0.83	0.66	0.96	1.01	0.75	1.02	0.81	1.01	0.93	0.80	0.89

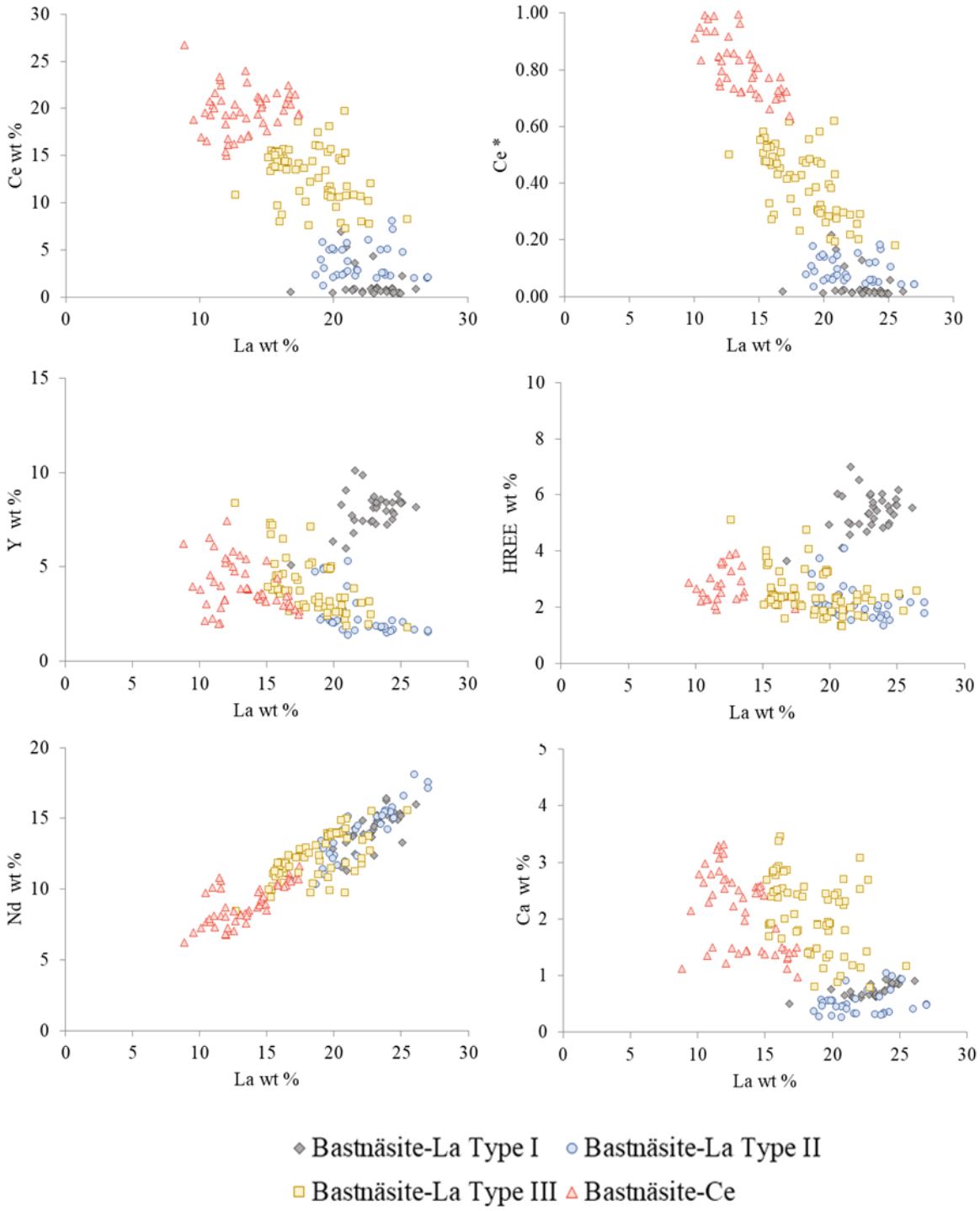


Figure 7.26. Element plots showing the compositions of REE-fluorcarbonates in saprolite, saprock and bedrock samples from DDH0161 and DDH0266.

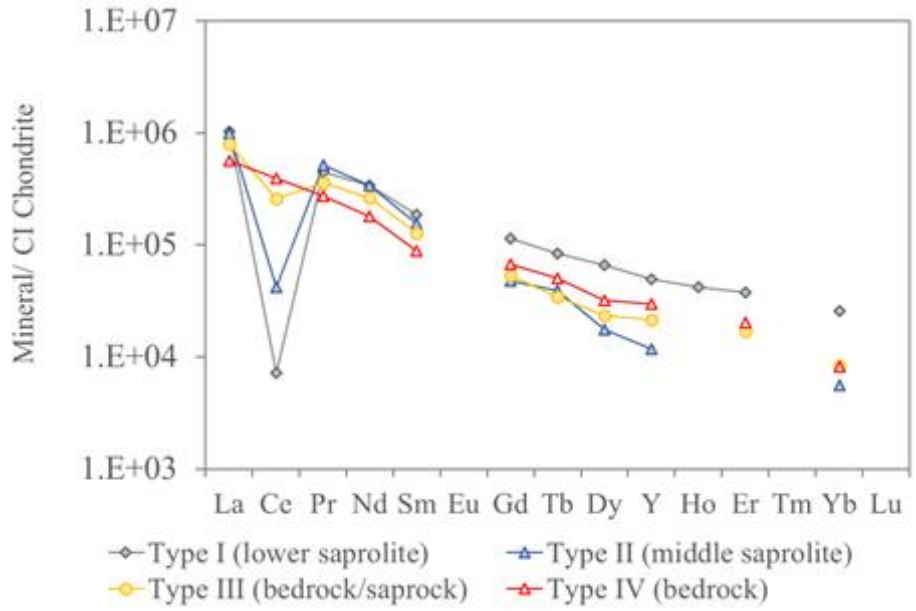


Figure 7.27. Chondrite-normalised REE patterns of LREE-fluorcarbonates present in saprolite, saprock, and bedrock samples of DDH0161.

7.5.2 Phosphates

REE-phosphate minerals are not common in the saprolite horizon but can be found in all of the samples prepared for SEM analysis. Samples with the highest abundance of REE-phosphate are SV10, SV11 and SV61 which also contain the highest phosphate concentrations in whole rock. No apatite grains were found in any of the saprolite samples, despite their common occurrence in the bedrock, which suggests they have been preferentially dissolved.

REE-enriched samples

In the REE-enriched saprolite samples, phosphate minerals are present as both crystalline grains, showing similar textures to those in the bedrock (see Chapter 5), and fine acicular clusters. The former are more common and easier to identify due to their large size (~ 100 microns in diameter). SEM analysis shows that primary REE-phosphates are not being chemically weathered, but rather broken up into smaller angular fragments due to their fractured nature (Figure 7.28Figure 7.28). These fragments either stay concentrated and form clusters, or are dispersed and mixed with other mineral weathering products. Fine-grained REE-phosphates are difficult to identify in saprolite samples. The few grains that were found exhibit acicular habits, and have proximal association with clay minerals (Figure 7.31).

A variety of REE-phosphates are observed in saprolite samples, including xenotime-(Y), monazite-(La), monazite-(Ce), and rhabdophane-(Ce). The monazite-La and xenotime-(Y) grains that were analysed have low Th contents, and high F contents respectively, with similar compositional characteristics as those found in the bedrock samples. None of the REE-phosphates analysed showed a negative Ce anomaly and all of the acicular minerals analysed have Ce-dominant compositions.

DDH0161 samples

SEM analysis of samples taken along drill hole DDH0161 shows that acicular Ce-rich phosphates become more common in the upper part of the saprolite horizon and transition zone. SEM-BSE images and EDX element maps show both micro-crystalline Ce-rich and Y-rich phosphates overprinting previous phases, or precipitating in the immediate vicinity of these crystals (Figure 7.29; panels A, B, Figure 7.30). Residual primary phosphates can still be found in the upper saprolite and transition zone but, due to their fragmentation and mixing, they cannot be as easily identified (Figure 7.29; panels C, D).

Clay veinlets:

REE-phosphates are also found in the clay-rich fracture infill samples. Phosphates are relatively common in the S3 and S9 samples which have elevated phosphate contents, but very scarce in all other samples, and particularly in S1 and S10. SEM-EDS analysis shows that the majority of REE-phosphates present in S3 occur as hexagonal radiating acicular crystals that are intergrown with clay minerals (Figure 7.32). This habit is characteristic of rhabdophane, a hydrated phosphate (Bideaux et al. 2000). Element analysis shows that these phosphates are La-dominant and display strong negative Ce anomalies (Figure 7.33). The phosphates found in sample S9 have a range of habits and compositions, which include rounded and elongate grains, and both LREE- and HREE-rich phosphates.

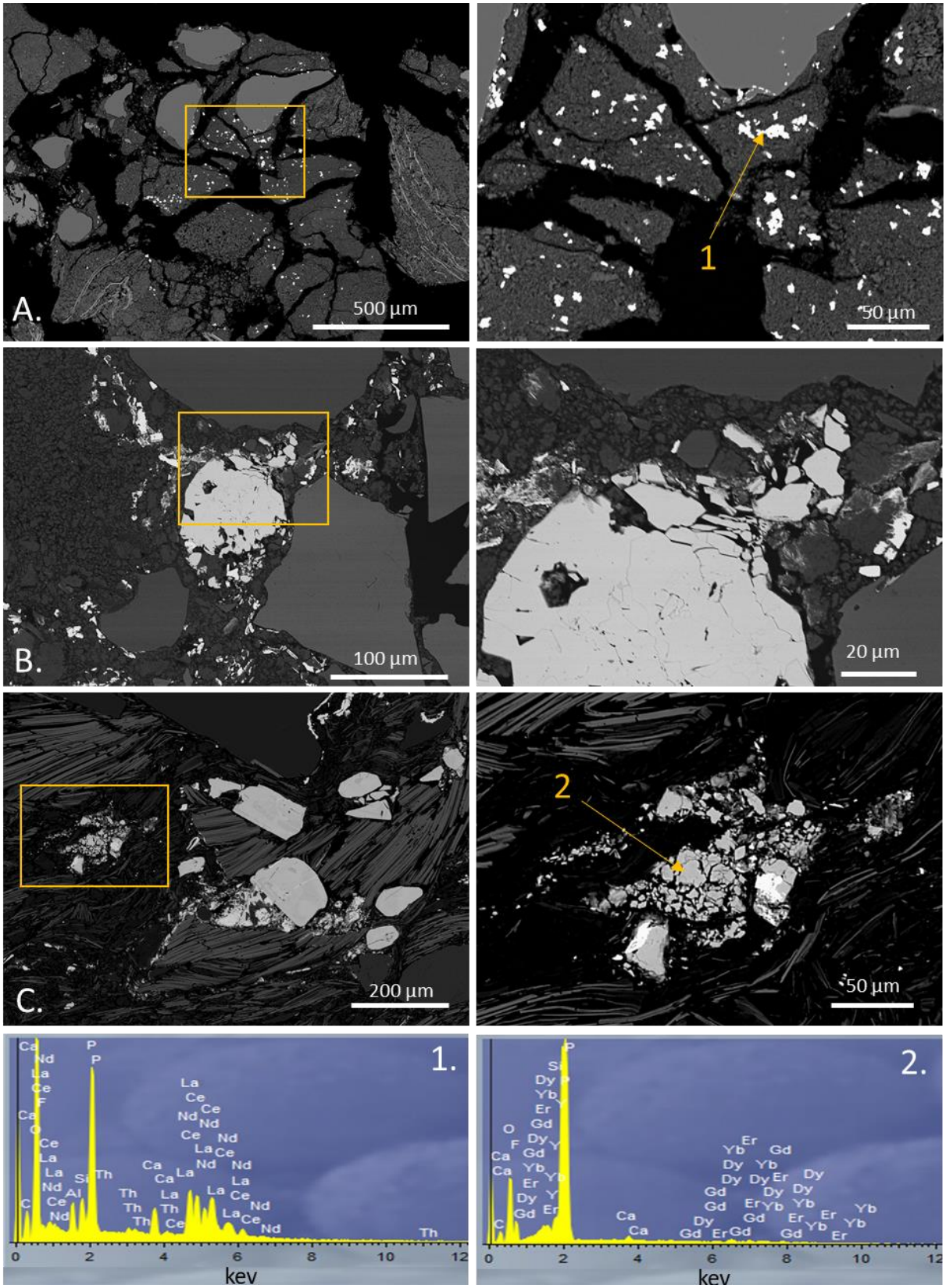


Figure 7.28. BSE images showing the variety of phosphate occurrences and habits in the saprolite. A. Fine monazite-La crystals found dispersed in a clay matrix. B and C. Large xenotime-(Y) that has been broken up into increasingly smaller fragments.

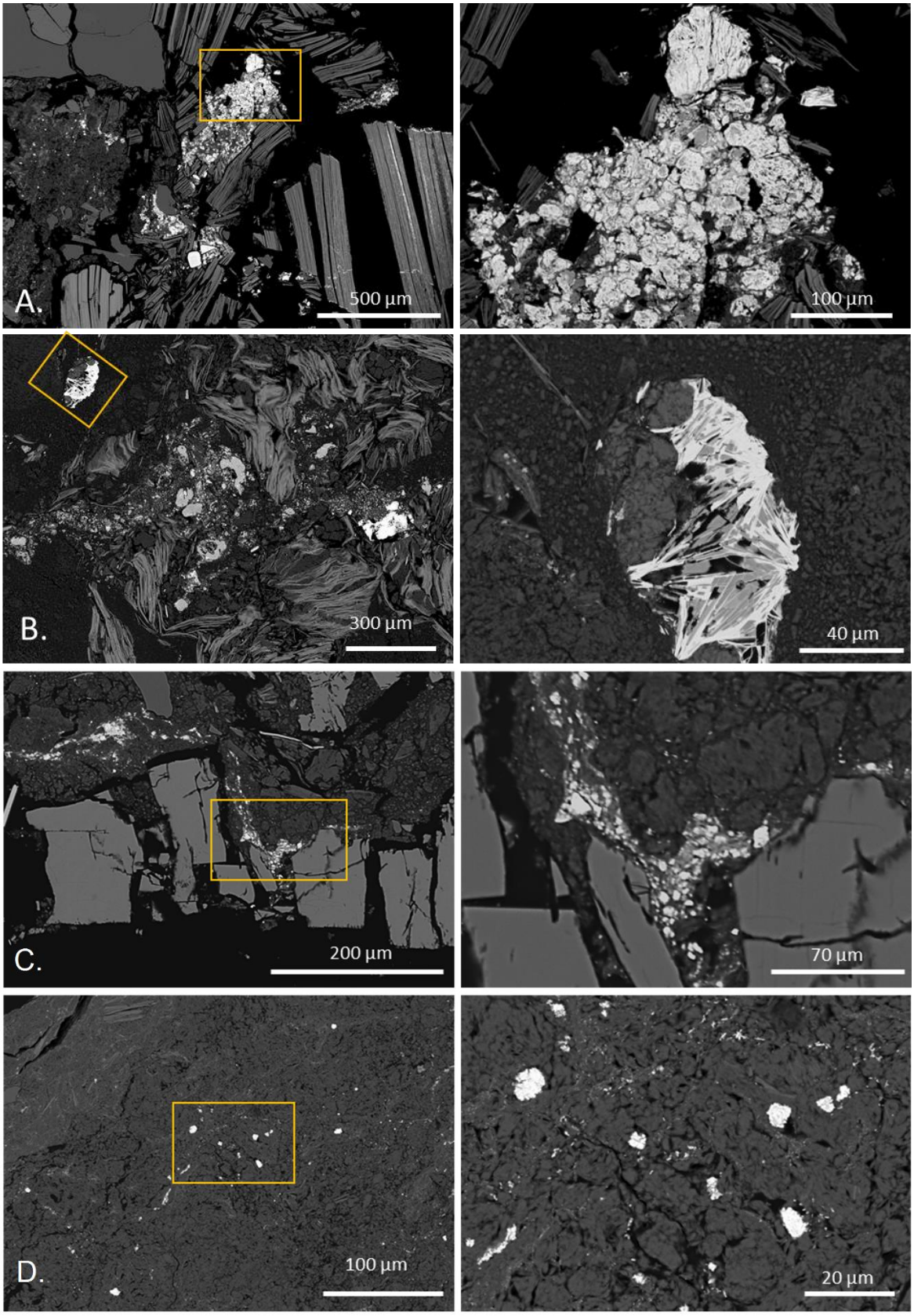


Figure 7.29. SEM-BSE images of fine REE-phosphate grains found in the upper saprolite and transition zone samples of DDH0161. A and B. local recrystallisation of phosphate (rhabdophane-(Ce)). C and D. fine fragmented crystals and clusters of phosphates.

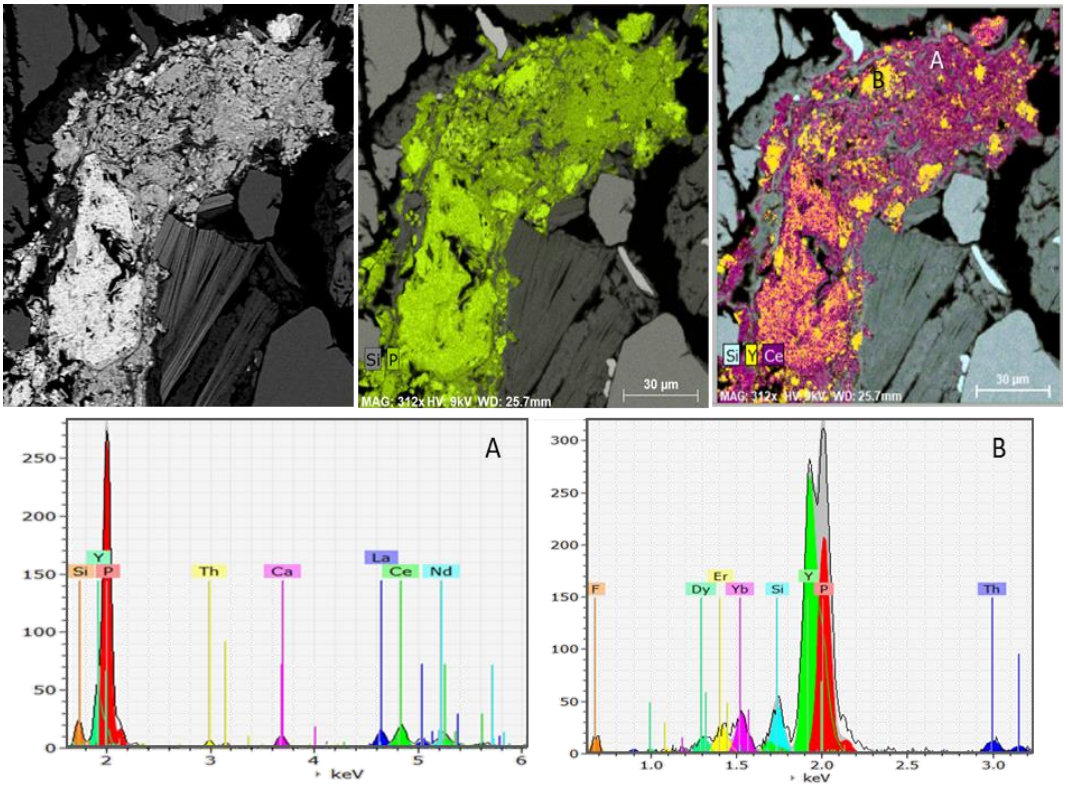


Figure 7.30. SEM-BSE and false-colour EDX element maps showing the dissolution and reprecipitation of intergrown Y- and Ce-rich phosphates in sample SV6.

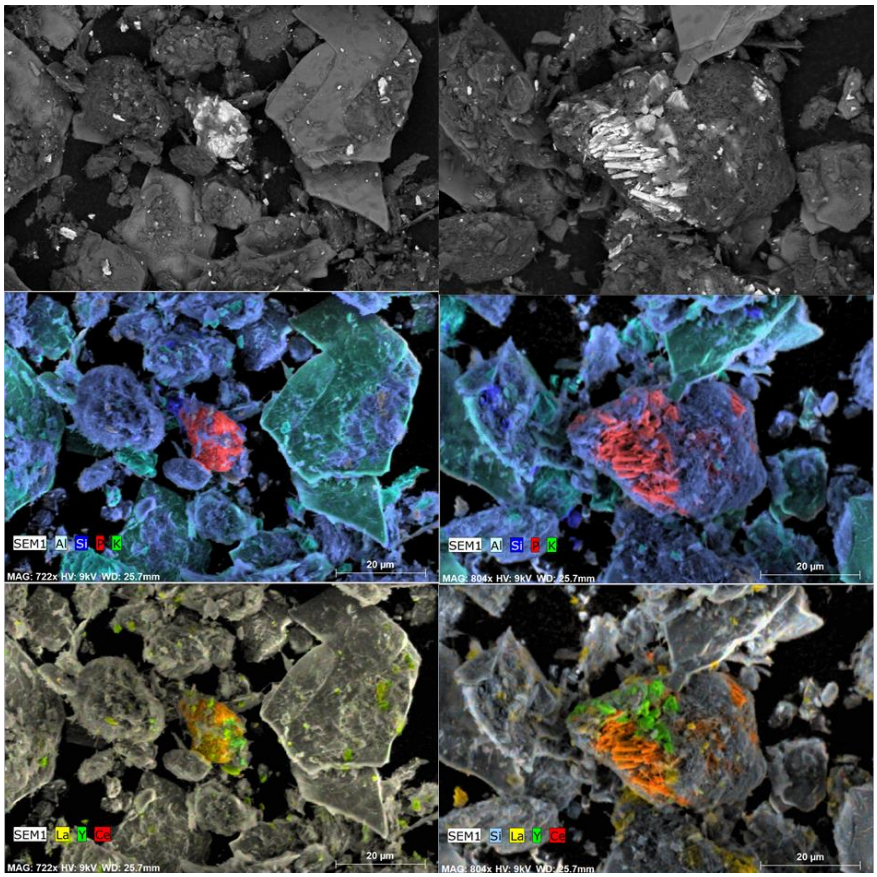


Figure 7.31. SEM-BSE and false-colour EDX element maps showing the representative habit and composition of bastnäsite-(La) and rhabdophane-(Ce) from sample SV14.

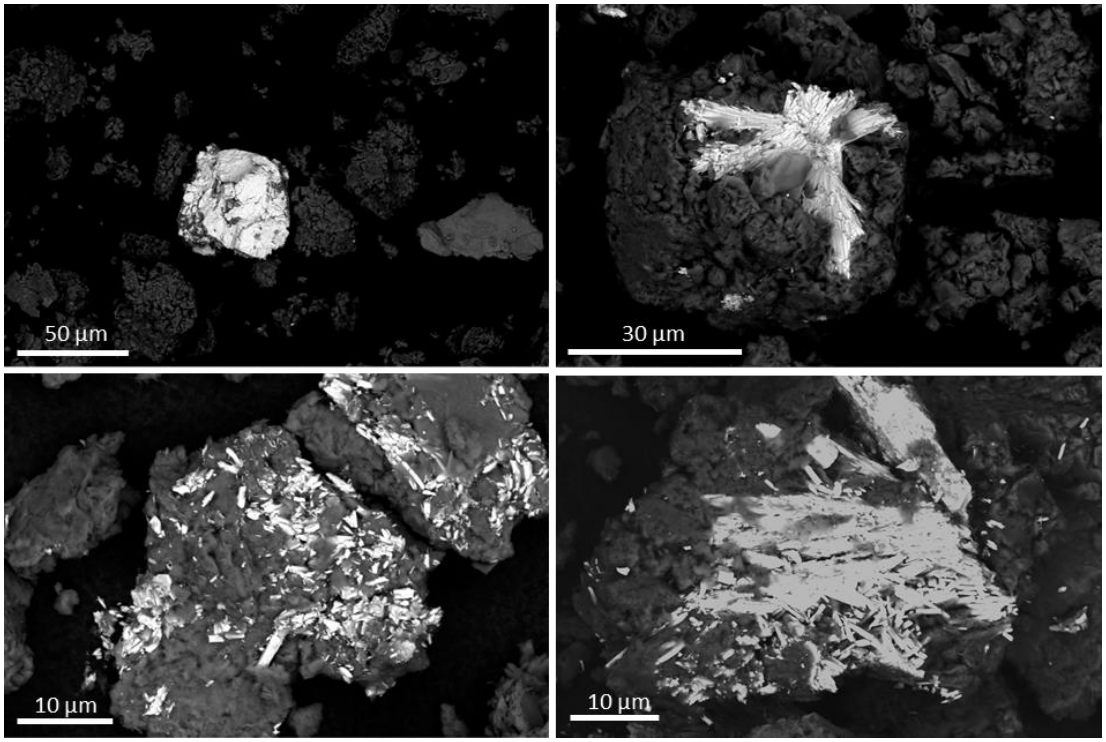


Figure 7.32. SEM-BSE images of acicular phosphates intergrown with clay minerals in clay-rich fracture-infill material collected in the weathered profile (sample S3).

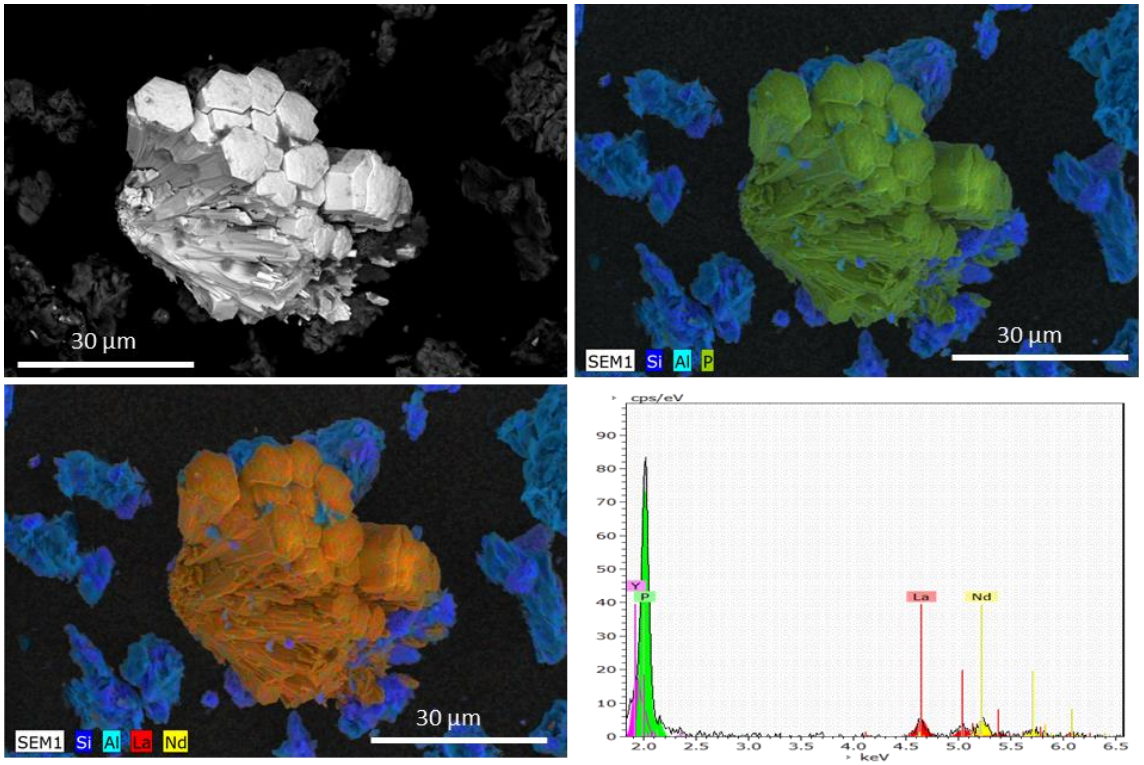


Figure 7.33. SEM-BSE image, false-colour EDX element maps and EDS spectrum showing composition of phosphate in a clay-rich fracture infill. Note: the Ce peak missing in EDS spectrum.

7.5.3 Niobiates

Niobiate minerals are not abundant in the saprolite horizon but can be found in all the samples studied. SEM analysis of the saprolite samples shows that niobiate minerals can be found as: whole, unaltered crystals locked within large quartz grains that have yet to fracture and break down; as rounded crystals concentrated around biotite clusters; and as broken up fragments intermixed with other weathered products (Figure 7.35).

SEM analysis suggests that niobiate minerals are resistant to dissolution in the saprolite but do breakdown into increasingly smaller grains. An image taken from sample SV12 in the lower saprolite shows nanoscale niobiate crystals intermixed with clay minerals (Figure 7.34). In the upper saprolite (SV5.1) and transition zone (SV5) of DDH0161, only niobiates locked in quartz crystals could be found. No niobiate minerals were found in any of the clay vein samples.

The resistant behaviour of niobiate minerals in the lower saprolite is also supported by EDS and EMP analyses, the results of which confirm that the compositions of saprolite niobiates are the same as those of niobiates found in the bedrock samples (analysed in Chapter 5). A representative EMP scan shows that niobiates are dominantly Ce- and HREE-rich species (Table 7.6).

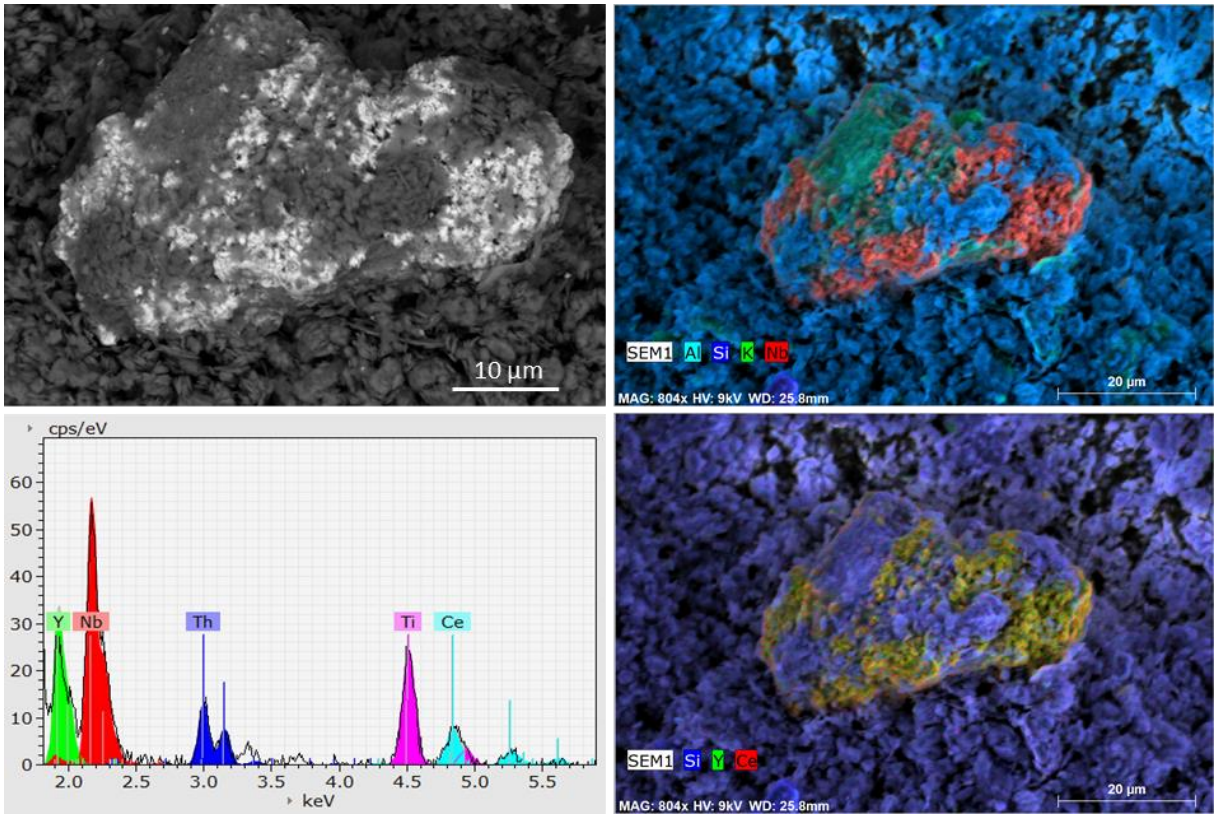


Figure 7.34. High resolution SEM-BSE and EDS false-colour maps of small niobiate grain intermixed with clay minerals from the saprolite, DDH0121.

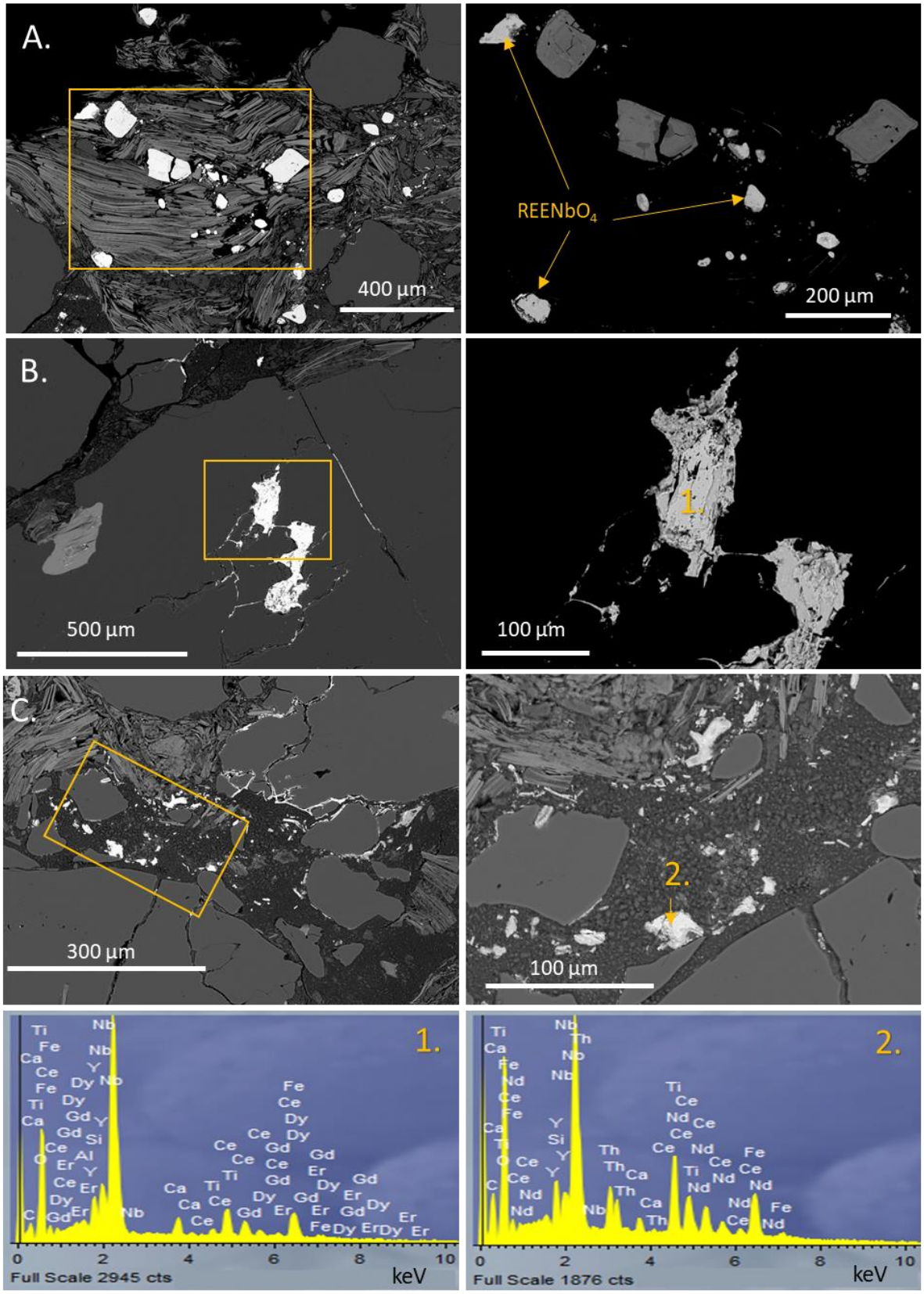


Figure 7.35. SEM-BSE images, enlargements, and EDS spectra of niobiates in saprolite samples: A. niobiate grains concentrated with zircon in partly weathered biotite; B. niobiates locked in quartz; C. niobiate crystal fragments.

7.5.4 Cerium oxides and silicates

Ce-oxides and Ce-silicates were identified in samples collected from drill hole DDH0161. SEM analysis shows that Ce silicates are more common in the saprolite, whereas Ce-oxides dominate in the transition zone.

Two types of Ce-silicate minerals were identified, and they appear to concentrate in different parts of the saprolite. In the lower saprolite, britholite-(Ce), a phosphorous-bearing silicate ($Ce(SiO_4,PO_4)_3,(OH,F)$), is observed, whereas in the upper half of the saprolite, cerite-Ce, a complex silicate ($Ce,Fe(SiO_4)(SiO_3)(OH)_4$), is more common. In the transition zone the Ce-oxides are identified as cerianite (CeO_2). Representative compositions of Ce silicates found in sample SV6.2 are presented in Table 7.6.

In the lower saprolite, britholite-(Ce) crystals retain the same habit as in the bedrock: large, elongate or anhedral grains, up to 1 mm in length, and associated with LREE-fluorcarbonates (Figure 7.36). Both Ce-silicates and Ce-oxides observed under the SEM occur as amorphous masses up to 300 μm across (Figure 7.37 and Figure 7.38). These masses are found concentrated in clusters, the shape of which suggests pseudomorphic replacement after another mineral. Both Ce-silicates and Ce-oxides are commonly found intergrown with Y-phosphate and Fe oxides (Figure 7.38).

Ce oxides are also found associated with manganese minerals that have precipitated in fissure surfaces in a saprock sample from DDH0099 (SV9.1). SEM-BSE images show Ce-oxides as coatings on the Mn minerals, which themselves occur as masses formed of concentric growths (Figure 7.39). SEM-EDS analysis of the Mn minerals show they contain small amounts of Ba and V and so they are interpreted to be a type of psilomelane, an amorphous, hydrous Ba-Mn oxide that has botryoidal habit, and which holds variable amounts of Ba (Koppi et al. 1996).

7.5.5 Other minerals

Zircons, which contain HREE-enriched zones, can be found in saprolite samples and show no signs of supergene alteration. Fractured zircon crystals are observed breaking into smaller fragments but are otherwise resistant to weathering.

REE-bearing minerals such as fluorite and apatite, which occur in bedrock samples, were not found in any of the samples studied and it is therefore assumed they have fully dissolved in the weathered profile.

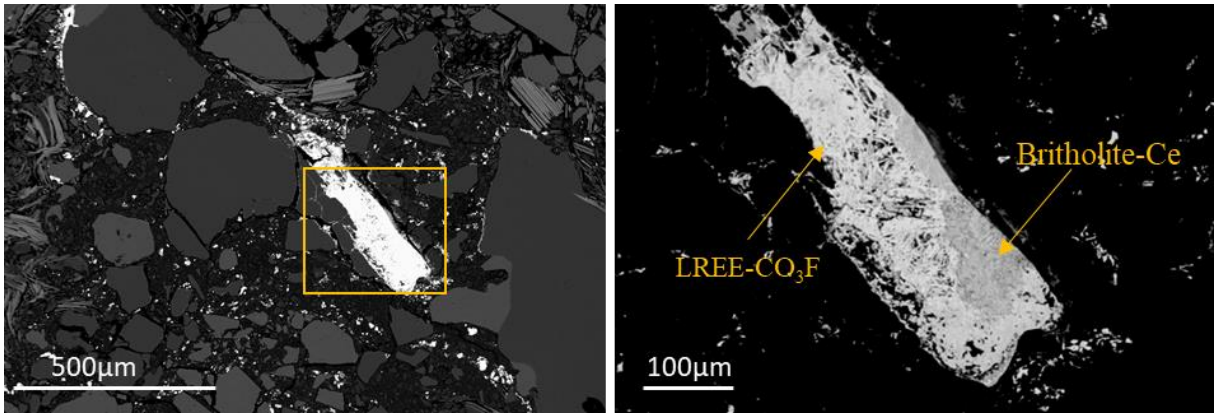


Figure 7.36. Britholite minerals intergrown with LREE-fluorcarbonates in lower saprolite sample SV6.1 from drill core DDH0161.

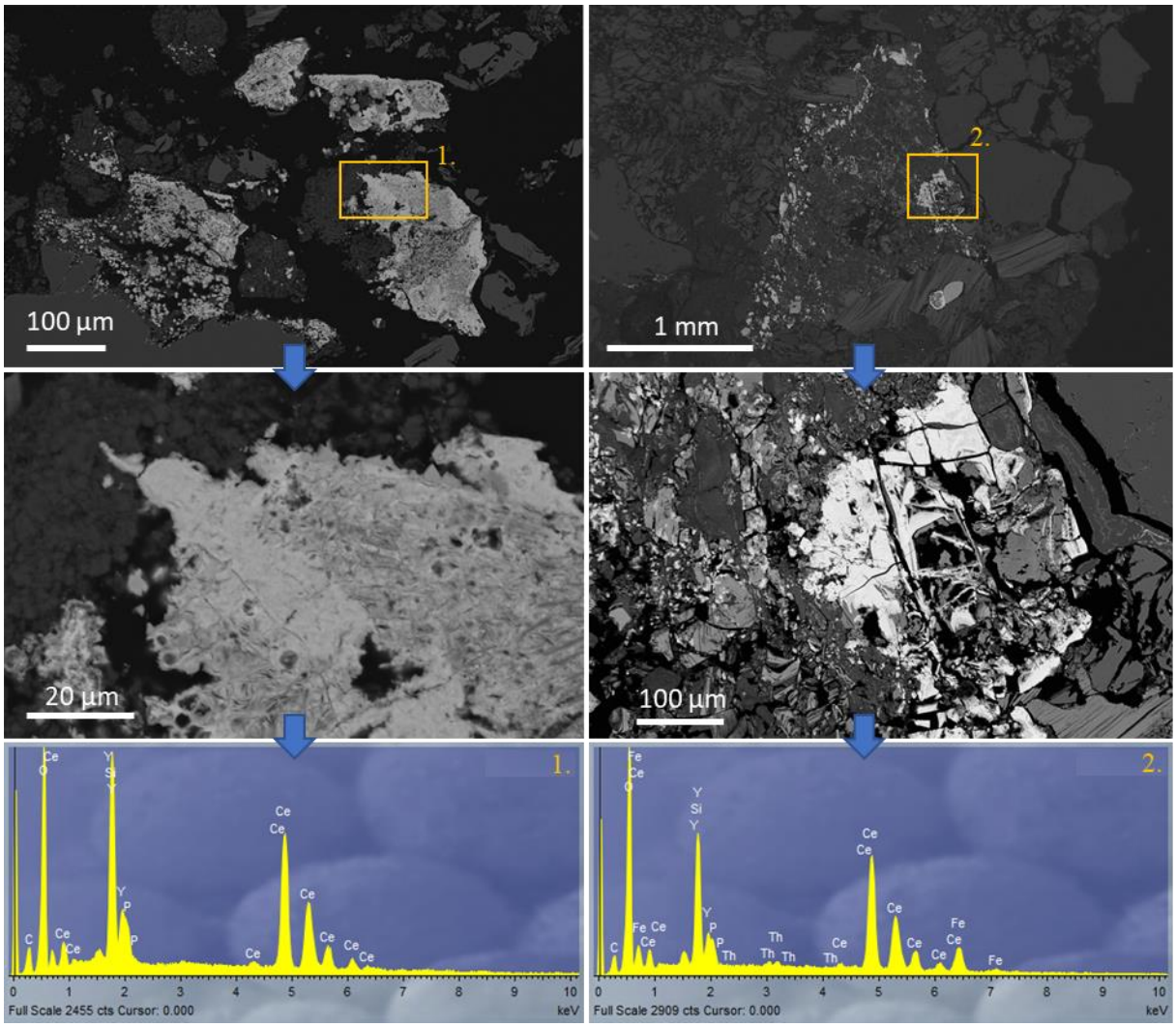


Figure 7.37. SEM-BSE images and EDS spectra of Ce-silicate minerals found in the upper-most part of the saprolite (sample SV5.1), with minor Y-phosphate also present.

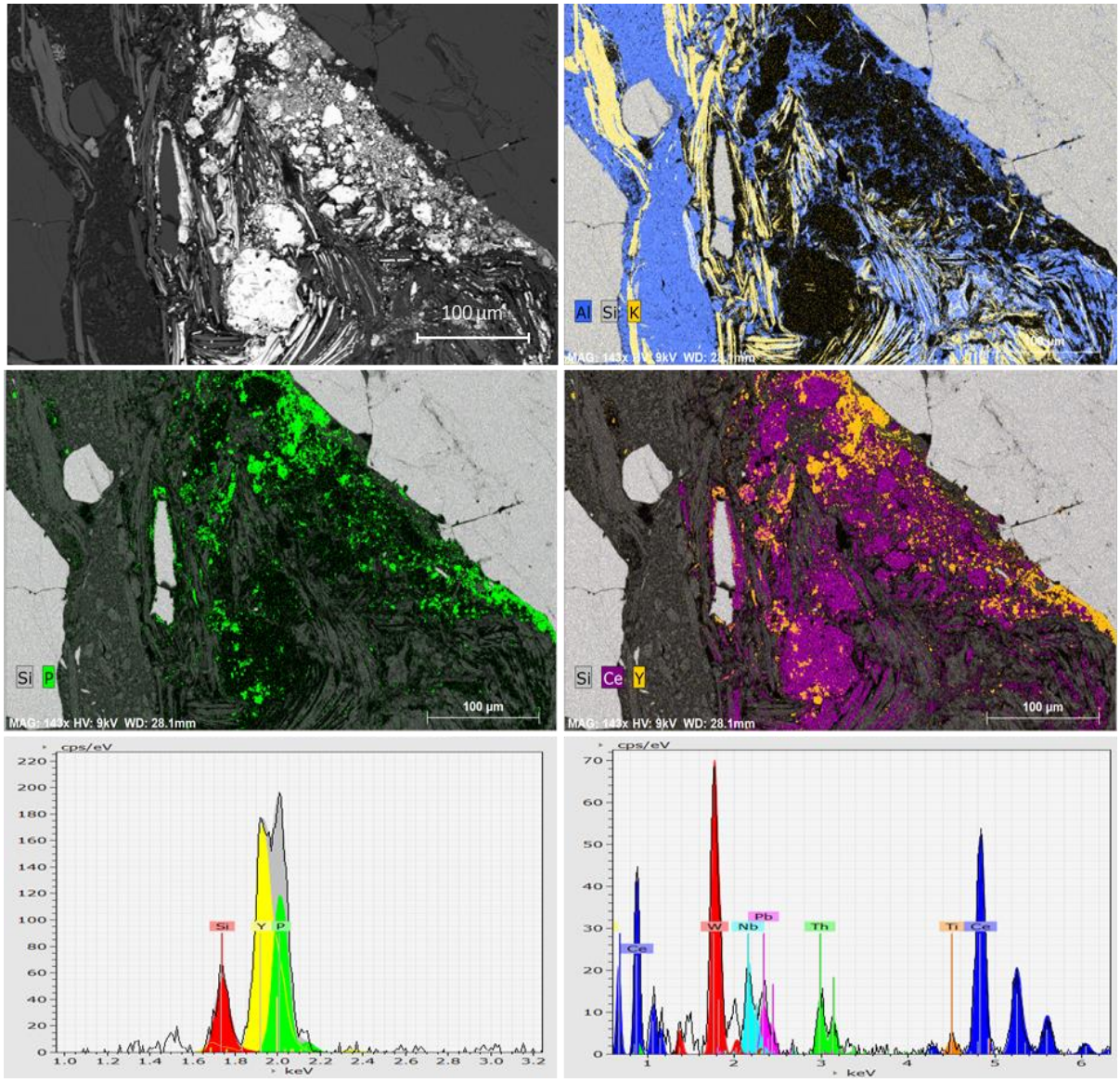


Figure 7.38. SEM-BSE image, element maps and EDX spectra showing Ce oxide and Y-phosphate clusters occurring in transition zone samples from DDH0161 (SV5). The left EDX gives a representative composition of green phosphate patches (left, middle panel; note that the Si content originated from the background content), and the right EDX gives the representative composition of purple Ce patches (right, middle panel).

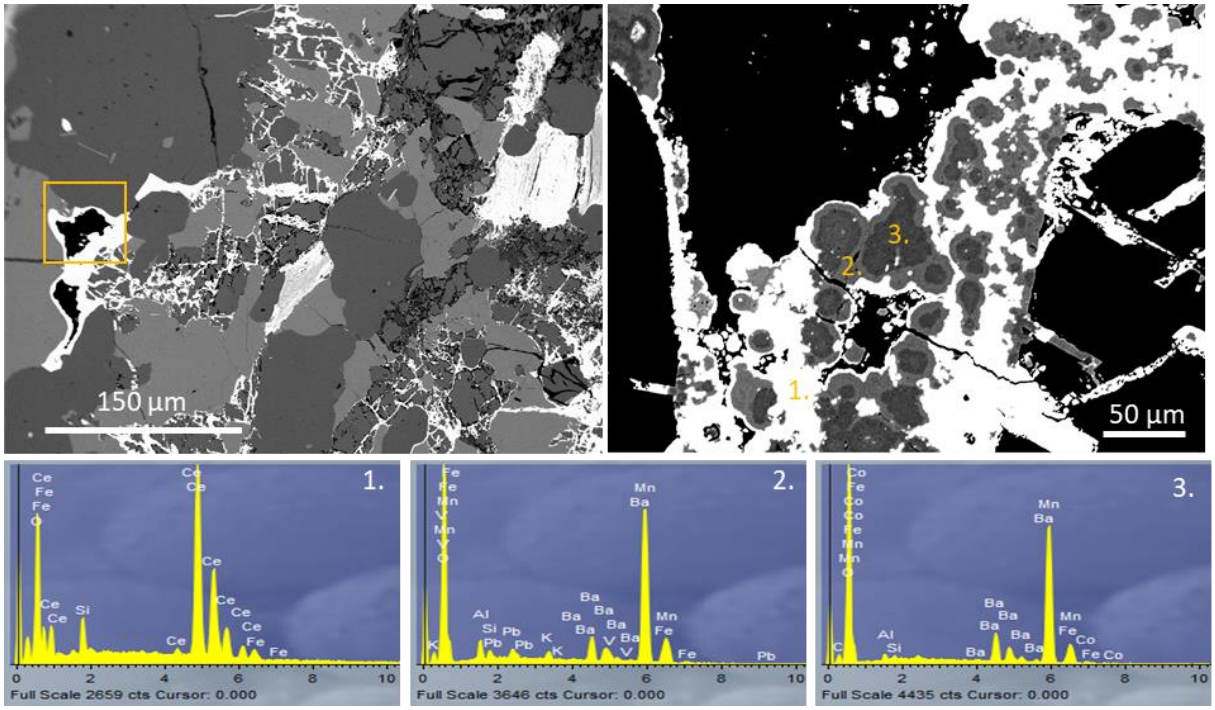


Figure 7.39. SEM-BSE images of Ce oxides associated with botryoidal Ba-Mn oxides (psilomelane) from DDH0099.

Table 7.6. Representative EMP analyses of phosphates, niobiates and Ce minerals from saprolite samples.

	Mineral	Xenotime-Y			Monazite-Ce	REE-Niobiates						Ce-Y-Silicates					
	Sample	SV6.2	SV6.2	SV8.2	SV6	SV6.2	SV6.2	SV6.2	SV6.2	SV8.2	SV8.2	SV8.2	SV6.2	SV6.2	SV6.2	SV8.2	SV6.2
	Analysis No.	PX-26	PX-28	PX-29	PM-103	Nb123	Nb125	Nb127	Nb134	Nb140	Nb143	CY-54	CY-50	CY-34	CY-30	CY-53	CY-35
F	wt %	6.61	5.82	6.61	0.70	0.42	0.48	<dt	<dt	<dt	<dt	3.79	3.09	2.78	2.61	3.60	2.21
P_2O_5	wt %	25.7	25.4	25.7	23.4	<dt	<dt	0.45	<dt	0.29	0.30	3.30	3.03	2.60	2.71	2.92	2.44
SiO_2	wt %	0.36	0.94	0.36	2.69	4.75	2.74	3.40	2.71	12.36	4.13	15.79	16.19	17.41	17.88	18.29	19.19
Al_2O_3	wt %	<dt	<dt	<dt	0.53	0.07	0.23	0.51	0.36	0.60	0.11	0.30	0.66	0.40	0.51	0.47	0.42
CaO	wt %	0.59	0.66	0.59	1.86	0.83	1.97	0.55	0.99	0.32	1.75	0.57	0.39	0.32	0.25	0.42	0.48
Na_2O	wt %	<dt	<dt	<dt	<dt	<dt	<dt	<dt	<dt	0.16	0.08	<dt	<dt	<dt	<dt	<dt	<dt
Nb_2O_5	wt %	<dt	<dt	<dt	0.28	39.3	46.4	30.8	40.3	44.9	45.0	0.34	0.33	0.31	0.36	0.98	0.16
Ta_2O_5	wt %	<dt	<dt	<dt	<dt	1.31	1.11	1.30	1.78	2.07	2.91	<dt	<dt	<dt	<dt	<dt	<dt
TiO_2	wt %	<dt	<dt	<dt	0.80	0.57	0.83	1.47	2.44	3.12	1.92	0.12	0.42	0.20	0.27	0.15	0.25
FeO	wt %	0.07	0.09	0.07	0.26	3.75	8.39	12.02	9.67	19.86	9.85	0.14	3.57	0.96	1.07	0.31	1.50
MnO	wt %	<dt	<dt	<dt	<dt	0.08	1.23	0.85	0.67	0.13	0.43	<dt	0.09	<dt	<dt	<dt	<dt
BaO	wt %	0.12	0.11	0.12	<dt	<dt	<dt	0.10	<dt	0.61	0.21	<dt	<dt	<dt	<dt	<dt	<dt
Th_2O	wt %	<dt	<dt	<dt	2.46	1.42	0.19	0.42	1.68	0.11	0.69	5.14	3.05	3.27	1.09	4.46	1.13
U_2O	wt %	0.38	0.26	0.38	<dt	<dt	0.35	0.79	0.81	2.94	<dt	1.52	1.88	1.79	1.80	0.98	1.56
Y_2O_3	wt %	53.2	51.5	53.2	3.23	13.41	10.78	1.17	3.22	0.80	6.84	11.3	13.5	12.8	13.2	11.5	11.2
La_2O_3	wt %	<dt	<dt	<dt	11.99	0.58	0.64	0.25	0.37	0.40	0.12	1.27	0.76	<dt	0.20	0.26	<dt
Ce_2O_3	wt %	<dt	0.04	<dt	20.3	9.18	4.91	32.41	20.53	2.14	9.63	43.6	37.6	43.0	42.6	42.2	46.9
Pr_2O_3	wt %	<dt	<dt	<dt	3.34	0.30	0.55	0.13	0.28	<dt	0.31	0.20	0.26	<dt	0.15	<dt	<dt
Nd_2O_3	wt %	<dt	<dt	<dt	11.73	1.46	2.57	0.59	1.13	0.29	1.69	0.85	0.86	0.36	0.51	0.33	0.36
Sm_2O_3	wt %	<dt	0.07	<dt	2.16	0.82	1.59	0.24	0.58	<dt	1.18	0.12	0.36	0.24	0.24	0.08	0.20
Gd_2O_3	wt %	<dt	<dt	<dt	1.23	1.23	2.04	0.40	0.90	0.16	0.90	<dt	0.64	0.54	0.56	<dt	0.64
Tb_2O_3	wt %	0.15	0.19	0.15	0.19	0.38	0.50	0.11	0.24	<dt	0.41	0.17	0.25	0.22	0.26	0.17	0.22
Dy_2O_3	wt %	2.14	2.27	2.14	0.74	3.05	3.40	0.67	1.66	0.25	2.98	1.16	1.77	1.50	1.63	1.27	1.48
Ho_2O_3	wt %	0.73	0.77	0.73	0.15	0.77	0.72	<dt	0.28	<dt	0.53	0.36	0.46	0.41	0.44	0.37	0.30
Er_2O_3	wt %	2.74	2.93	2.74	0.37	2.17	1.81	0.41	0.81	0.26	1.58	1.15	1.32	1.07	1.38	1.29	0.88
Tm_2O_3	wt %	0.36	0.36	0.36	<dt	0.30	0.21	0.09	0.10	<dt	0.17	0.16	0.20	0.18	0.21	0.17	0.14
Yb_2O_3	wt %	2.10	2.18	2.10	0.41	2.15	1.38	0.32	0.66	0.20	1.06	1.17	1.34	1.21	1.63	1.27	0.95
Lu_2O_3	wt %	0.40	0.34	0.40	<dt	0.19	<dt	<dt	<dt	<dt	0.09	0.16	0.20	0.17	0.22	0.13	0.12
Total	wt %	95.7	94.0	95.7	88.8	88.5	95.0	89.4	92.2	91.9	94.9	92.7	92.2	91.7	91.7	91.6	92.8
REE	wt %	8.6	9.2	8.6	52.6	22.6	20.3	35.6	27.5	3.7	20.7	50.4	46.1	48.9	50.0	47.5	52.2
REY	wt %	61.8	60.6	61.8	55.8	36.0	31.1	36.8	30.8	4.5	27.5	61.7	59.5	61.7	63.2	59.1	63.5

7.6 REE-Mineral Abundances in the Clay Fraction

7.6.1 SEM-BSE imagery

Representative SEM-BSE images of the surfaces of the saprolite CSF pressed discs are presented in Figure 7.40. The BSE images show that these samples contain variable amounts of bright phases which SEM-EDS analysis confirms are mostly REE-minerals. Although it is not possible to obtain pure mineral compositions due to the fine nature of the grains, the SEM-EDS analysis results suggests the minerals include niobiates, fluorcarbonates, and phosphates (Appendix E1).

The CSF samples with the highest concentration of bright REE phases are CS7 and CS14. In SEM-BSE images, hundreds of fine bright grains are found distributed throughout the imaged areas, the majority of which are LREE-fluorcarbonates (Figure 7.40). In comparison, the CSF samples CS9, CS11, CS12 and CS13 contain relatively few REE-minerals. The SEM-BSE images show only a handful of bright grains, which are coarser than those in CS7 and CS14. These are mainly phosphates and niobiates.

The SEM-BSE images also enable assessment of the quality of the CSF separates; they show that separation was not perfect as some coarser fragments managed to pass into the < 2 micron fraction. CS12 contains the greatest number of coarse fragments, some up to 20 microns in diameter (Figure 7.40). It is likely that coarse fragments were entrained during decantation of the centrifuged solution, which contained suspended clays that were separated from the coarser size fractions.

7.6.2 REE-mineral maps

Mineral maps were produced for two samples: three maps for CS7 and three maps for CS14 (Figure 7.41, Figure 7.42, and Appendix E2). No mineral maps were produced for other CSF samples as the REE grains were too scarce and scattered to obtain representative images.

Maps of both samples show that La-rich and Y-rich grains are present. No Ce-dominant minerals were found. The SEM-EDS spectra suggest that the majority of the La-rich grains are LREE-fluorcarbonates, and that the Y-rich grains are mainly Y-phosphates.

In each mineral map ~500 REE-rich grains (excluding 1 pixel size grains) were identified. Abundance calculations show that, altogether, the mapped REE grains account for 1.7 vol. % and 1.3 vol. % of samples CS7 and CS14 respectively. La-rich grains are significantly more

abundant (1.33 ± 0.43 vol% and 1.75± 0.46 vol% in CS7 and CS14 respectively) than Y-rich grains (0.37 ± 0.13 vol% and 0.47 ± 0.2 vol%).

Grain size distributions for each mineral map are presented as histograms (see Figure 7.41, Figure 7.42). The size distributions show that, excluding the 1 px data, La-rich grains have a mean diameter of 0.50 μm in CS7 and 0.72 μm in CS14, and that Y-rich grains have mean diameters of 0.45 μm in both CS7 and CS14. In both samples, > 90 % of REE-rich grains are < 1 micron across, and 50 % are < 0.5 micron across.

The grain size histograms for each grain type show that larger grains account for the majority of the calculated total REE mineral volume percent. In CS7, 66 % of the area covered by La-rich grains is taken up by grains that are > 0.5 μm in size. In sample CS14, where the overall REE-grain size is higher, the coverage is 84 % for > 0.5 μm. The histograms also show that 1 px grains have elevated counts, which may suggest those pixels contain significant noise. Removal of these pixels from the abundance estimates does not significantly affect the results as the area covered by 1 px grains is < 1 % of the total grain coverage.

7.6.3 Proportion of REE held in resistant and supergene minerals

7.6.3.1 Phosphates

The majority of phosphates found in bulk and CSF samples occur as REE-phosphate minerals, so the measured phosphate content in the bulk sample can be used to estimate their abundance. To estimate the proportion of REE residing in phosphate minerals, the REE composition is assumed to fall between the ideal composition of monazite and xi.

The estimates include the phosphate present in other accessory minerals such as britholite (Table 7.7). Therefore, the REE residing in phosphate minerals are slightly over-estimated. However, due to the scarcity of britholite in the samples, and the trace phosphate content in these minerals, this error is considered insignificant.

The P_2O_5 content in the samples studied ranges from 0.2 to 0.9 wt % in bulk samples and 0.2 to 0.14 wt %. Yet the calculated proportion of REE held in phosphate minerals ranges widely from 4 to 67 wt % in bulk rock and 2 to 73 % in the CSF. The large variation is attributed to the large differences in REE concentrations of the samples. Overall, samples with high total REY grades (> 0.7 wt %) have significantly fewer REE residing in phosphates compared to samples with low total REY grades (< 0.25 wt %; Table 7.7). This is illustrated by the contrasting phosphate REE residency of samples CS14 and CS11, which have similar bulk

phosphate contents. The amount of REY held in phosphates is therefore dependent on the amount of phosphate in the sample and the total content of REE in the saprolite.

Table 7.7. Estimates of total REY (REE+Y) residency in phosphates for the bulk samples of the saprolite, and corresponding clay size fraction separates.

	Bulk sample geochemistry		$REEPO_4$ REE residency			CSF sample geochemistry		$REEPO_4$ REE residency	
Samples	P_2O_5 wt%	REY wt %	REY wt %	%	Samples	P_2O_5 wt%	REY wt %	REY wt %	%
SV14	0.03	1.286	0.051	4%	CS14	0.07	2.64	0.120	5%
SV7	0.02	0.794	0.034	4%	CS7	0.02	1.83	0.034	2%
SV9	0.02	0.714	0.034	5%	CS9	0.03	1.284	0.051	4%
SV6	0.03	0.366	0.051	14%	CS6	0.14	1.57	0.239	15%
SV12	0.02	0.167	0.034	20%	CS12	0.05	0.323	0.086	26%
SV11	0.03	0.182	0.051	28%	CS11	0.03	0.173	0.051	30%
SV10	0.09	0.244	0.154	63%	CS10	0.04	0.194	0.068	35%
SV13	0.09	0.231	0.154	67%	CS13	0.13	0.306	0.222	73%

$REEPO_4$ composition between monazite and xenotime REE_2O_3 = 65 wt % P_2O_5 = 35 wt %

7.6.3.2 REE-fluorcarbonates

The proportion of REE held in REE-fluorcarbonates within clay separates sample CS14 and CS7 were calculated using the modal abundance estimates from section 7.6.2. Modal vol % abundances from the mineral maps were converted to wt % of abundance, using bastnäsite mineral density (4.9 gcm^{-3}) and the known weight and volume of the clay disk, before calculating the REE residency.

Calculations show that both CS14 and CS7 contain significant proportions of REE locked in supergene fluorcarbonates, at 64 ± 16 % and 67 ± 22 % respectively (Table 7.8). The large range is due to the differences in La-rich vol % between the three mineral maps for each sample. Mapping more samples, or larger areas would improve the estimates.

The abundance of REE-fluorcarbonates were not estimated for bulk saprolite samples. However, the preferential partitioning of REE into fine fraction (high DFx index, see Table 7.3) means that the results in the CSF are representative of the bulk saprolite residence.

Table 7.8. Calculated estimates of total REE (REY) residency in fluorcarbonates for the mapped CSF samples of the saprolite.

	CSF sample mineral abundance and geochemistry					$REECO_3F$ REE residency		
Samples	$REECO_3F$ vol%	STDV	$REECO_3F$ wt%	STDV	REY wt %	REY wt %	%	STDV
CS14	1.75	± 0.69	2.58	± 0.67	2.64	1.68	64%	± 16%
CS7	1.30	± 0.43	1.90	± 0.66	1.83	1.24	67%	± 22%

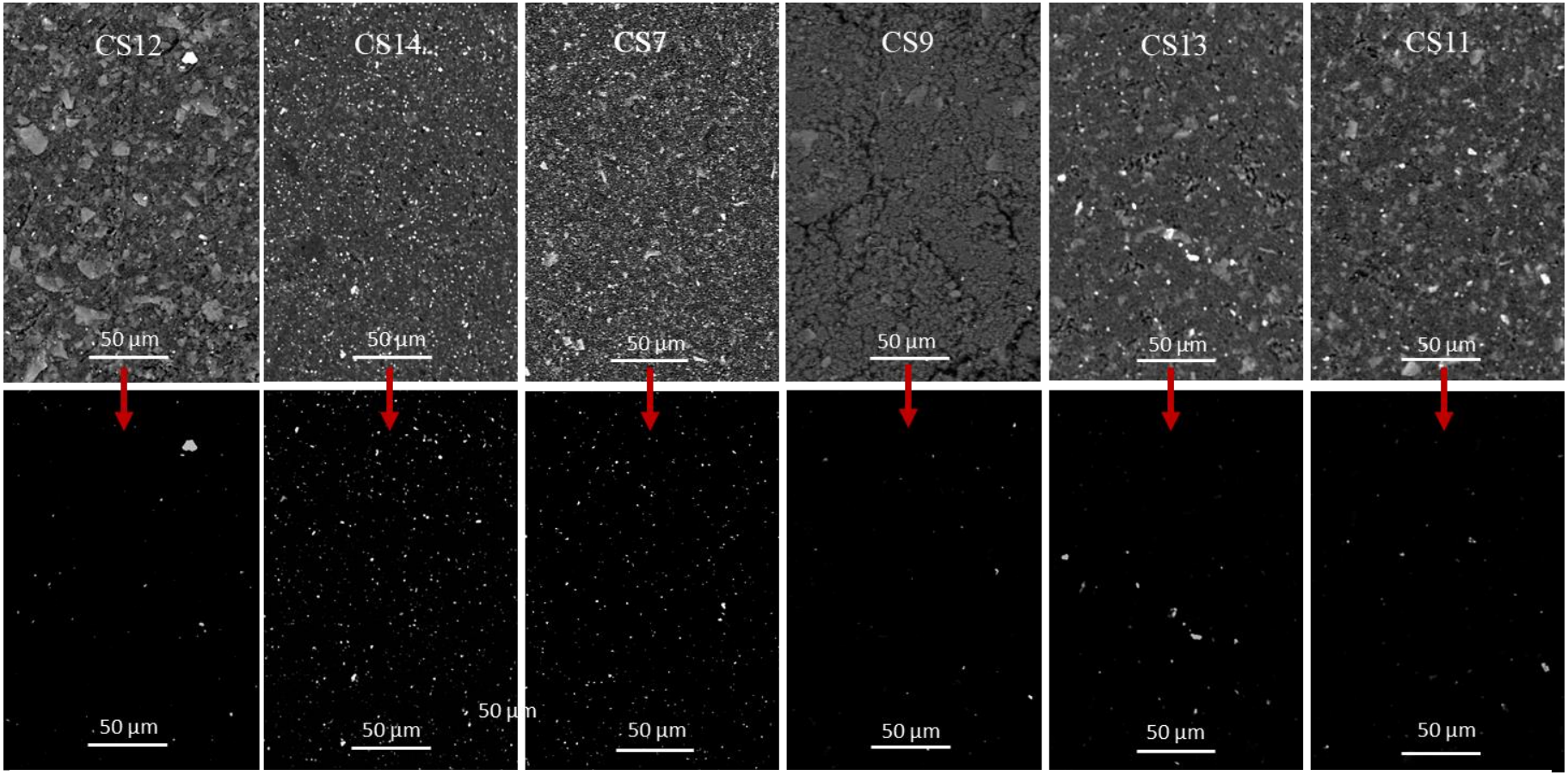


Figure 7.40. Representative SEM-BSE images of CSF samples from the saprolite. Upper image unmodified. Brightness and contrast adjusted in lower images to highlight bright phases.

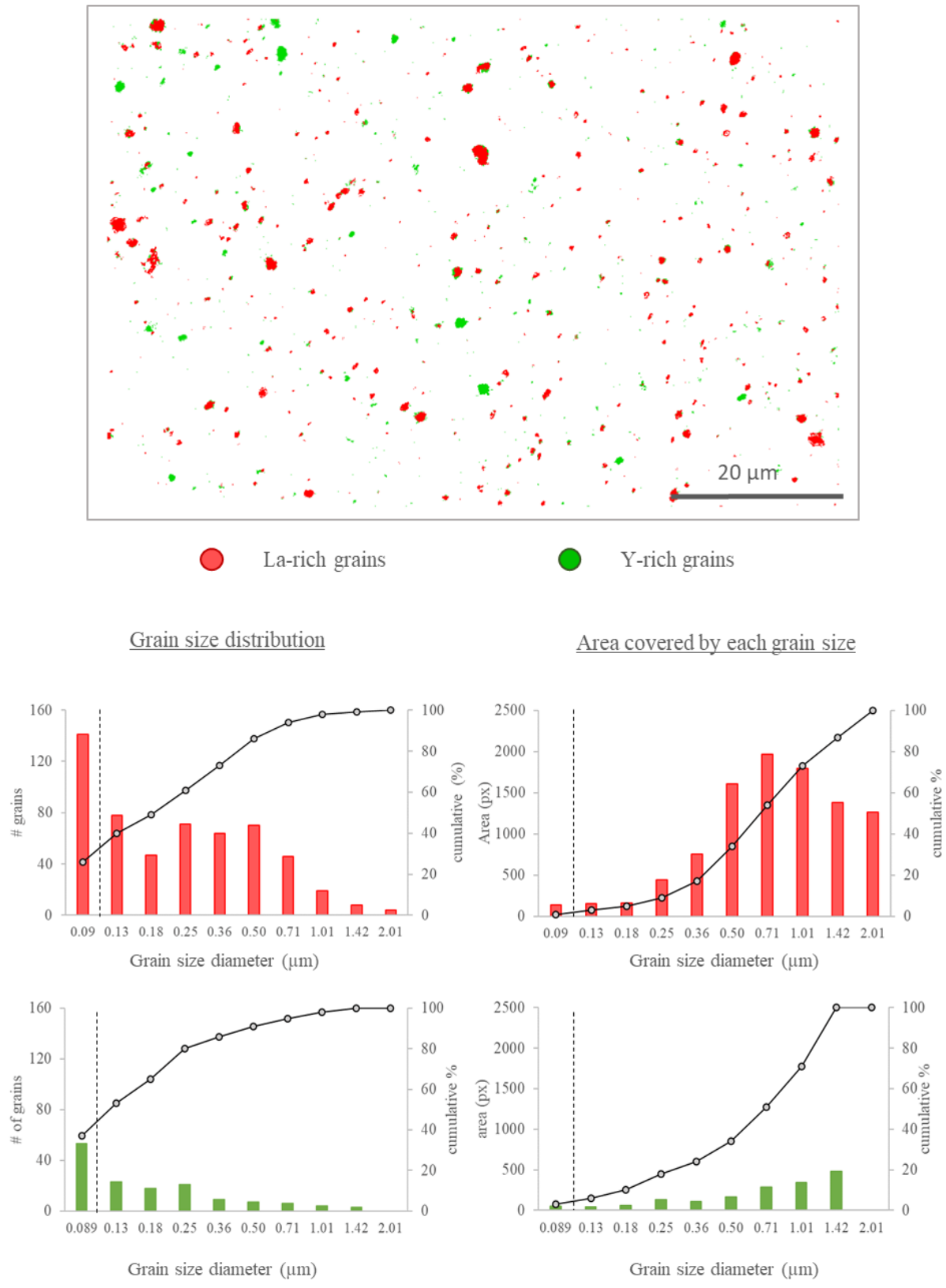


Figure 7.41. Mineral maps and grain size distribution analysis of La-rich and Y-rich mineral grains present in CS7. The mineral map was produced from SEM-EDS element maps (conditions and pixel size).

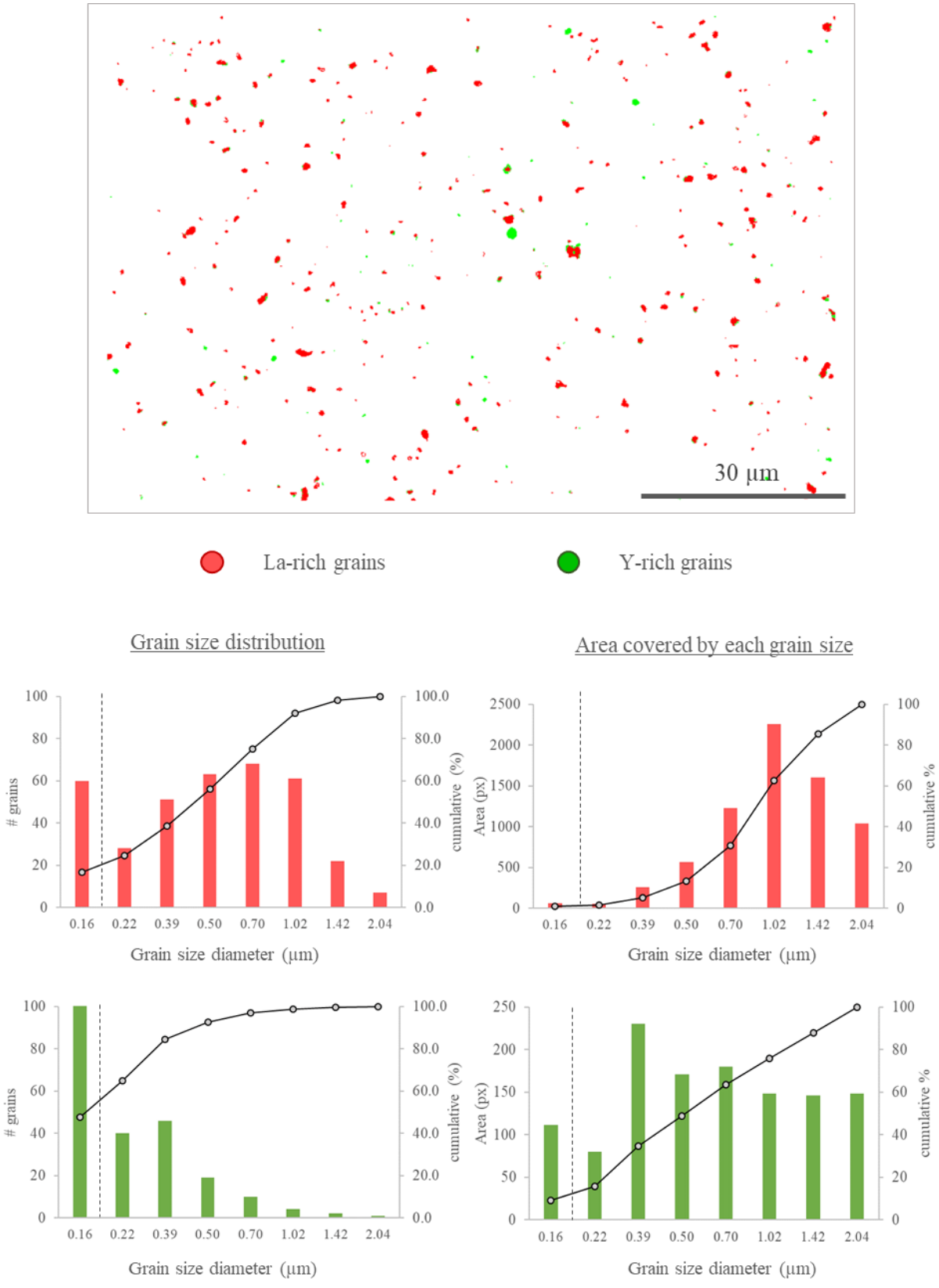


Figure 7.42. Mineral maps and grain size distribution analysis of La-rich and Y-rich mineral grains present in CS7. The mineral map was produced from SEM-EDS element maps (conditions and pixel size).

7.7 Discussion

7.7.1 Chemical and mineral characteristics of the saprolite ore horizon

Samples from six drill holes were selected from the most REE-enriched section of the saprolite to create a detailed picture of the vertical and lateral variations within the ore zone. The principal mineralogy of all saprolite samples is kaolinite, K-feldspar, biotite and quartz. All have low phosphate (< 0.1 wt % P_2O_5) and low radioactive element contents of Th (< 150 ppm) and U (< 15 ppm). The REE in of the bulk saprolite samples studied have concentrations that range widely between 0.17 wt % and 2.19 wt % REY and are preferentially concentrated in clay size fractions (DFx = 1.33 to 2.05). The preferential concentration of REE in clay size fraction confirms that the REE in the Serra Verde profile are hosted in clay minerals, and/or fine-grained REE-mineral bearing minerals. All samples show an enrichment in LREE and strong negative Ce anomalies.

Kaolinite is the most abundant clay mineral. Smectite is also present in some samples, which is detectable in the CSF. Only DDH0099 contains smectite as a main mineral. The dominant clay minerals available for REE adsorption are therefore limited to kaolinite, and perhaps smectite where present.

Kaolinite in the most REE-enriched part of the saprolite is interpreted to derive from the breakdown of Na-feldspar, which is entirely absent in the saprolite samples, as well as some biotite and K-feldspar which show signs of marginal mineral break down in SEM imagery. Bedrock with higher primary plagioclase contents are therefore more favourable for forming kaolinite-rich saprolite where the REE are most enriched. XRD patterns for the vertical saprolite profile show that clay content increases from the base to the top, coupled with a decrease in biotite crystallinity, and that K-feldspar and biotite are not fully broken down until the transition zone.

The smectite found in some samples is probably derived from the incomplete weathering of biotite in the saprolite, and has been linked to locally higher concentration of Na and Mg in a restricted percolating fluid (Fordham 1989). The elevated content of smectite in DDH0099 may have been a product of locally poorer drainage where this profile developed.

Quartz and K-feldspar are the least weathered due to their higher chemical resistance. The bulk geochemistry corroborates that K-feldspar is not breaking down in the saprolite; increases in

Ba, Rb, and Cs indicate that the abundance of K-feldspar has been increased as a residual phase in the saprolite.

REY-enriched saprolite samples from different drill holes show that the saprolite is laterally variable. The mineralogically and geochemically variation fall into three main groups;

Group 1 includes saprolite samples from DDH0161, DDH121 and DDH0266. It is characterised by low P concentrations, low LOI, strongly fractionated REE, and relatively higher DFx values (1.94 – 2.33) for the CSF. This REE-enriched part of the saprolite has experienced a moderate degree of mineral weathering of biotite and K-feldspar, which exhibit more intense XRD peaks than kaolinite.

Group 2 includes saprolite samples from DDH0096 and DDH0061. It is characterised by high P concentrations, high LOI, low Si, low K, moderately fractionated REE and relatively lower DFx values for the CSF. This REE-enriched part of the saprolite has experienced a high degree of mineral weathering of biotite and K-feldspar, which exhibit less intense XRD peaks than kaolinite.

Group 3 includes only the saprolite samples from DDH0099, is characterised by high Mg and REY concentrations, low P concentrations, and has experienced a high degree of mineral weathering with kaolinite and smectite as the dominant minerals.

It is evident that the saprolite geochemistry and mineralogy varies significantly, both vertically and laterally. This variation has important controls on the distribution and residence of REE in the saprolite.

7.7.2 REE distribution and mineral residence

In the granite, primary weathering-resistant minerals occur in grain sizes of tens of microns to several 100 microns in size. However, due to their fractured and metamict state, they break down into progressively smaller grains in the saprolite, occurring in fragments down to the single micron level. This fragmentation is most pronounced in the phosphates and niobiates, which can be found in the CSF. Very few zircon crystals are found in the CSF as the majority of fragments remain larger than < 2 μm. In the saprolite, broken up grains remain in clusters until they are dispersed, most likely by mechanical reworking from the internal strain identified in chapter 6. The break-up and disaggregation of these minerals leads to their concentration in the fine fraction, and therefore these phases cannot be separated from clays by sieving. The

REE held in these minerals remain locked-up and are unavailable for adsorption onto clays in the saprolite or incorporation into secondary REE-phases.

Fine-grained phosphates, which are found in addition to the resistant primary phosphates, most commonly occur between the upper saprolite and transition zone of DDH0161. The majority of phosphates are Y- and Ce-phosphates, in contrast to the monazite-La found in the bedrock. These REE-phosphates are concluded to be secondary due to their morphology (very fine, anhedral, amorphous) and their pseudomorphic habits, indicated that they have most likely formed from the breakdown of britholite and apatite, which are notably absent from the middle and upper saprolite horizons. No secondary apatite was observed in the samples studied, implying that secondary REE-phosphate formed from the breakdown of these primary minerals. Other studies have noted how the breakdown of apatite results in the formation of hydrated relatively insoluble supergene phosphates, linking with the strong affinity between phosphate and REE concentrations in solution (Banfield and Eggleton 1989, Braun et al. 1993, Laveuf and Cornu 2009, Köhler et al. 2005).

Cerium residence along the saprolite and transition zone horizons of drill hole DDH0161 varies systematically. In the lower saprolite, britholite-(Ce) is the dominant Ce phase, occurring as amorphous masses and grain sizes up to 300 microns; because this is also found in the bedrock samples it is interpreted as an inherited phase. Samples collected up through the profile above the saprolite track the gradual breakdown of britholite into secondary minerals. In the middle saprolite, britholite-(Ce) is observed breaking down into rhabdophane-(Y), rhabdophane-(Ce), and cerite. In the upper saprolite cerianite first appears as a breakdown product of cerite. Part of this Ce may also be sourced from nearby reprecipitation LREE-fluorcarbonates to explain their increasingly negative Ce anomaly. In the transition zone, rhabdophane-(Ce) and cerite are the main Ce phases. Supergene Ce-phosphates (rhabdophane) and Ce oxides are very stable in weathering profiles and therefore do not undergo further mobilisation (Braun 1990). Unlike LREE-fluorcarbonates, Ce-silicates and Ce-oxides do not appear to be mobilised through dissolution and reprecipitation process, but remain in-situ until they are physically dispersed.

The REE breakdown pathway from both britholite-(Ce) to Ce oxide, and from rhabdophane and primary bastnäsite-(Ce) to bastnäsite-(La) and Ce oxide, account for the negative Ce-anomalies observed in other supergene REE-minerals. The fractionation of Ce from the other REE, evident in both the bulk geochemistry and mineralogy, is simply explained by a change in the oxidation state of Ce^{3+} to Ce^{4+} (see chapter 6).

7.7.3 Occurrence and composition of supergene REE-fluorcarbonates

Detailed analysis of the samples from Serra Verde has led to the discovery of supergene fluorcarbonate phases forming in the saprolite ore, which have not previously been reported. These supergene REE-fluorcarbonates can be distinguished from primary fluorcarbonates by their negative Ce anomalies, smaller grain size, and their close intergrown occurrence with clays. The supergene species found are La-dominant, exhibit large negative Ce-anomalies, and have lower Ca and Th concentrations, in contrast to the Ce-dominant species in the bedrock. The negative Ce-anomaly indicates that the fluid from which the supergene REE-fluorcarbonates are precipitating are poor in Ce and Th. This is indicative of a fractionation process of Ce and Th separating from other REE begins to take place in the saprolite horizon.

LREE fluorcarbonates have been observed before in weathered granites (Styles and Young 1983, Hughes and Brown 1977, Sanematsu and Kon 2013) but they have been given little attention and their composition has not been studied. This is partly due to their low abundance, micron-scale grain size, and the assumption that they represent relict traces of the fluorcarbonates from the bedrock. The compositions and morphologies of the fluorcarbonates present in the saprolite, compared to those present in the bedrock (chapter 5) shows that this is not the case at Serra Verde.

SEM-BSE images taken from samples capture the dissolution, mobilisation, and recrystallisation of REE-fluorcarbonates in the weathered profile. A recurring reprecipitation process is proposed to have produced the progressively smaller grains, which dispersed the REE throughout the volume of the weathering profile, and may be associated with an increasingly negative Ce-anomaly as more Ce was being locked out of the supergene REE-fluorcarbonates. The occurrence of these minerals as nm-scale grains in small clusters is closely associated with areas of high clay mineral contents, matching white patches in hand samples. This association may indicate that the formation of the secondary REE-fluorcarbonates is occurring where the fluid is being buffered by feldspar weathering to clays.

Supergene REE-fluorcarbonates are ubiquitous in the saprock samples, but are variably present in the saprolite samples, and are entirely absent from the transition zone samples. In some saprolite samples the absence or traces of REE-fluorcarbonates suggest dissolution of these minerals has occurred (DDH0099, DDH0096, DDH0061). However, in two saprolite samples with the some of the highest REE grades (DDH0161, DDH0266), LREE-fluorcarbonates were found in abundance, occurring in fine veinlets. Together, this indicates that fluorcarbonates

began to form in the saprock, became enriched or dissolved in the lower saprolite due to dissolution-precipitation processes, and were completely dissolved in the upper saprolite (see summary Figure 7.43). There has been no work on the formation of LREE-fluorcarbonates at ambient pressures and temperatures. The recognition of these minerals at Serra Verde has implications for IADs, because the simple dissolution model for their enrichment into clays may not take into account the formation of other secondary phases. An investigation of the behaviour and stability of these supergene REE-minerals should therefore be the focus of further study.

Factors controlling the differences in supergene REE-fluorcarbonates occurrence in the saprolite are unclear, but two possible hypotheses are proposed here based on the data from this study:

1. The samples with higher fluorcarbonates content are less weathered, have lower clay contents, and therefore have a lower adsorption capacity for REE, which causes an excess of REE to precipitate in this form.
2. The saprolite has laterally variable physiochemical conditions, such as pH and Eh, that causes preferential formation of REE-fluorcarbonates rather that adsorption by clays in some regions of the weathering profile.

The nature of these supergene fluorcarbonates as relatively small grains at low absolute abundances in bulk samples precludes their detection by SEM or XRD. Similarly, their light element composition prevents the recognition of these species in bulk geochemistry.

Further work in understanding the controls on the formation of REE-fluorcarbonates under low temperature and pressure conditions is clearly necessary to predict their occurrence in the saprolite of IADs. Key variables to explore may include: the amount of clays and their REE-adsorption capacity, the availability of anions such as F^- and CO_3^{2-}, the dissolved concentration of REE, and the oxidation potential of the fluid.

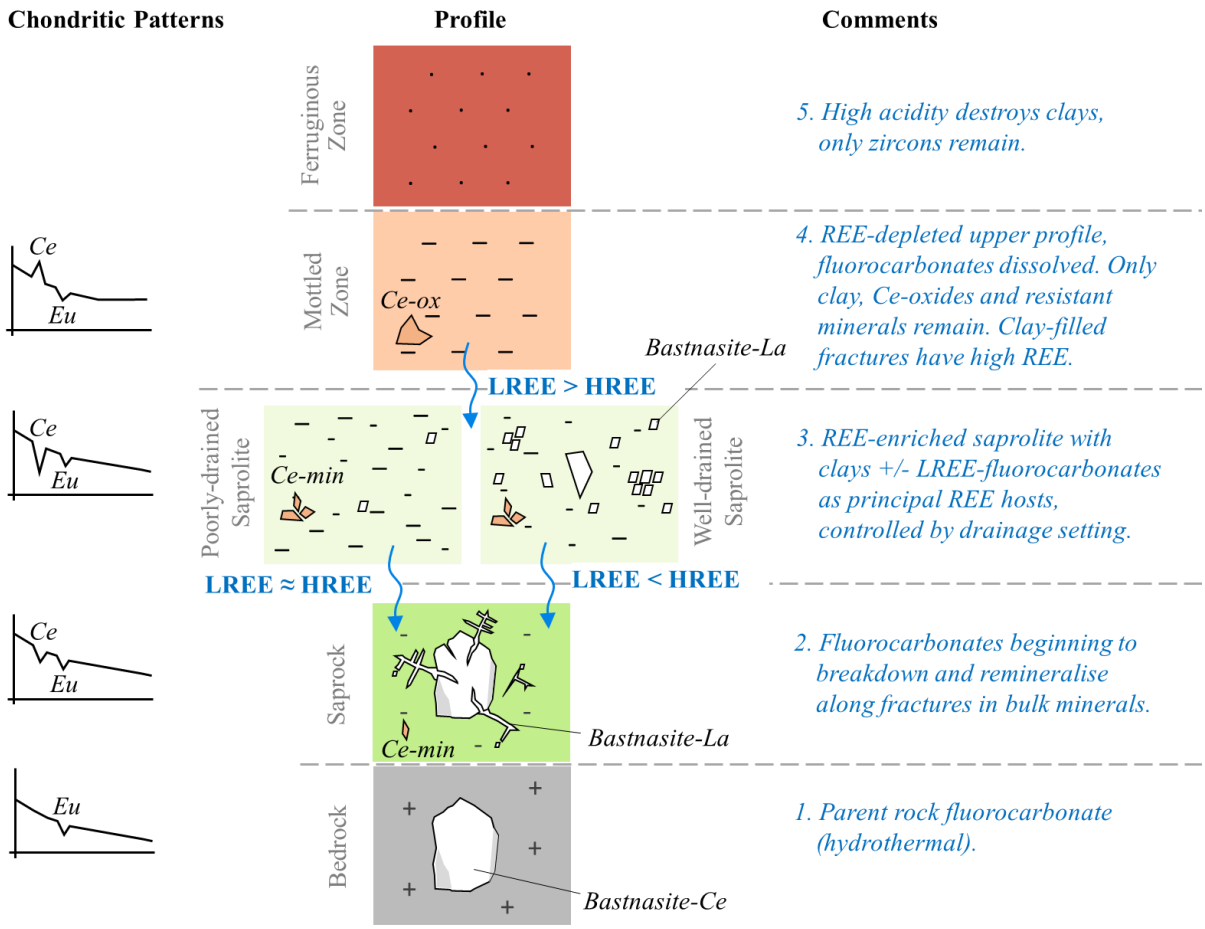


Figure 7.43. Schematic diagram of the occurrence and breakdown of LREE-fluorcarbonates in the different horizons.

7.7.4 Proportion of REE held in resistant and supergene minerals

Determining the proportion of REE held within resistant phases is useful for understanding the pathways that REE are taking in the weathering profile, the processes of enrichment, and the geometallurgical implications for clay leachability.

The calculated amount of REY held in phosphates is correlated the amount of phosphate in the sample, but also the total content of REE in the saprolite. Overall, samples with lower REE content (< 0.7 wt % REY) contain a range of phosphate contents (0.03 – 0.14 wt % P_2O_5), but have a consistently greater residency of REE locked in REE-phosphates (14 – 73 %) than high grade samples (> 0.7 wt % REY). This applies to both the bulk saprolite and CSF of the saprolite. The three samples with > 0.7 wt % REY have consistently < 5 % REY residing in phosphates, but also variable phosphate content (0.02 – 0.07 wt % P_2O_5). Therefore, the phosphate content alone is not a reliable indicator for the fraction of REE residing in phosphate

minerals. The similarity of the phosphate REE residency in the bulk and clay size fraction also indicates that the phosphate REE residency is not sensitive to the size of the mineral grains. Due to this relationship between bulk REE grade and REE residency in phosphates, IADs with lower grades will be more sensitive to phosphate content because a small fraction of resistant phosphate minerals can host a significant fraction of the REE in the ore.Other publications cite phosphate content as a negative control on the enrichment of IAD ores (Sanematsu et al. 2013, Sanematsu et al. 2015, Sanematstu and Watanabe 2016). These secondary phosphates originate from the breakdown of primary apatite and britholite from the bedrock, supporting the finding of Sanematsu et al. (2015) that phosphate-rich granites are unfavourable for the development of IADs.

Very fine-grained LREE-fluorcarbonates were identified in both SEM-BSE imagery and XRD analysis of two high grade saprolite samples, CS7 (0.8 wt % REY) and CS14 (1.3 wt % REY). Due to the small grainsize of fluorcarbonate, their abundance could only be measured in the CSF (1.8 and 2.6 wt % REY in CSF). Estimates from element map analysis show La-fluorcarbonate abundances of 1.30 ± 0.43 % for CS7 and 1.75 ± 0.69 % CS14, which hold the majority of REE in these samples (64 ± 16 % and 67 ± 22 % respectively). Despite the very low abundance of these minerals, the accumulation of supergene fluorcarbonates in the saprolite can lead to a significant fraction of the mobilised REE becoming locked in these minerals. In both samples, less than 5 % REY are held by phosphates, indicating that the formation of either phase can reduce the extractability of REE from IADs. Granites with LREE-fluorcarbonates are still considered favourable for the formation of IADs due to their high weathering susceptibility. However, due to the potential precipitation of secondary LREE-fluorcarbonates, more work needs to be carried out on the stability and conditions for their formation.

These calculations show that REE-fluorcarbonates and REE-phosphates forming or accumulating in the saprolite can host significant fractions of the REE. A relatively high abundance of these phases (> 0.1 wt % P_2O_5 and > 1 % fluorcarbonate) can therefore significantly reduce the amount of REE available for mobilisation and absorption onto clay minerals, and therefore the extractable REE content of the ore. Further mineral quantification work laterally along the saprolite will help to constrain this variability, and the principal controls on REE residency.

7.7.5 Clay-rich fracture fillings

The white to grey-green clay-rich material filling fractures found cutting through the weathered profile are strongly enriched in REE. These fracture fills are the most REE-enriched part of the whole profile and are therefore very important within the Serra Verde deposit.

The REE content of the fracture infill material is similar to the saprolite CSF, with concentrations ranging between 0.4 and 1.2 wt % REY. Fracture fillings hosted in the saprolite are more enriched than those hosted in other parts of the profile, but all fracture fillings are more REE-enriched than their respective host rocks.

XRD analysis shows that the infill material is composed of clay minerals (kaolinite/halloysite and smectites) as well as quartz grains, which is corroborated by the clay-dominant bulk geochemistry and lack of Na, K, and Ca. REE-fluorcarbonates occur in the saprock- and saprolite-hosted infills, whereas phosphate minerals only occur in the saprolite-hosted infills.

The infill material may be due to either precipitation from percolating fluids, mass transport of mineral grains into the fractures by percolating fluids, or in situ weathering of the wall rock into the fracture space. The lack of Zr in the bulk geochemistry indicates that zircon fragments were not transported into the fracture material.

The negative Ce-anomaly of the LREE-minerals found in these fractures suggests they are supergene. Their size and well-developed habits (including radiating hexagonal rhabdophane crystals and bastnäsite rosettes) further indicate that these minerals formed in the fractures instead of arriving through transportation.

These fractures are interpreted to be relatively high permeability conduits for acid meteoric water to percolate, locally producing an enhanced weathering regime at the wall rock interface with strong acid buffering, which caused LREE-minerals to precipitate. Their high REE contents suggest that the REE enrichment is either due to focused flow leading to concentrated REE precipitation, or that the fluid percolating along these fractures is REE enriched, resulting from the leaching of weathered bulk rock material.

7.8 Conclusions

1. The bulk of REE are concentrated in fine fraction of saprolite ore.
2. Differential breakdown of primary REE mineralogy occurs through the weathered profile. LREE-dominant minerals (fluorcarbonates, Ce-silicates) are more susceptible to weathering than HREE dominant phases (zircons, phosphates, niobiates), and contribute to the fractionation of REE in the ore zone.
3. Niobiates and phosphates, which are fractured and metamict in the parent rock, are intensely reworked and broken-down in the saprolite, and become increasingly concentrated in the finer fractions.
4. The liberation of REE from the dissolution of LREE-fluorcarbonates is not a simple process. The breakdown of primary fluorcarbonates can lead to the formation of supergene LREE-fluorcarbonates, which are chemically distinct, and are intimately associated with clay minerals.
5. Clay veinlets are strongly enriched in REE, and are characterised by kaolinite and smectite clays.
6. The proportion of REE held by phosphates in the saprolite is controlled by the REE grade. At bulk grades over 0.7 wt % REY, less than 5 % of REE are hosted in phosphates, while in low grade samples this increases to up to 67 %.
7. In samples containing abundant supergene LREE-fluorcarbonates, calculations show that a significant proportion of the total REE can be held in these minerals.

Chapter 8

Rare Earth Recovery by Ion-Exchange Leaching

8.1 Introduction

Ion-adsorption type deposits are REE-enriched weathered granites in which the majority of the REE exist as positively-charged trivalent ions that are weakly bound to the surfaces of clays. Kaolinite and halloysite are considered to be the main minerals holding the REE in IADs because their small size (< 2 μm), negative charge, and abundance provide a large surface area onto which significant amounts of REE can be accommodated (Yang et al. 1981, Huang et al. 1989, Wu et al. 1989, Murakami & Ishihara 2008). The weak bonding between REE ions and clay minerals facilitates economic processing of this type of low grade ore (0.05 – 0.5 wt % REE_2O_3), currently exploited from IADs in China.

The Serra Verde REE deposit, located in Goiás state of Brazil, is a newly discovered REE deposit that has been classified as an ion-adsorption type because the REEs in the enriched weathered profile are concentrated within the clay size fraction. However, detailed mineralogical work on drill core samples from this deposit have revealed the occurrence of very fine (< 2 μm) secondary REE phases (e.g. REE-fluorcarbonates and REE-phosphates; see Chapter 7) in varying amounts. This indicates that, in some parts of the deposit, a significant proportion of the total REE may not be associated with clay minerals, and therefore may not be readily processable by ion-exchange.

In order to help estimate the proportion of extractable REE (PER) bound to clay minerals in the ore material and to investigate the effect that the secondary REE phases have on the recovery of REE from the Serra Verde REE deposit, a small-scale ion-exchange leaching experiment was carried out.

The results presented in Chapter 6 have also shown that LREE were preferentially enriched in the saprolite ore zone. Previous work by Moldoveanu & Papangelakis (2012; 2013) indicate that LREE are preferentially absorbed by clays. Due to the relative higher economic value of HREE than LREE, it is therefore necessary to measure the relative extractability of these elements from the minerals that compose the Serra Verde ore. As the REE are principally

extracted via a supernatant solution during processing, this experiment also helps to identify impurities and deleterious non-REE that are readily leachable.

8.2 Experimental and Analytical Methods

8.2.1 Experimental samples

8.2.1.1 Sample composition

A total of 11 high grade samples were selected for the leaching experiment, including six bulk saprolite samples (labelled SV), two clay-size saprolite separates (CS), and three samples from clay-rich fracture infills observed cutting through the exposed weathered profiles on the plateau (S; clay veinlets; Table 8.1). These samples were studied in detail in Chapter 7, a summary of their geochemical and mineralogical compositions is presented in this chapter.

The samples selected for this experiment have high REE contents but variable REE mineralogy (see Table 8.1, Figure 8.1, Figure 8.2, and Figure 8.3). The highest-grade samples are the clay separates with concentrations of 1.28 and 1.85 wt % REY, followed by the clay veinlets with concentrations that range from 0.5 to 1.8 wt % REY. The bulk saprolite samples have a broad range of concentrations from 0.15 to 0.8 wt % REY. All samples, with the exception of SV12, have strong negative Ce anomalies.

Table 8.1. List and composition of samples used in ion-exchange experiment. The complete elemental analyses of these samples can be found in Table 7.2, Table 7.3 and Table 7.4.

Sample #	Sample type	Drill hole DDH	Depth (m)	Ca %	Mg %	Na %	K %	P_2O_5 %	REY (ppm)	LREE (ppm)	HREE (ppm)	Y (ppm)	Th (ppm)	U (ppm)	Ce/Ce*	Eu/Eu*	La_N/Yb_N
SV6	bulk saprolite	161	25.5	0.01	0.10	0.17	5.54	0.03	3664	3033	256	375	91.2	10.2	0.78	0.19	15.6
SV7	bulk saprolite	161	26.9	0.04	0.10	0.27	6.72	0.02	7939	6279	667	993	80.3	14.1	0.12	0.20	29.2
SV9	bulk saprolite	99	23.0	0.08	0.66	0.25	4.50	0.02	7139	4575	909	1655	69.7	10.9	0.12	0.18	11.6
SV11	bulk saprolite	96	29.8	< 0.01	0.13	0.08	2.77	0.05	1817	1366	174	276	96.2	12.4	0.38	0.26	12.6
SV12	bulk saprolite	121	21.0	0.01	0.07	0.15	4.33	0.02	1665	1226	171	268	91.6	14.4	1.47	0.22	4.3
SV13	bulk saprolite	61	30.5	0.02	0.15	0.14	4.31	0.09	2308	1361	332	615	79.3	13.1	0.40	0.24	5.6
CS7	< 2 µm fraction	161	26.9	0.10	0.25	0.06	2.36	0.04	18466	15207	1324	1935	179	37.1	0.09	0.16	39.6
CS9	< 2 µm fraction	99	23.0	0.16	1.29	0.05	0.77	0.03	12843	8239	1744	2860	106	17.8	0.09	0.18	12.2
S1	clay veinlet [1]		M.Z	0.01	0.70	<0.01	0.06	0.02	4866	3778	366	723	75.6	14.4	0.41	0.19	17.8
S3	clay veinlet [1]		SAP	0.02	0.69	<0.01	0.05	0.21	13960	11082	993	1885	88.9	17.1	0.17	0.17	28.6
S5	clay veinlet [1]		SAP	0.03	0.60	0.02	0.73	0.04	8709	6660	724	1325	82.0	8.06	0.06	0.24	25.4

$Ce/Ce^* = Ce_N/(La_N \cdot P_N)^{1/2}$, and $Eu/Eu^* = Eu_N/(Sm_N \cdot Gd_N)^{1/2}$. $_N$ subscript represents normalizatin by CI chondrite (McDonough and Sun, 1995).

[1] Samples collected from an exposed section of the weathered profile preserved on the plateau. Material analysed represents the < 53 µm fraction.

Clay veinlets are strongly depleted in CaO, Na_2O, and K_2O but have elevated MgO contents (0.7 wt %), while bulk saprolite are depleted in NaO (< 0.3 wt %), CaO (< 0.1 wt %), and MgO (< 0.15 wt %). The only exception is SV9 which shows elevated MgO concentrations (0.7 wt %). All samples have Th concentrations ranging from 75 to 200 ppm and, with the exception of two samples, phosphate contents below 0.05 wt %. Samples SV13 and S3 have concentrations of 0.9 and 0.21 wt % P_2O_5 respectively.

The clay separates from SV7 and SV9 were included in this experiment because they have similar high REY contents, but were shown to have different REE mineralogies (see chapter 7). In SV7, LREE-fluorcarbonates are found to occur in abundance, and hold a large proportion of the REE. Contrastingly, no LREE-fluorcarbonates are present in SV9, indicating that the clays are more REE-enriched.

The saprolite samples consist mainly of quartz, K-feldspar, biotite and kaolinite (Figure 8.1). The proportion and crystallinity of these minerals varies between samples. In sample SV9, smectite is also an important constituent and is responsible for the elevated MgO content. The mineral composition of the clay separate samples reflects the bulk saprolite samples (Figure 8.2). Clay veinlet samples are mainly composed of quartz, kaolin (kaolinite or halloysite) and smectite (Figure 8.3). No plagioclase was identified by X-ray diffraction in any of the samples, and is concluded to be the principal source of kaolin in the samples due to beakdown lower down in the profile.

Detailed mineralogical work of in Chapter 7 has also shown that saprolite samples contain variable amounts of resistant REE minerals, which include zircon, niobiates and REE-phoshates, and supergene REE minerals which include LREE-fluorcarbonates, Ce oxides and rhabdophane-Ce. These minerals hold variable amounts of REE.

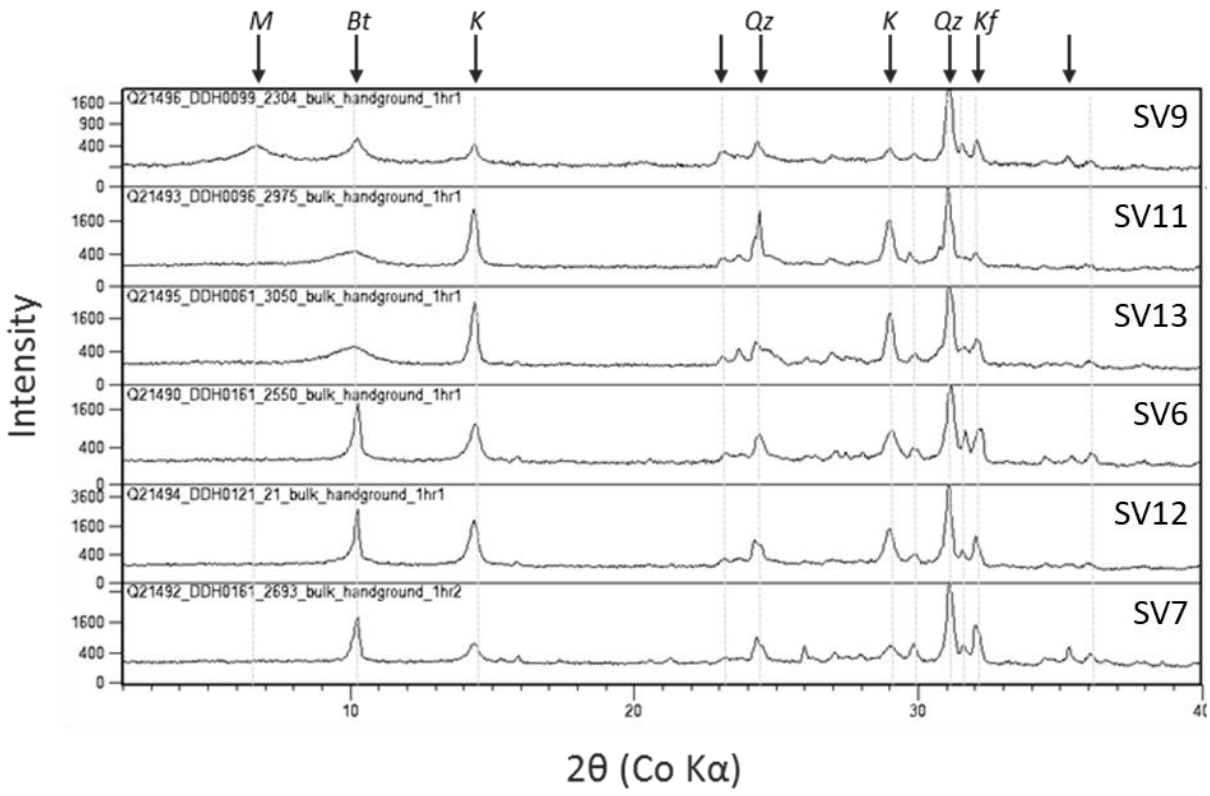


Figure 8.1. Representative X-ray diffraction patterns of bulk saprolite samples.

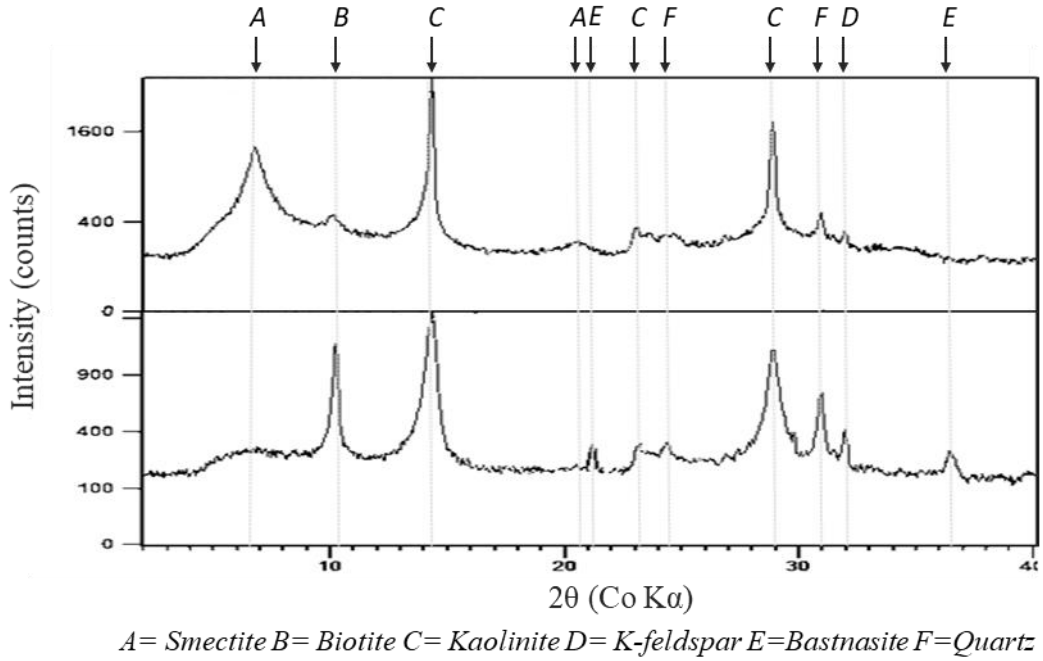


Figure 8.2 Representative X-ray diffraction patterns of < 2 micron fraction separates from the saprolite.

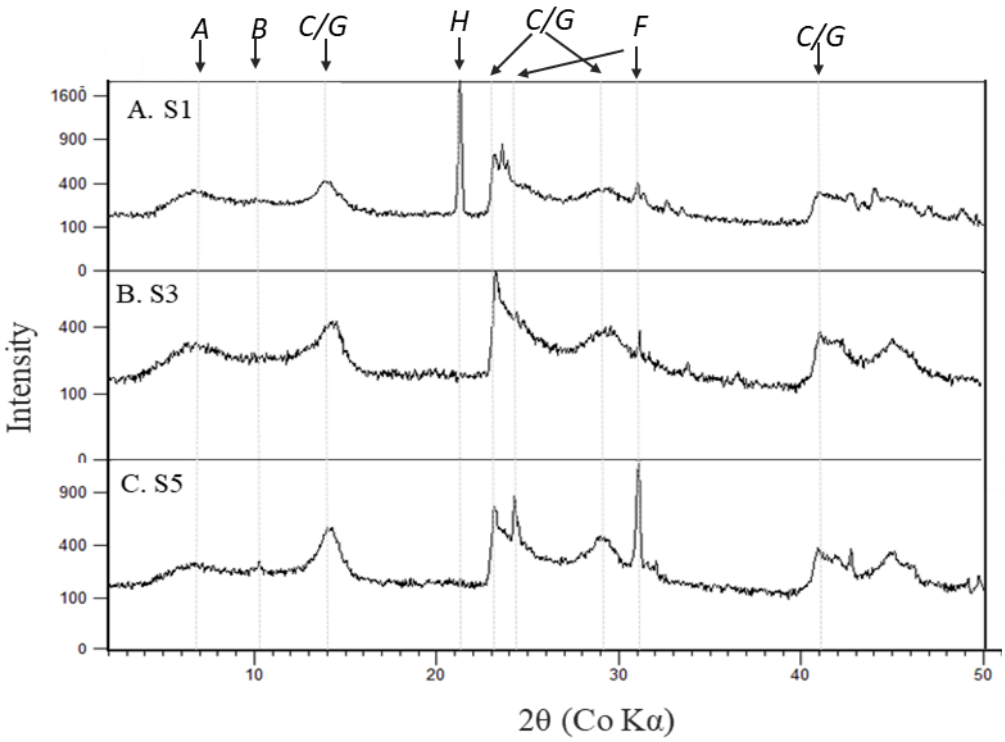


Figure 8.3 Representative X-ray diffraction patterns of clay veinlets samples (S1, S3, S5) collected from exposed sections of the weathered profile.

8.2.1.2 Sample preparation

Due to the small amount of material required for the batch leach experiments (0.5 g), sub-samples were split from the samples sent for bulk geochemical analysis. These parent samples include bulk saprolite samples, dried, crushed, and milled to < 75 microns; clay veinlets sieved to < 53 microns; and clay separates obtained through centrifugation of bulk saprolite samples. Filtering and sieving the samples to fine-grained material ensured representative and homogenous material was leached during the experiments. There is little visible difference between the prepared samples, only a slight colour contrast between the pale white clay veinlets and darker, dull brown saprolites (see Figure 8.4).

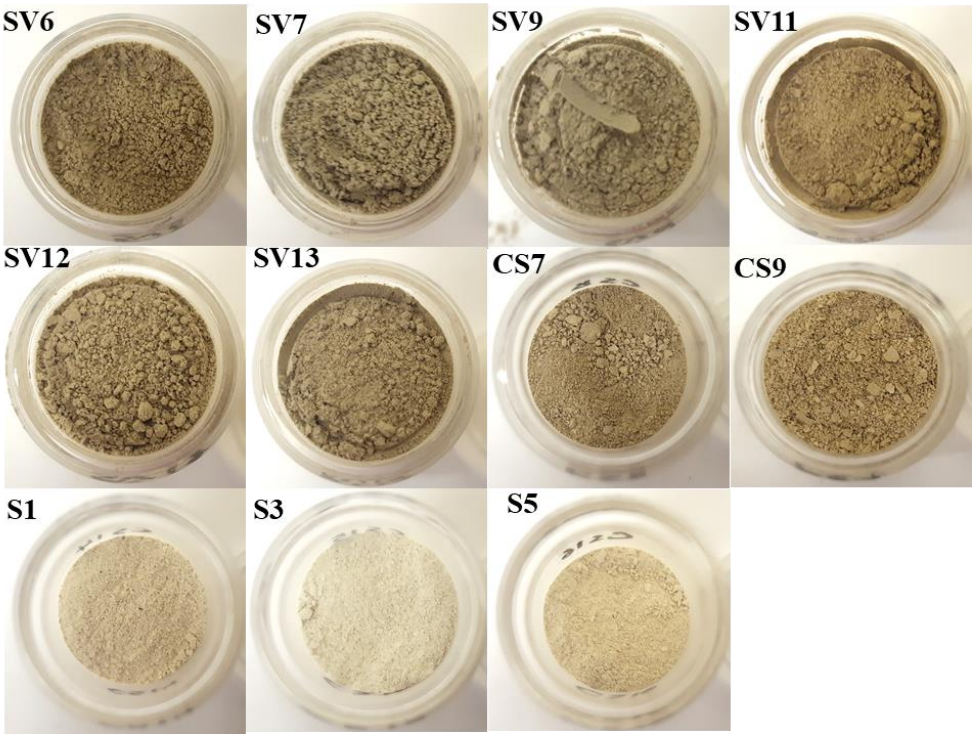


Figure 8.4.Photographs of prepared bulk saprolite (SV), clay fraction (CS) and clay veinlet (S) sample material used for the batch leach experiment. Note the variation in colour.

8.2.1.3 Experimental materials and reagents

The following materials and reagents were used in this experiment:

1. 15 ml polypropylene (PP) centrifuge test tubes with screw caps, and micro-pipettes.
2. Mechanical test tube roller for agitating the solid-liquid suspension.
3. Single use syringe filters (φ = 0.2 µm membranes).
4. Deionised water.
5. Ammonium sulphate solution (0.5 M) was used as the leaching solution, prepared by dissolving solid $(NH_4)_2SO_4$ salt with deionised water in a volumetric flask at pH 5.5, before being decanted into three flasks to prepare solutions at specific pH.
6. Dilute sulphuric acid (0.1 M) was used to adjust two batches of ammonium sulphate solutions of pH 4 and pH 3 respectively.
7. 0.2 ml of concentrated nitric acid was added to 9.8 ml of filtered solution after leaching to maintain the acidity during analysis of the solutions.

Ammonium sulphate was chosen for this experiment because it is currently the favoured monovalent salt used to recover REE from ion-adsorption ores by the industry and published experimental studies (Moldoveanu & Papangelakis 2016). It is considered to have good REE extraction capability, and is commercially available.

Concentrations of ammonium sulphate solution used by previous ion-exchange studies range between 0.05 and 2.5 M $(NH_4)_2SO_4$ (Tian et al. 2010, Moldoveanu & Papangelakis 2013, Yang & Zhang 2015.). Moldoveanu & Papangelakis (2013) showed that the percentage of REE extracted varied little between 0.5 and 0.25 M $(NH_4)_2SO_4$, but that below 0.05 M extraction levels dropped by 20 – 30 %. For this experiment, a reagent solution of 0.5 M $(NH_4)_2SO_4$ was considered sufficient to displace all exchangeable ions present in the sample, while also minimising the amount of sulphate being introduced into the ICP-MS apparatus during analysis.

Three ammonium sulphate solutions at pH 5.5, pH 4, and pH 3 were prepared to compare leaching at different pH levels in this study (Figure 8.5). Ammonium sulphate solutions are slightly acidic and naturally have pH values between 5 - 6 (Moldoveanu & Papangelakis 2016). Both the dilute sulphuric acid and the concentrated nitric acid were prepared by staff at NHM London.



Figure 8.5. Photographs showing the three 0.5 M ammonium sulphate solutions at different pH, and mechanical test tube roller used to agitate the solid-liquid mixture during the leaching experiment.

8.2.2 Experimental procedure

Small batch ion-exchange leach experiments were conducted at the Natural History Museum using ammonium sulphate to determine the amount and proportion of ion-exchangeable REE present in ore samples from the Serra Verde deposit. Leaching experiments with multiple pH conditions were carried out to investigate the effect on extraction of both REE and non-REE impurities (Ca, Al, Fe, Mg, Th, U), and the effect on supergene REE-phases identified in this

ore. In addition, leaching with D.I. water was carried out to determine the amount of free REE present in the ore material as aqueous-soluble REE ions. The experimental design of this study was based on the published work of Moldoveanu and Papangelakis (2012, 2013, 2016). A summary of the experimental conditions and procedures are presented in Table 8.2 and

Figure 8.6.

The experiments were carried out in 15 ml polypropylene (PP) centrifuge test tubes at room temperature conditions (~ 20 ºC). For bulk samples and clay veinlets, a 10 ml volume of 0.5 M ammonium sulphate solution was added to a test tube containing approximately 0.5 g of air-dried solid sample material (see Appendix F for exact sample weights). For the clay separates, the same solid to liquid ratio (L/S = 20 by mass) was used, but with only half the material (0.25 g solid, 5 ml solution) due to the limited material available. The test tubes containing the solid-liquid mixtures were placed on a mechanical roller to agitate slowly for 30 minutes. The reaction time was determined with preliminary timed leach experiment (see section 8.2.5).

After 30 minutes, the test tubes were centrifuged for 10 minutes at 12,000 rpm to separate the supernatant solution (SN solution) from the solid residue. The recovered supernatant solution was further filtered using a single use syringe filter (φ= 0.2 μm membrane) to remove any remaining particulate matter, and then acidified with 2 vol % HNO_3 to prevent the extracted metals from hydrolysing and precipitating out of solution. The acidified SN solutions were kept in polypropylene containers until analysis. Any remaining ammonium sulphate solution was removed from the separated solid residues by adding 10 ml D.I. water and centrifuging the test tubes a second time. The rinsed residues were then oven dried at 50 ºC for two days.

The leaching tests were repeated four times, using ammonium sulphate solutions adjusted to different pH's (~ 3 pH, ~ 4 pH and ~ 5.5 pH) and D.I. water (pH 7). Experiments with ammonium sulphate solution were not run above pH 6 to avoid lanthanide ions (REE^{+3}) from converting to insoluble hydroxide complexes, or below pH 3 to prevent dissolution of clay minerals (Piasecki and Sverjonsky 2008, Moldoveanu and Papangelakis 2016).

8.2.3 Analytical methods

Polished mounts of bulk saprolite fragments were prepared to observe and chemically analyse the clay clusters found in the saprolite samples SV9, SV7, SV11 and SV13 using SEM and EMPA.

The filtered and acidified SN leach solutions were submitted to the IAC at the NHM in London for chemical analysis by ICP-MS. For each sample, the concentration of the individual REE, and concentrations of non-rare earth impurities (Ca, Mg, Na, K, Ba, Rb, Sr, Al, Fe, Mn, Th, U, and Sc) were determined.

Powder X-ray diffraction (XRD) analysis and SEM imaging of the solid leach residues were employed to detect mineral alteration, formation of new phases caused by reaction with the leach solution, and occurrences of resistant REE-bearing minerals. Details of the sample preparation, procedures, and standards for these analyses can be found in Chapter 4.

8.2.4 Extraction calculations

Using the supernatant leach solution analysis results, the extracted percentage of both REE (PER), and non-REE, from the solid samples was calculated according to the following equation:

$$\% \, Extraction = (E_{(l)} / E_{(s)}) \cdot 100$$

$E_{(l)}$ (g) = total mass of element(s) in leaching solution after leaching 30 minutes.

$E_{(s)}$ (g) = total mass of element(s) present in the original ore sample.

The extraction cannot be measured directly because the adsorbed elements cannot be isolated from their bound state in the clays. Rather, the measured concentration of a given element in solution is assumed to be entirely the product of cationic exchange reactions. If the leaching is assumed to completed within the reaction time, the calculated extraction percentage (E) is the percentage of ion-exchangeable element in the sample.

Table 8.2. Experimental conditions of the batch ion-exchange experiments using Serra Verde ore samples.

Batch #	Reagent	pH	Temp. ºC	Reaction time (min.)	Samples leached #
1	0.5 M ammonium sulphate	~ 5.5	20	10 to 300	1
2	0.5 M ammonium sulphate	~ 5.5	20	30	11
3	0.5 M ammonium sulphate	~ 4	20	30	11
4	0.5 M ammonium sulphate	~ 3	20	30	11
5	D.I.water	~7	20	30	11

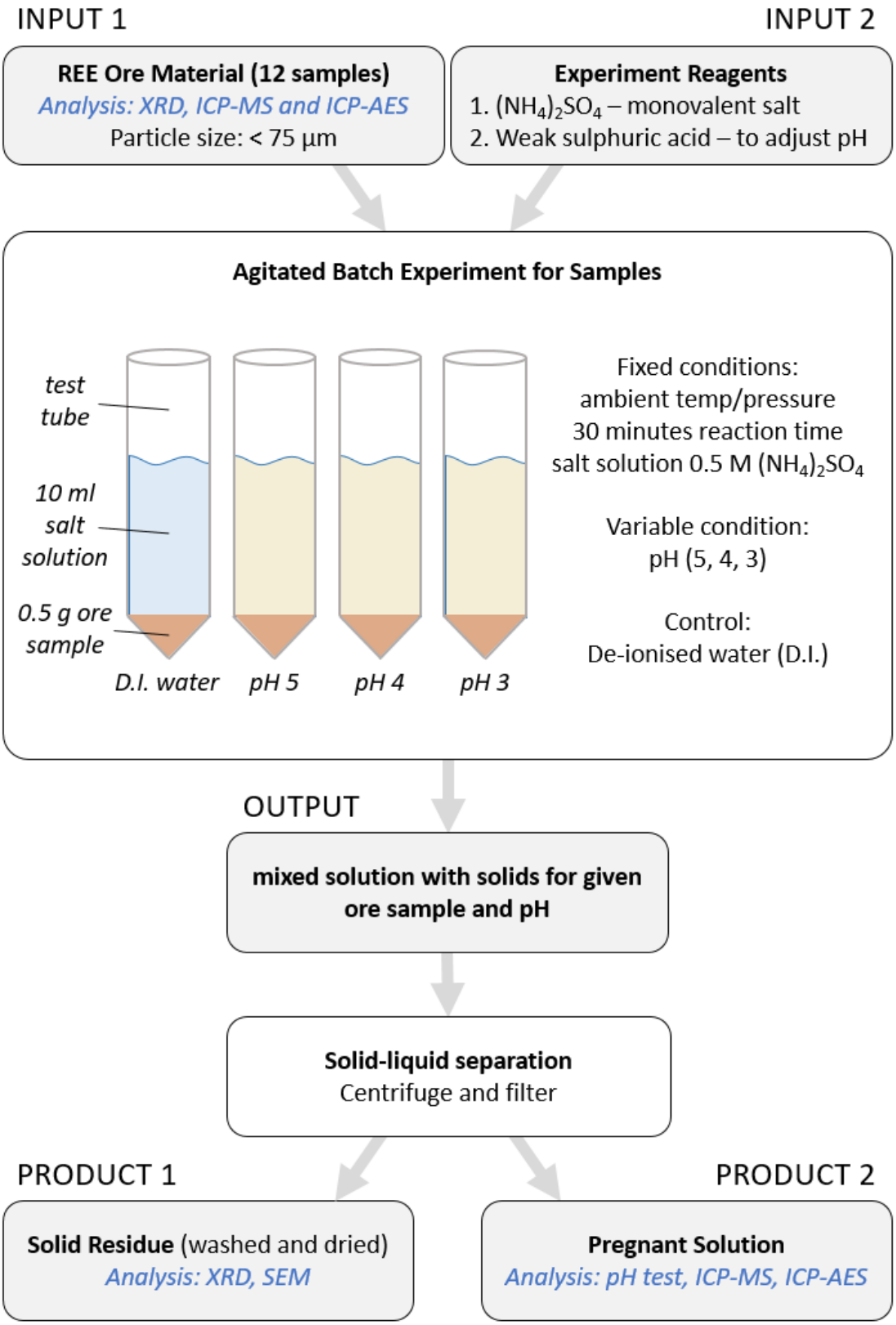


Figure 8.6. Work flow for single-step extraction experiments, using de-ionised water and ammonium sulphate solutions at varying pH, and showing the analytical methods for each product.

8.2.5 Preliminary experiment to determine leaching time

Studies that focused on establishing the optimum leach conditions for ion-adsorption of different clay ores have found that the leaching kinetics of ion-exchangeable REEs are generally fast, equilibrating within a few minutes, and that prolonged periods of leaching may decrease recovery. Tian et al. (2010) found that equilibrium was attained after 8 minutes, while Bruque et al. (1980) demonstrated that agitated leaching in excess of 1 hour led to a loss of dissolved REE. The optimal leaching time for the ore material in study was determined by a preliminary experiment. Batch leach experiments were run for varying time periods (10 min, 30 min. 1 hr., 2 hrs, and 5 hrs) using 10 ml of 0.5 M ammonium sulphate reagent solution at pH 5.5, 20 ºC, with 0.5 g of solid material from the bulk sample SV7.

The results of this preliminary experiments show that:

1. The concentrations of dissolved REY peaked shortly after exposure to the leach solution, and decreased progressively with leaching time (Figure 8.7A). The highest REY values were measured in the supernatant solution after 10-minutes leaching time, after which the dissolved REY in solution decreased by 3 %, 9%, 12% and 22 % for the 30-minute, 1-hour, 2-hour and 5-hour leaching times respectively (Figure 8.7A).

2. The rate of decrease of the dissolved REY, relative to the dissolved concentration after 10 minutes, is highest within the first hour. In the proceeding leaching times, the rate of concentration loss reduced significantly. Leaching times were not sufficient to observe a final equilibrated concentration (Figure 8.8).

3. Individual REE concentrations show the same decreasing trend with leaching time, but HREE and Ce are more strongly removed from solution than the LREE. For example, the concentrations of La, Ce, and Yb in the supernatant solution after 1 hour are 8 %, 13 % and 15 % lower than their peak concentrations after10-minutes (Figure 8.7B).

4. The results from most non-REE show similar trends to REE with concentrations decreasing over time (e.g. K, Mg, Mn and U; Figure 8.7, panels C to E). However, Al and Fe show a complex pattern with peak concentrations after 10 minutes, minimum concentrations at 30 min, and then either gradually increasing (Al) or stable (Fe) concentrations for longer leach times. Finally, there are a few elements such as Na, Ca and Ba which showed small fluctuations in concentration varying independently to leaching time.

The optimal leaching time tested for SV7 was shown to be 10 minutes. However, for practical reasons and to reduce the observed peaks in Al and Fe, a 30 minute leaching time was chosen for the main batch leaching experiments. From the results of the preliminary experiment, a 30 minute leach time with a further 10 min of centrifugation can be expected to result in a ~ 5 % loss of REE from solution due to reprecipitation. The results of this preliminary experiment corroborate the published observations that the kinetics of REE are fast, and that ion-exchange leach experiments should be run for short lengths of time to determine the maximum elemental concentrations in an ion-exchangeable state.

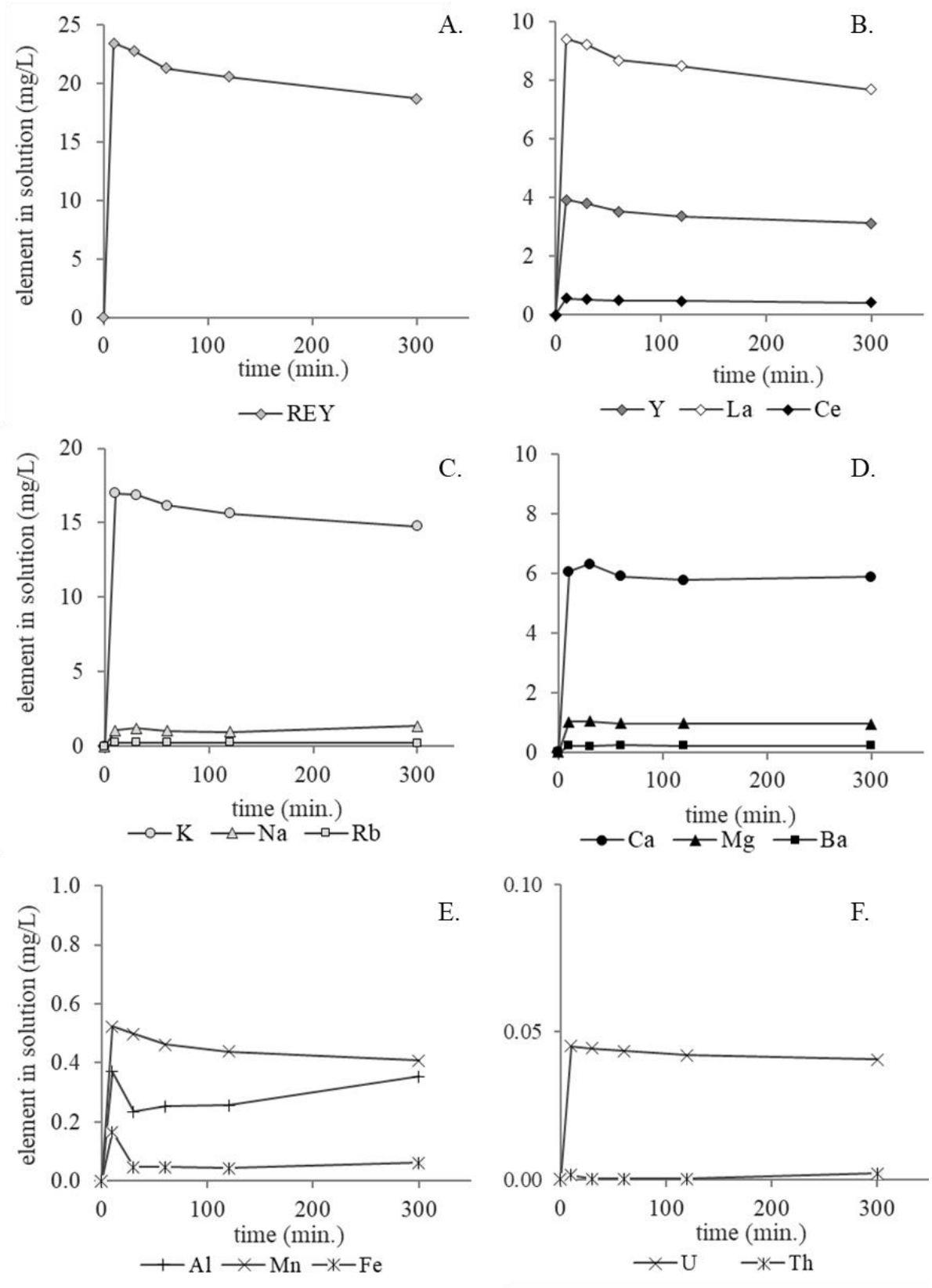


Figure 8.7. Plots showing the results of measured concentrations in the supernatant solution for sample SV7 at different leaching times. Note that most elements show similar decreasing concentration trends over time.

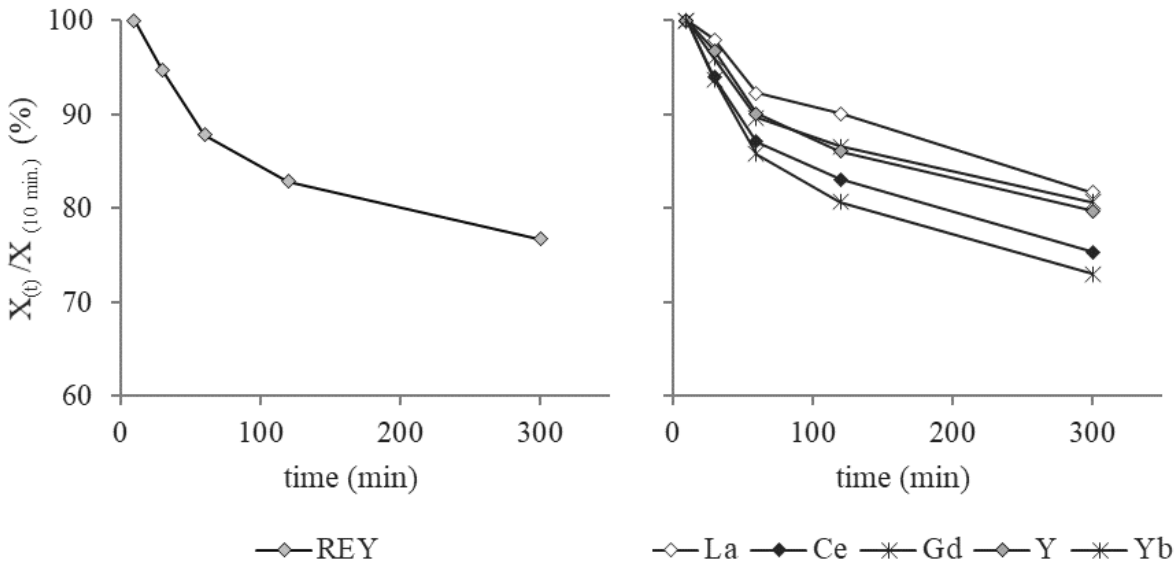


Figure 8.8. Changes in the proportion of REY (left) and selected individual REE (right) extracted in the supernatant solutions, relative to the shortest leaching run (10 minutes) over different leaching times.

8.3 Results

8.3.1 EMP and SEM analysis of clay minerals

EMP point analyses of leached saprolite samples SV7, SV9, SV11 and SV13 show that the clay minerals are principally composed of Si and Al, with small amounts of Mg, Ca, Fe and REE and Th and U concentrations below detection limit. In addition, clay minerals contain trace concentrations of F. Representative data points are present in Table 8.3 and a full table of EMP point analyses of clays in the saprolite samples can be found in Appendix C3.

The clays in samples SV11 and SV13 have the lowest Mg, Ca, and REE contents, with concentrations for all three elements falling below the detection limit (Table 8.3). Only SV13 contains F values above the detection limit, with an average value of 0.16 wt %. The Fe contents in both samples are highly variable, ranging from 0.6 to 5 wt %, and the average Si/Al value for these clays is ~1.1.

The clays analysed in SV7 have low Mg (0.02 – 0.8 wt %), Ca (0.03 – 0.42 wt %), and REE concentrations (average of 0.34 wt %). The clays in this sample have an average Si/Al value of ~1.2, moderate Fe (0.5 wt %) content and small amounts of F (0.22 wt %). Only La, Nd, and Y are present in high enough concentrations to be measured by EMPA. The results show

that La is the most abundant REE with mean concentrations of 0.18 wt % La. The mean concentration of Y in the clays is lower at 0.12 wt %, falling close to the detection limit. Element plots in Figure 8.10 show that neither La nor Y contents show any correlation with Ca or Mg concentrations.

The clays in SV9 have the highest Si/Al ratios, and Mg and REE concentrations. The clays in this sample have an average Si/Al of ~1.7, average Mg of 1.16 wt %, and average REE concentrations of 2.1 wt %. The Ca and Fe content in SV9 clays are very similar to SV7, with values Ca values ranging between 0.03 and 0.4 wt %, and mean Fe contents of 0.67 wt %. The point analyses also show that the clays contain small quantities of F, with a slightly higher average of 0.46 wt %.

The clays in SV9 have the highest REE measured, but individual point concentrations are highly variable and have an uneven distribution (Figure 8.10). The clays in this sample are generally LREE-enriched and have very low Ce concentrations that are at, or below the detection limit. The mean concentrations of La and Y in SV9 are 0.67 wt % and 0.5 wt % respectively, while values range from 0.07 to 1.83 % for La, and 0.06 to 0.15 wt % Y.

SEM-BSE imagery of clay-rich areas in sample SV9 show the uneven distribution of REE as irregular patches and rims on clay minerals with bright responses up to 50 microns across. EDS and EMP analyses of these bright areas reveals that they have higher REE concentrations and are particularly enriched in Y (Figure 8.9 and Figure 8.10). Separating the analyses between those from bright and dull SEM-BSE responses, reveal that bright areas have higher mean REE concentrations of 0.84 wt % La and 0.79 wt % Y, compared to dull areas with 0.56 wt % La and 0.26 wt % Y (Figure 8.10). EDS element maps clearly show that the Mg is concentrated in rounded clay patches, surrounded by low-Mg clays (Figure 8.9). The combined Y and Mg maps show that the distribution of these elements does not coincide in the clays.

The clay compositions show a weak relationship between Y and La, for compositions above ~0.5 wt % La (Figure 8.10). It appears that higher REE concentration are associated with lower La/Y ratios. The element plots also show that La has a weak, positive correlation with Si/La and Mg, in both SV7 and SV9, whereas Y shows no relationship with these elements. Y does however appear to have a negative relationship with Ca; points with elevated Y contents also have the lowest Ca concentrations.

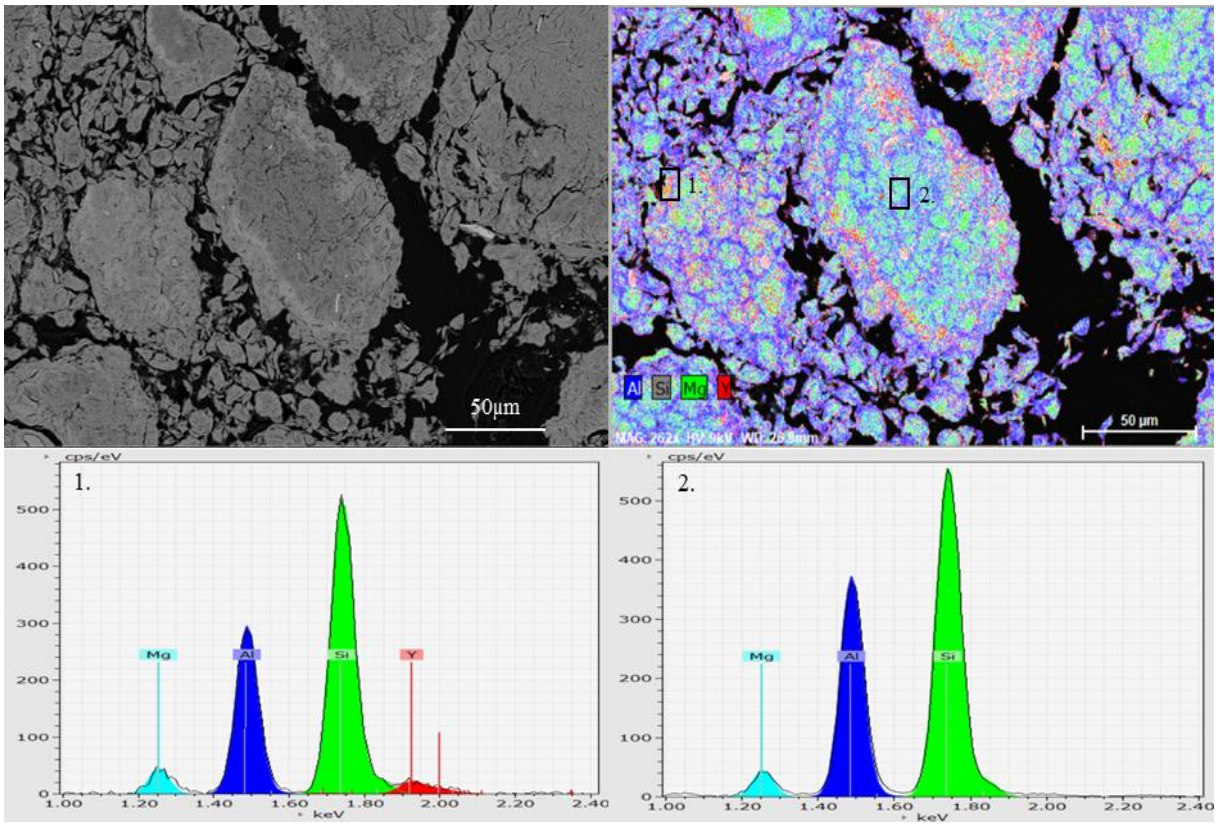


Figure 8.9. SEM-BSE image (top left) and corresponding false-colour EDX element map (top right) for a clay sample from drill hole DDH0099. Two spectra for element compositions of clays (black squares in top right map) are also given.

Table 8.3. EMPA results from clay-rich areas in saprolite samples. Results for sample SV9 are split between clays that have dark and light responses in SEM-BSE imagery (see Figure 8.10).

	SV9						SV7			SV11			SV13		
	dark clay			bright clay											
wt %															
F	0.53	0.42	0.28	0.55	0.42	0.50	0.23	<dt	0.30	<dt	<dt	<dt	<dt	0.17	0.20
Na	<dt	0.04	0.04	0.03	0.03	0.06	<dt	<dt	<dt	<dt	<dt	0.02	<dt	<dt	<dt
Mg	1.31	1.22	1.24	1.27	1.08	1.67	0.63	0.60	0.62	<dt	0.02	<dt	<dt	0.07	0.04
Al	14.6	14.1	13.9	13.8	15.9	11.6	17.8	17.7	17.0	18.3	19.9	17.7	18.6	18.2	19.2
Si	24.2	23.7	23.6	22.9	24.2	23.9	22.7	22.8	21.3	20.4	22.1	19.8	20.8	20.7	21.8
P	<dt	<dt	<dt	<dt	<dt	<dt	<dt	<dt	<dt	<dt	<dt	<dt	<dt	<dt	<dt
Ca	0.28	0.17	0.17	0.06	0.12	0.18	0.25	0.21	0.19	0.03	<dt	0.04	<dt	0.03	0.02
K	0.08	0.05	0.07	0.02	0.03	0.16	0.14	0.13	0.15	<dt	0.17	<dt	0.06	0.49	0.20
Ti	<dt	<dt	<dt	<dt	<dt	<dt	<dt	<dt	<dt	<dt	<dt	0.04	0.03	0.13	0.10
Mn	<dt	<dt	<dt	<dt	<dt	<dt	<dt	<dt	<dt	<dt	<dt	<dt	<dt	<dt	<dt
Fe	0.36	0.40	0.31	0.37	0.16	0.47	0.47	0.58	0.53	0.81	2.52	0.78	2.07	3.16	3.21
Th	<dt	<dt	<dt	<dt	<dt	<dt	<dt	<dt	<dt	<dt	<dt	<dt	<dt	<dt	<dt
U	<dt	<dt	<dt	<dt	<dt	<dt	<dt	<dt	<dt	<dt	<dt	<dt	<dt	<dt	<dt
Y	0.12	0.18	0.27	1.01	1.26	1.16	0.11	0.12	0.15	<dt	<dt	<dt	<dt	<dt	<dt
La	0.64	0.75	0.72	1.53	0.39	0.85	0.31	0.27	0.28	<dt	<dt	<dt	<dt	<dt	<dt
Ce	<dt	<dt	<dt	0.16	<dt	<dt	<dt	<dt	<dt	<dt	<dt	<dt	<dt	<dt	<dt
Pr	<dt	<dt	<dt	0.46	0.17	0.23	<dt	<dt	<dt	<dt	<dt	<dt	<dt	<dt	<dt
Nd	0.21	0.27	0.34	1.46	0.68	1.08	0.14	0.12	0.12	<dt	<dt	<dt	<dt	<dt	<dt
Sm	<dt	<dt	<dt	1.06	0.72	0.67	<dt	<dt	<dt	<dt	<dt	<dt	<dt	<dt	<dt
O	41.8	41.1	40.8	40.8	43.3	40.2	43.0	43.0	40.7	40.6	46.2	39.4	42.9	44.1	46.1

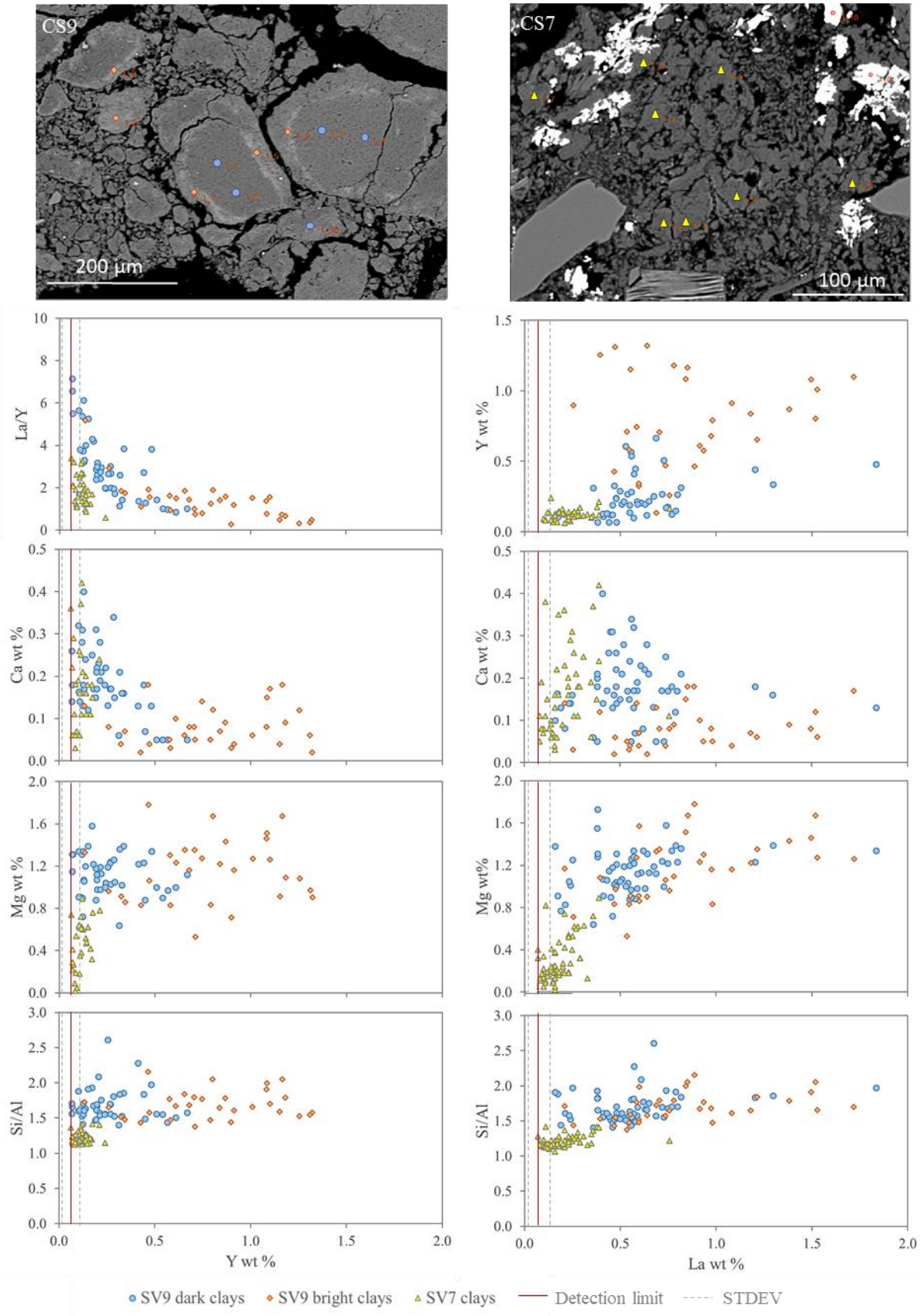


Figure 8.10. SEM-BSE images showing examples of clay rich areas analysed by EMPA in polished blocks of saprolite samples SV9 (top left) and SV7 (top right). Element plots of EMP results for these two samples are shown below.

8.3.2 Supernatant solutions

The PER extraction results from the small batch ion-exchange leach experiments are described in this section and presented in Figure 8.11. All results are presented in terms of aqueous-soluble ion concentrations, and ion-exchangeable element concentrations in the samples. For each group of samples, the aqueous soluble ion content, the ion-exchangeable REY content, and the non-REE leachable impurities are described. Raw concentration values from each solution (i.e. the measured element concentration) can be found in Appendix F.

8.3.1.1 Bulk saprolite samples

Aqueous soluble ions

The results from the experimental control run with D.I. water show that < 0.05 % REY in the bulk saprolite samples occur as free ions (Figure 8.11). The bulk saprolite samples with the highest concentration of aqueous soluble REE ions are SV7 and SV9 with values of 3.22 and 2.92 ppm REY respectively. The REE aqueous ions extracted by D.I. water are preferentially LREE, with La_N/Yb_N of 46.1 and 11.1 respectively.

The most abundant aqueous soluble ions in the bulk saprolite samples are Na and K with concentrations of up to 99 ppm Na and 50 ppm K extracted. All other elements analysed have aqueous soluble concentrations similar or lower to the REY.

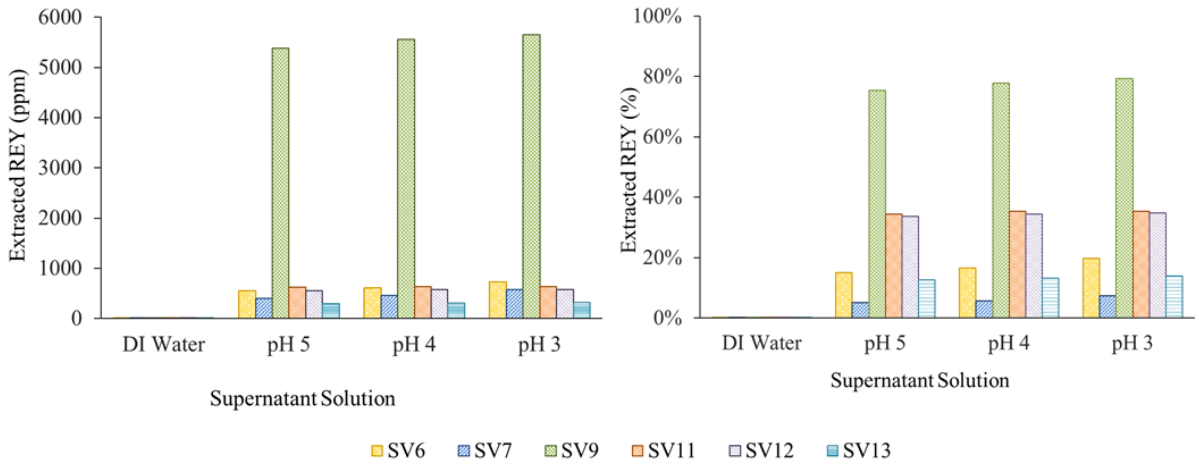


Figure 8.11. Extracted concentrations of REY in filtered supernatant solutions from leached bulk saprolite samples (left) and corresponding extracted percentages of REY (right).

However, in terms of proportion extracted, Na and Ca are the only elements with > 1 % present as aqueous soluble ions in the saprolite samples. The proportion of aqueous soluble Na ranges between 0.7 and 5.6 % with the highest values found in samples SV9 and SV6 and the lowest in sample SV7. The proportion of aqueous soluble Ca ranges from 0.38 to 3.38 % with the highest value found in SV11 and the lowest in SV9.

Ion-exchangeable REE at pH 5.5

The ion-exchangeable REY concentrations in bulk saprolite samples treated with ammonium sulphate at pH 5.5 range between 402 and 5387 ppm REY and are all LREE dominant (Figure 8.11). The large range is mainly caused by sample SV9, which has an ion-exchangeable REY concentration ten times higher compared to that of the other samples. Excluding SV9, the concentrations of ion-exchangeable REY in the bulk saprolite samples is < 700 ppm REY. The results in Table 8.4 show that in all samples 62 to 85 % of the REE is extracted are LREE.

The results presented in Figure 8.12 show that the percentage of ion-exchangeable REY relative to total REE content in bulk saprolite samples is highly variable with values ranging between 5 % and 75 %. The sample with the lowest percentage of ion-exchangeable REY is SV7 and the highest is SV9. The other four bulk saprolite samples have between 13 % and 35 % ion-exchangeable REY.

The extraction percentage for individual elements, presented in Figure 8.12 and Table 8.4 shows that all saprolite samples contain very low percentages of ion-exchangeable Ce. Sample SV9 has highest amount with 15 % ion-exchangeable Ce while all other samples contain < 3 % ion-exchangeable Ce. These results also show that, although the REE extracted are mainly LREE, similar percentages of individual REE (with the exception of Ce) are released by ion exchange leaching, in the majority of the samples. The only sample where this is not observed is SV12. In this sample LREE have much higher percentage of extraction than HREE (e.g. 83 % La vs 13 % Yb). There is a slight preferential extraction of LREE in samples SV9, SV11, SV13 and SV6 with samples SV9, SV11 and SV13 showing a slight preferential release of LREE, with < 15 % difference between La and Yb. For example, 47.6 % La vs 33.4 % for Yb was extracted from SV11. However, sample SV7 shows a small preferential extraction of HREE of a few percent.

Chondrite-normalised REE patterns

The graphs presented in Figure 8.13 show that the ion-exchangeable REE in the bulk saprolite samples have a LREE-enriched chondrite-normalised pattern, with strong negative Ce and Eu anomalies. Except for sample SV12, the ion-exchange REE closely follow the chondrite-normalised pattern of the total REE content in the bulk saprolite samples. However, the ion-exchange REE have a much larger negative Ce anomaly, and have a slightly more fractionated trend with higher LaN/YbN ratios. The negative Eu anomaly remains unchanged.

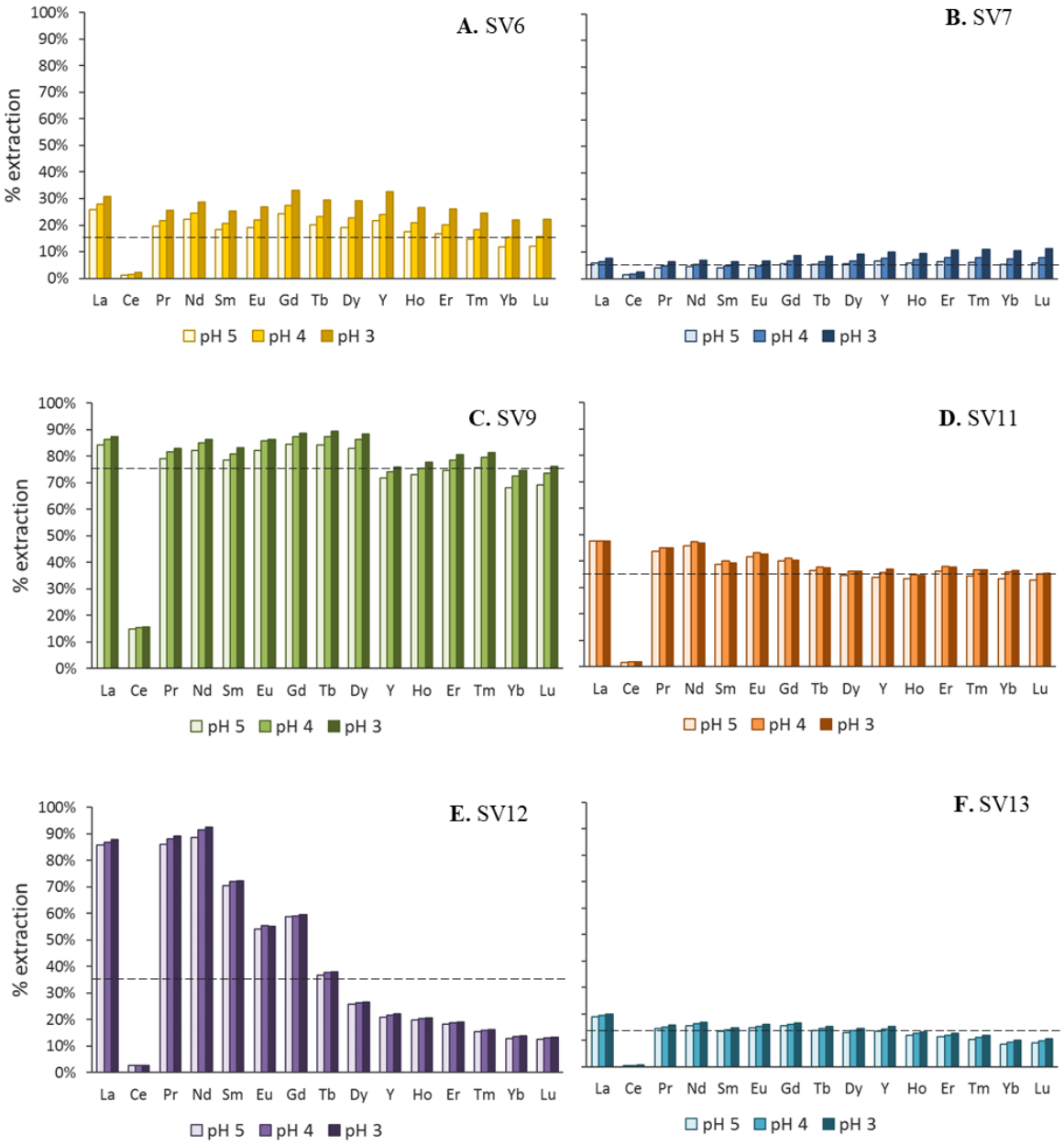


Figure 8.12. Extracted percentages of individual REE from bulk saprolite samples by leaching with ammonium sulphate solution at different pH values. The total percent of extracted REY for each sample is shown by the dashed line.

The negative Ce anomaly of the ion-exchangeable REE is < 0.05 Ce/Ce* for all samples, but the La_N/Yb_N ratio is variable with samples falling into two groups. Group 1, which includes SV9, SV11 and SV13 have La_N/Yb_N values ranging from 12 to 18. Group 2, which includes SV6, SV7 and SV12 have much higher La_N/Yb_N ratios with values ranging from 28 – 35 (see Table 8.4).

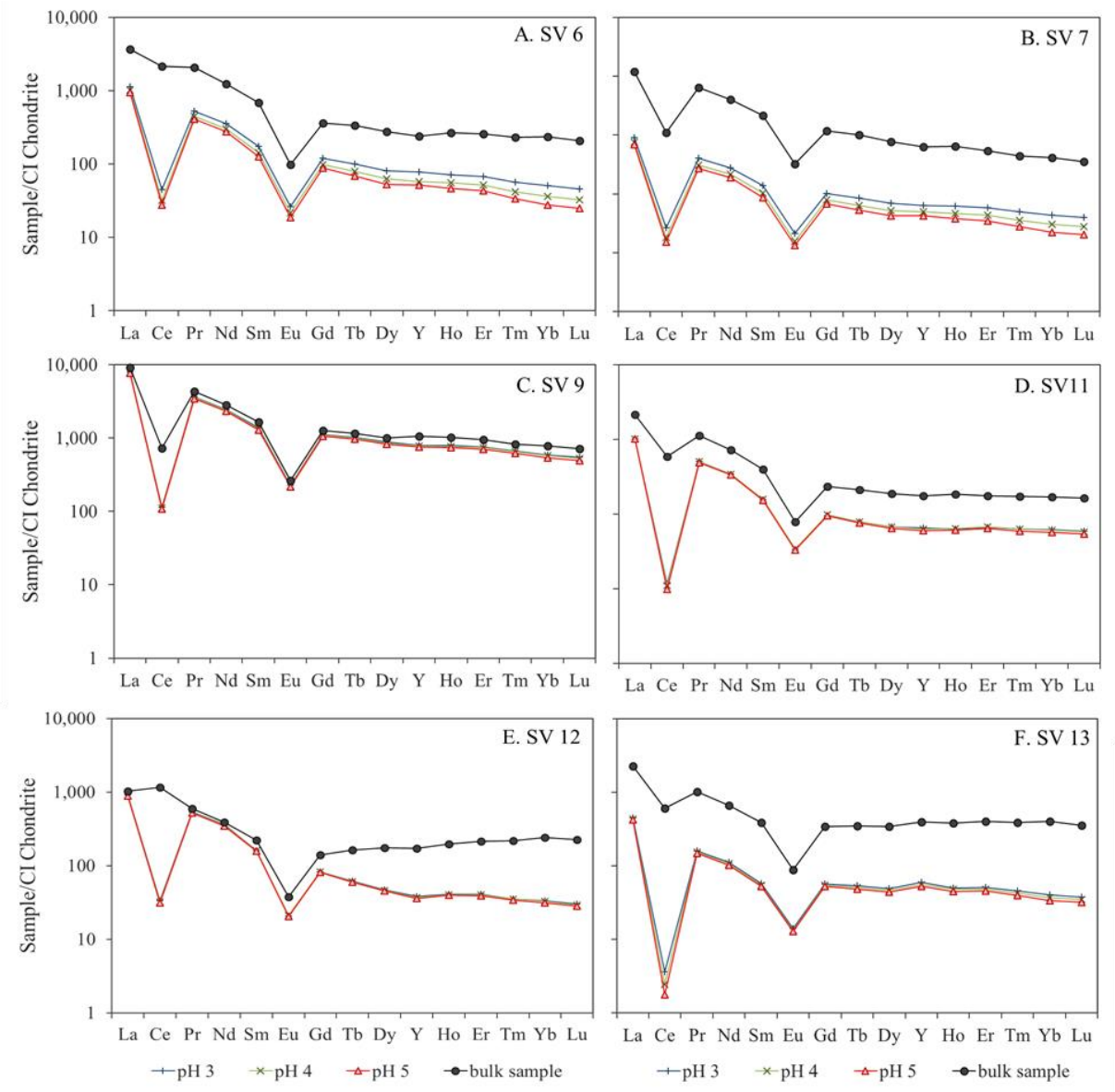


Figure 8.13. Chondrite-normalised REE patterns of untreated bulk saprolite samples (SV) and the REE extracted from these samples by ammonium sulphate solutions from batch experiments at different pH values. Note Y is plotted as a pseudolanthanide with atomic mass intermediate between Dy and Ho.

Effect of pH on REE extraction

Comparison of the composition of the supernatant solutions collected from ion-exchange experiments run at different pH conditions reveals the following:

1. The REE extraction is slightly higher when reagent solutions are more acidic (Figure 8.12 and Table 8.4). The supernatant solutions from pH 3 and pH 4 experiments have REE extraction concentrations that are 1 – 5 % higher compared to REE concentrations extracted with other solutions. The samples which showed the greatest increases are SV6 and SV9 with a REE concentration increases of 3.8 % and 4.7 % respectively. In all other samples, a 1 – 2 % increase in extraction was typically observed.
2. Extraction of HREE responds more strongly than LREE to changes in pH. With the exception of one sample (SV12), individual HREE show larger increases in ion-exchange concentration than LREE with increasing acidic reagent solutions. For example, the extracted La concentration in pH 3 solutions were 0.9 to 10.0 % higher than in pH 5.5 solutions, while extracted La/Yb concentrations showed a 0.01 to 4.76 % increase. Overall, increases in the concentration of HREE are 1.5 to 3 times higher than LREE. Samples with the largest HREE increases are SV6, SV7 and SV9; the three most REE-enriched bulk saprolite samples.
3. The least responsive REE to changes in pH is Ce, with an increase in concentration of < 1 % found in all samples.

Comparison of the results from different experimental batches shows that the chondrite-normalised patterns of the ion-exchange REE extracted at different pH conditions do not vary significantly (Figure 8.13). In all samples the Ce and Eu anomalies remain unchanged with changes in pH conditions. The most notable differences are observed in samples SV6 and SV7 where the chondrite-normalised patterns of ion-exchangeable REE extracted from under more acidic conditions have elevated REE content and are less strongly fractionated with La_N/Yb_N decreasing from 34 and 30 under pH 5.5 conditions to 22 and 20 under pH 3 conditions. The La_N/Yb_N for all the other samples also decreases but by a much smaller degree (Table 8.4).

Impurities: non-REE extracted

Chemical analysis of the superntant solution shows that non-REE are extracted from the saprolite samples by ion-exchange leaching using ammonium sulphate. Overall the results show that alkali and alkaline elements are more strongly extracted than both radioactive elements (Th & U) and transition metals (Al, Fe & Mn) (Figure 8.14 and Figure 8.15). In supernant solutions from experiments run at pH 5.5, Na, K, Ca, and Mg have the highest concentrations.

The ion-exchange concentrations of Ca, Na, K, and Mg in the bulk saprolite samples vary significantly with values ranging between 10's ppm to several 100 ppm (around one order of magnitude). Sample SV9 has the highest ion-exchangeable concentrations of Ca (416 ppm), Na (262 ppm) and Mg (102 ppm) while SV6 and SV7 have the highest K concentrations (283 ppm and 283 ppm respectively). However, the ion-exchange concentrations of these elements are proportional to the total element content in the sample and, as a result, the differences between samples are smaller when comparing the percentage extracted.

The data show that Ca is the most strongly leached element followed by Na. The sample with the highest ion-exchangeable Ca and Na is SV9 with extractions of 76 % and 14 %. The sample with the lowest ion-exchangeable Ca and Na is SV7 with extraction % of 45 % and 1.28 %. All other samples have > 50 % ion-exchangeable Ca and > 2 % Na. The extraction of K and Mg are much lower, with values of < 1 % and < 3 % respectively.

Very low concentrations of Th and U were extracted from saprolite sample in the leach experiment run at pH 5.5. The Th concentrations in the majority of the supernatant solution from this experiment were below detection limit of the ICP-MS (< 1.5 ppb) and therefore the ion-exchangeable Th concentration in these samples could not be determined. The two samples with detectable concentrations, contained 0.064 ppm and 0.08 ppm Th which represent < 0.1 % of the total Th content in the sample. The concentrations of extracted U ranged between 0.27 ppm and 0.89 ppm, which represent < 7 % of total U content in the sample.

The amount of Al, Fe and Mn extracted into the supernatant solution in experiment run at pH 5.5 were also low. The extracted concentrations for Al range between 6 to 18.4 ppm which represents < 0.01% of total content in the sample. The extracted concentration for Mn range between 2.07 ppm and 18.7 ppm, which represent < 5 %. The highest Mn extracted was from sample SV9. Fe remained below detection limit in the leach solutions.

Comparison of the results of from the leach experiments run at different pH (pH 3, pH 4, and pH 5.5) show that:

1. The reagent solution acidity has little effect on the extraction of alkali and alkaline elements. (Figure 8.14). No significant nor systematic increase in the concentration extraction was observed.
2. The reagent solution acidity has a strong effect on the release of Al, Fe, Th and U from bulk saprolite samples. The graphs in Figure 8.15 show that the extraction concentrations of these elements increase with decreasing pH of the reagent solution. The strongest effect is observed in Al and Fe graphs, which show the concentrations increasing from a few ppm to several hundred ppm in the supernatant solution. The effect is less significant with Th and U, with concentrations increasing by only a few ppm.

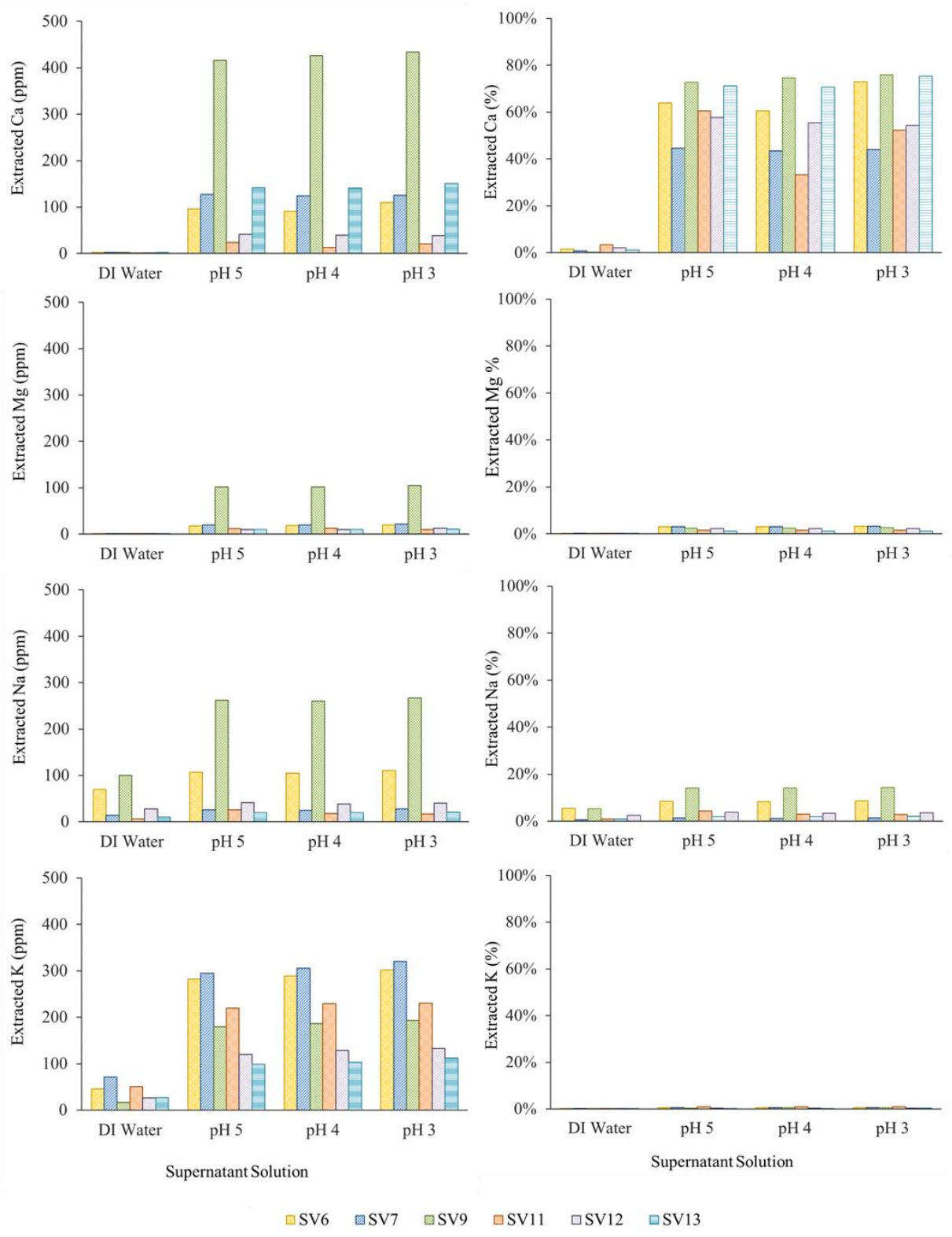


Figure 8.14. Extracted concentrations of alkali and alkaline earth metals in filtered supernatant solutions from leached bulk saprolite samples (left) and corresponding extracted percentages of REY (right) at different pH values.

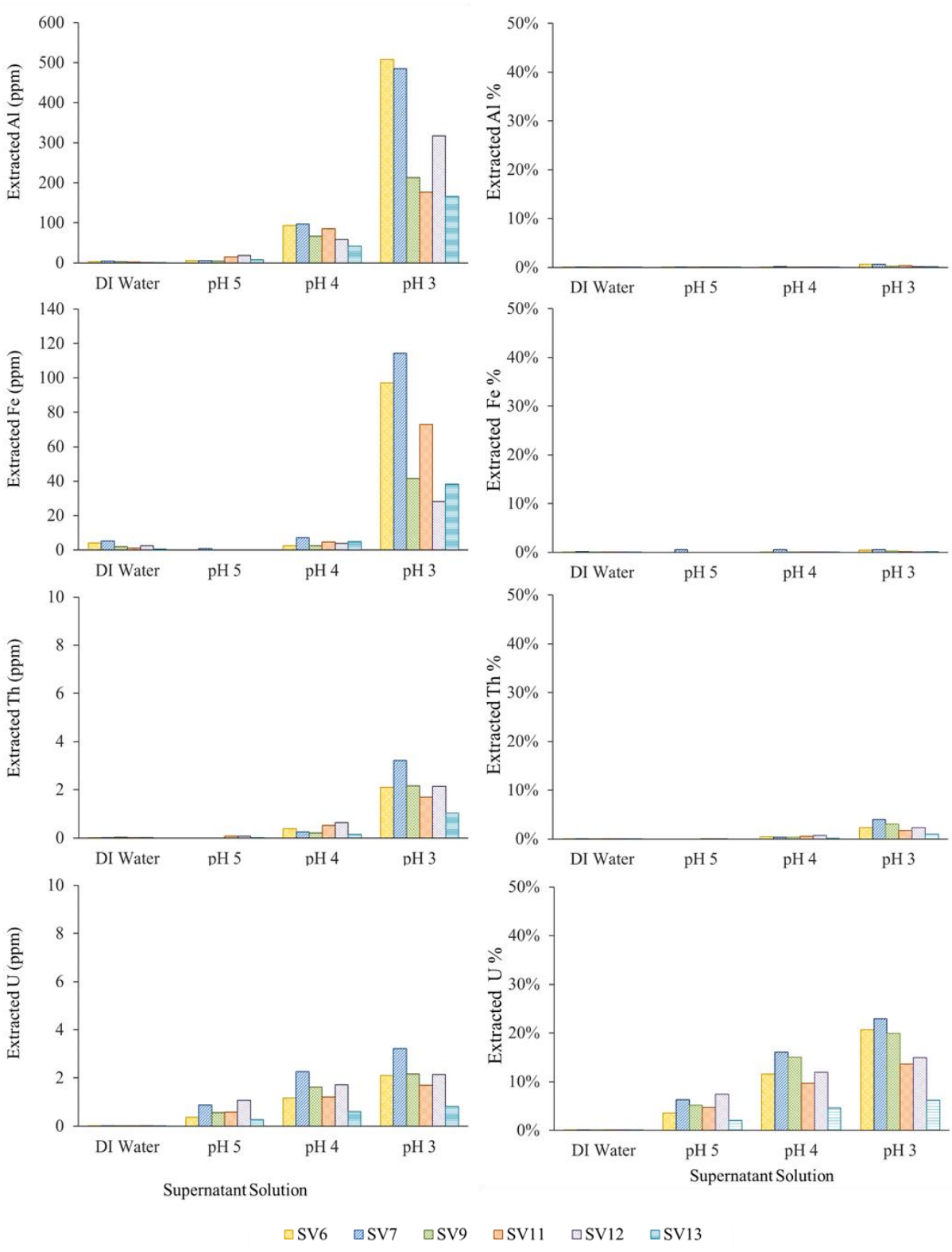


Figure 8.15. Extracted concentrations of selected elements in filtered supernatant solutions from leached bulk saprolite samples (left) and corresponding extracted percentages of REY (right) at different pH values.

8.3.2 Clay size fraction saprolite samples

The results show that the clay size fraction samples CS7 and CS9 leached with ammonium sulphate contain 2447 ppm and 6512 ppm ion-exchangeable REY. These concentrations are approximately 6 times and 1.2 times higher than the concentrations of ion-exchangeable REY obtained from the corresponding bulk saprolite samples, SV7 and SV9 (see Table 8.4).

The extraction percentage results presented in Figure 8.16A show that CS7 has a greater proportion of ion-exchangeable REE compared to the bulk sample but that the percentage remains low at 13.3 % REY. The opposite trend is observed for CS9, the extraction results show CS9 has 51 % ion-exchangeable REE compared to 75 % in the bulk sample. This lower extraction is observed in both of the experiments at different pH conditions, which indicates the reduction in extraction is not caused by sub-sample variations.

The calculated extraction percentage for individual REE show that in sample CS7, a greater proportion of HREE occur in ion-exchangeable form than LREE. The results in Figure 8.17 show that 26 % Yb was extracted compared to 18 % La. In sample CS9, individual REE show similar extraction values. A slight preferential extraction of LREE is observed, 53.9 % La vs 48 % Yb. In both samples, Cerium has much lower extraction values compared to all other REE.

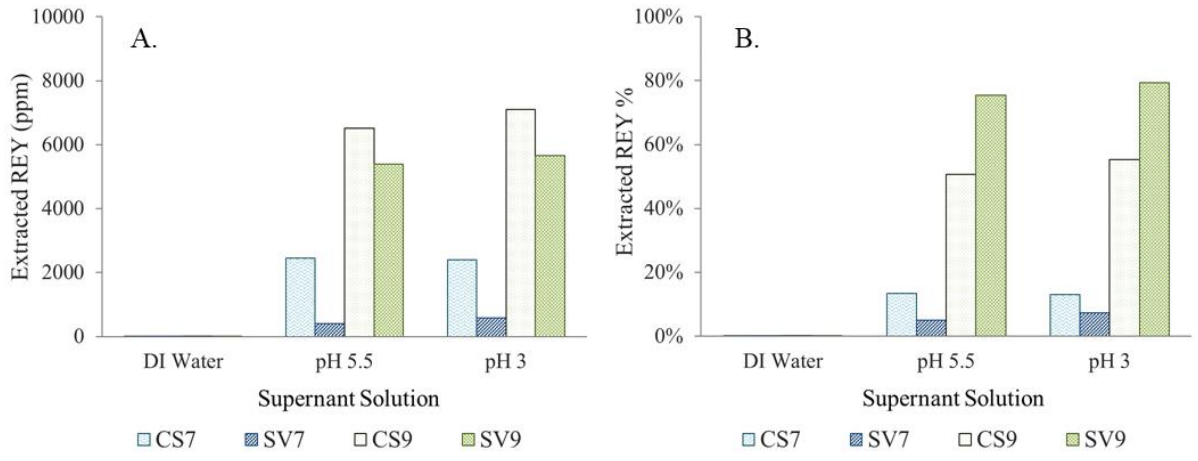


Figure 8.16. Extracted concentrations of REY in filtered supernatant solutions from leached bulk saprolite (SV7, SV9) with corresponding clay separates (CS7, CS9; A.) and extracted percentages of REY (B.) at different pH values, and for D.I. water.

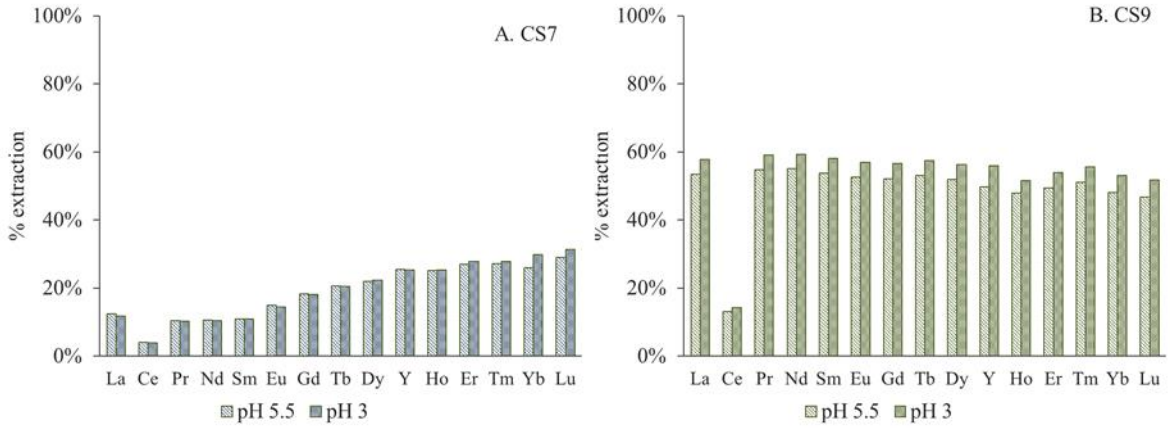


Figure 8.17. Percentage of REE extracted from saprolite clay separates at different pH values showing the influence of pH on the extraction level; for samples CS7 (left) and CS9 (right).

Ion-exchangeable REE in the CSF are both LREE-enriched and display the same chondrite-normalised pattern as the ion-exchangeable REE in the bulk saprolite samples (Figure 8.18). The ion-exchangeable REE in both CS7 and CS9 have the same negative Ce anomaly (0.02) and the same negative Eu anomaly (0.18) as the REE extracted from the bulk samples. The ion-exchangeable REE of CS9 also shows no change in the degree of LREE/HREE fractionation, with La_N/Yb_N remaining at 14. In contrast, ion-exchangeable REE from sample CS7 are less fractionated than the REE extracted from bulk saprolite sample SV7. The La_N/Yb_N value for CS7 is 19 compared to 30.9 for SV7. The ion-exchangeable REE in samples CS7 and CS9 have more similar fractionation compared to SV7 and SV9.

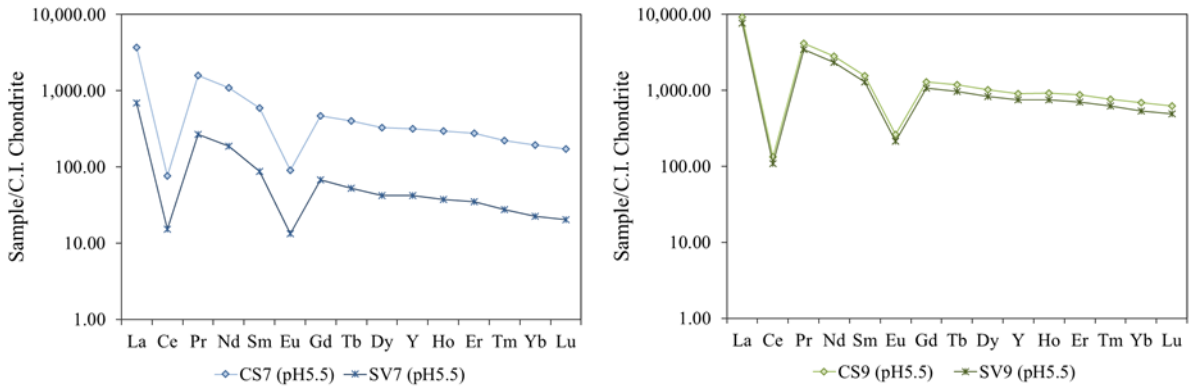


Figure 8.18. Chondrite-normalised REE patterns for REY extracted in filtered supernatant solutions from leached bulk saprolite samples (SV) and the corresponding clay separate samples (CS) by ammonium sulphate solutions from batch experiments at pH 5.5. Note Y is plotted as a pseudolanthanide with atomic mass intermediate between Dy and Ho.

8.3.3 Fracture infill samples

Aqueous soluble ions

The results from the D.I. water leach experiment show that the fracture infill samples also contain very low concentrations of aqueous soluble REY (Figure 8.19). The fracture infill samples from the saprolite horizon, S3 and S5, contain ~ 3 ppm aqueous soluble REY which represent ~ 0.03 % REY of total REY content of the sample. The fracture infill samples collected from the mottled zone, S1, contains slightly higher amounts with 13 ppm aqueous soluble REY which account for 0.26 % REY in the sample. In all three samples the aqueous soluble REY are dominantly LREE.

The results also show that the main non-REE aqueous soluble elements in the fracture infill samples are Na, K and Ca (Figure 8.22). In samples S3 and S5, the aqueous soluble concentrations of Na and K are lower than that of most of the saprolite samples studied but account for a higher percentage of the total Na and K content of the samples. This is particularly the case for Na where 10.5 % Na in S3 and 8.42 % Na in S5 is present in an aqueous-soluble form. The amount of aqueous-soluble calcium in S3 and S5 is slightly higher than in the saprolite samples (5 ppm vs 2 ppm Ca respectively) and accounts for ~ 3 % of the total Ca content.

The Na and K concentrations measured in supernatant solution of S1 collected from the D.I. water leach experiment are much higher than those observed in solution collected from the experiments with ammonium sulphate solution. Elevated values were not observed for any other element. This suggests that the S1 sub-sample used in the D.I. water experiment may have contained an anomalously elevated salt content, perhaps due to a nugget effect from coarse salts. Consequently, the results for Na, and K are probably not representative, and are omitted from the presented results.

Ion-exchangeable REY concentrations at pH 5.5

The results from the ammonium sulphate ion-exchange leach experiments show that the fracture infill samples contain high concentrations and high proportions of ion-exchangeable REE. The results presented in Figure 8.19 show that samples collected from fractures in the saprolite horizon, S3 and S5, contain 6360 ppm and 7251 ppm ion-exchange REY and that the sample collected from a fracture in the mottled zone, S1, contains 3130 ppm REY. These concentrations equate to 43.5 %, 83 % and 64.3 % of total REE content of each of the

samples (S3, S5 and S1 respectively). The concentrations extracted from samples S3 and S5 represent the highest of all samples leached in this study.

The results for individual REE, presented in Table 8.4, show that 80 % of the total concentration of REE extracted corresponds to LREE and the remaining 20 % to HREE & Y. However, the bar charts presented in Figure 8.20 show that, with the exception of Ce, the individual REE were extracted in the same proportion in each sample, which indicated that a greater proportion of LREE are held in clay minerals, but that there is no preferential adsorption of individual REE.

The proportion of ion-exchangeable Ce in fracture infill samples are significantly lower compared to all other REE. The bar charts in Figure 8.20 show that in sample S1 only 40 % of Ce was leached, and in samples S3 and S5 this value was less than 3 %. Most of the Ce in S3 and S5 therefore does not occur in ion-exchangeable form.

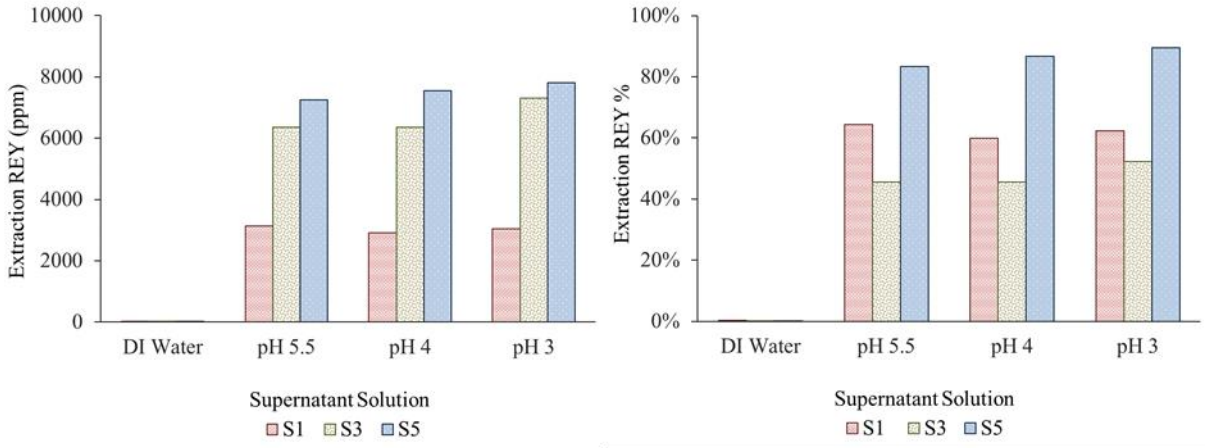


Figure 8.19. Extracted concentrations of REY in filtered supernatant solutions from leached clay veinlets (left) and corresponding extracted percentages of REY (right) at different pH values, and for D.I. water.

Chondrite-normalised REE patterns

Chondrite-normalised patterns of the REE extracted from the fracture infill samples by ammonium sulphate ion-exchange leaching are presented in Figure 8. 21. The graphs show that ion-exchangeable REE in fracture infill samples were measured to have very similar chondrite-normalised patterns to the total REE content of these samples. They are LREE-enriched, display a strong negative Ce anomaly, and have inherited the negative Eu feature.

The main difference observed is that ion-exchange REE have a stronger Ce negative anomaly. This difference is most noticeable in the chondrite-normalised patterns of S3 and S5 where the ion-exchange REE have Ce/Ce* values of 0.005 and 0.002 compared to 0.19 and 0.17 for the REE content of the sample. The difference is less pronounced S1 where ion-exchange REE have a Ce/Ce* value of 0.23 and the starting material is 0.33.

Apart from differences in Ce fractionation, no other differences in the chondrite-normalised patterns could be observed. The La_N/Yb_N, Gd/Lu, and Eu/Eu* ratio values remain unchanged (Table 8.4).

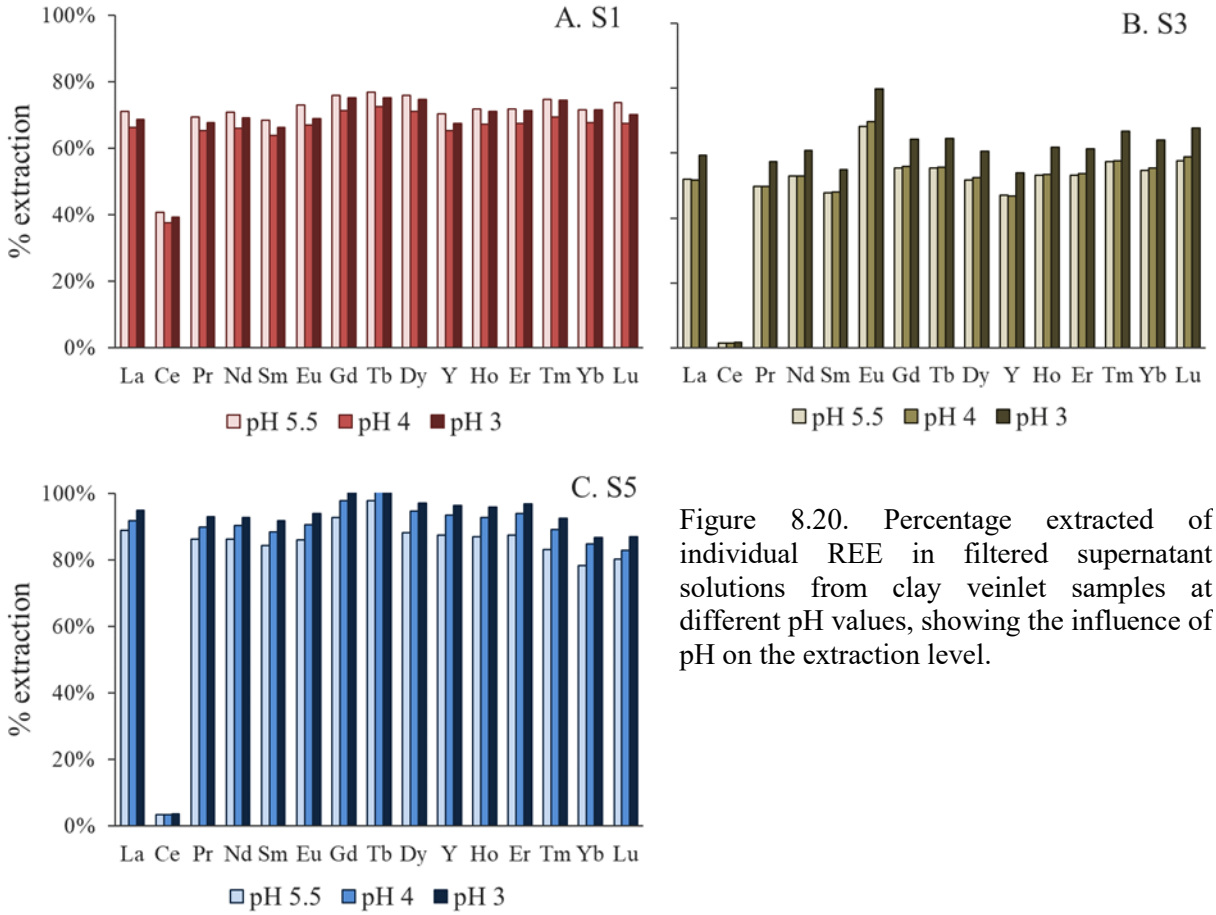


Figure 8.20. Percentage extracted of individual REE in filtered supernatant solutions from clay veinlet samples at different pH values, showing the influence of pH on the extraction level.

Effect of pH on REE extraction

The effects of pH conditions on the extraction of ion-exchange REE in fracture infill samples collected from saprolite horizon (S3 and S5) are the same as those observed in the bulk saprolite samples described above. The concentration of REY extraction increases with increasing acidity of the reagent solution and HREE respond more strongly than LREE. On the other hand, the fracture infill collected from mottled zone exhibit the opposite response.

The results presented in Figure 8.19 show that, for samples S3 and S5 the concentration of REY extracted is 6 % higher for experiments run at pH 3 than that of experiments run at pH 5.5. For sample S1, the results show that the concentrations of REY extracted are slightly lower, 2 – 4 %, in experiments run at pH 3 and pH 4 and that there is no systematic change as is observed in S3 and S5.

The results presented in Figure 8.20 show the difference in the response of LREE and HREE extraction to pH. For samples S3 and S5, the increase in HREE extraction is 9 % while the LREE extraction 6 %. In both samples, the increase in concentration of HREE released with increased acidity is ~1.5 times higher than for LREE; a lower ratio than what was found for bulk saprolite samples. For sample S1, LREE show a stronger decrease in concentration with increased acidity than HREE, with a drop of -1.9 % vs -0.8 % from the pH 5.5 to pH 3 experiment.

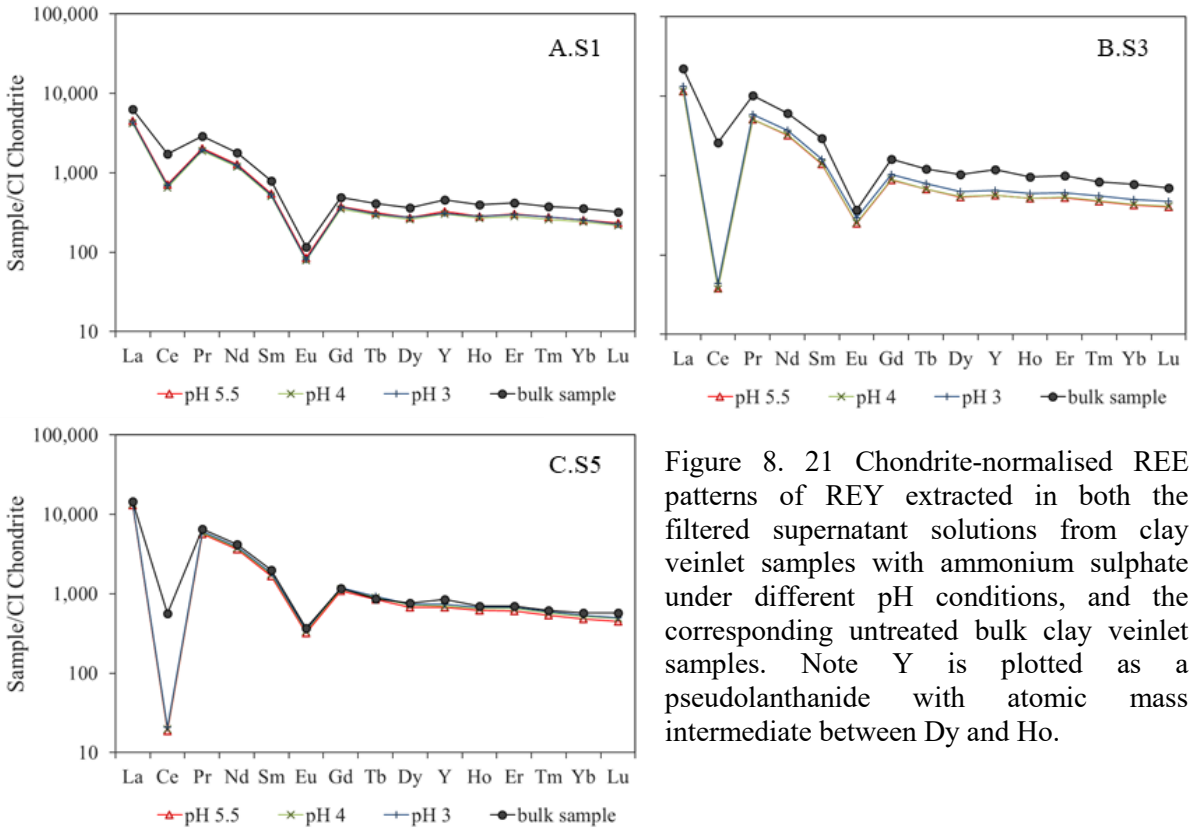


Figure 8. 21 Chondrite-normalised REE patterns of REY extracted in both the filtered supernatant solutions from clay veinlet samples with ammonium sulphate under different pH conditions, and the corresponding untreated bulk clay veinlet samples. Note Y is plotted as a pseudolanthanide with atomic mass intermediate between Dy and Ho.

Non-rare earth impurities

The results presented in Figure 8.22 show that the three fracture infill samples leached with ammonium sulphate at pH 5.5 have similar ion-exchangeable alkali and alkaline metal concentrations as bulk saprolite material (70 – 80 ppm K, 37 – 100 ppm Ca, 19 – 25 ppm Na, and 12 -24 ppm Mg). However, as a proportion of the total elemental content in the sample,

the ion-exchangeable K, Ca and Na in the infill fracture samples is variable with values ranging from 48 to 66 % Ca, 1 to 16 % K, and 13.5 to 25.3 % Na. For Mg, the percentage variation is narrower with values ranging between 0.3 to 0.5 % Mg. No significant differences in the extractable alkali and alkaline content between fracture infills collected in the saprolite horizon (S3 and S5) and mottled zone (S1) are observed. Compared to saprolite samples, the fracture infill samples contain much lower concentrations of ion-exchangeable alkali and alkaline elements.

The result presented in Figure 8.23 show that the amount of extractable Al in fracture infill samples using ammonium sulphate at pH 5.5 is widely variable, and values appear to relate to the position of samples along the weathered profile. The ion-exchangeable concentrations increase from 19.2 ppm in S5 (lower saprolite), to 140 ppm in S3 (upper saprolite sample) and to 800 ppm in S1 (mottled zone sample). Concentrations extracted from S5 are comparable to the results attained from the bulk saprolite samples, while Al concentrations extracted from S3 and S1 are of an order of magnitude higher.

The ion-exchangeable concentrations of Fe, Mn, Th and U are low for all three fracture infill samples with concentrations of < 5 ppm extracted for each element. As in the case of Al, greater concentrations of Fe, Th and Mn are recovered from sample S1 than the other two infill fracture samples. In terms of percentage extracted, < 2 % of Th, and < 15 % of U is leached, which although low, is higher compared to saprolite samples.

Comparison of experiments run at different pH conditions show that, except for Ca, the extraction of alkali and alkaline elements in the infill fractures does not change significantly with increased acidity of the reagent solution. The results for Ca are mixed and show no clear pattern. In samples S1 and S3, the percentage of extracted Ca decreases from 66.4 % and 37.1 % in experiments run at pH 5.5, to 44.1 % and 31 % in experiments run pH 3. However, no significant change is observed in the percentage of Ca extracted from sample S5.

The results in Figure 8.23 indicate that transition and radiative elements in fracture infill samples do respond to changes in pH conditions. For all of the elements analysed, Al, Fe, Mn, Th and U, higher concentrations in the supernatant solutions are found with increased acidic conditions. The largest effect is observed in the concentrations of Al which increases by 100 to 300 ppm with progressively more acidic experimental conditions. Th and U concentrations increase by small amounts, and remain low at <5 ppm.

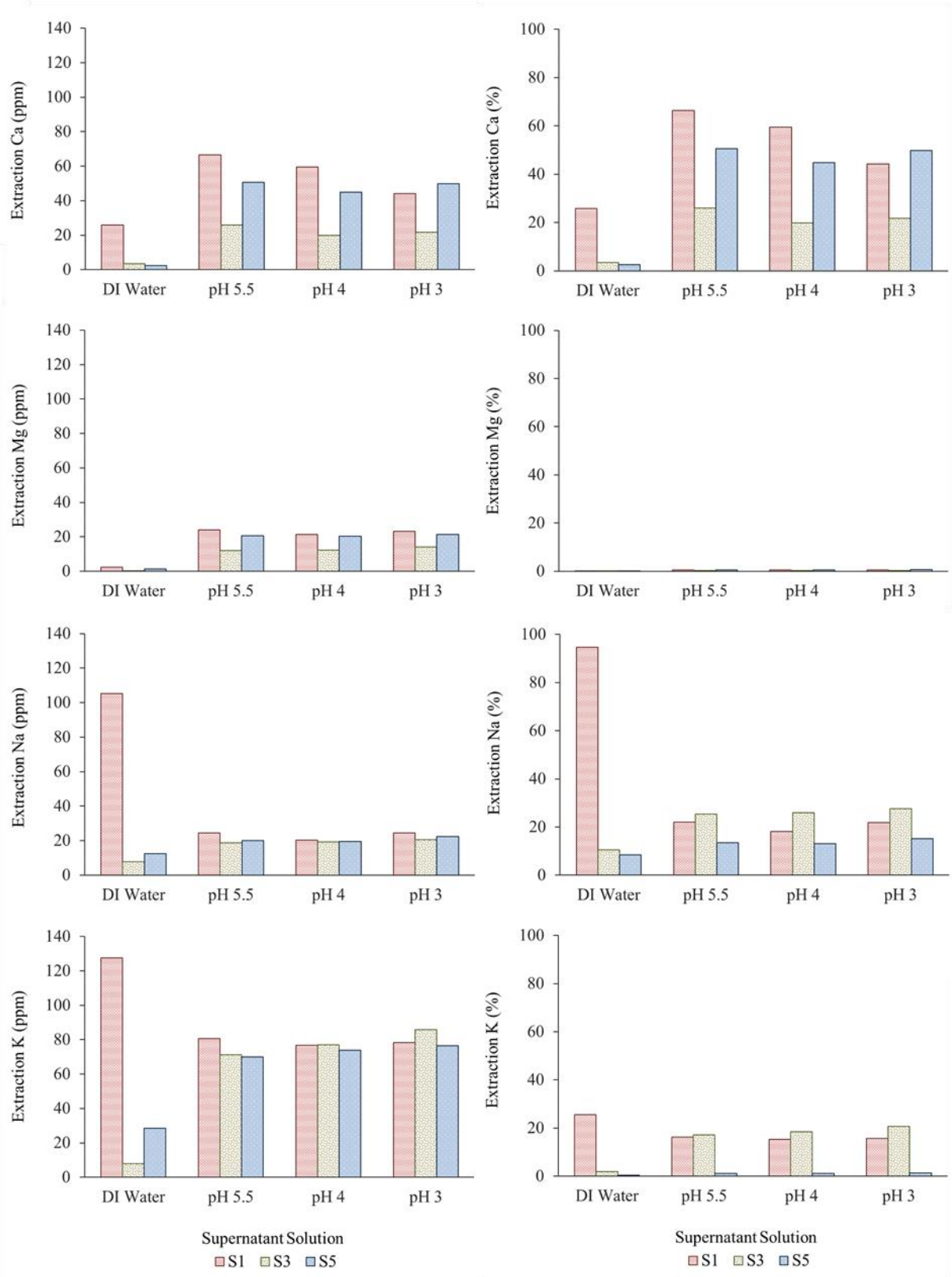


Figure 8.22. Extracted concentrations of Ca, Mg, Na, K in filtered supernatant solutions from leached clay veinlets (left) and corresponding extracted percentages of REY (right) at different pH values, and for D.I. water.

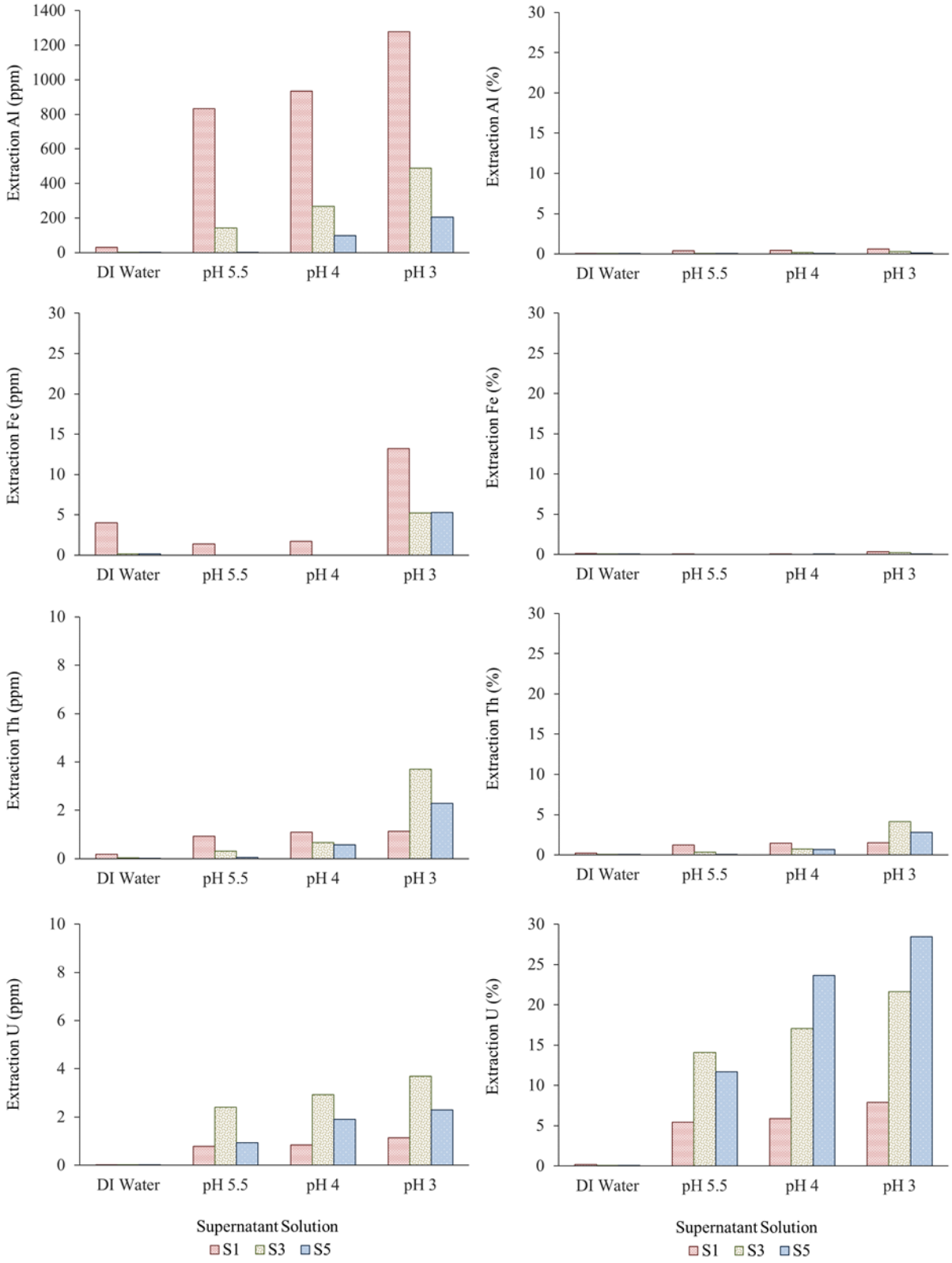


Figure 8.23. Extracted concentrations of Al, Fe, Th, U in filtered supernatant solutions from leached clay veinlets (left) and corresponding extracted percentages of REY (right) at different pH values, and for D.I. water.

Table 8.4. Extracted element concentrations in filtered supernatant solutions for all leached samples in the ion-exchange experiments, continued on next page.

Sample		batch experiment	Na (ppm)	(%)	Mg (ppm)	(%)	K (ppm)	(%)	Ca (ppm)	(%)	Rb (ppm)	(%)	Sr (ppm)	(%)	Ba (ppm)	(%)	Al (ppm)	(%)	Fe (ppm)	(%)	Mn (ppm)	(%)	REY (ppm)	(%)	LREE (ppm)	(%)	HREE (ppm)	(%)	Ce/Ce*	Eu/Eu*	La_N/Yb_N	Gd_N/Yb_N
	2.1	0.5 M $(NH_4)_2SO_4$ pH 5	24.4	22.0	24.0	0.57	80.7	16.2	47.5	66.4	1.93	11.8	0.24	26.4	3.39	27.50	832	0.42	1.38	0.03	3.96	6.26	3130	64.3	2426	62.6	196	73.5	0.24	0.19	17.7	1.48
S1	3.1	0.5 M $(NH_4)_2SO_4$ pH 4	20.2	18.1	21.3	0.50	76.7	15.4	42.5	59.5	1.75	10.8	0.22	24.6	3.33	28.8	933	0.47	1.71	0.04	3.73	5.91	2916	59.9	2259	58.3	185	69.0	0.23	0.19	17.4	1.46
	4.1	0.5 M $(NH_4)_2SO_4$ pH 3	24.3	21.9	23.2	0.55	78.4	15.7	31.5	44.1	1.8	11.0	0.22	23.9	3.25	28.3	1278	0.64	13.2	0.32	3.80	6.02	3035	62.4	2353	60.7	194	72.7	0.23	0.18	17.1	1.46
	5.1	D.I. water	105	94.7	2.32	0.05	128	25.6	18	25.8	1.06	6.52	0.04	4.5	0.288	2.4	31	0.02	4.02	0.10	0.32	0.51	12.8	0.26	10.7	0.3	0.58	0.22	0.66	0.17	20.5	1.84
	2.2	0.5 M $(NH_4)_2SO_4$ pH 5	18.8	25.3	12.1	0.29	71.2	17.1	37.1	26.0	2.26	17.5	0.23	5.04	6.98	44.3	143	0.08	nd	nd	1.41	2.22	6360	45.6	5116	44.9	359	53.3	0.00	0.22	27.3	2.09
S3	3.2	0.5 M $(NH_4)_2SO_4$ pH 4	19.2	25.9	12.2	0.29	77.0	18.6	28.4	19.8	2.20	17.1	0.25	4.94	6.84	40.4	268	0.15	nd	nd	1.47	2.32	6351	45.5	5105	44.8	363	53.9	0.00	0.23	26.7	2.09
	4.2	0.5 M $(NH_4)_2SO_4$ pH 3	20.4	27.6	14.1	0.34	85.9	20.7	31.0	21.7	2.22	17.2	0.22	5.54	7.67	39.5	489	0.28	5.25	0.25	1.69	2.68	7303	52.3	5868	51	419	62.2	0.01	0.23	26.6	2.08
	5.2	D.I. water	7.78	10.5	0.13	0.00	7.98	1.92	4.90	3.43	0.07	0.58	0.01	0.12	0.027	0.16	1.49	0.001	0.17	0.01	0.01	0.01	2.17	0.02	1.89	0.017	0.08	0.013	0.23	0.18	40.2	3.26
	2.3	0.5 M $(NH_4)_2SO_4$ pH 5	19.9	13.5	20.5	0.57	69.9	1.15	108	50.5	2.40	3.32	0.45	9.7	4.30	10.3	19.2	0.01	nd	nd	2.10	3.39	7251	83.3	5761	83.6	428	87.2	0.00	0.24	27.2	2.27
S5	3.3	0.5 M $(NH_4)_2SO_4$ pH 4	19.4	13.1	20.3	0.56	73.9	1.22	96	44.8	2.41	3.37	0.45	9.5	4.62	11.2	97	0.06	nd	0.01	2.26	3.57	7542	86.6	5986	86.8	458	93.3	0.00	0.24	26.2	2.23
	4.3	0.5 M $(NH_4)_2SO_4$ pH 3	22.4	15.1	21.4	0.59	76.4	1.26	107	49.8	2.41	3.37	0.47	9.9	4.63	11.2	205	0.13	5.28	0.09	2.42	3.83	7799	89.6	6177	89.6	472	96.1	0.00	0.24	26.1	2.22
	5.3	D.I. water	12.5	8.4	1.3	0.04	28.5	0.47	5.4	2.53	0.27	0.38	0.02	0.47	0.204	0.50	1.1	0.00	0.14	0.00	0.15	0.24	2.61	0.03	2.03	0.029	0.17	0.034	0.04	0.23	23.9	2.17
	2.5	0.5 M $(NH_4)_2SO_4$ pH 5	107	8.48	18.2	3.02	282	0.61	96	64.0	5.74	0.95	0.42	3.59	5.24	2.79	5.95	0.01	nd	nd	10.12	1.78	553	15.1	441	14.2	30.8	27.6	0.04	0.18	34.4	3.20
SV6	3.5	0.5 M $(NH_4)_2SO_4$ pH 4	105	8.32	18.3	3.04	289	0.63	91	60.5	5.80	0.96	0.48	3.63	5.04	3.13	94	0.11	2.38	0.01	13.31	2.34	611	16.7	483	15.5	37.2	33.3	0.05	0.18	28.1	2.73
	4.5	0.5 M $(NH_4)_2SO_4$ pH 3	110	8.75	19.7	3.26	301	0.66	110	73.0	5.85	0.97	0.42	4.17	4.67	3.01	508	0.62	97.0	0.43	22.1	3.88	726	19.8	555	17.9	48.7	43.6	0.06	0.18	22.0	2.35
	5.5	D.I. water	70.1	5.56	0.2	0.03	46.2	0.10	2.3	1.53	0.27	0.04	0.00	0.04	0.046	0.03	2.8	0.00	3.96	0.02	0.15	0.03	1.10	0.03	0.96	0.031	0.05	0.041	0.32	0.18	34.4	3.45
	2.6	0.5 M $(NH_4)_2SO_4$ pH 5	25.7	1.28	19.8	3.28	295	0.53	127	44.6	4.38	0.82	0.55	3.75	4.31	2.28	5.6	0.01	0.79	0.00	8.66	2.74	402	5.07	311	4.77	24.7	5.72	0.04	0.17	30.9	3.00
SV7	3.6	0.5 M $(NH_4)_2SO_4$ pH 4	24.7	1.23	20.1	3.33	305	0.55	124	43.4	4.45	0.84	0.56	3.63	4.03	2.56	96.6	0.12	7.04	0.03	10.8	3.42	456	5.75	348	5.34	30.9	7.15	0.04	0.17	24.7	2.57
	4.6	0.5 M $(NH_4)_2SO_4$ pH 3	27.8	1.39	21.5	3.57	320	0.57	126	43.9	4.38	0.82	0.54	3.78	3.83	2.40	485	0.61	114	0.55	18.2	5.77	580	7.30	438	6.73	42.2	9.77	0.04	0.18	20.8	2.32
	5.6	D.I. water	14.0	0.70	0.29	0.05	71.5	0.13	2.1	0.73	0.33	0.06	0.00	0.03	0.029	0.02	4.0	0.00	5.25	0.03	0.14	0.04	3.22	0.04	2.76	0.042	0.15	0.034	0.06	0.18	46.1	4.59
	2.7	0.5 M $(NH_4)_2SO_4$ pH 5	262	14.1	102	2.55	179	0.48	416	72.8	3.00	0.85	2.34	14.7	7.81	5.02	4.31	0.00	nd	nd	18.72	5.93	5388	75.5	3696	76.6	506	76.8	0.02	0.18	14.3	1.98
SV9	3.7	0.5 M $(NH_4)_2SO_4$ pH 4	260	14.0	102	2.57	186	0.50	426	74.6	2.95	0.83	2.30	14.6	8.70	5.60	66.8	0.07	2.38	0.01	20.3	6.41	5561	77.9	3807	78.9	529	80.4	0.02	0.19	13.8	1.92
	4.7	0.5 M $(NH_4)_2SO_4$ pH 3	267	14.4	105	2.64	193	0.52	434	76.0	2.94	0.83	2.32	14.4	8.28	5.33	213	0.23	41.6	0.24	22.6	7.17	5659	79.3	3860	80.0	543	82.5	0.02	0.18	13.6	1.90
	5.7	D.I. water	100	5.38	0.27	0.01	16	0.04	1.93	0.34	0.07	0.02	0.01	0.03	0.034	0.02	3.50	0.00	1.77	0.01	0.10	0.03	2.92	0.04	2.02	0.042	0.28	0.043	0.13	0.17	11.1	1.64
	2.8	0.5 M $(NH_4)_2SO_4$ pH 5	26.2	4.41	12.2	1.55	220	0.96	24.2	60.6	5.61	1.18	0.12	0.75	4.12	1.41	15.0	0.02	nd	nd	9.17	2.90	625	34.4	487	34.5	44.1	34.6	0.01	0.27	17.9	1.66
SV11	3.8	0.5 M $(NH_4)_2SO_4$ pH 4	17.9	3.02	12.9	1.64	229	1.00	13.4	33.4	5.81	1.22	0.13	0.71	4.52	1.55	85.7	0.09	4.59	0.02	9.58	3.03	642	35.4	497	35.2	46.5	36.6	0.02	0.27	16.7	1.59
	4.8	0.5 M $(NH_4)_2SO_4$ pH 3	17.3	2.91	10.1	1.66	231	1.00	20.9	52.2	5.61	1.18	0.12	0.80	4.54	1.56	177	0.19	72.9	0.22	9.58	3.03	642	35.4	494	34.9	46.5	36.6	0.02	0.28	16.4	1.53
	5.8	D.I. water	6.23	1.05	0.36	0.05	50.6	0.22	1.35	3.38	0.08	0.07	0.00	0.02	0.042	0.01	2.14	0.00	1.10	0.00	0.17	0.05	0.51	0.03	0.41	0.029	0.03	0.026	0.26	0.26	17.5	1.92
	2.9	0.5 M $(NH_4)_2SO_4$ pH 5	41.6	3.74	9.5	2.25	121	0.34	41.3	57.8	1.71	0.30	0.18	1.83	3.35	2.61	18.4	0.02	nd	nd	8.75	2.77	561	34.4	476	38.0	28.2	19.7	0.05	0.18	28.5	2.63
SV12	3.9	0.5 M $(NH_4)_2SO_4$ pH 4	38.8	3.49	9.7	2.29	129	0.36	39.7	55.5	1.78	0.31	0.19	1.97	3.50	2.73	58.5	0.07	3.78	0.01	9.72	3.08	573	35.4	486	38.8	29.0	20.2	0.05	0.18	27.6	2.53
	4.9	0.5 M $(NH_4)_2SO_4$ pH 3	40.4	3.63	13.0	2.39	133	0.37	38.9	54.4	1.74	0.31	0.19	1.91	3.70	2.89	317	0.21	28.1	0.12	10.7	3.38	581	35.4	492	39.2	29	20.5	0.05	0.18	27.3	2.48
	5.9	D.I. water	27.5	2.47	0.2	0.04	26.1	0.07	1.5	2.17	0.31	0.01	0.00	0.04	0.015	0.01	1.07	0.00	2.45	0.01	0.11	0.04	0.21	0.03	0.17	0.013	0.0	0.010	0.13	0.18	16.4	1.79
	2.10	0.5 M $(NH_4)_2SO_4$ pH 5	20.3	1.95	10.1	1.12	98.2	0.27	142	71.2	1.68	0.35	0.63	2.10	3.89	1.60	7.59	0.01	nd	nd	2.07	0.41	292	33.7	180	12.6	29.4	11.11	0.01	0.25	12.5	1.55
SV13	3.10	0.5 M $(NH_4)_2SO_4$ pH 4	19.5	1.88	10.4	1.14	103	0.29	141	70.7	1.74	0.36	0.63	2.05	4.12	1.69	41.4	0.05	4.93	0.02	2.61	0.52	305	34.4	186	13.0	31.4	11.87	0.01	0.24	11.7	1.47
	4.10	0.5 M $(NH_4)_2SO_4$ pH 3	21.2	2.04	11.3	1.25	112	0.31	151	75.5	1.72	0.36	0.61	2.10	4.17	1.71	166	0.34	38.3	0.14	3.59	0.71	321	34.9	194	13.6	33.4	12.62	0.01	0.25	11.1	1.40
	5.10	D.I. water	10.0	0.96	0.2	0.02	27.7	0.08	2.5	1.27	0.10	0.02	0.01	0.02	0.023	0.01	0.8	0.00	0.42	0.00	0.05	0.01	0.41	0.01	0.35	0.025	0.02	0.008	0.24	0.22	36.1	3.96
	2.11	0.5 M $(NH_4)_2SO_4$ pH 5	190	51.22	106	1.37	154	2.42	563	49.2	3.17	2.97	3.07	27.9	7.37	10.6	14.4	0.01	nd	nd	26.7	10.6	6512	50.7	4460	50.5	628	54.7	0.022	0.183	13.6	1.9
CS9	4.11	0.5 M $(NH_4)_2SO_4$ pH 3	208	56.1	117	1.50	172	2.70	633	55.4	0.00	0.00	3.34	30.3	3.73	5.35	347	0.22	44.4	0.27	31.8	12.6	7100	55.3	4816	54.5	684	59.5	0.022	0.183	13.3	1.9
	5.11	D.I. water	58	15.6	0.28	0.00	10	0.15	1.28	0.11	0.04	0.04	0.00	0.03	0.031	0.04	8.38	0.01	1.05	0.01	0.07	0.03	0.87	0.01	0.63	0.007	0.08	0.007	0.24	0.17	12.1	1.7
	2.12	0.5 M $(NH_4)_2SO_4$ pH 5	22	4.9	74	4.88	278	1.42	646	90.4	3.73	0.71	2.65	29.5	5.38	4.24	4.84	0.00	nd	nd	47.2	10.7	2447	13.3	1757	11.2	196	24.0	0.032	0.17	19.0	2.4
CS7	4.12	0.5 M $(NH_4)_2SO_4$ pH 3	19	4.34	67	4.42	248	1.27	545	76.3	nd	nd	2.24	24.9	3.22	2.53	227	0.15	118	0.33	46.3	10.5	2392	13.0	1697	10.8	204	24.9	0.032	0.17	15.7	2.1
	5.12	D.I. water	4.67	1.05	1.20	0.08	38	0.19	6.71	0.94	0.23	0.04	0.02	0.27	0.100	0.08	1.37	0.00	10.83	0.03	0.66	0.15	5.08	0.03	4.32	0.027	0.25	0.031	0.07	0.18	38.2	3.7

Ce/Ce*= $Ce_N/(La_N \cdot Pr_N)^{1/2}$, and Eu/Eu* = $Eu_N/(Sm_N \cdot Gd_N)^{1/2}$. N subscript represents nor **nd** not determined

Table 8.4 Continued

Sample		La (ppm)	(%)	Ce (ppm)	(%)	Pr (ppm)	(%)	Nd (ppm)	(%)	Sm (ppm)	(%)	Eu (ppm)	(%)	Gd (ppm)	(%)	Tb (ppm)	(%)	Dy (ppm)	(%)	Ho (ppm)	(%)	Er (ppm)	(%)	Tm (ppm)	(%)	Yb (ppm)	(%)	Lu (ppm)	(%)	Y (ppm)	(%)	Th (ppm)	(%)	U (ppm)	(%)
	2.1	1066	71.1	434	40.7	187	69.5	580	70.8	80.7	68.4	4.81	72.9	74.6	75.8	11.3	76.8	67.7	75.8	15.5	71.7	48.4	71.9	6.91	74.6	40.9	71.5	5.77	73.6	508	70.2	0.93	1.22	0.79	5.46
S1	3.1	993	66.2	400	65.2	175	66.1	541	63.8	75	67.1	4.42	71.2	70	72.4	10.6	71.1	63.5	67.2	14.5	67.4	45.4	69.5	6.43	67.7	38.7	67.5	5.29	65.4	473	66.2	1.09	1.45	0.84	5.9
	4.1	1031	68.7	418	37.5	182	67.6	565	69.0	78.1	66.2	4.54	68.8	73.8	75.0	11.1	75.2	66.7	74.7	15.3	71.0	48.0	71.2	6.88	74.3	40.9	71.6	5.49	70.0	487	67.4	1.14	1.51	1.14	7.9
	5.1	3.50	0.23	4.06	0.38	0.64	0.24	1.99	0.24	0.27	0.23	0.02	0.23	0.26	0.27	0.04	0.24	0.21	0.23	0.05	0.21	0.14	0.21	0.02	0.2	0.12	0.20	0.02	0.21	1.45	0.20	0.18	0.24	0.03	0.17
	2.2	2741	52.0	23.4	1.46	472	49.7	1480	52.9	209	47.8	14.1	68.3	177	55.4	24.4	55.4	133	51.8	28.1	53.3	84.4	53.2	11.7	57.3	68.3	54.6	9.86	57.7	885	47.0	0.31	0.35	2.41	14.1
S3	3.2	2722	51.7	23.0	1.4	473	53.0	1484	48.2	210	69.6	14.4	56.0	179	55.7	24.5	52.4	134	53.5	28.2	53.7	85.1	57.7	11.8	55.4	69.2	58.8	10.0	46.8	882	51.7	0.66	0.74	2.92	17.1
	4.2	3132	59.4	27.1	1.69	545	57.4	1703	60.8	239	54.9	16.5	79.8	205	64.4	28.4	64.5	155	60.7	32.6	61.9	97.3	61.4	13.7	66.7	80.0	64.0	11.6	67.7	1016	53.9	3.70	4.16	3.70	21.6
	5.2	0.83	0.02	0.33	0.02	0.15	0.02	0.46	0.02	0.07	0.02	0.00	0.02	0.06	0.02	0.01	0.02	0.03	0.01	0.01	0.01	0.02	0.01	0.00	0.01	0.01	0.01	0.00	0.01	0.19	0.01	0.025	0.03	0.00	0.03
	2.3	3083	88.9	11.5	3.33	528	86.2	1657	86.3	247	84.3	17.9	85.9	216	92.8	30.7	98	165	88.2	33.5	87.5	97	87.0	13.3	87.5	77.0	83.0	11.1	78.1	1062	80.2	0.055	0.07	0.94	11.7
S5	3.3	3187	91.8	12.1	3.5	550	89.8	1732	90.2	259	88.2	18.9	90	227	98	32.5	104	177	94.5	35.8	93.5	104	92.8	14.3	93.8	82.7	89.1	12.0	84.6	1098	82.9	0.57	0.70	1.91	23.7
	4.3	3290	94.8	12.8	3.73	569	93.0	1782	92.8	268	91.6	19.6	93.9	236	101	33.6	107	182	97	36.8	96	107	96	14.7	97	85.8	92.4	12.3	86.8	1150	86.8	2.29	2.80	2.29	28.5
	5.3	1.04	0.03	0.07	0.02	0.18	0.03	0.56	0.03	0.09	0.03	0.01	0.03	0.08	0.03	0.01	0.04	0.06	0.03	0.01	0.03	0.04	0.03	0.00	0.03	0.03	0.03	0.00	0.03	0.41	0.03	0.010	0.01	0.00	0.06
	2.5	225	25.9	16.8	1.29	37.7	19.7	125	22.2	18.6	18.2	1.05	19.1	17.5	24.4	2.46	20.2	13.0	19.2	2.54	17.5	6.92	16.9	0.83	14.6	4.44	11.8	0.61	12.0	81.33	21.7	nd	nd	0.36	3.5
SV6	3.5	241	27.8	19.6	1.5	42	24.6	138	20.7	21	21.9	1.20	27.3	19.7	23.3	2.84	22.8	15.4	20.8	3.02	20.2	8.26	18.3	1.04	15.5	5.83	15.8	0.80	24.2	90.6	27.8	0.38	0.42	1.18	11.5
	4.5	266	30.7	27.3	2.09	48.8	25.6	162	28.7	25.8	25.3	1.48	27.0	23.8	33.1	3.6	29.4	19.8	29.2	3.9	26.6	10.8	26.2	1.4	24.6	8.2	21.8	1.1	22.3	122	32.6	2.11	2.31	2.11	20.7
	5.5	0.36	0.04	0.22	0.02	0.08	0.04	0.24	0.04	0.04	0.04	0.00	0.04	0.03	0.04	0.00	0.03	0.02	0.03	0.00	0.02	0.01	0.02	0.00	0.02	0.01	0.02	0.00	0.02	0.09	0.02	0.019	0.02	0.00	0.02
	2.6	164	5.78	9.35	1.40	24.9	4.16	85.6	4.67	12.8	4.01	0.74	4.14	13.4	5.69	1.91	5.24	10.4	5.51	2.06	5.84	5.60	6.48	0.68	6.22	3.61	5.46	0.50	5.78	66.5	6.70	nd	nd	0.89	6.3
SV7	3.6	178	6.27	11.2	1.68	29	5.36	98	4.75	15	4.89	0.88	6.64	15.6	6.30	2.29	6.75	12.7	7.17	2.52	7.97	6.89	7.94	0.87	7.43	4.91	7.86	0.68	7.81	77.5	6.27	0.250	0.31	2.26	16.1
	4.6	215	7.57	16.5	2.47	37.6	6.28	127	6.93	20.4	6.39	1.19	6.63	20.2	8.59	3.1	8.43	17.2	9.15	3.4	9.54	9.3	10.8	1.2	11.2	7.0	10.6	1.0	11.2	99	10.0	3.22	4.00	3.22	22.9
	5.6	1.27	0.04	0.15	0.02	0.26	0.04	0.83	0.05	0.14	0.04	0.01	0.04	0.11	0.05	0.01	0.04	0.07	0.04	0.01	0.03	0.03	0.03	0.00	0.03	0.02	0.03	0.00	0.03	0.31	0.03	0.022	0.03	0.00	0.02
	2.7	1828	84.2	66.3	14.9	318	79.2	1067	82.1	192	78.6	12.2	82.1	212	84.5	35.0	84.1	203	82.9	40.8	73.1	113	74.7	15.3	75.6	86.5	68.1	12.2	69.1	1186	71.7	nd	nd	0.56	5.1
SV9	3.7	1875	86.4	68.6	15.4	328	85.0	1105	80.9	197	85.8	12.7	87.5	220	87.4	36.4	86.2	211	75.4	42.1	78.5	119	79.5	16	72.6	92	73.6	13	74.0	1224	74.0	0.209	0.30	1.63	15.0
	4.7	1896	87.4	69.9	15.7	334	83.0	1121	86.3	203	83.2	12.8	86.2	222	88.5	37.2	89.3	216	88.4	43.3	77.7	122	80.5	16.4	81.3	94.9	74.7	13.4	76.2	1256	75.9	2.16	3.10	2.16	19.9
	5.7	0.89	0.04	0.20	0.05	0.17	0.04	0.55	0.04	0.10	0.04	0.01	0.04	0.11	0.04	0.02	0.04	0.11	0.04	0.02	0.04	0.06	0.04	0.01	0.04	0.05	0.04	0.01	0.04	0.62	0.04	0.025	0.04	0.01	0.05
	2.8	241	47.6	6.0	1.67	45.3	43.7	152	45.8	22.6	38.8	1.85	41.6	18.8	40.0	2.75	36.3	15.9	34.7	3.33	33.3	10.18	36.1	1.46	34.4	9.16	33.4	1.33	32.8	93.15	33.7	0.064	0.07	0.58	4.7
SV11	3.8	243	48.1	6.7	2.8	46.6	47.3	157	40.0	23.4	43.1	1.92	41.3	19.3	37.7	2.86	36.3	16.6	35.0	3.49	38.1	10.74	36.6	1.55	35.9	9.83	35.2	1.42	35.6	98.2	35.6	0.52	0.54	1.20	9.69
	4.8	241	47.6	7.1	1.96	46.5	44.9	155	46.8	23.0	39.4	1.90	42.6	18.9	40.3	2.84	37.5	16.6	36.3	3.45	34.6	10.7	37.8	1.56	36.8	10.0	36.5	1.4	35.4	102	37.0	1.69	1.76	1.69	13.6
	5.8	0.16	0.03	0.08	0.02	0.03	0.03	0.10	0.03	0.02	0.03	0.00	0.03	0.02	0.03	0.00	0.03	0.01	0.03	0.00	0.02	0.01	0.03	0.00	0.02	0.01	0.02	0.00	0.02	0.07	0.03	0.014	0.01	0.00	0.02
	2.9	210	85.8	19.00	2.67	47.9	86.1	158	88.8	23.2	70.5	1.16	54.2	16.2	58.7	2.14	36.7	11.1	25.8	2.15	19.9	6.3	18.3	0.83	15.5	5.01	13.0	0.69	12.5	56.2	21.0	0.080	0.09	1.07	7.4
SV12	3.9	213	47.6	19.74	1.9	49.0	91.4	163	72.0	23.7	55.3	1.18	59.1	16.4	37.7	2.20	26.5	11.4	20.3	2.20	18.8	6.4	16.1	0.87	13.6	5.24	13.0	0.72	12.5	58.1	21.70	0.64	0.70	1.71	11.9
	4.9	215	87.9	20.32	2.85	49.7	89.2	165	92.4	23.8	72.3	1.17	55.1	16.5	59.4	2.22	37.9	11.5	26.7	2.2	20.6	6.5	19.0	0.87	16.2	5.4	13.9	0.7	13.4	60	22.3	2.14	2.34	2.14	14.9
	5.9	0.07	0.03	0.02	0.00	0.02	0.03	0.05	0.03	0.01	0.02	0.00	0.02	0.01	0.02	0.00	0.02	0.01	0.01	0.00	0.01	0.00	0.01	0.00	0.01	0.00	0.01	0.00	0.01	0.03	0.01	0.006	0.01	0.002	0.02
	2.10	99.8	18.79	1.08	0.29	13.7	14.5	46.7	15.6	7.75	13.4	0.72	14.7	10.4	15.4	1.72	13.7	10.8	12.8	2.45	11.8	7.29	11.3	0.98	10.3	5.41	8.39	0.78	8.94	82.8	13.5	nd	nd	0.27	2.04
SV13	3.10	102	19.3	1.51	0.4	14.2	16.2	48.5	14.0	8.07	15.2	0.75	16.0	10.8	14.4	1.81	13.6	11.5	12.5	2.60	12.0	7.73	11.1	1.05	9.19	5.93	9.75	0.85	14.1	86.9	19.3	0.119	0.15	0.60	4.60
	4.10	106	19.94	2.22	0.60	14.8	15.7	50.5	16.8	8.4	14.7	0.79	16.0	11.2	16.6	1.9	15.2	12.1	14.4	2.7	13.0	8.2	12.6	1.12	11.8	6.5	10.0	0.93	10.6	94	15.2	0.811	1.02	0.81	6.19
	5.10	0.15	0.03	0.06	0.02	0.03	0.03	0.09	0.03	0.01	0.03	0.00	0.02	0.01	0.02	0.00	0.02	0.01	0.01	0.00	0.01	0.00	0.01	0.00	0.01	0.00	0.00	0.00	0.00	0.04	0.01	0.008	0.01	0.00	0.01
	2.11	2199	53.5	82.0	13.1	385	54.8	1290	55.1	232	53.7	14.7	52.7	257	52.1	42.9	53.0	251	52.0	50.5	47.9	139	49.4	18.9	51.1	110	48.1	15.3	46.8	1423	49.8	0.03	0.03	1.71	9.6
CS9	4.11	2376	57.8	90.0	14.4	415	59.2	1388	59.3	251	58.1	15.9	57.0	279	56.6	46.4	57.4	272	56.2	54.4	51.5	152	53.9	20.6	55.6	122	53.1	17.0	51.7	1600	56.0	4.98	4.70	4.98	28.1
	5.11	0.26	0.01	0.11	0.02	0.05	0.01	0.16	0.01	0.03	0.01	0.00	0.01	0.03	0.01	0.01	0.01	0.03	0.01	0.01	0.01	0.02	0.01	0.00	0.01	0.01	0.01	0.00	0.01	0.16	0.01	0.019	0.0	0.01	0.03
	2.12	878	12.5	46.9	4.02	147	10.5	499	10.6	87.8	10.9	5.10	14.9	92.7	18.4	14.5	20.6	80.1	21.9	16.1	25.1	44.3	27.1	5.47	27.1	31.4	26.0	4.26	29.1	494	25.5	nd	nd	2.60	7.0
CS7	4.12	828	11.8	46.2	3.96	145	10.3	492	10.5	89.0	11.0	4.95	14.5	91.6	18.1	14.5	20.5	81.4	22.3	16.3	25.4	45.5	27.8	5.6	27.9	35.9	29.8	4.6	31.3	492	25.4	21.4	12.0	21.4	57.8
	5.12	1.98	0.03	0.28	0.02	0.41	0.03	1.27	0.03	0.21	0.03	0.01	0.03	0.16	0.03	0.02	0.03	0.11	0.03	0.02	0.03	0.05	0.03	0.01	0.03	0.04	0.03	0.00	0.03	0.52	0.03	0.044	0.02	0.02	0.04

8.3.3 Residual material

8.3.31 Bulk mineralogical changes – XRD analysis.

The XRD patterns of the leach residues of bulk saprolite, CSF and infill fracture samples from four leaching experimental runs, as well as the untreated material from these samples, are presented in Figure 8.24, Figure 8.25 and Figure 8.26. Overall, the patterns show that the leach residues remain similar to the untreated material. The bulk mineralogy (kaolinite, quartz, K-feldspar and biotite) remains unchanged and no new phases can be identified in the leach residue by XRD analysis. However, several small changes in XRD patterns of samples containing smectite and poorly crystalline biotite can be identified, which suggest small changes in the composition or structure of these minerals occurs during leaching.

The first observable change is found in the XRD patterns of the ammonium sulphate-treated leach residues of samples SV9 and CS9, where the low angle broad peak corresponding to smectite appears to have shifted to a higher angle position. The XRD patterns in Figure 8.24 A and Figure 8.25A show that the low angle smectite peak in the ammonium sulphate leach residues of these two samples has a d-spacing of 12.5 Å (8.2 2θ) instead of the 15 Å (6.8 2θ) and is the same for all leach residues run at different pH conditions. As well as changing position, the intensity of this low angle smectite peak also appears to be lower, with counts of < 400 compared to > 400 in the untreated material. The XRD patterns for these two samples show that that a second smectite peak found in the untreated material at 5 Å (20.6 θ) is absent after leaching. None of these changes to the smectite peaks are observed in XRD patterns of D.I. water treated leach residues.

In samples CS7, S1, S3 and S5, where smectites were also identified but in much smaller quantities or a less crystalline form (compared to SV9 and CS9), the low angle peaks which are very broad and only slightly above the background level are no longer present in ammonium sulphate treated leach residues (Figure 8.25A and Figure 8.26). It is possible that the peak has also shifted but its intensity is too low to be discriminated from background.

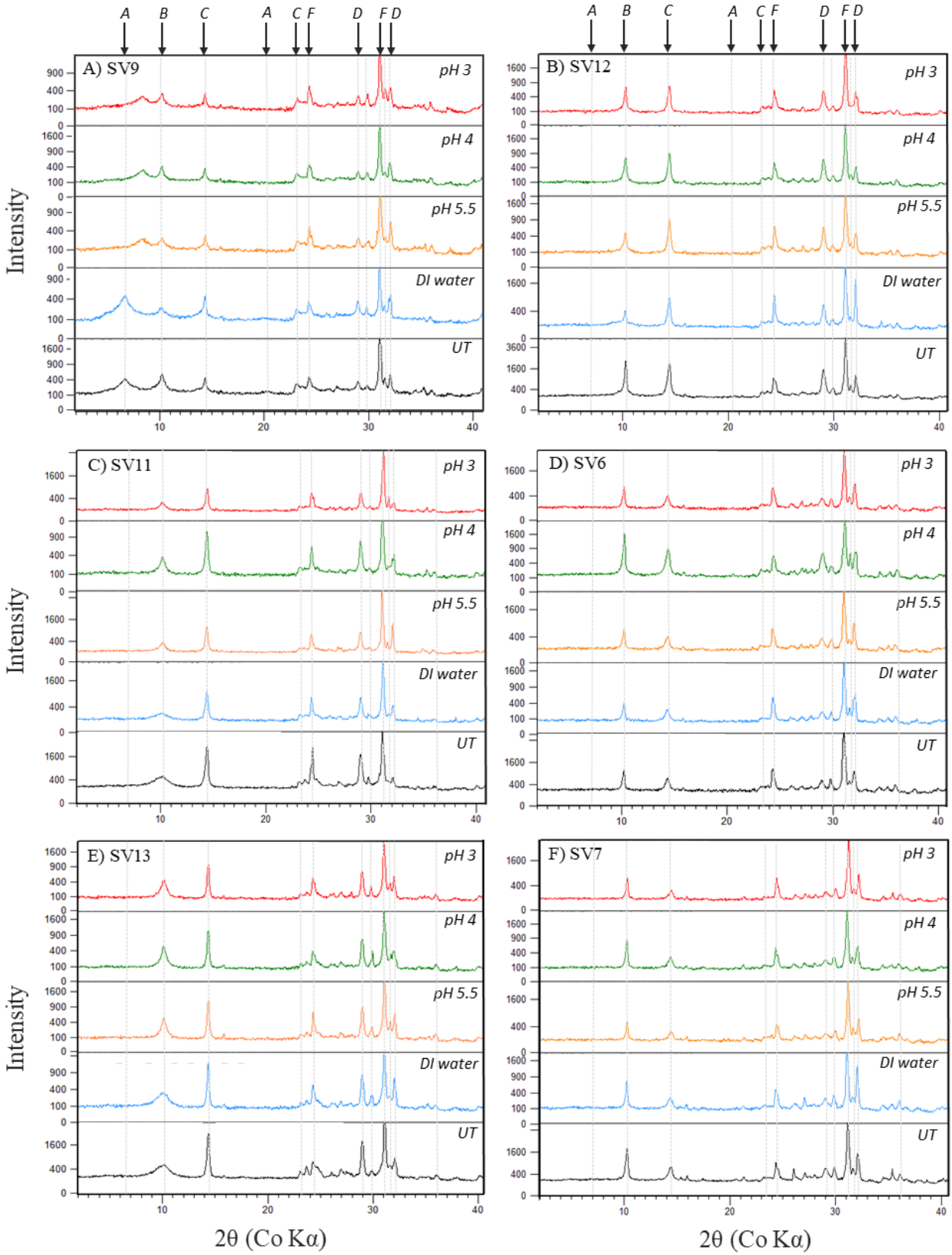


Figure 8.24. Representative XRD patterns of untreated bulk saprolite samples and corresponding washed and filtered leach residues. Note that bastnäsite was not detected in these samples.

The second observable change is related to the biotite peak 10 Å (10.2 *2θ*) in samples SV11 and SV13. In these samples, peaks corresponding to biotite are broad and of low intensity in untreated samples. However, in the ammonium sulphate-treated leach residue of these samples, the peak appears sharper and more intense (Figure 8.24 C & E). No shift in peak position is observed. This change is not observed in the XRD pattern of D.I. water treated solid residue.

All the other minerals present in the samples leached; kaolinite, K-feldspar, and quartz are unaffected by leaching. The intensity and position of the peaks associated with these minerals remain unchanged in solid residue of all experimental runs. The peaks identified as corresponding to bastnäsite in samples SV7 and CS7 are also unaltered during leaching (Figure 8.25).

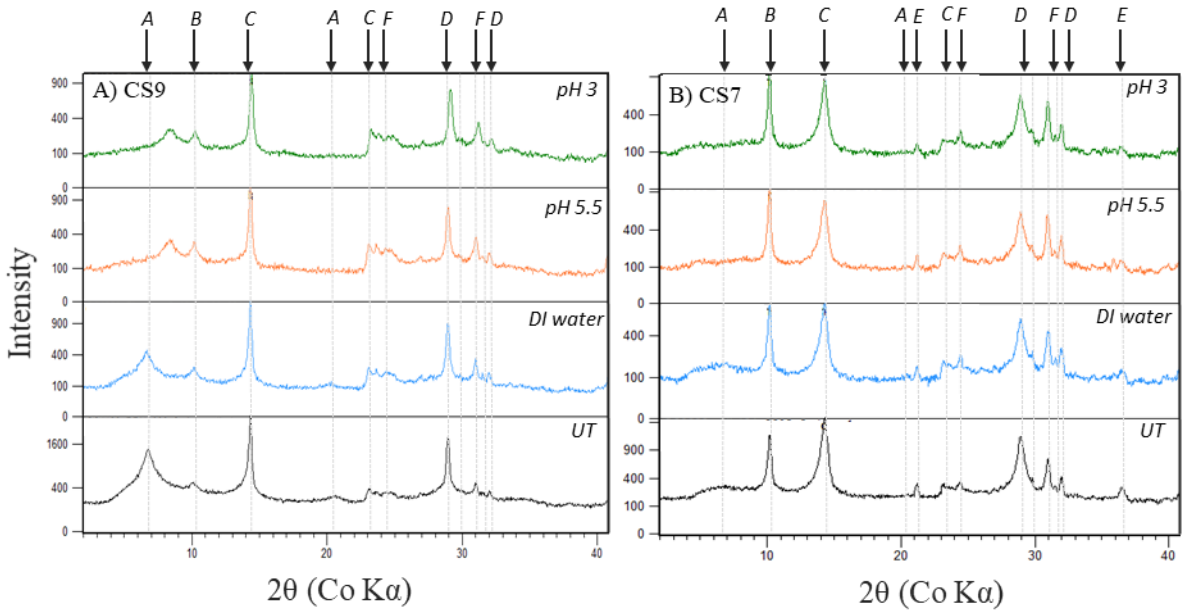


Figure 8.25. Representative XRD patterns of untreated clay separate samples and corresponding washed and filtered leach residues.

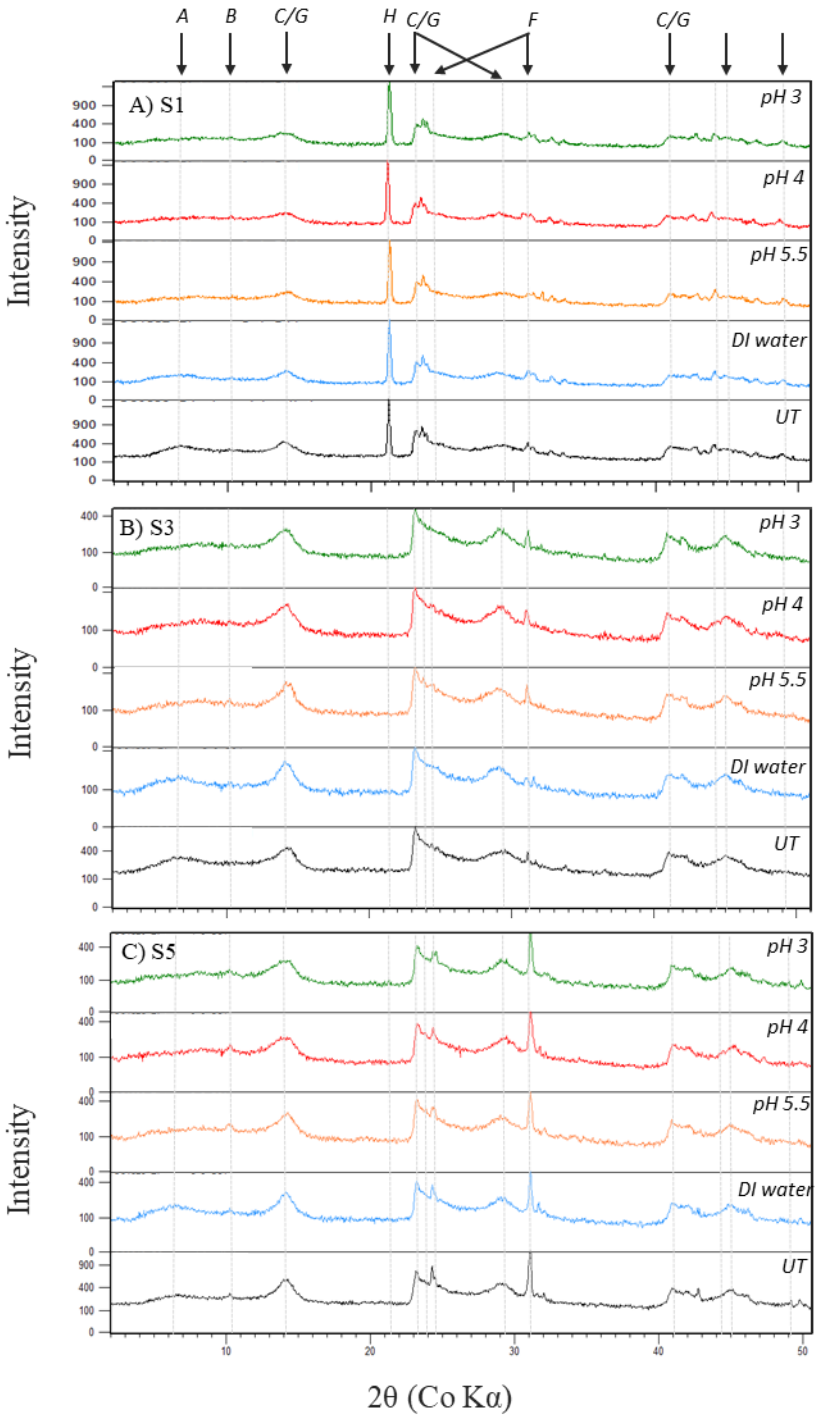


Figure 8.26. Representative XRD patterns of untreated clay veinlet samples and corresponding washed and filtered leach residues.

8.3.4.2 Residual material-SEM analysis

SEM analysis of the residual solids shows that the REE minerals present in the saprolite and fracture infill samples are unaffected by the ammonium sulphate, and the range of pH conditions used in these ion-exchange leaching experiments.

SEM-BSE images and SEM-EDS maps presented in Figure 8.27, Figure 8.28 and Figure 8.29 show preserved grains of LREE-fluorcarbonates, Y-phosphates, LREE-phosphates, Ce oxides, and niobiates in leach residue from the experiments using ammonium sulphate at pH 3. The images show that both composition and morphology remains unaffected by leaching.

SEM analysis shows that leach residues from samples with the lowest REE extraction % results contained the most abundant REE minerals. For example, in samples CS7 and SV7 which have among the lowest % extraction results, fine LREE-fluorcarbonates were commonly found in the leach residues of all experimental runs. In sample 61 and S3 REE phosphates were also easily identified, with grains occurring as large individual grains, as acicular crystals in clay clumps, or as amorphous grains coating coarse primary minerals such as quartz. In samples with very good extraction results e.g. SV9 and S5, very few REE mineral grains were observed in the residual solids.

Finally, although, XRD analysis of the residual solid showed no new mineral phases forming, SEM-EDS maps reveal clay rich zones with elevated S contents (Figure 8.29), suggesting the precipitation of Sulphur. It is not possible from the images to determine in which form the S is present (e.g. as elemental Sulphur or a Sulphur-bearing mineral).

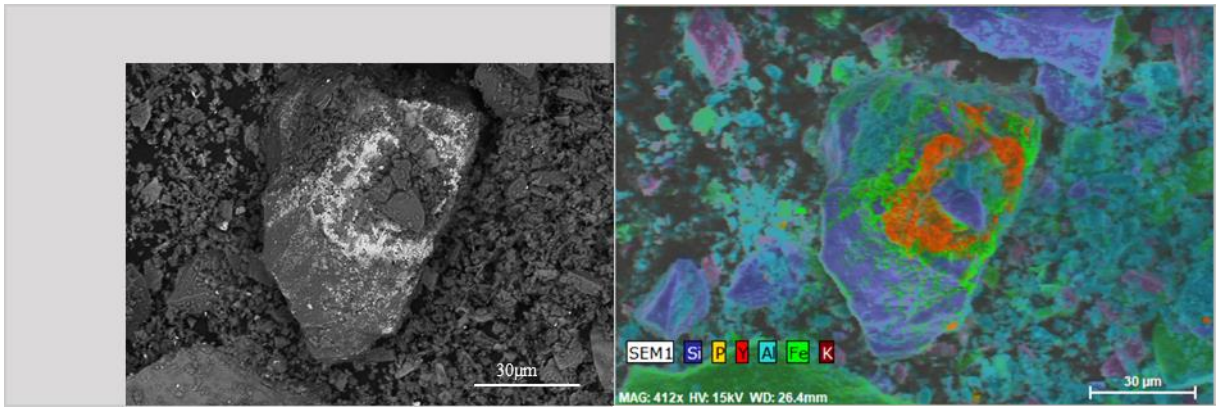


Figure 8.27. SEM-BSE image (left) and corresponding false-colour EDS element map (right) showing undissolved Y-phosphate amorphous grains within washed and filtered residue material from sample SV13 (leached with ammonium-sulphate solution of pH 3; run 4_10).

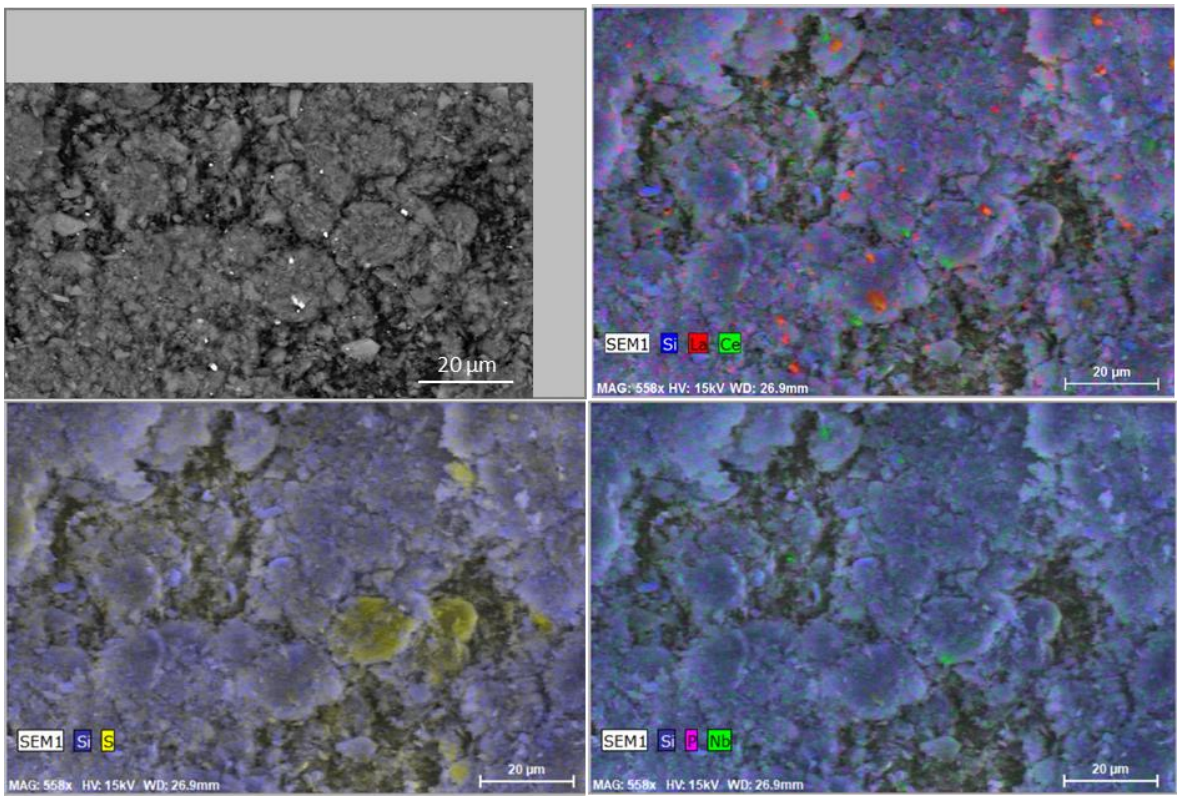


Figure 8.28. SEM-BSE image (top left) and corresponding false-colour EDS element maps overlaid overSEM-BSE imagery to show residual LREE-fluorcarbonates (top right), Ce-oxides (top right), REE-niobiates (lower right), and very fine-grained precipitated sulfur-bearing phase in the residual solid (lower left) from sample CS7 after leaching with ammonium sulphate solution at pH 3 (run 4_11).

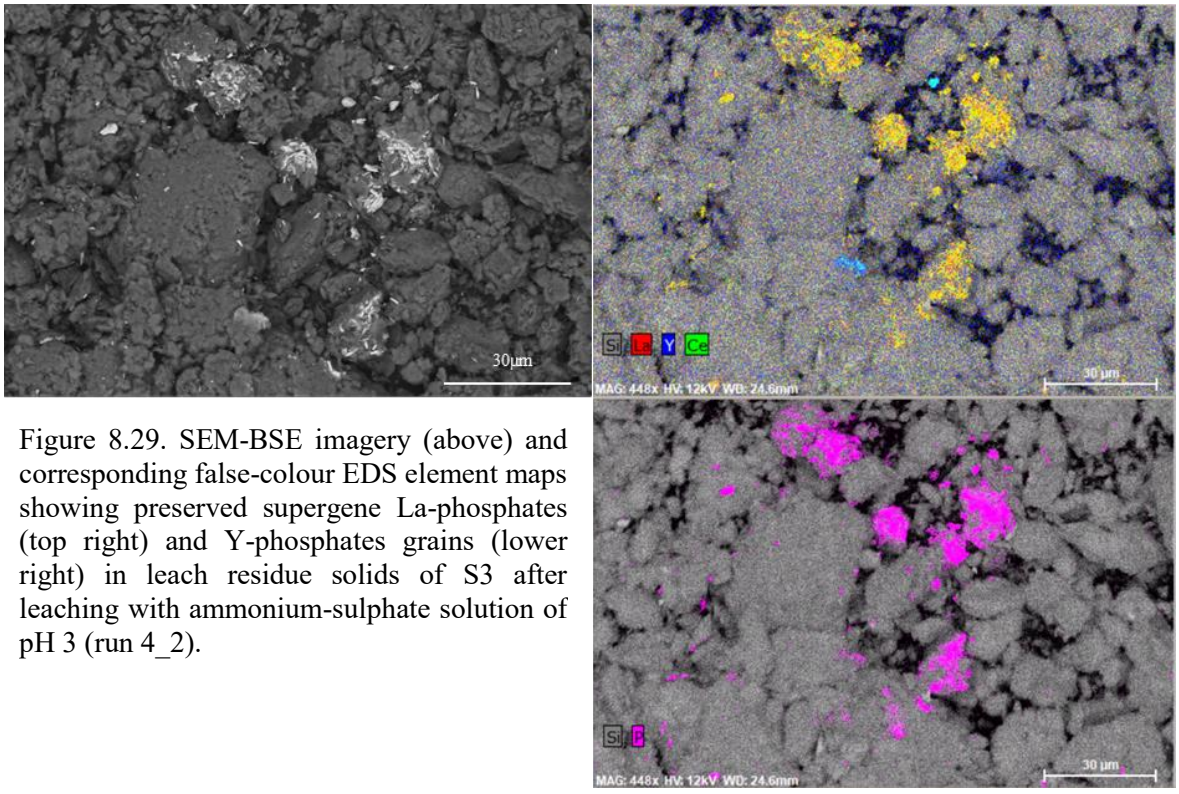


Figure 8.29. SEM-BSE imagery (above) and corresponding false-colour EDS element maps showing preserved supergene La-phosphates (top right) and Y-phosphates grains (lower right) in leach residue solids of S3 after leaching with ammonium-sulphate solution of pH 3 (run 4_2).

8.4 Discussion

8.4.1 Ion-exchangeable REE in Serra Verde ore

The ion-exchange leaching results of saprolite samples indicate that the PER in the REE-enriched saprolite horizon is highly variable, both laterally and vertically across the Serra Verde deposit. The ion-exchangeable REY in the saprolite samples leached with ammonium sulphate under pH 5.5 conditions range from 292 and 5388 ppm REY, which represent between 5 wt % and 75.5 % extraction of bulk saprolite REE content. Except for result of SV7 (5 wt % extraction), the values for all other samples are comparable with results published for Chinese ores which have between 30 – 100 % extractable REE (Sanematsu and Kon 2013, Sanematsu & Watanabe 2016) and clays leached other parts of the world at 40 – 80 % (Moldoveanu and Papangelakis 2016).

The saprolite samples used in these extraction experiment had high and wide ranging REE concentrations, 1665 ppm and 7000 ppm REY. However, neither the PER nor the amount of ion-exchangeable REE in the samples correlates with the total REE content in these samples. The results show that samples with similar REE concentrations may have very different ion-exchangeable REE and that samples with relatively low REE content can have a higher PER than samples that are more REE-enriched. For example, the two saprolite samples with the highest REE content, SV7 and SV9, contain the lowest and the highest PER respectively and SV11 which has the lowest REE content had the second highest PER.

The vertical variations in ion-exchangeable REE along the saprolite horizon are highlighted by the results from SV6 and SV7 which were collected from drill hole DDH0161. The results show that the more strongly REE-enriched lower saprolite (SV7) has a lower PER compared to the upper saprolite (SV6). More samples along the saprolite horizon from different locations need to be tested to determine if this saprolite REE distribution is found across the deposit, or if it represents a localised variation. The drill hole selected happens to have very low PER and therefore variations within it may not be representative of the deposit.

The variations in the ion-exchangeable REE content of saprolite samples studies are most likely controlled by variations in the REE mineralogy, clay content and the physiochemical conditions in the profile. The effect of the first two are discussed in the sections 8.4.3 and 8.4.4.

The analytical results show that the ion-exchangeable REE of Serra Verde deposit are significantly depleted in Ce. The depletion of Ce can be clearly seen in the chondrite-normalised REE patterns, which show that ion-exchangeable REE have much stronger negative Ce anomalies than REE in bulk saprolite sample (Figure 8.30). In all bulk and infill fracture samples collected from the saprolite, the REE extracted by ion-exchange contain < 3 % total Ce content and have negative Ce anomalies with values of < 0.05. These results suggest that the majority of the Ce in the saprolite horizon is not adsorbed onto clay minerals but held by other phases such REE bearing resistant minerals, Ce oxides, Mn oxides, or colloids. This finding follows results from previous studies which have shown that the depletion of ion-exchangeable Ce is common in ion-adsorption ores (e.g. Wu et al. 1990, Sanematsu et al 2013 Sanematsu & Kon 2013).

La_N/Yb_N ratios of the ion-exchangeable fraction of saprolite samples are generally higher than those of whole rock, suggesting that the ion-exchangeable REY, except Ce, are more strongly enriched in LREE than in HREE (Figure 8.30). This was also the case in the results from experiments carried out by Moldoveanu and Papangelakis (2016) and Sanematsu and Kon (2013). The preferential enrichment of LREE in exchangeable REE can be attributed to differences in the weathering resistance of REE bearing minerals in the parent rock. This suggests that LREE bearing minerals are preferentially breaking down in the Serra Verde deposit. However, except for two saprolite samples, the difference between bulk rock and extracted La_N/Yb_N ratios is small. No significant differences in the La_N/Yb_N of REE extracted from fracture infill samples was observed. In these samples the majority of REE are held in clays and therefore little fractionation can occur.

Eu content in the samples analysed and in the extracted REE is low. Comparison of Eu anomalies suggest a very small degree Eu fractionation is taking place between the ion-exchangeable fraction and bulk content of saprolite samples (Figure 8.30). The majority of the saprolite samples are Eu depleted while infill fracture samples the fracture infill samples collected are unchanged or enriched. The depletion of ion-exchangeable Eu has been observed in other ion-adsorption ores and is associated to the weathering of plagioclase, dominant Eu-bearing mineral (Wu et al. 1990, Bao and Zhao 2008, Sanematsu and Kon 2013).

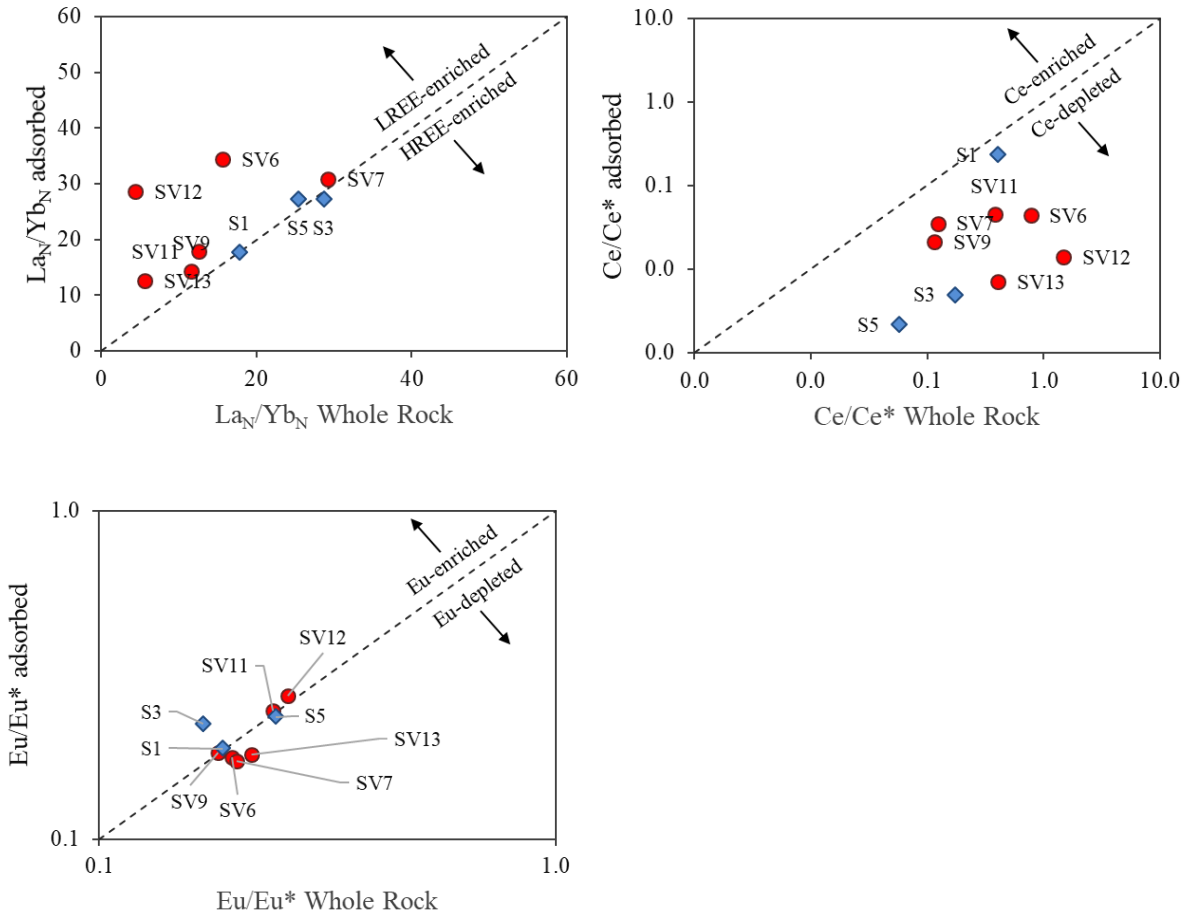


Figure 8.30. REE ratio plots comparing untreated bulk saprolite samples (Whole Rock) and corresponding ion-exchangeable REE for saprolite and clay veinlet samples. La/Yb and Ce/Ce* ratios indicate fractionation of REE between the bulk and ion-adsorbed fraction.

The fracture infill samples collected from saprolite and mottled zone horizons exposed in the plateau area have the highest amounts of ion-exchangeable REE of all samples studied. The ion-exchangeable REY in these samples ranges between 3130 and 7251 ppm REY and account for the majority of REE in the sample (53 to 87 %). The presence of these clays has not been reported before, and represent localised areas of extreme REE enrichment by percolating fluids.

The sensitivity of both REE and non-REE extraction to leaching times noted from the preliminary experiments indicate that significant improvements and optimisation of the leaching performance is possible, and should be a focus of further metallurgical test work.

8.4.2 Non-REE impurities

Other non-REE such as Ca, Na and Al were present in leached solutions from all samples. These elements are widely considered impurities that negatively impact the processing of REE solutions (Xiao et al. 2015). The extracted concentrations of these impurities varied between samples, but overall, Ca, Na and K were leached at the highest concentrations at pH 5.5, while Al was most leached at pH 3. In general, greater concentrations of non-REE impurities were released from saprolite samples than from clay veinlet samples.

Comparing the extracted concentrations of total REE and total non-REE shows that total REE are consistently extracted to higher concentrations. Only the individual species La, Nd, and in some cases Y, reach concentrations that exceed the most extracted non-REE.

Of the alkaline earth and alkali elements, Ca and Na are the most strongly leached. The high extractability of Ca (> 50 % in most samples) suggests that the majority of Ca is either held in carbonate minerals or adsorbed onto clays. The Mg and K show relatively low extractability from bulk saprolite samples, which is probably due to their high concentrations in bulk silicate minerals that have yet to breakdown in the saprolite, such as feldspars and biotite (see Chapter 7). In clay veinlets, higher proportions of Na and K are extracted than from saprolite samples, despite relatively low bulk concentration of these elements in the solid. Results from the D.I. water experiment show that, of the total amount of Na and K extracted with ammonium sulphate, 25 – 60 % of the Na, and 10 – 30 % of the K are present as readily soluble, free ions and are therefore not adsorbed onto clay minerals. The readily soluble Na and K probably indicate a minor salt content in the clay veinlets, which may be delivered by surface waters periodically flowing through these fractures in the profile and precipitating salt during drier periods.

The low extraction percentages of the transition metals and radioactive metals is interpreted to be due to their occurrence in primary and insoluble minerals. Fe and Al are present as structurally-bound elements in primary minerals, clays, and highly insoluble oxides. The high extraction of Al at pH 3 can be attributed to dissolution of clay minerals. Th and U are mostly hosted in insoluble minerals such as zircon, niobiates and phosphates. These results show that unlike REE, Th and U are not found as ion-exchangeable species in the Serra Verde saprolite ore.

8.4.3 Effect of supergene minerals on extraction of REE

Resistant primary and supergene REE-bearing minerals present in the weathered profile can hold a significant proportion of REE and limit the extraction of REE by ion-exchange methods. The ion-exchange leaching results show that samples with the highest phosphate contents (SV13 and S3) and samples containing supergene LREE-fluorcarbonates (SV7 and SV6). have the lowest percentages of ion-exchangeable REE. Contrastingly, samples with low REE-mineral contents (SV9, S3 and S5) have the highest percentages of ion-exchangeable REE. Bulk phosphate content of REE ore has been suggested to correlate with the percentage of extractable REE (Sanematsu et al. 2015), where high phosphate contents correlate with low PER, but low phosphate contents may have either high or low extractable REE. At Serra Verde, the same relationship is observed where high bulk phosphate contents correlate with lower extractable REE. These results are in agreement with the calculated proportions of REE carried by REE-minerals in Chapter 7. The differences in mineralogy partly explain why bulk REE grades cannot be used to predict ion-exchangeable REE.

Variation in the abundance and type of REE minerals found in the samples also explains some of the variations in the individual REE extractions between samples. For example, the preferential extraction of HREE in SV7 and SV6 can be attributed to the presence of LREE fluorcarbonates. Whereas the very low HREE extraction percentages in SV12 can be explained by the majority of the REE minerals present in this sample being HREE bearing niobiates and phosphates (Appendix E1).

Except for Ce oxides, organic matter, colloids and oxide phases have also been found to host REE in weathered granites (Sanematsu and Kon 2013, Sanematsu et al. 2013). These phases were not detected in the mineralogical study (Chapter 7), and there is no data to suggest whether they are present as REE hosts. The degree to which these minerals host REE in the saprolite ore, and their modes of occurrence at Serra Verde should be evaluated by further work such as sequential leaching (e.g. Sanematstu and Kon 2013). Sequential leaching would also help to produce better estimates of the amount of REE held by different REE minerals phases, namely phosphates, silicates, and oxides.

In summary, it can be concluded that, although the REE-minerals in the saprolite of the Serra Verde IAD are present in relatively low quantities, small variations in their abundance has a significant effect on the fraction of both total REE, and individual REE that are ion-exchangeable.

8.4.4 Effect of clay mineralogy on ion-exchangeable REE

The clay content, clay mineralogy and physiochemical conditions influence the absorption capacity of the weathered samples to accommodate REE. This section discusses the effects that variation in clay mineralogy and clay content have on the ion-exchangeable REE fraction.

Clay mineralogy

The clay mineralogy of the samples with mixed clay compositions of kaolinite and montmorillonite have higher PER compared to samples with only kaolinite as the dominant clay mineral. Samples containing montmorillonite can be distinguished geochemically by their high bulk Mg content (Figure 8.31).

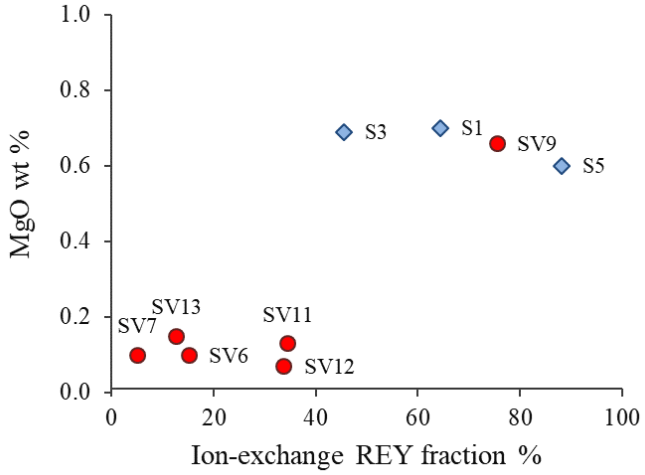


Figure 8.31. Plot showing the MgO content of bulk saprolite and clay veinlet samples, and corresponding percentages of extracted ion-exchangeable REY.

This effect is likely due to the higher cation exchange capacity of smectite (80 -150 meg/ 100 g for montmorrillonite) than kaolinite (3-15 meq/100 g), allowing smectite-bearing mixtures to accommodate greater amounts of REE cations through surface adsorption and chemisorption (Plant and Raiswell 1994). However, the zero-point charge of smectite is much higher (4.5-5.9) vs (3.6) in kaolinite (Helmy et al. 1994, Schroth and Sposito 1997), and therefore the clays in these samples likely captured REE under more neutral pH conditions. These neutral conditions are consistent with the poorer drainage setting which also encourage the formation of smectite clays (see Chapter 6). Smectite is therefore concluded to be a significant host to ion-exchangeable REE in all of the clay veinlets, and some of the saprolite samples.

However, the collapse of the basal layers of smectites in residual material after leaching with ammonium sulphate and the difference in measured La and Y content of clay minerals analysed from SV9 (mixed clay sample) and SV7 (kaolinite dominated sample), suggest that smectites in the sample probably do hold some of the REE. The collapse in the basal layers is caused by NH^{4+} substituting for the interlayer cations sitting in basal layers of the montmorillonite clays, characteristic of leaching with ammonium sulphate (Gautier et al. 2010).

More work will need to be carried out in order to determine whether smectite clay minerals have adsorbed REE in Serra Verde saprolite samples. What is evident however, is that in saprolite sections where smectite minerals have developed, high percentages of REE adsorbed can be found. This may be because smectite minerals adsorb a large amount of REE, or because of optimal physiochemical conditions for REE adsorption by kaolinite.

Clay content

CIA values represents the degree of feldspar weathering into clay minerals and LOI values the volatile content in bulk sample. Although the clay content of the leached samples was not measured, the calculated CIA and LOI values of the samples can be used to compare the relative clay content between each sample. Clay minerals hold relatively high amounts of water in their structure and may therefore contribute significantly to the bulk LOI. Samples with higher CIA and higher LOI values are therefore interpreted to contain higher clay mineral contents compared to samples with lower values.

The samples leached show a range of CIA values (0.7 to 1) and LOI (4.9 – 20 wt %), which suggests that the samples have variable amounts of clay minerals. Furthermore, the element plots in Figure 8.32 shows that the CIA and LOI values positively correlate with the percent of ion-exchangeable REE in the samples, which means that samples with higher clay contents also have higher ion-exchangeable fractions. This positive relationship is interpreted as follows: a greater proportion of clay minerals results in a higher capacity and absorption surface for the weathered rock to host REE, which are being delivered by percolating fluids.

Clay content appears to be a key factor in controlling the PER in weathered granite of Serra Verde, and may explain some of the differences observed between samples. For example, in the case of SV7 and SV9, which have the same REE content but very different ion-exchangeable REE fractions, the CIA and LOI would suggest SV7 has much lower clay content than SV9. A lower clay content in SV7 also explains why its clay size fraction was

several times more enriched in ion-exchangeable REE than its bulk sample, compared to sample SV9, because the clays hold most of the ion-exchangeable REE.

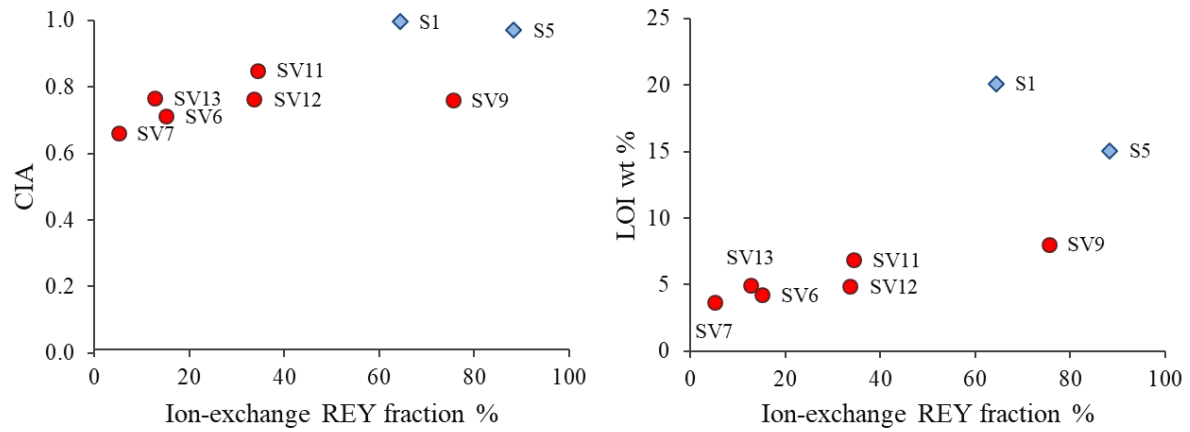


Figure 8.32. Plots showing the CIA and LOI of bulk saprolite and clay veinlet samples, and corresponding percentages of extracted ion-exchangeable REY.

REE fractionation

Samples with higher LOI and CIA values, interpreted to correlate with clay content, have less fractionated ion-exchangeable REE (La/Yb; see Figure 8.33). This suggests that HREE accumulation is partly controlled by clay content. Due to the preferential absorption of LREE onto clays, saprolites with low clay contents absorb relatively less HREE, resulting in HREE being lost from the system. When the clay contents during weathering are high, the adsorption capacity may be sufficient to host all of the exchangeable REE, and no fractionation between LREE and HREE occurs.

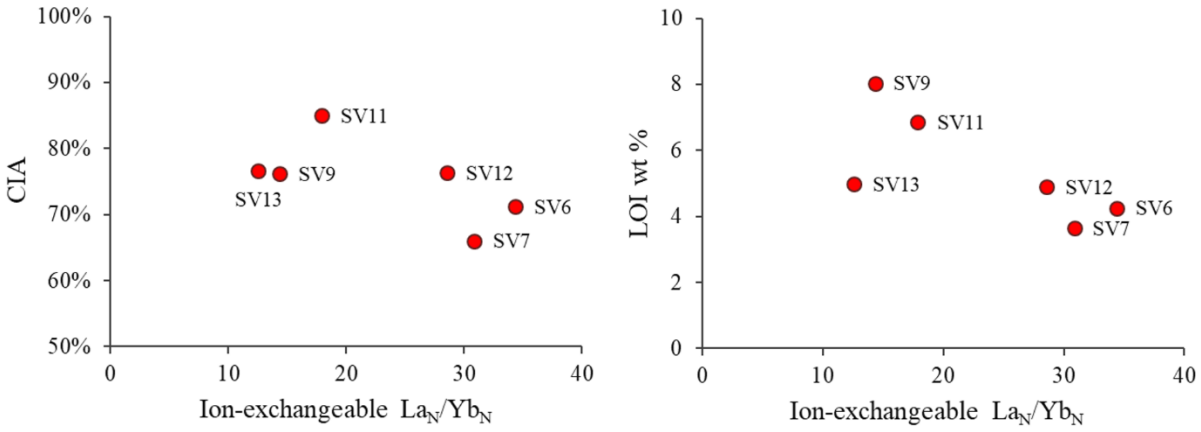


Figure 8.33. Plots showing the CIA and LOI of bulk saprolite samples, and corresponding La/Yb ratios of extracted ion-exchangeable REY.

8.4.5 Effect of pH on the leaching of REE and other elements

The three ion-exchange batch leach experiments with varying pH conditions (pH 5.5 to 3) show that a decrease in pH leads to an overall increase in extraction of REE, and a large increase in non-REE impurities. The increase in ion-exchangeable REY extraction with decreasing pH is small; the PER only increased by a few percent. In concentrations, increases of a few ppm to 200 ppm ion-exchangeable REY were observed, the highest of which are associated with samples of higher bulk REE concentrations. The extraction at pH 5.5 conditions is therefore effective at extracting the majority of the ion-exchangeable REY.

An improvement in the extraction of ion-exchangeable REE with higher acidity has been reported by other studies, such as Coppin et al. (2002) and Moldoveanu & Papangelakis (2013), and can be explained by changes in the variable charge of kaolinite from negative to positive, and by improved solubility conditions for REE ions. The point of zero charge for kaolinite is ~pH 3.6, indicating that below this pH value the variable charge of kaolinite switches to positive (Tchapek et al. 1974, Schroth and Sposito 1997). This charge switch will cause any positive REE ions adsorbed on kaolinite crystals to be released through desorption.

SEM images show that REE locked in resistant and supergene minerals such as phosphates and LREE-fluorcarbonates are unaffected by the more acidic leaching conditions. Contributions of these minerals to increased REE extraction are therefore considered to be negligible. The release of REE from phosphates, LREE-fluorcarbonates and niobiates requires a more aggressive treatment in order to leach their REE. For example, ore with large amounts of bastnäsite are usually calcinated and treated with strong acids (Peelman et al. 2014).

The experimental results also show that changes in pH conditions have stronger effect on the release of HREE than LREE. This difference in extraction is thought to be caused by HREE being more strongly bound to clays minerals resulting in preferential release of LREE into solution (Coppin et al. 2002). Ion-exchangeable HREE extraction is therefore favoured by more acidic conditions.

In the majority of solutions collected from experiments run at pH 5.5, the total concentrations of non-REE impurities are lower than the total concentration of REE. In solutions collected from experiments run at pH 3 however, the opposite result is observed. The large increase in non-REE impurities can mainly be attributed to increases in Al and Fe concentrations, which increase by one to two orders of magnitude from pH 5.5 to pH 3. The concentrations of alkaline and alkali elements, show no significant difference between experiments run at

different pH and concentrations of Th, and U only show a small increase with concentrations remaining low at < 5 ppm. The large increase in Al and Fe released under more acidic conditions can be explained by the vulnerability of clays minerals to breakdown in low pH solutions.

In this study, the absolute increase in Al and Fe concentrations are significantly higher than the increases in REE extraction with decreasing pH. Comparison of the REE/Al ratio between experiments shows that the values decrease from 10 – 100 down to 1 – 3 (Figure 8.34). This means that in supernatant solutions collected from batch experiment run at pH 3 conditions, 1 to 3 ppm REE are extracted with every 1 ppm Al.

Al and Fe are deleterious elements in supernatant solutions because they impact negatively on subsequent ore processing, producing longer and more costly separation. Before REE can be separated, these impurities need to be removed through complex processes such as centrifugal sedimentation, liquid membrane extraction, and selecting leaching (Xiao et al. 2015). The enhanced extraction of REE at more acidic conditions may therefore be outweighed by the accompanying elevated extraction of Al and Fe into the supernatant solutions. A cost-benefit analysis is recommended to assist in deciding the most economically feasible conditions for REE leaching from these types of ores.

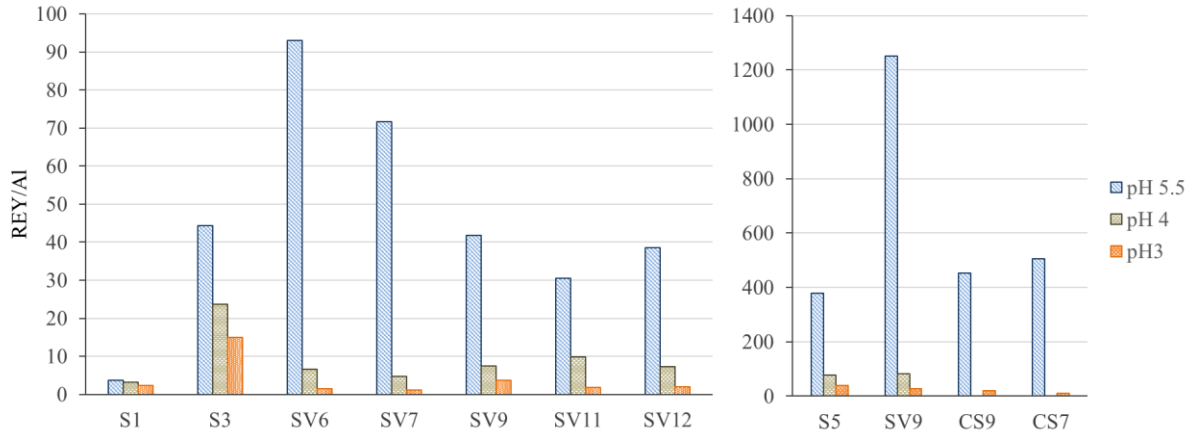


Figure 8.34. REE/Al ratio plot for the extracted Al and REE in the supernatant solutions for all leach experiments run under different pH conditions. Note the change in y-axis values for the right plot.

8.5 Conclusions

REE are readily leachable from the Serra Verde ore zone with 0.5 M ammonium sulphate supernatant solution at pH 5.5. REY concentrations of 500 ppm to 5000 ppm are attainable from milled bulk saprolite samples. Lower pH solutions increase the REE extraction, particularly of HREE, but cause considerable contamination from impurities such as Al and Fe due to clay dissolution, as well as detrimental elements such as U and Th from oxides.

Ion-exchangeable REE contents vary from 5 – 75 % in the bulk saprolite, and confirm that the ore zone at Serra Verde is principally a REE ion-adsorption deposit. Clay veinlets are highly enriched in REE-bearing clays, and contain the highest PER (up to 90 %). The extractability is controlled by differences in clay mineralogy, clay content, and the abundance of accessory REE-minerals. Samples with LREE-fluorcarbonates, niobiates, and phosphate contain lower PER due to their insolubility, while samples with clay mixtures including halloysite and montmorillonite have higher PER due to their cation absorption capacity. Separation of the CSF does not remove insoluble REE-minerals due to their extremely find grain size.

Higher CIA, LOI, and Mg values are useful indicators for predicting higher clay contents and clay type. Bulk P and Nb contents may be useful in estimating the abundances of insoluble REE-phosphates and niobiates, and therefore the relative proportion of non-extractable REE. Lower abundances of fluorcarbonates are a better indicator for higher extractable REE contents but require detailed mineralogical quantification. Crucially, bulk REE grade is not a good indicator of extractable REE as samples with similar grades were shown to contain incomparable REE extractions.

The relative extraction of LREE and HREE is highly variable and is principally controlled by the REE-mineralogy in each sample. Supernatant solutions either show no change in REE fractionation relative to the bulk composition or are more LREE-fractionated. The leachate is consistently depleted in Ce relative to the sample material, corroborating the results from Chapter 7 that Ce in the saprolite is mostly present as insoluble Ce^{4+} hosted in secondary Ce-minerals.

Chapter 9

Controls on the Formation and Enrichment of the Serra Verde REE Deposit

9.1 Assessment of the Controls on Formation and Enrichment

9.1.1 Composition and mineralogy of the protolith

The work in chapter 5 shows that the composition and history of the parent bedrock has played a key role in the development of the Serra Verde deposit.

The average REE enrichment in the lateritic profile at Serra Verde is shown to be ca. 2 – 3x higher than the starting bedrock concentrations (chapter 6). Initial high REE concentrations in the Serra Dourada biotite granite (800 – 1200 ppm REY) clearly contributed to the economic REE grades present in the Serra Verde IAD. These values are significantly higher than the protoliths underlying other economic IADs; Sanematsu and Watanabe (2016) showed that the protolith REE concentrations from several Chinese IADs were consistently below 600 ppm REY.

Hydrothermal alteration of the initial granite modified the primary REE-mineral assemblage, in the process increasing the HREE content, resulting in minerals that were considerably more susceptible to breakdown during weathering. Fluorcarbonates are the dominant LREE carriers in the altered granite, and these are shown to weather readily in the saprolite at Serra Verde (chapter 7), corroborating previous studies that suggest fluorcarbonates are favourable for IAD formation due to their high solubility (Sanematsu and Watanabe 2016). Hydrothermal addition of HREE increased the starting concentration for enrichment of these more valuable REE, residing within xenotimes, niobiates, and fluorite. While fluorite breaks down during weathering, xenotimes and niobiates are more resistant in the weathering profile (chapter 7), locking in the HREE, therefore partly explaining the preferential enrichment of LREE in the saprolite (chapter 6). The behaviour of these more resistant minerals above the saprolite of Serra Verde remains to be determined.

The formation of the Serra Verde IAD has also been favoured due to the low phosphate content of the granite protolith (< 0.01 – 0.04 wt % P_2O_5). Firstly, if REE phosphates were present, these would be resistant to weathering in the saprolite (chapter 7), so REE hosted in these minerals would not be available for clay adsorption in the saprolite. Secondly the breakdown of any apatite results in the formation of very stable supergene phosphates such as rhabdophane, which also locks up REE preventing secondary mobilisation. The preferential retention of REE in phosphates has been shown to be due to the strong affinity of REE and P_2O_5 (Banfield and Eggleton 1989).

The high feldspar content of the granite protolith, enabled a clay-rich saprolite to develop (chapter 6). Formation of abundant clay results in a high REE carrying capacity in the saprolite, adsorbing mobilised REE from the leaching zone, resulting in ion-adsorbed REE in the clays. A high feldspar content in the granite results in high acid buffering capacity, able to neutralise acidic REE-bearing fluids, resulting in precipitation of REE that become concentrated in the saprolite (chapter 6). Results from leaching experiments in chapter 8 showed that samples with higher proportions of clays contain a higher percentage of extractable REE (PER).

The A-type setting of the Serra Dourada granite contrasts the I- and S-type granite protoliths responsible for formation of Chinese IADs. However, several similar properties for the Serra Dourada granite as compared to the Chinese examples are apparent (Bao and Zhao 2008, Ishiara et al 2008, Sanematsu and Watanabe 2016 and references therein):

- A primary or hypogene enrichment of REE in the granite protolith.
- Hydrothermal alteration of REE-bearing minerals, forming less weathering resistant minerals as compared to the likely initial REE-bearing phases in the granite.
- An association with tin mineralisation.
- Alkali rich granite phase, with contrasting low phosphate content and elevated HFSE.

9.1.2 Climate

The rate of chemical weathering at the surface is promoted by elevated temperatures and a high input of water, both of which prevail in tropical climates (Gislason et al. 2009). Since the Paleogene, the rocks of the Tocantins province have been exposed to prolonged periods of such tropical conditions, and as a result, chemical weathering has resulted in the formation of deep weathering profiles across the region (Butt 1987). In Chapter 6, the characterisation of the Serra Verde profile shows that the thickness of the profile forms up to 40 m, with the weathering resulting in moderate lateritisation, a residual enrichment of insoluble minerals, and the

development of a strongly oxidised zone, all the result of pervasive incongruent chemical weathering.

The prolonged period of warm and wet conditions during the formation of the Serra Verde IAD has allowed sufficient volumes of bedrock to breakdown to form the clay-host minerals in abundance, and liberate the REE needed to form the grades present in the saprolite ore zone. Determining the rate of weathering, together with the results of the mass balance analysis, would enable an estimate of the duration of saprolite enrichment to be made.

Previous studies that compared the proportion of ion-exchangeable REE (PER) in kaolin-bearing profiles between Southern China and Southeast Asia suggested that temperate conditions are more favourable for the development of high PER ores than tropical conditions (Sanematsu and Watanabe 2016). Although variable, the PER of the Serra Verde IAD ore established in Chapter 8 suggests to the contrary, that the formation of high PER ores may occur during tropical weathering.

9.1.3 Topography and drainage

Several studies cite topography as being an important control on the formation and preservation of weathered profiles (e.g. Einsele 2000). In Southern China, low denudation rates controlled by low surface relief are argued to enhance the formation of IADs by preserving the in situ weathering material (Bao and Zhao 2008). In Brazil, the Cretaceous erosional cycle produced an extensive, flat peneplane (King 1956), which has protected the Serra Verde IAD from surface erosion during its formation, allowing chemical weathering processes to dominate.

In chapters 6, 7, and 8, the saprolite of the Serra Verde IAD is shown to be laterally variable in its thickness, geochemistry, mineralogy, and the proportion of PER. The variation seen presents a pattern, allowing the saprolite to be grouped into two end-members, that can be explained by differences in drainage setting across the profile (Marker & Oliviera 1994). The contour map of the underlying bedrock surface presented in chapter 6 shows the presence of significant relief of up to 40 m beneath the profile. This high relief, together with the impermeable property of the crystalline bedrock controlled the drainage behaviour of water within the overlying profile during formation of the IAD, and thus is responsible for the variability of the saprolite. Studies of lateral variations in other IADs have not been published, and therefore the degree to which drainage controls formation of IADs in general remains to be determined.

The origin of the bedrock topography beneath the Serra Verde IAD is not clear, and may be the product of inherited topography, or differences in bulk strength of the bedrock. The coincident location of a major bedrock channel feature in the plateau area with the contact of the Nb-rich and Nb-poor sectors of the biotite granite shown in chapter 5, suggest that the central fault has influenced the bedrock topography and drainage of the profile.

The drainage setting controls several important characteristics of the ore zone (Figure 9.1). The mass balance in chapter 6 showed that thinner saprolites, which overlie bedrock ridges, are associated with increased mobilisation and enrichment of REE through the profile, due to the higher rate of water flow in a relatively high drainage setting. However, the mineralogical abundance study in chapter 7, and the leaching experiments in chapter 8, showed that thinner saprolites have lower PER due to the presence of supergene LREE-fluorcarbonates. Conversely, thicker saprolites which developed in a relatively low drainage setting, were shown to have less concentrated REE, due to less enrichment, but were associated with higher PER. The optimum profiles, balancing the REE grade and PER, are suggested to have developed in intermediate drainage settings.

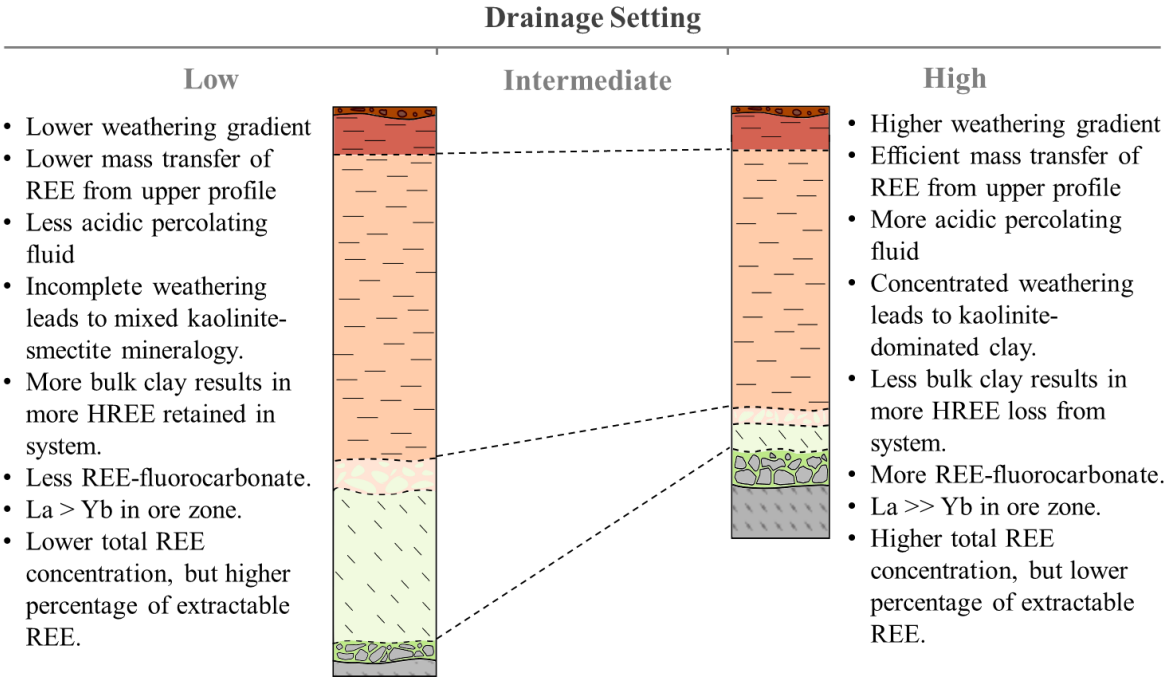


Figure 9.1. Summary of the relationship between drainage setting, and REE fractionation and residence in the saprolite. Note the difference in saprolite thickness.

9.2 The Mechanisms of REE Mobilisation, Fractionation, and Enrichment in the Serra Verde deposit

The XRD analysis of samples down the profile in chapter 6 show that the bulk minerals break down in order of chemical stability, starting with Na-feldspar, and followed by K-feldspar and biotite (quartz remains mostly resistant). The main breakdown products are kaolinite, Fe oxides and, in areas where drainage is limited and silica is not entirely removed, smectite (Figure 9.2). These are clays begin to concentrate in the saprolite, where they adsorb liberated REE ions from percolating fluid. When percolating acidic meteoric waters come into contact with the primary minerals, the acid hydrolyses the silicate structure, and are buffered by the resulting release of alkali cations and consumption of H^+ (White et al. 2001). This creates a gradient of increasing pH down the profile, with the least acidic conditions at the base of the saprolite.

The release of REE from breakdown of REE-minerals occurs principally in the saprock and saprolite, where SEM-BSE and EMP analysis show that apatite, britholite, bastnäsite, and fluorite from the bedrock are largely dissolved (chapter 7). For each of these minerals, intermediate products are formed which affect the liberation of REE. The breakdown of apatite releases phosphate in the saprolite which complexes with any free REE to precipitate rhabdophane due to their high affinity. Britholite weathers to cerite and Y-phosphate, which remain largely insitu in the saprolite, locking up REE. Cerite eventually breaks down to cerianite in the transition zone, causing Ce to fractionate from the other REE. Bastnäsite-Ce from the bedrock begins to weather in the saprock, forming supergene bastnäsite-La and some Ce oxide. As the bastnäsite-La enters the clay-bearing saprolite zone, it continues to dissolve and precipitate due to the lower pH, progressively releasing more REE along with F and carbonate, and becomes increasingly intermixed with other fine-grained breakdown products, eventually breaking down entirely. The conditions that control this supergene re-precipitation are currently unknown. Nonetheless, LREE-fluorcarbonates are the main source of REE in the saprolite, due to their high REE concentration, and complete breakdown.

REE hosted in niobiates, zircons, and phosphates exhibit minimal chemical breakdown in the saprolite, and so the REE in these minerals are retained into the mottled zone. These minerals are important hosts of HREE, which are not liberated in the saprolite, and as a result these elements become fractionated from LREE during mobilisation. However, niobiates and phosphates may be dissolved in the mottled zone were conditions are more acidic. For example,

Ruschel et al. (2010) found that the Y in highly metamict niobiates altered by low temperature fluids was released while Th and U were retained.

The liberated REE that are not re-precipitated into secondary minerals, become adsorbed onto clays. Previous work by Laveuf and Cornu (2009) has shown that REE adsorption onto clays is controlled by the pH, ionic strength, and clay surface charge. At the base of the saprolite, the clays have the maximum cationic-exchange capacity, because the pH is at its most buffered (Coppin et al. 2002, Aja 1998). In addition, the fluid has maximum ionic strength from the breakdown of feldspars occurring higher up in the saprolite, making the fluid highly-saturated in cations, enhancing the REE exchange onto clays (Coppin et al. 2002, Aja 1998). REE are preferentially adsorbed onto clays over alkali and alkaline earth cations due to their trivalent state (Roaldset 1975). Together with the availability of clay material, this results in the preferential REE-enrichment observed at the base of the saprolite (chapter 6). Mass balance analysis shows that not all liberated REE are adsorbed, and that HREE are preferentially lost from the weathering system. This suggests that clays are preferentially adsorbing LREE over HREE in the saprolite. Other studies have previously found that HREE are preferentially retained in percolating fluids, thought to be due to the relatively higher stability of aqueous HREE complexes (Braun 1990, Duddy 1980, Galan 2007, Scheepers & Rozendall 1993).

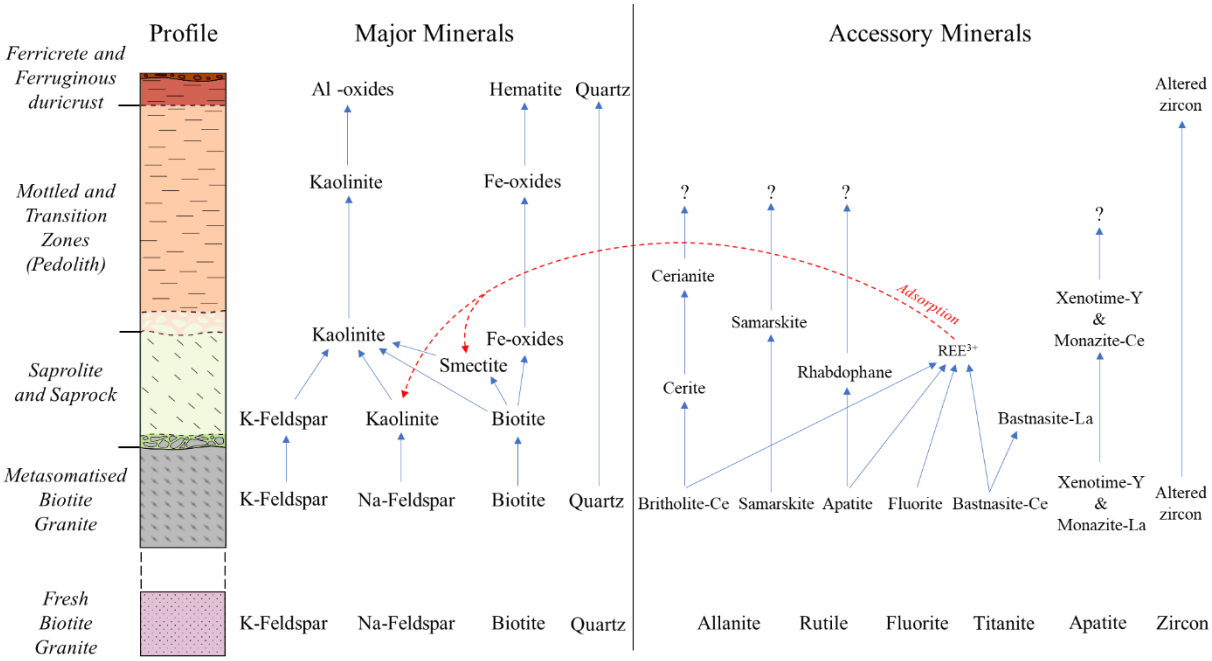


Figure 9.2. Schematic summary of the mineral breakdown pathways for the Serra Verde weathered profile.

Sanematsu et al. (2015) has proposed that a positive correlation exists between negative Ce anomalies and the percentage of ion-exchangeable REEs. This is due to the immobile behaviour of Ce in the mottled zone compared to other REE, leading to increasing fractionation as more REE are mobilised into the saprolite below. However, this assumes that all of the REE that are mobilised and accumulated in the saprolite are adsorbed onto clays. In addition, that same study suggested that profiles developing from high P_2O_5 granites, develop low PER ores, due to the retention of REE in primary and secondary phosphates during weathering, but that low phosphate ores show variable PER.

Several high-grade samples were found to show strong Ce anomalies, indicating that significant Ce has fractionated and that REE have been mobilised. However, the leaching results showed that only a small proportion of REE were in an ion-exchangeable state. In these samples, the majority of REE were found to be held in supergene LREE-fluorcarbonates. Therefore, caution should be exercised in using the Ce anomaly to predict the PER of ore, as it may not directly relate to the amount of REE available to adsorb onto clays (Figure 9.3). The presence of unidentified LREE-fluorcarbonates may also explain the low PER and low P contents noted by Sanematsu et al. (2015). In order to make reliable predictions of the PER, this study suggests that, in addition to Ce and P_2O_5 content of the ore, high resolution mineralogy of the IAD is required to identify other REE-mineral phases that may be taking up some of the mobilised REE from the leaching zone.

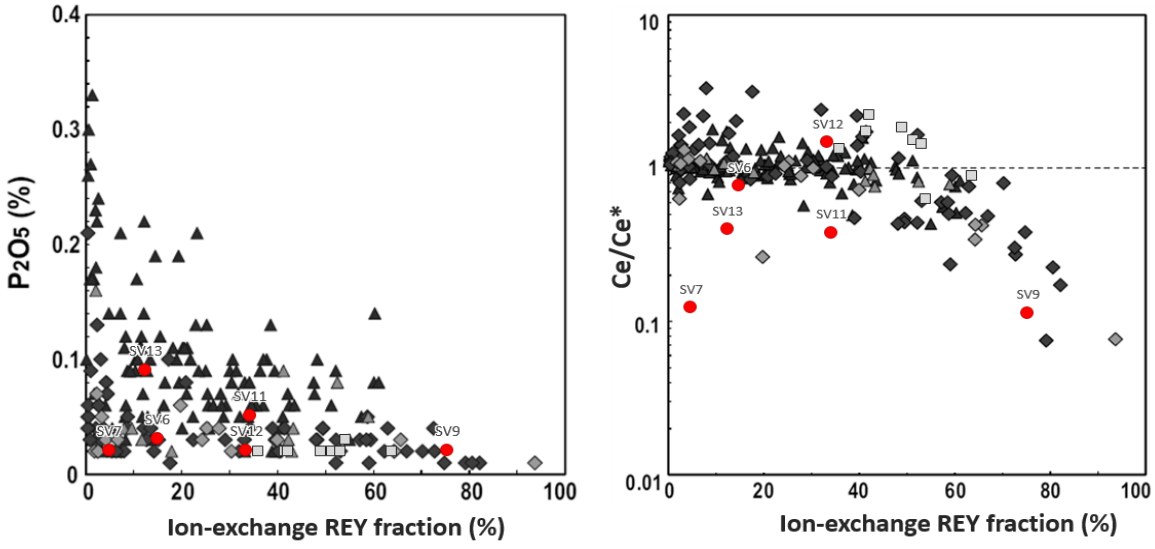


Figure 9.3. Plots of phosphate contents vs ion-exchangeable REYs as a percentage of total REE content in weathered granites (left); Ce anomalies vs ion-exchangeable REYs (right). The plots present data from Serra Verde deposit (red circles; this study), Thailand (triangles and diamonds; Sanematsu et al 2015), and China (squares; Murakami and Ishihara 2008, Sanematsu and Kon 2013). Graphs modified after (Sanematsu and Kon 2013). In all samples, the ion-exchange REE were extracted using 0.5 M ammonium sulphate solution at pH 5.5.

9.3 Proposed Model of Formation and Evolution of the Serra Verde REE Deposit

The geochemical and mineralogical studies presented in Chapters 5 to 8 together with literature of the geology of the area presented in Chapter 3 is used to develop an integrated model for the evolution of the Serra Verde REE deposit. A summary of the history is presented in Figure 9.4. The formation has the following sequence

1. The intrusion age of Serra Dourada granite complex is best bracketed by the ca. 1614 Ma late Paleoproterozoic U-Pb concordia intercept measured in zircons from the neighbouring Serra da Mesa biotite granite intrusion (Pimental et al. 1991), and the 1430 ± 30 Ma Rb-Sr whole rock age of the Serra Dourada granite itself (Reis Neto 1983). The alkali-rich biotite granite formed during a regional extension event, giving the Serra Dourada, and other g2 granites in the Tocantins province, a continental affinity with high initial REE and HFSE (Bilal et al. 1997).
2. During the cooling stage of the granite, a F-CO_2-alkali-rich volatile fluid likely exsolved from the silicate melt, and focused into the roof of the intrusive. The mineralogical study in Chapter 5 showed that alteration of primary apatite-allanite-titanite to hydrothermal fluorcarbonate-niobiate-phosphate accessory minerals occurred, together with the pervasive development of fluorite. The bulk geochemistry of the altered biotite granite was thus significantly enriched in F, carbonate, Nb, Ta, Ga, and most importantly HREE at the top of granitic cupola and at the edges of the granite body.
3. Multiple orogenic events subsequently deformed the intrusive complex, concluding with the regional Brasiliano event at ca. 530 Ma (Bilal 1991), which are likely responsible for the pervasive mineral foliation and elongation observed in the bedrock, and preserved in the lower weathering profile.
4. The geochemical bedrock mapping from Chapter 5 suggests development of a major central fault structure, striking NW-SE through the core of the biotite granite, which carries significant vertical displacement (see Figure 5.41, Figure 5.43). The timing of this fault is unknown, and its attitude could not be determined from the limited drill sections into the bedrock. However, the displacement of this structure by a set of Brasiliano-aged sinistral faults trending ENE-WSW indicate that the central fault zone is likely pre-Brasiliano in age (Hains, 2013).

5. Uplift and erosion cycles during the Proterozoic orogenic events, and perhaps extending into the Phanerozoic, uplifted and unroofed the biotite granite body. This uplift exposed the granite to the level of the hydrothermally altered cupola at the north-eastern half of the biotite granite.
6. Development of the South American peneplane from prolonged erosion during the Cretaceous-Paleogene levelled the surface in central Brazil (King 1956). The modern plateau surface overlying the weathered profile is likely the preservation of this peneplane, giving a maximum age for the start of laterisation.
7. Laterisation of the granite advanced during the Paleogene due to an increasingly wet and warm, tropical climate (Braun 1971). The deep weathering profile of the Serra Verde deposit formed during this prolonged period of stability, and allowed the development of a stratified column, with a well-defined zone of REE leaching in the upper, lateritised part of the profile and a zone of REE-accumulation in the lower, kaolinitised part of the profile (see Chapter 6). The release of REE from the hydrothermal mineral assemblage of the bedrock produced a saprolite ore on average 3 times more REE-enriched than the bedrock. The mineralogical analysis of the saprolite (Chapter 7) and the saprolite leaching experiments (Chapter 8) show that the majority of REE that were liberated, were ultimately adsorbed onto clay minerals, and in some cases, very fine-grained secondary REE-minerals.
8. The dominance of kaolinite in the clay minerals that form the bulk mineralogy of the lower profile determined in Chapter 7, indicate that the profile was well-drained during mineral breakdown (Marker and Oliviera 1994), which, together with the high influx of mildly acidic meteoric water, allowed efficient mass transfer of REE to form the saprolite ore zone. Lateral variations in the REE-mineralogy, and the proportion of ion-adsorbed REE (Chapter 7, Chapter 8) are explained by the topography of the bedrock surface (Chapter 6) producing relatively poorer drainage and lower weathering gradients over bedrock channel features.
9. In the late Paleogene, the Velhas erosional cycle caused a shift from a dominantly chemical weathering, to a dominantly erosional setting. This cycle was accompanied by a shift to drier climate conditions (Trescases et al. 1981), which greatly reduced the rate of weathering, preserving the enriched saprolite at the grade we see today. Over the Serra Dourada granite complex, incision by streams removed most of the weathered profile material. It is only in the small areas of topographic plateau highs that the complete original profile remains today. Today, the complete profile that hosts the Serra Verde IAD is only preserved on the topographic plateau highs. On the flanks of these plateaus, enriched saprolite material is still present but it has experienced reworking and dilution by surface processes.

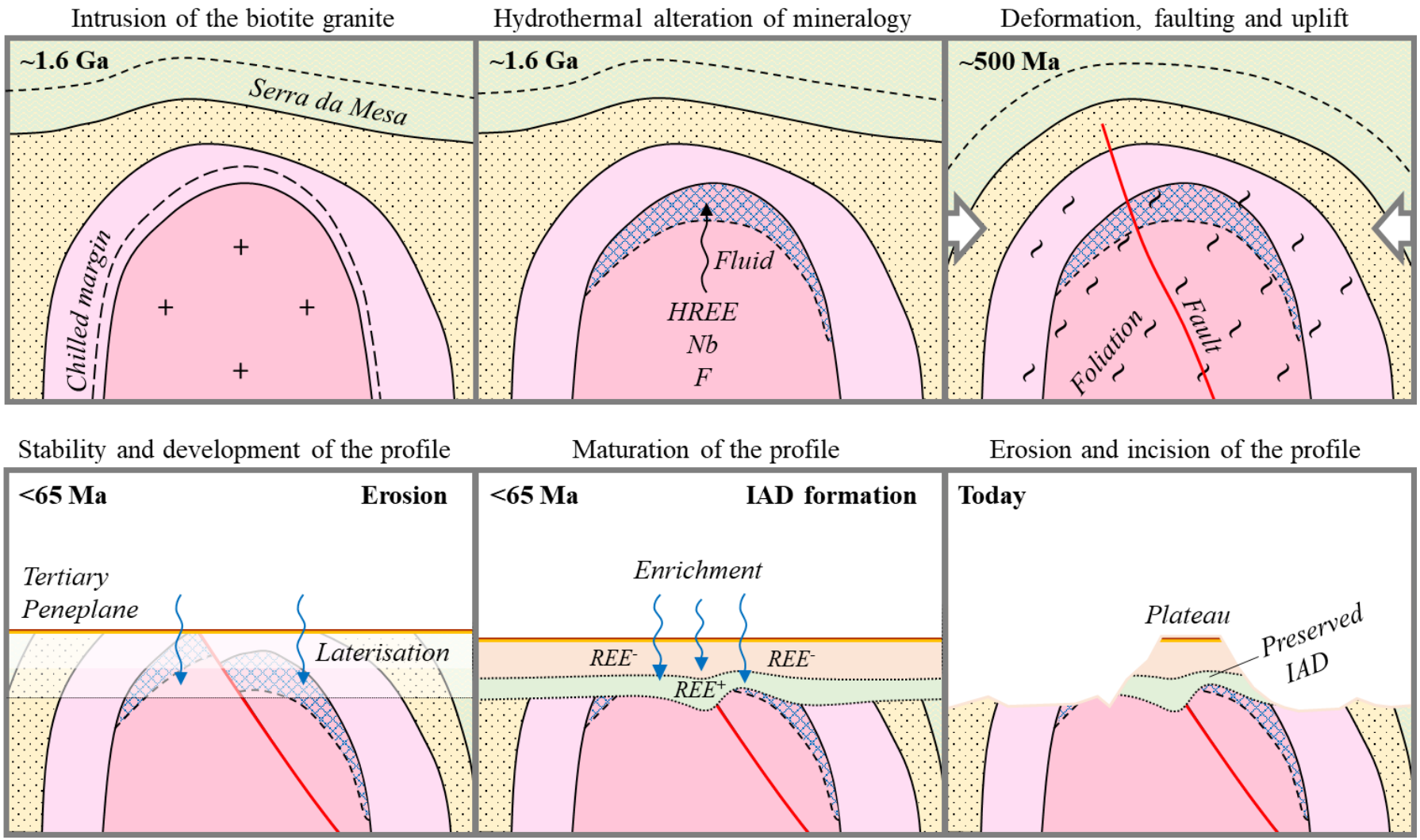


Figure 9.4. Schematic diagram illustrating the proposed genetic evolution that led to the formation of the Serra Verde REE deposit (intrusion, weathering and preservation), not to scale.

9.4 Exploration and Geometallurgical Implications

The high REE grades in the Serra Verde IAD are, in part, attributed to the high starting concentration of REE in the A-type granite protolith due to its highly evolved magmatic composition. As most of the Chinese IADs have been shown to develop from S-type and I-type granites (Sanematsu & Watanabe 2016), this finding suggests that A-type granite terranes may also be attractive IAD exploration targets if the magmatic differentiation is highly evolved, corroborating recent work by Wang et al. (2015).

Weathering processes have allowed efficient mass transfer of REE into the ore zone due to the readily soluble REE-accessory minerals from the granite. This weatherable accessory assemblage is shown to be the product of hydrothermal modification, common to the roof zones of large, evolved intrusive bodies (Pollard 1989). In Chinese IADs, some of the highest grade deposits have also developed over hydrothermally altered granite bedrock (Ishiara et al. 2008). Identifying the hydrothermally altered parts of the granite cupolas should therefore be prioritised to target profiles with the best potential for developing high REE enrichment.

In chapter 6, the concept of the bedrock topography drainage model was introduced to explain the thickness and variability of the saprolite ore zone. In chapter 8, the results from the leaching experiments showed that the highest leachable REE grades do not coincide with the highest bulk REE grades found in thin saprolite zones. The highest clay-hosted REE grades were shown to develop in intermediate drainage saprolites. Therefore, validation of the bedrock topography drainage model may enable its use in predicting the location of the highest leachable REE grades by mapping out the location and extent of intermediate-drainage areas. By predicting the leachability of the ore horizon, the drainage model may have a significant impact on the geometallurgical characterisation of the ore variability at other IADs.

Any REE present in residual and insoluble supergene minerals are shown to be un-extractable by ion-exchange leaching. The presence of LREE-fluorcarbonates which are not easily detectable in bulk geochemical samples can host significant REE and thus reduce the recovery of REE from IAD ores. Phosphate content and Ce/Ce* anomalies have already been suggested as tools to predict the PER of ore material. However, these will not account for the occurrence of possible supergene LREE-fluorcarbonates. Therefore, assay data has limited use in determining the amount of recoverable REE from IADs with these supergene minerals. High resolution mineralogical work of several different parts of the deposit is therefore needed to identify areas where these may be present in relatively high concentrations.

9.5 Conclusions and Further Work

The principal findings of this study were as follows:

1. The parent rock that weathered to form the Serra Verde IAD is a highly evolved, alkali-rich and phosphate-poor granite that was magmatically enriched in REE.
2. The REE deposit developed over a sector of the southern Serra Dourada granite complex that was hydrothermally altered by F-bearing fluids, which upgraded the HREE content, and altered the REE-bearing accessory mineral assemblage.
3. REE are held in a mature weathered profile that developed strong leaching and accumulation zones, dominantly due to a mass transfer enrichment process as a result of intense tropical weathering.
4. REE are most strongly concentrated and enriched in the lower saprolite, representing a 1.5 – 10x enrichment from the granite protolith.
5. Secondary fine-grained LREE-fluorcarbonates formed variably throughout the saprolite due to differences in drainage and bulk clay content during weathering.
6. The ion-extractability of the ore is highly variable with 5 – 75 % PER, and is principally controlled by the abundance of supergene REE-minerals in the saprolite. In some horizons, supergene phosphates and fluorcarbonates were found to hold up to 70 % of REE.
7. Clay veinlets running through the profile represent highly localised enrichment of REE, of which up to 90 % is ion-extractable.

Further work

The controls on IAD formation are still poorly understood despite the critical metals that they supply, and the ease of access to such ore systems in the near surface. In the course of this investigation at Serra Verde, several new potential pathways of further research were identified, which may impact scientific models of deposit formation, compositional variability, and geometallurgy.

The recognition of LREE-fluorcarbonate precipitation at ambient temperature and pressure conditions at Serra Verde has implications for IADs, because the simple dissolution model for the enrichment of REE into clays may not take into account the formation of other secondary phases. An investigation of the behaviour and stability of these supergene REE-minerals should therefore be the focus of further study to better understand the conditions that would lead to their formation in the saprolite horizon. This will provide additional constraints in the

conditions that favour the absorption of REE onto clays, producing an economic target for extraction, versus their precipitation into secondary REE-minerals where the REE are not extractable by simple leaching technologies. A preliminary study on the formation of LREE-fluorcarbonates should include experiments on mineral synthesis in a laboratory due to the apparently low pressures and temperatures required. The results from such work could be used to devise an alternative processing technology for such phases.

Very little work has been carried out on the Serra Dourada granite, and from the complex zonation of geochemistry, it is clear that more work is required to understand its composition and evolution. Furthermore, the REE mineralogy identified in the study area is not comparable to previous descriptions of the mineralogy from elsewhere in the complex. To understand the emplacement of this granite, and the relative timing of hydrothermal alteration and addition of HREE, further work that integrates zircon geochronology with dating of the other hydrothermal minerals should be pursued.

The Serra Dourada granite experience considerable deformation but the effects on the mineralogy were not considered in this study. Further work on the bulk and accessory mineralogy would help separate the magmatic-hydrothermal effects on the bedrock composition from metamorphic effects.

The hypothesis that different drainage settings control variation of both the ore mineralogy and extractability through the weathered profile is based on a small number of samples from the core of the Serra Verde IAD. Confirming or discounting the relationships between underlying bedrock topography and the ore composition requires more sampling work across the saprolite, perhaps extending to neighbouring plateaus or other deposits. This work would have potential to predictively map the ore composition and geometallurgy across the Serra Verde IAD.

References

Acosta J.A., Cano, A.F., Arocena, J.M., Debela, F., Martínez-Martínez, S. 2009. Distribution of metals in soil particle size fractions and its implication to risk assessment of playgrounds in Murcia City, Spain. *Geoderma*. **149,** 101-109.

Aide M. T. Aide C. 2012. Rare Earth Elements: Their Importance in Understanding Soil Genesis. *ISRN Soil Science* **2012.**

Agangi A., Kamenestsky, V.S., McPhie, J. 2000. The role of fluorine in the concentration and transport of lithophile trace elements in felsic magmas: Insights from the Gawler Range Volcanics, South Australia. *Chemical Geology*, **273,** 314-325.

Aja, S.U. 1998. The sorption of the rare earth element, Nd, onto kaolinite at 25 ºC. *Clays and Clay Minerals*, **46***,* 103-109.

Alderton D. J. M., Pearce J. A., Potts P.J. 1980. Rare earth element mobility during granite alteration – evidence from south west England. *Earth and Planetary Science Letters* **49**, 1, 149-165.

Almeida, F.F.M., Brito Neves, B.B. Dal Ré Carneiro, C. 2000. The origin and evolution of the South American Platform. *Earth-Science Reviews*, **50**, 77-111.

Alonso, E., Sherman, A. M., Wallington, T. J., Everson, M. P., Field, F. R., Roth, R., Kirchain, R. E. 2012. Evaluating rare earth element availability: A case with revolutionary demand from clean technologies. *Environmental science and technology*, **46**, 3406-3414.

Amundson R. 2003. Soil Formation. *In:* Holland, H.D., Turekian, K.K. (eds) Treatise on Geochemistry. Elsevier. 133-168.

Anderson, S.P., Dietrich, W.E., Brimhall, G.H., 2002. Weathering profiles, mass-balance analysis, and rates of solute loss: linkage between weathering and erosion in a small, steep catchment*. Geol. Soc.Am. Bull.* **114**, 1143-1158.

Aubert D., Stille P., Probost A. 2001. REE fractionation during granite weathering and removal by waters and suspended loads: Sr and Nd isotopic evidence*. Geochimica et Cosmochimica Acta*, **65**, 387-406.

Babechuk, M.G., Widdowson, M., Kamber, B.S. 2014. Quantifying chemical weathering intensity and trace element release from two contrasting basalt profiles, Deccan Traps, India. *Chemical Geology,* **363**, 56-75.

Banfield, J.F., Eggleton, R. 1989. Apatite replacement and rare earth mobilization, fractionation and fixation during weathering. *Clays and Clay Minerals*, **37**, 113-127.

Bao Z., Zhao Z. 2008. Geochemistry of mineralization with exchangeable REE in the weathering mantles of granitic rocks in South China. *Ore Geology Reviews* **33**. 519-535.

Bastos-Neto, A.C., Pereira, V. 2012. Fluorine-rich Xenotime from the Nb-Ta-Sn Madeira world-class deposit associated with the albite-enriched granite at Pitinga, Amazonia, Brazil. *Canadian Mineralogist*, **50**, 1019-1032.

Bau M. 1991. Rare-earth element mobility during hydrothermal and metamorphic fluid-rock interaction and the significance of the oxidation state of europium. *Chemical Geology,* **93**, 219-230.

Bau, M. 1996. Controls on the fractionation of isovalent trace elements in magmatic and aqueous systems: evidence from Y/Ho, Zr/Hf, and lanthanide tetrad effect. *Contributions to Mineralogy and Petrology*, **123**, 323-333.

Bea, F., 1996. Residence of REE, Y, Th and U in granites and crustal protoliths: implication for the chemistry of crustal melts. *J. Petrol.* **37**, 521-552.

Berner E.K. Berner R.A.1996. *Global Environment: water, air and geochemical Cycle*. Princeton,N,J: Princeton Univerity Press. 488 p.

Betkowski, W., Harlov, D. & Rokovan, J. 2014. Hydrothermal Mineral Replacement Reaction. *Goldschimdt Abstracts*, 193.

Berger, A., Gnos, E., Janots, E., Fernandez, A., Giese, J., 2008. Formation and composition of rhabdophane, bastnäsite and hydrated thorium minerals during alteration: implications for geochronology and low-temperature processes. *Chem. Geol*. **254**, 238–248.

Bideaux, R.A., Bladh, K.W., Nichols M.C. Anthony, J.W. 2000. *Handbook of Mineralogy: (Volume IV) Arsenates, Phosphates, Vanadates*. Mineral Data Publishing, Tucson, Arizona, 680 p.

Bilal, E. 1991. *Étude de Deux Massifs de La Province de Granitique Stannifère de l'Etat de Goiás - Bresil - et des Formations Métasomatiques Associées aux Mineralisations en Sn et Be*. Doutorado, École des Mines de Saint-Etienne.

Bilal, E., Moutte, J., Botelho, N.F., Marini, O.J. Andrade, G.F. 1997. Geochemistry of two proteroxoic A-type granites of Goiás state, Brazil: Possible links with Rapikivi Series. *Anais de Academia Brasileria de Ciencias*, **69**, 17 p.

Bilong, P. 1988. *Génèse et développement des sols ferralitiques sur syénite alkaline potassique en lilieu forestier du centre-sud Cameroun. Comparison avec les sols ferrallitiqus dévelopeés sur roches basiques.* PhD. Dissertation, Univ. of Yaoundé.

Botelho, N.F. Teixeira, L.M. 1995. Caracterização química de minerais de terras raras e sua aplicação à petrologia dos granitos da província estanífera de Goiás. V Congreso Brasileiro de Geocquímica e III Congreso de Geochímica dos países de Língua Portuguesa. (Abstract).

Brantley, S. L., Buss, H. L., Lebedeva, M., Fletcher, R. C., & Ma, L. 2011. Investigating the complex interface where bedrock transforms to regolith. *Applied Geochemistry*, **26**, S12-S15.

Braun J.J., Pagel M., M. J, Bilong P., Michard A., Guillet B.1990. Cerium anomalies in lateritic profiles. *Geochimica et Cosmochimica Acta*, **54**, 782-795.

Braun, J.J., Pagel, M., Herbillon, A., Rosin, C., 1993. Mobilization and redistribution of REEs and thorium in a syenitic lateritic profile: a mass balance study. *Geochim. Cosmochim. Acta* **57**, 4419-4434.

Braun, J.J., Viers, J., Dupré, B., Polve, M., Ndam, J., Muller, J.P., 1998. Solid/liquid REE fractionation in the lateritic system of Goyoum, East Cameroon: the implication for the present dynamics of the soil covers of the humid tropical regions. *Geochim. Cosmochim. Acta.* **62**, 273-299.

Braun, O.P.G. 1971. Contribuicao a geomofologia do Brasil central, *Revista Brasileira de Geografia*, **32**, 3-39.

Brimhall, G.H., Alpers, C. and Cunningham, A.B., 1985. Analysis of supergene ore-forming processes and ground-water solute transport using mass balance principles. *Econ. Geol.,* **80**, 1227-1254.

Brimhall, G.H., Dietrich,W.E., 1987. Constitutive mass balance relations between chemical composition, volume, density, porosity, and strain in metasomatic hydrochemical systems: results on weathering and pedogenesis. *Geochim. Cosmochim. Acta* **51**, 567-587.

Brimhall, G.H., Lewis, C.J., Ague, J.J., Dietrich, W.E., Hampel, J. and Rix, P.,1988. Metal enrichment in bauxites by deposition of chemically mature aeolian dust. *Nature* **333,** 819-824.

Brimhall, G.H., Lewis, C.J., Ford, C., Bratt, J., Taylor, G. Warin, O., 1991. Quantitative geochemical approach to pedogenesis: Importance of parent material reduction, volumetric expansion, and aeolian influx in laterization. *Geoderma*, 51, 51-91.

Brookins, D.G. (1988) *Eh-pH diagrams for geochemistry,* Springer-Verlag New York, 176 p.

Bruque, S., Mozas, T., and Rodriquez, A. 1980. Factors influencing retention of lanthanide ions by montmorillonite. *Clay Minerals*. **15**. 41-420.

Butt, C.R.M. 1987. A basis for geochemical exploration models for tropical terrains. *Chemical Geology*. 60, 5-16.

Castor S. B. Hedrick J. B. 2006. Rare Earth Elements. *In:* Kogel, J E, Trivedi, N C, Baker, J M, and Krukowski S T. (eds.). *Industrial Minerals and Rocks: Commodities, Markets, and Uses*, 7th edition. SME. P. 1568 p.

Catlos, E.J. 2013. Versatile Monazite: resolving geological records and solving challenges in materials science: Generalizations about monazite: Implications for geochronologic studies. *American Mineralogist*, **98**, 819-832.

Černý P., Ercit T.S. 1989. Mineralogy of niobium and tantalum: crystal chemical relationships, paragenetic aspects and their economic implications. In: *Lanthanides, Tantalum and Niobium*. Möller, P., Černý P. and Saupé, F. (Eds.) Springer-Verlag Berlin Heidelberg. 370 p.

Chadwick, O.A., Brimhall. G.H., Hendricks, D.M. 1990. From a black to a gray box- amass balance interpretation of pedogenesis. *Geomorphology*, **3**, 369-390.

Clarke, M.C.G., Beddoe-Stephens, B..1987. *Mineralogical Magazine*, **51**, 371-387.

Chi R., Tian J. 2008. *Weathered Mantle Elution-Deposited Rare Earth Ores*. Nova Science Publishers, Inc. New York. 286 p.

Clow D., Drever, J.I. 1996. Weathering rates as a function of flow through an alpine soil. *Chem. Geol.* **132**, 131 – 141.

Cook, R.J. 1992. A comparison of methods for the extraction of smectite from calcareous rocks by acid dissolution techniques. *Clay Minerals*, **27**, 73-80.

Coppin F., Berger G., Bauer A., Castet S. Loubet M. 2002. Sorption of lanthanides on smectite and kaolinite. *Chemical Geology*, 182, 57-68.

Cordani, U.G., Sato, K. 1999. Crustal evolution of the South American Platform, based on Nd isotopic systematics on granitoid rocks. *Episodes*, **22**, 3.

CPRM Serviço Geológico do Brasil 2008. Mapa Geológico do Estado de Goiás E Distrito Federal. 1:500.000.

Dardenne, M.A. 2000. The Brasilia fold Belt. *In*: Thomas, F. & Campos, D.A. (eds.) *Tectonic Evolution of South America.* 31 Int. Geol. Cong. Rio de Janeiro., Brazil.

Dall'Agnol, R., Costi, H.T., Leite, A.A., Magalhaes, M.S., 1999. Rapikivi granites from Brazil and adjacent areas. Precambrian Research **95,** 9-39.

Dequincey O., Chabaux F., Clauer N., Liewig N., Muller J. P. (1999) Dating of weathering profiles by radioactive disequilibria; contribution of the study of authigenic mineral fractions. Comptes Rendus de l'Academie des Sciences, Serie II. *Sciences de la Terre et des Planetes* **328** (10), 679–685.

Deer, W. A., Howie, R. A. & Zussman, J. (eds) 2013. 3rd edition *An Introduction to the Rock-forming Minerals*. Mineralogical Society, London, 498 pp.

Dostal, J. 2017. Rare Earth Element Deposits of Alkaline Igneous Rocks. *Resources* **6**, 34.

Du, X., Rate, A.W., Gee, M.A.M., 2012. Redistribution and mobilization of titanium, zirconium and thorium in an intensely weathered lateritic profile in Western Australia. *Chem. Geol*. **330-331**, 101-115.

Duddy I. 1980. Redistribution and fractionation of rare-earth and other elements in a weathering profile. *Chemical Geology*, **30**, 363-381.

Eby, G.N. 1990. The A-type granitoids: review of their occurrence and chemical characteristics and speculations on their petrogenesis. *Lithos*, **26**, 20.

Ecrit, T.S. 2005. Identification and alteration trends of granitic-pegmatite-hosted (Y,REE,U,Th)-(Nb,Ta,Ti) oxide minerals: a statistical approach. *Canadian Mineralogist* **43**, 1291-1303.

Einsele, G. 2000. *Sedimentary Basins: Evolution, Facies and Sediment Budget*. Second edition. Springer. Berlin, Heidelberg, New York, London, Paris, Tokyo, Hong Kong, 792 p.

Egli, M. Fitze, P. 2000. Formulation of pedologic mass balance based on immobile elements: a revision. Soil Science, 165, 437-443.

Fordham, A.W. 1990. Weathering of biotite into dioctahedral clay minerals. *Clay Minerals*, **25**. 51-63.

FÖRSTER, H.J. 1998. The chemical composition of REE–Y–Th–U-rich accessory minerals from peraluminous granites of the Erzgebirge–Fichtelgebirge region, Germany; Part I, The monazite-(Ce) - brabantite solid solution series. American Mineralogist, **83**, 259-272.

FÖRSTER, H.J. 2000. Cerite-(Ce) and thorian synchysite-Ce from the Niederbobritzsch granite, Erzgebrige, Germany: Implications for the differential mobility of the LREE and Th during alteration. The Canadian Mineralogist, **38**, 67-79.

Franz, G., Andrehs, G., Rhede, D. 1996. Crystal chemistry of monazite and xenotime from Saxothuringian- Moldanubian metapelites, NE Bavaria, Germany. *Eur. J. Mineral.* **8**, 1097-1118.

Freyssinet P., Butt C. R. M. & Morris R. C. 2005. Ore-Forming Processes Related to Lateritic Weathering. *Economic Geology*. 100th Anniversary Volume, 681-722.

Galan. E., Fernandez-Caliani, J.C, Miras, A., Aparicio, P. Marquez, M.G. 2007 Residence and fractionation of rare earth elements during kaolinitisation of alkaline peraluminous granites in NW Spain. Clay Minerals, **42**, 341-352.

Gautier, M., Muller, F., Le Forestier, F., Bény, Guégan R. 2010. NH4-smectite: characterization, hydration properties and hydro mechanical behaviour. *Applied Clay Science* **49**, 247-254

Giordano, D., Romano, C., Dingwell, D.B, Poe, D., Behrens, H., 2004. The combined effects of water and fluorine on the viscosity of silicic magmas. *Geochimica et Cosmochimica Acta* **68**, 24, 5159-5168.

Gislason, S. R., Oelkers, E. H., Eiriksdottir, E. S., Kardjilov, M. I., Gisladottir, G. Sigfusson, B., Snorrason, A., Elefsen, S., Hardardottir, J., Torssander, P., Oskarsson, N. 2009. Direct evidence of the feedback between climate and weathering, *Earth and Planetary Science Letters*, **277**, 213-222.

Grant, J.A., 1986. The isocon diagram—a simple solution to Gresens equation for metasomatic alteration. *Economic Geology* **81**, 1976-1982.

Grant, J.A. 2005. Isocon analysis: A brief review of the method and applications. *Physics and Chemistry of the Earth*, **30**, 997-1004.

Goldich S.S. 1938. A study of rock weathering. *J. Geol*.**46,** 17-58.

Goodnenough, K.M. Schilling, J. Jonsson, E. Kalvig, P. Charles, N. Tuduri, J. Deady, E.A. Sadegui, M. Schiellerup, H. Muller, A. Bertrand, G. Arvanitidis, N. Eliopoulos, D.G. Shaw, R.A, Thrane K. Keulen, N. 2016. Europe's rare earth element resource potential: An overview of REE metallogenetic provinces and their geodynamic setting. *Ore Geology Reviews,* **72**, 838-856.

Gutierrez, M. 2013. *Geomorphology.* Published by CRP Press.

Hains, D.H. 2013. *Technical Report and Preliminary Economic Assessment: Serra Verde Rare Earth Project, Goias,Brasil* 74-79.

Hanson, S.L., Simmons, W.B., Falster, A.U., Foord, E.E., Lichte, F.E. 1999.Proporsed nomenclature for samarskite-group minerals: new data on ishikawaite and calciosamarskite. *Mineralogical Magazine* **63**, 27-36.

Harlov, D.E. Förster, H.-J. 2002. High-Grade Fluid Metasomatism on both a Local and a Regional Scale: the Seward Peninsula, Alaska, and the Val Strona di Omegna, Ivrea–Verbano Zone, Northern Italy. Part II: Phosphate Mineral Chemistry. *Journal of Petrology*, **43**, 801-824.

Hasui, Y. Almeida, F.F.M. 1970. Geochronologia do centro-oeste brasilerio. Bol.Soc.Bras.Geol.,**19,** 15.

Hautmann S., Lippolt H. J. 2000. Ar-40/Ar-39 dating of central European K-Mn oxides—a chronological framework of supergene alteration processes during the Neogene. *Chem. Geol*. **170**, 37–80.

Hedrick J. B. 2010. *Rare-Earth Industry Overview and Defence Applications*. Presented at the 139th Society of Mining, Metallurgy & Exploration (SME) annual Meeting and Exhibit, Phoenix Arizona US. Slides retrieved from: www.slideshare.net/RareEarthsRareMetals/rare-earthindoverviewsme2010

Helmy, A.K., Ferreiro, E.A., Bussetti, S.G.1994. Cation exchange capacity and condition of zero charge of hydroxy-Al montmorillonite. *Clays and Clay minerals*. **42**, 444-450

Heroldová, N. 2011 *Low temperature alteration of metamictic Y,REE,-Nb,Ta,Ti minerals*. PhD thesis. Masaryk University.

Hoskin, P.W.O. Schaltegger, U. 2003. The Composition of Zircon and Igneous and Metamorphic Petrogenesis. *Reviews in Mineralogy and Geochemistry*, **53**, 27-62.

Huang, D. H, Wu, C. Y., Han, J. Z. Zhang, Q. D. 1989. Characteristics of isotopic systematics of U–Pb and Rb–Sr and their geological implications for Zudong and Guanxi granitic intrusives, Longnan County, Jiangxi. *Acta Petrologica Sinica* **5**, 37–48 (in Chinese with English abstract).

Huang, D.H., Wu, C.G., Han, J.Z., 1989. REE geochemistry and mineralization characteristics of the Zhundong and Guanxi Granites, Jiangxi Province. *Acta Geol. Sin*. **2**, 139-157.

Hughes, J.G., Brown, B. 1977. Two unusual minerals in a Nigerian soil: (I) Fibrous kaolin; (II) Bastnaesite. *Clay Minerals*. **12**, 319.

Imai A., Sanematsu K., Ishida S., Watanabe K. Boosayasak J. 2008. Rare Earth Elements in Weathered Mantle in Sn-bearing Granitic Rocks in Southern Thailand. Proceedings of the International Symposia on Geoscience Resources and Environments of Asian Terranes (GREAT 2008), 4th IGCP 516, and 5th APSEG; Bangkok, Thailand, 232-237.

Ishiara S. 2008. Granite Series, Type and Concentration of HREE in the Malay Peninsula Region. Proceedings of the International Symposia on Geoscience Resource and Environments of Asia Terranes (Great) 4th IGCP 516 and 5th APSEG. 31-35.

Ishiara S., Hua R., Hoshino M., Murakami H. 2008 REE abundances and REE minerals in granitic rocks in the Nanling Range, Jiangxi Province, Southern China and Generation of REE-rich Weathered Mantle Deposits. *Resource Geology* **58**, 355-372.

Kanazawa Y., Kamitani M. 2006. Rare earth minerals and resources in the world. *Journal of Alloys and Compounds,* **408–412**, 1339–1343.

Kempe, U., Lehmann, B., Wolf, D., Rodionov, N., Bombach, K., Schwengfelder, U. Dietrich, A. 2008. U–Pb SHRIMP geochronology of Th-poor, hydrothermal monazite: An example from the Llallagua tin-porphyry deposit, Bolivia. *Geochimica et Cosmochimica Acta*, **72**, 4352-4366.

Keppler, H., Wyllie, P.J., 1993. Influence of fluorine on the enrichment of high field strength trace elements in granitic rocks. *Contributions to Mineralogy and Petrology*, **114**, 479-488.

King, L.C. 1956. A geomorfologia do Brasil Oriental. Rev. Bras. Geografia, 18, 147-265.

Köhler, S.J, Harouiya, N., Chaïrat, C., Oelkers, E.H. 2005. Experimental studies of REE fractionation during water–mineral interactions: REE release rates during apatite dissolution from pH 2.8 to 9.2. *Chemical Geology*, **222,** 168-182.

Koppi, A.J., Edis, R., Field, D.J., Geering, H.R., Klessa, D.A., Cockayne, D.J.H. 1996. Rare earth element trends and cerium-uranium-manganese associations in weathered rocks from Koongarra, Northern Territory, Australia. *Geochimica et Cosmochimica Acta*, 60, 1695-1707.

Kynicky J., Martin P., Xu Ch. 2012. Diversity of Rare Earth deposits: The key examples of China. *Elements*, **8,** 361-367.

Laveuf, G., Cornu, S. 2009. A review on the potentiality of rare earth elements to trace pedogenetic processes. *Geoderma*, **154**, 415-423.

Le Maitre, R.W., Streckeisen, A., Zanettiun, B., LeBas, M.J., Bonin, B., Bateman, P., Bellieni, G., Dudek, A., Efremova, S., Keller, J., Lameyre, J., Sabine, P.A., Schmid, R., Sorensen, H., Wolley, A.R., 2002. *Igneous rocks. A classification and glossary of terms*. Cambridge University Press, Cambridge, U.K., 236 pp.

Littlejohn, A.L. 1981. Alteration products of accessory allanite in radioactive granites from the Canadian shield. *Papers Geol. Surv. Canada*, 81-1B, 95-104.

Ma, C., Eggleton, R.A. 1999. Cation exchange capacity of Kaolinite. *Clays and Clay Minerals*. 47, 174-180.

Ma, J. Wei, G., Xu, Y. Long, W. Sun, W. 2007 Mobilization and re-distribution of major and trace elements during extreme weathering of basalt in Hainan Island, South China. *Geochimica et Cosmochimica* Acta **71**, 3223-3237.

Macambira, M.J.B. 1983. *Ambiente Geologico e Mineralizacoes Associadas ao Granito Serra Dourada (Extremidade Meridional), Goias*. MSc Thesis, University of Para, 1-139.

Macambira, M. J. B. Villas, R. N. A. 1984. Geologia da extremidade meridional da Serra Dourada, Goiás: variedades litológicas, metamorfismo e mineralizações associadas. In: Congresso Brasileiro de Geologia, 33, 1984, Rio de Janeiro. Anais SBG, 123-124.

Machado de Mello, F., Bilal, E. (2009) Sucuri Massif albitites from Goiás tin Province Brazil, *Estudos Geológicos* **19**, 223 – 227.

Manning, D.A.C., 198. The effect of fluorine on liquidus phase relationships in the system Qz-Ab-Or with excess water at 1kb. *Contributions to Mineralogy and Petrology,* **76**, 206-215.

Marini, O.J., Botelho, N.F. Rossi, P. 1992. Elementos terras raras em granitóides da província estanífera de Goiás. *Revista Brasileira de Geosciencias*, **22**, 61-72.

Marini, O.J. Botelho, N.F. 1986. A Provincia de Granitos Estaníferos de Goiás. *Revista Brasileira de Geosciencias*, **16**, 12.

Marker A. Oliviera J. J. 1990. The formation of rare earth element scavenger minerals in weathering products derived from alkaline rocks of SE-Bahia, Brazil. *Chemical Geology*, **84**, 373-374.

Marker A. Oliviera J. J. 1994. Climatic and morphological control of rare earth element distribution in weathering mantles on alkaline rocks. *Catena*, **21.** 179-193.

McLennan, S.M., Hemming, S., McDanniel, D.K., Hanson, G.N. 1993.Geochemical approaches to sedimentation, provenance, and tectonics. In: Johnsson, M.J., Basu, A. (eds.). *Processes Controlling the Composition of Clastic Sediments.* Geological Society of America, Special Paper, **285**, 21-40.

McDonough, W.F., Sun, S.-S. 1995. Composition of the Earth. *Chemical Geology* **120,** 223-253.

Meinhold G. 2010. Rutile and its application in earth science. Earth-Science Reviews **102**, 1-28.

Meyerhoff, A. A., Kamen-Kaye, M., Chen, C., Taner, I., 1991, *China - Stratigraphy, Paleogeography and Tectonics.* Kluwer Academic Publishers, Dordrecht, 188 p.

Melfi, A. J., Cerri, C. C., Kronberg, B. I., Fyfe, W. S., McKinnon, B. 1983, Granitic weathering: a Brazilian study. *Journal of Soil Science*, **34**: 841–851.

Middleburg J.J., Van der Weijden C.V & Woittiez J.R.W. 1988. Chemical Processes affecting the mobility of major, minor and trace elements during weathering of granitic rocks. *Chemical Geology,* **68**, 263-273.

Migdisov, A. Williams-Jones, A.E. 2014. Hydrothermal transport and deposition of the rare earth elements by fluorine-bearing aqueous liquids. *Mineralium Deposita*, **49**, 987-997.

Miller, S.E., Heath, R., Gonzalez, R.D. 1982 Effects of temperature on the sorption of lanthanides by montmorillonite. *Clays and Clay Minera*ls, **30**, 111-122.

Miller, C.F., Mittlefehldt, D.W. 1982. Depletion of light rare-earth elements in felsic magmas. *Geology,* **10,** 3, 129-133.

Modenesi-Gauttieri M.C., Motta de Toledo, M.C., Hiruma S.T., Taioli, F., Shimada, H. 2011. Deep weathering and landscape evolution in a tropical plateau. *Catena*, **85**, 3, 221-230.

Moldoveanu , G.A., Papangelakis, V.G. 2012. Recovery of rare earth elements absorbed on clay minerals: I. Desorption mechanism. *Hydrometallurgy* **117-118**, 71-78.

Moldoveanu, G.A., Papangelakis, V.G. 2013. Recovery of rare earth elements adsorbed on clay minerals: II. Leaching with ammonium sulfate. *Hydrometallurgy* **131-132,** 158–166.

Moldoveanu, G.A., Papangelakis, V.G. 2016. An overview of rare-earth recovery by ion-exchange leaching from ion-adsorption clays of various origins. *Mineralogical Magazine*, **80**, 63-71.

Moore D.M., Reynolds, R.C. 1997. *X-ray diffraction and the identification and analysis of clay minerals.* Second Edition. Oxford University Press, USA, 378 pp.

Morteani, G., Preinfalk C. 1996. REE distribution and REE carriers in laterites formed on the alkaline complexes of Araxá and Catalão (Brazil). *In*: Jones A.P., Wall F., and Williams C.T. (eds) *Rare Earth Minerals: Chemistry, Origin and Ore Deposits*. Mineralogical Society, London: Chapman and Hall. 227-255.

Mongelli G. 1993. REE and other trace elements in a granitic weathering profile from Serre, southern Italy. *Chemical Geology*, **103**, 17-25.

Murakami H, Ishihara S. 2008. REE mineralization of Weathered Mantle and Clay Sediment on Granitic rocks in the Sanyo Belt, SW Japan and the Southern Jianxi Province, China. *Resource Geology*, **58**, 373-401.

Nesbitt W. 1979. Mobility and fractionation of rare earth elements during weathering of a granodiorite. *Nature*, **29**, 206-210.

Nesbitt, H.W., Young, G.M., 1982. Early Proterozoic climates and plate motions inferred from major element chemistry of lutites. *Nature* **299**, 715–717.

NPCS Board of Consultants & Engineers 2009 *Handbook on Rare Earth Metals and Alloys (Properties, Extraction, Preparation and Applications)*. Asia Pacific Business Press Inc.

Nasdala, L., Kronz, A., Wirth, R., Váczi, T., Pérez-Soba, C., Willner, A., Kennedy, A.K. 2009. The phenomenon of deficient electron microprobe totals in radiation-damaged and altered zircon. *Geochimica et Cosmochimica Acta*, **73**, 1637-1650.

Neves, J.M.C., Nunes, J.E.L. & Sahama, T.G. 1974. High hafnium members of the zircon-hafnon series from the granite pegmatites of Zambézia, Mozambique. *Contributions to Mineralogy and Petrology*, **48**, 73-80.

Oelkers, E., Poitrasson, F. 2002. An experimental study of the dissolution stoichiometry and rates of a natural monazite as a function of temperature from 50 to 230 °C and pH from 1.5 to 10. *Chemical Geology* **191.** 73-87.

Ogunleye, P.O., Garba, I., Ike, E.C. 2006. Factors contributing to enrichment and crystallization of niobium in pyrochlore in the Kaffo albite arfvedsonite granite, Ririwai Complex, Younger Granites province of Nigeria. *J. Afr. Earth Sci*. **44**, 372-382.

Parizek, J. R., Girty, G. H. 2014. Assessing volumetric strains and mass balance relationships resulting from biotite-controlled weathering: Implications for the isovolumetric weathering of the Boulder Creek Granodiorite, Boulder County, Colorado, USA. *CATENA*, **120**, 29-45.

Peccerillo, A., Taylor, S.R. 1976. Geochemistry of Eocene calc-alkaline volcanic rocks of the Kastamonu area, northern Turkey. Contributions Mineral Petrology 58, 63-81.

Peelman, S., Sun, Z.H.I., Sietsma, J. Yang, Y. 2014. Leaching of rare earth elements: Past and present. ERES 2014: 1st European Rare Earthe Resource Conference, Milos. 446 – 456.

Pérez-Soba, C., Villaseca, C., Del Tánago, J.G. Nasdala, L. 2007. The composition of zircon in the peraluminous hercynian granites of the spanish central system batholith. *The Canadian Mineralogist*, **45**, 509-527.

Petersen, J.K, Schultz-Guttler, R.A., Silveira, R.M. 2002 Alexandrita do Pela Ema, Minaçu/Go: Inclusões Fluidas E Condições Genéticas. *Revista Brasileira de Geociencias* **32**, 307-316.

Piasecki, W., Sverjensky, D.A.2008. Speciation of adsorbed yttrium and rare earth elements on oxide surfaces. *Geochemica et Cosmochimica Acta*, **72**, 3964-3979.

Pirajno F. 2009. Intrusion-Related Hydrothermal Mineral Systems. In: *Hydrothermal Processes and Mineral Systems*. Springer, Dordrecht, p.p.1250.

Pimentel, M.M., Heaman, L., Fuck, R.A. Marini, O.J. 1991. U-Zr geochronology of Precambrian tin-bearing continental-type acid magmatism in central Brazil. *Precambrian Research*, **52**, 15.

Pimentel M.M, Fuck, R.A., Botelho, N.F. 1999. Granites and the geodynamic history of the Neoproterozoic Brasília belt, Central Brazil: a review. *Lithos*, **46**, 463-483.

Pimentel, M.M. Botelho, N.F. 2001. Sr and Nd isotopic characteristics of 1.77-1.58 Ga rift-related granites and volcanics of the Goiás tin province, central Brazil. *Anais da Academia Brasileira de Ciências*, **73**, 263-276.

Pinto-Coelho, C.V., Vasconcellos, E.M.G., Ferreira C.H.N. 2007. Química mineral de micas do macico granítico Serra Branca, Goiás: processos de alteração hidrotermal como modificadores do reequilíbrio cristaloquimico. *Revista Brasileira de Geociências* **37**, 579-594.

Plant, J.A. Raiswell, R.W. 2013. Modifications to the geochemical signature of ore deposits and their associated rocks in different surface environments. In: *Drainage Geochemistry, Handbook of exploration geochemistr*y. Hale, M. and Plant, J.A.(eds). Elsevier Science publisher. 792 pages.

Pointer, C.M., Ashworth, J.R. Ixer, R.A. 1988. The zircon-thorite mineral group in metasomatized granite, Ririwai, Nigeria 2. zoning, alteration and exsolution in Zircon. *Mineralogy and Petrology*, **39**, 21-37.

Pollard, P.J. 1989. Geochemistry of granites associated with tantalum and niobium mineralization. In: *Lanthanides, Tantalum and Niobium*. Möller, P., Černý P. and Saupé, F. (eds) Springer-Verlag Berlin Heidelberg.

Praditwan J. 1988. Mineralogy of Tin and Niobium-Tantalum-Bearing Minerals in Thailand. In: Hutchison C.S. (eds) *Geology of Tin Deposits in Asia and the Pacific*. Springer, Berlin, Heidelberg

Prudencio, M.I. Braga, M.A.S., Gouveia M.A. 1993. REE mobilization, fractionation and precipitation during weathering of basalts. *Chemical Geoloy*, **107** (1993), 251-254.

Reis Neto, J.M. 1983. *Evolução Geotectonicada Bacia do Alto Tocantins, Goiás.* Dissertação de Mestrado, University of Sao Paulo. (unpublished).

Rhodes, J.M.1969. On the chemistry of potassium feldspars in granitic rocks. *Chem. Geology* **4**, 373-392.

Rossi, P., Andrade, G.F. A., C. 1992. The 1.58 Ga A-type granite of Serra da Mesa (GO): an example of NYF fertile granite pegmatite. *Cong.Bras.Geol. Bol. Res.*, **37.**

Rollinson, H. 1993. *Using geochemical data: evaluation, presentation, interpretation*. Longman Scientific & Technical.

Ruan C. Guocai Z. 1998 Rare earth partitioning of granitoid weathered mantle in southern China. *Trans. Nonferrous Met. Soc*. China. **8.**

Ru'an, C., 1988. Extraction of rare earths from a low-grade, kaolinitic ore by percolation leaching. In: Bautista, R.G., Wong, M.M. (Eds.), *Rare Earths: Extraction, Preparation and Applications*. The Minerals, Metals and Materials Society, Warrendale, 227–234.

Rubin, J.N., Hendry, C.D., Price, J.G. 1993. The mobility of zirconium and other "immobile" elements during hydrothermal alteration. *Chemical Geology* **110**, 29-47.

Sanematsu K., Murakami H., Watanabe Y., Duangsurigna S., Vilayhack S. 2009. Enrichment of rare earth elements (REE) in granitic rocks and their weathered mantles in central and southern Laos. *Bulletin of the Geological Survey of Japan*, **60**, 527-558.

Sanematsu K. Watanabe Y. 2013. Characteristics and genesis of ion-adsorption type REE ores. Presented at the Goldschmith Conference 2013, Florence, Italy. Abstract retrieved from: goldschmidt.info/2013/abstracts/originalPDFs/4319.pdf

Sanematsu, K., Kon, Y., Imai, A., Watanabe, K., Watanabe Y. 2013. Geochemical and mineralogical characteristics of ion-adsorption type REE mineralization in Phuket, Thailand. *Minerlium Deposita,* **48**, 437-451.

Sanematsu. K., Kon, Y., 2013. Geochemical characteristics determined by multiple extraction from ion-adsorption type REE ores in Dignan County of Jiangxi Province, South Asia. Bulletin of *Geological Survey of Japan* **64**. 313-330.

Sanematsu, K., Kon, Y., Imai, A., 2015. Influence of phosphate on mobility and adsorption of REE during weathering of granites in Thailand. *Journal of Asian Earth Sciences* **111**, 14-30.

Sanematsu, K., Watanabe, Y., 2016. Characteristics and genesis of ion-adsorption type REE deposits. *Reviews in Economic Geology* 18, 55-70.

Santana, I.V. 2013. *Caracterização mineralógica e geoquímica de ocorrencias de terras raras no maciço granítico Serra Dourada*, *Goiás/Tocantins, Brasil* dissertação de mestrado, Universidad de Brasília. (unpublished).

Santana, I.V. 2015 Occurrence and behaviour of monazite-Ce and xenotime-Y in detrital and saprolitic environments related to the Serra Dourada granite, Goias/Tocantins State, Brazil: Potential for REE deposits. *Journal of Geochemical Exploration*, **155,** 1-13.

Schellmann, W. 1981. Considerations on the definition and classification of laterites. Proceedings of the International Seminar on Lateritisation Processes, IGCP 129 and IAGC, Trivandrum, India. Oxford and IBH Publishing Company, New Delhi, pp. 1–10.

Schellmann, W. 1982. Eine neue laterit definition. *Geologische. Jahrbuch*. **D58**, 31–47.

Schellmann, W. 1986. A new definition of laterite. In: Banerji, P.K. (Ed.), *Lateritisation Processes. Memoirs of the Geological Survey of India*, 120, pp. 1–7.

Schellmann,W., 2003. Discussion of "A critique of the Schellmann definition and classification of laterite" by R.P. Bourman and C.D. Ollier (*Catena* 47, 117–131). *Catena* 52, 77–79.

Scheepers, R., Rozendaal, A. 1993. Redistribution and fractionation of U, Th and rare-earth elements during weathering of subalkaline granites in SW Cape Province, South Africa. *Journal of African Earth Sciences,* **17**, 41-50.

Schroth, B.K., Sposito, G. 1997 Surface charge properties of kaolinite. *Clays and Clay Minerals*, **45**, 85-91

Shand S.J. 1949. *Eruptive rocks their genesis composition, classification and their relation to ore deposits*. London, Thomas Murby and Co., 488p.

Stepanov, A.S., Hermann, J., Rubatto, D. & Rapp, R.P. 2012. Experimental study of monazite/melt partitioning with implications for the REE, Th and U geochemistry of crustal rocks. *Chemical Geology*, **300–301**, 200-220.

Suita, M.T.F. 1988. Late Paleo to Neoproterozoic geochronology & metallogeny of the Tocantins Province, Brazil: An outline. *Chinese Science Bulletin***, 43,** 123.

Takeno, N. 2005. *Atlas of Eh-pH diagrams. Intercomparison of thermodynamic databases*. Geological Survey of Japan. Open File Report **419**, 285p.

Tchapek, M., Tcheichvili, L., Wasowski, C.1974. The point of zero charge (pzc) of kaolinite and SiO2 and Al2O3 mixtures. Clay Minerals, 10, 219 – 229

Teixeira, L.M. 2002. *Caracterização de minerais portadores de terras raras e sua aplicação a petrologia e geocronologia de granitos das supbrovíncias Tocantins e Parana, Goias*.Thesis de Doutorado, Universidad de Brasília. (unpublished).

Teixeira, L.M. Botelho, N.F. 2002. Comportamento cristaloquímico de monazita primária e hidrotermal durante a evolução de granitos e greisens: exemplos das Sub-Províncias Tocantins e Paraná, Goiás. *Revista Brasileira de Geosciencias*, **32**, 8.

Teixeira, L.M. Botelho, N.F. 2006. Comportamiento Geoquímico de ETR durante evolução magmatica e alteração hidrotermal de granitos: exemplos da provínci estanífera de goiás. Revista Brasileira de Geosciencias, **36**, 13.

Tilley, D.B., Eggleton, R.A. 2005. Titanite low-temperature alteration and Ti-mobility. *Clays and Clay Minerals*, **53**, 100-107.

Tian, J., Jingqun, Y., Ruan, C., Guohua, R., Mintao, J., Kexian, O., 2010. Kinetics on leaching rare earth from the weathered crust-elution-deposited rare earth ores with ammonium sulfate solution. *Hydrometallurgy*, **101**, 166-170.

Trescases, J.J., Melfi, A., Barros De Oliveira, S.M. 1981. Nickeliferous laterites of Brazil. *In*: *Lateritization Processes*. Balkena Rotterdam, 170-1841.

Uher, P., Ondrejka,M., Bačík, P., Broska, I., Konečný, P., 2015. Britholite, monazite, REE carbonates and calcite: products of hydrothermal alteration of allanite and apatite in A-type granite from Stupné, Western Carpathians, Slovakia. *Lithos* 236-237, 212-225.

Valsami-Jones, E., E., Ragnarsdottir, K.V., Putnis, A., Bosbach, D., Kemp, A.J., Cressey, G. 1998. The dissolution of apatite in the presence of aqueous metal cations at pH 2–7, In Chemical Geology, Volume 151, 215-233.

Vasconcelos P. M., Brimhall G. H., Becker T. A., Renne P. R. (1994a) Ar-40/Ar-39 Analysis of Supergene Jarosite and Alunite—Implications to the Paleoweathering History of the Western USA and West-Africa. *Geochim. Cosmochim. Acta* **58** (1), 401-420.

Velde, B., Meunier, A., 2008. *The origin of clay minerals in soils and weathered rocks*. Springer.

Vlach, S.R.F., Gualda, G.A.R. 2007. Allanite and chevkinite in A-type granites and syenites of the Graciosa Province, southern Brazil. *Lithos,* **97,** 98-121.

Walters, A., Lusty P., Hill, A. 2011. Rare Earth Elements British Geological Survey. World Wide Web address: www.MineralsUK.com. Downloaded 17 January 2014.

Wang, L., Xu, C., Zhao, Z., Song, W., Kynicky, J. 2015. Petrological and geochemical characteristics of Zhaibei granites in Nanling region, Southeast China: Implications for REE mineralization. *Ore Geology Reviews,* **64,** 569-582.

Wan Y., Liu C. 2006. The effect of humic acid on the adsorption of REEs on kaolin. *Colloids and Surfaces A: Physicochemical and Engineering Aspects,* **290**, 112-117**.**

Williams-Jones, A. E., Wood, S.A. 1992. A preliminary petrogenic grid for REE fluorocarbonates and associated minerals. *Geochimica et Cosmochimica*, **56**, 725-738.

White A.F. 2003 Natural Weathering Rates of Silicate Minerals. *In:* Holland, H.D., and Turekian, K.K. (eds) Treatise on Geochemistry. Elsevier p133-168.

White, A.F., Bullen, T.D., Schulz, M.S., Blum, A.E., Huntington, T.G., Peters, N.E. 2001. Differential rates of feldspar weathering in granitic regoliths, *Geochimica et Cosmochimica Acta*, 65, 847-869.

Wu, C.Y., Huang, D.H., Guo, Z.X., 1989. REE geochemistry in the weathering process of granites in Longnan County, Jiangxi Province. *Acta Geologica Sinica* **63**, 349-362 (in Chinese with English abstract).

Wu, C.Y., Lu, H.L., Xu, L.M., Hou, L. 1993. A preliminary study on modes of occurrence of rare earth elements in the tropical subtropical weathering mantle of Nanling region. *Mineral Deposits,* **12**, 297-307 (in Chinese with English abstract).

Wu, C, Yuan, Z. Bai, G. (1996) Rare earth deposits in China. In: Jones, A.P., Wall, F. Williams, C.T., (eds), *Rare Earth Minerals: Chemistry origin and ore deposits*. The Mineralogical Society Chapman & Hall, Series 7, 281-310.

Yang, Z.M. 1987. A study on clay minerals from the REE-rich weathering mantle developed in the Longnan granite in Jiangxi. *Scientia Geologica Sinica* **22**, 70–80 (in Chinese with English abstract).

Yang, X., Zang, J. 2015. Recovery of rare earth from ion-adsorption rare earth ores with a compound lixiviant. *Separation and Purification Technology* **142**, 203-208.

Zhongxin Y., Changxu W., Leiming X., and Yunxing N. 1993. The distribution of trace elements in granitoids in the Nanling region of China. *Chinese Journal of Geochemistry*, **12.**

Zhang P., Zhuming Y., Kejie T., & Xueming Y. (1995*) Mineralogy and Geology of REE in China*. Science Press Beijing China.

Zhang, L., Deng, X., Li, W., Ding, Y., Chi, R., Zuo, X. 2013. Kinetics of weathered-crust elution-deposited rare-earth ore in a leaching process. *Materials and Technology*, **47**, 145-148.

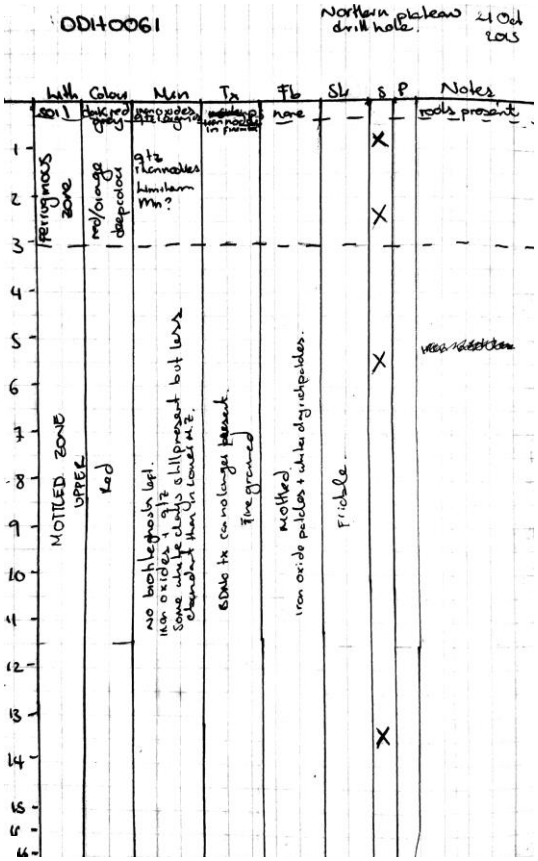
Zaraisky, G.P., Korzhinskaya, V., Kotova, N. 2010. Experimental studies of Ta_2O_5 and columbite–tantalite solubility in fluoride solutions from 300 to 550 ºC and 50 to 100 MPa. *Mineralogy and Petrology,* **99***,* 287-300.

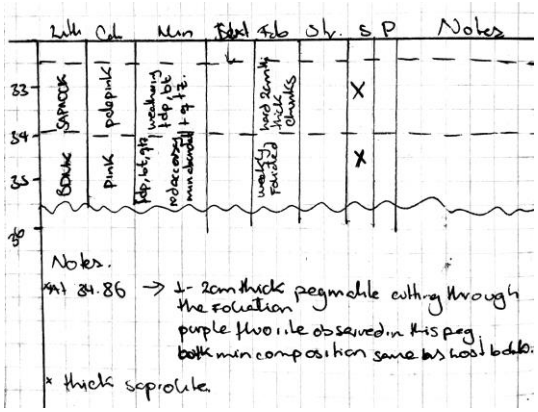
Xiao, Y., Chen, Y., Feng, Z., Huang, X., Huang, L., Long, Z., Cui, D. 2015. Leaching characteristics of ion-adsorption type rare earths ore with magnesium sulphate. *Trans Nonferrous Met. Soc. China*, **25**, 3784-3790.

APPENDIX

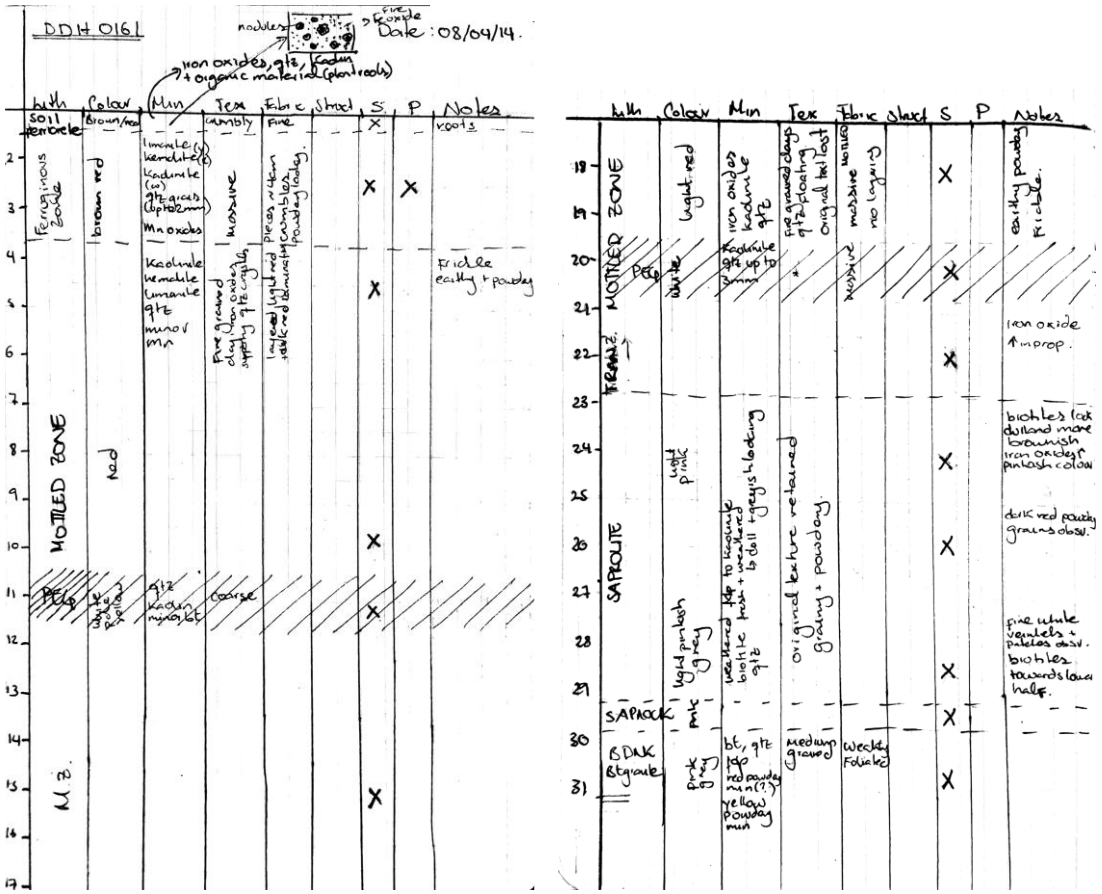
FIELD DRILL CORE LOGS A

DDH0061

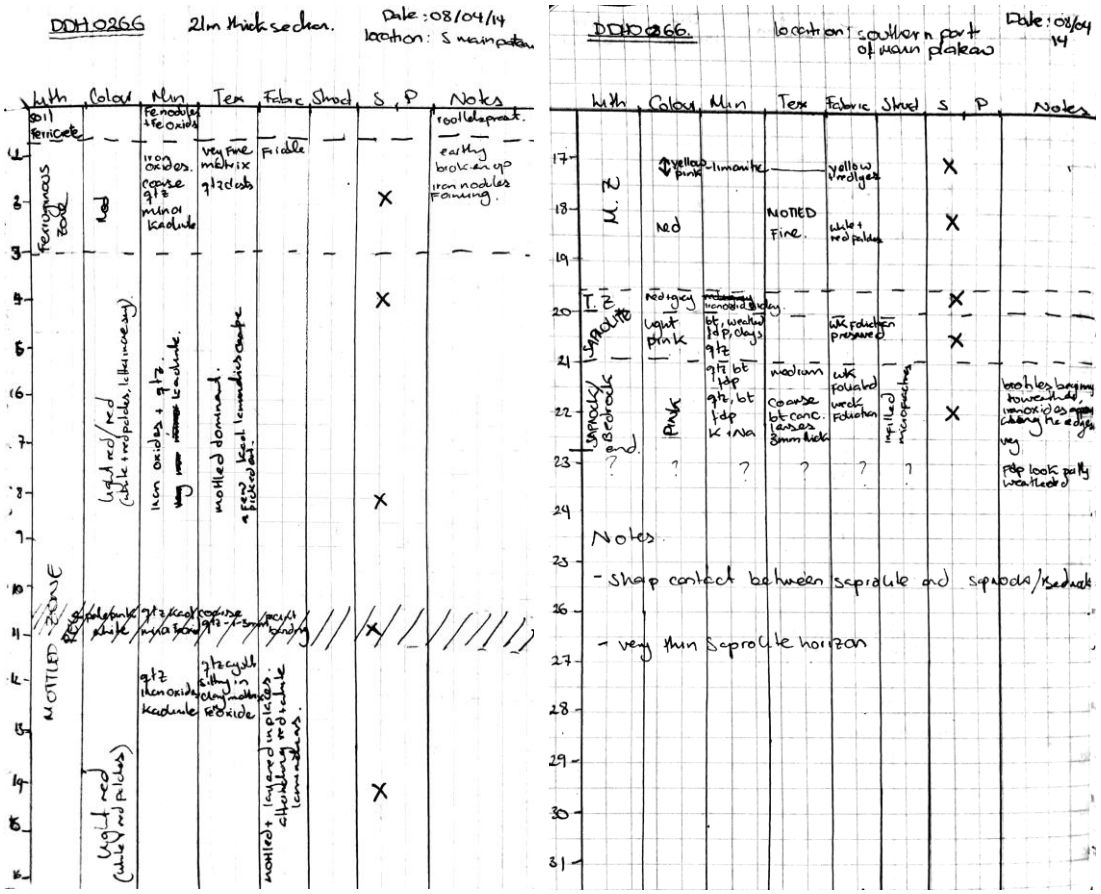




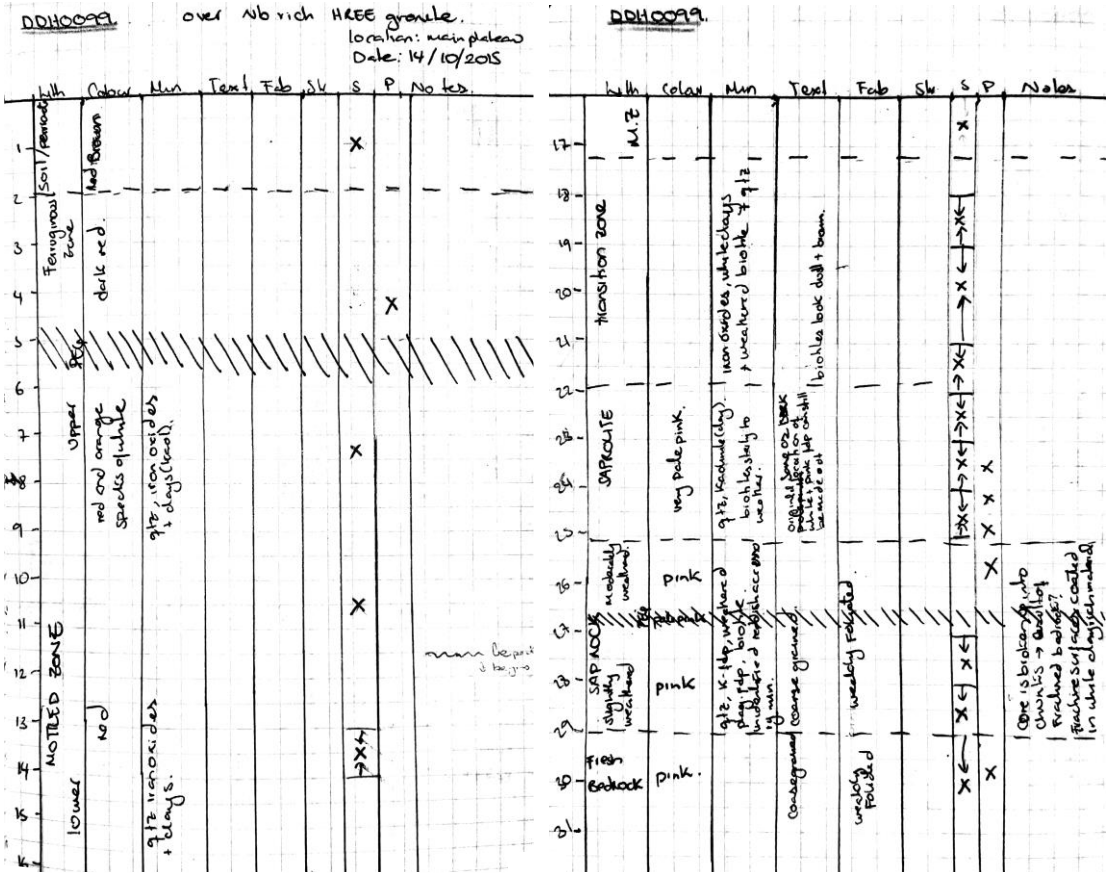
DDH0161


DDH 0161
Date: 08/04/14.
nodules
iron oxides, qtz, + organic material (plant roots)
Bulk
Colour
Min
Tex
Fabric
Struct
S
P
Notes
soil
ferricrete
ferruginous zone
MOTTLED ZONE
PEL
SAPROLITE
SAPROCK
BDAK
Btgravel
M.T.B.
brown red
red
kaolinite
hematite
limonite
qtz
Mn oxides
moisture
coarse
fine
roots
friable easily + powdery
iron oxide
↑ mprop.
birbles (ex dolland more brownish iron oxides pinkish colour
dark red powdery grains obsv.
fine white veinlets + pellets obsv. birbles towards lower half.
light red
light pink
pink
pink grey
grey
iron oxides
kaolinite
qtz up to 3mm
weathered bio to kaolinite bio + weakened by drill + joints loading
bt, qtz
red powder
yellow powdery mn
original texture retained
grainy + powdery
medium grained
massive
no layering
weak foliation

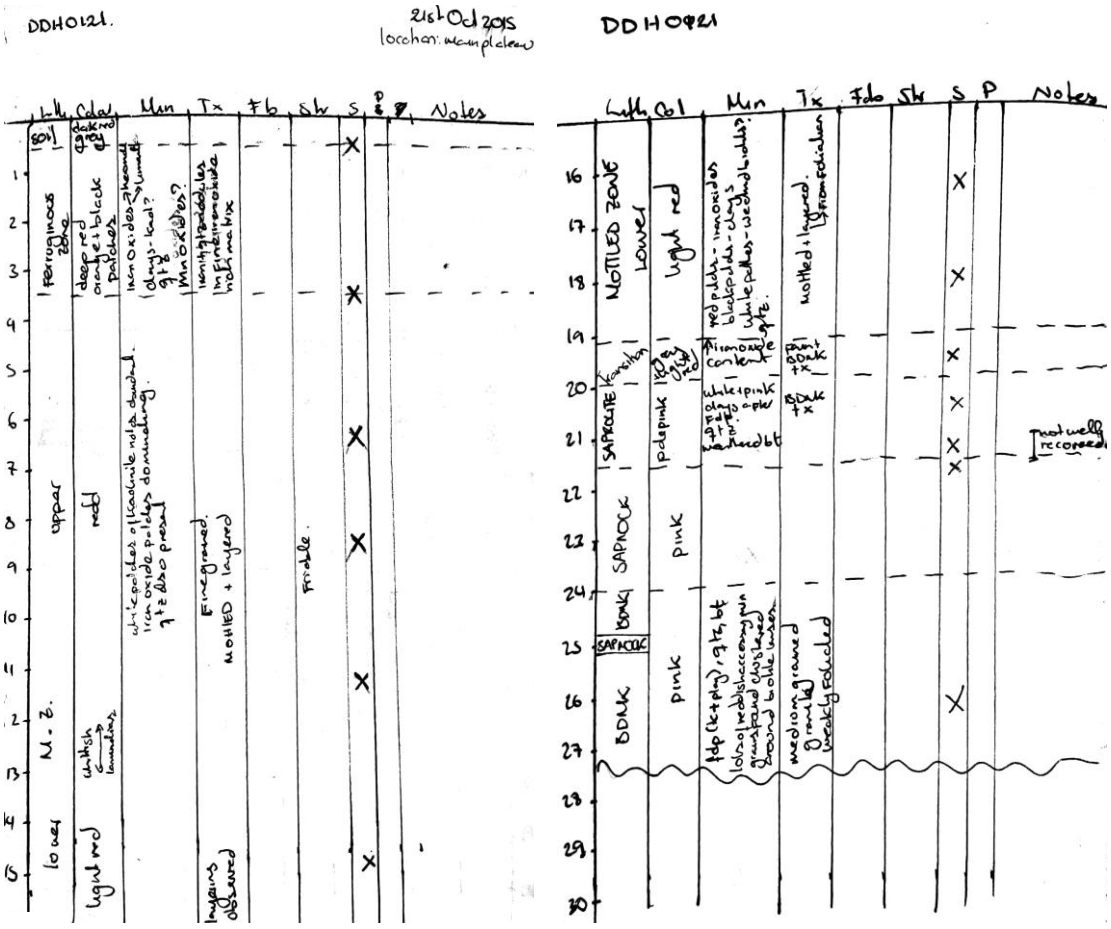
DDH0266


DDH0266
21m thick section.
Date: 08/04/14
location: S main plateau
Lith
Colour
Mun
Tex
Fabric
Struct
S
P
Notes
soil
ferricrete
ferruginous zone
MOTTLED ZONE
saprolite
saprock
Notes
- sharp contact between saprolite and saprock/bedrock
- very thin saprolite horizon

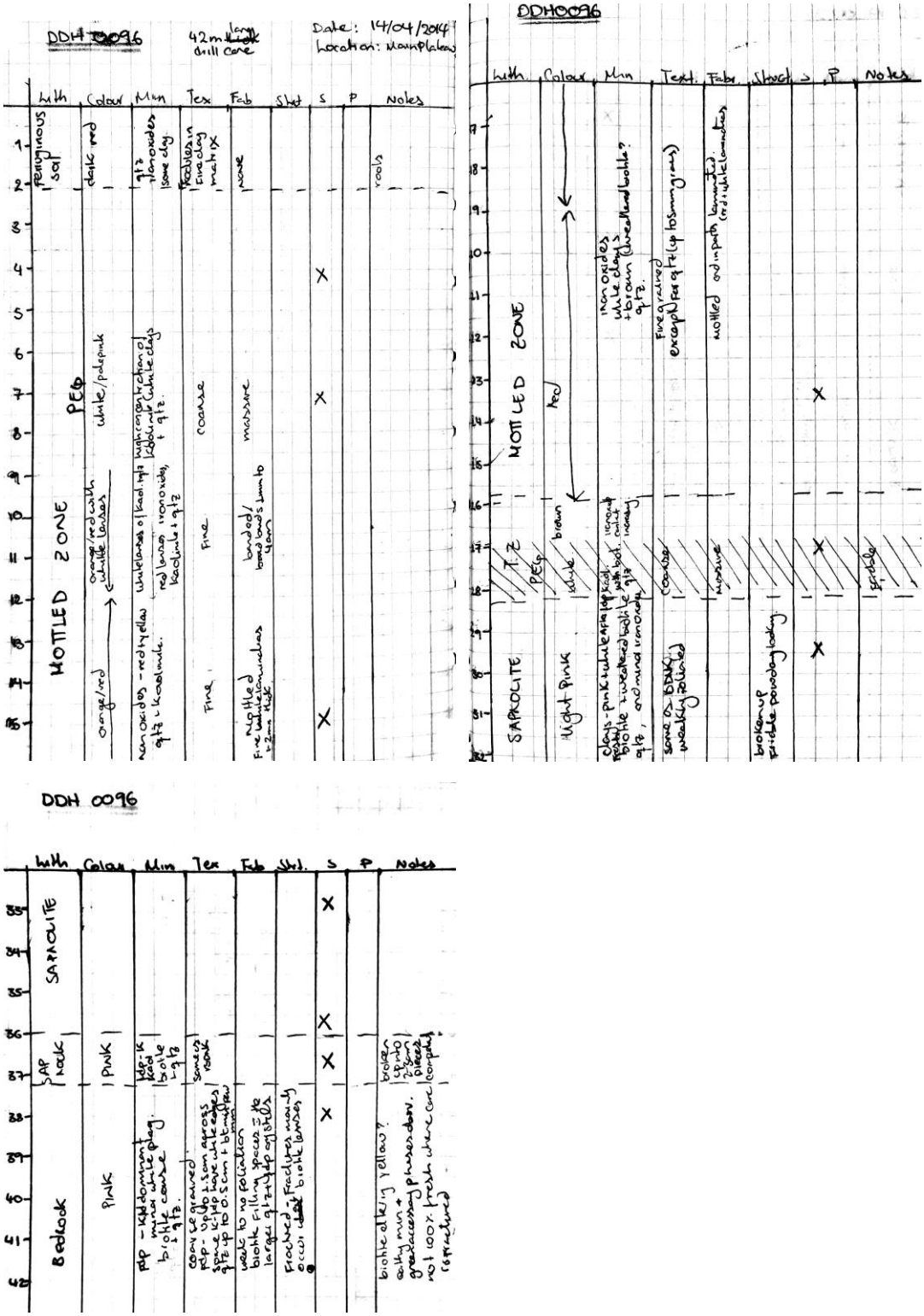
DDH0099


DDH0099
over Nb rich HREE granite.
location: main plateau
Date: 14/10/2015
DDH0099.
transition zone
SAPROLITE
NOTCHED ZONE
Upper
Lower
Fresh bedrock
pink.
very pale pink.
weakly weathered
slightly weathered
weakly FOLIATED
coarse grained.
dark red.
red and orange specks of white
Fe-Ti-oxides + clays(kaol).
Fe-Ti-oxides + clays.
bleached zone

DDH0121


DDH0121.
21st Oct 2015
location: near pipeline
DDH0921
Lith
Colour
Mun
Tx
Fab
Str
S
P
Notes
upper
N. 2.
lower
light red
red
deep red
orange-brown
patches
ferruginous
zone
MOTTLED ZONE
LOWER
SAPROLITE
SAPROCK
BDAK
pink
light red
pale pink
mottled + layered
fine-grained
fable
inclusions observed
root well recovered

DDH0096


DDH 0096
42m
drill core
Date: 14/04/2014
Location: Mamplaleu
MOTTLED ZONE
PEG
SAPROLITE
Bedrock
Width
Colour
Min
Tex
Fab
Str
S
P
Notes

BULK GEOCHEMICAL DATA B

B1. Analyses of reference standards and duplicates for bulk geochemical analysis at ALS and NHM

Table B1.1. ALS _ ME-ICP06 _ Duplicates

		Duplicates											
		SD10[1]			**SD21**[1]			**S11**[2]			**CS9**[2]		
Element	LOR	Main	DUP	*Difference*	Main	DUP	*Difference*	Main	DUP	*Difference*	Main	DUP	*Difference*
	wt %	wt %	wt %	*%*	wt %	wt %	*%*	wt %	wt %	*%*	wt %	wt %	*%*
SiO_2	0.01	71.1	71.9	*1.13*	74.4	73.9	*-0.67*	61.3	60.2	*-1.79*	48.6	47.4	*-2.47*
Al_2O_3	0.01	12.95	13.1	*1.16*	13.4	13.3	*-1.12*	14.45	14.2	*-1.73*	29.3	28.6	*-2.39*
Fe_2O_3	0.01	2.97	2.97	*0.00*	3.08	3.02	*-1.95*	0.88	0.86	*-2.27*	2.38	2.33	*-2.10*
CaO	0.01	1.21	1.23	*1.65*	0.63	0.62	*-1.59*	1.35	1.33	*-1.48*	0.16	0.16	*0.00*
MgO	0.01	0.1	0.1	*0.00*	0.13	0.13	*0.00*	2.72	2.69	*-1.10*	1.29	1.26	*-2.33*
Na_2O	0.01	3.11	3.07	*-1.29*	3.2	3.18	*-0.63*	0.24	0.22	*-8.33*	0.05	0.05	*0.00*
K_2O	0.01	5.8	5.81	*0.17*	5.9	5.87	*-0.51*	0.61	0.6	*-1.64*	0.77	0.75	*-2.60*
Cr_2O_3	0.01	<0.01	0.01	-	<0.01	<0.01	-	*na*	*na*	-	0.01	0.01	*0.00*
TiO_2	0.01	0.25	0.25	*0.00*	0.31	0.31	*0.00*	0.08	0.07	*-12.5*	0.16	0.15	*-6.25*
MnO	0.01	0.04	0.04	*0.00*	0.04	0.04	*0.00*	0.01	0.01	*0.00*	0.04	0.04	*0.00*
P_2O_5	0.01	0.03	0.02	*-33.3*	0.03	0.03	*0.00*	0.14	0.13	*-7.14*	0.03	0.05	*66.7*
SrO	0.01	<0.01	<0.01	-	<0.01	<0.01	-	<0.01	0.01	-	<0.01	<0.01	-
BaO	0.01	0.03	0.03	*0.00*	0.06	0.06	*0.00*	0.01	0.01	*0.00*	0.01	0.01	*0.00*

[1, 2] *respectively refer to batch numbers 1 and 2 of the standards analysed.*

Table B1.2. ALS _ ME-ICP06 _ Standards

		Standards																	
		OREAS-121		**AMIS0304**		**SY-4**						**GRE-3**							
Element	LOR	R.V.	STD1[2]	R.V.	STD1[2]	R.V.	STD1[1]	STD2[1]	STD3[2]	STD4[2]	*RSD*	R.V.	STD1[1]	STD2[1]	STD3[2]	STD4[2]	*RSD*	Mean Bias	1σ Error
	wt %	wt %	wt %	wt %	wt %	wt %	wt %	wt %	wt %	wt %	*%*	wt %	wt %	wt %	wt %	wt %	*%*	%	%
SiO_2	0.01	81.5	81.4	12.3	12.0	49.9	48.9	49.2	49.6	50.6	*1.49*	3.27	3.39	3.19	3.17	3.13	*3.60*	-1.19	2.48
Al_2O_3	0.01	9.11	9	1.52	1.59	20.69	20.7	20.4	21.1	20.1	*2.08*	0.94	0.99	0.94	0.92	0.96	*3.13*	0.65	2.87
Fe_2O_3	0.01	2.32	2.24	21.0	20.9	6.21	6	5.99	6.09	5.97	*0.88*	50.5	51.6	49.6	49.3	51.2	*2.27*	-1.70	2.17
CaO	0.01	0.105	0.13	28.5	28.9	8.05	7.92	7.75	8.07	7.96	*1.68*	18.4	18.2	17.9	18.25	18.85	*2.17*	1.79	1.95
MgO	0.01	0.425	0.39	2.83	2.75	0.54	0.5	0.5	0.5	0.5	*0.00*	0.14	0.16	0.16	0.16	0.16	*0.00*	1.66	11.04
Na_2O	0.01	0.32	0.3	0.09	0.07	7.1	7.01	7.15	6.83	7.07	*1.94*	*na*	0.05	0.05	0.05	0.05	*0.00*	-4.78	7.54
K_2O	0.01	3.29	3.4	0.28	0.25	1.66	1.57	1.61	1.74	1.61	*4.54*	*na*	<0.01	<0.01	<0.01	0.02	-	-2.33	5.60
Cr_2O_3	0.01	0.01	0.01	0.01	0.01	0.018	0.005	0.01	0.005	0.005		*na*	0.01	0.01	0.01	0.01	*0.00*	-42.86	31.30
TiO_2	0.01	0.43	0.43	1.8	1.83	0.287	0.28	0.27	0.29	0.29	*3.39*	1.63	1.58	1.54	1.55	1.59	*1.52*	-2.06	2.94
MnO	0.01	0.105	0.1	0.46	0.45	0.108	0.11	0.11	0.11	0.11	*0.00*	1.65	1.71	1.64	1.58	1.64	*3.24*	-0.13	2.48
P_2O_5	0.01	0.055	0.06	18.4	18.55	0.131	0.12	0.12	0.13	0.14	*7.51*	15.3	15.25	15.35	15.5	15.45	*0.72*	0.31	4.88
SrO	0.01	0.023	<0.01	0.4	0.45	0.14	0.13	0.12	0.14	0.13	*6.28*	0.24	0.23	0.23	0.21	0.23	*4.44*	-4.56	7.77
BaO	0.01	0.11	0.11	0.3	0.29	0.035	0.04	0.04	0.04	0.04	*6.28*	0.79	0.85	0.73	0.76	0.79	*6.55*	5.00	9.21

[1, 2] *respectively refer to batch numbers 1 and 2 of the standards analysed.*

Table B1.3. ALS _ ME-MS81 _ Standards and Duplicates

		Duplicates						Standards											
		SD10			**CS1**			**AMIS0304**		**SY-4**				**GRE-3**					
Element	LOR	Main	DUP	*Difference*	Main	DUP	*Difference*	R.V.	STD1[1]	R.V.	STD1[2]	STD2[1]	*Difference*	R.V.	STD1[2]	STD2[1]	*Difference*	Mean Bias	1σ Error
	ppm	ppm	ppm	*%*	ppm	ppm	*%*	ppm	ppm	ppm	ppm	ppm	*%*	ppm	ppm	ppm	*%*	%	%
Ba	0.5	291	294	*1.03*	69.6	73.0	*4.89*	2600	2580	340	347	326	*-6.05*	6975	6960	6960	*0.00*	-0.65	2.2
Ce	0.5	360	374	*3.89*	627	632	*0.80*	8090	8330	122	130	125	*-3.85*	4354	4120	4400	*6.80*	1.53	4.4
Cr	10	20.0	20.0	*0.00*	40.0	50.0	*25.00*	95	90.0	12	20	10	*-50.00*	50	50	50	*0.00*	8.95	33.0
Cs	0.01	2.39	2.01	*-15.9*	1.61	1.58	*-1.9*	0.4	0.44	1.5	1.55	1.48	*-4.5*	0.11	0.1	0.12	*20.0*	4.30	7.9
Dy	0.05	28.0	28.2	*0.71*	483	464	*-3.93*	132.3	129	18.2	19.1	18.15	*-4.97*	92.33	87.3	85.7	*-1.83*	-2.16	4.8
Er	0.03	18.2	19.7	*8.26*	282	270	*-4.26*	34	34.9	14.2	15.55	14.25	*-8.36*	28.84	27.5	28	*1.82*	0.99	5.5
Eu	0.03	1.60	1.59	*-0.63*	27.9	28	*0.36*	150	137	2	2.08	1.95	*-6.25*	75.24	75	73.5	*-2.00*	-2.03	4.7
Ga	0.1	38.0	38.5	*1.32*	60.5	64.3	*6.28*	53.25	48.4	35	38	37.5	*-1.32*	41.75	37.3	37.5	*0.54*	-2.85	9.8
Gd	0.05	25.7	26.0	*1.17*	494	476	*-3.64*	343	340	14	14.35	14.15	*-1.39*	191	176	177.5	*0.85*	-2.44	4.7
Hf	0.2	16.7	14.6	*-12.6*	2.50	2.70	*8.0*	28	27.6	10.7	11.2	11.9	*6.3*	19.8	19.9	19.8	*-0.5*	2.99	5.1
Ho	0.01	6.13	6.16	*0.49*	106	103	*-2.37*	18	17.45	4.3	4.55	4.46	*-1.98*	13.53	14.05	12.75	*-9.25*	0.91	5.0
La	0.5	208	216	*3.85*	4110	3860	*-6.08*	3610	3590	58	61.8	60.2	*-2.59*	2224	2150	2240	*4.19*	1.44	3.8
Lu	0.01	2.59	2.71	*4.63*	32.8	31.3	*-4.57*	2.045	1.94	2.1	2.2	2.09	*-5.00*	1.81	1.8	1.71	*-5.00*	-1.39	4.2
Nb	0.2	90.8	94.9	*4.52*	154	163	*5.52*	3970	>2500	13	14.1	13.9	*-1.42*	3524	>2500	>2500	-	-	-
Nd	0.1	144	150	*3.82*	2340	2360	*0.85*	3875	4090	57	59.5	60.2	*1.18*	1835	1755	1875	*6.84*	2.67	4.2
Pr	0.03	39.6	41.0	*3.54*	702	733	*4.42*	1007	>1000	15	16.15	14.95	*-7.43*	496.6	483	503	*4.14*	1.47	4.4
Rb	0.2	405	412	*1.73*	107	115	*7.98*	10.55	11.4	55	56.1	54.7	*-2.50*	***na***	0.7	1.8	*157*	3.17	4.4
Sm	0.03	24.2	25.4	*4.96*	432	443	*2.55*	603.5	603	12.7	13.35	13	*-2.62*	279	269	262	*-2.60*	-0.46	4.5
Sn	1	16.0	16.0	*0.00*	5.00	5.00	*0.00*	25.5	24	***na***	8	8	*0.00*	45.5	42	43	*2.38*	-6.36	1.2
Sr	0.1	41.6	41.8	*0.48*	11.0	11.2	*1.82*	3400	3420	1191	1225	1205	*-1.63*	2093	2110	2070	*-1.90*	0.88	1.4
Ta	0.1	7.70	7.30	*-5.19*	7.70	7.40	*-3.90*	12.45	11.8	0.9	0.8	0.8	*0.00*	161.5	147.5	156.5	*6.10*	-7.84	3.6
Tb	0.01	4.45	4.35	*-2.25*	80.9	81.0	*0.12*	34.25	32.1	2.6	2.86	2.75	*-3.85*	21.65	20.2	19.55	*-3.22*	-1.38	8.7
Th	0.05	65.4	69.2	*5.81*	106	103	*-2.83*	451	434	1.3	1.2	2.06	*71.67*	117.5	117	118.5	*1.28*	9.68	27.8
Tm	0.01	2.91	2.88	*-1.03*	37.1	36.0	*-2.96*	3.5	3.43	2.3	2.21	2.28	*3.17*	3.08	2.92	3.01	*3.08*	-2.85	1.7
U	0.05	8.36	8.37	*0.12*	17.8	17.8	*0.00*	24.1	24.5	0.8	0.75	0.81	*8.00*	111.8	116	113.5	*-2.16*	0.41	3.9
V	5	12.0	18.0	*50.0*	57.0	61.0	*7.0*	373	371	8	14	7	*-50.0*	1118	1190	1050	*-11.8*	12.48	35.6
W	1	4.00	4.00	*0.00*	23.0	23.0	*0.00*	5	4.00	1.8	2	1	*-50.00*	2.75	2	1	*-50.0*	-27.90	
Y	0.5	198	206	*4.30*	2860	2940	*2.80*	410	407	119	124	119	*-4.03*	320.6	311	313	*0.64*	-0.38	2.8
Yb	0.03	18.0	18.9	*5.00*	229	228	*-0.44*	17	16.55	14.8	14.8	15.05	*1.69*	14.8	14.6	14.4	*-1.37*	-1.00	1.9
Zr	2	549	469	*-14.6*	71.0	73.0	*2.8*	1118	1140	583	601	591	*-1.7*	969	1010	961	*-4.9*	1.98	1.9

[1, 2] respectively refer to batch numbers 1 and 2 of the standards analysed.

'na' denotes standards which do not have a certified reference value for a given element. For these elemental standards were omitted from the mean bias calculation.

Table B1.4. ALS _ ME-4AC81 _ Standards

		Standards									
		OGGeo08		**GEOMS-03**		**ICP-4**		**MRGeo08**			
Element	LOR	R.V.	STD1[1]	R.V.	STD1[1]	R.V.	STD1[2]	R.V.	STD1[2]	Mean Bias	1σ Error
	ppm	ppm	ppm	ppm	ppm	ppm	ppm	ppm	ppm	%	%
Ag	0.5	20.2	20.8	1.03	0.8	28	29	4.45	4.3	-4.70	11.9
As	5	119	120	633	618	1260	1260	33	35	1.13	3.56
Cd	0.5	18.6	18.7	0.68	0.5	18	18	2.25	2.2	-6.90	12.7
Co	1	96.0	98	12	11	31	35	20	20	1.66	8.74
Cu	1	8390	8460	134	128	1922.5	1920	631	634	-0.82	2.47
Li	10	28	30		40	305	300	27.5	30	5.51	6.20
Mo	1	935.5	944	2.63	2	80	74	15	15	-7.60	11.4
Ni	1	8885	8940	53	55	385.5	369	691	698	0.28	3.35
Pb	2	7240	7330	7	6	1932.5	1920	1080	1105	-2.83	7.74
Sc	1	10.5	10		12	23	22	12.5	11	-7.04	4.30
Zn	2	13725	7380	47	45	6350	6050	804	844	-1.33	5.47

[1, 2] respectively refer to batch numbers 1 and 2 of the standards analysed.

Table B1.5. ALS _ ME-4AC81 _ Duplicates

		Duplicates								
		SD10			**SV8**			**SV14**		
Element	LOR	Main	DUP	*Difference*[1]	Main	DUP	*Difference*	Main	DUP	*Differenc*
	ppm	ppm	ppm	*%*	ppm	ppm	*%*	ppm	ppm	*%*
Ag	0.5	<0.5	0.5		<0.5	<0.5		<0.5	<0.5	
As	5	<5	<5		6	<5	*58.3*	<5	12	
Cd	0.5	<0.5	<0.5		<0.5	<0.5		<0.5	<0.5	
Co	1	<1	1		1	2	*-100*	6	6	*0.00*
Cu	1	1	1	*0.00*	14	15	*-7.14*	12	12	*0.00*
Li	10	30	40	*-33.3*	20	20	*0.00*	160	160	*0.00*
Mo	1	1	1	*0.00*	<1	1		<1	1	
Ni	1	<1	<1		7	7	*0.00*	28	27	*3.57*
Pb	2	46	41	*10.9*	69	66	*4.35*	21	23	*-9.52*
Sc	1	3	3	*0.00*	1	1	*0.00*	11	10	*9.09*
Tl	10	<10	<10		<10	<10		<10	<10	
Zn	2	90	90	*0.00*	106	110	*-3.77*	11	11	*0.00*

[1, 2] respectively refer to batch numbers 1 and 2 of the standards analysed.

Table B1.6. ALS _ OAGRA05 _ Standards

		Standards													
		GBAP-3		**OREAS 90**					**OREAS-91**		**OREAS-93**			**All Standards**	
Element	LOR	R.V.	STD1[2]	R.V.	STD1[1]	STD2[2]	STD3[2]	RSD	R.V.	STD1[1]	R.V.	STD1[1]	STD2[2]	Mean Bias	1σ Error
	ppm	wt %	wt %	wt %	wt %	wt %	wt %	%	wt %	wt %	wt %	wt %	wt %	%	%
LOI	0.01	25.9	26.8	3.54	3.4	3.57	3.56	*2.72*	3.31	3.61	3.2	3.26	3.38	2.52	4.17

1, 2 respectively refer to batch numbers 1 and 2 of the standards analysed.

Table B1.7. ALS _ OAGRA05 _ Duplicates

		Duplicates					
		SD10			**SV14**		
Element	LOR	Main	DUP	*Difference*	Main	DUP	*Difference*
	ppm	wt %	wt %	*%*	wt %	wt %	*%*
LOI	0.01	0.7	0.6	*-14.29*	15.1	15.2	*0.33*

Table B1.8. ALS _ FIC881_ Standards and Duplicates

		Duplicates						Standards								
		SV10			**SD10**			**SARM-1**		**SARM-3**			**CCU-1d**			
Element	LOR	Main	DUP	*Difference*	Main	DUP	*Difference*	R.V.	STD1	R.V.	STD1	STD2	R.V.	STD1	Mean Bias	1σ Error
	ppm	ppm	ppm	*%*	ppm	ppm	*%*	ppm	ppm	ppm	ppm	ppm	ppm	ppm	%	%
F	20	1340	1320	*-1.49*	5320	5320	*0.00*	4200	4300	##	4220	4320	200	220	1.62	6.20

Table B1.9. NHM_ICP-AES_ Standards

			Major Element Standards													
			G-2		NIM-G		STM-1		GSP-2			SY-4		W-1		
Element	Unit	LOQ[1]	R.V.	STD1[1]	R.V.	STD1[1]	R.V.	STD1[1]	R.V.	STD1[1]	LOQ[2]	R.V.	STD1[2]	R.V.	STD1[2]	*Mean Bias (%,*	1σ Error (%)
Al_2O_3	wt%	0.1	15.4	15.5	12.1	12.5	18.4	18.5	14.9	15.0	0.1	20.7	21.1	15.0	15.2	*1.46*	1.05
CaO	wt%	0.05	1.96	1.96	0.780	0.793	1.09	1.15	2.10	2.14	0.05	8.05	8.06	11.0	10.9	*1.32*	2.34
Fe_2O_3	wt%	0.02	2.66	2.64	2.02	1.94	5.22	5.14	4.90	4.80	0.01	6.21	6.17	11.1	10.9	*-1.78*	1.15
K_2O	wt%	0.05	4.48	4.44	4.99	4.98	4.28	4.24	5.38	5.38	0.07	1.66	1.62	0.640	0.637	*-0.84*	0.88
MgO	wt%	0.01	0.750	0.748	*na*	0.0275	0.101	0.109	0.960	0.948	0.1	0.540	0.520	6.62	6.53	*0.31*	4.58
MnO	wt%	0	0.030	0.030	*na*	0.0165	0.220	0.217	0.039	0.039	0.005	0.108	0.108	0.170	0.171	*0.14*	0.87
Na_2O	wt%	0.05	4.08	4.07	3.36	3.37	8.94	8.96	2.78	2.82	0.5	7.10	7.03	2.16	2.18	*0.27*	0.86
P_2O_5	wt%	0.02	0.140	0.143	0.01	< 0.02	0.158	0.162	0.290	0.302	0.01	0.131	0.148	0.130	0.145	*6.54*	5.05
SiO_2	wt%	0.1	69.1	69.1	75.7	75.6	59.64	59.5	66.6	66.0	0.1	49.9	49.4	52.5	51.7	*-0.67*	0.61
TiO_2	wt%	0.05	0.480	0.488	0.090	0.092	0.135	0.131	0.660	0.665	0.01	0.287	0.290	1.07	1.04	*0.02*	2.20
Total	wt%		99.1	99.2	99.0	99.3	98.2	98.1	98.6	98.1			94.4		99.3	*1.25*	2.99
Ba	mg/g	5	1785	1888	109	113	568	583	1340	1340						*3.09*	2.43
Sr	mg/g	10	473	470	9	< 10	685	693	240	235						*-0.46*	1.63

[1, 2] respectively refer to batch numbers 1 and 2 of the standards analysed.

Table B1.10. NHM_CHN_ Standards

		CHN analysis					
		GA		SY-3			
Element	Unit	R.V.	STD1	R.V.	STD1	*Mean Bias (%)*	1σ Error (%)
H_2O	wt%	0.87	0.9726	0.67	0.5918	*0.06*	11.7

Table B1.11. NHM _ ICP-MS _ Standards

			Trace Element Standards								
			JLK-1		BCR-2			SCo-1			
Element	Unit	LOQ	R.V.	STD1	R.V.	STD1	STD2	R.V.	STD1	*Mean Bias (%)*	1σ Error (%)
Ba	ppm	1.2	565	636	683	699		578	606	*6.57*	5.31
Rb	ppm	0.03	138	151	48	49		113	114	*4.10*	4.88
Sr	ppm	0.1	66.2	70.4	346	334		169	169	*0.96*	5.00
Cr	ppm	1.8	59.4	57.2	18.0	10.3		68.0	71.5	*-13.7*	25.5
Hf	ppm	0.09	3.76	4.09	4.80	5.63		4.30	3.46	*2.14*	19.2
Li	ppm	0.13	49.3	54.2	9.00	7.99		45.0	39.7	*-4.30*	12.4
Nb	ppm	1	14.9	16.8		12.6		11.0	12.2	*11.9*	1.41
Pb	ppm	0.03	45.0	52.6	11.0	11.1	10.0	30.0	34.5	*5.82*	12.4
Sc	ppm	0.04	13.4	16.5	33.0	33.6	37.0	10.8	11.6	*11.2*	9.11
Th	ppm	0.07	19.2	21.8	6.20	6.34	6.31	9.5	10.1	*5.91*	5.35
U	ppm	0.002	3.80	4.24	1.69	1.79	1.75	3.10	3.32	*7.07*	3.43
Y	ppm	0.01	40.3	41.4	37.0	34.6	36.1	22.8	20.3	*-4.21*	5.77
Zr	ppm	1.3	134	115	188	191		153	107	*-14.0*	15.7
La	ppm	0.007	37.7	42.1	24.9	25.4	26.1	29.0	29.7	*5.17*	4.53
Ce	ppm	0.02	82.9	92.2	52.9	54.3	54.5	57.0	59.3	*5.25*	4.02
Pr	ppm	0.003	9.12	9.86	6.70	6.75	6.75	7.1	6.8	*1.38*	5.04
Nd	ppm	0.03	34.2	38.2	28.7	29.1	29.6	26.0	26.9	*4.95*	4.66
Sm	ppm	0.003	7.30	8.09	6.58	6.63	6.89	5.00	5.11	*4.62*	4.42
Eu	ppm	0.001	1.2	1.4	1.96	2.07	2.06	1.13	1.14	*6.68*	6.31
Gd	ppm	0.003	6.6	7.5	6.75	6.80	6.96	4.60	4.34	*2.89*	8.03
Tb	ppm	0.001	1.06	1.18	1.07	1.08	1.09	0.690	0.634	*1.64*	8.05
Dy	ppm	0.002	6.67	7.19	6.41	6.54	6.75	4.00	3.69	*1.85*	6.78
Ho	ppm	0.001	1.35	1.44	1.28	1.34	1.36	0.800	0.731	*2.25*	7.32
Er	ppm	0.001	3.95	4.22	3.66	3.84	3.83	2.38	2.12	*1.36*	8.26
Tm	ppm	0.001	0.600	0.624	0.540	0.549	0.548	0.350	0.317	*-0.57*	6.07
Yb	ppm	0.002	3.78	4.06	3.38	3.50	3.50	2.34	2.08	*0.85*	8.25
Lu	ppm	0.001	0.546	0.559	0.503	0.489	0.533	0.360	0.294	*-3.20*	10.8

B2. Serra Verde logs and assay results for drill holes studied

Table B.2.1. Samples analysed by ALS; Lithology = logging carried out by this study.

DDH0161

			Easting	**Northing**													
			768733	8504879													
From	To	Lithology	SiO_2	Al_2O_3	Fe_2O_3	CaO	MgO	Na_2O	K_2O	TiO_2	MnO	P_2O_5	LOI	Nb	Zr	Th	U
m	m		wt %	wt %	wt %	wt %	wt %	wt %	wt %	wt %	wt %	wt %	wt %	ppm	ppm	ppm	ppm
0.0	1.0	Ferricete	45.4	19.2	25.9	0.02	0.01	0.05	0.03	0.56	0.01	0.05	9.91	131	978	139	5.94
1.0	2.0	Ferruginous Zone	42.7	19.6	27.9	0.02	0.01	0.05	0.03	0.54	0.01	0.04	9.35	132.5	776	129	6.68
2.0	3.0	Ferruginous Zone	37.5	19.8	32.4	0.01	0.01	0.04	0.02	0.50	0.01	0.04	9.61	144	776	192	9.13
3.0	3.7	Ferruginous Zone	49.1	21.1	20.4	0.01	0.01	0.05	0.01	0.43	0.01	0.03	9.24	200	1090	156	6.04
3.7	4.5	Ferruginous Zone	52.8	19.6	19.68	0.01	0.02	0.05	0.02	0.40	0.01	0.03	7.97	207	952	171	5.60
4.5	5.6	U. Mottled Zone	64.8	20.5	6.66	0.01	0.03	0.05	0.02	0.42	0.01	0.01	7.73	220	1110	97	6.56
5.6	7.1	U. Mottled Zone	59.8	21.4	9.53	0.01	0.02	0.05	0.01	0.43	0.01	0.01	8.24	218	915	123	5.56
7.1	8.0	U. Mottled Zone	60.9	22.3	7.67	0.01	0.02	0.11	0.02	0.41	0.01	0.01	8.69	213	929	107	5.48
8.0	9.0	U. Mottled Zone	63.2	21.5	6.51	0.01	0.03	0.10	0.02	0.40	0.01	0.01	8.23	225	957	107	5.63
9.0	10.0	U. Mottled Zone	64.2	21.3	6.00	0.01	0.03	0.04	0.01	0.42	0.01	0.01	7.80	236	1020	109	5.75
10.0	11.0	U. Mottled Zone	65.9	22.3	3.80	0.01	0.03	0.04	0.05	0.30	0.01	0.01	8.04	185	707	77.2	4.44
11.0	12.0	Pematite	67.8	20.6	4.26	0.01	0.02	0.03	0.03	0.33	0.01	0.01	7.39	210	831	83.7	5.48
12.0	13.1	U. Mottled Zone	66.4	21.1	5.51	0.01	0.03	0.02	0.01	0.37	0.01	0.01	7.50	249	845	119	5.61
13.1	14.0	L. Mottled Zone	65.7	21.3	5.14	0.01	0.02	0.01	0.01	0.36	0.01	0.01	7.64	250	895	109	6.48
14.0	15.0	L. Mottled Zone	66.0	21.5	4.94	0.01	0.02	0.02	0.01	0.36	0.01	0.01	7.75	247	858	124	6.13
15.0	16.0	L. Mottled Zone	66.9	20.9	4.94	0.01	0.03	0.03	0.01	0.34	0.01	0.01	7.52	246	825	117	6.18
16.0	17.0	L. Mottled Zone	67.0	20.7	5.16	0.01	0.03	0.01	0.01	0.37	0.01	0.01	7.43	262	880	109	7.83
17.0	18.0	L. Mottled Zone	66.5	20.6	4.89	0.01	0.02	0.01	0.01	0.36	0.02	0.01	7.50	263	882	120	8.36
18.0	19.0	L. Mottled Zone	67.1	21.2	4.87	0.01	0.02	0.01	0.02	0.35	0.01	0.01	7.60	256	803	97.4	6.36
19.0	20.0	Pematite	70.4	19.7	2.97	0.01	0.03	0.02	0.05	0.18	0.01	0.01	7.04	200	441	62.7	5.39
20.0	20.6	Pematite	67.5	22.3	2.14	0.01	0.03	0.03	0.08	0.11	0.01	0.01	7.91	159	333	47.6	7.36
20.6	21.7	Pematite	67.6	22.4	3.14	0.01	0.04	0.03	0.08	0.20	0.01	0.01	7.90	212	587	81.8	9.55
21.7	22.3	Transition	69.9	18.5	4.48	0.01	0.06	0.02	0.76	0.31	0.04	0.02	6.33	228	820	95.4	9.93
22.3	23.0	Transition	70.6	17.0	4.18	0.02	0.08	0.08	2.45	0.29	0.06	0.02	5.06	203	687	89.9	10.6
23.0	24.0	SAPROLITE	70.8	16.6	3.84	0.02	0.08	0.11	3.24	0.28	0.05	0.01	4.53	190	665	87.5	10.2
24.0	25.1	SAPROLITE	71.1	15.9	3.96	0.02	0.08	0.14	4.17	0.27	0.06	0.02	3.83	185	643	83.0	10.7
25.1	26.0	SAPROLITE	71.4	15.6	3.73	0.03	0.11	0.20	5.39	0.27	0.06	0.02	3.26	180	686	79.8	10.4
26.0	26.9	SAPROLITE	70.7	14.8	3.61	0.04	0.12	0.24	5.91	0.26	0.06	0.02	2.95	182	596	78.1	12.4
26.9	28.3	SAPROLITE	71.1	14.5	3.65	0.06	0.10	0.43	6.07	0.24	0.05	0.02	2.60	173	586	76.3	12.7
28.3	29.6	Pegmatite	69.0	18.2	2.66	0.12	0.09	0.72	5.62	0.17	0.05	0.01	3.76	134	337	41.6	9.63
29.6	30.5	SAPROCK	74.0	12.8	3.17	0.68	0.11	2.84	5.60	0.22	0.05	0.01	0.55	146	515	70.8	8.08
30.5	31.6	SAPROCK	73.4	12.7	3.27	0.94	0.11	3.07	5.51	0.22	0.05	0.01	0.34	148	493	67.3	11.40

From	To	Lithology	La	Ce	Pr	Nb	Sm	Eu	Gd	Tb	Dy	Ho	Er	Tm	Yb	Lu	Y
m	m		ppm	ppm	ppm	ppm	ppm	ppm	ppm	ppm	ppm	ppm	ppm	ppm	ppm	ppm	ppm
0.0	1.0	Ferricete	17.30	32.8	2.59	8.10	2.08	0.24	2.63	0.59	4.36	1.08	4.56	0.85	6.83	1.16	31.3
1.0	2.0	Ferruginous Zone	19.10	27.2	2.82	8.80	2.13	0.24	2.66	0.64	4.74	1.21	4.81	0.89	6.80	1.13	33.7
2.0	3.0	Ferruginous Zone	15.00	23.1	2.31	7.40	1.86	0.21	2.41	0.59	4.33	1.13	4.51	0.87	6.71	1.11	29.4
3.0	3.7	Ferruginous Zone	5.00	26.5	0.96	3.20	1.02	0.10	1.55	0.42	3.48	0.95	3.83	0.81	6.36	1.10	28.5
3.7	4.5	Ferruginous Zone	3.90	22.6	0.70	2.40	0.79	0.07	1.28	0.40	3.21	0.81	3.73	0.77	6.02	1.00	26.2
4.5	5.6	U. Mottled Zone	4.30	22.1	0.71	2.50	0.78	0.11	1.38	0.40	3.52	1.00	4.25	0.95	7.29	1.25	33.4
5.6	7.1	U. Mottled Zone	3.90	29.4	0.67	2.40	0.78	0.11	1.68	0.46	3.82	1.00	4.41	0.87	7.08	1.15	32.5
7.1	8.0	U. Mottled Zone	3.50	40.5	0.62	2.50	1.02	0.15	1.81	0.46	4.01	1.12	4.61	0.90	6.98	1.16	31.9
8.0	9.0	U. Mottled Zone	2.70	40.7	0.56	2.10	0.80	0.08	1.85	0.51	4.20	1.13	4.67	0.87	7.20	1.17	33.4
9.0	10.0	U. Mottled Zone	3.20	83.8	0.70	2.90	1.12	0.14	2.05	0.60	4.80	1.26	5.64	0.98	8.21	1.44	37.6
10.0	11.0	U. Mottled Zone	2.90	128.5	0.55	2.10	0.89	0.11	1.77	0.47	3.82	1.07	4.52	0.86	6.80	1.14	30.7
11.0	12.0	Pematite	2.80	46.3	0.59	2.30	1.00	0.12	2.25	0.59	4.95	1.22	5.09	0.94	7.77	1.27	35.4
12.0	13.1	U. Mottled Zone	2.90	66.7	0.69	3.00	1.43	0.13	2.62	0.76	5.59	1.36	5.39	0.96	7.27	1.18	36.1
13.1	14.0	L. Mottled Zone	3.10	70.5	0.78	3.70	1.34	0.17	2.87	0.82	6.27	1.55	5.80	1.08	8.59	1.37	41.4
14.0	15.0	L. Mottled Zone	2.40	311	0.73	2.8	1.40	0.20	2.71	0.81	6.70	1.62	5.98	1.13	8.46	1.32	40.8
15.0	16.0	L. Mottled Zone	2.50	446	0.68	2.80	1.46	0.18	2.58	0.71	6.14	1.49	5.82	1.11	8.56	1.36	41.6
16.0	17.0	L. Mottled Zone	2.50	121	0.68	3.10	1.42	0.18	2.83	0.78	6.92	1.60	6.18	1.24	8.81	1.40	44.1
17.0	18.0	L. Mottled Zone	2.70	386	0.84	3.3	1.52	0.22	3.06	0.92	7.6	1.81	6.81	1.20	9.08	1.36	44.3
18.0	19.0	L. Mottled Zone	2.80	207	0.82	3.10	1.47	0.16	2.54	0.77	6.30	1.50	5.70	0.96	7.43	1.19	35.1
19.0	20.0	Pematite	3.70	159	1.01	3.70	1.41	0.13	2.82	0.79	6.6	1.70	6.08	1.05	7.71	1.10	34.6
20.0	20.6	Pematite	6.10	205	1.53	6.00	2.01	0.26	5.57	1.51	13.6	3.73	15.25	2.53	18.4	2.89	105
20.6	21.7	Pematite	12.1	454	3.18	12.1	3.57	0.35	5.74	1.65	12.9	3.22	12.3	1.95	14.5	2.16	72.3
21.7	22.3	Transition	200	586	43.8	159	29.0	1.77	25.0	4.52	30.3	6.15	19.4	2.99	20.1	2.68	157
22.3	23.0	Transition	298	1310	62.3	218	38.3	2.71	34.6	6.34	41.1	8.44	26.4	3.97	26.6	3.72	221
23.0	24.0	SAPROLITE	251	450	52.8	188	34.0	2.25	31.5	6.16	41.9	9.11	30.2	4.49	29.5	4.14	276
24.0	25.1	SAPROLITE	238	522	47.8	173	31.8	2.36	33.5	6.68	44.9	10.1	33.5	4.78	31.4	4.39	313
25.1	26.0	SAPROLITE	525	711	109	370	65.4	3.79	53.8	9.21	58.8	11.7	36.0	4.93	32.5	4.55	345
26.0	26.9	SAPROLITE	1905	757	388	1280	218	12.2	161	25.2	137	23.6	66.4	8.42	51.5	6.76	697
26.9	28.3	SAPROLITE	1865	436	346	1205	211	13.3	190	28.4	157	27.6	75.9	9.59	58.2	7.50	830
28.3	29.6	Pegmatite	246	738	43.5	153	27.2	2.43	31.9	5.90	39.2	9.16	30.6	4.41	28.6	4.25	297
29.6	30.5	SAPROCK	861	446	160	543	95.8	6.19	90.2	14.0	78.7	16.1	45.2	5.94	36.3	5.19	509
30.5	31.6	SAPROCK	352	427	65.2	223	40.0	2.80	43.1	7.18	45.9	11.1	34.9	5.11	30.7	4.74	384

DDH0099

Easting	Northing
768430	8505136

From	To	Lithology	SiO_2	Al_2O_3	Fe_2O_3	CaO	MgO	Na_2O	K_2O	TiO_2	MnO	P_2O_5	LOI	Nb	Zr	Th	U
m	m		wt %	wt %	wt %	wt %	wt %	wt %	wt %	wt %	wt %	wt %	wt %	ppm	ppm	ppm	ppm
0.0	0.6	Ferricete	41.0	16.5	33.4	0.02	0.03	0.02	0.05	0.46	0.01	0.06	9.16	129	900	185	5.48
0.6	1.7	Ferruginous Zone	41.6	17.0	31.9	0.02	0.03	0.02	0.02	0.46	0.01	0.06	8.55	135	753	179	5.22
1.7	3.0	Ferruginous Zone	55.0	15.6	22.1	0.02	0.03	0.03	0.02	0.36	0.01	0.03	7.37	135	716	153	5.80
3.0	4.0	Ferruginous Zone	62.9	20.5	8.1	0.02	0.03	0.02	0.02	0.47	0.01	0.02	8.16	181	1090	92.9	5.13
4.0	5.0	U. Mottled Zone	60.6	21.9	9.05	0.02	0.03	0.03	0.04	0.35	0.01	0.01	8.32	158	681	93.9	4.21
5.0	5.9	U. Mottled Zone	62.4	21.9	7.67	0.02	0.04	0.04	0.05	0.28	0.01	0.01	8.07	141	470	76.3	3.62
5.9	7.0	U. Mottled Zone	64.0	20.9	7.45	0.02	0.03	0.02	0.02	0.36	0.01	0.01	7.64	217	863	118	5.18
7.0	8.0	U. Mottled Zone	65.2	21.0	6.62	0.02	0.02	0.02	0.02	0.37	0.01	0.01	7.65	238	954	139	5.84
8.0	9.1	U. Mottled Zone	64.7	21.0	6.63	0.02	0.02	0.02	0.02	0.39	0.01	0.01	7.64	242	1140	128	7.21
9.1	10.1	U. Mottled Zone	65.7	21.2	5.70	0.02	0.03	0.02	0.02	0.37	0.01	0.01	7.59	222	943	118	5.25
10.1	11.1	L. Mottled Zone	66.1	20.8	5.09	0.02	0.02	0.01	0.01	0.37	0.01	0.01	7.56	233	878	97.6	4.69
11.1	12.1	L. Mottled Zone	67.4	20.6	4.62	0.02	0.03	0.02	0.01	0.36	0.01	0.01	7.44	221	906	96.8	5.94
12.1	13.1	L. Mottled Zone	68.7	20.5	4.38	0.02	0.03	0.02	0.01	0.34	0.08	0.02	7.35	212	830	99.0	6.85
13.1	14.0	L. Mottled Zone	66.6	20.4	4.78	0.02	0.04	0.03	0.02	0.35	0.02	0.02	7.65	216	825	108	12.6
14.0	15.0	L. Mottled Zone	67.0	20.5	4.69	0.02	0.06	0.03	0.02	0.34	0.02	0.02	7.89	210	806	102	17.0
15.0	16.0	L. Mottled Zone	66.3	20.6	4.61	0.02	0.04	0.02	0.02	0.35	0.02	0.02	8.03	218	837	102	14.5
16.0	17.0	L. Mottled Zone	65.2	20.9	4.71	0.02	0.05	0.02	0.04	0.36	0.03	0.02	8.51	226	784	106	18.0
17.0	18.1	Transition	67.4	19.5	4.99	0.02	0.11	0.03	0.41	0.36	0.07	0.03	7.53	225	852	103	14.1
18.1	19.0	Transition	65.7	20.6	4.47	0.02	0.07	0.04	0.70	0.33	0.03	0.03	8.16	217	835	102	20.2
19.0	20.0	Transition	69.2	16.8	5.94	0.02	0.15	0.09	2.01	0.33	0.06	0.03	5.45	198	748	103	9.80
20.0	21.0	Transition	70.5	17.4	4.61	0.04	0.19	0.15	2.34	0.33	0.06	0.03	5.60	189	722	94.2	11.5
21.0	22.0	SAPROLITE	69.9	16.6	3.74	0.03	0.38	0.18	3.70	0.29	0.08	0.02	4.68	172	597	71.9	9.31
22.0	23.0	SAPROLITE	68.9	17.5	3.30	0.03	0.35	0.21	4.54	0.23	0.10	0.02	4.60	152	594	64.5	11.0
23.0	24.1	SAPROLITE	72.0	15.1	3.44	0.08	0.60	0.29	4.78	0.22	0.08	0.02	3.75	142	521	76.2	11.0
24.1	25.1	SAPROLITE	74.3	12.2	3.18	0.27	0.38	1.65	5.50	0.22	0.08	0.01	1.53	143	503	62.9	11.0
25.1	26.0	SAPROCK	74.1	12.8	3.43	0.30	0.08	2.90	5.64	0.24	0.05	0.02	0.38	147	577	70.8	12.1
26.0	27.0	SAPROCK	74.2	13.6	2.67	0.51	0.09	3.75	5.08	0.19	0.04	0.01	0.27	125	416	53.5	10.5
27.0	28.0	SAPROCK	74.0	12.8	3.18	0.33	0.10	2.96	5.74	0.23	0.08	0.01	0.36	150	496	72.0	9.15
28.0	29.0	SAPROCK	73.5	12.9	3.28	0.75	0.08	3.33	5.56	0.23	0.05	0.02	0.29	150	534	69.8	10.6
29.0	30.1	BDRK	73.6	13.0	3.30	0.71	0.08	3.41	5.51	0.24	0.05	0.02	0.32	148	540	69.6	11.05

From	To	Lithology	La	Ce	Pr	Nb	Sm	Eu	Gd	Tb	Dy	Ho	Er	Tm	Yb	Lu	Y
m	m		ppm	ppm	ppm	ppm	ppm	ppm	ppm	ppm	ppm	ppm	ppm	ppm	ppm	ppm	ppm
0.0	0.6	Ferricete	17.00	73.5	2.28	7.40	1.79	0.17	2.28	0.46	3.46	0.89	3.65	0.68	5.10	0.82	26.3
0.6	1.7	Ferruginous Zone	19.00	59.9	2.50	7.80	1.89	0.20	2.08	0.43	3.36	0.79	3.04	0.59	4.46	0.74	21.6
1.7	3.0	Ferruginous Zone	7.40	64.7	1.31	4.50	1.22	0.13	1.64	0.36	2.79	0.72	2.98	0.56	4.22	0.71	19.2
3.0	4.0	Ferruginous Zone	5.80	114	0.88	3.00	0.76	0.10	1.39	0.36	2.76	0.77	3.20	0.66	5.21	0.89	24.0
4.0	5.0	U. Mottled Zone	3.20	57.8	0.55	2.10	0.56	0.07	0.96	0.24	2.12	0.59	2.40	0.50	3.96	0.69	16.6
5.0	5.9	U. Mottled Zone	2.40	40.9	0.44	1.60	0.48	0.05	0.89	0.19	1.84	0.51	2.14	0.42	3.41	0.59	15.5
5.9	7.0	U. Mottled Zone	3.70	65.3	0.71	2.80	0.86	0.10	1.62	0.38	2.92	0.78	3.27	0.65	4.97	0.85	23.3
7.0	8.0	U. Mottled Zone	2.60	232	0.64	2.60	0.89	0.13	1.78	0.49	3.55	1.01	4.08	0.74	5.98	0.98	27.2
8.0	9.1	U. Mottled Zone	3.30	78.8	0.82	3.00	1.17	0.10	2.14	0.50	4.12	1.07	4.16	0.80	6.24	1.05	28.6
9.1	10.1	U. Mottled Zone	3.30	48.0	0.78	3.20	1.23	0.12	2.25	0.51	4.00	0.97	3.80	0.68	5.11	0.84	24.7
10.1	11.1	L. Mottled Zone	1.90	136	0.54	2.20	1.04	0.14	2.34	0.52	4.38	1.05	3.87	0.74	5.21	0.82	25.0
11.1	12.1	L. Mottled Zone	2.20	132	0.71	3.20	1.55	0.16	3.09	0.75	5.65	1.34	4.80	0.83	6.00	0.92	29.9
12.1	13.1	L. Mottled Zone	3.00	1130	1.21	4.90	2.13	0.46	4.49	1.15	8.06	1.88	6.59	1.07	7.29	1.06	35.9
13.1	14.0	L. Mottled Zone	3.70	1645	1.84	7.20	3.15	0.65	5.20	1.49	9.91	2.25	7.89	1.34	9.12	1.26	40.4
14.0	15.0	L. Mottled Zone	4.20	1320	2.30	8.80	3.97	0.62	6.46	1.73	11.8	2.56	8.91	1.50	9.81	1.38	45.3
15.0	16.0	L. Mottled Zone	4.20	731	2.05	8.00	4.07	0.46	6.66	1.83	13.4	2.98	10.5	1.64	10.6	1.49	51.2
16.0	17.0	L. Mottled Zone	10.4	431	3.39	13.3	5.10	0.53	8.90	2.18	16.8	3.76	13.0	2.04	13.3	1.81	64.5
17.0	18.1	Transition	70.2	549	16.9	60.1	13.65	0.97	15.0	3.17	22.5	4.95	16.5	2.69	16.8	2.43	98.2
18.1	19.0	Transition	107	372	24.4	86.5	17.75	1.12	18.2	3.76	25.9	5.62	18.7	2.89	17.8	2.58	120
19.0	20.0	Transition	395	510	86.0	299	53.7	2.99	44.0	7.25	44.3	9.04	29.0	4.41	26.9	3.78	226
20.0	21.0	Transition	454	484	93.4	326	58.7	3.38	51.2	8.57	50.8	10.3	31.7	4.70	28.3	3.92	252
21.0	22.0	SAPROLITE	1325	366	252	862	157	10.4	155	23.8	140	26.8	78.7	11.1	64.9	9.08	776
22.0	23.0	SAPROLITE	1225	520	225	784	143	10.4	153	24.6	142	28.3	82.5	11.4	67.0	9.38	848
23.0	24.1	SAPROLITE	1820	530	331	1160	218	15.9	231	38.7	231	46.7	133	19.2	121	15.6	1445
24.1	25.1	SAPROLITE	1225	1050	212	742	142	11.1	163	27.4	170	36.3	107	15.4	98.8	12.8	1155
25.1	26.0	SAPROCK	566	355	102	358	69.5	5.37	79.3	13.3	81.6	16.2	46.1	6.50	38.9	4.96	467
26.0	27.0	SAPROCK	326	245	56.9	205	41.7	3.85	57.6	9.78	61.5	12.8	37.6	5.34	32.8	4.15	382
27.0	28.0	SAPROCK	320	508	57.9	207	42.5	3.66	59	10.0	65.4	14.1	42.1	6.26	39.9	5.31	420
28.0	29.0	SAPROCK	325	360	58.0	198	36.8	2.81	43.3	7.24	47.9	10.4	31.3	4.49	29.9	3.95	327
29.0	30.1	BDRK	282	357	51.1	172	31.3	2.25	35.0	6.04	40.6	9.14	28.6	4.18	26.7	3.60	270

DDH0061

Easting	Northing
768041	8507495

From	To	Lithology	SiO_2	Al_2O_3	Fe_2O_3	CaO	MgO	Na_2O	K_2O	TiO_2	MnO	P_2O_5	LOI	Nb	Zr	Th	U
m	m		wt %	wt %	wt %	wt %	wt %	wt %	wt %	wt %	wt %	wt %	wt %	ppm	ppm	ppm	ppm
0.0	0.5	Ferricete	40.6	18.3	30.7	0.02	0.03	0.01	0.04	0.39	0.01	0.06	9.49	172	643	137	6.20
0.5	1.4	Ferruginous Zone	43.0	20.1	27.4	0.02	0.02	0.01	0.04	0.42	0.01	0.05	9.47	199	655	178	7.52
1.4	2.0	Ferruginous Zone	48.9	24.5	16.4	0.02	0.03	0.01	0.03	0.48	0.01	0.04	10.45	239	773	150	6.72
2.0	3.0	Ferruginous Zone	54.8	23.9	11.8	0.02	0.03	0.01	0.02	0.43	0.01	0.03	9.53	248	784	136	6.07
3.0	4.0	U. Mottled Zone	58.9	23.1	9.12	0.02	0.03	0.01	0.01	0.38	0.01	0.02	8.81	231	669	108	4.88
4.0	5.1	U. Mottled Zone	62.9	22.0	6.40	0.02	0.02	0.01	0.01	0.35	0.01	0.01	8.32	219	723	91.2	4.93
5.1	6.4	U. Mottled Zone	66.5	20.5	5.01	0.02	0.03	0.01	0.01	0.31	0.01	0.01	7.51	200	610	80.1	4.94
6.4	7.8	U. Mottled Zone	65.6	21.3	4.75	0.02	0.02	0.01	0.01	0.31	0.01	0.01	7.77	229	631	75.7	4.79
7.8	8.6	U. Mottled Zone	67.5	21.6	4.24	0.02	0.03	0.01	0.01	0.29	0.01	0.01	7.71	233	577	83.4	4.75
8.6	9.8	U. Mottled Zone	64.8	21.5	5.83	0.02	0.02	0.01	0.01	0.25	0.01	0.01	7.88	225	509	88.3	4.80
9.8	10.9	U. Mottled Zone	66.3	21.6	4.82	0.02	0.03	0.01	0.01	0.24	0.01	0.01	7.58	233	600	80.5	5.05
10.9	12.1	U. Mottled Zone	67.4	21.0	4.02	0.02	0.03	0.01	0.01	0.23	0.01	0.01	7.42	223	611	86.1	5.45
12.1	13.1	U. Mottled Zone	68.5	20.9	3.94	0.02	0.03	0.01	0.01	0.21	0.03	0.01	7.31	225	485	80.4	5.43
13.1	14.0	L. Mottled Zone	69.4	19.8	3.69	0.02	0.02	0.01	0.01	0.20	0.10	0.01	7.01	214	480	97.3	5.91
14.0	15.2	L. Mottled Zone	70.7	19.5	3.69	0.02	0.02	0.01	0.01	0.21	0.01	0.02	6.66	183	419	71.3	4.80
15.2	16.8	L. Mottled Zone	71.9	18.8	3.84	0.02	0.03	0.02	0.01	0.21	0.02	0.02	6.50	225	539	72.8	7.36
17.9	19.9	L. Mottled Zone	72.4	17.4	4.28	0.02	0.02	0.01	0.01	0.21	0.02	0.02	5.99	192	529	75.9	7.21
19.9	21.4	L. Mottled Zone	69.1	19.2	4.63	0.02	0.03	0.01	0.01	0.23	0.04	0.03	7.05	213	621	84.7	8.52
21.4	22.4	L. Mottled Zone	70.5	19.1	3.80	0.02	0.02	0.01	0.01	0.20	0.01	0.02	6.84	239	500	80.1	6.80
22.4	24.0	Transition	72.9	17.4	3.63	0.02	0.03	0.02	0.33	0.21	0.08	0.02	6.11	235	487	82.1	6.65

21.4	22.4	L. Mottled Zone	70.5	19.1	3.80	0.02	0.02	0.01	0.01	0.20	0.01	0.02	6.84	239	500	80.1	6.80
22.4	24.0	Transition	72.9	17.4	3.65	0.02	0.05	0.02	0.53	0.21	0.08	0.02	6.11	233	487	82.1	6.63
24.0	26.0	Transition	81.0	11.8	2.52	0.03	0.07	0.08	1.96	0.11	0.28	0.02	3.28	144	374	46.7	5.22
26.0	28.6	SAPROLITE	75.1	14.3	3.47	0.02	0.10	0.15	3.93	0.17	0.04	0.02	3.41	172	511	68.0	7.24
28.6	29.6	SAPROLITE	71.7	16.3	3.51	0.03	0.10	0.15	4.34	0.18	0.08	0.02	3.94	202	439	76.1	7.04
29.6	30.5	SAPROLITE	71.2	16.7	4.09	0.04	0.28	0.09	2.98	0.34	0.08	0.07	4.72	201	500	72.2	7.65
30.5	31.1	SAPROLITE	71.9	15.9	4.07	0.05	0.16	0.14	3.94	0.27	0.14	0.14	3.96	206	599	81.4	12.4
31.1	32.5	SAPROLITE	72.1	15.6	3.48	0.05	0.12	0.20	5.36	0.21	0.07	0.08	3.28	190	492	69.2	8.68
32.5	33.5	SAPROLITE	74.1	13.4	2.87	0.32	0.13	2.42	5.89	0.15	0.03	0.02	0.68	159	370	57.0	6.08
33.5	34.5	SAPROCK	73.3	13.4	3.09	0.80	0.15	3.38	5.52	0.18	0.03	0.02	0.36	164	398	59.6	6.28
34.5	35.6	BDRK	73.0	13.4	3.07	1.04	0.14	3.29	5.81	0.16	0.03	0.02	0.41	155	413	56.1	7.60

From	To	Lithology	La	Ce	Pr	Nb	Sm	Eu	Gd	Tb	Dy	Ho	Er	Tm	Yb	Lu	Y
m	m		ppm	ppm	ppm	ppm	ppm	ppm	ppm	ppm	ppm	ppm	ppm	ppm	ppm	ppm	ppm
0.0	0.5	Ferricete	32.5	101	3.92	10.8	1.84	0.27	2.68	0.67	5.21	1.45	5.88	1.20	8.63	1.32	44.9
0.5	1.4	Ferruginous Zone	26.6	149	3.27	9.10	2.03	0.23	2.84	0.76	5.79	1.44	5.54	1.14	8.41	1.34	40.7
1.4	2.0	Ferruginous Zone	68.4	153	4.60	10.8	1.75	0.23	2.61	0.71	4.94	1.24	5.33	1.08	8.14	1.30	38.3
2.0	3.0	Ferruginous Zone	15.4	144	1.69	4.50	1.27	0.20	2.03	0.62	4.71	1.19	4.81	0.97	8.29	1.22	36.0
3.0	4.0	U. Mottled Zone	8.60	111	1.05	3.50	0.85	0.18	2.13	0.46	3.77	1.07	4.54	0.86	7.36	1.13	32.6
4.0	5.1	U. Mottled Zone	11.3	127	1.15	3.30	0.94	0.16	1.59	0.50	3.33	0.87	4.37	0.84	7.76	1.15	33.2
5.1	6.4	U. Mottled Zone	4.90	84.1	0.77	2.60	0.95	0.14	1.71	0.43	3.59	1.05	4.41	0.88	7.76	1.19	35.3
6.4	7.8	U. Mottled Zone	4.00	70.0	0.69	2.80	1.07	0.15	1.64	0.44	3.53	1.07	4.42	0.99	7.81	1.22	34.0
7.8	8.6	U. Mottled Zone	2.90	198	0.64	2.40	1.02	0.11	1.86	0.48	4.38	1.14	4.99	1.00	7.79	1.28	34.5
8.6	9.8	U. Mottled Zone	5.80	146	0.94	3.30	1.12	0.15	1.85	0.51	3.97	1.14	4.58	0.89	7.32	1.17	33.0
9.8	10.9	U. Mottled Zone	6.10	120	1.19	4.50	1.57	0.19	2.31	0.65	5.38	1.41	5.47	1.04	8.9	1.33	36.3
10.9	12.1	U. Mottled Zone	3.70	244	0.90	3.30	1.36	0.22	2.28	0.62	5.32	1.41	5.73	1.06	8.55	1.27	36.2
12.1	13.1	U. Mottled Zone	3.80	1040	1.30	4.90	1.88	0.42	3.11	0.95	6.39	1.58	6.19	1.11	8.96	1.27	36.0
13.1	14.0	L. Mottled Zone	4.50	1810	1.67	6.00	2.32	0.61	3.01	1.09	7.21	1.73	6.81	1.27	10.2	1.46	40.0
14.0	15.2	L. Mottled Zone	3.20	356	0.97	3.80	1.59	0.18	2.62	0.71	5.76	1.44	5.65	0.98	7.42	1.10	33.8
15.2	16.8	L. Mottled Zone	4.30	324	1.30	4.90	2.24	0.24	3.56	0.99	7.95	1.92	7.03	1.23	9.52	1.38	41.2
17.9	19.9	L. Mottled Zone	4.80	288	1.42	5.60	2.51	0.31	4.28	1.16	8.75	2.14	8.00	1.38	10.8	1.48	46.9
19.9	21.4	L. Mottled Zone	19.2	433	4.07	14.3	4.53	0.45	6.13	1.50	11.0	2.66	9.33	1.57	12.2	1.58	60.2
21.4	22.4	L. Mottled Zone	13.0	178	2.56	8.90	3.41	0.31	5.11	1.29	9.95	2.36	8.76	1.47	11.1	1.64	57.3
22.4	24.0	Transition	75.2	341	14.2	47.2	10.1	0.79	10.9	2.27	16.2	3.56	12.0	2.08	15.5	2.20	89.8
24.0	26.0	Transition	162	788	28.7	95.5	18.2	1.50	16.8	3.01	20.0	4.39	14.3	2.29	16.7	2.36	123
26.0	28.6	SAPROLITE	331	302	59.0	195	34.6	2.64	32.6	5.57	33.6	7.27	23.5	3.65	25.7	3.30	224
28.6	29.6	SAPROLITE	283	549	48.2	162	30.2	2.63	30.6	5.20	33.8	7.60	22.9	3.56	24.2	3.33	214
29.6	30.5	SAPROLITE	478	322	68.9	219	41.1	3.32	38.6	6.56	40.4	8.46	26.7	4.16	27.1	3.83	260
30.5	31.1	SAPROLITE	818	562	137	459	84.0	7.08	85.0	14.2	88.1	19.5	61.7	8.96	59.2	8.37	615
31.1	32.5	SAPROLITE	401	356	62.2	206	38.7	3.37	43.7	7.61	50.7	11.4	36.4	5.26	34.3	4.84	365
32.5	33.5	SAPROLITE	195	287	33.9	111	20.1	1.74	20.9	3.39	21.8	4.64	14.8	2.19	14.2	2.19	139
33.5	34.5	SAPROCK	243	321	39.7	134	24.6	2.04	24.6	4.05	25.3	5.10	15.6	2.32	14.7	1.98	153
34.5	35.6	BDRK	209	299	34.7	118	22.9	1.94	24.5	4.34	26.9	6.42	20.5	2.96	19.1	2.75	220

DDH0266

Easting	Northing
769021	8504380

From	To	Lithology	SiO_2	Al_2O_3	Fe_2O_3	CaO	MgO	Na_2O	K_2O	TiO_2	MnO	P_2O_5	LOI	Nb	Zr	Th	U
m	m		wt %	wt %	wt %	wt %	wt %	wt %	wt %	wt %	wt %	wt %	wt %	ppm	ppm	ppm	ppm
0.0	1.1	Ferruginous Soil	47.1	18.0	26.2	0.02	0.01	0.01	0.03	0.48	0.01	0.05	8.75	86.2	606	174	5.35
1.1	2.0	Ferruginous Soil	46.7	17.5	26.5	0.01	0.02	0.01	0.03	0.39	0.01	0.04	8.45	91.7	539	253	7.10
2.0	3.2	Ferruginous zone	59.1	19.4	13.2	0.01	0.01	0.01	0.02	0.42	0.01	0.03	7.85	121	898	191	6.78
3.2	4.0	U. Mottled Zone	67.0	21.3	3.47	0.01	0.01	0.07	0.02	0.41	0.01	0.02	8.19	132	970	80.1	6.67
4.0	5.0	U. Mottled Zone	68.2	19.2	4.44	0.01	0.01	0.05	0.02	0.39	0.01	0.02	7.65	117	789	92.6	5.40
5.0	7.0	U. Mottled Zone	70.6	18.8	3.13	0.01	0.01	0.07	0.02	0.37	0.01	0.02	7.00	108	838	74.8	6.01
7.0	9.0	U. Mottled Zone	66.7	21.1	4.15	0.01	0.01	0.01	0.02	0.38	0.01	0.02	7.73	108	670	99.1	7.19
9.0	10.0	U. Mottled Zone	68.1	19.9	5.15	0.01	0.01	0.02	0.02	0.38	0.01	0.02	7.11	131	838	97.0	6.12
10.0	11.0	U. Mottled Zone	67.2	22.2	3.29	0.01	0.01	0.01	0.02	0.20	0.01	0.01	7.73	129	376	80.1	5.28
11.0	12.0	L. Mottled Zone	64.7	22.2	4.92	0.01	0.01	0.01	0.01	0.37	0.01	0.03	7.92	105	595	266	5.67
12.0	13.0	L. Mottled Zone	64.8	22.5	4.39	0.01	0.01	0.01	0.02	0.32	0.01	0.02	8.06	106	637	155	7.19
13.0	14.0	L. Mottled Zone	66.9	19.6	4.94	0.01	0.04	0.06	0.04	0.37	0.02	0.02	7.04	124	844	128	12.5
14.0	15.0	L. Mottled Zone	67.8	20.1	4.96	0.01	0.02	0.02	0.04	0.37	0.02	0.03	7.02	121	710	125	9.95
15.0	16.0	L. Mottled Zone	66.9	19.7	4.90	0.01	0.04	0.04	0.03	0.35	0.03	0.02	7.17	130	722	118	18.3
16.0	17.0	L. Mottled Zone	69.8	18.8	5.43	0.01	0.04	0.02	0.03	0.38	0.02	0.02	6.69	135	719	128	25.0
17.0	18.0	L. Mottled Zone	68.9	19.7	4.91	0.01	0.06	0.03	0.04	0.34	0.03	0.02	6.89	113	668	113	16.8
18.0	19.0	L. Mottled Zone	68.9	19.3	4.49	0.01	0.10	0.02	0.05	0.31	0.02	0.01	6.85	110	638	105	14.1
19.0	20.0	Transition	67.8	18.8	5.40	0.01	0.10	0.05	0.86	0.38	0.05	0.02	6.66	130	732	144	12.7
20.0	20.9	Saprolite	69.7	14.6	5.23	0.06	0.19	0.37	5.19	0.39	0.08	0.03	3.14	140	1050	166	21.5

From	To	Lithology	La	Ce	Pr	Nb	Sm	Eu	Gd	Tb	Dy	Ho	Er	Tm	Yb	Lu	Y
m	m		ppm	ppm	ppm	ppm	ppm	ppm	ppm	ppm	ppm	ppm	ppm	ppm	ppm	ppm	ppm
0.0	1.1	Ferruginous Soil	16.20	88.5	2.22	6.70	1.60	0.20	1.86	0.39	2.82	0.71	2.59	0.51	3.68	0.59	18.3
1.1	2.0	Ferruginous Soil	13.90	71.5	2.13	7.00	1.50	0.20	1.99	0.43	3.00	0.72	2.72	0.53	4.10	0.64	18.8
2.0	3.2	Ferruginous zone	5.10	106	0.86	3.00	0.81	0.15	1.44	0.35	2.89	0.82	2.99	0.61	4.93	0.76	20.1
3.2	4.0	U. Mottled Zone	4.80	106	0.70	2.30	0.63	0.14	1.42	0.33	2.73	0.83	3.13	0.67	5.29	0.86	23.6
4.0	5.0	U. Mottled Zone	3.90	137	0.58	1.90	0.56	0.14	1.06	0.29	2.32	0.66	2.50	0.52	4.03	0.69	17.5
5.0	7.0	U. Mottled Zone	3.30	72.3	0.52	1.70	0.53	0.11	1.16	0.29	2.46	0.69	2.81	0.56	4.56	0.76	18.7
7.0	9.0	U. Mottled Zone	3.40	96.3	0.50	1.80	0.49	0.10	0.84	0.26	2.06	0.58	2.17	0.47	3.60	0.57	16.1
9.0	10.0	U. Mottled Zone	2.80	158	0.40	1.50	0.51	0.11	0.88	0.23	2.31	0.67	2.73	0.59	4.68	0.79	16.9
10.0	11.0	U. Mottled Zone	1.90	201	0.41	1.50	0.48	0.11	0.84	0.26	2.26	0.62	2.46	0.50	3.58	0.54	13.1
11.0	12.0	L. Mottled Zone	2.30	1895	0.82	2.60	0.81	0.57	1.78	0.63	4.43	1.16	4.35	0.90	7.70	1.00	24.2
12.0	13.0	L. Mottled Zone	2.90	1565	0.90	2.80	0.70	0.45	1.02	0.44	2.43	0.69	2.75	0.58	4.93	0.72	16.0
13.0	14.0	L. Mottled Zone	5.20	8700	3.53	10.80	3.33	2.28	3.12	1.66	6.31	1.50	5.69	1.19	9.95	1.33	32.0
14.0	15.0	L. Mottled Zone	4.10	2280	1.39	4.30	1.11	0.65	1.75	0.62	3.80	0.96	3.52	0.81	6.38	0.94	25.0
15.0	16.0	L. Mottled Zone	6.90	7210	5.10	15.60	4.53	3.25	3.93	2.24	7.91	1.63	6.01	1.30	12.35	1.45	29.6
16.0	17.0	L. Mottled Zone	4.40	1445	1.55	5.0	1.19	0.72	1.76	0.64	3.73	0.87	3.97	0.71	6.62	0.99	23.6
17.0	18.0	L. Mottled Zone	5.20	1235	1.53	5.30	1.20	0.63	1.69	0.54	3.65	0.92	3.62	0.77	6.61	0.87	23.2
18.0	19.0	L. Mottled Zone	19.50	2220	4.90	16.60	3.19	1.17	2.96	0.98	5.36	1.30	5.25	1.00	8.30	1.13	30.7
19.0	20.0	Transition	376	2050	81.3	262.0	40.90	2.93	20.4	3.63	20.5	3.65	11.8	2.00	15.65	1.99	82.2
20.0	20.9	Saprolite	4860	1805	874	2870	466	30.20	329	47.8	262	39.8	99.8	12.25	78.90	8.62	1080

DDH0121

Easting	Northing
768533	8505032

From	To	Lithology	SiO_2	Al_2O_3	Fe_2O_3	CaO	MgO	Na_2O	K_2O	TiO_2	MnO	P_2O_5	LOI	Nb	Zr	Th	U
m	m		wt %	wt %	wt %	wt %	wt %	wt %	wt %	wt %	wt %	wt %	wt %	ppm	ppm	ppm	ppm
0.0	1.0	Ferruginous Soil	39.0	15.1	36.5	0.01	0.01	0.01	0.03	0.43	0.01	0.06	9.12	113	906	178	7.33
1.0	2.0	Ferruginous Soil	67.5	11.3	15.6	0.01	0.01	0.01	0.02	0.29	0.01	0.03	6.01	81.7	675	86.3	3.75
2.0	3.0	Ferruginous zone	58.5	18.7	13.8	0.01	0.02	0.01	0.02	0.48	0.01	0.03	8.50	156	1230	119	5.04
3.0	4.0	Ferruginous zone	58.6	19.2	13.7	0.01	0.01	0.01	0.02	0.44	0.01	0.02	8.17	169	1255	125	5.59
4.0	5.0	U. Mottled Zone	66.6	19.5	6.40	0.01	0.02	0.01	0.02	0.45	0.01	0.01	7.62	180	1285	78.0	5.27
5.0	6.0	U. Mottled Zone	60.3	20.5	10.3	0.01	0.02	0.01	0.02	0.50	0.01	0.02	8.56	195	1260	109	5.69
6.0	7.0	U. Mottled Zone	63.0	21.6	6.88	0.01	0.02	0.01	0.02	0.51	0.01	0.02	8.44	203	1355	95.2	6.06
7.0	8.0	U. Mottled Zone	60.7	20.4	10.7	0.01	0.02	0.01	0.02	0.43	0.01	0.02	8.06	220	1145	123	5.71
8.0	9.0	U. Mottled Zone	62.6	20.6	9.09	0.01	0.02	0.01	0.01	0.37	0.01	0.01	7.59	235	998	129	5.48
9.0	10.0	U. Mottled Zone	64.8	21.1	6.27	0.01	0.01	0.01	0.01	0.35	0.01	0.01	7.70	225	1055	117	6.46
10.0	11.0	U. Mottled Zone	67.0	19.9	5.61	0.01	0.01	0.01	0.01	0.36	0.01	0.01	7.39	217	1095	95.3	6.12
11.0	12.0	U. Mottled Zone	66.6	21.3	3.79	0.01	0.02	0.01	0.01	0.41	0.01	0.01	7.78	227	1140	76.4	5.40
12.0	13.0	U. Mottled Zone	66.2	20.8	5.59	0.01	0.02	0.01	0.02	0.36	0.01	0.01	7.79	240	947	104	5.21
13.0	14.0	L. Mottled Zone	64.6	21.6	4.64	0.01	0.02	0.02	0.03	0.33	0.01	0.01	7.95	230	897	110	9.38
14.0	14.5	L. Mottled Zone	65.1	21.0	4.58	0.02	0.03	0.02	0.02	0.34	0.01	0.01	7.68	235	900	109	11.1
14.5	15.0	L. Mottled Zone	66.8	20.6	4.76	0.01	0.02	0.01	0.02	0.34	0.01	0.02	7.37	236	850	117	9.12
15.0	16.0	L. Mottled Zone	68.0	20.1	4.66	0.01	0.01	0.01	0.02	0.31	0.02	0.02	7.15	226	797	102	8.4
16.0	17.0	L. Mottled Zone	67.6	19.9	4.67	0.01	0.01	0.01	0.02	0.30	0.05	0.02	7.31	221	826	106	13.1
17.0	18.0	L. Mottled Zone	67.8	20.2	4.70	0.01	0.01	0.01	0.02	0.30	0.01	0.02	7.79	235	728	111	14.4
18.0	19.1	L. Mottled Zone	67.4	19.9	4.61	0.01	0.03	0.02	0.08	0.32	0.04	0.02	7.65	230	767	105	13.6
19.1	20.0	Transition	71.2	17.5	4.13	0.01	0.06	0.06	1.53	0.27	0.07	0.02	5.64	180	556	85.7	12.9
20.0	21.0	Saprolite	70.5	16.9	4.09	0.01	0.07	0.12	3.19	0.29	0.09	0.02	4.76	198	661	91.8	12.2
21.0	21.5	Saprolite	70.8	16.0	3.89	0.04	0.10	0.28	4.77	0.28	0.06	0.02	3.73	180	584	83.4	14.4
21.5	22.0	Saprock	73.7	12.9	3.26	0.93	0.08	3.36	5.46	0.22	0.05	0.02	0.38	147	494	67.9	10.5
22.0	23.0	Saprock	73.8	12.7	3.13	0.90	0.08	3.32	5.43	0.22	0.05	0.02	0.41	143	473	68.5	11.2
23.0	24.0	Saprock	73.2	12.9	3.45	0.95	0.08	3.40	5.46	0.21	0.05	0.02	0.30	150	504	65.6	11.4
24.0	25.0	Bedrock	73.5	12.8	3.11	0.93	0.08	3.37	5.50	0.22	0.05	0.02	0.34	146	510	67.7	11.4
25.0	26.0	Bedrock	73.2	12.9	3.28	0.97	0.08	3.39	5.42	0.23	0.05	0.02	0.30	146	477	69.4	10.8
26.0	27.3	Bedrock	73.3	13.0	3.07	0.98	0.07	3.42	5.52	0.20	0.05	0.01	0.27	138	474	63.1	9.36

From	To	Lithology	La	Ce	Pr	Nb	Sm	Eu	Gd	Tb	Dy	Ho	Er	Tm	Yb	Lu	Y
m	m		ppm	ppm	ppm	ppm	ppm	ppm	ppm	ppm	ppm	ppm	ppm	ppm	ppm	ppm	ppm
0.0	1.0	Ferruginous Soil	19.10	48.9	3.26	10.60	2.58	0.33	2.92	0.66	4.99	1.22	4.52	0.84	7.12	1.06	29.1
1.0	2.0	Ferruginous Soil	9.10	30.5	1.54	5.20	1.25	0.18	1.48	0.36	2.81	0.77	2.71	0.55	4.05	0.74	19.2
2.0	3.0	Ferruginous zone	9.10	32.5	1.35	4.70	1.15	0.19	1.67	0.44	3.57	1.12	4.08	0.87	6.90	1.17	33.8
3.0	4.0	Ferruginous zone	6.80	34.3	1.03	3.50	1.07	0.14	1.54	0.43	3.38	1.11	3.76	0.87	6.80	1.16	32.2
4.0	5.0	U. Mottled Zone	7.50	35.8	1.08	3.50	0.96	0.18	1.81	0.43	3.32	1.11	3.92	0.86	6.71	1.20	33.5
5.0	6.0	U. Mottled Zone	7.60	45.7	1.16	3.90	0.92	0.21	1.88	0.48	3.60	1.09	3.94	0.83	6.86	1.12	32.8
6.0	7.0	U. Mottled Zone	8.60	53.6	1.25	4.70	1.00	0.17	2.01	0.50	3.61	1.07	4.19	0.80	6.98	1.17	32.4
7.0	8.0	U. Mottled Zone	5.20	58.4	1.02	3.50	0.90	0.16	1.76	0.51	3.62	1.03	3.71	0.75	6.32	1.11	30.1
8.0	9.0	U. Mottled Zone	3.20	50.0	0.72	2.60	0.86	0.11	1.61	0.36	2.77	0.69	2.54	0.51	4.22	0.73	18.8
9.0	10.0	U. Mottled Zone	3.30	52.4	0.77	3.00	0.94	0.13	1.74	0.40	3.27	0.80	2.49	0.54	4.58	0.75	18.8
10.0	11.0	U. Mottled Zone	4.10	38.3	0.80	3.60	0.96	0.16	1.67	0.39	2.93	0.75	2.80	0.56	4.55	0.72	19.1
11.0	12.0	U. Mottled Zone	4.10	87.1	0.81	3.30	1.09	0.18	1.60	0.39	3.63	0.98	3.03	0.65	5.14	0.90	23.5
12.0	13.0	U. Mottled Zone	4.40	72.4	0.89	3.30	1.06	0.15	1.94	0.43	3.57	0.87	2.85	0.55	4.25	0.70	19.3
13.0	14.0	L. Mottled Zone	5.40	5860	2.47	9.00	2.42	2.13	3.21	1.72	5.84	1.30	4.29	0.86	7.28	0.99	26.4
14.0	14.5	L. Mottled Zone	6.40	7200	3.47	11.9	3.51	2.97	4.23	2.16	7.12	1.60	4.90	0.95	7.93	1.06	29.4
14.5	15.0	L. Mottled Zone	5.30	3060	2.26	8.50	2.59	1.26	3.39	1.26	6.09	1.42	4.19	0.80	6.22	0.93	26.5
15.0	16.0	L. Mottled Zone	4.20	1800	2.00	7.10	2.56	0.75	3.51	1.17	6.71	1.54	5.12	0.93	6.93	1.01	28.2
16.0	17.0	L. Mottled Zone	7.40	3960	4.72	15.7	5.34	1.63	5.37	1.97	10.0	2.29	6.74	1.23	9.21	1.28	34.1
17.0	18.0	L. Mottled Zone	7.80	911	3.05	11.7	4.05	0.62	5.13	1.43	9.49	2.19	6.76	1.19	8.34	1.30	38.9
18.0	19.1	L. Mottled Zone	20.9	845	6.22	22.8	5.61	0.67	6.31	1.68	12.1	2.81	8.47	1.55	10.6	1.47	47.0
19.1	20.0	Transition	145	706	28.0	93.2	16.1	1.20	14.25	3.20	23.6	5.26	17.55	2.77	18.7	2.61	135
20.0	21.0	Saprolite	285	472	66.2	226	35.9	2.12	30.5	5.65	37.6	9.09	27.9	4.60	31.6	4.60	279
21.0	21.5	Saprolite	2250	431	431	1465	263	14.1	185	29.2	156	26.5	69.6	9.55	61.1	7.85	721
21.5	22.0	Saprock	478	435	85.0	302	56.9	3.92	59.8	10.4	62.4	12.8	37.4	5.69	36.7	5.37	377
22.0	23.0	Saprock	460	423	80.1	285	53.6	3.84	56.3	9.76	60.5	12.85	37.0	5.52	33.2	4.94	410
23.0	24.0	Saprock	233	388	42.8	153	29.1	2.09	33.2	6.16	41.2	9.66	30.5	4.54	27.1	4.07	318
24.0	25.0	Bedrock	221	391	41.9	148	29.2	1.85	33.0	6.07	40.2	9.51	30.2	4.50	27.0	4.04	307
25.0	26.0	Bedrock	240	407	45.8	162	32.0	2.07	34.5	6.16	37.5	8.03	24.2	3.51	22.4	3.28	241
26.0	27.3	Bedrock	203	372	38.2	136	26.4	1.63	28.7	5.29	34.6	8.07	25.6	3.87	24.3	3.70	273

DDH0096

Easting	Northing
768437	8504986

From	To	Lithology	SiO_2	Al_2O_3	Fe_2O_3	CaO	MgO	Na_2O	K_2O	TiO_2	MnO	P_2O_5	LOI	Nb	Zr	Th	U
m	m		wt %	wt %	wt %	wt %	wt %	wt %	wt %	wt %	wt %	wt %	wt %	ppm	ppm	ppm	ppm
0.0	1.0	Ferricete	42.5	17.3	30.1	0.02	0.02	0.01	0.03	0.52	0.01	0.07	9.41	106	1000	152	5.48
1.0	2.0		43.8	18.6	28.3	0.02	0.02	0.01	0.02	0.56	0.01	0.05	8.77	114	916	139	5.10
2.0	3.0	Ferruginous Zone	41.9	19.6	28.9	0.02	0.02	0.01	0.02	0.55	0.01	0.05	9.24	124	971	179	7.09
3.0	4.2	Ferruginous Zone	47.8	18.1	25.8	0.02	0.02	0.01	0.01	0.50	0.01	0.04	8.04	119	982	212	5.53
4.2	5.0	Ferruginous Zone	52.8	20.8	17.61	0.03	0.02	0.01	0.03	0.57	0.01	0.03	8.67	131	1110	176	6.41
5.0	6.0	Pegmatite	73.1	16.4	3.84	0.02	0.02	0.01	0.03	0.33	0.01	0.02	6.17	83.5	698	47.3	3.46
6.0	7.0	Pegmatite	71.3	14.8	7.75	0.02	0.02	0.01	0.03	0.31	0.01	0.02	5.76	79.4	550	53.8	3.47
7.0	8.0	Pegmatite	74.9	15.3	4.04	0.02	0.01	0.01	0.04	0.27	0.01	0.02	5.73	74.8	471	43.2	3.22
8.0	9.0	U. Mottled Zone	62.7	21.8	7.19	0.02	0.02	0.02	0.04	0.55	0.01	0.02	8.32	127	1130	78.1	6.20
9.0	10.0	U. Mottled Zone	60.2	22.1	9.01	0.02	0.02	0.01	0.05	0.50	0.01	0.02	8.20	130	1010	126	6.16
10.0	11.0	Pegmatite	61.7	22.3	7.44	0.02	0.02	0.02	0.11	0.27	0.01	0.02	8.27	115	497	91.1	4.98
11.0	12.0	U. Mottled Zone	62.4	22.1	7.00	0.02	0.01	0.01	0.04	0.53	0.01	0.02	8.15	142	1150	138	6.59
12.0	13.0	U. Mottled Zone	66.1	21.0	5.23	0.02	0.01	0.01	0.03	0.51	0.01	0.02	7.56	126	969	99.0	6.37
13.0	14.0	U. Mottled Zone	64.4	22.0	5.53	0.02	0.01	0.01	0.03	0.51	0.01	0.02	7.90	140	1020	143	6.41
14.0	14.5	U. Mottled Zone	63.6	22.6	5.84	0.02	0.01	0.01	0.02	0.52	0.01	0.02	8.13	144	1040	122	6.54
14.5	15.0	U. Mottled Zone	62.2	22.3	7.31	0.02	0.01	0.01	0.02	0.55	0.02	0.02	8.17	140	1120	118	6.84
15.0	16.0	U. Mottled Zone	59.8	21.3	10.55	0.02	0.02	0.01	0.03	0.53	0.02	0.03	8.12	119	971	144	6.49
16.0	17.0	U. Mottled Zone	64.0	22.3	5.78	0.02	0.02	0.01	0.02	0.46	0.02	0.02	7.98	116	946	128	5.82
17.0	17.5	U. Mottled Zone	64.5	22.0	5.74	0.02	0.01	0.01	0.02	0.50	0.01	0.02	7.89	125	954	115	6.37
17.5	18.0	U. Mottled Zone	65.8	21.3	5.38	0.02	0.01	0.01	0.02	0.46	0.01	0.02	7.72	112	779	116	5.55

17.0	17.5	U. Mottled Zone	64.5	22.0	5.74	0.02	0.01	0.01	0.02	0.50	0.01	0.02	7.89	125	954	115	6.37
17.5	18.0	U. Mottled Zone	65.8	21.3	5.38	0.02	0.01	0.01	0.02	0.46	0.01	0.02	7.72	112	779	116	5.55
18.0	18.5	U. Mottled Zone	64.7	21.8	5.80	0.02	0.01	0.01	0.03	0.51	0.01	0.02	7.86	132	1045	126	6.64
18.5	19.0	U. Mottled Zone	66.1	21.3	5.16	0.02	0.01	0.01	0.03	0.45	0.01	0.03	7.73	115	948	95.4	6.23
19.0	20.0	L. Mottled Zone	63.6	21.5	6.49	0.02	0.01	0.01	0.03	0.57	0.05	0.05	7.87	138	1090	125	9.44
20.0	21.0	L. Mottled Zone	64.5	20.8	6.50	0.02	0.01	0.01	0.03	0.53	0.04	0.05	7.58	132	1080	122	9.37
21.0	21.5	L. Mottled Zone	67.4	19.1	6.10	0.02	0.01	0.01	0.03	0.53	0.07	0.06	6.78	161	1075	128	11.1
21.5	22.0	L. Mottled Zone	67.9	19.5	5.30	0.02	0.01	0.01	0.03	0.45	0.10	0.05	6.96	129	993	113	10.5
22.0	22.5	L. Mottled Zone	67.8	20.4	4.19	0.02	0.01	0.01	0.03	0.32	0.05	0.04	7.29	147	776	85.0	10.6
22.5	23.0	L. Mottled Zone	66.8	20.4	5.24	0.02	0.01	0.01	0.02	0.47	0.04	0.05	7.38	131	969	115	10.1
23.0	23.5	L. Mottled Zone	66.2	19.9	5.86	0.02	0.01	0.01	0.03	0.55	0.07	0.06	7.21	128	1265	128	10.3
23.5	24.5	L. Mottled Zone	65.5	19.7	7.24	0.02	0.01	0.01	0.04	0.50	0.04	0.06	7.21	120	979	116	9.54
24.5	25.3	L. Mottled Zone	66.4	20.0	5.71	0.02	0.02	0.01	0.07	0.50	0.08	0.06	7.24	126	963	109	9.52
25.3	26.0	L. Mottled Zone	66.2	19.8	5.98	0.02	0.05	0.01	0.26	0.52	0.05	0.07	7.10	131	1015	112	10.3
26.0	27.0	Transition	67.9	19.0	5.77	0.02	0.09	0.01	0.59	0.51	0.07	0.06	6.53	124	1100	106	11.3
27.0	28.0	Transition	68.8	19.7	3.95	0.01	0.08	0.01	0.63	0.31	0.16	0.04	6.64	89.4	606	90.4	8.77
28.0	28.5	Transition	65.1	21.0	4.55	0.01	0.12	0.04	1.70	0.36	0.22	0.04	6.80	113	653	66.2	8.19
28.5	29.0	SAPROLITE	67.6	18.8	5.21	0.01	0.14	0.05	1.80	0.43	0.07	0.05	6.02	108	805	97.8	9.93
29.0	29.5	SAPROLITE	67.5	18.4	5.29	0.01	0.15	0.06	2.34	0.45	0.05	0.05	5.64	116	993	101	14.8
29.5	30.0	SAPROLITE	68.3	17.8	5.01	0.01	0.14	0.08	2.62	0.42	0.05	0.05	5.36	110	1000	92.1	12.3
30.0	31.0	SAPROLITE	68.4	17.3	5.48	0.01	0.14	0.08	2.79	0.45	0.05	0.05	5.19	117	926	104	13.4
31.0	31.5	SAPROLITE	69.0	17.2	5.20	0.01	0.14	0.09	2.91	0.42	0.08	0.05	4.98	113	910	101	13.1
31.5	32.0	SAPROLITE	67.7	17.6	5.24	0.01	0.13	0.10	3.36	0.45	0.13	0.05	5.01	111	818	99.4	13.6
32.0	33.0	SAPROLITE	70.0	16.0	4.80	0.01	0.12	0.15	4.28	0.42	0.04	0.05	3.94	104	987	93.5	11.8
33.0	34.0	SAPROLITE	68.5	16.1	5.43	0.02	0.13	0.18	5.27	0.44	0.05	0.05	3.48	123	866	90.9	10.7
34.0	35.0	SAPROLITE	68.7	14.1	7.53	0.05	0.22	0.17	5.17	0.65	0.07	0.08	3.10	181	1310	114	15.8
35.0	36.7	SAPROLITE	69.8	14.8	5.58	0.12	0.16	0.51	6.18	0.36	0.05	0.04	2.46	144	733	80.3	9.15
36.7	37.3	SAPROCK	71.7	13.5	3.95	0.53	0.16	2.67	6.14	0.33	0.06	0.04	0.53	84.7	612	74.9	8.48
37.3	38.0	SAPROCK	71.6	13.5	4.04	0.99	0.16	3.01	5.94	0.34	0.04	0.04	0.46	95.4	651	75.4	9.74
38.0	39.0	SAPROCK	71.5	13.4	4.32	1.10	0.16	3.02	5.91	0.34	0.05	0.04	0.41	96.6	700	82.6	10.2
39.0	40.0	BDRK	72.3	13.2	3.84	1.02	0.14	2.96	5.95	0.31	0.05	0.03	0.39	93.1	634	84.3	10.9
40.0	41.0	BDRK	72.2	13.1	4.12	1.04	0.16	2.99	5.80	0.33	0.06	0.04	0.42	93.0	551	82.2	10.2
41.0	42.0	BDRK	73.0	13.5	2.99	0.86	0.12	3.02	6.22	0.26	0.04	0.03	0.26	73.5	576	63.3	7.54

DDH0096

From	To	Lithology	La	Ce	Pr	Nb	Sm	Eu	Gd	Tb	Dy	Ho	Er	Tm	Yb	Lu	Y
m	m		ppm	ppm	ppm	ppm	ppm	ppm	ppm	ppm	ppm	ppm	ppm	ppm	ppm	ppm	ppm
0.0	1.0	Ferricete	19.9	43.0	2.56	8.10	1.97	0.29	2.24	0.51	3.94	1.04	3.66	0.74	5.87	0.89	29.1
1.0	2.0		15.6	30.9	2.03	6.50	1.63	0.18	1.82	0.40	3.04	0.71	3.04	0.57	4.51	0.71	19.4
2.0	3.0	Ferruginous Zone	11.6	26.8	1.86	6.00	1.34	0.19	1.75	0.41	3.47	0.81	3.25	0.60	4.95	0.72	20.4
3.0	4.2	Ferruginous Zone	7.30	33.8	1.11	3.50	0.85	0.11	1.23	0.25	1.79	0.50	1.72	0.39	3.36	0.53	13.4
4.2	5.0	Ferruginous Zone	6.20	32.1	1.00	4.10	1.28	0.14	1.52	0.35	3.09	0.79	3.65	0.56	5.25	0.73	25.5
5.0	6.0	Pegmatite	5.80	20.2	0.77	2.50	0.67	0.15	1.30	0.33	2.67	0.82	3.23	0.63	4.68	0.71	25.1
6.0	7.0	Pegmatite	7.50	21.0	0.95	2.80	0.70	0.13	1.59	0.45	3.58	1.02	4.00	0.78	5.78	0.96	29.0
7.0	8.0	Pegmatite	6.50	22.9	0.88	2.70	0.94	0.13	1.67	0.35	3.29	0.91	3.68	0.62	5.20	0.77	28.7
8.0	9.0	U. Mottled Zone	8.40	49.2	1.17	4.20	1.14	0.13	1.46	0.43	3.04	0.84	3.54	0.63	5.69	0.85	28.5
9.0	10.0	U. Mottled Zone	4.90	161	0.93	3.70	1.03	0.19	1.42	0.35	2.48	0.70	2.93	0.56	4.85	0.77	23.1
10.0	11.0	Pegmatite	7.30	82.0	1.21	4.40	1.17	0.21	2.95	0.79	7.25	2.01	7.87	1.41	10.4	1.66	67.1
11.0	12.0	U. Mottled Zone	4.30	233	0.83	2.90	0.84	0.13	1.31	0.34	2.41	0.73	3.04	0.62	4.84	0.79	21.7
12.0	13.0	U. Mottled Zone	3.70	92.0	0.72	2.70	0.79	0.11	0.96	0.24	1.70	0.47	2.12	0.42	3.52	0.55	13.2
13.0	14.0	U. Mottled Zone	3.80	358	0.88	3.30	0.87	0.19	1.21	0.31	2.14	0.57	2.18	0.41	3.67	0.59	13.4
14.0	14.5	U. Mottled Zone	3.80	119	0.86	2.90	0.69	0.14	1.09	0.21	1.84	0.50	1.91	0.43	3.46	0.62	12.9
14.5	15.0	U. Mottled Zone	5.60	256	1.14	4.30	1.20	0.17	1.53	0.35	2.62	0.61	2.42	0.46	3.78	0.63	16.8
15.0	16.0	U. Mottled Zone	6.50	371	1.24	4.80	1.22	0.32	1.35	0.34	2.33	0.54	2.28	0.43	3.58	0.57	13.2
16.0	17.0	U. Mottled Zone	5.40	388	1.25	4.30	1.16	0.28	1.72	0.41	2.63	0.65	2.57	0.48	3.60	0.66	15.5
17.0	17.5	U. Mottled Zone	4.20	171	0.87	3.40	0.85	0.20	1.62	0.33	2.47	0.66	2.28	0.44	3.73	0.64	16.3
17.5	18.0	U. Mottled Zone	4.50	450	0.97	3.80	0.97	0.30	1.37	0.35	2.08	0.51	1.77	0.41	3.44	0.54	12.2
18.0	18.5	U. Mottled Zone	5.50	724	1.28	4.90	1.42	0.43	1.81	0.47	2.83	0.63	2.71	0.56	4.26	0.73	15.5
18.5	19.0	U. Mottled Zone	4.90	266	1.16	4.20	0.98	0.22	1.34	0.32	2.25	0.47	1.99	0.38	2.94	0.53	12.0
19.0	20.0	L. Mottled Zone	15.5	1325	3.59	12.1	2.62	0.74	2.44	0.68	3.80	0.85	3.10	0.56	4.91	0.71	17.6
20.0	21.0	L. Mottled Zone	32.5	1310	6.91	22.5	4.28	0.78	3.95	0.87	4.42	0.92	3.03	0.55	4.38	0.78	21.2
21.0	21.5	L. Mottled Zone	52.5	1425	11.2	36.1	7.05	0.95	5.70	1.19	5.86	1.21	4.13	0.72	5.76	0.94	26.5
21.5	22.0	L. Mottled Zone	52.0	1525	11.7	37.4	7.53	1.05	6.65	1.41	7.03	1.42	5.21	0.89	7.27	1.06	30.8
22.0	22.5	L. Mottled Zone	35.2	790	7.82	25.9	4.97	0.70	4.57	1.04	6.03	1.31	4.40	0.84	6.33	1.00	25.3
22.5	23.0	L. Mottled Zone	54.9	487	11.2	36.4	6.72	0.68	5.84	1.02	5.93	1.20	3.92	0.71	5.60	0.83	27.2
23.0	23.5	L. Mottled Zone	49.0	723	10.1	32.5	5.65	0.64	4.97	0.97	5.36	1.20	4.33	0.69	6.63	0.96	27.9
23.5	24.5	L. Mottled Zone	48.2	319	10.7	34.9	6.03	0.70	5.21	0.92	5.83	1.17	3.83	0.64	5.30	0.79	28.4
24.5	25.3	L. Mottled Zone	52.0	545	11.8	41.6	8.08	0.77	6.73	1.31	7.9	1.61	4.85	0.86	6.53	1.00	35.7
25.3	26.0	L. Mottled Zone	125	303	27.2	91.2	16.4	1.25	12.9	2.21	13.3	2.61	7.77	1.21	8.37	1.25	63.6
26.0	27.0	Transition	236	457	53.9	180	31.9	2.11	23.5	3.91	22.5	4.46	13.3	1.98	13.0	1.90	117
27.0	28.0	Transition	235	1150	53.9	185	31.9	2.44	24.3	4.21	25.7	5.02	16.1	2.48	17.7	2.50	132
28.0	28.5	Transition	361	1390	77.7	262	43.3	3.23	32.1	5.52	33.3	6.69	20.5	3.26	23.1	3.03	184
28.5	29.0	SAPROLITE	450	485	96.5	325	54.5	4.29	41.4	6.74	40.8	8.26	25.4	3.71	24.2	3.27	236
29.0	29.5	SAPROLITE	489	422	103	337	58.8	4.82	47.9	7.78	45.4	9.2	28.6	4.44	28.4	3.87	280
29.5	30.0	SAPROLITE	469	465	94.2	311	52.6	4.37	42.0	6.92	41.9	8.33	25.9	3.98	25.3	3.50	256
30.0	31.0	SAPROLITE	491	563	98.0	322	54.4	4.48	42.5	6.87	39.4	7.73	24.5	3.58	22.5	3.15	237
31.0	31.5	SAPROLITE	390	611	78.1	258	44.1	3.78	35.5	6.10	36.1	7.32	22.0	3.37	22.2	3.04	217
31.5	32.0	SAPROLITE	335	1050	66.1	223	39.6	3.77	37.1	6.40	38.1	7.70	23.0	3.49	21.9	3.03	213
32.0	33.0	SAPROLITE	329	416	63.7	221	38.3	3.48	36.6	6.13	37.2	7.68	22.9	3.39	21.6	3.09	226
33.0	34.0	SAPROLITE	297	419	58.1	195	36.5	3.35	37.8	6.31	37.3	7.65	23.6	3.48	21.3	2.97	239
34.0	35.0	SAPROLITE	377	506	77.4	268	50.3	3.84	53.5	9.47	56.7	12.2	37.0	5.43	34.5	5.07	385
35.0	36.7	SAPROLITE	278	411	50.7	180	32.8	3.04	32.4	5.31	32.7	6.84	22.8	3.28	21.2	2.88	235
36.7	37.3	SAPROCK	508	423	87.7	301	52.1	5.51	57.0	9.07	51.9	10.1	28.0	3.88	23.1	3.23	299
37.3	38.0	SAPROCK	402	387	69.7	244	44.2	4.83	52.7	8.60	52.0	10.9	30.7	4.23	24.8	3.54	372
38.0	39.0	SAPROCK	299	444	54.1	187	32.6	3.66	39.4	6.65	39.7	8.71	25.6	3.93	22.7	3.39	289
39.0	40.0	BDRK	251	424	46.2	157	27.5	2.91	29.9	5.14	29.7	6.26	18.1	2.87	17.9	2.51	195
40.0	41.0	BDRK	240	474	46.9	158	27.7	2.60	29.3	5.27	33.2	7.45	23.3	3.51	22.0	3.10	235
41.0	42.0	BDRK	184	315	32.5	108	17.2	2.03	16.1	2.72	16.0	3.60	10.8	1.70	11.0	1.56	119

DDH0004

Easting	Northing
768762	8504883

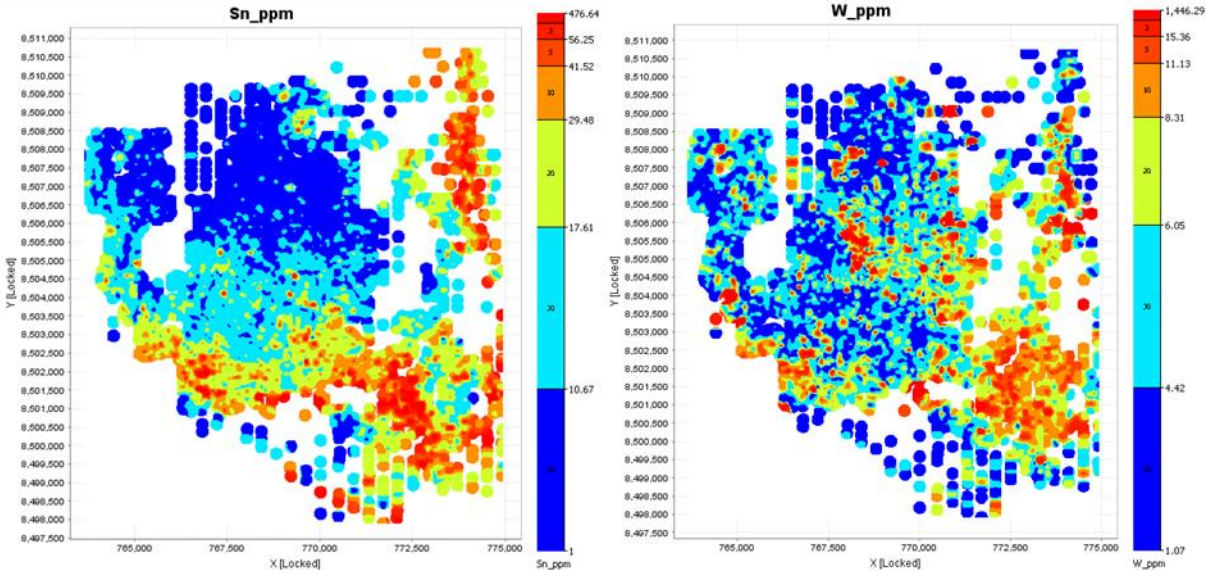
From	To	Lithology	SiO_2	Al_2O_3	Fe_2O_3	CaO	MgO	Na_2O	K_2O	TiO_2	MnO	P_2O_5	LOI	Nb	Zr	Th	U
m	m		wt %	wt %	wt %	wt %	wt %	wt %	wt %	wt %	wt %	wt %	wt %	ppm	ppm	ppm	ppm
26.0	27.0	Granite	73.5	13.4	3.15	0.94	0.11	3.19	5.54	0.23	0.06	0.02	0.41	125	549	66.7	7.17
27.0	28.5	Granite	74.0	13.3	3.02	0.98	0.11	3.48	5.51	0.22	0.05	0.02	0.21	134	632	69.7	8.21
28.5	30.0	Granite	73.1	12.9	3.07	0.99	0.10	3.33	5.50	0.22	0.05	0.02	0.24	153	545	62.2	7.85
30.0	31.5	Granite	72.9	12.8	3.25	0.95	0.12	3.28	5.41	0.23	0.07	0.01	0.31	129	566	67.7	6.67
31.5	33.0	Granite	72.5	13.1	3.09	1.00	0.23	3.08	5.56	0.23	0.05	0.01	0.69	125	468	64.9	5.88
33.0	34.5	Granite	74.2	12.6	2.94	0.76	0.51	2.26	5.43	0.21	0.09	0.02	1.16	109	458	60.6	7.77
34.5	36.0	Granite	73.5	12.9	3.20	0.98	0.10	3.63	5.47	0.23	0.05	0.02	0.27	118	511	66.3	9.70
36.0	37.5	Granite	73.2	12.8	3.13	1.00	0.10	3.49	5.39	0.22	0.06	0.02	0.45	122	546	68.5	11.8
37.5	39.0	Granite	73.3	12.8	3.28	0.99	0.10	3.41	5.49	0.23	0.09	0.02	0.37	115	538	70.0	13.2
39.0	40.5	Granite	72.9	13.1	3.53	0.94	0.10	3.58	5.50	0.24	0.06	0.02	0.38	123	571	72.5	12.8
40.5	42.0	Granite	73.2	12.7	3.15	0.97	0.09	3.39	5.45	0.22	0.06	0.02	0.36	122	560	69.2	10.3
42.0	43.5	Granite	72.7	12.8	3.16	0.97	0.09	3.53	5.38	0.21	0.06	0.02	0.39	119	545	67.0	12.1
43.5	45.0	Granite	73.1	12.8	3.11	0.97	0.10	3.41	5.49	0.22	0.05	0.01	0.33	126	562	64.6	10.7
45.0	46.5	Granite	73.1	12.8	3.27	0.99	0.10	3.42	5.47	0.23	0.05	0.02	0.40	124	581	70.0	10.7
46.5	48.0	Granite	73.4	12.8	3.27	0.98	0.10	3.45	5.44	0.23	0.05	0.02	0.42	129	533	73.1	10.1
48.0	49.5	Granite	73.3	13.1	3.13	0.78	0.10	3.57	5.57	0.22	0.07	0.01	0.36	139	555	73.8	12.9
49.5	51.0	Granite	73.4	12.0	3.07	2.07	0.09	3.23	5.09	0.21	0.05	0.01	0.75	109	480	66.6	10.0
51.0	52.5	Granite	73.0	13.5	3.00	0.77	0.11	3.72	5.59	0.22	0.04	0.01	0.42	126	494	70.0	10.1
52.5	54.0	Granite	72.8	12.7	3.24	0.96	0.10	3.39	5.47	0.22	0.05	0.01	0.45	126	486	74.3	11.8
54.0	55.5	Granite	73.3	12.9	3.24	1.00	0.10	3.41	5.53	0.23	0.04	0.02	0.41	126	545	69.6	13.1
55.5	57.0	Granite	73.2	12.8	3.19	1.00	0.09	3.41	5.48	0.23	0.04	0.02	0.47	120	587	71.5	11.6
57.0	58.5	Granite	73.0	12.8	3.29	1.03	0.09	3.34	5.50	0.23	0.04	0.02	0.45	134	452	61.7	10.0
58.5	59.5	Granite	72.9	12.7	3.14	0.98	0.08	3.29	5.53	0.20	0.04	0.01	0.48	144	558	66.2	11.7
59.5	60.5	Granite	73.4	12.7	3.00	0.98	0.08	3.20	5.53	0.21	0.04	0.01	0.38	142	443	70.3	12.3
60.5	61.6	Granite	72.9	12.8	3.06	1.06	0.08	3.20	5.55	0.20	0.06	0.01	0.37	144	501	62.3	14.7
61.6	63.0	Pegmatite	72.2	14.6	0.87	1.27	0.05	3.97	6.00	0.02	0.02	0.01	0.49	62.2	71	5.60	4.89
63.0	64.4	Pegmatite	74.0	15.1	0.82	1.03	0.08	5.44	3.78	0.02	0.02	0.01	0.38	56.3	77	4.42	4.97
64.4	65.5	Granite	73.8	12.9	3.23	1.06	0.11	3.31	5.19	0.20	0.06	0.01	0.46	148	510	66.6	20.6
65.5	67.0	Pegmatite	75.6	13.9	0.90	0.99	0.06	4.70	3.64	0.01	0.01	0.01	0.24	88.0	83.0	7.56	5.71
67.0	68.0	Pegmatite	71.7	15.7	0.78	0.97	0.07	4.51	5.79	0.01	0.01	0.01	0.33	39.4	42.0	6.57	3.00
68.0	69.0	Pegmatite	72.6	13.2	2.59	1.12	0.07	3.50	5.24	0.17	0.04	0.01	0.36	115	345	51.2	11.0
69.0	70.0	Granite	72.6	13.2	3.73	1.20	0.16	2.96	5.70	0.32	0.06	0.03	0.66	87.7	553	75.2	10.8
70.0	71.0	Granite	73.0	13.0	3.50	1.16	0.15	2.80	5.80	0.29	0.06	0.03	0.22	82.4	512	68.3	8.08
71.0	72.0	Granite	71.8	13.4	3.36	0.99	0.14	3.03	6.08	0.27	0.05	0.03	0.30	92.6	503	64.3	12.8
72.0	73.0	Granite	72.1	13.2	3.87	1.22	0.18	2.78	5.88	0.32	0.05	0.03	0.31	90.0	644	79.5	10.0
73.0	74.5	Granite	72.1	13.2	3.78	1.21	0.16	2.81	5.92	0.32	0.06	0.03	0.34	85.2	623	75.1	9.6
74.5	75.5	Granite	72.1	13.2	4.12	1.27	0.18	2.80	5.89	0.33	0.06	0.03	0.37	102	633	86.3	12.7
75.5	76.6	Granite	71.9	13.2	4.21	1.27	0.19	3.04	5.50	0.36	0.06	0.04	0.43	99.1	731	94.2	13.8
76.6	77.3	Pegmatite	75.6	13.5	1.59	1.06	0.11	4.49	3.63	0.02	0.02	0.01	0.41	72.2	87.0	12.1	4.54
77.3	78.2	Granite	71.3	13.0	3.85	1.18	0.18	2.88	5.54	0.26	0.05	0.03	0.32	85.9	597	81.6	12.1
78.2	79.5	Pegmatite	72.8	13.8	2.51	1.06	0.19	3.76	5.03	0.21	0.05	0.03	0.19	66.7	563	72.3	9.9
79.5	80.5	Granite	72.1	13.4	3.92	1.25	0.20	2.90	5.70	0.28	0.05	0.04	0.40	84.2	642	91.1	9.00
80.5	81.4	Granite	72.8	13.3	4.05	1.26	0.24	3.10	5.38	0.34	0.04	0.04	0.26	86.1	694	96.8	8.12
81.4	82.5	Granite	73.6	13.2	3.63	1.06	0.92	4.86	2.32	0.35	0.03	0.04	0.11	91.7	775	82.3	7.62
82.5	84.0	Granite	73.8	13.6	3.90	1.44	0.35	5.05	1.68	0.35	0.03	0.04	0.06	82.2	786	85.4	8.58
84.0	85.5	Granite	73.1	13.7	2.70	0.77	1.11	5.48	2.13	0.22	0.03	0.04	0.14	63.8	427	58.9	7.02
85.5	86.9	Granite	73.3	13.1	3.24	0.41	1.64	5.50	2.33	0.40	0.03	0.06	0.19	79.1	590	83.7	6.90
86.9	88.0	Granite	73.5	13.5	3.25	0.97	0.58	4.33	3.59	0.28	0.05	0.03	0.15	55.4	465	88.6	9.32
88.0	89.5	Granite	75.2	12.7	3.19	0.96	0.33	3.47	4.58	0.23	0.04	0.02	0.13	68.5	585	84.1	10.2
89.5	91.0	Granite	74.1	12.5	3.42	1.21	0.13	2.73	5.83	0.25	0.04	0.02	0.30	71.1	464	104.0	11.6
91.0	92.5	Granite	73.5	12.9	3.13	1.13	0.12	2.93	5.93	0.22	0.04	0.02	0.18	66.6	440	93.9	10.2
92.5	93.5	Granite	74.0	12.7	3.15	1.10	0.13	2.93	5.74	0.23	0.05	0.02	0.26	71.5	457	81.6	9.7
93.5	94.6	Granite	73.9	12.6	3.41	1.14	0.13	2.89	5.75	0.24	0.05	0.02	0.21	79.1	487	82.1	11.9
94.6	95.4	Pegmatite	70.2	17.8	1.48	1.13	0.18	6.74	3.28	0.07	0.02	0.01	0.34	69.2	117	29.2	4.89
95.4	96.5	Granite	73.9	12.8	3.41	0.91	0.15	2.90	5.77	0.25	0.05	0.03	0.06	74.4	514	79.2	8.46
96.5	98.0	Granite	73.9	12.7	3.17	1.12	0.15	2.80	5.77	0.24	0.04	0.02	0.29	67.9	488	80.2	7.08
98.0	99.0	Granite	75.5	12.5	3.21	0.63	0.21	2.40	5.89	0.23	0.04	0.02	0.27	66.9	466	82.6	8.08
99.0	100.2	Granite	75.0	13.0	3.04	0.53	0.20	2.33	5.78	0.22	0.04	0.01	0.49	64.5	457	81.9	6.77

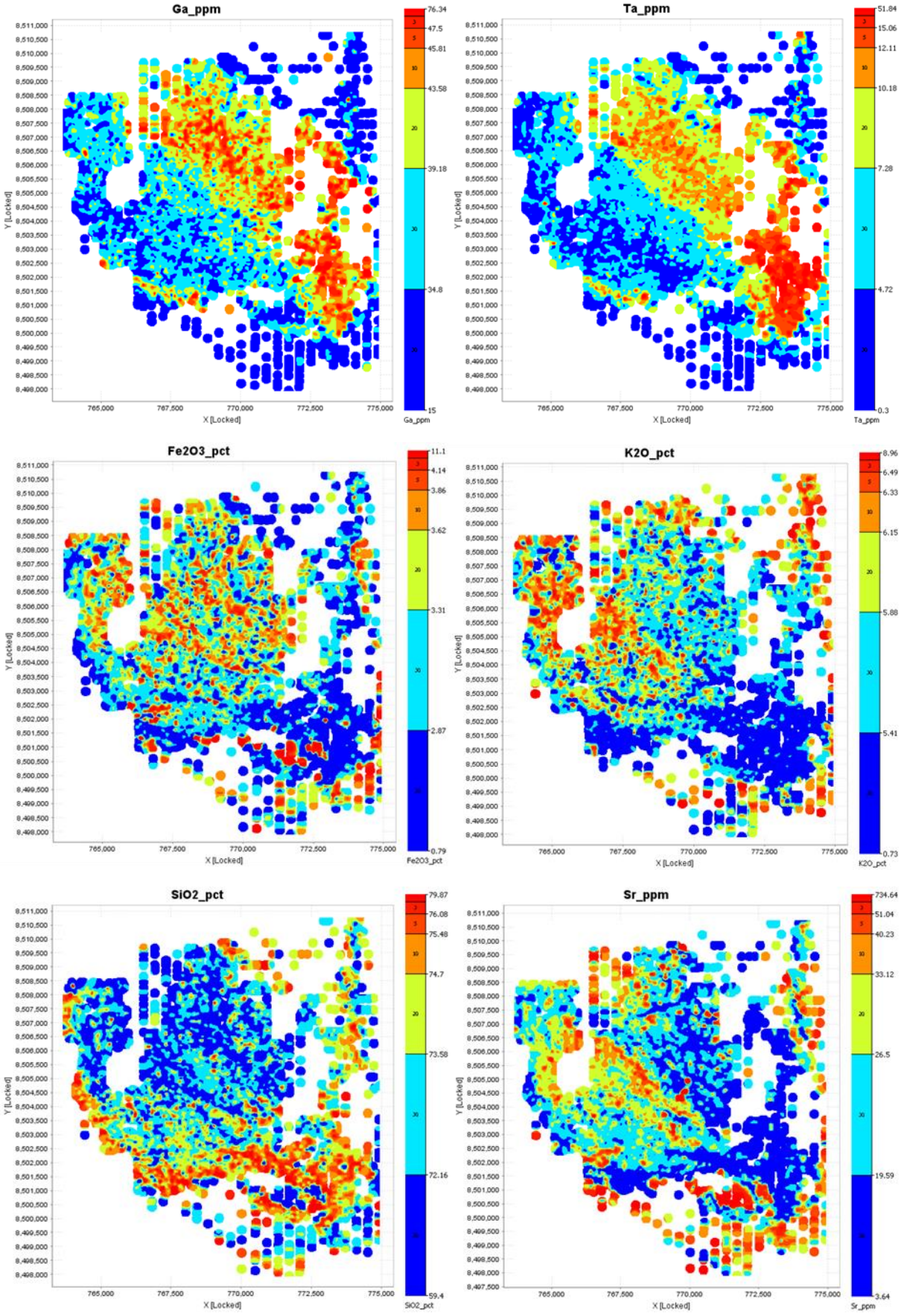
DDH0004

From	To	Lithology	La	Ce	Pr	Nb	Sm	Eu	Gd	Tb	Dy	Ho	Er	Tm	Yb	Lu	Y
m	m		ppm	ppm	ppm	ppm	ppm	ppm	ppm	ppm	ppm	ppm	ppm	ppm	ppm	ppm	ppm
26.0	27.0	Granite	453	409	81.4	312	64.3	4.72	76.5	13.3	80.8	16.3	44.8	6.06	39.4	5.37	454
27.0	28.5	Granite	294	420	57.7	212	41.9	2.69	48.8	8.65	54.7	12.1	35.7	5.26	35.8	4.96	351
28.5	30.0	Granite	243	377	47.2	165	32.5	2.80	42.1	7.38	47.4	10.5	32.0	4.42	32.8	4.96	302
30.0	31.5	Granite	253	584	49.5	178	35.2	2.44	40.5	7.72	48.6	11.3	34.8	5.32	36.6	5.01	322
31.5	33.0	Granite	217	554	41.6	148	27.8	2.17	36.6	7.19	50.6	12.3	40.5	6.00	42.1	6.20	398
33.0	34.5	Granite	194	574	37.0	133	26.3	2.02	36.4	7.39	54.8	14.4	48.5	7.55	50.5	7.73	505
34.5	36.0	Granite	219	396	45.0	156	30.5	1.76	31.4	5.52	34.7	7.48	21.8	3.13	19.3	2.94	215
36.0	37.5	Granite	223	428	46.0	163	32.3	1.83	34.1	6.00	38.8	9.11	29.6	4.18	28.3	4.21	297
37.5	39.0	Granite	249	491	51.0	179	34.1	1.97	34.0	6.47	41.3	9.73	31.2	4.73	30.4	4.60	353
39.0	40.5	Granite	222	437	45.4	161	31.0	2.01	34.3	6.40	40.7	10.1	32.1	4.65	31.1	4.57	346
40.5	42.0	Granite	202	425	40.9	140	26.4	1.43	26.9	4.99	31.8	7.97	26.7	3.94	25.0	3.79	275
42.0	43.5	Granite	192	395	39.0	133	25.2	1.70	29.4	5.28	33.7	8.12	26.2	3.82	24.5	3.49	253
43.5	45.0	Granite	181	343	37.0	128	23.3	1.63	28.2	5.04	32.1	8.18	25.1	3.84	24.5	3.54	287
45.0	46.5	Granite	213	413	43.0	144	27.7	1.73	30.7	5.31	33.0	7.35	22.9	3.42	20.5	2.87	230
46.5	48.0	Granite	247	477	51.5	180	33.4	1.55	29.0	5.10	33.3	7.89	25.2	3.53	21.7	3.14	285
48.0	49.5	Granite	257	435	52.9	193	36.8	1.73	33.0	5.86	36.8	8.80	28.6	4.19	27.0	3.96	301
49.5	51.0	Granite	229	436	47.3	166	31.8	1.52	27.0	5.20	31.9	7.38	22.8	3.38	21.2	3.20	286
51.0	52.5	Granite	216	407	45.0	158	29.9	1.57	28.6	5.07	32.8	7.76	24.2	3.47	21.3	3.23	260
52.5	54.0	Granite	215	426	43.9	150	28.9	1.51	26.5	4.78	29.5	6.90	20.8	2.93	18.8	2.82	224
54.0	55.5	Granite	207	401	42.3	147	27.8	1.45	26.0	4.48	27.2	6.21	18.75	2.61	17.25	2.38	199
55.5	57.0	Granite	212	411	43.0	147	28.2	1.53	26.5	4.52	27.3	5.91	18.0	2.54	16.2	2.28	182
57.0	58.5	Granite	195	389	42.7	135	25.1	1.80	24.9	4.12	25.1	5.47	15.8	2.20	14.6	2.12	152
58.5	59.5	Granite	206	395	42.6	137	25.6	1.79	24.9	4.25	25.6	5.66	17.4	2.44	16.1	2.32	172
59.5	60.5	Granite	224	399	46.2	150	26.9	1.82	28.2	4.59	27.0	6.20	18.0	2.64	16.5	2.28	186
60.5	61.6	Granite	189	357	39.3	127	23.8	1.79	24.3	4.24	26.0	5.92	18.4	2.65	18.8	2.76	189
61.6	63.0	Pegmatite	8.50	13.3	1.87	7.80	2.80	0.72	7.09	1.74	14.5	4.36	16.4	2.84	20.8	3.32	215
63.0	64.4	Pegmatite	7.70	8.20	1.63	6.20	2.08	0.62	4.16	1.00	8.53	2.60	10.4	1.61	11.7	1.90	86.2

61.6	63.0	Pegmatite	8.50	13.3	1.87	7.80	2.80	0.72	7.09	1.74	14.5	4.36	16.4	2.84	20.8	3.32	215
63.0	64.4	Pegmatite	7.70	8.20	1.63	6.20	2.08	0.62	4.16	1.00	8.53	2.60	10.4	1.61	11.7	1.90	86.2
64.4	65.5	Granite	214	385	43.7	141	26.5	1.62	30.0	5.11	34.4	7.88	27.0	3.97	26.8	4.05	253
65.5	67.0	Pegmatite	9.60	15.1	2.21	7.40	2.26	0.56	4.17	1.23	9.93	2.72	9.5	1.64	11.3	1.55	63.8
67.0	68.0	Pegmatite	5.20	7.30	1.08	3.80	1.46	0.54	3.25	0.95	7.14	2.24	8.4	1.45	10.7	1.71	94.3
68.0	69.0	Pegmatite	168	313	34.1	109	20.9	1.56	19.4	3.33	20.6	4.76	14.8	2.17	14.4	2.02	147
69.0	70.0	Granite	218	435	43.6	142	24.4	2.17	22.5	3.40	21.2	4.64	13.6	1.94	12.3	1.85	128
70.0	71.0	Granite	204	404	40.5	125	22.3	2.32	20.2	3.33	19.7	4.40	12.9	1.80	11.9	1.89	119
71.0	72.0	Granite	183	342	37.2	118	19.7	2.06	18.3	3.18	18.8	4.42	12.8	1.99	13.4	1.97	121
72.0	73.0	Granite	230	407	46.8	146	26.0	2.31	23.3	3.76	22.0	5.08	15.0	2.01	13.3	2.08	145
73.0	74.5	Granite	218	413	44.2	138	22.3	2.14	18.9	3.41	20.4	4.40	13.0	1.87	12.4	1.80	124
74.5	75.5	Granite	247	436	49.6	151	26.8	2.27	23.4	3.92	23.8	5.22	15.7	2.21	14.2	2.18	143
75.5	76.6	Granite	272	501	54.2	168	29.3	2.41	25.6	4.38	25.3	5.65	17.1	2.39	15.8	2.38	163
76.6	77.3	Pegmatite	20.1	53.8	4.74	15.8	3.53	0.74	5.60	1.23	9.49	2.72	9.02	1.48	11.5	1.59	87.1
77.3	78.2	Granite	225	441	44.8	134	24.5	2.39	22.1	3.55	22.1	4.91	15.5	2.08	14.5	2.12	138
78.2	79.5	Pegmatite	197	398	38.8	121	21.0	2.12	19.0	3.16	19.5	4.35	13.1	1.97	13.7	2.09	127
79.5	80.5	Granite	256	483	50.9	159	25.8	2.38	22.4	3.57	20.5	4.22	13.2	1.85	12.6	1.82	124
80.5	81.4	Granite	273	561	54.1	169	28.4	2.80	23.4	3.89	22.8	4.62	12.7	1.82	11.7	1.64	122
81.4	82.5	Granite	228	453	46.9	149	25.0	2.40	22.2	3.67	21.9	4.33	12.5	1.75	11.3	1.68	111
82.5	84.0	Granite	247	478	51.3	164	28.6	2.87	25.1	3.91	21.4	4.06	11.3	1.47	8.5	1.21	104
84.0	85.5	Granite	138	270	28.3	89	15.9	1.68	14.7	2.56	16.0	3.66	11.3	1.83	13.0	1.82	112
85.5	86.9	Granite	147	280	27.7	92	16.1	1.45	15.3	2.52	14.3	3.09	8.9	1.39	9.0	1.28	92.7
86.9	88.0	Granite	203	354	34.4	106	18.0	1.56	17.7	3.01	19.1	4.37	14.0	2.17	14.5	2.16	158
88.0	89.5	Granite	204	368	34.4	107	17.4	1.57	16.1	2.75	16.1	3.37	10.1	1.54	9.8	1.40	104
89.5	91.0	Granite	235	380	40.3	129	21.4	1.75	20.4	3.20	18.1	3.90	10.7	1.67	10.4	1.51	126
91.0	92.5	Granite	204	353	34.3	106	17.5	1.62	17.1	2.73	16.7	3.40	9.9	1.51	9.7	1.37	111
92.5	93.5	Granite	215	397	38.3	121	20.7	1.75	19.6	3.29	18.5	3.78	11.2	1.64	10.3	1.40	118
93.5	94.6	Granite	202	358	36.1	115	20.2	1.57	20.5	3.46	21.1	4.40	13.9	2.15	14.1	2.00	148
94.6	95.4	Pegmatite	23.7	59.6	4.34	14.4	3.30	0.60	5.42	1.33	10.6	3.06	11.5	1.94	15.7	2.15	95.2
95.4	96.5	Granite	217	352	39.2	128	22.8	1.88	20.6	3.22	19.1	3.81	11.4	1.83	11.3	1.68	124
96.5	98.0	Granite	209	334	36.9	116	20.0	1.61	17.7	2.76	16.3	3.30	10.2	1.47	10.1	1.46	109
98.0	99.0	Granite	183	281	32.2	101	17.5	1.64	16.8	2.82	17.0	3.29	10.0	1.50	9.7	1.40	101
99.0	100.2	Granite	207	319	34.4	109	17.6	1.56	15.9	2.59	15.6	3.20	9.52	1.48	9.7	1.35	98.8

B3. Bedrock element maps




Ga_ppm
Ta_ppm
Fe2O3_pct
K2O_pct
SiO2_pct
Sr_ppm
X [Locked]
Y [Locked]

C1 Standards and correction factors

Table C1.1. Standard glasses run as unknowns, element values highlighted in black are present in the standard. Note colour key at bottom.

		Weight%																																		
Standard	**#**	**F**	**Na**	**Mg**	**Al**	**Si**	**P**	**La**	**Ce**	**K**	**Ca**	**Ti**	**Mn**	**Fe**	**Sr**	**Y**	**Zr**	**Nb**	**Ba**	**Pr**	**Nd**	**Sm**	**Gd**	**Hf**	**Th**	**U**	**Ta**	**Cl**	**Tb**	**Dy**	**Ho**	**Er**	**Tm**	**Yb**	**Lu**	**O**	**Total**
Wolastonite	1	0.02	0.00	0.05	0.00	**24.34**	0.01	0.01	0.01	0.01	**34.31**	0.01	**0.25**	0.04	0.06	-0.08	-0.02	-0.02	-0.02	0.03	-0.06	0.01	-0.01	0.00	-0.02	0.00	0.01	0.00	-0.01	-0.03	0.01	-0.03	0.01	0.00	0.00	41.53	100.4
Wolastonite	2	-0.02	0.00	0.05	0.00	**24.45**	0.03	0.02	0.01	0.00	**34.40**	0.00	**0.25**	0.02	0.03	-0.09	-0.03	0.00	0.00	0.00	-0.05	0.00	0.01	-0.01	-0.03	0.03	0.00	0.00	-0.03	-0.01	-0.04	-0.02	0.00	-0.01	0.00	41.69	100.7
Wolastonite	3	-0.01	0.00	0.05	0.01	**24.43**	0.02	0.01	0.04	0.01	**34.15**	0.00	**0.23**	0.03	0.01	-0.08	0.01	-0.04	0.00	0.01	-0.05	0.01	-0.03	-0.05	-0.02	0.02	0.03	0.00	-0.02	-0.03	0.04	-0.04	-0.02	0.01	-0.02	41.56	100.3
Wolastonite	4	0.00	0.01	0.03	0.00	**24.32**	0.02	0.01	0.01	-0.02	**34.37**	-0.01	**0.25**	0.03	0.05	-0.09	-0.01	-0.01	-0.02	0.02	-0.04	0.02	0.05	-0.03	0.01	0.07	0.00	0.00	0.01	0.01	0.05	-0.02	0.00	0.00	0.00	41.55	100.6
Wolastonite	5	0.02	0.01	0.05	0.00	**24.39**	0.01	-0.02	-0.01	-0.01	**34.20**	0.00	**0.25**	0.04	0.03	-0.10	0.00	-0.01	-0.02	0.01	-0.04	0.01	-0.03	-0.02	0.00	0.00	0.00	0.00	-0.02	-0.02	-0.04	-0.01	0.02	0.02	-0.01	41.50	100.2
KBr	6	-0.06	0.00	-0.36	8.26	0.05	0.00	0.02	0.05	**32.33**	-0.11	0.01	0.01	-0.01	-0.02	-0.01	-0.01	0.00	-0.02	0.02	-0.11	0.02	-0.09	-0.03	0.00	1.98	0.03	0.03	-0.54	-0.01	-0.11	-0.03	0.01	0.00	-0.01	13.89	55.2
KBr	7	-0.02	0.01	-0.35	8.24	0.05	-0.01	-0.03	0.02	**32.38**	-0.07	0.01	0.00	0.02	-0.03	-0.04	-0.01	-0.02	0.02	-0.03	-0.12	0.07	-0.10	-0.07	-0.01	1.94	-0.02	0.03	-0.58	-0.05	0.00	-0.02	0.03	0.00	0.01	13.85	55.1
KBr	8	0.00	0.01	-0.36	8.25	0.07	-0.01	-0.01	0.04	**32.46**	-0.08	0.01	0.02	0.00	-0.02	-0.07	0.03	-0.04	0.02	0.02	-0.10	0.01	-0.10	-0.04	-0.01	2.05	0.00	0.02	-0.58	-0.05	0.03	-0.03	0.02	-0.01	0.00	13.91	55.4
KBr	9	0.05	0.01	-0.35	8.24	0.04	0.00	0.01	0.03	**32.58**	-0.07	0.01	0.00	0.01	0.01	-0.04	-0.01	0.00	-0.02	-0.01	-0.11	0.06	-0.13	-0.12	-0.06	2.27	0.01	0.03	-0.59	-0.10	-0.03	-0.02	-0.04	0.02	0.02	13.92	55.6
KBr	10	-0.03	0.00	-0.37	8.25	0.04	0.00	0.01	0.03	**32.27**	-0.07	-0.01	0.01	0.00	-0.05	-0.03	-0.01	-0.01	0.00	-0.02	-0.13	0.02	-0.12	-0.04	-0.02	1.89	0.01	0.03	-0.57	-0.01	-0.04	-0.04	0.00	0.01	0.00	13.80	54.8
MnTiO3	11	-0.07	0.04	0.01	0.03	0.04	0.01	-0.48	0.21	0.00	0.00	**32.32**	**35.49**	0.06	-0.01	-0.01	0.01	0.26	0.37	-0.02	-0.06	0.01	-0.14	-0.06	-0.36	0.02	0.00	0.02	-0.56	0.04	-0.01	0.01	-0.02	-0.01	0.04	31.97	99.1
MnTiO3	12	0.00	0.02	0.01	0.01	0.04	0.00	-0.43	0.19	0.00	0.01	**31.62**	**36.43**	0.07	-0.01	0.01	-0.03	0.22	0.36	-0.04	-0.05	0.05	-0.13	0.00	-0.35	0.07	0.00	0.02	-0.48	-0.04	-0.08	0.03	0.00	0.01	0.00	31.76	99.3
MnTiO3	13	-0.07	0.04	-0.01	0.01	0.03	-0.01	-0.45	0.21	0.00	0.02	**32.82**	**34.81**	0.06	0.04	-0.02	0.04	0.24	0.36	-0.05	-0.07	0.03	-0.15	-0.07	-0.33	-0.01	0.01	0.00	-0.47	-0.02	0.00	-0.04	0.00	-0.01	-0.02	32.08	99.0
MnTiO3	14	-0.02	-0.03	0.01	0.01	0.04	-0.01	-0.45	0.21	0.00	0.01	**31.97**	**35.82**	0.07	0.02	-0.05	0.01	0.23	0.35	0.02	-0.07	0.06	-0.16	-0.04	-0.38	0.01	-0.03	0.00	-0.54	0.03	-0.01	-0.01	-0.01	0.00	0.00	31.77	98.8
MnTiO3	15	0.00	0.00	0.01	0.00	0.04	0.00	-0.48	0.18	0.00	-0.01	**31.59**	**36.50**	0.05	-0.02	0.01	0.00	0.24	0.39	-0.03	-0.08	0.05	-0.10	-0.01	-0.38	-0.03	0.01	-0.01	-0.55	-0.04	0.02	-0.04	-0.01	0.01	-0.03	31.72	99.0
Baryte	16	-0.01	0.08	-0.02	0.43	0.04	0.01	-0.16	23.84	0.02	0.00	0.12	0.00	-0.01	0.28	-0.02	-0.05	0.06	**53.42**	0.00	0.00	0.00	-0.02	-0.07	-0.02	0.09	0.02	-0.03	-0.03	-0.05	0.03	0.00	0.01	-0.01	0.01	10.85	88.8
Baryte	17	-0.01	0.07	-0.02	0.39	0.05	-0.01	-0.13	23.88	0.01	-0.01	0.15	0.00	-0.01	0.29	-0.04	0.02	0.07	**53.58**	0.00	-0.05	0.00	-0.03	0.02	0.02	0.03	0.01	-0.01	-0.04	-0.02	-0.09	0.04	0.00	-0.02	0.02	10.86	89.0
Baryte	18	-0.01	0.04	-0.01	0.40	0.06	-0.01	-0.12	23.71	0.01	0.01	0.14	0.00	0.01	0.31	-0.03	-0.03	0.03	**53.48**	0.00	-0.02	0.00	-0.01	-0.04	-0.02	0.01	-0.02	-0.02	-0.04	0.04	-0.01	0.02	-0.01	-0.02	0.05	10.84	88.7
Baryte	19	-0.01	0.09	-0.02	0.42	0.06	0.00	-0.13	23.86	0.01	-0.01	0.15	0.00	0.00	0.27	0.01	0.02	0.08	**53.74**	0.00	-0.03	0.00	-0.05	-0.01	0.02	0.08	-0.04	-0.03	-0.04	-0.02	-0.04	0.01	-0.02	-0.01	0.02	10.95	89.3
Baryte	20	-0.01	0.08	-0.01	0.43	0.04	-0.01	-0.12	23.77	0.01	0.01	0.15	0.00	0.01	0.35	-0.04	-0.05	0.07	**53.73**	0.00	-0.04	0.00	-0.03	-0.01	-0.01	0.03	-0.03	-0.03	-0.04	0.05	-0.04	0.02	-0.02	-0.02	-0.03	10.88	89.1
Topaz	21	**22.07**	0.00	-0.01	**29.97**	**15.03**	0.00	0.01	0.02	0.00	0.01	0.01	-0.01	0.01	0.02	-0.03	-0.01	-0.01	0.00	0.00	-0.06	-0.01	0.00	-0.01	-0.01	0.01	-0.02	0.00	-0.01	-0.02	0.01	0.01	0.00	-0.02	0.01	43.76	110.7
Topaz	22	**21.67**	0.01	-0.01	**29.98**	**15.00**	0.01	-0.01	0.00	0.02	0.01	0.00	-0.01	0.00	0.00	-0.06	0.01	-0.01	-0.02	0.01	-0.02	0.02	0.03	-0.03	0.00	0.01	-0.01	0.00	-0.02	0.04	-0.05	0.04	-0.02	-0.03	0.01	43.76	110.4
Topaz	23	**21.73**	0.00	-0.01	**29.97**	**14.96**	-0.01	0.00	0.01	0.02	-0.01	0.00	0.00	0.01	0.03	-0.05	0.02	0.00	0.00	0.00	-0.03	0.01	-0.01	-0.02	-0.02	-0.01	-0.01	0.00	-0.02	-0.02	0.00	0.01	-0.02	-0.01	0.00	43.66	110.2
Topaz	24	**21.82**	0.01	0.00	**29.95**	**14.97**	0.00	-0.02	-0.01	0.03	0.00	0.01	-0.01	0.02	0.02	-0.05	-0.02	0.01	-0.01	-0.02	-0.03	0.02	-0.01	-0.04	-0.01	0.02	0.00	0.00	0.00	-0.04	0.00	0.00	-0.01	-0.01	0.02	43.67	110.3
Topaz	25	**21.58**	0.00	0.00	**29.92**	**14.98**	0.00	-0.01	0.00	0.01	-0.01	0.01	0.00	0.00	-0.01	-0.04	-0.03	-0.02	0.01	-0.02	-0.03	0.01	-0.01	0.00	-0.02	0.02	-0.01	0.01	-0.01	0.01	0.00	0.00	0.00	-0.01	0.01	43.64	110.0
Monazite	26	0.37	-0.04	-0.01	0.00	**1.11**	**11.87**	**11.15**	**23.39**	-0.01	**0.66**	0.00	0.02	0.00	-0.01	**0.15**	0.00	-0.06	0.02	**2.49**	**8.54**	**1.39**	**0.40**	-0.07	**11.68**	**0.22**	-0.01	0.04	**0.07**	**0.07**	0.03	0.04	**0.10**	0.01	0.00	26.58	100.2
Monazite	27	0.38	-0.04	-0.03	-0.03	**1.12**	**11.89**	**11.12**	**23.34**	-0.01	**0.69**	-0.01	0.00	0.01	-0.01	**0.10**	0.00	-0.03	0.07	**2.38**	**8.58**	**1.35**	**0.42**	0.01	**11.63**	**0.20**	0.00	0.04	**0.06**	**0.12**	0.01	0.06	**0.08**	-0.03	0.00	26.57	100.0
Monazite	28	0.41	-0.06	-0.02	-0.02	**1.12**	**12.00**	**11.15**	**23.39**	-0.01	**0.68**	0.01	0.00	0.02	0.00	**0.15**	0.00	-0.05	0.09	**2.47**	**8.52**	**1.33**	**0.49**	-0.04	**11.74**	**0.31**	-0.03	0.02	**0.08**	**0.07**	0.02	-0.02	**0.10**	-0.01	0.01	26.76	100.7
Monazite	29	0.42	-0.07	-0.01	-0.02	**1.12**	**12.00**	**11.11**	**23.40**	-0.01	**0.67**	0.00	-0.01	0.02	-0.01	**0.06**	0.00	-0.03	0.07	**2.43**	**8.56**	**1.34**	**0.45**	-0.02	**11.68**	**0.27**	-0.04	0.04	**0.07**	**0.08**	-0.02	0.07	**0.13**	-0.03	-0.02	26.74	100.5
Monazite	30	0.41	-0.06	-0.01	-0.02	**1.14**	**11.94**	**11.20**	**23.41**	-0.02	**0.67**	0.01	0.00	0.01	-0.01	**0.14**	0.00	-0.04	0.07	**2.47**	**8.57**	**1.40**	**0.42**	-0.04	**11.69**	**0.18**	0.00	0.06	**0.03**	**0.04**	-0.03	0.05	**0.07**	-0.03	0.02	26.71	100.5
LAG	31	-0.01	0.00	-0.01	**5.47**	**25.87**	-0.01	**14.23**	-0.20	0.02	**12.04**	0.00	0.00	0.01	0.04	-0.07	0.00	0.01	0.02	0.03	-0.02	0.00	0.03	0.05	0.01	0.02	0.01	0.00	0.01	0.02	0.03	-0.04	0.01	0.01	0.00	41.59	99.2
LAG	32	-0.01	0.01	0.00	**5.50**	**25.89**	0.00	**14.21**	-0.18	0.03	**12.12**	-0.01	-0.01	0.01	0.04	-0.08	-0.02	-0.01	-0.02	0.05	-0.04	0.05	0.02	0.00	-0.02	0.04	-0.05	0.00	0.01	0.01	0.04	0.02	-0.01	-0.01	-0.01	41.64	99.2
LAG	33	-0.02	0.01	0.00	**5.48**	**25.97**	0.02	**14.23**	-0.20	0.00	**12.02**	-0.01	0.00	0.01	0.04	-0.08	-0.03	0.01	0.02	-0.02	-0.03	0.04	-0.01	-0.04	-0.03	0.00	0.02	0.00	0.01	-0.05	0.07	-0.02	0.00	-0.02	0.00	41.68	99.1
LAG	34	-0.01	0.01	0.00	**5.52**	**26.02**	0.01	**14.28**	-0.18	-0.02	**12.09**	0.00	-0.01	0.02	0.05	-0.05	0.03	-0.02	0.01	0.02	-0.05	0.02	0.01	0.00	0.00	0.02	0.00	0.00	0.00	0.02	0.00	-0.04	-0.02	-0.01	0.02	41.83	99.6
LAG	35	-0.01	-0.01	-0.01	**5.47**	**25.81**	0.00	**14.19**	-0.16	0.00	**12.14**	-0.01	0.00	0.02	0.02	-0.09	0.02	0.00	0.01	0.01	-0.06	0.01	0.01	-0.01	-0.01	0.04	-0.02	0.00	0.02	0.03	-0.05	0.04	0.00	0.00	-0.02	41.52	98.9
CEG	36	0.34	0.04	0.00	**5.27**	**25.16**	0.02	-0.01	**16.77**	-0.01	**11.63**	0.01	0.00	0.01	0.02	-0.08	0.02	0.00	0.00	-0.02	0.11	0.20	-0.02	0.01	0.00	0.06	0.02	0.01	0.00	-0.03	0.01	0.04	0.00	-0.01	0.00	40.95	100.5
CEG	37	0.31	0.02	0.00	**5.31**	**25.26**	0.02	-0.02	**16.78**	0.01	**11.54**	0.00	-0.01	-0.01	0.01	-0.10	-0.01	-0.03	0.00	0.01	0.10	0.21	0.01	0.03	-0.01	0.06	0.02	0.00	0.00	-0.02	0.01	-0.06	0.01	0.00	-0.04	41.03	100.5
CEG	38	0.31	0.01	0.00	**5.29**	**25.18**	0.02	-0.02	**16.80**	-0.01	**11.55**	-0.01	-0.02	0.00	0.04	-0.10	-0.03	-0.01	-0.02	0.01	0.08	0.25	-0.01	-0.06	0.01	0.01	0.00	-0.01	0.03	0.01	-0.01	0.02	-0.01	0.02	0.00	40.91	100.2
CEG	39	0.35	0.03	0.01	**5.29**	**25.25**	0.01	0.00	**16.82**	0.00	**11.64**	0.00	0.00	0.01	0.03	-0.09	-0.03	-0.03	-0.02	0.00	0.14	0.23	0.00	-0.05	-0.01	0.05	0.04	0.01	-0.01	-0.02	0.04	0.01	0.01	-0.02	0.00	41.03	100.7
CEG	40	0.35	0.03	0.00	**5.31**	**25.32**	0.01	-0.01	**16.84**	0.01	**11.53**	-0.01	-0.01	0.01	0.03	-0.14	0.00	-0.01	-0.02	0.01	0.11	0.18	0.00	-0.03	-0.01	0.01	0.03	0.01	0.02	-0.01	-0.01	0.01	-0.01	-0.02	0.02	41.09	100.7
SrTiO3	41	-0.03	0.00	0.01	0.00	0.06	-0.01	-0.38	0.19	-0.01	-0.01	**26.25**	-0.01	-0.01	**48.11**	0.00	0.01	0.02	0.26	-0.04	-0.10	0.05	0.02	0.01	-0.01	0.02	-0.02	-0.01	-0.03	0.05	-0.08	0.03	-0.01	0.02	-0.02	26.36	100.7
SrTiO3	42	-0.01	0.01	0.01	0.00	0.04	-0.01	-0.38	0.17	0.02	0.00	**26.25**	0.00	0.01	**48.68**	0.00	0.00	0.02	0.31	-0.02	-0.10	0.03	0.01	-0.01	-0.03	0.05	-0.02	0.00	0.01	-0.01	-0.06	0.07	-0.02	0.03	0.01	26.46	101.5
SrTiO3	43	-0.01	-0.01	0.00	0.01	0.03	-0.01	-0.39	0.22	0.01	-0.01	**26.29**	-0.01	0.01	**48.49**	0.00	0.01	0.02	0.31	-0.04	-0.17	0.04	0.01	0.03	-0.05	0.08	-0.01	0.00	-0.02	-0.05	-0.01	-0.01	0.01	0.01	0.02	26.43	101.2
SrTiO3	44	0.01	0.02	0.01	0.00	0.03	-0.01	-0.41	0.17	0.02	0.01	**26.45**	-0.02	0.02	**48.35**	0.00	0.01	-0.02	0.28	0.01	-0.12	0.05	0.02	-0.07	-0.02	0.01	-0.04	0.01	-0.03	0.03	-0.05	-0.01	0.00	0.00	0.03	26.48	101.2
SrTiO3	45	0.00	0.00	0.00	0.00	0.02	-0.02	-0.38	0.18	0.03	-0.01	**26.30**	-0.02	0.00	**47.87**	0.00	-0.03	0.02	0.33	-0.01	-0.08	-0.01	-0.01	-0.01	0.01	-0.02	0.00	0.00	-0.02	-0.01	0.03	0.01	0.00	0.01	0.00	26.28	100.5
Zircon	46	-0.07	-0.04	**0.00**	-0.02	**15.16**	0.01	-0.01	-0.01	0.00	0.01	0.01	0.01	0.01	0.03	-0.28	**49.04**	-0.01	0.01	0.00	-0.08	0.02	0.02	**1.08**	-0.02	-0.02	0.00	0.00	0.01	-0.01	-0.02	0.02	0.01	0.02	-0.01	34.59	99.5
Zircon	47	-0.08	-0.02	**0.00**	**0.00**	**15.16**	0.01	-0.01	0.00	0.01	0.01	0.00	0.01	0.03	0.02	-0.31	**49.48**	-0.01	-0.02	-0.03	-0.06	0.04	0.02	**1.06**	-0.03	0.00	-0.03	0.01	0.01	-0.05	-0.04	0.01	0.01	0.06	0.00	34.75	100.0
Zircon	48	-0.04	-0.06	**0.00**	**0.00**	**15.31**	0.01	-0.02	0.01	0.01	0.01	0.00	0.02	0.01	0.05	-0.33	**48.89**	-0.02	-0.04	0.03	-0.05	0.02	0.00	**1.06**	0.02	-0.01	0.04	-0.02	0.00	0.01	-0.02	-0.07	-0.05	0.04	-0.02	34.69	99.5
Zircon	49	-0.06	-0.06	**0.00**	**-0.01**	**15.36**	0.01	0.01	0.03	-0.01	0.01	-0.01	0.04	0.04	0.01	-0.30	**49.13**	-0.03	0.05	0.00	-0.08	-0.02	-0.06	**1.09**	-0.04	0.04	0.04	0.00	0.00	-0.04	-0.02	-0.03	0.00	0.05	0.00	34.83	100.0
Zircon	50	-0.08	-0.04	**0.01**	**0.00**	**15.29**	0.03	-0.02	0.02	-0.02	0.00	0.01	0.02	0.02	0.02	-0.30	**49.06**	-0.03	0.00	-0.02	-0.09	0.02	-0.01	**1.09**	0.03	0.07	0.02	0.00	0.00	0.04	-0.04	0.01	0.01	0.06	0.03	34.79	100.0

Notes: peak overla background overlap not applicable - e.g. because element not in list

Weight%

Standard	#	F	Na	Mg	Al	Si	P	La	Ce	K	Ca	Ti	Mn	Fe	Sr	Y	Zr	Nb	Ba	Pr	Nd	Sm	Gd	Hf	Th	U	Ta	Cl	Tb	Dy	Ho	Er	Tm	Yb	Lu	O	Total
PNb	51	-0.03	0.01	-0.01	-0.02	0.02	-0.18	0.03	0.02	0.00	0.01	-0.01	0.00	0.06	0.01	0.13	-0.01	**99.84**	0.04	0.02	-0.15	0.04	0.00	-0.02	-0.04	0.02	-0.08	-0.01	0.00	-0.02	-0.01	0.01	-0.04	0.01	0.02	42.77	142.4
PNb	52	-0.03	0.01	0.01	0.00	0.04	-0.17	-0.01	0.02	-0.02	0.00	0.00	-0.01	0.08	0.02	0.09	-0.03	**99.98**	0.02	0.03	-0.14	0.02	0.05	-0.06	-0.03	0.06	-0.09	-0.01	-0.04	-0.02	0.03	0.05	-0.08	0.01	-0.02	42.87	142.7
PNb	53	0.00	-0.01	0.01	-0.01	0.01	-0.17	0.01	0.05	0.02	-0.01	-0.01	-0.01	0.07	0.04	0.09	-0.04	**99.40**	0.02	0.02	-0.17	0.03	-0.01	0.02	0.02	0.09	-0.07	0.01	-0.02	-0.06	-0.01	-0.01	-0.03	0.01	-0.02	42.59	141.9
PNb	54	0.00	0.00	0.00	-0.01	0.01	-0.16	-0.03	0.02	0.01	0.01	0.00	-0.01	0.18	0.00	0.12	-0.03	**100.0**	0.02	0.01	-0.12	0.06	0.00	0.01	-0.04	0.05	-0.14	-0.01	-0.02	0.03	-0.01	0.12	0.01	-0.02	-0.04	42.90	142.9
PNb	55	0.01	-0.01	-0.01	-0.01	0.01	-0.18	-0.03	0.08	-0.02	0.00	0.00	-0.01	0.06	0.04	0.11	-0.04	**100.2**	-0.03	0.01	-0.15	0.04	0.07	-0.04	0.00	0.03	-0.02	0.00	-0.02	-0.03	-0.03	-0.05	-0.01	-0.01	-0.04	42.91	142.8
Uranium Oxi	56	-0.02	-0.01	0.03	-0.04	0.01	-0.02	-0.02	0.06	0.16	0.02	0.02	-0.02	0.01	-0.27	-0.10	-0.03	-0.02	-0.19	-0.04	-0.21	0.03	0.03	-0.03	0.01	**88.43**	-0.01	-0.01	-0.06	-0.05	-0.04	-0.03	-0.02	-0.01	0.05	11.74	99.3
Uranium Oxi	57	-0.02	-0.01	0.01	-0.03	0.00	-0.01	-0.01	0.08	0.20	0.02	0.03	-0.03	0.01	-0.29	-0.07	0.01	0.02	-0.19	-0.06	-0.25	0.05	-0.04	-0.02	0.00	**87.90**	0.00	0.00	-0.03	-0.11	-0.04	-0.02	-0.04	-0.02	0.03	11.68	98.7
Uranium Oxi	58	-0.03	0.02	0.03	-0.04	0.02	0.00	0.02	0.06	0.15	0.01	0.01	-0.05	0.02	-0.30	-0.04	0.02	-0.01	-0.18	-0.08	-0.21	0.04	0.00	-0.03	-0.02	**88.28**	0.03	-0.01	-0.04	-0.01	-0.02	-0.07	0.00	0.00	0.04	11.79	99.4
Uranium Oxi	59	-0.01	0.01	0.03	-0.05	0.01	0.00	0.00	0.08	0.18	0.01	0.02	-0.01	0.00	-0.32	-0.08	-0.01	-0.04	-0.21	-0.06	-0.22	0.00	0.01	-0.01	0.00	**88.39**	-0.06	-0.01	-0.02	-0.02	-0.01	0.11	-0.02	-0.04	0.00	11.75	99.4
Uranium Oxi	60	0.00	-0.01	0.03	-0.03	0.00	-0.01	-0.03	0.07	0.20	0.01	0.03	-0.02	0.02	-0.27	-0.05	0.01	0.01	-0.19	-0.03	-0.17	0.06	-0.03	-0.05	-0.03	**88.08**	0.00	0.00	-0.05	0.02	-0.01	-0.04	-0.01	-0.04	-0.03	11.75	99.2
NaCl	61	0.00	**40.79**	-0.01	-0.01	0.02	-0.01	0.00	0.02	-0.01	0.00	0.00	-0.01	0.01	0.03	-0.02	-0.01	0.02	-0.02	0.02	-0.04	0.00	0.02	0.00	0.03	0.00	-0.04	**59.07**	-0.02	0.04	-0.01	0.04	-0.04	0.01	-0.01	14.19	114.0
NaCl	62	0.01	**41.80**	0.00	0.00	0.01	0.00	0.01	0.02	-0.02	-0.01	0.00	0.00	0.01	-0.01	-0.03	-0.03	0.00	-0.01	0.03	-0.04	0.01	0.03	-0.03	0.03	-0.02	-0.04	**59.68**	-0.04	-0.03	-0.01	-0.04	0.02	-0.03	-0.01	14.51	115.8
NaCl	63	-0.02	**41.34**	0.00	-0.01	0.02	0.00	-0.01	0.01	-0.01	0.00	-0.01	-0.01	0.01	-0.01	-0.04	0.00	0.01	0.01	0.02	-0.06	0.00	0.03	0.00	0.01	-0.01	0.04	**59.95**	-0.01	-0.05	-0.01	0.02	0.00	0.00	-0.04	14.37	115.5
NaCl	64	-0.02	**41.59**	-0.01	-0.01	0.02	-0.01	0.02	-0.01	0.02	0.00	0.00	-0.01	0.00	-0.01	-0.02	0.01	0.01	-0.01	-0.02	-0.04	0.03	-0.03	-0.06	0.00	0.00	-0.01	**59.63**	-0.02	0.03	-0.05	-0.02	0.01	0.01	0.03	14.45	115.5
NaCl	65	-0.01	**41.56**	-0.02	-0.01	0.02	-0.01	0.01	0.00	0.01	0.01	0.00	-0.01	0.01	0.03	-0.03	0.00	0.01	0.00	0.03	-0.06	0.02	-0.04	0.01	-0.01	0.07	-0.03	**59.69**	-0.01	-0.01	-0.03	0.02	0.02	0.01	0.00	14.45	115.7
Jadeite	66	-0.01	**11.04**	0.05	**13.42**	**28.31**	0.00	0.02	-0.01	-0.02	0.09	0.00	-0.01	0.14	0.02	-0.08	0.02	-0.01	0.02	-0.04	-0.04	0.02	0.02	-0.01	0.00	0.06	0.02	-0.01	-0.01	-0.04	-0.04	-0.02	-0.02	-0.02	0.02	48.12	101.0
Jadeite	67	0.00	**11.04**	0.03	**13.45**	**28.20**	0.01	-0.01	0.01	0.02	0.06	0.00	-0.01	0.03	0.00	-0.07	-0.01	0.00	-0.01	-0.01	-0.04	-0.01	0.02	-0.03	0.01	0.06	-0.02	0.00	0.00	0.01	0.02	-0.01	-0.01	0.00	0.01	47.98	100.7
Jadeite	68	-0.02	**11.07**	0.00	**13.56**	**28.14**	0.00	0.00	0.00	0.00	0.01	0.00	-0.01	0.01	0.02	-0.07	-0.02	0.01	-0.01	-0.01	-0.04	0.01	0.00	0.02	-0.01	0.01	-0.01	0.00	-0.01	-0.01	0.01	0.00	-0.01	-0.02	0.03	47.97	100.6
Jadeite	69	-0.05	**11.03**	0.05	**13.68**	**29.19**	0.00	-0.01	0.01	-0.01	0.06	0.01	0.01	0.13	0.03	-0.08	0.00	0.01	0.00	0.04	-0.03	0.01	0.01	0.01	0.00	0.04	-0.03	0.00	0.01	-0.03	0.03	0.01	0.01	-0.01	0.01	49.36	103.5
Jadeite	70	0.02	**11.02**	0.09	**13.32**	**28.14**	-0.01	0.00	0.01	0.02	0.15	0.00	-0.01	0.13	0.01	-0.10	0.02	-0.01	-0.02	-0.01	-0.03	0.00	-0.02	0.01	0.00	0.00	-0.01	0.00	0.00	-0.01	0.00	-0.02	-0.01	-0.03	0.04	47.86	100.6
Forsterite	71	0.01	0.00	**34.52**	-0.01	**20.14**	0.00	0.01	-0.01	0.00	-0.01	0.00	0.00	-0.01	0.01	-0.07	-0.02	0.02	0.01	-0.03	-0.05	0.00	-0.02	0.01	-0.02	0.01	-0.04	0.01	-0.01	-0.02	0.00	-0.07	-0.01	-0.02	-0.03	45.60	99.9
Forsterite	72	0.00	-0.01	**34.48**	-0.01	**20.14**	0.00	-0.01	0.01	-0.01	0.00	0.00	-0.01	0.00	-0.02	-0.08	0.02	0.00	0.00	0.01	-0.05	0.01	0.00	-0.02	-0.02	0.00	0.01	0.00	0.02	-0.03	0.00	0.01	-0.02	-0.01	-0.04	45.60	100.0
Forsterite	73	-0.03	-0.01	**34.41**	-0.01	**20.12**	0.01	0.00	0.02	-0.01	-0.01	0.01	-0.01	0.00	0.00	-0.05	0.00	0.01	-0.02	0.02	-0.05	0.03	0.00	0.02	-0.04	0.00	-0.04	0.00	0.01	-0.02	-0.01	-0.02	-0.01	-0.01	-0.01	45.54	99.8
Forsterite	74	-0.03	0.00	**34.56**	-0.01	**20.11**	0.00	0.00	0.00	-0.01	-0.01	-0.01	-0.01	0.00	0.02	-0.08	-0.01	0.03	-0.02	0.03	-0.04	0.02	0.01	-0.06	-0.01	0.03	-0.02	0.00	-0.02	-0.04	-0.01	-0.07	-0.01	-0.03	0.01	45.60	99.9
Forsterite	75	-0.03	0.01	**34.39**	-0.01	**20.08**	0.00	-0.01	0.00	0.01	0.00	0.00	-0.01	0.01	-0.01	-0.06	0.04	0.00	-0.01	-0.01	-0.03	0.00	-0.01	-0.02	-0.01	0.07	-0.02	0.01	0.00	0.00	-0.06	-0.01	0.00	0.00	0.00	45.49	99.8
Corundum	76	0.03	-0.01	0.00	**52.95**	0.03	0.00	0.00	0.02	-0.01	0.01	0.00	0.00	0.01	-0.02	0.01	-0.01	0.00	-0.02	0.01	-0.05	-0.01	0.00	-0.02	0.00	0.01	-0.01	0.01	0.02	-0.03	0.02	-0.04	0.00	-0.02	0.00	47.11	100.0
Corundum	77	-0.01	0.00	0.00	**52.87**	0.02	0.01	-0.02	-0.01	0.01	-0.01	0.00	-0.01	0.00	0.00	-0.03	0.01	0.02	0.01	0.04	-0.03	0.01	0.00	0.01	-0.01	-0.04	0.01	0.00	0.01	0.01	0.00	0.00	-0.02	0.01	0.00	47.06	99.9
Corundum	78	-0.01	-0.01	0.00	**52.82**	0.02	0.00	0.01	-0.01	-0.01	0.00	0.00	0.00	-0.01	-0.01	0.00	-0.01	-0.01	-0.01	0.01	-0.04	0.01	0.00	-0.03	0.00	0.06	0.01	0.00	-0.01	-0.03	0.05	0.01	0.01	0.01	0.01	47.00	99.8
Corundum	79	-0.02	0.00	0.00	**52.85**	0.02	0.00	0.00	0.00	0.01	-0.01	0.00	0.00	0.00	0.00	-0.04	0.02	-0.03	0.01	0.01	-0.01	-0.02	0.03	-0.04	0.01	0.06	0.02	-0.01	-0.01	0.00	-0.02	-0.03	0.01	0.00	-0.01	47.01	99.8
Corundum	80	-0.04	0.00	0.00	**52.96**	0.02	-0.01	0.01	0.00	0.00	0.00	0.00	-0.01	0.01	0.02	-0.02	0.00	0.00	0.00	0.01	-0.06	0.02	-0.02	-0.04	-0.01	0.04	0.01	0.00	0.00	-0.04	0.01	0.05	-0.02	0.01	0.00	47.12	100.0
YYG	81	0.01	0.00	0.01	**6.71**	**24.58**	0.00	0.02	-0.01	0.01	**15.00**	0.00	-0.02	0.02	0.05	**10.85**	-0.03	-0.02	0.00	-0.02	-0.06	0.03	-0.01	0.03	0.01	0.08	-0.02	0.00	0.01	-0.04	-0.01	0.05	0.02	0.01	-0.01	42.89	100.1
YYG	82	-0.02	-0.01	0.00	**6.69**	**24.60**	0.00	0.00	0.00	0.00	**14.97**	0.01	0.01	0.01	0.00	**10.95**	-0.01	-0.05	-0.01	-0.01	-0.04	0.04	0.06	-0.05	0.00	0.04	-0.01	0.00	0.00	0.02	0.04	0.00	-0.01	-0.01	0.00	42.90	100.1
YYG	83	-0.02	0.00	0.00	**6.71**	**24.60**	0.00	0.01	0.02	0.01	**14.91**	0.00	0.00	0.01	0.04	**10.93**	0.01	0.01	0.01	-0.05	-0.07	0.04	-0.02	0.00	0.01	0.01	-0.01	0.01	0.00	-0.02	0.02	0.02	0.00	0.00	0.00	42.92	100.1
YYG	84	0.00	0.00	-0.01	**6.71**	**24.67**	0.00	-0.02	0.01	0.00	**14.90**	-0.01	-0.01	0.01	0.01	**11.05**	0.03	-0.03	-0.01	-0.02	-0.05	0.03	0.03	-0.06	0.00	0.01	0.00	0.01	-0.01	-0.01	-0.07	-0.06	0.01	-0.01	0.00	42.96	100.1
YYG	85	-0.03	-0.01	0.00	**6.74**	**24.53**	0.00	0.01	0.01	0.02	**14.94**	0.00	0.00	0.01	0.03	**10.96**	-0.01	0.01	0.00	-0.04	-0.05	0.02	-0.01	-0.03	-0.02	0.01	-0.02	-0.01	0.00	0.00	0.03	0.00	0.00	0.00	-0.01	42.86	100.0
Fayerlite	86	-0.09	0.01	-0.01	**0.00**	**13.76**	0.00	0.00	0.00	0.00	0.01	0.00	-0.02	**54.60**	0.01	-0.06	0.02	0.02	-0.02	0.05	-0.08	0.01	-0.03	0.00	-0.07	0.04	-0.03	0.01	0.18	-0.09	-0.06	-0.01	0.03	-0.06	-0.03	31.29	99.4
Fayerlite	87	-0.08	0.00	-0.01	**0.01**	**13.75**	0.00	-0.01	-0.01	-0.01	0.00	0.01	-0.01	**54.55**	-0.02	-0.06	-0.03	-0.01	-0.01	0.04	-0.07	0.00	-0.04	-0.07	-0.04	-0.07	-0.01	-0.01	0.15	-0.11	-0.12	-0.07	0.01	-0.04	-0.04	31.18	98.8
Fayerlite	88	-0.07	-0.01	-0.01	**0.00**	**13.74**	-0.01	0.01	0.00	-0.02	-0.01	-0.01	0.00	**54.51**	0.01	-0.07	0.00	0.02	-0.01	0.05	-0.08	0.01	-0.02	-0.02	-0.06	-0.07	0.04	-0.01	0.13	-0.09	-0.06	0.00	0.04	-0.05	-0.01	31.21	99.1
Fayerlite	89	-0.09	-0.01	0.00	**0.00**	**13.75**	-0.01	0.01	0.01	0.00	0.00	-0.01	-0.01	**54.64**	-0.04	-0.03	0.02	0.00	0.00	0.00	-0.07	0.04	0.01	-0.01	-0.04	0.06	0.03	0.01	0.16	-0.10	-0.10	-0.07	-0.01	-0.04	-0.02	31.27	99.4
Fayerlite	90	-0.13	0.01	0.01	**0.02**	**13.71**	-0.01	0.01	0.03	0.00	0.01	0.00	0.00	**54.55**	0.00	-0.02	0.00	-0.01	0.00	-0.03	-0.04	0.00	-0.04	-0.03	-0.05	0.01	-0.02	-0.01	0.13	-0.15	-0.09	-0.01	0.05	-0.02	-0.05	31.21	99.0
PRG	91	-0.03	0.01	0.00	**5.39**	**26.18**	0.00	0.01	0.01	0.02	**12.19**	0.00	0.00	0.02	0.04	-0.06	0.00	0.00	0.29	**13.93**	-0.06	-0.12	-0.03	0.01	-0.01	-0.06	0.01	-0.01	0.03	0.00	-0.04	-0.03	0.00	-0.02	0.01	41.85	99.5
PRG	92	-0.04	0.01	-0.01	**5.46**	**26.33**	0.01	0.00	0.00	0.01	**12.20**	0.01	0.01	0.01	0.01	-0.07	-0.01	-0.03	0.27	**14.00**	-0.05	-0.10	-0.01	0.00	-0.01	0.04	0.00	0.00	0.03	0.01	0.07	-0.02	0.03	0.00	-0.03	42.12	100.3
PRG	93	-0.05	0.00	0.00	**5.44**	**26.16**	0.01	0.01	0.00	-0.01	**12.19**	0.01	0.01	0.02	0.01	-0.08	-0.01	-0.01	0.24	**14.00**	-0.07	-0.09	-0.02	-0.03	-0.03	0.03	-0.02	0.00	0.02	-0.04	0.02	0.00	-0.03	0.03	-0.02	41.87	99.6
PRG	94	-0.03	-0.01	0.00	**5.39**	**26.23**	0.01	-0.01	0.02	0.00	**12.17**	-0.01	0.00	0.02	0.06	-0.07	0.04	0.01	0.28	**13.83**	-0.05	-0.07	0.01	0.02	-0.02	0.01	-0.05	-0.01	0.03	-0.02	0.02	0.07	0.02	0.01	0.02	41.95	99.9
PRG	95	-0.02	-0.01	-0.02	**5.46**	**26.26**	0.00	-0.04	0.01	-0.01	**12.25**	-0.01	0.01	0.01	-0.01	-0.11	0.01	0.00	0.25	**13.76**	-0.03	-0.10	0.02	-0.01	-0.01	-0.01	0.03	-0.01	0.00	-0.04	0.02	0.03	-0.01	0.02	0.00	41.98	99.7
NDG	96	0.01	0.03	0.00	**5.48**	**26.05**	0.01	0.13	-0.02	0.03	**12.25**	0.00	0.03	0.05	0.06	-0.10	-0.02	-0.01	-0.01	-0.02	**14.55**	0.02	0.03	-0.01	-0.04	-0.12	-0.02	0.06	-0.05	0.00	0.00	0.02	-0.02	-0.01	-0.01	41.88	100.2
NDG	97	-0.03	0.03	0.00	**5.45**	**25.96**	0.01	0.13	-0.01	0.00	**12.17**	0.00	0.04	0.03	0.01	-0.05	-0.04	-0.02	0.00	0.02	**14.24**	0.03	0.01	-0.01	-0.03	-0.15	-0.01	0.06	0.00	-0.05	-0.05	-0.02	0.01	0.00	0.01	41.66	99.4
NDG	98	0.03	0.03	0.01	**5.48**	**26.01**	0.00	0.12	0.01	0.01	**12.08**	-0.01	0.03	0.03	0.01	-0.08	-0.06	0.01	-0.03	0.02	**14.25**	0.04	0.03	-0.02	0.00	-0.09	-0.04	0.04	-0.04	-0.03	0.00	0.01	-0.02	0.01	0.01	41.70	99.5
NDG	99	-0.02	0.02	0.01	**5.46**	**26.07**	0.01	0.09	-0.02	0.01	**12.18**	-0.02	0.04	0.04	0.01	-0.11	-0.05	-0.03	0.02	-0.02	**14.33**	0.04	0.04	0.00	0.00	-0.05	-0.01	0.05	-0.03	-0.04	-0.01	0.02	-0.01	0.00	-0.04	41.78	99.7
NDG	100	-0.02	0.02	0.00	**5.47**	**25.96**	0.00	0.12	0.04	0.01	**12.22**	-0.02	0.03	0.03	0.05	-0.07	-0.06	-0.01	0.00	0.02	**14.33**	0.01	0.00	-0.04	-0.01	-0.13	0.03	0.05	0.00	0.03	-0.02	-0.06	0.02	-0.01	-0.02	41.69	99.7

Notes: peak overla background overlap not applicable - e.g. because element not in list

Weight%

Standard	#	F	Na	Mg	Al	Si	P	La	Ce	K	Ca	Ti	Mn	Fe	Sr	Y	Zr	Nb	Ba	Pr	Nd	Sm	Gd	Hf	Th	U	Ta	Cl	Tb	Dy	Ho	Er	Tm	Yb	Lu	O	Total
SMG	101	-0.02	0.01	-0.03	**6.13**	**23.42**	0.01	0.02	0.01	0.01	**13.61**	0.00	0.00	-0.04	0.06	-0.47	0.02	0.03	0.04	-0.03	-0.08	**17.25**	0.04	-0.02	0.02	-0.31	-0.03	0.00	0.22	0.08	0.03	-0.01	1.65	0.05	0.00	40.44	102.1
SMG	102	-0.03	0.00	-0.03	**6.16**	**23.40**	0.00	-0.01	0.02	0.01	**13.70**	0.00	-0.01	-0.03	0.01	-0.49	-0.02	-0.02	0.01	-0.01	-0.05	**17.37**	0.02	-0.02	0.02	-0.26	-0.03	0.00	0.23	0.05	0.05	0.01	1.61	0.05	0.01	40.44	102.2
SMG	103	-0.03	0.00	-0.02	**6.12**	**23.42**	0.00	0.04	0.03	-0.01	**13.77**	0.00	-0.01	-0.04	0.02	-0.52	0.01	0.00	0.00	-0.04	-0.02	**17.29**	0.05	-0.02	0.02	-0.33	-0.06	0.01	0.20	0.08	0.07	0.02	1.60	0.09	0.02	40.47	102.2
SMG	104	-0.01	0.00	-0.03	**6.12**	**23.42**	0.00	0.02	0.04	-0.01	**13.78**	-0.01	-0.02	-0.05	0.05	-0.48	-0.02	-0.02	0.00	-0.05	-0.05	**17.11**	0.09	0.02	0.03	-0.32	-0.06	0.00	0.20	0.10	0.10	-0.03	1.68	0.05	0.04	40.44	102.1
SMG	105	0.02	0.01	-0.03	**6.15**	**23.46**	0.00	0.00	-0.01	0.02	**13.84**	-0.01	-0.01	-0.06	0.04	-0.49	-0.03	0.01	0.00	-0.05	-0.06	**17.27**	0.01	-0.01	0.04	-0.25	-0.02	0.00	0.20	0.10	0.11	-0.05	1.63	0.05	0.02	40.55	102.5
GDG	106	-0.01	0.02	-0.09	**5.91**	**22.11**	0.03	0.00	0.02	0.00	**13.76**	-0.02	-0.05	0.01	0.04	-0.07	-0.05	-0.01	0.00	0.03	-0.17	0.01	**18.12**	0.00	0.02	0.09	-0.04	0.00	-0.13	-0.17	-0.06	0.33	-0.01	-0.12	-0.03	38.60	98.1
GDG	107	-0.01	0.02	-0.08	**5.90**	**22.16**	0.02	-0.01	0.02	-0.02	**13.86**	-0.01	-0.03	0.01	0.06	-0.07	-0.01	-0.01	0.01	0.03	-0.16	0.04	**18.07**	0.00	-0.01	0.08	-0.03	-0.01	-0.09	-0.20	-0.16	0.33	-0.05	-0.10	-0.03	38.68	98.2
GDG	108	0.01	0.01	-0.05	**5.89**	**22.09**	0.01	-0.02	0.02	-0.01	**13.80**	0.00	-0.03	0.01	0.01	-0.10	-0.02	0.00	-0.01	0.03	-0.16	0.05	**18.14**	0.00	0.01	0.08	-0.05	0.00	-0.14	-0.17	-0.11	0.35	0.00	-0.08	-0.10	38.58	98.1
GDG	109	0.01	0.01	-0.07	**5.88**	**22.19**	0.01	-0.01	0.00	0.01	**13.84**	0.01	-0.03	0.01	0.03	-0.13	-0.03	-0.01	-0.01	-0.01	-0.15	0.03	**18.05**	0.00	0.00	0.13	-0.05	0.01	-0.15	-0.23	-0.21	0.43	0.01	-0.12	-0.06	38.66	98.1
GDG	110	0.01	0.02	-0.07	**5.94**	**22.13**	0.04	0.00	0.04	-0.02	**13.89**	-0.01	-0.04	0.02	0.03	-0.10	-0.01	-0.01	0.02	0.02	-0.17	-0.02	**18.21**	0.00	-0.01	0.06	-0.04	0.00	-0.11	-0.23	-0.17	0.36	-0.03	-0.11	-0.08	38.72	98.3
TBG	111	-0.01	0.01	0.07	**6.17**	**21.45**	0.01	0.02	0.02	0.00	**13.78**	0.01	-0.03	0.00	0.00	-0.10	0.00	0.01	0.01	-0.15	-0.04	-0.06	-0.03	0.04	-0.01	0.14	0.03	0.01	**19.24**	0.04	0.04	-0.07	0.02	0.20	-0.03	38.39	99.2
TBG	112	-0.01	0.04	0.06	**6.18**	**21.49**	0.01	0.01	0.02	0.02	**13.95**	-0.01	-0.03	0.00	0.01	-0.07	-0.04	0.00	-0.04	-0.18	-0.03	-0.07	0.00	-0.03	0.01	0.07	0.03	0.01	**19.38**	0.02	0.02	0.04	0.04	0.15	-0.03	38.51	99.5
TBG	113	0.00	0.01	0.07	**6.15**	**21.45**	0.01	0.01	0.01	0.00	**13.93**	0.01	-0.02	0.00	0.01	-0.07	-0.03	-0.03	0.01	-0.20	-0.04	-0.09	0.02	-0.03	0.01	0.14	0.04	0.00	**19.40**	0.08	-0.03	-0.03	0.09	0.17	-0.03	38.45	99.5
TBG	114	-0.02	0.02	0.06	**6.14**	**21.40**	0.01	-0.02	0.01	0.00	**13.78**	0.01	-0.02	0.00	0.05	-0.10	-0.01	0.02	-0.01	-0.19	-0.06	-0.06	-0.01	-0.04	-0.02	0.08	0.06	0.00	**19.15**	0.03	0.02	-0.04	0.05	0.19	-0.03	38.27	98.7
TBG	115	0.02	0.01	0.07	**6.08**	**21.46**	0.02	0.01	0.01	-0.02	**13.84**	0.00	-0.02	0.00	0.02	-0.11	-0.05	-0.04	0.01	-0.18	-0.08	-0.04	0.01	0.03	0.00	0.10	0.04	0.00	**19.40**	0.07	0.00	-0.03	0.05	0.17	-0.04	38.32	99.1
DYG	116	-0.02	0.02	-0.14	**5.95**	**22.26**	0.01	-0.02	0.02	0.01	**13.51**	-0.01	-0.01	0.06	0.09	-0.08	0.01	0.22	0.00	0.02	-0.04	0.04	0.05	-0.09	0.01	-0.01	-0.04	0.01	-0.03	**18.26**	0.10	0.01	0.27	0.14	0.71	38.93	100.2
DYG	117	0.00	0.00	-0.14	**6.07**	**22.32**	0.00	-0.01	0.00	-0.03	**13.48**	0.01	-0.01	0.05	0.01	-0.02	-0.02	0.23	-0.02	0.02	-0.03	0.01	0.02	-0.06	-0.01	0.02	-0.04	-0.01	-0.02	**18.55**	0.10	0.05	0.27	0.17	0.69	39.11	100.7
DYG	118	0.00	0.00	-0.15	**6.11**	**22.39**	0.01	0.01	0.04	-0.01	**13.59**	-0.01	-0.01	0.05	0.03	-0.04	-0.01	0.21	0.02	0.02	-0.07	0.04	0.01	-0.07	0.03	0.02	-0.02	0.00	0.01	**18.35**	0.13	0.02	0.25	0.17	0.71	39.25	101.0
DYG	119	0.01	0.01	-0.14	**6.06**	**22.47**	0.02	0.01	0.01	-0.02	**13.52**	-0.01	0.00	0.06	0.01	-0.06	0.00	0.18	-0.01	-0.03	-0.09	0.05	0.08	-0.06	0.03	0.02	-0.03	-0.01	-0.01	**18.62**	0.12	0.03	0.25	0.12	0.75	39.30	101.2
DYG	120	-0.01	0.02	-0.16	**6.08**	**22.38**	0.01	-0.01	0.03	-0.03	**13.61**	0.00	-0.01	0.05	0.01	-0.04	0.00	0.23	-0.01	0.02	-0.05	0.05	0.00	-0.09	0.01	0.01	-0.02	0.00	0.03	**18.53**	0.13	0.02	0.25	0.10	0.69	39.24	101.1
PHF	121	0.00	-0.01	-0.09	-0.01	0.00	0.00	0.00	0.05	-0.01	0.00	0.08	-0.02	0.01	0.06	0.00	2.87	-0.05	0.04	-0.07	-0.18	0.00	-0.02	**97.81**	-0.02	0.09	0.44	0.02	-0.02	0.00	0.00	0.42	0.00	0.00	0.00	18.64	120.0
PHF	122	0.00	0.03	-0.11	-0.02	0.00	-0.01	-0.02	0.08	0.00	0.01	0.08	-0.03	0.00	0.09	0.00	2.91	-0.10	0.02	0.00	-0.14	0.03	-0.04	**97.45**	0.06	0.09	0.41	0.00	-0.05	0.00	0.00	0.50	0.00	0.00	0.00	18.59	119.8
PHF	123	-0.02	0.02	-0.09	0.00	0.00	0.00	-0.02	0.10	0.02	0.00	0.06	-0.01	0.02	0.06	0.00	2.91	-0.08	0.00	0.04	-0.18	0.09	-0.02	**97.42**	0.05	0.08	0.43	0.00	-0.03	0.00	0.00	0.43	-0.49	0.00	0.00	18.55	119.3
PHF	124	-0.02	0.02	-0.09	-0.02	0.00	-0.02	0.06	0.09	0.01	-0.01	0.08	-0.04	0.00	0.01	0.00	2.84	-0.12	0.06	0.04	-0.21	0.00	-0.03	**97.43**	-0.07	0.05	0.47	0.00	-0.05	0.00	0.00	0.54	-0.50	0.00	0.00	18.46	119.0
PHF	125	-0.02	0.02	-0.09	-0.03	0.00	0.00	0.03	0.05	-0.01	0.02	0.06	-0.01	0.02	0.02	0.00	2.90	-0.10	0.07	0.00	-0.15	0.09	-0.01	**97.71**	0.02	0.01	0.35	0.02	-0.04	0.00	0.00	0.41	0.00	0.00	0.00	18.61	120.0
PTA	126	-0.02	0.05	0.00	0.02	-0.57	-0.01	0.06	0.20	0.02	-0.01	-0.01	-0.03	0.03	-0.49	-0.05	0.03	0.07	0.02	0.03	-0.29	0.11	-0.02	0.03	-0.05	0.10	**99.82**	0.00	-0.01	-0.13	-0.51	0.00	2.01	-0.21	-0.36	21.52	121.4
PTA	127	0.03	0.03	0.00	0.02	-0.56	-0.01	0.02	0.25	0.02	0.00	0.01	-0.01	0.06	-0.51	-0.11	-0.03	0.06	-0.04	-0.06	-0.31	0.15	-0.06	0.02	0.00	0.06	**100.0**	-0.03	0.00	-0.15	-0.50	0.00	1.95	-0.16	-0.34	21.52	121.3
PTA	128	0.02	0.03	0.00	0.06	-0.58	-0.02	0.04	0.25	-0.01	-0.01	-0.01	-0.01	0.04	-0.48	-0.08	-0.03	0.03	0.07	-0.05	-0.26	0.15	0.00	0.02	0.00	0.15	**99.94**	-0.01	-0.02	-0.11	0.00	0.00	1.94	-0.25	-0.34	21.60	122.1
PTA	129	-0.02	0.05	-0.01	0.03	-0.58	0.00	0.02	0.25	-0.02	0.03	0.02	-0.02	0.04	-0.48	-0.02	0.01	0.04	0.03	-0.02	-0.27	0.10	-0.02	0.02	0.06	0.13	**100.1**	0.01	-0.06	-0.12	0.00	0.00	1.94	-0.25	-0.37	21.67	122.3
PTA	130	-0.02	0.06	-0.01	0.03	-0.57	-0.03	0.09	0.23	-0.02	0.00	-0.01	-0.03	0.03	-0.34	-0.04	-0.07	0.01	0.02	0.01	-0.29	0.12	-0.03	-0.03	-0.04	0.05	**99.75**	0.01	0.04	-0.20	-0.50	0.00	2.02	-0.25	-0.31	21.44	121.1
HOG	131	0.00	0.05	0.00	**6.51**	**22.92**	0.03	-0.01	0.02	-0.01	**13.32**	-0.02	-0.07	0.01	0.11	-0.14	-0.04	0.00	-0.02	-0.03	-0.25	0.01	23.09	3.20	-0.06	0.16	-0.04	0.00	-0.27	-0.50	**18.64**	-0.17	-0.31	-0.20	1.20	43.94	131.1
HOG	132	0.00	0.03	-0.01	**6.52**	**22.90**	0.01	0.00	0.00	0.00	**13.37**	0.00	-0.07	0.02	0.04	-0.12	0.04	0.01	-0.01	0.00	-0.27	0.01	23.02	3.25	-0.03	0.24	-0.09	0.00	-0.32	-0.57	**18.56**	-0.19	-0.31	-0.18	1.19	43.92	131.0
HOG	133	-0.02	0.06	-0.01	**6.48**	**22.99**	0.02	0.01	0.01	0.01	**13.40**	0.01	-0.06	0.01	0.05	-0.15	-0.02	0.01	0.01	-0.02	-0.27	0.02	23.82	3.20	-0.04	0.19	-0.10	0.00	-0.27	-0.54	**18.34**	-0.18	-0.32	-0.16	1.21	44.09	131.8
HOG	134	-0.01	0.06	0.00	**6.43**	**23.04**	0.02	0.03	0.02	0.01	**13.39**	0.00	-0.07	0.00	0.05	-0.14	-0.02	-0.02	-0.03	-0.03	-0.29	0.05	24.08	3.38	-0.05	0.14	-0.09	-0.01	-0.27	-0.46	**18.28**	-0.20	-0.31	-0.25	1.17	44.12	132.0
HOG	135	0.01	0.06	-0.01	**6.42**	**22.90**	0.01	0.01	0.03	0.00	**13.25**	0.00	-0.06	0.01	0.03	-0.15	-0.02	-0.01	-0.02	0.01	-0.28	0.03	23.76	3.30	-0.04	0.15	-0.07	0.00	-0.25	-0.51	**18.20**	-0.17	-0.33	-0.23	1.20	43.84	131.1
ERG	136	0.02	0.00	-0.01	**5.71**	**20.76**	0.01	-0.01	0.01	0.01	**14.23**	0.00	-0.01	0.00	0.03	-0.08	0.03	-0.01	0.01	-0.03	-0.10	-0.01	0.01	0.00	-0.03	0.05	0.45	-0.01	-0.02	-0.12	-0.09	**19.70**	0.00	-0.05	-0.05	37.28	97.7
ERG	137	-0.03	0.01	0.00	**5.79**	**20.81**	0.00	-0.02	0.03	-0.02	**14.11**	-0.01	0.00	0.00	-0.01	-0.10	-0.02	0.00	0.01	0.02	-0.06	0.01	-0.01	0.00	0.01	-0.05	0.46	-0.01	-0.02	-0.08	-0.15	**19.76**	-0.02	-0.04	-0.03	37.33	97.7
ERG	138	0.01	0.01	0.00	**5.85**	**20.77**	0.03	-0.01	0.02	-0.01	**14.31**	0.01	-0.01	0.02	0.08	-0.10	0.00	-0.02	0.03	0.04	-0.07	0.01	-0.01	0.00	0.00	0.02	0.44	0.00	0.00	-0.07	-0.11	**19.70**	-0.06	-0.03	-0.04	37.49	98.3
ERG	139	-0.03	0.00	-0.01	**5.85**	**20.72**	0.01	0.01	0.04	-0.03	**14.36**	0.00	-0.01	0.01	0.03	-0.11	-0.04	-0.01	-0.01	0.01	-0.06	0.00	-0.06	0.00	-0.02	0.04	0.38	0.01	-0.01	-0.08	-0.13	**19.65**	-0.01	-0.07	-0.02	37.36	97.8
ERG	140	0.00	0.01	-0.01	**5.74**	**20.86**	0.00	-0.01	0.00	0.00	**14.30**	0.00	-0.01	0.00	0.03	-0.09	0.00	-0.01	0.03	0.01	-0.10	0.00	-0.03	0.00	0.01	0.02	0.47	0.00	0.01	-0.08	-0.11	**19.63**	-0.01	-0.07	-0.04	37.42	98.0
TMG	141	-0.01	0.00	0.00	**7.42**	**16.42**	0.01	0.05	0.00	-0.01	**16.55**	0.00	0.00	0.03	-0.01	-0.10	-0.07	0.00	0.02	0.01	-0.11	0.02	0.04	-0.01	0.00	-0.01	-0.05	-0.02	0.00	0.62	-0.38	-0.41	**22.86**	-0.12	-0.30	35.04	97.5
TMG	142	-0.05	0.01	0.01	**7.40**	**16.43**	0.01	-0.01	0.01	-0.01	**16.56**	-0.01	-0.01	0.03	0.00	-0.10	-0.07	0.01	-0.01	0.00	-0.08	0.03	-0.01	-0.04	0.00	0.00	0.02	0.00	0.03	0.58	-0.39	-0.46	**22.70**	-0.17	-0.28	34.98	97.1
TMG	143	-0.01	0.02	0.00	**7.40**	**16.43**	0.00	0.01	-0.01	-0.01	**16.64**	0.00	0.01	0.02	-0.01	-0.10	-0.03	0.01	0.02	0.01	-0.08	0.06	-0.01	-0.01	-0.02	0.04	-0.01	0.00	0.01	0.62	-0.47	-0.50	**22.66**	-0.14	-0.25	35.04	97.3
TMG	144	0.01	0.02	0.00	**7.39**	**16.50**	0.01	0.02	-0.02	0.01	**16.71**	0.01	0.00	0.02	-0.04	-0.07	-0.07	0.02	0.01	0.01	-0.06	0.02	0.00	0.03	-0.01	0.02	-0.01	-0.01	0.02	0.55	-0.38	-0.39	**22.62**	-0.12	-0.28	35.15	97.7
TMG	145	-0.04	0.02	0.00	**7.42**	**16.55**	0.01	0.01	0.01	0.02	**16.60**	0.00	-0.01	0.02	0.02	-0.07	-0.02	-0.05	0.03	-0.01	-0.09	0.02	-0.01	-0.03	-0.01	0.03	0.04	0.01	-0.01	0.61	-0.31	-0.43	**22.79**	-0.14	-0.22	35.22	97.9
YBG	146	0.00	0.02	0.00	**6.01**	**22.19**	0.00	0.00	0.01	0.01	**13.58**	0.01	0.00	0.00	0.01	-0.09	-0.02	0.01	-0.02	0.00	-0.07	0.02	-0.02	0.02	0.01	0.00	0.01	0.01	0.02	0.08	0.35	-0.01	0.02	**19.78**	0.03	38.85	100.8
YBG	147	-0.01	0.01	-0.01	**5.99**	**22.22**	-0.02	-0.01	0.03	0.01	**13.53**	-0.01	0.00	0.01	0.03	-0.09	-0.01	-0.01	-0.07	0.02	-0.04	0.03	0.03	-0.02	0.01	0.00	-0.04	-0.01	0.01	0.06	0.35	-0.02	-0.03	**19.79**	0.00	38.79	100.5
YBG	148	-0.02	0.00	-0.01	**5.98**	**22.25**	0.00	-0.02	0.00	0.01	**13.70**	0.00	0.00	0.01	0.01	-0.06	0.04	0.01	-0.03	-0.01	-0.08	0.01	0.04	0.02	0.02	0.05	-0.08	0.00	-0.02	0.04	0.36	0.00	0.01	**19.66**	0.06	38.91	100.9
YBG	149	0.02	0.00	0.00	**5.99**	**22.23**	-0.01	-0.03	0.03	0.02	**13.65**	0.00	-0.02	-0.01	0.02	-0.05	0.02	-0.02	-0.04	0.04	-0.05	0.01	-0.05	0.00	0.02	-0.02	-0.04	0.00	-0.01	0.00	0.28	0.00	0.03	**19.69**	0.01	38.85	100.6
YBG	150	-0.02	0.01	0.00	**5.97**	**22.21**	-0.01	0.01	-0.01	-0.01	**13.70**	0.00	-0.01	0.01	0.04	-0.10	-0.01	0.00	-0.02	0.01	-0.05	0.04	-0.03	0.04	0.00	0.02	-0.03	0.01	-0.03	0.06	0.39	0.04	0.03	**19.69**	0.03	38.86	100.8
LUG	151	-0.02	0.01	-0.02	**5.98**	**21.52**	0.01	0.00	-0.01	0.00	**13.85**	-0.01	-0.03	0.02	0.05	-0.08	0.00	0.01	-0.02	-0.02	-0.07	0.02	-0.09	-0.14	-0.01	0.02	-0.03	-0.02	-0.04	-0.02	0.15	0.15	-0.01	-0.02	**19.58**	38.01	98.7
LUG	152	0.00	0.02	0.00	**6.00**	**21.57**	0.00	0.02	0.00	-0.01	**13.77**	0.00	-0.01	0.01	0.06	-0.02	0.01	-0.01	-0.01	-0.01	-0.10	0.02	-0.03	-0.11	0.01	0.01	0.01	-0.01	-0.04	-0.06	0.09	0.09	-0.01	0.01	**19.44**	38.06	98.8
LUG	153	-0.01	0.03	-0.01	**5.96**	**21.58**	0.01	-0.05	-0.01	0.01	**13.70**	-0.01	-0.01	0.02	0.01	-0.04	0.03	-0.01	-0.03	0.01	-0.10	0.00	-0.06	-0.16	0.00	-0.05	0.00	0.01	-0.01	-0.07	0.11	0.11	-0.02	0.00	**19.59**	38.01	98.6
LUG	154	0.01	0.02	-0.01	**5.99**	**21.55**	0.01	-0.01	-0.01	-0.01	**13.81**	-0.01	-0.01	0.00	0.04	-0.05	0.00	0.00	-0.01	0.05	-0.05	0.01	0.02	-0.15	-0.02	0.02	-0.02	0.01	-0.06	-0.04	0.16	0.17	-0.03	0.01	**19.46**	38.07	98.9
LUG	155	0.00	0.02	0.00	**5.97**	**21.62**	0.01	0.01	-0.01	0.01	**13.84**	0.00	-0.03	0.02	0.04	-0.05	0.02	0.02	-0.06	0.01	-0.09	0.03	-0.04	-0.13	-0.01	0.03	-0.04	0.00	-0.02	-0.01	0.05	0.11	-0.05	-0.03	**19.63**	38.15	99.0

Notes: peak overla background overlap not applicable - e.g. because element not in list

Table C1.2. Calculated element interference corrections. Empirical corrections

Peak overalps						Background overlaps						
F / Ce	Zr/Hf	Ta/Hf	Ce/Ta	Ho/Dy	Tm/Dy	Mg/Dy	Hf/Lu	Y / Si	Nd/Nb	Sm/Pr	Mn/Ho	Yb/Ho
0.0183	0.0296	0.00431	0.00235	0.00627	0.0140	-0.00785	-0.00699	-0.00363	-0.00146	-0.00686	-0.00369	-0.01101
Mg/Tb	Hf/Ho	Ta/Er	Nd / Ce	Ho/Yb	Yb/Tb	Mg/Hf	Hf/Dy	Y / Zr	Nd/U	Gd / Mn	Ho/Gd	Yb/Tm
0.00353	0.177	0.0223	0.00646	0.0176	0.00923	-0.00097	-0.00408	-0.00617	-0.00244	-0.00377	-0.00776	-0.00603
Al/Ba	U / K	Ba / Ti	Sm/Ta	Ho/Lu	Yb/Dy	Mg/Gd	Th/Mn	Y/Sm	Nd/Hf	Tb / Mn	Ho/Er	Lu/Ta
0.00779	0.0624	0.0113	0.00126	0.0057	0.00753	-0.00391	-0.01008	-0.0284	-0.00177	-0.01452	-0.00589	-0.00342
K/U	U/Ta	Ba/Pr	Sm / Ce	Er/Gd	Lu/Dy	Si/Ta	U/Nd	La / Ti	Nd/Gd	Tb/Gd	Ho/Tm	F/Fe
0.00202	0.00099	0.0192	0.0127	0.0198	0.0385	-0.00572	-0.00748	-0.01454	-0.00903	-0.00673	-0.01709	-0.00166
Ti / Ba	U/Ho	Y / Nb	Gd/Ho	Er/Hf	Lu/Ho	P / Nb	U/Sm	La / Ba	Nd/Tm	Dy/Gd	Er/Ho	P/Y
0.00264	0.00949	0.00108	1.28	0.00470	0.0648	-0.00174	-0.01702	-0.00246	-0.00364	-0.01098	-0.00988	-0.03125
Fe / Mn	Nb/Mn	La/Nd	Tb/Fe	Er/Lu	Si/Ta	Ca / K	Nb/Hf	Ce / La	Nd/Ta	Dy/Fe	Er/Tm	Zr/P
0.00169	0.00665	0.00826	0.00274	0.00326	0.00779	-0.00243	-0.00093	-0.01285	-0.00285	-0.00193	-0.01931	-0.02768
Fe/Nb	Nb / Ba	Ce / Ba	Tb/Sm?	Tm/Ta		Sr/U	Ta/Ho	Pr/Tb	Nd/Lu	Dy/Ta	Yb/Gd	Zr/Y
0.00088	0.00111	0.444	0.0121	0.0197		-0.0033	-0.00416	-0.00924	-0.0041	-0.00144	-0.00569	-0.00996

X/Y X= element to be corrected. Y = element causing interference

Table C1.3. Limit of detection (LOD) and SEM analytical errors (standard error of the mean) for mineral type by EPMA. The LOD and SEM values presented here represent the mean values of individual point analysis for each mineral.

		F	Cl	Na	Mg	Al	Si	P	Ca	K	Ti	Mn	Fe	Ba	Sr	Zr	Hf	Nb
Apatite	LOI	4870	192	492	201	211	194	398	356	296	262	226	240	944	629	398	797	643
	Std error	*1171*	*17*	*48*	*22*	*20*	*18*	*79*	*33*	*26*	*19*	*17*	*18*	*66*	*65*	*252*	*76*	*61*
Britholite	LOI	2605	226	614	287	333	320	652	284	377	329	290	306	995	853	949	1117	826
	Std error	*852*	*17*	*59*	*17*	*20*	*21*	*102*	*13*	*18*	*12*	*10*	*13*	*46*	*60*	*99*	*81*	*65*
Fluorite	LOI	9331	186	558	239	235	216	312	387	295	287	241	250	886	767	522	843	542
	Std error	*1133*	*15*	*48*	*14*	*16*	*17*	*36*	*22*	*20*	*10*	*11*	*11*	*45*	*73*	*47*	*34*	*48*
Ilmenite	LOI	1851	227	580	217	240	217	236	226	345	278	228	255	937	851	593	920	607
	Std error	*136*	*12*	*130*	*12*	*12*	*8*	*21*	*10*	*25*	*6*	*7*	*7*	*30*	*61*	*67*	*29*	*30*
Fluorocabonate	LOI	3210	293	708	317	339	326	594	289	381	302	288	304	1057	1001	887	1114	822
	Std error	*441*	*20*	*73*	*28*	*25*	*19*	*146*	*13*	*22*	*13*	*11*	*12*	*63*	*83*	*140*	*83*	*61*
Monazite	LOI	1481	281	658	305	315	304	630	297	404	305	296	306	1009	991	822	1079	859
	Std error	*1834*	*14*	*85*	*25*	*19*	*13*	*166*	*13*	*25*	*14*	*13*	*12*	*53*	*61*	*352*	*61*	*52*
Niobiates	LOI	1594	272	602	274	301	281	516	283	394	309	271	310	1037	822	784	1181	1094
	Std error	*749*	*16*	*63*	*21*	*19*	*23*	*88*	*12*	*29*	*17*	*11*	*18*	*58*	*38*	*57*	*62*	*94*
Xenotime	LOI	3167	273	499	254	331	326	1297	301	337	315	271	281	1058	764	852	455	981
	Std error	*411*	*11*	*34*	*14*	*23*	*12*	*87*	*15*	*22*	*14*	*10*	*11*	*55*	*52*	*287*	*422*	*65*
Zircon	LOI	1607	277	395	188	218	301	357	291	387	298	263	278	1011	964	1244	1004	813
	Std error	*478*	*18*	*158*	*12*	*19*	*28*	*104*	*14*	*23*	*11*	*7*	*7*	*58*	*46*	*72*	*88*	*39*

		Ta	Th	U	Y	La	Ce	Pr	Nd	Sm	Gd	Tb	Dy	Ho	Er	Tm	Yb	Lu
Apatite	LOI	832	681	1520	394	427	523	805	559	463	520	473	897	947	959	463	480	481
	Std error	*73*	*50*	*1170*	*34*	*29*	*501*	*58*	*51*	*48*	*75*	*37*	*76*	*83*	*85*	*35*	*37*	*37*
Britholite	LOI	1058	921	1364	549	503	678	843	502	315	328	621	1182	1243	1247	617	647	640
	Std error	*47*	*49*	*224*	*29*	*29*	*43*	*38*	*143*	*129*	*62*	*28*	*51*	*60*	*60*	*28*	*29*	*29*
Fluorite	LOI	909	716	708	383	433	824	802	605	499	720	524	1006	1068	1086	525	547	547
	Std error	*30*	*46*	*1980*	*20*	*25*	*2951*	*40*	*24*	*75*	*627*	*23*	*38*	*42*	*42*	*18*	*19*	*19*
Ilmenite	LOI	870	762	923	490	472	140	936	646	520	634	529	1008	1064	1073	520	542	540
	Std error	*25*	*35*	*186*	*18*	*182*	*58*	*34*	*17*	*183*	*119*	*23*	*28*	*29*	*27*	*15*	*14*	*17*
Fluorocarbonate	LOI	1092	970	2142	605	636	775	1040	693	541	486	640	1212	1277	1290	632	657	655
	Std error	*42*	*53*	*5888*	*33*	*49*	*66*	*49*	*40*	*65*	*65*	*27*	*48*	*53*	*54*	*24*	*25*	*25*
Monazite	LOI	1014	954	1491	556	616	761	1013	688	536	482	618	1165	1222	1235	606	630	626
	Std error	*53*	*70*	*498*	*22*	*31*	*61*	*42*	*41*	*73*	*67*	*33*	*65*	*74*	*75*	*35*	*38*	*37*
Niobiates	LOI	936	985	1233	650	545	695	997	620	473	594	635	1207	1285	1293	636	663	663
	Std error	*31*	*50*	*321*	*40*	*26*	*64*	*44*	*28*	*47*	*31*	*25*	*47*	*44*	*52*	*23*	*23*	*26*
Xenotime	LOI	988	944	1010	554	490	1078	912	667	566	622	586	1128	1193	1208	585	609	604
	Std error	*36*	*47*	*1249*	*20*	*22*	*1205*	*36*	*84*	*30*	*47*	*21*	*37*	*39*	*42*	*19*	*21*	*21*
Zircon	LOI	1048	931	1319	532	497	775	941	734	414	581	578	1119	1189	1212	581	607	610
	Std error	*31*	*35*	*341*	*21*	*11*	*1656*	*27*	*866*	*1451*	*475*	*15*	*30*	*36*	*36*	*15*	*15*	*17*

C2 EMP Mineral Analysis

Table C2.1 EMPA analysis of fluorite minerals

#	Sample	F	Ca	Y	Cl	Na	Si	P	Mn	Fe	Sr	Ba	Th	U	La	Ce	Pr	Nd	Sm	Gd	Tb	Dy	Ho	Er	Tm	Yb	Lu	Total
		wt %	wt %	wt %	wt %	wt %	wt %	wt %	wt %	wt %	wt %	wt %	wt %	wt %	wt %	wt %	wt %	wt %	wt %	wt %	wt %	wt %	wt %	wt %	wt %	wt %	wt %	
F1	SV8.2	53.2	53.3	0.11	<dt	<dt	<dt	<dt	<dt	<dt	<dt	<dt	<dt	<dt	<dt	<dt	<dt	<dt	<dt	<dt	<dt	<dt	<dt	<dt	<dt	<dt	<dt	106.6
F2	SV8.2	53.8	53.4	0.10	<dt	<dt	<dt	<dt	<dt	<dt	<dt	<dt	<dt	<dt	<dt	<dt	<dt	<dt	<dt	<dt	<dt	<dt	<dt	<dt	<dt	<dt	<dt	107.3
F3	SV8.2	54.6	52.2	0.23	<dt	0.06	<dt	<dt	<dt	<dt	<dt	<dt	<dt	<dt	<dt	<dt	<dt	<dt	<dt	<dt	<dt	<dt	<dt	<dt	<dt	<dt	<dt	107.1
F4	SV8.2	54.4	52.4	0.23	<dt	<dt	0.03	<dt	<dt	<dt	<dt	<dt	<dt	<dt	<dt	<dt	<dt	<dt	<dt	<dt	<dt	<dt	<dt	<dt	<dt	<dt	<dt	107.1
F5	SV8.2	53.8	52.4	0.20	<dt	<dt	<dt	0.03	<dt	<dt	<dt	<dt	<dt	<dt	<dt	<dt	<dt	<dt	<dt	<dt	<dt	<dt	<dt	<dt	<dt	<dt	<dt	106.5
F6	SV8.2	54.0	52.8	0.20	<dt	<dt	<dt	0.03	<dt	<dt	<dt	<dt	<dt	<dt	<dt	<dt	<dt	<dt	<dt	<dt	<dt	<dt	<dt	<dt	<dt	<dt	<dt	107.0
F7	SV8.2	53.5	53.5	0.06	<dt	<dt	<dt	<dt	<dt	0.06	<dt	<dt	<dt	<dt	<dt	<dt	<dt	<dt	<dt	<dt	<dt	<dt	<dt	<dt	<dt	<dt	<dt	107.2
F8	SV8.2	53.3	53.5	0.08	<dt	<dt	<dt	<dt	<dt	0.10	<dt	<dt	<dt	<dt	<dt	<dt	<dt	<dt	<dt	<dt	<dt	<dt	<dt	<dt	<dt	<dt	<dt	106.9
F9	SV8.2	54.6	53.4	<dt	<dt	<dt	<dt	<dt	<dt	0.03	<dt	<dt	<dt	<dt	<dt	<dt	<dt	<dt	<dt	<dt	<dt	<dt	<dt	<dt	<dt	<dt	<dt	108.0
F10	SV8.2	56.3	52.6	0.07	<dt	<dt	<dt	<dt	<dt	0.05	<dt	<dt	<dt	<dt	<dt	<dt	<dt	<dt	<dt	<dt	<dt	<dt	<dt	<dt	<dt	<dt	<dt	109.0
F11	SV8.2	55.9	52.7	0.06	<dt	<dt	<dt	<dt	<dt	0.03	<dt	<dt	<dt	<dt	<dt	<dt	<dt	<dt	<dt	<dt	<dt	<dt	<dt	<dt	<dt	<dt	<dt	108.6
F12	SD4	54.9	51.9	0.08	<dt	<dt	<dt	<dt	<dt	<dt	<dt	<dt	<dt	<dt	<dt	<dt	<dt	<dt	<dt	<dt	<dt	<dt	<dt	<dt	<dt	<dt	<dt	107.0
F13	SD4	54.9	52.2	0.08	<dt	<dt	0.03	<dt	<dt	<dt	<dt	<dt	<dt	<dt	<dt	<dt	<dt	<dt	<dt	<dt	<dt	<dt	<dt	<dt	<dt	<dt	<dt	107.3
F14	SD4	55.4	52.2	0.06	<dt	<dt	0.02	<dt	<dt	0.09	<dt	<dt	<dt	<dt	<dt	<dt	<dt	<dt	<dt	<dt	<dt	<dt	<dt	<dt	<dt	<dt	<dt	107.8
F15	SD4	53.8	53.5	0.12	<dt	<dt	0.04	<dt	<dt	<dt	<dt	<dt	<dt	<dt	<dt	<dt	<dt	<dt	<dt	<dt	<dt	<dt	<dt	<dt	<dt	<dt	<dt	107.6
F16	SD4	55.3	53.0	0.21	<dt	<dt	0.05	0.04	<dt	<dt	<dt	<dt	<dt	<dt	<dt	<dt	<dt	<dt	<dt	<dt	<dt	<dt	<dt	<dt	<dt	<dt	<dt	108.8
F17	SD4	56.7	52.0	0.08	<dt	<dt	<dt	<dt	<dt	<dt	<dt	<dt	<dt	<dt	<dt	<dt	<dt	<dt	<dt	<dt	<dt	<dt	<dt	<dt	<dt	<dt	<dt	108.9
F18	SD4	56.3	51.4	0.11	<dt	<dt	<dt	<dt	<dt	<dt	<dt	<dt	<dt	<dt	<dt	<dt	<dt	<dt	<dt	<dt	<dt	<dt	<dt	<dt	<dt	<dt	<dt	107.9
F19	SD4	56.3	52.0	0.11	<dt	<dt	0.03	<dt	<dt	<dt	<dt	<dt	<dt	<dt	<dt	<dt	<dt	<dt	<dt	<dt	<dt	<dt	<dt	<dt	<dt	<dt	<dt	108.6
F20	SD4	54.4	53.0	0.14	<dt	<dt	<dt	<dt	<dt	<dt	<dt	<dt	<dt	<dt	<dt	<dt	<dt	<dt	<dt	<dt	<dt	<dt	<dt	<dt	<dt	<dt	<dt	107.5
F21	SD4	52.9	53.3	0.15	<dt	<dt	<dt	<dt	<dt	<dt	<dt	<dt	<dt	<dt	<dt	<dt	<dt	<dt	<dt	<dt	<dt	<dt	<dt	<dt	<dt	<dt	<dt	106.4
F22	SD4	54.4	53.7	0.07	<dt	<dt	<dt	<dt	<dt	0.22	<dt	<dt	<dt	<dt	<dt	<dt	<dt	<dt	<dt	<dt	<dt	<dt	<dt	<dt	<dt	<dt	<dt	108.5
F23	SD4	52.1	54.3	0.10	<dt	<dt	<dt	<dt	<dt	0.05	<dt	<dt	<dt	<dt	<dt	<dt	<dt	<dt	<dt	<dt	<dt	<dt	<dt	<dt	<dt	<dt	<dt	106.6
F24	SD4	53.0	53.5	0.17	<dt	<dt	<dt	<dt	<dt	<dt	<dt	<dt	<dt	<dt	<dt	<dt	<dt	<dt	<dt	<dt	<dt	<dt	<dt	<dt	<dt	<dt	<dt	106.7
F25	SD4	56.5	51.4	0.07	<dt	<dt	<dt	<dt	<dt	0.13	<dt	<dt	<dt	<dt	<dt	<dt	<dt	<dt	<dt	<dt	<dt	<dt	<dt	<dt	<dt	<dt	<dt	108.0
F26	SD4	56.6	51.8	0.07	<dt	<dt	0.03	<dt	<dt	0.13	<dt	<dt	<dt	<dt	<dt	<dt	<dt	<dt	<dt	<dt	<dt	<dt	<dt	<dt	<dt	<dt	<dt	108.6
F27	SD4	58.5	52.1	0.23	<dt	<dt	0.04	0.03	<dt	<dt	<dt	<dt	<dt	<dt	<dt	<dt	<dt	<dt	<dt	<dt	<dt	<dt	<dt	<dt	<dt	<dt	<dt	110.9
F28	SD4	58.7	52.4	0.17	<dt	0.06	0.02	0.03	<dt	<dt	<dt	<dt	<dt	<dt	<dt	<dt	<dt	<dt	<dt	<dt	<dt	<dt	<dt	<dt	<dt	<dt	<dt	111.4
F29	SD6	55.8	52.3	0.03	<dt	<dt	<dt	<dt	<dt	<dt	<dt	<dt	<dt	<dt	<dt	<dt	<dt	<dt	<dt	<dt	<dt	<dt	<dt	<dt	<dt	<dt	<dt	108.1
F30	SD6	55.8	52.2	<dt	<dt	<dt	<dt	<dt	<dt	<dt	<dt	<dt	<dt	<dt	<dt	<dt	<dt	<dt	<dt	<dt	<dt	<dt	<dt	<dt	<dt	<dt	<dt	107.9
F31	SD6	55.7	52.1	<dt	<dt	<dt	0.03	<dt	<dt	<dt	<dt	<dt	<dt	<dt	<dt	<dt	<dt	<dt	<dt	<dt	<dt	<dt	<dt	<dt	<dt	<dt	<dt	107.9
F32	SD6	56.8	51.8	0.09	<dt	<dt	0.04	0.03	<dt	<dt	<dt	<dt	<dt	<dt	<dt	<dt	<dt	<dt	<dt	<dt	<dt	<dt	<dt	<dt	<dt	<dt	<dt	108.9
F33	SD6	53.1	54.3	<dt	<dt	<dt	<dt	0.02	<dt	0.11	<dt	<dt	<dt	<dt	<dt	<dt	<dt	<dt	<dt	<dt	<dt	<dt	<dt	<dt	<dt	<dt	<dt	107.5
F34	SD6	52.8	53.5	<dt	<dt	<dt	0.04	<dt	<dt	0.12	<dt	<dt	<dt	<dt	<dt	<dt	<dt	<dt	<dt	<dt	<dt	<dt	<dt	<dt	<dt	<dt	<dt	106.6
F35	SD6	53.1	54.2	<dt	<dt	<dt	0.02	<dt	<dt	<dt	<dt	<dt	<dt	<dt	<dt	<dt	<dt	<dt	<dt	<dt	<dt	<dt	<dt	<dt	<dt	<dt	<dt	107.3
F36	SD27	57.1	51.7	0.19	<dt	<dt	0.05	<dt	<dt	<dt	<dt	<dt	<dt	<dt	<dt	<dt	<dt	<dt	<dt	<dt	<dt	<dt	<dt	<dt	<dt	<dt	<dt	109.1
F37	SD27	55.9	51.6	0.21	<dt	<dt	<dt	<dt	<dt	<dt	<dt	<dt	<dt	<dt	<dt	<dt	<dt	<dt	<dt	<dt	<dt	<dt	<dt	<dt	<dt	<dt	<dt	107.7
F38	SD8	50.6	54.4	<dt	<dt	<dt	0.04	<dt	<dt	0.11	<dt	<dt	<dt	<dt	<dt	<dt	<dt	<dt	<dt	<dt	<dt	<dt	<dt	<dt	<dt	<dt	<dt	105.1
F39	SD8	52.0	54.5	<dt	<dt	<dt	<dt	0.03	<dt	0.09	<dt	<dt	<dt	<dt	<dt	<dt	<dt	<dt	<dt	<dt	<dt	<dt	<dt	<dt	<dt	<dt	<dt	106.6
F40	SD8	51.9	54.4	<dt	<dt	<dt	0.03	<dt	<dt	0.12	<dt	<dt	<dt	<dt	<dt	<dt	<dt	<dt	<dt	<dt	<dt	<dt	<dt	<dt	<dt	<dt	<dt	106.5
F41	SD8	51.7	50.9	<dt	<dt	<dt	0.04	<dt	<dt	<dt	<dt	<dt	<dt	<dt	<dt	<dt	<dt	<dt	<dt	<dt	<dt	<dt	<dt	<dt	<dt	<dt	<dt	102.7
F42	SD9	53.4	52.8	0.39	<dt	<dt	<dt	<dt	<dt	<dt	<dt	<dt	<dt	<dt	<dt	<dt	<dt	<dt	<dt	<dt	<dt	<dt	<dt	<dt	<dt	<dt	<dt	106.6
F43	SD9	54.6	53.3	0.33	<dt	<dt	<dt	<dt	<dt	<dt	<dt	<dt	<dt	<dt	<dt	<dt	<dt	<dt	<dt	<dt	<dt	<dt	<dt	<dt	<dt	<dt	<dt	108.2
F44	SD9	52.3	54.1	0.04	<dt	<dt	0.05	<dt	<dt	<dt	<dt	<dt	<dt	<dt	<dt	<dt	<dt	<dt	<dt	<dt	<dt	<dt	<dt	<dt	<dt	<dt	<dt	106.6
F45	SD9	52.4	54.3	0.05	<dt	<dt	0.04	<dt	<dt	<dt	<dt	<dt	<dt	<dt	<dt	<dt	<dt	<dt	<dt	<dt	<dt	<dt	<dt	<dt	<dt	<dt	<dt	106.8

#	Sample	F	Ca	Y	Cl	Na	Si	P	Mn	Fe	Sr	Ba	Th	U	La	Ce	Pr	Nd	Sm	Gd	Tb	Dy	Ho	Er	Tm	Yb	Lu	Total
		wt %	wt %	wt %	wt %	wt %	wt %	wt %	wt %	wt %	wt %	wt %	wt %	wt %	wt %	wt %	wt %	wt %	wt %	wt %	wt %	wt %	wt %	wt %	wt %	wt %	wt %	
F45	SD9	52.4	54.3	0.05	<dt	<dt	0.04	<dt	<dt	<dt	<dt	<dt	<dt	<dt	<dt	<dt	<dt	<dt	<dt	<dt	<dt	<dt	<dt	<dt	<dt	<dt	<dt	106.8
F46	SD9	52.8	54.1	0.05	<dt	<dt	0.03	<dt	<dt	<dt	<dt	<dt	<dt	<dt	<dt	<dt	<dt	<dt	<dt	<dt	<dt	<dt	<dt	<dt	<dt	<dt	<dt	107.0
F47	SD9	52.7	54.3	<dt	<dt	<dt	0.03	<dt	<dt	<dt	<dt	<dt	<dt	<dt	<dt	<dt	<dt	<dt	<dt	<dt	<dt	<dt	<dt	<dt	<dt	<dt	<dt	107.0
F48	SD9	48.7	58.2	<dt	<dt	<dt	0.04	<dt	<dt	<dt	<dt	<dt	<dt	<dt	<dt	<dt	<dt	<dt	<dt	<dt	<dt	<dt	<dt	<dt	<dt	<dt	<dt	106.9
F49	SD9	52.8	52.8	0.28	<dt	<dt	<dt	<dt	<dt	<dt	<dt	<dt	<dt	<dt	<dt	<dt	<dt	<dt	<dt	<dt	<dt	<dt	<dt	<dt	<dt	<dt	<dt	106.0
F50	SD9	53.8	52.9	0.27	<dt	<dt	<dt	<dt	<dt	<dt	<dt	<dt	<dt	<dt	<dt	<dt	<dt	<dt	<dt	<dt	<dt	<dt	<dt	<dt	<dt	<dt	<dt	106.9
F51	SD9	55.6	50.9	0.33	<dt	<dt	<dt	0.04	<dt	<dt	<dt	<dt	<dt	<dt	<dt	<dt	<dt	<dt	<dt	<dt	<dt	<dt	<dt	<dt	<dt	<dt	<dt	106.9
F52	SD9	55.4	50.7	0.26	<dt	<dt	0.02	<dt	<dt	<dt	<dt	<dt	<dt	<dt	<dt	<dt	<dt	<dt	<dt	<dt	<dt	<dt	<dt	<dt	<dt	<dt	<dt	106.5
F53	SD9	55.5	51.0	0.35	<dt	<dt	<dt	<dt	<dt	<dt	<dt	<dt	<dt	<dt	<dt	<dt	<dt	<dt	<dt	<dt	<dt	<dt	<dt	<dt	<dt	<dt	<dt	106.9
F54	SD9	52.8	51.8	0.32	<dt	<dt	<dt	<dt	<dt	<dt	<dt	<dt	<dt	<dt	<dt	<dt	<dt	<dt	<dt	<dt	<dt	<dt	<dt	<dt	<dt	<dt	<dt	104.9
F55	SD9	53.2	51.3	0.36	<dt	<dt	<dt	<dt	<dt	<dt	<dt	<dt	<dt	<dt	<dt	<dt	<dt	<dt	<dt	<dt	<dt	<dt	<dt	<dt	<dt	<dt	<dt	104.8
F56	SD9	56.1	50.5	0.31	<dt	<dt	0.17	<dt	<dt	0.15	<dt	<dt	<dt	<dt	<dt	<dt	<dt	<dt	<dt	<dt	<dt	<dt	<dt	<dt	<dt	<dt	<dt	107.3
F57	SD9	53.8	50.8	0.31	<dt	<dt	0.22	<dt	<dt	0.03	<dt	<dt	<dt	<dt	<dt	<dt	<dt	<dt	<dt	<dt	<dt	<dt	<dt	<dt	<dt	<dt	<dt	105.1

Table C2.2 EMPA of apatite minerals

#	Sample	F	Ca	P	Si	Na	Mn	Fe	Sr	Ba	Y	Cl	Th	U	La	Ce	Pr	Nd	Sm	Gd	Tb	Dy	Ho	Er	Tm	Yb	Lu	O	Total
		wt %	wt %	wt %	wt %	wt %	wt %	wt %	wt %	wt %	wt %	wt %	wt %	wt %	wt %	wt %	wt %	wt %	wt %	wt %	wt %	wt %	wt %	wt %	wt %	wt %	wt %		
AP1	SD5	4.19	38.4	12.5	0.31	0.17	0.11	0.04	<dt	<dt	1.15	<dt	<dt	<dt	0.07	0.17	<dt	0.11	0.05	0.11	<dt	<dt	<dt	<dt	<dt	0.07	<dt	32.3	89.7
AP2	SD5	3.09	35.5	15.4	0.23	0.08	0.08	0.08	<dt	0.57	3.21	<dt	<dt	<dt	0.18	0.21	<dt	0.16	<dt	<dt	<dt	0.31	0.17	0.38	0.07	0.24	<dt	36.7	96.7
AP3	SD19	5.86	37.0	17.1	0.49	0.15	0.10	0.06	<dt	<dt	1.52	<dt	<dt	<dt	0.07	0.23	<dt	0.15	0.08	0.21	<dt	0.13	<dt	<dt	<dt	0.07	<dt	37.6	100.9
AP4	SD19	4.76	36.9	17.3	0.50	0.16	0.13	0.06	<dt	<dt	1.60	<dt	<dt	<dt	0.07	0.23	<dt	0.15	0.10	0.05	<dt	0.23	<dt	0.11	<dt	0.05	<dt	38.4	100.8
AP5	SD19	3.53	30.1	13.0	0.46	0.11	0.08	0.05	<dt	<dt	1.39	<dt	<dt	<dt	0.05	0.21	<dt	0.12	0.06	0.09	<dt	0.11	<dt	<dt	<dt	0.09	<dt	29.9	79.5
AP6	SD19	3.67	38.2	18.2	0.34	0.10	0.08	0.14	<dt	<dt	0.97	<dt	<dt	<dt	0.04	0.17	<dt	0.14	0.09	<dt	<dt	<dt	<dt	<dt	<dt	0.05	<dt	39.1	101.3
AP7	SD19	4.68	38.7	18.6	0.11	0.11	0.07	0.10	<dt	<dt	0.54	<dt	<dt	<dt	<dt	0.10	<dt	<dt	<dt	<dt	<dt	0.10	<dt	<dt	<dt	<dt	<dt	39.3	102.4
AP8	SD19	3.24	38.3	18.4	0.25	0.14	0.08	0.24	<dt	<dt	0.82	<dt	<dt	<dt	0.05	0.14	<dt	0.10	0.11	0.13	<dt	<dt	<dt	<dt	<dt	<dt	<dt	39.8	101.8
AP9	SD19	3.91	37.7	18.3	0.62	0.10	0.10	0.09	<dt	<dt	1.74	<dt	<dt	<dt	<dt	0.10	<dt	0.07	0.08	0.06	<dt	0.21	<dt	<dt	<dt	0.13	<dt	40.1	103.3
AP10	SD25	4.64	37.1	18.4	0.19	0.09	0.07	0.04	<dt	<dt	0.76	<dt	<dt	<dt	<dt	<dt	<dt	<dt	<dt	<dt	<dt	0.14	<dt	0.13	<dt	<dt	<dt	39.1	100.7
AP11	SD25	4.88	37.2	18.3	0.23	0.05	0.04	0.04	<dt	<dt	0.75	<dt	<dt	<dt	<dt	0.08	<dt	<dt	0.05	<dt	<dt	0.12	<dt	<dt	0.17	<dt	<dt	38.5	100.4
AP12	SD25	5.41	37.4	18.2	0.18	0.05	0.06	0.03	<dt	<dt	0.66	<dt	<dt	<dt	<dt	<dt	<dt	<dt	<dt	0.06	<dt	<dt	<dt	<dt	<dt	<dt	<dt	38.9	101.0
AP13	SD19	5.03	37.3	18.5	0.18	0.05	0.07	<dt	<dt	<dt	0.64	<dt	<dt	<dt	<dt	0.00	<dt	<dt	<dt	<dt	<dt	0.10	<dt	<dt	<dt	<dt	<dt	38.7	100.6
AP14	SD8	9.58	38.8	15.3	0.23	0.06	0.05	0.52	<dt	<dt	0.69	<dt	<dt	<dt	<dt	0.04	<dt	<dt	<dt	0.05	n.a.	n.a.	n.a.	n.a.	n.a.	n.a.	n.a.	35.9	101.3
AP15	SD8	5.67	37.5	18.3	0.60	0.09	0.05	0.23	<dt	<dt	1.70	<dt	<dt	<dt	0.04	0.07	<dt	<dt	<dt	0.07	n.a.	n.a.	n.a.	n.a.	n.a.	n.a.	n.a.	39.9	104.3
AP16	SD8	6.06	38.7	19.4	0.23	0.07	0.04	0.21	<dt	<dt	0.74	<dt	<dt	<dt	<dt	0.03	<dt	<dt	<dt	0.03	n.a.	n.a.	n.a.	n.a.	n.a.	n.a.	n.a.	41.5	106.9
AP17	SD8	6.65	39.4	19.7	0.11	<dt	<dt	0.03	<dt	<dt	0.37	<dt	<dt	<dt	<dt	<dt	<dt	<dt	<dt	<dt	n.a.	n.a.	n.a.	n.a.	n.a.	n.a.	n.a.	19.7	86.0
AP18	SD8	10.62	38.3	19.3	0.11	0.09	0.03	0.07	<dt	<dt	0.59	<dt	<dt	<dt	<dt	<dt	<dt	<dt	<dt	<dt	n.a.	n.a.	n.a.	n.a.	n.a.	n.a.	n.a.	40.5	109.6
AP19	SD8	4.97	38.9	19.1	0.12	0.09	0.05	0.06	<dt	<dt	0.57	<dt	<dt	<dt	<dt	<dt	<dt	<dt	<dt	<dt	n.a.	n.a.	n.a.	n.a.	n.a.	n.a.	n.a.	40.6	104.4
AP20	SD8	5.78	39.4	19.4	0.13	0.07	0.04	0.03	<dt	<dt	0.51	<dt	<dt	<dt	<dt	<dt	<dt	<dt	<dt	<dt	n.a.	n.a.	n.a.	n.a.	n.a.	n.a.	n.a.	41.1	106.5
AP21	SD8	5.10	39.7	19.4	0.09	0.08	0.04	0.10	<dt	<dt	0.35	<dt	<dt	<dt	<dt	<dt	<dt	<dt	<dt	<dt	n.a.	n.a.	n.a.	n.a.	n.a.	n.a.	n.a.	41.2	106.0
AP22	SD8	5.87	39.0	19.2	0.22	0.07	0.04	0.15	<dt	<dt	0.76	<dt	<dt	<dt	<dt	<dt	<dt	<dt	<dt	<dt	n.a.	n.a.	n.a.	n.a.	n.a.	n.a.	n.a.	40.9	106.3
AP23	SD8	6.02	39.7	19.3	0.05	<dt	0.03	0.13	<dt	<dt	0.29	<dt	<dt	<dt	<dt	<dt	<dt	<dt	<dt	<dt	n.a.	n.a.	n.a.	n.a.	n.a.	n.a.	n.a.	41.0	106.5
AP24	SD8	3.15	39.5	19.4	0.05	<dt	0.03	0.15	<dt	<dt	0.24	<dt	<dt	<dt	<dt	<dt	<dt	<dt	<dt	<dt	n.a.	n.a.	n.a.	n.a.	n.a.	n.a.	n.a.	41.5	104.0
AP25	SD8	5.05	37.8	18.6	0.60	0.07	0.07	0.09	<dt	<dt	1.28	<dt	<dt	<dt	<dt	0.03	<dt	<dt	<dt	0.08	n.a.	n.a.	n.a.	n.a.	n.a.	n.a.	n.a.	40.7	104.4
AP26	SD8	4.95	38.7	18.4	0.15	0.08	0.05	0.06	<dt	<dt	0.62	<dt	<dt	<dt	<dt	<dt	<dt	<dt	<dt	<dt	<dt	<dt	<dt	<dt	<dt	<dt	<dt	39.7	102.7
AP27	SD8	6.14	38.9	18.8	0.31	0.06	0.04	0.04	<dt	<dt	0.85	<dt	<dt	<dt	<dt	<dt	<dt	<dt	<dt	<dt	n.a.	n.a.	n.a.	n.a.	n.a.	n.a.	n.a.	40.5	105.7
AP28	SD8	4.99	39.0	18.6	0.22	0.06	0.04	0.09	<dt	<dt	0.77	<dt	<dt	<dt	<dt	<dt	<dt	<dt	<dt	<dt	<dt	<dt	<dt	<dt	<dt	<dt	<dt	39.5	103.2
AP29	SD8	5.62	38.9	19.2	0.40	<dt	0.04	0.14	<dt	<dt	0.79	<dt	<dt	<dt	<dt	<dt	<dt	<dt	<dt	<dt	n.a.	n.a.	n.a.	n.a.	n.a.	n.a.	n.a.	41.7	106.9
AP30	SD9	5.58	38.2	19.2	0.06	0.16	0.10	0.06	<dt	<dt	0.56	<dt	<dt	<dt	0.06	0.14	<dt	0.08	0.06	0.09	0.05	<dt	<dt	<dt	<dt	<dt	<dt	40.4	104.9

#	Sample	F	Ca	P	Si	Na	Mn	Fe	Sr	Ba	Y	Cl	Th	U	La	Ce	Pr	Nd	Sm	Gd	Tb	Dy	Ho	Er	Tm	Yb	Lu	O	Total
		wt %	wt %	wt %	wt %	wt %	wt %	wt %	wt %	wt %	wt %	wt %	wt %	wt %	wt %	wt %	wt %	wt %	wt %	wt %	wt %	wt %	wt %	wt %	wt %	wt %	wt %		
AP31	SD9	7.18	38.1	19.0	0.10	0.17	0.10	0.06	<dt	<dt	0.65	<dt	<dt	<dt	<dt	0.16	<dt	0.09	<dt	0.06	<dt	0.12	<dt	<dt	<dt	0.06	<dt	40.1	105.9
AP32	SD9	6.79	37.2	18.5	0.37	0.15	0.09	0.10	<dt	<dt	1.05	<dt	<dt	<dt	0.08	0.28	<dt	0.23	0.06	0.06	<dt	0.22	<dt	<dt	<dt	<dt	<dt	39.5	104.7
AP33	SD9	4.12	37.3	18.6	0.29	0.19	0.09	0.10	<dt	<dt	1.06	<dt	<dt	<dt	0.13	0.30	0.07	0.15	0.07	<dt	<dt	0.15	<dt	0.12	<dt	<dt	<dt	39.7	102.4
AP34	SD9	6.19	38.2	19.0	0.09	0.16	0.10	0.16	<dt	<dt	0.58	<dt	<dt	<dt	0.08	0.17	<dt	0.07	0.07	<dt	<dt	<dt	<dt	<dt	<dt	<dt	<dt	40.1	104.9
AP35	SD23	6.58	38.7	19.3	0.21	0.13	0.08	0.09	<dt	<dt	0.88	<dt	<dt	<dt	<dt	0.13	<dt	<dt	<dt	0.12	<dt	0.16	<dt	<dt	<dt	<dt	<dt	41.0	107.3
AP36	SD23	6.82	38.5	19.4	0.17	0.13	0.08	0.10	<dt	<dt	0.80	<dt	<dt	<dt	<dt	0.14	<dt	<dt	<dt	0.13	<dt	0.10	<dt	0.12	<dt	<dt	<dt	41.0	107.4
AP37	SD23	5.58	38.7	19.5	0.16	0.10	0.07	0.38	<dt	<dt	0.68	<dt	<dt	<dt	<dt	<dt	<dt	0.10	<dt	0.10	<dt	0.13	<dt	<dt	<dt	<dt	<dt	41.3	106.8
AP38	SD23	4.98	38.5	19.6	0.23	0.09	0.07	0.27	<dt	<dt	0.81	<dt	<dt	<dt	0.12	0.09	0.06	0.08	<dt	0.16	<dt	0.13	<dt	0.15	<dt	<dt	<dt	41.3	106.6
AP39	SD23	4.17	34.1	18.6	0.23	0.12	0.07	0.14	<dt	<dt	2.27	<dt	<dt	<dt	1.24	0.45	0.35	1.27	0.30	0.37	0.08	0.39	<dt	0.12	<dt	<dt	<dt	40.4	104.7
AP40	SD19	4.40	38.4	17.6	0.19	<dt	0.05	0.47	<dt	<dt	0.42	<dt	<dt	<dt	<dt	<dt	<dt	<dt	<dt	<dt	<dt	<dt	<dt	<dt	<dt	<dt	<dt	38.6	100.1
AP41	SD19	6.00	39.2	19.5	0.18	0.05	0.04	0.14	<dt	<dt	0.47	<dt	<dt	<dt	<dt	<dt	<dt	<dt	<dt	0.07	<dt	<dt	<dt	<dt	<dt	<dt	<dt	41.2	106.8
AP42	SD19	5.09	39.4	19.8	0.19	<dt	0.05	0.19	<dt	<dt	0.52	<dt	<dt	<dt	<dt	<dt	<dt	<dt	<dt	0.15	<dt	<dt	<dt	<dt	<dt	0.05	<dt	41.6	107.0
AP43	SD19	6.79	39.7	19.3	0.14	<dt	0.03	0.25	<dt	<dt	0.36	<dt	<dt	<dt	<dt	<dt	<dt	<dt	<dt	0.07	<dt	<dt	<dt	<dt	<dt	<dt	0.05	41.2	107.8
AP44	SD19	6.63	39.1	18.7	0.16	<dt	0.04	0.12	<dt	<dt	0.43	<dt	<dt	<dt	<dt	<dt	<dt	<dt	<dt	<dt	<dt	<dt	<dt	<dt	<dt	<dt	<dt	40.1	105.4
AP45	SD19	7.56	39.0	18.2	0.19	<dt	0.04	0.22	<dt	<dt	0.53	<dt	<dt	<dt	<dt	<dt	<dt	<dt	<dt	<dt	<dt	<dt	<dt	<dt	<dt	<dt	<dt	39.5	105.2
AP46	SD20	3.78	40.0	19.6	0.17	<dt	<dt	0.06	<dt	<dt	0.36	<dt	<dt	<dt	<dt	<dt	0.06	<dt	<dt	0.09	<dt	0.10	<dt	<dt	<dt	<dt	<dt	41.6	105.8
AP47	SD20	3.81	39.9	19.8	0.15	<dt	<dt	0.08	<dt	<dt	0.34	<dt	<dt	<dt	<dt	<dt	<dt	<dt	<dt	<dt	<dt	0.07	<dt	0.10	<dt	<dt	<dt	41.7	106.0
AP48	SD20	5.71	39.7	19.5	0.17	<dt	0.05	0.08	<dt	<dt	0.46	<dt	<dt	<dt	<dt	0.06	<dt	<dt	<dt	0.08	<dt	<dt	<dt	<dt	<dt	<dt	<dt	41.3	107.0
AP49	SD20	6.16	39.4	19.4	0.20	<dt	<dt	0.09	<dt	<dt	0.53	<dt	<dt	<dt	<dt	<dt	0.05	<dt	<dt	<dt	<dt	<dt	<dt	<dt	<dt	<dt	<dt	41.2	106.9
AP50	SD20	6.39	39.1	19.3	0.20	<dt	<dt	0.17	<dt	<dt	0.56	<dt	<dt	<dt	<dt	<dt	<dt	<dt	<dt	0.13	<dt	0.07	<dt	<dt	<dt	<dt	<dt	41.0	106.9

Table C2.3 EMPA of niobiate minerals

#	Sample	F	Cl	Nb	Ta	Ti	Na	Fe	Al	Si	P	Ca	Mn	Ba	Zr	Hf	Th	U	Y	La	Ce	Pr	Nd	Sm	Gd	Tb	Dy	Ho	Er	Tm	Yb	Lu	Pb	O	Total
		wt %	wt %	wt %	wt %	wt %	wt %	wt %	wt %	wt %	wt %	wt %	wt %	wt %	wt %	wt %	wt %	wt %	wt %	wt %	wt %	wt %	wt %	wt %	wt %	wt %	wt %	wt %	wt %	wt %	wt %	wt %	wt %		
Nb1	SD4	0.98	<dt	14.1	<dt	9.21	<dt	4.44	0.09	2.53	0.12	0.72	0.30	<dt	0.30	<dt	1.65	0.18	6.26	2.18	13.33	0.46	1.92	0.58	0.28	0.29	2.39	0.51	1.70	0.24	1.55	0.18	n.a	23.1	89.5
Nb2	SD4	1.83	0.04	14.0	6.37	0.21	0.36	1.35	0.25	5.47	1.52	0.48	0.09	0.42	7.25	0.25	0.19	3.38	7.53	0.50	2.74	<dt	0.20	<dt	<dt	<dt	0.83	0.20	1.23	0.24	2.19	0.30	n.a.	23.2	82.7
Nb3	SD4	0.22	<dt	33.3	2.07	0.65	0.06	5.45	0.10	1.63	0.19	1.03	0.34	0.16	0.60	<dt	1.52	0.53	8.03	0.14	5.05	0.17	1.13	0.81	0.39	0.35	3.04	0.67	1.86	0.22	1.49	0.12	n.a.	24.5	95.8
Nb4	SD4	0.21	<dt	36.1	1.26	0.47	<dt	5.76	0.08	1.46	0.16	1.56	0.61	<dt	0.15	<dt	0.21	0.32	8.54	0.20	3.15	0.33	1.82	1.29	0.86	0.42	3.13	0.67	1.66	0.17	1.20	0.14	n.a.	25.3	97.2
Nb5	SD4	0.21	0.03	33.0	1.97	0.85	<dt	4.93	0.07	1.38	0.12	1.23	0.30	0.16	0.28	<dt	1.31	<dt	7.22	0.16	7.90	0.18	0.93	0.62	0.07	0.29	2.90	0.68	1.90	0.25	1.57	0.15	n.a.	23.9	94.6
Nb6	SD4	0.42	<dt	25.6	0.52	4.20	<dt	4.92	0.11	1.50	0.14	0.93	0.34	0.12	0.17	<dt	2.32	<dt	7.22	0.64	8.70	0.27	1.67	0.78	0.37	0.27	2.45	0.59	1.73	0.18	1.29	0.11	n.a.	23.1	90.6
Nb7	SD4	0.35	<dt	29.1	0.40	5.60	0.07	3.49	0.13	1.57	0.18	1.14	0.56	<dt	0.12	<dt	1.87	0.20	8.84	0.13	4.18	0.28	1.70	1.10	0.63	0.40	2.93	0.66	1.83	0.22	1.26	0.11	n.a.	25.1	94.2
Nb8	SD4	0.67	0.05	24.3	0.85	0.70	<dt	1.09	<dt	3.16	0.28	0.41	0.07	<dt	1.28	<dt	1.37	0.17	13.48	0.16	7.48	0.14	0.62	0.55	0.12	0.35	3.26	0.79	2.53	0.37	2.22	0.22	n.a.	22.7	89.4
Nb9	SD4	1.08	<dt	23.8	0.92	0.85	<dt	1.40	<dt	3.08	0.28	0.53	0.08	<dt	1.25	<dt	1.54	0.18	13.69	0.16	7.98	<dt	0.65	0.50	0.20	0.36	3.49	0.74	2.68	0.37	2.38	0.23	n.a.	22.9	91.2
Nb10	SD4	0.80	<dt	36.9	0.67	1.11	0.07	5.00	0.19	1.33	0.16	1.50	0.74	<dt	0.29	<dt	0.25	0.28	7.83	0.20	5.05	0.29	1.47	0.99	0.57	0.34	2.97	0.63	1.74	0.17	1.02	<dt	n.a.	25.6	98.1
Nb11	SD4	0.52	<dt	22.6	0.22	10.19	<dt	2.89	0.13	2.08	0.29	1.06	0.65	0.15	0.08	<dt	1.38	0.18	10.75	0.22	3.08	0.22	1.48	1.09	0.67	0.40	3.32	0.79	2.02	0.24	1.64	0.15	n.a.	26.3	94.8
Nb12	SD5	<dt	<dt	33.5	1.61	0.60	<dt	5.73	0.07	1.21	<dt	1.39	0.41	0.14	<dt	<dt	1.16	0.18	7.67	0.09	5.32	0.22	1.19	0.76	0.47	0.34	2.79	0.53	1.82	0.24	1.46	0.17	n.a.	23.6	92.7
Nb13	SD5	<dt	<dt	30.4	1.98	1.27	0.11	4.06	0.13	1.78	0.13	0.95	0.11	0.12	0.51	<dt	3.25	0.58	7.52	0.17	5.42	0.11	0.63	0.41	<dt	0.34	3.14	0.75	2.30	0.34	2.18	0.22	n.a.	23.4	92.3
Nb14	SD5	0.56	0.07	23.0	3.05	0.53	0.13	1.83	<dt	3.17	<dt	0.55	0.06	<dt	1.57	<dt	1.67	0.95	9.69	0.32	5.97	<dt	0.62	0.48	0.26	0.28	2.79	0.58	2.18	0.36	2.30	0.25	n.a.	21.4	84.6
Nb15	SD5	<dt	0.03	28.0	2.11	0.81	0.14	4.67	0.14	2.28	<dt	1.07	0.35	0.29	1.83	<dt	0.74	0.87	6.32	0.25	8.44	0.11	0.78	0.54	0.26	0.25	2.18	0.52	1.57	0.19	1.47	0.17	n.a.	23.0	89.4
Nb16	SD5	0.21	<dt	29.9	1.53	0.68	0.06	5.03	0.13	2.31	<dt	1.12	0.39	0.22	2.93	<dt	0.96	0.26	6.70	0.09	9.14	<dt	0.84	0.61	0.24	0.24	2.35	0.57	1.59	0.21	1.33	0.17	n.a.	24.2	94.1
Nb17	SD5	<dt	<dt	31.3	1.22	0.62	0.07	5.63	0.10	1.53	<dt	1.22	0.45	0.23	1.04	<dt	0.88	0.34	6.28	0.10	10.15	0.17	0.96	0.61	0.32	0.33	2.56	0.53	1.71	0.22	1.32	0.12	n.a.	23.6	93.6
Nb18	SD5	<dt	<dt	32.6	1.24	0.38	<dt	5.40	0.06	1.15	<dt	1.89	0.82	0.16	0.14	<dt	0.36	0.17	7.21	0.29	5.74	0.32	1.36	0.83	0.57	0.31	2.60	0.56	1.60	0.23	1.31	0.15	n.a.	23.1	90.6
Nb19	SD5	0.24	0.03	26.7	1.72	0.37	<dt	1.55	<dt	3.09	<dt	0.44	0.07	<dt	1.26	<dt	2.27	0.31	13.29	0.22	5.81	<dt	0.75	0.66	0.34	0.36	3.41	0.78	2.73	0.39	2.70	0.29	n.a.	24.0	93.8
Nb20	SD5	0.25	0.03	27.3	2.08	0.57	<dt	2.36	<dt	2.45	<dt	0.55	0.11	0.12	1.02	<dt	1.86	0.24	11.09	0.21	6.23	0.12	0.76	0.66	0.19	0.38	3.35	0.82	2.63	0.35	2.43	0.27	n.a.	22.8	91.2
Nb21	SD5	0.28	<dt	26.8	1.81	0.41	<dt	1.82	<dt	2.75	<dt	0.47	0.08	<dt	1.16	<dt	2.10	0.27	12.41	0.25	5.43	0.15	0.84	0.62	0.28	0.37	3.41	0.77	2.57	0.34	2.57	0.25	n.a.	23.4	91.6
Nb22	SD5	0.44	0.03	18.4	<dt	7.18	<dt	3.47	0.11	1.87	<dt	0.82	0.27	0.22	0.57	<dt	2.65	0.18	6.77	2.51	12.40	0.45	1.84	0.59	0.33	0.27	2.38	0.51	1.71	0.26	1.52	0.20	n.a.	22.7	90.8
Nb23	SD5	<dt	<dt	31.1	2.20	1.22	<dt	4.81	0.11	1.40	<dt	1.49	0.50	0.20	0.25	<dt	0.63	0.30	8.63	0.14	5.42	0.16	0.95	0.77	0.45	0.38	2.87	0.61	1.89	0.19	1.50	0.18	n.a.	23.5	91.9
Nb24	SD5	<dt	0.03	31.8	0.96	0.83	<dt	6.67	0.09	1.30	<dt	1.40	0.57	0.15	0.29	<dt	0.34	0.18	6.63	0.11	9.00	0.17	1.09	0.80	0.35	0.33	2.69	0.63	1.64	0.25	1.34	0.12	n.a.	23.6	93.4
Nb25	SD5	<dt	<dt	30.1	1.50	1.71	<dt	6.19	0.08	1.40	<dt	1.25	0.53	0.12	0.34	<dt	0.59	0.24	6.30	0.11	9.80	0.17	0.95	0.69	0.42	0.34	2.69	0.54	1.72	0.23	1.41	0.14	n.a.	23.6	93.1
Nb26	SD5	0.75	0.04	25.4	0.93	0.63	<dt	1.27	0.09	2.70	<dt	0.82	0.13	<dt	1.00	<dt	1.36	0.22	12.15	0.96	6.64	0.25	1.29	0.73	0.39	0.32	3.09	0.75	2.37	0.33	2.27	0.26	n.a.	22.9	90.0
Nb27	SD5	<dt	0.03	33.0	2.07	0.94	0.09	4.16	0.19	1.69	<dt	1.48	0.39	0.23	0.63	<dt	1.03	0.39	8.03	0.16	6.94	0.13	0.92	0.68	0.40	0.33	2.69	0.58	1.95	0.26	1.56	0.22	n.a.	24.6	95.8
Nb28	SD5	0.38	0.04	19.0	5.40	0.46	0.25	1.29	0.21	3.83	0.32	0.81	0.20	0.31	4.15	<dt	0.34	2.30	5.40	0.59	4.28	<dt	0.39	0.15	<dt	0.12	1.14	0.28	1.11	0.19	1.64	0.23	n.a.	20.5	75.3
Nb29	SD6	<dt	0.04	21.7	1.85	6.71	<dt	6.41	0.10	2.43	0.13	1.19	0.26	0.26	0.51	<dt	1.37	<dt	4.66	0.08	14.60	<dt	0.68	0.46	0.16	0.26	1.94	0.43	1.24	0.13	0.77	<dt	n.a.	24.6	92.9
Nb30	SD6	<dt	0.03	21.5	1.87	6.81	<dt	6.18	0.07	2.43	0.10	1.19	0.26	0.39	0.47	<dt	1.48	<dt	4.41	0.11	14.76	0.10	0.69	0.48	0.32	0.22	2.01	0.38	1.19	0.15	0.73	0.10	n.a.	24.5	92.9

#	Sample	F	Cl	Nb	Ta	Ti	Na	Fe	Al	Si	P	Ca	Mn	Ba	Zr	Hf	Th	U	Y	La	Ce	Pr	Nd	Sm	Gd	Tb	Dy	Ho	Er	Tm	Yb	Lu	Pb	O	Total
		wt %	wt %	wt %	wt %	wt %	wt %	wt %	wt %	wt %	wt %	wt %	wt %	wt %	wt %	wt %	wt %	wt %	wt %	wt %	wt %	wt %	wt %	wt %	wt %	wt %	wt %	wt %	wt %	wt %	wt %	wt %	wt %	wt %
Nb31	SD6	<dt	0.03	29.6	1.88	3.52	<dt	5.79	0.09	1.71	0.15	2.14	0.31	0.29	0.23	<dt	1.33	0.24	5.91	0.16	8.03	0.19	1.05	0.71	0.39	0.30	2.23	0.44	1.18	0.15	0.91	0.09	n.a.	24.7	93.8
Nb32	SD6	<dt	<dt	27.6	1.74	3.34	0.06	6.31	0.08	1.84	0.18	1.72	0.45	0.30	0.24	<dt	0.93	0.19	6.01	0.10	9.44	0.15	0.92	0.69	0.46	0.29	2.29	0.43	1.33	0.16	1.01	0.10	n.a.	24.2	92.5
Nb33	SD6	<dt	<dt	24.5	1.93	4.03	0.06	6.54	0.08	2.02	0.26	1.49	0.40	0.32	0.35	<dt	1.42	<dt	4.94	0.10	13.55	0.09	0.63	0.46	0.20	0.23	1.82	0.37	1.14	0.14	0.84	0.09	n.a.	23.8	91.8
Nb34	SD6	<dt	<dt	27.3	1.59	2.91	<dt	6.62	0.09	1.82	0.16	1.70	0.44	0.32	0.23	<dt	1.10	<dt	5.00	<dt	12.14	0.12	0.72	0.51	0.20	0.24	1.98	0.47	1.24	0.16	0.82	0.09	n.a.	23.7	91.7
Nb35	SD6	<dt	<dt	31.6	2.23	0.66	<dt	6.16	0.09	1.65	0.14	1.96	0.55	0.41	0.45	<dt	1.24	0.17	5.34	0.11	10.07	<dt	0.90	0.54	0.36	0.24	2.05	0.39	1.19	0.15	0.79	<dt	n.a.	23.9	93.3
Nb36	SD6	0.16	0.03	21.6	0.98	0.15	0.06	2.55	0.16	2.67	0.27	0.87	0.20	0.14	0.98	<dt	1.01	0.23	10.96	0.11	4.66	0.08	0.52	0.36	<dt	0.24	2.07	0.50	1.71	0.25	1.53	0.17	n.a.	19.7	74.9
Nb37	SD6	<dt	<dt	32.2	2.24	0.49	0.06	5.86	0.11	1.62	0.17	1.98	0.61	0.35	0.41	<dt	0.84	0.21	6.04	0.12	8.51	0.09	1.02	0.63	0.33	0.28	2.18	0.45	1.36	0.17	0.91	0.09	n.a.	24.0	93.3
Nb38	SD6	<dt	<dt	32.6	1.97	0.60	<dt	6.14	0.13	1.58	0.14	2.06	0.62	0.36	0.38	<dt	0.97	0.25	5.85	0.09	8.73	0.20	0.95	0.65	0.40	0.27	2.20	0.45	1.31	0.16	0.94	0.09	n.a.	24.3	94.4
Nb39	SD6	0.18	0.03	23.5	1.34	0.25	0.05	2.15	<dt	2.24	0.27	1.00	0.19	0.18	0.97	<dt	1.19	0.18	10.73	0.08	5.59	0.13	0.53	0.38	0.10	0.27	2.06	0.51	1.64	0.25	1.50	0.19	n.a.	20.0	77.6
Nb40	SD6	<dt	0.06	34.5	3.02	0.65	0.29	5.41	0.17	2.25	<dt	1.98	0.22	0.76	0.46	<dt	0.75	1.82	3.63	0.12	5.35	<dt	0.84	0.42	0.34	0.19	1.46	0.29	0.85	0.10	0.55	<dt	n.a.	24.7	91.1
Nb41	SD6	<dt	0.06	35.6	1.88	0.83	0.18	10.31	0.18	1.60	0.11	1.92	0.24	0.77	0.43	<dt	0.48	0.55	2.04	0.10	3.52	<dt	0.43	0.26	0.26	0.10	0.84	0.14	0.49	0.08	0.35	<dt	n.a.	24.3	88.1
Nb42	SD6	<dt	0.05	32.5	2.29	1.06	0.10	5.32	0.10	1.97	0.14	2.04	0.23	0.34	0.57	<dt	1.20	0.32	5.16	0.14	6.81	0.25	1.27	0.85	0.57	0.33	2.31	0.47	1.35	0.15	0.79	0.08	n.a.	24.4	93.2
Nb43	SD6	<dt	<dt	33.0	2.22	0.80	0.06	5.27	0.10	1.87	0.14	2.05	0.27	0.41	0.38	<dt	0.82	0.46	5.52	0.17	6.11	0.22	1.35	0.89	0.66	0.33	2.44	0.42	1.33	0.14	0.88	0.09	n.a.	24.3	92.7
Nb44	SD6	0.47	<dt	26.2	2.31	0.89	0.09	4.47	0.15	3.34	0.72	1.63	0.20	0.48	3.98	<dt	1.06	0.79	7.19	0.15	3.86	0.12	1.08	0.69	0.46	0.29	2.18	0.43	1.29	0.18	1.15	0.13	n.a.	24.7	90.7
Nb45	SD6	<dt	0.04	34.3	2.20	0.74	0.12	5.00	0.10	1.75	0.11	2.33	0.32	0.44	0.32	<dt	0.90	0.34	5.56	0.13	5.53	0.19	1.53	0.98	0.48	0.35	2.47	0.58	1.40	0.20	0.82	0.07	n.a.	24.6	93.9
Nb46	SD6	<dt	<dt	31.4	2.80	1.32	0.08	5.76	0.08	1.87	0.13	2.01	0.23	0.47	0.55	<dt	1.05	0.19	4.82	0.10	9.08	0.14	1.02	0.69	0.36	0.30	2.22	0.46	1.19	0.14	0.75	<dt	n.a.	24.2	93.4
Nb47	SD6	<dt	<dt	32.9	2.28	1.08	0.07	5.85	0.08	1.70	0.13	2.10	0.23	0.47	0.44	<dt	1.23	0.39	4.97	0.11	8.49	0.16	1.12	0.70	0.46	0.31	2.34	0.41	1.27	0.13	0.78	<dt	n.a.	24.5	94.8
Nb48	SD6	0.21	<dt	33.9	1.57	0.77	0.07	6.28	0.08	1.44	0.17	2.10	0.36	0.38	0.30	<dt	0.69	0.35	6.61	0.16	4.58	0.20	1.40	0.90	0.62	0.33	2.60	0.51	1.48	0.16	1.03	<dt	n.a.	24.4	93.7
Nb49	SD6	<dt	0.03	32.2	0.80	0.61	<dt	0.09	<dt	<dt	0.34	0.36	<dt	<dt	0.36	<dt	1.80	0.59	20.99	0.06	0.54	0.16	1.36	1.05	1.14	0.47	3.77	0.78	2.62	0.36	2.52	0.32	n.a.	23.3	96.7
Nb50	SD7	<dt	0.03	28.0	3.53	0.52	0.17	5.16	0.65	2.37	0.13	1.07	0.16	0.63	0.35	<dt	0.65	1.95	3.55	0.06	7.28	<dt	0.31	0.17	0.18	0.11	1.21	0.21	0.89	0.09	0.66	0.07	n.a.	22.0	82.1
Nb51	SD7	<dt	<dt	27.4	4.67	0.40	0.33	3.74	0.13	2.54	0.18	1.06	0.18	0.80	0.38	<dt	0.36	2.82	2.18	<dt	7.23	<dt	0.24	0.03	<dt	0.09	0.66	0.17	0.47	<dt	0.38	<dt	n.a.	20.9	77.3
Nb52	SD7	<dt	<dt	23.2	0.92	13.64	<dt	5.41	0.43	1.92	<dt	0.84	0.21	0.16	0.19	<dt	0.32	1.04	6.79	0.11	3.08	0.18	0.88	0.56	0.33	0.24	2.07	0.41	1.37	0.14	1.03	0.13	n.a.	27.6	93.2
Nb53	SD7	0.32	<dt	27.7	2.01	0.68	0.08	6.51	0.34	2.43	<dt	1.21	0.21	0.38	0.25	<dt	0.96	0.59	7.43	0.20	4.76	0.21	0.89	0.52	0.32	0.22	2.23	0.48	1.58	0.24	1.30	0.17	n.a.	22.8	87.1
Nb54	SD7	<dt	<dt	31.6	1.88	0.47	0.09	7.45	0.08	1.59	<dt	1.36	0.28	0.39	0.09	<dt	0.65	0.51	8.35	0.30	3.72	0.20	1.17	0.64	0.43	0.30	2.56	0.54	1.64	0.21	1.28	0.17	n.a.	23.6	91.6
Nb55	SD8	0.22	<dt	37.5	1.64	0.38	0.56	0.14	0.55	5.92	0.32	3.00	<dt	2.98	0.54	<dt	0.34	4.30	<dt	0.39	1.12	<dt	0.16	<dt	0.06	n.a.	n.a.	n.a.	n.a.	n.a.	n.a.	n.a.	n.a.	n.a.	27.7	87.8
Nb56	SD8	<dt	<dt	38.5	1.51	1.03	0.37	0.59	0.26	4.06	0.20	3.47	<dt	1.69	0.49	<dt	1.23	2.80	1.87	0.26	1.67	<dt	0.98	0.46	0.27	0.24	1.89	0.32	0.98	0.12	0.57	<dt	n.a.	27.1	93.0
Nb57	SD8	0.13	<dt	37.6	1.45	0.40	0.55	0.15	0.57	5.69	0.39	2.86	<dt	3.10	0.45	<dt	0.37	4.52	<dt	0.37	1.17	<dt	0.20	<dt	<dt	<dt	0.15	<dt	<dt	<dt	0.08	<dt	n.a.	27.5	87.7
Nb58	SD8	0.19	<dt	37.0	1.92	1.21	0.45	1.03	0.23	3.65	0.22	3.40	<dt	1.51	0.48	<dt	2.37	2.48	1.50	0.22	2.30	<dt	0.79	0.38	0.59	n.a.	n.a.	n.a.	n.a.	n.a.	n.a.	n.a.	n.a.	n.a.	25.8	87.7
Nb59	SD8	0.15	<dt	37.8	1.91	0.34	0.28	0.34	0.49	5.57	0.36	2.89	<dt	3.63	0.36	<dt	<dt	6.75	<dt	0.31	1.09	<dt	0.17	<dt	<dt	<dt	0.14	<dt	<dt	<dt	<dt	<dt	n.a.	27.5	90.1
Nb60	SD8	<dt	<dt	39.0	1.13	1.47	0.14	1.13	0.12	2.37	0.10	3.91	<dt	0.91	0.52	<dt	1.55	0.97	2.93	0.17	2.52	0.12	1.41	0.95	1.13	n.a.	n.a.	n.a.	n.a.	n.a.	n.a.	n.a.	n.a.	n.a.	25.3	87.8
Nb61	SD8	0.73	<dt	39.5	1.08	1.44	0.14	1.11	0.26	2.45	0.13	3.83	<dt	0.88	0.51	<dt	1.60	1.06	3.13	0.19	2.45	0.15	1.30	0.89	0.43	0.37	3.10	0.49	1.61	0.20	0.98	<dt	n.a.	26.6	96.6
Nb62	SD8	<dt	<dt	29.6	2.32	0.32	0.54	0.25	0.50	5.77	0.32	2.92	<dt	2.85	0.63	<dt	0.20	3.02	<dt	0.35	1.12	<dt	0.14	<dt	0.03	n.a.	n.a.	n.a.	n.a.	n.a.	n.a.	n.a.	n.a.	n.a.	23.9	74.9
Nb63	SD8	<dt	<dt	38.2	2.53	0.38	0.36	0.27	0.47	5.89	0.35	3.03	<dt	3.07	0.42	<dt	0.43	4.65	<dt	0.38	1.29	<dt	0.18	<dt	0.05	<dt	<dt	<dt	<dt	<dt	0.08	<dt	n.a.	28.0	90.0
Nb64	SD8	<dt	<dt	33.3	2.97	0.17	0.08	3.35	0.09	3.77	1.29	2.43	<dt	3.80	0.29	<dt	<dt	10.19	<dt	0.12	0.76	<dt	<dt	<dt	<dt	n.a.	n.a.	n.a.	n.a.	n.a.	n.a.	n.a.	n.a.	n.a.	25.3	87.9
Nb65	SD8	<dt	<dt	31.2	0.57	0.33	<dt	22.06	0.06	2.20	0.10	0.91	<dt	0.78	1.13	<dt	0.59	0.32	2.24	0.13	1.19	<dt	0.12	<dt	0.19	n.a.	n.a.	n.a.	n.a.	n.a.	n.a.	n.a.	n.a.	n.a.	24.6	88.8
Nb66	SD8	0.23	<dt	27.7	0.60	0.27	0.08	23.06	0.08	2.71	0.12	0.95	<dt	0.51	1.40	<dt	0.71	0.42	3.02	0.10	1.22	<dt	0.17	<dt	0.24	n.a.	n.a.	n.a.	n.a.	n.a.	n.a.	n.a.	n.a.	n.a.	24.2	87.8
Nb67	SD8	0.36	<dt	34.5	2.45	0.81	0.10	5.99	0.10	1.80	0.12	1.58	<dt	0.56	0.35	<dt	0.81	1.15	4.93	0.16	1.46	0.10	0.89	0.55	0.91	n.a.	n.a.	n.a.	n.a.	n.a.	n.a.	n.a.	n.a.	n.a.	22.9	82.6
Nb68	SD8	<dt	<dt	37.6	1.73	0.90	0.16	5.44	0.08	2.71	0.09	2.06	<dt	0.88	0.22	<dt	0.47	0.45	3.39	0.22	6.28	<dt	1.01	0.40	0.65	n.a.	n.a.	n.a.	n.a.	n.a.	n.a.	n.a.	n.a.	n.a.	25.4	90.1
Nb69	SD8	0.17	<dt	27.4	0.52	0.24	0.07	21.99	0.06	2.92	0.12	0.99	<dt	0.53	1.36	<dt	0.77	0.49	3.52	0.08	1.36	<dt	0.17	0.10	0.23	n.a.	n.a.	n.a.	n.a.	n.a.	n.a.	n.a.	n.a.	n.a.	24.1	87.2
Nb70	SD8	<dt	<dt	32.7	3.16	0.18	<dt	3.56	0.10	3.76	1.17	2.48	<dt	3.97	0.28	<dt	<dt	10.25	<dt	0.16	1.03	<dt	0.11	<dt	0.02	<dt	<dt	<dt	<dt	<dt	0.07	<dt	n.a.	25.1	88.1
Nb71	SD8	<dt	<dt	31.7	1.06	0.43	0.09	14.87	0.03	2.27	0.12	1.49	<dt	0.71	1.22	<dt	0.73	0.50	3.01	0.11	5.00	<dt	0.43	0.21	<dt	0.10	1.42	0.27	0.97	0.13	0.82	0.08	n.a.	24.8	92.6
Nb72	SD8	0.15	<dt	28.1	0.45	0.24	0.06	22.15	0.07	2.76	0.11	0.90	<dt	0.49	1.33	<dt	0.73	0.45	3.20	0.08	1.33	<dt	0.14	0.10	<dt	0.07	0.93	0.18	0.86	0.12	0.86	<dt	n.a.	24.7	90.5
Nb73	SD8	0.12	<dt	30.9	0.42	0.21	0.07	20.46	0.04	2.37	0.12	0.89	<dt	0.70	1.28	<dt	0.65	0.43	3.13	0.10	1.46	<dt	0.22	0.06	<dt	<dt	0.91	0.21	0.84	0.13	0.85	0.07	n.a.	24.9	91.6
Nb74	SD8	0.16	<dt	27.3	0.52	0.26	<dt	22.86	0.06	2.77	0.12	1.03	<dt	0.52	1.28	<dt	0.71	0.47	3.06	0.11	1.20	<dt	0.17	0.07	<dt	0.08	0.84	0.18	0.77	0.10	0.81	<dt	n.a.	24.5	89.9
Nb75	SD8	<dt	<dt	32.8	1.03	0.51	<dt	16.71	0.05	2.67	0.09	1.14	<dt	0.89	1.11	<dt	0.71	0.35	2.51	0.13	2.83	<dt	0.31	0.08	<dt	0.09	0.92	0.24	0.82	0.11	0.67	0.06	n.a.	25.4	92.3
Nb76	SD8	0.16	<dt	32.0	1.31	3.14	0.31	0.14	0.29	4.50	0.16	3.12	<dt	1.42	0.99	<dt	3.79	4.86	1.38	0.26	1.20	<dt	0.76	0.31	<dt	0.18	1.55	0.37	0.83	0.09	0.58	<dt	n.a.	26.0	89.7
Nb77	SD8	0.20	<dt	36.9	1.59	1.01	0.69	0.34	0.46	6.21	0.27	3.09	<dt	2.58	1.11	<dt	0.55	4.68	<dt	0.36	1.28	<dt	0.19	<dt	<dt	<dt	<dt	<dt	<dt	<dt	0.11	<dt	n.a.	28.3	90.0
Nb78	SD8	<dt	<dt	49.8	0.96	1.41	0.43	0.66	0.20	1.97	0.13	4.27	<dt	1.09	0.34	<dt	0.27	1.22	<dt	0.13	0.76	<dt	0.12	<dt	0.03	<dt	<dt	<dt	<dt	<dt	<dt	<dt	n.a.	28.1	91.9
Nb79	SD8	0.14	<dt	31.5	2.16	1.46	0.94	0.31	0.52	6.66	0.22	2.97	<dt	2.00	1.05	<dt	0.67	7.86	0.09	0.30	1.15	<dt	0.21	<dt	0.08	<dt	0.18	<dt	0.14	<dt	0.11	<dt	n.a.	27.3	88.1
Nb80	SD8	0.38	<dt	43.9	0.69	0.67	0.32	0.78	0.22	3.09	0.31	4.56	0.09	1.29	0.59	<dt	0.59	1.69	3.54	0.18	0.73	<dt	0.27	<dt	0.06	0.11	1.39	0.22	1.04	0.14	0.85	0.10	n.a.	28.4	96.2

#	Sample	F	Cl	Nb	Ta	Ti	Na	Fe	Al	Si	P	Ca	Mn	Ba	Zr	Hf	Th	U	Y	La	Ce	Pr	Nd	Sm	Gd	Tb	Dy	Ho	Er	Tm	Yb	Lu	Pb	O	Total
		wt %	wt %	wt %	wt %	wt %	wt %	wt %	wt %	wt %	wt %	wt %	wt %	wt %	wt %	wt %	wt %	wt %	wt %	wt %	wt %	wt %	wt %	wt %	wt %	wt %	wt %	wt %	wt %	wt %	wt %	wt %	wt %	wt %	
Nb81	SD8	0.33	<dt	25.6	1.76	1.08	0.89	0.12	0.42	5.57	0.26	3.07	<dt	2.25	0.83	<dt	0.38	4.04	<dt	0.40	1.17	<dt	0.12	<dt	0.05	n.a.	n.a.	n.a.	n.a.	n.a.	n.a.	n.a.	n.a.	22.5	70.9
Nb82	SD8	0.49	<dt	32.4	2.42	1.12	0.74	0.46	0.48	6.37	0.23	3.26	<dt	2.28	1.07	<dt	0.52	5.74	<dt	0.37	1.24	<dt	0.17	<dt	0.04	n.a.	n.a.	n.a.	n.a.	n.a.	n.a.	n.a.	n.a.	27.0	86.5
Nb83	SD8	0.43	<dt	37.3	0.19	0.55	0.15	1.22	0.10	1.00	0.17	4.71	0.18	0.37	0.19	<dt	0.70	0.37	3.76	0.11	0.49	<dt	0.41	0.29	0.52	n.a.	n.a.	n.a.	n.a.	n.a.	n.a.	n.a.	n.a.	21.7	74.9
Nb84	SD8	<dt	<dt	32.7	1.35	4.29	0.11	0.58	0.14	2.67	0.11	3.60	<dt	0.74	1.01	<dt	2.52	0.90	3.24	0.16	1.28	0.11	1.26	0.82	1.10	n.a.	n.a.	n.a.	n.a.	n.a.	n.a.	n.a.	n.a.	24.6	83.4
Nb85	SD8	0.34	<dt	32.1	2.27	1.32	0.89	0.24	0.52	6.47	0.20	3.25	<dt	2.03	0.97	<dt	0.49	7.03	<dt	0.39	1.23	<dt	0.22	<dt	0.05	n.a.	n.a.	n.a.	n.a.	n.a.	n.a.	n.a.	n.a.	27.1	87.1
Nb86	SD9	<dt	<dt	35.1	1.29	0.83	0.17	4.14	0.08	1.70	0.08	2.84	0.46	0.99	0.52	<dt	1.26	0.84	0.80	0.21	16.15	<dt	0.75	0.35	0.43	n.a.	n.a.	n.a.	n.a.	n.a.	n.a.	n.a.	n.a.	14.2	83.1
Nb87	SD9	<dt	<dt	34.8	1.02	0.75	0.11	5.11	0.07	1.57	0.07	2.81	0.46	0.86	0.64	<dt	0.79	0.47	0.68	0.16	17.33	<dt	0.72	0.27	0.42	n.a.	n.a.	n.a.	n.a.	n.a.	n.a.	n.a.	n.a.	22.2	91.2
Nb88	SD9	<dt	<dt	33.0	1.25	1.18	<dt	5.91	0.11	1.41	0.10	2.85	0.47	0.45	0.32	<dt	1.52	0.50	2.75	0.15	12.06	0.19	0.88	0.41	0.62	n.a.	n.a.	n.a.	n.a.	n.a.	n.a.	n.a.	n.a.	34.2	100.4
Nb89	SD9	<dt	<dt	38.7	1.27	0.85	0.15	1.92	0.17	1.43	0.08	3.88	0.86	0.86	0.27	<dt	0.77	0.79	1.76	0.20	11.09	<dt	0.90	0.38	0.52	n.a.	n.a.	n.a.	n.a.	n.a.	n.a.	n.a.	n.a.	32.3	99.2
Nb90	SD9	<dt	<dt	33.4	1.05	0.94	0.08	5.11	0.08	1.51	0.09	2.80	0.40	0.70	0.48	<dt	1.51	0.50	1.33	0.19	15.55	<dt	0.84	0.37	0.50	n.a.	n.a.	n.a.	n.a.	n.a.	n.a.	n.a.	n.a.	14.4	81.8
Nb91	SD9	<dt	0.03	15.1	1.73	3.63	0.09	6.27	0.25	4.42	0.27	1.13	0.41	0.25	2.99	<dt	1.09	0.20	2.03	<dt	21.81	<dt	0.43	0.17	0.11	0.10	0.68	<dt	0.42	0.09	0.47	<dt	n.a.	23.2	87.3
Nb92	SD9	<dt	0.05	17.1	1.67	3.93	<dt	6.62	0.28	4.34	0.29	1.13	0.42	0.27	2.57	<dt	1.14	0.21	1.93	<dt	20.46	<dt	0.39	0.18	0.05	0.13	0.76	0.13	0.46	0.08	0.42	<dt	n.a.	23.9	88.8
Nb93	SD10	<dt	0.03	25.4	1.14	3.86	0.10	6.45	0.20	2.32	0.06	1.98	0.43	0.39	0.75	<dt	2.02	0.18	1.18	0.26	20.71	0.11	0.68	0.31	0.42	n.a.	n.a.	n.a.	n.a.	n.a.	n.a.	n.a.	n.a.	15.8	84.8
Nb94	SD10	0.28	0.04	12.3	2.52	0.93	<dt	0.93	0.14	3.71	0.30	0.66	0.04	<dt	0.71	<dt	0.88	0.38	10.78	0.23	4.66	<dt	0.45	0.31	0.05	0.20	1.95	0.49	1.76	0.24	1.66	0.23	n.a.	17.0	63.9
Nb95	SD10	0.16	0.03	24.1	2.58	2.37	<dt	4.67	0.41	2.45	0.17	0.76	0.16	0.20	0.72	<dt	1.44	0.31	7.92	0.17	7.97	<dt	0.72	0.51	0.13	0.26	2.24	0.60	1.75	0.25	1.60	0.21	n.a.	22.8	87.7
Nb96	SD10	<dt	0.04	21.9	2.74	0.72	0.07	2.51	0.53	4.75	0.42	0.49	0.05	<dt	1.47	<dt	1.81	0.66	11.85	0.17	4.94	<dt	0.50	0.35	<dt	0.22	2.32	0.59	1.93	0.29	1.97	0.22	n.a.	24.0	87.5
Nb97	SD10	<dt	0.05	18.0	2.85	0.80	0.06	1.51	0.72	4.30	0.26	0.59	0.05	<dt	1.55	<dt	1.41	0.60	8.71	0.18	4.63	<dt	0.46	0.35	0.05	0.22	2.11	0.55	1.82	0.26	1.85	0.24	n.a.	20.6	74.8
Nb98	SD10	<dt	<dt	22.4	2.67	2.23	<dt	4.08	0.38	2.39	0.10	0.71	0.14	0.15	0.63	<dt	1.39	0.24	6.55	0.14	7.71	0.09	0.59	0.43	0.13	0.27	2.23	0.58	1.87	0.29	1.63	0.23	n.a.	12.2	72.4
Nb99	SD10	0.27	0.05	19.7	2.78	0.77	<dt	1.10	0.27	2.04	<dt	0.56	0.04	<dt	1.07	<dt	1.41	0.51	3.79	0.20	5.05	0.09	0.48	0.40	0.13	0.28	2.39	0.56	2.01	0.31	2.00	0.21	n.a.	16.6	65.1
Nb100	SD10	0.52	0.08	20.9	5.60	0.28	0.72	1.47	0.11	2.89	1.42	0.61	0.10	0.72	0.14	<dt	0.12	4.89	5.53	0.69	2.93	<dt	0.28	<dt	<dt	0.07	0.77	0.18	0.82	0.13	1.39	0.19	n.a.	20.2	73.8
Nb101	SD10	0.76	0.06	20.3	5.17	0.36	0.53	2.28	0.21	2.77	1.68	0.57	0.08	0.67	0.20	<dt	0.29	4.24	6.66	0.60	3.31	<dt	0.32	0.07	<dt	0.10	0.95	0.27	1.09	0.20	1.75	0.24	n.a.	20.7	76.4
Nb102	SD10	0.52	0.04	26.1	2.94	0.74	0.28	3.79	0.08	2.08	1.33	0.73	0.10	0.42	0.18	<dt	0.85	1.94	9.02	0.31	5.91	<dt	0.43	0.22	<dt	0.20	2.17	0.54	1.93	0.29	2.23	0.31	n.a.	23.3	89.0
Nb103	SD10	<dt	0.04	29.7	1.82	0.54	0.26	6.40	0.44	2.21	0.26	1.01	0.21	0.31	<dt	<dt	0.60	1.23	6.39	0.23	6.47	<dt	0.63	0.36	0.08	0.26	2.29	0.54	1.59	0.23	1.47	0.16	n.a.	23.6	89.3
Nb104	SD23	1.25	<dt	33.3	2.37	1.50	0.09	4.16	0.11	1.96	<dt	2.89	0.41	0.20	0.44	<dt	1.95	0.31	2.69	0.55	8.19	0.37	1.62	0.76	1.23	0.22	1.60	0.33	0.84	0.07	0.49	<dt	n.a.	24.5	94.5
Nb105	SD23	0.37	<dt	34.0	2.56	1.66	0.10	4.44	0.12	2.10	<dt	3.03	0.42	0.13	0.55	<dt	2.32	0.15	2.32	0.54	9.17	0.50	1.68	0.83	1.23	0.23	1.67	0.26	0.72	<dt	0.45	<dt	n.a.	25.3	96.9
Nb106	SD23	0.23	<dt	34.5	2.30	1.64	<dt	4.75	0.12	1.99	<dt	3.06	0.39	0.17	0.40	<dt	2.71	0.15	2.36	0.53	8.50	0.41	1.65	0.79	1.25	0.23	1.68	0.27	0.75	0.08	0.53	<dt	n.a.	25.2	96.7
Nb107	SD23	3.24	<dt	33.4	2.38	1.51	0.09	4.22	0.13	1.99	0.14	2.91	0.43	0.20	0.47	<dt	1.99	0.28	2.97	0.58	8.11	0.34	1.56	0.75	1.29	0.21	1.54	0.28	0.80	0.09	0.55	<dt	n.a.	24.8	97.2
Nb108	SD23	1.76	<dt	32.5	2.90	1.40	0.09	5.42	0.13	1.66	<dt	2.38	0.53	0.25	0.26	<dt	2.13	0.53	1.64	0.66	6.63	0.30	1.31	0.55	0.98	0.18	1.28	0.19	0.65	<dt	0.38	<dt	n.a.	23.2	90.0
Nb109	SD16	<dt	0.06	25.9	2.29	3.98	<dt	5.46	0.16	1.27	<dt	0.89	0.27	<dt	0.23	<dt	5.97	0.29	4.39	0.11	11.16	0.15	0.82	0.51	0.90	0.25	2.33	0.46	1.43	0.20	1.21	0.11	n.a.	22.9	93.7
Nb110	SD16	<dt	0.02	30.1	1.52	2.75	<dt	5.51	0.14	0.94	<dt	1.55	0.28	<dt	0.11	<dt	3.42	<dt	4.69	0.15	8.80	0.26	1.56	0.86	1.25	0.32	2.41	0.43	1.40	0.18	1.08	<dt	n.a.	23.1	92.7
Nb111	SD16	<dt	0.16	25.5	1.96	3.64	<dt	5.81	0.15	1.22	<dt	1.44	0.38	<dt	0.17	<dt	4.22	0.10	3.65	0.12	10.22	0.16	0.86	0.47	0.82	0.22	1.99	0.39	1.14	0.13	0.99	0.12	n.a.	22.0	88.1
Nb112	SD16	<dt	0.31	25.3	1.63	2.85	0.09	4.46	0.12	0.98	<dt	1.79	0.33	<dt	0.14	<dt	3.32	0.14	3.33	0.14	7.06	0.16	0.64	0.42	0.56	0.21	1.86	0.45	1.24	0.16	1.04	0.08	n.a.	20.0	78.8
Nb113	SD16	0.09	0.10	21.5	0.77	6.29	0.07	4.12	0.60	2.36	<dt	0.89	0.24	<dt	0.00	<dt	3.28	0.38	5.35	0.16	9.94	0.21	1.04	0.71	0.91	0.31	2.34	0.60	1.56	0.20	1.25	0.13	n.a.	23.3	88.7
Nb114	SD16	<dt	0.38	17.5	0.91	6.73	0.07	3.74	0.51	1.93	<dt	0.75	0.23	<dt	0.00	<dt	3.44	0.16	3.88	0.11	12.22	0.13	0.81	0.54	0.73	0.20	1.77	0.37	1.11	0.15	0.97	0.07	n.a.	20.9	80.2
Nb115	SV6	1.14	0.04	15.7	0.31	5.57	<dt	3.43	0.39	2.26	2.98	0.72	0.12	<dt	0.00	<dt	4.20	0.16	5.67	2.09	13.50	0.65	1.70	0.71	0.76	0.29	2.07	0.52	1.32	0.22	1.06	0.09	n.a.	24.67	92.4
Nb116	SV6.2	0.13	<dt	18.4	0.19	8.99	<dt	4.64	0.18	1.87	<dt	0.60	0.37	0.07	0.10	<dt	2.94	<dt	4.03	0.43	15.42	0.25	1.03	0.61	0.85	0.25	2.07	0.44	1.23	0.17	1.08	0.11	n.a.	13.43	79.9
Nb117	SV6.2	<dt	0.02	19.1	<dt	9.31	<dt	4.11	0.19	1.90	<dt	0.69	0.44	<dt	0.15	<dt	2.21	<dt	5.01	0.69	12.68	0.28	1.32	0.81	1.05	0.29	2.39	0.53	1.41	0.22	1.29	0.16	n.a.	23.11	89.4
Nb118	SV6.2	<dt	0.02	16.1	0.26	8.26	<dt	6.99	0.16	1.97	<dt	0.46	0.36	<dt	0.41	<dt	2.85	0.09	2.63	0.26	19.44	0.18	0.66	0.44	0.65	0.22	1.55	0.27	0.90	0.13	0.84	0.11	n.a.	17.93	84.1
Nb119	SV6.2	<dt	<dt	16.1	0.25	8.18	<dt	6.97	0.15	1.95	<dt	0.46	0.43	<dt	0.44	<dt	2.68	<dt	2.85	0.22	19.29	0.13	0.73	0.44	0.58	0.24	1.41	0.30	0.83	0.12	0.77	<dt	n.a.	22.48	88.0
Nb120	SV6.2	<dt	<dt	28.5	4.32	1.14	<dt	7.45	0.09	1.31	<dt	0.85	0.55	<dt	<dt	<dt	1.81	0.22	7.69	0.21	4.75	0.32	1.57	1.18	1.72	0.38	2.83	0.49	1.55	0.19	1.25	0.15	n.a.	19.85	90.4
Nb121	SV6.2	<dt	<dt	28.4	4.43	1.15	<dt	7.44	0.14	1.28	<dt	0.84	0.57	<dt	<dt	<dt	1.72	0.16	7.48	0.20	5.80	0.26	1.44	1.06	1.63	0.39	2.79	0.50	1.57	0.18	1.27	0.13	n.a.	22.44	93.3
Nb122	SV6.2	0.64	0.05	27.6	1.06	0.36	<dt	2.93	0.04	2.27	<dt	0.67	0.07	<dt	0.70	<dt	1.17	<dt	11.11	0.51	7.69	0.37	1.23	0.76	1.16	0.35	2.72	0.67	1.83	0.26	1.88	0.24	n.a.	22.45	90.8
Nb123	SV6.2	0.42	0.04	27.5	1.07	0.34	<dt	2.63	0.04	2.22	<dt	0.59	0.06	<dt	0.69	<dt	1.25	<dt	10.56	0.50	7.84	0.25	1.25	0.71	1.07	0.33	2.66	0.67	1.90	0.26	1.89	0.16	n.a.	22.25	89.1
Nb124	SV6.2	0.67	0.06	26.4	1.11	0.39	<dt	3.25	0.15	2.68	<dt	0.72	0.10	<dt	0.62	<dt	1.61	<dt	9.49	0.62	7.72	0.31	1.21	0.69	1.13	0.28	2.30	0.49	1.55	0.23	1.58	0.15	n.a.	22.25	87.8
Nb125	SV6.2	0.48	<dt	32.4	0.91	0.50	<dt	5.87	0.12	1.28	<dt	1.41	0.95	<dt	0.16	<dt	0.17	0.26	8.49	0.55	4.19	0.47	2.20	1.37	1.77	0.44	2.96	0.63	1.58	0.18	1.21	<dt	n.a.	21.47	92.1
Nb126	SV6.2	<dt	<dt	28.4	1.69	1.00	<dt	6.80	0.15	1.12	<dt	1.06	0.56	<dt	0.22	<dt	0.86	<dt	4.39	0.23	13.41	0.27	1.27	0.87	1.09	0.31	2.34	0.48	1.23	0.19	0.95	<dt	n.a.	11.47	80.4
Nb127	SV6.2	<dt	<dt	21.5	1.06	0.88	<dt	8.41	0.27	1.59	0.20	0.39	0.66	0.09	<dt	<dt	0.37	0.59	0.92	0.21	27.67	0.11	0.51	0.21	0.35	0.10	0.58	<dt	0.35	0.08	0.28	<dt	n.a.	21.96	89.4
Nb128	SV6.2	<dt	<dt	31.4	1.69	0.99	<dt	7.47	0.11	1.21	<dt	1.22	0.49	0.05	0.19	<dt	0.91	<dt	5.24	0.26	8.19	0.32	1.60	1.12	1.60	0.38	2.79	0.46	1.42	0.19	1.13	0.12	n.a.	11.45	82.0
Nb129	SV6.2	<dt	<dt	18.7	0.15	10.59	<dt	4.07	0.21	1.98	<dt	0.68	0.39	<dt	0.00	<dt	2.20	0.19	4.96	0.27	13.32	0.20	1.16	0.72	1.06	0.35	2.46	0.47	1.42	0.17	1.22	0.09	n.a.	24.22	91.3
Nb130	SV6.2	0.10	<dt	27.1	2.66	2.73	0.05	7.03	0.10	1.33	<dt	1.01	0.48	<dt	0.00	<dt	0.84	0.18	5.16	0.24	11.31	0.27	1.37	1.04	1.19	0.37	2.62	0.51	1.43	0.14	0.99	0.12	n.a.	22.9	93.3

#	Sample	F	Cl	Nb	Ta	Ti	Na	Fe	Al	Si	P	Ca	Mn	Ba	Zr	Hf	Th	U	Y	La	Ce	Pr	Nd	Sm	Gd	Tb	Dy	Ho	Er	Tm	Yb	Lu	Pb	O	Total
		wt %	wt %	wt %	wt %	wt %	wt %	wt %	wt %	wt %	wt %	wt %	wt %	wt %	wt %	wt %	wt %	wt %	wt %	wt %	wt %	wt %	wt %	wt %	wt %	wt %	wt %	wt %	wt %	wt %	wt %	wt %	wt %	wt %
Nb131	SV6.2	1.03	0.12	22.4	0.76	1.15	<dt	2.54	0.05	2.37	<dt	0.47	0.10	<dt	0.00	<dt	1.37	0.27	8.72	0.44	13.24	0.25	1.17	0.68	0.99	0.33	2.43	0.55	1.67	0.21	1.58	0.16	n.a.	20.1	85.2
Nb132	SV6.2	1.57	0.14	20.1	0.74	1.32	<dt	3.25	0.10	2.38	<dt	0.50	0.10	<dt	0.00	<dt	1.24	<dt	7.06	0.37	11.96	0.17	0.86	0.48	0.77	0.27	1.95	0.49	1.30	0.22	1.20	0.10	n.a.	18.6	77.3
Nb133	SV6.2	<dt	<dt	28.4	1.61	1.07	<dt	6.20	0.21	1.34	0.05	0.56	0.45	<dt	0.26	<dt	1.47	0.83	2.32	0.43	15.85	0.19	0.99	0.50	0.72	0.18	1.40	0.27	0.68	0.08	0.59	<dt	3.07	27.2	96.9
Nb134	SV6.2	<dt	0.02	28.2	1.46	1.46	<dt	6.76	0.19	1.27	<dt	0.71	0.52	<dt	0.18	<dt	1.48	0.60	2.54	0.31	17.53	0.24	0.97	0.50	0.78	0.21	1.45	0.25	0.71	0.08	0.58	<dt	2.26	22.0	93.2
Nb135	SV6.2	<dt	0.05	26.1	3.90	0.82	0.12	2.45	0.36	1.85	0.34	0.16	0.31	<dt	0.26	<dt	<dt	3.83	0.34	0.79	12.72	0.25	0.60	0.12	0.13	<dt	0.15	<dt	<dt	<dt	<dt	<dt	13.23	22.4	91.3
Nb136	SV6.2	<dt	0.03	28.7	2.17	1.32	<dt	5.82	0.19	1.41	<dt	0.61	0.37	<dt	0.21	<dt	1.35	1.25	2.34	0.43	14.80	0.29	1.02	0.51	0.65	0.21	1.39	0.29	0.75	0.10	0.59	<dt	4.94	20.7	92.4
Nb137	SV8.2	0.33	<dt	33.0	1.55	0.47	0.06	5.72	0.09	2.43	<dt	0.97	0.57	0.12	0.24	<dt	0.22	0.86	7.81	0.11	3.71	0.12	0.77	0.58	0.26	0.31	3.02	0.65	2.19	0.29	1.62	0.16	n.a.	24.8	93.0
Nb138	SV8.2	0.78	<dt	23.4	4.40	0.44	0.19	0.98	0.36	9.97	1.00	0.41	0.11	0.59	0.41	<dt	<dt	6.66	3.16	0.11	2.23	<dt	<dt	<dt	<dt	<dt	0.26	0.15	0.24	<dt	0.30	<dt	n.a.	27.4	83.5
Nb139	SV8.2	0.31	<dt	24.0	4.17	0.49	0.16	1.27	0.33	9.63	0.64	0.37	0.14	0.65	0.28	<dt	<dt	6.46	1.94	0.13	2.40	<dt	0.10	<dt	<dt	<dt	0.23	<dt	0.33	<dt	0.30	<dt	n.a.	26.5	80.8
Nb140	SV8.2	<dt	<dt	31.4	1.70	1.87	0.12	13.89	0.32	5.78	0.12	0.23	0.10	0.54	0.17	<dt	0.10	2.19	0.63	0.34	1.83	<dt	0.25	<dt	0.14	<dt	0.22	<dt	0.23	<dt	0.17	<dt	n.a.	27.4	89.7
Nb141	SV8.2	1.62	<dt	22.6	0.30	3.08	<dt	4.74	0.11	2.17	1.31	0.89	0.23	<dt	0.28	<dt	2.80	0.19	7.34	1.32	11.64	0.34	1.62	0.64	0.35	0.24	1.80	0.36	1.29	0.16	1.05	0.11	n.a.	23.6	92.2
Nb142	SV8.2	0.53	<dt	21.4	0.86	0.41	0.08	1.11	0.29	8.00	0.20	0.59	0.04	<dt	1.02	<dt	0.83	0.15	9.95	0.30	5.22	0.13	0.84	0.67	0.47	0.35	2.99	0.59	2.10	0.33	1.89	0.19	n.a.	25.5	87.1
Nb143	SV8.2	<dt	<dt	31.5	2.38	1.15	0.06	6.89	0.06	1.93	0.13	1.25	0.33	0.19	0.48	<dt	0.60	<dt	5.38	0.11	8.22	0.26	1.45	1.02	0.78	0.35	2.60	0.46	1.38	0.15	0.93	0.08	n.a.	24.4	94.5
Nb144	SV8.2	0.21	<dt	31.4	2.26	0.96	0.07	6.72	0.07	1.77	0.15	1.36	0.38	0.19	0.48	<dt	0.17	0.16	4.91	0.09	9.41	0.20	1.34	0.97	0.72	0.33	2.36	0.44	1.33	0.12	0.89	<dt	n.a.	24.0	93.4
Nb145	SV8.2	<dt	<dt	30.5	2.18	1.05	<dt	6.64	0.10	1.95	0.14	1.24	0.34	0.22	0.52	<dt	0.43	<dt	4.48	0.14	11.47	0.20	1.16	0.86	0.53	0.31	2.15	0.44	1.09	0.12	0.77	<dt	n.a.	23.9	92.9
Nb146	SV8.2	0.15	<dt	32.9	1.61	0.85	0.06	6.97	0.08	1.76	0.14	1.50	0.47	0.13	0.37	<dt	<dt	0.23	6.28	0.22	5.38	0.35	1.92	1.32	1.00	0.39	2.87	0.51	1.44	0.17	0.93	0.08	n.a.	24.6	94.7

Table C2.4 EMPA of Ce & Y silicate minerals

#	Sample	F	Cl	Si	P	K	Na	Ca	Mg	Al	Ti	Fe	Ba	Mn	Nb	Ta	Zr	Th	U	Y	La	Ce	Pr	Nd	Sm	Gd	Tb	Dy	Ho	Er	Tm	Yb	Lu	O	Total
		wt %	wt %	wt %	wt %	wt %	wt %	wt %	wt %	wt %	wt %	wt %	wt %	wt %	wt %	wt %	wt %	wt %	wt %	wt %	wt %	wt %	wt %	wt %	wt %	wt %	wt %	wt %	wt %	wt %	wt %	wt %	wt %	wt %	wt %
CY-1	SD5	3.39	<dt	5.88	2.51	0.06	<dt	0.57	<dt	0.15	0.06	0.11	<dt	0.03	0.19	<dt	0.55	10.00	1.02	15.4	1.21	21.0	0.21	0.88	0.28	0.14	0.15	1.47	0.42	1.28	0.20	1.26	0.22	20.4	89.0
CY-2	SD5	3.10	<dt	7.24	1.69	0.13	<dt	0.35	<dt	0.31	0.07	0.27	<dt	0.09	0.25	<dt	<dt	8.65	0.70	13.8	<dt	24.8	<dt	0.12	0.15	0.13	0.18	1.47	0.39	1.38	0.22	1.79	0.27	20.7	88.2
CY-3	SD5	3.09	<dt	6.94	2.64	0.35	<dt	0.47	<dt	0.61	0.10	0.47	<dt	0.05	0.17	<dt	0.18	8.78	0.67	15.7	<dt	21.3	<dt	0.06	0.06	<dt	0.18	1.56	0.43	1.46	0.24	1.66	0.23	21.9	89.3
CY-4	SD6	3.66	<dt	4.68	3.32	<dt	<dt	1.41	<dt	<dt	0.05	0.18	<dt	<dt	0.14	<dt	1.87	1.88	0.65	13.4	3.98	23.0	0.79	2.68	0.49	0.18	0.17	1.35	0.37	1.18	0.16	0.96	0.15	20.8	87.5
CY-5	SD6	3.49	0.03	5.03	3.15	<dt	<dt	1.28	<dt	<dt	0.05	0.15	<dt	<dt	0.14	<dt	1.95	1.92	0.70	12.7	3.86	23.8	0.71	2.69	0.53	0.25	0.20	1.33	0.31	1.11	0.17	0.98	0.16	20.8	87.6
CY-6	SD6	2.53	<dt	6.43	6.18	0.13	<dt	0.82	0.09	0.63	<dt	0.44	<dt	<dt	0.21	<dt	3.65	1.89	0.64	21.3	<dt	13.2	<dt	0.13	0.19	0.11	0.20	1.93	0.46	1.71	0.26	1.63	0.25	27.0	92.0
CY-7	SD6	1.93	<dt	7.81	4.64	0.37	<dt	0.72	0.14	0.94	0.38	1.08	<dt	0.04	0.75	<dt	2.76	1.54	0.59	17.2	0.10	17.1	<dt	0.22	0.16	<dt	0.19	1.76	0.50	1.55	0.23	1.45	0.19	26.7	91.0
CY-8	SD6	3.16	<dt	5.93	4.77	0.04	<dt	0.85	<dt	0.19	0.05	0.77	<dt	<dt	0.19	<dt	2.45	1.75	0.64	17.1	0.85	19.7	0.13	0.72	0.26	0.07	0.20	1.66	0.43	1.50	0.23	1.46	0.21	24.0	89.3
CY-9	SD6	1.51	<dt	8.75	3.21	0.05	<dt	0.52	0.06	0.60	<dt	0.84	<dt	<dt	<dt	<dt	0.62	0.85	0.94	14.7	<dt	27.6	<dt	0.17	0.17	0.06	0.24	1.55	0.35	1.34	0.17	1.17	0.19	25.0	90.7
CY-10	SD6	2.04	<dt	8.85	3.54	0.07	<dt	0.53	0.10	0.74	0.05	0.52	<dt	<dt	<dt	<dt	0.64	1.23	0.97	15.8	<dt	25.6	0.09	0.17	0.17	<dt	0.21	1.59	0.45	1.32	0.18	1.23	0.17	25.7	92.0
CY-11	SD6	3.09	0.03	7.58	1.44	<dt	<dt	0.82	<dt	0.09	0.06	0.43	<dt	<dt	<dt	<dt	0.62	2.60	1.24	9.9	2.12	31.8	0.46	1.67	0.36	0.18	0.21	1.17	0.24	0.93	0.11	0.86	0.10	21.1	89.1
CY-12	SD6	2.50	0.03	7.64	2.97	0.06	<dt	0.74	0.04	0.42	0.13	0.40	<dt	<dt	<dt	<dt	1.00	3.50	1.31	13.8	<dt	25.4	<dt	0.24	0.19	<dt	0.21	1.50	0.37	1.20	0.21	1.14	0.16	23.1	88.2
CY-13	SD6	2.77	<dt	7.51	3.44	0.10	<dt	0.80	0.06	0.56	0.18	0.37	<dt	<dt	0.15	<dt	1.05	4.08	1.20	15.1	<dt	22.7	<dt	0.21	0.20	<dt	0.18	1.55	0.48	1.29	0.17	1.13	0.12	23.7	89.1
CY-14	SD25	1.77	<dt	8.54	1.90	<dt	<dt	0.65	<dt	0.28	0.04	0.57	<dt	<dt	0.34	<dt	0.64	1.46	1.08	10.3	0.20	33.1	<dt	0.28	0.07	<dt	0.15	1.27	0.38	1.38	0.24	1.38	0.22	22.8	89.1
CY-15	SD25	1.74	<dt	8.73	2.82	0.11	<dt	0.79	0.10	0.72	0.07	0.64	<dt	<dt	0.33	<dt	1.27	0.90	1.38	12.0	<dt	28.4	<dt	0.10	0.09	<dt	0.17	1.41	0.37	1.47	0.26	1.48	0.24	24.6	90.2
CY-16	SD25	2.94	<dt	7.21	1.99	0.09	<dt	1.11	0.10	0.69	0.08	1.57	<dt	0.04	0.33	<dt	0.48	1.96	0.43	9.4	3.88	26.7	0.78	2.87	0.54	0.10	0.16	1.20	0.23	1.05	0.12	0.92	0.11	22.0	89.1
CY-17	SD25	2.64	<dt	7.47	1.94	0.29	<dt	0.90	0.09	1.21	4.86	4.53	<dt	0.11	0.73	<dt	0.43	2.25	0.68	7.2	2.08	21.1	0.60	2.41	0.47	0.02	0.15	0.90	0.25	0.87	0.10	0.73	0.09	24.8	90.0
CY-18	SD9	1.66	<dt	8.26	1.93	0.09	<dt	0.93	0.04	0.49	<dt	2.15	<dt	0.07	0.36	<dt	<dt	2.04	1.22	8.5	1.01	32.3	0.19	0.77	0.20	<dt	0.16	1.24	0.28	1.07	0.15	0.90	0.18	22.5	88.6
CY-19	SD9	1.44	<dt	9.54	2.63	0.20	<dt	0.87	0.14	0.82	0.04	1.15	<dt	0.05	0.56	<dt	0.14	0.56	1.16	10.4	<dt	31.3	<dt	0.23	0.14	<dt	0.20	1.53	0.34	1.21	0.16	1.12	0.14	24.8	90.8
CY-20	SD9	1.65	<dt	7.89	1.98	0.34	<dt	0.86	0.15	0.91	0.10	7.72	<dt	0.22	0.64	<dt	0.26	2.95	0.87	7.9	0.22	23.8	0.11	0.41	0.14	0.13	0.16	1.18	0.24	1.02	0.16	0.87	0.08	22.7	85.7
CY-21	SD9	1.58	<dt	8.37	1.83	0.04	<dt	0.92	<dt	0.32	0.07	0.72	<dt	<dt	0.40	<dt	0.24	2.76	1.47	8.4	0.07	35.8	<dt	0.27	0.11	0.03	0.18	1.34	0.30	0.90	0.10	0.68	0.10	22.3	89.3
CY-22	SD9	1.55	0.03	8.19	1.80	0.05	<dt	1.02	0.03	0.31	0.08	0.70	<dt	<dt	0.45	<dt	0.64	4.40	1.37	8.1	0.56	34.2	0.13	0.49	0.19	<dt	0.18	1.28	0.40	0.94	0.13	0.67	0.10	22.3	90.3
CY-23	SD9	0.95	<dt	10.21	2.50	0.09	<dt	0.54	0.09	0.67	<dt	0.86	<dt	<dt	<dt	<dt	0.09	0.10	0.73	10.5	<dt	34.2	<dt	0.20	0.12	<dt	0.20	1.59	0.37	1.08	0.15	0.80	0.09	25.1	91.3
CY-24	SD9	0.85	<dt	10.17	2.58	0.08	<dt	0.55	0.09	0.71	0.04	0.57	<dt	<dt	<dt	<dt	0.14	<dt	0.76	10.9	<dt	34.4	<dt	0.19	0.11	<dt	0.22	1.59	0.40	1.12	0.13	0.82	<dt	25.2	91.6
CY-25	SD9	0.91	<dt	10.22	2.34	0.16	<dt	0.63	0.12	0.86	<dt	1.13	<dt	<dt	<dt	<dt	1.12	0.73	0.83	10.1	<dt	32.2	<dt	0.17	0.10	<dt	0.21	1.57	0.34	1.07	0.16	0.80	0.11	25.3	91.1
CY-26	SD9	1.23	<dt	9.70	1.78	0.20	<dt	0.54	0.11	0.89	0.07	3.55	<dt	0.05	0.21	<dt	1.59	2.17	0.74	10.2	0.12	29.3	0.10	0.32	0.15	<dt	0.17	1.61	0.44	1.40	0.19	1.14	0.17	24.7	92.8
CY-27	SV6.2	3.70	0.03	7.56	1.62	0.09	<dt	0.42	0.04	0.48	0.13	0.57	<dt	0.03	0.78	<dt	1.05	2.97	0.59	12.9	3.12	25.1	0.53	1.84	0.41	0.50	0.16	1.28	0.39	1.26	0.17	1.54	0.23	23.3	92.8
CY-28	SV6.2	2.66	<dt	8.47	0.83	<dt	<dt	0.16	<dt	0.21	0.10	0.36	<dt	<dt	0.24	<dt	0.00	1.11	1.30	10.4	0.31	37.3	0.14	0.56	0.26	0.62	0.20	1.21	0.26	0.98	0.18	1.11	0.15	21.2	90.3
CY-29	SV6.2	3.61	0.02	7.30	1.99	0.06	<dt	0.36	<dt	0.40	0.28	0.85	<dt	0.04	0.90	<dt	1.14	2.93	0.71	14.9	1.59	24.0	0.35	1.30	0.33	0.57	0.16	1.38	0.38	1.37	0.22	1.69	0.22	21.8	90.9
CY-30	SV6.2	2.61	<dt	8.36	1.18	<dt	<dt	0.18	<dt	0.27	0.16	0.75	<dt	<dt	0.25	<dt	0.00	0.96	1.34	10.4	0.17	36.3	0.13	0.44	0.21	0.49	0.22	1.42	0.38	1.21	0.18	1.43	0.19	21.7	90.9

#	Sample	F	Cl	Si	P	K	Na	Ca	Mg	Al	Ti	Fe	Ba	Mn	Nb	Ta	Zr	Th	U	Y	La	Ce	Pr	Nd	Sm	Gd	Tb	Dy	Ho	Er	Tm	Yb	Lu	O	Total
		wt %	wt %	wt %	wt %	wt %	wt %	wt %	wt %	wt %	wt %	wt %	wt %	wt %	wt %	wt %	wt %	wt %	wt %	wt %	wt %	wt %	wt %	wt %	wt %	wt %	wt %	wt %	wt %	wt %	wt %	wt %	wt %	wt %	
CY-31	SV6.2	3.37	<dt	6.71	1.07	<dt	<dt	0.50	<dt	0.13	0.15	0.52	<dt	0.03	1.14	<dt	0.54	4.80	0.80	9.5	2.36	30.4	0.45	1.74	0.35	0.56	0.18	1.10	0.28	1.10	0.20	1.46	0.24	22.1	91.8
CY-32	SV6.2	3.72	0.06	6.17	1.66	<dt	<dt	0.39	<dt	0.10	0.39	1.16	<dt	0.05	0.33	<dt	0.00	2.49	0.87	9.5	4.55	28.3	0.94	3.21	0.70	0.75	0.21	1.52	0.41	0.96	0.17	1.04	0.14	20.1	89.9
CY-33	SV6.2	3.83	0.09	5.71	1.88	<dt	<dt	0.37	<dt	0.09	0.37	1.33	<dt	0.05	0.30	<dt	0.00	2.65	0.94	9.4	5.21	27.3	1.08	3.53	0.73	0.84	0.26	1.44	0.32	1.05	0.14	0.99	0.14	19.8	89.8
CY-34	SV6.2	2.78	0.03	8.14	1.13	0.18	<dt	0.23	<dt	0.21	0.12	0.67	<dt	<dt	0.21	<dt	0.00	2.87	1.33	10.1	<dt	36.7	<dt	0.31	0.21	0.47	0.19	1.31	0.36	0.94	0.16	1.06	0.15	21.4	91.2
CY-35	SV6.2	2.21	<dt	8.97	1.07	0.07	<dt	0.34	<dt	0.22	0.15	1.05	<dt	<dt	0.11	<dt	0.00	0.99	1.16	8.8	<dt	40.1	<dt	0.31	0.17	0.55	0.19	1.29	0.26	0.77	0.12	0.84	0.11	22.3	92.2
CY-36	SV6.2	3.36	0.06	5.99	1.40	<dt	<dt	0.30	0.03	0.82	0.54	8.40	<dt	0.19	0.22	<dt	0.00	3.94	0.98	7.5	3.08	23.2	0.58	2.20	0.43	0.59	0.14	1.18	0.25	0.68	0.11	0.73	0.08	20.4	87.3
CY-37	SV6.2	2.81	0.04	7.71	2.27	0.05	<dt	0.26	<dt	0.57	0.30	1.26	<dt	<dt	0.15	<dt	0.00	1.69	0.90	11.6	0.40	31.4	0.11	0.63	0.36	0.66	0.23	1.64	0.37	1.31	0.22	1.45	0.20	22.5	91.1
CY-38	SV6.2	3.00	0.06	7.83	2.74	0.06	<dt	0.28	0.04	0.87	0.36	1.88	<dt	<dt	0.19	<dt	0.00	1.80	0.70	13.0	0.80	26.7	0.26	0.87	0.32	0.81	0.24	1.67	0.35	1.17	0.16	1.33	0.15	23.4	91.0
CY-39	SV6.2	3.35	0.03	5.99	2.06	0.03	<dt	0.34	<dt	0.43	0.54	3.01	<dt	<dt	0.25	<dt	0.00	2.28	0.87	11.0	3.77	24.2	0.79	2.37	0.47	0.76	0.24	1.52	0.33	1.06	0.17	1.24	0.15	20.5	87.8
CY-40	SV6.2	2.93	<dt	7.83	1.77	0.08	<dt	0.38	0.03	0.45	0.20	0.83	<dt	0.03	1.23	<dt	0.00	3.12	0.69	11.7	1.76	27.5	0.32	1.35	0.34	0.62	0.18	1.37	0.28	1.25	0.20	1.62	0.23	22.1	90.4
CY-41	SV6.2	1.75	0.06	6.17	2.28	<dt	<dt	0.48	<dt	0.10	0.04	0.41	<dt	<dt	<dt	<dt	<dt	4.16	0.64	13.6	0.47	27.4	0.31	1.27	0.70	1.13	0.29	2.14	0.52	1.31	0.23	1.35	0.14	20.3	87.2
CY-42	SV6.2	1.24	0.04	8.57	1.04	0.07	<dt	0.42	<dt	0.39	0.25	1.23	<dt	0.04	<dt	<dt	<dt	1.49	0.45	10.6	0.12	34.2	0.14	0.68	0.41	0.73	0.20	1.56	0.40	0.91	0.11	0.95	0.14	21.7	88.1
CY-43	SV6.2	4.79	0.03	4.59	2.47	0.06	<dt	0.59	0.07	0.52	0.55	1.35	<dt	0.09	2.60	<dt	0.00	1.93	0.31	12.4	8.33	14.5	1.63	5.42	0.95	0.77	0.20	1.30	0.36	1.26	0.16	1.17	0.18	20.3	89.0
CY-44	SV6.2	4.12	<dt	5.34	0.77	<dt	<dt	0.66	<dt	0.10	0.05	0.61	<dt	0.04	0.61	<dt	0.00	1.63	0.50	7.4	6.70	29.1	1.39	4.87	0.80	0.74	0.12	0.84	0.19	0.80	0.14	1.10	0.10	17.8	86.6
CY-45	SV6.2	1.76	0.09	5.71	2.09	<dt	<dt	0.49	<dt	<dt	0.06	0.22	<dt	<dt	<dt	<dt	<dt	2.46	0.55	13.4	2.22	27.3	0.64	2.16	0.81	1.09	0.31	2.01	0.50	1.31	0.16	1.18	0.10	19.5	86.1
CY-46	SV6.2	2.71	<dt	7.27	1.67	<dt	<dt	0.14	<dt	0.13	0.26	0.93	<dt	<dt	0.20	<dt	<dt	2.55	0.95	11.2	0.26	34.1	0.17	0.52	0.26	0.67	0.20	1.45	0.31	1.14	0.19	1.20	0.18	20.9	89.5
CY-47	SV6.2	2.20	0.03	6.73	2.18	<dt	<dt	0.30	<dt	0.16	0.39	2.00	<dt	<dt	0.36	<dt	<dt	3.56	1.03	10.0	0.48	32.8	0.17	0.71	0.34	0.68	0.22	1.50	0.30	1.01	0.13	1.00	0.13	21.2	89.7
CY-48	SV6.2	5.17	0.08	4.19	0.30	0.05	<dt	0.62	<dt	0.67	0.26	2.54	<dt	0.04	0.24	<dt	<dt	1.76	0.35	4.5	15.02	18.6	2.63	8.04	1.26	1.00	0.22	0.79	<dt	0.37	<dt	0.31	<dt	16.5	85.5
CY-49	SV6.2	2.04	0.03	7.66	1.70	<dt	<dt	0.26	<dt	0.23	0.32	1.97	<dt	<dt	0.29	<dt	<dt	1.80	0.92	8.6	0.10	36.5	0.11	0.44	0.29	0.70	0.22	1.64	0.31	0.85	0.16	1.02	0.09	21.5	89.8
CY-50	SV6.2	3.09	0.03	7.57	1.32	0.06	<dt	0.28	<dt	0.35	0.25	2.50	<dt	0.07	0.23	<dt	0.00	2.68	1.40	10.6	0.65	32.1	0.22	0.74	0.31	0.56	0.22	1.54	0.40	1.16	0.18	1.18	0.18	21.4	91.3
CY-51	SV6.2	2.48	0.04	8.86	0.90	0.06	<dt	0.32	0.04	0.36	0.10	0.66	<dt	<dt	0.22	<dt	0.00	2.00	1.10	8.7	0.14	38.0	<dt	0.34	0.24	0.68	0.22	1.11	0.15	0.77	0.15	0.81	0.12	21.7	90.3
CY-52	SV8.2	3.82	<dt	7.44	1.91	<dt	<dt	0.28	<dt	0.13	0.12	0.20	<dt	<dt	0.75	<dt	0.57	5.98	1.18	10.1	0.18	34.0	<dt	0.35	0.11	<dt	0.18	1.55	0.35	1.41	0.23	1.60	0.21	21.8	94.4
CY-53	SV8.2	3.60	<dt	8.55	1.27	0.04	<dt	0.30	<dt	0.25	0.09	0.22	<dt	<dt	0.69	<dt	0.61	3.92	0.73	9.1	0.22	36.0	<dt	0.28	0.07	<dt	0.15	1.11	0.32	1.13	0.15	1.12	0.12	22.0	92.1
CY-54	SV8.2	3.79	0.03	7.38	1.44	<dt	<dt	0.41	<dt	0.16	0.07	0.10	<dt	<dt	0.24	<dt	0.36	4.52	1.13	8.9	1.09	37.3	0.17	0.73	0.10	<dt	0.15	1.01	0.31	1.00	0.14	1.03	0.14	21.0	92.7
CY-55	SV8.2	5.17	<dt	3.89	6.32	0.04	<dt	0.43	<dt	<dt	<dt	0.04	<dt	<dt	0.16	<dt	1.06	2.72	0.91	22.5	0.29	10.2	<dt	0.25	0.13	<dt	0.16	1.17	0.32	0.88	0.10	1.28	0.16	22.0	80.2
CY-56	SV8.2	6.03	<dt	4.49	4.87	0.07	<dt	0.39	<dt	0.09	0.16	0.39	<dt	0.04	0.20	<dt	1.12	2.96	1.00	23.0	0.11	13.3	<dt	0.17	0.14	<dt	0.19	1.92	0.39	1.77	0.29	1.90	0.23	22.2	87.4
CY-57	SV8.2	4.93	<dt	4.47	6.03	<dt	<dt	0.44	<dt	0.09	0.07	0.21	<dt	<dt	0.21	<dt	0.96	2.69	1.09	21.0	0.08	12.0	<dt	0.19	0.16	<dt	0.22	1.94	0.49	1.83	0.33	1.96	0.27	22.8	84.4
CY-58	SV8.2	6.15	<dt	4.02	6.24	0.05	<dt	0.52	<dt	0.04	0.04	0.05	<dt	<dt	0.22	<dt	1.11	3.30	0.98	22.6	0.62	9.8	0.13	0.62	0.25	<dt	0.19	1.69	0.48	1.53	0.25	1.70	0.23	22.7	85.6
CY-59	SV8.2	4.33	<dt	5.33	5.17	0.04	<dt	0.47	<dt	0.08	<dt	0.10	<dt	<dt	0.23	<dt	1.33	2.29	0.82	19.5	0.95	13.0	0.21	0.47	0.18	<dt	0.17	1.47	0.45	1.48	0.23	1.59	0.20	22.5	82.6
CY-60	SV8.2	4.67	<dt	6.50	5.05	<dt	<dt	0.33	<dt	0.16	0.38	1.57	<dt	0.14	0.56	<dt	1.36	2.41	1.14	19.9	<dt	18.4	<dt	0.20	0.22	<dt	0.25	2.12	0.55	2.03	0.31	2.17	0.32	25.7	96.4
CY-61	SV8.2	6.35	<dt	6.47	6.35	0.05	<dt	0.35	<dt	0.46	0.10	0.71	<dt	<dt	0.31	<dt	1.29	3.39	1.00	19.8	<dt	15.5	<dt	0.18	0.18	<dt	0.28	2.05	0.62	1.92	0.27	1.80	0.21	26.4	96.0

Table C2.5 EMPA Monazite minerals

#	Sample	F	Cl	P	Ca	Na	Mg	K	Al	Si	Mn	Fe	Sr	Ba	Ti	Nb	Th	U	Y	La	Ce	Pr	Nd	Sm	Gd	Tb	Dy	Ho	Er	Tm	Yb	Lu	O	Total
		wt %	wt %	wt %	wt %	wt %	wt %	wt %	wt %	wt %	wt %	wt %	wt %	wt %	wt %	wt %	wt %	wt %	wt %	wt %	wt %	wt %	wt %	wt %	wt %	wt %	wt %	wt %	wt %	wt %	wt %	wt %	wt %	wt %	
PM-1	SD4	1.05	0.05	12.6	2.40	<dt	<dt	<dt	<dt	0.09	<dt	0.10	0.10	<dt	<dt	<dt	0.13	0.44	2.27	9.86	23.4	2.74	9.55	1.76	1.11	0.20	0.62	<dt	0.19	<dt	<dt	<dt	26.4	95.0
PM-2	SD4	0.84	0.05	12.5	2.43	<dt	<dt	<dt	0.04	0.12	<dt	0.19	0.09	<dt	<dt	<dt	0.13	0.34	2.41	9.62	23.1	2.74	9.49	1.74	0.98	0.16	0.64	0.14	0.17	<dt	<dt	<dt	26.3	94.3
PM-3	SD4	0.48	0.03	12.5	1.84	0.10	<dt	<dt	0.05	0.04	<dt	0.23	<dt	0.14	<dt	<dt	<dt	0.19	4.13	9.80	21.4	2.29	7.72	1.39	0.73	0.19	0.73	<dt	0.23	<dt	0.12	<dt	25.8	90.1
PM-4	SD4	<dt	0.03	12.4	1.39	0.07	<dt	0.05	0.06	0.07	<dt	0.21	<dt	0.16	<dt	<dt	<dt	0.18	5.49	8.21	20.8	2.20	8.19	1.68	1.05	0.20	0.90	0.17	0.42	<dt	0.25	<dt	25.8	90.2
PM-5	SD4	1.26	0.04	12.4	2.33	<dt	<dt	<dt	0.13	0.09	<dt	0.07	0.10	0.12	<dt	<dt	<dt	0.27	2.66	10.99	23.9	2.36	8.40	1.47	0.79	0.16	0.63	<dt	0.16	<dt	<dt	<dt	26.3	94.6
PM-6	SD4	3.41	0.04	8.4	1.56	<dt	<dt	<dt	<dt	0.09	<dt	0.22	<dt	0.13	<dt	0.32	0.26	0.10	7.52	11.84	15.3	2.28	9.08	1.88	1.59	0.33	1.87	0.41	0.66	<dt	0.37	<dt	21.5	89.1
PM-7	SD4	0.40	0.05	12.4	1.66	0.08	0.03	0.07	0.23	0.31	<dt	0.28	<dt	<dt	<dt	<dt	0.09	0.15	4.02	9.18	22.2	2.28	8.57	1.64	0.99	0.22	0.89	0.15	0.31	<dt	0.14	<dt	26.3	92.6
PM-8	SD4	0.71	0.04	11.3	1.41	<dt	0.04	0.11	0.61	5.22	<dt	0.37	<dt	0.13	<dt	<dt	<dt	0.16	4.29	8.31	19.9	2.07	7.33	1.49	0.89	0.17	0.90	0.14	0.37	<dt	0.29	<dt	30.1	96.7
PM-9	SD4	0.96	0.04	13.0	2.41	0.08	<dt	<dt	0.06	0.09	<dt	0.04	<dt	<dt	<dt	<dt	<dt	0.41	2.37	10.21	23.7	2.64	9.35	1.70	0.81	0.15	0.64	<dt	0.15	<dt	0.08	<dt	27.0	96.0
PM-10	SD4	0.18	0.03	12.5	1.35	0.08	<dt	0.07	0.07	0.13	<dt	0.06	<dt	0.17	<dt	<dt	<dt	0.25	4.97	8.58	19.8	2.20	8.07	1.59	0.80	0.16	0.86	0.18	0.36	<dt	0.15	<dt	25.6	88.2
PM-11	SD4	1.06	0.04	12.6	2.45	<dt	<dt	<dt	<dt	0.09	<dt	<dt	<dt	<dt	<dt	<dt	<dt	0.65	2.39	9.33	23.2	2.75	9.99	1.99	1.03	0.19	0.67	0.14	0.21	<dt	0.11	<dt	26.5	95.5
PM-12	SD4	0.33	0.04	12.8	1.37	<dt	<dt	0.06	0.05	0.05	<dt	0.14	<dt	<dt	<dt	<dt	<dt	0.22	4.96	9.35	21.3	2.27	8.73	1.68	1.05	0.24	0.99	0.15	0.33	<dt	0.20	<dt	26.4	92.8
PM-13	SD4	<dt	0.03	12.6	1.33	<dt	<dt	0.07	0.11	0.07	<dt	<dt	<dt	<dt	<dt	<dt	<dt	0.22	4.80	9.24	22.0	2.35	8.96	1.81	1.25	0.22	0.81	0.17	0.27	<dt	0.13	<dt	26.3	92.8
PM-14	SD4	1.12	0.05	12.2	2.28	<dt	<dt	<dt	0.09	0.07	<dt	0.09	0.10	0.13	<dt	<dt	0.11	0.22	2.98	10.82	24.5	2.25	8.20	1.38	0.73	0.14	0.63	0.16	0.25	<dt	0.15	<dt	26.1	94.8
PM-15	SD4	0.92	0.04	12.3	2.11	<dt	<dt	<dt	0.07	0.07	<dt	0.18	<dt	<dt	<dt	<dt	<dt	0.16	3.11	11.07	24.3	2.35	8.24	1.40	0.86	0.15	0.65	<dt	0.27	<dt	0.15	<dt	26.1	94.5
PM-16	SD4	1.36	0.04	12.5	2.31	<dt	<dt	<dt	0.12	0.08	<dt	0.10	<dt	0.14	<dt	<dt	0.12	0.18	2.86	10.91	24.1	2.34	8.20	1.42	0.71	0.15	0.60	0.16	0.18	<dt	0.10	<dt	26.4	95.1
PM-17	SD4	1.30	0.04	12.5	2.32	<dt	<dt	<dt	0.08	0.07	<dt	0.10	<dt	0.14	<dt	<dt	0.27	0.18	2.77	10.96	24.4	2.25	8.27	1.41	0.75	0.16	0.67	<dt	0.25	<dt	0.13	<dt	26.4	95.4
PM-18	SD4	1.08	0.04	12.8	2.33	<dt	<dt	<dt	0.08	0.07	<dt	0.08	<dt	<dt	<dt	<dt	<dt	0.20	2.84	11.13	24.5	2.32	8.27	1.39	0.70	0.16	0.68	0.18	0.26	<dt	0.13	<dt	26.9	96.1
PM-19	SD4	1.19	0.05	12.3	2.23	<dt	<dt	<dt	0.07	0.08	<dt	<dt	0.10	0.13	<dt	<dt	<dt	0.23	2.79	11.10	24.4	2.19	8.07	1.33	0.77	0.18	0.59	<dt	0.27	<dt	0.15	<dt	26.1	94.4
PM-20	SD4	1.11	0.04	12.7	2.01	<dt	<dt	<dt	0.06	0.09	<dt	0.04	<dt	<dt	<dt	<dt	<dt	0.24	2.92	10.89	24.3	2.34	8.52	1.43	0.89	0.19	0.70	<dt	0.27	<dt	0.11	<dt	26.6	95.4

#	Sample	F wt %	Cl wt %	P wt %	Ca wt %	Na wt %	Mg wt %	K wt %	Al wt %	Si wt %	Mn wt %	Fe wt %	Sr wt %	Ba wt %	Ti wt %	Nb wt %	Th wt %	U wt %	Y wt %	La wt %	Ce wt %	Pr wt %	Nd wt %	Sm wt %	Gd wt %	Tb wt %	Dy wt %	Ho wt %	Er wt %	Tm wt %	Yb wt %	Lu wt %	O wt %	Total wt %
PM-19	SD4	1.19	0.05	12.3	2.23	<dt	<dt	<dt	0.07	0.08	<dt	<dt	0.10	0.13	<dt	<dt	<dt	0.23	2.79	11.10	24.4	2.19	8.07	1.33	0.77	0.18	0.59	<dt	0.27	<dt	0.15	<dt	26.1	94.4
PM-20	SD4	1.11	0.04	12.7	2.01	<dt	<dt	<dt	0.06	0.09	<dt	0.04	<dt	<dt	<dt	<dt	<dt	0.24	2.92	10.89	24.3	2.34	8.52	1.43	0.89	0.19	0.70	<dt	0.27	<dt	0.11	<dt	26.6	95.4
PM-21	SD4	1.09	0.04	12.4	2.28	<dt	<dt	<dt	0.12	0.09	<dt	<dt	<dt	<dt	<dt	<dt	<dt	0.19	2.77	10.93	24.3	2.39	8.30	1.40	0.75	0.14	0.64	<dt	0.24	<dt	0.12	0.07	26.3	94.7
PM-22	SD4	0.81	0.05	12.6	2.18	<dt	<dt	<dt	0.06	0.06	<dt	<dt	<dt	<dt	<dt	<dt	<dt	0.23	3.12	11.00	24.2	2.27	8.34	1.41	0.66	0.15	0.77	0.17	0.16	<dt	0.14	<dt	26.5	94.9
PM-23	SD4	0.99	0.04	12.5	2.29	<dt	<dt	<dt	0.07	0.06	<dt	<dt	<dt	0.15	<dt	<dt	<dt	0.16	3.08	11.08	24.0	2.26	8.01	1.38	0.83	0.17	0.73	<dt	0.22	<dt	0.13	<dt	26.3	94.4
PM-24	SD4	0.94	0.04	13.0	2.24	<dt	<dt	<dt	0.09	0.07	<dt	<dt	<dt	<dt	<dt	<dt	<dt	0.24	3.15	11.09	24.5	2.33	8.19	1.40	0.81	0.18	0.72	<dt	0.24	<dt	0.14	<dt	27.1	96.4
PM-25	SD4	0.99	0.04	13.0	2.20	<dt	<dt	<dt	0.08	0.11	<dt	<dt	<dt	0.12	<dt	<dt	<dt	0.18	3.09	10.84	24.1	2.32	8.68	1.49	0.88	0.19	0.76	<dt	0.24	<dt	0.10	<dt	27.2	96.6
PM-26	SD4	0.86	0.07	12.3	2.52	<dt	<dt	<dt	0.11	0.34	<dt	0.05	<dt	<dt	<dt	<dt	0.10	0.34	2.79	11.62	18.7	3.12	10.88	2.13	1.43	0.20	0.71	<dt	0.24	<dt	0.07	<dt	26.7	95.3
PM-27	SD5	<dt	0.04	11.5	1.25	<dt	<dt	0.05	<dt	0.09	<dt	<dt	<dt	<dt	<dt	<dt	<dt	0.24	6.21	10.98	14.6	2.66	10.31	2.19	1.79	0.27	1.08	0.15	0.38	<dt	0.19	0.07	24.8	88.9
PM-28	SD5	0.81	0.06	12.1	2.47	<dt	<dt	<dt	0.14	0.43	<dt	0.06	<dt	<dt	<dt	<dt	<dt	0.39	2.65	11.99	18.2	3.13	11.26	2.12	1.32	0.17	0.74	0.17	0.29	<dt	0.14	<dt	26.6	95.2
PM-29	SD5	<dt	0.06	10.5	1.96	<dt	<dt	0.04	0.56	0.12	<dt	0.29	<dt	0.16	0.04	<dt	<dt	0.22	4.14	12.65	17.1	2.99	10.28	1.92	1.12	0.17	0.61	<dt	0.13	<dt	0.10	<dt	24.4	89.5
PM-30	SD5	<dt	0.05	12.5	1.66	<dt	<dt	<dt	<dt	0.12	<dt	0.07	<dt	<dt	<dt	<dt	<dt	0.26	3.56	11.63	17.6	3.29	11.91	2.34	1.56	0.17	0.80	<dt	0.22	<dt	0.07	<dt	26.6	94.3
PM-31	SD5	0.42	0.05	10.6	2.92	<dt	<dt	<dt	0.11	0.17	<dt	0.04	<dt	0.16	<dt	<dt	<dt	0.23	4.04	13.20	15.8	2.70	10.04	1.70	1.22	0.18	0.80	0.16	0.29	<dt	0.14	<dt	24.2	89.2
PM-32	SD5	0.53	0.05	11.6	2.46	<dt	<dt	<dt	0.04	0.10	<dt	0.04	<dt	<dt	<dt	<dt	<dt	0.17	2.75	12.90	18.1	3.24	11.25	2.03	1.35	0.18	0.56	<dt	0.13	<dt	0.10	<dt	25.4	92.9
PM-33	SD5	0.47	0.04	12.1	2.54	<dt	<dt	<dt	0.05	0.13	<dt	0.09	<dt	<dt	<dt	<dt	<dt	0.33	2.80	12.85	17.4	2.91	10.67	2.11	1.58	0.23	0.74	<dt	0.24	<dt	0.07	<dt	26.2	93.6
PM-34	SD27	<dt	0.04	13.0	1.98	<dt	<dt	0.09	<dt	0.10	<dt	0.20	<dt	<dt	<dt	<dt	5.28	0.77	2.83	12.19	9.0	2.95	9.86	1.61	0.73	0.10	0.51	0.14	0.17	<dt	0.10	<dt	25.4	87.0
PM-35	SD27	<dt	0.04	11.5	1.41	<dt	<dt	0.06	<dt	0.26	<dt	0.13	<dt	<dt	<dt	<dt	3.91	0.63	3.24	12.08	6.7	3.29	10.27	1.66	0.89	0.12	0.47	<dt	<dt	<dt	0.08	<dt	23.0	79.7
PM-36	SD27	<dt	0.04	12.4	2.15	<dt	<dt	0.08	0.03	0.42	<dt	0.34	<dt	<dt	0.04	<dt	6.15	0.93	3.16	10.59	9.7	2.83	8.79	1.54	0.85	0.18	0.56	<dt	0.19	<dt	0.12	<dt	24.9	86.1
PM-37	SD27	<dt	0.06	13.0	1.09	0.14	<dt	0.06	<dt	0.06	<dt	0.04	<dt	<dt	<dt	<dt	<dt	0.40	5.26	12.11	9.0	3.48	11.34	2.18	1.28	0.20	0.91	0.14	0.27	<dt	0.24	<dt	25.8	87.1
PM-38	SD27	<dt	0.05	13.0	1.15	0.13	<dt	0.07	<dt	0.08	<dt	<dt	<dt	<dt	<dt	<dt	<dt	0.58	4.40	13.41	9.9	3.50	10.85	1.89	0.90	0.20	0.79	0.19	0.25	<dt	0.17	<dt	25.7	87.3
PM-39	SD27	<dt	0.04	13.2	1.20	0.07	<dt	0.07	<dt	0.12	<dt	0.04	<dt	<dt	<dt	<dt	<dt	0.71	4.00	15.65	7.8	4.03	13.91	2.33	1.23	0.13	0.66	<dt	0.21	<dt	0.15	<dt	26.7	92.3
PM-40	SD27	<dt	0.03	13.1	1.77	0.07	<dt	0.08	<dt	0.09	<dt	0.66	<dt	<dt	0.04	<dt	4.41	0.70	3.17	9.91	16.4	2.19	7.27	1.19	0.74	0.16	0.44	<dt	0.19	<dt	0.11	<dt	25.7	88.4
PM-41	SD27	<dt	<dt	13.1	1.90	0.07	<dt	0.12	0.83	0.19	<dt	0.72	<dt	<dt	0.07	<dt	5.71	0.74	3.46	9.59	17.8	2.18	7.64	1.37	0.94	0.16	0.62	<dt	0.24	<dt	0.16	<dt	27.2	94.8
PM-42	SD25	<dt	0.03	11.8	0.98	0.06	<dt	0.13	<dt	0.11	<dt	<dt	<dt	<dt	<dt	<dt	<dt	0.39	4.40	9.17	11.7	3.16	12.01	2.36	1.48	0.23	0.97	<dt	0.30	<dt	0.14	<dt	24.1	83.5
PM-43	SD25	<dt	0.03	11.9	2.32	<dt	<dt	0.07	<dt	0.13	<dt	0.03	<dt	<dt	<dt	<dt	<dt	0.33	2.82	11.73	15.0	3.54	12.48	2.49	1.16	0.21	0.83	0.17	0.21	<dt	0.14	<dt	25.4	91.1
PM-44	SD25	0.64	0.04	11.8	2.13	<dt	<dt	0.05	<dt	0.44	<dt	0.04	0.09	<dt	<dt	<dt	<dt	0.32	2.82	12.41	14.5	3.27	11.75	2.24	1.36	0.23	0.87	0.15	0.22	<dt	0.08	<dt	25.3	90.7
PM-45	SD25	0.80	0.04	12.0	2.10	<dt	<dt	<dt	<dt	0.16	<dt	<dt	<dt	<dt	<dt	<dt	<dt	0.32	3.08	12.64	14.8	3.56	12.28	2.47	1.49	0.18	0.76	<dt	0.18	<dt	0.13	<dt	25.6	92.6
PM-46	SD25	<dt	0.04	12.8	1.51	0.07	<dt	0.08	<dt	<dt	<dt	0.20	<dt	<dt	<dt	<dt	1.35	0.59	5.93	8.21	9.9	2.83	9.88	2.14	1.41	0.24	1.09	0.15	0.31	<dt	0.19	0.08	25.1	84.1
PM-47	SD25	<dt	0.04	12.9	1.39	<dt	0.05	<dt	0.87	1.29	<dt	0.29	<dt	<dt	<dt	<dt	2.32	0.55	5.54	8.04	11.3	3.19	11.69	2.71	1.78	0.28	1.52	0.25	0.49	<dt	0.27	<dt	28.3	95.1
PM-48	SD25	1.11	0.03	12.8	6.29	<dt	0.06	<dt	0.56	1.63	<dt	0.25	<dt	<dt	<dt	<dt	<dt	0.23	3.41	9.01	12.1	2.82	9.45	2.02	1.28	0.21	1.00	0.14	0.32	<dt	0.20	<dt	29.4	95.6
PM-49	SD25	<dt	0.04	12.1	1.89	0.17	<dt	0.12	0.15	0.65	<dt	0.06	<dt	<dt	<dt	<dt	<dt	0.45	5.93	6.00	10.7	2.73	10.90	2.94	2.07	0.37	1.76	0.25	0.48	<dt	0.30	<dt	25.4	85.6
PM-50	SD25	<dt	0.06	12.3	1.31	0.70	<dt	0.07	0.93	2.72	<dt	0.15	<dt	<dt	<dt	<dt	<dt	0.62	5.78	8.50	11.5	3.16	11.76	2.58	1.73	0.30	1.40	0.21	0.49	<dt	0.25	<dt	29.2	95.7
PM-51	SD25	<dt	0.04	12.4	1.82	0.11	<dt	0.11	<dt	0.19	<dt	0.05	<dt	<dt	<dt	<dt	<dt	0.87	4.20	8.88	13.0	3.10	11.65	2.57	1.81	0.32	1.32	0.16	0.38	<dt	0.20	<dt	25.6	88.7
PM-52	SD25	<dt	0.04	11.8	1.42	0.08	<dt	0.10	<dt	0.19	<dt	0.06	<dt	<dt	<dt	<dt	0.12	0.69	4.69	8.53	12.0	3.02	11.16	2.42	1.54	0.27	1.16	0.15	0.39	<dt	0.20	<dt	24.4	84.7
PM-53	SD25	<dt	0.03	11.8	1.78	<dt	<dt	0.08	<dt	0.06	<dt	0.21	<dt	<dt	<dt	<dt	2.07	0.65	4.54	8.26	11.1	2.65	9.50	2.18	1.49	0.28	1.21	0.14	0.34	<dt	0.17	<dt	23.8	82.4
PM-54	SD25	<dt	<dt	13.0	2.00	<dt	<dt	0.06	<dt	0.08	<dt	0.16	<dt	<dt	<dt	<dt	1.96	0.53	4.84	8.94	10.8	2.79	9.50	2.10	1.31	0.25	1.00	0.21	0.27	<dt	0.14	<dt	25.4	85.3
PM-55	SD25	0.12	0.04	12.4	1.51	0.07	<dt	0.07	0.38	1.07	<dt	0.41	<dt	<dt	<dt	<dt	0.26	0.61	4.82	8.69	12.2	2.95	11.60	2.57	1.85	0.30	1.39	0.18	0.43	<dt	0.23	<dt	26.8	90.8
PM-56	SD25	0.41	0.03	12.2	1.89	<dt	<dt	<dt	0.24	0.75	<dt	0.26	<dt	<dt	<dt	<dt	0.40	0.43	3.51	9.74	13.0	3.16	10.19	2.02	1.16	0.23	0.89	0.15	0.29	<dt	0.12	<dt	25.6	86.7
PM-57	SD10	<dt	0.03	12.3	1.28	<dt	<dt	0.04	<dt	0.16	<dt	0.04	<dt	0.12	<dt	<dt	<dt	0.19	4.10	9.38	19.2	2.71	10.03	1.98	1.25	0.22	0.91	0.17	0.28	<dt	0.22	<dt	25.9	90.5
PM-58	SD10	0.63	0.03	12.1	2.24	<dt	<dt	<dt	0.21	0.16	<dt	0.04	<dt	<dt	<dt	<dt	<dt	0.31	2.90	11.40	19.7	2.72	10.12	1.91	1.18	0.20	0.71	<dt	0.29	<dt	0.15	<dt	26.1	93.0
PM-59	SD10	0.69	0.04	12.3	2.48	<dt	<dt	<dt	0.05	0.17	<dt	<dt	<dt	<dt	<dt	<dt	<dt	0.40	2.32	10.61	19.2	3.11	11.50	2.29	1.48	0.17	0.76	<dt	<dt	<dt	0.14	<dt	26.4	94.2
PM-60	SD10	<dt	0.04	12.3	1.28	<dt	<dt	0.06	0.10	0.10	<dt	0.03	<dt	<dt	<dt	<dt	<dt	0.22	5.70	8.59	17.4	2.60	10.14	2.28	1.67	0.28	1.37	0.25	0.48	<dt	0.27	<dt	26.1	91.2
PM-61	SD10	0.40	0.05	12.1	1.87	<dt	<dt	0.07	0.09	0.22	<dt	<dt	<dt	0.12	<dt	<dt	<dt	0.39	3.89	9.76	18.2	2.70	10.18	2.10	1.30	0.23	0.92	0.16	0.35	<dt	0.24	<dt	25.9	91.2
PM-62	SD10	<dt	0.04	12.3	1.46	<dt	<dt	0.06	0.45	0.69	0.03	<dt	<dt	<dt	<dt	<dt	<dt	0.28	4.66	9.93	17.8	2.73	10.12	2.11	1.55	0.24	1.08	<dt	0.45	<dt	0.28	<dt	26.9	93.1
PM-63	SD10	0.70	0.05	12.7	2.29	<dt	<dt	0.04	0.11	0.23	<dt	0.23	<dt	0.12	<dt	<dt	<dt	0.25	3.76	11.14	19.9	2.78	9.82	1.82	1.20	0.14	0.76	0.15	0.24	<dt	0.15	<dt	27.2	95.8
PM-64	SD10	<dt	<dt	13.0	1.16	0.10	<dt	0.07	<dt	0.93	<dt	0.44	<dt	<dt	<dt	<dt	<dt	0.26	6.43	9.24	15.6	2.58	9.80	2.28	1.86	0.27	1.33	0.28	0.45	0.07	0.29	<dt	27.9	94.4
PM-65	SD10	0.49	0.06	12.6	2.24	<dt	<dt	0.04	0.09	0.13	<dt	0.21	<dt	<dt	<dt	<dt	<dt	0.28	3.59	11.42	18.7	2.81	10.14	2.12	1.41	0.28	0.96	0.14	0.36	<dt	0.19	<dt	26.9	95.2
PM-66	SD10	<dt	0.03	12.9	1.47	0.11	<dt	0.08	<dt	0.08	<dt	0.10	<dt	0.15	<dt	<dt	<dt	0.25	5.23	9.53	18.0	2.50	10.04	2.12	1.61	0.27	1.13	0.16	0.36	<dt	0.29	<dt	26.9	93.3
PM-67	SD10	<dt	0.05	13.1	1.96	<dt	<dt	0.04	0.34	0.18	<dt	0.15	<dt	<dt	<dt	<dt	<dt	0.26	3.91	9.70	20.5	2.67	9.89	1.83	1.34	0.20	0.83	<dt	0.26	<dt	0.19	<dt	27.6	95.0
PM-68	SD10	0.55	0.05	12.9	2.33	<dt	<dt	<dt	0.06	0.11	<dt	0.19	<dt	0.15	<dt	<dt	<dt	0.26	3.37	11.17	20.4	2.82	10.01	1.86	1.22	0.17	0.75	0.13	0.27	<dt	0.15	<dt	27.3	96.3
PM-69	SD10	<dt	0.04	12.6	1.44	<dt	<dt	0.05	0.04	0.03	<dt	0.11	<dt	0.16	<dt	<dt	<dt	0.21	4.93	9.37	18.7	2.70	10.11	2.04	1.38	0.24	0.92	0.17	0.42	<dt	0.25	<dt	26.3	92.2
PM-70	SD10	0.25	0.04	12.5	1.87	<dt	<dt	0.05	<dt	0.08	<dt	0.26	<dt	<dt	<dt	<dt	<dt	0.39	4.05	10.89	18.6	2.74	10.11	2.04	1.39	0.20	0.93	0.18	0.33	<dt	0.18	<dt	26.4	93.5
PM-71	SD10	<dt	<dt	12.7	1.54	<dt	<dt	0.05	<dt	0.06	<dt	0.18	<dt	<dt	<dt	<dt	<dt	0.25	4.83	10.61	17.1	2.65	10.02	2.12	1.67	0.22	1.18	0.16	0.39	<dt	0.25	<dt	26.4	92.4
PM-72	SD10	1.01	0.04	10.3	2.17	<dt	<dt	<dt	0.46	0.50	0.06	0.88	0.09	0.13	0.16	4.56	0.68	0.43	5.31	7.69	15.6	2.31	8.90	1.91	1.08	0.24	1.03	0.26	0.71	<dt	0.61	0.08	26.1	93.5

#	Sample	F wt %	Cl wt %	P wt %	Ca wt %	Na wt %	Mg wt %	K wt %	Al wt %	Si wt %	Mn wt %	Fe wt %	Sr wt %	Ba wt %	Ti wt %	Nb wt %	Th wt %	U wt %	Y wt %	La wt %	Ce wt %	Pr wt %	Nd wt %	Sm wt %	Gd wt %	Tb wt %	Dy wt %	Ho wt %	Er wt %	Tm wt %	Yb wt %	Lu wt %	O wt %	Total wt %
PM-73	SD10	<dt	0.05	12.8	1.16	0.07	<dt	0.08	0.51	0.14	<dt	0.34	<dt	0.12	<dt	<dt	<dt	0.24	4.85	9.46	18.1	2.76	10.43	2.08	1.42	0.23	1.12	0.18	0.30	<dt	0.24	<dt	27.1	93.7
PM-74	SD10	<dt	0.04	12.5	1.20	<dt	<dt	0.07	0.13	0.08	<dt	0.38	<dt	<dt	<dt	<dt	0.14	0.28	4.10	9.49	18.4	2.93	10.63	2.04	1.46	0.22	0.90	<dt	0.30	<dt	0.23	<dt	26.2	91.7
PM-75	SD10	<dt	0.04	12.3	1.13	0.09	<dt	0.09	0.63	0.15	<dt	0.14	<dt	<dt	<dt	<dt	<dt	0.24	5.30	9.55	15.9	2.59	10.11	2.31	1.92	0.33	1.33	0.26	0.43	<dt	0.31	<dt	26.5	91.7
PM-76	SD10	0.57	0.05	10.5	2.16	<dt	0.07	0.10	0.83	1.25	0.05	0.44	0.09	<dt	<dt	<dt	0.09	0.27	2.33	9.63	17.6	2.67	9.89	2.00	1.26	0.16	0.72	<dt	0.15	<dt	0.13	<dt	25.1	88.1
PM-77	SD10	<dt	0.04	12.4	1.30	<dt	<dt	0.06	<dt	0.07	<dt	0.09	<dt	<dt	<dt	<dt	0.33	0.23	4.35	9.20	18.5	3.05	10.91	2.08	1.18	0.21	0.83	0.14	0.25	<dt	0.18	<dt	25.9	91.4
PM-78	SD23	<dt	0.05	12.6	0.42	<dt	<dt	<dt	<dt	<dt	<dt	0.11	0.05	0.17	<dt	<dt	<dt	0.09	15.22	11.96	1.7	2.17	7.25	1.73	2.73	0.38	2.05	0.36	1.00	0.14	0.81	0.12	25.2	86.3
PM-79	SD23	0.36	0.05	12.4	0.27	<dt	<dt	0.04	<dt	0.05	<dt	0.19	<dt	0.04	<dt	<dt	<dt	<dt	7.50	14.12	0.7	4.28	12.45	2.48	1.83	0.23	1.14	0.23	0.41	<dt	0.40	<dt	24.2	83.4
PM-80	SD23	0.17	0.05	12.8	0.40	<dt	<dt	0.05	0.06	0.22	<dt	0.43	0.21	0.14	<dt	<dt	<dt	<dt	14.67	11.84	1.7	2.54	8.57	2.09	3.09	0.42	2.52	0.49	1.16	0.14	0.97	0.13	26.3	91.2
PM-81	SD23	0.37	0.10	12.4	0.28	<dt	<dt	<dt	<dt	0.08	<dt	0.34	<dt	<dt	0.36	<dt	<dt	<dt	9.16	13.19	0.7	3.97	12.79	2.80	2.43	0.36	1.93	0.32	0.78	0.08	0.77	<dt	25.3	88.5
PM-82	SD23	0.38	0.06	12.9	0.40	<dt	<dt	<dt	<dt	0.04	<dt	0.11	<dt	0.07	<dt	<dt	<dt	0.26	9.62	12.22	4.3	2.85	8.80	1.87	1.85	0.20	1.25	0.24	0.48	<dt	0.43	<dt	24.9	83.3
PM-83	SD23	0.46	0.05	12.7	0.34	<dt	<dt	<dt	<dt	<dt	<dt	0.10	<dt	0.11	<dt	0.01	<dt	<dt	8.96	13.34	3.7	2.98	9.52	1.97	1.87	0.27	1.39	0.27	0.52	<dt	0.50	<dt	24.7	83.8
PM-84	SD21	<dt	<dt	12.7	0.92	<dt	<dt	0.03	<dt	0.06	<dt	0.17	<dt	0.08	0.74	<dt	0.28	0.13	6.01	11.49	20.5	2.13	7.73	1.20	1.25	0.15	0.92	0.17	0.43	<dt	0.27	<dt	26.7	94.0
PM-85	SD21	<dt	<dt	13.0	0.92	<dt	<dt	0.04	<dt	0.05	<dt	0.11	<dt	0.14	0.09	<dt	0.11	0.17	6.43	11.59	19.6	2.17	7.84	1.26	1.20	0.16	0.89	0.17	0.38	<dt	0.29	<dt	26.5	93.1
PM-86	SD21	<dt	0.03	13.1	1.02	<dt	<dt	<dt	<dt	0.03	<dt	0.11	<dt	0.06	0.33	<dt	<dt	<dt	5.01	12.34	22.0	2.17	7.39	1.06	0.90	0.15	0.64	<dt	0.35	<dt	0.23	<dt	26.8	93.7
PM-87	SD21	0.11	0.06	9.8	0.98	<dt	<dt	0.03	0.12	0.26	<dt	1.26	<dt	<dt	9.64	0.63	1.39	0.21	4.54	6.52	15.8	2.10	7.50	1.82	1.55	0.25	1.50	0.28	0.55	<dt	0.41	<dt	28.3	95.8
PM-88	SD21	<dt	0.03	12.4	1.04	0.09	<dt	0.07	0.06	<dt	<dt	0.04	<dt	0.13	<dt	<dt	1.32	0.43	5.96	7.03	15.3	2.01	7.48	1.51	1.20	0.25	1.18	0.22	0.52	0.07	0.55	<dt	83.7	142.6
PM-89	SD21	<dt	0.04	12.5	1.10	<dt	<dt	0.05	<dt	0.12	<dt	0.06	<dt	0.14	<dt	<dt	2.00	0.47	6.63	7.64	17.1	2.54	9.31	2.03	1.85	0.36	1.83	0.29	0.77	0.10	0.60	<dt	93.9	161.4
PM-90	SD21	<dt	0.04	12.3	2.30	<dt	<dt	0.07	<dt	<dt	<dt	0.11	0.11	0.16	<dt	<dt	10.11	0.40	4.61	6.32	12.1	1.68	5.37	1.21	1.05	0.20	0.87	<dt	0.32	<dt	0.27	<dt	84.3	143.8
PM-91	SD21	<dt	<dt	12.9	1.18	0.06	<dt	0.04	<dt	<dt	<dt	<dt	<dt	0.13	<dt	<dt	<dt	0.26	8.41	9.92	15.9	2.07	6.74	1.24	1.24	0.21	1.20	0.24	0.59	0.09	0.45	<dt	25.8	88.7
PM-92	SD21	<dt	0.03	12.8	1.09	0.05	<dt	0.07	<dt	<dt	<dt	<dt	<dt	0.16	<dt	<dt	<dt	0.16	9.57	10.01	15.2	1.93	6.56	1.35	1.39	0.25	1.26	0.27	0.56	0.10	0.58	0.07	25.8	89.3
PM-93	SD21	<dt	0.04	13.2	1.33	<dt	<dt	0.06	<dt	<dt	<dt	<dt	<dt	0.26	<dt	<dt	<dt	0.17	7.14	11.70	18.9	2.05	6.70	1.09	1.21	0.14	0.90	0.14	0.47	<dt	0.28	<dt	26.7	92.5
PM-94	SD21	<dt	0.06	11.4	0.08	<dt	<dt	<dt	<dt	1.61	<dt	<dt	<dt	<dt	<dt	<dt	13.04	0.39	<dt	14.43	25.6	2.00	4.71	0.43	0.11	0.06	<dt	<dt	<dt	<dt	<dt	<dt	26.5	100.5
PM-95	SD21	1.56	0.04	7.4	0.83	<dt	<dt	<dt	0.24	4.88	<dt	0.60	0.13	0.03	0.03	<dt	13.33	0.34	3.47	8.30	16.9	1.39	3.80	0.43	0.41	0.06	0.42	<dt	0.43	0.08	0.44	<dt	26.2	91.7
PM-96	SD21	<dt	<dt	11.3	0.08	<dt	<dt	<dt	<dt	1.68	<dt	<dt	<dt	0.04	<dt	<dt	13.17	0.45	<dt	14.21	25.3	2.08	4.57	0.39	0.16	<dt	<dt	<dt	<dt	<dt	<dt	<dt	26.4	99.8
PM-97	SD21	0.58	<dt	12.4	0.44	<dt	<dt	<dt	0.05	1.14	<dt	0.26	0.06	<dt	<dt	<dt	5.05	<dt	0.71	13.42	27.8	2.48	5.96	0.56	0.33	0.05	0.18	<dt	<dt	<dt	<dt	<dt	27.0	98.5
PM-98	SD21	<dt	<dt	11.7	0.13	<dt	<dt	<dt	<dt	1.37	<dt	0.23	0.05	<dt	<dt	<dt	9.91	0.29	<dt	14.48	26.7	2.16	5.22	0.42	0.24	0.08	<dt	<dt	<dt	<dt	<dt	<dt	26.6	99.5
PM-99	SD21	0.09	0.40	8.3	0.87	<dt	0.27	0.22	0.85	3.02	0.03	1.53	0.32	<dt	0.07	0.22	3.08	0.06	2.39	8.36	15.1	2.74	8.63	1.67	0.92	0.13	0.54	0.17	0.30	<dt	0.31	<dt	23.8	84.4
PM-100	SV6	0.22	0.16	9.8	0.90	<dt	0.03	0.05	0.34	1.45	<dt	0.35	0.29	<dt	<dt	0.10	2.83	0.13	3.76	9.03	15.6	2.94	9.42	1.71	1.25	0.18	0.77	<dt	0.34	0.07	0.37	<dt	23.6	85.6
PM-101	SV6	1.65	0.05	9.4	1.12	<dt	<dt	0.04	0.14	1.95	<dt	0.37	0.10	<dt	0.05	0.24	2.38	0.16	8.71	7.51	13.7	2.23	7.35	1.41	1.08	0.18	1.04	0.22	0.87	0.14	0.99	0.11	23.8	87.1
PM-102	SV6	1.29	0.07	10.0	1.16	<dt	<dt	0.05	0.16	1.36	<dt	0.55	<dt	<dt	0.05	0.12	1.99	0.22	8.73	8.33	15.3	2.43	8.48	1.58	1.30	0.20	1.18	0.29	0.88	0.11	0.78	0.13	24.5	91.2
PM-103	SV6	0.70	0.09	10.2	1.33	<dt	<dt	<dt	0.28	1.26	<dt	0.18	<dt	<dt	0.48	0.19	2.16	<dt	2.55	10.22	17.3	2.85	10.06	1.86	1.06	0.17	0.64	0.13	0.32	<dt	0.36	<dt	24.5	88.9

Table C2.5 EMPA Xenotime minerals

#	Sample	F wt %	Cl wt %	P wt %	Ca wt %	Na wt %	Mg wt %	K wt %	Al wt %	Si wt %	Mn wt %	Fe wt %	Sr wt %	Ba wt %	Ti wt %	Nb wt %	Th wt %	U wt %	Y wt %	La wt %	Ce wt %	Pr wt %	Nd wt %	Sm wt %	Gd wt %	Tb wt %	Dy wt %	Ho wt %	Er wt %	Tm wt %	Yb wt %	Lu wt %	O wt %	Total wt %
PX-1	SD4	8.78	<dt	4.5	1.27	<dt	<dt	<dt	<dt	1.23	<dt	0.50	<dt	<dt	0.04	<dt	2.14	0.27	22.5	4.76	7.53	0.91	3.89	1.11	1.39	0.38	2.96	0.66	2.03	0.27	1.79	0.22	19.3	90.2
PX-2	SD5	6.94	<dt	11.2	0.39	<dt	0.07	0.07	0.79	2.34	<dt	0.61	<dt	<dt	<dt	<dt	<dt	0.29	41.0	<dt	0.07	<dt	<dt	<dt	<dt	0.10	1.55	0.60	2.56	0.36	1.75	0.28	30.4	101.3
PX-3	SD6	8.70	<dt	7.0	0.23	0.05	<dt	0.04	<dt	0.43	<dt	0.04	<dt	<dt	<dt	<dt	<dt	0.26	39.0	<dt	<dt	<dt	<dt	0.09	<dt	0.15	2.62	0.84	3.32	0.58	5.15	0.77	22.3	91.8
PX-4	SD6	8.29	<dt	8.4	2.71	<dt	<dt	0.06	<dt	0.04	<dt	<dt	<dt	<dt	<dt	<dt	<dt	0.21	41.3	<dt	0.07	<dt	<dt	0.06	<dt	0.13	1.64	0.57	2.09	0.29	1.83	0.30	24.1	92.1
PX-5	SD7	9.18	<dt	9.7	0.20	0.09	<dt	<dt	<dt	0.76	<dt	0.07	<dt	<dt	<dt	<dt	0.22	0.49	38.9	<dt	0.19	<dt	<dt	<dt	<dt	0.10	1.72	0.71	2.77	0.45	2.91	0.43	25.4	94.3
PX-6	SD7	9.94	<dt	8.8	0.19	0.08	<dt	0.04	<dt	0.86	<dt	0.05	<dt	<dt	<dt	<dt	0.16	0.52	40.3	<dt	0.22	<dt	<dt	<dt	<dt	0.07	1.51	0.60	2.23	0.31	2.24	0.33	24.5	93.1
PX-7	SD7	6.97	0.03	7.1	0.15	0.07	<dt	0.05	0.30	1.10	<dt	0.12	<dt	<dt	<dt	<dt	0.13	0.39	31.5	<dt	0.14	<dt	<dt	0.05	<dt	0.08	1.40	0.58	2.24	0.37	2.37	0.37	20.3	75.7
PX-8	SD7	8.97	<dt	9.3	0.20	0.11	<dt	0.06	<dt	0.90	<dt	0.33	<dt	0.11	<dt	<dt	0.25	0.48	40.2	<dt	0.19	<dt	<dt	<dt	<dt	0.09	1.66	0.64	2.65	0.41	2.76	0.43	25.5	95.2
PX-9	SD27	<dt	<dt	15.1	0.15	<dt	<dt	0.04	0.10	0.53	<dt	0.36	<dt	<dt	<dt	<dt	0.07	<dt	36.0	0.71	1.23	0.19	0.80	0.44	0.36	0.37	2.92	0.78	2.40	0.36	3.03	0.47	32.2	98.6
PX-10	SD27	0.19	<dt	15.1	0.29	<dt	<dt	0.17	0.17	0.67	<dt	0.63	<dt	<dt	<dt	<dt	<dt	<dt	34.7	1.30	2.05	0.26	1.00	0.41	0.46	0.31	2.84	0.63	2.21	0.37	3.01	0.51	32.6	100.2
PX-11	SD9	<dt	<dt	16.3	<dt	<dt	<dt	<dt	<dt	0.25	<dt	0.45	<dt	<dt	<dt	<dt	0.74	0.38	37.8	<dt	<dt	<dt	<dt	0.12	<dt	0.30	3.17	0.80	2.65	0.39	3.02	0.47	31.8	99.1
PX-12	SD9	<dt	<dt	16.1	0.04	<dt	<dt	<dt	<dt	0.31	<dt	0.46	<dt	<dt	<dt	<dt	1.04	0.37	36.3	<dt	<dt	<dt	<dt	0.17	<dt	0.36	3.87	1.03	3.35	0.48	3.11	0.45	31.7	99.6
PX-13	SD9	<dt	<dt	12.7	0.12	<dt	<dt	<dt	<dt	2.76	0.03	0.15	<dt	<dt	0.05	0.18	0.58	0.71	28.0	<dt	<dt	<dt	<dt	0.09	<dt	0.18	2.53	0.96	4.17	0.66	4.99	0.67	30.1	94.9
PX-14	SD9	<dt	<dt	16.1	<dt	<dt	<dt	<dt	<dt	0.07	<dt	0.53	<dt	<dt	<dt	<dt	0.75	0.21	34.2	<dt	<dt	<dt	0.09	0.32	<dt	0.50	4.86	1.31	4.02	0.50	3.39	0.43	31.2	98.5
PX-15	SD9	<dt	<dt	16.1	<dt	<dt	<dt	<dt	<dt	0.12	<dt	0.41	<dt	<dt	<dt	<dt	0.87	0.18	33.9	<dt	<dt	<dt	<dt	0.34	<dt	0.44	4.99	1.35	4.31	0.50	3.47	0.46	31.2	98.7
PX-16	SD9	<dt	<dt	16.1	<dt	<dt	<dt	<dt	<dt	0.08	<dt	0.58	<dt	<dt	<dt	<dt	0.83	0.19	34.4	<dt	<dt	<dt	0.09	0.35	<dt	0.49	4.90	1.34	4.10	0.52	3.31	0.40	31.3	98.9
PX-17	SV6	3.16	0.12	7.1	0.69	0.09	<dt	0.14	0.42	3.62	<dt	0.71	<dt	<dt	0.04	0.35	2.41	0.30	21.6	1.62	6.71	0.50	1.93	0.62	0.98	0.24	2.30	0.64	1.99	0.32	2.29	0.30	23.1	84.4

#	Sample	F wt %	Cl wt %	P wt %	Ca wt %	Na wt %	Mg wt %	K wt %	Al wt %	Si wt %	Mn wt %	Fe wt %	Sr wt %	Ba wt %	Ti wt %	Nb wt %	Th wt %	U wt %	Y wt %	La wt %	Ce wt %	Pr wt %	Nd wt %	Sm wt %	Gd wt %	Tb wt %	Dy wt %	Ho wt %	Er wt %	Tm wt %	Yb wt %	Lu wt %	O wt %	Total wt %
PX-18	SV6	3.27	0.18	6.7	0.47	0.04	<dt	<dt	0.06	2.42	<dt	0.10	<dt	<dt	<dt	0.23	4.67	0.41	25.1	0.75	2.49	0.31	0.99	0.48	0.87	0.27	2.59	0.70	2.57	0.39	3.03	0.41	20.8	80.3
PX-19	SV6	2.44	0.27	6.8	0.59	<dt	<dt	<dt	0.16	3.07	<dt	0.08	<dt	<dt	<dt	0.28	4.25	0.31	18.6	2.65	5.87	0.86	2.89	0.71	0.84	0.20	2.00	0.49	1.86	0.33	2.35	0.33	21.1	79.3
PX-20	SV6	6.22	<dt	8.3	0.71	0.05	<dt	0.05	0.05	1.03	0.04	3.05	<dt	0.09	0.17	0.86	1.57	0.48	32.8	0.38	6.04	0.10	0.31	0.21	0.75	0.16	2.08	0.64	2.15	0.25	1.57	0.19	23.9	94.2
PX-21	SV6	6.38	<dt	7.8	0.72	<dt	<dt	0.07	0.12	1.65	0.05	2.25	<dt	0.07	0.12	0.53	3.38	0.68	30.5	0.23	7.78	<dt	0.33	0.23	0.82	0.20	2.13	0.63	2.16	0.27	1.67	0.18	23.6	94.6
PX-22	SV6	4.47	0.05	7.1	0.67	<dt	<dt	0.07	<dt	0.99	0.13	3.44	<dt	<dt	0.10	0.25	4.07	0.59	28.3	0.34	5.83	0.12	0.42	0.29	0.74	0.27	2.44	0.78	2.22	0.32	1.86	0.18	21.5	87.5
PX-23	SV6.2	8.80	<dt	9.1	0.47	0.05	<dt	0.10	<dt	<dt	<dt	0.23	<dt	0.10	<dt	<dt	<dt	0.16	40.4	<dt	0.01	<dt	<dt	0.08	0.57	0.21	2.00	0.66	2.42	0.40	2.66	0.39	22.8	91.6
PX-24	SV6.2	8.65	<dt	9.0	0.45	0.06	<dt	0.09	<dt	<dt	<dt	0.09	<dt	0.11	<dt	<dt	<dt	<dt	37.9	<dt	0.04	<dt	<dt	0.08	0.41	0.16	1.95	0.70	2.39	0.37	2.49	0.40	22.0	87.3
PX-25	SV6.2	8.39	<dt	9.3	0.54	0.04	<dt	0.07	0.08	0.46	<dt	0.15	<dt	0.08	<dt	<dt	<dt	0.15	38.6	0.08	0.10	<dt	<dt	0.09	0.47	0.23	2.39	0.87	2.73	0.45	2.66	0.42	23.5	91.8
PX-26	SV6.2	6.61	<dt	11.2	0.42	<dt	<dt	0.08	<dt	0.17	<dt	0.05	<dt	0.11	<dt	<dt	<dt	0.28	41.9	<dt	<dt	<dt	<dt	<dt	<dt	0.13	1.86	0.64	2.39	0.32	1.85	0.35	27.3	95.7
PX-27	SV6.2	10.56	<dt	11.4	0.33	<dt	<dt	0.07	<dt	0.14	<dt	0.32	<dt	<dt	<dt	<dt	<dt	0.21	41.6	0.05	<dt	<dt	<dt	0.06	<dt	0.15	2.29	0.76	2.94	0.38	2.33	0.35	27.8	101.8
PX-28	SV6.2	5.82	<dt	11.1	0.47	<dt	<dt	0.07	<dt	0.44	<dt	0.06	<dt	0.10	<dt	<dt	<dt	0.19	40.6	<dt	0.03	<dt	<dt	0.06	<dt	0.16	1.98	0.68	2.56	0.32	1.92	0.30	27.2	94.0
PX-29	SV8.2	6.61	<dt	11.2	0.42	<dt	<dt	0.08	<dt	0.17	<dt	0.05	<dt	0.11	<dt	<dt	<dt	0.28	41.9	<dt	<dt	<dt	<dt	<dt	<dt	0.13	1.86	0.64	2.39	0.32	1.85	0.35	27.3	95.7
PX-30	SV8.2	10.56	<dt	11.4	0.33	<dt	<dt	0.07	<dt	0.14	<dt	0.32	<dt	<dt	<dt	<dt	<dt	0.21	41.6	0.05	<dt	<dt	<dt	0.06	<dt	0.15	2.29	0.76	2.94	0.38	2.33	0.35	27.8	101.8
PX-31	SV8.2	5.82	<dt	11.1	0.47	<dt	<dt	0.07	<dt	0.44	<dt	0.06	<dt	0.10	<dt	<dt	<dt	0.19	40.6	<dt	0.03	<dt	<dt	0.06	<dt	0.16	1.98	0.68	2.56	0.32	1.92	0.30	27.2	94.0
PX-32	SV8.2	7.09	<dt	11.0	0.44	<dt	<dt	0.17	<dt	0.29	<dt	0.12	<dt	0.14	<dt	<dt	<dt	0.20	44.1	<dt	0.01	<dt	<dt	<dt	<dt	0.15	2.32	0.80	3.07	0.40	2.47	0.35	28.2	101.4
PX-33	SV8.2	8.38	<dt	11.6	0.48	0.10	<dt	0.09	<dt	0.12	<dt	0.43	<dt	0.16	<dt	<dt	<dt	<dt	39.8	0.05	<dt	<dt	<dt	<dt	<dt	0.15	2.07	0.73	2.70	0.37	2.15	0.39	27.6	97.4
PX-34	SV8.2	7.09	<dt	11.0	0.44	<dt	<dt	0.17	<dt	0.29	<dt	0.12	<dt	0.14	<dt	<dt	<dt	0.20	44.1	<dt	0.01	<dt	<dt	<dt	<dt	0.15	2.32	0.80	3.07	0.40	2.47	0.35	28.2	101.4
PX-35	SV8.2	8.38	<dt	11.6	0.48	0.10	<dt	0.09	<dt	0.12	<dt	0.43	<dt	0.16	<dt	<dt	<dt	<dt	39.8	0.05	<dt	<dt	<dt	<dt	<dt	0.15	2.07	0.73	2.70	0.37	2.15	0.39	27.6	97.4
PX-36	SV8.2	9.61	<dt	11.5	0.40	<dt	<dt	0.07	<dt	0.13	<dt	0.18	<dt	<dt	<dt	<dt	<dt	0.18	42.4	<dt	0.00	<dt	<dt	<dt	<dt	0.16	2.42	0.84	3.29	0.47	2.83	0.43	28.1	103.0
PX-37	SV8.2	6.75	<dt	11.2	0.44	0.05	<dt	0.08	<dt	0.23	<dt	0.07	<dt	<dt	<dt	<dt	<dt	0.27	41.0	<dt	<dt	<dt	<dt	<dt	<dt	0.16	2.40	0.81	3.16	0.43	2.57	0.39	27.5	97.5
PX-38	SV8.2	8.77	<dt	10.9	0.32	0.06	<dt	0.09	<dt	0.28	<dt	0.15	<dt	0.15	<dt	<dt	<dt	0.18	42.1	<dt	0.01	<dt	<dt	<dt	<dt	0.16	2.20	0.77	3.09	0.46	2.82	0.47	27.5	100.4
PX-39	SV8.2	9.61	<dt	11.5	0.40	<dt	<dt	0.07	<dt	0.13	<dt	0.18	<dt	<dt	<dt	<dt	<dt	0.18	42.4	<dt	0.00	<dt	<dt	<dt	<dt	0.16	2.42	0.84	3.29	0.47	2.83	0.43	28.1	103.0
PX-40	SV8.2	6.75	<dt	11.2	0.44	0.05	<dt	0.08	<dt	0.23	<dt	0.07	<dt	<dt	<dt	<dt	<dt	0.27	41.0	<dt	<dt	<dt	<dt	<dt	<dt	0.16	2.40	0.81	3.16	0.43	2.57	0.39	27.5	97.5
PX-41	SV8.2	6.89	<dt	10.5	1.07	0.09	<dt	0.09	0.20	0.69	<dt	0.88	0.21	0.07	<dt	<dt	<dt	0.24	39.8	<dt	0.13	<dt	<dt	<dt	1.38	0.15	1.68	0.61	1.70	0.17	0.97	0.13	25.4	93.0
PX-42	SV8.2	8.65	<dt	10.7	1.59	0.07	<dt	0.07	<dt	<dt	<dt	0.09	0.20	0.04	<dt	<dt	<dt	0.14	42.4	<dt	<dt	<dt	<dt	<dt	1.49	0.17	2.14	0.64	2.34	0.24	1.10	0.17	25.5	97.7
PX-43	SV8.2	7.16	<dt	13.6	11.07	0.06	<dt	<dt	<dt	<dt	<dt	0.07	0.14	0.11	<dt	<dt	<dt	0.22	32.5	<dt	<dt	<dt	0.06	<dt	1.08	0.11	1.49	0.52	1.81	0.23	0.95	0.13	30.4	101.7
PX-44	SD20	8.21	<dt	10.4	1.20	0.08	<dt	<dt	<dt	<dt	<dt	0.18	0.19	0.13	<dt	<dt	<dt	0.37	41.8	<dt	<dt	<dt	<dt	<dt	1.30	0.16	1.81	0.62	2.05	0.22	1.09	0.16	24.6	94.6
PX-45	SD20	8.80	<dt	9.5	0.66	<dt	<dt	0.08	<dt	<dt	<dt	0.04	0.20	0.11	<dt	<dt	<dt	0.14	40.6	<dt	<dt	<dt	<dt	<dt	1.18	0.13	2.01	0.69	2.38	0.26	1.30	0.19	23.0	91.3
PX-46	SD20	7.77	<dt	10.7	1.53	0.08	<dt	<dt	<dt	<dt	<dt	0.20	0.19	0.11	<dt	<dt	<dt	0.21	43.1	<dt	<dt	<dt	<dt	<dt	1.46	0.15	2.18	0.80	2.47	0.24	1.10	0.18	25.6	98.0
PX-47	SD20	8.59	<dt	9.4	0.59	0.08	<dt	0.05	<dt	<dt	<dt	0.15	0.20	0.13	<dt	<dt	<dt	0.17	44.0	<dt	<dt	<dt	<dt	<dt	1.44	0.17	2.21	0.77	2.62	0.30	1.63	0.21	23.9	96.7
PX-48	SD20	8.21	<dt	10.2	0.85	0.06	<dt	0.07	<dt	0.17	<dt	0.37	0.20	0.06	0.17	<dt	0.84	0.28	41.9	<dt	0.17	<dt	<dt	<dt	1.29	0.15	1.81	0.71	2.24	0.25	1.04	0.16	24.8	96.0
PX-49	SD20	8.43	<dt	9.1	0.64	0.08	<dt	0.09	0.33	0.90	<dt	0.99	0.18	0.14	0.35	<dt	0.42	0.19	41.8	<dt	<dt	<dt	<dt	<dt	1.43	0.13	1.96	0.66	2.37	0.27	1.30	0.21	24.6	96.5
PX-50	SD20	7.33	<dt	17.8	0.94	<dt	<dt	<dt	0.08	1.72	<dt	1.72	0.20	0.06	0.04	<dt	6.83	0.36	41.1	<dt	0.20	0.12	0.47	0.35	1.96	0.23	1.86	0.46	1.32	0.16	1.35	0.16	24.6	87.1
PX-51	SD20	7.01	<dt	18.8	1.02	<dt	<dt	0.05	<dt	1.73	0.06	1.64	0.21	<dt	0.03	<dt	6.21	0.43	43.1	0.17	0.29	0.15	0.49	0.38	2.33	0.27	2.70	0.71	2.30	0.30	1.92	0.25	23.9	92.9
PX-52	SD20	7.27	<dt	9.6	0.73	0.10	<dt	0.10	0.44	0.87	<dt	0.21	<dt	<dt	<dt	<dt	0.56	<dt	34.8	0.21	0.330	<dt	0.17	0.15	0.55	0.26	3.36	1.12	4.10	0.65	4.94	0.68	25.0	96.2

Table C2.5 EMPA REE-flurocaronate minerals

#	Sample	F wt %	Cl wt %	Na wt %	Mg wt %	Al wt %	Si wt %	P wt %	Ca wt %	K wt %	Ti wt %	Mn wt %	Fe wt %	Ba wt %	Sr wt %	Th wt %	U wt %	Y wt %	La wt %	Ce wt %	Pr wt %	Nd wt %	Sm wt %	Gd wt %	Tb wt %	Dy wt %	Ho wt %	Er wt %	Tm wt %	Yb wt %	Lu wt %	O wt %	Total wt %
B-1	SD4	7.04	0.05	<dt	<dt	<dt	0.08	<dt	1.30	<dt	0.06	<dt	0.08	0.11	<dt	2.92	0.17	3.50	16.63	22.49	2.96	10.75	1.67	0.96	0.14	0.53	<dt	0.16	<dt	<dt	<dt	11.6	83.1
B-2	SD4	7.39	0.05	<dt	<dt	<dt	0.10	0.11	1.37	<dt	0.08	<dt	0.47	<dt	<dt	2.85	0.16	3.23	15.75	21.62	2.91	10.38	1.64	0.97	0.17	0.56	<dt	<dt	<dt	<dt	<dt	11.2	81.0
B-3	SD4	7.35	0.04	<dt	<dt	<dt	0.07	<dt	1.32	<dt	0.04	<dt	<dt	<dt	<dt	2.93	<dt	2.87	16.69	21.59	3.03	10.63	1.67	0.99	0.16	0.50	<dt	0.20	<dt	<dt	<dt	11.1	81.2
B-4	SD4	7.37	0.05	<dt	<dt	<dt	0.17	0.17	1.46	<dt	0.05	<dt	0.14	<dt	<dt	3.49	0.16	3.43	16.46	20.51	2.84	10.28	1.60	1.06	0.18	0.64	<dt	0.29	<dt	0.12	<dt	11.5	82.1
B-5	SD4	7.18	0.03	<dt	<dt	<dt	0.16	0.12	1.41	<dt	0.04	<dt	0.07	<dt	<dt	3.50	<dt	2.98	16.78	20.44	2.95	10.57	1.59	1.15	0.16	0.51	<dt	0.27	<dt	0.08	<dt	11.3	81.4
B-6	SD4	7.20	0.04	<dt	<dt	<dt	0.15	0.11	1.40	<dt	0.04	<dt	0.19	0.12	<dt	3.56	<dt	2.78	17.12	21.45	3.01	10.73	1.63	0.90	0.12	0.42	0.15	0.17	<dt	0.12	<dt	11.5	83.0
B-7	SD4	7.06	0.05	<dt	<dt	0.27	0.86	0.14	1.69	0.05	0.35	0.06	1.85	<dt	0.16	4.07	0.17	7.18	15.32	13.28	2.64	9.39	1.68	1.38	0.23	1.37	0.21	0.59	<dt	0.21	<dt	13.0	83.4
B-8	SD4	7.53	0.05	<dt	<dt	0.07	0.35	0.16	1.89	<dt	0.26	<dt	1.23	0.12	0.14	4.71	<dt	7.32	15.31	14.81	2.74	9.62	1.63	1.27	0.22	1.35	0.29	0.45	<dt	0.20	<dt	12.4	84.3
B-9	SD4	6.54	0.04	<dt	<dt	0.05	0.27	0.16	1.91	<dt	0.15	<dt	0.75	0.21	0.16	4.79	0.15	7.19	15.46	15.08	2.76	10.16	1.74	1.29	0.24	1.21	0.18	0.47	<dt	0.19	<dt	12.2	83.3
B-10	SD4	8.01	0.05	<dt	<dt	<dt	1.04	0.24	1.29	<dt	0.05	0.04	1.58	<dt	0.13	2.14	<dt	8.71	13.05	17.02	2.20	8.90	1.84	1.62	0.33	1.84	0.37	0.68	<dt	0.32	<dt	13.1	84.5

#	Sample	F	Cl	Na	Mg	Al	Si	P	Ca	K	Ti	Mn	Fe	Ba	Sr	Th	U	Y	La	Ce	Pr	Nd	Sm	Gd	Tb	Dy	Ho	Er	Tm	Yb	Lu	O	Total
		wt %	wt %	wt %	wt %	wt %	wt %	wt %	wt %	wt %	wt %	wt %	wt %	wt %	wt %	wt %	wt %	wt %	wt %	wt %	wt %	wt %	wt %	wt %	wt %	wt %	wt %	wt %	wt %	wt %	wt %	wt %	wt %
B-11	SD4	8.89	0.04	<dt	<dt	<dt	0.09	0.07	1.79	<dt	<dt	<dt	0.19	0.17	<dt	2.27	<dt	2.53	20.99	11.69	4.13	13.57	2.05	1.15	0.15	0.45	<dt	0.16	<dt	<dt	<dt	11.0	81.4
B-12	SD4	8.19	0.05	<dt	<dt	<dt	0.11	0.09	1.89	<dt	0.19	0.04	0.99	0.15	0.12	2.59	0.16	3.10	18.90	12.61	3.64	12.36	1.89	1.06	0.14	0.49	<dt	0.13	<dt	0.07	<dt	11.2	80.3
B-13	SD4	7.26	0.04	<dt	<dt	<dt	0.22	0.18	1.44	<dt	0.04	0.05	2.08	0.12	<dt	3.32	<dt	3.55	14.74	18.46	2.65	9.47	1.42	0.69	0.16	0.62	0.13	0.25	<dt	0.11	<dt	11.3	78.6
B-14	SD4	7.31	0.04	<dt	<dt	0.07	0.38	0.17	1.49	<dt	0.08	0.03	2.85	<dt	0.11	2.98	0.13	5.01	12.52	19.30	2.35	8.44	1.39	0.92	0.17	0.80	0.14	0.29	<dt	0.14	<dt	11.7	79.1
B-15	SD4	7.62	0.03	<dt	<dt	<dt	0.17	0.18	1.49	<dt	0.08	0.05	3.27	<dt	<dt	2.86	0.17	6.10	11.07	20.01	2.21	8.12	1.45	1.02	0.25	0.98	0.15	0.45	<dt	0.23	<dt	11.7	79.8
B-16	SD4	7.25	0.04	<dt	<dt	<dt	0.17	0.10	1.79	<dt	0.04	0.05	1.15	0.13	<dt	2.58	<dt	3.71	17.49	11.23	3.56	12.82	2.24	1.29	0.17	0.58	<dt	0.24	<dt	0.11	<dt	11.0	77.9
B-17	SD4	9.05	0.03	<dt	<dt	0.03	1.37	1.96	1.40	<dt	0.05	<dt	0.14	0.12	<dt	3.06	0.51	11.04	12.57	16.09	2.18	6.16	1.01	<dt	0.18	1.56	0.39	1.27	0.15	1.25	0.15	16.7	92.4
B-18	SD4	9.89	0.04	<dt	<dt	<dt	0.11	0.10	1.51	<dt	<dt	<dt	0.06	0.17	<dt	3.75	<dt	2.47	17.37	19.31	3.10	10.68	1.54	0.92	0.10	0.38	<dt	0.15	<dt	0.08	<dt	10.9	82.7
B-19	SD4	8.16	0.04	<dt	<dt	0.04	0.36	0.12	1.50	<dt	<dt	<dt	0.09	0.14	<dt	3.52	0.17	2.98	16.28	19.77	2.90	10.19	1.47	0.82	0.13	0.52	<dt	0.19	<dt	0.11	<dt	11.3	81.0
B-20	SD5	6.55	0.05	<dt	<dt	0.15	0.62	<dt	1.87	0.11	0.15	0.04	3.33	<dt	0.13	3.02	0.13	17.56	9.38	6.70	1.93	7.99	1.91	2.81	0.59	3.51	0.62	1.44	0.12	0.65	<dt	14.7	71.8
B-21	SD5	7.63	0.04	<dt	<dt	<dt	0.58	<dt	1.87	<dt	0.16	0.04	3.99	<dt	0.11	2.24	<dt	15.59	9.27	6.12	1.76	7.91	1.91	2.93	0.59	3.78	0.64	1.54	0.15	0.68	0.08	14.0	70.2
B-22	SD5	7.01	0.04	<dt	<dt	0.08	1.02	<dt	1.82	0.10	0.17	0.08	4.50	0.11	0.12	3.79	0.21	14.59	8.97	8.10	1.98	7.47	1.63	2.17	0.41	2.74	0.50	1.29	0.14	0.76	<dt	14.2	71.3
B-23	SD5	7.46	0.03	<dt	<dt	0.04	2.21	0.78	1.22	<dt	0.14	<dt	0.22	<dt	<dt	4.16	0.34	7.43	12.08	16.79	1.98	7.26	1.12	0.72	0.12	0.82	0.23	0.69	0.07	0.59	0.12	14.8	69.5
B-24	SD5	8.04	0.06	<dt	<dt	<dt	0.21	<dt	1.36	<dt	0.04	<dt	0.13	0.13	<dt	2.83	<dt	2.79	19.80	15.65	3.32	11.45	1.65	0.98	0.10	0.34	<dt	0.22	<dt	<dt	<dt	11.0	69.4
B-25	SD5	7.49	0.04	<dt	<dt	<dt	0.24	<dt	1.47	<dt	0.04	<dt	0.08	<dt	<dt	3.64	<dt	2.83	18.86	17.46	3.09	11.02	1.60	1.02	0.15	0.38	<dt	0.18	<dt	<dt	<dt	11.2	69.7
B-26	SD5	7.66	0.05	<dt	<dt	<dt	0.85	0.40	1.38	<dt	0.14	0.06	1.37	0.10	<dt	2.58	0.18	5.35	15.00	17.60	2.46	8.48	1.30	0.85	0.14	0.79	0.17	0.41	<dt	0.29	<dt	12.3	67.6
B-27	SD5	8.08	0.05	<dt	<dt	<dt	0.09	<dt	1.33	<dt	0.07	<dt	0.12	<dt	0.12	1.94	<dt	2.19	20.88	15.27	3.52	11.83	1.72	0.93	0.10	0.28	<dt	<dt	<dt	<dt	<dt	10.8	68.5
B-28	SD5	7.46	0.05	<dt	<dt	0.15	0.50	<dt	1.31	0.12	0.05	<dt	0.79	<dt	<dt	2.09	0.09	2.39	19.55	15.37	3.14	10.80	1.51	0.89	0.10	0.42	<dt	0.16	<dt	<dt	<dt	11.2	66.9
B-29	SD6	7.30	0.04	<dt	<dt	<dt	0.17	0.09	2.42	<dt	0.11	<dt	0.33	0.22	<dt	2.60	<dt	3.15	14.93	21.12	2.68	8.92	1.43	0.73	0.13	0.51	0.13	0.18	<dt	0.07	<dt	11.2	78.6
B-30	SD6	6.03	0.04	<dt	<dt	<dt	0.91	0.37	2.12	<dt	0.07	<dt	0.08	0.13	<dt	2.35	0.22	3.90	13.52	22.82	2.43	8.14	1.27	0.68	0.14	0.58	<dt	0.27	<dt	0.18	<dt	12.3	78.8
B-31	SD6	6.95	0.05	<dt	<dt	<dt	0.12	0.07	2.57	<dt	0.11	<dt	0.54	0.20	<dt	2.74	<dt	3.62	14.60	20.10	2.65	9.29	1.52	0.92	0.18	0.65	0.14	0.22	<dt	0.10	<dt	11.3	78.8
B-32	SD6	7.42	0.05	<dt	<dt	<dt	0.12	0.09	2.59	<dt	0.11	<dt	0.48	0.19	<dt	2.75	0.16	3.46	14.69	20.46	2.55	9.13	1.49	1.00	0.18	0.60	<dt	0.13	<dt	<dt	<dt	11.3	79.1
B-33	SD6	7.28	0.06	<dt	<dt	<dt	0.12	0.09	2.57	<dt	0.13	<dt	0.58	0.17	<dt	2.75	0.19	3.39	14.45	21.10	2.58	8.88	1.48	0.93	0.17	0.55	0.14	0.22	<dt	0.08	<dt	11.3	79.4
B-34	SD6	6.64	0.05	<dt	<dt	<dt	0.11	0.08	2.56	<dt	0.10	<dt	0.68	0.18	<dt	2.75	0.16	3.50	14.31	21.24	2.52	8.73	1.47	0.96	0.19	0.57	<dt	<dt	<dt	<dt	<dt	11.2	78.2
B-35	SD6	6.22	0.06	<dt	<dt	0.23	0.71	0.08	2.70	0.07	0.05	<dt	0.70	0.16	<dt	3.24	0.22	3.36	20.86	7.28	4.02	14.25	2.32	1.23	0.16	0.56	<dt	0.16	<dt	0.08	<dt	12.2	81.0
B-36	SD6	7.08	0.07	<dt	<dt	0.12	0.33	<dt	2.42	<dt	0.05	<dt	0.98	0.18	<dt	1.90	<dt	2.62	20.19	9.54	3.91	13.92	2.30	1.06	0.16	0.47	0.14	<dt	<dt	<dt	<dt	11.5	78.9
B-37	SD6	6.90	0.07	<dt	<dt	<dt	0.17	<dt	2.45	<dt	0.07	0.04	0.39	0.18	<dt	2.08	<dt	2.61	20.43	10.59	4.08	13.98	2.18	1.12	0.15	0.48	0.14	0.19	<dt	<dt	<dt	11.3	79.6
B-38	SD6	7.17	0.08	<dt	<dt	<dt	0.20	<dt	2.31	0.03	0.06	<dt	0.09	0.14	<dt	1.27	<dt	1.87	20.97	10.70	4.22	14.96	2.40	1.12	0.16	0.37	<dt	<dt	<dt	<dt	<dt	11.1	79.2
B-39	SD6	6.13	0.08	<dt	<dt	0.09	0.38	0.09	2.44	<dt	0.12	<dt	0.59	0.17	<dt	1.56	<dt	2.55	19.55	11.29	4.04	13.93	2.25	1.29	0.12	0.46	<dt	<dt	<dt	<dt	<dt	11.6	78.8
B-40	SD6	8.31	0.05	<dt	<dt	<dt	0.29	0.12	2.54	<dt	0.17	<dt	0.11	0.12	<dt	2.43	0.23	4.60	16.28	14.65	3.21	11.12	1.93	1.17	0.17	0.70	<dt	0.25	<dt	0.08	<dt	11.7	80.6
B-41	SD6	8.54	0.05	<dt	<dt	<dt	0.33	0.12	2.51	0.03	0.15	<dt	0.15	0.18	<dt	2.24	0.13	4.52	15.93	15.33	3.11	11.07	1.92	1.13	0.15	0.72	0.16	0.20	<dt	<dt	<dt	11.7	80.8
B-42	SD6	8.00	0.06	<dt	<dt	<dt	0.30	0.10	2.48	<dt	0.17	<dt	0.21	0.17	0.12	2.12	0.14	4.54	15.72	15.40	3.12	11.17	1.98	1.19	0.18	0.74	0.15	0.28	<dt	<dt	<dt	11.7	80.5
B-43	SD6	6.78	0.05	<dt	<dt	<dt	0.12	<dt	2.45	<dt	0.06	<dt	0.06	0.13	<dt	1.84	0.16	3.50	14.33	19.35	2.84	9.80	1.64	0.96	0.17	0.57	<dt	0.15	<dt	<dt	<dt	10.9	75.8
B-44	SD6	7.13	0.05	<dt	<dt	<dt	0.12	0.09	2.47	<dt	0.08	<dt	0.07	0.15	<dt	1.92	<dt	3.27	14.47	20.77	2.93	9.99	1.66	0.91	0.17	0.58	0.14	0.17	<dt	0.07	<dt	11.2	78.5
B-45	SD6	8.20	0.05	<dt	<dt	0.05	0.59	0.24	2.47	<dt	0.19	<dt	0.14	0.16	0.12	2.25	0.27	5.14	15.65	15.34	3.11	10.87	1.90	1.19	0.22	0.80	0.14	0.21	<dt	0.13	<dt	12.5	82.6
B-46	SD6	7.53	0.07	<dt	<dt	<dt	0.19	0.08	2.39	<dt	0.09	<dt	0.40	0.16	<dt	2.36	0.21	3.00	17.81	13.61	3.53	12.21	1.97	1.16	0.16	0.52	<dt	0.22	<dt	<dt	<dt	11.2	79.0
B-47	SD6	7.73	0.07	<dt	<dt	0.12	0.40	0.10	2.43	0.04	0.05	<dt	0.18	0.20	<dt	2.78	<dt	2.98	17.42	14.09	3.63	12.28	2.01	1.12	0.19	0.53	<dt	0.24	<dt	<dt	<dt	11.5	80.1
B-48	SD6	7.05	0.05	<dt	<dt	0.06	0.26	<dt	2.45	<dt	0.09	<dt	0.59	0.19	<dt	2.32	0.19	2.63	16.69	15.54	3.29	11.58	1.93	0.95	0.14	0.43	<dt	<dt	<dt	0.07	<dt	11.2	77.8
B-49	SD6	7.38	0.05	<dt	<dt	<dt	0.17	0.09	2.82	<dt	0.10	<dt	1.24	0.20	<dt	3.18	0.20	4.12	15.61	13.78	3.14	11.27	2.02	1.09	0.18	0.68	0.14	0.16	<dt	<dt	<dt	11.4	79.0
B-50	SD6	8.74	0.06	<dt	<dt	<dt	0.10	0.08	2.86	<dt	0.09	<dt	0.07	0.19	<dt	3.57	<dt	3.73	16.63	14.27	3.53	12.40	2.12	1.20	0.14	0.63	0.14	0.17	<dt	0.09	<dt	11.4	82.2
B-51	SD6	8.42	0.05	<dt	<dt	<dt	0.12	0.08	2.88	<dt	0.18	<dt	0.06	0.22	<dt	3.59	0.18	3.80	15.84	14.33	3.40	11.84	2.05	1.28	0.17	0.63	<dt	0.22	<dt	0.09	<dt	11.3	80.7
B-52	SD6	7.95	0.05	<dt	<dt	<dt	0.09	0.06	2.83	<dt	0.08	<dt	0.36	0.21	<dt	3.39	<dt	3.74	16.40	14.40	3.37	11.76	2.06	1.12	0.17	0.64	0.13	0.17	<dt	0.08	<dt	11.3	80.3
B-53	SD6	7.50	0.05	<dt	<dt	<dt	0.13	0.10	2.93	<dt	0.08	<dt	0.09	0.19	<dt	3.63	0.17	3.80	16.03	14.81	3.32	11.91	2.10	1.29	0.14	0.70	<dt	0.20	<dt	<dt	<dt	11.4	80.6
B-54	SD6	8.47	0.06	<dt	<dt	<dt	0.11	0.06	2.84	<dt	0.09	<dt	0.27	0.19	<dt	3.45	0.23	4.12	15.62	15.05	3.09	11.25	1.90	1.10	0.20	0.61	0.14	0.19	<dt	<dt	<dt	11.2	80.2
B-55	SD6	6.76	0.06	<dt	<dt	0.11	0.44	0.05	2.33	<dt	0.26	0.05	2.88	0.22	<dt	2.33	0.15	2.53	17.95	9.19	3.74	12.71	2.13	1.05	0.16	0.46	<dt	<dt	<dt	<dt	<dt	11.5	77.1

#	Sample	F	Cl	Na	Mg	Al	Si	P	Ca	K	Ti	Mn	Fe	Ba	Sr	Th	U	Y	La	Ce	Pr	Nd	Sm	Gd	Tb	Dy	Ho	Er	Tm	Yb	Lu	O	Total
		wt %	wt %	wt %	wt %	wt %	wt %	wt %	wt %	wt %	wt %	wt %	wt %	wt %	wt %	wt %	wt %	wt %	wt %	wt %	wt %	wt %	wt %	wt %	wt %	wt %	wt %	wt %	wt %	wt %	wt %	wt %	wt %
B-56	SD6	6.55	0.07	<dt	<dt	0.08	0.37	0.07	2.56	<dt	0.13	0.04	2.01	0.20	<dt	2.80	0.18	2.83	17.94	10.06	3.71	12.94	2.15	1.19	0.14	0.54	<dt	0.17	<dt	<dt	<dt	11.5	78.3
B-57	SD7	7.78	0.05	<dt	<dt	0.05	0.25	<dt	2.35	<dt	<dt	0.04	0.27	0.20	<dt	1.91	0.14	2.76	11.38	24.78	2.61	8.85	1.44	0.88	0.18	0.63	<dt	0.17	<dt	<dt	<dt	11.0	77.7
B-58	SD7	7.53	0.03	<dt	<dt	0.07	0.28	<dt	2.31	0.04	<dt	<dt	0.46	0.15	<dt	1.83	<dt	2.63	11.23	24.79	2.57	8.74	1.39	0.79	0.13	0.55	<dt	0.21	<dt	<dt	<dt	10.9	76.7
B-59	SD7	7.80	0.05	<dt	<dt	0.26	0.72	<dt	2.36	0.07	0.06	0.04	1.25	0.16	<dt	1.81	0.08	2.84	11.00	23.88	2.53	8.45	1.42	0.78	0.14	0.61	<dt	0.17	<dt	<dt	<dt	11.7	78.2
B-60	SD7	7.65	0.04	<dt	<dt	<dt	0.09	<dt	2.07	<dt	<dt	<dt	0.07	0.16	<dt	1.52	<dt	2.86	13.01	24.43	2.42	8.45	1.35	0.70	0.17	0.37	<dt	0.16	<dt	<dt	<dt	10.6	76.1
B-61	SD7	7.05	0.07	<dt	<dt	0.04	0.31	<dt	2.17	0.03	0.07	<dt	0.96	0.14	<dt	1.52	0.10	3.19	12.88	23.62	2.39	8.13	1.28	0.64	0.12	0.39	0.13	0.19	<dt	<dt	<dt	11.2	76.8
B-62	SD7	6.94	0.04	<dt	<dt	<dt	0.12	<dt	2.14	<dt	<dt	<dt	0.46	0.13	<dt	1.69	<dt	3.11	13.09	24.04	2.38	8.29	1.33	0.77	0.13	0.42	<dt	<dt	<dt	<dt	<dt	10.8	75.8
B-63	SD7	7.06	0.07	<dt	<dt	0.09	0.82	0.24	2.08	0.04	0.04	<dt	1.12	0.19	<dt	3.33	<dt	4.44	11.44	20.54	2.16	7.31	1.15	0.74	0.12	0.53	0.14	0.30	<dt	0.21	<dt	12.0	77.2
B-64	SD7	6.85	0.03	<dt	<dt	0.12	0.96	0.64	2.17	<dt	0.04	<dt	1.08	0.13	<dt	3.42	<dt	5.73	11.26	20.47	2.04	7.03	1.13	0.61	0.13	0.64	0.16	0.35	<dt	0.39	0.07	13.0	79.6
B-65	SD7	7.44	0.06	<dt	<dt	<dt	0.14	<dt	2.17	<dt	<dt	<dt	0.42	0.13	<dt	1.64	<dt	2.80	13.04	24.21	2.46	8.40	1.32	0.76	0.16	0.39	0.12	<dt	<dt	<dt	<dt	10.7	76.4
B-66	SD7	7.66	0.05	<dt	0.09	0.49	1.53	<dt	2.28	0.07	0.04	<dt	0.48	0.15	<dt	2.67	0.18	4.43	11.24	20.79	2.30	8.00	1.39	1.03	0.17	0.65	<dt	0.26	<dt	0.10	<dt	12.7	78.9
B-67	SD7	7.46	0.04	<dt	0.05	0.35	2.01	<dt	1.92	0.05	1.80	0.04	4.19	<dt	<dt	3.56	0.30	15.70	5.75	8.01	1.15	4.40	0.82	0.43	0.14	1.15	0.33	1.09	0.17	1.05	0.12	15.1	79.2
B-68	SD7	7.71	0.05	<dt	0.18	0.70	1.97	<dt	2.46	0.11	0.10	<dt	1.56	<dt	<dt	2.22	0.07	3.23	11.50	20.27	2.27	8.16	1.37	0.92	0.17	0.46	<dt	0.20	<dt	<dt	<dt	13.3	79.0
B-69	SD7	7.41	0.05	<dt	<dt	0.28	0.88	0.05	2.78	0.10	0.05	<dt	2.15	<dt	<dt	2.16	0.10	3.59	11.62	20.45	2.30	8.49	1.36	0.84	0.11	0.46	<dt	0.23	<dt	<dt	<dt	12.1	77.6
B-70	SD27	5.87	0.05	<dt	<dt	0.16	0.70	0.28	2.43	<dt	0.07	<dt	1.30	0.12	<dt	4.46	0.17	1.98	19.54	12.97	2.93	9.47	1.29	0.64	0.08	0.36	<dt	<dt	<dt	0.12	<dt	11.7	76.8
B-71	SD27	6.92	0.05	<dt	<dt	<dt	0.11	0.07	2.14	0.04	0.05	<dt	0.47	0.14	<dt	3.74	0.18	1.58	20.60	14.58	3.10	10.17	1.41	0.75	0.10	0.30	<dt	0.15	<dt	<dt	<dt	10.7	77.3
B-72	SD27	6.92	0.06	<dt	<dt	0.12	0.33	0.06	2.18	<dt	0.07	<dt	0.45	0.18	<dt	3.77	<dt	1.60	20.10	14.81	2.99	9.82	1.45	0.80	0.10	0.28	<dt	<dt	<dt	<dt	<dt	10.9	77.0
B-73	SD27	6.79	0.05	<dt	<dt	<dt	0.14	0.06	2.13	<dt	0.07	<dt	0.55	0.16	<dt	3.76	0.25	1.61	19.94	15.08	3.02	9.92	1.46	0.71	0.15	0.37	<dt	0.13	<dt	<dt	<dt	10.7	77.0
B-74	SD27	6.09	0.05	<dt	<dt	<dt	0.12	0.20	2.79	<dt	0.04	<dt	0.10	0.20	<dt	6.66	0.21	1.85	17.89	14.84	2.72	9.14	1.37	0.69	0.12	0.36	<dt	0.20	<dt	<dt	<dt	10.6	76.2
B-75	SD27	5.35	0.04	<dt	<dt	<dt	0.57	0.48	2.79	<dt	<dt	<dt	0.16	0.18	<dt	6.24	0.20	2.91	17.77	14.62	2.65	8.82	1.29	0.71	0.13	0.44	<dt	0.16	<dt	0.12	<dt	11.8	78.0
B-76	SD27	6.02	0.05	<dt	<dt	<dt	0.12	0.17	2.93	<dt	0.04	<dt	0.06	0.23	<dt	6.97	0.21	1.77	18.35	14.17	2.79	9.20	1.32	0.68	0.11	0.36	<dt	<dt	<dt	0.07	<dt	10.6	76.3
B-77	SD27	5.58	0.04	<dt	<dt	0.09	0.60	0.26	2.56	<dt	<dt	<dt	0.15	0.18	<dt	5.09	0.29	2.16	17.97	14.85	2.77	9.41	1.35	0.49	0.11	0.40	0.21	0.20	<dt	0.08	<dt	11.4	76.6
B-78	SD27	5.78	0.04	<dt	<dt	<dt	0.10	0.12	2.90	<dt	<dt	<dt	0.11	0.17	<dt	6.88	0.20	1.68	18.55	13.84	2.78	9.40	1.35	0.70	0.12	0.37	<dt	0.18	<dt	<dt	<dt	10.5	75.7
B-79	SD27	6.78	0.06	<dt	<dt	<dt	0.59	0.18	3.12	<dt	0.05	<dt	0.39	0.24	<dt	8.33	0.23	1.73	19.60	12.11	2.86	9.87	1.41	0.80	0.10	0.41	<dt	0.16	<dt	<dt	<dt	11.5	80.8
B-80	SD27	6.08	0.04	<dt	<dt	<dt	0.19	0.10	3.05	<dt	<dt	<dt	0.13	0.30	<dt	7.86	0.23	1.53	19.65	12.47	2.94	9.82	1.34	0.72	0.11	0.26	<dt	<dt	<dt	<dt	<dt	10.7	77.5
B-81	SD27	6.81	0.05	<dt	<dt	<dt	0.37	0.12	2.51	<dt	0.05	<dt	0.46	0.21	<dt	5.75	0.21	1.78	19.96	12.27	3.13	10.30	1.46	0.78	0.10	0.42	<dt	0.17	<dt	<dt	<dt	11.0	78.0
B-82	SD27	6.00	0.04	<dt	<dt	<dt	0.11	0.11	2.59	<dt	0.14	<dt	0.47	0.20	<dt	5.12	<dt	1.62	20.75	12.29	3.17	9.98	1.40	0.64	0.09	0.33	<dt	0.17	<dt	<dt	<dt	10.6	75.9
B-83	SD27	6.30	0.05	<dt	<dt	<dt	0.08	0.09	2.60	<dt	0.05	<dt	0.14	0.19	<dt	5.43	<dt	1.71	20.77	12.59	3.31	10.93	1.51	0.65	0.11	0.32	0.14	<dt	<dt	<dt	<dt	10.7	77.7
B-84	SD25	6.54	0.04	<dt	<dt	0.04	0.58	0.13	2.43	<dt	0.30	<dt	0.87	0.11	<dt	2.85	0.21	3.27	13.03	22.54	2.43	8.52	1.32	0.85	0.17	0.74	<dt	0.34	<dt	0.13	<dt	12.3	80.6
B-85	SD25	6.33	0.04	<dt	<dt	<dt	0.49	0.12	2.39	<dt	0.27	<dt	0.61	0.18	<dt	3.04	0.22	3.34	13.85	21.00	2.62	9.13	1.45	0.74	0.18	0.68	0.15	0.18	<dt	0.12	<dt	12.0	79.9
B-86	SD25	8.39	0.04	<dt	<dt	<dt	0.26	0.12	2.86	<dt	<dt	<dt	0.31	0.22	<dt	4.25	0.20	3.23	18.17	12.95	3.33	11.22	1.81	0.93	0.15	0.65	0.16	0.17	<dt	0.07	<dt	11.4	81.2
B-87	SD25	7.60	0.05	<dt	<dt	<dt	0.15	0.12	2.80	<dt	<dt	<dt	0.79	0.29	<dt	4.45	0.17	3.29	18.28	12.89	3.29	11.32	1.88	1.00	0.18	0.60	<dt	0.22	<dt	0.08	<dt	11.4	81.0
B-88	SD25	9.96	0.04	<dt	<dt	<dt	0.26	0.11	2.89	<dt	<dt	<dt	0.54	0.20	<dt	4.39	0.14	3.13	17.89	12.91	3.29	11.29	1.82	1.03	0.17	0.65	<dt	0.20	<dt	<dt	<dt	11.3	82.4
B-89	SD8	9.12	0.06	<dt	<dt	<dt	0.09	0.08	2.28	<dt	<dt	<dt	0.26	<dt	<dt	1.53	<dt	4.22	12.61	25.43	2.57	8.93	1.55	0.91	0.20	0.84	<dt	0.28	<dt	0.10	<dt	11.5	82.5
B-90	SD8	8.62	0.04	<dt	<dt	<dt	0.09	0.07	2.13	<dt	<dt	<dt	0.24	0.16	<dt	1.51	<dt	4.23	12.47	25.47	2.52	8.77	1.55	0.90	0.19	0.87	<dt	0.32	<dt	0.09	<dt	11.4	81.6
B-91	SD8	7.73	0.04	<dt	<dt	<dt	0.09	0.07	2.47	<dt	<dt	<dt	0.28	0.15	<dt	1.55	<dt	4.41	12.38	24.90	2.47	8.75	1.48	0.83	0.21	0.89	<dt	0.27	<dt	0.09	<dt	11.5	80.5
B-92	SD8	9.42	0.04	<dt	<dt	<dt	0.14	0.11	2.19	<dt	<dt	<dt	0.40	0.17	<dt	1.68	<dt	4.20	12.47	25.47	2.56	8.85	1.50	0.92	0.21	0.81	<dt	0.28	<dt	0.10	<dt	11.6	83.1
B-93	SD8	7.72	0.04	<dt	<dt	<dt	0.08	0.13	2.99	<dt	0.05	<dt	0.15	0.21	<dt	3.33	<dt	5.08	11.59	24.94	2.57	9.35	1.73	1.34	n.a.	n.a.	n.a.	n.a.	n.a.	n.a.	n.a.	12.0	83.3
B-94	SD8	7.78	0.04	<dt	<dt	<dt	0.09	0.12	3.12	<dt	0.04	<dt	0.19	0.21	<dt	3.87	<dt	5.21	11.48	24.32	2.50	9.15	1.77	1.36	n.a.	n.a.	n.a.	n.a.	n.a.	n.a.	n.a.	12.0	83.2
B-95	SD8	7.76	0.04	<dt	<dt	<dt	0.23	0.12	2.85	0.03	0.05	<dt	0.31	0.17	<dt	3.59	<dt	5.24	11.15	24.72	2.59	9.08	1.79	1.36	n.a.	n.a.	n.a.	n.a.	n.a.	n.a.	n.a.	12.1	83.2
B-96	SD8	5.39	0.04	<dt	0.12	0.54	2.41	0.08	2.34	0.07	0.06	<dt	1.05	<dt	<dt	0.83	<dt	3.00	13.12	23.88	2.29	8.44	1.41	1.08	n.a.	n.a.	n.a.	n.a.	n.a.	n.a.	n.a.	0.0	66.2
B-97	SD8	7.31	0.04	<dt	<dt	0.06	0.33	0.15	3.43	<dt	0.04	<dt	0.20	0.14	<dt	5.29	<dt	3.52	11.01	21.68	2.16	7.79	1.29	0.65	0.17	0.79	0.13	0.27	<dt	0.12	<dt	11.3	78.1
B-98	SD8	7.15	0.04	<dt	<dt	0.72	1.38	<dt	3.15	<dt	0.04	<dt	0.38	0.17	<dt	3.30	0.17	4.93	10.84	23.42	2.44	8.75	1.58	1.30	n.a.	n.a.	n.a.	n.a.	n.a.	n.a.	n.a.	13.7	83.5
B-99	SD8	8.35	0.03	<dt	0.06	0.90	1.72	0.16	3.18	0.05	0.05	<dt	0.55	0.16	<dt	3.93	0.07	4.54	10.67	23.21	2.46	8.60	1.59	1.34	n.a.	n.a.	n.a.	n.a.	n.a.	n.a.	n.a.	14.3	85.9
B-100	SD8	7.39	0.03	<dt	<dt	0.36	0.83	0.17	3.27	0.03	0.04	<dt	0.11	0.18	<dt	3.37	<dt	4.92	11.03	24.16	2.53	8.91	1.58	1.21	n.a.	n.a.	n.a.	n.a.	n.a.	n.a.	n.a.	12.9	83.0

#	Sample	F wt %	Cl wt %	Na wt %	Mg wt %	Al wt %	Si wt %	P wt %	Ca wt %	K wt %	Ti wt %	Mn wt %	Fe wt %	Ba wt %	Sr wt %	Th wt %	U wt %	Y wt %	La wt %	Ce wt %	Pr wt %	Nd wt %	Sm wt %	Gd wt %	Tb wt %	Dy wt %	Ho wt %	Er wt %	Tm wt %	Yb wt %	Lu wt %	O wt %	Total wt %
B-101	SD8	6.51	0.04	<dt	<dt	0.58	0.93	<dt	3.33	0.04	0.05	<dt	0.13	0.18	<dt	3.45	0.19	5.01	10.90	24.84	2.55	9.20	1.62	1.30	n.a.	n.a.	n.a.	n.a.	n.a.	n.a.	n.a.	13.5	84.3
B-102	SD8	7.96	0.05	<dt	0.07	0.50	1.84	0.09	2.68	0.05	<dt	<dt	0.29	0.13	<dt	2.57	<dt	3.96	11.78	23.41	2.40	8.55	1.59	1.41	n.a.	n.a.	n.a.	n.a.	n.a.	n.a.	n.a.	13.5	82.9
B-103	SD8	8.59	0.03	<dt	<dt	0.06	0.35	0.16	3.46	0.03	0.05	<dt	0.37	0.17	<dt	5.43	0.17	3.72	11.68	23.64	2.43	8.58	1.45	1.09	n.a.	n.a.	n.a.	n.a.	n.a.	n.a.	n.a.	12.3	84.0
B-104	SD8	8.59	0.03	<dt	<dt	<dt	0.50	0.13	3.35	<dt	0.11	<dt	0.26	0.12	0.27	4.31	0.34	3.87	10.89	22.77	2.28	8.83	1.45	1.25	n.a.	n.a.	n.a.	n.a.	n.a.	n.a.	n.a.	12.6	83.7
B-105	SD9	9.48	0.05	<dt	<dt	0.10	0.29	0.13	4.43	<dt	0.04	<dt	1.03	<dt	0.17	11.42	0.33	2.55	18.03	9.05	3.05	10.47	1.65	1.11	0.12	0.52	<dt	0.15	<dt	0.10	<dt	12.5	86.9
B-106	SD9	8.44	0.06	<dt	0.13	0.73	1.90	0.10	3.40	0.07	0.07	<dt	0.71	<dt	0.21	6.21	0.33	2.47	18.91	9.19	3.12	10.60	1.71	0.91	0.12	0.56	0.16	0.15	<dt	<dt	<dt	14.1	84.9
B-107	SD9	6.17	0.06	<dt	<dt	0.10	1.00	0.10	3.13	0.06	0.34	0.05	1.18	0.16	0.11	5.73	0.34	2.67	15.38	14.27	2.80	9.57	1.60	1.00	0.15	0.61	<dt	0.19	<dt	0.07	<dt	13.2	81.8
B-108	SD9	3.40	0.04	<dt	<dt	<dt	1.88	0.14	2.34	<dt	0.87	0.08	0.97	0.15	<dt	4.02	0.20	1.95	9.24	29.18	1.71	5.71	0.93	0.45	0.16	0.53	<dt	0.28	<dt	0.10	<dt	14.6	81.8
B-109	SD9	2.97	0.03	<dt	<dt	0.07	2.28	0.10	2.05	<dt	0.94	0.08	0.87	<dt	<dt	3.77	0.18	1.75	7.42	35.01	1.40	4.59	0.79	0.26	0.08	0.44	<dt	0.25	<dt	0.14	<dt	15.5	84.5
B-110	SD9	4.23	0.03	<dt	<dt	0.04	1.70	0.15	2.28	<dt	0.48	0.05	0.44	0.13	<dt	3.04	0.19	2.17	10.55	29.16	2.01	6.29	1.00	0.46	0.14	0.57	0.13	0.22	<dt	0.11	<dt	13.9	81.5
B-111	SD9	3.99	0.05	<dt	<dt	0.08	1.82	0.18	2.07	<dt	0.39	0.06	0.45	0.14	<dt	2.26	0.24	2.09	9.13	34.01	1.73	5.53	0.89	0.12	0.13	0.52	0.21	0.22	<dt	0.15	<dt	14.2	82.6
B-112	SD9	8.70	0.04	<dt	0.14	0.99	2.66	0.10	2.87	0.14	0.08	0.04	1.58	<dt	0.12	4.66	0.23	2.14	14.91	10.70	2.40	9.04	1.44	0.90	0.15	0.45	<dt	0.16	<dt	<dt	<dt	13.9	78.5
B-113	SD9	8.04	0.05	<dt	0.08	0.50	1.28	0.10	4.20	0.04	0.05	<dt	0.90	<dt	0.18	9.46	0.33	2.36	17.60	9.62	3.11	10.35	1.58	0.95	0.18	0.53	<dt	<dt	<dt	0.07	<dt	13.5	85.0
B-114	SD9	5.30	0.04	<dt	<dt	0.07	1.60	0.15	2.44	<dt	0.33	0.06	1.48	0.13	<dt	3.01	<dt	2.32	14.22	24.75	2.64	9.17	1.38	0.94	n.a.	n.a.	n.a.	n.a.	n.a.	n.a.	n.a.	22.2	93.4
B-115	SD9	5.28	0.03	<dt	<dt	0.17	1.84	0.12	2.51	0.08	0.80	0.08	1.52	<dt	<dt	2.64	0.21	1.72	13.01	26.37	2.41	7.95	1.24	0.73	n.a.	n.a.	n.a.	n.a.	n.a.	n.a.	n.a.	14.1	83.7
B-116	SD9	4.12	0.04	<dt	<dt	<dt	1.69	0.18	1.84	<dt	0.30	0.09	0.53	<dt	<dt	1.83	0.21	2.18	11.68	35.32	2.09	6.63	1.01	0.74	n.a.	n.a.	n.a.	n.a.	n.a.	n.a.	n.a.	0.0	70.8
B-117	SD9	6.72	0.03	<dt	0.13	0.93	2.96	0.08	3.15	0.08	0.07	0.06	1.19	0.18	<dt	4.96	0.21	2.01	17.33	8.34	2.78	8.90	1.44	1.00	n.a.	n.a.	n.a.	n.a.	n.a.	n.a.	n.a.	22.0	84.9
B-118	SD9	9.47	0.03	<dt	<dt	0.14	0.68	0.12	4.60	0.04	0.06	<dt	1.18	0.29	<dt	10.83	0.20	2.62	19.18	9.72	3.27	11.03	1.75	1.19	n.a.	n.a.	n.a.	n.a.	n.a.	n.a.	n.a.	21.2	97.6
B-119	SD9	8.38	0.03	<dt	<dt	0.11	0.35	0.12	3.89	<dt	0.07	<dt	0.58	0.23	<dt	6.94	0.26	3.04	21.12	10.75	3.51	12.06	1.93	1.34	n.a.	n.a.	n.a.	n.a.	n.a.	n.a.	n.a.	13.4	88.1
B-120	SD9	7.53	0.04	<dt	<dt	<dt	0.06	0.11	3.88	<dt	0.04	<dt	0.27	0.25	<dt	8.70	0.38	2.81	20.28	10.77	3.42	11.56	1.88	1.27	n.a.	n.a.	n.a.	n.a.	n.a.	n.a.	n.a.	34.3	107.5
B-121	SD9	8.37	0.03	<dt	0.04	0.35	0.92	0.11	4.29	<dt	0.05	<dt	0.74	0.26	<dt	9.16	0.24	2.60	19.00	11.57	3.37	11.09	1.83	1.26	n.a.	n.a.	n.a.	n.a.	n.a.	n.a.	n.a.	14.4	89.7
B-122	SD9	7.08	0.04	<dt	0.16	0.84	1.99	0.09	3.29	0.10	0.10	0.04	3.00	0.13	<dt	5.31	<dt	2.29	16.88	11.69	2.99	10.53	1.69	1.24	n.a.	n.a.	n.a.	n.a.	n.a.	n.a.	n.a.	21.7	91.3
B-123	SD9	7.18	0.04	<dt	<dt	<dt	0.27	0.09	3.35	<dt	0.10	0.04	0.91	0.29	<dt	5.50	0.25	2.66	20.25	12.63	3.53	11.56	1.86	1.25	n.a.	n.a.	n.a.	n.a.	n.a.	n.a.	n.a.	34.6	106.5
B-124	SD10	7.88	0.04	<dt	<dt	0.21	0.43	0.07	2.44	<dt	0.05	<dt	0.21	0.19	0.19	4.61	0.19	7.11	11.60	16.08	2.35	7.89	1.39	0.85	0.22	1.05	0.24	0.42	<dt	0.23	<dt	11.3	77.3
B-125	SD10	6.79	0.03	<dt	<dt	0.94	2.01	0.09	2.13	0.04	0.20	<dt	0.95	0.17	0.14	4.87	0.20	9.30	10.95	11.14	2.08	7.53	1.50	1.35	0.31	1.70	0.32	0.64	<dt	0.33	0.08	13.8	79.5
B-126	SD10	6.68	0.03	<dt	<dt	0.26	0.83	0.07	2.10	<dt	1.28	<dt	1.69	0.11	0.19	4.44	0.17	9.74	10.57	10.68	2.07	7.50	1.41	1.40	0.27	1.69	0.26	0.64	<dt	0.33	<dt	12.7	77.4
B-127	SD10	7.11	<dt	<dt	<dt	0.28	0.60	0.09	2.32	<dt	<dt	<dt	0.15	0.19	0.19	4.58	0.21	7.38	11.92	16.09	2.25	7.92	1.31	0.93	0.20	1.14	0.20	0.43	<dt	0.23	<dt	11.6	77.3
B-128	SD10	7.75	0.03	<dt	<dt	0.54	0.76	0.07	2.36	<dt	0.06	<dt	0.27	0.21	0.18	5.28	0.17	7.55	11.94	14.69	2.19	7.83	1.35	0.99	0.20	1.13	0.24	0.48	<dt	0.25	<dt	11.9	78.4
B-129	SD10	7.16	0.04	<dt	<dt	<dt	0.14	0.04	1.48	<dt	<dt	0.03	0.45	0.18	<dt	1.50	<dt	1.58	24.77	6.03	4.02	14.63	2.09	0.99	0.07	0.21	<dt	<dt	<dt	<dt	<dt	10.5	75.9
B-130	SD10	6.89	0.03	<dt	0.05	0.85	1.88	<dt	2.27	0.06	0.13	<dt	3.91	0.16	0.14	5.87	0.18	8.05	10.18	10.32	1.92	7.03	1.36	1.17	0.28	1.41	0.30	0.55	<dt	0.27	<dt	13.6	78.9
B-131	SD23	8.98	0.09	<dt	<dt	0.07	0.65	0.16	5.18	<dt	0.14	<dt	0.26	0.04	0.28	14.30	0.30	3.48	23.12	8.46	3.67	11.84	1.66	1.35	0.12	0.57	<dt	0.17	<dt	<dt	<dt	85.5	170.7
B-132	SD23	7.52	0.06	<dt	<dt	0.08	0.80	<dt	4.31	<dt	0.14	<dt	0.62	0.09	0.35	9.01	0.25	3.33	24.10	10.44	3.81	12.72	1.78	1.32	0.12	0.61	<dt	0.28	<dt	<dt	<dt	82.6	165.0
B-133	SD23	8.83	0.09	<dt	<dt	0.05	0.38	<dt	4.36	<dt	0.05	<dt	0.11	<dt	0.28	7.69	0.21	4.07	26.46	7.29	4.32	14.48	2.11	1.66	0.16	0.76	<dt	<dt	<dt	<dt	<dt	83.6	167.1
B-134	SD23	8.87	0.08	<dt	<dt	0.13	0.73	0.08	4.28	<dt	0.12	<dt	0.42	0.04	0.19	8.35	0.25	3.85	25.13	8.71	4.01	13.54	1.99	1.52	0.13	0.62	<dt	0.20	<dt	<dt	<dt	83.8	167.5
B-135	SD23	8.49	0.12	<dt	<dt	0.12	0.25	<dt	2.69	<dt	<dt	<dt	0.30	0.06	0.18	3.86	0.17	3.18	22.69	7.76	3.80	12.71	1.81	1.38	0.14	0.64	<dt	0.17	<dt	<dt	<dt	11.5	82.0
B-136	SD23	8.18	0.09	<dt	<dt	0.10	0.23	<dt	2.52	<dt	0.04	<dt	0.92	0.04	0.20	3.61	0.10	3.07	22.08	8.00	3.59	12.18	1.74	1.42	0.15	0.66	<dt	0.23	<dt	<dt	<dt	11.5	80.6
B-137	SD19	9.29	0.06	<dt	<dt	0.22	0.98	<dt	3.29	0.12	<dt	<dt	1.95	<dt	<dt	0.11	<dt	2.05	11.5	23.0	2.73	10.61	1.60	1.26	0.18	0.45	<dt	<dt	<dt	<dt	<dt	12.5	82.0
B-138	SD19	6.82	0.07	<dt	<dt	0.09	0.41	<dt	3.22	<dt	<dt	<dt	1.35	<dt	0.14	0.00	<dt	2.01	11.4	23.4	2.66	10.84	1.67	1.21	0.12	0.49	<dt	0.147	<dt	0.07	<dt	11.6	77.7
B-139	SD19	5.71	0.05	<dt	<dt	0.59	2.30	0.18	3.15	0.12	0.04	<dt	2.20	<dt	<dt	4.44	0.09	3.30	11.90	18.35	2.32	8.07	1.42	1.21	0.15	0.79	<dt	0.23	<dt	0.14	<dt	14.3	81.0
B-140	SD19	6.77	0.06	<dt	<dt	0.17	0.59	0.79	3.32	<dt	<dt	<dt	0.63	<dt	0.10	4.53	<dt	3.25	11.90	19.31	2.55	8.69	1.55	1.13	0.19	0.92	0.17	0.32	<dt	0.12	<dt	12.6	79.7
B-141	SD19	7.66	0.06	<dt	0.04	0.47	1.65	<dt	2.65	0.42	<dt	<dt	2.69	<dt	<dt	0.19	<dt	2.14	10.4	19.5	2.37	9.72	1.66	1.37	0.15	0.49	<dt	0.22	<dt	<dt	<dt	12.5	76.4
B-142	SD19	6.39	0.07	<dt	0.12	0.64	2.26	<dt	2.79	0.29	<dt	<dt	2.26	<dt	0.09	0.24	<dt	2.28	11.0	20.4	2.52	10.10	1.72	1.44	0.13	0.49	<dt	0.23	<dt	<dt	<dt	13.8	79.2
B-143	SD19	7.20	0.07	<dt	<dt	0.18	0.61	<dt	3.08	<dt	0.04	<dt	1.69	<dt	<dt	2.19	0.11	4.00	11.6	22.5	2.47	8.10	1.36	1.04	0.21	0.80	0.16	0.39	<dt	0.17	<dt	12.0	80.0
B-144	SD19	5.70	0.08	<dt	<dt	0.19	0.76	0.11	2.85	0.12	<dt	<dt	1.67	<dt	<dt	1.03	<dt	2.83	11.6	20.8	2.49	10.05	1.74	1.38	0.15	0.58	<dt	0.14	<dt	0.06	<dt	11.9	76.2
B-145	SD21	7.26	0.11	0.24	<dt	1.69	2.87	<dt	0.67	0.11	<dt	<dt	0.13	<dt	<dt	<dt	<dt	7.09	17.29	1.68	2.46	10.04	1.87	2.00	0.27	1.64	0.32	0.68	0.08	0.44	<dt	13.0	72.0

#	Sample	F	Cl	Na	Mg	Al	Si	P	Ca	K	Ti	Mn	Fe	Ba	Sr	Th	U	Y	La	Ce	Pr	Nd	Sm	Gd	Tb	Dy	Ho	Er	Tm	Yb	Lu	O	Total
		wt %	wt %	wt %	wt %	wt %	wt %	wt %	wt %	wt %	wt %	wt %	wt %	wt %	wt %	wt %	wt %	wt %	wt %	wt %	wt %	wt %	wt %	wt %	wt %	wt %	wt %	wt %	wt %	wt %	wt %	wt %	wt %
B-146	SD21	8.96	0.09	<dt	<dt	0.04	0.38	<dt	1.37	<dt	<dt	<dt	<dt	<dt	<dt	2.70	<dt	5.22	18.43	14.36	2.86	10.37	1.75	1.75	0.24	1.13	0.19	0.53	<dt	0.22	<dt	11.0	81.6
B-147	SD21	8.16	0.10	<dt	<dt	0.33	0.29	<dt	1.11	<dt	<dt	<dt	<dt	<dt	<dt	1.47	<dt	9.05	20.94	5.270	2.84	11.31	2.05	2.37	0.29	1.85	0.35	0.68	<dt	0.40	<dt	11.1	80.0
B-148	SD21	9.16	0.09	<dt	<dt	<dt	0.17	<dt	0.97	<dt	<dt	<dt	<dt	<dt	<dt	1.42	<dt	8.13	22.97	4.320	2.94	12.40	2.25	2.44	0.34	1.77	0.32	0.68	<dt	0.42	<dt	10.8	81.6
B-149	SD21	9.82	0.10	<dt	<dt	<dt	0.06	<dt	0.68	<dt	<dt	<dt	<dt	<dt	<dt	0.00	<dt	8.40	25.09	2.24	3.36	13.31	2.31	2.39	0.32	1.87	0.34	0.73	0.08	0.44	<dt	10.6	82.2
B-150	SD21	8.70	0.08	<dt	<dt	0.34	1.52	0.45	1.65	<dt	<dt	<dt	0.14	<dt	<dt	5.29	0.23	6.08	14.98	14.56	2.27	8.12	1.31	1.42	0.17	1.05	0.19	0.55	0.07	0.49	0.10	13.6	84.7
B-151	SD21	9.45	0.07	<dt	<dt	0.04	0.38	<dt	1.97	<dt	0.13	<dt	0.56	0.14	<dt	4.75	0.18	5.42	13.45	19.0	2.24	7.60	1.22	1.34	0.24	1.04	<dt	0.52	<dt	0.35	<dt	11.7	82.3
B-152	SD21	8.52	0.08	<dt	<dt	0.14	0.52	<dt	1.42	<dt	0.05	<dt	0.37	0.12	<dt	3.47	<dt	7.11	18.28	12.14	2.58	9.75	1.66	1.85	0.26	1.47	0.27	0.52	<dt	0.38	<dt	11.9	83.3
B-153	SD21	7.33	0.08	<dt	<dt	0.21	0.28	<dt	2.43	<dt	<dt	<dt	2.83	0.12	<dt	4.43	0.18	4.23	11.10	21.6	2.12	7.33	1.25	1.08	0.19	1.00	0.17	0.41	<dt	0.20	<dt	11.8	80.7
B-154	SD21	7.70	<dt	<dt	<dt	0.21	0.65	<dt	2.47	0.05	0.46	<dt	1.60	0.25	0.17	8.72	0.17	4.71	11.38	14.47	1.74	6.40	1.15	1.22	0.20	1.06	0.20	0.44	<dt	0.27	<dt	12.3	80.0
B-155	SD21	8.27	0.05	<dt	<dt	0.07	0.51	<dt	2.64	<dt	0.04	<dt	0.18	<dt	<dt	9.56	0.27	5.81	12.53	16.19	2.06	7.06	1.28	1.38	0.18	1.17	0.24	0.53	<dt	0.38	<dt	12.2	83.5
B-156	SD21	8.75	0.05	<dt	<dt	0.21	0.60	<dt	2.71	0.05	0.13	<dt	0.58	0.19	0.15	9.39	0.18	5.33	12.10	16.16	1.99	7.01	1.20	1.36	0.22	1.11	0.24	0.43	<dt	0.27	<dt	12.2	83.4
B-157	SD21	7.98	0.04	<dt	<dt	0.08	0.34	<dt	2.53	<dt	0.41	<dt	1.24	0.24	<dt	9.41	0.17	5.20	11.96	15.02	2.00	6.79	1.21	1.29	0.20	1.12	0.21	0.45	<dt	0.27	<dt	12.1	82.2
B-158	SD21	7.66	0.05	<dt	<dt	0.09	0.38	<dt	2.70	<dt	0.27	<dt	0.84	0.20	0.14	9.64	0.17	5.46	11.92	15.45	2.03	6.82	1.24	1.31	0.19	1.17	0.27	0.42	<dt	0.25	<dt	12.0	82.2
B-159	SD21	6.32	0.07	0.36	<dt	0.28	0.53	<dt	0.75	<dt	<dt	<dt	0.04	<dt	<dt	0.30	<dt	8.29	20.57	6.9	2.88	11.54	2.21	2.31	0.34	1.91	0.33	0.72	<dt	0.42	<dt	11.3	78.3
B-160	SD21	8.21	0.12	<dt	<dt	0.04	0.21	<dt	0.62	<dt	<dt	<dt	<dt	<dt	<dt	0.22	<dt	10.12	21.57	3.630	3.08	12.47	2.32	2.64	0.40	2.13	0.35	0.84	0.10	0.51	<dt	10.7	80.3
B-161	SV6.1	7.04	0.18	<dt	<dt	0.18	0.47	0.09	0.35	<dt	0.07	<dt	0.17	<dt	0.14	2.11	<dt	1.60	24.24	2.25	4.79	15.44	2.21	0.89	0.11	0.56	<dt	0.18	<dt	<dt	<dt	10.4	73.5
B-162	SV6.1	6.43	0.20	<dt	<dt	0.07	0.32	0.10	0.31	<dt	<dt	<dt	0.08	<dt	<dt	2.20	<dt	1.84	23.80	2.57	4.79	15.45	2.30	0.95	0.14	0.43	<dt	<dt	<dt	0.09	<dt	10.1	72.5
B-163	SV6.1	5.70	0.29	<dt	<dt	0.08	0.61	0.25	0.29	<dt	0.05	<dt	1.54	0.10	0.09	1.64	<dt	2.03	19.97	2.06	4.07	13.26	1.91	0.83	0.09	0.54	<dt	0.20	<dt	0.15	<dt	10.1	66.8
B-164	SV6.1	5.52	0.31	<dt	<dt	0.10	0.41	0.15	0.26	<dt	0.05	0.04	1.46	<dt	<dt	1.58	<dt	1.67	20.69	2.30	4.38	13.88	2.02	0.86	0.10	0.45	<dt	0.19	<dt	0.10	<dt	9.6	66.3
B-165	SV6.1	7.43	0.12	<dt	<dt	0.04	0.30	0.11	0.34	<dt	<dt	<dt	0.09	<dt	<dt	1.79	0.15	1.71	23.85	2.29	4.84	15.56	2.25	0.97	0.15	0.58	<dt	<dt	<dt	<dt	<dt	10.0	72.9
B-166	SV6.1	6.74	0.19	<dt	<dt	0.19	0.65	0.25	0.33	<dt	0.31	0.04	0.37	<dt	<dt	1.83	<dt	2.19	21.82	2.78	4.54	14.45	2.15	0.93	0.12	0.60	<dt	0.20	<dt	0.18	<dt	11.2	73.7
B-167	SV6.1	8.33	0.11	<dt	<dt	<dt	0.19	0.10	0.31	<dt	<dt	<dt	0.05	<dt	<dt	1.94	<dt	1.86	23.21	1.95	4.74	15.10	2.15	0.96	0.13	0.51	<dt	<dt	<dt	<dt	<dt	9.5	71.4
B-168	SV6.1	7.53	0.15	<dt	<dt	<dt	0.29	0.11	0.30	<dt	0.14	<dt	0.17	<dt	0.10	1.87	<dt	1.81	23.61	2.54	4.85	15.17	2.28	1.00	0.14	0.61	<dt	0.18	<dt	0.13	<dt	10.3	74.2
B-169	SV6.1	6.33	0.32	<dt	<dt	0.24	0.39	<dt	0.45	<dt	<dt	<dt	0.12	<dt	<dt	0.53	<dt	2.76	20.67	4.94	4.19	14.16	2.27	1.18	0.16	0.75	<dt	0.22	<dt	0.13	<dt	9.8	69.6
B-170	SV6.2	8.47	0.04	<dt	<dt	2.60	0.20	0.10	0.85	<dt	<dt	<dt	<dt	<dt	<dt	0.20	<dt	8.52	22.84	0.94	3.75	13.66	2.36	2.00	0.30	1.56	0.26	0.73	0.09	0.38	<dt	13.2	83.1
B-171	SV6.2	6.14	0.05	<dt	<dt	0.09	2.49	0.64	0.73	<dt	0.09	0.03	0.76	<dt	<dt	3.71	0.34	5.47	14.42	14.17	2.77	10.41	1.69	1.22	0.13	0.72	<dt	0.41	<dt	0.37	<dt	11.8	67.3
B-172	SV6.2	6.59	0.05	<dt	<dt	<dt	0.22	<dt	1.16	<dt	0.17	0.06	0.81	<dt	<dt	1.54	<dt	1.80	25.50	8.24	4.81	15.5	2.29	1.14	0.10	0.46	<dt	0.15	<dt	<dt	<dt	11.6	82.3
B-173	SV6.2	6.80	0.07	<dt	<dt	0.18	0.58	<dt	1.04	0.09	0.63	0.16	3.48	<dt	<dt	1.80	<dt	1.50	24.00	5.07	4.34	14.2	1.93	0.90	0.13	0.31	<dt	<dt	<dt	<dt	<dt	12.2	79.7
B-174	SV6.2	7.62	0.06	<dt	<dt	0.07	0.20	<dt	0.99	<dt	0.21	0.06	1.07	<dt	<dt	1.39	<dt	1.67	24.44	7.20	4.57	15.0	2.21	1.00	0.11	0.41	<dt	<dt	<dt	<dt	<dt	11.1	79.4
B-175	SV6.2	7.42	0.05	<dt	<dt	0.05	1.46	0.27	1.17	0.04	0.63	0.05	1.01	<dt	<dt	2.86	0.41	3.86	21.54	10.84	3.67	11.3	1.65	0.97	0.09	0.47	0.14	0.18	<dt	0.11	<dt	13.3	83.7
B-176	SV6.2	8.70	0.03	<dt	<dt	<dt	0.18	<dt	1.42	0.04	0.32	0.07	1.40	<dt	<dt	1.52	<dt	1.95	22.60	10.19	4.14	13.7	2.01	1.03	0.10	0.41	<dt	<dt	<dt	0.08	<dt	11.4	81.2
B-177	SV6.2	7.02	0.06	<dt	<dt	0.22	0.67	<dt	1.14	0.08	0.75	0.13	3.05	<dt	0.09	2.29	<dt	1.78	22.14	7.19	4.11	13.5	1.98	1.10	0.09	0.49	<dt	<dt	<dt	<dt	<dt	12.4	80.7
B-178	SV6.2	8.13	0.06	<dt	<dt	0.06	0.36	<dt	0.93	<dt	0.04	0.03	0.07	<dt	<dt	3.32	<dt	2.08	25.19	4.71	4.82	16.58	2.50	1.27	0.16	0.70	<dt	0.16	<dt	0.10	<dt	13.7	71.3
B-179	SV6.2	6.74	0.05	<dt	<dt	0.20	1.69	0.58	0.91	<dt	0.06	<dt	0.14	0.08	<dt	3.43	<dt	3.95	21.03	5.71	4.26	15.12	2.47	1.12	0.13	0.69	0.18	0.35	<dt	0.27	<dt	22.4	69.2
B-180	SV6.2	4.80	0.20	<dt	<dt	0.13	0.31	<dt	0.49	<dt	0.12	<dt	0.74	<dt	<dt	1.97	<dt	1.40	21.07	3.77	4.22	13.8	2.12	1.00	0.12	0.47	<dt	0.25	<dt	<dt	<dt	9.5	66.5
B-181	SV6.2	6.64	0.16	<dt	<dt	0.30	0.80	<dt	0.62	0.06	0.14	0.04	0.79	<dt	<dt	2.01	<dt	1.79	23.52	4.98	4.43	14.6	2.16	0.98	0.10	0.50	0.15	0.14	0.07	<dt	<dt	11.2	76.2
B-182	SV6.2	8.15	0.18	<dt	<dt	0.40	0.47	<dt	0.61	<dt	<dt	0.02	<dt	<dt	<dt	0.07	<dt	7.47	21.56	0.84	3.84	14.30	2.70	2.10	0.27	1.46	0.23	0.53	<dt	0.36	<dt	11.0	65.6
B-183	SV6.2	8.27	0.11	<dt	<dt	0.16	0.38	<dt	0.64	<dt	<dt	<dt	<dt	<dt	<dt	<dt	<dt	8.14	23.20	0.84	4.14	15.23	2.84	2.21	0.28	1.71	0.27	0.61	0.09	0.44	<dt	10.2	69.6
B-184	SV6.2	8.34	0.09	<dt	<dt	<dt	0.07	<dt	0.76	<dt	<dt	0.03	<dt	<dt	<dt	<dt	<dt	8.75	23.01	0.40	3.68	14.42	2.71	2.23	0.33	1.79	0.38	0.74	0.07	0.50	<dt	11.4	68.3
B-185	SV6.2	6.58	0.03	<dt	<dt	<dt	0.18	<dt	0.97	<dt	0.08	<dt	0.09	<dt	<dt	1.49	<dt	2.67	17.43	19.49	3.26	11.63	1.93	1.25	0.15	0.55	<dt	<dt	<dt	<dt	<dt	11.1	67.9
B-186	SV6.2	7.05	0.05	<dt	<dt	<dt	0.13	<dt	1.12	<dt	0.08	<dt	<dt	<dt	<dt	1.44	<dt	3.16	16.63	21.16	3.06	11.15	1.86	1.41	0.19	0.61	<dt	0.16	<dt	<dt	<dt	22.9	69.4
B-187	SV6.2	7.46	0.05	<dt	<dt	<dt	0.48	0.06	0.80	<dt	0.13	<dt	0.04	<dt	<dt	1.56	<dt	3.26	18.66	16.03	3.63	13.06	2.12	1.53	0.17	0.65	<dt	0.23	<dt	0.15	<dt	11.1	70.2
B-188	SV6.2	7.56	0.04	<dt	<dt	<dt	0.14	<dt	0.88	<dt	0.08	<dt	<dt	<dt	<dt	1.45	<dt	2.67	20.44	14.70	3.95	13.88	2.19	1.28	0.14	0.66	<dt	0.15	<dt	0.10	<dt	11.2	70.3
B-189	SV6.2	8.11	0.05	<dt	<dt	<dt	0.13	<dt	0.99	<dt	0.07	<dt	<dt	<dt	0.10	1.66	<dt	2.94	20.61	14.42	4.03	13.89	2.31	1.40	0.16	0.59	<dt	0.21	<dt	<dt	<dt	11.0	71.7
B-190	SV6.2	7.86	0.06	<dt	<dt	<dt	0.19	<dt	0.79	<dt	0.07	<dt	0.06	<dt	<dt	1.46	<dt	2.47	22.79	11.99	4.42	15.48	2.55	1.44	0.21	0.68	<dt	0.17	<dt	0.12	<dt	11.1	72.8

#	Sample	F	Cl	Na	Mg	Al	Si	P	Ca	K	Ti	Mn	Fe	Ba	Sr	Th	U	Y	La	Ce	Pr	Nd	Sm	Gd	Tb	Dy	Ho	Er	Tm	Yb	Lu	O	Total
		wt %	wt %	wt %	wt %	wt %	wt %	wt %	wt %	wt %	wt %	wt %	wt %	wt %	wt %	wt %	wt %	wt %	wt %	wt %	wt %	wt %	wt %	wt %	wt %	wt %	wt %	wt %	wt %	wt %	wt %	wt %	wt %
B-191	SV6.2	11.14	0.05	<dt	<dt	<dt	0.06	<dt	0.90	<dt	0.04	0.03	0.28	0.08	<dt	0.32	<dt	8.17	26.12	0.82	4.33	15.97	2.78	2.35	0.32	1.70	0.20	0.58	<dt	0.39	<dt	20.9	76.6
B-192	SV6.2	9.07	0.06	<dt	<dt	0.11	0.22	<dt	0.72	<dt	<dt	0.04	0.10	<dt	<dt	<dt	0.01	8.43	23.91	0.71	4.35	16.41	3.10	2.34	0.32	1.90	0.35	0.65	<dt	0.47	<dt	44.5	73.3
B-193	SV6.2	7.69	0.05	<dt	<dt	<dt	0.30	<dt	1.12	<dt	0.03	0.04	0.43	<dt	<dt	1.57	<dt	2.89	19.38	13.42	3.68	13.17	1.99	1.24	0.14	0.54	<dt	0.25	<dt	0.11	<dt	11.1	79.3
B-194	SV6.2	6.88	0.12	<dt	<dt	0.17	0.37	<dt	0.49	0.10	0.08	0.03	0.55	<dt	<dt	1.90	<dt	1.54	27.03	2.02	5.25	17.58	2.72	1.13	0.14	0.60	0.17	<dt	<dt	0.12	<dt	11.2	69.0
B-195	SV6.2	7.47	0.11	<dt	<dt	0.04	0.25	<dt	0.48	<dt	0.06	0.03	0.23	<dt	<dt	1.71	<dt	1.62	27.03	2.04	5.12	17.14	2.50	1.08	0.09	0.52	<dt	<dt	<dt	0.07	<dt	10.6	67.6
B-196	SV6.2	4.84	0.15	<dt	<dt	<dt	2.78	0.52	0.39	<dt	0.07	0.04	0.23	<dt	<dt	2.29	<dt	4.71	16.74	12.12	3.29	11.68	1.89	1.02	0.22	0.94	0.22	0.47	<dt	0.42	<dt	13.8	65.0
B-197	SV6.2	6.83	0.14	<dt	<dt	0.13	0.26	<dt	0.41	0.06	0.21	0.07	1.78	<dt	<dt	1.42	<dt	1.67	26.01	1.98	5.15	18.07	2.79	1.21	0.15	0.59	<dt	0.14	<dt	0.07	<dt	11.3	69.1
B-198	SV6.2	8.49	0.10	<dt	<dt	<dt	0.07	<dt	0.62	<dt	<dt	<dt	<dt	<dt	<dt	<dt	<dt	8.27	23.25	1.03	4.13	15.0	2.78	2.26	0.23	1.52	0.20	0.58	<dt	0.37	<dt	10.6	79.5
B-199	SV6.2	8.92	0.07	<dt	<dt	<dt	0.07	<dt	0.81	<dt	<dt	<dt	<dt	<dt	<dt	<dt	<dt	7.52	24.40	0.91	4.11	15.1	2.69	2.05	0.27	1.49	0.25	0.56	<dt	0.36	<dt	10.7	80.2
B-200	SV6.2	8.37	0.08	<dt	<dt	<dt	0.06	<dt	0.61	0.03	<dt	0.03	<dt	<dt	<dt	<dt	<dt	9.84	22.16	0.60	4.14	14.8	2.99	2.34	0.36	2.01	0.43	0.77	0.07	0.55	<dt	10.7	81.0
B-201	SV6.2	9.44	0.07	<dt	<dt	<dt	0.06	<dt	0.87	<dt	<dt	<dt	0.08	<dt	<dt	<dt	<dt	7.82	24.47	0.44	4.16	15.5	2.79	2.27	0.30	1.62	0.23	0.61	<dt	0.41	<dt	10.7	81.8
B-202	SV6.2	9.03	0.12	<dt	<dt	<dt	0.05	<dt	0.68	0.05	<dt	0.03	0.29	<dt	<dt	<dt	<dt	8.57	23.51	0.58	3.99	14.7	2.75	2.24	0.30	1.65	0.32	0.52	<dt	0.40	<dt	10.5	80.3
B-203	SV6.2	8.81	0.08	<dt	<dt	0.80	0.81	<dt	0.86	0.05	0.03	<dt	0.53	<dt	<dt	<dt	<dt	7.91	24.37	0.87	4.16	15.3	2.74	2.18	0.27	1.41	0.23	0.47	<dt	0.37	<dt	12.6	84.9
B-204	SV6.2	8.92	0.10	<dt	<dt	0.36	0.49	<dt	0.65	0.03	<dt	<dt	0.26	<dt	<dt	<dt	<dt	8.39	23.21	0.82	3.97	14.9	2.80	2.26	0.30	1.76	0.31	0.57	0.08	0.44	<dt	11.5	82.1
B-205	SV6.2	8.97	0.05	<dt	<dt	<dt	0.06	<dt	0.75	<dt	<dt	0.03	0.27	<dt	<dt	<dt	<dt	7.96	23.91	0.80	4.48	16.3	3.03	2.41	0.34	1.69	0.22	0.68	<dt	0.44	<dt	11.1	83.4
B-206	SV6.2	8.22	0.04	<dt	<dt	0.22	0.30	<dt	0.80	0.04	<dt	0.03	0.44	<dt	<dt	<dt	<dt	8.41	24.36	0.47	4.02	14.9	2.67	2.31	0.33	1.65	0.19	0.56	0.09	0.45	<dt	11.3	81.8
B-207	SV6.2	8.61	0.06	<dt	<dt	0.09	0.18	<dt	0.86	<dt	<dt	0.04	0.29	<dt	<dt	<dt	<dt	8.86	24.75	0.45	4.16	14.9	2.66	2.21	0.29	1.55	0.28	0.49	0.07	0.41	<dt	11.1	82.3
B-208	SV6.2	8.36	0.12	<dt	0.04	1.86	2.54	<dt	0.76	<dt	<dt	<dt	0.10	<dt	<dt	<dt	<dt	6.37	19.93	0.47	3.53	12.86	2.37	2.05	0.29	1.45	0.24	0.49	0.07	0.34	<dt	41.1	64.2
B-209	SV7	7.44	0.12	<dt	<dt	<dt	0.10	<dt	0.70	<dt	0.03	<dt	<dt	<dt	<dt	<dt	0.00	7.29	23.11	0.65	3.93	14.59	2.64	2.09	0.28	1.46	0.21	0.51	<dt	0.36	<dt	41.3	65.5
B-210	SV7	9.33	0.03	<dt	<dt	<dt	0.08	<dt	0.85	<dt	0.03	<dt	<dt	<dt	<dt	<dt	<dt	8.45	24.91	0.48	4.13	15.36	2.78	2.38	0.32	1.64	0.28	0.54	<dt	0.42	0.07	13.3	72.1
B-211	SV7	8.12	0.14	<dt	<dt	1.06	1.25	<dt	0.72	0.05	0.03	<dt	0.12	<dt	<dt	<dt	<dt	7.72	21.38	0.65	3.78	13.73	2.58	2.13	0.27	1.53	0.22	0.49	<dt	0.38	<dt	41.3	66.3
B-212	SV7	7.47	0.10	<dt	<dt	<dt	0.07	<dt	0.73	<dt	<dt	<dt	<dt	<dt	<dt	<dt	<dt	7.44	22.91	0.49	3.92	14.20	2.62	2.28	0.31	1.50	0.17	0.60	0.09	0.40	<dt	0.4	65.3
B-213	SV7	7.35	0.20	<dt	<dt	0.07	0.09	<dt	0.66	<dt	<dt	0.03	<dt	<dt	<dt	<dt	-0.01	7.46	22.17	0.47	3.80	13.87	2.48	2.20	0.24	1.49	0.17	0.52	<dt	0.35	<dt	10.1	63.6
B-214	SV7	8.56	0.05	<dt	<dt	0.10	0.18	<dt	0.85	<dt	<dt	<dt	<dt	<dt	<dt	<dt	<dt	8.50	24.93	0.47	4.12	15.35	2.81	2.41	0.31	1.77	0.22	0.62	0.08	0.42	<dt	10.9	71.8
B-215	SV7	9.06	0.04	<dt	<dt	<dt	0.06	<dt	0.94	<dt	0.03	<dt	<dt	0.07	<dt	<dt	<dt	8.35	25.00	0.39	4.02	15.18	2.79	2.42	0.31	1.70	0.26	0.58	<dt	0.35	<dt	11.2	71.5
B-216	SV7	7.61	0.05	<dt	<dt	0.06	0.23	<dt	0.75	<dt	0.09	<dt	0.10	<dt	<dt	2.03	<dt	2.16	24.37	8.05	4.65	15.75	2.37	1.24	0.14	0.59	<dt	<dt	<dt	0.07	<dt	22.4	70.3
B-217	SV7	7.04	0.05	<dt	0.31	0.67	2.24	<dt	0.74	0.29	0.07	0.05	0.89	<dt	<dt	1.91	0.02	1.85	22.63	6.07	4.16	13.87	2.09	1.04	0.11	0.51	<dt	0.18	<dt	0.07	<dt	11.2	66.9
B-218	SV8	5.89	0.21	<dt	<dt	<dt	0.65	1.02	0.52	<dt	<dt	<dt	0.26	<dt	<dt	3.02	0.21	4.95	19.29	3.00	3.42	11.04	1.67	0.96	0.14	0.74	0.17	0.35	<dt	0.35	<dt	11.2	70.0
B-219	SV8	5.65	0.29	<dt	<dt	<dt	0.12	0.08	0.46	<dt	<dt	<dt	0.14	<dt	<dt	2.70	<dt	2.23	20.81	2.49	3.61	11.97	1.76	0.93	0.12	0.59	<dt	<dt	<dt	0.08	<dt	8.6	62.6
B-220	SV8	5.26	0.34	<dt	<dt	<dt	0.15	0.08	0.44	<dt	<dt	<dt	0.47	<dt	0.09	2.57	<dt	2.14	20.29	2.28	3.54	11.69	1.73	0.86	0.13	0.51	0.12	0.13	<dt	0.06	<dt	8.5	61.3
B-221	SV8	6.62	0.13	<dt	0.36	0.74	2.43	0.28	0.59	0.22	<dt	<dt	1.02	<dt	0.13	2.97	0.10	3.09	21.72	2.84	3.70	12.35	1.77	1.04	0.10	0.68	0.19	0.25	<dt	0.35	<dt	13.5	77.5
B-222	SV8.1	7.12	0.06	<dt	0.11	0.62	1.46	0.11	1.45	<dt	0.06	0.04	2.80	<dt	0.12	1.11	<dt	3.81	13.65	17.20	2.43	8.47	1.28	0.89	0.16	0.79	0.21	0.34	<dt	0.15	<dt	14.2	82.5
B-223	SV8.1	7.00	0.07	<dt	0.10	0.64	1.42	0.10	1.43	<dt	0.07	0.04	2.80	<dt	0.10	1.08	0.16	3.83	13.57	17.05	2.42	8.33	1.25	0.87	0.14	0.78	0.14	0.29	<dt	0.16	<dt	14.1	81.9
B-224	SV8.1	5.67	0.06	<dt	0.08	0.62	1.42	0.10	1.40	<dt	0.08	0.10	2.83	<dt	0.13	1.02	0.13	3.86	13.05	16.82	2.36	8.24	1.31	0.84	0.15	0.71	0.14	0.29	<dt	0.18	<dt	13.8	79.1
B-225	SV8.1	7.63	0.03	<dt	0.05	0.31	1.12	0.71	1.36	<dt	0.09	<dt	3.72	<dt	<dt	1.34	<dt	5.41	13.36	14.19	2.53	9.02	1.50	1.04	0.17	0.71	0.17	0.44	<dt	0.25	<dt	13.1	78.5
B-226	SV8.2	6.89	0.04	<dt	<dt	<dt	0.46	<dt	2.24	<dt	0.15	<dt	0.20	<dt	<dt	1.45	<dt	2.25	20.83	19.73	2.86	9.73	1.30	0.66	0.08	0.33	<dt	0.16	<dt	0.11	<dt	11.9	81.3
B-227	SV8.2	7.21	0.06	<dt	<dt	0.05	0.83	0.09	2.33	<dt	0.30	0.04	0.28	0.14	<dt	1.88	0.15	3.17	19.71	18.05	2.88	9.90	1.45	0.73	0.13	0.57	<dt	0.20	<dt	0.10	<dt	12.7	83.5
B-228	SV8.2	7.99	0.07	<dt	<dt	0.04	1.25	0.75	1.65	<dt	0.20	<dt	0.17	0.09	<dt	2.01	0.20	6.48	16.28	15.66	3.05	10.41	1.73	1.14	0.21	0.90	0.14	0.44	0.09	0.34	<dt	14.0	86.2
B-229	SV8.2	7.33	0.06	<dt	<dt	<dt	0.46	0.11	1.90	<dt	0.13	<dt	0.41	<dt	<dt	1.61	<dt	3.39	18.93	15.96	3.35	12.01	1.90	1.05	0.12	0.58	0.14	0.27	<dt	0.13	<dt	12.0	82.1
B-230	SV8.2	7.04	0.04	<dt	<dt	<dt	0.69	0.15	1.77	<dt	0.16	<dt	0.33	<dt	<dt	1.24	<dt	4.28	17.35	18.58	3.07	11.12	1.73	1.17	0.18	0.78	0.16	0.25	<dt	0.12	<dt	12.5	83.0
B-231	SV8.2	7.21	0.05	<dt	<dt	0.04	1.52	0.49	1.84	<dt	0.16	<dt	0.36	<dt	<dt	2.87	0.23	4.41	15.83	18.56	2.92	10.30	1.60	0.93	0.16	0.64	<dt	0.30	<dt	0.26	<dt	13.6	84.6
B-232	SV8.2	7.98	0.06	<dt	<dt	0.08	2.25	0.72	2.00	<dt	0.22	0.07	1.08	<dt	<dt	1.63	0.41	5.48	16.47	13.46	3.49	11.77	1.86	0.78	0.18	0.79	0.21	0.49	<dt	0.42	<dt	14.9	86.8
B-233	SV8.2	7.74	0.06	<dt	0.10	0.94	2.21	0.08	2.30	0.11	0.14	0.06	1.05	0.12	<dt	2.23	<dt	3.35	20.54	7.78	4.25	14.88	2.35	1.28	0.14	0.60	<dt	0.15	<dt	0.11	<dt	14.8	87.3
B-234	SV8.2	8.45	0.06	<dt	<dt	0.10	2.41	0.41	2.08	<dt	0.24	0.05	1.22	0.12	<dt	1.80	0.37	4.44	17.19	13.44	3.60	12.23	1.99	0.94	0.13	0.73	<dt	0.29	<dt	0.24	<dt	14.7	87.2
B-235	SV8.2	7.46	0.06	<dt	<dt	<dt	0.40	0.12	1.91	<dt	0.13	<dt	0.09	0.17	<dt	1.95	0.17	4.91	19.79	10.59	3.87	13.82	2.49	1.64	0.25	0.86	<dt	0.35	<dt	0.12	<dt	12.1	83.5

#	Sample	F	Cl	Na	Mg	Al	Si	P	Ca	K	Ti	Mn	Fe	Ba	Sr	Th	U	Y	La	Ce	Pr	Nd	Sm	Gd	Tb	Dy	Ho	Er	Tm	Yb	Lu	O	Total
		wt %	wt %	wt %	wt %	wt %	wt %	wt %	wt %	wt %	wt %	wt %	wt %	wt %	wt %	wt %	wt %	wt %	wt %	wt %	wt %	wt %	wt %	wt %	wt %	wt %	wt %	wt %	wt %	wt %	wt %	wt %	wt %
B-236	SV8.2	7.75	0.06	<dt	<dt	<dt	0.34	0.14	1.91	<dt	0.10	<dt	0.09	0.12	0.11	2.06	<dt	5.03	19.86	11.16	3.94	13.97	2.48	1.71	0.19	0.94	<dt	0.30	<dt	0.13	<dt	12.2	84.7
B-237	SV8.2	8.24	0.06	<dt	<dt	<dt	0.47	0.19	1.78	<dt	0.12	<dt	0.06	0.12	<dt	2.03	0.18	4.93	19.74	11.69	3.93	13.72	2.49	1.49	0.23	0.93	0.19	0.34	<dt	0.14	<dt	12.4	85.7
B-238	SV8.2	7.59	0.07	<dt	<dt	<dt	0.49	<dt	1.87	<dt	0.15	<dt	0.07	0.14	<dt	1.97	<dt	4.93	19.56	10.73	3.84	13.71	2.45	1.61	0.22	0.95	<dt	0.24	<dt	0.13	<dt	12.2	83.1
B-239	SV8.2	7.72	0.06	<dt	<dt	<dt	0.44	<dt	1.94	<dt	0.14	<dt	0.08	0.11	<dt	1.98	<dt	4.86	19.69	11.03	3.87	13.86	2.40	1.54	0.21	0.87	0.16	0.29	<dt	0.15	<dt	12.3	83.8
B-240	SV8.2	7.39	0.09	<dt	<dt	<dt	0.18	<dt	2.06	<dt	0.07	0.04	0.12	0.17	<dt	1.40	<dt	2.88	24.48	3.82	5.13	17.59	2.64	1.22	0.09	0.47	0.14	<dt	<dt	0.09	<dt	11.5	81.6
B-241	SV8.2	7.40	0.09	<dt	<dt	<dt	0.19	<dt	1.75	<dt	0.06	0.04	0.09	<dt	0.11	0.70	<dt	2.46	25.84	3.67	5.50	18.54	2.78	1.20	0.14	0.46	<dt	0.16	<dt	0.10	<dt	11.7	83.0
B-242	SV8.2	7.72	0.08	<dt	0.09	0.60	1.33	0.08	1.85	0.11	0.07	0.06	0.41	0.14	<dt	1.58	<dt	2.82	25.25	3.51	5.27	17.71	2.68	1.37	0.10	0.54	<dt	0.19	<dt	0.07	<dt	13.6	87.2
B-243	SV8.2	7.40	0.09	<dt	<dt	<dt	0.19	<dt	1.75	<dt	0.06	0.04	0.09	0.11	<dt	0.70	<dt	2.46	25.84	3.67	5.50	18.54	2.78	1.20	0.14	0.46	<dt	0.16	<dt	0.10	<dt	11.68	71.3
B-244	SV8.2	7.72	0.08	<dt	0.09	0.60	1.33	0.08	1.85	0.11	0.07	0.06	0.41	<dt	0.14	1.58	<dt	2.82	25.25	3.51	5.27	17.71	2.68	1.37	0.10	0.54	<dt	0.19	<dt	0.07	<dt	13.61	73.6
B-245	SV8.2	7.39	0.09	<dt	<dt	<dt	0.18	<dt	2.06	<dt	0.07	0.04	0.12	<dt	0.17	1.40	<dt	2.88	24.48	3.82	5.13	17.59	2.64	1.22	0.09	0.47	0.14	<dt	<dt	0.09	<dt	11.5	70.1
B-246	SV8.2	8.54	0.07	<dt	<dt	<dt	0.09	0.19	1.47	<dt	<dt	0.03	0.04	<dt	<dt	0.69	<dt	10.62	23.94	1.08	3.92	15.03	2.74	2.30	0.39	2.10	0.32	0.83	<dt	0.49	<dt	12.7	87.6
B-247	SV8.2	7.07	0.07	<dt	<dt	<dt	0.08	0.24	1.47	<dt	0.04	<dt	<dt	<dt	<dt	0.52	<dt	11.23	23.96	0.77	3.78	14.39	2.65	2.09	0.36	1.97	0.39	0.84	<dt	0.43	<dt	12.7	85.1
B-248	SV8.2	9.32	0.07	<dt	<dt	0.04	0.16	0.30	1.27	0.03	<dt	<dt	<dt	<dt	<dt	1.92	0.25	7.67	23.67	5.02	3.74	14.04	2.38	1.89	0.28	1.57	0.20	0.59	<dt	0.29	<dt	12.4	87.0
B-249	SV8.2	9.32	0.07	<dt	<dt	0.04	0.16	0.30	1.27	0.03	<dt	<dt	<dt	<dt	<dt	1.92	0.25	7.67	23.67	5.02	3.74	14.04	2.38	1.89	0.28	1.57	0.20	0.59	<dt	0.29	<dt	12.37	74.7
B-250	SD 20	7.60	0.07	<dt	0.05	0.98	2.05	<dt	2.22	0.07	<dt	<dt	0.95	0.06	0.11	2.18	<dt	4.78	12.63	20.5	2.31	7.77	1.39	1.65	0.22	1.08	0.18	<dt	<dt	0.16	<dt	13.7	82.7
B-251	SD 20	8.05	<dt	<dt	<dt	<dt	0.11	<dt	2.37	<dt	0.06	<dt	0.51	0.15	0.11	1.95	<dt	4.65	13.39	24.0	2.53	8.27	1.31	1.34	0.18	0.79	0.17	0.33	<dt	0.13	<dt	11.4	81.7
B-252	SD 20	7.57	0.06	<dt	<dt	0.09	0.28	0.52	2.51	<dt	<dt	<dt	0.35	0.18	0.18	4.42	0.13	5.64	13.02	19.65	2.36	8.15	1.49	1.87	0.27	1.09	0.18	0.34	<dt	0.16	<dt	12.2	82.8

Table C2.5 EMPA Fe-oxide and Ti-oxide minerals

		F	Cl	Mg	Na	Al	Si	P	Ca	K	Ti	Fe	Nb	Mn	Ta	Th	U	Y	La	Ce	Pr	Nd	Sm	Gd	Tb	Dy	Ho	Er	Tm	Yb	Lu	O	Total
		wt %	wt %	Mg	Na	wt %	wt %	wt %	wt %	wt %	wt %	wt %	wt %	wt %	wt %	wt %	wt %	wt %	wt %	wt %	wt %	wt %	wt %	wt %	wt %	wt %	wt %	wt %	wt %	wt %	wt %	wt %	wt %
O-1	SD4	<dt	<dt	<dt	<dt	0.52	1.89	<dt	0.07	0.15	0.20	61.97	0.22	0.33	<dt	<dt	<dt	0.13	<dt	<dt	<dt	<dt	<dt	<dt	<dt	<dt	<dt	<dt	0.07	<dt	<dt	20.8	86.3
O-2	SD4	<dt	<dt	0.07	<dt	0.79	2.42	<dt	0.06	0.27	0.28	60.60	0.31	0.31	<dt	<dt	<dt	0.13	<dt	<dt	<dt	<dt	<dt	<dt	<dt	<dt	<dt	<dt	<dt	<dt	<dt	21.4	86.6
O-3	SD6	<dt	<dt	<dt	<dt	0.16	0.66	<dt	0.04	0.07	0.40	65.48	0.64	0.15	<dt	<dt	<dt	0.05	<dt	<dt	<dt	<dt	<dt	0.08	<dt	<dt	<dt	<dt	<dt	<dt	<dt	20.3	88.0
O-4	SD6	<dt	<dt	<dt	<dt	0.21	0.81	<dt	0.04	0.07	0.56	64.59	0.88	0.16	<dt	<dt	<dt	<dt	0.04	<dt	<dt	<dt	<dt	0.06	<dt	<dt	<dt	<dt	<dt	<dt	<dt	20.5	87.9
O-5	SD6	<dt	<dt	0.06	<dt	1.03	2.83	<dt	0.14	0.43	0.08	60.78	0.30	0.11	<dt	<dt	0.00	0.05	<dt	<dt	<dt	<dt	<dt	<dt	<dt	<dt	<dt	<dt	<dt	<dt	<dt	22.0	87.8
O-6	SD6	<dt	<dt	0.04	<dt	0.78	2.35	0.07	0.12	0.23	5.17	52.88	0.69	0.20	<dt	<dt	<dt	0.43	0.05	0.04	<dt	<dt	<dt	0.07	<dt	<dt	<dt	<dt	<dt	<dt	<dt	22.8	86.3
O-7	SD6	<dt	<dt	0.03	<dt	0.80	2.19	<dt	0.15	0.22	0.16	61.34	0.63	0.13	<dt	<dt	0.18	0.08	<dt	<dt	<dt	<dt	<dt	0.10	<dt	<dt	<dt	<dt	0.08	<dt	<dt	21.4	87.5
O-8	SD6	<dt	<dt	<dt	<dt	0.73	2.03	<dt	0.12	0.20	0.12	61.46	0.51	0.13	<dt	<dt	0.13	0.07	<dt	<dt	<dt	<dt	<dt	<dt	<dt	<dt	<dt	<dt	0.07	<dt	<dt	21.0	86.6
O-9	SD27	<dt	<dt	<dt	<dt	0.71	1.67	<dt	0.15	0.04	0.86	60.52	0.39	0.27	<dt	<dt	<dt	<dt	0.17	0.14	0.08	<dt	<dt	0.11	<dt	<dt	<dt	<dt	<dt	<dt	<dt	20.8	86.0
O-10	SD27	<dt	<dt	0.45	<dt	0.93	1.60	0.05	0.12	0.12	0.15	50.17	1.85	0.12	<dt	0.15	<dt	0.07	0.08	0.21	<dt	<dt	<dt	<dt	<dt	<dt	<dt	<dt	<dt	<dt	<dt	18.5	74.8
O-11	SD27	<dt	<dt	<dt	<dt	0.46	2.60	<dt	0.15	0.10	<dt	61.28	0.09	0.03	<dt	<dt	<dt	<dt	<dt	<dt	<dt	<dt	<dt	0.14	<dt	<dt	<dt	<dt	<dt	<dt	<dt	21.0	85.9
O-12	SD27	<dt	<dt	0.50	<dt	0.96	1.69	0.03	0.11	0.12	0.14	50.34	1.64	0.12	<dt	<dt	<dt	0.06	0.06	0.15	<dt	<dt	<dt	0.07	<dt	<dt	<dt	<dt	<dt	<dt	<dt	18.6	74.7
O-13	SD27	<dt	<dt	0.07	<dt	0.83	2.63	<dt	0.20	0.06	0.35	60.14	0.88	0.03	<dt	<dt	<dt	<dt	0.06	<dt	<dt	<dt	<dt	0.16	<dt	<dt	<dt	<dt	<dt	<dt	<dt	21.8	87.2
O-14	SD27	<dt	<dt	0.14	<dt	0.86	2.89	<dt	0.23	0.10	0.33	59.34	0.73	0.03	<dt	<dt	<dt	<dt	0.06	0.05	<dt	<dt	<dt	<dt	<dt	<dt	<dt	<dt	<dt	<dt	<dt	21.8	86.6
O-15	SD8	<dt	<dt	<dt	0.42	<dt	<dt	<dt	<dt	0.06	<dt	48.50	<dt	<dt	<dt	<dt	<dt	<dt	<dt	<dt	<dt	<dt	<dt	<dt	n.a.	n.a.	n.a.	n.a.	n.a.	n.a.	n.a.	14.1	63.0
O-16	SD8	0.17	<dt	0.11	<dt	1.70	5.41	0.08	0.37	0.24	1.02	43.50	5.97	<dt	<dt	<dt	<dt	0.46	0.12	0.29	<dt	0.06	<dt	<dt	<dt	<dt	<dt	<dt	<dt	0.16	<dt	26.1	92.0
O-17	SD8	<dt	<dt	<dt	0.37	<dt	0.05	<dt	<dt	0.08	0.04	48.66	<dt	<dt	<dt	<dt	<dt	<dt	<dt	<dt	<dt	<dt	<dt	<dt	n.a.	n.a.	n.a.	n.a.	n.a.	n.a.	n.a.	14.2	63.4
O-18	SD8	<dt	<dt	<dt	0.38	<dt	<dt	<dt	<dt	0.08	0.07	48.55	<dt	<dt	<dt	<dt	<dt	<dt	<dt	<dt	<dt	<dt	<dt	<dt	n.a.	n.a.	n.a.	n.a.	n.a.	n.a.	n.a.	14.1	63.2
O-19	SD8	<dt	<dt	0.04	0.33	0.11	0.18	<dt	<dt	0.08	0.06	48.57	<dt	<dt	<dt	<dt	<dt	<dt	<dt	<dt	<dt	<dt	<dt	<dt	n.a.	n.a.	n.a.	n.a.	n.a.	n.a.	n.a.	14.4	63.8
O-20	SD8	<dt	<dt	<dt	<dt	0.98	2.37	0.03	0.15	0.06	0.60	59.10	0.34	0.62	<dt	0.31	<dt	0.06	0.05	0.05	<dt	<dt	<dt	<dt	<dt	<dt	<dt	<dt	0.07	<dt	<dt	21.5	86.2
O-21	SD8	<dt	<dt	0.09	<dt	1.02	2.83	0.04	0.19	0.07	0.67	58.44	0.70	0.51	<dt	0.19	<dt	0.11	0.05	0.09	<dt	<dt	<dt	<dt	<dt	<dt	<dt	<dt	0.06	<dt	<dt	22.1	87.3
O-22	SD8	<dt	<dt	<dt	<dt	1.02	2.58	0.09	0.17	0.08	0.47	58.93	0.41	0.65	<dt	0.24	<dt	0.18	<dt	0.06	<dt	<dt	<dt	0.14	<dt	<dt	<dt	<dt	<dt	<dt	<dt	21.7	86.9
O-23	SD9	<dt	<dt	0.08	<dt	1.28	2.84	<dt	0.20	0.05	0.30	57.94	0.29	0.47	<dt	0.11	<dt	<dt	0.28	0.18	<dt	0.16	<dt	0.09	<dt	<dt	<dt	<dt	<dt	<dt	<dt	21.7	86.0
O-24	SD9	<dt	<dt	0.06	<dt	1.30	2.85	<dt	0.19	0.05	0.28	58.14	0.35	0.52	<dt	<dt	<dt	<dt	0.16	0.09	<dt	0.06	<dt	0.13	<dt	<dt	<dt	<dt	<dt	<dt	<dt	21.7	85.9
O-25	SD9	<dt	<dt	<dt	<dt	1.01	2.51	<dt	0.15	0.09	0.44	60.08	0.27	0.57	<dt	<dt	<dt	<dt	0.05	0.04	<dt	<dt	<dt	0.13	<dt	<dt	<dt	<dt	<dt	<dt	<dt	21.7	87.0

#	Sample	F	Cl	Na	Mg	Al	Si	P	Ca	K	Ti	Mn	Fe	Ba	Sr	Th	U	Y	La	Ce	Pr	Nd	Sm	Gd	Tb	Dy	Ho	Er	Tm	Yb	Lu	O	Total
		wt %	wt %	wt %	wt %	wt %	wt %	wt %	wt %	wt %	wt %	wt %	wt %	wt %	wt %	wt %	wt %	wt %	wt %	wt %	wt %	wt %	wt %	wt %	wt %	wt %	wt %	wt %	wt %	wt %	wt %	wt %	wt %
B-236	SV8.2	7.75	0.06	<dt	<dt	<dt	0.34	0.14	1.91	<dt	0.10	<dt	0.09	0.12	0.11	2.06	<dt	5.03	19.86	11.16	3.94	13.97	2.48	1.71	0.19	0.94	<dt	0.30	<dt	0.13	<dt	12.2	84.7
B-237	SV8.2	8.24	0.06	<dt	<dt	<dt	0.47	0.19	1.78	<dt	0.12	<dt	0.06	0.12	<dt	2.03	0.18	4.93	19.74	11.69	3.93	13.72	2.49	1.49	0.23	0.93	0.19	0.34	<dt	0.14	<dt	12.4	85.7
B-238	SV8.2	7.59	0.07	<dt	<dt	<dt	0.49	<dt	1.87	<dt	0.15	<dt	0.07	0.14	<dt	1.97	<dt	4.93	19.56	10.73	3.84	13.71	2.45	1.61	0.22	0.95	<dt	0.24	<dt	0.13	<dt	12.2	83.1
B-239	SV8.2	7.72	0.06	<dt	<dt	<dt	0.44	<dt	1.94	<dt	0.14	<dt	0.08	0.11	<dt	1.98	<dt	4.86	19.69	11.03	3.87	13.86	2.40	1.54	0.21	0.87	0.16	0.29	<dt	0.15	<dt	12.3	83.8
B-240	SV8.2	7.39	0.09	<dt	<dt	<dt	0.18	<dt	2.06	<dt	0.07	0.04	0.12	0.17	<dt	1.40	<dt	2.88	24.48	3.82	5.13	17.59	2.64	1.22	0.09	0.47	0.14	<dt	<dt	0.09	<dt	11.5	81.6
B-241	SV8.2	7.40	0.09	<dt	<dt	<dt	0.19	<dt	1.75	<dt	0.06	0.04	0.09	<dt	0.11	0.70	<dt	2.46	25.84	3.67	5.50	18.54	2.78	1.20	0.14	0.46	<dt	0.16	<dt	0.10	<dt	11.7	83.0
B-242	SV8.2	7.72	0.08	<dt	0.09	0.60	1.33	0.08	1.85	0.11	0.07	0.06	0.41	0.14	<dt	1.58	<dt	2.82	25.25	3.51	5.27	17.71	2.68	1.37	0.10	0.54	<dt	0.19	<dt	0.07	<dt	13.6	87.2
B-243	SV8.2	7.40	0.09	<dt	<dt	<dt	0.19	<dt	1.75	<dt	0.06	0.04	0.09	0.11	<dt	0.70	<dt	2.46	25.84	3.67	5.50	18.54	2.78	1.20	0.14	0.46	<dt	0.16	<dt	0.10	<dt	11.68	71.3
B-244	SV8.2	7.72	0.08	<dt	0.09	0.60	1.33	0.08	1.85	0.11	0.07	0.06	0.41	<dt	0.14	1.58	<dt	2.82	25.25	3.51	5.27	17.71	2.68	1.37	0.10	0.54	<dt	0.19	<dt	0.07	<dt	13.61	73.6
B-245	SV8.2	7.39	0.09	<dt	<dt	<dt	0.18	<dt	2.06	<dt	0.07	0.04	0.12	<dt	0.17	1.40	<dt	2.88	24.48	3.82	5.13	17.59	2.64	1.22	0.09	0.47	0.14	<dt	<dt	0.09	<dt	11.5	70.1
B-246	SV8.2	8.54	0.07	<dt	<dt	<dt	0.09	0.19	1.47	<dt	<dt	0.03	0.04	<dt	<dt	0.69	<dt	10.62	23.94	1.08	3.92	15.03	2.74	2.30	0.39	2.10	0.32	0.83	<dt	0.49	<dt	12.7	87.6
B-247	SV8.2	7.07	0.07	<dt	<dt	<dt	0.08	0.24	1.47	<dt	0.04	<dt	<dt	<dt	<dt	0.52	<dt	11.23	23.96	0.77	3.78	14.39	2.65	2.09	0.36	1.97	0.39	0.84	<dt	0.43	<dt	12.7	85.1
B-248	SV8.2	9.32	0.07	<dt	<dt	0.04	0.16	0.30	1.27	0.03	<dt	<dt	<dt	<dt	<dt	1.92	0.25	7.67	23.67	5.02	3.74	14.04	2.38	1.89	0.28	1.57	0.20	0.59	<dt	0.29	<dt	12.4	87.0
B-249	SV8.2	9.32	0.07	<dt	<dt	0.04	0.16	0.30	1.27	0.03	<dt	<dt	<dt	<dt	<dt	1.92	0.25	7.67	23.67	5.02	3.74	14.04	2.38	1.89	0.28	1.57	0.20	0.59	<dt	0.29	<dt	12.37	74.7
B-250	SD 20	7.60	0.07	<dt	0.05	0.98	2.05	<dt	2.22	0.07	<dt	<dt	0.95	0.06	0.11	2.18	<dt	4.78	12.63	20.5	2.31	7.77	1.39	1.65	0.22	1.08	0.18	<dt	<dt	0.16	<dt	13.7	82.7
B-251	SD 20	8.05	<dt	<dt	<dt	<dt	0.11	<dt	2.37	<dt	0.06	<dt	0.51	0.15	0.11	1.95	<dt	4.65	13.39	24.0	2.53	8.27	1.31	1.34	0.18	0.79	0.17	0.33	<dt	0.13	<dt	11.4	81.7
B-252	SD 20	7.57	0.06	<dt	<dt	0.09	0.28	0.52	2.51	<dt	<dt	<dt	0.35	0.18	0.18	4.42	0.13	5.64	13.02	19.65	2.36	8.15	1.49	1.87	0.27	1.09	0.18	0.34	<dt	0.16	<dt	12.2	82.8

Table C2.5 EMPA Fe-oxide and Ti-oxide minerals

		F	Cl	Mg	Na	Al	Si	P	Ca	K	Ti	Fe	Nb	Mn	Ta	Th	U	Y	La	Ce	Pr	Nd	Sm	Gd	Tb	Dy	Ho	Er	Tm	Yb	Lu	O	Total
		wt %	wt %	Mg	Na	wt %	wt %	wt %	wt %	wt %	wt %	wt %	wt %	wt %	wt %	wt %	wt %	wt %	wt %	wt %	wt %	wt %	wt %	wt %	wt %	wt %	wt %	wt %	wt %	wt %	wt %	wt %	wt %
O-1	SD4	<dt	<dt	<dt	<dt	0.52	1.89	<dt	0.07	0.15	0.20	61.97	0.22	0.33	<dt	<dt	<dt	0.13	<dt	<dt	<dt	<dt	<dt	<dt	<dt	<dt	<dt	<dt	0.07	<dt	<dt	20.8	86.3
O-2	SD4	<dt	<dt	0.07	<dt	0.79	2.42	<dt	0.06	0.27	0.28	60.60	0.31	0.31	<dt	<dt	<dt	0.13	<dt	<dt	<dt	<dt	<dt	<dt	<dt	<dt	<dt	<dt	<dt	<dt	<dt	21.4	86.6
O-3	SD6	<dt	<dt	<dt	<dt	0.16	0.66	<dt	0.04	0.07	0.40	65.48	0.64	0.15	<dt	<dt	<dt	0.05	<dt	<dt	<dt	<dt	<dt	0.08	<dt	<dt	<dt	<dt	<dt	<dt	<dt	20.3	88.0
O-4	SD6	<dt	<dt	<dt	<dt	0.21	0.81	<dt	0.04	0.07	0.56	64.59	0.88	0.16	<dt	<dt	<dt	<dt	0.04	<dt	<dt	<dt	<dt	0.06	<dt	<dt	<dt	<dt	<dt	<dt	<dt	20.5	87.9
O-5	SD6	<dt	<dt	0.06	<dt	1.03	2.83	<dt	0.14	0.43	0.08	60.78	0.30	0.11	<dt	<dt	0.00	0.05	<dt	<dt	<dt	<dt	<dt	<dt	<dt	<dt	<dt	<dt	<dt	<dt	<dt	22.0	87.8
O-6	SD6	<dt	<dt	0.04	<dt	0.78	2.35	0.07	0.12	0.23	5.17	52.88	0.69	0.20	<dt	<dt	<dt	0.43	0.05	0.04	<dt	<dt	<dt	0.07	<dt	<dt	<dt	<dt	<dt	<dt	<dt	22.8	86.3
O-7	SD6	<dt	<dt	0.03	<dt	0.80	2.19	<dt	0.15	0.22	0.16	61.34	0.63	0.13	<dt	<dt	0.18	0.08	<dt	<dt	<dt	<dt	<dt	0.10	<dt	<dt	<dt	<dt	0.08	<dt	<dt	21.4	87.5
O-8	SD6	<dt	<dt	<dt	<dt	0.73	2.03	<dt	0.12	0.20	0.12	61.46	0.51	0.13	<dt	<dt	0.13	0.07	<dt	<dt	<dt	<dt	<dt	<dt	<dt	<dt	<dt	<dt	0.07	<dt	<dt	21.0	86.6
O-9	SD27	<dt	<dt	<dt	<dt	0.71	1.67	<dt	0.15	0.04	0.86	60.52	0.39	0.27	<dt	<dt	<dt	<dt	0.17	0.14	0.08	<dt	<dt	0.11	<dt	<dt	<dt	<dt	<dt	<dt	<dt	20.8	86.0
O-10	SD27	<dt	<dt	0.45	<dt	0.93	1.60	0.05	0.12	0.12	0.15	50.17	1.85	0.12	<dt	0.15	<dt	0.07	0.08	0.21	<dt	<dt	<dt	<dt	<dt	<dt	<dt	<dt	<dt	<dt	<dt	18.5	74.8
O-11	SD27	<dt	<dt	<dt	<dt	0.46	2.60	<dt	0.15	0.10	<dt	61.28	0.09	0.03	<dt	<dt	<dt	<dt	<dt	<dt	<dt	<dt	<dt	0.14	<dt	<dt	<dt	<dt	<dt	<dt	<dt	21.0	85.9
O-12	SD27	<dt	<dt	0.50	<dt	0.96	1.69	0.03	0.11	0.12	0.14	50.34	1.64	0.12	<dt	<dt	<dt	0.06	0.06	0.15	<dt	<dt	<dt	0.07	<dt	<dt	<dt	<dt	<dt	<dt	<dt	18.6	74.7
O-13	SD27	<dt	<dt	0.07	<dt	0.83	2.63	<dt	0.20	0.06	0.35	60.14	0.88	0.03	<dt	<dt	<dt	<dt	0.06	<dt	<dt	<dt	<dt	0.16	<dt	<dt	<dt	<dt	<dt	<dt	<dt	21.8	87.2
O-14	SD27	<dt	<dt	0.14	<dt	0.86	2.89	<dt	0.23	0.10	0.33	59.34	0.73	0.03	<dt	<dt	<dt	<dt	0.06	0.05	<dt	<dt	<dt	<dt	<dt	<dt	<dt	<dt	<dt	<dt	<dt	21.8	86.6
O-15	SD8	<dt	<dt	<dt	0.42	<dt	<dt	<dt	<dt	0.06	<dt	48.50	<dt	<dt	<dt	<dt	<dt	<dt	<dt	<dt	<dt	<dt	<dt	<dt	n.a.	n.a.	n.a.	n.a.	n.a.	n.a.	n.a.	14.1	63.0
O-16	SD8	0.17	<dt	0.11	<dt	1.70	5.41	0.08	0.37	0.24	1.02	43.50	5.97	<dt	<dt	<dt	<dt	0.46	0.12	0.29	<dt	0.06	<dt	<dt	<dt	<dt	<dt	<dt	<dt	0.16	<dt	26.1	92.0
O-17	SD8	<dt	<dt	<dt	0.37	<dt	0.05	<dt	<dt	0.08	0.04	48.66	<dt	<dt	<dt	<dt	<dt	<dt	<dt	<dt	<dt	<dt	<dt	<dt	n.a.	n.a.	n.a.	n.a.	n.a.	n.a.	n.a.	14.2	63.4
O-18	SD8	<dt	<dt	<dt	0.38	<dt	<dt	<dt	<dt	0.08	0.07	48.55	<dt	<dt	<dt	<dt	<dt	<dt	<dt	<dt	<dt	<dt	<dt	<dt	n.a.	n.a.	n.a.	n.a.	n.a.	n.a.	n.a.	14.1	63.2
O-19	SD8	<dt	<dt	0.04	0.33	0.11	0.18	<dt	<dt	0.08	0.06	48.57	<dt	<dt	<dt	<dt	<dt	<dt	<dt	<dt	<dt	<dt	<dt	<dt	n.a.	n.a.	n.a.	n.a.	n.a.	n.a.	n.a.	14.4	63.8
O-20	SD8	<dt	<dt	<dt	<dt	0.98	2.37	0.03	0.15	0.06	0.60	59.10	0.34	0.62	<dt	0.31	<dt	0.06	0.05	0.05	<dt	<dt	<dt	<dt	<dt	<dt	<dt	<dt	0.07	<dt	<dt	21.5	86.2
O-21	SD8	<dt	<dt	0.09	<dt	1.02	2.83	0.04	0.19	0.07	0.67	58.44	0.70	0.51	<dt	0.19	<dt	0.11	0.05	0.09	<dt	<dt	<dt	<dt	<dt	<dt	<dt	<dt	0.06	<dt	<dt	22.1	87.3
O-22	SD8	<dt	<dt	<dt	<dt	1.02	2.58	0.09	0.17	0.08	0.47	58.93	0.41	0.65	<dt	0.24	<dt	0.18	<dt	0.06	<dt	<dt	<dt	0.14	<dt	<dt	<dt	<dt	<dt	<dt	<dt	21.7	86.9
O-23	SD9	<dt	<dt	0.08	<dt	1.28	2.84	<dt	0.20	0.05	0.30	57.94	0.29	0.47	<dt	0.11	<dt	<dt	0.28	0.18	<dt	0.16	<dt	0.09	<dt	<dt	<dt	<dt	<dt	<dt	<dt	21.7	86.0
O-24	SD9	<dt	<dt	0.06	<dt	1.30	2.85	<dt	0.19	0.05	0.28	58.14	0.35	0.52	<dt	<dt	<dt	<dt	0.16	0.09	<dt	0.06	<dt	0.13	<dt	<dt	<dt	<dt	<dt	<dt	<dt	21.7	85.9
O-25	SD9	<dt	<dt	<dt	<dt	1.01	2.51	<dt	0.15	0.09	0.44	60.08	0.27	0.57	<dt	<dt	<dt	<dt	0.05	0.04	<dt	<dt	<dt	0.13	<dt	<dt	<dt	<dt	<dt	<dt	<dt	21.7	87.0

		F	Cl	Mg	Na	Al	Si	P	Ca	K	Ti	Fe	Nb	Mn	Ta	Th	U	Y	La	Ce	Pr	Nd	Sm	Gd	Tb	Dy	Ho	Er	Tm	Yb	Lu	O	Total
		wt %	wt %	Mg	Na	wt %	wt %	wt %	wt %	wt %	wt %	wt %	wt %	wt %	wt %	wt %	wt %	wt %	wt %	wt %	wt %	wt %	wt %	wt %	wt %	wt %	wt %	wt %	wt %	wt %	wt %	wt %	wt %
O-26	SD9	<dt	<dt	<dt	<dt	1.04	2.63	<dt	0.16	0.12	0.53	59.50	0.27	0.55	<dt	<dt	<dt	<dt	0.07	0.09	<dt	<dt	<dt	<dt	<dt	<dt	<dt	<dt	0.06	<dt	<dt	21.8	86.8
O-27	SD9	<dt	<dt	0.18	<dt	1.99	4.47	<dt	0.20	0.18	0.33	54.56	0.23	0.43	<dt	<dt	<dt	0.07	0.08	0.09	<dt	<dt	<dt	<dt	<dt	<dt	<dt	<dt	<dt	<dt	<dt	23.3	86.1
O-28	SD9	<dt	<dt	0.23	<dt	2.10	4.69	<dt	0.22	0.20	0.41	55.08	0.26	0.33	<dt	<dt	<dt	0.05	0.05	<dt	<dt	<dt	<dt	<dt	<dt	<dt	<dt	<dt	<dt	<dt	<dt	23.8	87.4
O-29	SD9	<dt	0.02	0.06	<dt	1.21	2.91	<dt	0.19	0.10	0.65	57.28	0.28	0.42	<dt	<dt	<dt	<dt	0.17	0.14	<dt	0.08	<dt	0.06	<dt	<dt	<dt	<dt	<dt	<dt	<dt	21.7	85.3
O-30	SD9	<dt	<dt	0.27	0.07	2.51	5.47	<dt	0.24	0.28	0.35	52.92	0.22	0.32	<dt	<dt	<dt	<dt	0.06	<dt	<dt	<dt	<dt	<dt	<dt	<dt	<dt	<dt	<dt	<dt	<dt	24.4	87.1
O-31	SD9	<dt	<dt	0.09	<dt	1.35	3.11	<dt	0.17	0.14	0.63	59.29	0.29	0.41	<dt	<dt	<dt	<dt	0.12	0.10	<dt	<dt	<dt	<dt	n.a.	n.a.	n.a.	n.a.	n.a.	n.a.	n.a.	21.7	87.4
O-32	SD9	<dt	<dt	<dt	<dt	0.95	2.45	0.16	0.19	0.09	0.56	59.88	0.39	0.66	<dt	0.68	<dt	0.32	0.06	0.10	<dt	<dt	<dt	<dt	n.a.	n.a.	n.a.	n.a.	n.a.	n.a.	n.a.	14.2	80.9
O-33	SD9	<dt	<dt	<dt	<dt	1.00	2.41	<dt	0.12	0.10	0.42	61.24	0.26	0.54	<dt	<dt	<dt	<dt	0.07	<dt	<dt	<dt	<dt	<dt	n.a.	n.a.	n.a.	n.a.	n.a.	n.a.	n.a.	17.4	83.6
O-34	SD9	<dt	<dt	0.08	<dt	1.31	2.87	<dt	0.17	0.11	0.52	59.92	0.27	0.49	<dt	<dt	<dt	<dt	0.14	0.08	<dt	<dt	<dt	0.03	n.a.	n.a.	n.a.	n.a.	n.a.	n.a.	n.a.	22.1	88.2
O-35	SD9	<dt	<dt	0.25	<dt	2.29	4.72	<dt	0.21	0.26	0.29	56.05	0.27	0.38	<dt	<dt	<dt	<dt	0.20	0.13	<dt	<dt	<dt	<dt	n.a.	n.a.	n.a.	n.a.	n.a.	n.a.	n.a.	21.8	86.9
O-36	SD9	<dt	<dt	0.22	<dt	2.03	4.50	<dt	0.21	0.16	0.54	57.88	0.27	0.32	<dt	<dt	<dt	<dt	0.14	0.10	<dt	<dt	<dt	<dt	n.a.	n.a.	n.a.	n.a.	n.a.	n.a.	n.a.	21.7	88.0
O-37	SD21	<dt	0.04	0.20	<dt	2.10	7.87	<dt	0.24	0.45	0.15	54.21	<dt	<dt	<dt	<dt	<dt	<dt	<dt	<dt	<dt	<dt	<dt	0.17	<dt	<dt	<dt	<dt	<dt	<dt	<dt	26.8	92.2
O-38	SD21	<dt	<dt	<dt	<dt	<dt	0.11	<dt	<dt	<dt	0.03	69.84	<dt	<dt	<dt	<dt	<dt	<dt	<dt	<dt	<dt	<dt	0.00	<dt	<dt	<dt	<dt	<dt	<dt	<dt	<dt	20.1	90.1
O-39	SD21	<dt	<dt	<dt	<dt	0.03	0.16	<dt	<dt	<dt	0.04	70.41	<dt	<dt	<dt	<dt	<dt	<dt	<dt	<dt	<dt	<dt	<dt	0.14	<dt	<dt	<dt	<dt	<dt	<dt	<dt	20.3	91.1
O-40	SD21	<dt	<dt	0.07	<dt	0.80	3.33	<dt	0.11	0.20	0.11	59.16	<dt	<dt	<dt	<dt	<dt	<dt	<dt	<dt	<dt	<dt	<dt	<dt	<dt	<dt	<dt	<dt	<dt	<dt	<dt	21.6	85.4
O-41	SD21	<dt	<dt	<dt	<dt	0.47	1.88	<dt	0.08	0.09	0.43	64.27	0.07	<dt	<dt	<dt	<dt	<dt	0.07	0.11	<dt	<dt	<dt	<dt	<dt	<dt	<dt	<dt	<dt	<dt	<dt	21.4	88.9
O-42	SD21	<dt	<dt	0.05	<dt	0.92	2.15	<dt	0.04	0.26	0.09	64.29	<dt	0.08	<dt	<dt	<dt	<dt	<dt	0.09	<dt	<dt	<dt	0.08	<dt	<dt	<dt	<dt	<dt	<dt	<dt	21.9	89.9
O-43	SD21	<dt	<dt	0.03	<dt	1.08	2.57	<dt	<dt	0.22	0.23	61.99	0.09	0.15	<dt	<dt	<dt	<dt	0.06	0.12	<dt	<dt	<dt	0.11	<dt	<dt	<dt	<dt	<dt	<dt	<dt	22.0	88.6
O-44	SD21	<dt	0.29	0.03	<dt	2.89	3.61	<dt	0.04	0.29	13.06	30.41	0.34	1.15	<dt	<dt	<dt	<dt	<dt	0.08	<dt	<dt	<dt	<dt	<dt	<dt	<dt	<dt	<dt	<dt	<dt	24.9	77.9
O-45	SD21	<dt	0.07	0.11	<dt	1.96	4.15	0.06	<dt	0.85	0.25	56.36	<dt	0.39	<dt	<dt	<dt	<dt	<dt	0.04	<dt	<dt	<dt	<dt	<dt	<dt	<dt	<dt	<dt	<dt	<dt	23.2	87.5
O-46	SD21	<dt	0.07	<dt	<dt	0.53	1.13	0.03	<dt	0.05	12.89	48.20	1.26	0.07	<dt	<dt	<dt	<dt	0.08	0.15	<dt	<dt	<dt	<dt	<dt	<dt	<dt	<dt	<dt	<dt	<dt	24.8	89.3
O-47	SD21	<dt	<dt	0.03	<dt	0.53	1.11	<dt	0.08	0.14	1.34	62.41	0.38	0.07	<dt	<dt	<dt	0.04	<dt	<dt	<dt	<dt	<dt	0.12	<dt	<dt	<dt	<dt	<dt	<dt	<dt	20.8	87.1
O-48	SD6	<dt	<dt	<dt	<dt	0.03	0.07	<dt	<dt	<dt	56.6	1.49	0.61	<dt	<dt	<dt	<dt	<dt	0.05	<dt	<dt	<dt	<dt	<dt	<dt	<dt	<dt	<dt	<dt	<dt	<dt	38.8	97.9
O-49	SD6	<dt	<dt	<dt	<dt	0.56	0.87	0.02	0.12	0.05	31.2	26.67	0.86	0.15	<dt	<dt	<dt	0.16	<dt	0.10	<dt	<dt	0.00	0.07	<dt	<dt	<dt	<dt	<dt	<dt	<dt	30.6	91.4
O-50	SD6	<dt	<dt	<dt	<dt	0.81	1.07	0.15	0.14	0.18	36.8	16.20	1.74	0.36	<dt	<dt	<dt	0.72	<dt	0.09	<dt	<dt	<dt	<dt	<dt	<dt	<dt	<dt	<dt	0.08	<dt	32.7	91.5
O-51	SD6	<dt	<dt	<dt	<dt	0.24	0.35	0.03	0.06	0.04	38.0	20.07	0.57	0.14	<dt	<dt	<dt	0.13	<dt	0.06	<dt	<dt	<dt	0.08	<dt	<dt	<dt	<dt	<dt	<dt	<dt	32.2	92.0
O-52	SD6	<dt	<dt	<dt	<dt	0.77	1.16	0.23	0.18	0.11	38.0	13.27	2.39	0.28	<dt	<dt	<dt	1.15	<dt	0.27	<dt	<dt	<dt	<dt	<dt	<dt	<dt	0.13	<dt	0.14	<dt	33.3	92.1
O-53	SD8	<dt	0.02	0.05	<dt	0.10	0.30	<dt	0.13	0.07	38.9	15.73	2.36	0.28	<dt	<dt	<dt	<dt	0.07	0.10	<dt	<dt	<dt	<dt	<dt	<dt	<dt	<dt	<dt	<dt	<dt	32.2	91.1
O-54	SD8	<dt	<dt	0.03	<dt	0.13	0.30	<dt	0.16	<dt	39.7	13.77	2.42	0.43	<dt	<dt	<dt	<dt	0.07	0.12	<dt	<dt	<dt	<dt	<dt	<dt	<dt	<dt	<dt	<dt	<dt	32.3	90.1
O-55	SD8	<dt	<dt	0.02	<dt	0.06	0.16	<dt	0.10	<dt	38.1	17.61	1.24	1.39	<dt	<dt	<dt	<dt	<dt	0.06	<dt	<dt	<dt	<dt	<dt	<dt	<dt	<dt	<dt	<dt	<dt	31.8	91.0
O-56	SD8	<dt	<dt	0.03	<dt	0.04	0.20	<dt	0.13	<dt	37.4	18.75	1.07	0.57	<dt	<dt	<dt	<dt	<dt	0.05	<dt	<dt	<dt	<dt	<dt	<dt	<dt	<dt	<dt	<dt	<dt	31.4	90.2
O-57	SD8	<dt	<dt	0.02	<dt	0.12	0.27	<dt	0.16	<dt	47.6	5.29	3.29	0.55	<dt	<dt	<dt	<dt	<dt	0.10	<dt	<dt	<dt	<dt	<dt	<dt	<dt	<dt	<dt	<dt	<dt	35.7	93.9
O-58	SD8	<dt	<dt	0.03	<dt	0.08	0.32	<dt	0.21	0.08	39.1	17.83	1.24	0.10	<dt	<dt	0.58	<dt	<dt	0.07	<dt	<dt	<dt	<dt	n.a.	n.a.	n.a.	n.a.	n.a.	n.a.	n.a.	32.3	92.7
O-59	SD8	<dt	<dt	<dt	<dt	<dt	0.18	<dt	0.18	<dt	38.1	20.13	0.75	0.18	<dt	<dt	0.24	<dt	<dt	<dt	<dt	<dt	<dt	<dt	n.a.	n.a.	n.a.	n.a.	n.a.	n.a.	n.a.	31.7	91.8
O-60	SD8	<dt	<dt	<dt	<dt	0.44	0.58	0.04	0.53	<dt	37.9	19.22	1.08	0.12	<dt	<dt	<dt	<dt	<dt	<dt	<dt	<dt	<dt	0.02	n.a.	n.a.	n.a.	n.a.	n.a.	n.a.	n.a.	0.0	60.4
O-61	SD8	<dt	<dt	<dt	<dt	0.04	0.17	<dt	0.14	<dt	39.1	18.57	0.84	0.45	<dt	<dt	0.02	<dt	<dt	0.06	<dt	<dt	<dt	<dt	n.a.	n.a.	n.a.	n.a.	n.a.	n.a.	n.a.	32.1	92.0
O-62	SD8	<dt	<dt	<dt	<dt	0.06	0.11	<dt	0.09	0.03	41.2	17.65	0.87	0.84	<dt	<dt	<dt	<dt	<dt	<dt	<dt	<dt	<dt	<dt	n.a.	n.a.	n.a.	n.a.	n.a.	n.a.	n.a.	33.2	94.6
O-63	SD8	<dt	0.02	0.07	<dt	0.16	0.66	<dt	0.43	0.10	43.2	8.07	3.39	0.36	<dt	<dt	2.67	<dt	0.08	0.19	<dt	<dt	<dt	<dt	n.a.	n.a.	n.a.	n.a.	n.a.	n.a.	n.a.	34.5	95.3
O-64	SD8	<dt	<dt	0.06	<dt	0.21	0.53	<dt	0.32	0.12	39.9	14.05	1.75	0.09	<dt	<dt	1.19	<dt	0.11	0.15	<dt	<dt	<dt	0.03	n.a.	n.a.	n.a.	n.a.	n.a.	n.a.	n.a.	32.8	92.5
O-65	SD8	<dt	<dt	0.02	<dt	0.03	0.16	<dt	0.12	0.07	37.7	20.44	0.72	0.16	<dt	<dt	0.32	<dt	0.05	0.05	<dt	<dt	<dt	<dt	n.a.	n.a.	n.a.	n.a.	n.a.	n.a.	n.a.	31.9	92.1
O-66	SD8	<dt	0.02	0.08	<dt	0.17	0.76	<dt	0.41	0.08	40.8	8.46	3.13	0.47	<dt	<dt	2.40	<dt	0.09	0.17	<dt	<dt	<dt	<dt	<dt	<dt	<dt	<dt	<dt	<dt	<dt	33.0	91.4
O-67	SD8	<dt	<dt	0.03	<dt	0.06	0.23	<dt	0.18	0.07	37.5	18.98	0.78	0.14	<dt	<dt	0.43	<dt	<dt	0.05	<dt	<dt	<dt	0.00	<dt	<dt	<dt	<dt	<dt	<dt	<dt	31.4	90.5
O-68	SD8	<dt	<dt	0.08	<dt	0.16	0.52	<dt	0.30	0.21	38.8	14.38	1.79	0.11	<dt	<dt	1.25	<dt	0.12	0.16	<dt	<dt	<dt	0.03	<dt	<dt	<dt	<dt	<dt	<dt	<dt	32.1	91.2
O-69	SD8	<dt	<dt	0.06	<dt	0.16	0.48	<dt	0.27	0.04	39.2	15.23	1.91	0.11	<dt	<dt	0.45	<dt	0.11	0.18	<dt	<dt	<dt	<dt	n.a.	n.a.	n.a.	n.a.	n.a.	n.a.	n.a.	32.5	91.9
O-70	SD8	<dt	<dt	0.03	<dt	0.07	0.20	<dt	0.41	<dt	39.2	17.63	1.15	0.06	<dt	<dt	0.20	<dt	0.10	0.12	<dt	<dt	<dt	<dt	n.a.	n.a.	n.a.	n.a.	n.a.	n.a.	n.a.	32.4	91.9

		F	Cl	Mg	Na	Al	Si	P	Ca	K	Ti	Fe	Nb	Mn	Ta	Th	U	Y	La	Ce	Pr	Nd	Sm	Gd	Tb	Dy	Ho	Er	Tm	Yb	Lu	O	Total
		wt %	wt %	Mg	Na	wt %	wt %	wt %	wt %	wt %	wt %	wt %	wt %	wt %	wt %	wt %	wt %	wt %	wt %	wt %	wt %	wt %	wt %	wt %	wt %	wt %	wt %	wt %	wt %	wt %	wt %	wt %	wt %
O-71	SD8	<dt	0.02	0.03	<dt	0.05	0.22	<dt	0.17	<dt	39.1	17.86	0.62	0.41	<dt	<dt	<dt	<dt	<dt	0.12	<dt	<dt	<dt	0.11	<dt	<dt	<dt	<dt	<dt	<dt	<dt	32.1	91.3
O-72	SD8	<dt	<dt	<dt	<dt	<dt	0.12	<dt	0.12	<dt	37.5	20.11	0.41	0.22	<dt	<dt	<dt	<dt	<dt	0.04	<dt	<dt	<dt	0.12	<dt	<dt	<dt	<dt	<dt	<dt	<dt	31.3	90.5
O-73	SD8	<dt	<dt	0.03	<dt	0.12	0.30	<dt	0.19	0.06	39.3	14.97	1.82	0.69	<dt	<dt	<dt	<dt	<dt	0.12	<dt	<dt	<dt	<dt	<dt	<dt	<dt	<dt	<dt	<dt	<dt	32.2	90.6
O-74	SD29	<dt	<dt	<dt	<dt	0.03	0.17	<dt	<dt	<dt	34.6	23.88	0.56	2.43	<dt	<dt	<dt	<dt	<dt	<dt	0.10	<dt	<dt	<dt	<dt	<dt	<dt	<dt	<dt	<dt	<dt	31.1	92.9
O-75	SD29	<dt	<dt	0.03	<dt	0.22	0.58	<dt	<dt	0.24	32.8	24.54	0.40	2.43	<dt	<dt	<dt	<dt	<dt	<dt	<dt	<dt	<dt	<dt	<dt	<dt	<dt	<dt	<dt	<dt	<dt	30.7	92.0
O-76	SD29	<dt	<dt	<dt	<dt	0.11	0.38	<dt	0.03	0.22	33.1	24.77	0.36	1.82	<dt	<dt	<dt	<dt	<dt	<dt	<dt	<dt	<dt	<dt	<dt	<dt	<dt	<dt	<dt	<dt	<dt	30.5	91.3
O-77	SD29	<dt	<dt	<dt	<dt	<dt	0.13	<dt	<dt	<dt	34.0	25.54	0.35	2.48	<dt	<dt	<dt	<dt	0.08	<dt	<dt	<dt	<dt	<dt	<dt	<dt	<dt	-0.02	<dt	<dt	<dt	31.0	93.60
O-78	SD19	<dt	<dt	0.06	<dt	1.00	2.87	<dt	0.35	0.09	46.7	4.17	2.64	<dt	0.19	<dt	0.18	<dt	<dt	0.07	<dt	<dt	<dt	<dt	<dt	<dt	<dt	<dt	<dt	<dt	<dt	<dt	38.1	96.6
O-79	SD19	<dt	<dt	0.06	<dt	0.92	2.90	0.024	0.33	0.07	46.6	4.21	2.46	<dt	0.20	<dt	0.20	<dt	<dt	0.08	<dt	<dt	<dt	<dt	<dt	<dt	<dt	<dt	<dt	<dt	<dt	<dt	37.9	96.0
O-80	SD19	0.32	<dt	0.20	<dt	2.50	5.79	<dt	0.48	0.10	39.1	3.87	2.06	<dt	0.17	<dt	0.18	<dt	<dt	0.10	<dt	<dt	<dt	<dt	<dt	<dt	<dt	<dt	<dt	<dt	<dt	<dt	37.4	92.2
O-81	SD19	0.30	<dt	0.03	<dt	0.46	2.21	<dt	0.28	<dt	42.9	4.91	2.35	<dt	0.26	<dt	0.31	<dt	<dt	0.12	<dt	<dt	<dt	<dt	<dt	<dt	<dt	<dt	<dt	<dt	<dt	<dt	34.4	88.7
O-82	SD19	0.27	<dt	0.19	<dt	2.64	5.74	<dt	0.56	0.13	42.4	3.36	2.00	<dt	0.20	<dt	0.11	<dt	<dt	0.09	<dt	<dt	<dt	<dt	<dt	<dt	<dt	<dt	<dt	<dt	<dt	<dt	39.6	97.4
O-83	SD19	0.43	<dt	0.19	<dt	2.13	4.86	<dt	0.58	0.10	42.6	3.49	2.10	<dt	0.20	<dt	0.16	<dt	<dt	0.09	<dt	<dt	<dt	<dt	<dt	<dt	<dt	<dt	<dt	<dt	<dt	<dt	38.4	95.5
O-84	SD19	0.26	<dt	0.10	<dt	1.36	3.63	<dt	0.41	0.05	45.0	4.32	2.54	<dt	0.35	<dt	0.17	<dt	<dt	0.14	<dt	<dt	0.00	<dt	<dt	<dt	<dt	<dt	<dt	<dt	<dt	<dt	38.2	96.7
O-85	SD19	<dt	<dt	0.06	<dt	0.96	2.83	<dt	0.39	0.08	47.1	4.13	2.26	<dt	0.11	<dt	0.21	<dt	<dt	0.09	<dt	<dt	<dt	<dt	<dt	<dt	<dt	<dt	<dt	<dt	<dt	<dt	38.1	96.4
O-86	SD19	0.24	<dt	0.05	<dt	0.75	2.81	<dt	0.38	0.08	45.1	4.65	3.57	<dt	0.39	<dt	0.14	<dt	<dt	0.09	<dt	<dt	<dt	0.08	<dt	<dt	<dt	<dt	<dt	<dt	<dt	<dt	37.4	96.0
O-87	SD19	0.31	<dt	0.11	0.05	1.64	3.73	0.034	0.43	0.12	46.7	3.34	1.86	<dt	<dt	<dt	<dt	<dt	<dt	0.09	<dt	<dt	<dt	<dt	<dt	<dt	<dt	<dt	<dt	<dt	<dt	<dt	39.1	97.5
O-88	SD21	<dt	0.08	<dt	<dt	0.90	1.40	0.07	<dt	0.02	45.0	4.54	2.15	<dt	0.26	0.32	0.11	<dt	<dt	0.07	<dt	<dt	<dt	<dt	<dt	<dt	<dt	<dt	<dt	<dt	<dt	<dt	35.0	89.9
O-89	SD21	<dt	0.08	<dt	<dt	0.56	0.98	0.08	<dt	<dt	48.7	4.63	1.98	<dt	0.23	0.37	0.15	<dt	<dt	0.16	<dt	<dt	<dt	<dt	<dt	<dt	<dt	<dt	<dt	<dt	<dt	<dt	36.6	94.6
O-90	SD21	<dt	0.07	<dt	<dt	0.57	1.06	0.05	<dt	<dt	48.6	4.23	2.16	<dt	0.24	0.33	0.16	<dt	<dt	0.09	<dt	<dt	<dt	<dt	<dt	<dt	<dt	<dt	<dt	<dt	<dt	<dt	36.6	94.2
O-91	SD21	<dt	0.09	<dt	<dt	0.69	1.08	0.05	<dt	0.04	45.5	4.72	2.43	<dt	0.24	0.34	0.20	<dt	<dt	0.12	<dt	<dt	<dt	<dt	<dt	<dt	<dt	<dt	<dt	<dt	<dt	<dt	34.8	90.3
O-92	SD21	<dt	0.10	0.03	<dt	0.75	1.30	0.03	<dt	0.05	43.5	8.02	2.96	<dt	0.20	0.19	0.10	<dt	<dt	0.09	<dt	<dt	<dt	<dt	<dt	<dt	<dt	<dt	<dt	<dt	<dt	<dt	34.9	92.2
O-93	SD21	<dt	0.07	<dt	<dt	1.40	1.68	0.07	<dt	0.03	46.8	5.49	2.11	<dt	<dt	0.76	0.16	<dt	<dt	0.10	<dt	<dt	<dt	<dt	<dt	<dt	<dt	<dt	<dt	<dt	<dt	<dt	37.2	95.9
O-94	SD21	<dt	<dt	<dt	<dt	0.21	0.45	<dt	<dt	<dt	25.7	24.91	0.33	9.84	<dt	<dt	<dt	<dt	<dt	0.10	<dt	<dt	<dt	<dt	<dt	<dt	<dt	<dt	<dt	<dt	<dt	<dt	28.0	89.5
O-95	SD21	<dt	0.08	<dt	<dt	1.03	1.42	0.06	<dt	0.02	48.4	5.29	1.74	<dt	<dt	0.83	0.17	<dt	<dt	0.06	<dt	<dt	<dt	<dt	<dt	<dt	<dt	<dt	<dt	<dt	<dt	<dt	37.5	96.6

Table C2.5 EMPA zircon minerals

#	Sample	F	Cl	Al	Si	P	Ca	K	Ti	Mn	Fe	Zr	Hf	Nb	Ta	Th	U	Y	La	Ce	Pr	Nd	Sm	Gd	Tb	Dy	Ho	Er	Tm	Yb	Lu	O	Total
		wt %	wt %	wt %	wt %	wt %	wt %	wt %	wt %	wt %	wt %	wt %	wt %	wt %	wt %	wt %	wt %	wt %	wt %	wt %	wt %	wt %	wt %	wt %	wt %	wt %	wt %	wt %	wt %	wt %	wt %	wt %	wt %	
Z-1	SD4	3.09	<dt	0.43	10.5	1.00	0.18	<dt	<dt	0.04	0.60	31.5	0.41	0.26	<dt	0.13	0.46	9.19	<dt	0.81	<dt	0.01	<dt	<dt	<dt	0.75	0.26	1.22	0.21	1.98	0.29	28.6	92.1
Z-2	SD3	<dt	<dt	<dt	14.6	0.03	<dt	<dt	<dt	<dt	0.09	46.1	1.65	<dt	<dt	<dt	<dt	0.34	<dt	<dt	<dt	0.09	<dt	<dt	<dt	<dt	<dt	<dt	<dt	<dt	<dt	33.3	96.2
Z-3	SD4	<dt	<dt	0.09	14.6	0.06	<dt	<dt	<dt	<dt	0.27	37.6	1.44	<dt	<dt	0.23	<dt	1.27	<dt	0.25	<dt	<dt	<dt	<dt	<dt	<dt	<dt	<dt	<dt	0.21	<dt	30.8	86.8
Z-4	SD4	<dt	<dt	<dt	14.9	0.05	<dt	<dt	<dt	<dt	0.22	39.8	1.13	<dt	<dt	<dt	0.14	0.48	<dt	<dt	<dt	<dt	<dt	<dt	<dt	<dt	<dt	<dt	<dt	<dt	<dt	31.0	87.8
Z-5	SD4	<dt	<dt	<dt	15.0	0.04	<dt	<dt	<dt	<dt	0.32	39.3	1.26	<dt	<dt	<dt	<dt	0.46	<dt	<dt	<dt	<dt	<dt	<dt	<dt	<dt	<dt	<dt	<dt	<dt	<dt	31.1	87.6
Z-6	SD4	<dt	<dt	<dt	15.0	<dt	<dt	<dt	<dt	<dt	0.16	39.4	1.28	<dt	<dt	<dt	<dt	0.35	<dt	<dt	<dt	<dt	<dt	<dt	<dt	<dt	<dt	<dt	<dt	0.07	<dt	31.1	87.4
Z-7	SD4	1.22	<dt	0.33	13.0	0.34	0.28	<dt	<dt	0.08	0.59	33.3	1.22	0.29	<dt	0.10	0.22	3.46	<dt	0.34	<dt	<dt	0.08	<dt	0.06	0.39	<dt	0.35	<dt	0.49	<dt	31.5	87.6
Z-8	SD4	0.13	<dt	0.04	14.6	0.07	0.05	<dt	<dt	<dt	0.41	38.5	1.37	<dt	<dt	<dt	<dt	0.79	<dt	<dt	<dt	<dt	<dt	<dt	<dt	<dt	<dt	0.13	<dt	0.07	<dt	31.4	87.4
Z-9	SD4	<dt	<dt	0.03	15.1	0.03	<dt	<dt	<dt	<dt	0.38	40.5	1.29	<dt	<dt	<dt	<dt	0.39	<dt	<dt	<dt	<dt	<dt	0.07	<dt	<dt	<dt	<dt	<dt	<dt	<dt	31.4	89.2
Z-10	SD4	<dt	<dt	0.06	14.8	0.04	<dt	<dt	<dt	<dt	0.31	46.7	1.36	<dt	<dt	<dt	<dt	0.72	<dt	<dt	<dt	<dt	<dt	<dt	<dt	<dt	<dt	<dt	<dt	0.07	<dt	33.9	98.0
Z-11	SD4	<dt	<dt	<dt	15.0	0.02	<dt	<dt	<dt	<dt	0.05	47.1	1.33	<dt	<dt	<dt	<dt	0.42	<dt	<dt	<dt	<dt	<dt	0.09	<dt	<dt	<dt	<dt	<dt	0.06	<dt	34.1	98.2
Z-12	SD4	<dt	<dt	<dt	14.8	0.03	<dt	<dt	<dt	<dt	<dt	48.5	0.89	<dt	<dt	<dt	<dt	0.46	<dt	<dt	<dt	<dt	<dt	<dt	<dt	<dt	<dt	<dt	<dt	<dt	<dt	34.2	98.8
Z-13	SD4	<dt	<dt	0.04	14.3	0.08	<dt	<dt	<dt	<dt	0.30	46.3	2.09	<dt	<dt	<dt	<dt	0.80	<dt	<dt	<dt	<dt	<dt	<dt	<dt	<dt	<dt	<dt	<dt	0.11	<dt	33.4	97.3
Z-14	SD4	<dt	<dt	<dt	14.8	0.04	<dt	<dt	<dt	<dt	<dt	47.6	2.55	<dt	<dt	<dt	<dt	0.37	<dt	<dt	<dt	<dt	<dt	<dt	<dt	<dt	<dt	<dt	<dt	<dt	<dt	34.2	99.6
Z-15	SD4	1.94	<dt	0.48	11.3	0.69	0.29	<dt	<dt	0.04	0.94	36.0	1.20	0.24	<dt	0.12	0.47	6.96	<dt	0.48	<dt	<dt	0.07	<dt	0.06	0.60	0.20	0.80	0.14	1.04	0.17	30.1	94.5

#	Sample	F wt %	Cl wt %	Al wt %	Si wt %	P wt %	Ca wt %	K wt %	Ti wt %	Mn wt %	Fe wt %	Zr wt %	Hf wt %	Nb wt %	Ta wt %	Th wt %	U wt %	Y wt %	La wt %	Ce wt %	Pr wt %	Nd wt %	Sm wt %	Gd wt %	Tb wt %	Dy wt %	Ho wt %	Er wt %	Tm wt %	Yb wt %	Lu wt %	O wt %	Total
Z-16	SD4	2.28	<dt	0.44	12.3	0.65	0.26	<dt	<dt	0.03	0.66	42.5	1.60	0.21	<dt	<dt	0.23	3.21	<dt	0.27	<dt	<dt	<dt	<dt	<dt	0.21	<dt	0.26	<dt	0.45	<dt	31.9	97.4
Z-17	SD4	<dt	<dt	<dt	15.0	0.03	0.04	<dt	<dt	<dt	0.03	39.4	1.22	<dt	<dt	<dt	<dt	0.42	<dt	<dt	<dt	<dt	<dt	<dt	<dt	<dt	<dt	<dt	<dt	<dt	<dt	31.5	87.6
Z-18	SD4	<dt	<dt	<dt	15.0	0.05	0.05	<dt	<dt	<dt	<dt	39.4	1.25	<dt	<dt	<dt	<dt	0.45	<dt	<dt	<dt	<dt	<dt	0.05	<dt	<dt	<dt	<dt	<dt	0.10	<dt	31.3	87.6
Z-19	SD4	2.02	<dt	0.47	11.0	0.88	0.31	0.04	<dt	<dt	0.26	27.3	0.66	0.56	<dt	0.15	0.28	8.58	<dt	0.46	<dt	0.07	0.06	<dt	0.07	0.82	0.24	0.99	0.19	1.66	0.23	31.0	88.4
Z-20	SD5	2.61	<dt	0.83	10.7	0.95	0.40	<dt	<dt	<dt	0.31	26.6	1.18	0.51	<dt	0.15	0.47	8.79	<dt	0.57	<dt	<dt	0.08	<dt	0.06	0.80	0.22	1.07	0.22	1.80	0.27	30.9	89.7
Z-21	SD5	0.25	<dt	0.11	14.5	0.10	0.13	<dt	<dt	<dt	0.07	35.2	3.27	0.11	<dt	<dt	0.18	1.81	<dt	0.22	<dt	<dt	<dt	<dt	<dt	0.18	<dt	0.17	<dt	0.44	<dt	30.6	87.3
Z-22	SD5	<dt	<dt	<dt	14.9	<dt	<dt	0.03	<dt	<dt	0.18	39.9	1.76	<dt	<dt	<dt	<dt	0.33	<dt	<dt	<dt	<dt	<dt	0.07	<dt	<dt	<dt	<dt	<dt	<dt	<dt	30.7	87.9
Z-23	SD5	<dt	<dt	0.05	14.7	0.04	<dt	<dt	<dt	<dt	0.05	46.7	1.84	<dt	<dt	<dt	<dt	0.59	<dt	<dt	<dt	<dt	<dt	<dt	<dt	<dt	<dt	<dt	<dt	<dt	<dt	33.7	97.7
Z-24	SD5	<dt	<dt	<dt	14.8	<dt	<dt	<dt	<dt	<dt	0.03	46.7	1.81	<dt	<dt	<dt	<dt	0.47	<dt	<dt	<dt	<dt	<dt	<dt	<dt	<dt	<dt	<dt	<dt	<dt	<dt	33.7	97.6
Z-25	SD5	<dt	<dt	<dt	14.9	<dt	<dt	0.03	<dt	<dt	0.12	48.7	1.32	<dt	<dt	<dt	<dt	0.49	<dt	<dt	<dt	<dt	<dt	0.07	<dt	<dt	<dt	<dt	<dt	<dt	<dt	34.5	100.2
Z-26	SD5	0.63	<dt	0.42	13.1	<dt	0.26	0.03	<dt	0.11	0.36	40.2	1.00	0.33	<dt	0.15	<dt	3.86	<dt	0.49	<dt	<dt	0.07	<dt	<dt	0.26	0.12	0.40	0.06	0.65	0.13	31.3	94.0
Z-27	SD5	<dt	<dt	<dt	15.0	<dt	<dt	<dt	<dt	<dt	0.05	48.1	1.28	<dt	<dt	<dt	<dt	0.46	<dt	<dt	<dt	<dt	<dt	<dt	<dt	<dt	<dt	<dt	<dt	<dt	<dt	34.3	99.2
Z-28	SD5	1.30	<dt	0.46	11.7	0.24	0.24	<dt	<dt	0.04	0.24	35.6	0.77	0.42	<dt	0.17	0.29	7.20	<dt	0.59	<dt	<dt	0.07	<dt	<dt	0.61	0.17	0.93	0.16	1.48	0.25	29.7	92.8
Z-29	SD5	1.10	<dt	0.53	11.5	0.22	0.20	0.06	0.05	0.04	0.71	31.7	1.41	0.79	<dt	0.35	0.35	8.30	<dt	1.30	<dt	<dt	0.06	<dt	<dt	0.68	0.20	1.09	0.19	2.09	0.36	29.1	92.4
Z-30	SD5	<dt	<dt	<dt	14.7	0.05	<dt	<dt	<dt	<dt	0.13	46.8	1.73	<dt	<dt	0.19	0.31	0.70	<dt	<dt	<dt	<dt	<dt	0.08	<dt	<dt	<dt	<dt	<dt	0.12	<dt	33.8	98.5
Z-31	SD5	<dt	<dt	<dt	14.9	0.03	<dt	<dt	<dt	<dt	0.12	47.7	1.68	<dt	<dt	<dt	<dt	0.35	<dt	<dt	<dt	<dt	<dt	<dt	<dt	<dt	<dt	<dt	<dt	<dt	<dt	34.2	99.0
Z-32	SD5	<dt	<dt	<dt	14.9	0.04	<dt	<dt	<dt	<dt	0.03	48.0	1.28	<dt	<dt	<dt	<dt	0.47	<dt	<dt	<dt	<dt	<dt	0.08	<dt	<dt	<dt	<dt	<dt	<dt	<dt	34.2	99.0
Z-33	SD5	<dt	<dt	<dt	14.7	0.03	<dt	<dt	<dt	<dt	0.04	47.8	1.18	<dt	<dt	0.07	<dt	0.48	<dt	<dt	<dt	<dt	<dt	<dt	<dt	<dt	<dt	<dt	<dt	<dt	<dt	33.9	98.2
Z-34	SD5	<dt	<dt	<dt	14.7	0.04	<dt	<dt	<dt	<dt	0.06	46.4	1.38	<dt	<dt	0.29	0.39	0.83	<dt	<dt	<dt	<dt	<dt	<dt	<dt	<dt	<dt	<dt	<dt	0.16	<dt	33.6	97.9
Z-35	SD5	0.45	<dt	0.21	13.3	0.15	0.16	<dt	<dt	<dt	0.22		1.17	<dt	<dt	0.13	0.21	2.96	<dt	0.24	<dt	<dt	<dt	<dt	<dt	0.26	<dt	0.31	0.06	0.53	0.08	16.9	37.4
Z-36	SD5	<dt	<dt	<dt	14.8	0.03	<dt	<dt	<dt	<dt	0.16	48.5	1.36	<dt	<dt	0.08	<dt	0.44	<dt	0.01	<dt	<dt	<dt	<dt	<dt	<dt	<dt	<dt	<dt	<dt	<dt	34.4	99.8
Z-37	SD5	<dt	<dt	<dt	14.9	<dt	<dt	<dt	<dt	<dt	0.37	47.9	1.35	<dt	<dt	<dt	<dt	0.46	<dt	<dt	<dt	<dt	<dt	<dt	<dt	<dt	<dt	<dt	<dt	<dt	<dt	34.3	99.3
Z-38	SD5	<dt	<dt	<dt	14.9	<dt	<dt	<dt	<dt	<dt	0.32	47.5	1.39	<dt	<dt	<dt	<dt	0.46	<dt	<dt	<dt	<dt	<dt	0.11	<dt	<dt	<dt	<dt	<dt	0.07	<dt	34.2	98.9
Z-39	SD5	<dt	<dt	<dt	14.9	<dt	0.03	<dt	<dt	<dt	<dt	46.9	1.82	<dt	<dt	<dt	<dt	0.38	<dt	<dt	<dt	<dt	<dt	0.09	<dt	<dt	<dt	<dt	<dt	<dt	<dt	33.8	98.0
Z-40	SD5	0.95	<dt	0.57	12.9	<dt	0.30	0.04	<dt	0.16	0.22	36.3	1.06	0.18	<dt	0.13	0.24	4.75	0.37	1.29	<dt	0.18	0.09	<dt	<dt	0.51	<dt	0.46	0.09	0.79	0.12	30.3	92.0
Z-41	SD5	<dt	<dt	<dt	14.7	0.03	<dt	<dt	<dt	<dt	<dt	47.6	1.29	<dt	<dt	<dt	<dt	0.43	<dt	<dt	<dt	<dt	<dt	<dt	<dt	<dt	<dt	<dt	<dt	<dt	<dt	33.9	98.0
Z-42	SD5	0.48	<dt	0.21	13.8	<dt	0.20	0.03	<dt	0.04	0.19	43.8	1.41	0.11	<dt	<dt	0.15	1.80	<dt	0.10	<dt	<dt	<dt	<dt	<dt	0.11	<dt	0.20	<dt	0.28	<dt	32.3	95.2
Z-43	SD5	0.33	<dt	0.97	13.7	0.09	0.10	<dt	<dt	<dt	0.07	43.5	1.75	0.15	<dt	0.12	0.21	2.10	<dt	0.24	<dt	<dt	<dt	<dt	<dt	0.15	<dt	0.23	<dt	0.42	0.07	33.0	97.2
Z-44	SD5	<dt	<dt	<dt	14.6	0.03	<dt	<dt	<dt	<dt	0.08	47.2	1.87	<dt	<dt	<dt	0.21	<dt	<dt	<dt	<dt	<dt	<dt	<dt	<dt	<dt	<dt	<dt	<dt	<dt	<dt	33.7	97.7
Z-45	SD5	<dt	<dt	<dt	14.6	0.03	<dt	<dt	<dt	<dt	<dt	47.7	1.27	<dt	<dt	<dt	<dt	0.56	<dt	<dt	<dt	<dt	<dt	<dt	<dt	<dt	<dt	<dt	<dt	<dt	<dt	33.8	98.0
Z-46	SD5	<dt	<dt	<dt	14.9	0.03	<dt	<dt	<dt	<dt	0.07	48.3	1.32	<dt	<dt	<dt	<dt	0.44	<dt	<dt	<dt	<dt	<dt	<dt	<dt	<dt	<dt	<dt	<dt	<dt	<dt	34.4	99.5
Z-47	SD5	<dt	<dt	<dt	14.8	<dt	<dt	<dt	<dt	<dt	0.06	47.7	1.25	<dt	<dt	<dt	<dt	0.46	<dt	<dt	<dt	<dt	<dt	<dt	<dt	<dt	<dt	<dt	<dt	<dt	<dt	33.9	98.1
Z-48	SD5	<dt	<dt	<dt	15.0	<dt	<dt	<dt	<dt	<dt	0.06	48.2	1.51	<dt	<dt	<dt	<dt	0.34	<dt	<dt	<dt	<dt	<dt	<dt	<dt	<dt	<dt	<dt	<dt	<dt	<dt	34.3	99.4
Z-49	SD5	1.15	<dt	0.79	12.1	0.17	0.28	<dt	<dt	0.07	0.25	31.8	1.08	0.28	<dt	0.17	0.23	8.30	<dt	1.21	<dt	<dt	0.05	<dt	<dt	0.63	0.19	1.04	0.15	1.41	0.17	29.4	91.0
Z-50	SD5	0.72	<dt	0.43	12.9	0.11	0.35	<dt	<dt	0.11	0.35	41.0	1.34	0.16	<dt	0.10	0.31	3.32	<dt	0.12	<dt	<dt	0.08	<dt	<dt	0.31	0.11	0.36	<dt	0.44	<dt	31.3	93.9
Z-51	SD5	0.53	<dt	0.39	12.9	0.09	0.28	<dt	<dt	0.07	0.25	40.1	1.33	0.29	<dt	0.07	0.16	3.66	<dt	0.40	<dt	<dt	<dt	0.06	<dt	0.42	<dt	0.43	0.07	0.61	0.08	31.1	93.4
Z-52	SD5	<dt	<dt	<dt	14.9	0.03	<dt	<dt	<dt	<dt	0.10	48.6	1.52	<dt	<dt	<dt	<dt	0.46	<dt	<dt	<dt	<dt	<dt	0.09	<dt	<dt	<dt	<dt	<dt	<dt	<dt	34.5	100.1
Z-53	SD5	<dt	<dt	<dt	14.7	<dt	<dt	<dt	<dt	<dt	0.08	48.7	0.84	<dt	<dt	<dt	<dt	0.43	<dt	<dt	<dt	<dt	<dt	<dt	<dt	<dt	<dt	<dt	<dt	<dt	<dt	34.1	98.9
Z-54	SD6	<dt	<dt	<dt	14.8	0.04	0.05	<dt	<dt	<dt	<dt	47.7	1.35	<dt	<dt	<dt	<dt	0.42	<dt	<dt	<dt	<dt	<dt	0.11	<dt	<dt	<dt	<dt	<dt	<dt	<dt	34.1	98.6
Z-55	SD6	<dt	<dt	<dt	14.7	<dt	<dt	<dt	<dt	<dt	<dt	48.0	1.32	<dt	<dt	<dt	<dt	0.51	<dt	<dt	<dt	<dt	<dt	<dt	<dt	<dt	<dt	<dt	<dt	<dt	<dt	33.9	98.4
Z-56	SD6	0.71	<dt	0.54	13.0	0.25	0.36	<dt	<dt	0.24	0.28	38.8	1.07	0.18	<dt	0.12	0.24	4.23	<dt	0.18	<dt	<dt	<dt	<dt	<dt	0.33	<dt	0.53	0.13	0.84	0.10	31.3	93.5
Z-57	SD6	0.37	<dt	0.03	14.7	0.07	0.08	<dt	<dt	0.08	0.26	38.5	1.22	<dt	<dt	0.19	0.27	1.04	<dt	0.00	<dt	<dt	<dt	<dt	<dt	<dt	<dt	<dt	<dt	0.19	<dt	30.8	87.8
Z-58	SD6	0.77	<dt	0.49	12.8	0.23	0.32	0.06	<dt	0.24	0.42	38.1	1.88	0.14	<dt	<dt	0.23	3.92	<dt	0.22	<dt	<dt	<dt	<dt	<dt	0.28	<dt	0.40	0.09	0.68	<dt	30.8	92.1
Z-59	SD6	<dt	<dt	<dt	15.0	0.05	<dt	<dt	<dt	<dt	0.27	39.3	1.16	<dt	<dt	<dt	<dt	0.54	<dt	<dt	<dt	<dt	<dt	<dt	<dt	<dt	<dt	<dt	<dt	<dt	<dt	30.9	87.2
Z-60	SD6	0.88	<dt	0.46	13.7	0.12	0.22	<dt	<dt	0.11	0.41	33.3	1.09	0.09	<dt	0.15	0.40	3.80	<dt	0.22	<dt	<dt	<dt	<dt	<dt	0.21	<dt	0.26	<dt	0.53	0.09	30.6	86.6
Z-61	SD6	0.13	<dt	0.16	14.4	0.08	0.09	<dt	<dt	0.05	0.12	43.8	1.36	<dt	<dt	0.10	0.22	1.81	<dt	0.08	<dt	<dt	<dt	<dt	<dt	<dt	<dt	0.20	<dt	0.37	0.08	33.0	96.1
Z-62	SD6	0.79	<dt	0.42	14.1	0.11	0.21	<dt	<dt	0.09	0.42	34.3	1.00	<dt	<dt	0.17	0.35	3.58	<dt	0.15	<dt	<dt	<dt	<dt	<dt	0.23	<dt	0.35	0.07	0.50	0.09	30.7	87.7
Z-63	SD6	<dt	<dt	<dt	15.1	0.04	<dt	<dt	<dt	<dt	<dt	38.3	1.21	<dt	<dt	<dt	<dt	0.41	<dt	<dt	<dt	<dt	<dt	<dt	<dt	<dt	<dt	<dt	<dt	<dt	<dt	31.4	86.5
Z-64	SD6	<dt	<dt	<dt	15.1	0.04	<dt	<dt	<dt	<dt	<dt	38.0	1.18	<dt	<dt	<dt	<dt	0.41	<dt	<dt	<dt	<dt	<dt	<dt	<dt	<dt	<dt	<dt	<dt	<dt	<dt	31.3	86.1
Z-65	SD6	0.24	<dt	0.25	14.7	0.09	0.06	0.03	<dt	<dt	0.15	35.7	1.53	<dt	<dt	<dt	<dt	1.11	<dt	0.13	<dt	<dt	<dt	0.11	<dt	<dt	<dt	<dt	<dt	0.17	<dt	29.1	83.4

#	Sample	F	Cl	Al	Si	P	Ca	K	Ti	Mn	Fe	Zr	Hf	Nb	Ta	Th	U	Y	La	Ce	Pr	Nd	Sm	Gd	Tb	Dy	Ho	Er	Tm	Yb	Lu	O	Total
		wt %	wt %	wt %	wt %	wt %	wt %	wt %	wt %	wt %	wt %	wt %	wt %	wt %	wt %	wt %	wt %	wt %	wt %	wt %	wt %	wt %	wt %	wt %	wt %	wt %	wt %	wt %	wt %	wt %	wt %	wt %	
Z-66	SD6	<dt	<dt	<dt	15.0	0.06	<dt	<dt	<dt	<dt	<dt	37.9	1.72	<dt	<dt	<dt	<dt	0.34	<dt	<dt	<dt	<dt	<dt	<dt	<dt	<dt	<dt	<dt	<dt	<dt	<dt	30.8	85.9
Z-67	SD6	0.80	<dt	0.79	12.3	<dt	0.38	0.05	0.05	0.18	2.39	24.7	0.73	0.38	<dt	0.15	0.57	6.33	<dt	1.25	<dt	<dt	0.06	<dt	<dt	0.62	0.16	0.79	0.14	1.44	0.23	31.9	86.6
Z-68	SD6	1.23	<dt	0.83	12.1	0.31	0.40	0.04	<dt	<dt	0.49	20.7	0.55	0.59	<dt	0.17	0.42	8.71	<dt	4.85	<dt	0.03	0.04	<dt	<dt	0.77	0.24	0.99	0.19	1.82	0.32	31.1	87.1
Z-69	SD6	0.19	<dt	0.22	14.2	0.07	0.13	<dt	<dt	0.05	0.13	33.3	2.40	0.18	<dt	<dt	0.27	2.15	<dt	0.30	<dt	<dt	<dt	<dt	<dt	0.16	<dt	0.29	<dt	0.58	0.08	31.3	86.1
Z-70	SD6	<dt	<dt	0.61	18.7	0.05	0.06	0.05	<dt	<dt	0.28	29.5	1.35	<dt	<dt	<dt	0.19	0.35	<dt	<dt	<dt	<dt	<dt	<dt	<dt	<dt	<dt	<dt	<dt	<dt	<dt	29.6	81.1
Z-71	SD6	<dt	<dt	<dt	14.9	0.05	<dt	<dt	<dt	<dt	0.04	37.5	1.88	<dt	<dt	<dt	<dt	0.31	<dt	0.01	<dt	<dt	<dt	0.10	<dt	<dt	<dt	<dt	<dt	<dt	<dt	31.1	85.8
Z-72	SD6	<dt	<dt	<dt	14.9	0.04	<dt	<dt	<dt	<dt	0.04	37.6	1.82	<dt	<dt	<dt	<dt	0.31	<dt	<dt	<dt	<dt	<dt	0.10	<dt	<dt	<dt	<dt	<dt	<dt	<dt	27.9	82.7
Z-73	SD6	<dt	<dt	<dt	15.1	0.05	<dt	<dt	<dt	<dt	0.06	38.1	1.17	<dt	<dt	<dt	<dt	0.49	<dt	<dt	<dt	<dt	<dt	<dt	<dt	<dt	<dt	<dt	<dt	0.08	<dt	30.6	85.6
Z-74	SD6	<dt	<dt	0.07	15.0	<dt	<dt	<dt	<dt	<dt	0.04	37.6	1.26	<dt	<dt	<dt	<dt	0.58	<dt	<dt	<dt	<dt	<dt	<dt	<dt	<dt	<dt	<dt	<dt	0.07	<dt	28.4	82.9
Z-75	SD6	<dt	<dt	<dt	15.0	<dt	<dt	<dt	<dt	<dt	0.05	38.1	1.17	<dt	<dt	<dt	<dt	0.36	<dt	<dt	<dt	<dt	<dt	<dt	<dt	<dt	<dt	<dt	<dt	<dt	<dt	27.5	82.2
Z-76	SD6	<dt	<dt	<dt	15.0	0.04	<dt	<dt	<dt	<dt	0.06	38.6	1.15	<dt	<dt	<dt	<dt	0.57	<dt	<dt	<dt	<dt	<dt	<dt	<dt	<dt	<dt	<dt	<dt	<dt	<dt	31.3	86.8
Z-77	SD6	<dt	<dt	<dt	14.9	0.04	<dt	<dt	0.04	<dt	0.06	38.3	1.93	<dt	<dt	<dt	<dt	0.30	<dt	<dt	<dt	<dt	<dt	<dt	<dt	<dt	<dt	<dt	<dt	<dt	<dt	31.3	87.0
Z-78	SD6	1.39	<dt	0.61	12.0	0.62	0.71	<dt	<dt	0.05	0.21	29.5	1.03	<dt	<dt	0.18	0.46	5.39	<dt	0.43	<dt	0.07	<dt	<dt	<dt	0.52	0.15	0.50	0.06	0.69	0.11	27.3	82.1
Z-79	SD6	<dt	<dt	<dt	14.9	0.06	<dt	<dt	<dt	<dt	<dt	46.2	1.13	<dt	<dt	<dt	0.18	0.58	<dt	<dt	<dt	<dt	<dt	<dt	<dt	<dt	<dt	0.19	<dt	0.09	<dt	33.7	97.1
Z-80	SD6	<dt	<dt	0.02	14.8	<dt	<dt	<dt	<dt	<dt	0.04	37.5	1.84	<dt	<dt	<dt	<dt	0.47	<dt	<dt	<dt	<dt	<dt	<dt	<dt	<dt	<dt	<dt	<dt	<dt	<dt	27.4	82.1
Z-81	SD6	<dt	<dt	<dt	14.9	0.03	<dt	<dt	<dt	<dt	0.26	46.3	1.19	<dt	<dt	<dt	<dt	0.47	<dt	<dt	<dt	<dt	<dt	0.06	<dt	<dt	<dt	<dt	<dt	0.06	<dt	33.7	97.0
Z-82	SD6	1.41	<dt	0.44	12.9	0.32	0.50	<dt	<dt	0.05	0.19	31.9	1.15	<dt	<dt	<dt	0.22	3.57	<dt	0.20	<dt	<dt	<dt	<dt	<dt	0.25	<dt	0.26	<dt	0.36	<dt	30.4	84.4
Z-83	SD6	<dt	<dt	0.10	14.6	0.03	0.07	<dt	<dt	0.03	<dt	44.9	1.96	<dt	<dt	<dt	0.17	0.72	<dt	<dt	<dt	<dt	<dt	0.11	<dt	<dt	<dt	<dt	<dt	<dt	<dt	33.1	95.8
Z-84	SD6	1.12	<dt	0.66	12.1	0.48	0.75	<dt	<dt	0.04	0.24	28.7	1.13	<dt	<dt	0.10	0.39	5.31	<dt	0.57	<dt	0.00	0.08	<dt	<dt	0.50	0.14	0.59	0.11	0.78	0.09	30.8	84.7
Z-85	SD6	<dt	<dt	<dt	14.8	<dt	<dt	<dt	<dt	<dt	<dt	46.6	1.17	<dt	<dt	<dt	<dt	0.46	<dt	<dt	<dt	<dt	<dt	<dt	<dt	<dt	<dt	<dt	<dt	<dt	<dt	33.6	96.6
Z-86	SD6	<dt	<dt	<dt	14.9	0.03	<dt	<dt	<dt	<dt	0.05	46.8	1.24	<dt	<dt	<dt	<dt	0.43	<dt	<dt	<dt	<dt	<dt	<dt	<dt	<dt	<dt	<dt	<dt	0.06	<dt	33.8	97.3
Z-87	SD6	<dt	<dt	<dt	14.8	0.02	<dt	<dt	<dt	<dt	0.11	47.1	1.33	<dt	<dt	<dt	<dt	0.43	<dt	<dt	<dt	<dt	<dt	<dt	<dt	<dt	<dt	<dt	<dt	<dt	<dt	33.8	97.7
Z-88	SD6	0.74	<dt	0.90	12.5	0.18	0.31	0.06	<dt	0.08	4.84	35.3	1.85	0.13	<dt	<dt	0.41	4.34	0.12	0.27	<dt	<dt	0.07	<dt	<dt	0.46	<dt	0.51	0.08	1.04	0.17	31.2	95.7
Z-89	SD6	<dt	<dt	<dt	14.8	0.05	<dt	<dt	<dt	<dt	0.04	47.7	1.08	<dt	<dt	<dt	<dt	0.57	<dt	<dt	<dt	<dt	<dt	<dt	<dt	<dt	<dt	<dt	<dt	<dt	<dt	34.0	98.2
Z-90	SD6	0.64	<dt	0.50	13.6	0.14	0.27	<dt	<dt	0.18	0.17	40.5	1.00	0.19	<dt	0.11	0.22	3.55	<dt	0.56	<dt	<dt	<dt	<dt	<dt	0.27	0.13	0.45	0.08	0.70	<dt	32.1	95.4
Z-91	SD6	0.19	<dt	0.15	14.2	0.07	0.10	<dt	<dt	<dt	0.33	43.1	3.45	<dt	<dt	<dt	0.15	1.47	<dt	0.18	<dt	<dt	<dt	0.19	<dt	<dt	<dt	<dt	<dt	0.21	<dt	32.7	96.5
Z-92	SD6	0.79	<dt	0.72	11.2	0.16	0.37	<dt	0.04	0.25	9.37	29.9	2.69	0.08	<dt	<dt	0.25	4.56	<dt	0.35	<dt	0.01	<dt	0.06	<dt	0.36	<dt	0.36	0.07	0.65	0.09	29.1	91.4
Z-93	SD6	1.04	<dt	0.74	11.9	0.28	0.41	<dt	<dt	0.31	3.08	32.5	2.58	0.30	<dt	0.13	0.39	5.46	<dt	1.30	<dt	<dt	<dt	0.13	0.06	0.42	<dt	0.57	0.07	0.88	0.13	29.8	92.5
Z-94	SD7	0.46	<dt	0.38	12.3	0.10	0.22	0.05	<dt	0.08	8.20	35.9	3.95	<dt	<dt	<dt	0.21	2.34	<dt	0.34	<dt	<dt	<dt	0.09	<dt	0.12	<dt	0.25	<dt	0.40	<dt	31.1	96.5
Z-95	SD7	1.25	<dt	0.88	12.7	0.16	0.44	0.06	<dt	0.42	0.28	34.9	0.90	0.32	<dt	0.21	0.37	5.73	<dt	1.20	<dt	<dt	<dt	<dt	<dt	0.51	0.17	0.55	0.11	1.10	0.15	30.6	93.1
Z-96	SD7	1.01	<dt	0.90	13.0	0.15	0.46	<dt	<dt	0.43	0.34	35.4	0.95	0.32	<dt	0.26	0.47	5.91	<dt	1.17	<dt	<dt	0.05	<dt	<dt	0.45	0.13	0.68	0.14	1.10	0.15	31.2	94.7
Z-97	SD7	<dt	<dt	<dt	15.0	<dt	<dt	<dt	<dt	<dt	0.29	48.5	1.21	<dt	<dt	<dt	<dt	0.53	<dt	<dt	<dt	<dt	<dt	<dt	<dt	<dt	<dt	<dt	<dt	<dt	<dt	34.6	100.1
Z-98	SD7	<dt	<dt	<dt	14.9	<dt	<dt	<dt	<dt	<dt	0.15	48.0	1.21	<dt	<dt	0.07	<dt	0.64	<dt	<dt	<dt	<dt	<dt	<dt	<dt	<dt	<dt	<dt	<dt	0.07	<dt	34.3	99.3
Z-99	SD7	<dt	<dt	0.07	14.9	<dt	<dt	0.13	<dt	<dt	0.37	48.2	1.08	<dt	<dt	<dt	<dt	0.50	<dt	<dt	<dt	<dt	<dt	<dt	<dt	<dt	<dt	<dt	<dt	<dt	<dt	34.4	99.6
Z-100	SD7	0.97	<dt	0.70	12.4	<dt	0.42	<dt	<dt	0.04	1.17	36.6	1.04	<dt	<dt	0.36	0.16	5.65	<dt	0.06	<dt	<dt	<dt	<dt	<dt	0.43	0.16	0.59	0.11	1.01	0.15	30.2	92.3
Z-101	SD7	<dt	<dt	<dt	14.8	<dt	<dt	<dt	<dt	<dt	0.13	47.9	1.27	<dt	<dt	<dt	<dt	0.49	<dt	0.00	<dt	<dt	<dt	<dt	<dt	<dt	<dt	<dt	<dt	<dt	<dt	34.0	98.6
Z-102	SD7	<dt	<dt	<dt	14.5	<dt	<dt	<dt	<dt	<dt	0.12	46.6	1.44	<dt	<dt	0.27	0.40	0.89	<dt	-0.01	<dt	<dt	<dt	<dt	<dt	<dt	<dt	<dt	<dt	0.14	<dt	33.5	97.8
Z-103	SD7	0.96	<dt	0.18	13.8	0.07	0.29	<dt	<dt	<dt	0.41	42.6	1.85	<dt	<dt	0.33	0.17	1.54	0.88	1.02	0.17	0.64	0.12	0.13	<dt	<dt	<dt	0.13	<dt	0.12	<dt	32.5	97.9
Z-104	SD7	0.32	<dt	<dt	14.0	<dt	0.07	<dt	<dt	<dt	0.48	44.9	2.01	<dt	<dt	0.15	0.26	0.85	0.14	0.24	<dt	<dt	<dt	0.02	<dt	<dt	<dt	0.12	<dt	0.15	<dt	32.6	96.3
Z-105	SD27	0.43	<dt	0.20	14.0	<dt	0.14	0.04	<dt	<dt	0.26	44.3	1.33	<dt	<dt	<dt	0.16	2.26	<dt	<dt	<dt	<dt	<dt	<dt	<dt	0.13	<dt	0.26	<dt	0.45	<dt	32.8	96.7
Z-106	SD27	2.16	<dt	0.76	11.1	<dt	0.47	0.04	<dt	0.14	0.74	33.9	1.49	0.15	<dt	0.21	0.57	7.16	<dt	0.17	<dt	<dt	0.06	<dt	<dt	0.44	<dt	0.65	0.11	1.31	0.23	28.5	90.7
Z-107	SD27	<dt	<dt	<dt	14.6	<dt	0.03	<dt	<dt	<dt	0.11	46.4	1.70	<dt	<dt	0.10	0.23	0.78	<dt	<dt	<dt	<dt	<dt	<dt	<dt	<dt	<dt	<dt	<dt	0.14	<dt	33.5	97.7
Z-108	SD27	0.15	<dt	0.09	14.6	<dt	0.11	<dt	<dt	0.03	0.22	35.4	4.02	<dt	<dt	<dt	0.22	0.61	<dt	0.06	<dt	<dt	<dt	0.08	<dt	<dt	<dt	<dt	<dt	0.07	<dt	30.2	85.8
Z-109	SD27	<dt	<dt	0.02	15.1	<dt	<dt	<dt	<dt	<dt	0.13	36.7	2.18	<dt	<dt	<dt	<dt	0.40	<dt	<dt	<dt	<dt	<dt	0.08	<dt	<dt	<dt	<dt	<dt	<dt	<dt	30.7	85.2
Z-110	SD27	0.80	<dt	0.92	12.5	0.13	0.50	0.07	<dt	0.14	1.13	26.2	1.97	0.47	<dt	0.11	0.50	5.27	<dt	1.26	<dt	0.10	0.12	<dt	0.07	0.58	0.13	0.52	<dt	0.84	0.14	27.6	82.1
Z-111	SD27	0.69	<dt	0.79	13.0	0.11	0.70	0.04	<dt	0.34	0.41	29.2	2.14	0.28	<dt	<dt	0.45	3.49	<dt	0.83	<dt	<dt	0.08	<dt	<dt	0.34	<dt	0.38	0.07	0.57	<dt	28.3	82.3
Z-112	SD27	0.91	<dt	0.93	12.5	0.18	0.56	0.07	0.05	0.12	1.14	26.1	2.16	0.44	<dt	0.19	0.40	4.97	<dt	1.14	<dt	0.11	0.10	0.07	<dt	0.55	<dt	0.58	0.10	0.94	0.15	27.51	82.0
Z-113	SD27	<dt	<dt	<dt	14.8	<dt	<dt	<dt	<dt	<dt	0.04	38.6	1.31	<dt	<dt	<dt	<dt	0.29	<dt	<dt	<dt	<dt	<dt	<dt	<dt	<dt	<dt	<dt	<dt	<dt	<dt	28.2	83.3
Z-114	SD27	<dt	<dt	<dt	14.8	0.03	<dt	<dt	<dt	<dt	0.19	39.0	1.35	<dt	<dt	<dt	<dt	0.36	<dt	<dt	<dt	<dt	<dt	<dt	<dt	<dt	<dt	<dt	<dt	<dt	<dt	31.2	86.8
Z-115	SD27	0.78	<dt	0.63	12.5	0.13	0.52	0.09	<dt	0.09	1.54	29.6	2.15	<dt	<dt	<dt	0.84	3.50	<dt	0.00	<dt	0.22	0.12	0.21	<dt	0.28	<dt	0.25	<dt	0.26	<dt	31.1	84.8
Z-116	SD27	0.51	<dt	0.75	13.1	<dt	0.82	<dt	<dt	0.27	0.33	31.5	1.53	<dt	<dt	<dt	0.61	2.41	<dt	0.20	<dt	0.15	0.11	0.17	<dt	0.15	<dt	0.15	<dt	0.17	<dt	30.6	83.5

#	Sample	F wt %	Cl wt %	Al wt %	Si wt %	P wt %	Ca wt %	K wt %	Ti wt %	Mn wt %	Fe wt %	Zr wt %	Hf wt %	Nb wt %	Ta wt %	Th wt %	U wt %	Y wt %	La wt %	Ce wt %	Pr wt %	Nd wt %	Sm wt %	Gd wt %	Tb wt %	Dy wt %	Ho wt %	Er wt %	Tm wt %	Yb wt %	Lu wt %	O wt %	Total
Z-116	SD27	0.51	<dt	0.75	13.1	<dt	0.82	<dt	<dt	0.27	0.33	31.5	1.53	<dt	<dt	<dt	0.61	2.41	<dt	0.20	<dt	0.15	0.11	0.17	<dt	0.15	<dt	0.15	<dt	0.17	<dt	30.6	83.5
Z-117	SD27	0.21	<dt	0.35	12.1	0.09	0.24	<dt	0.09	0.05	6.44	28.0	1.62	0.20	<dt	<dt	0.22	1.19	<dt	0.11	<dt	<dt	<dt	<dt	<dt	<dt	<dt	0.13	<dt	0.16	<dt	27.7	78.9
Z-118	SD27	<dt	<dt	<dt	14.7	0.06	<dt	<dt	<dt	<dt	0.07	37.2	2.96	<dt	<dt	<dt	0.15	0.32	<dt	<dt	<dt	<dt	<dt	0.13	<dt	<dt	<dt	<dt	<dt	<dt	<dt	28.4	84.0
Z-119	SD27	0.64	<dt	0.71	12.2	0.16	0.55	0.09	0.04	0.05	3.04	28.3	0.93	0.41	<dt	0.16	0.65	4.37	<dt	0.59	<dt	0.07	0.14	0.13	<dt	0.43	<dt	0.46	0.06	0.48	0.08	26.8	81.5
Z-120	SD27	<dt	<dt	0.19	14.3	0.08	0.15	<dt	<dt	<dt	0.71	36.6	1.47	<dt	<dt	<dt	0.24	1.10	<dt	0.13	<dt	<dt	<dt	0.10	<dt	0.13	<dt	<dt	<dt	0.18	<dt	27.8	83.2
Z-121	SD27	<dt	<dt	<dt	14.8	0.04	<dt	<dt	<dt	<dt	0.42	38.7	1.27	<dt	<dt	<dt	<dt	0.37	<dt	<dt	<dt	<dt	<dt	0.05	<dt	<dt	<dt	<dt	<dt	<dt	<dt	30.3	86.0
Z-122	SD27	0.55	<dt	0.67	13.0	0.10	0.64	0.06	<dt	0.18	0.50	31.5	1.15	0.29	<dt	<dt	0.52	2.88	<dt	<dt	<dt	0.13	0.10	0.10	<dt	0.27	<dt	0.28	<dt	0.23	<dt	30.9	84.2
Z-123	SD27	0.14	<dt	0.20	14.1	0.08	0.14	<dt	0.05	<dt	0.37	36.3	1.20	0.14	<dt	<dt	0.19	0.97	<dt	<dt	<dt	<dt	<dt	0.12	<dt	<dt	<dt	<dt	<dt	0.11	<dt	28.4	82.5
Z-124	SD27	<dt	<dt	<dt	15.0	0.05	<dt	<dt	<dt	<dt	0.11	38.5	1.09	<dt	<dt	<dt	<dt	0.38	<dt	<dt	<dt	<dt	<dt	<dt	<dt	<dt	<dt	<dt	<dt	<dt	<dt	29.9	85.0
Z-125	SD27	<dt	<dt	<dt	14.8	<dt	<dt	0.03	<dt	<dt	0.44	38.1	1.43	<dt	<dt	<dt	<dt	0.33	<dt	<dt	<dt	<dt	<dt	<dt	<dt	<dt	<dt	<dt	<dt	<dt	<dt	31.0	86.1
Z-126	SD27	<dt	<dt	<dt	14.9	0.03	<dt	<dt	<dt	<dt	0.28	37.8	1.12	<dt	<dt	<dt	<dt	0.37	<dt	<dt	<dt	<dt	<dt	<dt	<dt	<dt	<dt	<dt	<dt	<dt	<dt	30.7	85.2
Z-127	SD24	0.53	<dt	0.80	12.9	0.19	0.63	0.06	0.04	0.08	0.74	30.6	0.96	0.31	<dt	<dt	0.58	3.60	<dt	0.71	<dt	0.09	<dt	0.08	0.08	0.46	<dt	0.41	0.06	0.58	0.09	28.7	83.3
Z-128	SD24	0.74	<dt	0.85	12.7	0.16	0.60	0.07	0.05	0.07	0.97	28.7	1.17	0.41	<dt	0.09	0.66	4.59	<dt	0.96	<dt	0.10	0.11	0.10	0.09	0.54	<dt	0.42	0.08	0.62	0.10	28.3	83.4
Z-129	SD24	0.12	<dt	0.11	14.8	0.04	0.11	0.03	<dt	0.03	0.47	36.6	1.55	<dt	<dt	<dt	<dt	0.71	<dt	0.12	<dt	<dt	<dt	<dt	<dt	<dt	<dt	<dt	<dt	0.10	<dt	30.6	85.3
Z-130	SD24	<dt	<dt	<dt	14.3	0.03	0.03	<dt	<dt	<dt	0.19	46.0	1.62	<dt	<dt	<dt	<dt	0.38	<dt	<dt	<dt	<dt	<dt	<dt	<dt	<dt	<dt	<dt	<dt	<dt	<dt	32.9	95.5
Z-131	SD24	<dt	<dt	<dt	14.4	0.02	<dt	<dt	<dt	<dt	0.15	46.9	0.98	<dt	<dt	<dt	<dt	0.39	<dt	<dt	<dt	<dt	<dt	0.08	<dt	<dt	<dt	<dt	<dt	<dt	<dt	33.2	96.2
Z-132	SD24	<dt	<dt	<dt	14.4	0.08	<dt	<dt	<dt	<dt	0.12	45.7	1.25	<dt	<dt	0.19	0.37	0.64	<dt	<dt	<dt	<dt	<dt	0.08	<dt	<dt	<dt	0.14	<dt	0.07	<dt	33.1	96.1
Z-133	SD24	0.31	<dt	0.40	13.1	0.12	0.30	<dt	<dt	0.12	0.43	40.3	0.85	0.28	<dt	0.24	0.39	2.71	<dt	0.14	<dt	<dt	<dt	<dt	<dt	0.25	<dt	0.44	0.10	0.86	0.14	31.2	92.7
Z-134	SD24	<dt	<dt	<dt	14.7	0.03	<dt	<dt	<dt	<dt	0.07	46.7	1.18	<dt	<dt	<dt	0.14	0.46	<dt	<dt	<dt	<dt	<dt	<dt	<dt	<dt	<dt	<dt	<dt	<dt	<dt	33.5	96.8
Z-135	SD24	0.72	<dt	0.54	13.0	0.14	0.35	0.07	<dt	0.21	0.45	39.7	1.06	<dt	<dt	<dt	0.30	3.47	<dt	0.05	<dt	<dt	<dt	<dt	<dt	0.29	<dt	0.30	<dt	0.35	<dt	31.1	92.2
Z-136	SD24	<dt	<dt	<dt	14.4	0.03	<dt	<dt	<dt	<dt	0.09	46.4	1.12	<dt	<dt	<dt	<dt	0.40	<dt	<dt	<dt	<dt	<dt	<dt	<dt	<dt	<dt	<dt	<dt	<dt	<dt	33.0	95.3
Z-137	SD24	<dt	<dt	<dt	14.7	0.03	<dt	<dt	<dt	<dt	0.19	45.8	1.14	<dt	<dt	<dt	0.14	0.57	<dt	<dt	<dt	<dt	<dt	<dt	<dt	<dt	<dt	<dt	<dt	0.08	<dt	33.3	95.9
Z-138	SD24	<dt	<dt	<dt	14.4	0.04	<dt	<dt	<dt	<dt	0.14	46.2	1.08	<dt	<dt	<dt	<dt	0.41	<dt	<dt	<dt	<dt	<dt	<dt	<dt	<dt	<dt	<dt	<dt	<dt	<dt	32.9	95.2
Z-139	SD24	<dt	<dt	<dt	14.0	0.12	<dt	<dt	<dt	<dt	0.28	44.0	1.07	<dt	<dt	0.40	0.55	1.51	<dt	<dt	<dt	<dt	<dt	<dt	<dt	<dt	<dt	0.28	<dt	0.32	<dt	32.4	95.0
Z-140	SD24	<dt	<dt	<dt	14.1	0.15	<dt	<dt	<dt	<dt	0.39	43.4	1.09	<dt	<dt	0.46	0.62	1.50	<dt	<dt	<dt	<dt	<dt	<dt	<dt	<dt	<dt	0.22	<dt	0.34	<dt	32.4	94.6
Z-141	SD24	<dt	<dt	<dt	14.6	0.02	<dt	<dt	<dt	<dt	0.19	46.9	1.15	<dt	<dt	<dt	<dt	0.34	<dt	<dt	<dt	<dt	<dt	<dt	<dt	<dt	<dt	<dt	<dt	<dt	<dt	33.5	96.8
Z-142	SD24	0.32	<dt	0.10	13.4	0.10	0.14	<dt	<dt	<dt	0.23	43.1	1.20	0.14	<dt	0.22	0.41	1.25	<dt	<dt	<dt	<dt	<dt	<dt	<dt	<dt	<dt	0.18	<dt	0.29	<dt	31.5	92.7
Z-143	SD24	<dt	<dt	<dt	14.4	0.04	<dt	<dt	<dt	<dt	0.41	46.8	1.15	<dt	<dt	<dt	<dt	0.43	<dt	<dt	<dt	<dt	<dt	<dt	<dt	<dt	<dt	<dt	<dt	<dt	<dt	33.3	96.6
Z-144	SD24	<dt	<dt	<dt	14.5	0.08	<dt	<dt	<dt	<dt	0.39	45.5	1.06	<dt	<dt	0.50	0.62	1.04	<dt	<dt	<dt	<dt	<dt	0.09	<dt	<dt	<dt	<dt	<dt	0.22	<dt	33.3	97.2
Z-145	SD24	<dt	<dt	<dt	14.3	0.06	<dt	<dt	<dt	<dt	0.36	45.3	0.97	<dt	<dt	0.31	0.36	1.09	<dt	<dt	<dt	<dt	<dt	<dt	<dt	<dt	<dt	<dt	<dt	0.20	<dt	33.0	95.9
Z-146	SD24	<dt	<dt	<dt	14.5	0.02	<dt	<dt	<dt	<dt	0.41	46.9	1.10	<dt	<dt	<dt	<dt	0.40	<dt	<dt	<dt	<dt	<dt	<dt	<dt	<dt	<dt	<dt	<dt	<dt	<dt	33.5	96.8
Z-147	SD24	<dt	<dt	0.06	14.7	0.06	<dt	<dt	<dt	<dt	0.56	47.4	1.26	<dt	<dt	<dt	<dt	0.56	<dt	<dt	<dt	<dt	<dt	<dt	<dt	<dt	<dt	<dt	<dt	0.07	<dt	34.1	98.8
Z-148	SD24	0.16	<dt	0.25	14.9	0.05	0.14	0.10	<dt	<dt	0.52	49.2	1.48	<dt	<dt	<dt	<dt	1.18	<dt	0.06	<dt	<dt	<dt	0.04	<dt	<dt	<dt	0.20	<dt	0.12	<dt	35.4	103.8
Z-149	SD24	0.22	<dt	0.26	14.1	0.10	0.22	<dt	<dt	0.11	0.31	44.1	1.55	<dt	<dt	<dt	0.16	1.75	<dt	0.29	<dt	<dt	<dt	<dt	<dt	<dt	<dt	0.24	<dt	0.43	0.07	33.0	96.9
Z-150	SD24	<dt	<dt	<dt	14.6	<dt	<dt	<dt	<dt	<dt	0.23	48.2	1.32	<dt	<dt	<dt	0.15	0.33	<dt	<dt	<dt	<dt	<dt	<dt	<dt	<dt	<dt	<dt	<dt	<dt	<dt	34.0	98.8
Z-151	SD24	<dt	<dt	<dt	14.4	0.18	<dt	<dt	<dt	<dt	0.25	45.6	1.59	<dt	<dt	0.14	0.53	1.05	<dt	<dt	<dt	<dt	<dt	<dt	<dt	<dt	<dt	0.17	<dt	0.25	<dt	33.4	97.5
Z-152	SD24	<dt	<dt	<dt	14.2	0.20	<dt	<dt	<dt	<dt	0.23	45.3	1.36	<dt	<dt	0.31	0.66	1.15	<dt	<dt	<dt	<dt	<dt	0.10	<dt	<dt	<dt	0.16	<dt	0.28	<dt	33.1	96.9
Z-153	SD24	<dt	<dt	<dt	14.2	0.03	<dt	<dt	<dt	<dt	0.50	46.6	1.30	<dt	<dt	<dt	<dt	0.45	<dt	<dt	<dt	<dt	<dt	<dt	<dt	<dt	<dt	<dt	<dt	0.07	<dt	33.1	96.3
Z-154	SD24	<dt	<dt	<dt	14.8	0.03	<dt	<dt	<dt	<dt	0.05	47.9	0.93	<dt	<dt	<dt	<dt	0.52	<dt	<dt	<dt	<dt	<dt	<dt	<dt	<dt	<dt	<dt	<dt	0.06	<dt	34.0	98.2
Z-155	SD8	<dt	<dt	<dt	14.7	0.05	<dt	<dt	<dt	<dt	0.10	48.0	0.84	<dt	<dt	<dt	<dt	0.57	<dt	-0.01	<dt	<dt	<dt	<dt	<dt	<dt	<dt	<dt	<dt	<dt	<dt	34.0	98.2
Z-156	SD8	<dt	<dt	<dt	14.7	0.03	<dt	<dt	<dt	<dt	0.09	47.9	1.06	<dt	<dt	<dt	<dt	0.42	<dt	0.00	<dt	<dt	<dt	0.08	<dt	<dt	<dt	<dt	<dt	<dt	<dt	33.9	98.1
Z-157	SD8	<dt	<dt	<dt	14.5	0.03	<dt	<dt	<dt	<dt	0.13	47.8	0.87	<dt	<dt	<dt	0.00	0.49	<dt	<dt	<dt	<dt	<dt	<dt	<dt	<dt	<dt	<dt	<dt	<dt	<dt	33.6	97.4
Z-158	SD8	<dt	<dt	<dt	14.7	0.04	<dt	<dt	<dt	<dt	0.09	47.6	0.89	<dt	<dt	<dt	<dt	0.55	<dt	<dt	<dt	<dt	<dt	0.04	<dt	<dt	<dt	<dt	<dt	<dt	<dt	33.8	97.7
Z-159	SD8	<dt	<dt	<dt	14.9	0.03	<dt	<dt	<dt	<dt	0.05	48.2	1.03	<dt	<dt	<dt	<dt	0.41	<dt	<dt	<dt	<dt	<dt	<dt	<dt	<dt	<dt	<dt	<dt	<dt	<dt	34.2	98.8
Z-160	SD8	<dt	<dt	<dt	14.8	<dt	<dt	<dt	<dt	<dt	<dt	47.4	1.07	<dt	<dt	<dt	<dt	0.48	<dt	<dt	0.08	<dt	<dt	<dt	<dt	<dt	<dt	<dt	<dt	<dt	<dt	33.8	97.6
Z-161	SD8	0.96	<dt	0.29	12.8	0.23	0.34	0.03	<dt	<dt	1.55	39.3	1.50	0.20	<dt	<dt	<dt	4.06	<dt	<dt	<dt	<dt	<dt	<dt	n.a	n.a	n.a	n.a	n.a	n.a	n.a	30.9	92.2
Z-162	SD8	1.04	<dt	0.26	13.1	0.17	0.31	0.04	<dt	<dt	1.41	40.5	1.46	0.19	<dt	<dt	0.14	3.78	<dt	<dt	<dt	<dt	<dt	<dt	n.a	n.a	n.a	n.a	n.a	n.a	n.a	31.4	93.8
Z-163	SD8	<dt	<dt	<dt	14.8	0.06	<dt	<dt	<dt	<dt	0.10	48.0	2.02	<dt	<dt	<dt	<dt	0.39	<dt	<dt	<dt	<dt	<dt	<dt	n.a	n.a	n.a	n.a	n.a	n.a	n.a	34.4	99.9
Z-164	SD8	<dt	<dt	0.17	14.4	<dt	<dt	0.03	<dt	<dt	4.09	46.4	1.68	<dt	<dt	<dt	<dt	0.52	<dt	<dt	<dt	<dt	<dt	<dt	n.a	n.a	n.a	n.a	n.a	n.a	n.a	34.6	102.0
Z-165	SD8	<dt	<dt	<dt	14.9	<dt	<dt	<dt	<dt	<dt	0.08	48.9	0.93	<dt	<dt	<dt	<dt	0.38	<dt	<dt	<dt	<dt	<dt	<dt	n.a	n.a	n.a	n.a	n.a	n.a	n.a	34.5	99.7
Z-166	SD8	<dt	<dt	<dt	14.6	0.04	<dt	0.04	<dt	<dt	0.35	48.3	1.47	<dt	<dt	<dt	<dt	0.34	<dt	<dt	<dt	<dt	<dt	<dt	n.a	n.a	n.a	n.a	n.a	n.a	n.a	34.2	99.3

#	Sample	F wt %	Cl wt %	Al wt %	Si wt %	P wt %	Ca wt %	K wt %	Ti wt %	Mn wt %	Fe wt %	Zr wt %	Hf wt %	Nb wt %	Ta wt %	Th wt %	U wt %	Y wt %	La wt %	Ce wt %	Pr wt %	Nd wt %	Sm wt %	Gd wt %	Tb wt %	Dy wt %	Ho wt %	Er wt %	Tm wt %	Yb wt %	Lu wt %	O wt %	Total
Z-166	SD8	<dt	<dt	<dt	14.6	0.04	<dt	0.04	<dt	<dt	0.35	48.3	1.47	<dt	<dt	<dt	<dt	0.34	<dt	<dt	<dt	<dt	<dt	<dt	n.a	n.a	n.a	n.a	n.a	n.a	n.a	34.2	99.3
Z-167	SD8	<dt	<dt	<dt	14.9	0.03	<dt	<dt	<dt	<dt	0.12	48.3	1.28	<dt	<dt	<dt	<dt	0.38	<dt	<dt	<dt	<dt	<dt	<dt	n.a	n.a	n.a	n.a	n.a	n.a	n.a	34.3	99.3
Z-168	SD8	<dt	<dt	<dt	14.7	0.06	<dt	<dt	<dt	<dt	0.14	47.3	1.28	<dt	<dt	0.15	0.27	0.60	<dt	<dt	<dt	<dt	<dt	<dt	n.a	n.a	n.a	n.a	n.a	n.a	n.a	34.0	98.6
Z-169	SD8	<dt	<dt	<dt	14.8	0.03	<dt	<dt	<dt	<dt	0.34	47.5	1.25	<dt	<dt	<dt	<dt	0.50	<dt	<dt	<dt	<dt	<dt	<dt	n.a	n.a	n.a	n.a	n.a	n.a	n.a	34.1	98.5
Z-170	SD8	<dt	<dt	<dt	14.7	0.04	<dt	<dt	<dt	<dt	0.21	48.1	0.94	<dt	<dt	0.10	<dt	0.52	<dt	<dt	<dt	<dt	<dt	<dt	n.a	n.a	n.a	n.a	n.a	n.a	n.a	34.2	98.8
Z-171	SD8	<dt	<dt	<dt	14.9	0.02	<dt	<dt	<dt	<dt	0.16	48.2	1.14	<dt	<dt	<dt	<dt	0.43	<dt	<dt	<dt	<dt	<dt	<dt	n.a	n.a	n.a	n.a	n.a	n.a	n.a	34.3	99.2
Z-172	SD8	<dt	<dt	<dt	14.6	<dt	<dt	<dt	<dt	<dt	0.05	47.8	1.32	<dt	<dt	<dt	<dt	0.35	<dt	<dt	<dt	<dt	<dt	<dt	<dt	<dt	<dt	<dt	<dt	<dt	<dt	33.8	97.9
Z-173	SD8	<dt	<dt	<dt	14.8	0.03	<dt	<dt	<dt	<dt	0.07	47.6	1.53	<dt	<dt	<dt	<dt	0.34	<dt	<dt	<dt	<dt	<dt	<dt	<dt	<dt	<dt	<dt	<dt	<dt	<dt	33.9	98.3
Z-174	SD8	<dt	<dt	<dt	14.8	<dt	<dt	<dt	<dt	<dt	0.34	48.0	1.27	<dt	<dt	<dt	<dt	0.49	<dt	<dt	<dt	<dt	<dt	<dt	<dt	<dt	<dt	<dt	<dt	<dt	<dt	34.2	99.1
Z-175	SD8	0.14	<dt	0.48	14.5	0.07	0.22	<dt	<dt	<dt	0.27	44.2	1.54	<dt	<dt	<dt	<dt	0.63	0.82	1.52	0.12	0.37	<dt	0.07	n.a	n.a	n.a	n.a	n.a	n.a	n.a	33.8	98.8
Z-176	SD8	<dt	<dt	<dt	14.9	<dt	<dt	<dt	<dt	<dt	0.29	49.0	1.63	<dt	<dt	<dt	<dt	0.36	<dt	0.04	<dt	<dt	<dt	<dt	n.a	n.a	n.a	n.a	n.a	n.a	n.a	34.8	101.0
Z-177	SD8	<dt	<dt	<dt	14.6	<dt	<dt	<dt	<dt	<dt	0.19	48.1	1.73	<dt	<dt	<dt	0.08	0.38	<dt	<dt	<dt	<dt	<dt	0.03	n.a	n.a	n.a	n.a	n.a	n.a	n.a	34.0	99.1
Z-178	SD8	1.02	<dt	0.81	12.1	0.15	0.62	<dt	<dt	<dt	2.36	33.7	2.24	<dt	<dt	<dt	0.29	4.92	<dt	0.08	<dt	<dt	<dt	<dt	<dt	0.44	<dt	0.76	0.11	1.22	0.20	29.7	90.9
Z-179	SD8	<dt	<dt	<dt	14.9	<dt	<dt	<dt	<dt	<dt	0.09	48.4	1.43	<dt	<dt	<dt	<dt	0.37	<dt	<dt	<dt	<dt	<dt	<dt	n.a	n.a	n.a	n.a	n.a	n.a	n.a	34.4	99.7
Z-180	SD8	0.90	<dt	0.82	11.9	0.16	0.60	<dt	<dt	<dt	2.60	33.5	2.21	<dt	<dt	<dt	0.23	4.88	<dt	0.10	<dt	<dt	<dt	<dt	<dt	0.40	0.16	0.65	0.11	1.18	0.17	29.4	90.0
Z-181	SD8	<dt	<dt	0.03	14.5	0.17	0.08	<dt	<dt	<dt	0.23	47.2	1.48	0.09	<dt	<dt	<dt	0.87	<dt	<dt	<dt	<dt	<dt	<dt	<dt	<dt	<dt	<dt	<dt	<dt	0.17	<dt	34.0	98.8
Z-182	SD8	<dt	<dt	<dt	14.8	0.03	<dt	<dt	<dt	<dt	0.25	48.2	0.96	<dt	<dt	<dt	<dt	0.49	<dt	<dt	<dt	<dt	<dt	<dt	n.a	n.a	n.a	n.a	n.a	n.a	n.a	34.2	98.9
Z-183	SD8	<dt	<dt	<dt	14.7	0.05	<dt	<dt	<dt	<dt	0.38	47.4	1.36	<dt	<dt	<dt	<dt	0.43	<dt	<dt	<dt	<dt	<dt	<dt	<dt	<dt	<dt	<dt	<dt	<dt	<dt	33.9	98.2
Z-184	SD8	<dt	<dt	<dt	14.9	<dt	0.03	<dt	<dt	<dt	0.07	48.6	1.41	<dt	<dt	<dt	<dt	0.46	<dt	<dt	<dt	<dt	<dt	<dt	n.a	n.a	n.a	n.a	n.a	n.a	n.a	34.5	100.0
Z-185	SD8	0.31	<dt	0.13	14.8	0.12	0.12	<dt	<dt	<dt	0.73	46.7	1.22	<dt	<dt	<dt	<dt	0.83	0.05	<dt	<dt	<dt	<dt	<dt	<dt	<dt	<dt	<dt	<dt	0.12	<dt	34.3	99.4
Z-186	SD8	<dt	<dt	<dt	14.8	0.02	<dt	<dt	<dt	<dt	<dt	48.0	1.49	<dt	<dt	<dt	<dt	0.35	<dt	<dt	<dt	<dt	<dt	0.06	<dt	<dt	<dt	<dt	<dt	<dt	<dt	34.2	99.0
Z-187	SD8	<dt	<dt	<dt	14.8	0.03	<dt	<dt	<dt	<dt	<dt	47.9	1.33	<dt	<dt	<dt	<dt	0.40	<dt	<dt	<dt	<dt	<dt	<dt	<dt	<dt	<dt	<dt	<dt	<dt	<dt	34.1	98.7
Z-188	SD8	<dt	<dt	<dt	14.9	0.03	<dt	<dt	<dt	<dt	0.06	49.0	1.46	<dt	<dt	<dt	<dt	0.35	<dt	0.02	<dt	<dt	<dt	<dt	n.a	n.a	n.a	n.a	n.a	n.a	n.a	34.7	100.5
Z-189	SD8	<dt	<dt	<dt	14.7	0.07	<dt	<dt	<dt	<dt	0.09	47.9	2.49	<dt	<dt	<dt	<dt	0.40	<dt	0.00	<dt	<dt	<dt	<dt	n.a	n.a	n.a	n.a	n.a	n.a	n.a	34.3	99.9
Z-190	SD8	<dt	<dt	<dt	14.6	0.05	<dt	<dt	<dt	<dt	0.08	48.3	0.87	<dt	<dt	<dt	<dt	0.66	<dt	<dt	<dt	<dt	<dt	<dt	n.a	n.a	n.a	n.a	n.a	n.a	n.a	34.1	98.6
Z-191	SD8	<dt	<dt	<dt	14.9	<dt	<dt	<dt	<dt	<dt	0.07	48.9	1.41	<dt	<dt	<dt	<dt	0.35	<dt	<dt	<dt	<dt	<dt	<dt	n.a	n.a	n.a	n.a	n.a	n.a	n.a	34.6	100.3
Z-192	SD8	<dt	<dt	<dt	14.8	<dt	<dt	<dt	<dt	<dt	<dt	47.8	1.21	<dt	<dt	<dt	<dt	0.37	<dt	<dt	<dt	<dt	<dt	<dt	n.a	n.a	n.a	n.a	n.a	n.a	n.a	34.0	98.2
Z-193	SD8	<dt	<dt	<dt	14.8	0.03	<dt	<dt	<dt	<dt	<dt	47.7	1.94	<dt	<dt	<dt	<dt	0.35	<dt	<dt	<dt	<dt	<dt	<dt	<dt	<dt	<dt	<dt	<dt	<dt	<dt	34.0	98.8
Z-194	SD8	<dt	<dt	<dt	15.0	0.03	<dt	<dt	<dt	<dt	0.03	48.7	1.20	<dt	<dt	<dt	0.22	0.37	<dt	<dt	<dt	<dt	<dt	<dt	<dt	<dt	<dt	<dt	<dt	<dt	<dt	34.5	100.0
Z-195	SD8	<dt	<dt	<dt	14.7	0.06	0.04	<dt	<dt	<dt	0.25	47.0	1.20	<dt	<dt	0.28	0.20	0.75	<dt	<dt	<dt	<dt	0.00	<dt	<dt	<dt	<dt	0.13	<dt	0.10	<dt	33.9	98.7
Z-196	SD8	1.41	<dt	0.27	11.6	0.83	0.58	<dt	0.10	<dt	0.44	38.2	0.65	0.43	<dt	0.21	<dt	3.78	<dt	<dt	<dt	<dt	<dt	0.11	n.a	n.a	n.a	n.a	n.a	n.a	n.a	29.7	88.2
Z-197	SD8	<dt	<dt	<dt	14.4	0.06	<dt	<dt	<dt	<dt	0.09	46.1	1.16	<dt	<dt	1.59	1.42	0.45	<dt	<dt	<dt	<dt	<dt	-0.02	<dt	<dt	<dt	<dt	<dt	0.07	<dt	33.4	98.7
Z-198	SD8	<dt	<dt	<dt	14.6	0.07	0.04	<dt	<dt	<dt	0.09	47.5	1.20	<dt	<dt	0.41	0.46	0.54	<dt	<dt	<dt	<dt	<dt	<dt	<dt	<dt	<dt	<dt	<dt	0.13	<dt	33.9	98.9
Z-199	SD8	<dt	<dt	<dt	14.9	0.03	<dt	<dt	<dt	<dt	0.14	48.1	1.34	<dt	<dt	<dt	<dt	0.41	<dt	<dt	<dt	<dt	<dt	<dt	n.a	n.a	n.a	n.a	n.a	n.a	n.a	34.3	99.1
Z-200	SD8	<dt	<dt	<dt	14.7	0.10	<dt	<dt	<dt	<dt	0.18	47.2	1.36	<dt	<dt	0.19	0.45	0.95	<dt	-0.02	<dt	<dt	<dt	<dt	n.a	n.a	n.a	n.a	n.a	n.a	n.a	34.1	99.1
Z-201	SD8	<dt	<dt	<dt	14.3	0.17	<dt	<dt	<dt	<dt	0.26	46.0	1.51	<dt	<dt	0.22	0.69	1.12	<dt	<dt	<dt	<dt	<dt	<dt	n.a	n.a	n.a	n.a	n.a	n.a	n.a	33.5	97.9
Z-202	SD8	<dt	<dt	0.18	14.5	0.18	0.07	<dt	<dt	<dt	0.18	44.2	1.06	<dt	<dt	<dt	0.36	1.21	<dt	<dt	<dt	<dt	<dt	0.02	n.a	n.a	n.a	n.a	n.a	n.a	n.a	33.1	95.1
Z-203	SD8	<dt	<dt	<dt	14.8	<dt	<dt	<dt	<dt	<dt	0.12	47.8	1.41	<dt	<dt	<dt	<dt	0.53	0.08	0.15	<dt	<dt	<dt	<dt	n.a	n.a	n.a	n.a	n.a	n.a	n.a	34.2	99.1
Z-204	SD8	<dt	<dt	<dt	14.8	0.04	<dt	<dt	<dt	<dt	0.11	48.0	0.87	<dt	<dt	<dt	<dt	0.40	<dt	<dt	<dt	<dt	<dt	<dt	<dt	<dt	<dt	<dt	<dt	<dt	<dt	34.1	98.4
Z-205	SD9	<dt	<dt	<dt	14.8	0.03	<dt	<dt	<dt	<dt	0.13	47.8	1.02	<dt	<dt	<dt	<dt	0.46	<dt	0.00	<dt	<dt	<dt	<dt	<dt	<dt	<dt	<dt	<dt	<dt	<dt	34.0	98.1
Z-206	SD9	<dt	<dt	<dt	14.8	0.06	<dt	<dt	0.03	<dt	0.29	47.9	1.24	<dt	<dt	0.14	0.20	0.56	<dt	<dt	<dt	<dt	<dt	<dt	n.a	n.a	n.a	n.a	n.a	n.a	n.a	34.3	99.6
Z-207	SD9	<dt	<dt	<dt	14.7	0.04	<dt	<dt	<dt	<dt	0.11	48.0	1.19	<dt	<dt	<dt	<dt	0.43	<dt	<dt	<dt	<dt	<dt	<dt	<dt	<dt	<dt	<dt	<dt	<dt	<dt	34.0	98.5
Z-208	SD9	0.95	<dt	0.88	12.9	0.17	0.71	0.05	<dt	0.38	0.26	30.7	1.24	0.09	<dt	0.20	0.44	3.93	<dt	0.27	<dt	<dt	<dt	<dt	<dt	0.37	<dt	0.33	<dt	0.43	0.06	28.48	82.9
Z-209	SD9	<dt	<dt	<dt	14.9	<dt	<dt	<dt	<dt	<dt	<dt	39.3	1.23	<dt	<dt	<dt	<dt	0.38	<dt	<dt	<dt	<dt	<dt	<dt	<dt	<dt	<dt	<dt	<dt	<dt	<dt	31.06	86.9
Z-210	SD9	<dt	<dt	<dt	15.2	0.03	<dt	<dt	<dt	<dt	0.09	39.2	1.26	<dt	<dt	<dt	<dt	0.37	<dt	<dt	<dt	<dt	<dt	<dt	<dt	<dt	<dt	<dt	<dt	<dt	<dt	31.33	87.4
Z-211	SD9	0.37	<dt	0.34	14.0	0.07	0.26	0.04	<dt	0.12	0.12	35.5	1.11	<dt	<dt	<dt	0.25	1.85	<dt	0.16	<dt	<dt	<dt	<dt	<dt	0.21	<dt	0.31	<dt	0.41	<dt	29.84	85.0
Z-212	SD9	0.78	<dt	0.77	13.3	0.14	0.68	<dt	<dt	0.46	0.35	30.5	0.83	0.14	<dt	0.12	0.61	4.04	<dt	0.32	<dt	<dt	<dt	<dt	<dt	0.39	0.15	0.46	0.07	0.78	0.12	28.8	83.8
Z-213	SD9	<dt	<dt	<dt	14.9	0.04	<dt	<dt	<dt	<dt	0.26	39.4	0.92	<dt	<dt	<dt	<dt	0.44	<dt	<dt	<dt	<dt	<dt	<dt	<dt	<dt	<dt	<dt	<dt	<dt	<dt	31.06	87.0
Z-214	SD9	<dt	<dt	<dt	14.8	0.05	<dt	<dt	<dt	<dt	0.24	38.5	1.01	<dt	<dt	<dt	<dt	0.46	<dt	<dt	<dt	<dt	<dt	<dt	<dt	<dt	<dt	<dt	<dt	<dt	<dt	30.68	85.7
Z-215	SD9	<dt	<dt	<dt	15.0	0.05	<dt	<dt	<dt	<dt	0.25	38.7	1.00	<dt	<dt	<dt	<dt	0.38	<dt	<dt	<dt	<dt	<dt	<dt	<dt	<dt	<dt	<dt	<dt	0.06	<dt	31.05	86.5

#	Sample	F	Cl	Al	Si	P	Ca	K	Ti	Mn	Fe	Zr	Hf	Nb	Ta	Th	U	Y	La	Ce	Pr	Nd	Sm	Gd	Tb	Dy	Ho	Er	Tm	Yb	Lu	O	Total
		wt %	wt %	wt %	wt %	wt %	wt %	wt %	wt %	wt %	wt %	wt %	wt %	wt %	wt %	wt %	wt %	wt %	wt %	wt %	wt %	wt %	wt %	wt %	wt %	wt %	wt %	wt %	wt %	wt %	wt %	wt %	
Z-216	SD9	<dt	<dt	<dt	15.1	0.04	<dt	<dt	<dt	<dt	0.57	38.9	1.48	<dt	<dt	<dt	<dt	0.30	<dt	<dt	<dt	<dt	<dt	<dt	<dt	<dt	<dt	<dt	<dt	<dt	<dt	31.34	87.7
Z-217	SD9	<dt	<dt	0.16	14.4	0.07	0.17	<dt	<dt	0.05	0.42	35.9	1.82	0.08	<dt	<dt	0.22	1.31	<dt	0.09	<dt	<dt	<dt	<dt	<dt	<dt	<dt	<dt	<dt	0.22	<dt	30.11	84.9
Z-218	SD9	1.47	<dt	0.93	12.2	0.18	0.69	0.07	<dt	0.30	0.14	29.1	0.91	<dt	<dt	0.18	0.82	5.56	<dt	0.89	0.08	<dt	0.07	<dt	<dt	0.63	<dt	0.59	0.08	0.80	0.10	27.76	83.6
Z-219	SD9	<dt	<dt	<dt	14.7	0.04	0.06	<dt	<dt	<dt	0.04	38.1	1.29	<dt	<dt	<dt	<dt	0.62	<dt	0.00	<dt	<dt	<dt	<dt	<dt	<dt	<dt	<dt	<dt	<dt	<dt	30.57	85.4
Z-220	SD9	1.62	<dt	1.09	11.0	0.43	0.99	0.08	<dt	0.36	2.71	23.6	0.83	0.36	<dt	0.31	0.83	5.62	0.06	0.86	<dt	0.24	0.13	<dt	0.08	0.69	0.20	0.63	0.08	0.77	0.08	26	79.7
Z-221	SD9	<dt	<dt	<dt	14.9	0.05	0.05	<dt	<dt	<dt	0.04	38.3	1.21	<dt	<dt	<dt	<dt	0.46	<dt	<dt	<dt	<dt	<dt	<dt	<dt	<dt	<dt	<dt	<dt	0.11	<dt	30.79	85.9
Z-222	SD9	3.99	<dt	0.71	7.5	2.06	2.32	0.07	0.07	0.03	1.78	17.1	<dt	0.27	<dt	13.06	0.87	7.41	4.99	3.51	0.67	1.24	0.32	0.46	n.a	n.a	n.a	n.a	n.a	n.a	n.a	47.6	116.1
Z-223	SD9	<dt	<dt	0.04	14.6	0.05	0.06	<dt	<dt	0.03	0.05	47.3	1.31	<dt	<dt	<dt	0.16	0.63	<dt	<dt	<dt	<dt	<dt	<dt	n.a	n.a	n.a	n.a	n.a	n.a	n.a	46.3	110.6
Z-224	SD9	0.84	<dt	0.76	13.1	0.09	0.65	0.07	<dt	0.34	0.05	41.4	1.77	0.12	<dt	<dt	0.75	2.45	<dt	<dt	<dt	0.10	0.06	0.13	n.a	n.a	n.a	n.a	n.a	n.a	n.a	12.4	75.0
Z-225	SD9	<dt	<dt	<dt	14.7	<dt	<dt	<dt	<dt	<dt	0.09	46.1	3.71	<dt	<dt	<dt	<dt	0.38	<dt	<dt	<dt	<dt	<dt	<dt	n.a	n.a	n.a	n.a	n.a	n.a	n.a	36.4	101.3
Z-226	SD9	1.31	<dt	0.69	13.0	0.11	0.70	<dt	<dt	0.26	0.23	41.1	1.26	0.17	<dt	0.19	0.76	2.68	<dt	0.08	<dt	0.08	0.06	0.13	n.a	n.a	n.a	n.a	n.a	n.a	n.a	21.2	84.0
Z-227	SD9	0.24	<dt	0.23	13.8	0.12	0.21	<dt	<dt	0.04	0.08	41.4	5.03	0.08	<dt	<dt	0.30	1.58	<dt	0.17	<dt	<dt	<dt	0.09	n.a	n.a	n.a	n.a	n.a	n.a	n.a	21.2	84.6
Z-228	SD9	0.89	<dt	0.52	13.3	0.11	0.33	0.04	0.04	<dt	0.07	37.9	3.91	0.08	<dt	<dt	0.45	2.92	0.05	0.30	<dt	<dt	<dt	0.09	n.a	n.a	n.a	n.a	n.a	n.a	n.a	18.2	79.2
Z-229	SD9	<dt	<dt	0.05	14.6	0.06	0.13	<dt	<dt	0.03	<dt	47.3	1.41	<dt	<dt	<dt	<dt	0.67	<dt	<dt	<dt	<dt	<dt	<dt	n.a	n.a	n.a	n.a	n.a	n.a	n.a	22.1	86.3
Z-230	SD9	1.32	<dt	0.66	12.0	0.50	0.90	<dt	<dt	0.20	0.16	37.3	1.27	0.29	<dt	0.11	0.91	4.63	0.05	0.94	<dt	0.12	0.12	0.16	n.a	n.a	n.a	n.a	n.a	n.a	n.a	25.2	86.9
Z-231	SD9	1.25	<dt	0.78	11.8	0.29	0.84	0.04	<dt	0.36	0.14	35.9	1.29	0.38	<dt	0.73	0.78	4.50	0.05	0.58	<dt	0.10	0.11	0.20	n.a	n.a	n.a	n.a	n.a	n.a	n.a	33.8	94.0
Z-232	SD9	<dt	<dt	<dt	14.7	<dt	<dt	<dt	<dt	<dt	0.03	46.0	3.76	<dt	<dt	<dt	<dt	0.33	<dt	<dt	<dt	<dt	<dt	<dt	n.a	n.a	n.a	n.a	n.a	n.a	n.a	31.8	96.7
Z-233	SD9	0.81	<dt	0.61	13.0	0.09	0.70	<dt	<dt	0.36	0.06	41.2	1.13	<dt	<dt	0.14	0.62	2.83	<dt	0.07	<dt	<dt	0.07	0.11	n.a	n.a	n.a	n.a	n.a	n.a	n.a	22.2	84.1
Z-234	SD9	4.13	<dt	0.56	7.1	0.77	1.92	0.14	0.07	0.07	3.12	19.2	0.60	0.39	<dt	3.87	0.60	5.55	6.75	4.84	1.11	3.74	0.64	0.62	n.a	n.a	n.a	n.a	n.a	n.a	n.a	22.0	87.9
Z-235	SD9	<dt	<dt	<dt	14.8	<dt	<dt	<dt	<dt	<dt	0.07	48.1	1.46	<dt	<dt	<dt	0.14	0.45	<dt	<dt	<dt	<dt	<dt	<dt	n.a	n.a	n.a	n.a	n.a	n.a	n.a	40.5	105.6
Z-236	SD9	1.32	<dt	0.80	11.9	0.18	0.50	0.05	<dt	0.38	0.38	35.2	0.68	1.03	<dt	0.19	0.27	4.39	<dt	1.27	<dt	<dt	<dt	0.11	n.a	n.a	n.a	n.a	n.a	n.a	n.a	16.0	74.7
Z-237	SD9	0.55	<dt	0.55	13.5	0.08	0.49	0.05	<dt	0.22	0.53	42.7	1.21	0.09	<dt	<dt	0.33	2.30	<dt	0.07	<dt	<dt	<dt	<dt	n.a	n.a	n.a	n.a	n.a	n.a	n.a	40.6	103.3
Z-238	SD9	0.64	<dt	0.34	13.9	0.08	0.33	<dt	<dt	0.23	0.41	44.7	1.34	<dt	<dt	0.09	0.16	2.13	<dt	<dt	<dt	<dt	<dt	0.06	n.a	n.a	n.a	n.a	n.a	n.a	n.a	41.1	105.6
Z-239	SD9	0.21	<dt	0.35	13.4	0.06	0.27	0.03	<dt	0.12	0.44	42.6	1.39	0.21	<dt	<dt	0.26	1.84	<dt	0.23	<dt	<dt	0.06	<dt	n.a	n.a	n.a	n.a	n.a	n.a	n.a	42.0	103.5
Z-240	SD9	0.61	<dt	0.44	13.4	0.08	0.41	0.05	<dt	0.09	0.34	42.0	1.10	0.23	<dt	0.12	0.35	2.26	<dt	0.11	<dt	<dt	<dt	0.04	n.a	n.a	n.a	n.a	n.a	n.a	n.a	32.5	94.2
Z-241	SD9	<dt	<dt	<dt	14.9	<dt	<dt	<dt	<dt	<dt	0.18	47.9	1.30	<dt	<dt	<dt	<dt	0.33	<dt	<dt	<dt	<dt	<dt	<dt	n.a	n.a	n.a	n.a	n.a	n.a	n.a	14.0	78.6
Z-242	SD9	1.07	<dt	0.81	12.3	0.16	0.71	0.05	<dt	0.46	0.40	38.3	1.25	0.09	<dt	0.11	0.57	4.05	<dt	0.40	<dt	<dt	0.08	0.11	n.a	n.a	n.a	n.a	n.a	n.a	n.a	33.1	94.1
Z-243	SD9	1.05	<dt	0.40	13.7	0.09	0.41	0.03	<dt	0.21	0.27	44.8	1.63	<dt	<dt	<dt	0.30	1.94	<dt	0.17	<dt	<dt	<dt	0.06	n.a	n.a	n.a	n.a	n.a	n.a	n.a	31.9	97.0
Z-244	SD9	<dt	<dt	<dt	14.7	<dt	<dt	<dt	<dt	<dt	0.07	48.2	1.43	<dt	<dt	<dt	<dt	0.40	<dt	<dt	<dt	<dt	<dt	<dt	n.a	n.a	n.a	n.a	n.a	n.a	n.a	26.9	91.7
Z-245	SD9	1.35	<dt	0.96	11.6	0.20	0.67	0.06	<dt	0.18	0.34	34.3	1.14	<dt	<dt	0.44	0.76	5.91	<dt	0.46	<dt	0.17	0.13	0.23	n.a	n.a	n.a	n.a	n.a	n.a	n.a	29.3	88.2
Z-246	SD9	<dt	<dt	<dt	15.0	0.04	<dt	<dt	<dt	<dt	0.30	48.6	1.05	<dt	<dt	<dt	<dt	0.42	<dt	<dt	<dt	<dt	<dt	<dt	n.a	n.a	n.a	n.a	n.a	n.a	n.a	16.6	82.0
Z-247	SD9	1.42	<dt	0.97	12.3	0.17	0.67	0.07	<dt	0.33	0.56	36.1	1.14	0.15	<dt	<dt	0.66	4.94	<dt	0.48	<dt	<dt	<dt	0.14	n.a	n.a	n.a	n.a	n.a	n.a	n.a	23.3	83.5
Z-248	SD9	<dt	<dt	<dt	14.9	<dt	<dt	0.04	0.04	<dt	0.67	48.0	1.43	<dt	<dt	<dt	<dt	0.41	<dt	<dt	<dt	<dt	<dt	<dt	n.a	n.a	n.a	n.a	n.a	n.a	n.a	20.9	86.4
Z-249	SD9	0.84	<dt	0.65	13.1	0.11	0.56	0.04	0.04	0.39	0.61	40.2	0.97	0.21	<dt	0.15	0.39	3.28	<dt	0.24	<dt	<dt	<dt	0.09	n.a	n.a	n.a	n.a	n.a	n.a	n.a	20.5	82.4
Z-250	SD10	<dt	<dt	<dt	14.7	0.03	<dt	<dt	<dt	<dt	0.35	47.5	2.03	<dt	<dt	<dt	<dt	0.48	<dt	<dt	<dt	<dt	<dt	<dt	n.a	n.a	n.a	n.a	n.a	n.a	n.a	25.7	90.9
Z-251	SD10	<dt	<dt	<dt	15.0	<dt	<dt	<dt	<dt	<dt	0.29	48.5	0.98	<dt	<dt	<dt	<dt	0.50	<dt	<dt	<dt	<dt	<dt	<dt	n.a	n.a	n.a	n.a	n.a	n.a	n.a	22.8	88.1
Z-252	SD10	<dt	<dt	<dt	14.8	<dt	<dt	<dt	<dt	<dt	0.20	48.6	0.97	<dt	<dt	<dt	<dt	0.46	<dt	<dt	<dt	<dt	<dt	<dt	n.a	n.a	n.a	n.a	n.a	n.a	n.a	37.2	102.1
Z-253	SD10	<dt	<dt	<dt	14.8	<dt	<dt	<dt	<dt	<dt	<dt	47.9	1.31	<dt	<dt	<dt	<dt	0.51	<dt	<dt	<dt	<dt	<dt	<dt	<dt	<dt	<dt	<dt	<dt	<dt	<dt	34.0	98.5
Z-254	SD10	<dt	<dt	<dt	14.8	<dt	<dt	<dt	<dt	<dt	0.03	47.7	1.30	<dt	<dt	<dt	0.15	0.49	<dt	<dt	<dt	<dt	<dt	<dt	<dt	<dt	<dt	<dt	<dt	<dt	0.07	<dt	34.0	98.5
Z-255	SD10	<dt	<dt	<dt	14.7	<dt	<dt	<dt	<dt	<dt	0.05	46.7	1.31	<dt	<dt	0.22	0.39	0.83	<dt	<dt	<dt	<dt	<dt	<dt	<dt	<dt	<dt	<dt	<dt	0.13	<dt	33.7	98.1
Z-256	SD10	<dt	<dt	<dt	14.6	<dt	<dt	<dt	<dt	<dt	0.05	47.0	1.28	<dt	<dt	0.17	0.28	0.88	<dt	<dt	<dt	<dt	<dt	<dt	<dt	<dt	<dt	<dt	<dt	0.16	<dt	33.7	98.2
Z-257	SD10	0.86	<dt	0.35	12.2	0.30	0.21	<dt	<dt	<dt	0.27	37.9	1.23	0.11	<dt	0.13	0.26	5.57	<dt	0.55	<dt	<dt	<dt	<dt	<dt	0.39	<dt	0.66	0.13	1.32	0.19	30.4	93.2
Z-258	SD10	0.90	<dt	0.38	12.2	0.34	0.22	<dt	<dt	<dt	0.45	36.5	1.41	0.12	<dt	0.56	0.17	6.23	<dt	0.52	<dt	<dt	<dt	<dt	<dt	0.47	<dt	0.73	0.14	1.36	0.21	30.2	93.2
Z-259	SD10	<dt	<dt	0.07	14.4	<dt	0.06	<dt	<dt	<dt	0.09	46.7	1.89	<dt	<dt	<dt	0.20	1.18	<dt	0.13	<dt	<dt	<dt	0.07	<dt	<dt	<dt	0.12	<dt	0.22	<dt	33.6	98.7
Z-260	SD10	1.12	0.03	0.29	11.5	0.58	0.23	<dt	<dt	<dt	0.20	35.2	1.76	0.35	<dt	0.07	0.26	7.03	<dt	0.51	<dt	<dt	0.05	<dt	<dt	0.59	0.15	0.81	0.19	1.66	0.24	29.7	92.5
Z-261	SD10	1.59	<dt	0.57	12.0	0.64	0.25	<dt	0.05	0.03	0.29	34.9	2.58	0.36	<dt	<dt	0.24	5.09	1.05	2.09	0.25	0.92	0.18	<dt	<dt	0.40	0.13	0.57	0.10	1.13	0.19	30.6	96.2
Z-262	SD10	<dt	<dt	<dt	14.6	<dt	<dt	<dt	<dt	<dt	0.08	48.4	1.19	<dt	<dt	<dt	<dt	0.52	<dt	<dt	<dt	<dt	<dt	-0.03	<dt	<dt	<dt	<dt	<dt	0.08	<dt	34.0	98.9
Z-263	SD10	1.08	0.03	0.70	11.7	0.40	0.18	<dt	<dt	0.03	0.20	30.9	0.87	0.71	<dt	0.25	0.21	9.09	<dt	1.40	<dt	<dt	<dt	<dt	<dt	0.66	0.15	1.13	0.21	2.11	0.32	29.3	91.6
Z-264	SD10	<dt	<dt	0.19	14.0	<dt	0.07	0.09	<dt	<dt	0.09	43.7	1.79	0.12	<dt	<dt	0.14	1.68	<dt	0.11	<dt	<dt	<dt	<dt	<dt	<dt	<dt	0.15	<dt	0.39	<dt	32.5	95.0
Z-265	SD10	<dt	<dt	0.27	13.6	<dt	0.05	0.07	<dt	<dt	0.07	42.8	1.81	0.10	<dt	<dt	0.20	1.72	<dt	0.14	<dt	<dt	<dt	<dt	<dt	0.12	<dt	0.23	<dt	0.44	<dt	31.8	93.4

#	Sample	F	Cl	Al	Si	P	Ca	K	Ti	Mn	Fe	Zr	Hf	Nb	Ta	Th	U	Y	La	Ce	Pr	Nd	Sm	Gd	Tb	Dy	Ho	Er	Tm	Yb	Lu	O	Total
		wt %	wt %	wt %	wt %	wt %	wt %	wt %	wt %	wt %	wt %	wt %	wt %	wt %	wt %	wt %	wt %	wt %	wt %	wt %	wt %	wt %	wt %	wt %	wt %	wt %	wt %	wt %	wt %	wt %	wt %	wt %	
Z-266	SD10	1.98	<dt	0.36	9.5	2.67	0.23	<dt	<dt	<dt	0.10	24.3	0.60	1.17	<dt	0.25	0.15	13.63	<dt	0.76	<dt	<dt	<dt	<dt	<dt	0.95	0.38	1.94	0.39	3.53	0.60	28.9	92.4
Z-267	SD10	<dt	<dt	0.07	14.2	<dt	0.04	<dt	<dt	<dt	0.53	45.3	1.24	0.13	<dt	0.06	<dt	1.61	<dt	<dt	<dt	<dt	<dt	<dt	<dt	<dt	<dt	0.23	<dt	0.37	<dt	33.1	97.0
Z-268	SD10	1.38	<dt	0.59	11.4	0.63	0.28	0.32	0.08	0.04	1.83	33.2	1.10	0.31	<dt	0.14	0.24	6.92	<dt	0.57	<dt	<dt	0.06	<dt	<dt	0.55	<dt	0.75	0.17	1.39	0.22	29.5	91.8
Z-269	SD10	<dt	<dt	<dt	14.7	<dt	<dt	<dt	<dt	<dt	0.39	46.1	1.19	<dt	<dt	0.07	<dt	0.86	<dt	<dt	<dt	<dt	<dt	<dt	<dt	<dt	<dt	<dt	<dt	0.15	<dt	33.5	96.9
Z-270	SD10	<dt	<dt	<dt	14.7	<dt	<dt	<dt	<dt	<dt	0.64	46.2	1.26	<dt	<dt	<dt	<dt	0.60	<dt	<dt	<dt	<dt	<dt	<dt	<dt	<dt	<dt	<dt	<dt	<dt	<dt	33.6	97.1
Z-271	SD10	1.90	<dt	0.34	10.2	1.32	0.27	0.04	0.05	<dt	0.68	29.2	0.82	0.99	<dt	0.28	0.21	10.42	<dt	0.50	<dt	<dt	<dt	<dt	<dt	0.78	0.27	1.34	0.28	2.29	0.39	28.5	91.2
Z-272	SD10	<dt	<dt	<dt	14.8	<dt	<dt	<dt	<dt	<dt	0.43	46.8	1.11	<dt	<dt	<dt	<dt	0.54	<dt	<dt	<dt	<dt	<dt	<dt	<dt	<dt	<dt	<dt	<dt	<dt	<dt	33.8	97.5
Z-273	SD10	1.76	<dt	0.39	10.4	0.68	0.33	<dt	0.04	<dt	0.77	31.3	0.88	0.29	<dt	0.39	0.32	8.15	<dt	0.76	<dt	<dt	<dt	<dt	<dt	0.61	0.20	1.13	0.21	2.06	0.33	27.8	88.9
Z-274	SD23	<dt	<dt	<dt	14.6	<dt	<dt	<dt	<dt	<dt	0.23	46.6	1.35	<dt	<dt	<dt	<dt	0.49	<dt	<dt	<dt	<dt	<dt	<dt	<dt	<dt	<dt	<dt	<dt	0.07	<dt	33.4	96.8
Z-275	SD23	<dt	<dt	<dt	14.9	<dt	0.03	<dt	<dt	<dt	0.43	46.7	1.39	<dt	<dt	<dt	<dt	0.57	<dt	<dt	<dt	<dt	<dt	<dt	<dt	<dt	<dt	<dt	<dt	0.07	<dt	33.9	98.0
Z-276	SD23	0.57	<dt	0.56	13.4	0.19	0.16	<dt	<dt	<dt	0.97	37.7	1.19	0.16	<dt	0.11	0.14	4.10	<dt	0.62	<dt	<dt	<dt	<dt	<dt	0.30	0.19	0.49	0.08	0.83	0.13	31.4	93.4
Z-277	SD23	0.94	<dt	0.64	13.2	<dt	0.44	0.08	0.04	0.06	0.82	39.0	1.38	0.14	<dt	0.20	0.49	3.63	<dt	1.10	<dt	<dt	<dt	0.29	<dt	0.47	0.15	0.58	0.10	0.94	<dt	31.51	96.4
Z-278	SD23	0.69	<dt	0.74	12.1	<dt	0.46	0.07	0.14	0.12	6.16	35.0	1.27	0.51	<dt	0.30	0.38	3.08	<dt	0.46	<dt	<dt	<dt	0.25	<dt	0.43	<dt	0.60	0.11	1.29	0.18	30.15	93.6
Z-279	SD23	<dt	<dt	<dt	14.9	<dt	<dt	<dt	<dt	<dt	0.40	48.9	1.38	<dt	<dt	<dt	0.15	0.20	<dt	<dt	<dt	<dt	<dt	<dt	<dt	<dt	<dt	<dt	<dt	<dt	<dt	34.46	100.4
Z-280	SD23	<dt	<dt	<dt	14.8	<dt	<dt	<dt	<dt	<dt	0.21	48.5	1.90	<dt	<dt	<dt	0.11	0.21	<dt	<dt	<dt	<dt	<dt	<dt	<dt	<dt	<dt	<dt	<dt	<dt	<dt	34.30	100.0
Z-281	SD23	0.54	<dt	0.47	13.4	<dt	0.44	0.07	<dt	0.14	0.90	41.8	1.43	<dt	<dt	<dt	0.40	2.83	<dt	0.23	<dt	<dt	<dt	0.21	<dt	0.31	<dt	0.48	<dt	0.60	<dt	32.13	96.6
Z-282	SD23	<dt	<dt	<dt	14.8	0.03	<dt	<dt	<dt	<dt	0.23	47.7	1.41	<dt	<dt	0.11	0.20	0.40	<dt	<dt	<dt	<dt	<dt	<dt	<dt	<dt	<dt	0.14	<dt	<dt	<dt	34.11	99.5
Z-283	SD23	<dt	<dt	0.05	14.7	<dt	0.06	<dt	<dt	<dt	0.17	48.3	1.40	<dt	<dt	<dt	0.10	0.43	<dt	<dt	<dt	<dt	<dt	<dt	<dt	<dt	<dt	<dt	<dt	<dt	<dt	34.22	99.9
Z-284	SD23	0.58	<dt	0.52	13.4	<dt	0.37	0.06	<dt	0.08	0.69	41.2	1.50	<dt	<dt	<dt	0.30	2.68	<dt	0.63	<dt	<dt	<dt	0.24	<dt	0.32	<dt	0.49	0.09	0.85	<dt	31.95	96.3
Z-285	SD23	0.99	<dt	0.23	14.2	<dt	0.12	<dt	<dt	<dt	0.21	45.3	1.73	<dt	<dt	<dt	0.10	1.14	<dt	0.26	<dt	<dt	<dt	0.08	<dt	0.16	<dt	0.26	<dt	0.46	<dt	33.19	98.7
Z-286	SD23	0.57	<dt	0.12	14.2	0.14	0.09	<dt	<dt	<dt	0.12	46.5	1.41	<dt	<dt	<dt	0.11	1.14	<dt	0.15	<dt	<dt	<dt	0.14	<dt	0.13	<dt	0.15	<dt	0.24	<dt	33.38	98.6
Z-287	SD23	0.99	<dt	0.72	11.9	<dt	0.72	0.09	<dt	0.07	1.95	36.7	0.74	0.36	<dt	2.35	0.80	4.03	<dt	0.68	<dt	<dt	<dt	0.37	0.06	0.49	0.24	0.68	0.13	0.96	0.15	29.93	94.3
Z-288	SD23	1.93	<dt	0.77	11.5	0.27	1.09	0.11	<dt	<dt	1.64	35.3	0.73	0.23	<dt	1.02	0.88	4.80	<dt	0.86	<dt	<dt	<dt	0.38	<dt	0.56	0.20	0.75	0.11	1.08	<dt	29.25	92.7
Z-289	SD23	0.85	<dt	0.33	13.7	<dt	0.39	0.06	<dt	<dt	1.23	44.5	1.16	<dt	<dt	0.20	0.30	1.67	<dt	0.28	<dt	<dt	<dt	0.16	<dt	0.17	<dt	0.19	<dt	0.35	<dt	32.85	98.6
Z-290	SD23	2.16	<dt	0.95	12.4	<dt	0.93	<dt	<dt	<dt	0.64	35.1	0.65	<dt	<dt	0.31	1.02	5.26	<dt	1.15	<dt	<dt	<dt	0.41	0.06	0.64	<dt	0.93	0.11	1.09	0.14	29.56	92.7
Z-291	SD23	<dt	<dt	<dt	14.7	<dt	<dt	<dt	<dt	<dt	0.11	48.0	1.18	<dt	<dt	0.45	0.52	0.56	<dt	<dt	<dt	<dt	<dt	<dt	<dt	<dt	<dt	<dt	<dt	0.16	<dt	34.10	100.0
Z-292	SD23	<dt	<dt	<dt	14.9	<dt	<dt	<dt	<dt	<dt	<dt	49.1	1.28	<dt	<dt	<dt	0.10	0.16	<dt	<dt	<dt	<dt	<dt	<dt	<dt	<dt	<dt	<dt	<dt	<dt	<dt	34.38	99.8
Z-293	SD23	<dt	<dt	0.04	14.8	<dt	0.04	<dt	<dt	<dt	0.28	47.3	1.47	<dt	<dt	<dt	0.09	0.34	<dt	<dt	<dt	<dt	<dt	<dt	<dt	<dt	<dt	<dt	<dt	<dt	<dt	33.91	98.5
Z-294	SD19	<dt	<dt	<dt	15.0	<dt	<dt	<dt	<dt	<dt	0.31	47.9	1.64	<dt	<dt	<dt	<dt	<dt	<dt	<dt	<dt	<dt	<dt	<dt	<dt	<dt	<dt	<dt	<dt	<dt	<dt	34.24	99.1
Z-295	SD19	0.52	<dt	0.22	13.2	0.19	0.12	<dt	<dt	0.08	6.02	40.8	1.08	0.19	<dt	0.16	0.17	1.38	<dt	0.13	<dt	<dt	<dt	0.09	<dt	0.16	<dt	0.13	<dt	0.33	<dt	32.39	97.7
Z-296	SD19	<dt	<dt	0.08	14.7	<dt	<dt	<dt	<dt	<dt	0.54	47.5	1.69	<dt	<dt	<dt	<dt	0.12	<dt	<dt	<dt	<dt	<dt	<dt	<dt	<dt	<dt	<dt	<dt	<dt	<dt	33.91	98.7
Z-297	SD19	<dt	<dt	<dt	15.0	<dt	<dt	<dt	<dt	<dt	0.19	45.3	1.31	<dt	<dt	<dt	<dt	0.19	<dt	0.020	<dt	<dt	<dt	<dt	<dt	<dt	<dt	<dt	<dt	<dt	<dt	33.18	94.6
Z-298	SD19	<dt	<dt	<dt	15.1	0.035	<dt	<dt	<dt	<dt	0.37	44.7	1.47	<dt	<dt	<dt	<dt	0.17	<dt	<dt	<dt	<dt	<dt	0.08	<dt	<dt	<dt	<dt	<dt	<dt	<dt	33.25	95.0
Z-299	SD19	0.54	<dt	0.11	15.7	0.532	1.04	0.09	0.03	<dt	1.45	38.2	1.39	<dt	<dt	0.50	0.46	0.98	<dt	0.080	<dt	<dt	<dt	<dt	<dt	<dt	<dt	0.17	<dt	0.28	0.07	33.63	95.3
Z-300	SD19	<dt	<dt	<dt	14.9	<dt	<dt	<dt	<dt	<dt	0.29	45.1	1.28	<dt	<dt	0.11	<dt	0.25	<dt	####	<dt	<dt	<dt	<dt	<dt	<dt	<dt	<dt	<dt	0.07	<dt	33.18	95.1
Z-301	SD19	<dt	<dt	<dt	14.9	0.039	<dt	<dt	<dt	<dt	1.01	44.2	1.62	<dt	<dt	<dt	<dt	0.29	<dt	<dt	<dt	<dt	<dt	0.10	<dt	<dt	<dt	<dt	<dt	<dt	<dt	33.08	94.9
Z-302	SD19	<dt	<dt	<dt	15.0	<dt	0.03	<dt	<dt	<dt	0.05	45.2	1.13	<dt	<dt	<dt	<dt	0.21	<dt	<dt	<dt	<dt	<dt	0.13	<dt	<dt	<dt	<dt	<dt	<dt	<dt	33.08	94.3
Z-303	SD19	<dt	<dt	<dt	14.9	<dt	<dt	<dt	<dt	<dt	0.05	44.7	2.01	<dt	<dt	<dt	<dt	0.08	<dt	<dt	<dt	<dt	<dt	<dt	<dt	<dt	<dt	<dt	<dt	<dt	<dt	33.07	94.6
Z-304	SD19	<dt	<dt	<dt	14.9	<dt	<dt	<dt	<dt	<dt	<dt	45.5	1.11	<dt	<dt	<dt	<dt	0.29	<dt	<dt	<dt	<dt	<dt	<dt	<dt	<dt	<dt	<dt	<dt	<dt	<dt	33.15	94.6
Z-305	SD19	<dt	<dt	0.05	14.8	0.160	<dt	<dt	<dt	<dt	<dt	44.3	1.64	<dt	<dt	<dt	0.27	0.32	<dt	<dt	<dt	<dt	<dt	0.08	<dt	<dt	<dt	0.13	<dt	0.08	<dt	33.03	94.4
Z-306	SD19	<dt	<dt	<dt	14.6	0.078	0.07	<dt	<dt	<dt	0.05	43.7	1.31	<dt	<dt	<dt	<dt	0.59	<dt	<dt	<dt	<dt	<dt	<dt	<dt	<dt	<dt	<dt	<dt	0.12	<dt	32.41	92.8
Z-307	SD19	<dt	<dt	<dt	14.8	0.054	<dt	<dt	<dt	<dt	0.03	43.9	1.66	<dt	<dt	0.24	0.45	0.45	<dt	<dt	<dt	<dt	<dt	<dt	<dt	<dt	<dt	<dt	<dt	0.13	<dt	32.74	94.2
Z-308	SD19	<dt	<dt	<dt	15.0	<dt	<dt	<dt	<dt	<dt	0.04	45.2	1.40	<dt	<dt	<dt	<dt	0.14	<dt	<dt	<dt	<dt	<dt	<dt	<dt	<dt	<dt	<dt	<dt	<dt	<dt	33.22	94.8
Z-309	SD19	<dt	<dt	<dt	15.0	<dt	<dt	<dt	<dt	<dt	0.05	44.9	1.40	<dt	<dt	<dt	<dt	<dt	<dt	<dt	<dt	<dt	<dt	<dt	<dt	<dt	<dt	<dt	<dt	<dt	<dt	33.04	93.9
Z-310	SD19	<dt	<dt	<dt	14.8	<dt	<dt	<dt	<dt	<dt	0.14	45.5	1.03	<dt	<dt	<dt	<dt	0.23	<dt	<dt	<dt	<dt	<dt	<dt	<dt	<dt	<dt	<dt	<dt	<dt	<dt	33.08	94.6
Z-311	SD19	<dt	<dt	<dt	15.0	<dt	<dt	<dt	<dt	<dt	0.40	44.9	1.12	<dt	<dt	<dt	<dt	0.16	<dt	<dt	<dt	<dt	<dt	<dt	<dt	<dt	<dt	<dt	<dt	<dt	<dt	33.17	94.4
Z-312	SD19	<dt	<dt	<dt	14.8	0.058	0.06	<dt	<dt	<dt	0.48	45.0	1.55	<dt	<dt	<dt	0.24	0.25	<dt	<dt	<dt	<dt	<dt	<dt	<dt	<dt	<dt	<dt	<dt	0.09	<dt	33.2	95.7
Z-313	SD21	<dt	<dt	<dt	15.0	<dt	<dt	<dt	<dt	<dt	0.35	46.9	1.23	<dt	<dt	<dt	0.15	0.25	<dt	<dt	<dt	<dt	<dt	<dt	<dt	<dt	<dt	<dt	<dt	0.07	<dt	33.87	97.6
Z-314	SD22	<dt	<dt	<dt	15.0	<dt	<dt	<dt	<dt	<dt	0.11	43.8	0.88	<dt	<dt	<dt	<dt	0.31	<dt	<dt	<dt	<dt	<dt	<dt	<dt	<dt	<dt	<dt	<dt	<dt	<dt	32.69	92.6
Z-315	SV8.2	<dt	<dt	<dt	14.9	<dt	<dt	<dt	<dt	<dt	0.15	44.6	0.95	<dt	<dt	<dt	<dt	0.25	<dt	<dt	<dt	<dt	<dt	<dt	<dt	<dt	<dt	<dt	<dt	<dt	<dt	32.91	93.6

#	Sample	F	Cl	Al	Si	P	Ca	K	Ti	Mn	Fe	Zr	Hf	Nb	Ta	Th	U	Y	La	Ce	Pr	Nd	Sm	Gd	Tb	Dy	Ho	Er	Tm	Yb	Lu	O	Total
		wt %	wt %	wt %	wt %	wt %	wt %	wt %	wt %	wt %	wt %	wt %	wt %	wt %	wt %	wt %	wt %	wt %	wt %	wt %	wt %	wt %	wt %	wt %	wt %	wt %	wt %	wt %	wt %	wt %	wt %	wt %	
Z-316	SV8.2	<dt	<dt	0.05	14.5	0.230	0.05	<dt	<dt	<dt	0.06	41.7	2.94	0.32	<dt	0.13	0.28	0.93	<dt	0.100	<dt	<dt	<dt	0.20	<dt	<dt	<dt	0.18	<dt	0.33	<dt	32.5	94.3
Z-317	SV8.2	0.33	<dt	0.08	14.1	0.132	0.09	0.05	<dt	<dt	0.28	41.6	1.87	<dt	<dt	0.18	0.44	1.02	<dt	<dt	<dt	<dt	<dt	0.14	<dt	<dt	<dt	<dt	<dt	0.21	<dt	31.75	92.1
Z-318	SV8.2	<dt	<dt	<dt	14.9	0.05	<dt	<dt	<dt	<dt	0.39	40.5	1.54	<dt	<dt	0.11	0.39	0.70	<dt	-0.01	<dt	<dt	<dt	<dt	<dt	<dt	<dt	<dt	<dt	0.15	<dt	31.0	89.8
Z-319	SV8.2	<dt	<dt	<dt	14.9	0.05	<dt	<dt	<dt	<dt	0.49	40.7	1.60	<dt	<dt	0.19	0.42	0.67	<dt	-0.02	<dt	<dt	<dt	<dt	<dt	<dt	<dt	<dt	<dt	0.13	<dt	31.0	90.1
Z-320	SV8.2	<dt	<dt	0.18	13.4	0.36	0.11	<dt	0.04	<dt	0.29	36.4	1.51	0.15	<dt	<dt	0.21	2.23	0.05	0.13	<dt	<dt	<dt	<dt	<dt	0.21	<dt	0.22	<dt	0.47	<dt	30.3	86.4
Z-321	SV8.2	<dt	<dt	<dt	15.2	0.04	<dt	<dt	<dt	<dt	0.06	40.7	1.33	<dt	<dt	<dt	<dt	0.49	<dt	<dt	<dt	<dt	<dt	<dt	<dt	<dt	<dt	<dt	<dt	<dt	<dt	27.8	85.5
Z-322	SV8.2	0.21	<dt	0.04	14.6	0.13	<dt	<dt	0.04	<dt	0.05	36.8	1.82	0.20	<dt	<dt	<dt	1.14	<dt	0.25	<dt	<dt	<dt	<dt	<dt	<dt	<dt	0.18	<dt	0.22	<dt	27.4	83.1
Z-323	SV8.2	2.56	<dt	0.60	10.6	0.84	0.30	<dt	<dt	<dt	0.22	25.5	1.16	0.74	<dt	0.21	0.34	6.82	<dt	0.59	<dt	<dt	0.06	<dt	0.06	0.72	0.14	0.90	0.14	1.28	0.20	29.5	83.6
Z-324	SV8.2	2.67	<dt	0.76	12.4	0.34	0.28	<dt	0.04	0.06	0.18	28.6	1.05	0.49	<dt	0.10	0.32	6.19	<dt	0.89	<dt	<dt	0.06	<dt	<dt	0.55	0.12	0.65	0.12	1.11	0.17	32.0	89.3
Z-325	SV8.2	<dt	<dt	<dt	14.9	0.06	<dt	<dt	<dt	<dt	<dt	40.3	1.25	<dt	<dt	<dt	<dt	0.58	<dt	<dt	<dt	<dt	<dt	<dt	<dt	<dt	<dt	<dt	<dt	0.07	<dt	27.8	85.0
Z-326	SV8.2	1.92	<dt	0.74	12.1	0.19	0.26	<dt	<dt	0.12	0.15	28.0	1.22	0.65	<dt	0.12	0.27	5.81	<dt	1.40	<dt	0.00	0.06	<dt	0.06	0.55	0.12	0.73	0.17	1.29	0.19	30.7	86.9
Z-327	SV8.2	2.23	<dt	0.55	12.9	0.26	0.36	0.03	<dt	0.03	0.11	32.5	1.57	0.15	<dt	<dt	0.30	4.24	<dt	0.13	<dt	<dt	0.06	<dt	<dt	0.32	<dt	0.47	0.10	0.64	0.09	31.0	88.0
Z-328	SV8.2	<dt	<dt	<dt	14.8	<dt	<dt	0.04	<dt	<dt	<dt	39.2	1.69	<dt	<dt	<dt	<dt	0.39	<dt	<dt	<dt	<dt	<dt	<dt	<dt	<dt	<dt	<dt	<dt	<dt	<dt	31.2	87.3
Z-329	SV8.2	2.10	<dt	0.67	11.8	0.80	0.40	<dt	<dt	<dt	0.16	28.5	1.23	0.46	<dt	0.16	0.53	7.01	<dt	0.70	<dt	<dt	0.09	<dt	<dt	0.68	0.16	0.77	0.16	1.04	0.12	34.6	92.3
Z-330	SV8.2	<dt	<dt	<dt	14.8	0.03	<dt	<dt	<dt	<dt	0.29	39.0	2.04	<dt	<dt	<dt	<dt	0.30	<dt	<dt	<dt	<dt	<dt	0.09	<dt	<dt	<dt	<dt	<dt	<dt	<dt	31.6	88.1
Z-331	SV8.2	<dt	<dt	<dt	15.1	0.03	<dt	<dt	<dt	<dt	0.16	39.6	1.42	<dt	<dt	<dt	<dt	0.32	<dt	<dt	<dt	<dt	<dt	<dt	<dt	<dt	<dt	<dt	<dt	<dt	<dt	27.5	84.1
Z-332	SV8.2	<dt	<dt	<dt	15.2	0.04	<dt	<dt	<dt	<dt	<dt	38.9	1.50	<dt	<dt	<dt	0.16	0.29	<dt	<dt	<dt	<dt	<dt	<dt	<dt	<dt	<dt	<dt	<dt	<dt	<dt	28.9	85.0
Z-333	SV8.2	<dt	<dt	<dt	15.1	0.06	<dt	<dt	<dt	<dt	<dt	38.5	1.56	<dt	<dt	<dt	<dt	0.57	<dt	<dt	<dt	<dt	<dt	<dt	<dt	<dt	<dt	<dt	<dt	0.07	<dt	31.0	86.8
Z-334	SV8.2	<dt	<dt	<dt	15.0	0.03	<dt	<dt	<dt	<dt	<dt	38.6	1.18	<dt	<dt	<dt	<dt	0.44	<dt	<dt	<dt	<dt	<dt	<dt	<dt	<dt	<dt	<dt	<dt	0.06	<dt	28.3	83.6
Z-335	SV8.2	<dt	<dt	<dt	15.1	0.03	<dt	<dt	<dt	<dt	0.04	38.9	2.20	<dt	<dt	<dt	<dt	0.29	<dt	<dt	<dt	<dt	<dt	0.07	<dt	<dt	<dt	<dt	<dt	<dt	<dt	30.6	87.2
Z-336	SV8.2	<dt	<dt	<dt	14.7	0.14	<dt	<dt	<dt	<dt	0.09	35.8	4.60	<dt	<dt	0.12	0.39	0.69	<dt	<dt	<dt	<dt	<dt	0.11	<dt	<dt	<dt	<dt	<dt	0.16	<dt	25.9	82.7
Z-337	SV8.2	<dt	<dt	<dt	14.8	0.11	<dt	<dt	<dt	<dt	0.10	36.9	1.52	<dt	<dt	0.21	0.51	1.10	<dt	<dt	<dt	<dt	<dt	<dt	<dt	<dt	<dt	<dt	<dt	0.26	<dt	27.4	82.9
Z-338	SV8.2	<dt	<dt	<dt	15.2	<dt	<dt	<dt	<dt	<dt	0.06	38.2	1.36	<dt	<dt	<dt	<dt	0.36	<dt	<dt	<dt	<dt	<dt	<dt	<dt	<dt	<dt	<dt	<dt	<dt	<dt	26.8	81.9
Z-339	SV8.2	<dt	<dt	0.03	14.6	0.12	<dt	0.04	<dt	<dt	0.11	35.9	1.27	<dt	<dt	0.31	0.61	1.30	<dt	-0.01	<dt	<dt	<dt	<dt	<dt	<dt	<dt	<dt	<dt	0.21	<dt	29.6	84.0
Z-340	SV8.2	2.97	<dt	0.87	12.1	0.54	0.27	<dt	<dt	0.08	0.16	27.1	1.10	<dt	<dt	0.22	0.25	7.54	<dt	0.54	<dt	<dt	0.09	<dt	0.06	0.67	0.17	0.80	0.13	1.18	0.17	32.9	90.1
Z-341	SV8.2	3.04	<dt	0.25	12.5	0.07	0.15	<dt	<dt	<dt	0.43	35.5	1.31	<dt	<dt	<dt	<dt	0.67	0.59	0.64	<dt	0.21	<dt	<dt	<dt	<dt	<dt	<dt	<dt	0.12	<dt	36.4	91.8
Z-342	SV8.2	<dt	<dt	<dt	14.8	0.11	<dt	<dt	<dt	<dt	0.09	37.2	1.61	<dt	<dt	0.26	0.53	0.81	<dt	<dt	<dt	<dt	<dt	<dt	<dt	<dt	<dt	<dt	<dt	0.16	<dt	31.0	86.6
Z-343	SV8.2	<dt	<dt	<dt	14.9	0.04	<dt	<dt	<dt	<dt	0.21	38.7	1.88	<dt	<dt	<dt	0.20	0.31	<dt	<dt	<dt	<dt	<dt	<dt	<dt	<dt	<dt	<dt	<dt	<dt	<dt	30.7	87.0
Z-344	SV8.2	<dt	<dt	<dt	15.0	0.06	<dt	<dt	<dt	<dt	0.12	37.8	1.66	<dt	<dt	0.14	0.29	0.64	<dt	<dt	<dt	<dt	<dt	<dt	<dt	<dt	<dt	<dt	<dt	0.11	<dt	32.0	87.8
Z-345	SV8.2	<dt	<dt	<dt	15.1	<dt	<dt	<dt	<dt	<dt	0.10	38.9	1.31	<dt	<dt	<dt	<dt	0.41	<dt	<dt	<dt	<dt	<dt	<dt	<dt	<dt	<dt	<dt	<dt	<dt	<dt	32.1	87.9
Z-346	SD20	<dt	<dt	0.36	16.8	0.04	<dt	0.39	0.14	<dt	1.14	39.8	1.70	<dt	<dt	<dt	0.10	0.90	<dt	<dt	<dt	<dt	<dt	<dt	<dt	<dt	<dt	<dt	<dt	0.09	<dt	29.9	91.4
Z-347	SD20	3.47	<dt	0.72	11.9	0.64	0.35	<dt	<dt	0.04	0.29	27.4	1.08	0.09	<dt	0.22	0.33	6.62	<dt	0.33	<dt	0.07	<dt	<dt	0.08	0.62	0.25	0.75	0.15	0.99	0.16	30.7	87.4
Z-348	SD21	2.18	<dt	0.61	13.2	0.29	0.31	<dt	<dt	<dt	0.29	32.1	1.03	0.10	<dt	0.17	0.46	5.20	<dt	0.11	<dt	<dt	<dt	<dt	0.06	0.42	0.14	0.55	0.08	0.78	0.09	30.1	88.3
Z-349	SD22	<dt	<dt	<dt	14.9	<dt	<dt	<dt	<dt	<dt	0.07	49.4	1.44	<dt	<dt	0.10	0.27	0.29	<dt	<dt	<dt	<dt	<dt	<dt	<dt	<dt	<dt	<dt	<dt	<dt	<dt	34.59	101.1
Z-350	SD23	<dt	<dt	<dt	14.7	0.06	<dt	<dt	<dt	<dt	0.12	48.6	1.03	<dt	<dt	0.13	0.17	0.57	<dt	<dt	<dt	<dt	<dt	<dt	<dt	0.11	<dt	<dt	<dt	0.33	<dt	34.27	100.4
Z-351	SD24	<dt	<dt	<dt	14.9	<dt	<dt	<dt	<dt	<dt	<dt	49.9	0.97	<dt	<dt	<dt	<dt	0.20	<dt	<dt	<dt	<dt	<dt	<dt	<dt	<dt	<dt	<dt	<dt	<dt	<dt	34.58	100.6
Z-352	SD25	8.00	<dt	0.27	5.1	0.15	0.77	0.15	0.03	<dt	0.67	32.6	0.61	<dt	<dt	<dt	<dt	1.14	4.89	7.65	0.91	3.36	0.46	0.32	<dt	<dt	<dt	<dt	<dt	<dt	<dt	21.37	88.1
Z-353	SD23	<dt	<dt	<dt	14.9	<dt	<dt	<dt	<dt	<dt	0.13	50.0	0.97	<dt	<dt	<dt	<dt	0.12	<dt	<dt	<dt	<dt	<dt	<dt	<dt	<dt	<dt	<dt	<dt	<dt	<dt	34.65	100.6
Z-354	SD24	<dt	<dt	<dt	14.7	<dt	<dt	<dt	<dt	<dt	<dt	49.2	1.28	<dt	<dt	<dt	<dt	0.21	<dt	<dt	<dt	<dt	<dt	<dt	<dt	<dt	<dt	<dt	<dt	<dt	<dt	34.23	99.8
Z-355	SD25	<dt	<dt	<dt	14.7	<dt	<dt	<dt	<dt	<dt	0.14	48.8	1.31	<dt	<dt	<dt	<dt	0.19	<dt	<dt	<dt	<dt	<dt	<dt	<dt	<dt	<dt	<dt	<dt	<dt	<dt	34.12	99.0

C3. Clay analysis

Table C3.1. Microprobe analysis of clays in saprolite samples

No.	Sample	F	Na	Mg	Al	Si	P	Ca	K	Ti	Mn	Fe	Th	Y	La	Ce	Pr	Nd	Sm	Gd	Dy	Ho	Er	Yb	O	Total
1	SV6	0.25	0.05	0.41	17.5	21.6	<0.02	0.22	0.08	<0.02	<0.02	0.50	<0.06	0.07	0.17	<0.02	<0.06	<0.05	<0.05	<0.06	<0.09	<0.09	<0.09	<0.05	40.90	81.8
2	SV6	0.18	0.05	0.35	17.7	21.3	<0.02	0.16	0.05	<0.02	<0.02	0.41	<0.06	0.11	0.23	<0.02	<0.06	0.10	<0.05	<0.06	<0.09	<0.09	<0.09	<0.05	40.1	80.7
3	SV6	0.28	0.03	0.55	16.2	20.7	<0.02	0.35	0.07	<0.02	<0.02	0.38	<0.06	<0.06	0.18	<0.02	<0.06	0.08	<0.05	<0.06	<0.09	<0.09	<0.09	<0.05	38.4	77.3
4	SV6	0.27	0.09	0.29	18.6	21.8	<0.02	0.06	<0.03	<0.02	<0.02	0.28	<0.06	0.07	0.17	<0.02	<0.06	0.07	<0.05	<0.06	<0.09	<0.09	<0.09	<0.05	41.4	83.0
5	SV6	<0.16	0.08	0.22	17.3	20.3	<0.02	0.06	<0.03	<0.02	<0.02	0.28	<0.06	0.07	0.15	<0.02	<0.06	0.05	<0.05	<0.06	<0.09	<0.09	<0.09	<0.05	38.8	77.3
6	SV6	0.35	0.03	0.64	16.6	21.7	<0.02	0.19	0.07	<0.02	<0.02	0.39	<0.06	0.10	0.35	<0.02	0.06	0.18	0.06	<0.06	<0.09	<0.09	<0.09	<0.05	39.5	80.2
7	SV6	0.25	0.14	0.49	16.5	20.6	<0.02	0.08	0.08	<0.02	<0.02	0.29	<0.06	0.14	0.25	<0.02	0.06	0.11	<0.05	<0.06	<0.09	<0.09	<0.09	<0.05	38.2	77.2
8	SV6	0.33	0.09	0.61	15.4	20.5	<0.02	0.11	0.08	0.02	<0.02	0.37	<0.06	0.12	0.28	<0.02	<0.06	0.14	0.06	<0.06	<0.09	<0.09	<0.09	<0.05	37.1	75.2
9	SV6	<0.16	0.03	0.18	15.2	18.0	0.03	0.06	0.05	<0.02	<0.02	0.26	<0.06	0.11	0.35	0.10	0.08	0.25	0.06	0.07	<0.09	<0.09	<0.09	<0.05	33.4	68.2
10	SV6	0.28	0.08	0.76	14.1	20.0	<0.02	0.15	0.05	<0.02	<0.02	0.36	<0.06	0.17	0.38	<0.02	<0.06	0.22	0.06	<0.06	0.09	<0.09	<0.09	<0.05	35.1	71.8
11	SV6	0.24	<0.03	0.42	18.2	22.1	<0.02	0.11	0.05	0.02	<0.02	0.34	<0.06	0.16	0.76	0.05	0.18	0.59	0.11	0.11	<0.09	<0.09	<0.09	<0.05	40.0	83.5
12	SV6	0.29	0.07	0.78	15.6	21.9	<0.02	0.24	0.15	0.02	<0.02	0.37	<0.06	0.21	0.39	<0.02	<0.06	0.21	0.07	<0.06	<0.09	<0.09	<0.09	<0.05	38.7	79.0
13	SV6	0.23	0.05	0.48	17.8	22.3	<0.02	0.11	0.04	0.02	<0.02	0.38	<0.06	0.14	0.26	<0.02	<0.06	0.15	<0.05	<0.06	<0.09	<0.09	<0.09	<0.05	41.3	83.3
14	SV6	0.14	0.04	0.19	15.2	17.6	<0.02	0.06	<0.03	<0.02	<0.02	0.36	<0.06	0.08	0.14	<0.02	<0.06	0.07	<0.05	<0.06	<0.09	<0.09	<0.09	<0.05	33.6	67.5
15	SV6	0.24	0.06	0.05	18.9	20.3	<0.02	0.04	<0.03	<0.02	<0.02	0.32	<0.06	<0.06	0.05	<0.02	<0.06	<0.05	<0.05	<0.06	<0.09	<0.09	<0.09	<0.05	40.1	80.0
16	SV7	<0.16	<0.03	0.04	9.8	11.1	<0.02	0.03	<0.03	<0.02	<0.02	0.31	<0.06	<0.06	<0.04	<0.02	<0.06	<0.05	<0.05	<0.06	<0.09	<0.09	<0.09	<0.05	22.5	43.9
17	SV7	0.16	<0.03	0.02	10.3	11.7	<0.02	0.03	0.13	<0.02	<0.02	0.42	<0.06	0.08	0.16	<0.02	<0.06	0.06	<0.05	<0.06	<0.09	<0.09	<0.09	<0.05	22.8	45.9
18	SV7	<0.16	<0.03	<0.02	12.8	13.7	<0.02	0.03	0.48	<0.02	<0.02	0.31	<0.06	<0.06	<0.04	<0.02	<0.06	<0.05	<0.05	<0.06	<0.09	<0.09	<0.09	<0.05	27.6	54.9
19	SV7	0.23	<0.03	0.02	13.0	14.3	<0.02	0.04	<0.03	<0.02	<0.02	0.28	<0.06	<0.06	0.05	<0.02	<0.06	<0.05	<0.05	<0.06	<0.09	<0.09	<0.09	<0.05	28.6	56.5
20	SV7	<0.16	0.03	0.25	13.9	16.9	<0.02	0.13	0.07	<0.02	<0.02	0.34	<0.06	<0.06	0.16	<0.02	<0.06	0.08	<0.05	<0.06	<0.09	<0.09	<0.09	<0.05	32.0	63.8
21	SV7	0.20	<0.03	0.09	14.6	16.4	<0.02	0.11	0.06	<0.02	<0.02	0.47	<0.06	0.08	0.11	<0.02	<0.06	0.05	<0.05	<0.06	<0.09	<0.09	<0.09	<0.05	31.8	63.9
22	SV7	<0.16	<0.03	<0.02	15.1	16.8	<0.02	0.07	<0.03	<0.02	<0.02	0.34	<0.06	<0.06	<0.04	<0.02	<0.06	<0.05	<0.05	<0.06	<0.09	<0.09	<0.09	<0.05	33.2	65.5
23	SV7	<0.16	<0.03	0.05	15.0	17.1	<0.02	0.06	<0.03	0.042	<0.02	0.42	<0.06	<0.06	0.06	1.32	<0.06	0.04	<0.05	<0.06	<0.09	<0.09	<0.09	<0.05	32.3	66.5
24	SV7	0.15	<0.03	0.15	16.1	17.7	<0.02	0.09	0.09	<0.02	<0.02	0.66	<0.06	<0.06	0.13	<0.02	<0.06	0.06	<0.05	<0.06	<0.09	<0.09	<0.09	<0.05	35.1	70.2
25	SV7	<0.16	<0.03	0.32	15.9	19.0	<0.02	0.18	0.11	<0.02	<0.02	0.33	<0.06	0.17	0.29	<0.02	0.09	0.19	<0.05	<0.06	<0.09	<0.09	<0.09	<0.05	35.6	72.2
26	SV7	0.21	<0.03	0.09	16.5	18.8	<0.02	0.07	0.06	<0.02	0.02	0.64	<0.06	<0.06	0.15	<0.02	<0.06	0.09	<0.05	<0.06	<0.09	<0.09	<0.09	<0.05	36.5	73.1
27	SV7	0.30	<0.03	0.05	17.4	18.6	<0.02	0.04	0.06	<0.02	<0.02	0.37	<0.06	<0.06	0.16	<0.02	<0.06	0.12	0.05	<0.06	<0.09	<0.09	<0.09	<0.05	36.7	73.9
28	SV7	<0.16	<0.03	0.15	17.1	19.2	<0.02	0.16	0.12	<0.02	<0.02	0.51	<0.06	<0.06	0.12	<0.02	<0.06	<0.05	<0.05	<0.06	<0.09	<0.09	<0.09	<0.05	37.5	75.0
29	SV7	0.16	<0.03	0.17	16.5	19.7	<0.02	0.19	0.04	<0.02	<0.02	0.43	<0.06	<0.06	0.09	<0.02	<0.06	<0.05	<0.05	<0.06	<0.09	<0.09	<0.09	<0.05	37.7	75.0
30	SV7	<0.16	<0.03	0.05	17.3	19.6	<0.02	0.07	<0.03	<0.02	<0.02	0.39	<0.06	0.09	0.10	<0.02	<0.06	0.09	<0.05	<0.06	<0.09	<0.09	<0.09	<0.05	38.0	75.7
31	SV7	0.30	<0.03	0.89	15.3	21.5	<0.02	0.42	0.17	<0.02	<0.02	0.37	<0.06	0.12	0.39	<0.02	<0.06	0.20	<0.05	<0.06	<0.09	<0.09	<0.09	<0.05	38.4	78.1
32	SV7	0.23	0.10	0.42	17.1	20.9	<0.02	0.09	0.11	<0.02	<0.02	0.27	<0.06	<0.06	0.14	0.03	<0.06	0.06	<0.05	0.06	<0.09	<0.09	<0.09	<0.05	39.3	78.9
33	SV7	0.15	<0.03	0.38	17.2	20.9	<0.02	0.16	0.15	<0.02	<0.02	0.44	<0.06	0.12	0.16	<0.02	<0.06	<0.05	<0.05	<0.06	<0.09	<0.09	<0.09	<0.05	39.4	79.0
34	SV7	0.26	<0.03	0.54	16.7	21.1	<0.02	0.18	0.26	<0.02	<0.02	0.43	<0.06	0.09	0.23	<0.02	<0.06	0.10	<0.05	<0.06	<0.09	<0.09	<0.09	<0.05	39.1	79.0
35	SV7	<0.16	<0.03	0.24	17.8	20.5	<0.02	0.10	0.12	<0.02	<0.02	0.56	<0.06	<0.06	0.14	<0.02	<0.06	0.06	<0.05	<0.06	<0.09	<0.09	<0.09	<0.05	39.5	79.0
36	SV7	<0.16	<0.03	0.52	16.8	21.5	<0.02	0.20	0.18	<0.02	<0.02	0.52	<0.06	0.14	0.23	<0.02	<0.06	0.10	<0.05	<0.06	<0.09	<0.09	<0.09	<0.05	39.7	79.8
37	SV7	0.13	<0.03	0.04	18.0	20.7	<0.02	0.04	0.05	<0.02	<0.02	0.76	<0.06	<0.06	0.04	<0.02	<0.06	<0.05	<0.05	<0.06	<0.09	<0.09	<0.09	<0.05	40.1	79.9
38	SV7	0.29	0.17	0.74	16.0	21.9	<0.02	0.36	0.22	<0.02	<0.02	0.29	<0.06	0.06	0.21	<0.02	<0.06	0.08	0.07	<0.06	<0.09	<0.09	<0.09	<0.05	39.8	80.3
39	SV7	0.30	<0.03	0.62	17.0	21.3	<0.02	0.19	0.15	<0.02	<0.02	0.48	<0.06	0.15	0.28	<0.02	<0.06	0.12	0.05	<0.06	<0.09	<0.09	<0.09	<0.05	39.6	80.3
40	SV7	<0.16	<0.03	0.53	16.9	21.7	<0.02	0.31	0.09	<0.02	<0.02	0.37	<0.06	<0.06	0.25	<0.02	<0.06	<0.05	<0.05	<0.06	<0.09	<0.09	<0.09	<0.05	40.3	80.5
41	SV7	<0.16	<0.03	0.09	18.5	20.8	<0.02	0.06	0.06	<0.02	<0.02	0.58	<0.06	<0.06	0.05	<0.02	<0.06	<0.05	<0.05	<0.06	<0.09	<0.09	<0.09	<0.05	40.6	80.8
42	SV7	<0.16	<0.03	0.48	17.5	22.0	<0.02	0.16	0.12	<0.02	<0.02	0.35	<0.06	0.14	0.18	<0.02	<0.06	0.08	<0.05	<0.06	<0.09	<0.09	<0.09	<0.05	40.9	82.0
43	SV7	0.21	<0.03	0.82	16.0	22.8	<0.02	0.38	0.18	<0.02	<0.02	0.35	<0.06	<0.06	0.11	<0.02	<0.06	<0.05	<0.05	<0.06	<0.09	<0.09	<0.09	<0.05	41.1	82.0

No.	Sample	F	Na	Mg	Al	Si	P	Ca	K	Ti	Mn	Fe	Th	Y	La	Ce	Pr	Nd	Sm	Gd	Dy	Ho	Er	Yb	O	Total
44	SV7	0.19	<0.03	0.13	18.5	21.5	<0.02	0.11	0.07	<0.02	<0.02	0.36	<0.06	<0.06	0.08	<0.02	<0.06	<0.05	<0.05	<0.06	<0.09	<0.09	<0.09	<0.05	41.2	82.1
45	SV7	0.20	<0.03	0.72	16.7	22.7	<0.02	0.37	0.20	<0.02	<0.02	0.47	<0.06	0.11	0.36	<0.02	0.06	0.19	0.06	<0.06	<0.09	<0.09	<0.09	<0.05	40.9	83.1
46	SV7	0.18	<0.03	0.37	18.7	22.1	<0.02	0.13	0.11	<0.02	<0.02	0.30	<0.06	<0.06	0.16	<0.02	<0.06	0.05	<0.05	0.07	<0.09	<0.09	<0.09	<0.05	42.1	84.3
47	SV7	<0.16	<0.03	0.60	17.7	22.8	<0.02	0.21	0.13	<0.02	<0.02	0.52	<0.06	0.12	0.27	<0.02	<0.06	0.12	<0.05	<0.06	<0.09	<0.09	<0.09	<0.05	41.9	84.3
48	SV7	0.17	<0.03	0.42	18.3	22.4	<0.02	0.24	0.17	<0.02	<0.02	0.46	<0.06	<0.06	0.21	<0.02	<0.06	0.06	0.04	<0.06	<0.09	<0.09	<0.09	<0.05	42.2	84.6
49	SV7	0.23	<0.03	0.63	17.8	22.7	<0.02	0.25	0.14	<0.02	<0.02	0.42	<0.06	0.11	0.31	<0.02	<0.06	0.14	0.07	<0.06	<0.09	<0.09	<0.09	<0.05	42.0	84.8
50	SV7	0.24	<0.03	0.62	18.3	22.9	<0.02	0.26	0.15	<0.02	<0.02	0.35	<0.06	0.10	0.26	<0.02	0.07	0.12	0.05	0.07	<0.09	<0.09	<0.09	<0.05	42.6	86.0
51	SV7	0.13	<0.03	0.17	19.6	22.3	<0.02	0.08	0.10	<0.02	<0.02	0.50	<0.06	<0.06	0.10	<0.02	<0.06	<0.05	<0.05	<0.06	<0.09	<0.09	<0.09	<0.05	43.1	86.1
52	SV7	0.21	<0.03	0.11	19.6	22.6	<0.02	0.09	0.05	<0.02	<0.02	0.55	<0.06	<0.06	0.09	<0.02	<0.06	<0.05	<0.05	<0.06	<0.09	<0.09	<0.09	<0.05	43.5	86.7
53	SV7	<0.16	<0.03	0.05	19.9	22.6	<0.02	0.04	<0.03	<0.02	<0.02	0.43	<0.06	<0.06	0.06	<0.02	<0.06	<0.05	<0.05	<0.06	<0.09	<0.09	<0.09	<0.05	43.8	86.9
54	SV7	0.17	<0.03	0.28	18.7	23.2	<0.02	0.29	0.20	<0.02	<0.02	0.50	<0.06	0.08	0.24	<0.02	<0.06	0.05	<0.05	<0.06	<0.09	<0.09	<0.09	<0.05	43.4	87.1
55	SV7	<0.16	<0.03	0.06	20.1	22.8	<0.02	0.05	<0.03	<0.02	<0.02	0.38	<0.06	<0.06	0.06	<0.02	<0.06	<0.05	<0.05	<0.06	<0.09	<0.09	<0.09	<0.05	44.1	87.6
56	SV7	<0.16	<0.03	0.11	20.1	23.0	<0.02	0.06	0.10	<0.02	<0.02	0.84	<0.06	<0.06	0.08	<0.02	<0.06	<0.05	<0.05	<0.06	<0.09	<0.09	<0.09	<0.05	44.5	88.8
57	SV7	<0.16	<0.03	0.03	20.8	23.1	<0.02	0.02	0.05	<0.02	<0.02	0.67	<0.06	<0.06	<0.04	<0.02	<0.06	<0.05	<0.05	<0.06	<0.09	<0.09	<0.09	<0.05	45.1	89.8
58	SV7	<0.16	<0.03	0.05	20.9	23.3	<0.02	0.04	0.07	<0.02	<0.02	0.64	<0.06	<0.06	0.04	<0.02	<0.06	<0.05	<0.05	0.08	<0.09	<0.09	<0.09	<0.05	45.4	90.5
59	SV9	0.60	<0.03	1.33	13.0	22.4	<0.02	0.13	0.03	<0.02	<0.02	0.18	<0.06	0.13	0.69	<0.02	0.07	0.21	0.07	<0.06	<0.09	<0.09	<0.09	<0.05	36.9	75.6
60	SV9	0.47	0.04	0.96	12.7	20.9	<0.02	0.08	<0.03	<0.02	<0.02	0.21	<0.06	0.26	0.76	<0.02	0.11	0.37	0.07	0.07	<0.09	<0.09	<0.09	<0.05	34.2	71.1
61	SV9	0.51	<0.03	0.91	12.8	19.4	<0.02	0.04	<0.03	<0.02	<0.02	0.22	<0.06	0.32	0.60	<0.02	0.13	0.41	0.10	0.08	0.10	<0.09	<0.09	<0.05	32.5	68.2
62	SV9	0.38	0.01	0.86	13.3	19.7	<0.02	0.07	0.12	<0.02	<0.02	0.36	<0.06	0.34	0.60	<0.02	0.08	0.36	0.07	<0.06	<0.09	<0.09	<0.09	<0.05	33.6	69.7
63	SV9	0.47	<0.03	0.83	14.3	20.5	<0.02	0.02	<0.03	<0.02	<0.02	0.26	<0.06	0.43	0.47	<0.02	0.06	0.26	<0.05	<0.06	0.09	<0.09	<0.09	<0.05	35.4	73.1
64	SV9	0.62	<0.03	1.78	11.8	25.3	<0.02	0.18	<0.03	0.02	<0.02	0.35	<0.06	0.46	0.89	<0.02	0.16	0.43	0.09	<0.06	0.10	<0.09	<0.09	<0.05	38.8	81.0
65	SV9	0.31	<0.03	1.06	13.5	21.3	<0.02	0.04	<0.03	<0.02	<0.02	0.24	<0.06	0.47	0.74	<0.02	0.16	0.51	0.14	0.11	0.10	<0.09	<0.09	0.07	34.8	73.5
66	SV9	0.50	0.04	1.30	12.9	22.8	<0.02	0.05	<0.03	<0.02	<0.02	0.32	<0.06	0.58	0.93	0.06	0.16	0.63	0.15	0.11	0.12	<0.09	<0.09	<0.05	35.7	76.3
67	SV9	0.39	<0.03	0.83	14.7	21.6	<0.02	0.04	<0.03	<0.02	<0.02	0.27	<0.06	0.58	0.55	<0.02	0.16	0.44	0.10	<0.06	<0.09	<0.09	<0.09	<0.05	36.5	76.1
68	SV9	0.54	<0.03	1.23	14.2	23.7	<0.02	0.10	<0.03	<0.02	<0.02	0.18	<0.06	0.61	0.91	<0.02	0.20	0.67	0.12	<0.06	0.18	<0.09	<0.09	0.09	37.7	80.4
69	SV9	0.53	0.16	1.35	12.3	22.6	<0.02	0.06	0.03	0.02	<0.02	0.28	<0.06	0.66	1.21	<0.02	0.26	0.81	0.12	0.12	0.16	<0.09	<0.09	<0.05	34.4	75.0
70	SV9	0.68	0.08	1.16	13.9	23.4	<0.02	0.08	0.07	<0.02	<0.02	0.89	<0.06	0.68	0.97	<0.02	0.17	0.64	0.13	0.14	0.13	<0.09	<0.09	<0.05	37.5	80.7
71	SV9	0.33	<0.03	0.54	15.2	20.9	<0.02	0.05	<0.03	<0.02	<0.02	0.31	<0.06	0.71	0.54	<0.02	0.17	0.60	0.13	0.13	0.09	<0.09	<0.09	<0.05	35.5	75.3
72	SV9	0.53	0.03	1.27	12.7	22.4	<0.02	0.14	0.07	<0.02	<0.02	0.27	<0.06	0.75	0.59	<0.02	0.18	0.61	0.16	0.13	0.23	<0.09	0.10	0.10	34.9	75.1
73	SV9	0.35	0.07	0.83	13.6	20.0	<0.02	0.05	<0.03	<0.02	<0.02	0.20	<0.06	0.79	0.98	<0.02	0.29	1.08	0.27	0.29	0.16	<0.09	<0.09	0.07	31.7	70.8
74	SV9	0.62	0.06	1.67	11.7	24.0	<0.02	0.12	0.13	0.02	0.02	0.54	<0.06	0.80	1.52	0.18	0.40	1.40	0.18	0.18	0.12	<0.09	<0.09	<0.05	34.4	78.0
75	SV9	0.49	0.04	1.22	14.0	23.1	<0.02	0.07	<0.03	0.02	0.02	0.37	<0.06	0.84	1.18	0.07	0.33	1.14	0.17	0.12	0.17	<0.09	<0.09	0.06	35.8	79.2
76	SV9	0.41	0.04	1.44	12.4	22.2	<0.02	0.09	0.04	<0.02	<0.02	0.22	<0.06	0.87	1.38	<0.02	0.25	1.06	0.25	0.10	0.23	<0.09	<0.09	0.09	33.2	74.3
77	SV9	0.42	<0.03	0.71	13.8	19.8	<0.02	0.03	<0.03	<0.02	<0.02	0.20	<0.06	0.90	0.25	<0.02	0.19	0.64	0.22	0.15	0.21	<0.09	0.10	0.07	32.6	70.3
78	SV9	0.42	0.04	1.16	14.8	23.8	<0.02	0.04	0.02	<0.02	0.02	0.27	<0.06	0.91	1.08	0.08	0.28	0.98	0.20	0.18	0.18	<0.09	<0.09	0.06	37.3	81.8
79	SV9	0.55	0.03	1.27	13.8	22.9	<0.02	0.06	0.02	<0.02	<0.02	0.33	<0.06	1.01	1.53	0.12	0.46	1.46	0.25	0.11	0.16	0.10	0.13	0.07	34.0	78.4
80	SV9	0.49	0.08	1.46	12.4	23.6	<0.02	0.08	0.07	0.02	0.03	0.99	<0.06	1.08	1.50	0.14	0.50	1.77	0.22	0.21	0.11	<0.09	<0.09	<0.05	33.9	78.6
81	SV9	0.60	0.09	1.51	12.2	24.3	<0.02	0.15	0.10	<0.02	0.02	1.16	<0.06	1.08	0.84	0.09	0.27	1.01	0.22	0.20	0.20	<0.09	0.11	0.05	36.1	80.3
82	SV9	0.51	0.05	1.26	13.6	23.1	<0.02	0.17	0.02	<0.02	0.02	0.17	<0.06	1.10	1.72	0.08	0.41	1.38	0.23	0.23	0.19	<0.09	0.12	0.13	33.8	78.3
83	SV9	0.59	<0.03	0.91	12.7	20.3	<0.02	0.04	<0.03	<0.02	0.04	0.71	<0.06	1.15	0.55	0.12	0.26	0.96	0.28	0.20	0.25	<0.09	0.12	0.08	31.4	70.7
84	SV9	0.50	0.06	1.67	11.6	23.9	<0.02	0.18	0.16	<0.02	<0.02	0.42	<0.06	1.16	0.85	0.05	0.23	1.08	0.26	0.27	0.25	<0.09	<0.09	0.13	34.7	77.5
85	SV9	0.52	0.04	1.09	11.3	20.2	<0.02	0.09	0.07	<0.02	0.04	0.97	<0.06	1.18	0.78	0.15	0.35	1.20	0.27	0.25	0.26	<0.09	0.13	0.07	29.6	68.5
86	SV9	0.42	0.03	1.08	15.9	24.2	<0.02	0.12	0.03	<0.02	<0.02	0.14	<0.06	1.25	0.39	<0.02	0.17	0.68	0.22	0.21	0.25	<0.09	0.15	0.18	39.0	84.5
87	SV9	0.40	<0.03	0.97	15.0	23.2	<0.02	0.06	<0.03	<0.02	0.02	0.36	<0.06	1.31	0.47	0.06	0.17	0.78	0.20	0.25	0.25	<0.09	0.21	0.11	36.8	80.6

No.	Sample	F	Na	Mg	Al	Si	P	Ca	K	Ti	Mn	Fe	Th	Y	La	Ce	Pr	Nd	Sm	Gd	Dy	Ho	Er	Yb	O	Total
88	SV9	0.40	<0.03	0.90	12.3	19.4	<0.02	0.02	<0.03	<0.02	0.04	0.29	<0.06	1.32	0.64	<0.02	0.26	1.17	0.36	0.37	0.41	<0.09	0.15	0.15	29.0	67.1
89	SV9	0.45	0.03	1.43	10.4	21.0	<0.02	0.04	<0.03	<0.02	0.05	0.28	<0.06	2.04	0.94	0.13	0.42	1.91	0.42	0.41	0.40	0.11	0.18	0.11	27.3	68.1
90	SV9	0.55	<0.03	1.52	9.9	20.9	<0.02	0.04	<0.03	<0.02	0.06	0.36	<0.06	2.29	1.20	0.14	0.66	2.53	0.53	0.48	0.39	0.10	0.12	0.11	25.2	67.1
91	SV9	0.40	0.03	1.19	10.4	19.7	<0.02	0.06	<0.03	<0.02	<0.02	0.69	<0.06	2.77	0.82	0.09	0.68	2.82	0.69	0.58	0.55	0.15	0.19	0.15	23.4	65.4
92	SV9	0.59	0.04	1.57	12.2	24.1	<0.02	0.07	<0.03	<0.02	<0.02	0.34	<0.06	<0.06	0.60	<0.02	0.10	0.18	<0.05	<0.06	<0.09	<0.09	<0.09	<0.05	38.7	78.5
93	SV9	0.43	0.21	1.17	13.5	23.1	<0.02	0.14	0.10	<0.02	<0.02	0.37	<0.06	<0.06	0.21	<0.02	<0.06	0.05	<0.05	<0.06	<0.09	<0.09	<0.09	<0.05	39.1	78.4
94	SV9	0.54	0.19	0.64	13.7	19.3	<0.02	0.06	<0.03	<0.02	<0.02	0.13	<0.06	0.31	0.36	<0.02	<0.06	0.20	0.07	<0.06	0.08	<0.09	<0.09	<0.05	33.8	69.4
95	SV9	0.52	<0.03	0.98	12.5	20.7	<0.02	0.22	0.07	<0.02	<0.02	0.80	<0.06	0.20	0.63	<0.02	0.07	0.30	0.08	0.10	<0.09	<0.09	<0.09	<0.05	34.4	71.6
96	SV9	0.38	<0.03	1.03	13.6	21.1	<0.02	0.16	0.04	<0.02	<0.02	0.20	<0.06	0.27	0.54	<0.02	0.09	0.31	0.08	<0.06	<0.09	<0.09	<0.09	<0.05	35.6	73.4
97	SV9	0.57	0.12	0.90	13.7	21.2	<0.02	0.05	0.07	<0.02	0.02	0.39	<0.06	0.54	0.56	<0.02	0.11	0.38	0.09	0.07	<0.09	<0.09	<0.09	<0.05	35.4	74.2
98	SV9	0.44	<0.03	1.13	12.2	21.3	<0.02	0.21	0.04	<0.02	<0.02	0.92	<0.06	0.22	0.65	<0.02	0.09	0.29	0.06	<0.06	<0.09	<0.09	<0.09	<0.05	35.0	72.6
99	SV9	0.36	0.06	0.83	13.4	21.6	<0.02	0.08	0.67	0.13	0.03	1.71	<0.06	<0.06	0.21	1.13	<0.06	<0.05	0.04	<0.06	<0.09	<0.09	<0.09	<0.05	36.8	77.0
100	SV9	0.38	<0.03	0.88	14.8	21.8	<0.02	0.14	0.03	<0.02	<0.02	0.24	<0.06	0.19	0.55	<0.02	0.10	0.30	<0.05	<0.06	<0.09	<0.09	<0.09	<0.05	37.7	77.1
101	SV9	0.27	0.02	0.90	14.4	21.9	<0.02	0.31	0.05	<0.02	<0.02	0.24	<0.06	0.12	0.45	<0.02	0.07	0.17	<0.05	<0.06	<0.09	<0.09	<0.09	<0.05	37.8	76.7
102	SV9	0.39	<0.03	1.04	14.1	21.9	<0.02	0.22	0.04	<0.02	<0.02	0.24	<0.06	0.24	0.48	<0.02	0.07	0.30	0.06	<0.06	<0.09	<0.09	<0.09	<0.05	37.2	76.3
103	SV9	0.62	0.04	1.34	13.7	21.9	<0.02	0.32	0.08	<0.02	<0.02	0.29	<0.06	0.10	0.57	<0.02	<0.06	0.15	<0.05	<0.06	<0.09	<0.09	<0.09	<0.05	37.5	76.6
104	SV9	0.46	0.05	1.01	14.4	21.9	<0.02	0.14	0.04	<0.02	<0.02	0.23	<0.06	<0.06	0.24	<0.02	<0.06	<0.05	<0.05	<0.06	<0.09	<0.09	<0.09	<0.05	38.4	76.9
105	SV9	0.48	0.04	1.18	14.9	22.0	0.03	0.31	0.07	<0.02	<0.02	0.15	<0.06	0.19	0.46	0.01	0.07	0.17	<0.05	<0.06	<0.09	<0.09	<0.09	<0.05	38.5	78.6
106	SV9	0.30	<0.03	0.77	15.4	22.2	<0.02	0.13	0.04	<0.02	<0.02	0.21	<0.06	<0.06	0.19	<0.02	<0.06	<0.05	<0.05	<0.06	<0.09	<0.09	<0.09	<0.05	39.4	78.6
107	SV9	0.33	0.04	1.24	11.4	22.4	<0.02	0.16	0.07	<0.02	<0.02	0.23	<0.06	<0.06	0.25	<0.02	<0.06	<0.05	<0.05	0.07	<0.09	<0.09	<0.09	<0.05	36.3	72.5
108	SV9	0.41	<0.03	1.19	14.6	22.5	<0.02	0.28	0.05	<0.02	<0.02	0.18	<0.06	0.21	0.52	<0.02	0.10	0.26	0.07	<0.06	<0.09	<0.09	<0.09	<0.05	38.4	78.7
109	SV9	0.44	<0.03	1.26	12.5	22.5	<0.02	0.34	<0.03	<0.02	<0.02	0.28	<0.06	0.28	0.56	<0.02	0.10	0.29	0.08	<0.06	<0.09	<0.09	<0.09	<0.05	36.6	75.2
110	SV9	0.34	<0.03	0.72	16.0	22.6	<0.02	0.13	<0.03	<0.02	<0.02	0.35	<0.06	0.12	0.46	<0.02	<0.06	0.10	<0.05	<0.06	<0.09	<0.09	<0.09	<0.05	39.9	80.7
111	SV9	0.33	<0.03	0.98	14.4	22.7	<0.02	0.19	0.05	<0.02	<0.02	0.24	<0.06	0.21	0.59	<0.02	0.09	0.28	<0.05	<0.06	<0.09	<0.09	<0.09	<0.05	38.3	78.4
112	SV9	0.41	<0.03	1.23	13.3	22.7	<0.02	0.17	0.04	<0.02	<0.02	0.26	<0.06	0.27	0.80	<0.02	0.13	0.36	0.09	<0.06	<0.09	<0.09	<0.09	<0.05	37.1	76.9
113	SV9	0.41	0.04	1.07	14.1	22.8	<0.02	0.21	0.03	<0.02	<0.02	0.31	<0.06	0.20	0.51	<0.02	0.06	0.26	0.08	0.07	<0.09	<0.09	<0.09	<0.05	38.4	78.6
114	SV9	0.54	0.06	0.97	15.9	22.8	<0.02	0.05	0.04	<0.02	0.02	0.22	<0.06	0.57	0.56	0.06	0.18	0.56	0.09	<0.06	0.09	<0.09	<0.09	<0.05	38.8	81.6
115	SV9	0.54	0.04	1.36	12.4	22.9	<0.02	0.21	0.07	<0.02	<0.02	0.30	<0.06	0.32	0.82	<0.02	0.12	0.45	0.08	<0.06	<0.09	<0.09	<0.09	<0.05	36.5	76.1
116	SV9	0.30	<0.03	1.13	11.0	23.0	<0.02	0.23	0.10	<0.02	<0.02	0.81	<0.06	0.21	0.61	0.02	0.12	0.30	0.06	<0.06	<0.09	<0.09	<0.09	<0.05	35.9	73.9
117	SV9	0.39	0.08	1.05	14.6	23.0	<0.02	0.14	0.50	0.13	0.02	1.74	<0.06	<0.06	0.23	<0.02	<0.06	<0.05	<0.05	<0.06	<0.09	<0.09	<0.09	<0.05	40.7	82.6
118	SV9	0.50	0.03	1.12	14.6	23.0	<0.02	0.05	<0.03	<0.02	<0.02	0.13	<0.06	0.67	0.69	0.05	0.13	0.50	0.14	0.11	0.14	<0.09	<0.09	<0.05	37.7	79.6
119	SV9	0.39	<0.03	1.02	15.3	23.3	<0.02	0.16	0.04	<0.02	<0.02	0.20	<0.06	0.33	0.47	<0.02	<0.06	0.26	0.09	<0.06	<0.09	<0.09	<0.09	<0.05	39.8	81.3
120	SV9	0.55	0.12	1.34	13.6	23.3	<0.02	0.18	0.11	<0.02	<0.02	0.22	<0.06	0.13	0.77	0.04	0.07	0.21	<0.05	<0.06	<0.09	<0.09	<0.09	<0.05	38.6	79.2
121	SV9	0.50	<0.03	1.00	15.0	23.3	<0.02	0.05	0.10	0.04	<0.02	0.67	<0.06	0.51	0.73	<0.02	0.10	0.42	0.11	<0.06	<0.09	<0.09	<0.09	<0.05	39.0	81.5
122	SV9	0.33	0.03	1.12	13.7	23.3	<0.02	0.17	0.06	0.02	<0.02	0.27	<0.06	0.20	0.59	<0.02	0.08	0.23	0.06	<0.06	<0.09	<0.09	<0.09	<0.05	38.6	78.8
123	SV9	0.72	0.05	1.73	12.8	23.4	<0.02	0.21	0.06	<0.02	<0.02	0.21	<0.06	<0.06	0.38	<0.02	0.06	<0.05	<0.05	<0.06	<0.09	<0.09	<0.09	<0.05	38.9	78.5
124	SV9	0.41	0.06	1.34	13.2	23.4	<0.02	0.08	0.04	<0.02	<0.02	0.29	<0.06	<0.06	0.62	<0.02	0.07	0.14	<0.05	<0.06	<0.09	<0.09	<0.09	<0.05	38.6	78.3
125	SV9	0.33	<0.03	1.07	15.1	23.4	<0.02	0.40	0.04	<0.02	<0.02	0.33	<0.06	0.13	0.41	<0.02	<0.06	0.25	0.06	<0.06	<0.09	<0.09	<0.09	<0.05	40.3	81.9
126	SV9	0.42	<0.03	1.20	14.3	23.5	<0.02	0.24	0.07	<0.02	<0.02	0.25	<0.06	0.14	0.55	<0.02	0.08	0.18	<0.05	<0.06	<0.09	<0.09	<0.09	<0.05	39.6	80.5
127	SV9	0.45	<0.03	1.00	15.6	23.6	<0.02	<0.02	<0.03	<0.02	0.02	0.34	<0.06	0.61	0.53	<0.02	0.10	0.41	0.10	0.09	0.09	<0.09	<0.09	<0.05	39.7	82.6
128	SV9	0.28	0.04	1.24	13.9	23.6	<0.02	0.17	0.07	<0.02	<0.02	0.28	<0.06	0.27	0.72	<0.02	0.10	0.34	0.07	<0.06	<0.09	<0.09	<0.09	<0.05	38.8	79.9
129	SV9	0.42	0.04	1.22	14.1	23.7	<0.02	0.17	0.05	<0.02	<0.02	0.36	<0.06	0.18	0.75	<0.02	0.13	0.27	0.07	<0.06	<0.09	<0.09	<0.09	<0.05	39.2	80.6
130	SV9	0.41	0.01	1.00	15.4	23.9	<0.02	0.18	0.04	<0.02	<0.02	0.27	<0.06	0.24	0.48	<0.02	0.10	0.23	<0.05	<0.06	<0.09	<0.09	<0.09	<0.05	40.7	83.0
131	SV9	0.53	0.06	1.31	14.0	23.9	<0.02	0.14	0.07	0.02	<0.02	0.42	<0.06	0.07	0.48	<0.02	0.06	0.09	<0.05	<0.06	<0.09	<0.09	<0.09	<0.05	40.1	81.3

No.	Sample	F	Na	Mg	Al	Si	P	Ca	K	Ti	Mn	Fe	Th	Y	La	Ce	Pr	Nd	Sm	Gd	Dy	Ho	Er	Yb	O	Total
132	SV9	0.53	0.04	1.15	15.3	23.9	<0.02	0.26	0.13	<0.02	<0.02	0.22	<0.06	0.07	0.44	0.00	<0.06	<0.05	<0.05	<0.06	<0.09	<0.09	<0.09	<0.05	41.3	83.4
133	SV9	0.35	0.03	0.91	14.8	23.9	<0.02	0.14	0.07	<0.02	<0.02	0.41	<0.06	0.11	0.41	<0.02	<0.06	<0.05	<0.05	<0.06	<0.09	<0.09	<0.09	<0.05	40.8	82.0
134	SV9	0.60	0.07	1.38	12.5	23.9	<0.02	0.10	0.05	<0.02	<0.02	1.30	<0.06	<0.06	0.16	<0.02	<0.06	<0.05	<0.05	<0.06	<0.09	<0.09	<0.09	<0.05	39.8	79.9
135	SV9	0.50	0.03	1.05	15.7	24.0	<0.02	0.15	<0.03	<0.02	<0.02	0.21	<0.06	0.29	0.50	<0.02	0.09	0.24	<0.05	<0.06	<0.09	<0.09	<0.09	<0.05	41.1	83.9
136	SV9	0.53	<0.03	1.31	14.6	24.2	<0.02	0.28	0.08	<0.02	<0.02	0.32	<0.06	0.12	0.64	<0.02	0.08	0.21	<0.05	<0.06	<0.09	<0.09	<0.09	<0.05	40.6	82.9
137	SV9	0.45	0.07	1.21	15.1	24.3	<0.02	0.26	0.12	<0.02	<0.02	0.24	<0.06	<0.06	0.48	<0.02	<0.06	0.09	<0.05	<0.06	<0.09	<0.09	<0.09	<0.05	41.6	83.9
138	SV9	0.71	0.17	1.06	15.1	24.3	<0.02	0.17	0.16	<0.02	<0.02	0.52	<0.06	0.13	0.43	<0.02	<0.06	0.10	0.05	<0.06	<0.09	<0.09	<0.09	<0.05	41.6	84.5
139	SV9	0.42	0.12	1.23	13.3	24.4	<0.02	0.18	0.09	0.02	<0.02	2.01	<0.06	0.44	1.20	0.07	0.27	0.83	0.09	0.14	<0.09	<0.09	<0.09	<0.05	38.5	83.3
140	SV9	0.50	0.10	1.39	12.8	24.5	<0.02	0.12	0.09	0.02	<0.02	1.80	<0.06	0.15	0.79	0.01	0.08	0.23	<0.05	<0.06	<0.09	<0.09	<0.09	<0.05	39.8	82.3
141	SV9	0.45	0.07	1.31	14.8	24.6	<0.02	0.18	0.09	<0.02	<0.02	0.32	<0.06	0.07	0.38	<0.02	<0.06	<0.05	<0.05	<0.06	<0.09	<0.09	<0.09	<0.05	41.8	84.1
142	SV9	0.66	0.07	1.58	12.8	24.7	<0.02	0.25	0.09	<0.02	<0.02	1.05	<0.06	0.17	0.74	<0.02	0.08	0.23	<0.05	<0.06	<0.09	<0.09	<0.09	<0.05	40.0	82.4
143	SV9	<0.16	0.32	1.22	10.9	24.9	<0.02	0.13	0.26	0.88	<0.02	2.64	<0.06	0.41	0.57	0.04	0.08	0.27	0.06	<0.06	<0.09	<0.09	<0.09	<0.05	39.5	82.1
144	SV9	0.51	0.07	1.28	13.7	24.9	<0.02	0.17	0.07	<0.02	<0.02	1.93	<0.06	<0.06	0.57	<0.02	<0.06	0.08	<0.05	<0.06	<0.09	<0.09	<0.09	<0.05	41.7	85.0
145	SV9	0.44	0.07	1.28	13.8	25.1	<0.02	0.20	0.08	<0.02	<0.02	0.32	<0.06	<0.06	0.38	<0.02	<0.06	<0.05	<0.05	0.09	<0.09	<0.09	<0.09	<0.05	41.5	83.2
146	SV9	0.12	0.41	1.19	9.7	25.2	0.03	0.13	0.54	0.41	<0.02	4.73	<0.06	0.25	0.67	0.05	0.08	0.33	0.07	<0.06	<0.09	<0.09	<0.09	<0.05	39.3	83.2
147	SV9	0.75	0.05	1.55	13.5	26.0	<0.02	0.05	0.06	<0.02	<0.02	1.41	<0.06	<0.06	0.38	<0.02	0.07	0.11	<0.05	<0.06	<0.09	<0.09	<0.09	<0.05	42.7	86.6
148	SV11	<0.16	<0.03	<0.02	14.8	16.7	<0.02	<0.02	<0.03	0.02	<0.02	0.95	<0.06	<0.06	<0.04	<0.02	<0.06	<0.05	<0.05	<0.06	<0.09	<0.09	<0.09	<0.05	32.6	65.1
149	SV11	<0.16	<0.03	<0.02	16.9	18.6	<0.02	<0.02	<0.03	0.02	<0.02	0.67	<0.06	<0.06	<0.04	<0.02	<0.06	<0.05	<0.05	<0.06	<0.09	<0.09	<0.09	<0.05	36.6	72.9
150	SV11	<0.16	<0.03	<0.02	14.5	16.7	<0.02	<0.02	<0.03	0.04	<0.02	0.49	<0.06	<0.06	<0.04	<0.02	<0.06	<0.05	<0.05	<0.06	<0.09	<0.09	<0.09	<0.05	32.1	63.7
151	SV11	<0.16	<0.03	<0.02	16.0	17.4	<0.02	<0.02	0.05	0.04	<0.02	4.57	<0.06	<0.06	<0.04	<0.02	<0.06	<0.05	<0.05	<0.06	<0.09	<0.09	<0.09	<0.05	36.1	74.1
152	SV11	<0.16	<0.03	0.02	16.5	18.7	<0.02	<0.02	<0.03	0.04	<0.02	0.57	<0.06	<0.06	<0.04	<0.02	<0.06	<0.05	<0.05	<0.06	<0.09	<0.09	<0.09	<0.05	36.3	72.1
153	SV11	<0.16	<0.03	0.03	17.0	19.3	<0.02	<0.02	0.12	0.04	<0.02	1.26	<0.06	<0.06	<0.04	<0.02	<0.06	<0.05	<0.05	<0.06	<0.09	<0.09	<0.09	<0.05	37.7	75.5
154	SV11	<0.16	<0.03	<0.02	17.7	19.8	<0.02	0.04	<0.03	0.04	<0.02	0.70	<0.06	<0.06	<0.04	<0.02	<0.06	<0.05	<0.05	<0.06	<0.09	<0.09	<0.09	<0.05	38.7	77.0
155	SV11	<0.16	<0.03	<0.02	17.2	18.9	<0.02	<0.02	<0.03	0.05	<0.02	0.62	<0.06	<0.06	<0.04	<0.02	<0.06	<0.05	<0.05	<0.06	<0.09	<0.09	<0.09	<0.05	37.2	73.9
156	SV11	<0.16	<0.03	0.05	14.4	15.7	<0.02	<0.02	0.22	0.14	0.10	14.54	<0.06	<0.06	<0.04	<0.02	<0.06	<0.05	<0.05	<0.06	<0.09	<0.09	<0.09	<0.05	37.2	82.3
157	SV11	<0.16	<0.03	0.11	15.3	18.1	<0.02	<0.02	1.33	0.23	0.05	5.03	<0.06	<0.06	<0.04	<0.02	<0.06	<0.05	<0.05	<0.06	<0.09	<0.09	<0.09	<0.05	37.1	77.3
158	SV11	<0.16	<0.03	0.02	17.6	18.7	<0.02	<0.02	0.06	1.65	<0.02	3.30	<0.06	<0.06	<0.04	<0.02	<0.06	<0.05	<0.05	<0.06	<0.09	<0.09	<0.09	<0.05	39.6	81.0
159	SV11	<0.16	<0.03	<0.02	14.0	15.8	<0.02	<0.02	<0.03	<0.02	<0.02	0.86	<0.06	<0.06	<0.04	<0.02	<0.06	<0.05	<0.05	<0.06	<0.09	<0.09	<0.09	<0.05	30.9	61.6
160	SV11	<0.16	<0.03	<0.02	14.6	16.5	<0.02	<0.02	<0.03	<0.02	<0.02	0.51	<0.06	<0.06	<0.04	<0.02	<0.06	<0.05	<0.05	<0.06	<0.09	<0.09	<0.09	<0.05	32.0	63.5
161	SV11	<0.16	<0.03	<0.02	14.4	16.5	<0.02	<0.02	<0.03	<0.02	<0.02	0.38	<0.06	<0.06	<0.04	<0.02	<0.06	<0.05	<0.05	<0.06	<0.09	<0.09	<0.09	<0.05	31.8	63.1
162	SV11	<0.16	<0.03	<0.02	14.6	16.5	<0.02	<0.02	0.06	<0.02	<0.02	1.93	<0.06	<0.06	<0.04	<0.02	<0.06	<0.05	<0.05	<0.06	<0.09	<0.09	<0.09	<0.05	32.6	65.6
163	SV11	<0.16	<0.03	<0.02	14.7	16.8	<0.02	<0.02	0.03	<0.02	<0.02	0.87	<0.06	<0.06	<0.04	<0.02	<0.06	<0.05	<0.05	<0.06	<0.09	<0.09	<0.09	<0.05	32.6	65.0
164	SV11	<0.16	<0.03	<0.02	15.5	17.9	<0.02	<0.02	0.05	<0.02	<0.02	0.95	<0.06	<0.06	<0.04	<0.02	<0.06	<0.05	<0.05	<0.06	<0.09	<0.09	<0.09	<0.05	34.6	69.0
165	SV11	<0.16	<0.03	0.02	15.7	18.0	<0.02	<0.02	<0.03	<0.02	<0.02	0.51	<0.06	<0.06	<0.04	<0.02	<0.06	<0.05	<0.05	<0.06	<0.09	<0.09	<0.09	<0.05	34.7	68.9
166	SV11	<0.16	<0.03	<0.02	18.6	19.6	<0.02	<0.02	<0.03	<0.02	<0.02	0.79	<0.06	<0.06	<0.04	<0.02	<0.06	<0.05	<0.05	<0.06	<0.09	<0.09	<0.09	<0.05	39.3	78.4
167	SV11	<0.16	<0.03	<0.02	18.3	20.4	<0.02	0.03	<0.03	<0.02	<0.02	0.73	<0.06	<0.06	<0.04	<0.02	<0.06	<0.05	<0.05	<0.06	<0.09	<0.09	<0.09	<0.05	39.8	79.3
168	SV11	<0.16	<0.03	0.04	19.8	22.0	<0.02	<0.02	0.15	<0.02	<0.02	2.04	<0.06	<0.06	<0.04	<0.02	<0.06	<0.05	<0.05	<0.06	<0.09	<0.09	<0.09	<0.05	43.7	87.8
169	SV11	<0.16	<0.03	0.02	19.9	22.1	<0.02	<0.02	0.17	<0.02	<0.02	2.27	<0.06	<0.06	<0.04	<0.02	<0.06	<0.05	<0.05	<0.06	<0.09	<0.09	<0.09	<0.05	43.9	88.4
170	SV13	<0.16	<0.03	<0.02	14.4	16.5	<0.02	0.02	0.05	0.02	<0.02	0.76	<0.06	<0.06	<0.04	<0.02	<0.06	<0.05	<0.05	<0.06	<0.09	<0.09	<0.09	<0.05	31.9	63.6
171	SV13	0.18	<0.03	0.02	17.9	19.9	<0.02	0.03	0.12	0.03	<0.02	1.50	<0.06	<0.06	<0.04	<0.02	<0.06	<0.05	<0.05	<0.06	<0.09	<0.09	<0.09	<0.05	39.4	79.1
172	SV13	<0.16	<0.03	<0.02	18.6	20.8	<0.02	<0.02	0.06	0.03	<0.02	1.86	<0.06	<0.06	<0.04	<0.02	<0.06	<0.05	<0.05	<0.06	<0.09	<0.09	<0.09	<0.05	41.1	82.4
173	SV13	<0.16	<0.03	<0.02	16.2	18.4	<0.02	0.01	0.06	0.04	<0.02	2.25	<0.06	<0.06	<0.04	<0.02	<0.06	<0.05	<0.05	<0.06	<0.09	<0.09	<0.09	<0.05	36.3	73.3

No.	Sample	F	Na	Mg	Al	Si	P	Ca	K	Ti	Mn	Fe	Th	Y	La	Ce	Pr	Nd	Sm	Gd	Dy	Ho	Er	Yb	O	Total
174	SV13	<0.16	<0.03	0.04	14.9	17.5	<0.02	0.02	0.21	0.06	<0.02	2.42	<0.06	<0.06	<0.04	<0.02	<0.06	<0.05	<0.05	<0.06	<0.09	<0.09	<0.09	<0.05	34.3	69.4
175	SV13	0.20	<0.03	0.04	19.2	21.8	<0.02	0.02	0.20	0.10	<0.02	2.89	<0.06	<0.06	<0.04	<0.02	<0.06	<0.05	<0.05	<0.06	<0.09	<0.09	<0.09	<0.05	43.2	87.6
176	SV13	0.17	<0.03	0.07	18.2	20.7	<0.02	0.03	0.49	0.13	<0.02	2.84	<0.06	<0.06	<0.04	<0.02	<0.06	<0.05	<0.05	<0.06	<0.09	<0.09	<0.09	<0.05	41.3	83.9
177	SV13	<0.16	<0.03	<0.02	14.8	17.0	<0.02	0.01	<0.03	<0.02	<0.02	0.63	<0.06	<0.06	<0.04	<0.02	<0.06	<0.05	<0.05	<0.06	<0.09	<0.09	<0.09	<0.05	32.9	65.4
178	SV13	<0.16	<0.03	<0.02	14.8	17.1	<0.02	<0.02	<0.03	<0.02	<0.02	0.64	<0.06	<0.06	<0.04	<0.02	<0.06	<0.05	<0.05	<0.06	<0.09	<0.09	<0.09	<0.05	33.0	65.5
179	SV13	0.16	0.03	<0.02	15.0	17.4	<0.02	0.03	<0.03	<0.02	<0.02	0.64	<0.06	<0.06	<0.04	<0.02	<0.06	<0.05	<0.05	<0.06	<0.09	<0.09	<0.09	<0.05	33.5	66.9
180	SV13	<0.16	<0.03	<0.02	14.9	17.4	<0.02	<0.02	<0.03	<0.02	<0.02	0.65	<0.06	<0.06	<0.04	<0.02	<0.06	<0.05	<0.05	<0.06	<0.09	<0.09	<0.09	<0.05	33.5	66.5
181	SV13	0.20	<0.03	<0.02	15.7	17.7	<0.02	0.03	0.05	<0.02	<0.02	0.61	<0.06	<0.06	<0.04	<0.02	<0.06	<0.05	<0.05	<0.06	<0.09	<0.09	<0.09	<0.05	34.4	68.8
182	SV13	0.17	<0.03	<0.02	15.9	17.8	<0.02	0.02	<0.03	<0.02	<0.02	0.97	<0.06	<0.06	<0.04	<0.02	<0.06	<0.05	<0.05	<0.06	<0.09	<0.09	<0.09	<0.05	34.9	69.8
183	SV13	<0.16	<0.03	<0.02	15.9	18.0	<0.02	0.02	<0.03	<0.02	<0.02	0.66	<0.06	<0.06	<0.04	<0.02	<0.06	<0.05	<0.05	<0.06	<0.09	<0.09	<0.09	<0.05	35.1	69.6
184	SV13	<0.16	<0.03	<0.02	16.0	18.0	<0.02	0.02	<0.03	<0.02	<0.02	0.64	<0.06	<0.06	<0.04	<0.02	<0.06	<0.05	<0.05	<0.06	<0.09	<0.09	<0.09	<0.05	35.0	69.7
185	SV13	<0.16	<0.03	0.02	17.7	20.1	<0.02	0.01	0.12	<0.02	<0.02	1.09	<0.06	<0.06	<0.04	<0.02	<0.06	<0.05	<0.05	<0.06	<0.09	<0.09	<0.09	<0.05	39.2	78.2
186	SV14	0.31	<0.03	0.4	18.5	21.9	<0.02	0.02	<0.03	<0.02	<0.02	0.36	<0.06	<0.06	0.13	0.06	<0.06	0.05	<0.05	<0.06	<0.09	<0.09	<0.09	<0.05	43.0	84.8
187	SV14	0.40	<0.03	0.4	17.2	21.0	<0.02	0.03	0.04	<0.02	<0.02	0.41	<0.06	<0.06	0.13	<0.02	<0.06	<0.05	<0.05	<0.06	<0.09	<0.09	<0.09	<0.05	40.8	80.6
188	SV14	0.26	0.08	0.7	16.8	22.4	<0.02	0.02	<0.03	<0.02	<0.02	0.73	<0.06	<0.06	0.17	0.07	<0.06	0.09	<0.05	0.09	<0.09	<0.09	<0.09	<0.05	42.4	83.8
189	SV14	0.48	0.03	0.4	18.1	22.5	<0.02	0.02	<0.03	<0.02	<0.02	0.48	<0.06	<0.06	0.13	0.06	<0.06	0.05	<0.05	<0.06	<0.09	<0.09	<0.09	<0.05	43.5	85.9
190	SV14	0.33	0.10	0.4	17.2	21.0	<0.02	<0.02	0.08	<0.02	<0.02	0.46	<0.06	<0.06	0.11	0.05	<0.06	<0.05	<0.05	0.07	<0.09	<0.09	<0.09	<0.05	40.6	80.4
191	SV14	0.47	0.04	0.4	18.2	21.9	<0.02	<0.02	0.04	<0.02	<0.02	0.50	<0.06	<0.06	0.11	0.04	<0.06	<0.05	<0.05	<0.06	<0.09	<0.09	<0.09	<0.05	42.7	84.4
192	SV14	0.49	0.05	0.5	17.0	21.1	<0.02	0.03	<0.03	<0.02	<0.02	0.67	<0.06	<0.06	0.12	0.06	<0.06	0.06	<0.05	0.12	<0.09	<0.09	<0.09	<0.05	40.8	80.9
193	SV14	0.57	0.06	0.4	18.2	22.5	<0.02	0.06	0.04	<0.02	<0.02	0.54	<0.06	<0.06	0.11	0.04	<0.06	<0.05	<0.05	<0.06	<0.09	<0.09	<0.09	<0.05	43.4	85.9
194	SV14	0.57	0.08	0.4	17.8	21.9	<0.02	0.08	0.05	<0.02	<0.02	0.54	<0.06	<0.06	0.13	0.04	<0.06	0.05	<0.05	<0.06	<0.09	<0.09	<0.09	<0.05	42.2	83.9
195	SV14	0.33	0.04	0.2	19.4	22.1	<0.02	<0.02	<0.03	<0.02	<0.02	0.32	<0.06	<0.06	0.04	<0.02	<0.06	<0.05	<0.05	<0.06	<0.09	<0.09	<0.09	<0.05	43.8	86.2
196	SV14	0.27	0.10	0.5	18.5	23.1	<0.02	0.03	0.05	<0.02	<0.02	1.18	<0.06	<0.06	0.12	<0.02	<0.06	<0.05	<0.05	0.07	<0.09	<0.09	<0.09	<0.05	44.7	88.6
197	SV14	0.42	0.13	0.4	17.8	22.3	<0.02	0.02	0.04	<0.02	<0.02	1.04	<0.06	<0.06	0.11	<0.02	<0.06	<0.05	<0.05	<0.06	<0.09	<0.09	<0.09	<0.05	43.0	85.3
198	SV14	0.40	0.12	0.6	18.0	23.4	<0.02	0.03	0.04	<0.02	<0.02	1.07	<0.06	<0.06	0.14	0.07	<0.06	0.07	<0.05	<0.06	<0.09	<0.09	<0.09	<0.05	44.7	88.7
199	SV14	0.35	0.04	0.4	15.9	19.8	<0.02	0.02	<0.03	<0.02	<0.02	0.49	<0.06	<0.06	0.11	0.04	<0.06	0.06	<0.05	0.11	<0.09	<0.09	<0.09	<0.05	38.2	75.5
200	SV14	0.44	0.14	0.8	17.0	23.5	<0.02	0.05	0.05	<0.02	<0.02	0.86	<0.06	<0.06	0.18	<0.02	<0.06	0.06	<0.05	<0.06	<0.09	<0.09	<0.09	<0.05	44.0	87.0
201	SV14	0.36	<0.03	0.2	14.9	19.1	<0.02	0.16	0.04	<0.02	<0.02	1.87	<0.06	0.13	0.56	0.12	0.10	0.33	0.06	<0.06	<0.09	<0.09	<0.09	<0.05	37.2	75.0
202	SV14	<0.16	<0.03	0.6	16.8	22.3	<0.02	0.18	0.15	<0.02	<0.02	0.69	<0.06	0.15	0.46	0.10	0.08	0.25	<0.05	<0.06	<0.09	<0.09	<0.09	<0.05	42.7	84.5
203	SV14	0.28	0.04	0.1	17.5	20.0	<0.02	0.10	0.06	<0.02	<0.02	1.18	<0.06	0.16	1.03	0.22	0.31	0.88	0.18	<0.06	0.12	<0.09	<0.09	0.05	40.4	82.6
204	SV14	0.23	0.07	0.4	17.5	22.2	0.09	1.33	0.12	<0.02	<0.02	1.23	<0.06	0.11	0.42	0.09	0.06	0.20	<0.05	<0.06	<0.09	<0.09	<0.09	<0.05	43.6	87.6
205	SV14	<0.16	0.03	0.1	19.6	22.9	<0.02	0.06	<0.03	<0.02	<0.02	0.59	<0.06	<0.06	0.13	<0.02	<0.06	0.10	<0.05	<0.06	<0.09	<0.09	<0.09	<0.05	45.4	89.0
206	SV14	0.20	0.03	0.3	16.8	21.6	<0.02	0.22	0.07	<0.02	<0.02	2.07	<0.06	0.15	0.47	0.12	0.10	0.24	0.06	<0.06	<0.09	<0.09	<0.09	<0.05	42.0	84.6
207	SV14	<0.16	0.04	0.1	19.2	21.9	<0.02	0.08	0.07	<0.02	<0.02	1.13	<0.06	0.09	0.19	0.06	<0.06	0.08	<0.05	<0.06	<0.09	<0.09	<0.09	<0.05	43.7	86.6
208	SV14	0.30	0.09	0.5	14.3	21.2	<0.02	0.31	0.20	<0.02	<0.02	1.88	<0.06	0.13	0.59	0.13	0.10	0.24	<0.05	<0.06	<0.09	<0.09	<0.09	<0.05	39.5	79.5
209	SV14	0.18	0.10	0.4	16.5	21.4	<0.02	0.27	0.31	<0.02	<0.02	1.12	<0.06	<0.06	0.38	0.09	0.07	0.22	<0.05	0.09	<0.09	<0.09	<0.09	<0.05	41.1	82.2
210	SV14	0.23	0.07	0.4	16.3	21.3	<0.02	0.16	<0.03	<0.02	<0.02	0.51	<0.06	0.10	0.32	0.09	<0.06	0.11	<0.05	<0.06	<0.09	<0.09	<0.09	<0.05	40.8	80.4
211	SV14	<0.16	<0.03	0.0	19.8	21.9	<0.02	0.03	<0.03	<0.02	<0.02	0.27	<0.06	<0.06	0.06	<0.02	<0.06	<0.05	<0.05	<0.06	<0.09	<0.09	<0.09	<0.05	43.8	85.9
212	SV14	0.23	0.10	0.3	17.7	22.2	<0.02	0.14	0.15	<0.02	<0.02	0.62	<0.06	0.10	0.27	0.07	<0.06	0.16	<0.05	<0.06	<0.09	<0.09	<0.09	<0.05	42.7	84.8
213	SV14	<0.16	<0.03	0.3	17.2	21.2	<0.02	0.15	0.09	<0.02	<0.02	0.63	<0.06	<0.06	0.32	0.07	<0.06	0.10	<0.05	<0.06	<0.09	<0.09	<0.09	<0.05	41.3	81.4
214	SV14	0.76	0.08	1.1	12.0	22.5	0.07	0.43	0.27	0.03	<0.02	3.99	<0.06	0.40	1.01	0.25	0.22	0.60	0.12	<0.06	<0.09	<0.09	<0.09	<0.05	40.9	84.7
215	SV14	0.50	0.08	1.0	13.0	21.2	0.15	0.38	0.24	0.10	<0.02	1.96	<0.06	0.58	0.57	0.18	0.09	0.33	0.08	0.07	<0.09	<0.09	<0.09	0.10	39.2	79.8
216	SV14	0.60	<0.03	1.0	13.4	22.1	0.29	0.27	1.79	0.08	<0.02	2.83	<0.06	0.30	0.60	0.15	0.09	0.33	<0.05	<0.06	0.11	<0.09	0.10	0.10	41.2	85.4
217	SV14	0.38	<0.03	0.4	16.6	21.9	<0.02	0.15	0.21	<0.02	<0.02	2.58	<0.06	0.24	0.36	0.11	<0.06	0.20	<0.05	<0.06	<0.09	<0.09	<0.09	<0.05	42.9	86.2

ISOCON ANALYSIS TABLES D

DDH00161

Element		Least weathered (bedrock)	Most weathered (ferruginous zone)	Slope to data point		Rescaled	Rescaled
		C_i^O (BR_29)	C_i^A (FZ_2)	C_i^A/C_i^O	*Scale*	C_i^A	C_i^O
Al_2O_3	wt %	12.5	15.6	1.24	1	15.6	12.5
TiO_2	wt %	0.22	0.4	1.64	70	25.2	15.4
Th	ppm	69.6	153	2.20	0.2	30.6	13.9
Zr	ppm	540	716	1.33	0.04	28.6	21.6
Hf	ppm	17.1	22.3	1.30	0.5	11.2	8.6
Nb	ppm	148	134.5	0.91	0.18	24.2	26.6

Element		Least weathered (bedrock)	Most weathered (mottled zone)	Slope to data point		Rescaled	Rescaled
		C_i^O (BR_29)	C_i^A (FZ_6.5)	C_i^A/C_i^O	*Scale*	C_i^A	C_i^O
Al_2O_3	wt %	12.5	20.9	1.67	1	20.9	12.5
TiO_2	wt %	0.22	0.36	1.64	70	25.2	15.4
Th	ppm	69.6	118	1.69	0.2	23.5	13.9
Zr	ppm	540	863	1.60	0.04	34.5	21.6
Hf	ppm	17.1	26.9	1.57	0.5	13.5	8.6
Nb	ppm	148	217	1.47	0.18	39.1	26.6

DDH0096

Element		Least weathered (bedrock)	Most weathered (ferruginous zone)	Slope to data point		Rescaled	Rescaled
		C_i^O (BR_39)	C_i^A (FZ_2)	C_i^A/C_i^O	*Scale*	C_i^A	C_i^O
Al_2O_3	wt %	13.2	19.6	1.48	1	19.6	13.2
TiO_2	wt %	0.31	0.6	1.77	70	38.5	21.7
Th	ppm	84.3	179	2.12	0.2	35.7	16.9
Zr	ppm	634	971	1.53	0.04	38.8	25.4
Hf	ppm	17.3	26.3	1.52	0.5	13.2	8.7
Nb	ppm	93	124.0	1.33	0.18	22.3	16.8

Element		Least weathered (bedrock)	Most weathered (mottled zone)	Slope to data point		Rescaled	Rescaled
		C_i^O (BR_39)	C_i^A (FZ_20)	C_i^A/C_i^O	*Scale*	C_i^A	C_i^O
Al_2O_3	wt %	13.2	20.8	1.58	1	20.8	13.2
TiO_2	wt %	0.31	0.53	1.71	70	37.1	21.7
Th	ppm	84.3	122	1.45	0.2	24.4	16.9
Zr	ppm	634	1080	1.70	0.04	43.2	25.4
Hf	ppm	17.3	28.1	1.62	0.5	14.1	8.7
Nb	ppm	93	132	1.41	0.18	23.7	16.8

DDH0061

Element		Least weathered (bedrock)	Most weathered (ferruginous zone)	Slope to data point		Rescaled	Rescaled
		C_i^O (BR_34.5)	C_i^A (FZ_2.5)	C_i^A/C_i^O	*Scale*	C_i^A	C_i^O
Al_2O_3	wt %	13.4	23.9	1.79	1	23.9	13.4
TiO_2	wt %	0.16	0.4	2.69	70	30.1	11.2
Th	ppm	56.1	136	2.42	0.2	27.2	11.2
Zr	ppm	413	784	1.90	0.04	31.4	16.5
Hf	ppm	14.0	26.0	1.86	0.5	13.0	7.0
Nb	ppm	155	248.0	1.60	0.18	44.6	27.9

Element		Least weathered (bedrock)	Most weathered (mottled zone)	Slope to data point		Rescaled	Rescaled
		C_i^O (BR_34.5)	C_i^A (FZ_15)	C_i^A/C_i^O	*Scale*	C_i^A	C_i^O
Al_2O_3	wt %	13.4	20.5	1.54	1	20.5	13.4
TiO_2	wt %	0.16	0.31	1.94	70	21.7	11.2
Th	ppm	56.1	80	1.43	0.2	16.0	11.2
Zr	ppm	413	610	1.48	0.04	24.4	16.5
Hf	ppm	14.0	20.2	1.44	0.5	10.1	7.0
Nb	ppm	155	200	1.29	0.18	36.0	27.9

DDH0266

Element		Least weathered (bedrock)	Most weathered (ferruginous zone)	Slope to data point		Rescaled	Rescaled
		C_i^O (BR_)	C_i^A (FZ_2.5)	C_i^A/C_i^O	*Scale*	C_i^A	C_i^O
Al_2O_3	wt %	13.2	19.4	1.47	1	19.4	13.2
TiO_2	wt %	0.38	0.4	1.11	70	29.4	26.6
Th	ppm	83.3	191	2.29	0.18	34.4	15.0
Zr	ppm	767	898	1.17	0.04	35.9	30.7
Hf	ppm	19.6	27.3	1.39	0.5	13.7	9.8
Nb	ppm	102	121.0	1.19	0.18	21.8	18.3

Element		Least weathered (bedrock)	Most weathered (mottled zone)	Slope to data point		Rescaled	Rescaled
		C_i^O (BR_)	C_i^A (FZ_7)	C_i^A/C_i^O	*Scale*	C_i^A	C_i^O
Al_2O_3	wt %	13.2	19.7	1.49	1	19.7	13.2
TiO_2	wt %	0.38	0.38	1.00	70	26.6	26.6
Th	ppm	83.3	97	1.16	0.18	17.5	15.0
Zr	ppm	767	838	1.09	0.04	33.5	30.7
Hf	ppm	19.6	23.6	1.20	0.5	11.8	9.8
Nb	ppm	102	131	1.29	0.18	23.6	18.3

DDH0121

Element		Least weathered (bedrock)	Most weathered (ferruginous zone)	Slope to data point		Rescaled	Rescaled
		C_i^O (BR_26)	C_i^A (FZ_2.5)	C_i^A/C_i^O	*Scale*	C_i^A	C_i^O
Al_2O_3	wt %	12.5	18.7	1.50	1	18.7	12.5
TiO_2	wt %	0.22	0.5	2.18	80	38.4	17.6
Th	ppm	69.6	119	1.70	0.2	23.7	13.9
Zr	ppm	540	1230	2.28	0.04	49.2	21.6
Hf	ppm	17.1	39.1	2.29	0.5	19.6	8.6
Nb	ppm	148	155.5	1.05	0.2	31.1	29.6

Element		Least weathered (bedrock)	Most weathered (mottled zone)	Slope to data point		Rescaled	Rescaled
		C_i^O (BR_26)	C_i^A (FZ_16)	C_i^A/C_i^O	*Scale*	C_i^A	C_i^O
Al_2O_3	wt %	13.0	19.9	1.53	1	19.9	13.0
TiO_2	wt %	0.20	0.30	1.50	80	24.0	16.0
Th	ppm	63.1	106	1.67	0.2	21.1	12.6
Zr	ppm	474	826	1.74	0.04	33.0	19.0
Hf	ppm	15.5	28.6	1.85	0.5	14.3	7.8
Nb	ppm	138	221	1.61	0.2	44.2	27.5

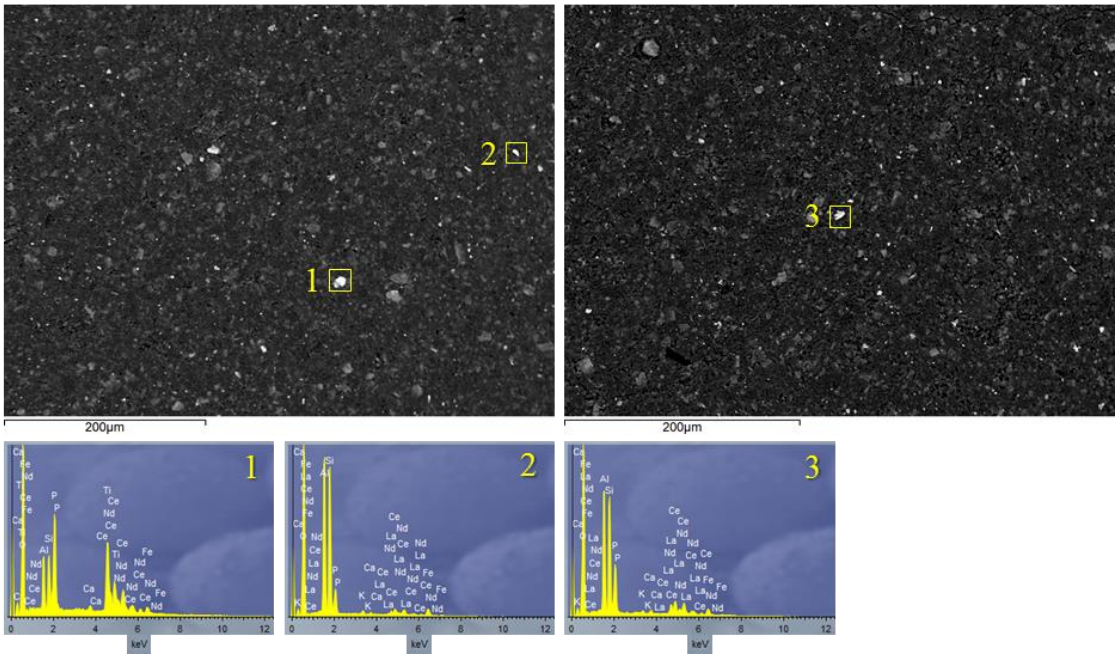
DDH0099

Element		Least weathered (bedrock)	Most weathered (ferruginous zone)	Slope to data point		Rescaled	Rescaled
		C_i^O (BR_29)	C_i^A (FZ_2)	C_i^A/C_i^O	*Scale*	C_i^A	C_i^O
Al_2O_3	wt %	12.5	15.6	1.24	1	15.6	12.5
TiO_2	wt %	0.22	0.4	1.64	70	25.2	15.4
Th	ppm	69.6	153	2.20	0.2	30.6	13.9
Zr	ppm	540	716	1.33	0.04	28.6	21.6
Hf	ppm	17.1	22.3	1.30	0.5	11.2	8.6
Nb	ppm	148	134.5	0.91	0.18	24.2	26.6

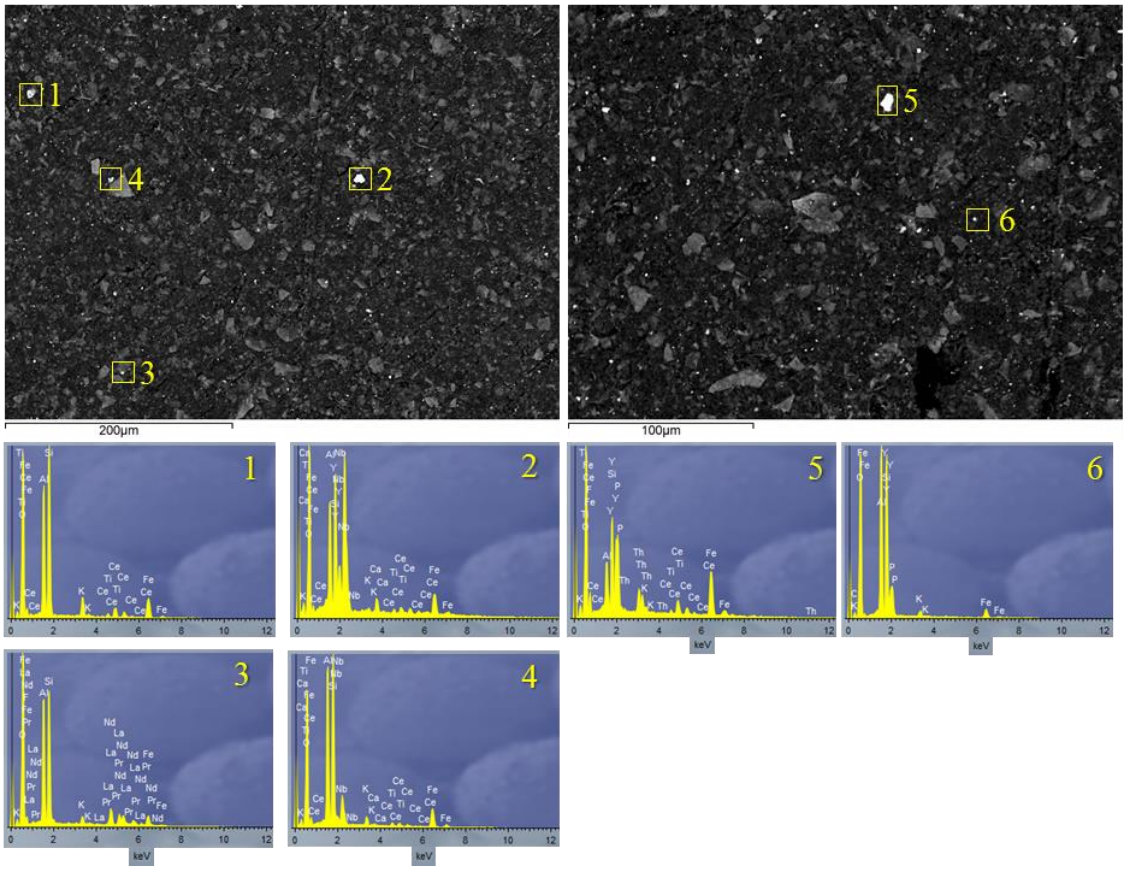
Element		Least weathered (bedrock)	Most weathered (mottled zone)	Slope to data point		Rescaled	Rescaled
		C_i^O (BR_29)	C_i^A (FZ_6.5)	C_i^A/C_i^O	*Scale*	C_i^A	C_i^O
Al_2O_3	wt %	12.5	20.9	1.67	1	20.9	12.5
TiO_2	wt %	0.22	0.36	1.64	70	25.2	15.4
Th	ppm	69.6	118	1.69	0.2	23.5	13.9
Zr	ppm	540	863	1.60	0.04	34.5	21.6
Hf	ppm	17.1	26.9	1.57	0.5	13.5	8.6
Nb	ppm	148	217	1.47	0.18	39.1	26.6

E1. Clay separates analysis

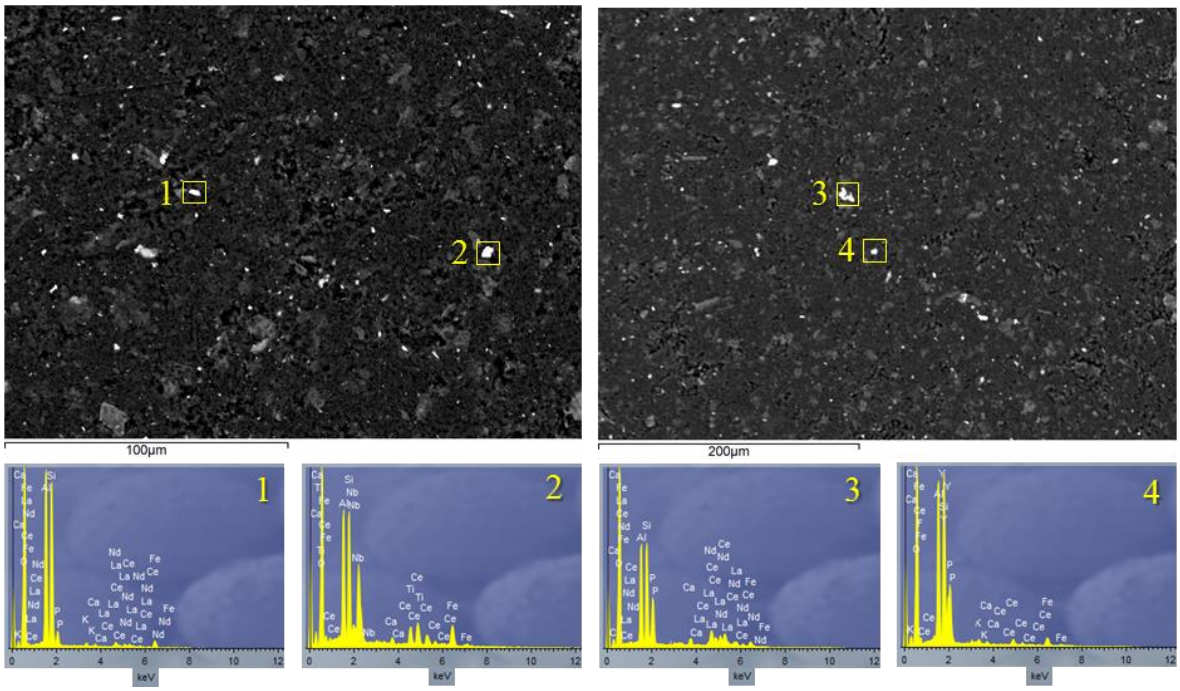
CS11-96



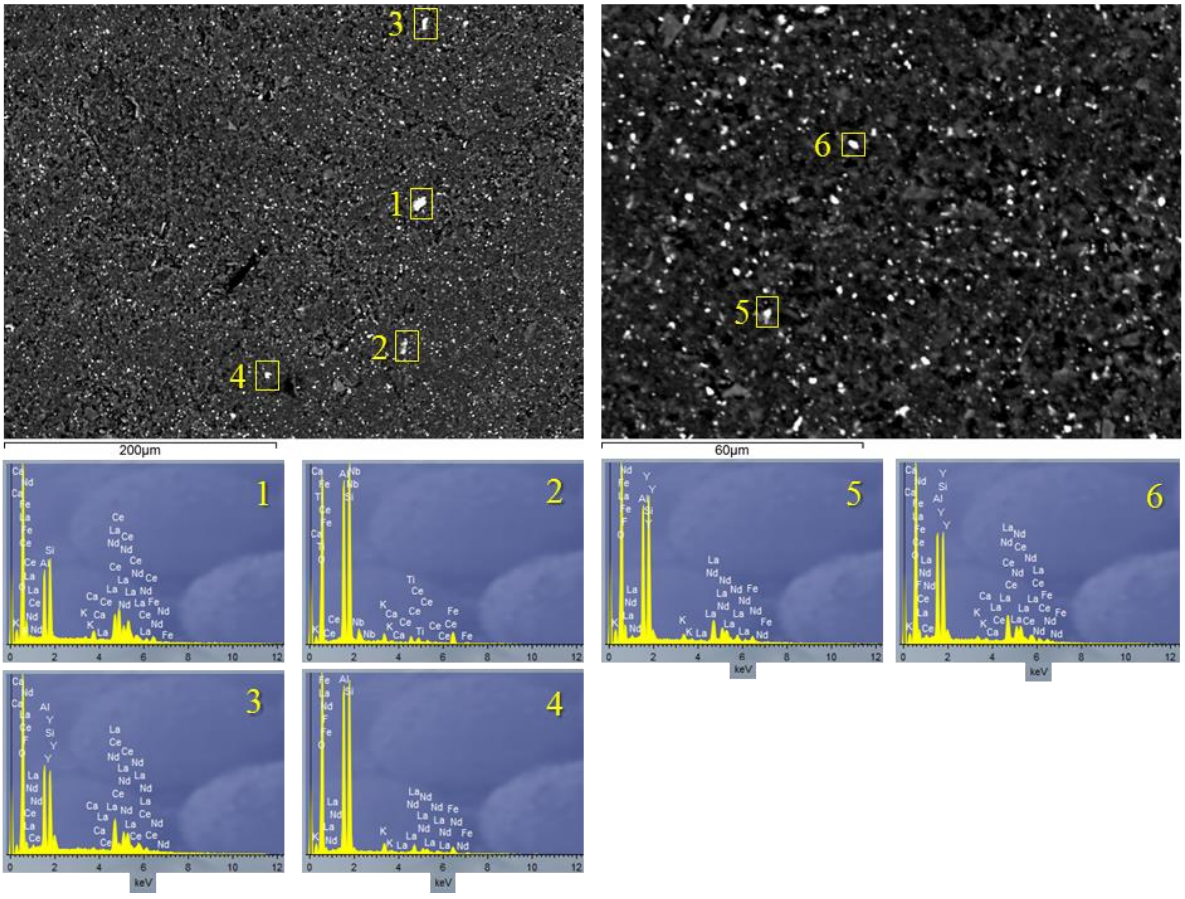
CS12-121



CS13-61

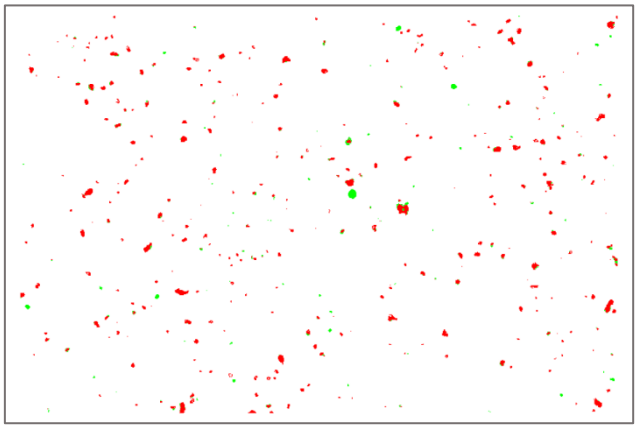


CS16-266



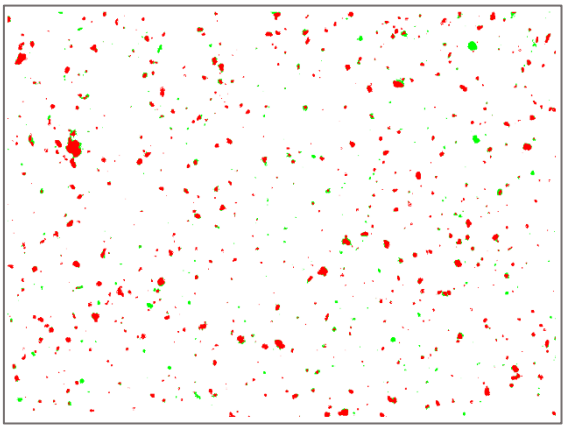
E2. Mineral maps

Map 1: DDH0266



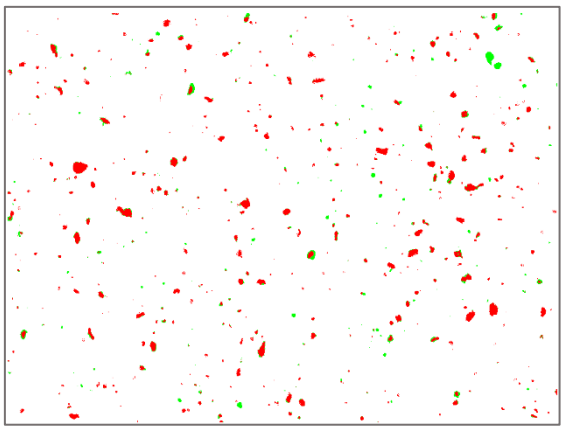
La grains =1.2 vol % Y grains = 0.21 vol %

Map 2: DDH00266



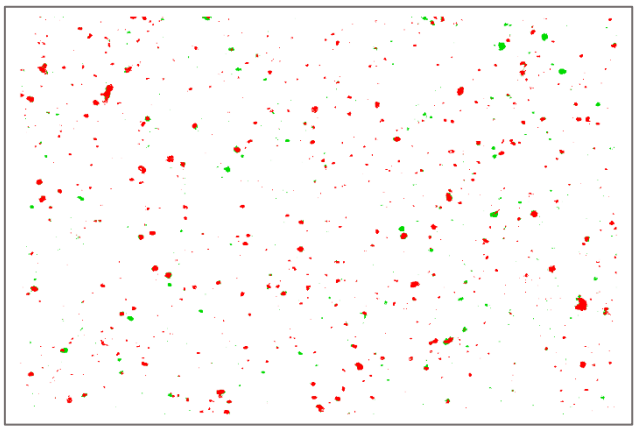
La grains = 1.8 vol %Y grains = 0.5 vol %

Map 3: DDH0266



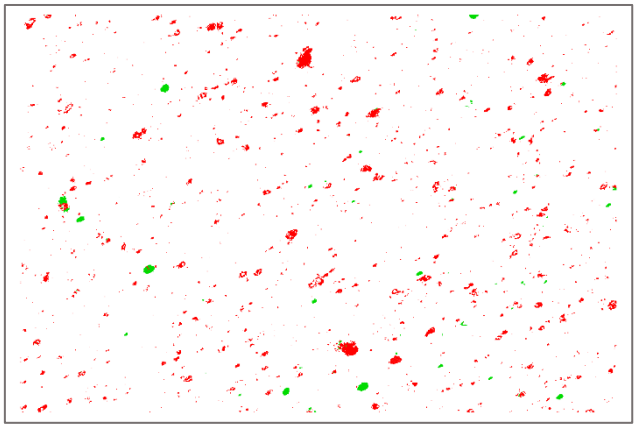
La grains = 2.4 vol % Y grains= 0.7 vol %

Map 1: DDH0161_26.9



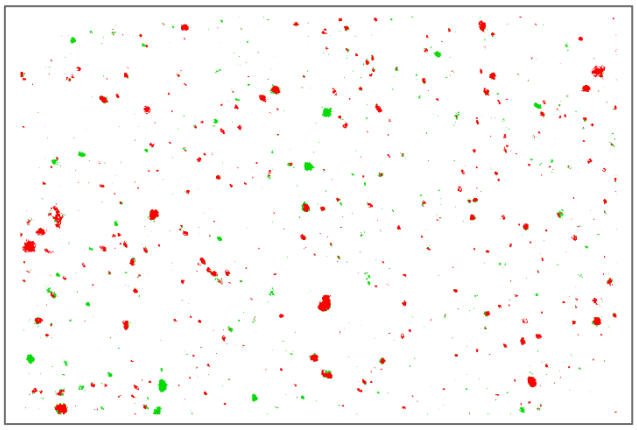
La grains = 1.49 % vol Y grains = 0.46 % vol

Map 2: DDH0161_26.9



La grains = 1.4 % vol Y grains = 0.26 % vol

Map 3: DDH0161_26.9



La grains = 1.8 % vol Y grains =0.25 % vol

LEACHING EXPERIMENTS RAW DATA F

ICP-MS analysis of supernatant solutions from leaching experiments

Sample	Batch experiment	Weight g	Na ppb	Mg ppb	Al ppb	K ppb	Ca ppb	Sc ppb	Mn ppb	Fe ppb	Rb ppb	Sr ppb	Ba ppb	Th ppb	U ppb	Y ppb
	LOQ, ppb		19.7	0.298	1.02	19.1	11.4	0.12	0.04	0.77	0.01	0.03	0.53	0.03	0.01	0.20
Run 1	0.5 M $(NH_4)_2SO_4$ pH 5															
1.1	10 min	0.5073	1061	1022	370	16995	6068	<1	523	166	241	28.7	222	1.52	45.2	3925
1.2	30 min	0.508	1203	1049	235	16874	6316	<1	498	46.4	237	29.4	208	<0.3	44.5	3800
1.3	1 hr	0.5132	1024	974	253	16143	5909	<1	461	47.6	225	27.5	229	0.337	43.6	3535
1.4	2 hr	0.5199	958	963	256	15615	5777	<1	439	43.1	219	26.7	224	<0.3	42.1	3377
1.5	5 hr	0.5125	1362	959	355	14780	5898	<1	408	61.2	212	24.1	215	2.01	40.6	3129
Run 2	0.5 M $(NH_4)_2SO_4$ pH 5															
2.1	S1	0.505	1234	1213	42015	4074	2398	<5	200	69.5	97.5	12.0	171	46.7	39.7	25639
2.2	S3	0.524	<985	633	7519	3731	1945	<5	73.7	<38	118	11.9	366	16.1	127	46398
2.3	S5	0.540	1077	1109	1039	3773	5848	<5	116	<38	128	24.5	230	2.95	50.8	57367
2.4	kaolinite STD	0.516	1343	5619	147	1340	87720	<5	22.7	43.4	7.09	143	104	<1.5	<0.3	16.2
2.5	SV6	0.516	5517	940	307	14572	4956	<5	522	<38	296	21.5	270	<1.5	18.6	4198
2.6	SV7	0.508	1304	1006	285	15002	6474	<5	440	40.1	222	28.2	219	<1.5	45.0	3380
2.7	SV9	0.515	13497	5237	222	9241	21438	<5	965	<38	155	121	402	<1.5	28.7	61118
2.8	SV11	0.513	2133	488	945	6185	2119	<5	449	<38	87.9	9.13	172	4.08	54.8	2883
2.9	SV12	0.550	1441	669	823	12100	1334	<5	505	<38	308	6.70	226	3.51	32.0	5123
2.1	SV13	0.508	1028	514	385	4985	7227	<5	105	<38	85.2	31.8	198	<1.5	13.6	4203
2.12	CS9	0.255	1116	3752	247	14153	32939	<5	2409	<38	190	135	275	<1.5	133	25190
2.11	CS7	0.259	9825	5504	746	7985	29105	<5	1381	<38	164	159	381	1.70	88.4	73649
Run 3	0.5 M $(NH_4)_2SO_4$ pH 4															
3.1	S1	0.5123	1033	1091	47823	3928	2178	6.51	191	87.4	89.8	11.33	171	56.1	43.2	24211
3.2	S3	0.5135	<985	624	13769	3956	1456	<5	75.3	<38	113	11.4	351	34.0	150	45308
3.3	S5	0.540	1047	1097	5220	3990	5190	<5	122	48.0	130	24.2	250	30.9	103	59288
3.4	kaolinite STD	0.500	1212	5602	1473	1349	86675	<5	18.8	132	6.45	142	97.6	2.53	0.621	20
3.5	SV6	0.5162	5416	947	4828	14905	4686	<5	687	123	300	21.7	260	19.7	60.7	4675
3.6	SV7	0.5014	1237	1008	4845	15315	6228	<5	541	353	223	26.9	202	12.5	113	3886
3.7	SV9	0.510	13266	5208	3405	9487	21729	<5	1033	121	150	118	443	10.7	82.9	62382
3.8	SV11	0.507	1967	489	2965	6541	2011	<5	493	191	90.0	9.68	177	32.5	86.7	2946
3.9	SV12	0.550	<985	709	4714	12620	735	<5	527	252	320	6.34	249	28.4	66.1	5400
3.1	SV13	0.5053	<985	523	2094	5226	7141	<5	132	249	88.0	30.8	208	6.00	30.4	4391
3.13	control		<985	24.2	70.3	<955	<569	<5	<2.1	<38	<0.5	<1.2	<26	<1.5	<0.3	<10
Run 4	0.5 M $(NH_4)_2SO_4$ pH 3															
4.1	S1	0.500	1217	1160	63949	3922	1578	13.3	190	659	89.92	10.8	163	172	56.9	24381
4.2	S3	0.5105	1043	719	24988	4385	1584	10.7	86.47	268	127	12.7	384	101	189	51860
4.3	S5	0.540	1210	1155	11096	4125	5764	9.54	131	285	134	25.2	250	87.2	124	62113
4.4	kaolinite STD	0.5118	1467	5651	3312	1508	88158	<5	30.23	427	7.11	143	93.7	7.83	0.928	14
4.5	SV6	0.512	5648	1007	26014	15432	5609	<5	1130	4913	315	24.8	234	308	108	6255
4.6	SV7	0.510	1416	1097	24728	16331	6403	<5	929	5832	239	28.5	192	93.6	164	5068
4.7	SV9	0.511	13647	5373	10890	9884	22200	<5	1157	2128	147	117	414	67.6	111	64186
4.8	SV11	0.5161	2085	520	9123	6838	2007	<5	551	1449	96	9.58	185	100	110	3086
4.9	SV12	0.570	<985	740	18046	13143	1190	9.60	546	4158	338	7.44	227	149	96.5	5820
4.1	SV13	0.511	1085	577	8486	5719	7713	<5	183	1957	94.36	32.02	208	16.0	41.5	4791
4.11	CS9	0.2549	<985	3397	17710	12649	27787	<5	2361	5988	151	114	322	108	1093	25062
4.12	CS7	0.260	10806	6069	11800	8955	32881	<5	1650	2306	178	173	373	96.7	259	83104
4.13	control		<985	21.06	90.89	<955	<569	<5	<2.1	<38	<0.5	<1.2	<26	<1.5	<0.3	<10
Run 5	D.I water															
5.10	S1	0.505	5321	117	1545	6446	931	2.03	16.1	203	53.6	2.05	14.5	9.11	1.27	73.0
5.20	S3	0.507	394	6.82	75.5	404	248	0.189	0.394	8.55	3.79	0.284	1.36	1.28	0.221	9.73
5.30	S5	0.504	630	64.3	56.2	1438	274	0.135	7.65	6.94	13.7	1.12	10.3	0.487	0.248	20.5
5.4	kaolinite STD	0.502	866	281	14.3	537	3859	<0.1	1.11	1.68	1.07	5.69	7.23	<1.5	<0.3	<10
5.50	SV6	0.515	3608	10.5	144	2376	118	0.125	7.92	204	13.9	0.224	2.39	0.990	0.0884	4.75
5.6	SV7	0.501	700	14.4	198	3583	105	0.127	6.95	263	16.3	0.237	1.44	1.12	0.149	15.7
5.7	SV9	0.516	5154	14.1	181	849	99.7	0.130	5.34	91.2	3.56	0.282	1.77	1.27	0.264	32.0
5.8	SV11	0.506	1390	8.67	54.0	1318	78.3	<0.1	5.65	55.9	4.27	0.179	0.782	0.297	0.115	1.53
5.9	SV12	0.514	320	18.3	110	2599	69.5	0.122	8.79	126	16.1	0.208	2.15	0.695	0.110	3.54
5.1	SV13	0.505	503	9.64	41.0	1397	128	<0.1	2.71	21.2	5.30	0.372	1.18	0.414	0.0599	2.07
5.11	CS9	0.255	238	61.1	427	1929	342	0.336	33.8	552	11.6	1.23	5.07	2.26	0.784	26.3
5.12	CS7	0.258	2988	14.7	70.6	495	66.3	0.150	3.53	54.3	1.94	0.152	1.61	0.996	0.280	8.47
5.13	control		<985	22.8	59.0	<955	<569	<5	<2.1	<38	<0.5	<1.2	<26	3.05	<0.3	<10

Sample	Batch experiment	Weight g	La ppb	Ce ppb	Pr ppb	Nd ppb	Sm ppb	Eu ppb	Gd ppb	Tb ppb	Dy ppb	Ho ppb	Er ppb	Tm ppb	Yb ppb	Lu ppb	Y ppb
LOQ, ppb			0.55	0.04	0.08	0.25	0.05	0.01	0.05	0.01	0.05	0.01	0.02	0.01	0.02	0.01	0.20
Run 1	0.5 (NH4)2SO4 pH 5																
1.1	10 min	0.5073	9419	576	1480	5005	743	43.4	765	111	605	120	330	40.5	219	30.2	3925
1.2	30 min	0.508	9227	542	1429	4888	708	41.8	735	106	576	114	312	38.2	205	28.4	3800
1.3	1 hr	0.5132	8689	502	1349	4570	660	38.4	686	98.7	535	106	289	35.1	188	26.1	3535
1.4	2 hr	0.5199	8487	479	1296	4375	628	36.5	663	93.3	506	101	272	32.8	177	24.2	3377
1.5	5 hr	0.5125	7697	434	1163	3931	588	34.0	617	87.0	470	93.9	253	30.1	160	22.3	3129
Run 2	0.5 M $(NH_4)_2SO_4$ pH 5																
2.10	S1	0.505	53838	21907	9437	29282	4075	243	3765	570	3420	782	2446	349	2064	291	25639
2.20	S3	0.524	143676	1225	24742	77614	10932	741	9264	1282	6951	1472	4424	616	3580	517	46398
2.30	S5	0.540	166490	619	28488	89480	13344	969	11676	1658	8927	1809	5260	718	4157	597	57367
2.40	kaolinite STD	0.516	33.3	3.61	5.70	18.70	2.76	<0.3	2.68	<0.3	<2.5	<0.4	1.19	<0.3	<1	<0.3	16.2
2.50	SV6	0.516	11593	868	1944	6458	957	54.2	905	127	669	131	357	42.8	229	31.3	4198
2.60	SV7	0.508	8332	475	1265	4348	652	37.8	679	96.9	526	104	285	34.6	183	25.5	3380
2.70	SV9	0.515	94182	3416	16394	54987	9879	626	10932	1804	10464	2100	5815	787	4459	627	61118
2.80	SV11	0.513	10788	975	2460	8132	1190	59.3	834	110	568	110	322	42.8	257	35.3	2883
2.90	SV12	0.550	13262	332	2490	8343	1245	102	1032	152	873	183	560	80.3	504	73.2	5123
2.1	SV13	0.508	5066	54.84	695	2369	393	36.7	527	87.5	548	125	370	49.5	275	39.7	4203
2.12	CS9	0.255	44846	2393	7483	25465	4480	257	4734	740	4084	822	2258	279	1637	217	25190
2.11	CS7	0.259	113690	4242	19901	66722	11997	759	13311	2219	12982	2611	7209	980	5703	794	73649
Run 3	0.5 M $(NH_4)_2SO_4$ pH 4																
3.1	S1	0.5123	50855	20479	8984	27725	3858	226	3588	545	3255	744	2326	330	1983	271	24211
3.2	S3	0.5135	139778	1182	24306	76190	10781	740	9174	1260	6886	1447	4370	607	3556	516	45308
3.3	S5	0.540	172083	653	29692	93531	13961	1021	12285	1756	9571	1934	5613	770	4467	647	59288
3.4	kaolinite STD	0.500	46.95	5.03	8.42	27.23	4.46	0.42	3.96	0.605	3.11	0.706	1.94	<0.3	1.41	<0.3	20
3.5	SV6	0.5162	12444	1012	2151	7150	1088	62.0	1015	147	795	156	427	53.6	301	41.4	4675
3.6	SV7	0.5014	8934	561	1438	4935	762	44.1	782	115	636	126	345	43.6	246	34.2	3886
3.7	SV9	0.510	95555	3494	16711	56323	10058	647	11185	1853	10758	2145	6043	819	4701	660	62382
3.8	SV11	0.507	10794	1001	2486	8275	1201	59.7	830	112	575	111	327	43.9	266	36.3	2946
3.9	SV12	0.550	13386	370	2561	8609	1285	105	1064	157	914	192	591	85.4	541	78.3	5400
3.1	SV13	0.5053	5173	76.2	718	2453	408	37.8	544	91.7	580	131	391	53.2	299	43.1	4391
3.13	control		<27.5	<1.7	<4	<12.5	<2.5	<0.3	<2.5	<0.3	<2.5	<0.4	<1	<0.3	<1	<0.3	<10
Run 4	0.5 M $(NH_4)_2SO_4$ pH 3																
4.1	S1	0.500	51582	20923	9097	28284	3909	227	3690	553	3336	767	2401	344	2048	275	24381
4.2	S3	0.5105	159880	1383	27821	86960	12225	844	10482	1452	7933	1665	4969	698	4082	591	51860
4.3	S5	0.540	177646	694	30733	96201	14496	1059	12723	1817	9819	1989	5794	794	4632	663	62113
4.4	kaolinite STD	0.5118	28	8	4.42	15.7	2.83	<	2.61	<	<	0.443	1.31	<0.3	<1	<0.3	14
4.5	SV6	0.512	13609	1399	2500	8282	1319	75.8	1220	183	1012	198	551	71.6	421	57.7	6255
4.6	SV7	0.510	10962	839	1917	6485	1042	60.8	1029	156	876	171	476	62.3	358	49.5	5068
4.7	SV9	0.511	96907	3572	17057	57305	10372	652	11356	1899	11062	2215	6214	839	4847	685	64186
4.8	SV11	0.5161	11115	1048	2564	8514	1228	60.5	850	114	591	115	336	45.0	277	38.1	3086
4.9	SV12	0.570	13746	404	2651	8835	1312	108	1077	162	946	197	607	88.9	570	81.8	5820
4.1	SV13	0.511	5410	114	755	2582	432	40.2	572	97.8	620	139	416	57.5	331	47.3	4791
4.11	CS9	0.2549	42224	2353	7368	25096	4535	252	4669	739	4150	830	2319	287	1832	234	25062
4.12	CS7	0.260	123392	4672	21576	72078	13037	826	14508	2411	14104	2824	7893	1072	6319	881	83104
4.13	control		<27.5	3.59	<4	<12.5	<2.5	<0.3	<2.5	<0.3	<2.5	<0.4	<1	<0.3	<1	<0.3	<10
Run 5	D.I water																
5.10	S1	0.505	177	205	32.2	100	13.9	0.78	13.3	1.78	10.5	2.32	7.06	0.992	5.84	0.846	73.0
5.2	S3	0.507	41.9	16.8	7.60	23.2	3.39	0.18	2.85	0.351	1.73	0.333	0.946	0.123	0.708	0.100	9.73
5.3	S5	0.504	52.7	3.58	9.27	28.2	4.43	0.32	4.02	0.585	3.26	0.653	1.88	0.252	1.50	0.210	20.5
5.4	kaolinite STD	0.502	<27.5	<1.7	<4	<12.5	<2.5	<0.3	<2.5	<0.3	<2.5	<0.4	<1	<0.3	<1	<0.3	<10
5.5	SV6	0.515	18.3	11.2	4.01	12.3	2.03	0.10	1.54	0.209	1.02	0.179	0.483	0.061	0.360	0.0466	4.75
5.6	SV7	0.501	63.5	7.49	13.0	41.7	6.78	0.36	5.31	0.731	3.49	0.569	1.41	0.164	0.936	0.112	15.7
5.7	SV9	0.516	45.7	10.3	8.66	28.2	5.32	0.32	5.68	0.955	5.69	1.13	3.19	0.447	2.81	0.381	32.0
5.8	SV11	0.506	3.52	0.87	0.77	2.51	0.405	0.02	0.323	0.0495	0.276	0.0556	0.165	0.0232	0.146	0.0198	1.53
5.9	SV12	0.514	8.40	4.04	1.64	5.29	0.893	0.07	0.774	0.114	0.640	0.127	0.368	0.0526	0.326	0.0464	3.54
5.1	SV13	0.505	7.51	3.12	1.36	4.31	0.752	0.05	0.691	0.0955	0.457	0.0783	0.203	0.0260	0.141	0.0197	2.07
5.11	CS9	0.255	101	14.1	20.6	64.9	10.6	0.56	8.31	1.17	5.75	0.977	2.52	0.307	1.80	0.225	26.3
5.12	CS7	0.258	13.2	5.63	2.48	8.23	1.52	0.09	1.57	0.259	1.52	0.300	0.849	0.118	0.740	0.102	8.47
5.13	control		<27	<1.7	<4	<12	<2.5	<0.3	<2.5	<0.3	<2.5	<0.4	<1	<0.3	<1	<0.3	<10